PHYSIOLOGY AND PATHOPHYSIOLOGY OF THE HEART

edited by

Nicholas Sperelakis

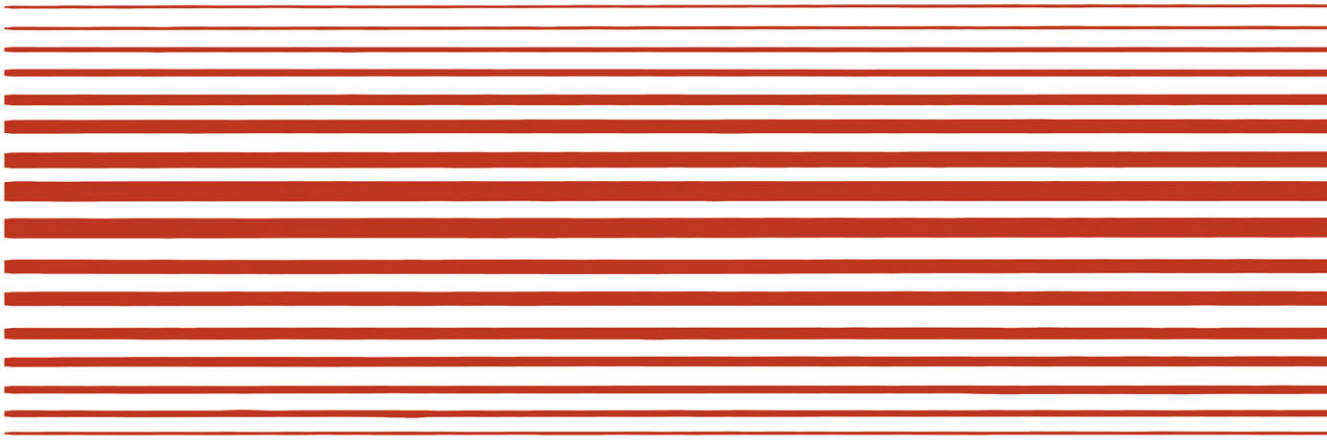

Springer-Science+Business Media, B.V.

PHYSIOLOGY AND PATHOPHYSIOLOGY OF THE HEART

Developments in Cardiovascular Medicine

Other volumes in this series:

Lancée CT, ed: Echocardiology, 1979, ISBN 90-247-2209-8.

Baan J, Arntzenius AC, Yellin EL, eds: Cardiac dynamics. 1980. ISBN 90-247-2212-8.

Thalen HJT, Meere CC, eds: Fundamentals of cardiac pacing. 1970. ISBN 90-247-2245-4.

Kulbertus HE, Wellens HJJ, eds: Sudden death. 1980.
ISBN 90-247-2290-X.

Dreifus LS, Brest AN, eds: Clinical applications of cardiovascular drugs. 1980. ISBN 90-247-2295-0.

Spencer MP, Reid JM, eds: Cerebrovascular evaluation with Doppler ultrasound. 1981.
ISBN 90-247-2348-1.

Zipes DP, Bailey JC, Elharrar V, eds: The slow inward current and cardiac arrhythmias. 1980.
ISBN 90-247-2380-9.

Kesteloot H, Joossens JV, eds: Epidemiology of arterial blood pressure. 1980. ISBN 90-247-2386-8.

Wackers FJT, ed: Thallium-201 and technetium-99m-pyrophosphate myocardial imaging in the coronary care unit. 1980. ISBN 90-247-2396-5.

Maseri A, Marchesi C, Chierchia S, Trivella MG, eds: Coronary care units. 1981. ISBN 90-247-2456-2.

Morganroth J, Moore EN, Dreifus LS, Michelson EL, eds: The evaluation of new antiarrhythmic drugs. 1981. ISBN 90-247-2474-0.

Alboni P: Intraventricular conduction disturbances. 1981.
ISBN 90-247-2483-X.

Rijsterborgh H, ed: Echocardiology. 1981. ISBN 90-247-2491-0.

Wagner GS, ed: Myocardial infarction: Measurement and intervention. 1982. ISBN 90-247-2513-5.

Meltzer RS, Roelandt J, eds: Contrast echocardiography. 1982. ISBN 90-247-2531-3.

Amery A, Fagard R, Lijnen R, Staessen J, eds: Hypertensive cardiovascular disease; pathophysiology and treatment. 1982. ISBN 90-247-2534-8.

Bouman LN, Jongsma HJ, eds: Cardiac rate and rhythm. 1982. ISBN 90-247-2626-3.

Morganroth J, Moore EN, eds: The evaluation of beta blocker and calcium antagonist drugs. 1982.
ISBN 90-247-2642-5.

Rosenbaum MB, ed: Frontiers of cardiac electrophysiology. 1982. ISBN 90-247-2663-8.

Roelandt J, Hugenholtz PG, eds: Long-term ambulatory electrocardiography. 1982. ISBN 90-247-2664-8

Adgey AAJ, ed: Acute phase of ischemic heart disease and myocardial infarction. 1982.
ISBN 90-247-2675-1.

Hanrath P, Bleifeld W, Souquet, J. eds: Cardiovascular diagnosis by ultrasound. Transesophageal, computerized, contrast, Doppler echocardiography. 1982. ISBN 90-247-2692-1.

Roelandt J, ed: The practice of M-mode and two-dimensional echocardiography. 1983.
ISBN 90-247-2745-6.

Meyer J, Schweizer P, Erbel R, eds: Advances in noninvasive cardiology. 1983. ISBN 0-89838-576-8.

Morganroth Joel, Moore EN, eds: Sudden cardiac death and congestive heart failure: Diagnosis and treatment. 1983. ISBN 0-89838-580-6.

Perry HM, ed: Lifelong management of hypertension. ISBN 0-89838-582-2.

Jaffe EA, ed: Biology of endothelial cells. ISBN 0-89838-587-3.

Surawicz B, Reddy CP, Prystowsky EN, eds: Tachycardias.
ISBN 0-89838-588-1.

Spencer MP, ed: Cardiac Doppler diagnosis. ISBN 0-89838-591-1.

Villareal HV, Sambhi MP, eds: Topics in pathophysiology of hypertension. ISBN 0-89838-595-4.

Messerli FH, ed: Cardiovascular disease in the elderly.
ISBN 0-89838-596-2.

Simoons ML, Reiber JHC, eds: Nuclear imaging in clinical cardiology. ISBN 0-89838-599-7.

Ter Keurs HEDJ, Schipperheym JJ, eds: Cardiac left ventricular hypertrophy. ISBN 0-89838-612-8.

PHYSIOLOGY AND PATHOPHYSIOLOGY OF THE HEART

Edited By

Nicholas Sperelakis

SPRINGER-SCIENCE+BUSINESS MEDIA, B.V.

Library of Congress Cataloging in Publication Data
Main entry under title:

Physiology and pathophysiology of the heart.

(Developments in cardiovascular medicine ; v. 34)
Includes bibliographical references and index.
1. Heart—Addresses, essays, lectures. 2. Coronary circulation—Addresses, essays, lectures. 3. Heart—Diseases—Addresses, essays, lectures. I. Sperelakis, Nick, 1930- . II. Series. [DNLM: 1. Heart—Physiology. 2. Heart—Physiopathology. WG 202 P5787]
QP111.4.P53 1984 612'.17 83-21926
ISBN 978-1-4757-1173-8 ISBN 978-1-4757-1171-4 (eBook)
DOI 10.1007/978-1-4757-1171-4

CONTENTS

CONTRIBUTING AUTHORS

Dr. Tai Akera
Department of Pharmacology and Toxicology
Life Sciences Building
Michigan State University
East Lansing, MI 48824 USA
Chicago, IL 60611 USA

Dr. Morton F. Arnsdorf
Department of Medicine
School of Medicine
University of Chicago
Chicago, IL 60637 USA

Dr. Roger C. Barr
Department of Biomedical Engineering
Duke University School of Medicine
Durham, NC 27706 USA

Dr. Arthur L. Bassett
Department of Pharmacology
Northwestern University Medical School
Chicago, IL 60611 USA

Dr. Clive Marc Baumgarten
Department of Physiology
Medical College of Virginia
Box 551
Richmond, VA, 23298 USA

Dr. Richard J. Bing
Huntington Memorial Hospital
100 Congress Street
Pasadena, CA 91105 USA
Dallas, TX 75235 USA

Dr. Allan J. Brady
Medical Center
University of California
Los Angeles, CA 90024 USA

Prof. Hans Jürgen Bretschneider
Institute of Physiology
University of Göttingen
D-3400 Göttingen
West Germany

Dr. Theodore M. Brody
Department of Pharmacology and Toxicology
Life Sciences Building
Michigan State University
East Lansing, MI 48824 USA

Dr. L. Maximilian Buja
Department of Pathology
School of Medicine
University of Texas
5232 Harry Hines Boulevard
Dallas, TX 75235 USA

Prof. R. Casteels
Laboratorium voor Fysiologie
K.U.L. Campus Gasthuisberg
Herestraat
B-300 Leuven, Belgium

Dr. M.J. Daly
Department of Medicine
University of Melbourne
Austin Hospital
Heidelberg
Victoria, Australia

Prof. Walmor C. De Mello
Department of Pharmacology
Medical Sciences Campus
University of Puerto Rico
GPO Box 5067
San Juan, Puerto Rico 00936

Dr. Donald F. DeWitt
Department of Physiology
School of Medicine
Michigan State University
East Lansing, MI 48824 USA

Dr. Steven R. Driska
Physiology Department, Box 551
Medical College of Virginia
Virginia Commonwealth University
MCV Station
Richmond, VA 23298 USA

Dr. G. Droogmans
Laboratorium voor Fysiologie
K.U.L. Campus Gasthuisberg
Herestraat
B-300 Leuven, Belgium

Dr. Alexandre Fabiato
Department of Physiology
Medical College of Virginia
Box 551
Richmond, VA 23298 USA

Dr. Victor J. Ferrans
Pathology Branch
National Heart, Lung, and Blood Institute
National Institutes of Health
Bethesda, MD 20014 USA

Prof. A. Fleckenstein
Albert-Ludwigs-Universität
Physiologisches Institut
Hermann-Herder-Strasse 7
D7800 Freiburg, West Germany

Dr. G. Fleckenstein-Grün
Albert-Ludwigs-Universität
Physiologisches Institut
Hermann-Herder-Strasse 7
D-7800 Freiburg, West Germany

Prof. Michael S. Forbes
Department of Physiology
School of Medicine
University of Virginia
Charlottesville, VA 22908 USA

Dr. Martha Maria Gebhard
Institute of Physiology
University of Göttingen
D-3400 Göttingen
West Germany

Dr. S. David Gertz
Department of Anatomy and Embryology
Hebrew University
Hadassah Medical School
PO Box 102
Jerusalem, Israel

Dr. Philip D. Henry
Department of Medicine
Cardiovascular Division
Baylor College of Medicine
Methodist Hospital
6516 Bertner Avenue
Houston, TX 77030 USA

Dr. Kent Hermsmeyer
Department of Pharmacology
College of Medicine
University of Iowa
Bowen Science Building
Iowa City, IA 52242 USA

Dr. Luc M. Hondeghem
Department of Pharmacology
University of California/San Francisco
San Francisco, CA 94143 USA

Prof. H. Irisawa, M.D.
National Institute for Physiological Sciences
Okazaki
Myodiji, 444 Japan

Dr. Robert S. Kass
Physiology Department
School of Medicine
University of Rochester
601 Elmwood Avenue
Rochester, NY 14642 USA

Dr. Bertram G. Katzung
Department of Pharmacology
School of Medicine
University of California/San Francisco
San Francisco, CA 94143 USA

Dr. S. Kokubun
National Institute for Physiological Sciences
Okazaki
Myodiji, 444 Japan

Dr. Y. Kurachi
National Institute for Physiological Sciences
Okazaki
Myodiji, 444 Japan

Dr. Adi Kurgan
Department of Anatomy and Embryology
Hebrew University
Hadassah Medical School
PO Box 102
Jerusalem, Israel

Dr. Edward G. Lakatta, Chief
Cardiovascular Section
National Institute on Aging
4940 Eastern Avenue
Baltimore, MD 21224 USA

Prof. Michel Lazdunski
Centre de Biochimie
Faculte S.P.C.N.I.
Universite de Nice/Parc Valrose
F-06034 Nice, France

Dr. Ralph Lazzara
Med./Cardiol. Sec.
Oklahoma Univ. Health Science Center
PO Box 26901
Oklahoma City, OK 73190 USA

Dr. Matthew N. Levy
Department of Investigative Medicine
Mount Sinai Hospital
Cleveland, OH 44106 USA

Dr. Jon P. Lindemann
Richard L. Roudebush Veterans Administration Medical Center
and Krannert Institute of Cardiology
1001 W. 10th Street
Indianapolis, IN 46202

Dr. Paul J. Martin
Department of Investigative Medicine
Mount Sinai Hospital
Cleveland, OH 44106 USA

Dr. Terence F. McDonald
Department of Physiology and Biophysics
Dalhousie University
Halifax NS B3H 4H7
Canada

Dr. Eugene Morkin
Division of Cardiology
College of Medicine
University of Arizona
Tucson, AZ 85724 USA

Dr. Lorin J. Mullins
Biophysics Department
University of Maryland
Baltimore, MD 21201 USA

Dr. Winifred G. Nayler
Department of Medicine
University of Melbourne
Austin Hospital
Heidelberg
Victoria, Australia

Dr. A. Noma
National Institute for Physiological Studies
Okazaki
Myodiji, 444
Japan

Dr. Yasuharu Nimura
National Cardiovascular Research Institute
Suita 565, Japan

Prof. L.H. Opie
Department of Medicine
School of Medicine
University of Cape Town
Observatory 7925
Cape Town, South Africa

Dr. Achilles J. Pappano
Department of Pharmacology
University of Connecticut Health Center
2 Holcomb Street
Farmington, CT 06032 USA

Dr. John W. Peterson
Neurosurgical Services
Warren–4 Building
Massachusetts General Hospital
Boston, MA 02114 USA

Dr. Margaret G. Pratila
Anesthesiology Department
Memorial/Sloane Kettering Hospital
New York, NY USA

Dr. Vasilios Pratilas
Anesthesiology Department
Mount Sinai School of Medicine
1 Gustave Levy Place
New York, NY 10029 USA

Dr. Claus Jürgen Preusse
Institute of Physiology
University of Göttingen
D-3400 Göttingen
West Germany

Dr. Jean-Francois Renaud
University of Nice
Centre de Biochimie
Faculte des Sciences, Parc Valrose
F-06034 Nice, France

Dr. Benjamin J. Scherlag
University of Oklahoma College of Med.
VA Hospital
Oklahoma City, OK 73104 USA

Dr. Munekazu Shigekawa
National Cardiovascular Research Institute
Suita 565, Japan

Dr. Harvey V. Sparks, Jr.
Department of Physiology
Michigan State University
East Lansing, MI 48824 USA

Prof. Nicholas Sperelakis
Department of Physiology
University of Cincinnati Medical Center
231 Bethesda Avenue
Cincinnati, Ohio 45267 USA

Dr. Michihiko Tada
First Department of Internal Medicine
University of Osaka
Kukushima-ku
Osaka 553, Japan

Dr. Robert E. Ten Eick
Department of Pharmacology
Northwestern University Medical School
Chicago, IL 60611 USA

Dr. Roger D. Wangler
Department of Physiology
School of Medicine
Michigan State University
East Lansing, MI 48824 USA

Dr. August M. Watanabe
Department of Medicine & Pharmacology
Indiana University School of Medicine
1100 W. Michigan Street
Indianapolis, IN 46223 USA

FOREWORD

This book emphasizes the fundamental, functional aspects of cardiology. Within the last thirty years, the rift between clinical and investigative cardiology has widened, because of the overwhelming development of new clinical procedures, both diagnostic and therapeutic. Almost forgotten is the fact that we owe most of the clinical advances to theoretical and experimental observations. I need not remind the reader of the work of Carrel, who performed the first experimental coronary bypass in 1902, or the work of the brothers Curie in 1880, both physicists, who discovered piezoelectricity, the keystone in echogradiography; of the works of Langley, who introduced the receptors concept; of Ahlquist in 1946, who first differentiated between alpha and beta receptors; of Fleckenstein, a physiologist who pioneered the field of Ca^{2+} antagonists. This list could go on for several pages. Thus the book edited by Sperelakis is a potent reminder of the almost forgotten fact that cardiology has two sites, inextricably related.

The book deals with subjects in which Dr. Sperelakis has pioneered: ultrastructure of heart muscle, electrophysiology, cardiac contractility, and ion exchange. An extension of these subjects is the chapter dealing with fundamental topics of the coronary circulation.

This book is indeed a timely reminder of the importance of the fundamental aspects of cardiology. Emphasis on clinical aspects of cardiology alone will result in a sterile and unproductive future for a field that has made such stunning advances during the last thirty years to the benefit of millions of people.

Richard J. Bing

PREFACE

The theme of this book is the physiology and function of the heart in the normal state and in various pathologic states. The two major sections are on (1) cardiac muscle and related tissues, such as nodal cell and Purkinje fiber systems, and (2) coronary circulation, including properties of the vascular smooth muscle cells. Not only are the relevant physiology and biophysics discussed, but, in addition, the ultrastructure, biochemistry, and pharmacology—that is, the book attempts to integrate all relevant aspects of the factors influencing the function of the heart as a vital organ under normal and abnormal conditions and states. The book also attempts to set the foundation for an understanding of the action of, and mechanism of action of, a number of classes of cardioactive drugs, including the calcium antagonistic drugs, antianginal drugs, antiarrthythmic drugs, and cardiac glycosides.

Each chapter is written by one or more experts in the area who have been selected from around the world. The authors were asked to aim for a clear, concise, accurate, and up-to-date summary of the topic in a didactic and textbook teaching style. it was suggested that the authors present key references only, with heavy emphasis on review-type and summary-type articles. The reader should be able to obtain the important facts, concepts, and hypotheses from the chapters and, if he or she wishes to go into greater depth and examine more of the evidence on some particular aspect, he or she can look up the appropriate reference.

The book is intended for practicing and academic cardiologists, related medical specialists, and researchers. However, resident physicians, graduate students, and medical students should find the book useful as a reference volume to supplement and amplify specific points covered in lectures and in broader textbooks. The authors were made aware of the audience intended for the book, and were requested to pitch their chapter at the appropriate level. It was suggested that they present sufficient detail, documentation, and illustrations as required for the readership that the book was aimed at. The clinician undoubtedly recognizes the importance of basic science aspects of the heart that underlie his or her practice of cardiology, and this undertaking attempts to help bridge the gap between basic science and clinical science.

As mentioned above, the chapters have been written by a distinguished group of experts and outstanding researchers in their respective fields from around the world. It has been my great pleasure in assembling and working with this distinguished group of individuals in this rather massive undertaking. I hope that the readers will recognize the merits of the book and will agree that it represents a clear, concise, up-to-date, and multidisciplinary book on the heart.

Nicholas Sperelakis

PHYSIOLOGY AND PATHOPHYSIOLOGY OF THE HEART

I. CARDIAC MUSCLE

1. ULTRASTRUCTURE OF MAMMALIAN CARDIAC MUSCLE

Michael S. Forbes
Nicholas Sperelakis

Introduction

The great majority of muscle cells of the mammalian heart are superbly organized entities. It is impressive to consider that observations on these myocytes are in most cases being made on cells which are roughly the same age as the entire animal; only a scant bit of evidence is yet available to suggest that any substantial capability for regeneration is intrinsic to the myocardia of higher vertebrates (see the section on *Nuclei*). Still these venerable cells can respond admirably under trying circumstances, such as those necessitating osmotic shrinkage or hypertrophy, in which cases they adjust their sarcolemmal and myoplasmic components to maintain an extraordinarily constant surface–volume ratio [1, 2]. In this chapter, we provide a sketch of the fine structure of cardiac muscle cells in mammalian heart. The many electron microscopic studies of such cells have served to point out the difficulty of making generalizations when considering the numerous aspects of myocardial substructure. We will, nevertheless, describe the salient features of myocardial cells, while pointing out along the way some of the variations on these basic themes which have been discovered to date.

Myocardial cells are commonly classified either in terms of their location within the heart (i.e., atrial vs ventricular) or according to their primary function (*working* [contractile] vs *conductive*). For the purposes of this description, we have chosen to deal with cardiac muscle cells primarily on the basis of the latter system of classification. "Working" cells are those which carry out the bulk of the mechanical activity of the heart, whereas cells of the AVCS (atrioventricular conducting system) are responsible for the generation and delivery of action potentials which regulate the rate and direction of heart contractions. Depending on the species being examined, the differences in morphology between working and AVCS cells may be profound, or may be scarcely appreciable.

Other comprehensive reviews of cardiac ultrastructure are available [e.g., 3–5], and there also have been published detailed compilations addressed to one or more specific cytologic feature of cardiac muscle cells, notably the membrane systems [6–8]. The efficacy of our summary sketch will be to present a picture of myocardial ultrastructure against which the results of microscopic studies—be they of normal or pathologic tissue—can be effectively compared. In addition, this study will serve to some degree as an anatomic reference for the remaining chapters in this volume. Because of the requisite interest in the structure and function of human heart, we have weighted this chapter on the side of the myocardial cells of the monkey, which offer both the advantages of reasonably ready availability and the ethical possibility of optimum fixation by means of vascular perfusion.

Synopsis of Myocardial Cell Structure

The generalizations of microscopic appearance which can be applied to the cardiac muscle cells of mammals are briefly described in this

N. Sperelakis (ed.), PHYSIOLOGY AND PATHOPHYSIOLOGY OF THE HEART.

Martinus Nijhoff Publishing, Boston/The Hague/
Dordrecht/Lancaster.

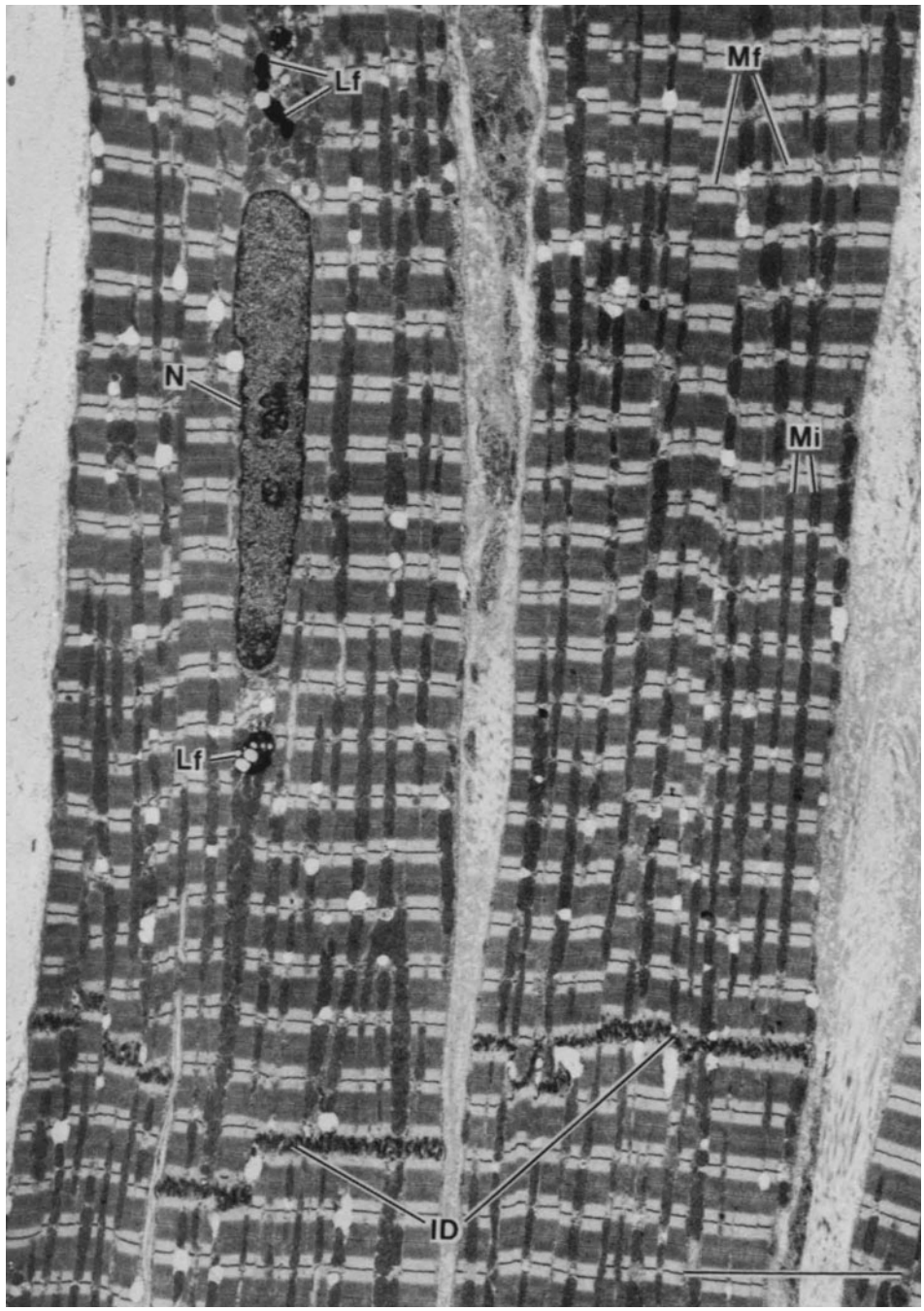

FIGURE 1–1. Transmission electron micrograph. Survey of longitudinal thin section of myocardium from right papillary muscle of monkey (vervet: *Cercopithecus aethiops*). A characteristic feature of these typical cardiac muscle cells is the longitudinal alignment of their major constituents; these include the myofibrils (Mf), which frequently exhibit branched profiles, mitochondria (Mi), which are arranged in intermyofibrillar rows for the most part, and nuclei, one of which (N) appears in this field. Regions of mitochondrion-rich myoplasm extend from each pole of the nucleus; examples of lipofuscin bodies (Lf) are most often located in this "nuclear pole myoplasm." The cell tips incorporate numerous intermembranous junctions, which collections form the intercalated discs (ID). Scale bar represents 10 μm.

section; the details and variations of cell structure are considered at greater length in the sections on *Working (contractile) myocardial cells* and *Conductive myocardial cells.*

WORKING VENTRICULAR CELLS

The contractile myocytes of the ventricular walls, papillary muscles, and interventricular septum are elongate, densely packed cells which are grouped into muscular rods or bands. Such cells display a distinct longitudinal polarity of the majority of their internal contents, including myofibrils, mitochondria, and nuclei (figs. 1–1 and 1–2). The closely apposed portions of cells—primarily the cell tips—contain numerous junctions which collectively form *intercalated discs,* the extensive regions of adhesion which are obvious even with light microscopy [9, 10]. Myofibrils, bundles of contractile protein filaments, are the primary cell constituent, followed in incidence by mitochondria, which fall into rows in the intermyofibrillar spaces and into less well organized masses in the subsarcolemmal and nuclear pole regions. Ventricular myocardial cells frequently possess two or more nuclei. The two membrane systems—(a) transverse (T) and axial tubules (which together comprise the T-axial tubular system: TATS), and (b) the sarcoplasmic reticulum (SR)—are well developed and frequently arranged in patterns seemingly directed by the presence of sarcomeric segmentation of the myofibrils. Working ventricular cells are thicker and more voluminous than their atrial counterparts.

WORKING ATRIAL CELLS

Although many of their cytologic features resemble those of ventricular muscle cells, the contractile cells of the atrium are substantially thinner (figs. 1–5 and 1–36) and frequently lack a system of T tubules. The packing of muscle cells within atrial walls and trabeculae is less dense than is the case for ventricular musculature. Intercalated discs are less elaborate and often consist largely of side-to-side attachments (figs. 1–5 and 1–36). The hallmark of atrial myocytes is the presence of *atrial specific granules* (figs. 1–36 and 1–38), dense-cored spheroids which appear in the nuclear pole cytoplasm, between myofibrils, and in the subsarcolemmal myoplasm.

CONDUCTIVE CELLS

Cells of the AVCS are the most varied in terms of interspecific comparison, as will be further considered in the section on *conductive myocardial cells.* Suffice it to say that the majority of nodal cells (i.e., those of the sinoatrial and atrioventricular nodes) are small and highly interdigitated to form characteristic cell groups (fig. 1–6). Nodal cells may, however, be difficult to distinguish from adjacent atrial cells, save on the basis of the numerous specific granules of the latter and the frequent Z-disc alterations in the former. The so-called *Purkinje cells,* which for the most part form subendocardial networks on the inner ventricular surfaces, are in many mammals thin cells with poorly developed intercalated discs and a fair amount of myofibrillar material. However, myofibril-poor cells can be seen as well, and in mammals such as the ungulates such Purkinje fibers are extremely large and are occupied by great quantities of glycogen and intermediate filaments [e.g., 11, 12]. There is general consensus that AVCS cells lack a system of T tubules, although they sometimes display pleimorphic sarcolemmal invaginations (see *Nodal cells*).

Working (Contractile) Myocardial Cells

CELL SHAPE AND SIZE

The overall forms of myocardial cells are not always apparent upon inspection of their profiles in the various tissue sections utilized for light and electron microscopy (fig. 1–1). A further degree of uncertainty is imposed by the existence within the mammalian heart of several rather distinct categories of cardiac muscle cells. To date, much of the investigation of three-dimensional structure has been carried out in the working ventricular myocardial cell, the classic form of the cardiomyocyte. This has been accomplished for the most part by the isolation of intact individual cells and the examination of those cells by various modes of microscopy (light, scanning electron, and

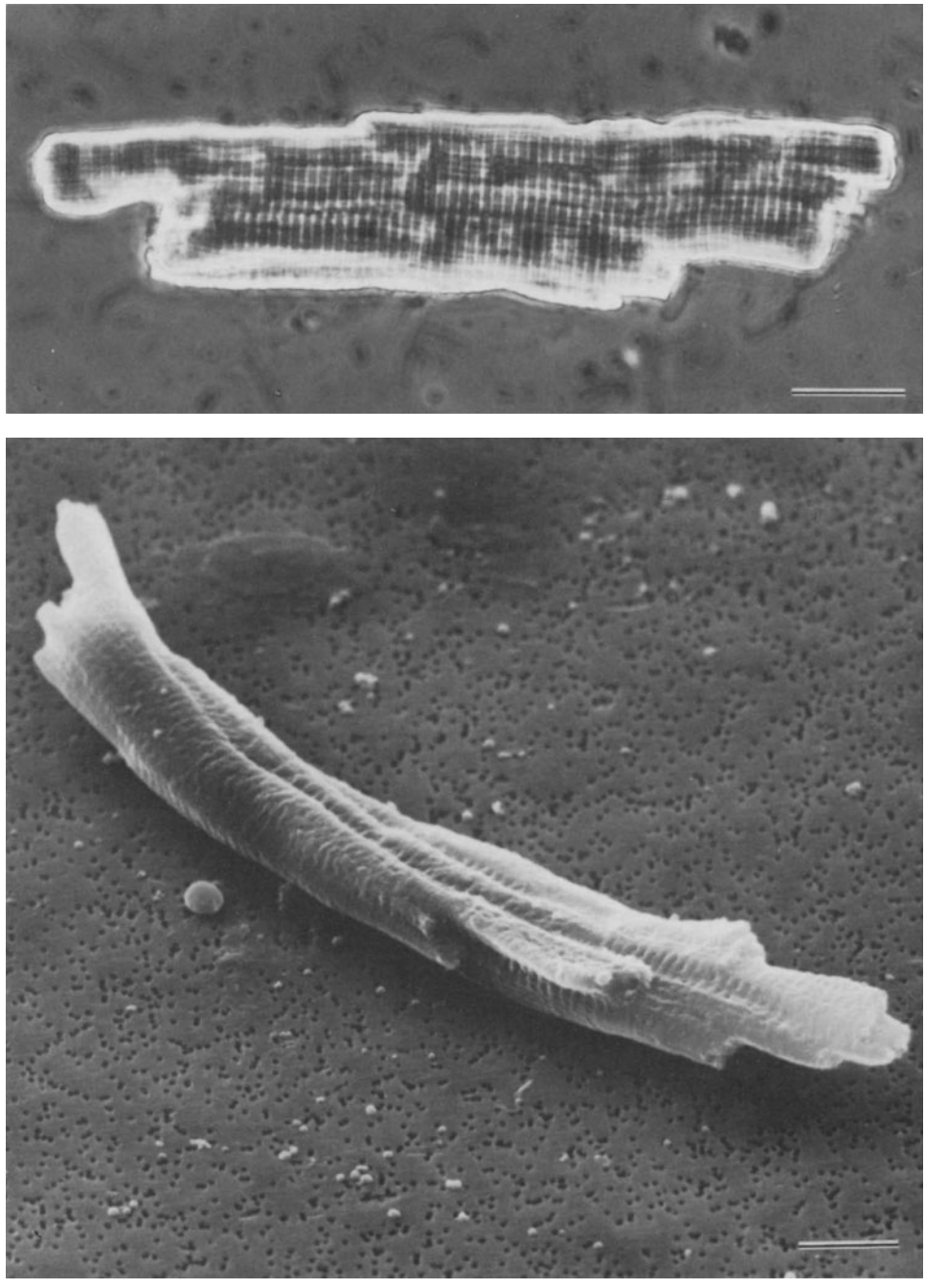

FIGURE 1–2. Phase-contrast light micrograph of ventricular cardiac muscle cell, isolated from rat heart by means of enzymatic digestion and mechanical dispersion [13]. The longitudinal array of myofibrils is obvious, and the myofibrillar banding pattern is clearly discernible (cf. fig. 1–1). The uneven profile of the cell tips is typical, derived from the cell's content of myofibrils of different lengths. Scale bar represents 20 μm.

FIGURE 1–3. Scanning electron micrograph of isolated rat ventricular myocyte. Staggered cell ends are evident; these are the basis of the steplike intercalated disc profiles found in thin sections (cf. figs. 1–1 and 1–27). The transverse striations seen over the entire lateral cell surface are likely "Z ridges," which probably are exaggerated by shrinkage of the sarcolemma over the Z discs of subsarcolemmal myofibrils. The curvature of this cell suggests origin from the ventricular wall. Scale bar represents 10 μm.

transmission electron [e.g., 13–15]). The shape of the "typical" cardiac muscle cell is largely the product of its internal construction, the cell appearing as a fasceslike assemblage of myofibrils, about which an external covering (the sarcolemma) is wrapped. The enveloped myofibrils may assume a variety of lengths, and thus frequently create staggered cell ends which are the basis of the steplike intercalated disc profiles (see *Intermembranous junctions* and figs. 1–1 and 1–3). In situ, the shape of the cardiac muscle cell is dictated also to some degree by its surroundings, the ventricular cell's profile in particular conforming to the contours of the numerous blood vessels of the heart (fig. 1–4). It has been pointed out that ventricular cells are not the simple cylindrical entities implied to exist by some histology texts, but in fact may be band- or ribbonlike, displaying in addition a goodly amount of branching [16, 17]. There has been increasing utilization of computer-based imaging of heart shape [18, 19]; recently this has been profitably used to describe the forms of both atrial and atrioventricular bundle cells [18].

The length of the "average" mammalian ventricular myocardial cell is commonly given as ca. 100 μm, with diameters on the order of 15–20 μm. In fact, the flattened configuration of ferret ventricular cells establishes for them both major and minor "diameters" of 26.8 μm and 8.3 μm, respectively [17]. Though it cannot be stated with certainty that individual myocardial cells retain their original shapes once they have become detached from one another, much of the recent data relating to cellular dimensions is derived from studies of single-cell preparations (figs. 1–2 and 1–3). There is variation between the results obtained by different investigators for similar preparations, however. Nag et al. [20] have given figures of 80 μm length and 12 μm diameter for isolated rat ventricular cells. On the other hand, Bishop and Drummond [21] record corresponding average values of 94 μm and 18 μm, but point out that two distinct cell types, mononucleate and binucleate, exist in adult rat ventricle. The binucleate cells constitute 85% of the total myocardial cell population, each possessing twice the volume of a typical mononucleate cell, and being both a third longer and a fifth again wider. Polyploidy is in fact common in ventricular cells (see *Nuclei*) and would be expected to create different populations—in terms of cell size—in a number of mammalian species.

FIBRILLAR COMPONENTS

Myofibrils and Myofilamentous Masses. In tonic, "fast-twitch" skeletal muscle, the discrete bundles of proteinaceous filaments (myofibrils) constitute the major portion of each cell. Since a great deal of cardiac muscle terminology has been derived from the study of skeletal muscle morphology, the term "myofibrils" was automatically applied to the collections of contractile material found in heart cells (fig. 1–7). Few cardiac myofibrils attain in cross section the circular profiles and regular, small diameters of skeletal myofibrils, however, instead forming more massive assemblages of filaments which partially or totally envelop the associated mitochondria (fig. 1–8). For this reason, McNutt and Fawcett [4] proposed the term "myofilamentous masses" as better descriptive of myocardial filament bundles. In this respect, myocardial cells of larger mammals are in fact reminiscent of phasic or of slow-twitch tonic skeletal muscle, whose myofibrils display a pleiomorphic *Felderstruktur,* as opposed to the *Fibrillenstruktur* typical of fast-twitch muscles such as frog sartorius. Conversely, *Fibrillenstruktur* of a sort can be detected in smaller, fast-beating hearts such as those of mouse and shrew (which arrangement apparently provides substantially greater expanses of surface upon which the system of sarcoplasmic reticulum tubules can form [fig. 1–22]). Most investigators have thus far elected to retain *myofibril* as the preeminent term for all bodies in muscle which are composed of actin, myosin, and α actinin (along with various accompanying proteins such as tropomyosin.)

A longitudinally arrayed, striped pattern is obvious in cardiac myofibrils (figs. 1–1, 1–7, and 1–19). The details of this pattern are essentially the same for all mammals examined, and comprise the I bands, A bands, and Z bands (or "Z lines," "Z discs"). These desig-

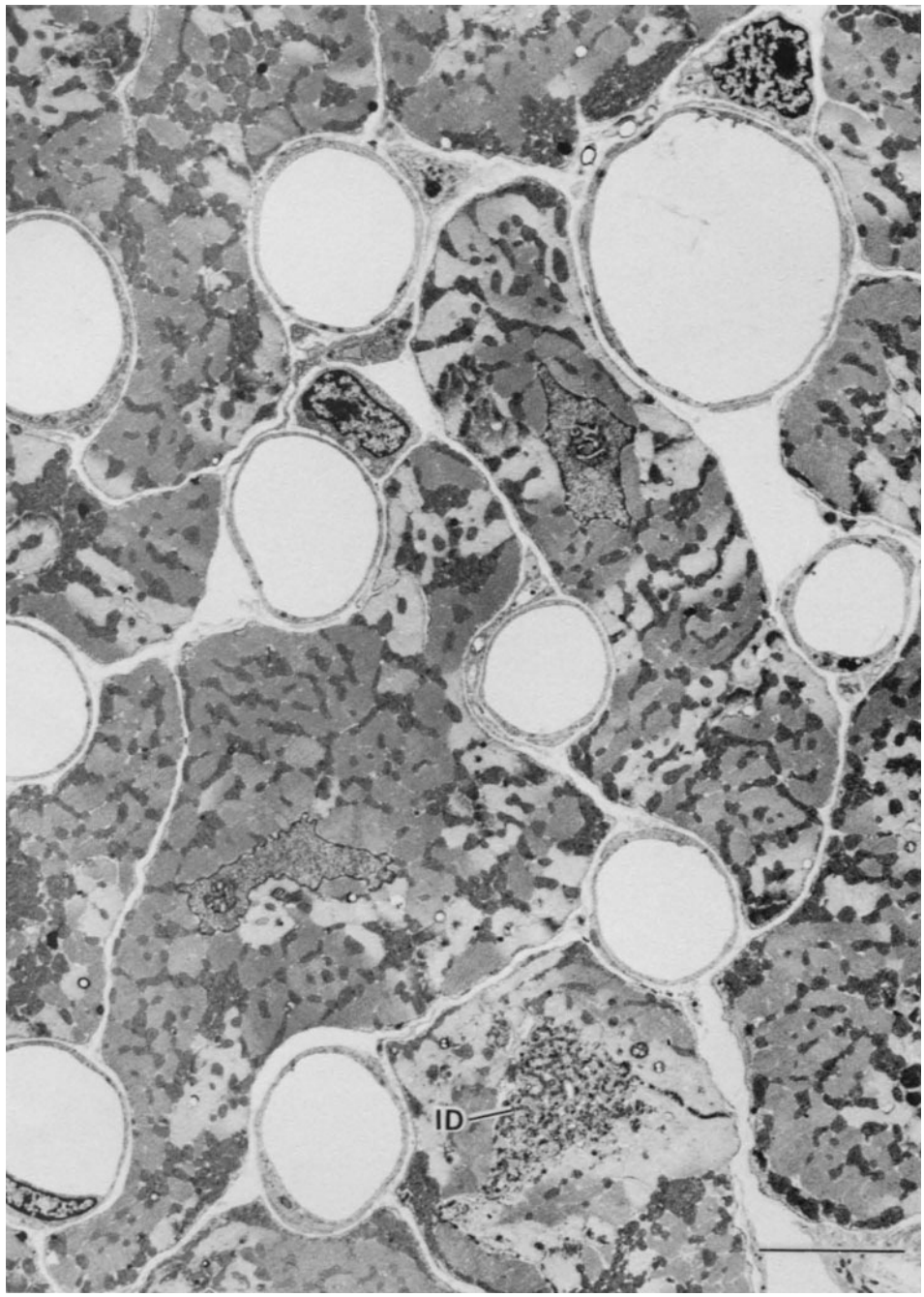

FIGURES 1–4 to 1–6. Survey transmission electron micrographs of the three major categories of myocardial cells (samples taken from rhesus monkey), presented at the same magnification for comparison of the relative degrees of packing, shape, and size of the muscle cells.

FIGURE 1–4. Right papillary muscle. In transverse section, these ventricular myocardial cells display extreme pleiomorphism. Profiles of cardiac myocytes are indented to accommodate the numerous blood vessels. In this field, myocardial nuclei are located in more-or-less central positions, and in one region a sizeable expanse of an intercalated disc (ID) is caught in section. Scale bar represents 5 μm.

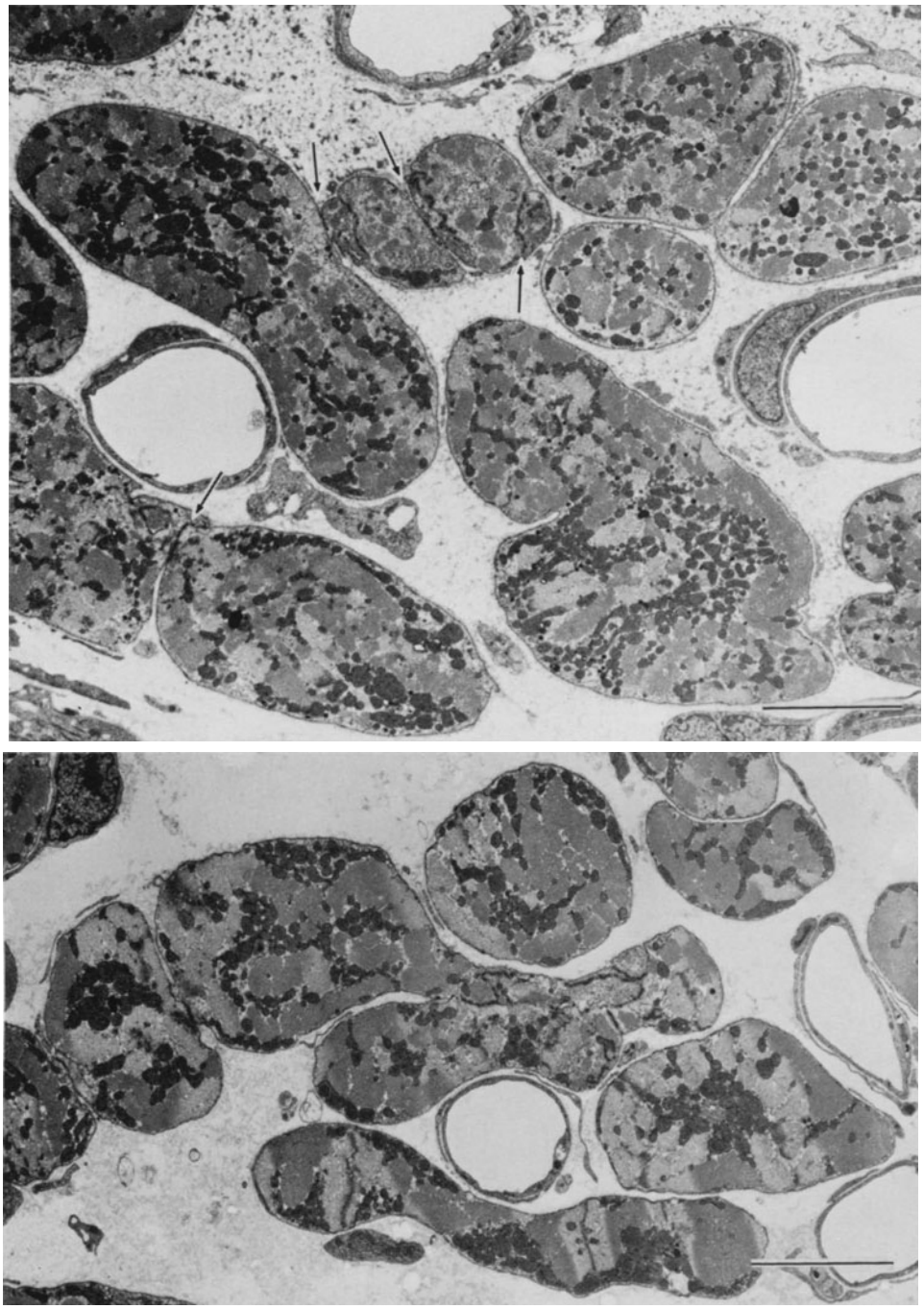

FIGURE 1–5. Left atrial trabecula. Cell profiles are arranged in a loosely packed array. Although the cells vary widely in size, all are considerably smaller than ventricular cells (cf. fig. 1–4). Atrial intercellular attachments are largely invested in simple, side-to-side "spot-weld" appositions (arrows). Scale bar represents 5 μm.

FIGURE 1–6. Sinoatrial node. These small cell profiles are characteristically joined together in groups by complex interdigitations (also see fig. 1–39). Scale bar represents 5 μm.

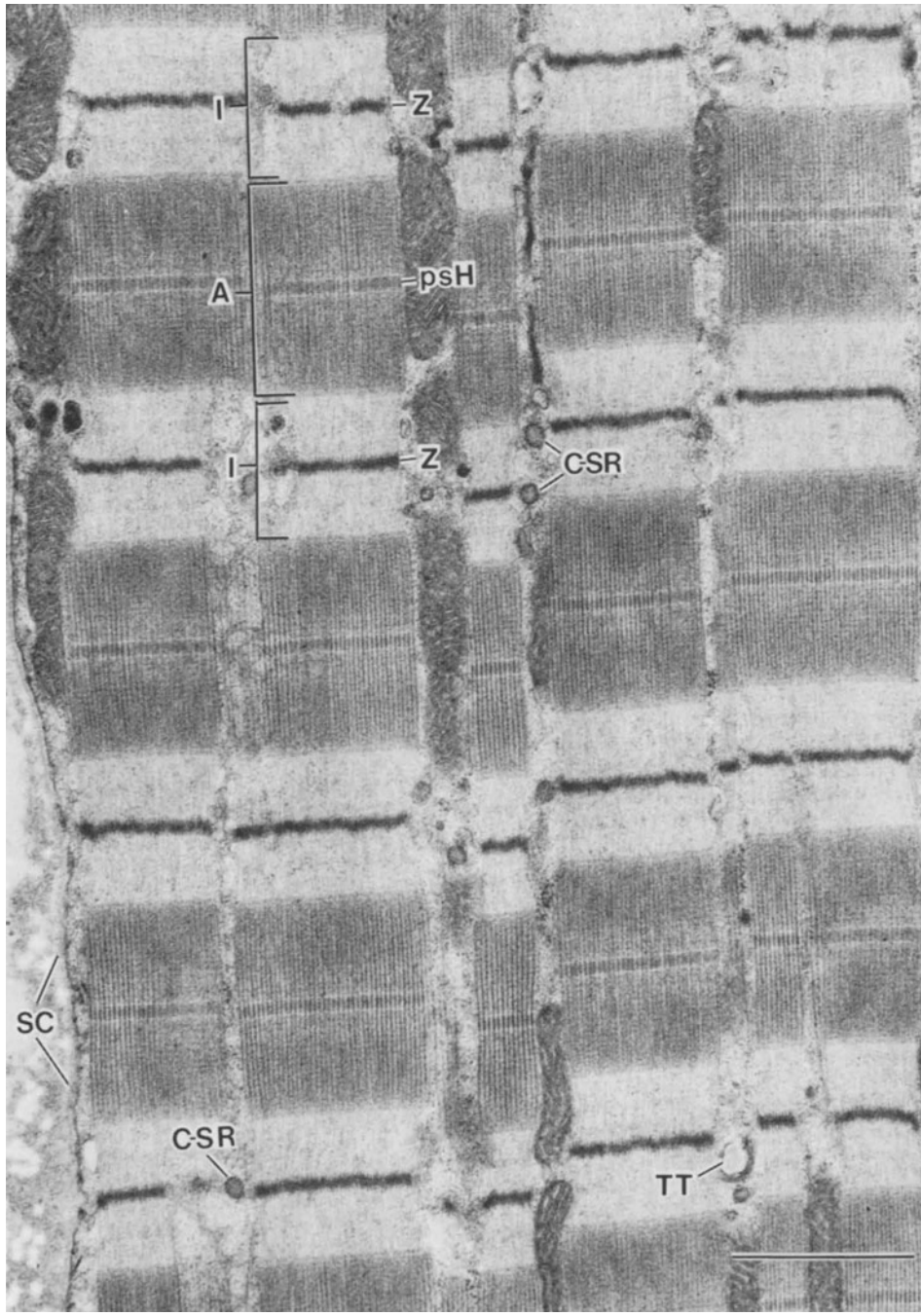

FIGURE 1–7. Rhesus monkey right papillary muscle. In this longitudinally cut cell, the classic banding pattern of relaxed myofibrils is evident. Each sarcomere is delimited by Z bands (Z), and consists in addition of two "half" I bands (entire I bands are denoted: I) and the opaque A band (A), which occupies much of the sarcomere length. At the center of the sarcomere there appears the M-band–L-line complex or "pseudo-H zone" (psH), which is shown in greater detail in figure 1–11. A number of cell structures are known to be located preferentially at the Z-band level of the myofibrils [28]. Among these are transverse tubules (TT) and spheroidal expansions of the sarcoplasmic reticulum ("corbular" SR: C-SR), here seen as individual profiles (cf. 1–19 and 1–26). The sarcomere pattern of the centermost myofibril is out of register with respect to the remaining myofibrils, a common occurrence in myocardial cells (also see figs. 1–1, 1–8, and 1–19). At the left of the micrograph is the cell surface (sarcolemma), which bears a lightly opaque covering (the surface coat: SC) on its extracellular side. The electron-lucent profiles near the surface coat are negatively stained collagen fibrils. Scale bar represents 1 μm.

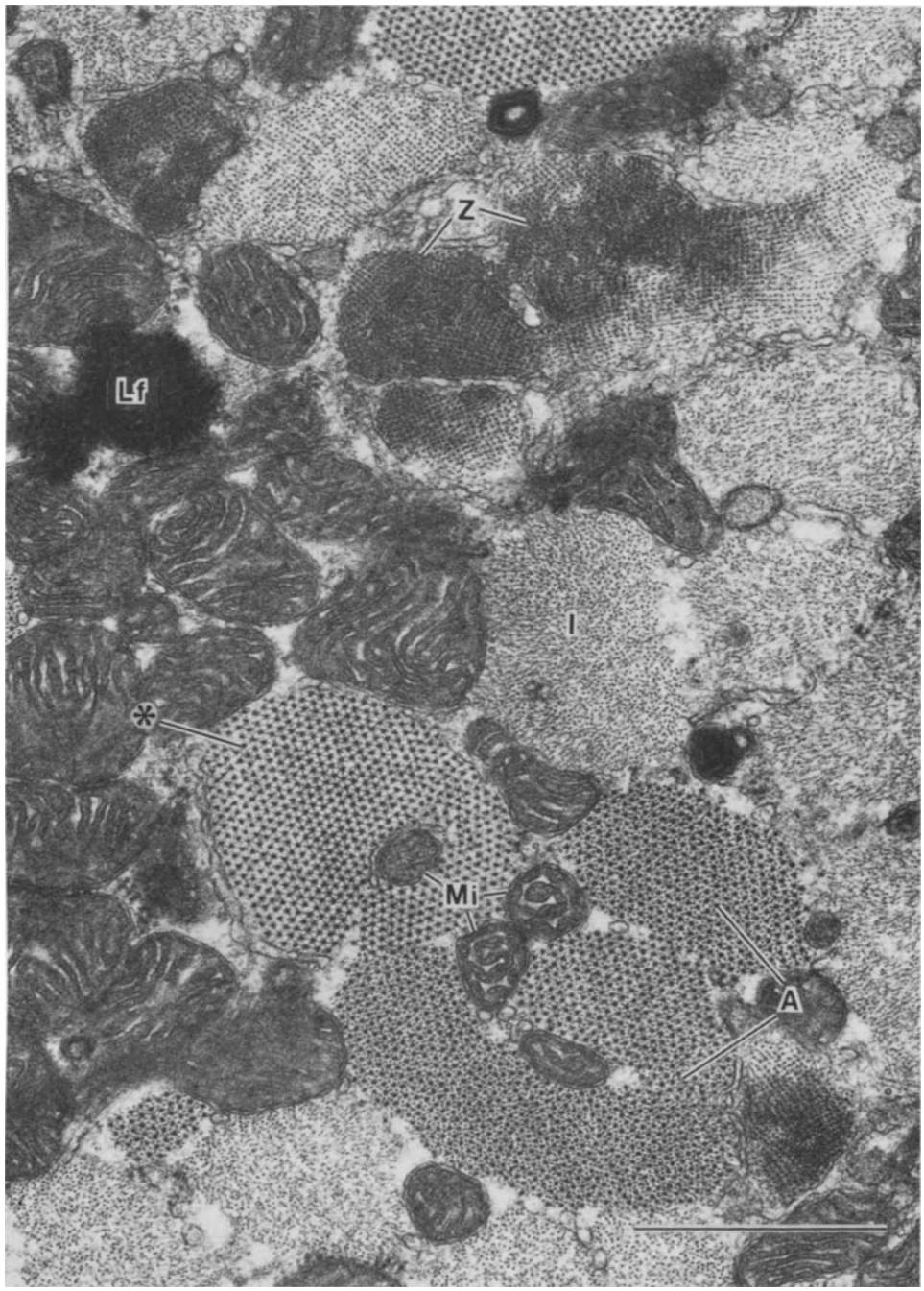

FIGURE 1–8. Rhesus papillary muscle cell in transverse section. In this field, all the divisions of the sarcomere appear in cross section (cf. fig. 1–7). Several areas of Z-line substance ("Z discs") appear at the top of the field (Z); other regions contain elements of the I band (I) and A band (A). One myofibril is cut at its midlevel (*), a detail of which is shown in figure 1–10. Note that the myofibrillar profiles are pleiomorphic, forming a *Felderstruktur* similar to that of slow skeletal muscle. Mitochondria are massed between myofibrils, and some (Mi) are enveloped by them. Lf, lipofuscin body. Scale bar represents 1 μm.

nations correspond to the terms derived from examinations of muscle with polarized light (I, isotropic; A, anisotropic) and from observations by German histologists (Z, *Zwischenscheibe,* "dividing line"; H, *helle Zone,* "light zone"; M, *Mittellinie,* "middle line"). The classic longitudinal unit of each myofibril is the *sarcomere,* which contains two "half" I bands and one A band (see fig. 1–7). Strictly speaking, each sarcomere length also incorporates the transversely bisected halves of two Z bands; a more practical view is to consider a sarcomere as constituted by each region bracketed by adjacent Z bands. The construction of cardiac myofibrils has been actively studied [e.g., 4], but exact details of structure, particularly the architecture of Z bands and of the "pseudo-H" zones at the midsection of the myocardial sarcomere, remain obscure.

In transverse view, cardiac Z bands may display an assortment of patterns, each known by a descriptive term: "basket weave," "large square," and "small square." Combinations of patterns may be observed in the same transverse Z-band profile (figs. 1–8 and 1–9). The various appearances may depend on such factors as tilt of the plane of section (fig. 1–9) and the level through which the Z band has been cut [22, 23]. The type of fixation used may also play a role in the generation of Z-band patterns in muscle [24]. A system containing both large axial and finer oblique "connecting" filaments makes up the Z-band latticework, which itself is likely a labile complex, judging from its coexistent variations in substructure [23]. Z bands of ventricular (fig. 1–7) and atrial (fig. 1–37) working fibers differ considerably in appearance; it remains for intensive study of the sort described above to be carried out on atrial Z discs.

Under conditions of myofibrillar relaxation, actin filaments do not project into the central zone of the sarcomere, the M-band–L-line complex ("pseudo-H zone" [4]). Three alternating striations, in the longitudinal order of L line/M band/L line, compose this region (figs. 1–7 and 1–11). The two L lines encompass those segments of myosin filaments which are neither connected by myosin–actin crosslinks (such connections, together with the overlap of actin and myosin, are the structural basis of the A band) nor by myosin–myosin crossbridges (the presence of which contributes to the opacity of the M band: figs. 1–10 and 1–11). The presence of M bands is the colophon of the mature sarcomere; in rat heart, for example, the appearance of M-band crossbridges begins only postnatally [25]. In the heart of the guinea pig, which is virtually fully developed at the time of birth [26, 27], M bands are evident by the eighth week of gestation (unpublished observations).

The characteristic resting length of sarcomeres in mammalian ventricular cells is on the order of 2.2 μm. Approximate values for the dimensions of the various sarcomere segments are: Z band, 80–160 nm; I band (each half) 0.35 μm; A band, 1.45–1.65 μm; M band,

FIGURE 1–9. Rhesus papillary. Stereoscopic pair of micrographs (20° angle of convergence) taken of a transversely sectioned Z disc. The substructure within the disc is the product of interdigitation of longitudinal and transverse filamentous components. The predominant pattern formed in this disc is that called the "small square" (exemplary region indicated by arrow); in other areas, the "basket-weave" pattern—actually the product of a negative image formed by the included fibrils—can be discerned (*). If, however, the latter region of the Z disc is compared on a "right-eye, left-eye" basis in the individual micrographs, it can be seen that the basket-weave apparent in the left-hand micrograph is converted into a pattern approaching the small-square configuration in the right-hand micrograph. Scale bar represents 0.2 μm.

FIGURE 1–10. Detail of figure 1–8. Plane of section passes through the A band of the myofibrils. At the right, the six-around-one actin–myosin configuration is seen (circled), denoting a region located to one side of the midlevel of the sarcomere. At the left, the substructure of the pseudo-H zone is revealed; at the edge of the myofibril, naked, roughly triangular myosin filaments appear (L: L-line level), and toward the center of the myofibril prominent crossbridges are present between the myosin filaments, thus indicating passage of the section through the M band (M) (cf. fig. 1–11). Note the scalloped appearance of some of the mitochondrial cristae, and the transversely sectioned microtubules (MT) in the myofibrillar interstices. Scale bar represents 0.5 μm.

FIGURE 1–11. Longitudinal section through the pseudo-H zone of a cardiac myofibril. Short, bare stretches of myosin filaments constitute the L lines (L), whereas the myosin segments of the broad central M band (M) are characterized by thin crossbridges (arrows). Scale bar represents 0.1 μm.

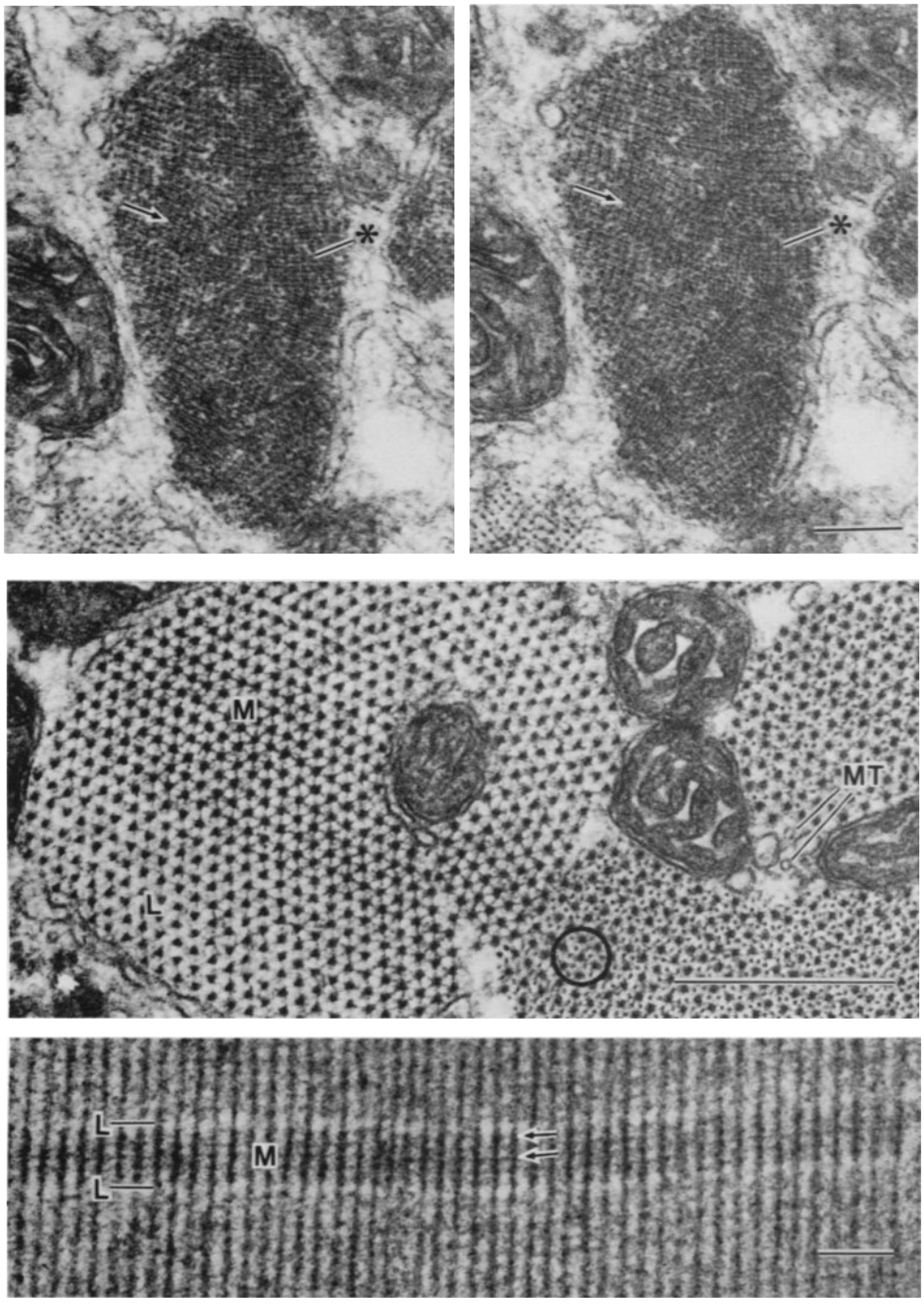
M
MT
L
L
L
M

70–90 nm; L lines, 10–20 nm. The contribution of each actin filament to the individual sarcomere is 1.25 μm or less (much of the actin filament being obscured in the relaxed sarcomere because of its overlap with myosin within the A band). It is not yet clear whether actin filaments traverse the Z band, form—or fuse with—other, thicker filament segments, or terminate in some fashion inside the Z lattice [5].

Adjacent myocardial myofibrils seldom achieve side-to-side sarcomeric register (figs. 1–1, 1–7, and 1–36), and for this reason thin transverse sections of cells are found which capture examples of basic levels of the sarcomere (fig. 1–8). Misalignment of myofibrils is related to the uneven contours of the intercalated discs at the myocardial cell tips (figs. 1–1, 1–27, and 1–37). Given that the point of each sarcomere's insertion into the intercalated disc occurs at the level at which the Z bands would be formed (figs. 1–1 and 1–27), and considering the varying lengths of excursions of the intercalated disc, the skewed alignment of adjacent myofibrils naturally follows (though the degree of individual myofibrillar growth obviously is involved as well).

The early formation of the myofibrils during embryony appears to influence the formation of segmented portions of sarcoplasmic reticulum, as well as the orientation of the transversely arranged components of the T-axial tubular system (TATS: see *Transverse-axial tubular system*). The Z band of the sarcomere seemingly dictates the positioning of certain myocardial cell components, among them T tubules, junctional SR saccules, "Z tubules" of SR, and intermediate filaments, most examples of which gravitate so as to be aligned parallel to the Z disc (figs. 1–14, 1–15, 1–20 to 1–22, and 1–26). Because of this preferential orientation of many cell structures, there is exclusion by them of other organelles such as mitochondria (figs. 1–1, 1–7, and 1–19), which ordinarily do not occupy the regions which constitute the "Z-level myoplasm" [28].

Microtubules. Microtubules are, in the majority of cells, the premier element of the cytoskeletal system. In the highly organized cardiac muscle cell, the system of myofibrils, whose own elements are closely packed, oriented in predominantly longitudinal array, and securely anchored in the substance of the intercalated disc, there seems minimal need for an organized intracellular framework. Despite this seemingly logical conclusion, several studies have already demonstrated the presence of numerous microtubules in heart cells [e.g., 8, 29, 30]. Cardiac microtubules run largely in the longitudinal axis of the cell, are particularly concentrated about the nucleus (fig. 1–13), and also appear between the myofibrils—especially near mitochondria—and at the cell periphery (fig. 1–13). Goldstein and Entman [30] report, further, that microtubules in dog heart wind in helical patterns about the nuclei and myofibrils; this may account for the finding of some nearly transversely oriented microtubules near the I- or Z-band levels of heart (figs. 1–12 and 1–24; also see Forbes and Sperelakis [8, 28]). Microtubules in heart muscle range from 24 to 30 nm in diameter and may achieve lengths of several micrometers (fig. 1–12).

Intermediate (10-nm) Filaments. These fibrils, so named because of their diameters (range of ca. 7–11 nm, average of ca. 10 nm), which are roughly intermediate between the diameters of actin and myosin, are the second major cytoskeletal component of most cells. Their contribution to the myocardial cytoskeleton occurs primarily in the transverse plane of the cell, and most particularly at the Z-band level (figs. 1–14 and 1–15) [8, 28, 29, 31]. Such filaments may be attached to the inner sarcolemmal surface and to the nuclear membrane [29], thus contributing in substantial part to a series of parallel strata which apparently confer rigidity in the transverse axis to myocardial cells [8, 28]. Particularly in rodents, bundles of intermediate filaments encircle the myofibrils (fig. 1–15) and may contain upward of 50 filaments. The incidence of intermediate filaments seems considerably lower in carnivore and primate hearts than is the case in rodent heart. In thin sections, intermediate filaments are seldom encountered in substantial quantities along the longitudinal axis of the main body of the myocardial cell, a finding confirmed by immunologic observations [32, 33]. When found,

small numbers of longitudinal intermediate filaments appear at the cell periphery and in myofibrillar interstices (fig. 1–35). The intercalated disc is a prominent site at which intermediate filaments are found, specifically inserted into the intracellular plaques of desmosomes (figs. 1–16 and 1–29).

MITOCHONDRIA

These organelles are the second most populous constituent of ventricular myocardial cells (myofibrils forming the greatest portion [5]). The typical locations for mitochondria are the myoplasmic spaces, where they form longitudinal columns among the myofibrils (figs. 1–1, 1–2, 1–7, 1–8, 1–19, 1–22, and 1–27), in the subsarcolemmal spaces, and in the myoplasm leading away from the nucleus (figs. 1–17 and 1–32). Speculation has been offered that the intermyofibrillar mitochondria constitute a population which in functional nature is different from the subsarcolemmal collection of mitochondria [34–36]. Subsarcolemmal mitochondria have the singular quality, in a variety of mammalian myocardial cells, of forming "tailored" appositions with gap junctions [37]. Such complexes frequently incorporate connecting strands that seem to form an adhesive bond between the juxtaposed structures; this seemingly specific attachment may be related to regulation of $[Ca^{++}]_i$ in the immediate vicinities of gap junctions, which in turn may affect the electrochemical functioning of such junctions [38, 39].

Mitochondria in conventionally preserved heart cells, even though they assume orthodox (metabolically inactive) configurations, nevertheless exhibit a number of variations in internal pattern, e.g., the rather densely packed, shelflike cristae of mouse ventricle (figs. 1–14 and 1–27) and the elaborate scalloped cristae of cat [40], dog (fig. 1–19), and monkey (figs. 1–7 and 1–13). Rarely are mitochondria of working myocardial cells small or poorly endowed with internal membranes. In fact, in apparently normal cells, mitochondria may assume proportions that are truly gigantic, though giant mitochondria also may be symptomatic of pathology [41].

Mitochondria in cells of the mammalian AVCS can vary widely in size, even within the same cells, and sometimes are small and poorly supplied with cristae (figs. 1–39, 1–42 to 1–44, and 1–46).

NUCLEI

As mentioned in the section on *Cell shape and size,* multinucleate cells are the rule rather than the exception in mammalian ventricular cells. Binuclearity attains the majority (70%) by the end of the first postnatal week of life in the mouse [42], and in the rat 85% of muscle cells are binucleate in the adult [21]. Swine heart [43] and human heart [44] both achieve a high degree of binuclearity and polynuclearity, with as many as 22 nuclei observed in single myocardial cells of the pig [43]. The presence of multiple nuclei is likely the result of the persistence of karyokinesis, past the neonatal state, without the accompaniment of cytokinesis. This conclusion is supported by the discovery of single tetraploid nuclei in cells of neonatal mouse [42]. Complete mitosis ceases early in the postnatal life of the mammal [e.g., 45], and in adults only atrial cells display any ability to divide [46]. It seems likely that the development of a stratified, oriented internal architecture is partly responsible for the inhibition of cytokinesis in ventricular muscle cells [e.g., 47], though additional structural pecularities of the myocardial cell may be involved (see *Centrioles*).

Myocardial nuclei generally are fusiform (figs. 1–1 and 1–18) and conform to the overall longitudinal arrangement of other major organelles (particularly myofibrils and mitochondria). Numerous infoldings and identations may be present in nuclear envelopes (fig. 1–18). The elongate form of the nucleus may be controlled not only by the presence of surrounding myofibrils, but also by the microtubules which envelop them [29, 30]. The lateral insertion and/or attachment of intermediate filaments [29] may be the agent responsible for the nuclear crenations which develop upon contraction of the myocardial cell [48].

Myocardial nuclei may be located in peripheral or interior positions within the myoplasm (figs. 1–1, 1–7, 1–8, 1–13, and 1–19). Each nuclear pole has associated with it a conical myoplasmic region in which there appear Golgi saccules, centrioles (when present), mitochon-

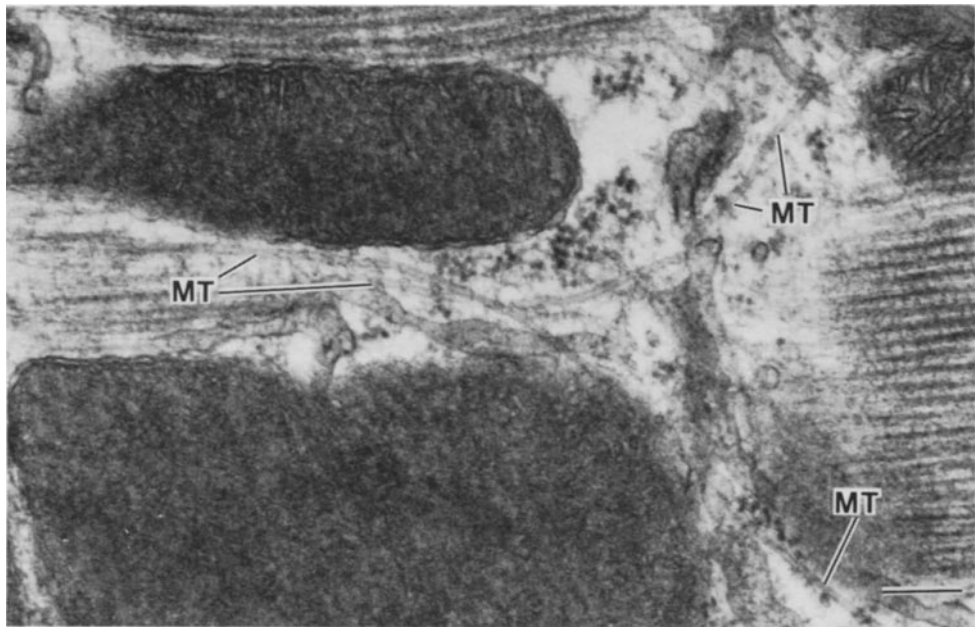

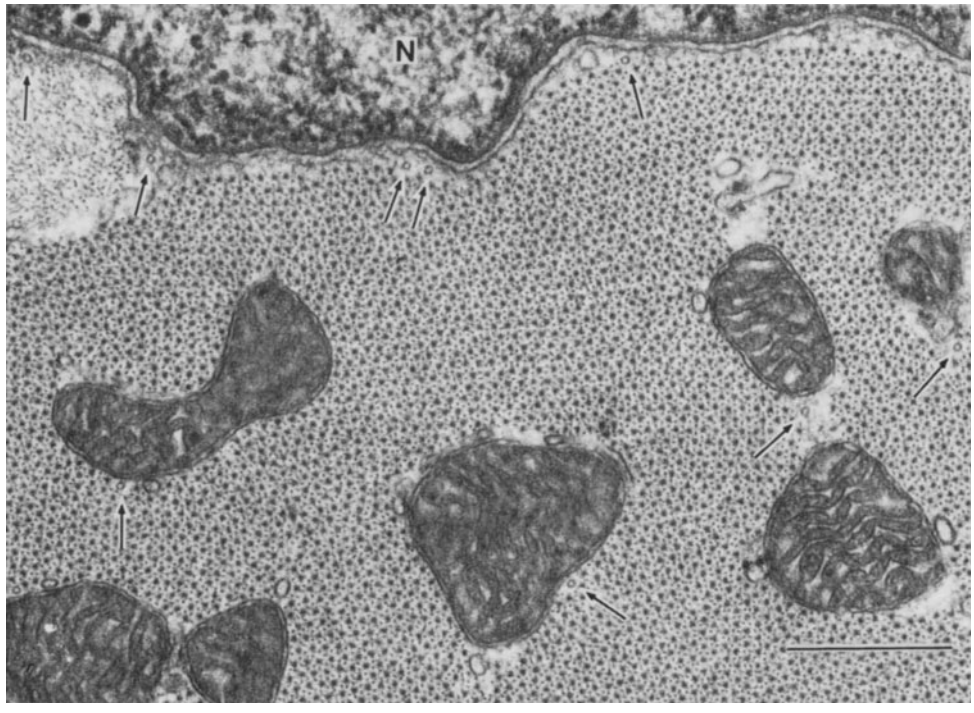

FIGURE 1–12. Mouse ventricular myocardial cell. Microtubules (MT) run both longitudinally and obliquely in this field, the individual tubules tending to bend over the level of the I band. Scale bar represents 0.2 μm.

FIGURE 1–13. Rhesus monkey papillary muscle. Cross sections of microtubules (arrows) can be found near the border of the nucleus (N), as well as in the myoplasm between the myofibrils, and thus often are located adjacent to mitochondria. Scale bar represents 0.5 μm.

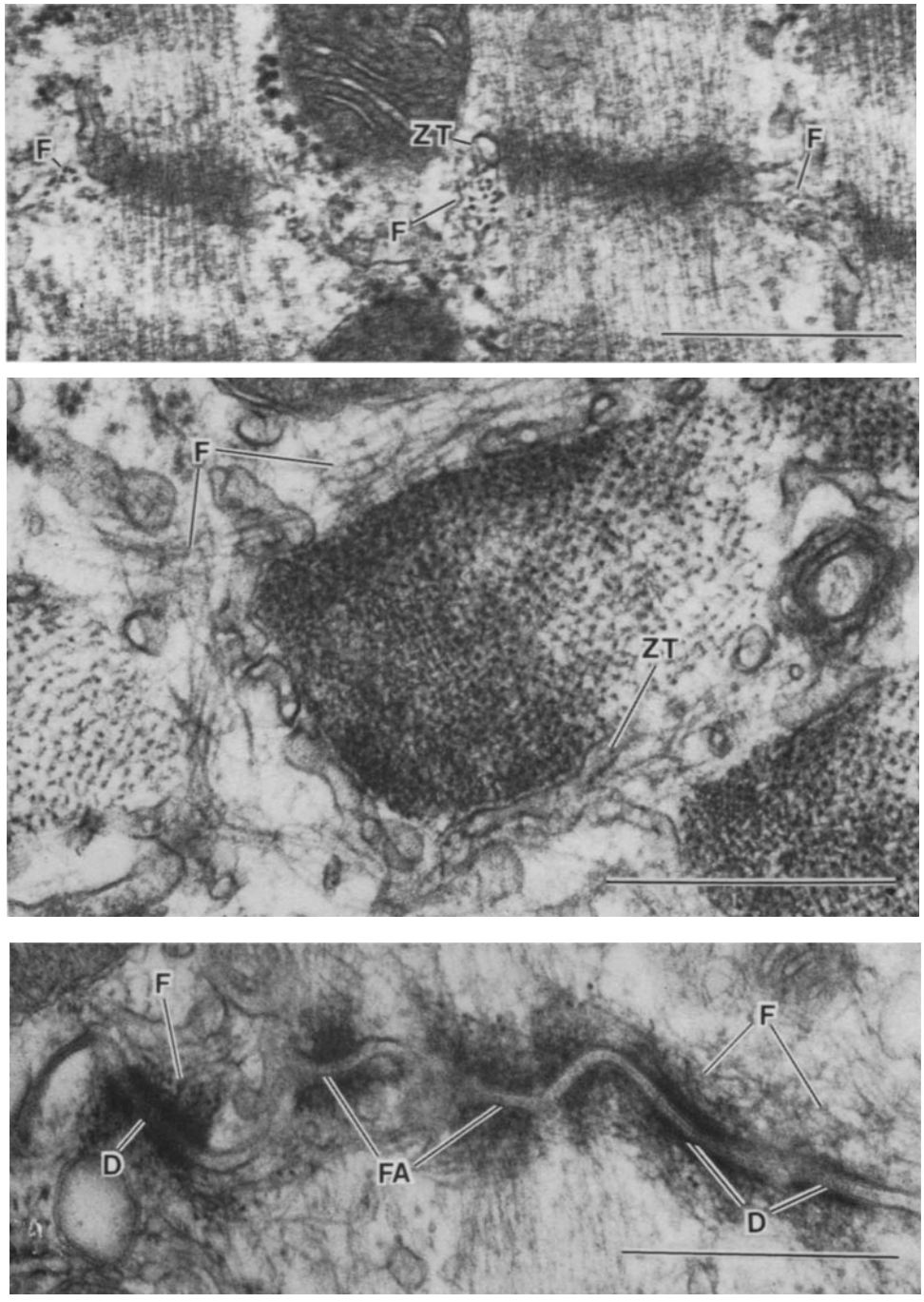

FIGURE 1–14. Longitudinally sectioned cell of mouse ventricular wall. Intermediate filaments (F) appear in groups adjacent to the Z bands of the myofibrils. The transverse section of a "Z tubule" of sarcoplasmic reticulum (ZT) is also present in the Z-level myoplasm. Scale bar represents 0.5 μm.

FIGURE 1–15. Transverse section of mouse ventricular myocardial cell. A Z disc is partially encircled by bundles of intermediate filaments (F). Z tubules (ZT) adhere closely to the surface of the myofibril. Scale bar represents 0.5 μm.

FIGURE 1–16. Mouse ventricle. Intercalated disc formed between two apposed cell tips. Webworks of intermediate filaments (F) are closely associated with the intracellular plaques of desmosomes (D). Note the termination of actin filaments in the opaque substance of the *fasciae adherentes* junctions (FA). Scale bar represents 0.5 μm.

dria, rough and smooth endoplasmic (sarcoplasmic) reticulum, and a variety of lysosomes (including lipofuscin) (fig. 1–17). Within individual cells examined in the same sample, the regions of "nuclear pole myoplasm" may range from being quite limited to occupying extensive volume (fig. 1–32).

The surfaces of myocardial nuclei possess numerous rounded depressions ("pores") (fig. 1–18) at whose peripheries the outer and inner nuclear membranes fuse, and across which amorphous "diaphragms" extend.

MEMBRANE SYSTEMS

Surface Sarcolemma and Caveolae. The unit membrane which encloses the myocardial cell is usually referred to as the *sarcolemma.* The fact that there exist numerous folds, invaginations, and inpocketings of the sarcolemma has necessitated its terminological subdivision into: (1) the *surface* or *peripheral sarcolemma,* that portion composing the large planar portions of the myocardial cell surface; (b) the *interior sarcolemma,* more commonly known as *transverse (T) tubules* or as the *transverse-axial tubular system* (TATS [8]; see the following section); and (c) *caveolae,* membrane-bounded vesicular structures which project inward from the cell surface, retaining luminal continuity with the extracellular fluid. The intercalated discs, which comprise sarcolemmal regions containing specialized junctions and which are located at and near the cell ends, are considered separately (see *Intermembranous junctions*).

The majority of the surface sarcolemma is invested with a glycoproteinaceous covering, the least committal term for which is the *surface coat* (also referred to as "glycocalyx" and "basal lamina"). The surface coat is indistinct and largely amorphous in most electron-microscopic preparations (figs. 1–7, 1–19, 1–33, and 1–35). It is continuous over the mouths of caveolae, but does not appear to fill the caveolar lumina (fig. 1–35). In regions of close cell-to-cell apposition (e.g., the intercalated discs), the surface coat thins or disappears altogether. The surface coat has been thought to function in the trapping of certain ions, notably Ca^{2+} [49], but the contribution of this particular external Ca^{2+} pool to the process of excitation–contraction coupling may not be especially significant [50].

Caveolae bestow significant amounts of surface area to myocardial cells [51, 52], particularly to those cells which lack a TATS [53, 54]. The evidence now available suggests strongly that proliferation of caveolae, from the surface of the muscle cell toward its interior, is the means whereby the TATS is formed in the course of myocardial development [8, 26, 55, 56].

Transverse-Axial Tubular System (TATS). The myocardial cells of mammals are essentially unique among vertebrates in their possession of extensive invaginations conventionally referred to as transverse (T) tubules. Even in mammals, all cardiac muscle cells do not form T tubules; for example, certain atrial cells of the rat heart [53], all atrial myocardial cells of guinea pig [57], and many elements of the atrioventricular conducting system lack them. Where "T" tubules are found, they often are accompanied by longitudinally oriented (axial) tubules [8, 57, 58]. The interconnection in myocardial cells of transversely and axially oriented tubules has produced the concept of a "transverse-axial tubular system" or *TATS* [6, 8, 57]. The constituents of the TATS vary considerably among mammals. The tubules of mouse heart are characterized by small diameters and irregular profiles (fig. 1–20); on the other hand, the TATS of guinea pig and monkey hearts (for example) is a collection of large-diameter tubules which often anastomose in rather regular latticeworks (fig. 1–21) that pervade the entire ventricular cell [6, 8, 57].

The points of invagination of the transverse members of the TATS usually form at or near the successive sarcolemmal levels nearest the Z lines of the outermost myofibrils, and quite regular arrays of T-tubule openings are frequently apparent (figs. 1–19 to 1–21). Even if a T tubule does not originate squarely across from a Z line, it usually veers into a configuration so as to become aligned with the Z-line myoplasm [8, 28] (figs. 1–20 and 1–21). As mentioned in the preceding section, the vectorial proliferation of caveolar elements from the

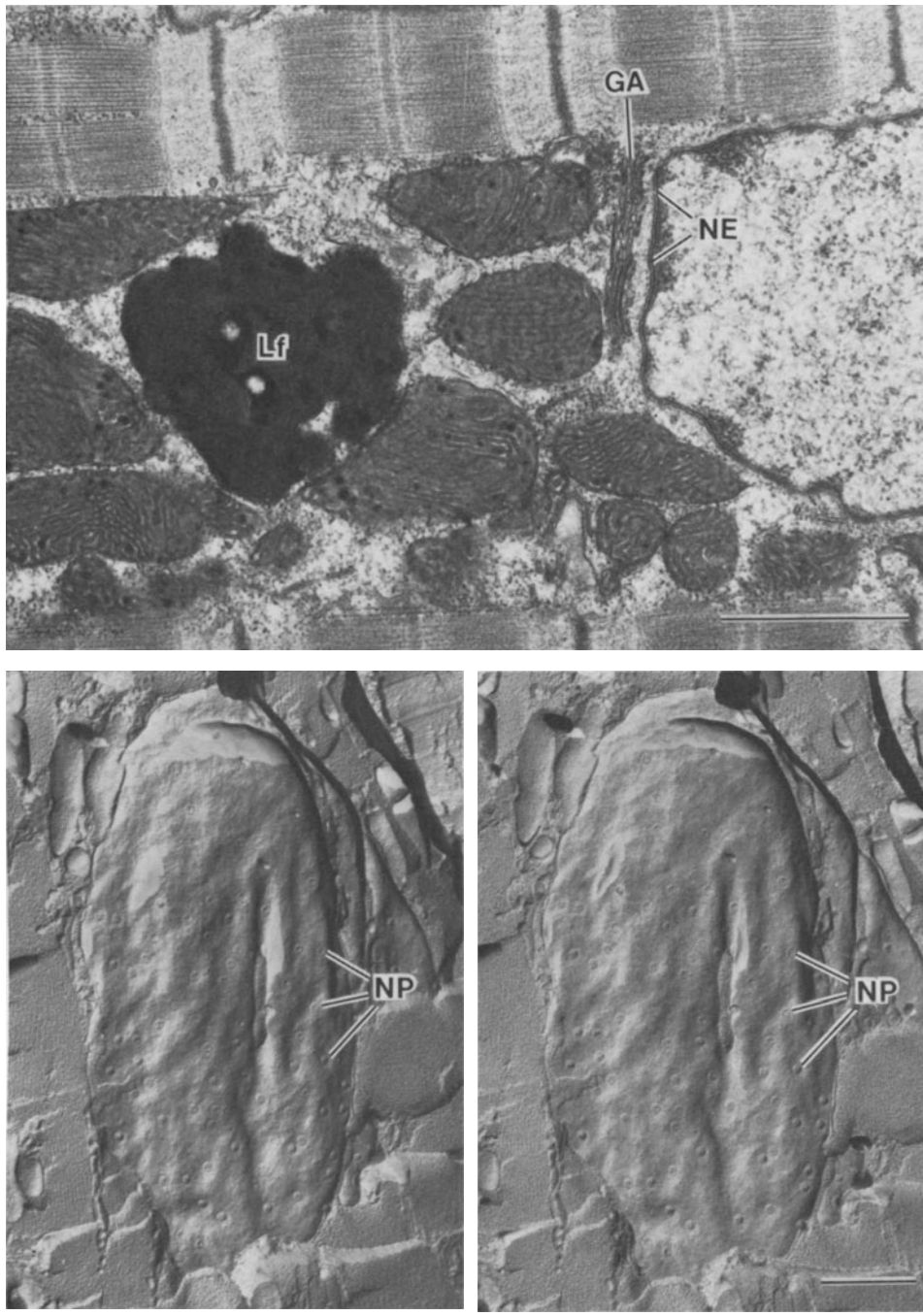

FIGURE 1–17. Right ventricular wall of dog heart. This field, from a longitudinally sectioned myocardial cell, demonstrates typical contents of the "nuclear pole myoplasm," which extends longitudinally from the nuclear tips. A large lipofuscin body (Lf) dominates the field. Numerous mitochondria, which display dense granules and a variety of crystal configurations, also are packed into this myoplasmic compartment. The Golgi apparatus (GA) in this cell is a simple stack of saccules closely apposed to the nuclear envelope (NE). Scale bar represents 1 μm.

FIGURE 1–18. Stereo micrographs which demonstrate the surface contours of a nucleus in mouse ventricular myocardium (stereo angle 20°). Numerous nuclear pores (NP) are distributed rather evenly in the nuclear membrane. Creases and folds also characterize the nuclear surface. Scale bar represents 1 μm.

sarcolemma, as well as from the caveolar chains themselves, is likely the mechanism by which the TATS comes to exist. Profiles of the TATS in mouse heart very often reflect its caveolar origin (fig. 1–20; also see Forbes and Sperelakis [8, 59]), and in addition caveolae are prominent along fully formed tubules (fig. 1–21). The significance of this latter finding is unclear, but it may indicate that the process of caveolation continues to a limited degree in the adult heart cell and can be called upon conditions such as cardiac hypertrophy which necessitate additional growth of the TATS. In both neonatal and adult hearts, the caveolae directly connected to the surface sarcolemma are seldom found as individual entities, but instead form alveolar collections of 3–5 fused caveolae; these have been found on occasion to form couplings with saccules of peripheral junctional SR [59].

The larger examples of TATS elements are lined with surface-coat material (fig. 1–19), and it is likely that many of the smaller, more "primitive" transverse and axial tubules, such as those of mouse heart, are also coated [8]. A great deal of polymorphism is evident when comparing the TATSs of various mammals; average diameters of the tubules can range from ca. 50 to 500 nm (see the summary in Forbes and Sperelakis [8]), various cardiac muscle cells of mouse, rat, and shrew providing the lower values, and ventricular cells of guinea pig [57], seal [60], and golden hamster [61] achieving values at the upper end of the scale. The use of electron-opaque "tracer" materials such as colloidal lanthanum hydroxide, horseradish peroxidase-diaminobenzidine-H_2O_2 reaction product, and the precipitate formed by postfixation in ferrocyanide-reduced osmium tetroxide (OsFeCN) has been vital in achieving appreciation of the form and extent of development of the TATS in the mammalian heart (see Forbes and Sperelakis [8] for further discussion).

The contribution of the TATS to myocardial cells is considerably greater than that of the skeletal muscle T system. If the function of the cardiac TATS is primarily to bestow optimum surface–volume ratio to each muscle cell, there would seem to be some physiologic disparity, since skeletal myocytes possess far greater volumes (though the constitution of the TATS elements may be considerably different between the two types of muscle [5]). Substantial additional surface area is conferred to myocardial cells by caveolae, whether joined to the surface sarcolemma or to the TATS, or participating in extensive three-dimensional tubulovesicular arrays ("labyrinths") found in mouse [8, 55, 56, 58, 62] and shrew hearts [8]. The development of a TATS is not directly attributable to the attainment of a certain cell diameter; it has been shown that large (30–50 μm diameter) conducting system muscle cells lack a TATS [e.g., 5] and that T-tubule development in dog is initiated in cells of the left ventricle, which are of smaller average diameter than their counterparts in the right ventricle [63]. It has been suggested [5] that the TATS is an accommodative feature of these myocardial cells which are capable of undergoing hypertrophy, since cells of the AVCS lack a TATS and do not undergo enlargement. The fact remains that regions of excitable membrane and extracellular fluid are provided to all levels of the myocardial cells which contain a TATS [6], thus potentially optimizing the conditions and processes which result in excitation–contraction coupling.

The TATS is the final system to develop in myocardial cells, and under culture conditions may not develop at all [64]. The majority of mammalian hearts have not achieved TATS development by the time of birth, but the precocity of some species has been documented (e.g., the guinea pig [26, 27]). It has been pointed out, however, that for different species the stages during which the TATS begins development are the same, i.e., the heart of guinea pig and rat are equivalent in structural development when T tubules form, even though, in the two species, these stages occur, respectively, at the eighth week of gestation and 1–2 weeks postnatally [27].

Sarcoplasmic Reticulum. The equivalent of endoplasmic reticulum in muscle cells, *sarcoplasmic reticulum* (SR), exists in heart muscle in a variety of configurations which are structurally distinct, yet contiguous. The bulk of the SR is made up of the "network" SR (N-SR), which appears in the form of meshworks which

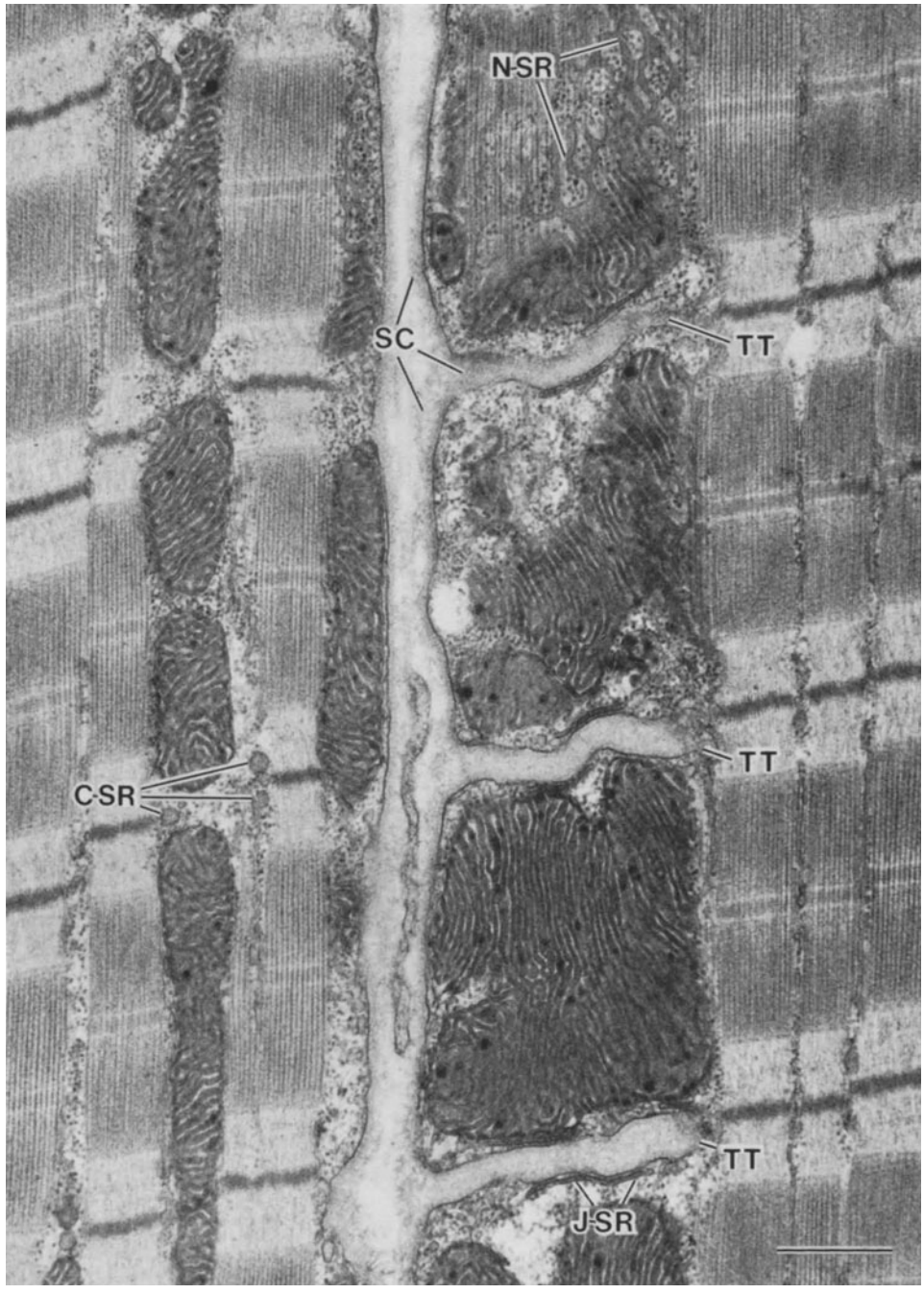

FIGURE 1–19. Ventricular myocardial cells from dog right ventricular wall. The sarcolemma of the right-hand cell forms three T tubules (TT) oriented in register with Z bands of the nearest myofibrils. The substance of the myocardial surface coat (SC) can be seen both in association with the surface sarcolemma and within the T tubules' lumina. Three categories of sarcoplasmic reticulum can be discerned: network SR (N-SR) on the face of one myofibril; junctional SR (J-SR), flattened saccules apposed to the T tubules; and corbular SR (C-SR) (cf. figs. 1–7 and 1–26). Note mitochondria, either arranged in intermyofibrillar row or located just beneath the surface sarcolemma. Scale bar represents 0.5 μm.

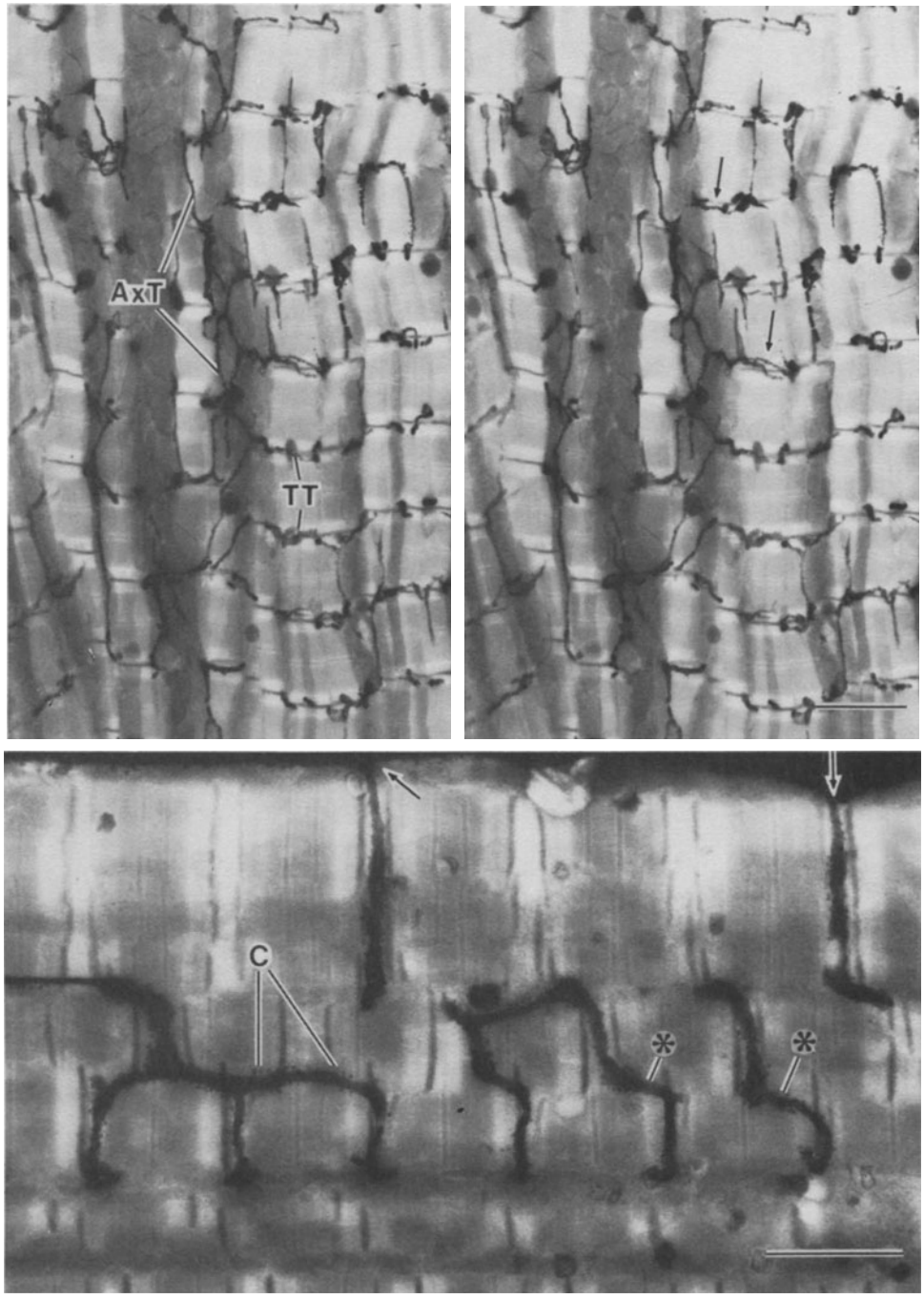
AxT
TT
C

are closely applied to the myofibrillar surfaces (figs. 1–22 and 1–23). Specialization and segmentation of the N-SR according to the pattern of the underlying sarcomeres is commonly observed (figs. 1–22 and 1–23); in particular, closely packed tubules may anastomose over the central regions of A bands to form fenestrated collars [65], and "Z tubules" of SR encircle the myofibrils at their Z-line levels in the mouse and other mammals [e.g., 8, 28] (figs. 1–14 and 1–15). Recently, distended regions of N-SR have been described [8, 66, 67]. Such "cisternal" SR is not limited in incidence to any particular level of the sarcomere, and can thus be readily distinguished from "extended junctional" SR (see below), which is formed primarily at the Z-line level.

The second major division of myocardial SR comprises the various categories of "junctional" SR (J-SR), the most noticeable examples of which form couplings (figs. 1–19 and 1–23 to 1–25). Myocardial couplings have often been called "triads" (two elements of J-SR complexed with a single T tubule), the term being derived from the study of skeletal muscle ultrastructure. Although the derivative "diad"—which describes the apposition of a single J-SR element with the sarcolemma (see fig. 1–25)—seems adequate, the use of "triad" has been vitiated by the finding of numerous couplings (in the mouse, for example [8, 58]) which incorporate widely varying configurations, including circles of J-SR around TATS elements, "reversed triads" in which two TATS profiles flank a single J-SR saccule, S-shaped entwinements of J-SR and the TATS, and other formation.

Viewed en face, junctional SR saccules appear as roughly discoidal or oblong expansions into which N-SR tubules lead (figs. 1–23 and 1–24). In sagittal section (side view, so to speak), the J-SR is flattened in the vertical plane relative to the associated tubules of N-SR (in contrast to the situation in skeletal muscle, in which each example of the J-SR ["terminal cisterna"] is substantially distended). In the vertical plane of section, the two hallmarks of cardiac J-SR are apparent. These are: (a) the intrasaccular *junctional granules,* which fall into a somewhat linear array along the length of the J-SR (fig. 1–25); and (b) the *junctional processes,* which are represented by a variety of amorphous and membranelike profiles (fig. 1–25). The subject of junctional process structure in muscle (skeletal, cardiac, and smooth muscle cells inclusive) has recently received intense attention, which has now led to the description in the junctional gap of "pillars" [59, 68–70], which are thin bodies which exist in apparent continuity with the unit membranes of the J-SR and sarcolemma (or, in addition, the T-axial tubules, in the case of striated and cardiac myocytes). The elucidation of pillars among the population of junctional processes has been fomented by such techniques as membrane intensification by tannic acid mordanting [68, 71] or en bloc staining with uranyl acetate solution combined with stereoscopic analysis [59]. In the latter instance, it appears that even small degrees of tilt of the plane of section with respect to the incident electron beam are sufficient to resolve quasi-membranous bodies in spaces where before in the junctional gap there appeared only amorphous substance [59].

The spatial configuration of myocardial junctional processes remains unresolved. Modifications of freeze-fracture technology which have

FIGURE 1–20. Mouse ventricle. "Semithin" (ca. 1 μm thick) longitudinal section (stereo separation of 12°) of tissue whose system of extracellular spaces has been infiltrated with opaque material by means of postfixation in ferrocyanide-reduced osmium tetroxide (OsFeCN). Although many transversely oriented tubular structures are present (TT), numerous longitudinal and oblique tubules (collectively known as "axial" tubules: AxT) can be seen which frequently form connections between transverse tubules. "Beaded" segment profiles can be discerned (examples shown at arrows), the presence of which implies origin of the tubules from the proliferation of caveolar elements. The irregular contours, dilatations, and branching are typical of the mouse TATS. Scale bar represents 2 μm.

FIGURE 1–21. A 2-μm-thick section of OsFeCN-infiltrated T-axial tubular system (TATS) of rhesus monkey papillary muscle cell. The continuity of some T tubules with the surface sarcolemma is clearly shown (arrows). Deeper in the cell, transverse tubules are anastomosed with truly axial tubules (at the left), and toward the right half of the micrograph, obliquely oriented "axial" segments (*) connect T tubules oriented along Z lines of out-of-register myofibrils. The small opaque dots which decorate the TATS along much of its profile are caveolae (C). Scale bar represents 2 μm.

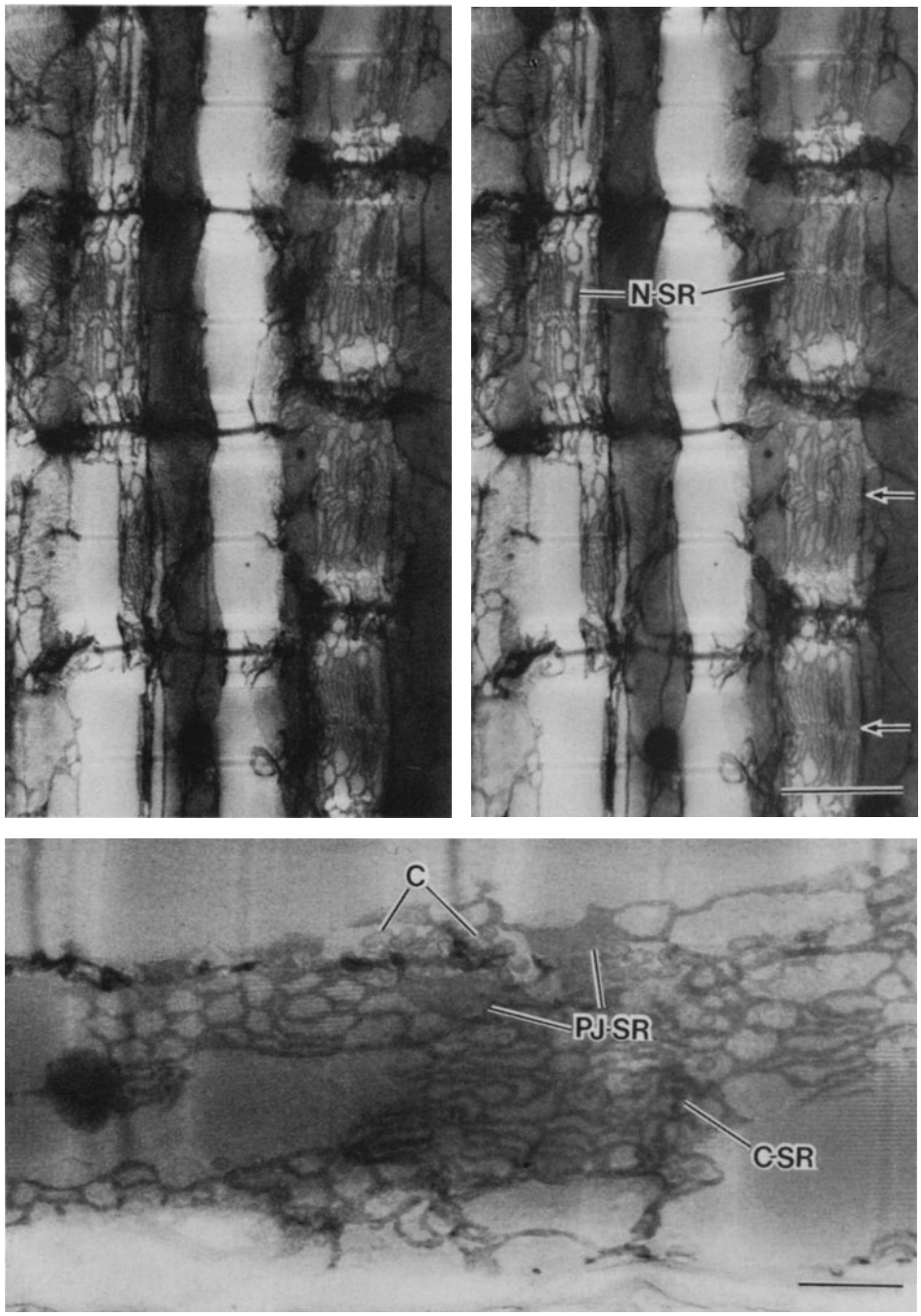

FIGURE 1–22. Stereoscopic micrograph pair (12° stereo angle) of mouse ventricular tissue treated in such a manner that OsFeCN postfixation results in opacification of the sarcoplasmic reticulum (SR). In this semithin (ca. 0.3 μm) section, extensive arrays of SR are superimposed on the faces of myofibrils. Although the SR is continuous across the Z lines, it nevertheless forms a similar segmented pattern over each sarcomere. Over the A bands, most elements of network SR (N-SR) are found in the form of closely packed, parallel longitudinal tubules which mass in perforated retes ("fenestrated collars": arrows) over the M-band level. Over the I bands, a looser meshwork of SR tubules appears. Such a pattern is typical of deep regions of the mouse myocardial cell (cf. fig. 1–23). Scale bar represents 1 μm.

FIGURE 1–23. Tissue same as figure 1–22. The section passes close to the surface of an SR-stained cell (note caveolae, C), where the loose-mesh N-SR configuration tends to dominate, the tubules anastomosing with expanded areas of junctional SR (in this case, "peripheral" J-SR, PJ-SR). Corbular SR (C-SR) also appears over a Z line. Scale bar represents 0.5 μm.

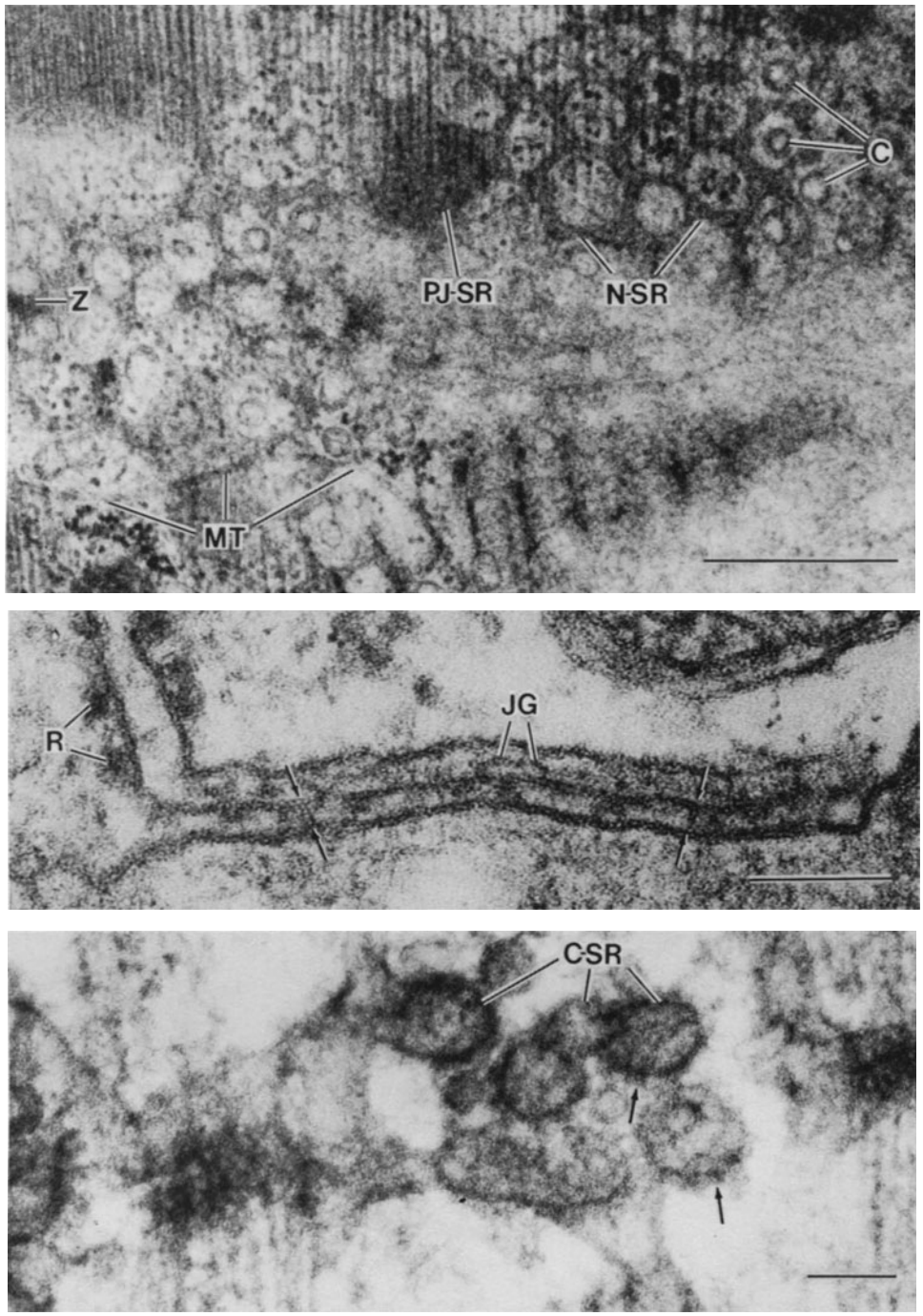

FIGURE 1–24. Thin section, grazing surface of myocardial cell from vervet right ventricular wall. Note caveolae (C) interspersed with meshes of network SR (N-SR) (cf. fig. 1–23). In this conventionally stained tissue, the greater opacity (relative to the N-SR) of the contents of the junctional SR saccule (PJ-SR) can be readily appreciated; this results in part from the presence of junctional granules and processes. The undulating profile of a microtubule (MT), oriented transversely across a myofibrillar face (Z, Z band), appears at lower left. Scale bar represents 0.5 μm.

FIGURE 1–25. Mouse ventricle. High magnification of peripheral J-SR saccule, showing its connection with N-SR tubule, here studded with ribosomes (R). Salient J-SR features are present, including the intrasaccular junctional granules (JG) and the junctional processes in the gap between the J-SR and surface sarcolemma. Some processes ("pillars": between arrows) appear to join the apposed membranes, and themselves appear membranelike. Scale bar represents 0.1 μm.

FIGURE 1–26. Mouse ventricle. At the Z-line level, several examples of corbular SR (C-SR) are found, fused with N-SR tubules. Opaque contents and surface-connected projections, some membranelike (arrows), characterize these spherules of "extended junctional SR." Scale bar represents 0.1 μm.

demonstrated junctional processes of skeletal J-SR [72] have not yet been successfully applied to cardiac muscle. In addition, thin-section analysis is made difficult by the superposition of the various layers of the coupling (see discussions in Forbes and Sperelakis [8, 73]). Nevertheless it has been deemed likely that junctional processes of cardiac muscle, like those of skeletal muscle, are disposed in rows [5, 7].

Additional forms of junctional SR have been described in heart, all of which anastomose with N-SR, contain electron-opaque granules, and bear external projections which resemble junctional processes, but which do not come into apposition with the sarcolemma or TATS. The overall classification for these bodies is "extended junctional SR" (EJ-SR) [5, 7, 8, 74]. A commonly encountered variety of EJ-SR is *corbular SR* ("coated SR" [4]), 80- to 120-nm spherules which appear to bud from the N-SR or exist in vesicular chains, usually near the Z lines (figs. 1–7, 1–26, 1–40). Corbular SR appears with widely varying frequency among different species and between different regions of the myocardium, and when found may exist singly, in small groups, or in clusters containing 5–10 vesicles.

Cisternal or saccular expansions of the SR have now been described in mouse heart [8]; these lie in deeper myoplasmic regions and are positioned over Z lines. They resemble nothing so much as J-SR components of interior couplings which have formed in the absence of contact with the TATS, a phenomenon first described in avian heart [74].

Additional variations of myocardial SR structure have been noted, including proliferations of J-SR [e.g., 75] and of N-SR [8], as well as dense-cored segments of the N-SR [8].

Enzymes and other proteins associated with cardiac SR are likely involved primarily in the sequestration and release of Ca^{2+} ion, and the pillarlike structures within couplings may be electromechanical devices whereby the action potential or other signals are relayed to the J-SR, thence to the rest of the internal SR membrane system which envelops the myofibrils [e.g., 59, 70].

During myocardial development, couplings first appear at the cell periphery, but as the TATS forms, increasing numbers of interior couplings arise, to the degree that the latter preponderate by far in adult heart [76, 77]. The mechanism(s) by which couplings are formed may be related to an inductive effect derived from sarcolemma–SR contact; however, in consideration of the presence of EJ-SR, other influences—such as that of the Z lines and associated myoplasm [28]—should be considered.

INTERMEMBRANOUS JUNCTIONS: INTERCALATED DISCS

Myocardial cells are joined to one another by numerous intermembranous junctions, most of which are collected into adhesive complexes known as *intercalated discs*. These complexes incorporate that sarcolemma which borders the ends of the cells, as well as additional, variable expanses of lateral sarcolemma near the cell ends (figs. 1–1 and 1–27). The sarcolemma of the intercalated disc is divided into four structural areas, those occupied by: (a) *fasciae adherentes* ("intermediate" junctions), (b) *maculae adherentes* (desmosomes), (c) *maculae communicantes* (gap junctions, nexuses), and (d) unspecialized or "general" sarcolemma [78].

For the most part, *fasciae adherentes* are regions in which the myofibrils terminate, the actin filaments apparently anchoring in the vague, opaque substance underneath the sarcolemma (figs. 1–16 and 1–27). Structured material is sometimes found in the intercellular gap of the *fascia adherens* [3], but at best this extracellular material does not approach the complexity of the central lamella of desmosomes, a structure which may to a large degree be the basis of adhesion between adjacent myocardial cells [79]. Desmosomes are characterized additionally by discrete collections of opaque subsarcolemmal material ("plaques") which face one another across the intercellular space and are matched in length in each of the apposed cells (fig. 1–29). The central lamella appears to receive filamentous projections from the sarcolemma; it has been proposed that different linking proteins are present between intermediate filaments and the intracellular portions of the desmosome [80]. The third

junctional category, gap junctions, as well may be instrumental in cell-to-cell connection, both in mechanical and in electrical terms. In the mechanical sense, the integrity of the gap junction has been shown to be resistant both to pathologic conditions [81] and to processes which attempt by enzymatic and/or ionic means to separate the cells [82]; such findings necessarily ascribe to the gap junction some measure of adhesion. The more generally acclaimed function of gap junctions, particularly those of myocardium, is one of electrical communications via fluid-filled channels which may exist in continuity with the myoplasm of both connected cells. The intercalated disc is a patchwork of the three types of junction, which are interspersed with areas of general sarcolemma that bear no intra- or extracellular adornments (figs. 1–27 to 1–29 and 1–31). The contours of intercalated discs can be both species-specific—and also region-specific—within the same heart. Among mammalian ventricles, the discs in rodent heart exhibit a "wavy" pattern because of the presence of extensive, fingerlike longitudinal excursions and incursions (fig. 1–27). On the other hand, the tips of carnivore and primate ventricular cells are far more geometric in contour; wide expanses of the intercalated discs in such hearts are truly discoidal (figs. 1–1 and 1–28), and the longitudinal deviations are rectangular in profile, thus creating the classic "steplike" appearance of the intercalated disc (fig. 1–1). Intercalated discs of atrial and conductive cells incorporate a great deal of longitudinal sarcolemma (figs. 1–37, 1–39, and 1–42), and the disc segments are much less tightly corrugated than is usually the case in working ventricular muscle cells (fig. 1–28).

The interdigitation of the various junctional categories is largely the product of the positions taken by the myofibrils, which specifically terminate in the *fasciae adherentes* (fig. 1–27). Therefore the majority of the transversely oriented sarcolemma—as well as some of the longitudinal component—of the disc is immutably occupied. Desmosomes and gap junctions therefore are relegated for the most part to the longitudinal folds, and only secondarily appear in the limited available sarcolemma in the intermyofibrillar spaces of the transverse component of the intercalated disc (figs. 1–27 to 1–30). Perhaps because of their greater investment in lateral sarcolemma, the ventricular cells of mouse and guinea pig exhibit gap junctions which are quite extensive [83]; this possible interspecies disparity in total contribution of gap junction membrane is deserving of morphometric study, in view of the controversy which remains concerning the electric properties of myocardial intercalated discs [e.g., 84].

Freeze-fracture replication and extracellular tracer techniques have both led to a better understanding of gap junctions, collectively revealing the distribution of subunits ("connexons") in hexagonally packed aggregates (at least in conventionally prepared tissue: see Raviola et al. [85]) and the central dot [86] within each connection (figs. 1–30 and 1–31), which cavity may be the basis of cell-to-cell ionic communication. Gap junctions, desmosomes, and, to a lesser degree, *fasciae adherentes,* are recognizable in freeze-fracture replicas which afford a two dimensional view of the distribution and extent of such junctions (fig. 1–31).

As pointed out in the section on *Intermediate (10-nm) Filaments,* myocardial desmosomes are frequently associated with intermediate filaments. As stated above, the specific intracellular associate of the *fascia adherens* junction is the myofibril. We have recently demonstrated [37], furthermore, that there may be gravitation of subsarcolemmal mitochondria to myocardial gap junctions (see *Mitochondria*).

OTHER ORGANELLES

Golgi Apparatus and Associated Structures. Stacks of flattened, fenestrated sacs form the major portion of Golgi apparati. Each Golgi apparatus may be limited, in the heart, to a few saccules which lie against the tips of nuclei (fig. 1–17)—this is often the case in ventricular fibers—or may comprise, in a single cell, numerous sets of lamellae throughout the nuclear pole myoplasm (fig. 1–32). This latter configuration is especially characteristic of atrial myocytes. An additional feature of the atrial Golgi apparati is their generation of atrial

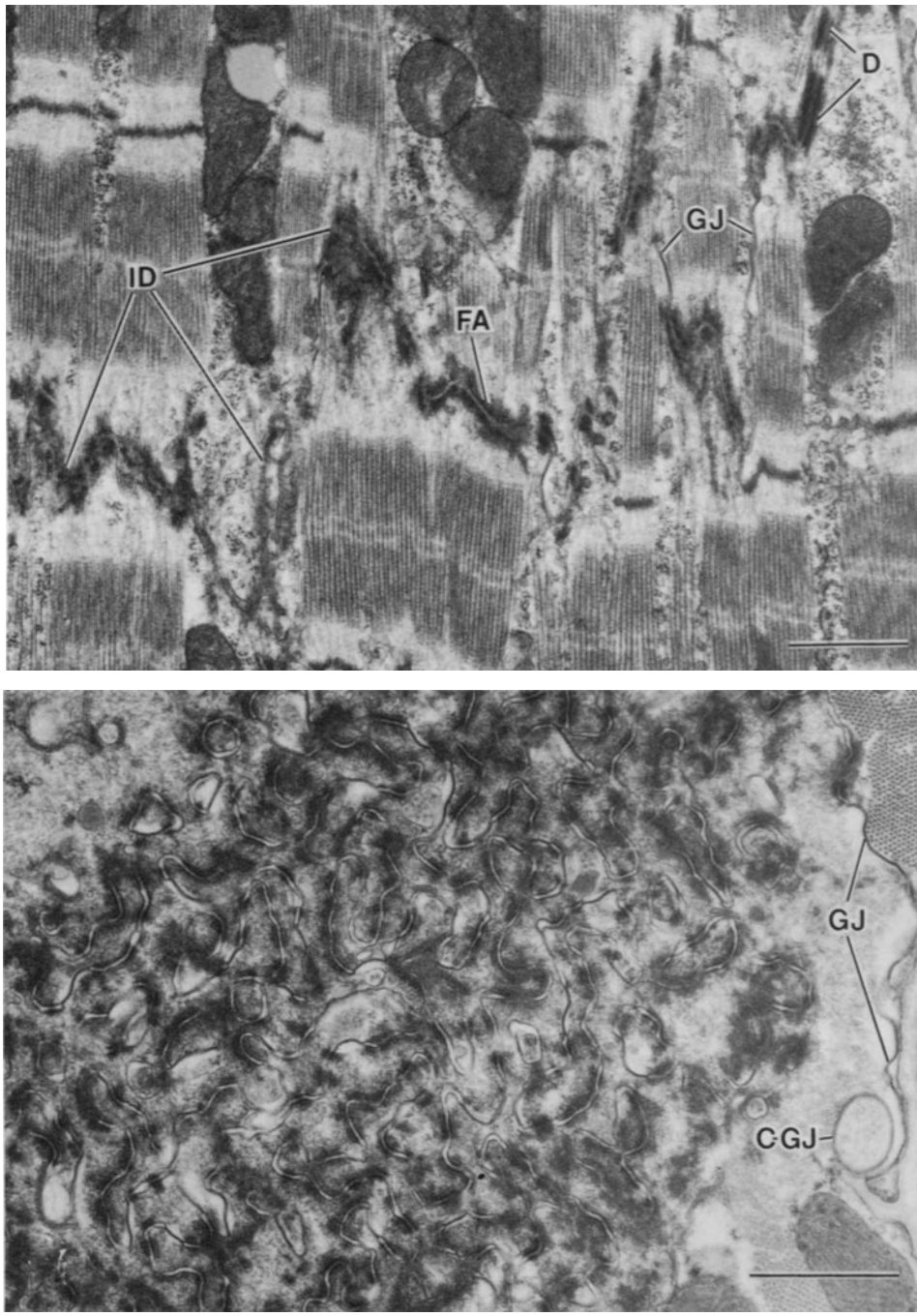

FIGURE 1–27. Longitudinal thin section through intercalated disc (ID) of mouse ventricular wall. The actin filaments of the subjacent myofibrils terminate in the opaque intracellular material of the *fasciae adherentes* junctions (FA). The transverse portions of the intercalated disc thus substitute at these sarcomere levels for Z lines. Extensive, longitudinally aligned stretches of cell-to-cell appositions are common in hearts of rodents such as mouse and guinea pig, and these are the sarcolemmal sites at which desmosomes (D) and gap junctions (GJ) typically appear. Scale bar represents 1 μm.

FIGURE 1–28. Transverse section of intercalated disc in dog ventricular myocardium. In working ventricular cells of carnivores and primates, the intercellular attachments form transverse planar arrays (cf. fig. 1–1) which in fact are disclike, and thus large expanses may be captured in a single transverse section (cf. fig. 1–4). As in the case of rodent heart (fig. 1–27), the longitudinal disc surfaces are the primary repository of desmosomes and gap junctions. An extensive gap junction (GJ) is present, in addition to a circular profile of gap junction membrane (C-GJ). Scale bar represents 1 μm.

specific granules, opaque spheroidal bodies which have been extensively investigated and found to comprise several morphologic subcategories, to contain both carbohydrate and protein moieties, but not to consist of catecholamines [e.g., 87]. Specific granules of one subcategory or another are found throughout atrial cells (fig. 1–36), but are particularly concentrated in the nuclear pole myoplasm.

Associated with the Golgi apparatus in all cardiac cells are numerous vesicles of various sizes and appearances, including large and small pleiomorphic dense-cored bodies (fig. 1–32) and small clear-cored coated vesicles (fig. 1–32). Short segments of rough endoplasmic reticulum and of smooth-surfaced (sarcoplasmic) reticulum are frequent occupants of the nuclear pole cytoplasm, and thus can be found in apparent association with the Golgi region; it is not yet clear, however, what confluency may exist between the membranes of the Golgi and the ER or SR [88].

Centrioles. When found, centrioles are located in the nuclear pole myoplasm, often in the vicinity of the Golgi apparatus. There are few published micrographs of centrioles in the ventricular cells of adult mammalian heart; however, centrioles are often discernible in atrial cells. It has been historically difficult to explain the exact function of centrioles, since they are not the intrinsic point from which microtubules become assembled to form the mitotic spindle. The paucity of centrioles in ventricular myocytes has been attributed to the low probability of encountering, in thin sections, these small, presumably paired bodies within large volumes of myoplasm [40]. In view of the great frequency with which centrioles are encountered in developing ventricular myocytes of guinea pig and mouse (unpublished observations), an alternative—though speculative—explanation comes to mind, namely, that centrioles degenerate and disappear as a consequence of the completion of development of ventricular cells, which lose their cytokinetic competence in the adult heart (see *Nuclei*).

Coated Vesicles. A variety of different vesicular structures appears in heart cells. As noted above (*Golgi apparatus and associated structures*), small coated vesicles are characteristically associated with the Golgi apparatus, and may exist—in the static thin section—either free in the myoplasm or fused with a Golgi saccule (fig. 1–32), indicating the participation of such vesicles in a dynamic process. Larger coated vesicles are present in small numbers throughout myocardial cells (figs. 1–33 to 1–35); neither their origin nor function has yet been explained. The vesicles may be found fused with the sarcolemma (fig. 1–33) or TATS, or free in the myoplasm (figs. 1–34 and 1–35).

Lysosomes and Other Inclusions. The incidence of lysosomes per se is quite low in heart [5], but membrane-bounded lipofuscin bodies (fig. 1–17) (also known collectively as "aging pigment") become increasingly common in the nuclear pole myoplasm as the animal grows older [89]. Lipofuscin is likely a form of residual body, the product of lysosomal engulfment and degradation of other organelles, most likely mitochondria [4, 5]. Multivesicular bodies are found on occasion, and these have been likened to lysosomes [4].

Lipid bodies and peroxisomes (microbodies) have been noted in myocardial intermyofibrillar and subsarcolemmal spaces, and can be distinguished cytochemically from one another. Peroxisomes, in addition to their reaction with diaminobenzidine and H_2O_2, also are characterized by their positions at the A-I levels of the sarcomeres [90].

Glycogen particles occur with varying frequency in myocardial cells; β particles are more prominent in slower-beating hearts (such as those of cat and dog) than in fast-beating myocardia such as that of the mouse. Glycogen granules grouped together to form α particles appear in developing and neonatal hearts, and in some conductive cells [91], but are not a common feature of mature working myocytes. McNutt and Fawcett [4] have noted the rather specific disposition of β particles between the myofilaments in the I bands, and glycogen particles can be found in the various myoplasmic spaces such as those adjacent to the nuclear poles, where they and ribosomes may easily be confused with one another (fig. 1–32).

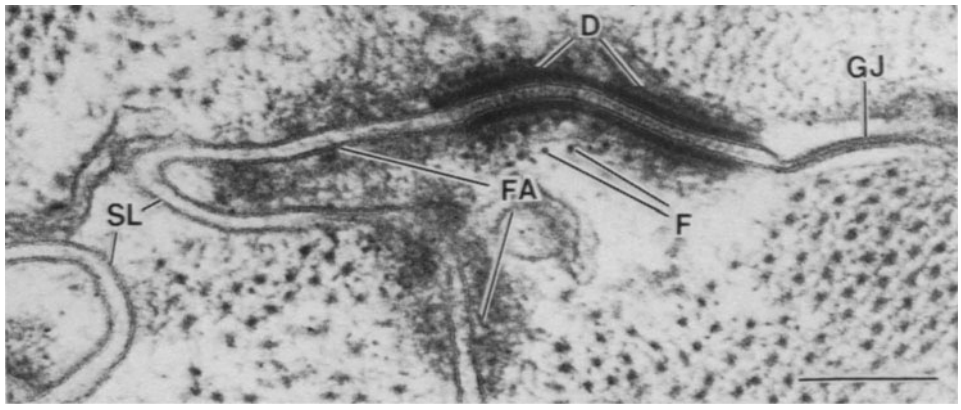
D
GJ
FA
F
SL

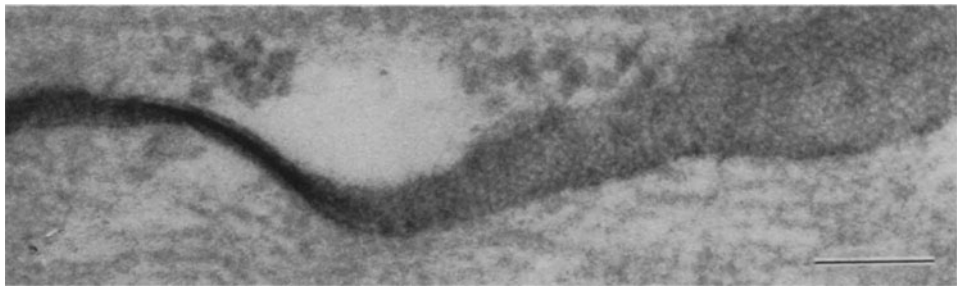

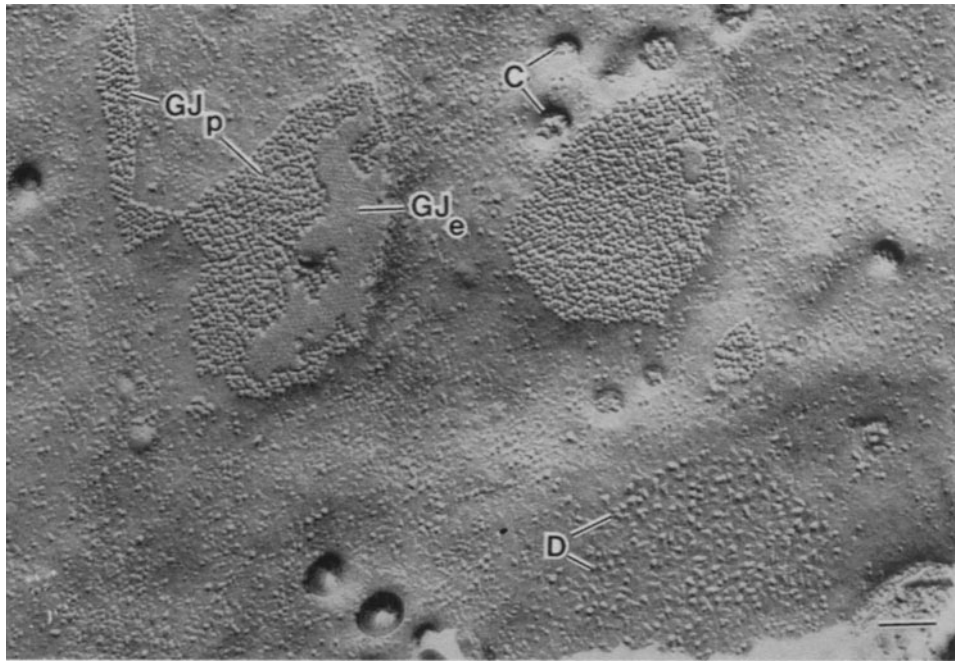
C
GJp
GJe
D

Conductive Myocardial Cells: the Atrioventricular Conducting System

Several relatively recent reviews are concerned with characterization of the conductive cells and pathways of the mammalian heart [e.g., 91–95]. These and other, broader reviews of myocardial structure point out the great deal of anatomic variation that can exist between physiologically similar cells of different species. No attempt will be made here to summarize all these variations, but some of the more salient ultrastructural features of conductive cells will be considered, largely in the context of descriptions of working myocardial cells given in the preceding sections.

NODAL CELLS

The major nodes of the AVCS, found in the right atrial region, are the sinoatrial (SA) and atrioventricular (AV) nodes. The two are connected by pathways often dismissed as practically being more physiologic than anatomic; the AV node in turn gives rise to pathways which penetrate into the ventricles and ramify there in the form of the so-called "Purkinje cell" network. (Other pathways, from SA node to left atrium, apparently exist, however [92, 95]). There often are described two major cell types in the nodes, those that are relatively myofibril-rich, and those that possess rather little contractile material; forms transitional between working atrial muscle cells and conductive cells have also been discerned [91].

In thin sections, a reasonably dependable distinguishing characteristic of nodal cells is their tendency to group into clusters which contain several cells (figs. 1–4 and 1–39); this grouping appears to be the result of the involved interdigitation of cells via their "intercalated discs," which in such cell groups are far less disclike than those of working myocardium, instead consisting largely of laterally placed junctional complexes (fig. 1–39). The interdigitation of cells within a nodal group typically is sufficiently involved that some cells may be wound about others, with tiny cell protrusions appearing in the midst of the intertwined members (fig. 1–39). The three main types of intermembranous junctions (see *Intermembranous junctions*) can usually be identified, but opinion has it that nexuses do not occupy a major portion of nodal cell sarcolemma [5].

The Z substance of myofibrils in SA and AV nodal cells often displays unusual morphologies. In some instances circular perforations appear in transversely cut Z discs (fig. 1–40). Longitudinal sections confirm the discontinuity of the Z bands across the widths of some myofibrils. An additional oddity of conductive cell myofibrils is the occasional presence of proliferated Z substance [96] which forms intensely opaque myofibril segments (figs. 1–44 and 1–45) that resemble the nemaline rods of skeletal myopathy. Similar bodies are seen in working myocardium, particularly in older animals [97]. Such "Z rods" [22] are likely made up in large part (but not in their entirety) of tropomyosin. Their function in normal cells is not clear, but morphologically similar bodies have

FIGURE 1–29. Transverse section of mouse ventricular wall. Examples of the four sarcolemmal constituents of the intercalated disc are shown: the gap junction (GJ), septilaminar and the most narrow region of the disc; the desmosome (D), characterized by a linear extracellular structure (the central lamella) and extremely opaque intracellular plaques, near which appear profiles of intermediate filaments (F); the *fascia adherens* (FA) which lacks the distinctly organized extra- and intracellular components of the desmosome; and general sarcolemma (SL), the region in which caveolae and peripheral couplings are formed (see fig. 1–35). Scale bar represents 0.2 μm.

FIGURE 1–30. Guinea pig papillary. Gap junction infiltrated with electron-opaque precipitate formed as a result of block-staining with uranyl acetate. The thin section passes through a region in which the plane of the sarcolemma tilts, thus revealing the gap junction in sideview at the *left* and en face at the *right*. At the upper right the characteristic hexagonal packing of gap junction subunits ("connexons"), as well as the opaque central dots within each connexon, is made clear by the presence of the uranium precipitate. Scale bar represents 0.1 μm.

FIGURE 1–31. Mouse ventricle. Freeze-fracture replica of lateral sarcolemmal region of intercalated disc (cf. fig. 1–27). In addition to the evenly distributed intramembranous particles on the P face of the general sarcolemma, there appear several groups of larger, tightly packed P-face particles of gap junctions (GJ_p); atop these aggregates appear small portions of the gap junctional E face (GJ_e), which separated from the cell above. The large particles distributed in a discoidal array at the lower right of the field are characteristic of a desmosome (D). C, caveolar openings. Scale bar represents 0.1 μm.

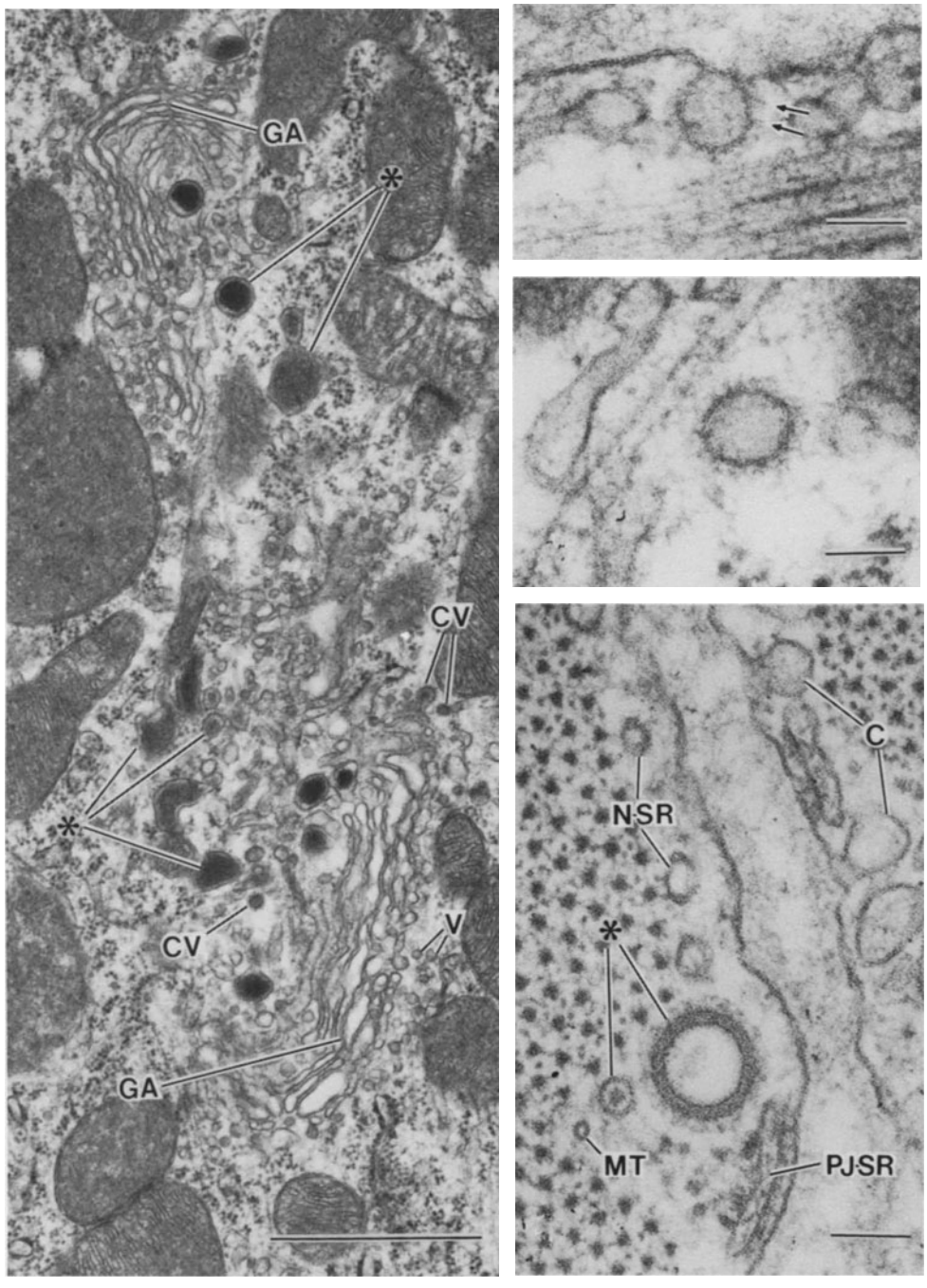
GA
*
CV
*
CV
V
GA
C
NSR
*
MT
PJSR

been proposed as the framework on which new sarcomeres are produced [98]. Their presence in pathologic skeletal muscle is thought to compromise myofibrillar contractility, but such impediment is probably of minor consequence to cells of the AVCS, since their primary function is electrical rather than mechanical.

The sarcoplasmic reticulum of nodal cells consists of network SR, peripheral junctional SR, and numerous examples of corbular (extended junctional) SR (fig. 1–40; see *Sarcoplasmic reticulum*). In some cells, collections of N-SR are not specifically associated with the myofibrils, but instead occupy subsarcolemmal locations, intermingling there with filamentous material and glycogen particles [99].

No clear-cut evidence has been presented to support the general presence of transverse tubules, much less a TATS (cf. *Transverse-axial tubular system*), in cells of the AVCS. Nevertheless a number of observations suggest that a variety of invaginations can form in such cells. For example, Osculati and Garibaldi [100, 101], Osculati et al. [102, 103], and Rybicka [99] have published micrographs which display indentations which emanate from the surface sarcolemma of Purkinje-type cells. In the SA node of cat myocardium, certain cells (fig. 1–41) contain large, membrane-bounded, granule-filled cavities which appear to be continuous with the sarcolemma, in view of occasional J-SR saccules which are attached to them. Some sarcolemmal intrusions, similar in form to T tubules, can be found as well (fig. 1–41). The above findings cast some doubt on the pat concept that AVCS cells can be distinguished de facto by their lack of a TATS. Whether or not the invaginations described are generated by a process similar to that which creates the TATS of working myocardial cells remains to be investigated. Such a determination will be significant in defining the parallels in construction which exist between contractile and conductive cells of the heart.

FIGURE 1–32. Mouse ventricular myocardial cell. Nuclear pole myoplasm, occupied in large part by Golgi apparati (GA). Although an extensive Golgi system is not a frequent constituent of ventricular cells, these profiles provide a composite view of the numerous aspects of the Golgi region. In addition to the dense-cored vesicles of varying sizes and shapes (*) which appear at the concave faces of the stacks of curved cisternae, there are numbers of small vesicles (V), largely associated with the forming, concave Golgi saccules. Coated vesicles (CV) are present as well at both Golgi faces. Ribosomes, microtubules, and mitochondria coexist with the Golgi in nuclear pole myoplasm. Scale bar represents 1 μm.

FIGURES 1–33 to 1–35. Coated vesicles of various configurations and locations in mouse ventricular myocardium.

FIGURE 1–33. Coated vesicle fused with surface sarcolemma. Bristlelike projections (arrows) form part of the characteristic coating. Scale bar represents 0.1 μm.

FIGURE 1–34. Coated vesicle deep in myoplasm. Note similarity of its coating to that of the vesicle shown in figure 1–33. Scale bar represents 0.1 μm.

FIGURE 1–35. Transverse section of portions of two cells, demonstrating a variety of vesiclelike profiles, some of which are not truly spheroidal bodies, including cross sections of network SR (N-SR) at the myofibril periphery, and a microtubule (MT). Associated with the sarcolemma are surface-connected caveolae (C) and saccules of peripheral junctional SR (PJ-SR). Two atypical vesicles are present (*), one of which exhibits an opaque core. Scale bar represents 0.1 μm.

PURKINJE CELLS

A great deal of controversy has developed over the conductive network of mammalian ventricle, beginning presumably with the work of Purkinje himself [104] and continuing with numerous other investigations which have questioned the singular identity and regional specificity of such cells (e.g., see Sherf and James [95]). The term continues to be readily recognized, however, even though exact definition seems yet forthcoming. Suffice it to say that the AVCS within the ventricle is largely composed of a highly ramified network of cells, subendocardial in location, which can be distinguished from the sometimes adjacent working fibers on the basis of one, or another, or more structural criteria. At this point the collection of qualified cells burgeons. Rodent Purkinje cells differ from working ventricular myocytes by little more than the lack of the TATS, it seems [105, 106]. Purkinje-type cells of certain other species, however, display T-tubule-like structures (see the preceding section). Ungulates occupy an extreme of the spectrum, in having extraordinarily enlarged

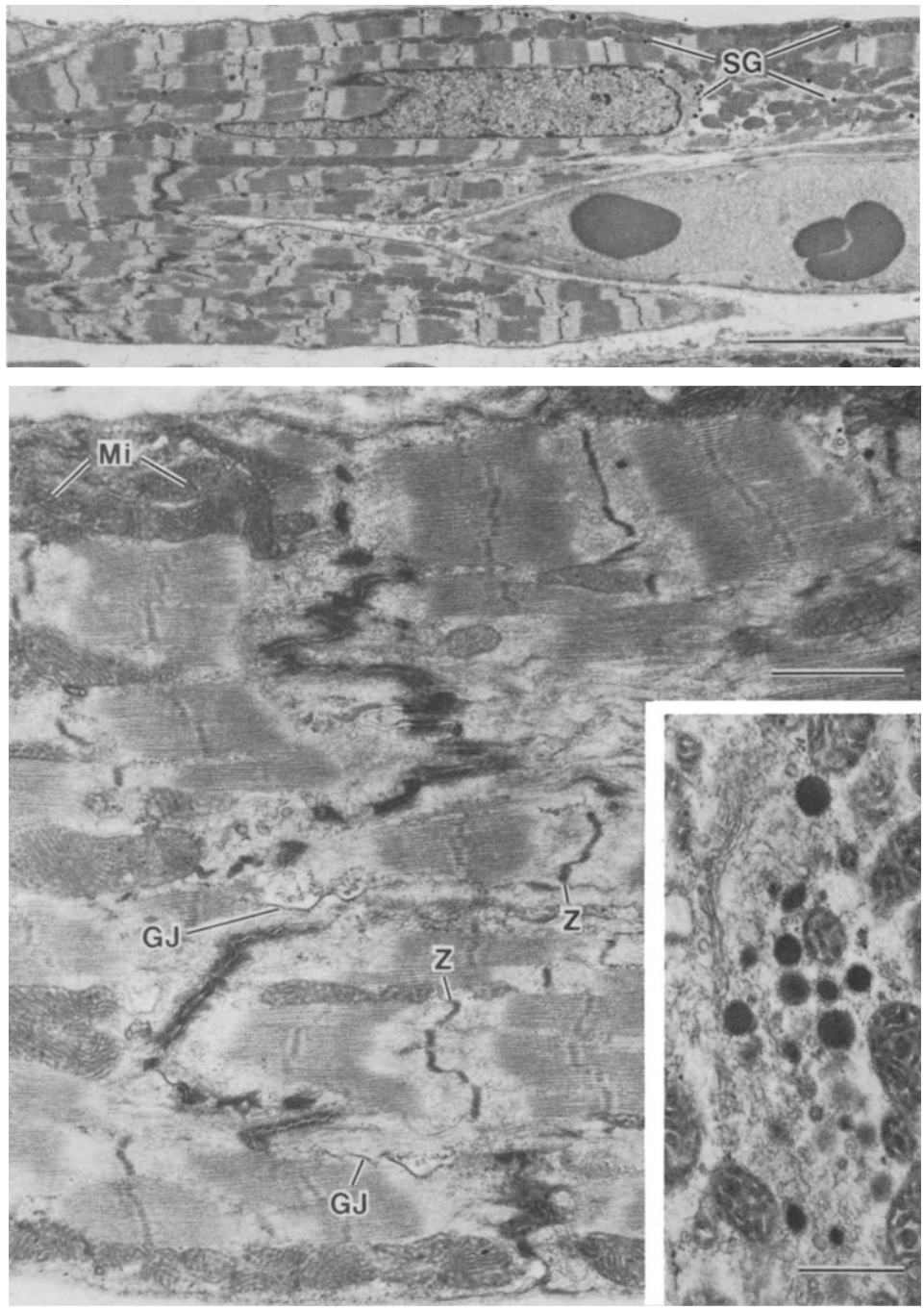

FIGURES 1–36 to 1–38. Left atrial wall (longitudinal sections) from rhesus monkey heart.

FIGURE 1–36. This section illustrates the thinness of the muscle cells of the atrium (cf. fig. 1–5). Atrial specific granules (SG) are scattered through the myoplasm of the upper cell. Scale bar represents 5 μm.

FIGURE 1–37. The contours of this intercalated disc are irregular and largely involved in longitudinal folds, some of which contain gap junctions (GJ). Mitochondria (Mi) are smaller and less numerous than in working ventricular cells (e.g., cf. fig. 1–7). The lower degree of organization of these atrial cells also is denoted by their sarcomeric components (including Z bands: Z), which may be misaligned even in the same myofibril. Scale bar represents 1 μm.

FIGURE 1–38. Golgi region, illustrating forming and mature atrial specific granules. Scale bar represents 0.5 μm.

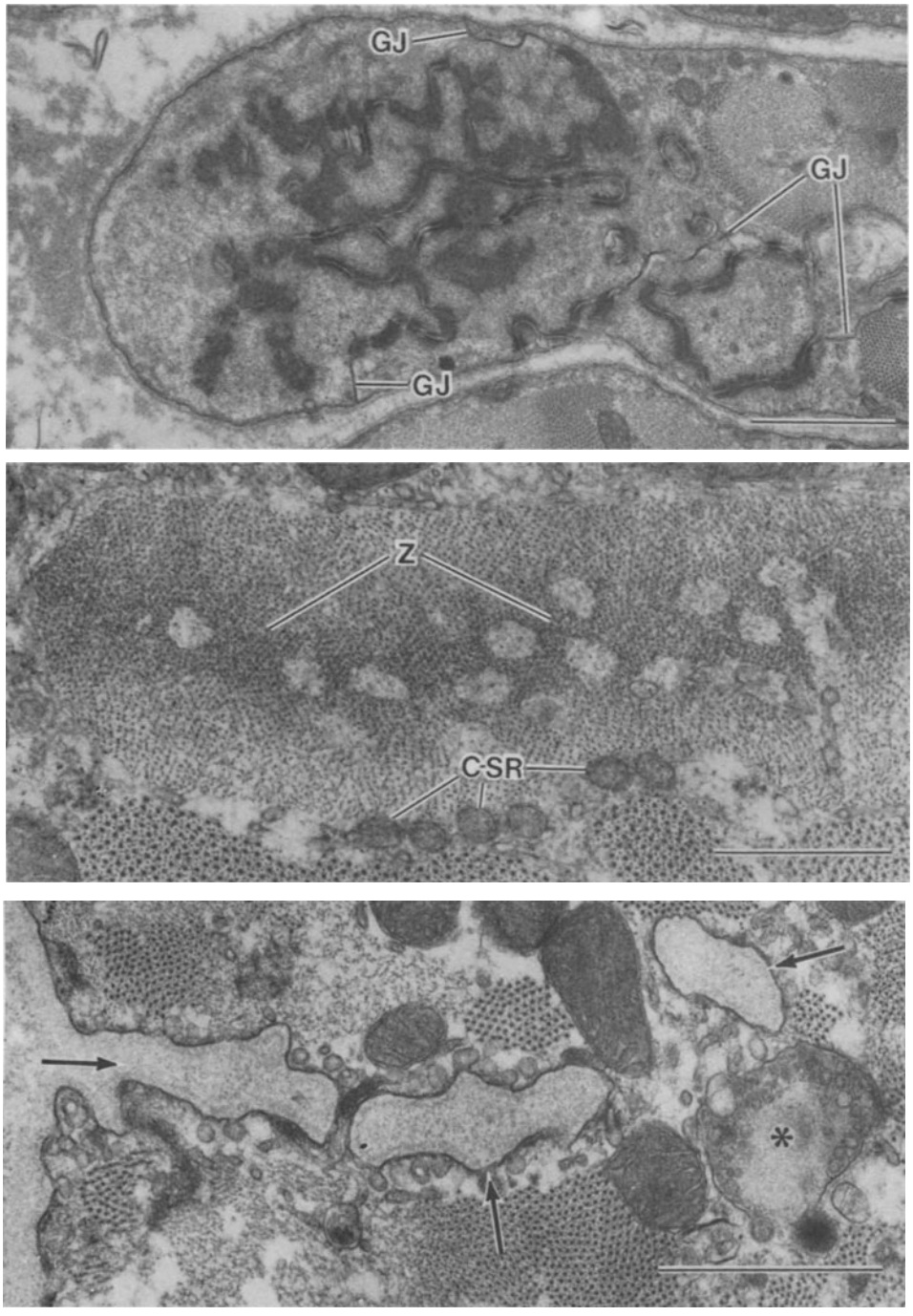

FIGURE 1–39. Rhesus sinoatrial node. The complex interdigitation of apposed cells typifies nodal groupings (also see fig. 1–6). Gap junctions (GJ) are prominent in these intercalated disc profiles. Scale bar represents 1 μm.

FIGURE 1–40. Rhesus SA nodal cell. Z discs (Z) in many of these cells exhibit numbers of circular defects ("perforations"). Numerous spherules of corbular SR (C-SR) also are characteristic of such cells. Scale bar represents 0.5 μm.

FIGURE 1–41. Cat SA node. Certain nodal cells exhibit definite sarcolemmal infoldings (arrows) which are filled with surface-coat meterial. Granule-filled bodies (*) are common in these cells, and some of these can be traced to connection with the surface sarcolemma. Scale bar represents 1 μm.

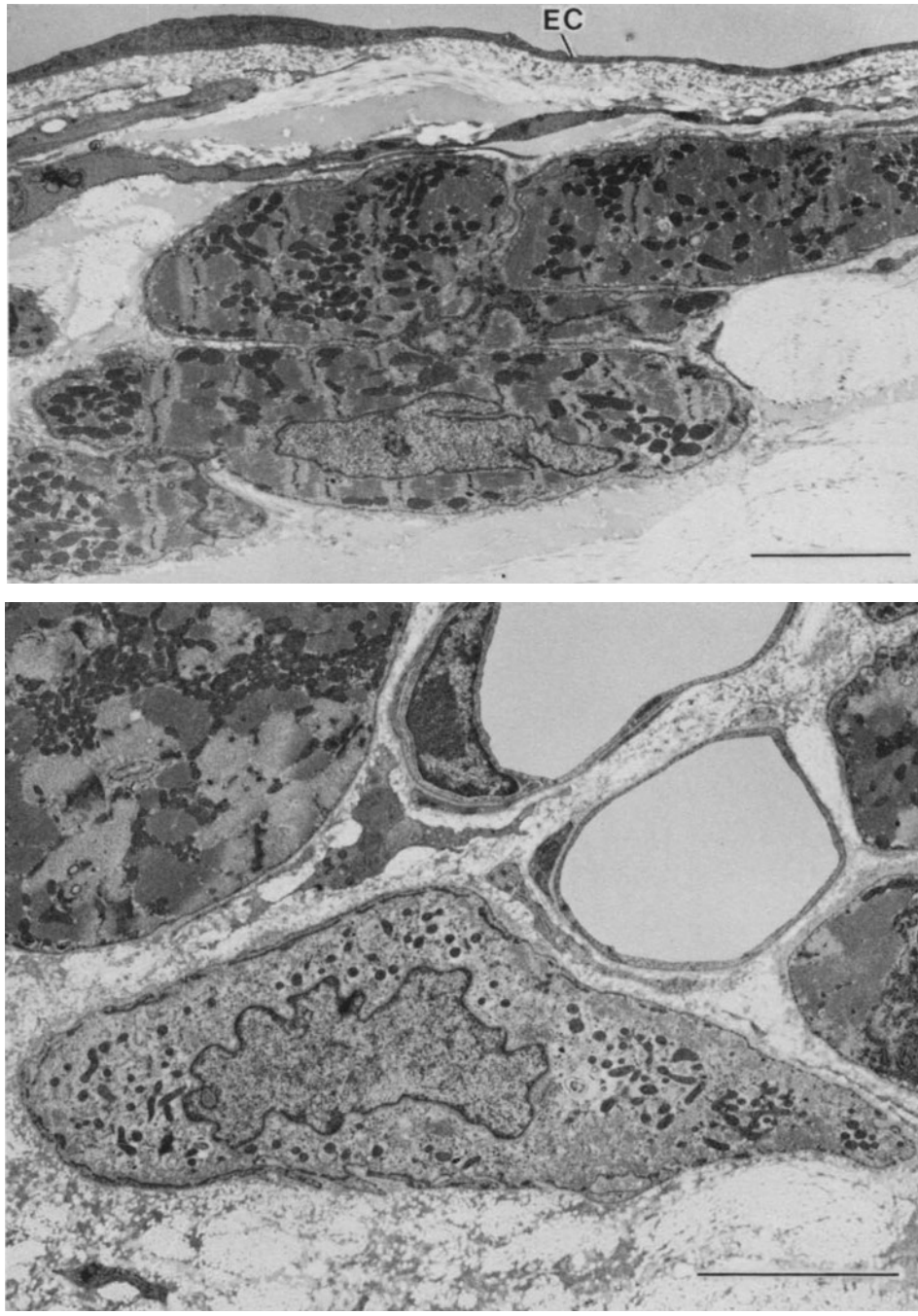

FIGURES 1–42 and 1–43. "Purkinje" cells from ventricular subendocardial network of conductive cells in rhesus monkey heart.

FIGURE 1–42. Small, myofibril-rich Purkinje cells, connected to one another by short, side-to-side appositions (see fig. 1–44) to form a thin network just beneath the endocardium (EC). Scale bar represents 5 μm.

FIGURE 1–43. Transverse section of subendocardial "type I" [91] Purkinje fiber, identifiable by its overall lucent appearance relative to the adjacent working ventricular cells. Detail shown in figure 1–46. Scale bar represents 5 μm.

conductive fibers, often grossly discernible on ventricular surface, whose contractile apparati are virtually nil, which are devoid of T tubules, and whose volume is largely taken up by glycogen [e.g., 107, 108]. Subdivision into categories of the Purkinje fibers of monkey heart has been attempted as well [91].

Our own observations on rhesus monkey heart confirm the existence of at least two general types of cells in the subendocardial network. As in the case of nodal cells, the dichotomy is based on greater and lesser incidence of myofibrillar material (figs. 1–42 and 1–43). The conductive cell having a prominent complement of myofibrils seems predominant; each example of this category, like nodal cells, is joined to its fellow cells by intercalated discs which are heavily invested in longitudinally oriented expanses of sarcolemma (fig. 1–42). There is also significant occurrence of nemalinelike aggregates of Z-disc substance (figs. 1–44 and 1–45), a phenomenon seen also in Purkinje cells of cow [109] and dog [110]. Myofibril-poor cells (probably equivalent to the type-I cells described by Virágh and Challice [91]) are spectacularly evident because of their "clear" appearance relative to other cells in their immediate vicinity (figs. 1–43 and 1–46). The contractile elements of such cells, like those of ungulate Purkinje fibers, are located primarily at the cell periphery. Their boundaries are convoluted, and the intermyofibrillar spaces (fig. 1–46) contain small mitochondria, microtubules, and some loosely arranged filamentous material (possibly composed in part of intermediate filaments [cf. 111]). Short sarcolemmal invaginations create undulated surfaces along stretches of cell border, and junctional SR of exceptional length—which becomes "extended" J-SR at some points (fig. 1–46)—is a notable characteristic of such cells.

Conclusion

Heart muscle, by dint of its essentiality to the survival of the body—particularly in regard to that of man—has enjoyed commensurate interest in the form of scientific research. Understanding of the structure of heart muscle has been almost unbelievably expanded over the relatively short period during which cardiac ultrastructure has been studied [112]. Still the adjurations of Raymond Truex [94] come to mind as particularly apt. He has pointed out that the limitations imposed by light and electron microscopy are both significant and very different. By means of the first mode, light microscopy, the cell boundaries cannot be clearly identified; in the other (specifically transmission electron microscopy), the small sample size offered by thin sections is potentially deceptive, in terms of such tasks as measuring maximal cell diameters, even though resolution is increased as much as a thousandfold. In recent years the use of evolved techniques, for example, scanning electron microscopy in combination with single-cell isolation, freeze-fracture replication, stereoscopic thick-section examination of selectively opacified heart tissue, and computer-based reconstruction of cell shapes, has helped to close the informational gap that existed, in 1974, between 5-μm and 50-nm tissue sections. Nevertheless there remain additional problems which are largely a product of the global Heisenberg principle: nothing can be evaluated without being somehow altered. Isolation of myocardial cells can rupture their intercalated discs, procedures such as dehydration and critical-point drying may shrink cells severely, and so forth. Yet, if the various limitations can be recognized and countered insofar as possible, in future reviews there will continue to be demonstrated the fact that the study of heart has been well served by the broad technical field of ultrastructure research.

Acknowledgments

This work was supported by grants from both the Public Health Service (HL-28329 to M.S.F., HL-18711 to N.S.) and the American Heart Association (grant-in-aid 78-753, and a grant-in-aid from the Virginia Affiliate of the A.H.A., both to M.S.F.). Dr. Forbes is recipient of Research Career Development Award 5 KO4 HL-00550-05 from the National Institutes of Health.

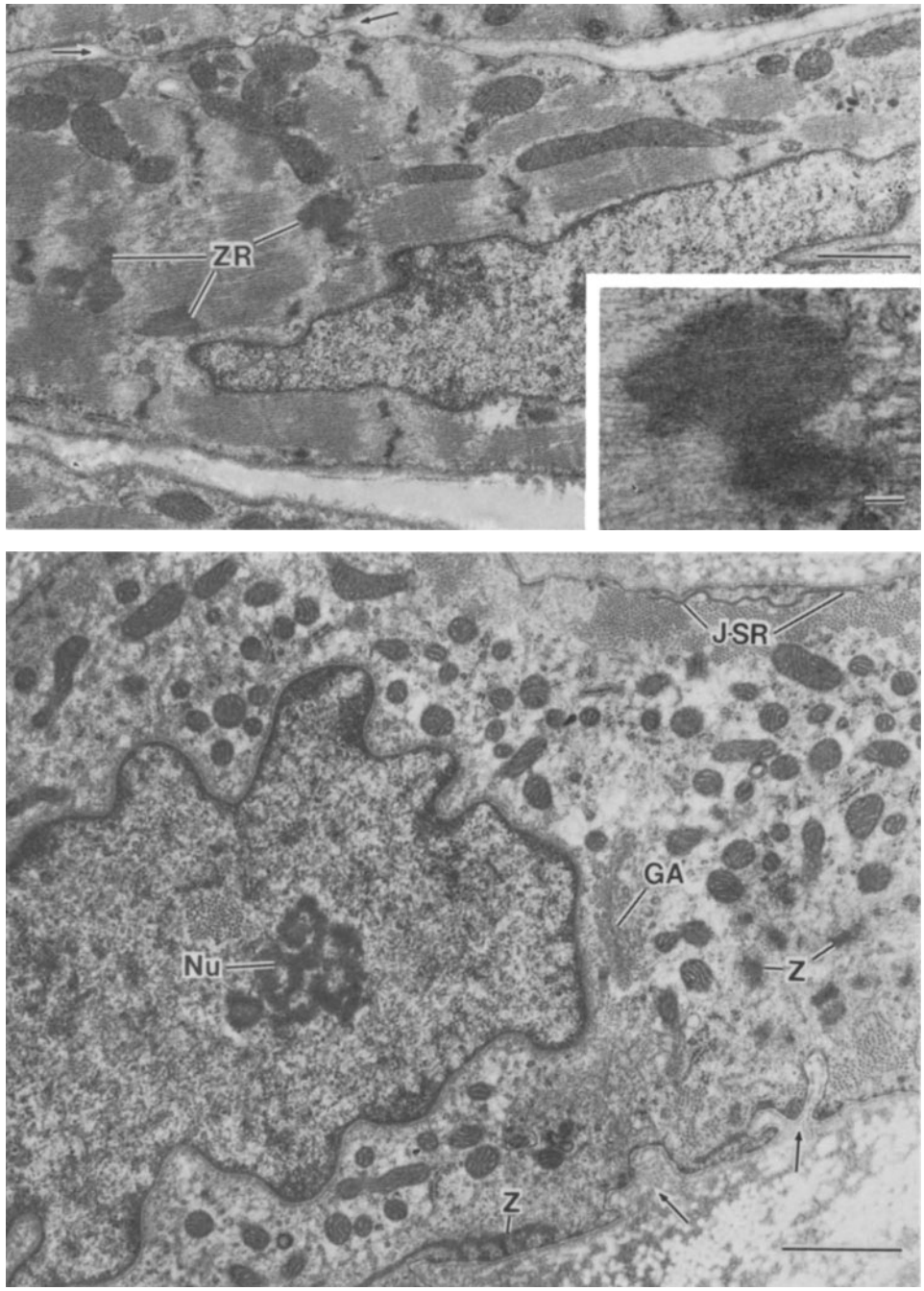

FIGURE 1–44. Purkinje fibers in section alternate to that shown in figure 1–42. Cell-to-cell adhesions are short (between arrows), and the substance of Z bands frequently proliferates to form "Z rods" (ZR). Scale bar represents 1 μm.

FIGURE 1–45. Detail of Purkinje Z rod, illustrating its distinct substructure. Scale bar represents 0.1 μm.

FIGURE 1–46. Detail of "clear" Purkinje cell. The nucleus exhibits a prominent nucleolus (Nu) and a crenated envelope. Myofibrillar material is sparse and tends to be located at the outer rim of the cell. Z-band material (Z) forms small dense profiles of various shapes. A limited Golgi apparatus (GA) is juxtaposed to the nucleus, and numerous small mitochondria are present in the electron-lucent myoplasm. Short sarcolemmal invaginations, lined with surface coat material, are seen (arrows). An elongate saccule of junctional SR (J-SR) undulates into and away from contact with the surface sarcolemma. Scale bar represents 1 μm.

The various monkey heart specimens were donated by Drs. S.K. Jirge and K.R. Brizzee of the Tulane University Delta Regional Primate Research Center at Covington, Louisiana (Dr. Peter Gerone, Director). Single-cell preparations of rat ventricular muscle were generously provided by Dr. S.L. Jacobsen (Carleton University, Ottawa, Canada). The technical assistance of Mr. Lawrence A. Hawkey is acknowledged with special thanks. Studies with freeze-fracture, as well as some of the stereoscopic analysis, were carried out by means of the personnel and equipment of the Central Electron Microscope Facility of the University of Virginia School of Medicine. Preparation of the manuscript was aided greatly by the efforts of Ms. Jane A. Forbes and Ms. Emilie Worrall.

References

1. Sperelakis N, Rubio R: Ultrastructural changes produced by hypertonicity in cat cardiac muscle. J Mol Cell Cardiol 3:139–156, 1971.
2. Page E, McCallister LP: Quantitative electron microscopic description of heart muscle cells: application to normal, hypertrophied and thyroxin-stimulated hearts. Am J Cardiol 31:172–181, 1973.
3. Simpson FO, Rayns DG, Ledingham JM: The ultrastructure of ventricular and atrial myocardium. In: Challice CE, Virágh S (eds) Ultrastructure of the mammalian heart. New York: Academic, 1973, pp 1–41.
4. McNutt NS, Fawcett DW: Myocardial ultrastructure. In: Langer GA, Brady AJ (eds) The mammalian myocardium. New York: John Wiley and Sons, 1974, pp 1–49.
5. Sommer JR, Johnson EA: Ultrastructure of cardiac muscle. In: Berne RM, Sperelakis N, Geiger SR (eds) Handbook of physiology, sect 2: The cardiovascular system, vol 1: The heart, Bethesda MD: American Physiological Society, 1979, pp 113–186.
6. Sperelakis N, Forbes MS, Rubio R: The tubular systems of myocardial cells: ultrastructure and possible function. In: Dhalla NS (ed) Recent advances in studies on cardiac structure and metabolism, vol 4: Myocardial biology. Baltimore: University Park, 1974, pp 163–194.
7. Sommer JR, Waugh RA: The ultrastructure of the mammalian cardiac muscle cell—with special emphasis on the tubular membrane systems. Am J Pathol 82:191–232, 1976.
8. Forbes MS, Sperelakis N: The membrane systems and cytoskeletal elements of mammalian myocardial cells. In: Shay JW, Dowben RM (eds) Cell and muscle motility, vol 3. New York: Plenum, 1983, pp 89–155.
9. Jordan HE, Banks JB: A study of the intercalated discs of the heart of the beef. Am J Anat 22:285–339, 1917.
10. Sjöstrand FS, Andersson-Cedergren E, Dewey MM: The ultrastructure of the intercalated disc of frog, mouse and guinea pig cardiac muscle. J Ultrastruct Res 1:271–287, 1958.
11. Rhodin JAG, del Missier P, Reid LC: The structure of the specialized impulse-conduction system of the steer heart. Circulation 24:349–367, 1961.
12. Hayashi K: An electron microscope study on the conduction system of the cow heart. Jpn Circ J 26:765–842, 1962.
13. Jacobson SL: Culture of spontaneously contracting myocardial cells from adult rats. Cell Struct Function 2:1–9, 1977.
14. Vahouny GV, Wei RW, Tamboli A, Albert EN: Adult canine myocytes: isolation, morphology and biochemical characterizations. J Mol Cell Cardiol 11:339–357, 1979.
15. Robinson TF, Hayward BS, Krueger, JW, Sonnenblick EH, Wittenberg, BA: Isolated heart myocytes: ultrastructural case study technique. J Microscopy (Oxford) 124:135–142, 1981.
16. Phillips SJ, Dacey DM: Mammalian ventricular heart cell shape, surface and fiber organization as seen with the scanning electron microscope (SEM). J Cell Biol 70:85a, 1976.
17. Phillips SJ, Dacey DM, Bove A, Conger AD: Quantitative data on the shape of the mammalian ventricular heart cell. Fed Proc 36:601, 1977.
18. Marino TA, Cook PN, Cook LT, Dwyer SJ III: The use of computer imaging techniques to visualize cardiac muscle cells in three dimensions. Anat Rec 198:537–546, 1980.
19. Janicki JS, Weber KT, Gochman RF, Shroff S, Geheb FJ: Three-dimensional myocardial and ventricular shape: a surface representation. Am J Physiol 241:H1–H11, 1981.
20. Nag AC, Fischman DA, Aumont MC, Zak R: Studies of isolated adult rat heart cells: the surface morphology and the influence of extracellular calcium ion concentration on cellular viability. Tissue Cell 9:419–436, 1977.
21. Bishop SP, Drummond JL: Surface morphology and cell size measurement of isolated rat cardiac myocytes. J Mol Cell Cardiol 11:423–433, 1979.
22. Goldstein MA, Schroeter JP, Sass RL: Optical diffraction of the Z lattice in canine cardiac muscle. J Cell Biol 75:818–836, 1977.
23. Goldstein MA, Schroeter JP, Sass RL: The Z lattice in canine cardiac muscle. J Cell Biol 83:187–204, 1979.
24. Landon DN: The influence of fixation upon the fine structure of the Z-disk of rat striated muscle. J Cell Sci 6:257–276, 1970.
25. Anversa P, Olivetti G, Bracchi P-G, Loud AV:

Postnatal development of the M-band in rat cardiac myofibrils. Circ Res 48:561–568, 1981.
26. Forbes MS, Sperelakis N: The presence of transverse and axial tubules in the ventricular myocardium of embryonic and neonatal guinea pigs. Cell Tissue Res 166:83–90, 1976.
27. Hirakow R, Gotoh T: Quantitative studies on the ultrastructural differentiation and growth of mammalian cardiac muscle cells. II. The atria and ventricles of the guinea pig. Acta Anat 108:230–237, 1980.
28. Forbes MS, Sperelakis N: Structures located at the level of the Z bands in mouse ventricular myocardial cells. Tissue Cell 12:467–489, 1980.
29. Ferrans VJ, Roberts WC: Intermyofibrillar and nuclear-myofibrillar connections in human and canine myocardium: an ultrastructural study. J Mol Cell Cardiol 5:247–257, 1973.
30. Goldstein MA, Entman ML: Microtubules in mammalian heart muscle. J Cell Biol 80:183–195, 1979.
31. Behrendt H: Effect of anabolic steroids on rat heart muscle cells. I. Intermediate filaments. Cell Tissue Res 180:303–315, 1977.
32. Fuseler JW, Shay JW, Feit H: The role of intermediate (10-nm) filaments in the development and integration of the myofibrillar contractile apparatus in the embryonic mammalian heart. In: Dowben RM, Shay JW (eds) Cell and muscle motility, vol 1. New York: Plenum, 1981, pp 205–259.
33. Carlsson E, Kjörell U, Thornell L-E, Lambertsson A, Strehler E: Differentiation of the myofibrils and the intermediate filament system during postnatal development of the rat heart. Eur J Cell Biol 27:62–78, 1982.
34. Palmer JW, Tandler B, Hoppel CL: Biochemical properties of subsarcolemmal and interfibrillar mitochondria isolated from rat cardiac muscle. J Biol Chem 252:8731–8739, 1977.
35. Wolkowicz PE, McMillan-Wood J: Respiration-dependent calcium ion uptake by two preparations of cardiac mitochondria. Biochem J 186:257–266, 1980.
36. Matlib MA, Rebman D, Ashraf M, Rouslin W, Schwartz A: Differential activities of putative subsarcolemmal and interfibrillar mitochondria from cardiac muscle. J Mol Cell Cardiol 13:163–170, 1981.
37. Forbes MS, Sperelakis N: Association between gap junctions and mitochondria in mammalian myocardial cells. Tissue Cell 14:25–37, 1982.
38. Peracchia C: Calcium effects on gap junction structure and cell coupling. Nature (Lond) 271: 669–671, 1978.
39. Baldwin KM: Cardiac gap junction configuration after an uncoupling treatment as a function of time. J Cell Biol 82:66–75, 1979.
40. Fawcett DW, McNutt NS: The ultrastructure of the cat myocardium. I. Ventricular papillary muscle. J Cell Biol 42:1–45, 1969.
41. Kraus B, Cain H: Giant mitochondria in the human myocardium—morphogenesis and fate. Virchows Arch [B] 33:77–89, 1980.
42. Brodsky WK, Arefyeva AM, Uryvaeva IV: Mitotic polyploidization of mouse heart myocytes during the first postnatal week. Cell Tissue Res 210:133–144, 1980.
43. Gräbner W, Pfitzer P: Number of nuclei in isolated myocardial cells of pigs. Virchows Arch [B] 15:279–294, 1974.
44. Schneider R, Pfitzer P: Die Zahl der Kerne in isolierten Zellen des menschlichen Myokards. Virchows Arch [B] 12:238–258, 1973.
45. Bugaisky L, Zak R: Cellular growth of cardiac muscle after birth. Tex Rep Biol Med 39:123–138, 1979.
46. Rumyantsev PP: Ultrastructural reorganization, DNA synthesis and mitotic division of myocytes in atria of rats with left ventricle infarction: an electron microscopic and autoradiographic study. Virchows Arch [B] 15:357–378, 1974.
47. Rumyantsev PP, Snigirevskaya ES: The ultrastructure of differentiating cells of the heart muscle in the state of mitotic division. Acta Morphol Acad Sci Hung 16:271–283, 1968.
48. Bloom S, Cancilla PA: Conformational changes in myocardial nuclei of rats. Circ Res 24:189–196, 1969.
49. Langer GA: Ionic movements and the control of contraction. In: Langer GA, Brady AJ (eds) The mammalian myocardium. New York: John Wiley and Sons, 1974, pp 193–217.
50. Isenberg G, Klöckner U: Glycocalyx is not required for slow inward calcium current in isolated rat heart myocytes. Nature 284:358–360, 1980.
51. Gabella G: Inpocketings of the cell membrane (caveolae) in the rat myocardium. J Ultrastruct Res 65:135–147, 1978.
52. Levin KR, Page E: Quantitative studies on plasmalemmal folds and caveolae of rabbit ventricular myocardial cells. Circ Res 46:244–255, 1980.
53. Forssmann WG, Girardier L: A study of the T system in rat heart. J Cell Biol 44:1–19, 1970.
54. Masson-Pévet M, Gros D, Besselsen E: The caveolae in rabbit sinus node and atrium. Cell Tissue Res 208:183–196, 1980.
55. Forbes MS, Sperelakis N: A labyrinthine structure formed from a transverse tubule of mouse ventricular myocardium. J Cell Biol 56:865–869, 1973.
56. Ishikawa H, Yamada E: Differentiation of the sarcoplasmic reticulum and T-system in developing mouse cardiac muscle. In: Lieberman M, Sano T (eds) Developmental and physiological correlates of cardiac muscle. New York: Raven, 1976, pp 21–35.
57. Sperelakis N, Rubio R: An orderly lattice of axial tubules which interconnect adjacent transverse tubules in guinea-pig ventricular myocardium. J Mol Cell Cardiol 2:211–220, 1971.
58. Forbes MS, Sperelakis N: Myocardial couplings:

their structural variations in the mouse. J Ultrastruct Res 58:50–65, 1977.
59. Forbes MS, Sperelakis N: Bridging junctional processes in couplings of striated, cardiac, and smooth muscle cells. Muscle Nerve 5:674–681, 1982.
60. Ayettey AS, Navaratnam V: The fine structure of myocardial cells in the grey seal. J Anat 131:748, 1980.
61. Ayettey AS, Navaratnam V: The ultrastructure of myocardial cells in the golden hamster *Cricetus auratus*. J Anat 132:519–524, 1981.
62. Forbes MS, Plantholt BA, Sperelakis N: Cytochemical staining procedures selective for sarcotubular systems of muscle: applications and modifications. J Ultrastruct Res 60:306–327, 1977.
63. Legato MJ: Cellular mechanisms of normal growth in the mammalian heart. II. A quantitative and qualitative comparison between the right and left ventricular myocytes in the dog from birth to five months of age. Circ Res 44:263–279, 1979.
64. Legato MJ: Ultrastructural characteristics of the rat ventricular cell grown in tissue culture, with special reference to sarcomerogenesis. J Mol Cell Cardiol 4:299–317, 1972.
65. Van Winkle WB: The fenestrated collar of mammalian cardiac sarcoplasmic reticulum: a freeze-fracture study. Am J Anat 149:277–282, 1977.
66. Dolber PC, Sommer JR: Freeze-fracture appearance of rabbit cardiac sarcoplasmic reticulum. In: Bailey G (ed) Thirty-eighth annual EMSA meeting. Baton Rouge: Claitor's, 1980, pp 630–631.
67. Scales DJ: Aspects of the cardiac sarcotubular system revealed by freeze fracture electron microscopy. J Mol Cell Cardiol 13:373–380, 1981.
68. Somlyo AV: Bridging structures spanning the junctional gap at the triad of skeletal muscle. J Cell Biol 80:743–750, 1979.
69. Eisenberg BR, Gilai A: Structural changes in single muscle fibers after stimulation at a low frequency. J Gen Physiol 74:1–16, 1979.
70. Eisenberg BR, Eisenberg RS: The T-SR junction in contracting single skeletal muscle fibers. J Gen Physiol 79:1–19, 1982.
71. Brunschwig JP, Brandt N, Caswell AH, Lukeman DS: Ultrastructural observations of isolated intact and fragmented junctions of skeletal muscle by use of tannic acid mordanting. J Cell Biol 93:533–542, 1982.
72. Kelly DE, Kuda AM: Subunits of the triadic junction in fast skeletal muscle as revealed by freeze-fracture. J Ultrastruct Res 68:220–233, 1979.
73. Forbes MS, Sperelakis N: Spheroidal bodies in the junctional sarcoplasmic reticulum of lizard myocardial cells. J Cell Biol 60:602–615, 1974.
74. Jewett PH, Sommer JR, Johnson EA: Cardiac muscle: its ultrastructure in the finch and hummingbird with special reference to the sarcoplasmic reticulum. J Cell Biol 49:50–65, 1971.
75. Waugh RA, Sommer JR: Lamellar junctional sarcoplasmic reticulum: a specialization of cardiac sarcoplasmic reticulum. J Cell Biol 63:337–343, 1974.
76. Bossen EH, Sommer JR, Waugh RA: Comparative stereology of the mouse and finch left ventricle. Tissue Cell 10:773–784, 1978.
77. Page E, Surdyk-Droske M: Distribution, surface density, and membrane area of diadic junctional contacts between plasma membrane and terminal cisterns in mammalian ventricle. Circ Res 45:260–267, 1979.
78. McNutt NS: Ultrastructure of the myocardial sarcolemma. Circ Res 37:1–13, 1975.
79. Rayns DG, Simpson FO, Ledingham JM: Ultrastructure of desmosomes of mammalian intercalated disc: appearances after lanthanum treatment. J Cell Biol 42:322–326, 1969.
80. Kelly DE, Kuda AM: Traversing filaments in desmosomal and hemidesmosomal attachments: freeze-fracture approaches toward their characterization. Anat Rec 199:1–14, 1981.
81. Kawamura K, James TN: Comparative ultrastructure of cellular junctions in working myocardium and the conduction system under normal and pathologic conditions. J Mol Cell Cardiol 3:31–60, 1971.
82. Berry MN, Friend DS, Scheuer J: Morphology and metabolism of intact muscle cells isolated from adult rat heart. Circ Res 26:679–687, 1970.
83. Kensler RW, Goodenough DA: Isolation of mouse myocardial gap junctions. J Cell Biol 86:755–764, 1980.
84. Sperelakis N: Propagation mechanisms in heart. Annu Rev Physiol 41:441–457, 1979.
85. Raviola E, Goodenough DA, Raviola G: Structure of rapidly frozen gap junctions. J Cell Biol 87:273–279, 1980.
86. McNutt NS, Weinstein RS: The ultrastructure of the nexus: a correlated thin-section and freeze-cleave study. J Cell Biol 47:666–688, 1970.
87. Cantin M, Benchimol S, Castonguay Y, Berlinguet J-C, Huet M: Ultrastructural cytochemistry of atrial muscle cells. V. Characterization of specific granules in the human left atrium. J Ultrastruct Res 52:179–192, 1975.
88. Goldfischer S: The internal reticular apparatus of Camillo Golgi: a complex, heterogeneous organelle, enriched in acid, neutral, and alkaline phosphatases, and involved in glycosylation, secretion, membrane flow, lysosome formation, and intracellular digestion. J Histochem Cytochem 30:717–733, 1982.
89. Tomanek J, Karlsson UL: Myocardial ultrastructure of young and senescent rats. J Ultrastruct Res 42:201–220, 1973.
90. Herzog V, Fahimi HD: Identification of peroxisomes (microbodies) in mouse myocardium. J Mol Cell Cardiol 8:271–281, 1976.
91. Virágh S, Challice CE: The impulse generation and conduction system of the heart. In: Challice CE, Virágh S (eds) Ultrastructure of the mammalian heart. New York: Academic, 1973, pp 43–90.

92. James TN, Sherf L: Specialized tissues and preferential conduction in the atria of the heart. Am J Cardiol 28:414–427, 1971.
93. James TN, Sherf L, Urthaler F: Fine structure of the bundle-branches. Br Heart J 36:1–18, 1974.
94. Truex RC: Structural basis of atrial and ventricular conduction. Cardiovasc Clin 6:2–24, 1974.
95. Sherf L, James RN: Fine structure of cells and their histological organization within internodal pathways of the heart: clinical and electrocardiographic implications. Am J Cardiol 44:345–369, 1979.
96. Colborn GL, Carsey E Jr: Electron microscopy of the sinoatrial node of the squirrel monkey *Saimiri sciureus*. J Mol Cell Cardiol 4:525–536, 1972.
97. Fawcett DW: The sporadic occurrence in cardiac muscle of anomalous Z bands exhibiting a periodic structure suggestive of tropomyosin. J Cell Biol 36:266–270, 1968.
98. Legato MJ: Sarcomerogenesis in human myocardium. J Mol Cell Cardiol 1:425–437, 1970.
99. Rybicka K: Sarcoplasmic reticulum in the conducting fibers of the dog heart. Anat Rec 189:237–262, 1977.
100. Osculati F, Garibaldi E: Particolari strutturali delle fibre del Purkinje del cuore di ratto; osservazioni al microscopio elettronico effuttuate anche applicando la tecnica della perossidasi. Boll Soc Med Chir (Pavia) 88:403–437, 1974.
101. Osculati F, Garibaldi E: Fine structural aspects of the Purkinje fibres of the dog's heart. J Submicr Cytol 6:39–53, 1974.
102. Osculati F, Amati S, Petrini E, Francheschini F, Cinti S: Ultrastructural investigation on the Purkinje fibres of rabbit's and cat's heart. J Submicr Cytol 10:185–197, 1978.
103. Osculati F, Amati S, Petrini E, Marelli M, Gazzanelli G: A study on the organization of the tubular endoplasmic reticulum in the rat heart conduction fibres. J Submicr Cytol 10:371–380, 1978.
104. Robb JS: Comparative basic cardiology. New York: Grune and Stratton, 1965.
105. Sommer JR, Johnson EA: Cardiac muscle: a comparative study of Purkinje fibers and ventricular fibers. J Cell Biol 36:497–526, 1968.
106. Kim S, Baba N: Atrioventricular node and Purkinje fibers of the guinea pig heart. Am J Anat 132:339–354, 1971.
107. Thornell L-E: The fine structure of Purkinje fiber glycogen: a comparative study of negatively stained and cytochemically stained particles. J Ultrastruct Res 49:157–166, 1974.
108. Thornell LE: An ultrahistochemical study on glycogen in cow Purkinje fibers. J Mol Cell Cardiol 6:439–448, 1974.
109. Thornell LE: Ultrastructural variations of Z bands in cow Purkinje fibers. J Mol Cell Cardiol 5:409–417, 1973.
110. Martinez-Palomo A, Alanis J, Benitez D: Transitional cardiac cells of the conductive system of the dog heart: distinguishing morphological and electrophysiological features. J Cell Biol 47:1–17, 1970.
111. Thornell L-E, Ericksson A: Filament systems in the Purkinje fibers of the heart. Am J Physiol 241:H291–H305, 1981.
112. Weinstein HJ: An electron microscope study of cardiac muscle. Exp Cell Res 7:130–146, 1954.

2. BASIC PATHOLOGIC PROCESSES OF THE HEART

Relationship to Cardiomyopathies

L. Maximilian Buja

Introduction

Cardiomyopathy is broadly defined as heart muscle disease. This chapter reviews certain basic pathologic processes affecting the heart and discusses the relationship of these processes to various cardiomyopathies. Additional information regarding several of these pathologic processes is provided in other chapters of this book.

Myocardial Ischemia

Myocardial ischemia is a state of relative deficiency of oxygen supply in relation to the global or regional oxygen demands of the heart [1, 2]. The initial consequence of ischemia is altered excitation–contraction coupling, leading to a decrease or loss of contractile activity. Ischemic myocardium also has abnormal electrical activity which may lead to the generation of arrhythmias. The third consequence of ischemia, when it is of sufficient severity and duration, is the progression of cell injury to an irreversible phase of cell death (myocardial infarction).

ETIOLOGY AND PATHOPHYSIOLOGY

Ischemic heart disease in humans usually occurs as a consequence of coronary atherosclerosis, a disease which impairs coronary perfusion by accumulation of atherosclerotic plaque and thrombus [2]. The coronary arteries also are subject to nonatheromatous diseases, including congenital anomalies, embolization, dissection, and aneurysms. Coronary diseases ordinarily affect the epicardial arteries, but involvement of intramural (small) arteries may be significant in some cases of ischemic heart disease.

The dynamic nature of ischemic heart disease is indicated by the imperfect relationship between the severity of anatomic lesions of the coronary vasculature and the variety and severity of clinical manifestations of ischemic heart disease [2–5]. A number of factors influence the interplay between the myocardium and the coronary vasculature. It is known that the primary determinants of myocardial oxygen demand are heart rate, myocardial contractile state, and stress on the myocardial wall (influenced by blood pressure). It is also known that ventricular hypertrophy and failure create a state of increased oxygen demand by their influence on these parameters.

With a discrete area of coronary obstruction, 50% reduction in luminal diameter (75% reduction in area) is needed to reduce hyperemic blood flow and 80% reduction in diameter is required to impair resting blood flow [2]. However, a number of factors can influence the functional significance of a coronary stenosis, including the presence of multiple stenoses, the degree of development of the coronary collat-

N. Sperelakis (ed.), PHYSIOLOGY AND PATHOPHYSIOLOGY OF THE HEART.

Martinus Nijhoff Publishing, Boston/The Hague/ Dordrecht/Lancaster.

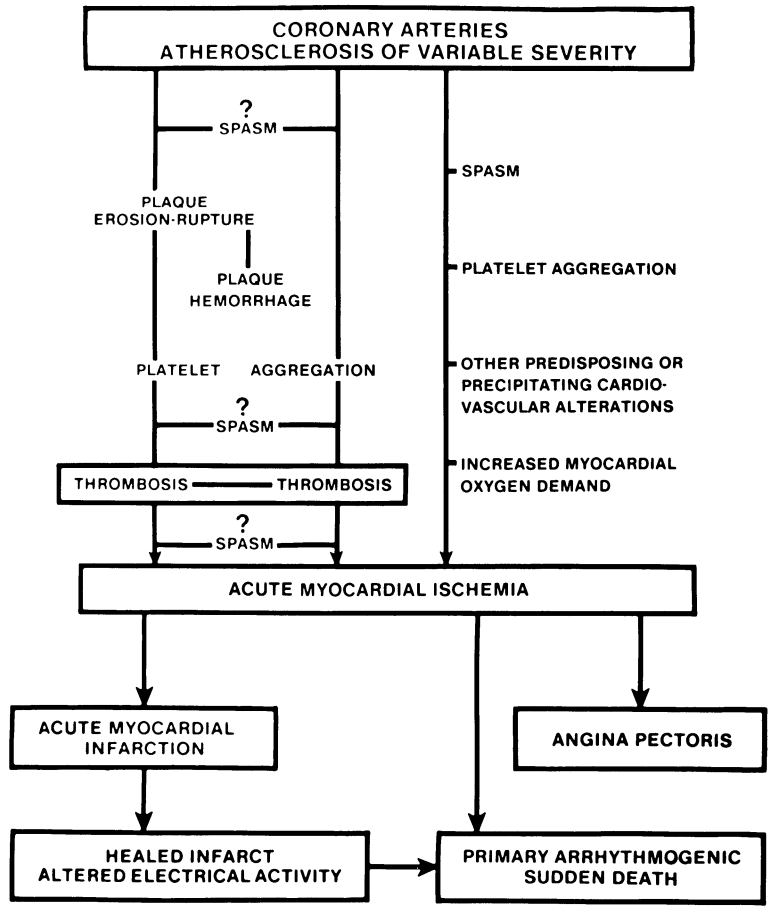

FIGURE 2–1. Pathogenetic mechanisms operative in the major syndromes of acute ischemic heart disease. From Buja et al. [6].

eral circulation, and an excessive myocardial oxygen demand. Coronary perfusion is also influenced by coronary tone, blood pressure (particularly diastolic perfusion pressure), and hemic factors, including blood volume, hematocrit, viscosity, oxygen–hemoglobin dissociation properties, coagulation, and platelet function.

Localized alterations in the coronary arterial wall lead to many episodes of acute ischemic heart disease. The triggering mechanisms include coronary spasm, platelet aggregation, and thrombosis (fig. 2–1). [1–7].

Coronary thrombosis plays an important role in the progression of coronary heart disease [2]. Thrombi are composed of granular aggregates of platelets, deposited at the site of thrombus initiation, as well as coagulated blood components deposited proximal and distal to the initiation site. Repeated episodes of formation of small thrombi contribute to the growth of complicated atherosclerotic plaques. In addition, occlusive mural thrombi are involved in the pathogenesis of major episodes of ischemic heart disease, including acute transmural myocardial infarction.

Occlusive coronary thrombi are frequently associated with evidence of plaque erosion, ulceration, rupture, and/or hemorrhage [2–5]. These findings suggest that the primary events leading to coronary thrombosis occur in the vessel wall. These phenomena typically involve soft plaques with prominent atheromatous cores and thin fibrous capsules. Causative factors may involve chronic hemodynamic trauma,

inflammatory or chemical injury to endothelium and subendothelial tissue, or increased intraplaque pressure due to infiltration of blood and vasospasm. Some coronary thrombi develop without identifiable lesions in the arterial wall.

Occlusive coronary thrombi occur in over 90% of cases of transmural infarction, a third to a half of cases of subendocardial infarction, and a lower percentage of patients with unstable angina pectoris (without evidence of major infarction) and in those who die suddenly prior to hospitalization [2–5]. The available evidence indicates that occlusive coronary thrombosis is of major importance in the ultimate extent of an evolving myocardial infarction, and additional factors are involved in the initiation of acute ischemic events which may or may not ultimately involve thrombus formation and further progression of the severity of the insult. In some cases, the important factor may be an excessive increase in myocardial oxygen demand. In other cases, the factors are vessel wall injury, platelet aggregation, and coronary vasospasm.

It is now clear that there is an important distinction between the pathophysiology of the common form of sudden cardiac death and acute myocardial infarction [1–6]. Most cases of sudden cardiac death are produced by a primary ventricular arrhythmia, usually ventricular fibrillation. This arrhythmia may be induced by an episode of acute ischemia or by an ectopic focus generated in an area of chronic myocardial damage with altered electrical activity. Most of the resuscitated survivors of sudden death do not evolve evidence of a major myocardial infarction. A minority of subjects with sudden cardiac death show evidence of a coronary thrombosis and/or an acute myocardial infarct. In these patients, arrhythmia presumably developed secondary to the coronary and myocardial lesions.

Coronary spasm is a localized, exaggerated increase in vascular tone leading to an acute narrowing or occlusion of an artery [2, 5–7]. Spasm of a major coronary artery has been shown to be the cause of Prinzmetal variant angina pectoris. Spasm of large and small coronary arteries also may play a role in other forms of ischemic heart disease. The etiology of coronary spasm is uncertain. One possibility is an alteration of the autonomic nervous system. Although generalized autonomic dysfunction has not been found in patients with coronary spasm, an association of coronary spasm with other vasospastic disorders has been reported. In addition, activation of the alpha-adrenergic system by the cold pressor maneuver in patients with ischemic heart disease can result in coronary vasoconstriction and reduced coronary blood flow. Recent studies indicate a complex interaction between vascular endothelium and platelets, since the former produces prostacyclin, a substance with vasodilator and antiplatelet aggregation properties, whereas the latter produce thromboxane A_2, which promotes vasoconstriction and platelet aggregation. Several recent studies have demonstrated enhanced platelet aggregation and increased thromboxane levels in patients with active ischemic heart disease. Platelet aggregation is associated with the release of thromboxane A_2, a potent coronary vasoconstrictor, that could, in turn, be involved in the initiation of spasm or the perpetuation of spasm initiated by other mechanisms. These findings suggest that an imbalance of the prostacyclin–thromboxane system may be involved in the initiation of platelet aggregation and spasm. Another possibility is that spasm may be induced by primary alterations in medial smooth muscle, and that these changes may involve alterations in calcium and/or magnesium homeostasis.

Further work is needed to elucidate the interrelationship of coronary spasm and platelet aggregation in various clinical syndromes of ischemic heart disease. In patients with classic Prinzmetal angina pectoris, particularly those with minimal coronary artery disease, the primary event likely is coronary spasm, with platelet aggregation possibly contributing as a secondary phenomenon. In other patients with unstable angina pectoris, particularly those with significant atherosclerosis, platelet aggregation on atheromatous plaques could be the primary event which develops without vasospasm as a triggering mechanism.

Survivors of one or more episodes of acute ischemic damage may develop significant chronic ischemic heart disease. Manifestations include recurrent angina pectoris, arrhythmias, conduction abnormalities, cardiomegaly, and congestive heart failure. Pathologically, the

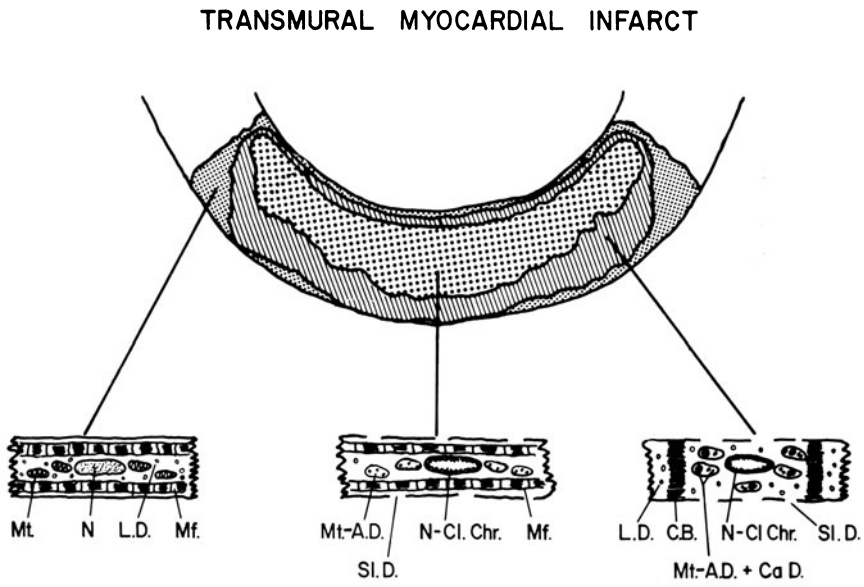

FIGURE 2–2. Patterns of myocytic injury in acute myocardial infarction: C.B., myofibrillar contraction band; L.D., lipid droplet; Mf., myofibril; Mt., mitochondrion; Mt-A.D., mitochondrion with amorphous matrix (flocculent) densities; Mt.-A.D. + CaD., mitochondrion with amorphous matrix densities and calcium phosphate deposits; N., nucleus; N.-Cl. Chr., nucleus with clumped chromatin; Sl.D., sarcolemmal defect.

heart shows coronary atherosclerosis, frequently with one or more occlusions; cardiac enlargement with left ventricular hypertrophy and dilatation; and extensive patchy myocardial fibrosis and/or one or more healed regional myocardial infarcts. Advanced cases with severe clinical and pathologic changes have been termed ischemic cardiomyopathy.

EXPERIMENTAL ISCHEMIC INJURY

Important information regarding mechanisms of myocardial cell injury has been obtained from the study of myocardial ischemia produced by coronary occlusion in experimental animals [1]. Myocardial infarction evolves within a risk region (bed-at-risk) supplied by the occluded vessel [8]. The ultimate basic lesion is coagulative necrosis. However, within the risk region, topographic differences occur in the pattern of myocyte injury (fig. 2–2) [9, 10]. In the central, mostly subendocardial region, the predominant cell type exhibits stretched myofibrils, clumped nuclear chromatin, mitochondria with flocculent (amorphous) matrix densities, and plasma membrane defects. The latter three features are indicative of irreversible injury. An intermediate region contains necrotic muscle cells with evidence of calcium overloading manifested by myofibrillar hypercontraction with contraction bands and, in some cells, by mitochondria with calcium phosphate deposits. These cells also exhibit amorphous matrix densities in the mitochondria, plasma membrane defects, clumped chromatin, and variable numbers of lipid droplets. In the outer region, the muscle cells exhibit marked accumulation of lipid droplets and other changes of cell injury, but they lack the changes of advanced necrosis.

Many studies have addressed the question of progression of irreversible injury within the bed-at-risk [2, 8]. The observations indicate that the rate of progression is a function of a severity–time index. The progression of necrosis is influenced by the size of the bed-at-risk and the severity of the ischemia which, in turn, is influenced by the amount of collateral blood flow into the bed-at-risk shortly after the onset of coronary occlusion [8]. When ischemia is severe (less than 10%–15% of normal blood flow), extensive irreversible injury is present

throughout the subendocardium after 40–60 min of coronary occlusion. The predisposition of the subendocardium is related to the more tenuous oxygen supply–demand relationship of this region under basal conditions and the severe alteration of this relationship with coronary occlusion. After 3–6 h of coronary occlusion, a wavefront of necrosis has progressed into the subepicardium. Little further progression of necrosis occurs thereafter.

The different patterns of myocardial injury observed in an established infarct are related to the rate of progression of damage in different regions of the bed-at-risk. In addition to coagulative necrosis, ischemia also may produce myocytolysis [2, 11]. This pattern of injury is characterized by hydropic change and lysis of myofibrils with potential progression to complete cytolysis.

MECHANISMS OF IRREVERSIBLE INJURY

Following the onset of ischemia or hypoxia, numerous metabolic alterations occur in the oxygen-starved myocytes [1]. Progressive dysfunction of the plasma membrane also occurs [12–14]. Early alterations involve dysfunction of specific membrane pumps, such as the Na^+-K^+ ATPase. Progressive increases in membrane permeability also occur. Experimental evidence suggests that the onset of irreversibility correlates with the development of a severe permeability defect to polyvalent ions and with phospholipid degradation [13, 14].

The functional consequences of altered membrane function involve: (a) altered flux of sodium, potassium, chloride, and water leading to cell swelling, and (b) net influx of calcium leading to toxic effects of this cation. The magnitude of the cell swelling and calcium accumulation is determined by access to extracellular fluid. In severely ischemic areas, however, subtle shifts in electrolytes and water between the intracellular and extracellular spaces could have important consequences on progression of cell injury.

A number of pathophysiologic factors may influence the progression of irreversible ischemic injury. Certain observations have implicated alterations of the adrenergic nervous system. Coronary occlusion is followed by an increase in the population of detectable beta- and alpha-adrenergic receptors in the ischemic myocardium [15, 16]. Ischemia also results in a release of norepinephrine from nerve endings [17]. Thus, exposure of ischemic myocytes with altered receptor populations to increased amounts of catecholamines may contribute to the progression of ischemic injury.

Toxic Myocardial Injury

It is known that a number of toxic insults produce myocardial injury independent of interruption in coronary blood flow [18–21]. The classic example of acute toxic myocardial injury is the damage produced by administration of excessive amounts of isoproterenol or other biogenic amines [22, 23]. Catecholamine-induced cardiotoxicity is characterized by damaged muscle cells with myofibrillar hypercontraction, contraction bands, and mitochondrial calcium deposition. The pattern of injury is similar to that observed in peripheral regions of myocardial infarcts. This pattern of injury appears to be a general response of the myocardium when severe injury develops and some degree of coronary perfusion exists (either as occlusion–reperfusion, collateral perfusion, or toxic injury with normal perfusion). A similar pattern of acute myocardial injury has been observed with many other toxic insults to the heart (fig. 2–3) [18, 19].

The progression of catecholamine-induced myocardial injury involves activation of adrenergic receptors, stimulation of myocardial metabolism, and increased oxygen consumption. A relatively severe mismatch in the oxygen supply–demand ratio may result and trigger phenomena operative in ischemic injury. The irreversible phase of injury is associated with a marked defect in sarcolemmal permeability [22, 23].

Another pattern of toxic injury is characterized by the myocardial response to the anthracycline antibiotics, daunomycin and adriamycin [19, 20, 24, 25]. In addition to acute effects, these agents produce chronic cardiotoxicity which can lead to severe cardiac failure. Biologically, the phenomenon is characterized by a delayed response to the cumulative effects of the drug. Affected subjects exhibit cardiac dilatation and serous effusions. Microscopi-

THE CLINICOPATHOLOGIC SPECTRUM OF DRUG-RELATED CARDIOMYOPATHIES

	Acute Toxic or Allergic Cardiomyopathy	Anthracycline Cardiomyopathy	Cobalt Cardiomyopathy	Alcoholic Cardiomyopathy
Drug or Chemical	Most cardiotoxic drugs	Daunorubicin, Adriamycin	Cobalt	Ethyl alcohol
Toxicology	Onset during therapy; unequivocal dose-response relationship	Delayed response to cumulative dose	Equivocal dose-response relationship; probable multifactorial etiology	Probable multifactorial etiology
Clinical Features	Ischemic changes, arrhythmias, acute CHF, sudden death	Fulminant CHF	Fulminant CHF	Progressive CHF
Pathology	Multifocal myocardial lesions without generalized cardiomegaly	Cardiomegaly with mural thrombosis, interstitial fibrosis and myocardial degeneration	Cardiomegaly with mural thrombosis, interstitial fibrosis and myocardial degeneration	Cardiomegaly with mural thrombosis, interstitial and replacement fibrosis, and myocardial degeneration

FIGURE 2–3. The clinicopathologic spectrum of drug-related cardiomyopathies. From Buja et al. [19].

cally, the characteristic lesion is a multifocal vacuolar change of the myocytes associated ultrastructurally with variable amounts of dilatation of the sarcoplasmic reticulum and T tubules, lysis of myofibrils, and degeneration of mitochondria. Morphologically, these lesions represent a distinctive type of myocytolysis, which represents another general pattern of response to myocardial injury [11].

The pathogenesis of adriamycin cardiotoxicity has not been fully defined. Potential mechanisms involve membrane damage, possibly mediated by the generation of free radicals [25, 26], impaired protein synthesis mediated through effects on nucleic acids [27], and alterations in catecholamines and histamine [28].

Toxic injury to the heart has been implicated in the etiology and pathogenesis of cardiomyopathy, but progression from an acute to a chronic stage of disease has not been proven for many agents. Anthracycline cardiotoxicity is conceptually important because this entity demonstrates that cardiomyopathy can result as a delayed response to the cumulative effects of an exogenous chemical (fig. 2–3).

Infection and Inflammation

A number of viruses, bacteria, and other microbes can produce acute myocarditis [29–32]. The end result may be death or complete resolution, but some cases can have a recurrent course resulting in a picture resembling cases of idiopathic cardiomyopathy [29–32]. Studies of the pathogenesis of viral myocarditis suggest that, although the process is initiated by viral infection, the disease may be perpetuated by the host response. One such mechanism is the proliferation of a specific population of cytotoxic lymphocytes which may attack the myocytes altered by the initial viral infection [31].

Heart disease can result from autoimmune injury, as shown by the entities of acute rheumatic fever and chronic rheumatic heart disease. It is possible that less well defined autoimmune phenomena can contribute to the development or progression of certain cardiomyopathies [33–37].

Hypertrophy and Failure

Hypertrophy is a basic response of the heart in which one or both of the ventricles or atria increase in mass in response to an increased load [38–40]. This process is accomplished primarily by an increase in the mass of the cardiac myocytes without an increase in their number.

Normal growth and development of the mammalian heart is influenced by important changes occurring at the time of parturition. During early fetal development, growth of the heart involves multiplication and differentiation of myocytes. At or around the time of birth, myocytes lose the ability to undergo mitotic division. At this time a significant percentage of myocytes become binucleate probably as a result of a final nuclear division without cytokinesis [41]. Subsequent normal growth of the heart is mediated by synthesis of myofibrils and other organelles in the existing myocytes.

Hypertrophy implies a further increase in cardiac mass above the normal value in response to an increased hemodynamic load: an afterload (pressure load), preload (volume load), or both. Hypertrophy occurs in response to physiologic stimuli, such as exercise, and in a variety of pathologic states. There is debate as to whether or not the processes of physiologic hypertrophy and pathologic hypertrophy, at least in early stages, represent the same or different patterns of response [42, 43]. There is also uncertainty as to the basic stimulus for hypertrophy at the cellular level [38–48]. One view is that the physical forces of the increased stress directly stimulate a burst of protein synthesis leading to increased cell mass. At the level of the whole ventricle, normalization of an increased wall stress by an appropriate hypertrophic response, according to the law of La Place, is an important predictor of the cardiac response to a variety of stimuli [42, 48]. Alternative hypotheses emphasize the importance of other factors, such as transient ischemia, changes in high-energy phosphates, or other alterations in cellular metabolism. These factors are postulated to function as couplers of the hemodynamic stimuli to increased protein synthesis and myocyte enlargement. A schema for the potential interactions of these factors leading to myocardial hypertrophy in one disease state, namely, coronary heart disease, is shown in figure 2–4 [49]. Additional insight into the molecular basis of hypertrophy awaits further basic studies of the regulation of nucleic acid and protein metabolism in the heart.

Cardiac failure is another important pathophysiologic process affecting the heart [50, 51]. This alteration is a pathophysiologic state in which the heart loses its ability to provide an output sufficient for the metabolic demands of the peripheral tissues. Cardiac failure usually is the result of myocardial failure of the left, right, or both ventricles. However, cardiac failure also can result from pericardial disease, mitral stenosis, massive acute valvular insufficiency, or other causes. Cardiac failure may occur in a previously normal heart or one with hypertrophy. The usual response is chamber dilatation, but the presence of chamber dilatation does not have a one-to-one relationship with overt failure because a ventricle with a chronic volume load may exhibit dilatation when the subject does not show evidence of cardiac failure.

Experimental studies have identified a number of biochemical alterations in the failing heart [52–55]. The critical lesion could involve defective energy production, defective energy utilization, or defective excitation–contraction coupling. Available evidence has implicated defective excitation–contraction coupling, due to defective calcium homeostasis, as the earliest alteration in certain models of myocardial failure. Specifically, these studies have identified defective uptake and release of Ca^{2+} from the sarcoplasmic retriculum with the potential result that less Ca^{2+} is available for activation of cardiac contraction [52–55].

The above considerations imply a diffuse

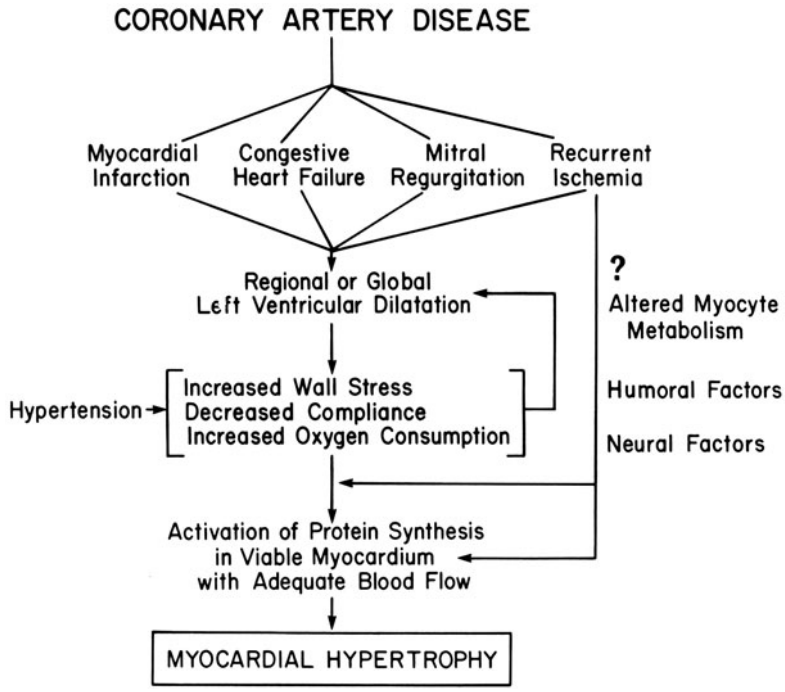

FIGURE 2–4. Pathophysiologic mechanisms leading to cardiac hypertrophy in chronic ischemic heart disease. From Buja et al. [49].

subcellular defect as the basis for myocardial failure. An alternative hypothesis for the pathogenesis of myocardial failure has been proposed by Sonnenblick and associates [56]. According to their hypothesis, myocardial failure is initiated by factors which produce multifocal necrosis of myocardial fibers. Myocardial failure results when a critical mass of myocytes is lost such that the remaining myocytes, although functionally normal, are no longer able to maintain adequate ventricular function. Sonnenblick et al. have suggested that vasospasm may be the initiating cause of multifocal myocyte necrosis in several models of cardiomyopathy and cardiac failure.

Alterations of the autonomic nervous system also contribute to the pathophysiology of congestive heart failure [55, 57]. Progressive loss of catecholamines from failing myocardium and elevated circulating levels of catecholamines in subjects with cardiac failure have been documented. Recently, myocardium from subjects with end-stage cardiac failure has been shown to have a decreased population of beta-adrenergic receptors [58]. A depressed response of the heart to adrenergic stimulation appears to be important in the progression of cardiac dysfunction.

Patterns of Cardiomegaly

Patterns of cardiomegaly provide important information regarding the nature of the underlying pathologic process (fig. 2–5) [39, 40, 59]. Cardiac dilatation without hypertrophy is indicative of acute cardiac failure involving a previously normal heart. The process is characterized by a normal heart weight, chamber enlargement, and reduced thickness of the wall. Ventricular dilation involves the Frank–Starling mechanism with progressive recruitment of myocytes with an optimal diastolic sarcomere length of 2.2 microns (L_{max}) [50, 60]. Slippage and loss of registration of myocytes also may contribute [50]. A major factor, however, is a geometric rearrangement of myocytes within the ventricular wall rather than in pro-

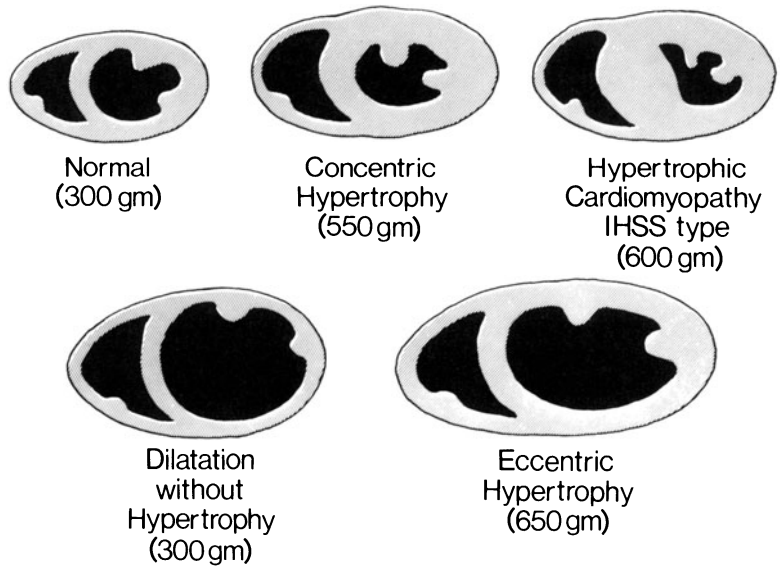

FIGURE 2–5. Patterns of cardiomegaly shown in transverse sections through the cardiac ventricles. Values in parentheses represent corresponding heart weights. From Buja and Petty [59].

gressive stretching of the myocytes. As a result of the rearrangement of myocytes, the wall of the dilated ventricle becomes thinner and exhibits fewer myocytes in a given transmural cross section [39, 40]. Disease processes producing acute cardiac dilatation without hypertrophy include the acute phase of myocarditis, infective endocarditis, valvular insufficiency, and ischemia-induced cardiac decompensation.

Concentric hypertrophy is characterized by a relative or absolute increase in ventricular weight, a small chamber size, and a symmetric, excessively thickened chamber wall [39, 40, 59]. This type of cardiomegaly is produced by a pressure load (afterload) on the involved ventricle. Common etiologies of concentric hypertrophy are valvular stenosis and systemic hypertension.

Eccentric hypertrophy is characterized by increased ventricular weight and chamber dilatation [39, 40, 59]. The dilated ventricle has an eccentric configuration. Even though the weight is increased, the thickness of the involved chamber wall can vary from less than to greater than normal depending upon the degrees of hypertrophy and dilatation. Eccentric hypertrophy is the typical response of the heart to a chronic volume load (preload).

This pattern of cardiomegaly can result from: (a) acute chamber dilatation followed by compensatory hypertrophy, (b) progressive dilatation and hypertrophy developing in parallel, and (c) concentric hypertrophy followed by dilatation. Eccentric hypertrophy may be due to chronic valvular insufficiency of any cause, cardiac failure superimposed on chronic coronary heart disease or hypertensive heart disease, or congestive (dilated) cardiomyopathy. The latter is distinguished by diffuse cardiac involvement producing symmetric, four-chamber hypertrophy and dilatation.

The natural history of cardiac hypertrophy involves an early stage characterized by stable cardiac function and the potential for regression of hypertrophy and a late stage characterized by progressive myocardial failure and progressive decrease in the potential for regression [38–40]. Linzbach has proposed that a critical cardiac mass in the range of 550 g occurs at a point of transition from the early to the late stage of hypertrophy [39]. After the critical

cardiac mass is surpassed, important structural changes develop in the hypertrophied ventricle which predispose to myocardial failure and hinder regression. The greatly hypertrophied heart may develop an increase in myocyte number as a result of amitotic, longitudinal fission of enlarged myocytes [39]. Progressive degeneration of myocytes and fibrosis develop, and these changes tend to be more extensive in the subendocardium [61, 62]. Degeneration and fibrosis occur in part because the oxygen demands of the greatly hypertrophied ventricle exceed the capability of the vasculature to supply blood [39, 49, 62]. Increasing wall stress may be another factor. The end result is a fixed structural dilatation of the involved chamber of the heart. Specific disease processes and mechanisms of hypertrophy undoubtedly influence the progression of hypertrophy and the potential for regression [63].

Cardiomyopathies

The cardiomyopathies encompass a wide spectrum of disease processes [64–66]. They may be classified according to etiology and pathophysiology (clinicopathologic features) (table 2–1). Unfortunately the cause of many cases of cardiomyopathy in man is unknown or uncertain. The typical idiopathic cardiomyopathy is characterized by heart muscle disease occurring in the absence of hypertension, coronary artery disease, valvular lesions, congenital cardiac defects, or other recognized forms of heart disease. These cardiomyopathies may have a congenital, familial, or genetic basis, or they may be acquired secondary to injury from some exogenous agent. Primary (idiopathic) cardiomyopathies arise from poorly understood causes which exert major or exclusive effects on the myocardium. Secondary cardiomyopathies have a known cause or arise as part of a well-defined systemic or multiorgan disease [64].

TABLE 2–1. General classification of cardiomyopathy

A. Etiology
   1. Isolated heart muscle disease (primary or idiopathic CMP)
      a) congenital, familial, or genetic
      b) acquired
   2. Heart muscle disease secondary to
      a) recognized etiology
      b) systemic disease
      c) other cardiovascular disease

B. Pathophysiology
   1. Congestive (dilated) CMP
   2. Hypertrophic CMP
      a) with obstruction (IHSS)
      b) without obstruction
   3. Restrictive (constrictive) CMP

Secondary cardiomyopathy may occur with neuromuscular diseases such as Friedreich's ataxia and various muscular dystrophies; with connective tissue diseases, including systemic lupus erythematosus; with neoplastic diseases when cardiac metastases occur; with metabolic diseases, including diabetes mellitus, thyrotoxicosis, myxedema, and glycogen storage disease; with nutritional diseases, notably beriberi and kwashiorkor; with hematologic diseases, including various hypereosinophilia syndromes; with viral, parasitic, protozoal, and bacterial infections; with granulomatous diseases, notably sarcoidosis; with infiltrative diseases, notably amyloidosis; and with drugs and other toxins [64].

Heart muscle disease also may result from an initial cardiac or cardiovascular lesion of the types described above. The heart muscle disease may come to dominate the clinical course even if the underlying cardiac lesion is ameliorated. Examples of this phenomenon are the progression of ischemic cardiomyopathy following coronary bypass surgery [2, 49] and the persistence of cardiac disease following valve replacement [63]. The basis for this phenomenon relates to the general factors governing the natural history of cardiac hypertrophy discussed in the previous section.

Cardiomyopathies also are classified according to their pathophysiologic manifestations with associated clinical and pathologic features. The pathophysiologic classification proposed by Goodwin is a practical and clinically useful approach [65]. It must be stressed, however, that this classification is not an etiologic one per se. Nevertheless, the pathophysiologic manifestations of the cardiomyopathy frequently provide useful information in assigning the case to a broad etiologic group.

CONGESTIVE CARDIOMYOPATHY

Most primary cardiomyopathies are of the congestive type. Congestive cardiomyopathy is a subacute or chronic disorder characterized clinically by congestive cardiac failure, which is usually recurrent or progressive and leads to progressive cardiac enlargement. Arrhythmias are another important clinical manifestation. They may occur as the presenting feature, and they may dominate the clinical picture at later stages of the disease. The prognosis is poor once chronic congestive heart failure develops. Clinical episodes resulting from systemic emboli frequently occur. At necropsy, the heart is flabby, enlarged with a globular shape, and exhibits hypertrophy and dilatation (eccentric hypertrophy) of all four chambers [66]. Mural thrombi are frequently present, especially in the left ventricle, and explain the frequency of systemic embolization. Less advanced cases may exhibit mild hypertrophy with mild dilatation. Histologic changes are nonspecific and consist of variation in size, shape, and staining of muscle cells and their nuclei and variable degrees of muscle cell degeneration and fibrosis. Congestive cardiomyopathy typically presents as an acquired condition. Reports of familial occurrence of congestive cardiomyopathy are rare.

Circumstantial evidence has implicated viral myocarditis and chronic alcoholism as the most likely etiologic factors in many cases of primary congestive cardiomyopathy [21, 29–31]. Many viruses, including those in the influenza, poliomyelitis, and Coxsackie-B groups, have a known propensity for infecting the myocardium and producing acute cardiac failure (acute myocarditis). It has been documented that acute myocarditis may progress into a subacute or chronic disorder with features indistinguishable from those of idiopathic congestive cardiomyopathy. In most cases of congestive cardiomyopathy, however, proof of a preceding or active viral infection cannot be obtained. The incidence of congestive cardiomyopathy is higher in chronic alcoholics than in the general population. Only a small percentage of chronic alcoholics, however, develop congestive cardiomyopathy, and the heart disease tends to occur in those alcoholics without severe liver disease.

The terms *postpartum cardiomyopathy* and *peripartum cardiomyopathy* are applied to congestive cardiomyopathy which occurs within 3–5 months after childbirth or in the last trimester to 3–5 months after childbirth, respectively [64]. A predisposition exists for women over 30 who have had three or more pregnancies. Specific factors related to pregnancy, including autoimmune phenomena, have been implicated in the pathogenesis of peripartum cardiomyopathy, but there is no definitive evidence regarding pathogenetic factors.

Another form of congestive cardiomyopathy occurs in cancer patients treated with adriamycin. An increased incidence of congestive cardiomyopathy occurs in patients who have received a total cumulative dose of 550 mg/m^2 of the drug [25]. Further study is needed regarding the roles of chemical agents, including drugs (Fig. 2–3), and immunologic phenomena [32–37] in the genesis of congestive cardiomyopathy.

HYPERTROPHIC CARDIOMYOPATHY

Hypertrophic cardiomyopathy includes hypertrophic obstructive cardiomyopathy (HOCM) and idiopathic hypertrophic subaortic stenosis (IHSS). Most patients with clinicopathologic features of hypertrophic cardiomyopathy have a genetically induced disease which is inherited as an autosomal dominant with incomplete penetrance [67, 68]. Manifestations of typical hypertrophic cardiomyopathy include cardiac murmur, reduced arterial pulse, angina, dyspnea, and sudden death [65, 69]. Laboratory evaluation may reveal evidence of asymmetric septal hypertrophy (ASH) and/or systolic anterior motion (SAM) of the mitral valve [64]. Characteristic pathologic features include cardiac hypertrophy without dilatation; left ventricular hypertrophy with excessive thickening of the ventricular septum (asymmetric septal hypertrophy); a widespread disorganized arrangement of muscle cells (muscle cell disarray), primarily in the ventricular septum; endocardial fibrous plaque in the left ventricle outflow tract; focal thickening of the anterior leaflet of the mitral valve; and normal aortic valve [66, 70].

Patients with hypertrophic cardiomyopathy

frequently develop left ventricular outflow tract obstruction which simulates valvular aortic stenosis (hence the designation IHSS). Outflow tract obstruction probably results from an abnormal pattern of ventricular contraction which produces abnormal systolic anterior movement of the anterior mitral leaflet toward the bulging ventricular septum. The abnormal movement of the mitral valve can also produce variable degrees of mitral insufficiency. Anatomic markers of the functional left ventricular outflow obstruction are the areas of fibrosis involving the anterior mitral leaflet and endocardium of the left ventricular outflow tract. The abnormally hypertrophied left ventricle also causes resistance to ventricular filling (inflow resistance), even when features of outflow tract obstruction are not prominent [65, 68]. Patients may develop progressive congestive cardiac failure and ventricular dilatation late in the course of the disease. Characteristic pathologic features, including asymmetric septal hypertrophy and extensive muscle cell disarray, are still recognizable, even in the heart with end-stage hypertrophic cardiomyopathy and ventricular dilatation.

The genetic basis of typical hypertrophic cardiomyopathy is suggested by the high incidence of a positive family history with this disease. In addition, the noninvasive clinical technique of echocardiography has documented the familial occurrence of asymmetric septal hypertrophy in asymptomatic relatives of patients with clinical disease in over 90% of families studied [67]. Some features of inherited hypertrophic cardiomyopathy, including asymmetric septal hypertrophy, can rarely develop in patients with other forms of heart disease, including cardiac hypertrophy induced by severe hypertension [68]. An important distinguishing feature of inherited hypertrophic cardiomyopathy versus secondary hypertrophic cardiomyopathy appears to be the presence of extensive muscle cell disarray indicating an unusual pattern of myocardial hypertrophy [70]. An inherited pattern of abnormal response of the myocardium to catecholamines beginning during cardiac development has been suggested as the basis for the development of asymmetric left ventricular hypertrophy and extensive muscle cell disarray in patients with hypertrophic cardiomyopathy [68].

RESTRICTIVE (CONSTRICTIVE) CARDIOMYOPATHY

Restrictive (constrictive) cardiomyopathy is a rare form of cardiomyopathy which is characterized by impaired diastolic ventricular filling due to reduced compliance of the myocardium [64, 65]. Restrictive cardiomyopathy frequently mimics constrictive pericarditis clinically. Patients typically show signs of elevated central venous pressure without cardiomegaly. Restrictive cardiomyopathy most commonly results from involvement of the heart by amyloidosis [71], and also can occur in cases of hemochromatosis (although most cases of hemochromatosis have a congestive pattern) [72] and on an idiopathic basis.

Some cases of cardiomyopathy are characterized by massive filling of the ventricular cavities by mural thrombi, necrosis and/or fibrosis of the subendocardial myocardium, and variable degrees of mitral or tricuspid valvular insufficiency. These cases are sometimes designated as obliterative cardiomyopathy [65]. They occur with endomyocardial fibrosis of Africa and with Loffler fibroplastic endocarditis which is associated with chronic hypereosinophilia syndromes.

MYOCARDIAL BIOPSY

Myocardial biopsy can be safely used to obtain tissue from cardiomyopathy patients during life [73, 74]. Biopsy has been useful in the separation of constrictive pericarditis from restrictive cardiomyopathy due to amyloidosis and other causes. Muscle fiber disarray indicative of hypertrophic cardiomyopathy can be identified, but the diagnostic sensitivity is relatively low because of the small sample size and focal nature of the lesion [70]. Myocardial biopsy also is useful in identification and staging of transplant rejection and adriamycin cardiotoxicity [73, 74]. In most cases, however, biopsy reveals nonspecific changes of hypertrophy and myocyte degeneration, and a specific etiologic diagnosis cannot be made. A recent area of in-

terest is the identification of a subgroup of patients with active inflammation in myocardial tissue obtained at biopsy [74, 75]. Current studies are underway to evaluate the therapeutic efficacy of treatment of these patients with steroids or other antiinflammatory agents [74–76].

ANIMAL MODELS

Most animal models of cardiac hypertrophy and failure have involved the imposition of a hemodynamic overload [77]. As previously mentioned, much information regarding acute toxic and viral injury has come from animal models, but documentation that these acute insults lead to chronic cardiomyopathy is often unavailable. Two extensively studied models of chronic disease are the cardiomyopathic Syrian hamster and adriamycin cardiotoxicity.

Summary

This chapter has summarized important pathologic responses of the heart to injury. These responses are involved in complex and often poorly understood ways in the development of cardiomyopathy. Much further work is needed to establish the causes and mechanisms of progression of the various types of cardiomyopathies.

References

1. Hillis LD, Braunwald E: Myocardial ischemia. N Engl J Med 296:971–978, 1034–1041, 1093–1096, 1977.
2. Willerson JT, Hillis LD, Buja LM: Pathogenesis and pathology of ischemic heart disease. In: Ischemic heart disease: clinical and pathophysiological aspects. New York: Raven, 1982.
3. Willerson JT, Buja LM: Cause and course of acute myocardial infarction. Am J Med 69:903–914, 1980.
4. Buja LM, Willerson JT: Clinicopathologic findings in acute ischemic heart disease syndromes. Am J Cardiol 47:343–356, 1981.
5. Oliva PB: Pathophysiology of acute myocardial infarction, 1981. Ann Intern Med 94:236–250, 1981.
6. Buja LM, Hillis LD, Petty CS, Willerson JT: The role of coronary arterial spasm in ischemic heart disease. Arch Pathol Lab Med 105:221–226, 1981.
7. Hirsh PD, Campbell WB, Willerson JT, Hillis LD: Prostaglandins and ischemic heart disease. Am J Med 71:1009–1026, 1981.
8. Reimer KA, Jennings RB: The "wavefront phenomenon" of myocardial ischemic cell death. II. Transmural progression of necrosis within the framework of ischemic bed size (myocardium at risk) and collateral flow. Lab Invest 40:633–644, 1979.
9. Willerson JT, Parkey RW, Bonte FJ, Lewis SE, Corbett J, Buja LM: Pathophysiologic considerations and clinicopathological correlates of technetium-99m stannous pyrophosphate myocardial scintigraphy. Semin Nucl Med 10:54–69, 1980.
10. Hagler H, Burton K, Buja L: Electron probe x-ray microanalysis of normal and injured myocardium: methods and results. In: Hutchinson TE, Somlyo AP (eds), Microprobe analysis of biological systems. New York: Academic, 1981, pp 245–281.
11. Schlesinger MJ, Reiner L: Focal myocytolysis of the heart. Am J Pathol 31:443–459, 1955.
12. Buja LM, Willerson JT: Abnormalities of volume regulation and membrane integrity in myocardial tissue slices after early ischemic injury in the dog: effects of mannitol, polyethylene glycol and propranolol. Am J Pathol 103:79–95, 1981.
13. Burton, KP, Hagler HK, Willerson JT, Buja LM: Relationship of abnormal intracellular lanthanum accumulation to progression of ischemic injury in isolated perfused myocardium: effect of chlorpromazine. Am J Physiol 241:H714–H723, 1981.
14. Chien KR, Reeves JP, Buja LM, Bonte F, Parkey RW, Willerson JT: Phospholipid alterations in canine ischemic myocardium: temporal and topographical correlations with Tc-99m-PPi accumulation and an in vitro sarcolemmal Ca^{2+} permeability defect. Circ Res 48:711–719, 1981.
15. Mukherjee A, Bush LR, McCoy KE, Duke RJ, Hagler H, Buja LM, Willerson JT: Relationship between β-adrenergic receptor numbers and physiological responses during experimental canine myocardial ischemia. Circ Res 50:735–741, 1982.
16. Corr PB, Shayman JA, Kramer JB, Kipnis RJ: Increased alpha adrenergic receptors in ischemic cat myocardium: a potential mediator of electrophysiological derangements. J Clin Invest 67:1232–1236, 1981.
17. Muntz KH, Hagler HK, Boulos HJ, Willerson JT, Buja LM: Redistribution of catecholamines in the ischemic zone of the dog heart. Am J Path 114:64–78, 1984.
18. Reichenbach DD, Benditt EP: Catecholamines and cardiomyopathy: the pathogenesis and potential importance of myofibrillar degeneration. Hum Pathol 1:125–150, 1970.
19. Buja LM, Ferrans VJ, Roberts WC: Drug-induced cardiomyopathies. In: Homburger F (ed) Comparative pathology of the heart. Advances in cardiology, vol 13. Basel: Karger, 1974, pp 330–348.
20. Buja LM, Ferrans VJ: Myocardial injury produced by antineoplastic drugs. In: Fleckenstein A, Rona G (eds) Pathophysiology and morphology of myocardial

cell alteration. Recent advances in studies on cardiac structure and metabolism, vol 6. Baltimore: University Park, 1975, pp 487–497.
21. Rubin E: Alcohol: toxic or tonic? Cardiovasc Rev Rep 2:23–29, 1981.
22. Csapó Z, Dušek J, Rona G: Early alterations of the cardiac muscle cells in isoproterenol-induced necrosis. Arch Pathol 93:356–365, 1972.
23. Rona G, Boutet M, Hüttner I, Peters H: Pathogenesis of isoproterenol-induced myocardial alterations: functional and morphological correlates. In: Dhalla NS (ed) Myocardial metabolism. Recent advances in studies on cardiac structure and metabolism, vol 3. Baltimore: University Park, 1973, pp 507–525.
24. Ferrans VJ: Overview of cardiac pathology in relation to anthracycline cardiotoxicity. Cancer Treat Rep 62:995–961, 1978.
25. Young RC, Ozols RF, Myers CE: The anthracycline antineoplastic drugs. N Engl J Med 305:139–153, 1981.
26. Olson RD, Boerth RC, Gerber JG, Nies AS: Mechanisms of adriamycin cardiotoxicity: evidence for oxidative stress. Life Sci 29:1393–1401, 1981.
27. Dalbow DG, Jaenke RS: In vivo RNA synthesis in the hearts of adriamycin-treated rats. Cancer Res 42:79–83, 1982.
28. Bristow MR, Minobe WA, Billingham ME, Marmor JB, Johnson GA, Ishimoto BM, Sageman WS, Daniels JR: Anthracycline-associated cardiac and renal damage in rabbits: evidence for mediation by vasoactive substances. Lab Invest 45:157–168, 1981.
29. Lerner AM, Wilson FM: Virus myocardiopathy. Prog Med Virol 15:63–91, 1973.
30. Abelman WH: Viral myocarditis and its sequelae. Annu Rev Med 22:145–152, 1973.
31. Woodruff JF: Viral myocarditis: a review. Am J Pathol 101:425–484, 1980.
32. Cambridge G, MacArthur CGC, Waterson AP, Goodwin JF, Oakley CM: Antibodies to Coxsackie B viruses in congestive cardiomyopathy. Br Heart J 41:692–696, 1979.
33. Kirsner AB, Hess EV, Fowler NO: Immunologic findings in idiopathic cardiomyopathy: a prospective serial study. Am Heart J 86:625–630, 1973.
34. Bolte HD, Schultheiss P: Immunological results in myocardial diseases. Postgrad Med J 54:500–503, 1978.
35. Jacobs B, Matsuda Y, Deodhar S, Shirey E: Cell-mediated cytotoxicity to cardiac cells of lymphocytes from patients with primary myocardial disease. Am J Clin Pathol 72:1–4, 1979.
36. Fowles RE, Dieber CP, Stinson EB: Defective in vitro suppressor cell function in idiopathic congestive cardiomyopathy. Circulation 59:483–491, 1979.
37. Hang LM, Izui S, Dixon FJ: (NZW × BXSB) F_1 hybrid: a model of acute lupus and coronary vascular disease with myocardial infarction. J Exp Med 154:216–221, 1981.
38. Meerson FZ: The myocardium in hyperfunction, hypertrophy and heart failure. Circ Res (Suppl 2) 24 and 25:II-1–163, 1969.
39. Linzbach AJ: Heart failure from the point of view of quantitative anatomy. Am J Cardiol 5:370–382, 1960.
40. Hort W: Quantitative morphology and structural dynamics of the myocardium. In: Bajusz E, Jasmin G (eds) Methods and achievements in experimental pathology, vol 5. Basel: Karger, 1971, pp 3–21.
41. Bishop SP, Hine P: Cardiac muscle cytoplasmic and nuclear development during canine neonatal growth. In: Roy P-E, Harris P (eds) The cardiac sarcoplasm. Recent advances in studies on cardiac structure and metabolism, vol 8. Baltimore: University Park, 1975, pp 77–98.
42. Grossman W: Cardiac hypertrophy: useful adaptation or pathologic process? Am J Med 69:576–584, 1980.
43. Wikman-Coffelt J, Parmley WW, Mason DR: The cardiac hypertrophy process: analysis of factors determining pathological vs. physiological development. Circ Res 45:697–707, 1979.
44. Rabinowitz M, Zak R: Biochemical and cellular changes in cardiac hypertrophy. Annu Rev Med 23:245–262, 1972.
45. Morkin E: Activation of synthetic processes in cardiac hypertrophy. Circ Res (Suppl 2) 34 and 35: II-37–48, 1974.
46. Cohen J: Role of endocrine factors in the pathogenesis of cardiac hypertrophy. Circ Res (Suppl 2) 34 and 35: II-49–57, 1974.
47. Schreiber SS, Evans CD, Oratz M, Rothschild MA: Protein synthesis and degradation in cardiac stress. Circ Res 48:601–611, 1981.
48. Grossman W, Jones D, McLaurin LP: Wall stress and patterns of hypertrophy in the human left ventricle. J Clin Invest 56:56–64, 1975.
49. Buja LM, Muntz KH, Lipscomb K, Willerson JT: Cardiac hypertrophy in chronic ischemic heart disease. In: Tarazi R (ed) Mechanisms of left ventricular hypertrophy. New York: Raven, 1983 (in press).
50. Braunwald E, Ross J Jr, Sonnenblick EH: Mechanisms of contraction of the normal and failing heart, 2nd edn. Boston: Little, Brown and Company, 1976.
51. Braunwald E: Historical overview and pathophysiologic considerations. In: Braunwald E, Mock MB, Watson J (eds) Congestive heart failure: current research and clinical applications. New York: Grune and Stratton, 1982, pp 3–9.
52. Schwartz A, Sordahl LA, Entman ML, Allen JC, Reddy YS, Goldstein MA, Luchi RJ, Wyborny LE: Abnormal biochemistry in myocardial failure. Am J Cardiol 32:407–422, 1973.
53. Dhalla NS, Das PK, Sharma GP: Subcellular basis of cardiac contractile failure. J Mol Cell Cardiol 10:363–385, 1978.
54. Chidsey CA: Calcium metabolism in the normal and failing heart. In: The myocardium: failure and

infarction. New York: HP Publishing, 1975, pp 37–47.
55. Willerson JT: What is wrong with the failing heart? N Engl J Med 307:243–245, 1982.
56. Sonneblick EH, Factor S, Strobeck JE, Capasso JM, Fein F: The pathophysiology of heart failure: the primary role of microvascular hyperactivity and spasm in the development of congestive cardiomyopathies. In: Braunwald E, Mock MB, Watson J (eds) Congestive heart failure: current research and clinical applications. New York: Grune and Stratton, 1982, pp 87–97.
57. Sole MJ: Alterations in sympathetic and parasympathetic neurotransmitter activity. In: Braunwald E, Mock MB, Watson J (eds) Congestive heart failure: current research and clinical applications. New York: Grune and Stratton, 1982, pp 101–113.
58. Bristow MR, Ginsbury R, Minobe W, Cubicciotti RS, Sageman WS, Lurie K, Billingham M, Harrison DC, Stinson EB: Decreased catecholamine sensitivity and β-adrenergic-receptor density in failing human hearts. N Engl J Med 307:205–211, 1982.
59. Buja LM, Petty CS: Heart disease, trauma, and death. In: Curran WJ, McGarry AL, Petty CS (eds) Modern legal medicine, psychiatry, and forensic science. Philadelphia: FA Davis, 1980, pp 187–206.
60. Yoran C, Covell JW, Ross J Jr: Structural basis for the ascending limb of left ventricular function. Circ Res 32:297–303, 1973.
61. Maron BJ, Ferrans VJ: Ultrastructural features of hypertrophied human ventricular myocardium. Prog Cardiovasc Dis 11:207–238, 1978.
62. Dick MR, Unverferth DV, Baba N: The pattern of myocardial degeneration in nonischemic congestive cardiomyopathy. Hum Pathol 13:740–744, 1982.
63. Tarazi RC, Sen S, Fouad FM: Regression of myocardial hypertrophy. In: Braunwald E, Mock MB, Watson J (eds) Congestive heart failure: current research and clinical applications. New York: Grune and Stratton, 1982, pp 151–163.
64. Wynne J, Braunwald E: The cardiomyopathies and myocardities. In: Braunwald E (ed) Heart disease: a textbook of cardiovascular medicine. Philadelphia: Saunders, 1980, pp 1437–1498.
65. Goodwin JF: Congestive and hypertrophic cardiomyopathies: a decade of study. Lancet 1:731–739, 1970.
66. Roberts WC, Ferrans VJ: Pathologic anatomy of the cardiomyopathies: idiopathic dilated and hypertrophic types, infiltrative types, and endomyocardial disease with and without eosinophilia. Hum Pathol 6:287–342, 1975.
67. Clark CE, Henry WL, Epstein SE: Familial prevalence and genetic transmission of idiopathic hypertrophic subaortic stenosis. N Engl J Med 289:709–714, 1973.
68. Goodwin JF: ?IHSS. ?HOCM. ?ASH. a plea for unity. Am Heart J 89:269–277, 1975.
69. Maron BJ, Roberts WC, McAllister HA, Rosing DR, Epstein SE: Sudden death in young athletes. Circulation 62:218–229, 1980.
70. Maron BJ, Roberts WC: Quantitative analysis of cardiac muscle cell disorganization in the ventricular septum of patients with hypertrophic cardiomyopathy. Circulation 59:689–706, 1979.
71. Buja LM, Khoi NB, Roberts WC: Clinically significant cardiac amyloidosis: clinicopathologic findings in 15 patients. Am J Cardiol 26:394–405, 1970.
72. Cutler DJ, Isner JM, Bracey AW, Hufnagel CA, Conrad PW, Roberts WC, Kerwin DM, Weintraub AM: Hemochromatosis heart disease: an unemphasized cause of potentially reversible restrictive cardiomyopathy. Am J Med 69:923–928, 1980.
73. Billingham ME, Bristow MR, Mason JW, Joseph LJ: Endomyocardial biopsy. In: Braunwald E, Mock MB, Watson J (eds) Congestive heart failure: current research and clinical applications. New York: Grune and Stratton, 1982, pp 237–251.
74. Nippoldt TB, Edwards WD, Holmes DR Jr, Reeder GS, Hartzler GO, Smith HC: Right ventricular endomyocardial biopsy: clinicopathologic correlates in 100 consecutive patients. Mayo Clin Proc 57:407–418, 1982.
75. Mason JW, Bilingham ME, Ricci DR: Treatment of acute inflammatory myocarditis by endomyocardial biopsy. Am J Cardiol 45:1037–1044, 1980.
76. O'Connell JB, Robinson JA, Henkin RE, Gunnar RM: Immunosuppressive therapy in patients with congestive cardiomyopathy and myocardial uptake of gallium-67. Circulation 64:780–786, 1981.
77. Bishop SP: Animal models. In: Braunwald E, Mock MB, Watson J (eds) Congestive heart failure: current research and clinical applications. New York: Grune and Stratton, 1982, pp 125–149.

3. ELECTRICAL PROPERTIES OF CELLS AT REST AND MAINTENANCE OF THE ION DISTRIBUTIONS

Nicholas Sperelakis

Introduction

Cardiac muscle is a unique excitable tissue. The peculiar electrical properties of heart muscle determine the special mechanical properties of the heart, enabling it to serve as an effective pump for circulating the blood. The entire ventricle is rapidly activated, within several hundredths of a second, by virtue of the rapidly conducting (2–3 m/s) specialized Purkinje fiber system and by rapid propagation (0.3–0.4 m/s) through the myocardium. The ventricular myocardium normally contracts in an all-or-none manner because of the rapid spread of excitation throughout the muscle. Cardiac muscle cannot normally be tetanized because of the long functional refractory period resulting from the long-duration action potential. The long-duration plateau component of the action potential allows the mechanical active state to be maximally developed and maintained for a sufficiently long period.

The pumping action of the heart can be increased when required or decreased when conditions permit by various mechanisms, including release of the neurotransmitters, norepinephrine and acetylcholine, at the autonomic nerve terminals and by action of circulating hormones or autacoids (e.g., angiotensin-II, histamine). Cardiac output can be increased by increasing heart rate (by increasing automaticity of the normal pacemaker for the heart, the SA node), and by increasing the force of contraction of the ventricles. In addition to the Starling mechanism, one key mechanism for increasing force of contraction is by increasing the number of Ca^{2+} slow channels in the cell membrane available for voltage activation, and hence increasing the Ca^{2+} ion influx per each cardiac cycle. A greater Ca^{2+} influx causes a greater activation of the contractile machinery.

It is obvious then that the cell membrane exerts tight control over the contractile machinery during the process of excitation–contraction coupling (or electromechanical coupling). In addition, numerous drugs and toxins exert primary or secondary effects on the electrical properties of the cell membrane, and thereby exert effects on automaticity, arrhythmias, and force of contraction. Therefore, for an understanding of the mode of action of cardioactive and cardiotoxic agents, neurotransmitters, hormones, and plasma electrolytes on the electrical and mechanical activity of the heart, it is necessary to understand the electrical properties and behavior of the myocardial cell membrane at rest and during excitation. The first step in gaining such an understanding is to examine the electrical properties of myocardial cells at rest, including the origin of the resting membrane potential. The resting potential and action potential are the direct result of special properties of the cell membrane.

The work of the author and his associates summarized in this chapter was supported by NIH grant HL-18711.

N. Sperelakis (ed.), PHYSIOLOGY AND PATHOPHYSIOLOGY OF THE HEART.

Martinus Nijhoff Publishing, Boston/The Hague/ Dordrecht/Lancaster.

TABLE 3–1. Comparison of the resting potentials and action potentials of cells in different regions of the mammalian heart.

Parameter	Ventricular cell	Atrial cell	Sinoatrial nodal cell	Atrioventricular nodal cell	Purkinje fiber
Resting potential (mV)	−80 to 90	−80 to 90	−50 to 60	−60 to 70	−90 to 95
Action potential					
Magnitude (mV)	110–120	110–120	60–70	70–80	120
Overshoot (mV)	30	30	0–10	5–15	30
Duration (ms)	200–300	100–300	100–300	100–300	300–500
Maximal rate of rise (V/s)	100–200	100–200	1–10	5–15	500–700
Propagation velocity (m/s)	0.3–0.4	0.3–0.4	<0.05	0.1	2–3
Fiber diameter (μm)	10–16	10–15	5–10	5–10	100

The action potential duration is about 120 ms in avian heart and about 400–500 ms in amphibian heart. In any species, the duration is a function of heart rate and temperature. The propagation velocity at the atrial–atrioventricular nodal junction is considerably less than in the atrioventricular node proper. Cell length is about 100–200 μm for myocardial cells. Adapted from Sperelakis [3].

Some of the electrical characteristics of the cells of the various tissues of the heart are summarized in table 3–1.

Passive Electrical Properties and Cable Properties

MEMBRANE STRUCTURE AND COMPOSITION

The cell membrane is composed of a bimolecular leaflet of phospholipid molecules (e.g., phosphatidylcholine and phosphatidylethanolamine) sandwiched inbetween two layers of adsorbed protein. The nonpolar hydrophobic ends of the phospholipid molecules project toward the middle of the membrane, and the polar hydrophilic ends project toward the edges of the membrane bordering on the water phases (fig. 3–1). This orientation is thermodynamically favorable. The cell membrane is about 70–100 Å thick, and the phospholipid molecules are about the right length (30–40 Å) to stretch across half of the membrane thickness. Cholesterol molecules are also in high concentration in the cell membrane (of animal cells), giving a phospholipid—cholesterol ratio of about 1.0, and are inserted inbetween the phospholipid molecules. Large protein molecules are also inserted in the lipid bilayer matrix. Some proteins protrude through the entire membrane thickness, e.g., the (Na, K)-ATPase and the various ion channel proteins, whereas other proteins are inserted into one leaflet (inner or outer) only, e.g., neurotransmitter receptors and adenylate cyclase enzyme. These proteins "float" in the lipid bilayer matrix, and the membrane has fluidity (reciprocal of microviscosity) such that the protein and lipid molecules can move around laterally in the plane of the membrane.

The outer surface of the cell membrane is lined with strands of mucopolysaccharides (the cell coat) that endow the cell with immunochemical properties. The cell coat is highly charged negatively, and therefore can bind cations, such as Ca^{2+} ion. Treatment with neuraminidase, to remove sialic acid residues, destroys the cell coat.

MEMBRANE CAPACITANCE AND RESISTIVITY

Lipid bilayer membranes of the Mueller–Rudin type made artificially have a specific membrane capacitance (C_m) of 0.4–1.0 μF/cm^2, which is close to the value for biologic membranes; that is, capacitance of myocardial cell membranes is due to the lipid bilayer matrix. Calculation of membrane thickness (δ) from the equation for capacitance for a measured membrane capacitance (C_m) of 0.7 μF/cm^2, and assuming a dielectric constant (ϵ) of 5, gives 63 Å:

$$C_m = \frac{\epsilon A_m}{\delta} \frac{1}{4\pi k}$$

where A_m is the membrane area (in cm^2) and k is a constant (9.0×10^{11} cm/F). Most oils

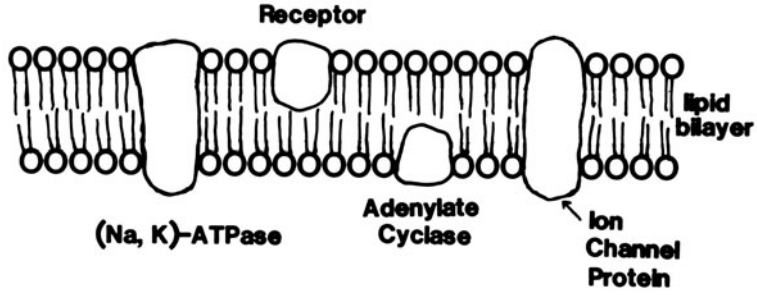

FIGURE 3–1. Diagrammatic illustration of cell membrane substructure showing the lipid bilayer. Nonpolar hydrophobic tail ends of the phospholipid molecules project toward the middle of the membrane, and polar hydrophilic heads border on the water phase at each side of the membrane. Lipid bilayer is about 50–100 Å thick. For simplicity, the cholesterol molecules are not shown. Large protein molecules protrude through entire membrane thickness or are inserted into one leaflet only, as illustrated. These proteins include various enzymes associated with the cell membrane as well as membrane ionic channels. Membrane has fluidity, so that the protein and lipid molecules can move around in the plane of the membrane and fluorescent probe molecules inserted into the hydrophobic region of the membrane have freedom to rotate. Adapted from Singer and Nicolson [42].

have dielectric constants of 3–5. The more dipolar the material, the greater the dielectric constant (e.g., water has a value of 81).

The artificial lipid bilayer membrane, on the other hand, has an exceedingly high ionic resistivity (R_m) of 10^6–10^9 Ω-cm^2, which is several orders of magnitude higher than the biologic cell membrane (about 10^3 Ω-cm^2). But if the bilayer is doped with certain substances, such as macrocyclic-polypeptide antibiotics (known as ionophores), R_m is greatly lowered. (The added ionophores may be of the ion-carrier type, such as valinomycin; or of the channel-former type, such as gramicidin.) Therefore, the presence of proteins that span across the thickness of the cell membrane must account for the relatively low resistance of the biologic cell membrane. These proteins include those associated with the voltage-dependent gated ion channels of the excited membrane, and the voltage-independent ungated ion channels of the resting membrane. To repeat, the C_m component is due to the lipid bilayer matrix, and the R_m component is due to the proteins inserted into the lipid bilayer.

MEMBRANE FLUIDITY

Thus, the electrical properties and the ion transport properties of the cell membrane are determined by the molecular composition of the membrane. The lipid bilayer matrix even influences the function of the membrane proteins, e.g., the (Na, K)-ATPase activity is affected by the surrounding lipid. A high cholesterol content lowers the fluidity of the membrane, and a high degree of unsaturation and branching of the tails of the phospholipid molecules raises the fluidity; chain length also affects fluidity. The polar portion of cholesterol lodges in the hydrophilic part of the membrane, and the nonpolar part of the planar cholesterol molecule is wedged inbetween the fatty acid tails, thus restricting their motion and lowering fluidity. Phospholipids with unsaturated and branched-chain fatty acids cannot be packed tightly because of steric hindrance due to their greater rigidity; hence such phospholipids increase membrane fluidity. Low temperature decreases membrane fluidity, as might be expected. Ca^{2+} and Mg^{2+} may diminish the charge repulsion between the phospholipid head groups; this allows the bilayer molecules to pack more tightly, thereby constraining the motion of the tails and reducing fluidity. The density of packing of the phospholipid tails is about 20–30 Å^2 per chain, and the average packing of the head group is about 60 Å^2 [1]. Membrane fluidity changes occur in muscle de-

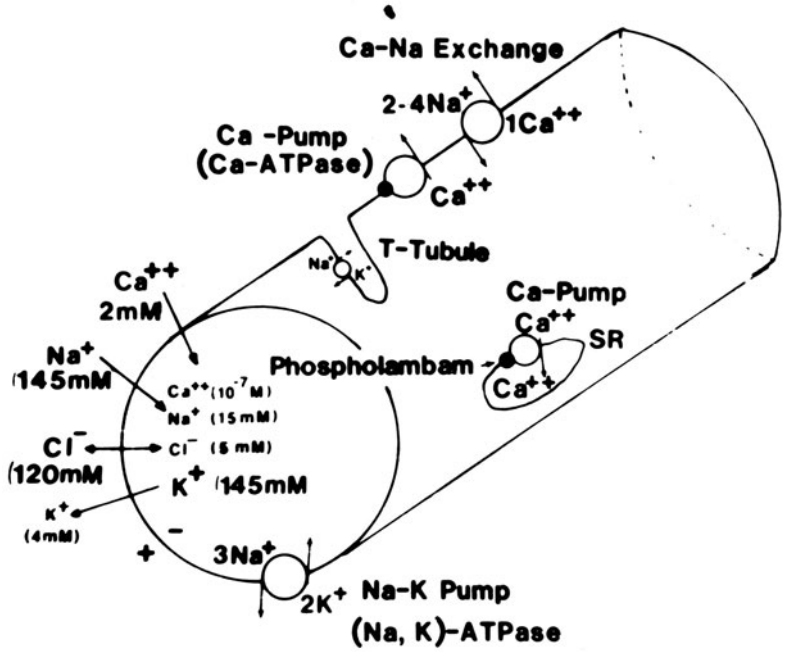

FIGURE 3–2. Intracellular and extracellular ion distributions in a vertebrate myocardial cell. Also given are polarity and magnitude of the resting potential. Arrows give direction of the net electrochemical gradient. Invaginating transverse (T) tubules found in mammalian ventricular cells are continuations of the cell surface membrane into the cell interior. Na^+-K^+ pump is located in the cell surface and the T-tubule membranes. A Ca-ATPase/Ca pump, similar to that in the SR, may be located in the cell membrane. A Ca-Na exchange carrier is located in the cell membrane. Redrawn from Sperelakis [3].

velopment and in certain disease states, such as cancer, muscular dystrophy (Duchenne type), and myotonic dystrophy.

The hydrophobic portion of local anesthetic molecules may interpose between the lipid molecules; this separates the acyl chain tails of the phospholipid molecules further, reducing the Van der Waals forces of interaction between adjacent tails, and so increasing the fluidity of the membrane. Local anesthetics are known to depress the resting conductance of the membrane for K^+ and Na^+ and to depress the voltage-dependent changes in g_{Na} and g_K, and the anesthetics also depress the voltage-dependent slow-cation channels; that is, the local anesthetics produce a nonselective depression of most conductances of the resting and the excited membrane. This depression presumably could come about indirectly by the anesthetics' effect on the fluidity of the lipid matrix. At the concentration of local anesthetics that is required to completely block excitability, the estimated concentration of local anesthetic molecules in the lipid bilayer is more than 100,000/μm^2. The depression of the (Na, K)-ATPase activity by local anesthetics [2] also could be explained by an effect on the fluidity of the lipid matrix, although a direct effect on the protein enzyme is also possible.

Ion Distributions and Their Maintenance

ION DISTRIBUTIONS

The transmembrane resting potential in the atrial and ventricular myocardial cells is about −80 mV. The resting potential or maximum diastolic potential in the Purkinje fibers is somewhat greater (about −90 mV), whereas that in the nodal cells is lower (about −60 mV). The ionic composition of the extracellular fluid bathing the heart cells is similar to that of the blood plasma. It is high in Na^+ (about 145 m*M*) and Cl^- (about 120 m*M*), but low

in K^+ (about 4 m*M*). The free Ca^{2+} concentration is about 2 m*M*. In contrast, the intracellular fluid has a low concentration of Na^+ (about 15 m*M* or less) and Cl^- (about 6 m*M*), but a high concentration of K^+ (about 150 m*M*). The free intracellular Ca^{2+} concentration ($[Ca]_i$) is about 10^{-7} *M* or less, but during contraction it may rise as high as 10^{-5} or 10^{-4}*M*. The total intracellular Ca^{2+} is much higher (about 2 mmol/kg), but most of this is bound to molecules such as proteins or is sequestered into compartments such as mitochondria and the sarcoplasmic reticulum (SR). Most of the intracellular K^+ is free, and it has a diffusion coefficient only slightly less than K^+ in free solution. Thus, under normal conditions, the myocardial cell maintains an internal ion concentration markedly different from that in the medium bathing the cells, and it is these ion concentration differences that underlie the resting potential and excitability. The ion distributions and related pumps are depicted in figure 3–2.

Na-K PUMP

The intracellular ion concentrations are maintained differently from those in the extracellular fluid by active ion transport mechanisms that expend metabolic energy to push specific ions against their concentration or electrochemical gradients. These ion pumps are located in the cell membrane at the cell surface and probably also in the transverse tubular membrane. The major ion pump is the Na-K-linked pump, which pumps Na^+ out of the cell against its electrochemical gradient while simultaneously pumping K^+ in against its electrochemical gradient (fig. 3–2). The coupling of Na^+ and K^+ pumping is obligatory, since in zero $[K]_0$ the Na^+ can no longer be pumped out. The coupling ratio of Na^+ pumped out to K^+ pumped in may vary from 3:3 to 3:2 to 3:1, with the 3:2 ratio being the most common. When the ratio is 3:3, the pump is electrically neutral or nonelectrogenic: a potential difference (PD) across the membrane is not directly produced because the pump pulls in one positive charge (K^+) for every positive charge (Na^+) it pushes out. When the ratio is 3:2, the pump is electrogenic and directly produces a PD that causes the membrane potential (E_m) to be greater (more negative) than it would be otherwise (on the basis of the ion concentration gradients and relative permeabilities or net diffusion potential [E_{diff}] alone.) Under normal steady-state conditions, the contribution of the Na^+ electrogenic pump potential (V_{ep}) to E_m in myocardial cells is only a few millivolts.

The driving mechanism for the Na-K pump is a membrane ATPase, the (Na, K)-ATPase, that requires both Na^+ and K^+ ions for activation. This enzyme requires Mg^{2+} for activity, and it is inhibited by Ca^{2+}. ATP, Mg^{2+}, and Na^+ are thus required at the inner surface of the membrane, and K^+ is required at the outer surface. A phosphorylated intermediate of the (Na, K)-ATPase occurs in the transport cycle, its phosphorylation being Na^+ dependent and its dephosphorylation being K^+ dependent (for references, see Sperelakis [3]). The pump enzyme usually drives three Na^+ ions in for each ATP molecule hydrolyzed. The (Na, K)-ATPase is specifically inhibited by the cardiac glycosides acting on the outer surface. The pump enzyme is also inhibited by sulfhydryl reagents (such as N-ethylmaleimide, mercurial diuretics, and ethacrynic acid), thus indicating that the SH groups are crucial for activity.

Blockade of the Na-K pump produces only a small immediate effect on the resting E_m: a small depolarization of about 2–6 mV, representing the contribution of V_{ep} to E_m. Excitability and the generation of an action potential (AP) are only slightly affected at short times: excitability is independent of active ion transport. However, over a period of many minutes, depending on the ratio of surface area to volume of the cell, the resting E_m slowly declines because of gradual dissipation of the ionic gradients. The progressive depolarization depresses the rate of rise of the AP and hence the propagation velocity, and eventually all excitability is lost. Thus, a large resting potential and excitability, although not immediately dependent on the Na-K pump, are ultimately dependent on it.

The rate of Na-K pumping in myocardial cells must change with the heart rate in order to maintain the intracellular ion concentrations relatively constant, because a higher frequency

of APs results in a greater overall movement of ions down their electrochemical gradients (e.g., the cells tend to gain Na^+, Cl^-, and Ca^{2+} and to lose K^+), and these ions must be repumped. The factors that control the rate of Na-K pumping include $[Na]_i$ and $[K]_0$. In cells that have a large surface area to volume ratio (such as small diameter heart cells), $[Na]_i$ may increase by a relatively large percentage during a train of APs, and this would stimulate the pumping rate. Likewise, an accumulation of K^+ externally would stimulate the pump (the K_m for K^+ is about 2 m*M*).

Cl^- DISTRIBUTION

In many invertebrate and vertebrate nerve or muscle cells, Cl^- ion does not appear to be actively transported: that is, there is no Cl^- ion pump. In such cases, Cl^- distributes itself passively (no energy used) in accordance with E_m:E_{Cl} becomes equal to E_m if the cell is at rest. In mammalian myocardial cells, Cl^- also seems to be close to passive distribution because $[Cl]_i$ is at (or only slightly above) the value predicted by the Nernst equation from the resting E_m (for references, see Sperelakis [3]). When passively distributed, $[Cl]_i$ is low because the negative potential inside the cell (the resting potential) pushes out the negatively charged Cl^- ion until the Cl^- distribution is at equilibrium with the resting E_m. Hence, for a resting E_m of -80 mV, and taking $[Cl]_0$ to be 120 m*M*, $[Cl]_i$ would be a 5.9 m*M* [$E_m = +61$ mV log $([Cl]_i/[Cl]_0)$]. However, during the AP, the inside of the cell goes in a positive direction, and a net Cl^- influx (outward Cl^- current, I_{Cl}) will occur and thus increase $[Cl]_i$. The magnitude of the Cl^- influx depends on the Cl^- conductance (g_{Cl}) of the membrane [$I_{Cl} = g_{Cl}(E_m - E_{Cl})$]. Thus, the average level of $[Cl]_i$ in myocardial cells of the beating heart should depend on the frequency and duration of the AP, that is, on the mean E_m averaged over many AP cycles.

Ca^{2+} DISTRIBUTION

Need for Calcium Pumps. For the positively charged Ca^{2+} ion, there must be some mechanism for removing Ca^{2+} from the myoplasm; otherwise the myocardial cell would continue to gain Ca^{2+} until there was no electrochemical gradient for net influx of Ca^{2+}. This would occur until the free $[Ca]_i$ in the myoplasm was even greater than that outside (2 m*M*), because of the negative potential inside the cell. Therefore, there must be one or more Ca^{2+} pumps in effect. The SR membrane contains a Ca^{2+}-activated ATPase (which also requires Mg^{2+}) that actively pumps Ca^{2+} from the myoplasm into the SR lumen at the expense of ATP, and is capable of pumping down the Ca^{2+} to less than 10^{-7} *M*. This sequestration of Ca^{2+} by the SR is essential for muscle relaxation. (The mitochondria also can actively take up Ca^{2+} [to about the same degree as the SR], but this Ca^{2+} pool probably does not play an important role in normal excitation–contraction coupling processes.) However, the resting Ca^{2+} influx and the extra Ca^{2+} influx that enters with each AP must be returned to the interstitial fluid. Several mechanisms have been proposed for this (for references, see Sperelakis [3]): (a) a Ca-ATPase, similar to that in the SR, may be present in the sarcolemma, and (b) a Ca-Na exchange occurs across the cell membrane.

It has been reported [4, 5] that there is a Ca-ATPase in the sarcolemma of myocardial cells that actively transports Ca^{2+} outward against an electrochemical gradient, utilizing ATP in the process. A similar conclusion was reached for smooth muscle [6]. In cardiac muscle, it has been speculated that Ca^{2+} sequestered into the SR network may be transported across the junctional coupling formed between the junctional SR and the sarcolemma. This would allow a more direct reequilibration of the Ca^{2+} taken up by the SR with the ISF space.

Ca-Na Exchange Reaction. The Ca-Na exchange reaction exchanges one internal Ca^{2+} ion for 2, 3, or 4 external Na^+ ions via a membrane carrier molecule (for references, see Sperelakis [3]) (fig. 3–2). This reaction is facilitated by ATP, but ATP is not hydrolyzed. Instead, the energy for the pumping of Ca^{2+} against its large electrochemical gradient comes from the Na^+ electrochemical gradient. That is, the

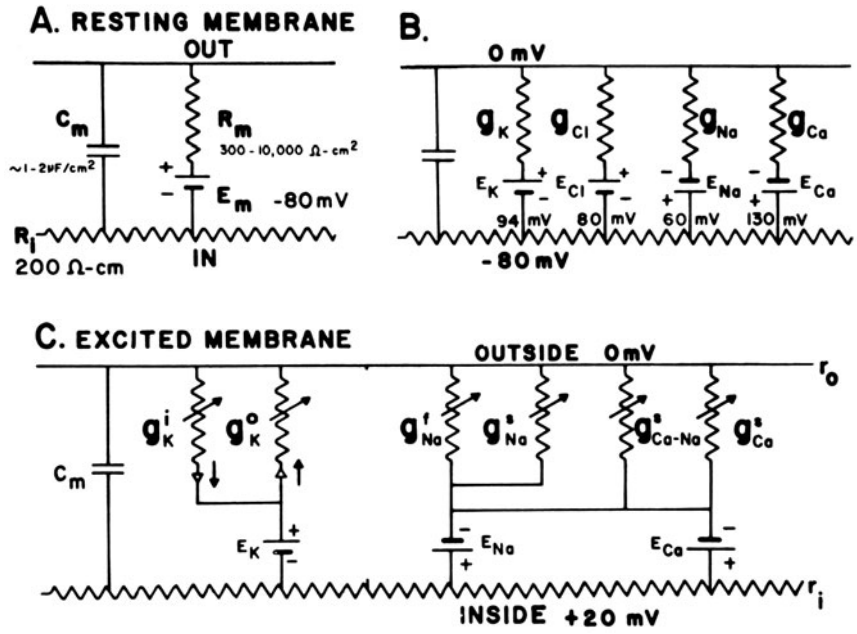

FIGURE 3–3. Electrical equivalent circuits for a myocardial cell membrane at rest *(A* and *B)* and during excitation *(C). (A)* Membrane as a parallel resistance–capacitance circuit, the membrane resistance (R_m) being in parallel with the membrane capacitance (C_m). Resting potential (E_m) is represented by an 80-mV battery in series with the membrane resistance, the negative pole facing inward. *(B)* Membrane resistance is divided into its four component parts, one for each of the four major ions of importance: K^+, Cl^-, Na^+, and Ca^{2+}. Resistances for these ions (R_K, R_{Cl}, R_{Na}, and R_{Ca}) are parallel to one another, and represent totally separate and independent pathways for permeation of each ion through the resting membrane. These ion resistances are depicted as their reciprocals, namely, ion conductances (g_K, g_{Cl}, g_{Na}, and g_{Ca}). Equilibrium potential for each ion (e.g., E_K), determined solely by the ion distribution in the steady state and calculated from the Nernst equation, is shown in series with the conductance path for that ion. Resting potential of −80 mV is determined by the equilibrium potentials and by the relative conductances. *(C)* Equivalent circuit is further expanded to illustrate that for the voltage-dependent conductances there are at least two separate K^+-conductance pathways (labeled here g^o_K and g^i_K). Arrowheads in series with the K^+ conductances represent rectifiers, the arrowhead points giving the direction of least resistance to current flow. Thus g^o_K allows K^+ flux to occur more readily in the outward direction (so-called outwardly directed rectification, whereas g^i_K allows K^+ flux to occur more readily in the inward direction (inwardly directed rectification). There are two separate Na^+-conductance pathways, one a kinetically fast Na^+ conductance (g^f_{Na}) and the other a kinetically slow Na^+ conductance (g^s_{Na}). In addition, there is a nonspecific kinetically slow pathway that allows both Na^+ and Ca^{2+} to pass through, perhaps by competition with one another. Ca^{2+}-selective pathway (g^s_{Ca}) is also kinetically slow. Arrows drawn through the resistors represent that the conductances are variable, depending on membrane potential and time. The three types of slow channels are not necessarily all present in any one type of cell. Redrawn from Sperelakis [3].

uphill transport of Ca^{2+} is coupled to the downhill movement of Na^+. Effectively, the energy required for this Ca^{2+} movement is derived from the (Na, K)-ATPase. Thus, the Na-K pump, which uses ATP to maintain the Na^+ electrochemical gradient, indirectly helps to maintain the Ca^{2+} electrochemical gradient. Hence, the inward Na^+ leak is greater than it would be otherwise. The energy cost (ΔG_{Ca}, in joules/mol) for pumping out Ca^{2+} ion is directly proportional to its electrochemical gradient, namely, $\Delta G_{Ca} = zF(E_m - E_{Ca})$. The energy available from the Na^+ distribution is directly proportional to its electrochemical gradient [$\Delta G_{Na} = zF(E_m - E_{Na})$]. Depending on the exact values of $[Na]_i$ and $[Ca]_i$ at any time during the cardiac cycle, the energetics would be adequate for an exchange ratio of 2 Na^+ : 1 Ca^{2+} or 3 Na^+ : 1 Ca^{2+}. An exchange ratio of 2 : 1 would be electroneutral, whereas a ratio of

3:1 would produce a small depolarization (unless the three Na^+ ions were accompanied by a univalent counter-ion such as Cl^-). The exchange reaction depends on relative concentrations of Ca^{2+} and Na^+ on each side of the membrane and on relative affinities of the binding sites to Ca^{2+} and Na^+. Because of this Ca-Na exchange reaction, whenever the cell gains Na^+ it will also gain Ca^{2+} because the exchange reaction becomes slowed (e.g., the Na^+ electrochemical gradient is reduced). In addition, when an elevated $[Na]_i$ occurs, some of the exchange carriers will exchange the ions in reverse (internal Na^+ for external Ca^{2+}) and thus increase Ca^{2+} influx. The net effect of both mechanisms is to elevate $[Ca]_i$. The Ca-Na exchange process has been proposed as the mechanism of the positive inotropic action of cardiac glycosides. A complete discussion of the Ca-Na exchange is given in chapter 10.

Equilibrium Potentials

For each ionic species distributed unequally across the cell membrane, an equilibrium potential (E_i) or battery can be calculated for that ion from the Nernst equation (for 37°C): $E_i = -61 \text{ mV}/z \log (C_i/C_0)]$ where C_i is the internal concentration of the ion, C_0 is the extracellular concentration, and z is the valence (with sign). The Nernst equation gives the PD (electrical force) that would exactly oppose the concentration gradient (diffusion force). Only very small charge separation (Q, in coulombs) is required to build up a very large PD($E_m = Q/C_m$, where C_m is the membrane capacitance). For the ion distributions given previously, the approximate equilibrium potentials are $E_{Na} = +60$ mV, $E_{Ca} = +129$ mV, $E_K = -94$ mV, and $E_{Cl} = -80$ mV (fig. 3–3). The sign of the equilibrium potential gives the direction of the concentration gradient, with the side of higher concentration being negative for positive ions (cations) and positive for negative ions (anions). Any ion whose equilibrium potential is different from the resting potential (−80 mV) is off equilibrium, and therefore must effectively be pumped at the expense of energy. In the myocardial cell, only Cl^- ion appears to be at or near equilibrium, whereas Na^+, Ca^{2+}, and K^+ are actively transported. Extensive discussion of concentration cells and diffusion is given by Sperelakis [3], and the mechanisms for development of the equilibrium potential is depicted in figure 3–4 and discussed in its legend.

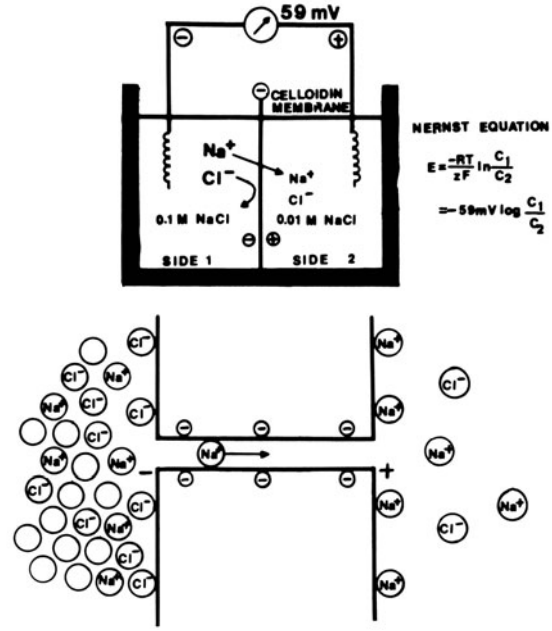

FIGURE 3–4. *(Upper diagram)* Concentration cell diffusion potential developed across artificial membrane containing negatively charged pores. The membrane is impermeable to Cl^- ions, but permeable to cations such as Na^+. Concentration gradient for Na^+ causes a potential to be generated, the side of higher Na^+ concentration becoming negative. *(Lower diagram)* Expanded diagram of a water-filled pore in the membrane, showing the permeability to Na^+ ions, but lack of penetration of Cl^- ions. Potential difference is generated by charge separation, a slight excess of Na^+ ions being held close to the right-hand surface of the membrane; a slight excess of Cl^- ions is plastered up close to the left surface. From Sperelakis [3].

Electrochemical Driving Forces and Membrane Ionic Currents

The electrochemical driving force for each species of ion is the algebraic difference between its equilibrium potential, E_i, and the mem-

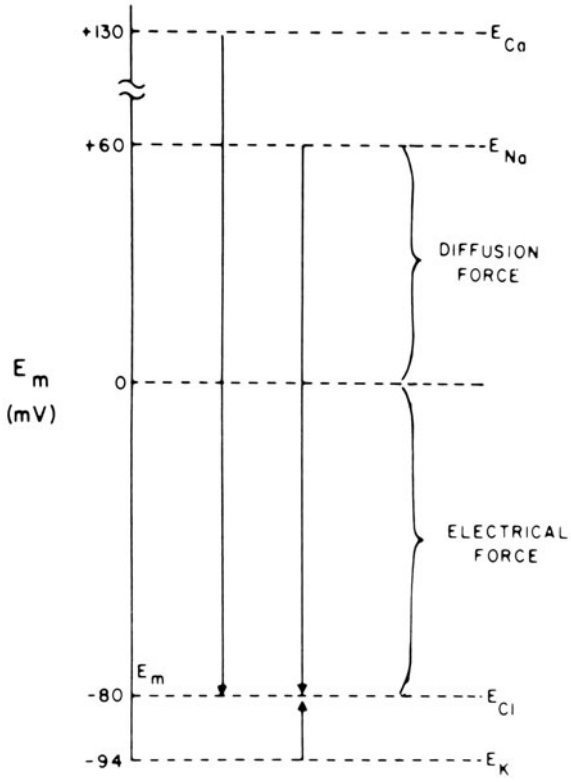

FIGURE 3–5. Representation of the electrochemical driving forces for Na^+, Ca^{2+}, K^+, and Cl^-. Equilibrium potentials for each ion (e.g., E_{Na}) are positioned vertically according to their magnitude and sign; they were calculated from Nernst equation for given set of extracellular and intracellular ion concentrations. Measured resting potential is assumed to be −80 mV. Electrochemical driving force for an ion is the difference between its equilibrium potential (E_i) and the membrane potential (E_m), that is ($E_i - E_m$). Thus, at rest, the driving force for Na^+ is the difference between E_{Na} and the resting E_m; if E_{Na} is +60 mV and resting E_m is −80 mV, the driving force is 140 mV; that is, the driving force is the algebraic sum of the diffusion force and the electrical force, and is represented by the length of the arrows in the diagram. Driving force for Ca^{2+} (about 210 mV) is even greater than that for Na^+, whereas that for K^+ is much less (about 14 mV). Direction of the arrows indicates the direction of the net electrochemical driving force, namely, the direction for K^+ is outward, whereas that for Na^+ and Ca^{2+} is inward. If Cl^- is passively distributed, then its distribution across the cell membrane can only be determined by the net membrane potential; for a cell sitting a long time at rest, $E_{Cl} = E_m$ and there is no net driving force. Redrawn from Sperelakis [3].

brane potential, E_m. The total driving force is the sum of two forces: an electrical force (e.g., the negative potential in the cell tends to pull in positively charged ions) and a diffusion force (based on the concentration gradient) (fig. 3–5). Thus, in a resting cell, the driving force for Na^+ is $(E_m - E_{Na}) = -80$ mV $- (-60$ mV$) = -140$ mV. The negative sign means that the driving force is directed to bring about net movement of Na^+ inward. The driving force for Ca^{2+} is $(E_m - E_{Ca}) = -80$ mV $- (+129$ mV$) = -209$ mV. The driving force for K^+ is $(E_m - E_K) = -80$ mV $- (-94$ mV$) = +14$ mV; hence, the driving force for K^+ is small and directed outward. The driving force for Cl^- is zero for a cell at rest: $(E_m - E_{Cl}) = -80$ mV $- (-80$ mV$) = 0$. However, during the AP, when E_m is changing, the driving force for Cl^- is not zero, and there is a net driving force for inward Cl^- movement. Similarly, the driving force for K^+ outward movement increases during the AP, whereas those for Na^+ and Ca^{2+} decrease.

The net current for each ionic species (I_i) is equal to its driving force times its conductance (g_i, reciprocal of the resistance) through the membrane. This is essentially Ohm's law, $I = V/R = g \cdot V$, modified for the fact that in an electrolytic system the total force tending to drive net movement of a charged particle must take into account both the electrical force and the concentration (or chemical) force. Thus, for the four ions, the net current can be expressed as $I_{Na} = g_{Na}(E_m - E_{Na})$, $I_{Ca} = g_{Ca}(E_m - E_{Ca})$, $I_K = g_K(E_m - E_K)$, and $I_{Cl} = g_{Cl}(E_m - E_{Cl})$. In a resting cell, Cl^- and Ca^{2+} can be neglected, and the Na^+ current (inward) must be equal and opposite to the K^+ current (outward) in order to maintain a steady resting potential: $I_K = -I_{Na}$. Thus, although in the resting membrane the driving force for Na^+ is much greater than that for K^+, g_K is much larger than g_{Na}, so the currents are equal. Hence, there is a continual leak of Na^+ inward and K^+ outward even in a resting cell, and the system would run down if active pumping were blocked. Since the ratio of the Na^+/K^+ driving forces (-140 mV/-14 mV) is 10, the ratio of conductances (g_{Na}/g_K) will be about

1:10. The fact that g_K is much greater than g_{Na} accounts for the resting potential being close to E_K and not E_{Na}.

The myocardial membrane has at least two separate voltage-dependent K^+ channels (fig. 3–3C). One allows K^+ ion to pass more readily inward (against the usual net electrochemical gradient for K^+) than outward, the so-called inward-going rectifier. This ungated channel is responsible for anomalous rectification, and instantaneously decreases its conductance upon depolarization and increases its conductance with repolarization. The second type of voltage-dependent K^+ channel is similar to the usual K^+ channel found in other excitable membranes, which slowly opens (increasing total g_K) upon depolarization, the so-called delayed rectifier. This channel allows K^+ to pass more readily outward (down the usual electrochemical gradient for K^+) than inward, and so is also known as the outward-going rectifier. This delayed rectifier channel turns on much more slowly than in nerve or skeletal muscle. The activation of this channel produces the large increase in total g_K that terminates the cardiac AP.

Determination of Resting Potential and Net Diffusion Potential (E_{diff})

For given ion distributions, which normally remain nearly constant under usual steady-state conditions, the resting potential is determined by the relative membrane conductances *(g)* or permeabilities (P) for Na^+ and K^+ ions. That is, the resting potential (of about -80 mV) is close to E_K (about -94 mV) because $g_K >> g_{Na}$ or $P_K >> P_{Na}$. From simple circuit analysis (using Ohm's law and Kirchhoff's laws), one can prove that this should be true. Therefore, the membrane potential will always be closer to the battery (equilibrium potential) having the lowest resistance (highest conductance) in series with it (figs. 3–3 and 3–5). In the resting membrane, this battery is E_K, whereas in the excited membrane it will be E_{Na} (or E_{Ca}) because there is a large increase in g_{Na} (and g_{Ca}) during the AP. Any ion that is passively distributed cannot determine the resting potential; instead, the resting potential determines the distribution of that ion. Therefore, Cl^- drops out of the consideration for myocardial cells because it seems to be passively distributed. (However, transient net movements of Cl^- across the membrane do influence E_m. For example, washout of Cl^- from the cell (in Cl^--free solution) produces a transient depolarization, and reintroduction of Cl^- produces a small in myocardial cells.) Because of its relatively low concentration coupled with its relatively low resting conductance, the Ca^{2+} distribution has only a relatively small effect on the resting E_m, and so it can be ignored. Therefore, a simplified version of the Goldman–Hodgkin–Katz constant-field equation can be given (for 37° C):

$$E_m = -61 \text{ mV } \ln \frac{[K]_i + P_{Na}/P_K [Na]_i}{[K]_o + P_{Na}/P_K [Na]_o}$$

This equation shows that for a given ion distribution, the resting E_m is determined by the P_{Na}/P_K ratio, the relative permeability of the membrane to Na^+ and K^+. There is a direct proportionality between P_K and g_K and between P_{Na} and g_{Na} at constant E_m and concentrations. For myocardial cells, the P_{Na}/P_K ratio is about 0.05.

Inspection of the constant-field equation shows that the numerator of the log term will be dominated by the $[K]_i$ term [since (P_{Na}/P_K) $[Na]_i$ will be very small], whereas the denominator will be affected by both the $[K]_o$ and (P_{Na}/P_K) $[Na]_o$ terms. This relationship thus accounts for the deviation of the E_m versus log $[K]_o$ curve from a straight line (having a slope of 61 mV/decade) in normal Ringer solution (fig. 3–6). When $[K]_o$ is elevated ($[Na]_o$ reduced by an equimolar amount), the denominator becomes more and more dominated by the $[K]_o$ term and less and less by the (P_{Na}/P_K) $[Na]_o$ term. Therefore, in bathing solutions of high K^+, the constant-field equation approaches the simple Nernst equation for K^+, and E_m approaches E_K. As $[K]_o$ is raised, E_K becomes correspondingly reduced since $[K]_i$ stays relatively constant; therefore, the membrane becomes more and more depolarized (fig. 3–6).

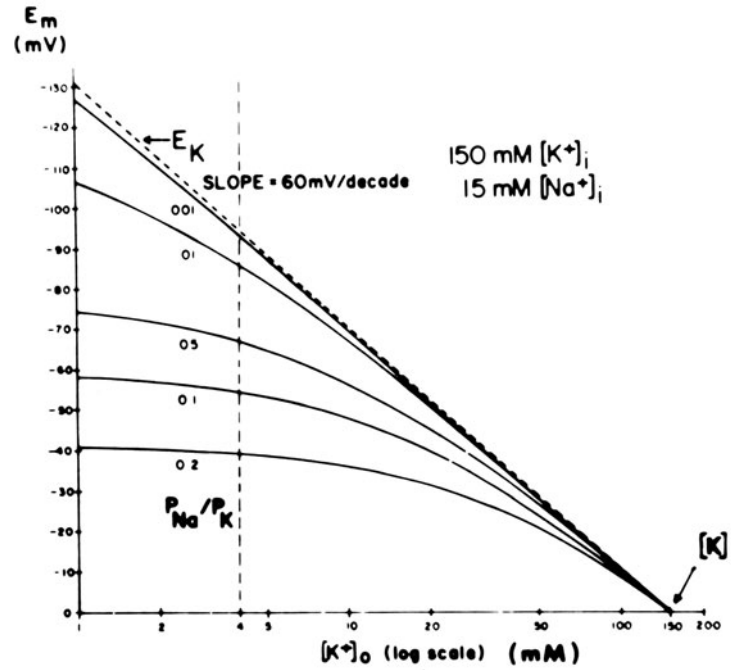

FIGURE 3–6. Theoretical curves calculated from the Goldman constant-field equation for resting potential (E_m) as a function of $[K]_0$. Family of curves is given for various P_{Na}/P_K ratios (0.001, 0.01, 0.05, 0.1, and 0.2). K^+ equilibrium potential (E_K) calculated from the Nernst equation (broken straight line). Curves calculated for a $[K]_i$ of 150 m*M* and a $[Na]_i$ of 15 m*M*. Calculations made holding $[K]_0 + [Na]_0$ constant at 154 m*M;* i.e., as $[K]_0$ was elevated, $[Na]_0$ was lowered by an equimolar amount. Change in P_K as a function of $[K]_o$ was not taken into account for these calculations. Point at which E_m is zero gives $[K]_i$. The potential reverses in sign when $[K]_0$ exceeds $[K]_i$. Modified from Sperelakis [3].

An alternative method of approximating the resting potential is by the chord-conductance equation:

$$E_m = \frac{g_K}{g_K + g_{Na}} E_K + \frac{g_{Na}}{g_K + g_{Na}} E_{Na}$$

This equation can be derived simply from Ohm's law and circuit analysis for the condition when net current is zero. The chord-conductance equation again illustrates the important fact that the ratio g_K/g_{Na} determines the resting potential. When $g_K >> g_{Na}$, then E_m is close to E_K; conversely, when $g_{Na} >> g_K$ (as during the spike part of the cardiac AP), E_m shifts to close to E_{Na}.

When $[K]_0$ is elevated (e.g., to 10 m*M*) in some cells, a hyperpolarization of up to about 10 mV may be produced. Such behavior is often observed in cells with a high P_{Na}/P_K ratio (due to low P_K) and therefore a low resting E_m, such as in young embryonic hearts. This hyperpolarization could be explained by several factors: (a) stimulation of the electrogenic Na^+ pump (V_{ep}), (b) an increase in P_K (and therefore g_K), and (c) an increase in g_K (but not P_K) due to the concentration effect.

Inhibition of the Na-K pump will gradually run down the ion concentration gradients. The cells lose K^+ and gain Na^+, and therefore E_K and E_{Na} become smaller. The cells thus become depolarized (even if the relative permeabilities are unaffected), which causes them to gain Cl^- and therefore also water (cells swell). In summary, in the presence of ouabain (short-term exposure only) to inhibit V_{ep}, the resting potential or net diffusion potential E_{diff} is determined by the ion concentration gradients for K^+ and Na^+ and by the relative permeability

for K^+ and Na^+. When the Na-K pump is operating, there is normally a small additional contribution of V_{ep} to the resting E_m of about 3–6 mV in myocardial cells.

Electrogenic Sodium Pump Potentials

The Na-K pump is responsible for maintaining the cation concentration gradients. The diffusion potentials for K^+ (E_K) and Na^+ (E_{Na}) are about −94 mV and +60 mV, respectively. The resting potential value is usually near E_K, because the K^+ permeability (P_K) is much greater than P_{Na} in a resting membrane. The exact resting membrane potential (E_m) depends on the P_{Na}/P_K ratio, myocardial cells having P_{Na}/P_K ratios of 0.01–0.05, whereas smooth muscle or nodal cells of the heart have a ratio closer to 0.15. In the various types of heart cells, the resting E_m has a smaller magnitude (i.e., is less negative) than E_K by 10–30 mV. Therefore, although it would appear that there were no electrogenic pump potential contribution to the resting potential (that is, as though the Na-K pump could be only indirectly responsible for the resting potential by its role in producing the ionic gradients), a direct contribution of the pump to the resting E_m can be demonstrated. For example, if the Na-K pump is blocked by the addition of ouabain, there usually is an immediate depolarization of 3–8 mV, depending on the type of heart cell. That is, the contribution of an electrogenic pump to the measured resting E_m is small under physiologic conditions.

But under conditions in which the pump is stimulated to pump at a high rate—e.g., when [Na] is abnormally high—the direct electrogenic contribution of the pump to the resting potential can be much greater, and E_m can actually exceed E_K by as much as 30 mV or more. For example, if the ionic concentration gradients are allowed to run down (e.g., by storing the tissues at low temperatures for several hours), then after allowing the tissues to restart pumping, the measured E_m can exceed the calculated E_K (e.g., by 10–20 mV) for a period of time (fig. 3–7). The Na^+ loading of the muscle cells can be facilitated by placing them in cold low-K^+ or zero-K^+ Ringer solutions, since external K^+ is necessary for the

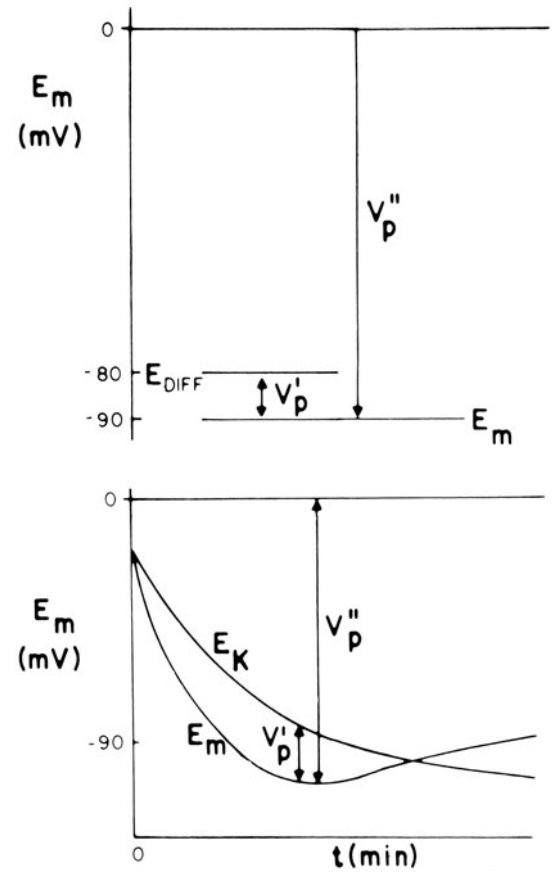

FIGURE 3–7. Diagrammatic representation of an electrogenic sodium pump potential. *(Upper graph)* Muscle cell whose net ionic diffusion potential (E_{diff}, function of ion equilibrium potentials and relative conductances) is −80 mV, yet exhibits a measured membrane resting potential (E_m) that is greater. Difference between E_m and E_{diff} represents the contribution of the electrogenic pump to the resting potential. Usual direct contribution of the pump is only a few millivolts and can be measured by the amount of depolarization produced immediately after complete inhibition of the (Na, K)-ATPase by cardiac glycosides. Because the pump pathway is separate from and parallel to the ionic conductance pathways, the electrogenic pump potential must be equal to V_p''. The contribution of the electrogenic pump potential to the resting potential ($E_m - E_{diff}$) is equal to V_p' *(Lower graph)* Cell that was run down (Na loaded, K depleted) over several hours by inhibition of Na-K pumping, resulting in a low resting potential. Returning the muscle cell to a pumping solution allows the resting E_m to build back up as a function of time. Buildup in E_m occurs faster than buildup in E_K, as illustrated. Whenever E_m is greater (more negative) than the K^+ equilibrium potential (E_K), the difference (V_p') must reflect (as a minimum) the contribution of the sodium pump potential. The actual pump potential may be represented by V_p''. From Sperelakis [3].

Na-K-linked pump to operate; K_m of the (Na, K)-ATPase for K^+ is about 2 m*M*. After several hours in such a solution, the internal concentrations of Na^+, K^+, and Cl^- approach the concentrations in the bathing Ringer solution, and the resting potential is very low (< -20 mV). The tissue is then transferred to a pumping solution, which is the appropriate Ringer solution containing normal K^+ and at normal temperature. Under such conditions, the pump turns over at a maximal rate, because the major control over pump rate is $[Na]_i$. (The low initial E_m also might stimulate the pump rate, because the energy required to pump out Na^+ is much less.) The measured E_m of such Na^+ preloaded cells increases rapidly and more rapidly than E_K, as shown in figure 3–7. After this transient phase, however, a crossover of the two curves occurs, so that E_K again exceeds E_m, as in the physiologic condition. Any method used to increase membrane resistance (R_m) enhances the electrogenicity of the pump (fig. 3–8). Cardiac glycoside reverses the transient hyperpolarization beyond E_K [7].

Rewarming cardiac muscles previously cooled leads to the rapid restoration of the normal resting potential (within 10 min), whereas recovery of the intracellular Na^+ and K^+ concentrations is much slower [8]. During prolonged hypoxia, the resting potential of cardiac muscle decreases much less than E_K (a difference of about 25 mV) [9]. In such a situation, the electrogenic pump acts in an attempt to hold the resting potential constant despite dissipating ionic gradients; that is, the degree of electrogenicity of the pump (Na/K coupling ratio) might increase to compensate for a slowing pump rate.

Another method used to demonstrate that the pump is electrogenic is to inject Na^+ ions into the cell through a microelectrode, which produces a small transient hyperpolarization. This rapid hyperpolarization is immediately abolished by ouabain. The pump current and the rate of Na^+ extrusion increase in proportion to the amount of Na^+ injected.

It is often difficult to prove that the pump is electrogenic: (a) It must be unequivocally demonstrated that, for example, hyperpolarization produced upon Na^+ injection is not the result of enhanced pumping of an electroneutral pump. This could cause depletion of external K^+ in a restricted diffusion space just outside the cell membrane, the depletion thus leading to a larger E_K and thereby to hyperpolarization. Depletion might occur because the Na-K pump pumps in K^+ faster than replenishment (by diffusion from the bulk interstitial fluid) can occur. (b) If the hyperpolarization is really due to an electrogenic Na^+ pump, the hyperpolarization must be augmented under conditions that increase membrane resistance. (c) It must be demonstrated that ionic conductance changes (e.g., an increase in g_K or a decrease in g_{Na}) cannot account for the observed hyperpolarization. This possibility could be ruled out whenever E_m exceeds (is more negative than) E_K.

It has been suggested that the electrogenic Na^+ pump may be influenced by the membrane potential. From energetic considerations, depolarization should enhance the electrogenic Na^+ pump, whereas hyperpolarization should inhibit it. This is because depolarization reduces the electrochemical gradient (and hence the energy requirements) against which Na^+ must be extruded, whereas hyperpolarization increases the gradient. If the energetics are important, there should be a distinct potential, more negative than E_K, at which Na^+ pumping is prevented (e.g., a pump equilibrium potential).

In general, Cl^- ions are known to have a short-circuiting effect on the electrogenic Na^+ pump potential. For example, if the external Cl^- is replaced by less permeant anions, the magnitude of the hyperpolarization produced by the electrogenic Na^+ pump is greatly increased. The mechanism of the Cl^- lowering of the magnitude of the pump potential could be caused by the lowering of membrane resistance in the presence of Cl^-. The greater R_m is, the greater is the electrogenic pump potential.

The density of Na-K pump sites, estimated by specific binding of [^{3}H] ouabain, is usually about $1000/\mu m^2$. The turnover rate of the pump is generally estimated to be 20–100 s^{-1}. The pump current (I_p) has been estimated ($I_p = V_p/R_m$, where V_p is the pump potential), and values of about 10 pmol/cm^2-s were obtained. A density of 1000 sites/μm^2 (10^{11} sites/cm^2) times a turnover rate of 20/s gives 2 $\times$

10^{12} turnovers/cm^2-s. If 3 Na^+ are pumped with each turnover, this gives 6×10^{12} Na^+ ions/cm^2-s; dividing by Avogadro's number (6.02×10^{23} ions/mol) yields 10×10^{-12} mol/cm^2-s, which is the same value as the 10 pmol/cm^2-s measured. The net pump current would be less, depending on the amount of K^+ pumped in the opposite direction (i.e., on the coupling ratio).

One possible scheme for a hypothetical carrier mechanism for a Na-K-linked active transport may be constructed. Because 3 Na^+ are known to be transported per molecule of ATP spent, it is assumed that the carrier has a net negative charge of 3. The carrier, while at the inner surface of the membrane, may have a much higher affinity for Na^+ than for K^+, whereas the converse may be true at the outer surface. It is assumed that the carrier cannot move forward, i.e., diffuse from the inner surface of the membrane to the outer surface, unless fully loaded with 3 Na^+ ions. 1–3 K^+ ions must be carried in for every 3 Na^+ ions moved out. If the pump is electrogenic, i.e., produces a net current (and hence potential) across the membrane, then the amount of K^+ pumped in must be less than the amount of Na^+ pumped out; e.g., the Na/K coupling ratios must be 3:2 or 3:1. The coupling ratio cannot be 3:0, because of the well-known fact that external K^+ must be present for the pump to operate. A coupling ratio of 3:2 or 3:1 could be produced if the carrier were allowed to diffuse backward (outer surface to inner) only partially loaded with K^+. The most usual coupling ratio found is 3:2. The coupling ratio apparently can be altered, however, in the same cell under different conditions.

Whenever the Na-K pump is stimulated to turn over faster, e.g., by increasing $[Na]_i$ or $[K]_0$, for a given coupling ratio (e.g., 3:2), the electrogenic pump potential contribution to E_m becomes larger. The pump potential contribution also becomes larger, for a constant pumping rate, if the coupling ratio is increased (e.g., to 3:1). It is not certain which factors control the coupling ratio. The Na^+/K^+ coupling ratio increases as $[Na]_i$ is increased. K^+ ion is the main ion acting as a shunt on the pump potential. The Na-K pump in several cell types can switch from a Na^+-K^+ exchanging mode of operation to a Na^+-Na^+ exchanging mode of operation, and the mode is governed by the intracellular ATP/ADP/P_i ratios. There is some evidence that the Na/K coupling ratio may be affected by the ADP concentration.

The contribution of the pump potential to the measured E_m is the difference in E_m when the pump is operating versus immediately after the pump has been stopped by the addition of ouabain. Consequently, it appears as though the pump potential (V_p) were in series with the net cationic diffusion potential (E_{diff}):[1]

$$E_m = E_{diff} + R_m i_p$$

where i_p is the electrogenic component of the pump current. (E_{diff} is the E_m that would exist solely on the basis of the ionic gradients and relative permeabilities in the absence of an electrogenic pump potential, as calculated from the constant-field equation.) This equation states that E_m is the sum of E_{diff} and a voltage drop produced by the electrogenic pump. It seems, however, that the pump potential should be considered to be in parallel with E_{diff} (fig. 3–8). Because the density of pump sites is more than 1000-fold greater than that of Na^+ and K^+ channels in resting membrane, there should be no relation between the pump pathway (the active flux path) and R_m (the passive flux paths). The pump path and the passive conductance paths are in parallel. The true pump potential must be much greater than the ΔE_m measured in the absence and presence of ouabain; namely, the pump potential should be considered as the full potential between zero and the maximum negative pump potential (V_p'') while the pump is pumping (fig. 3–7).

One possible equivalent circuit for an electrogenic Na^+ pump, which takes into account many of the known facts, is given in figure 3–8. The pump pathway is in parallel with the resistance pathways, and the pump potential is the full potential (and not the ΔV). The pump pathway is shown as a battery with a switch in series. The switch opens (infinite resistance) when the pump potential is low or zero so that it cannot act as short-circuit path to E_{diff}. A relatively fixed resistance of moderate value in

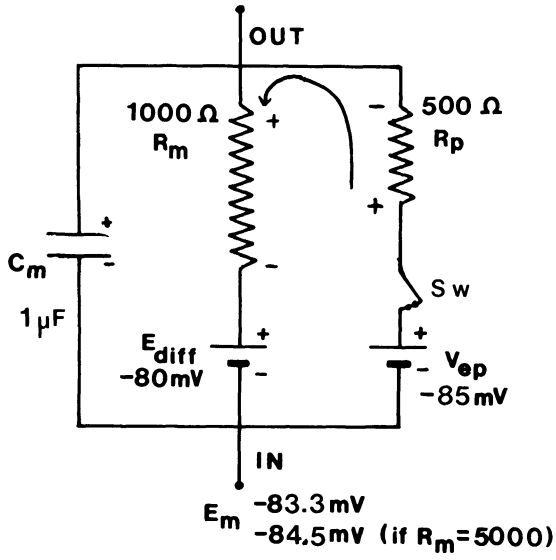

FIGURE 3–8. Hypothetical electrical equivalent circuit for electrogenic sodium pump. Model consists of a pump pathway in parallel with the membrane resistance (R_m) pathway and the membrane capacitance (C_m) pathway. This model fits the evidence that the pump is independent of short-range membrane excitability and that the pump proteins and channel proteins are probably embedded in the lipid bilayer as parallel elements. Net diffusion potential (E_{diff}, determined by the ion equilibrium potentials and relative conductances) of −80 mV is depicted in series with R_m. Pump leg is assumed to consist of a battery in series with a fixed resistor (pump resistance, R_p) that does not change with changes in R_m and whose value is not much different from R_m. Pump battery is charged up to some voltage (V_{ep} of −85 mV, for example) by a pump current generator. Net electrogenic pump current may be developed, for example, by the pumping in of only 2 K^+ ions for every 3 Na^+ ions pumped out. For the values given in the figure (namely, R_m of 1000 Ω, E_{diff} of −80 mV, R_p of 500 Ω, and V_{ep} of −85 mV), it may be calculated by circuit analysis that the measured membrane potential (E_m) is −83.3 mV; that is, the direct electrogenic pump potential contribution to the resting potential is −3.3 mV. If R_m were raised to 5000 Ω (e.g., by placing the membrane in Cl^--free solution, or by adding Ba^{2+} ion to decrease P_K, or both), then the calculated E_m would be −84.5 mV, i.e., much closer to V_{ep} (−85 mV). Modified from Sperelakis [3].

series with the pump (R_p) gives the circuit the feature that the observed pump potential contribution to E_m (ΔV) is a function of membrane resistance (R_m): the higher R_m is (R_p constant), the more nearly E_m approaches V_p. The pump battery is charged to some voltage by a pump current generator. If the pump is stopped by ouabain, the pump potential rapidly dissipates through R_m with a time constant of $(R_p + R_m)C_m$. If $V_p < E_{diff}$ (−80 mV), then E_m = −80 mV; i.e., the pump potential is masked by E_{diff}. If $V_p > E_{diff}$, then E_m is somewhere between E_{diff} and V_p. The exact E_m measured depends on the magnitude of V_p and on R_m. Using circuit analysis for the values of the parameters given in figure 3–8, E_m would be −83.3 mV, i.e., moderately close to the value of V_p (−85 mV) (table 3–2). If R_m is raised fivefold (to 5000 Ω), E_m would be −84.5 mV, i.e., closer to V_p (table 3–2). Thus, this circuit clearly gives a pump potential contribution to E_m that is dependent on R_m. Another way to state this is that the higher R_m is (relative to R_p), the more E_m reflects V_p, because of less short-circuiting of V_p by R_m. If E_{diff} is made smaller (e.g., in cells with a higher P_{Na}/P_K ratio or if E_K were lowered by the elevation of $[K]_o$), then the relative contribution of the pump potential to E_m becomes greater. For example, for the same values indicated in figure 3–8, if E_{diff} is changed from −80 mV to −50 mV, then E_m would be −76.7 mV (table 3–2); i.e., the ΔV is now much larger: 26.7 mV vs 6.7 mV (table 3–2). As expected, an increase of V_p (by stimulating the pump rate or by increasing the coupling ratio) hyperpolarizes (compare D and C in table 3–2), and the amount of hyperpolarization produced by an increase in V_p is greater when E_{diff} is smaller (compare H and D in table 3–2).

The physiologic importance of an electrogenic pump potential is not fully known for myocardial cells. Although small, the electrogenic pump potential contribution to the membrane resting potential could have significant effects on the level of inactivation of the fast Na^+ channels. Further, an electrogenic pump potential could act to delay depolarization under adverse conditions (e.g., ischemia and hypoxia), and would act to speed repolarization of the normal resting potential during recovery from the adverse conditions. It is crucial that the excitable cell maintain its normal resting potential as much as possible, because of the effect on the action potential's rate of rise

TABLE 3–2. Summary of calculations of resting potential (E_m) for a model having an electrogenic pump potential (V_p) in parallel with the net diffusion potential (E_{diff})

	E_{diff} (mV)	R_m (Ω-cm^2)	R_p (Ω-cm^2)	V_p (mV)	Resting E_m (mV)	ΔV ($E_m - E_{diff}$) (mV)
(1)	−80	1000	500	−85	−83.3	−3.3
(2)	−80	1000	500	−90	−86.7	−6.7
(3)	−80	1000	500	−80	−80.0	0
(4)	−80	1000	500	−70	−73.3	+6.7
(5)	−80	1000	500	0	−26.6	+53.4
(6)	−80	2000	500	−85	−84.0	−4.0
(7)	−80	4000	500	−85	−84.5	−4.5
(8)	−80	500	500	−85	−82.5	−2.5
(9)	−80	1000	1,000	−85	−82.5	−2.5
(10)	−75	1000	500	−85	−81.6	−6.6
(11)	−75	1000	1,000	−85	−80.0	−5.0

R_m = membrane resistivity; R_p = pump resistance; ΔV = contribution of V_p to the measured E_m. E_m was calculated from the following equation:

$$E_m = \frac{R_m}{R_m + R_p} V_p + \frac{R_p}{R_m + R_p} E_{diff}$$

Adapted from Sperelakis [3].

and conduction velocity with small depolarizations, and complete loss of excitability with larger depolarizations.

In cells in which there are lower resting potentials (e.g., vascular smooth muscle cells and cardiac nodal cells) (table 3–1), the electrogenic pump potential can be considerably larger. Sinusoidal oscillations in the Na-K pumping rate could produce oscillations in E_m, which could exert important control over the spontaneous firing of the cell. The period of enhanced pumping hyperpolarizes the cell and suppresses automaticity, whereas slowing of the pump leads to depolarization and consequently to triggering of action potentials. Oscillation of the pump may be brought about by changes in $[Na]_i$. For example, the firing of several APs should raise $[Na]_i$ (nodal cells have a small volume–surface area ratio) and stimulate the electrogenic pump. The increased pumping rate, in turn, hyperpolarizes and suppresses firing, thus allowing $[Na]_i$ to become lower again and removing the stimulation of the pump; the latter depolarizes and triggers spikes; and the cycle could be repeated. Noma and Irisawa [10] concluded that, in rabbit sinoatrial nodal cells, the electrogenic Na^+ pump might be one factor that modulates the heart rate under physiologic conditions. When stimulated at a high rate, cardiac Purkinje fibers and nodal cells undergo a transient period of inhibition of automaticity after cessation of the stimulation, known as overdrive suppression of automaticity. Stimulation of the electrogenic pump due to elevation in $[Na]_i$ is the major cause of this phenomenon [11, 12].

Pacemaker Potentials and Automaticity

In order to maintain a steady resting potential, the outward K^+ current must be equal and opposite to the inward Na^+ current (primarily Na^+ but also Ca^{2+}), assuming Cl^- is passively distributed. If the inward current exceeds the outward current, then the membrane will depolarize along a certain time course (i.e., slope of the pacemaker potential or diastolic or phase-4 depolarization), depending on the excess (or net) inward current. The inward leak of Na^+ and Ca^{2+} currents is often called the background inward current. For the inward current to exceed the outward current (i.e., for a net inward current), either the inward current can be increased or the outward current I_K can be decreased. Both of these mechanisms are used for genesis of pacemaker potentials (auto-

maticity). For example, if a time-dependent decrease in g_K occurs following an AP and hyperpolarizing afterpotential, then I_K decreases and the membrane depolarizes (g_{Na}/g_K progressively increases). Conversely, if an agent such as acetylcholine (ACh) were to increase the resting g_K, then the outward I_K is increased, the membrane hyperpolarizes, and the slope of the pacemaker potential decreases, thus reducing the frequency of firing. Some agents, such as norepinephrine, may increase the background inward current and decrease the outward current, thereby increasing the slope of the pacemaker potential by both mechanisms.

A prerequisite for automaticity is that the cells must have a relatively low Cl^- conductance (g_{Cl}). This condition holds true for all or most cell types in the heart. A high g_{Cl} acts to clamp E_m, making it difficult for a pacemaker potential to be developed. For example, addition of Ba^{2+} (0.5 m*M*) to frog sartorius muscle fibers, which have a high g_{Cl}/g_K ratio of about 4.0, has very little immediate effect. However, when the fibers are first equilibrated in Cl-free solution to reduce g_{Cl} to zero, Ba^{2+} produces a prompt depolarization, an increase in R_m, and automaticity [13]. Another way to view this effect of Cl^- is by Cole's [14] parallel capacitance–inductance (C_mL_m) circuit for an excitable membrane that tends to oscillate spontaneously when the R_{Cl} shunt resistance (and R_{Na}) is very high. The membrane inductance L_m arises because of the peculiar behavior of the K^+ resistance: namely, anomalous rectification. This rectifier causes an instantaneous decrease in g_K with depolarization or increase with hyperpolarization.

During the time course of the pacemaker potential V_p, R_m, increases progressively due to a decrease in g_K [15, 16]. There is a progressive turnoff of the g_K increase (delayed rectification) responsible for the rapid repolarizing phase of the AP and the subsequent hyperpolarizing ("positive") afterpotential usually exhibited by pacemaker cells. The decreasing g_K produces the depolarization. The pacemaker depolarization in heart cells is usually linear (or a ramp).

In some cases, heart cells can exhibit automaticity of another type, which is a large depolarizing afterpotential arising from the hyperpolarizing afterpotential [17]. The depolarizing afterpotential triggers the subsequent spike once the threshold potential (V_{th}) is reached. In this type of automaticity, each AP is triggered by the preceding one. Thus, a train of spikes can be turned off by simply stopping one spike in the train from developing (e.g., by a brief hyperpolarizing current pulse) [18, 19]. The depolarizing afterpotential is depressed by verapamil and is facilitated by cardiac glycosides [20, 21], thus tending to produce ectopic pacemaker activity.

All heart cells are capable of exhibiting automaticity under certain conditions. For example, ventricular cells placed into cell culture develop automaticity [16, 18]. Myocardial cells exposed to Ba^{2+} to decrease their g_K and depolarize them develop automaticity [18, 19, 22, 23]. Ventricular muscle depolarized by the application of current also fires spontaneously during the current pulse [16, 24–26]; that is, when E_m is brought into the voltage region that can develop pacemaker potentials, automaticity occurs. In any cardiac pacemaker cell, if the membrane potential is hyperpolarized by a current pulse, the frequency of spontaneous firing is slowed and stopped; that is, automaticity is suppressed at high resting potentials [16]. Conversely, application of depolarizing current increases the frequency of discharge. Thus, the slope of the pacemaker potential is exquisitely sensitive to small changes in E_m. The further E_m is above E_K (within limits), the greater the degree of automaticity (and of anomalous rectification). A low g_K, which also means a relatively lower resting E_m, facilitates automaticity. Elevation of $[K]_0$, which increases g_K although it depolarizes, suppresses automaticity [22, 27].

Under normal circumstances in the heart, the hierarchy of automaticity capability is: SA nodal cells > AV nodal cells > Purkinje fibers. Ventricular or atrial myocardial cells develop automaticity only under pathologic conditions such as regional ischemia. The genesis of automaticity in Purkinje fibers is somewhat different from that in nodal cells [28–30]. Normally the automaticity of the cells lower in the hierarchy (e.g., the Purkinje cells) is latent ("latent pacemakers") because the cells are driven at

higher rates by the primary pacemaker (SA node). Because of the phenomenon of overdrive suppression of automaticity (fast drives of a pacemaker cell tend to hyperpolarize the cell and cause a pause in automaticity after the drive is terminated), the latent pacemakers normally may be partly in a state of overdrive suppression. Thus, a pacemaker potential may or may not be seen during diastole. One factor in production of overdrive suppression is stimulation of the electrogenic Na^+ pump by the increase in $[Na]_i$ accompanying a high rate of driving [12, 31]. In addition, K^+ tends to accumulate extracellularly during the fast drive.

One characteristic of a pacemaker cell is that accommodation does not occur normally; the cell fires, no matter how slowly E_m is brought to the threshold potential V_{th}. This could reflect a homogeneous population of ionic channels with nearly identical voltage-sensitive gating, the low g_{Cl} (less clamping effect of Cl^-), and the decrease in g_K due to anomalous rectification. Little or no inactivation of slow channels occurs during the pacemaker depolarization because inactivation of slow channels occurs at less-negative potentials (between about -45 mV and -10 mV).

Automaticity of the heart (nodal cells) is normally under control of the autonomic nerves. The release of ACh from the parasympathetic nerves increases g_K and thereby hyperpolarizes (toward E_K) and depresses automaticity. ACh also depresses the inward slow current, which also would tend to depress automaticity (for references, see Josephson and Sperelakis [32]). The release of norepinephrine from the sympathetic nerves tends to increase the inward slow current and to decrease g_K (kinetics of turnon), both of which tend to enhance automaticity.

For a complete discussion of the electrogenesis of pacemaker potentials, the reader is referred to chapter 5.

Effect of Resting Potential on the Action Potential

Any agent that affects the resting potential (e.g., depolarizes) will have important repercussions on the cardiac AP. Depolarization reduces the rate of rise of the AP, and thereby also slows its velocity of propagation. A slow spread of excitation throughout the heart will interfere with the heart's ability to act as an efficient blood pump. This effect is progressive as a function of the degree of depolarization. If the myocardial cells and Purkinje fibers are depolarized to about -50 mV, then the rate of rise goes to zero and all excitability (and contraction) is lost, leading to cardiac arrest. Hyperpolarization usually produces only a small increase in rate of rise, and large hyperpolarizations may actually slow propagation velocity (because the critical depolarization required to bring the membrane to threshold is increased) or cause propagation block.

The explanation of the effect of resting E_m (or takeoff potential) on maximum rate of rise ($+\dot{V}_{max}$) of the AP is based on the sigmoidal h_∞ versus E_m curve. In Hodgkin–Huxley notation, h is the inactivation variable for the fast Na^+ conductance; it is a probability factor that deals with the open ($h = 1.0$) versus closed ($h = 0$) positions of the inactivation (I) gate of the channel (figs. 3–9 and 3–10). The value of h is a function of E_m and time *(t)*, and h_∞ is the h value at steady state or infinite time (practically, $t > 20$ ms). h_∞ is 0.9–1.0 at the normal resting potential (-80 mV) and diminishes with depolarization, becoming zero at about -50 mV. The I gates are open in a resting membrane and close slowly (time constant of several milliseconds) upon depolarization, thus inactivating the fast Na^+ conductance (figs. 3–9 and 3–10).

The slow channels in myocardial cells are similar to the fast Na^+ channels, except that their A gates and I gates operate much more slowly kinetically; that is, they turn on (activate) more slowly, turn off (inactivate) more slowly, and recover more slowly (figs. 3–9 and 3–10). In addition, their voltage inactivation curve is shifted to the right, so the inactivation begins at about -45 mV and is not complete until about 0 mV [33, 34]. The slow channels also have a lower activation (threshold) potential of about -35 mV (compared to about -60 mV for the fast Na^+ channels). When the fast Na^+ channels are either blocked by tetrodotoxin (TTX) or voltage-inactivated in ele-

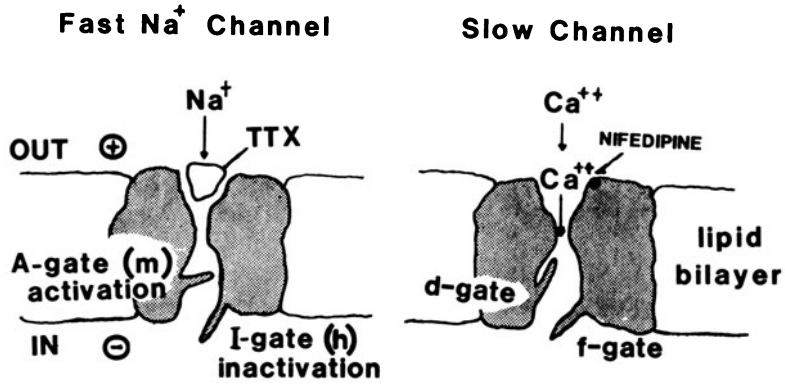

FIGURE 3–9. Cartoon models for a fast Na^+ channel *(left)* and for a slow channel *(right)* in myocardial cell membrane. As depicted, two gates are associated with each type of channel: activation (A) gate and inactivation (I) gate. Gates are presumably charged positively so that they can sense membrane potential. I gate moves more slowly than A gate. Gates of the slow channel are kinetically much slower than those of the fast Na^+ channel. The fast Na^+ channel is depicted in resting state (A gate closed, I gate open) and just beginning the process of activation, whereas the slow channel is depicted in the active state (both gates open) and just beginning the process of inactivation. Depolarization causes the A gate to open quickly so that the channel becomes conducting (active state). However, the I gate slowly closes during depolarization and inactivates the channel (inactive state). During recovery upon repolarization, the A gate closes and the I gate opens (returns to resting state). Not depicted is the hypothesis that protein constituent of the slow channel must be phosphorylated in order for the channel to be in a functional state available for voltage activation. Tetrodotoxin (TTX) blocks the fast Na^+ channel from the outside, presumably by binding in the channel mouth. Verapamil and Mn^{2+} block the slow channel. Redrawn from Sperelakis [43].

vated $[K]_0$ (25 m*M;* E_m of about -40 mV), positive inotropic agents, such as catecholamines or histamine, restore excitability in the form of slowly rising APs by increasing the number of slow channels available for voltage activation. The rate of rise of the slow AP is also dependent on the h_∞ variable (often termed the f_∞ variable for myocardial slow channels), with depression of $+\dot{V}_{max}$ beginning at -45 mV and going to zero at about -20 mV. (The apparent discrepancy between the E_m values at which $f_\infty = 0$ and at which $+\dot{V}_{max} = 0$ is due to failure of propagation occurring below a minimal inward slow current.) These relationships are depicted in figure 3–11.

The resting potential also affects duration of the cardiac AP. With polarizing current, depolarization lengthens the AP whereas hyperpolarization shortens it. In contrast, when elevated $[K]_0$ is used to depolarize the cells, the AP is usually shortened. (Under special conditions, such as Cl^--free solution, the AP may be prolonged with elevation of $[K]_0$ [30]). One important determinant of the AP duration is the K^+ conduction (g_K). Agents or conditions that increase g_K, such as elevation of $[K]_0$, tend to shorten the duration. In contrast, agents that decrease g_K or slow the activation of g_K, such as Ba^{2+} ion or tetraethylammonium ion (TEA^+), tend to lengthen the AP duration. Due to anomalous rectification (i.e., a decrease in g_K with depolarization and an increase with hyperpolarization), depolarization by current prolongs the AP and hyperpolarization shortens it.

Other factors are also important in determining the AP duration. For example, agents that slow the closing of the I gates of the fast Na^+ channels, such as veratridine, prolong the AP. Agents that affect the inward slow current (I_{si}) also affect the AP duration. Prolongation or stimulation of I_{si} tends to prolong the AP; conversely, agents that depress I_{si}, such as verapamil or Mn^{2+}, slightly shorten the AP. Agents that depress metabolism of the heart, such as valinomycin or hypoxia, primarily depress I_{si}

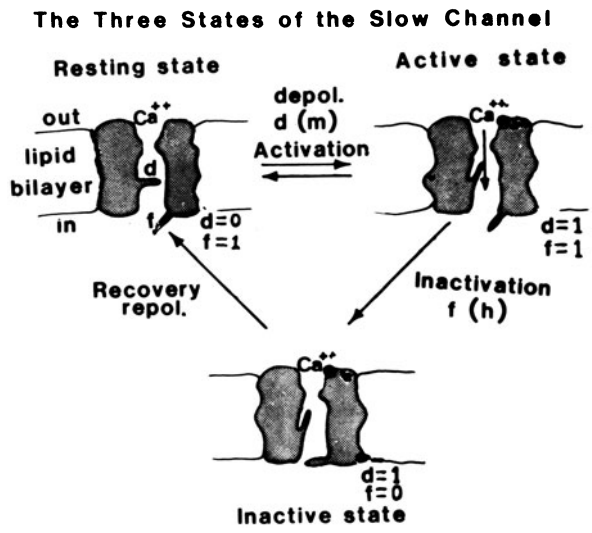

FIGURE 3–10. Cartoon model of the three states of the myocardial calcium slow channel, patterned after that for the Hodgkin–Huxley fast sodium channel. In the resting state, the activation (d) gate is closed and the inactivation (f) gate is open. In the active state, the d gate is open while the f gate is still open. In the inactivated state, the d gate remains open, but the f gate has closed. During the recovery process, the inactivated channel is reverted back to the resting state by closing of the d gate and opening of the f gate.

and the slow conductance g_s, but secondarily also act to turn on g_K earlier and so greatly abbreviate the cardiac AP [35–38].

Finally, the cardiac AP shortens markedly at high heart rates, and three factors could contribute toward this effect: (a) the increase in $[Ca]_i$ (resulting from increase in $[Na]_i$) produces an increase in resting g_K and enhances g_K activation kinetics (the Gardos–Meech effect) [39–41]; (b) K^+ accumulates outside the cell membrane, thereby increasing g_K; and (c) recovery of the slow channels is incomplete, thereby depressing I_{si}.

Potential Profile across Membrane

The cell membrane has fixed negative charges at its outer and inner surfaces. The charges are presumably due to acidic phospholipids in the bilayer and to protein molecules either embedded in the membrane (islands floating in the lipid bilayer matrix) or tightly adsorbed to the surface of the membrane. Most proteins have an acid isoelectric point, so that at a pH near 7.0 they possess a net negative charge. The charge at the outer surface of the cell membrane, with respect to the solution bathing the cell, is known as the zeta potential. This charge is responsible for the electrophoresis of cells in an electric field, the cells moving toward the anode (positive electrode), because unlike charges attract. The surface charge affects the true potential difference (PD) across the membrane, as illustrated in figure 3–12A. At each surface, the fixed charge produces an electric field that extends a short distance into the solution and causes each surface of the membrane to be slightly more negative (by a few millivolts) than the extracellular and intracellular solutions. The potential theoretically recorded by an ideal electrode as the electrode is driven through the solution perpendicular to the membrane surface should become negative as the electrode approaches within a few Angstrom units of the surface; that is, the potential difference between the membrane surface and the solution declines exponentially as a function of distance from the surface. The length constant is a function of the ionic strength (or resistivity) of the solution: the lower the ionic strength, the greater the length constant is.

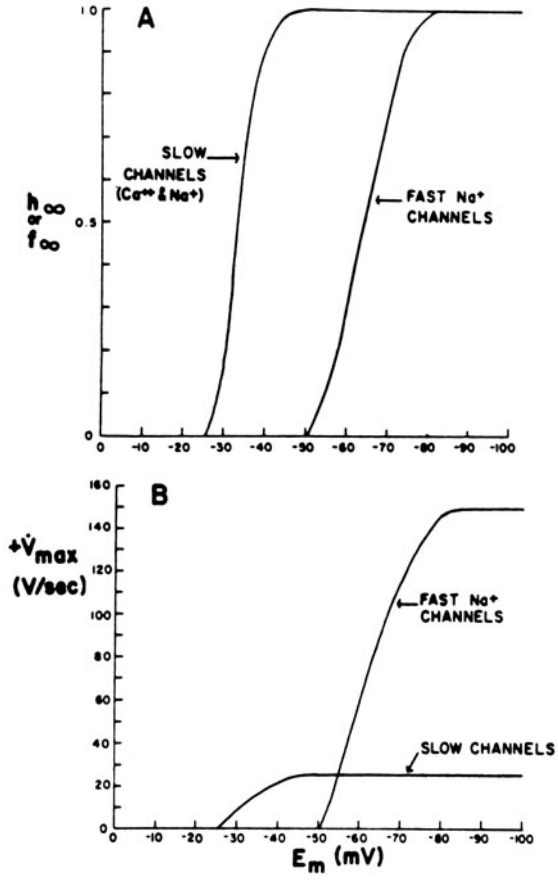

FIGURE 3–11. Graphic representation of differences in behavior, with respect to voltage inactivation, of the fast Na^+ channels and slow (Na^+ and Ca^{2+}) channels. *(A)* h_∞ inactivation factor of Hodgkin–Huxley ($g_{Na} = \bar{g}_{Na} m^3 h$, where g_{Na} is the Na^+ conductance, m and h are probability variables, and overbar means maximal) for fast Na^+ channels or the comparable f_∞ factor for slow channels as a function of resting potential (E_m). The h_∞ or f_∞ represents h or f at t = infinity or steady state (practically, after 20 ms for h and after 1 s for f). This graph illustrates that fast Na^+ channels of myocardial cells begin to inactivate at about −75 mV, and complete inactivation occurs at about −50 mV ($h = 0$). In contrast, slow channels inactivate between about −45 mV (f = about 1.0) and −25 mV ($f_\infty = 0$). *(B)* Maximal rate of rise of the action potential ($+\dot{V}_{max}$) as a function of resting E_m for the normal cardiac action potential (dependent on inward current through the fast Na^+ channels) and for the slow action potential (dependent on inward current through the slow channels) elicited in cells whose fast Na^+ channels are blocked (by TTX or by depolarization to about −45 mV). $^+\dot{V}_{max}$ is a measure of the inward current intensity (everything else, such as membrane capacitance, held constant), which in turn is dependent on the number of channels available for activation.

The magnitude of the PD depends on the density of charge sites (number per unit of membrane area); the number of charges is also affected by the ionic strength and pH.

In figure 3–12A, the membrane potential measured by an intracellular microelectrode (E_m) is the potential of the outer solution (ψ_0, the reference electrode) minus the potential of the inner solution (ψ_i, the active microelectrode): $E_m = \psi_0 - \psi_i$. The true PD across the membrane (E'_m), however, is really that PD directly across the membrane, as shown in the figure. If the surface charges at each surface of the membrane are equal, then $E'_m = E_m$. If the outer surface charge is decreased to zero by extra binding of cations, such as Ca^{2+}, then the membrane becomes slightly hyperpolarized ($E'_m > E_m$), although this is not measurable by the intracellular microelectrode (fig. 3–12B). Conversely, if the outer surface charge were restored, and if the inner surface charge were neutralized, then the membrane would become slightly depolarized ($E'_m < E_m$); again this change is not measurable by the microelectrode.

Because the membrane ionic conductances are controlled by the PD directly across the membrane (i.e., by E'_m, and not by E_m), changes in the surface charges (e.g., by drugs, ionic strength, or pH) can lead to apparent shifts in the threshold potential and in the E_m vs h_∞ curve. For example, elevated $[Ca]_0$ is known to raise the threshold potential (i.e., the critical depolarization required to reach electrical threshold), as expected from the small increase in E'_m that should occur. The apparent mechanical threshold (the E_m value at which contraction of muscle just begins) can also be shifted by a similar mechanism.

Summary

In this chapter most of the factors that determine or influence the resting potential of heart cells were discussed. The structural and chemical composition of the cell membrane was briefly examined and correlated with the membrane's resistive and capacitative properties. The factors that determine the intracellular ion concentrations in myocardial cells under steady-

state conditions were examined. These factors include the Na-K coupled pump, the Ca-Na exchange reaction, a sarcolemmal Ca pump, and the intracellular polyvalent macroelectrolytes. The Na-K pump is mediated by the membrane-bound (Na, K)-ATPase enzyme. This enzyme requires both Na^+ and K^+ for activity, and transports 3 Na^+ ions outward and usually 2 K^+ ions inward per ATP hydrolyzed. Cardiac glycosides are specific blockers of this transport ATPase. The Na-K pump is not directly related to excitability, but only indirectly related by its role in maintaining the Na^+ and K^+ concentration gradients (i.e., blockage of the pump does not produce an immediate large depolarization or cessation of action potentials and contractions). The Ca-Na exchange reaction seems to be carrier mediated and may be driven by the Na^+ electrochemical gradient; i.e., the energy for pumping out internal Ca^{2+} by this mechanism comes from the (Na, K)-ATPase. The Ca-Na exchange reaction exchanges one internal Ca^{2+} ion for two, three, or four external Na^+ ions.

The mechanism whereby the ionic distributions give rise to diffusion potentials was discussed, as were the factors that determine the magnitude and polarity of each ionic equilibrium potential. The equilibrium potential for any ion and the transmembrane potential determine the total electrochemical driving force for that ion, and the product of this driving force and membrane conductance for that ion determine the net ionic current or flux. The net ionic movement can be inward or outward across the membrane, depending on the direction of the electrochemical gradient.

The key factor that determines the resting potential—in the absence of any electrogenic pump potential contributions and for fixed ionic distributions—is the relative permeability of the various ions, particularly of K^+ and Na^+, i.e., the P_{Na}/P_K ratio (or g_{Na}/g_K ratio), as calculated from the Goldman constant-field equation. The major physiologic ions that have some effect on the resting potential or on the action potentials are K^+, Na^+, Ca^{2+}, and Cl^-. The Ca^{2+} electrochemical gradient has only a small direct effect on the resting potential, although low external Ca^{2+} can affect the permeabilities and conductances for the other

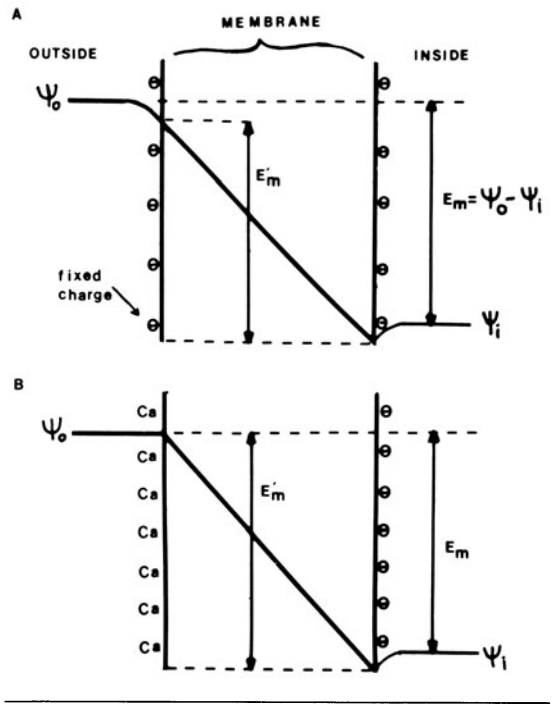

FIGURE 3–12. Potential profile across the cell membrane. *(A)* Because of fixed negative charges (at pH 7.4) at outer and inner surfaces of the membrane, there is a negative potential that extends from the edge of the membrane into the bathing solution on both sides of the membrane. This surface potential falls off exponentially with distance into the solution. Magnitude of the surface potential is a function of the charge density. ψ_o is the electrical potential of the outside solution, ψ_i is that of the inside solution, and membrane potential (E_m) is the difference ($\psi_o - \psi_i$). E_m is determined by the equilibrium potentials and relative conductances. Profile of the potential through the membrane is shown as linear (the constant-field assumption), although this need not be true for the present purpose. If the outer surface potential is exactly equal to that in the inner surface, then the true transmembrane potential (E'_m) is exactly equal to the (microelectrode) measured membrane potential (E_m). *(B)* If the outer surface potential is different from the inner potential, in this example done by elevating the extracellular Ca^{2+} concentration to bind Ca^{2+} to more of the negative charges, then the E'_m is greater than the measured E_m. Diminution of the inner surface charge decreases E'_m. The membrane ion channels are controlled by E'_m. From Sperelakis [3].

ions, such as Na^+ and K^+. (Elevation of internal Ca^{2+} can sometimes increase the permeability to K^+ by activating voltage-independent Ca^{++}-operated K^+-selective channels.) The Cl^- ion is passively distributed according to

the membrane potential, i.e., not actively transported. However, there is some evidence indicating that $[Cl]_i$ is about two or three times as great as that predicted according to the E_m, thus giving an E_{Cl} value of about -35 to -50 mV compared to a resting potential of about -80 mV. Before one can conclude that there is a Cl^- pump directed inward, however, the calculated E_{Cl} (concentrations corrected for activity coefficients) must be proved to be significantly more positive than the mean resting potential of the cell averaged over a period of time; i.e., for example, any spontaneous action potentials must be taken into account. If Cl^- is passively distributed, it cannot determine the resting potential. But transient net movements of Cl^- ions, e.g., during the action potential, can and do affect the E_m, particularly when g_{Cl} is high.

The elevation of $[K]_0$ to more than the normal concentration of about 4 m*M* decreases the K^+ equilibrium potential (E_K) as predicted from the Nernst equation ($[K]_i$ about constant), and depolarization is produced. Sometimes, however, some hyperpolarization is produced at a $[K]_0$ level between 5 and 10 m*M*. In addition, lowering $[K]_0$ to values of 1.0–0.1 m*M* often produces a prominent depolarization. These effects are usually explained on the basis that: (a) g_K is a function of P_K and $[K]_0$, (b) P_K is lowered in low $[K]_0$ and elevated in higher $[K]_0$, and (c) an electrogenic Na-K pump potential is inhibited at a low $[K]_0$.

The resting potential not only is the potential energy storehouse that is drawn upon for propagation of the action potentials, but because the membrane voltage-dependent cationic channels are inactivated with sustained depolarization, the rate of rise of the action potential, and hence propagation velocity, are critically dependent on the level of the resting potential. For example, a small elevation of K^+ concentration in the blood has dire consequences for functioning of the heart.

The Na-K pump can be electrogenic, depending on the coupling ratio of Na^+ pumped out to K^+ pumped in and depending on the magnitude of the membrane resistance. The electrogenic pump potential may be in parallel to the net ionic diffusion potential (E_{diff}, determined by the ionic equilibrium potentials and by the relative permeabilities). The contribution of the electrogenic pump potential to the measured resting potential of myocardial cells is generally small (only a few millivolts) so that the immediate depolarization produced by complete Na-K pump stoppage with cardiac glycosides is only a few millivolts. Of course, long-term pump stoppage produces a larger and larger depolarization as the ionic gradients are dissipated. The rate of Na-K pumping, and hence the magnitude of the electrogenic pump contribution to E_m, is controlled by $[Na]_i$ and by $[K]_0$, among other factors. The electrogenic pump potential might be physiologically important to the heart under certain conditions that tend to depolarize the cells, such as transient ischemia or hypoxia. In such cases, the actual depolarization produced may be less because of a constant pump potential in parallel with diminishing E_{diff}. The electrogenic pump potential may also affect automaticity of the nodal cells.

References

1. Jain MK: The bimolecular lipid membrane: a system. New York: Van Nostrand, 1972.
2. Henn FA, Sperelakis N: Stimulative and protective action of Sr^{2+} and Ba^{2+} on (Na^+, K^+)-ATPase from cultured heart cells. Biochem Biophys Acta 163:415–417, 1968.
3. Sperelakis N: Handbook of physiology. Berne RM, Sperelakis N (eds) Vol 1: The cardiovascular system. Bethesda: American Physiological Society, 1979, pp 187–267.
4. Dhalla NS, Ziegelhoffer A, Hazzow JA: Regulatory role of membrane systems in heart function. Can J Physiol Pharmacol 55:1211–1234, 1977.
5. Jones LR, Maddock SW, Besch HR Jr: Unmasking effect of alamethicin on the (Na^+, K^+)-ATPase, beta-adrenergic receptor-coupled adenylate cyclase, and cAMP-dependent protein kinase activities of cardiac sarcolemmal vesicles. J Biol Chem 255:9971–9980, 1980.
6. Daniel EE, Kwan CY, Matlib MA, Crankshaw D, Kidwai A: Characterization and Ca^{2+}-accumulation by membrane fractions from myometrium and artery. In: Casteels R, Godfraind T, Ruegg JC (eds) Excitation–contraction coupling in smooth muscle. Amsterdam: Elsevier/North-Holland, 1977, pp 181–188.
7. Glitsch HG: Activation of the electrogenic sodium pump in guinea-pig auricles by internal sodium ions. J Physiol (Lond) 220:565–582, 1972.
8. Page E, Storm SR: Cat heart muscle in vitro. VIII.

Active transport of sodium in papillary muscles. J Gen Physiol 48:957–972, 1965.
9. McDonald TF, MacLeod DP: Maintenance of resting potential in anoxic guinea pig ventricular muscle: electrogenic sodium pumping. Science 172:570–572, 1971.
10. Noma A, Irisawa H: Electrogenic sodium pump in rabbit sinoatrial node cell. Pflugers Arch Eur J Physiol 351:177–182, 1974.
11. Vassalle M: Electrogenic suppression of automaticity in sheep and dog Purkinje fibers. Circ Res 27:361–377, 1970.
12. Pelleg A, Vogel S, Belardinelli L, Sperelakis N: Overdrive suppression of automaticity in cultured chick myocardial cells. Am J Physiol 238:H24–H30, 1980.
13. Sperelakis N, Schneider M, Harris EJ: Decreased K^+ conductance produced by Ba^{++} in frog sartorius fibers. J Gen Physiol 50:1565–1583, 1967.
14. Cole KS: Membranes, ions and impulses: a chapter of classical biophysics. Berkeley: University of California, 1968.
15. Trautwein W, Kassebaum DG: On the mechanism of spontaneous impulse generation in the pacemaker of the heart. J Gen Physiol 45:317–330, 1961.
16. Sperelakis N, Lehmkuhl D: Effect of current on transmembrane potentials in cultured chick heart cells. J Gen Physiol 47:895–927, 1964.
17. Sperelakis N, Lehmkuhl D: Effects of temperature and metabolic poisons on membrane potentials of cultured heart cells. Am J Physiol 213:719–724, 1967.
18. Sperelakis N: Electrophysiology of cultured chick heart cells. In: Sano T, Mizuhira V (eds) Electrophysiology and ultrastructure of the heart.
19. Sperelakis N: (Na^+,K^+)-ATPase activity of embryonic chick heart and skeletal muscles as a function of age. Biochem Biophys Acta 266:230–237, 1972.
20. Ferrier GR, Moe GK: Effects of calcium on acetylstrophanthidin-induced transient depolarizations in canine Purkinje tissue. Circ Res 33:508–515, 1973.
21. Kass RS, Tsien RS, Weingart R: Ionic basis of transient inward current induced by strophanthidin in cardiac Purkinje fibres. J Physiol (Lond) 281:209–226, 1978.
22. Sperelakis N, Lehmkuhl D: Ionic interconversion of pacemaker and nonpacemaker cultured chick heart cells. J Gen Physiol 49:867–895, 1966.
23. Hermsmeyer K, Sperelakis N: Decrease in K^+ conductance and depolarization of frog cardiac muscle produced by Ba^{++}. Am J Physiol 219:1108–1114, 1970.
24. Katzung BG: Effects of extracellular calcium and sodium on depolarization-induced automaticity in guinea papillary muscle. Circ Res 37:118–127, 1975.
25. Imanishi S, Surawicz B: Automatic activity in depolarized guinea pig ventricular myocardium. Circ Res 39:751–759, 1976.
26. Reuter H, Scholz H: The regulation of the calcium conductance of cardiac muscle by adrenaline. J Physiol (Lond) 264:49–62, 1977.
27. Vassalle M: Cardiac pacemaker potentials at different extra- and intracellular K concentrations. Am J Physiol 208:770–775, 1965.
28. Noble D: Initiation of the heartbeat. Oxford: Clarendon, 1975.
29. Irisawa H: Comparative physiology of the cardiac pacemaker mechanism. Physiol Rev 58:461–498, 1978.
30. Carmeliet E, Vereecke J: Electrogenesis of the action potential and automaticity. In: Berne RM, Sperelakis N (eds) Handbook of physiology. Bethesda: American Physiological Society, 1979, pp 269–334.
31. Vassalle M: Electrogenic suppression of automaticity in sheep and dog Purkinje fibers. Circ Res 27:361–377, 1970.
32. Josephson I, Sperelakis N: On the ionic mechanism underlying adrenergic–cholinergic antagonism in ventricular muscle. J Gen Physiol 79:69–86, 1982.
33. New W, Trautwein W: Inward membrane currents in mammalian myocardium. Pflugers Arch 334:1–23, 1972.
34. McDonald TF, Trautwein W: Membrane currents in cat myocardium: separation of inward and outward components. J Physiol 274:193–216, 1978.
35. McDonald TF, MacLeod DP: Metabolism and the electrical activity of anoxic ventricular muscle. J Physiol 229:559–582, 1973.
36. Schneider JA, Sperelakis N: The demonstration of energy dependence of isoproterenol-induced transcellular Ca^{2+} current in isolated perfused guinea pig hearts—an explanation for mechanical failure of ischemic myocardium. J Surg Res 16:389–403, 1974.
37. Sperelakis N, Schneider JA: A metabolic control mechanism for calcium ion influxes that may protect the ventricular myocardial cell. Am J Cardiol 37:1079–1085, 1976.
38. Vluegels A, Carmeliet E, Bosteels S, Zaman M: Differential effects of hypoxia with age on the chick embryonic heart. Pflugers Arch 365:159–166, 1976.
39. Meech RW: Intracellular calcium injection causes increased potassium conductance in Aplysia nerve cells. Comp Biochem Physiol 42A:493–499, 1972.
40. Isenberg G: Is potassium conductance of cardiac Purkinje fibres controlled by $[Ca^{2+}]_i$? Nature (Lond) 253:273–274, 1975.
41. Bassingwaighte JB, Fry CH, McGuigan JAS: Relationship between internal calcium and outward current in mammalian ventricular muscle: a mechanism for the control of the action potential duration? J Physiol 262:15–37, 1976.
42. Singer SJ, Nicolson GL: The fluid mosaic model of the structure of cell membranes. Science 175:720–731, 1972.
43. Sperelakis N: Changes in membrane electrical properties during development of the heart. In: Zipes DP, Bailey JC, Elharrar V (eds) The slow inward current and cardiac arrhythmias. The Hague: Martinus Nijhoff, pp 221–262, 1980.

4. THE IONIC BASIS OF ELECTRICAL ACTIVITY IN THE HEART

Robert S. Kass

Introduction

Cardiac muscle, like skeletal muscle and nerve, belongs to a class of tissues referred to as excitable cells. This classification reflects the ability of these cells to propagate impulses in a regenerative manner. The electrical activity of nerve and skeletal muscle is rather uniform and is generated by similar ionic mechanisms. In contrast, the electrical activity in different regions of the heart consists of clearly distinguishable action potentials. This diversity of action potential configuration reflects the multiple roles of electrical activity in the heart. Despite regional differences, however, these electrical impulses are generated by membrane permeability mechanisms that generally resemble those in other excitable cells.

This chapter presents a review of the major ionic currents in the heart and relates these currents both to the electrical activity of different regions and to some of the characteristic roles of this activity. Emphasized are time-dependent currents that have been studied in various mammalian cardiac cells. It is not intended to be a detailed review of each of these currents, but instead a source from which the reader may then pursue selected areas in more detail.

Excitation in the Heart

NORMAL SPREAD OF THE IMPULSE: ROLES OF SPECIALIZED TISSUE

Electrical impulses in excitable cells are generated by local changes in the relative permeabilities of the surface membranes of these cells to various ions (see chapter 3). These local permeability changes, in turn, regulate the electrical potential difference across the surface membrane through the electrochemical potential differences of the permeant ions. As a consequence of these local changes in membrane potential, voltage gradients are established both across the cell membrane and between local and distal longitudinal sites. These gradients force the movement of intracellular and extracellular ions. Ionic currents in combination with the cable properties (see chapter 6) and morphology of different regions of the heart are responsible for the orderly pattern of cardiac excitation and contraction. This process depends on the unique electrical properties that have evolved for tissues that carry out specialized functions.

Electrical activity begins at the sinoatrial (SA) node, a strip of fine muscle fibers near the junction of the superior vena cava and the right atrium. The SA node generates electrical activity in a cyclic pattern, depolarizing and repolarizing spontaneously. The process of spontaneous depolarization is known as pacemaker activity. This region is not the only cardiac tissue that has this property (fig. 4–2), but it beats at the fastest rate and is thus the dominant pacemaker in the heart under normal conditions. In several pathologic states, impulses from the SA node may not reach other regions of the heart consists of clearly distinguishable action potentials. This diversity of action podrive the heart at a much lower than normal rate.

Under normal conditions, the impulse spreads rapidly from the SA node throughout the atrial muscle, where conduction is aided by

N. Sperelakis (ed.), PHYSIOLOGY AND PATHOPHYSIOLOGY OF THE HEART.

Martinus Nijhoff Publishing, Boston/The Hague/ Dordrecht/Lancaster.

special conducting tissue that resembles ventricular Purkinje fibers [1]. Electrical activity in the atrium is conducted into the ventricles through the atrioventricular (AV) node, a small strip of fine fibers that connects ventricular and atrial tissue. The small size of this tissue along with its electrical properties results in very slow impulse propagation through this node (typically on the order of 0.2 m/s). This slow AV nodal conduction ensures an adequate delay between atrial and ventricular contraction that is essential to proper filling and pumping of the ventricles.

From the AV node, the impulse is then conducted by specialized conducting tissue, the Purkinje fibers. In contrast to AV nodal tissue, Purkinje fibers consist of bundles of large cells that are well suited for rapid impulse conduction. Conduction velocity in the Purkinje network is on the order of 5 m/s (more than ten times the velocity in the AV node) and this ensures that the impulse spreads rapidly and uniformly throughout the ventricles. This rapid excitation of the ventricular muscle cells results in nearly synchronous contraction of these cells and a uniform pumping action on the blood in the ventricular chambers. When Purkinje fiber conduction is slowed in diseased states, ventricular ejection is compromised due to the loss of synchrony in the contraction of individual muscle cells (see chapters 19–21 and Noble [2] and Cranefield [3]).

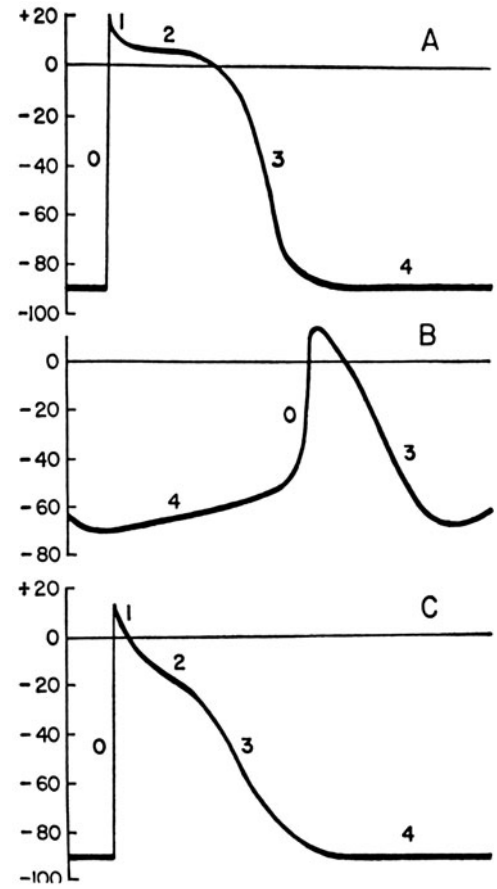

FIGURE 4–1. Representative schematic records of transmembrane action potentials recorded from ventricular muscle *(A)*, sinoatrial node *(B)*, and atrial muscle *(C)*. The vertical scale is in millivolts. From Hoffman and Cranefield [4].

CARDIAC ACTION POTENTIALS

As already suggested in the previous section, the distinct functional roles of electrical activity in each of these regions are closely related to the differences that have been found in the action potentials recorded in each area.

NODAL TISSUE

An example of electrical activity recorded from an SA nodal preparation is shown in figure 4–1. The duration of this action potential, and all other cardiac action potentials, is very long (on the order of 100 ms). The SA node shows spontaneous activity. The membrane potential changes from a negative value (near −65 mV) to a value greater than 0 mV and then returns (repolarizes) to the negative potential where the cycle is repeated. Because the SA node determines heart rate, the slow change toward positive potentials (depolarization) occurring between beats is called the pacemaker depolarization. The most negative potential reached in this action potential is near −65 mV, a value much more positive than resting potentials of nerve or skeletal muscle. However, because the SA node is spontaneously active, it is not proper to refer to this as a resting potential. Instead the term "maximum diastolic" potential (MDP) is used to characterize this part of the nodal action potential. Another characteristic of this action potential is its maximum rate of depolarization. This rate, on the

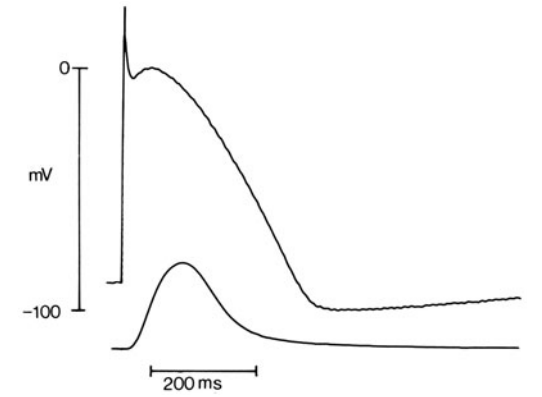

FIGURE, 4–2. Action potential and associated twitch tension in isolated Purkinje fiber. The *upper trace* is an intracellular recording of membrane potential obtained in an isolated Purkinje fiber that was driven by an external stimulus. Note the slow pacemaker activity following repolarization of the action potential. The *lower trace,* obtained using an optical monitor of contractions, shows the phasic tension developed by this fiber during the action potential. R.S. Kass and D. Krafte, unpublished data.

order of 10 V/s, reflects the magnitude of the current that generates the voltage change (see eq. 4.4).

Electrical activity of cells in the AV node resembles that of the SA node, except that pacemaker activity is less pronounced (see Hoffman and Cranefield [4]). Thus, like SA nodal fibers, the maximum rate of rise of the action potential is on the order of 10 V/s, and MDP is around −60 mV.

PURKINJE FIBERS

Cells in Purkinje fiber bundles often also show some pacemaker activity (fig. 4–2), but this is much slower than pacing in the SA node. The Purkinje fiber MDP is much more negative (−90 mV) and the maximum rate of depolarization is much greater (500 V/s) than comparable parameters of the nodes. These differences are not entirely independent of each other and suggest the possibility that these action potentials are generated by two distinct mechanisms.

In the action potential shown, the membrane rapidly returns to approximately 0 mV following the initial depolarization. This rapid phase of repolarization seems to be most prominent in the Purkinje fiber (see *Calcium-activated currents*). After this rapid repolarization, there is a long-lasting phase of the action potential where the membrane potential remains near −20 mV to 0 mV with only a very slow repolarization evident. This is the plateau phase of the action potential. It is maintained by a delicate balance of small ionic currents and is easily altered by conditions such as drive rate or temperature.

ATRIAL AND VENTRICULAR MUSCLE

Like the Purkinje fiber, the most negative potential reached in these cells is near −90 mV, but under normal conditions these cells do not show pacemaker activity (fig. 4–1). The term "resting potential" is appropriate in describing these negative potentials. Neither atrial nor ventricular muscle cells have a rapid repolarization phase following the initial upstroke, but both have plateau phases of various shapes. Also, the maximum rate of rise of the rapid upstrokes of these cells resembles that of the Purkinje fiber.

Action potentials in the heart are the result of a complex interaction of several ionic currents. Regional differences in electrical activity often result from the varying contributions of different currents. The next section discusses measurement of cardiac ionic currents and identification of some key current components that characterize electrical activity of the different anatomic regions.

Electrical Analogues: Equivalent Circuits

The mathematical description of impulse conduction based on local currents in nerve [5] is basically the same formalism originally developed by Kelvin to describe transmission of electrical signals along submerged telegraph cables and is thus referred to as "cable theory". In addition to describing impulse conduction, cable theory provides the foundation upon which methods for measuring membrane currents in excitable cells are built. The cable properties of heart tissue are presented in more detail in chapter 6, but some of the consequences of these properties will be briefly discussed here in the context of ionic current measurement.

One of the simplest and oldest biophysical representations of the permeability properties of cell membranes is the linear (ohmic) equivalent circuit. This circuit corresponds to the lumped electrical properties of local patches of membrane. It consists of membrane capacitance (C_m) and ionic conductances that provide pathways for transmembrane movement of permeant ions. Although such a model does not provide insight into how ions actually move across membranes [6], it is extremely useful in studying both the cable properties and the electrical responses of excitable cells.

Membrane structure accounts for the membrane capacitance [2], which is fairly constant in most biologic membranes ($\sim 1\ \mu F\ cm^{-2}$). Charge must be added to one side of the cell membrane and subtracted from the other in order to change the voltage across the membrane capacitance, as is the case for any two conducting surfaces that form a capacitor. This charge movement comprises a displacement, or capacity, current that is related to the rate of change in voltage across the membrane capacitance (C_m) as follows:

$$I_c = C_m dV_m/dt \tag{4.1}$$

According to this expression, membrane potential (V_m) will not change if there is no change in charge across the membrane capacitance. This equation also shows that, when there is capacity current, the rate of change of voltage is proportional to the magnitude of the current flowing into and out of the capacitor's conducting surfaces.

A region of membrane is referred to as "active" when the permeability to one or more ions suddenly increases in this region. Then, positively charged ions move down their electrochemical gradients through open channels. This excitatory inward current adds positive charge to the inner surface of the cell membrane and thus leads to local depolarization. Intracellularly a longitudinal voltage difference is established between this depolarized region and more distant regions still at rest. This voltage drop forces ion movement (mostly K^+) from active to passive areas and sets up the local circuit currents that spread the depolarization.

At each patch of membrane, the total transmembrane current (I_m) divides between capacity current (that changes the voltage across the membrane) and ionic current (I_i) that flows through the conductive pathways shunting the membrane capacitance. Total membrane current is thus the sum of these two components:

$$I_m = I_i + I_c \tag{4.2}$$

or, using equation 4.1 for I_c,

$$I_m = I_i + C_m dV_{m/dt} \tag{4.3}$$

Measurement of Ionic Current

Two important experimental conditions can be imposed to simplify equation 4.3 and permit analysis of membrane current. In one case, longitudinal voltage gradients are considerably reduced, and that minimizes local circuit currents. In the squid axon, this can be accomplished by short-circuiting the axon interior with an intracellular, low-resistance, axial electrode. This condition has been termed "space clamp" and active electrical activity measured under space-clamp conditions is called a "membrane action potential". In this case the net transmembrane current must be zero, and equation 4.3 simplifies to

$$C_m dV/dt = -I_{ionic} \tag{4.4}$$

Although the multicellular nature of heart muscle precludes the experimental simplification used in nerve, equation 4.4 can be applied to small isolated cardiac preparations. Then, under conditions approximating zero longitudinal current, equation 4.4 can be used to estimate net ionic current from time-dependent changes in membrane potential. However, this approach must be used with caution as it is restricted by frequency-dependent changes in membrane capacity [7, 8] as well as nonlinear characteristics of cardiac currents [9].

Another simplification of equation 4.3 occurs when membrane potential is measured and experimentally controlled by passing current from an intracellular current source. This technique is referred to as "voltage clamp". Since

voltage is controlled, capacity current (excluding brief transients) is eliminated, and the total applied current (which is measured) becomes transmembrane ionic current (I_i). Once again this requires uniform voltage control, a condition which can be attained in squid axon with axial wire arrangements, but only approximated in multicellular cardiac preparations. Several recent advances, however, have improved the reliability of cardiac voltage-clamp measurements. These include the computation of limiting properties of multicellular heart preparations [10] and the introduction of single isolated cardiac cells that can be voltage clamped [11].

The Ionic Basis of Cardiac Electrical Activity

SOME BASIC NOMENCLATURE

Before discussing the ionic basis of cardiac electrical activity, it will be useful to review some basic concepts that are used in descriptions of ionic currents. From the preceding section (eq. 4.4), it is clear that, under experimental conditions that minimize impulse propagation (space clamp), the rate of change of membrane potential is given by the magnitude and direction of the total ionic current flowing across the membrane. By convention, negative current (inward movement of positive charge) depolarizes the membrane and thus produces a positive dV_m/dt. Total membrane current generally is the summation of several component ionic currents, and it is the experimenter's goal to characterize each current component. Each current is described as the product of a conductance (G_i) and a driving force ($V_m - V_i$):

$$I_i = G_i \times (V_m - V_i) \tag{4.5}$$

where V_i is the equilibrium potential for a given channel (see chapter 3) and E_m is membrane potential. In general, the conductance G_i may be a function of membrane potential and time.

Ions move across membranes through channels that can discriminate between possible charge carriers. The relative permeability of a channel to various ions, the channel selectivity, is reflected in the equilibrium potential. This is the potential of zero *net* current through the channel, and it is a function of the transmembrane concentration gradients of the permeant ions.

TWO INWARD CURRENTS IN THE HEART

Action potentials in the heart may be divided into two general groups based on rate of depolarization. In one group (atrial and ventricular muscle, Purkinje fibers), the action potentials are characterized by very rapid (500 V/s) upstrokes; whereas in the second group (SA and AV nodal fibers), the action potential rises with a markedly slower upstroke (10 V/s). Using equation 4.4 as a guide, this contrast in upstroke velocity suggests that the regenerative inward current in the nodes might be much smaller than in other cardiac tissues. Another distinction between these groups is the voltage range from which these upstrokes emerge. The nodal tissues are activated over a considerably more positive voltage range than the other cardiac preparations.

These two observations provide clues to the existence of two inward currents in cardiac cells which may be distinguished both by the voltage range over which they contribute to ionic current and by the differences in their sizes. Considerable experimental evidence now supports this view and provides several criteria for distinguishing these excitatory currents. One current, carried by sodium ions, resembles regenerative sodium current in nerve and skeletal muscle and is responsible for the rapid upstroke and fast impulse conduction in atrial and ventricular muscle as well as the special conducting tissue. A second current, carried principally by calcium ions, generates the nodal upstroke, underlies slow impulse conduction in the AV node, and maintains the plateau phase of the action potential in other parts of the heart.

Sodium Current. The upstroke of the action potential of working cardiac muscle and cells of the specialized conducting tracts, like action potentials in nerve and skeletal muscle, is due to a transient increase in membrane permeabil-

ity to sodium ions. The very rapid rates of rise of the action potentials in these tissues predict (from eq. 4.4), that the current responsible for these voltage changes is large (about 1 mA/cm^2).

Before the introduction of preparations that were suitable for voltage-clamp analysis of large inward cardiac currents [10–12], experiments on the upstroke and overshoot of the Purkinje fiber action potential demonstrated the sodium dependence of these parameters [13]. Later, this same approach was used to probe the gating mechanisms of this channel [14] and to study interactions of calcium ions and some local anesthetics on them [15].

Sodium currents have now been studied under voltage clamp in several cardiac preparations [11, 12, 16–18]. These currents appear similar to sodium currents in nerve and skeletal muscle. When the cell membrane is depolarized beyond −65 mV, an inward current is initiated that rises to a peak and then declines within a few milliseconds (fig. 4–3A). As in other excitable cells, this current is described as current flow through channels regulated by time- and voltage-dependent activation and inactivation gates. At a particular time and voltage, the fraction of open sodium channels is determined by the product of the activation and inactivation gating parameters. The steady-state voltage dependence of these parameters obtained in the rabbit Purkinje fiber is given in figure 4–3B.

As this product is zero at all potentials in figure 4–3B, these curves predict that the sodium conductance must also be zero in the steady state. These data were obtained at low temperatures. However, at more physiologic temperatures, there appears to be a region of overlap of these two parameters that results in a "window" of steady-state sodium current over the plateau voltage range [19–21]. This current accounts for the effects of tetrodotoxin (TTX) and sodium removal on the cardiac action potential plateau [22, 23].

Membrane potential affects the fraction of sodium channels that are open and thus determines the number of sodium channels available for impulse conduction. In the plateau potential range (fig. 4–3B), most of these channels

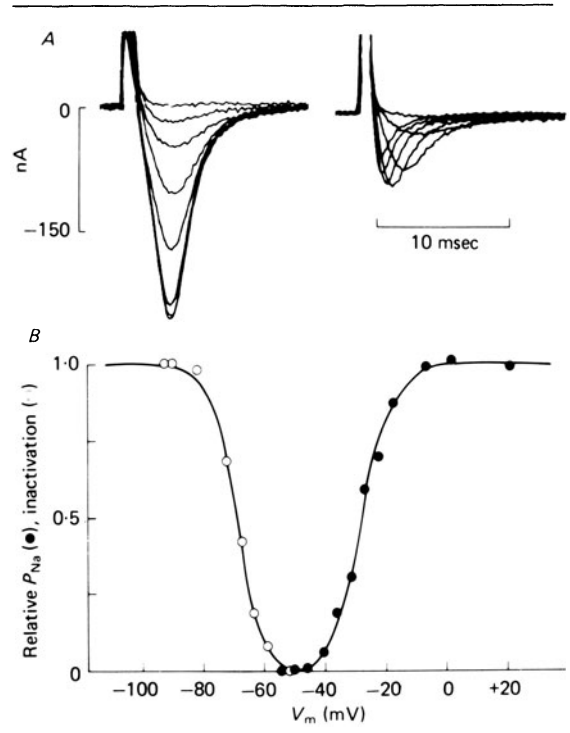

FIGURE 4–3. Sodium current in the rabbit Purkinje fiber. *(A)* Families of total membrane current obtained using conventional protocols for inactivation (left) and permeability (right). The inactivation curve was measured at a constant test pulse voltage (−38 mV) following 500-ms prepulses. Permeability was measured from peak inward currents measured at various test pulses from a −58-MV holding potential. *(B)* Voltage dependence of relative sodium current inactivation (o) and permeability (●). Data from Colatsky [16].

are closed (inactivated). The time course of removal of sodium channel inactivation at diastolic potentials determines the availability of these channels for impulse conduction and consequently the periods in which the cells remain inexcitable (refractory). Sodium channels in the heart thus resemble sodium channels in other excitable cells in their voltage dependence and sensitivity to local anesthetic drugs. But some clues such as a distinctly low TTX sensitivity as well as voltage-dependent TTX block [24] suggest that cardiac sodium channels may display marked differences from those of other cells. This interesting possibility is one example of the important questions presently being

investigated using voltage-clamp analysis of sodium currents in the heart.

Calcium Current

ACTION POTENTIAL EXPERIMENTS. The action potential of the Purkinje fiber or of working myocardial muscle can be made to resemble electrical activity of the SA or AV nodes by a variety of experimental conditions that depolarize the cells. Then, the Purkinje fiber action potential is characterized by a very slow upstroke (about 10 V/s) and conduction velocity (0.1–0.01 m/s). Consequently, it is referred to as a slow-response action potential [3, 25]. Characteristics of the slow response are discussed in chapter 8.

The current which generates the slow response is now referred to as the slow inward current (I_{si}). It is carried principally by calcium ions and is as much as 100 times smaller than peak sodium currents. In addition to the slow response, it underlies impulse conduction in nodal tissue [26, 27] and is crucial to maintenance of the plateau phase of action potentials of myocardial and special conducting tissues [28, 29].

VOLTAGE-CLAMP STUDIES OF I_{si}. Voltage-clamp investigations in Purkinje fibers [30, 31] and other preparations [32–34] demonstrated the existence of a calcium-sensitive inward current (Is_i). This current has many of the properties suggested by slow-response experiments: it is enhanced by catecholamines and blocked by Mn^{2+} and other metallic cations, and it has a voltage dependence distinct from I_{Na}.

In intact preparations, I_{si} has been analyzed by Reuter, Trautwein and others (see Reuter [35] for review). More recently, this current has been measured in isolated single-cell cardiac preparations [36–39] and in patches of membrane obtained from cultured heart cells [40]. It is described analogously to the sodium current as current through a gated channel:

$$I_{si} = \overline{G}_{si} * d * f * (V_m - V_{si}) \qquad (4.6)$$

$\overline{G}_{si}$ is the conductance when all I_{si} channels are fully open, d is the activation parameter, f, the inactivation parameter, and V_{si} is the equilibrium potential. The voltage dependence and kinetics of these gating parameters differ from those of the sodium channel and account for the properties of calcium-dependent upstrokes. As suggested by the slow-response data, the voltage range of I_{si} inactivation is so different from I_{Na} inactivation that calcium current can be activated from potentials at which the sodium current is almost completely inactivated.

Examples of calcium channel current recorded from calf Purkinje fiber and rabbit SA nodal preparations are shown in figure 4–4. Comparison of the records shows that calcium current is quite similar in both cell types as it apppears to be in each of the cardiac preparations in which it has been measured (for recent reviews, see Hagiwara and Byerly [41] and Tsien [42]).

Reuter and Scholz [43] found that I_{si} channels are not perfectly selective for calcium ions. They found that Na or K ions also move through this channel, but are approximately 100 times less permeant than calcium. Lee and Tsien [39] have confirmed that K ions move through this channel in isolated rat ventricular cells, thus linking properties of cardiac channels to those of other excitable cells [41, 42].

PHARMACOLOGY AND SENSITIVITY TO NEUROHORMONES. Calcium channels are not blocked by tetrodotoxin, but instead are inhibited by a rather diverse group of compounds. This group includes the metalic cations La^{3+}, Mn^{2+}, Co^{2+}, and Ni^{2+} as well as several organic agents such as D600, verapamil, nifedipine, nisoldipine, and diltiazem. Although each of these agents blocks calcium channel current (see fig. 4–4A), investigations are beginning to reveal differences in their specificities and modes of action [39, 44, 45].

Calcium current in the heart is modulated by neurohormones. It is decreased by muscarinic agents [46, 47] and increased by catecholamines [48]. Reuter and Scholz [49] have suggested that the principal action of epinephrine on I_{si} is to increase the maximal conductance ($\overline{G}_{si}$) of this channel. This can occur either by increasing the maximal conductance of each I_{si} channel or by creating more channels, each with a constant single-channel conductance. These investigators suggested the former, but

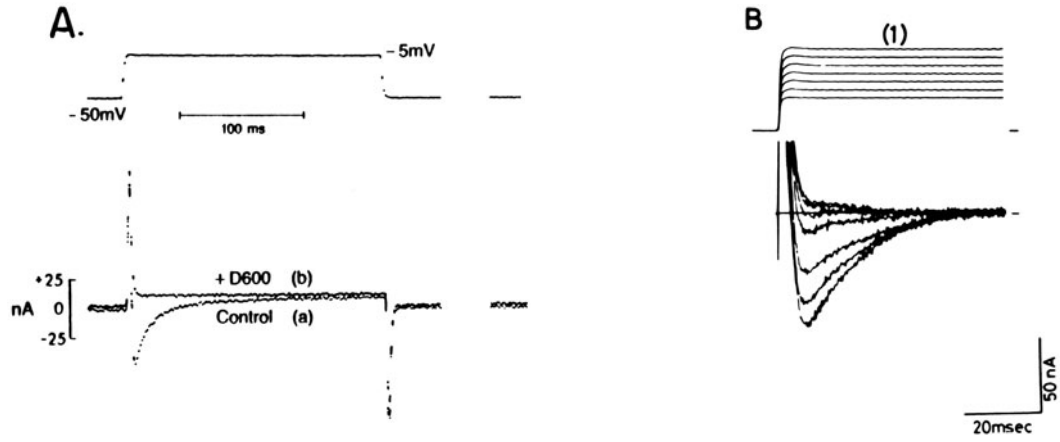

FIGURE 4–4. Calcium current in two cardiac cell types. *(A)* Calf Purkinje fiber membrane current measured in response to 250-ms voltage step before (a) and after application of the calcium current blocker D600 (b). The rapid downward current deflection is the calcium current (I_{si}) in control, and this is completely blocked by D600. R.S. Kass, unpublished data. *(B)* Calcium current recorded in the rabbit SA node. The current shown is in response to six voltage steps applied in 10-mV intervals from 0 to 60 mV. Data from Noma et al. [78].

this remains to be confirmed in studies in which single-channel conductances are directly measured [40].

OUTWARD CURRENTS: REPOLARIZATION OF THE ACTION POTENTIAL

Delayed Rectification. The plateau phase of the Purkinje fiber (as well as ventricular muscle) action potential is maintained by a fine balance between small inward and outward currents. During the plateau phase, the membrane potential changes very slowly, indicating little net charge transfer across the membrane capacitance (see eq. 4.4). Then, as the balance tips in favor of outward current, the net movement of positive charge is from the inner surface to the outer surface of the membrane, and repolarization of the cell begins. The gradual transition to outward current is due both to the inactivation (decrease) of the calcium current I_{si} and to the slow activation (increase) of a time-dependent outward current.

Noble and Tsien [50] investigated the repolarization process in the Purkinje fiber. They found a time-dependent outward current that is activated over a potential range similar to the plateau of the action potential. Its time dependence consists of two components: one relatively fast time constant (~500 ms) and the other much slower (~5 s). When they used voltage-clamp protocols to determine the equilibrium potential for this current, Noble and Tsien found the charge carrier of this current to be largely, but not exclusively, potassium ions. Because this channel is not completely selective for one charge carrier, it was labeled I_x and expressed as the sum of its two components:

$$I_x = I_{x1} + I_{x2} \tag{4.7}$$

I_{x1} is the faster component and I_{x2} is the slower component. This current is often also referred to as the delayed rectifier in order to relate it to repolarizing outward currents in nerve and skeletal muscle. Figure 4–5A shows records of I_x taken from Noble and Tsien [50].

Computer-generated reconstruction of the Purkinje fiber action potential confirmed that I_x is crucial to the repolarization process in these fibers [28]. Similar time-dependent outward currents have now been reported in SA nodal preparations (fig. 4–5B and Di Francesco et al. [51]), atrial preparations, and in ventricular fibers [52, 53]. Although not as crucial to repolarization in the ventricle as in the Pur-

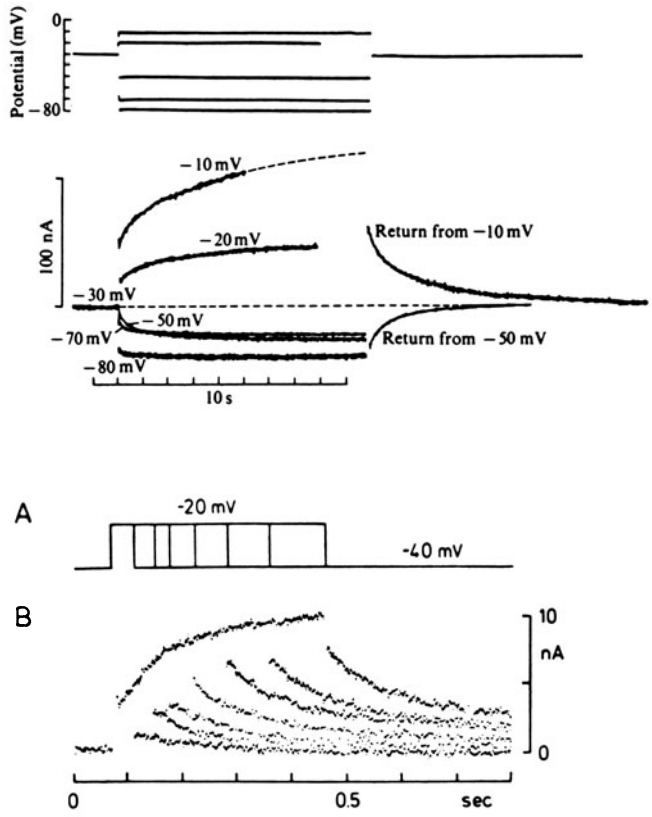

FIGURE 4–5. Repolarizing outward currents in the Purkinje fiber and SA node. *(A)* The slow activation of I_x in the sheep Purkinje fiber. Depolarizations to −20 mV and −10 mV produce slow increase in outward current. Hyperpolarization decreases the current. The tails of current that follow these pulses are used to monitor changes in the amount of I_x turned on (or off) during the preceding voltage pulse. *(B)* A similar procedure shows faster outward current in the rabbit SA node. In this case, current is shown in response to depolarizations of different durations to a test potential of −20 mV. The envelope of the current tails that follow each test pulse is a measure of the time course of the increase of this current. From Di Francesco et al. [51].

kinje fiber [29], it does contribute to this process in each of these cell types and even participates in pacemaker activity in the SA node (see Brown [54] for review) as well as in partially depolarized ventricular [53] and Purkinje [55] fibers.

I_x is blocked by intra- [63] and extracellular cesium ions [53] and by intracellular injection of quaternary ammonium compounds [56]. It is also very sensitive to norepinephrine [57], increasing by as much as fourfold in maximal concentrations of this neurohormone [48].

Transient Outward Current. The very rapid repolarization that follows the sodium-dependent upstroke of the Purkinje fiber action potential is also generated by a transition from inward to outward current, but in this case the transition is due to the inactivation of I_{Na} along with the activation and subsequent inactivation of a large outward current.

Early voltage-clamp studies showed a transient outward current component that dominated the early periods of currents recorded during strong depolarizing voltage pulses. These initial studies suggested that this was a chloride current because it was greatly reduced by chloride removal [58, 59], but these effects of chloride substitution were later attributed to

indirect effects on intracellular Ca activity [60].

More recent studies have provided evidence that potassium ions are the most likely charge carrier for this transient outward current. This conclusion is based on pharmacologic grounds: the transient outward current has been shown to be sensitive to compounds or procedures that block K channels in other excitable cells. It is sensitive to 4-aminopyridine and extracellular tetraethylammonium [60, 61], intracellular quaternary ammonium ion compounds, [56] and to replacement of intracellular potassium by cesium [62, 63].

This current was initially labeled I_{qr} but now is referred to as I_{to} (for transient outward current). Its kinetic properties have not been completely analyzed, but it is clear that I_{to} activates quickly and inactivates, at least partially, with time constants near 50 ms. Recent studies have suggested that I_{to} may also consist of two components: one sensitive to intracellular calcium and a second component that is not calcium activated [64].

I_{to} is most prominent in the Purkinje fiber, where it contributes to the "notch" configuration of the action potential. It is also present in other cardiac cells, such as ventricular muscle, although not as important in these tissues (see McDonald et al. [65]).

Calcium-activated Currents. Calcium-activated K currents are known to exist in a wide variety of cells, and evidence has been presented that I_{to} is, at least in part, such a current. Siegelbaum et al. [66] first demonstrated a possible role of Ca_i in regulating the conductance of the I_{to} channel, and this work has been supported by further studies [64, 67]. In this view, the time-dependent changes in I_{to} are not entirely due to modulation of the I_{to} conductance by voltage-dependent gates. Instead, this conductance is enhanced by intracellular calcium ion concentration which changes in a phasic manner during depolarizations.

Several properties of the delayed rectifier (I_x) have suggested that it too may be a calcium-activated current. Calcium influx (I_{si}) precedes the slower onset of I_x, and several compounds that block I_{si} also reduce I_x [44]. In addition, catecholamine-induced increases in I_{si} are accompanied by dramatic increases in I_x. However, recent experimental evidence has shown that I_x activation can be separated from I_{si} activation by a new calcium channel blocker, nisoldipine [45]. Nisoldipine, as well as D600, also prevents the increase of I_{si}, but not I_x, by norepinephrine [48]. Thus it is not likely that I_x is activated by intracellular calcium ions [68].

Pacemaker Current. Although the Purkinje fibers are not the dominant pacemaker cells in the heart, the ionic basis of pacemaker activity was first investigated in these cells because of their experimental accessibility. Once again, using equation 4.4 as a guide, it is evident that slow pacemaker depolarization must be due to the unmasking of net inward ionic current. Weidmann (see Tsien et al. [69]) suggested three possible explanations:

1. a slow increase in sodium permeability,
2. a slow decline in potassium permeability, and
3. a slow decline in outward current carried by an Na pump (see below).

Vassalle [70] combined voltage-clamp and current clamp techniques and found support for explanation 2. Later, Noble and Tsien [71], in a very detailed investigation, characterized the properties of this pacemaker current, which they called I_{K_2}. Their data provided evidence that this current is carried via gated potassium channels (see fig. 4–6). All of these channels are in an open state when the membrane potential is more positive than -60 mV, and they begin to close as the membrane becomes more negative during the repolarization process. The time course of the transition of these channels from open to closed states determines the rate at which total membrane current becomes less outward, and thus accounts for the slope of the pacemaker depolarization (eq. 4.4). A similar mechanism is responsible for SA nodal pacing (see Brown [54]).

Although pharmacologic evidence supports the theory that Purkinje fiber pacemaker current is largely carried by K ions, recent exper-

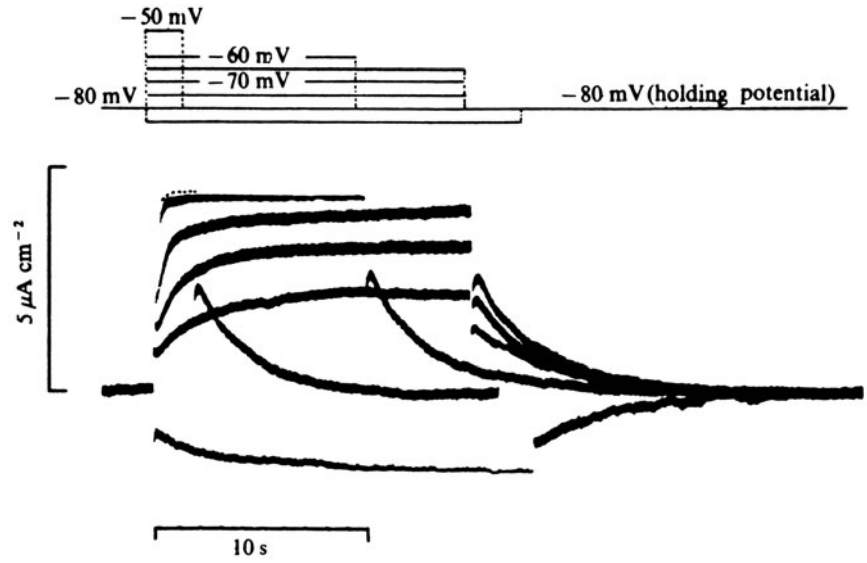

FIGURE 4–6. Pacemaker current (I_{K_2}) in the sheep Purkinje fiber. Membrane current is shown in response to step voltage changes in the diastolic range of potentials. This is the superposition of six records in which current tails were used to monitor changes in this current [71].

iments have raised the possibility that the situation is more complicated due in part to accumulation or depletion of K^+ ions in the intracellular spaces of this preparation [72–74]. Di Francesco [75] has suggested that I_{K_2} may be due, at least in part, to a time-dependent inward current. Future studies of pacemaker currents in isolated Purkinje cells will help resolve these views.

Chronotropic Actions of Neurotransmitters. Norepinephrine increases heart rate; acetylcholine slows it. Although the best-known action of vagal stimulation (causing release of acetylcholine) is to increase a passive potassium conductance, both of these neurotransmitters also affect gated channels, and it is the sum of all of these effects that determines the overall response of the heart.

The effects of norepinephrine on heart rate also were first well characterized in the Purkinje fiber. Tsien [76] found that this catecholamine affects the kinetics of the I_{K_2} channel in a manner that speeds its decay in the diastolic potential range. This increase in the "turnoff" of outward current results in an increased slope of depolarization (eq. 4.4). A similar situation exists in the SA node, but the effects of norepinephrine on I_{si} also contribute to the faster pacing in these cells. Similarly the slowing of nodal pacing by acetylcholine is due, in part, to is inhibitory actions on nodal calcium current (see the preceding section).

Summary

This chapter has focused on the major time-dependent ionic currents that contribute to cardiac electrical activity. It has not discussed time-independent, background currents (see Noble [2]) electrogenic Na-K pump currents (see chapter 18 and Vaughn-Jones et al. [77]), or possible roles of Na-Ca exchange in cardiac electrical activity (see chapter 10).

On the other hand, it has presented a review of several currents that have been characterized in the heart and has provided references for more detailed study of each of them. Cardiac electrophysiology is an exciting area of study that is rapidly changing as newer and more quantitative experimental techniques are introduced. As this field of study expands, we increase our understanding of the mechanisms that underlie the complicated patterns of elec-

trical activity in the normal heart, and we further our ability to correct electrical disturbances in diseased states.

References

1. Hogan PM, Davis LD: Evidence for specialized fibers in the canine right atrium. Circ Res 23:387–396, 1968.
2. Noble D: The initiation of the heartbeat. London: Oxford, 1979.
3. Cranefield PF: The conduction of the cardiac impulse. Mt Kisco NY: Futura, 1975.
4. Hoffman BF, Cranefield PF: Electrophysiology of the heart. Mt Kisco NY: Futura, 1976.
5. Hodgkin AL, Rushton WAH: The electrical constants of a crustacean nerve fiber. Proc R Soc B133:444–479, 1946.
6. Hille B: Rate theory models of ion flow in ionic channels of nerve and muscle. In: Stevens CF, Tsien RW (eds) Membrane transport processes, vol 3. New York: Raven, 1979.
7. Fozzard HA: Membrane capacity of the cardiac Purkinje fibre. J Physiol 182:255–267, 1966.
8. Carmeliet E, Willems J: The frequency dependent character of the membrane capacity in cardiac Purkinje fibres. J Physiol 213:85–84, 1971.
9. Strichartz GR, Cohen IS: $\dot{V}_{max}$ as a measure of G_{Na} in nerve and cardiac membranes. Biophysical J 23:153–156, 1978.
10. Kass RS, Siegelbaum SA, Tsien RW: Three-microelectrode voltage clamp experiments in calf cardiac Purkinje fibers: is slow inward current adequately measured? J Physiol 290:201–225, 1979.
11. Lee KS, Weeks TA, Kao RL, Akaike N, Brown AM: Sodium current in single heart muscle cells. Nature 278:269–271, 1979.
12. Colatsky TJ, Tsien RW: Sodium channels in rabbit cardiac Purkinje fibres. Nature 278:265–268, 1979.
13. Draper MH, Weidmann S: Cardiac resting and action potentials recorded with an intracellular electrode. J Physiol 115:74–94, 1951.
14. Weidman S: The effect of the cardiac membrane potential on the rapid availability of the sodium carrying system. J Physiol 127:213, 1955.
15. Weidmann S: Effects of calcium ions and local anaesthetics on electrical properties of Purkinje fibres. J Physiol 129:568–582, 1955.
16. Colatsky TJ: Voltage clamp measurements of sodium channel properties in rabbit cardiac Purkinje fibres. J Physiol 305:215–234, 1980.
17. Ebihara L, Shigeto N, Lieberman M, Johnson EA: The initial inward current in spherical clusters of chick embryonic heart cells. J Gen Physiol 75:437–456, 1980.
18. Brown AM, Lee KS, Powell T: Sodium current in single rat heart muscle cells. J Physiol 318:479–500, 1981.
19. Attwell D, Cohen I, Eisner D, Ohba M, Ojeda C: The steady state TTX-sensitive ("window") sodium current in cardiac Purkinje fibres. Pflugers Arch 379:137–142, 1979.
20. Colatsky TJ, Gadsby DC: Is tetrodotoxin block of background sodium channels voltage-dependent? J Physiol 306:20P, 1980.
21. Coltasky TJ: Mechanisms of action of lidocaine and quinidine on action potential duration in rabbit cardiac Purkinje fibers: an effect on steady state sodium currents. Circ Res 50:17–27, 1982.
22. Dudel J, Peper K, Rudel R, Trautwein W: Excitatory membrane current in heart muscle (Purkinje fibres). Pflugers Arch 292:255–273, 1966.
23. Coraboeuf E, Derobaix E, Coulombe A: Effect of tetrodotoxin on action potentials of the conducting system in the dog heart. Am J Physiol 236:H561–H567, 1979.
24. Cohen CJ, Bean BP, Colatsky TJ, Tsien RW: Tetrodotoxin block of sodium channels in rabbit Purkinje fibers. J Gen Physiol 78:383–411, 1981.
25. Cranefield PF: Action potentials, afterpotentials, and arrhythmias. Circ Res 41:415–423, 1977.
26. Noma A, Yanagihara K, Irisawa H: Inward current of the rabbit sinoatrial node cell. Pflugers Arch 372:43–51, 1977.
27. Brown H, Di Francesco D: Voltage-clamp investigations of membrane currents underlying pace-maker activity in rabbit sino-atrial node. J Physiol 308:331–351, 1980.
28. McAllister RE, Noble D, Tsien RW: Reconstruction of the electrical activity of cardiac Purkinje fibres. J Physiol 251:1–59, 1975.
29. Beeler GW, Reuter H: Reconstruction of the action potential of ventricular myocardial fibres. J Physiol 268:177–210, 1977.
30. Reuter H: The dependence of slow inward current in Purkinje fibres on the extracellular calcium concentration. J Physiol 192:479–492, 1967.
31. Vitek M, Trautwein W: Slow inward current and action potential in cardiac Purkinje fibres: the effect of Mn ions. Pflugers Arch 323:204, 1971.
32. Beeler GW Jr, Reuter H: Membrane calcium current in ventricular myocardial fibres. J Physiol 207: 191–209, 1970.
33. Rougier O, Vassort G, Garnier D, Gargouil YM, Coraboeuf E: Existence and role of a slow inward current during the frog atrial action potential. Pflugers Arch 308:91–110, 1969.
34. New W, Trautwein W: Inward membrane currents in mammalian myocardium. Pflugers Arch 334: 1–23, 1972.
35. Reuter H: Properties of two inward membrane currents in the heart. Annu Rev Physiol 41:413–424, 1979.
36. Isenberg G, Klockner U: Glycocalyx is not required for slow inward calcium current in isolated rat heart myocytes. Nature 284:358–360, 1980.
37. Hume JR, Giles W: Active and passive electrical

properties of single bullfrog cells. J Gen Physiol 78:19–42, 1981.
38. Lee KS, Lee EW, Tsien RW: Slow inward current carried by Ca^{2+} or Ba^{2+} in single isolated heart cells. Biophys J 33:143a, 1981.
39. Lee KS, Tsien RW: Reversal of current through calcium channels in dialyzed single heart cells. Nature 297:498–501, 1982.
40. Reuter H, Stevens CF, Tsien RW, Yellen G: Properties of single calcium channels in cultured cardiac cells. Nature 297:501–504, 1982.
41. Hagiwara S, Byerly L: Calcium channel. Annu Rev Neurosci 4:69–125, 1981.
42. Tsien RW: Calcium channels in excitable cell membranes. Annu Rev Physiol 45:341–58, 1983.
43. Reuter H, Scholz A: A study of the ion selectivity and the kinetic properties of the calcium dependent slow inward current in mammalian cardiac muscle. J Physiol 264:17–47, 1977.
44. Kass RS, Tsien RW: Multiple effects of calcium antagonists on plateau currents in cardiac Purkinje fibers. J Gen Physiol 66:169–192, 1975.
45. Kass RS: Nisoldipine: a new, more selective calcium current blocker in the cardiac Purkinje fiber. J Pharmacol Exp Ther 223:446–456, 1982.
46. Giles W, Noble SJ: Changes in membrane currents in bullfrog atrium produced by acetylcholine. J Physiol 261:103–123, 1976.
47. Ten Eick R, Nawrath H, McDonald TF, Trautwein W: On the mechanism of the negative inotropic effect of acetylcholine. Pfluger Arch 361:207–213, 1976.
48. Kass RS, Wiegers SE: Ionic basis of concentration-related effects of noradrenaline on the action potential of cardiac Purkinje fibres. J Physiol 322:541–558, 1982.
49. Reuter H, Scholz H: The regulation of Ca conductance of cardiac muscle by adrenaline. J Physiol 264:49–62, 1977.
50. Noble D, Tsien RW: Outward membrane currents activated in the plateau range of potentials in cardiac Purkinje fibers. J Physiol 200:205–231, 1969.
51. Di Francesco D, Noma A, Trautwein W: Kinetics and magnitude of the time-dependent potassium current in the rabbit S-A node. Pflugers Arch 381: 271–279, 1979.
52. McDonald TF, Trautwein W: Membrane currents in cat myocardium: separation of inward and outward components. J Physiol 274:193–216, 1978.
53. Meier CF, Katzung BG: Cesium blockade of delayed outward currents and electrically induced pacemaker in mammalian ventricular myocardium. J Gen Physiol 77:531–547, 1981.
54. Brown HF: Electrophysiology of the sinoatrial node. Physiol Rev 62:505–530, 1982.
55. Hauswirth O, Noble D, Tsien RW: The mechanism of oscillatory activity at low membrane potentials in cardiac Purkinje fibres. J Physiol 200:255–265, 1969.
56. Kass RS, Scheuer T, Malloy KJ: Block of outward current in cardiac Purkinje fibers by injection of quaternary ammonium ions. J Gen Physiol 79:1041–1063, 1982.
57. Tsien RW, Giles WR, Greengard P: Cyclic AMP mediates the action of epinephrine on the action potential plateau of cardiac Purkinje fibres. Nature [New Biol] 240:181–183, 1972.
58. Dudel J, Peper K, Rudel R, Trautwein W: The dynamic chloride component of membrane current in Purkinje fibers. Pflugers Arch 295:197–212, 1967.
59. Fozzard HA, Hiraoka M: The positive dynamic current and its inactivation properties in cardiac Purkinje fibers. J Physiol 234:569–586, 1973.
60. Kenyon JL, Gibbons WR: Influence of chloride, potassium, and tetraethylammonium on the early outward current of sheep cardiac Purkinje fibers. J Gen Physiol 73:117–138, 1979.
61. Kenyon JL, Gibbons WR: 4-Amminopyridine and the early outward current of sheep cardiac Purkinje fibers. J Gen Physiol 73:139–157, 1979.
62. Marban E: Inhibition of transient outward current by intracellular ion substitution unmasks slow inward current in cardiac Purkinje fibers. Pflugers Arch 390:102–106, 1981.
63. Marban E, Tsien RW: Effects of nystatin-mediated intracellular ion substitution on membrane currents in calf Purkinje fibres. J Physiol 329:569–81, 1982.
64. Coraboeuf E, Carmeliet E: Existence of two transient outward currents in sheep cardiac Purkinje fibers. Pflugers Arch 392:352–359, 1982.
65. McDonald TF, Pelzer D, Trautwein W: On the mechanism of slow calcium channel block in heart. Pflugers Arch 385:175–179, 1980.
66. Siegelbaum SA, Tsien RW, Kass RS: Role of intracellular calcium in the transient outward current of calf Purkinje fibers. Nature 269:611–613, 1977.
67. Siegelbaum SA, Tsien RW: Calcium-activated outward current in calf cardiac Purkinje fibres. J Physiol 299:485–506, 1980.
68. Kass RS: Delayed rectification is not a calcium activated current in cardiac Purkinje fibers. Biophys J 37:342a, 1982.
69. Tsien RW, Siegelbaum S: Excitable tissues: the heart. In: Andreoli T, Hoffman JF, Fanestil D (eds) The physiological basis of biomembranes. New York: Plenum, 1978.
70. Vassale M: Analysis of cardiac pacemaker potential using a "voltage clamp" technique. Am J Physiol 210:1335–1341, 1966.
71. Noble D, Tsien RW: The kinetics and rectifier properties of the slow potassium current in cardiac Purkinje fibres. J Physiol 195:185–213, 1968.
72. Maylie JM, Morad M, Weiss J: A study of pacemaker potential in rabbit sinoatrial node measurement of potassium activity under voltage clamp conditions. J Physiol 311:161–178, 1981.
73. Baumgarten CM, Isenberg G: Depletion and accumulation of potassium in the extracellular clefts of

cardiac Purkinje fibers. Pflugers Arch 368:19–31, 1977.
74. Di Francesco D, Ohba M, Ojeda C: Measurement and significance of the reversal potential for the pacemaker current (I_{K_2}) in sheep Purkinje fibres. J Physiol 297:135–162, 1979.
75. Di Francesco D: A new interpretation of the pacemaker current I_{K_2} in Purkinje fibers. J Physiol 314:359–376, 1981.
76. Tsien RW: Effects of epinephrine on the pacemaker potassium current of cardiac Purkinje fibers. J Gen Physiol 64:293–319, 1977.
77. Vaughan-Jones RD, Lederer WJ, Eisner DA: The electrogenic Na-K pump in the sheep cardiac Purkinje fibre. In: Progress in enzyme and ion-selective electrodes. Berlin: Springer-Verlag, 1981, pp 156–163.
78. Noma A, Kotake H, Irisawa H: Slow inward current and its role mediating the chronotropic effect of epinephrine in the rabbit sinoatrial node. Pflugers Arch 388:1–9, 1980.

5. ELECTROGENESIS OF PACEMAKER POTENTIAL AS REVEALED BY AV NODAL EXPERIMENTS

H. Irisawa,
A. Noma,
S. Kokubun,
and Y. Kurachi

Introduction

The atrioventricular (AV) node has two vitally important functions. One is its role in the conduction through atrium to ventricle. The slow conduction of excitation within the node [1, 2] provides an adequate time delay between the contraction of atria and that of ventricles and enables the heart to function as an efficient pump. Another function of the AV node is its secondary pacemaker activity. When the sinoatrial (SA) node fails to control cardiac rhythm, as a result either of depressed automaticity or impaired conduction, the AV node functions as a pacemaker of the heart.

After the discovery of the AV node [3], there were major developments of the physiologic concept of the AV node in the late 1950s, when the membrane potentials of the AV node were thoroughly studied. Today, almost all of the basic concepts of AV node have been investigated. However, because the studies have been mostly limited to the analysis of the action potential pattern and the maximum rate of depolarization, it is still unclear whether measurements reflect the membrane property of the AV nodal cell or the propagated action potential. Does slurred upstroke with steps or notches frequently described in the N cell represent a strange characteristic of the inward-current system or simply an artifact due to the conduction block? Does acetylcholine increase the membrane potassium conductance or depress the slow inward current? Is action potential generation independent from the membrane potential? In order to answer these questions, direct measurement of the membrane current is essential.

In 1976, Noma and Irisawa [4] developed the small SA nodal preparation useful for the voltage-clamp experiment on the primary pacemaker cell. This method has become a conventional technique in several different laboratories for study of the SA node (for review, see Irisawa [5] and Brown [6]). In this chapter, results of our study on AV nodal cells are reviewed. The small preparation of AV nodal cells showed very similar electrophysiologic characteristics to those observed in the SA node.

Materials and Methods

Rabbit AV node lies between the ostium of the coronary sinus and the leaflet of the tricuspid valve [7]. Its size is approximately 5 × 3 mm. Before preparing the small specimen, we examined the configuration of the action potentials of the intact AV node (fig. 5–1B). We

N. Sperelakis (ed.), PHYSIOLOGY AND PATHOPHYSIOLOGY OF THE HEART.

Martinus Nijhoff Publishing, Boston/The Hague/ Dordrecht/Lancaster.

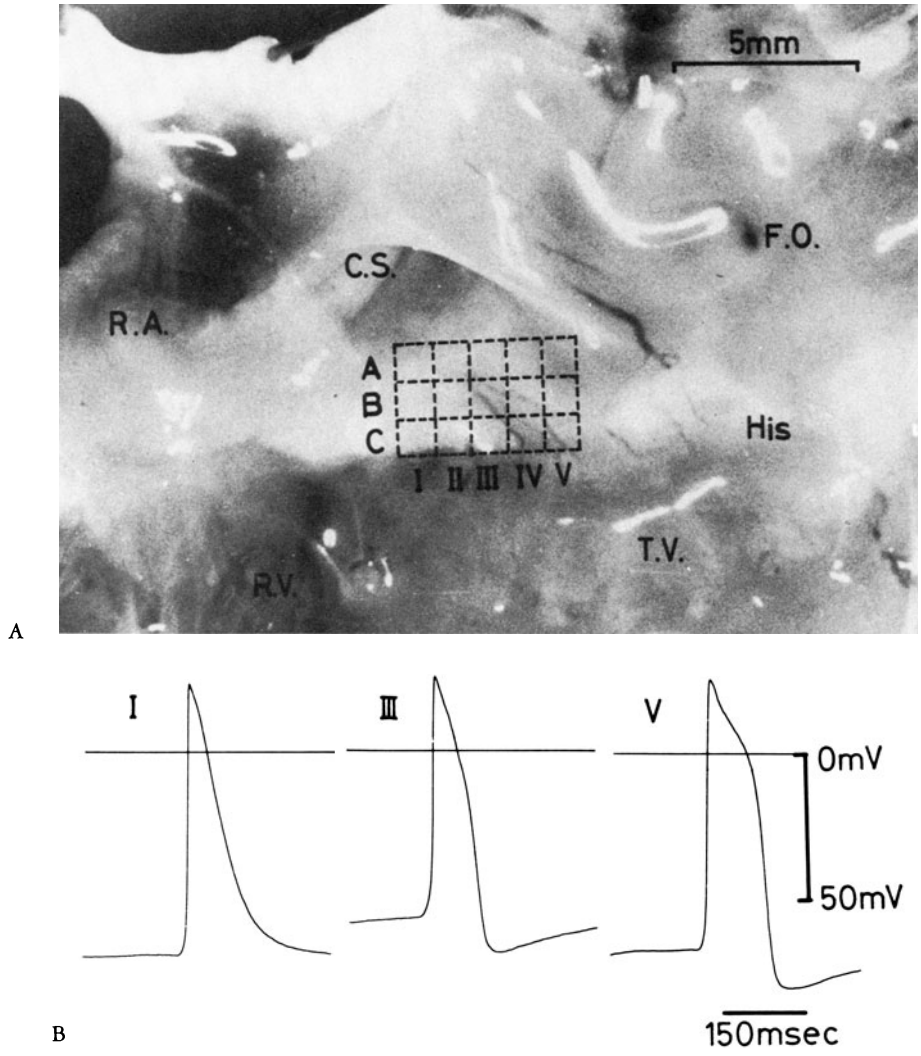

FIGURE 5–1. *(A)* Photograph showing the AV nodal region of the heart: CS, coronary sinus; RA, right atrium; FO, foramen ovale; RV, right ventricle; TV, tricuspid valve; HIS, His bundle; A, B, and C, I–V, see text. *(B)* Action potentials recorded in intact AV nodal specimens I, III, and V correspond to those of I-B, III-B, and V-B in figure 5–1A. From Kokubun et al. [30].

subdivided the nodal region into 15 small portions as shown in figure 5–1A. From region I, the action potential pattern which was similar to those of atria was recorded, but the maximum rate of rise of this potential was 28.6 V/s, which was smaller than those usually observed in atrial tissue. From region V, the pattern similar to the NH cells (original nomenclature) was recorded, but the maximum rate of rise was very small compared with that observed in the His bundle. In region III, the amplitude of the action potential was smallest, the resting potential being less negative than the two other potentials. All of these action potentials comprised the conducted action potential. These potentials, which we recorded from the intact sheet preparation, were similar to those observed by Akiyama and Fozzard [8], Ruiz-Cretti and Zumino, [9], and Zipes and Mendez

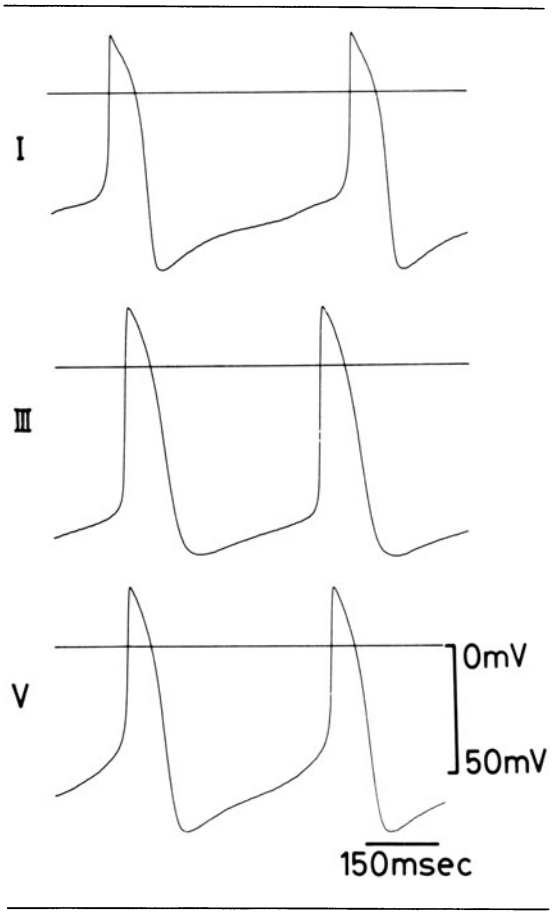

FIGURE 5–2. Action potentials recorded in the small specimens of AV node: I, III, and V correspond to I-B, III-B, and V-B in figure 5–1A. From Kokubun et al. [30].

[10], indicating that the region we investigated was in fact the AV node defined by the previous authors.

We then transected the AV nodal region perpendicularly to the AV ring into five 1-mm-wide strands. Both sides of each strand were trimmed bit by bit to a width of 0.5 mm. These strands were numbered from I to V (fig. 5–1A). We removed the epicardial side of these thin-strand preparations, while the endocardial side remained intact. Each strand was then ligated by a silk suture into three equal portions, which were labeled A, B, and C.

When we used the voltage-clamp method, this size was not sufficiently small. We had to trim the preparation stepwise to 0.25 × 0.25 × 0.1 mm. The trimming procedure was deliberate, using a fragment of razor blade.

Action Potentials in the Small AV Nodal Specimen

Figure 5–2 shows one example of the action potentials recorded from such a small specimen. In ten experiments, 4–6 specimens of regions I-A, I-B, II-A, and V-C were quiescent, but mostly the individual small preparation revealed spontaneous activity, as seen by the slowly rising pacemaker depolarization (fig. 5–2). In contrast to the regional variation of the action potential configuration observed in the intact AV nodal specimens, the action potential parameters from the small AV nodal specimens showed similar values in every 15 portions.

The amplitude of the action potential in the small specimens was slightly larger than that in N cell reported in the references [8, 10] but the maximum rate of rise and the duration of action potentials were comparable to those described in many reports, including the most recent one (fig. 6 in Mendez [11]).

The resting potential of the small AV nodal specimen was approximately −44 mV, and this value was obviously more positive than the resting potential in the intact AV nodal specimen (−62 mV in three quiescent specimens). The latter value is in good agreement with the data reported by other investigators [8–10]. In the small preparation, resting potential and maximum rate of rise of action potential were low, but the amplitude and the overshoot were normal and no slurred upstroke was observed. In the small AV nodal specimen, action potentials recorded from three different sites coincided well, indicating a synchronous excitation within the specimen.

In the small AV nodal specimen, acetylcholine hyperpolarizes the membrane in a same manner as in the SA nodal cell (fig. 5–3). Membrane hyperpolarized by the superfusion of acetylcholine (10^{-7} g/ml) and cessation of the spontaneous activity was observed.

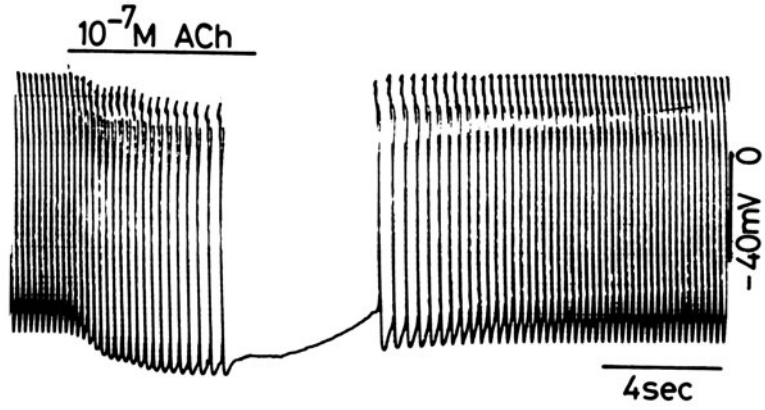

FIGURE 5–3. Effect of acetylcholine on the small AV nodal specimen; 10^{-7} g/ml acetylcholine was superfused. Original trace by S. Kokubun.

RESPONSE TO THE CURRENT INJECTION

The membrane potential of the small AV nodal specimen could be controlled by injecting currents through a second microelectrode. When the size of the specimen was larger than 0.5 mm, point injection of the current with the second microelectrode produced no frequency modulation [12]. In the larger specimen, current injected by using a suction electrode with a tip diameter of 0.1 mm caused frequency and amplitude modulation [13, 14]. Mendez [11] repeated Shigeto and Irisawa's experiment using a large-diameter micropipette located over the His bundle. They found the maximum rate of rise of N cell action potential only very slightly reduced. Knowing the space constant of this region [15], it is rather clear that the point of injection of the electric current from His bundle cannot change the frequency of the midnodal cells.

In the small AV nodal specimen, any portion of the AV node shown in figure 5–1, both frequency and amplitude modulation occurred in response to the injection of current (fig. 5–4). With depolarizing current pulses, the maximum diastolic potential decreased and the frequency of the spontaneous discharge increased, whereas cessation of spontaneous activity occurred during application of hyperpolarizing current.

In this example, the lowest membrane potential supressing automaticity was −60 mV, which was close to the resting potential of the intact quiescent AV nodal specimen.

PRESENCE OF ELECTROGENIC Na PUMP IN THE SMALL AV NODAL SPECIMEN

The electrogenic Na-K pump has also been found in the small AV nodal specimen [16, 17]. The electrogenicity of the Na-K pump

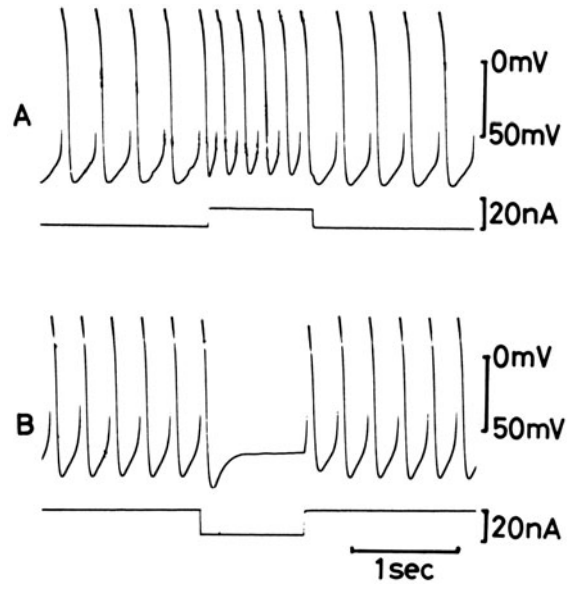

FIGURE 5–4. Current clamp experiment in the small specimens. In each panel the top trace represents the membrane potential, while the bottom the applied current: *(A)* depolarization of 11.4 nA; *(B)* hyperpolarization of 17.1 nA. From Kokubun et al. [30].

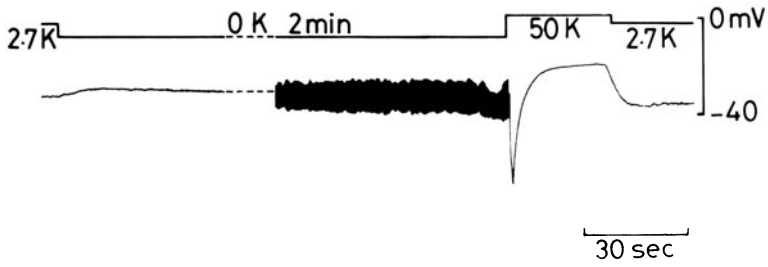

FIGURE 5–5. Effect of 50 m*M* K solution on transient hyperpolarization. The experiment was carried out in 10^{-6} g/ml D-600 solution. From Kurachi et al. [16].

was determined by using a procedure of K-induced transient hyperpolarization after brief exposure to K-free Tyrode solution (fig. 5–5). K-free Tyrode solution was perfused for as long as 2 min, followed by the perfusion of 50 m*M* K-Tyrode solution. The oscillatory potential changes were observed after the long exposure to K-free solution. As the perfusion fluid was switched to the high-K Tyrode solution, membrane hyperpolarized as negative as -69.3 mV, which is obviously more negative than the K equilibrium potential of -28 mV when intracellular K concentration was 150 m*M*. This transient hyperpolarization was abolished after the application of 10^{-5}M strophantidin. The membrane slope conductance remained unchanged during the transient hyperpolarization. The order of potencies of monovalent cations to activate the K site of the Na pump was $Tl > Rb \doteqdot K > NH_4 \doteqdot Cs > Li$, which was similar to the sequences reported in the literature. These findings indicate that the Na pump in the AV nodal cells shares common characteristics with those other excitable tissues and confirm that the small AV nodal specimen maintains normal physiologic characteristics well even after the repeated trimming procedure.

MEMBRANE CURRENTS IN THE AV NODAL CELL

Use of the small AV nodal specimen also enabled us to study the voltage-clamp experiment. The conventional two-microelectrode voltage-clamp method was applied [18]. Membrane current systems were extensively studied in mammalian Purkinje fiber, ventricle fiber, and SA nodal cells [19]. Noma et al. [20] and Kokubun et al. [15] have reported the ionic current systems of the AV nodal cells. In the following, we summarize these results.

For the purpose of the voltage-clamp experiment, the dimensions of the small AV nodal specimen should be as small as $0.2 \times 0.2 \times 0.1$ mm. The specimen continued to contract spontaneously at this size and revealed normal action potential patterns. Voltage homogeneity within the small specimen was examined using three microelectrodes. We confirmed no serious deviation from the command pulse except for a deviation of 5 mV during the initial 10 ms into the clamp pulse [20].

Figure 5–6 presents a family of voltage-clamp traces, from the holding potential of -40 mV to either $+10$ mV or -100 mV in 10-mV steps. Before this clamp experiment, the specimen showed spontaneous activity: the amplitude of action potential was 98 mV and the maximum rate of rise of depolarization was 11 V/s. When the clamp was initiated, the transient current change due to the previous action potentials subsided and was followed by a steady membrane current. The steady current level was outward at holding potentials more positive than -35 to -40 mV and was inward at more negative holding potentials. On depolarization, the slow inward current was elicited, which was sensitive to D-600 but insensitive to tetrodotoxin (TTX). The progressively activating outward current was followed after the inactivation of the slow inward current, and it decayed gradually after the clamp pulse was repolarized to the holding potential.

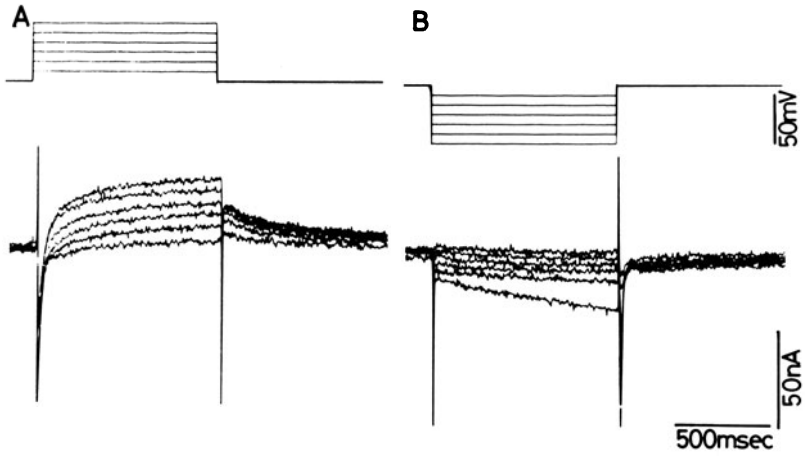

FIGURE 5–6. Voltage-clamp records from AV nodal cells in Tyrode solution: upper traces, the potential; lower traces, the corresponding current traces. Holding potential (−40 mV) duration of each test pulse was 1 s and the clamp pulsing rate was 0.1 Hz From Kokubun et al. [15].

This outward current component was a potassium current, similar to the i_K in the SA node. The outward current tail has two components, fast and slow. When the membrane potential was clamped at + 10 mV for as long as 1 s and then held back to the holding potential, the fast component revealed a time constant of 133 ms while the slow component showed 1234 ms. These findings were also in good agreement with i_K in the SA node [5, 6].

In AV nodal cells, we also observed the hyperpolarization-activated current (i_h [22], i_f [21], and i_p [23]). On hyperpolarization from the holding potential of −40 mV, at the first two or three steps (−50 to −60 mV), a gradually decaying i_K was observed, but at the potential more negative than −70 mV, i_h was activated. On return to the holding potential, the sodium current (i_{Na}) and the slow inward current were activated and the inward current was observed after the capacitive surge. In some specimens, we could not register the i_h while the specimen showed spontaneous activity.

When the clamp circuit was switched off, the specimen immediately resumed spontaneous activity. The configuration of the action potential was almost the same as before the clamp.

Partial Participation of i_{Na}

There is accumulating evidence that AV nodal cells, especially at the midnodal region or the N cell region, have a slow inward channel [10, 24, 25]. True nodal cells (N cells) are resistant to the effect of TTX, but are suppressed by an application of manganese as well as verapamil. However, Ponce Zumino et al. [26] and De Ceretti et al. [27] have suggested that even in the midnodal region there is a fast Na channel. The response of the individual researcher to these findings may vary. One can state that their midnodal cell is not an N cell, but a transitional cell. On the other hand, others may claim that the N cell is insensitive to TTX at its normal resting potential, where most of the Na channels are inactivated. If the membrane hyperpolarized more negative than −70 mV, i_{Na} became activated. This is indeed so in the SA nodal cell [28, 29]. These questions can only be answered in the AV node, where the membrane potential can be varied quantitatively.

Kokubun et al. [30] have shown the presence of i_{Na} in the small AV nodal specimen isolated from the mid-AV-nodal area (fig. 5–7). TTX in a concentration of 10^{-6} g/ml caused a very small (6%) reduction of both the amplitude and maximum rate of rise. The spontaneous activity never ceased within this TTX concentration, but application of 4 m*M* Mn^{2+}

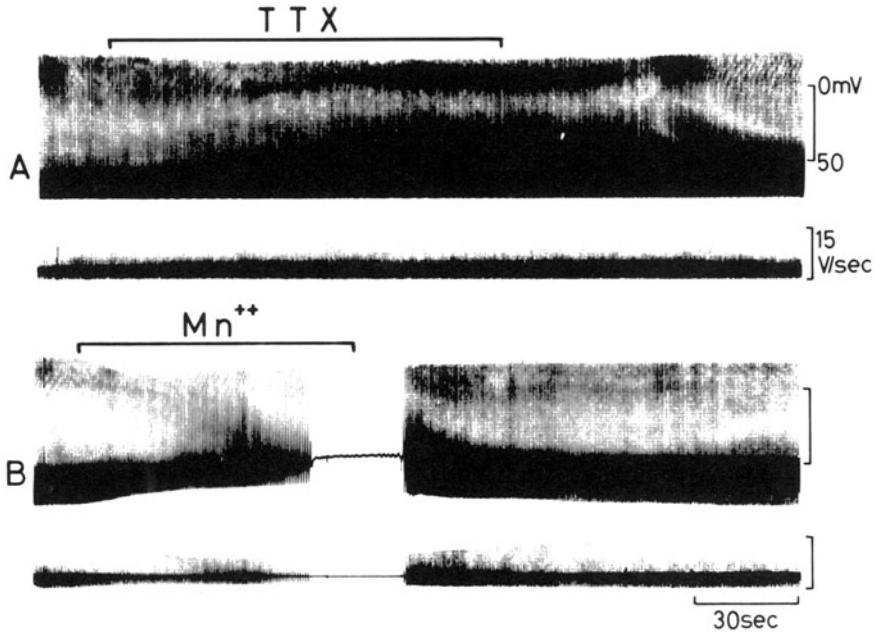

FIGURE 5–7. Effects of TTX and Mn^{2+} on the AV nodal action potential. In each panel the upper trace is the maximum rate of rise of depolarization. From Kokubun et al. [30].

suppressed the action potential within 2 min. Verapamil 10^{-6} g/ml had a similar effect. These facts correspond fairly well with other reports and support the possibility that we are recording from the N cell of classic nomenclature. Using the voltage-clamp method, we then hyperpolarized the cell to −83 mV for 0.5 s to restore the availability of i_{Na}. On releasing the feedback circuit, the anodal break excitation was registered. The upstroke of this break excitation contains two phases, fast (75 V/s) and slow (4.2 V/s). After superfusing TTX (10^{-7} g/ml) the fast-rising phase disappeared. The slow phase was activated after the initial foot, which reflects the time constant of the resting membrane. It should be noted that the peaks of the two anodal break excitations are similar (fig. 5–8). Based on these findings, we concluded that even in the midnodal region there are partial contributions of i_{Na} to the action potential, but the major current at the normal resting potential range is the slow inward current.

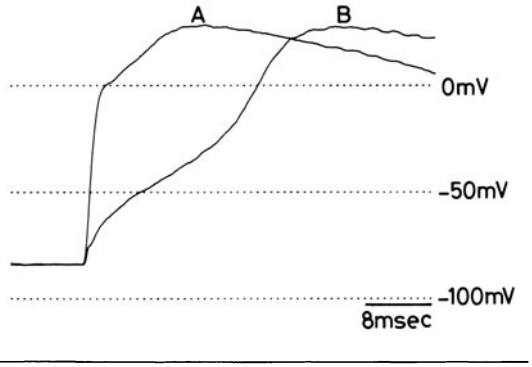

FIGURE 5–8. Effect of TTX on the upstroke of the anodal break excitation: *(A)* in Tyrode solution; *(B)* 10^{-7} g/ml TTX was added to the control Tyrode solution. From Kokubun et al. [15].

Effects of Na-free and Ca-free Tyrode Solutions on the AV Node

When all Na within the normal Tyrode solution was removed and replaced with Tris, the AV nodal specimen immediately became quiescent. The holding current level became more outward by 20 nA under this condition. The slow inward current was still present, but its amplitude relative to the holding current was

slightly smaller than that in the control. The time-dependent increase of the outward current in Na-free solution seemed to be larger than that in the control, and the leak current was also increased in Na-free solutions. As is illustrated in figure 5–9A, the outward current component at 250 ms into the clamp pulse gives an almost linear relationship against membrane potentials. These results clearly show that AV nodal cells can be excitable within Na-free solutions. Because of the increased outward current and leak current, the duration of action potential within Na free solution is brief.

In Na-free solution, spontaneous activity failed to occur because the marked increase in the holding current in an outward direction hyperpolarized the membrane. Under this condition, if the perfusate contains 5 m*M* Ba, the AV node can resume spontaneous activity. A similar phenomenon was observed by Wiggins and Cranefield [31], who observed sustained rhythmic activity in Purkinje fiber exposed to Na-free solution containing 4 m*M* Ba, 16 m*M* Ca, and 128 m*M* TEA. These observations also can be explained from the I–V relation shown in figure 5–9A.

The AV nodal specimen also became quiescent when the perfusate contained 0.5 m*M* EGTA and Ca was not added to the solution. The holding current shifted outward by about 10 nA (fig. 5–9B). The amplitude of the slow inward current gradually decreased and, within 3 min, disappeared. On continuing the perfusion of Ca-free solution, an inward current having the slow-inactivation time course began to appear within 2 min. This inward current was completely blocked by an application of D-600. The current and voltage relationship in Ca-free solution is illustrated in figure 5–9B. At 330 ms into the clamp pulse, the negative slope was between −40 and −20 mV. This negative slope was abolished by the influence of verapamil and therefore must be an incomplete inactivation of the slow inward current. These findings indicate that the inward current recorded in Ca-free solutions is carried by Na ions through the slow inward current channels. Existence of the slow inward current in Na-free or Ca-free solution strongly suggests that the

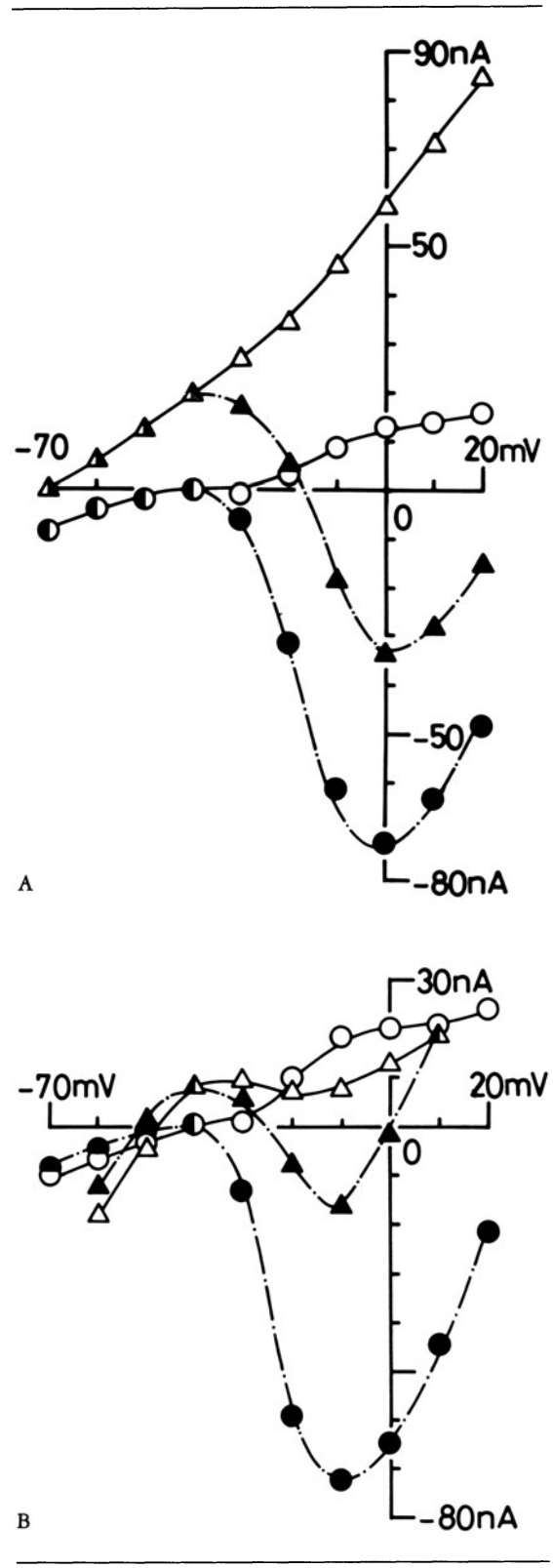

slow inward current in the AV nodal cell may not be carried by a single ionic species.

The slow inward current found in the heart muscle was identical to the Ca current in many other excitable tissues. This was confirmed in a single ventricular cell experiment and in single-channel analysis. It might therefore be safe to state that the AV node has a Ca channel through which both Ca and Na can pass. This finding is in good accord with previous findings in the AV node [8]. Action potential elicited within Ca-free solution had a long plateau phase. This pattern of action potential can also be explained from the I–V relationship described above.

Latent Pacemaker Activity of the AV Nodal Cell

The voltage-clamp experiment described above revealed that AV nodal cells possess dynamic current systems quite similar to those in SA nodes, and thus in the case of failure of the SA nodal rhythm and impaired atrial conduction AV nodal cells can play the role of a pacemaker. In the normal intact heart, however, AV nodal cells never excite spontaneously. The resting potential of the intact quiescent AV nodal specimen was approximately -60 mV, while in the spontaneous small AV nodal specimen, it was approximately -40 mV. It is well known that the resting potentials of the His fiber and the atrial fiber are more negative than -70 mV. In the current clamp experiment we knew that spontaneous excitation ceased at a membrane potential of -60 mV. These findings indicate that a low resting potential is one condition necessary for the AV node to retain its spontaneity.

It was recently shown [32] that in the SA node the current i_h is entirely different from the inward rectifier that has been commonly observed in ventricular cells [33] and skeletal muscle cells [34]. The hyperpolarization-activated current i_h is carried by several ions while the inward rectifier is carried by K^+. The i_h is insensitive to the external application of Ba, while the inward rectifier is abolished. Both i_h and inward rectifier are abolished by application of Cs^+ [32]. The inward rectifier hyperpolarizes the membrane to the resting potential close to the E_K value. If the AV nodal cell has no such channel, then presence of i_h may depolarize the membrane of the AV node to -60 mV. At this potential, the membrane is still quiescent, but if some increase in the leakage current occurs, the membrane will further depolarize, which will initiate spontaneous activity. In fact, Kokubun managed to reconstruct the action potential of the AV node and, by reducing the leakage current component, the model became quiescent.

FIGURE 5–9. Effect of Na or Ca depletion on the slow inward current. The holding potential was -40 mV. The current voltage relations measured at the peak of the inward current (closed symbols) and at 250 ms *(A)* or 330 msec *(B)* into the clamp pulse (open symbols): circles, control Tyrode; triangles, in test solutions in *(A)* Na free solution and in *(B)* Ca-free solution. From Kokubun et al. [15].

Findings in Isolated AV Nodal Cluster Cells

The small AV nodal specimen was convenient for the study of the ionic currents of the AV node. Taniguchi et al. [35] recently isolated the AV nodal cell after collagenase treatment. Compared with the size of ventricular cells, diameters of AV nodal cells are small; in 85 measurements in Tyrode solution, 93 ± 23 μm long and 14 ± 6 μm wide. On the other hand, ventricular cells were 115 ± 33 μm long and 29 ± 9 μm wide (in 102 measurements). The ventricular cells are not spontaneously active within Tyrode solution, containing 1.8 m*M* Ca. When AV nodal tissue was dispersed within Tyrode solution, another marked finding was the presence of cluster cells. The cluster contains 3–10 rounded cells. These rounded cells are unstained by trypan blue, suggesting that the cells are alive. In ventricular cells, such a round cell showed no resting potential, but AV nodal cluster cells showed action potential configurations very similar to those in the intact AV nodal specimen. Figure 5–10 illustrates the voltage-clamp experiments in the flat AV nodal cell cluster, about 50 μm wide and 100 μm long. A two-microelectrode voltage clamp was used. The slow inward current,

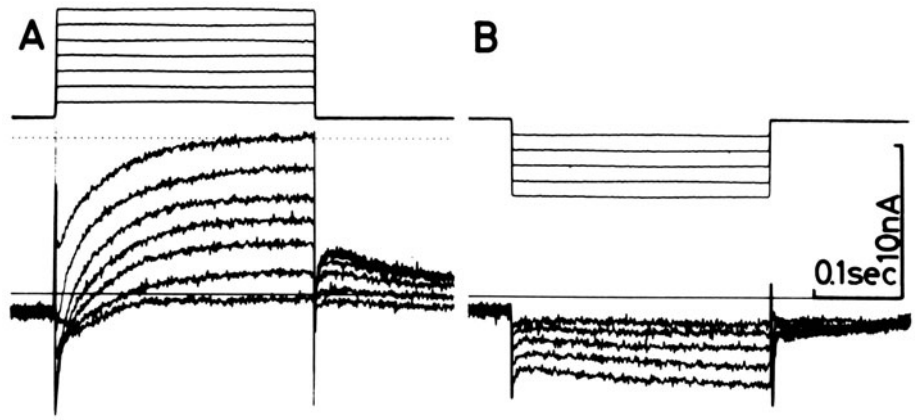

FIGURE 5–10. Voltage clamp experiments in the flat AV nodal cell cluster, about 50 μm wide and 100 μm long. The holding potential was −40 mV and the clamp pulses were applied in 10-mV steps at depolarization (−30 to +30 mV) and hyperpolarization (−90 to +50 mV). Straight lines on the current traces represent 0 level and dotted lines represent 10 nA outward current. From Taniguchi et al. [35].

outward K current, and its tail current were all comparable to those obtained in the small AV nodal specimen. These cluster cells respond to acetylcholine and adrenaline in the same way as the small AV nodal specimen. Moreover, we can inject chemicals into the cluster cells through the microelectrode. We found this cluster preparation is also useful for the study of the AV node.

Conclusion

Although fundamental knowledge about the electrophysiology of AV nodal cells has accumulated during the past decade, the ionic currents underlying the slow conduction and the latent pacemaker activity of the AV nodal cell have not been studied because of the lack of a voltage-clamp method. Instead of the traditional sheet specimen of the AV node, which contains a mixture of information about membrane action potentials, and propagated action potentials, either the small AV nodal specimen or the AV nodal cluster will provide more definitive knowledge about AV nodal function.

In the midnodal region, it was difficult to find a cell that could not be voltage clamped by the conventional method. AV nodal cells have a Ca channel through which both Na^+ and Ca^{2+} flow.

All discrepancies found in this experiment and those in the previous reports [36, 37, 38] resulted from the difference of the specimens, small and large. There are indeed nodal cells in the AV nodal region, having a low resting potential, smaller size, and the Ca channel, and the difference between the midnodal region and the transitional region may be a quantitative one.

References

1. Hoffman BF, Cranefield PF: Electrophysiology of the heart. Mount Kisco NY: Futura, 1960 [reprinted 1976].
2. Matsuda K, Hoshi T, Kameyama S: Action potential of the atrioventricular node (Tawara). Tohoku J Exp Med 68:8, 1958.
3. Tawara S: Das Reizleitungssystem des Saugetierherzens. Jena: Gustav Fischer, 1906.
4. Noma A, Irisawa H: Membrane current in the rabbit sinoatrial node cell as studied by the double microelectrode method. Pflugers Arch 364:45–52, 1976.
5. Irisawa H: Comparative physiology of the cardiac pacemaker mechanism. Physiol Rev 58:461–498, 1978.
6. Brown HF: Electrophysiology of the sinoatrial node. Physiol Rev 62:505–530, 1982.
7. Paes de Carvalho A, De Almeida DF: Spread of activity through the atrioventricular node. Circ Res 8:801–809, 1960.
8. Akiyama T, Fozzard HA: (1979) Ca and Na selectivity of the active membrane of rabbit AV node cells. Am J Physiol 236:C1–C8, 1979.

9. Ruiz-Ceretti E, Ponce Zumino A: Action potential changes under varied $(Na)_0$ and $(Ca)_0$ indicating the existence of two inward currents in cells of the rabbit atrioventricular node. Circ Res 39:326–336, 1976.
10. Zipes DP, Mendez C: Action of manganese ions and tetrodotoxin on atrioventricular nodal transmembrane potentials in isolated rabbit hearts. Circ Res 32:447–454, 1973.
11. Mendez C: The slow inward current and AV nodal propagation. In: Zipes DP, Bailey JC, Elharrar V (eds) The slow inward current and cardiac arrhythmias. The Hague: Martinus Nijhoff, 1980, pp 285–294.
12. Hoffman BF: The specialized tissues of the heart. Paes de Carvalho A, De Mello WC, Hoffman BB (eds). Amsterdam: Elsevier, 1961.
13. Shigeto N, Irisawa H: Slow conduction in the atrioventricular node of the cat: a possible explanation. Experientia 28:1442–1443, 1972.
14. Shigeto N, Irisawa H: Effect of polarization on the action potentials of the rabbit AV node cells. Jpn J Physiol 24:605–616, 1974.
15. Kokubun S, Nishimura M, Noma A, Irisawa H: Membrane currents in the rabbit atrioventricular node cells. Pflugers Arch 393:15–22, 1982.
16. Kurachi Y, Noma A, Irisawa H: Electrogenic sodium pump in rabbit atrio-ventricular node cell. Pflugers Arch 391:261–266, 1981.
17. Kurachi Y, Noma A, Irisawa H: Electrogenic Na pump evidenced by injecting various Na salts into the isolated A-V node cells of rabbit heart. Pflugers Arch 392:89–91, 1981.
18. Deck KA, Kern R, Trautwein W: Voltage clamp technique in mammalian cardiac fibres. Pflugers Arch 280:50–62, 1964.
19. Carmeliet E, Vereecke J: Electrogenesis of the action potential and automaticity. In: Bern RM, Sperelakis N, Geiger SR (eds) Handbook of physiology. Sect 2: The cardiovascular system. Vol 1: The heart. Bethesda MD: American Physiological Society, 1979, pp 269–334.
20. Noma A, Irisawa H, Kokubun S, Kotake H, Nishimura M, Watanabe Y: Slow current systems in the A-V node of the rabbit heart. Nature 285:228–229, 1980.
21. Brown HF, Di Francesco D, Noble SJ: How does adrenaline accelerate the heart? Nature 280: 235–236, 1979
22. Yanagihara K, Irisawa H: Inward current activated during hyperpolarization in the rabbit sinoatrial node cell. Pflugers Arch 385:11–19, 1980.
23. Maylie J, Morad M, Weiss J: A study of pace-maker potential in rabbit sino-atrial node: measurement of potassium activity under voltage-clamp conditions. J Physiol (Lond) 311:161–178, 1981.
24. Mendez C, Moe GK: Atrioventricular transmission. In: De Mello WC (ed) Electrical phenomena in the heart. New York: Academic, 1972, pp 263–291.
25. Wit AL, Cranefield PF: Effect of verapamil on the sinoatrial and atrioventricular nodes of the rabbit and the mechanism by which it arrests reentrant atrioventricular nodal tachycardia. Circ Res 35:413–425, 1974.
26. Ponce Zumino AZ, Parisii IM, De Ceretti ERP: Effect of ischemia and low sodium medium on atrioventricular conduction. Am J Physiol 218:1489–1494, 1970.
27. De Ceretti E, Ruiz P, Ponce Zumino A, Parissi IM: Resolution of two components in the upstroke of the action potential in atrioventricular fibers of the rabbit heart. Can J Physiol Pharmacol 49:642–648, 1971.
28. Irisawa H: Ionic currents underlying spontaneous rhythm of the cardiac primary pacemaker cells. In: Bonke FIM (ed) The sinus node. The Hague: Martinus Nijhoff, 1980, pp 368–375.
29. Kreitner D: Effects of polarization and inhibitors of ionic conductances on the action potentials of nodal and perinodal fibers in rabbit sinoatrial node. In: Bonke FIM (ed) The sinus node. The Hague: Martinus Nijhoff, 1980, pp 270–278.
30. Kokubun S, Nishimura M, Noma A, Irisawa H: The spontaneous action potential of rabbit atrioventricular node cells. Jpn J Physiol 30:529–540, 1980.
31. Wiggins JR, Cranefield PF: The effect of membrane potential and electrical activity of adding sodium to sodium-depleted cardiac Purkinje fibers. J Gen Physiol 64:473–493, 1974.
32. Morad M, Kurachi Y: Cs and Ba block the inward rectifier K channel from the outside site in single isolated ventricular cells. 1982 (in preparation).
33. Cleemann L, Morad M: Potassium currents in frog ventricular muscle: evidence from voltage clamp currents and extracellular K accumulation. J Physiol (Lond) 283:113–143, 1979.
34. Standen NB, Stanfield PR: A potential- and time-dependent blockade of inward rectification in frog skeletal muscle fibres by barium and strontium ions. J Physiol (Lond) 280:169–191, 1978.
35. Taniguchi J, Kokubun S, Noma A, Irisawa H: Spontaneously active cells isolated from the sino-atrial and atrio-ventricular nodes of the rabbit heart. Jpn J Physiol 31:547–558, 1981.
36. Cranefield P, Hoffman B, Paes de Carvalho A: Effects of acetylcholine on single fibers of the atrioventricular node. Circ Res 7:19–23, 1959.
37. Cranefield PF: The conduction of the cardiac impulse: the slow response and cardiac arrhythmias. Mount Kisco NY: Futura, 1975.
38. Hoffman, BF: Neural influences on cardiac electrical activity and rhythm. In: Randall WC (ed) The neural regulation of the heart. New York: Oxford University, 1977, pp 291–312.

6. CABLE PROPERTIES AND CONDUCTION OF THE ACTION POTENTIAL

Excitability, Sources, and Sinks

Morton F. Arnsdorf

Introduction

Cardiac excitability has a certain intuitive meaning suggesting the ease with which cardiac cells undergo individual and sequential regenerative depolarization and repolarization, communicate with each other, and propagate electrical activity in a normal or abnormal manner. The heartbeat arises from a highly organized control of ionic flow through channels in the cardiac membrane, the myoplasm, the gap junctions between cells, and the extracellular space. These bioelectrical events are regulated within very tight limits to allow the coordinated propagation of excitation and contraction of the heart that is necessary for an efficient cardiac output. Abnormalities in the regulatory mechanisms often accompany cardiac disease.

The topic of cardiac excitability is very complex and seems to be getting more complex. In 1962, Noble described cardiac membrane events in terms of two currents [1]. The most recent reviews by Trautwein in 1973 [2], by McAllister et al. as well as by Fozzard and Beeler in 1975 [3, 4], and by Fozzard both in 1977 and 1979 [5, 6] require at least two or three inward currents and four, or perhaps more, outward currents with numerous control mechanisms for the passive and active membrane properties. A quantitative theoretical and experimental scientific definition of cardiac excitability has proven to be a severe challenge to the researcher and the clinician.

As a first approximation, the components of cardiac excitability fall into two general categories: passive and active membrane properties. Passive membrane properties are characterized by a response proportional to the stimulus; active membrane properties by a response out of proportion to the stimulus. Passive membrane properties include the determinants of the resting potential such as intracellular and extracellular ionic activities as well as the energy-requiring pumps that maintain the ionic gradients and both linear and nonlinear cable properties. Active generator properties include the liminal length, which is the critical amount of tissue that must be raised above threshold to overcome the repolarizing effects of adjacent resting tissues and to result in explosive regenerative depolarization, and the voltage- and time-dependent membrane ionic conductances which control the ionic currents responsible for normal and abnormal depolari-

I would like to acknowledge the efforts of Mrs. Clarice Connor and Ms. Antonia Blake in the preparation of this manuscript. Some of the work included was made possible, in part, by NHLBI grants HL-21788 and HL-26591.

N. Sperelakis (ed.), PHYSIOLOGY AND PATHOPHYSIOLOGY OF THE HEART.

Martinus Nijhoff Publishing, Boston/The Hague/ Dordrecht/Lancaster.

zation, repolarization, and automaticity. It is the active membrane properties that are unique to excitable cells. Propagation of the action potential depends on both passive and active membrane properties as they relate to the resting potential, subthreshold events, the fulfillment of the requirements of liminal length, regenerative depolarization, regenerative repolarization, and automaticity.

In this chapter, cable properties and conduction of the action potential will be considered in the context of the determinants of cardiac excitability. The approach will be to make a qualitative statement, an *approximation,* and then to discuss the approximation. Structure–function relationships relevant to electrical events will be discussed. The effects of cable properties and the determinants of conduction can be approached in terms of a few equations. The less mathematically inclined should not feel intimidated since the equations will be used qualitatively as a starting point for discussion. In the sections that follow, certain general principles were selected for discussion and some simplification was required. The more venturesome are referred to the valuable collection of essays in the *Handbook of Physiology* [7] and in the comprehensive book by Jack et al. [8]. Finally, experimental work in electrophysiology, electropharmacology, and arrhythmogenesis will be woven into the discussion to illustrate the principles at hand.

The purpose of this chapter is to create an intellectual framework for the reader that is based on biophysical theory. Such a framework will allow him to appreciate what is known and what is unknown, to decide whether our current hypotheses are reasonable or unreasonable, and to critically assess extrapolations which have been made from the basic laboratory to the clinical situation.

Structure and Bioelectrical Equivalents

THE CELL MEMBRANE: STRUCTURE AND FUNCTION

Approximation 1: The heartbeat results from the generation and organized control of bioelectricity across the cardiac membrane, within and between cells, and throughout the extracellular space.

The ultrastructure of cardiac muscle has been extensively reviewed by Sommer and Johnson [9] as has the molecular biology of membrane by Quinn [10]. The sarcolemma is the boundary of the muscle fiber which has several components. One component is the plasma membrane or plasmalemma which is 6–9 nm thick; another is the glycocalyx, the cell-covering material that stains for sugars and is often associated with collagen, which is 50 nm or more thick.

The plasma membrane is a thin, lipid bilayer that separates the aqueous phases inside and outside the cells. The phospholipids, and some other components of the lipid bilayer, have a hydrophobic portion that is oriented toward the interior of the lipid membrane and a charged hydrophilic portion that is oriented toward the internal or external aqueous phase. The hydrophilic groups vary in extent and affinity for water from single hydroxyl groups, as in cholesterol, to the zwitterionic and charged groups of the glycerophosphatides, to the complex oligosaccharides of the glycosphingolipids. This amphipathicity is characteristic of membrane lipids and largely determines their interactions and orientations in the membrane. Many of the lipid constituents can be polarized with the result that the membrane can act as a capacitor or condenser: that is, it can store charge. The lipid bilayer is a resistive barrier to the flow of ions and charged species, yet the plasmalemma is much more permeable to ions and water than would be expected for such a bilayer. It is assumed that specialized structures allow and control such permeability. These structures seem to be of two types: aqueous channels or pores that extend through the membrane; and protein carriers that either extend or "shuttle" from the inside to the outside of the membrane.

Approximation 2: The cardiac membrane can be modeled in terms of an electrical analogue containing resistors and capacitors (V_m and C_m, respectively, in fig. 6–1B). Models of varying complexity have been proposed.

The plasmalemma, then, has both capacitive and resistive elements, and this is depicted in figure 6–1. Referring to figure 6–1, the cur-

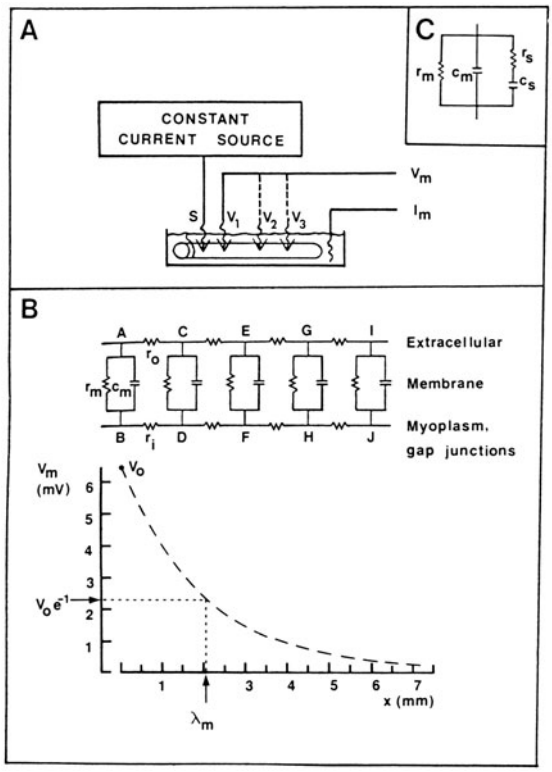

FIGURE 6–1. *(A)* Experimental arrangement for cable analysis. Constant current is injected intracellularly through a microelectrode positioned near the ligated end of a cardiac Purkinje fiber (S). The response in transmembrane voltage (V_m) is recorded by microelectrodes at several points along the preparation (V_1, V_2, V_3, etc.). Measurement of current (I) is obtained from the bath ground. *(B)* The electrical analogue of the passive properties of the membrane, extracellular space, and the combined myoplasm and gap junctions is shown. Below is plotted the transmembrane voltage as a function of distance after intracellular current application. The abbreviations are as in the text. *(C)* This is a more complex electrical analogue which includes series resistance and capacitance (r_s, c_s, respectively).

rent flow through any one unit length of cable (e.g., i_m in element A-B) consists of two components: a capacitive current (i_c) through the capacitor c_m and an ionic current (i_i) through resistor r_m:

$$i_m = i_c + i_{ion} \tag{6.1}$$

where the units for i_m are A/cm.

In reality, the situation is more complex. Equation 6.1 fairly well describes the outer membrane of the plasmalemma which conducts regenerative action potentials down the length of the preparation. In many types of mammalian myocardium, a system of transverse tubules (the T system) conducts action potentials into the interior of the fiber. It is the junction between the T system and the sarcoplasmic reticulum (SR) that links the extracellular and intracellular membrane systems. The membrane that faces these extracellular clefts contributes resistance and capacitance in series to that of the outer membrane (c_s and r_s in the electrical analogue shown in panel C of fig. 6–1). Three-dimensional geometry, of course, further adds complexity to the electrical analogue of membrane geometry [8, 11, 12]. Nevertheless, equation 6.1 serves as a useful approximation, particularly when a preparation is used as its own control and not much anatomic change is anticipated.

Returning again to equation 6.1, i_c is determined by the capacitance of this unit length of cable, c_m which is expressed as F/cm, and controls the rate at which the transmembrane voltage (V_m) changes. This can be described as:

$$i_c = c_m (\partial V_m/\partial t) \tag{6.2}$$

According to Ohm's Law, the ionic current will be directly related to the transmembrane voltage, V_m, and inversely related to the membrane resistance for a unit length of cable, r_m, expressed as Ω.cm. Therefore,

$$i_{ion} = V_m/r_m \tag{6.3}$$

and combining equations 6.1–6.3,

$$i_m = c_m (\partial V_m/\partial t) + (V_m/r_m) \tag{6.4}$$

Approximatic ı 3: The cardiac membrane is selectively permeable to different ionic species that pass through channels controlled by gates which open and close in response to voltage and/or time. The control of these currents can be described in terms in membrane conductance and driving force. The driving force, in turn, depends in part on the maintenance of ionic distribution across the membrane by ionic pumps.

Often the term membrane conductance (g_m) rather than membrane resistance is used when speaking of biologic membranes. Conductance is the reciprocal of resistance (i.e., $g_m = 1/r_m$) and refers to the ease with which an ionic species can flow through a membrane channel. In general, the flow of an ionic species through a membrane channel is determined by the conductance to that ionic species and by the driving force behind that ionic species. For a given ionic species, say y, the driving force is the difference between V_m and the equilibrium potential (E_y) or:

$$i_y = \underbrace{g_y}_{\text{conductance}} \underbrace{(V_m - E_y)}_{\text{driving force}} \tag{6.5}$$

Equations 6.3 and 6.5 imply a linear or ohmic relationship, but this is not the case. The conductance term may depend on voltage, time, or both. Recent evidence suggests the same may be true for intracellular ionic activities [13, 14] which, in part, determine the equilibrium potential. Energy-requiring ionic pumps determine and maintain the transmembrane ionic gradients and may also affect V_m and the equilibrium potential. The equilibrium potential, then, depends on the ionic activities and on the ionic pumps. Many of the linear and nonlinear properties of the membrane have been reviewed by Jack et al. [8] and in other chapters of this book.

In the resting cell, the intracellular voltage is negative with respect to the outside, and the cell is polarized. Negative charges are stored along the inside of the cell membrane and are balanced by positive charges outside the membrane. When current is applied intracellularly, it takes time for the capacitive charge to change so that V_m is not altered instantaneously. The time required for V_m to reach a certain percent of its final value after current onset or offset is termed the time constant of the membrane (τ_m): 84% in a long cablelike structure (see eq. 6.21 below from Hodgkin and Rushton [15]; also see Fozzard and Schoenberg [16]) and 63% in short fibers [16]. It follows then that:

$$\tau_m = r_m c_m \tag{6.6}$$

INTERCELLULAR COMMUNICATION

Approximation 4: Cardiac cells are connected by gap junctions. Gap junctions normally have a low resistance and little impede ionic flow. Injury and other factors may partially or completely uncouple a cell from its neighbor. Longitudinal resistance is determined largely by the gap junctions, and this is represented in the electrical analogue in figure 6–1B by r_i.

Largely as a result of the influence of German pathologists such as Heidenhain [17], the heart was considered by most investigators as being an anatomic and electrical syncytium. The electron microscopic studies by Sjöstrand and Andersson in 1954 [18], however, showed that cardiac cells were bound by membranes and that there was no direct cytoplasmic connection between cells. The manner by which cells communicate has received a great deal of attention from anatomists and electrophysiologists.

In 1952, Weidmann [19] studied the electrophysiologic properties of cardiac Purkinje fibers. Purkinje fibers conduct action potentials rapidly (0.5–5.0 m/s) and constitute the cell type of the conduction system between the atrioventricular node and the ventricles including the bundle of His, the bundle branches and fascicles, and the terminal branching system. Many of the strands of Purkinje fibers are essentially cylindrical and are arranged in columns that are 2–3 cells in diameter. These columns are surrounded by connective tissue. Since structurally the columns are cytoplasm surrounded by membrane and connective tissue and since the cells connect with each other, long Purkinje fiber preparations resemble cables. Weidmann applied subthreshold depolarizing and hyperpolarizing currents intracellularly through one microelectrode and recorded V_m at various points along the length of such Purkinje fibers. He observed a graded drop in V_m with distance from the point of stimulation which was well described by uniform cable theory. An example of such a recording is shown in figure 6–2. Electrotonic potential could be recorded several millimeters from the site of current application, indicating that several cells were between the stimulating and re-

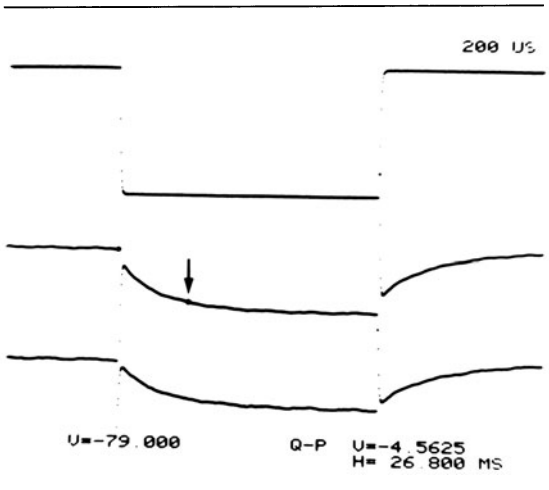

FIGURE 6–2. Experimental records obtained during cable analysis in a long sheep Purkinje fiber. The *top trace* is the current recording; the *lower traces* are recordings of the transmembrane voltage made at different sites along the Purkinje fiber. The *middle trace* was recorded at a site nearer the stimulating microelectrode than was the *lower trace,* and the difference in amplitudes is apparent. Note the nearly exponential change in voltage in response to rectangular current step, a shape caused by the resistance and capacitance of the membrane. One cursor was positioned at the resting potential immediately before current onset; the second cursor was placed at the point where the transmembrane voltage has reached 84% of its final value after current onset (arrow). The number at the lower left is the resting potential; the numbers at the lower right give the coordinates of the cursor indicated by the arrow as compared to the cursor positioned immediately before current onset.

cording microelectrodes, and that the resistance to ionic flow of the structure, allowing communication between cells, must be low. Moreover, the magnitude of the change in V_m was quite linearly related to small intracellularly applied depolarizing and hyperpolarizing currents; characteristics which favored low-resistance electrical coupling rather than chemical coupling.

Weidmann later studied the diffusion of ^{42}K in ventricular muscle [20]. The theoretical distribution of ^{42}K was calculated according to cable theory, and observation was found to agree well with prediction in that ^{42}K diffused freely between cells with the upper limit for resistance between cells being 3 Ω.cm, almost 700-fold less than for the outer cell membrane.

The low-resistance structures responsible for the electrical communication seem to be the gap junctions, specializations of the membrane that allow intercellular communication and mediate transport of small molecules and ions between cells (see reviews by De Mello [21], Lowenstein [22], and Page and Shibata [23]). The gap junction is a specialized portion of the intercalated disc where the membranes of neighboring cells are some 30 Å from each other and are linked by hydrophilic channels that connect the interiors of the two cells. A geometric array of subunits is grouped about a central channel or pore to form a *connexon* which extends from the myoplasm through the inner hydrophilic layer, the hydrophobic lipid bilayer, and the outer hydrophilic layer of the membrane into the gap between the cells where it meets the connexon extending from the neighboring cell. The central channels of the connexons are continuous and connect the interiors of the two cells. Despite the similar electron microscopic appearances, recent studies of isolated gap junctions indicate that the protein compositions between hearts of two different species are similar, but differ from those in the liver and the lens [24, 25].

A number of factors seem to increase the resistance at the gap junction, including an increase in intracellular calcium concentration, a decrease in pH, some metabolic poisons, and digitalis [21–23, 26, 27]. The "healing over" capability of heart cells is of interest, and evidence suggests that cellular uncoupling rather than the formation of a new membrane seems to be responsible [28–31]. Recently, ischemia has been shown to alter the geometric characteristics of the gap junction [32]. Teleologically, the regulation of current flow through the gap junction may have several purposes. It will isolate injured cells, prevent the leakage of the contents of normal neighboring cells through the gap junction to the injured cell to the outside, and will eliminate the current flows and resultant potential for arrhythmias. Other influences on electrical communication between cells may include capacitive coupling [33, 34] and the accumulation and depletion of ions in limited intercellular spaces [35].

Having said all this, there is a longitudinal

or inside resistance resistor (r_i in fig. 6–1) which is determined primarily by the gap junctions and to a lesser extent by cytoplasmic components and perhaps other determinants. There is also an extracellular resistance resistor r_o in figure 6–1, which, for the reasons to be discussed in next section, is negligible in normal tissues. In tissues of small diameter and in injury, however, r_o may not be negligible and this will be discussed below.

Cable Properties

ONE-DIMENSIONAL CABLE CIRCUIT

Approximation 5: The electrical analogue in figure 6–1 resembles a telegraph cable in that a low-resistance core (the myoplasm and normally low-resistance gap junctions) is surrounded by insulation of relatively high resistance (the cell membrane). The so-called cable equations, therefore, have been applied to cardiac structures. In many instances, experimental data have been well described by these cable equations.

Cable properties influence the coordination of electrical activity, conduction, and aspects both of normal and abnormal cardiac excitability. The central importance of passive membrane properties is the reason for this chapter. We may now experimentally examine and quantify many of the passive membrane properties relevant to excitability and conduction.

Many electrocardiographers and some electrophysiologists respond to the topic of the cable equations with a sense of panic. We have attempted to minimize this panic by devoting a fair amount of space to a discussion of structure and bioelectrical equivalents in the preceding sections. This should prepare the reader for a reasoned approach to these equations. The meaning and implications of the components in the simple electrical analogue depicted in figure 6–1 should now be understood conceptually. As a first approximation, we will now analyze passive membrane behavior in terms of membrane resistance (r_m), membrane capacitance (c_m), the longitudinal or inside resistance (r_i), and the time constant (τ_m).

Concept and Assumptions. We will assume that the preparation resembles a transmission line and can be modeled as a one-dimensional cable circuit with the resistances and capacitances in this circuit as depicted in figure 6–1. The cells are considered to be a column with a low-resistance cytoplasm, a high-resistance outer membrane, and low-resistance connections at the end and between cells. The column is assumed to be cylindrical and, for the moment, uncomplicated by invagination of the membrane, three-dimensional considerations, and the accumulation and depletion of ions in limited intercellular spaces. Other simplifying assumptions are also made: the membrane and longitudinal resistances are ohmic and linear for small changes in V_m; longitudinal current flow is uniform and radial currents are negligible; the membrane capacity is perfect and uniform; and the outside solution is large so that the resistance of the outside (r_o) is negligible.

The Classic Cable Equation: One-dimensional Cable Circuit

Approximation 6: The insulation of the cable (the membrane) is leaky, and the loss of current through the membrane will result in less current being available for longitudinal flow. Longitudinal flow, in turn, is also influenced by resistances in the myoplasm and at the gap junctions. The circuit is completed by ionic flow in the extracellular space.

In the mid-19th century, Lord Kelvin considered the case of the decrement in the signal carried by transatlantic telegraph cable. This one-dimensional cable circuit included terms to account for the internal and external resistances and for the leak through the insulation. In a classic study, Hodgkin and Rushton in 1946 [15] showed that a modified cable equation rather well fit experimental observation in a nerve axon. Weidmann in 1952 [19] applied one-dimensional cable theory to cardiac Purkinje fibers and found the experimental data to be well described by the cable equation. The basic equation, assuming r_o is negligible is:

$$i_m = \frac{1}{r_i}\frac{\partial^2 V_m}{\partial x} = \frac{V_m}{r_m} + c_m\frac{\partial V_m}{\partial t} \qquad (6.7)$$

where i_m is the current flow through any unit length of membrane; r_i is the longitudinal resistance of a unit length of the inside conductor

or core of the cable (Ω/cm); V_m is the transmembrane voltage; and r_m and c_m, as previously defined, are the membrane resistance and capacitance for a unit length of cable (Ω.cm and F/cm, respectively).

This equation looks formidable, but can be understood if considered in the context of the earlier descriptions of structure and function. Referring to figure 6–1, the current flow (i_i) inside the cell to the right for a given length of inside conductor must return to the left through the parallel segment of the outer conductor. The resistance for a given length (termed Δx) of the inside and outside conductors would be $r_i\Delta x$ and $r_o\Delta x$, respectively. According to Ohm's Law, the potential difference across any of the resistors (say, the resistor r_i between elements B and D in fig. 6–1) is:

$$\Delta V_i = i_i r_i \Delta x \tag{6.8}$$

The length can be made smaller and smaller so that Δx approaches zero. Mathematically, this is written:

$$\frac{\partial V_i}{\partial x} = \lim_{x \to 0} \frac{\Delta V_i}{\Delta x} = -i_i r_i \tag{6.9}$$

The negative sign indicates that the potential drops as the current passes across the resistor.

As mentioned before, r_o is negligible because the outside solution is large although it could be considered in the same manner as r_i. Since r_o is negligible, V_m may be identified with V_i since the extracellular voltage will be constant. Conventionally, the extracellular current is assumed to be zero. Equation 6.9, therefore can be rewritten:

$$\frac{\partial V_m}{\partial x} = -i_i r_i \tag{6.10}$$

The membrane of the cell is leaky, and a certain amount of current is lost ($-i_m$) per unit length of the cable (Δx). It follows that a loss through the membrane will result in less longitudinal current flow through the core. The change in longitudinal current (Δi_i) can be described as:

$$\Delta i_i = -i_m \Delta x \tag{6.11}$$

Once again, the length of membrane can be made smaller and smaller. If we take the limit as Δx approaches zero, we have:

$$\frac{\partial i_i}{\partial x} = \lim_{x \to 0} \frac{\Delta i_i}{\Delta x} = i_m \tag{6.12}$$

and rearranging,

$$i_m = -\frac{\partial i_i}{\partial x} \tag{6.13}$$

Differentiation of equation 6.10 results in,

$$\frac{\partial^2 V_m}{\partial x^2} = r_i\left(\frac{\partial i_i}{\partial x}\right) \tag{6.14}$$

and substituting from equation 6.13, the relationship becomes,

$$\frac{\partial^2 V_m}{\partial x^2} = r_i i_m \tag{6.15}$$

We obtain the *cable equation,* equation 6.7, by substitution from equation 6.4 and rearranging,

$$i_m = \frac{1}{r_i}\frac{\partial^2 V_m}{\partial x^2} = \frac{V_m}{r_m} + c_m \frac{\partial V_m}{\partial_t} \qquad \text{(eq. 6.7 again)}$$

Cable Analysis Based on a One-dimensional Cable Circuit

Approximation 7: Biophysical theory is powerful when it is amenable to experimental testing. One-dimensional cable theory has been used as the basis of experimental cable analysis. The cable equations required some modification to contain terms that could be assessed experimentally: terms that could be expressed as voltage, distance or space, and time.

Equation 6.7 is the fundamental equation of one-dimensional linear cable theory and serves as the basis for cable analysis. The object is to derive equations which contain terms that can be assessed experimentally. Cable analysis has defined certain temporal and spatial constants: the *time constant,* $\tau_m = r_m c_m$ (eq. 6.6); and the *length* or *space constant,* $\lambda_m = \sqrt{r_m/(r_i + r_o)}$ or,

when r_o can be neglected, $\lambda_m = \sqrt{r_m/r_i}$. The length constant is the distance over which V_m falls to e^{-1} (about 37%) of its value at the point of steady-state current application (see fig. 6–1).

Given these two definitions, multiplying equation 6.7 by r_m, substituting, and rearranging, we obtain,

$$-\lambda_m^2 \left(\frac{\partial^2 V_m}{\partial x^2}\right) + \tau_m \left(\frac{\partial V_m}{\partial t} + V_m\right) = 0 \qquad (6.16)$$

Equation 6.16 provides a relationship between V_m, x, and t that is amenable to experimental description. The solution of this equation requires transform methods and a consideration of error functions. The interested reader is referred to Hodgkin and Rushton [15]. The solution leads to the description of the transmembrane voltage at the point of stimulation (V_0) for a constant current long duration (I_0) as:

$$V_0 = r_i I_o \lambda_m / 2 \qquad (6.17)$$

The denominator of 2 is used since half the current flows in one direction down the cable and the other half flows in the opposite direction. If current is introduced near a high-resistance barrier such as the cut or ligated end of a Purkinje fiber, division by 2 is not required.

The distribution of the transmembrane voltage along the cable after the intracellular application of a long constant current can be rather well described. For V_x, defined as V_m at any point x along the cable, the relationship to V_0 is approximated by:

$$V_x = V_0 e^{-x/\lambda_m} \qquad (6.18)$$

Equation 6.18 says that V_x reaches $1/e$ the value of V_0 at one length constant. The decline is exponential. The use of this relationship will be considered below.

Another special solution is the time course of a voltage change at $x = 0$. This can be described as:

$$V_t = V_0 \operatorname{erf} \sqrt{t/\tau_m} \qquad (6.19)$$

The erf of 1 is 0.84, so V_m will reach 84% of its final value at $t = \infty$ in one time constant. The use of this relationship will also be considered in the following section.

Input resistance (R_{in}) describes the relationship between the step constant current and the response in the transmembrane voltage at the point of stimulation.

$$R_{in} = V_0/I_0 \qquad (6.20)$$

Realizing that $\lambda_m = \sqrt{r_m/r_i}$ and combining equations 6.17 and 6.20, the input resistance can be expressed as:

$$R_{in} = \frac{\sqrt{r_m/r_i}}{2} \qquad (6.21)$$

When geometric terms are added so that resistance and capacitance are considered in terms of surface area or cross-sectional area, we obtain:

$$R_m = 2\pi a r_m \qquad (6.22)$$
$$R_i = \pi a^2 r_i \qquad (6.23)$$
$$C_m = c_m/2\pi a \qquad (6.24)$$

where a is the radius of the cable; R_m is the resistance of 1 cm^2 of membrane ($\Omega.cm^2$); R_i is the intracellular or longitudinal resistance in Ω.cm; and C_m is the capacitance of 1 cm^2 of membrane is F/cm^2.

Weidmann's classic study in 1952 [19] first defined these constants in cardiac Purkinje fibers. He also presented special cases for fibers terminating in branches, a short circuit, or a cut end. The latter has been particularly useful in explaining voltage-clamp data in short segments of Purkinje fibers [4, 16].

Cable Analysis Using Theory Based on a One-dimensional Cable Circuit: Limitations

Approximation 8: To understand the power of cable analysis, one must appreciate its limitations. Once the limitations are appreciated, the technique can be applied with care. A number of very important and useful experiments in physiology and pharmacology have employed cable analysis based on one-dimensional cable circuits.

The assumptions underlying the one-dimensional cable analysis considered in the section

Concept and assumptions are not strictly true and limit the method. The most serious deviation from simplified theory results from complex cardiac ultrastructure. Nonhomogeneity of charge during point stimulation has been recognized since the early studies by Weidmann in ungulate Purkinje fibers of several species. In his classic study of 1952 [19], Weidmann found the following in long kid Purkinje fibers: an R_i of about 100 Ω.cm, R_m of about 2000 Ωcm^2, λ_m of about 2 mm, τ_m of about 20 ms, and a C_m of about 12$\mu F/cm^2$. R_m was comparable although somewhat lower than nerve; R_i was greater than the extracellular solution; but C_m was ten times higher than nerve. Weidmann suggested that his geometric assumptions might be in error. Mobley and Page [36] later found that the cleft membrane accounted for some 80% of the total surface membrane, meaning that the total area was 10–12 times greater than that assumed by Weidmann for a simple cylinder. This suggests that C_m should be about 1 $\mu F/cm^2$ and R_m should be about 20,000 Ωcm^2. Hellam and Studt [37] came to a similar conclusion and calculated C_m at 0.9 $\mu F/cm^2$. Fozzard in 1966 [38] found the equivalent membrane circuit to contain not only a resistance and capacitance in parallel, but also a resistance in series with a capacitance (see panel C of fig. 6–1). The Purkinje strand is made up of many cells that are separated by narrow intercellular clefts [9, 36] and these clefts may be the source of the series capacitance. Freygang and Trautwein [33] suggested that the intercalated discs might be a capacitive component in a longitudinal direction. Schoenberg et al. [39] used a more complex model based on the ratios provided by Mobley and Page, and discussed in some detail the differences in cable properties depending on the assumed geometry. These investigators determined that the internal membrane of the passive Purkinje fiber is accessible to charge injected at the surface and, for a 100-μm fiber, the charging time constant is 1–2 ms and the d.c. length constant for the clefts appears to be in the order of 100 μm. It seems reasonable to conclude that the rapidity of the charging time and the magnitude of the length constant as compared to the diameter of the column is the reason that experimental observations have been fit so well by the simplified theory except for extreme cases such as for stimuli of short duration. Potassium accumulation and depletion in the extracellular clefts has been documented during voltage clamping [40, 41], but the error introduced by this type of change is uncertain. Other comments on structure will be made in the section on *The sink: discontinuous propagation,* where the concept of structural and functional discontinuities is introduced.

As discussed above, membrane resistances often are not ohmic and linear except for very small electrical perturbations. Such nonlinearities are seen in figure 6–3 and will be discussed below. Nonlinear theory, therefore, needed to be developed (see *Multidimensional cable circuits and nonlinear theory).* Longitudinal current flow may or may not be uniform and radial currents may or not be negligible. Theories which considered two-dimensional and three-dimensional characteristics needed to be developed (see the sections on *Multidimensional cable circuits and nonlinear theory; Sources, sinks, and propagation;* and *Safety factor).*

Cable Analysis Using Theory Based on a One-dimensional Cable Circuit: Practice. The successful and useful description of experimental results using such simplified theory, however, has been demonstrated in physiologic [16, 19, 20, 28, 38, 39, 42, among others], pharmacologic [43–47] and other interventional studies [48, 49].

We have recently been interested in the effects that lysophosphatidylcholine (LPC) has on electrical properties of Purkinje fibers [48] and that lidocaine has on the membrane properties altered by LPC [49]. The reason for our interest is that LPC accumulates in ischemic but not in normal myocardium and has electrophysiologic actions. A strong case has been made for the role of LPC and similar compounds in arrhythmias that accompany acute myocardial ischemia [50–52, among others]. Given the descriptive background and the relatively rigorous mathematical treatment in the preceding sections, it seems reasonable to describe an experiment and the manner in which it is analyzed.

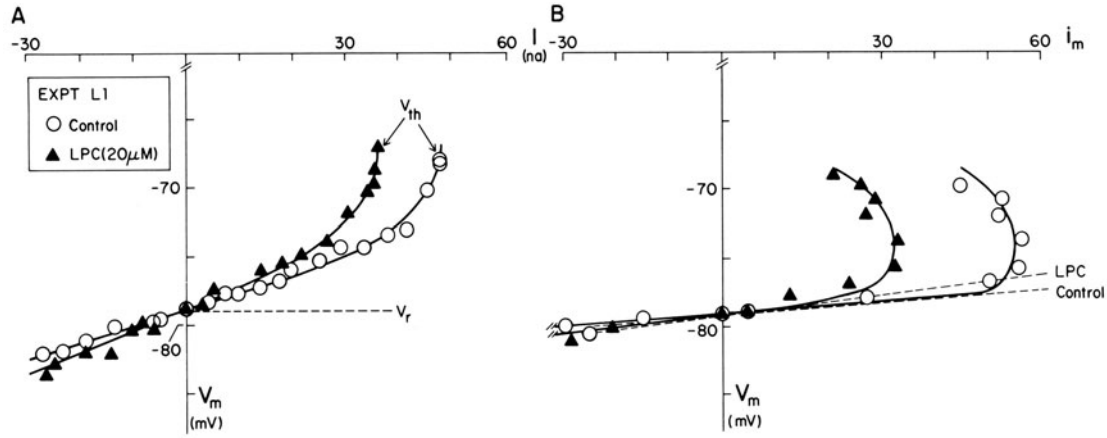

FIGURE 6–3. Current–voltage relationships demonstrating nonlinear behavior in the subthreshold potential range before and after lysophosphatidylcholine (LPC), a toxic metabolite of ischemia. *(A)* I vs V_m. *(B)* i_m vs V_m where i_m is the mathematically derived membrane current density; t = 100 ms. Tangents to the curves (dashed lines) allow estimation of slope conductance, in this case at $i_m = 0$, which is equivalent to the chord conductance. From Arnsdorf and Sawicki [48].

Small hyperpolarizing constant currents were applied intracellularly through a glass microelectrode positioned near the ligated end of a long unbranched Purkinje fiber, thereby permitting the modification of equation 6.17 that holds for unidirectional current flow, $V_0 = r_i I_0 \lambda m$. The fiber radius was 80 μm. The bath was kept at virtual ground using an operational amplifier and produced a voltage signal proportional to the current collected by the bath ground (fig. 6–1B). This transmembrane current was termed I_0 and is depicted in the upper trace of figure 6–2. The value for I_0 was 45.4 nA. The intracellularly applied current was of 100 ms duration and produced a 5.44 and 4.05 mV change in V_m at recording microelectrodes located 300 μm (middle trace) and 900 μm (lower trace), respectively, from the stimulating microelectrode. V_m at these and other sites can be plotted on a logarithmic scale as a function of the distance from the stimulating microelectrode *(x)* or, as in this case, the data can be subjected to linear regression analysis and a curve generated V_0 is determined by extrapolation of the line to $x = 0$ and was 6.30 mV. λ_m is defined as x at which $V_m = e^{-1}V_0$ and was 2.03 mm. τ_m was the time at which the change in V_m had reached 84% of its final value in the microelectrode nearest to the stimulating electrode and was 26.8 ms (arrow in fig. 6–2). Using this data, R_{in} was 139 kΩ (eq. 6.20), R_m was 1771 Ωcm^2 (eq. 6.22), R_i was 215 Ωcm (eq. 6.23), and C_m was 15.1 μF/cm^2 (eq. 624). After LPC, V_0 was 8.4 mV and λ_m was 2.47 mm. R_{in} increased to 186 kΩ, R_m increased to 2883 Ωcm^2, R_i increased to 236 Ωcm, and C_m was little changed at 12.0 μF/cm^2.

The limitations of the assumption that the current–voltage relationship is ohmic or linear are illustrated in figure 6–3, which shows the voltage response in the proximal microelectrode to hyperpolarizing and depolarizing intracellularly applied constant currents in the same preparation before and after LPC [48]. The panel on the left is uncorrected and shows the relatively linear or ohmic changes near the resting potential and the clear nonlinearities as the voltage threshold for regenerative depolarization (V_{th}) is approached. The long Purkinje fiber can be considered an infinite cable, and the relationship suggested by Cole and Curtis in 1941 [53] can be applied to the heart [45, 48, 50, 53], thereby providing an estimate of the current density (i_m) where i_m is approximated by I (dI/dV_m). The current, I, can be measured

directly and dI/dV_m determined from tangents constructed to the curve of the V_m vs I plot (fig. 6–3A). V_m is plotted as a function of i_m in figure 6–3B. This calculation corrects mathematically for cable properties that tend to smooth out current–voltage relationships and allows for approximation of a uniform depolarized membrane resulting in an accentuation of the membrane current–voltage relationship. The negative slope in panel B may represent inward rectification, although possibly the contribution of inward currents is increasing as threshold is approached. Membrane slope conductance (G_m) can be estimated from the relationships $G_m \simeq dI/dV_m$ in panel A or di_m/dV_m in panel B. As can be seen in figure 6–3A, at this point in the experiment neither the resting potential (V_r) nor the threshold voltage (V_{th}) was affected by LPC. In both panels, LPC caused the curve to become steeper and shifted it to the left for depolarizing currents, resulted in a crossing over of the two curves, and resulted in a given hyperpolarizing current producing a large change in V_m. This reflects a decrease in slope conductance or an increase in its reciprocal, slope resistance. Identical curves fit both the control and LPC periods in both panels, suggesting that the current–voltage nonlinearities were little changed.

MULTIDIMENSIONAL CABLE CIRCUITS AND NONLINEAR THEORY

Approximation 9: Reality requires nonlinear theory in three dimensions. Such mathematical and analytic approaches are formidable. The advantage of the simpler linear, one-dimensional model is the ease of calculation; the cost is the loss of information and precision. Computer technology presents an opportunity for utilizing more complex models in the analysis of experimental data.

Without doubt, one-dimensional cable circuits and linear theory have been useful in a variety of tightly controlled experimental conditions. Clearly, however, more dimensions exist and current–voltage responses are not linear. A problem has been the development of mathematical and analytic theories suitable for considering experimental results in two or three dimensions. It is beyond the scope of this chapter to consider the several approaches in detail and the interested reader is referred to Jack et al.[8]. A few comments, however, should be made.

Woodbury and Crill over 20 years ago [54] observed that electrotonic potential distribution from a point source of current in a two-dimensional sheet of cells did not follow the exponential decay consistent with unidimensional cable theory, but rather had a form of a Bessel function. They also observed that the decay in potential in rat atrium was much sharper perpendicular to the fiber axis than along the long axis, although both decays could be fit by a Bessel function. Sperelakis and MacDonald [55] considered the bulk resistivities in ventricular muscle and found that the resistivity longitudinally was much lower than transversely. This and other work suggests that internal coupling and the resistance of the gap junction are of great importance in the electrotonic spread of currents and in the determination of input resistance. Conduction velocity should and is affected, and this will be discussed later in this chapter, particularly in *Sinks, sources, and propagation* and *Safety factor.*

Active Membrane Properties and Excitation

THRESHOLD; LIMINAL LENGTH; AND STRENGTH– AND CHARGE–DURATION RELATIONSHIPS

Approximation 10: Under certain conditions in excitable cells, a stimulus produces a regenerative response. These conditions have been described in terms of threshold, threshold current, charge, and liminal length. The concept of liminal length emphasizes the importance of passive membrane properties to cardiac excitability.

The passive membrane properties in which the stimulus produces a proportional response in the membrane potential have been discussed. At a certain point in excitable cells, the response is regenerative and out of proportion to the stimulus. This point has often been called the threshold voltage or, more simply, the threshold. Threshold, however, is somewhat of a metaphysical concept since it depends in a given fiber on a number of factors.

Lapicque in 1907 [56] recognized in nerve

that the current required to attain threshold was greater for stimuli of short duration than for stimuli of long duration. The rheobasic current was the smallest current regardless of length that could cause a regenerative response. The current strength–duration relationship was described by Lapicque as:

$$I_{th} = I_{rh}/ [1 - e^{t/\tau}] \quad (6.25)$$

where I_{th} is the current required to provoke a regenerative response, I_{rh} is the rheobasic current, t is the duration of I_{th} and τ approximates the membrane time constant. The data suggested that the charge threshold, $I_{th} \times t$, was relatively constant, and the relationship could be interpreted in terms of a constant threshold and a simple RC circuit.

Hodgkin and Huxley [57], however, found threshold to be quite complicated even in nerve. Sodium conductance needed to be described in terms of voltage- and time-dependent activation and inactivation variables (see the following section). Noble and Stein [58] and Cooley and Dodge [59], among others, concluded that threshold was the situation where depolarizing inward current equals repolarizing outward current, with the kinetics of the former being more rapid than those of the latter.

Dominguez and Fozzard [42] utilized intracellular current application and intracellular potential recording to study strength–duration relationships in sheep Purkinje fibers. They found that the time constant of the strength–duration curve in heart muscle was much shorter than was the membrane time constant. Moreover, they observed that the voltage which defined threshold differed with the duration of the stimulus. Fozzard and Schoenberg [16] studied strength–duration relationships in both short and long Purkinje fibers and concluded that the characteristics described by Dominguez and Fozzard resulted from the cable properties of the Purkinje fibers. They applied the concept of "liminal length", first proposed by Rushton [60] in nerve, to the results in short and long preparations. For the unidimensional cable, the liminal length is that length of tissue required to be raised above threshold so that the inward depolarizing current from that region is greater than the repolarizing influences of adjacent tissues. For the reasons discussed above when comparing unidimensional to multidimensional circuits or tissues, point excitation is more difficult in a three-dimensional tissue than in a sheet, and more difficult in a sheet than in a simple cable. The complex calculation of the liminal length and of strength–duration curves from a liminal length model can be found in the paper by Fozzard and Schoenberg [16], but it is useful to simply include the equation since it shows the type of influences relevant to the attainment of the liminal length and threshold in heart tissue:

$$\text{liminal length} = \frac{0.855\ Q_{th}}{2\ (\pi)^{3/2}\ a\ C_m\ \lambda_m\ V_{th}} \quad (6.26)$$

where Q_{th} is the charge threshold, a is the radius, and the other terms are as previously defined. This shows that cable properties are not only important in the passive cell, but to a great extent define the conditions under which regenerative depolarization can occur.

FAST AND SLOW RESPONSES

Approximation 11: Some cardiac tissues, such as those of the atrium, the Purkinje fibers of the His–bundle branch system, and ventricular muscle, normally depend on i_{Na} for phase-0 regenerative depolarization. Others, such as the SA and AV nodes, normally depend on i_{si} for phase 0. These have been termed "fast-" and "slow-response" tissues, respectively, and the characteristics are summarized in table 6–1.

The characteristics of these responses are considered in detail elsewhere in this book and in recent reviews [2, 5, 61, 62, among others]. The regenerative action potential in some tissues depends on the inrush of sodium ions (i_{Na}) through a kinetically rapid channel that is blocked by tetrodotoxin (TTX); while in other tissues depends on the inrush of a mixed $Ca^{2+} - Na^{+}$ current (the slow inward current, i_{si}) through a kinetically slow channel that is little affected by TTX, but which can be blocked by compounds such as D-600 and verapamil. The former has been termed a fast response; the latter a slow response. The electro-

TABLE 6–1. Characteristics of "fast" and "slow" response cardiac tissues

	"Fast" response tissues	"Slow" response tissues
Passive Membrane Properties		
Normal resting potential (V_r)	Appx −80 to −90 mV	Appx −40 to −65 mV
Subthreshold membrane conductable	Components of g_K, particularly g_{K_1}	Probably a component of g_K
Active Membrane Properties		
"Threshold" voltage	Appx −60 to −75 mV	Appx −40 to −60 mV
Current responsible for phase 0 depolarization	i_{Na}	i_{si} (mixed current with both Ca++ and Na+
Activation and inactivation kinetics of channel responsible for phase 0 depolarization	Fast	Slow
Maximal rise velocity of phase 0 (dV/dt_{max} or V_{max})	300–1000 + V/sec	1–50 V/sec
Peak overshoot	Appx +20 to +40 mV	−5 to +20 mV
Overall amplitude of action potential	Appx +90 to +135 mV	Appx −30 to +70 mV
Refractoriness and reactivation	Partial reactivation during phases 3; complete reactivation in normal tissue 10 to 50 msec after return to normal V_r.	Partial and complete reactivation returns after (>100 msec) attainment of V_r.
Conduction velocity	0.5 to 5 m/sec	0.01 to 0.1 m/sec
Characteristics conducive to reentry	Only with inactivation of the sodium system	Yes, even in normally i_{si}-dependent tissues
Automaticity	yes	yes
Automaticity depressed by physiological increases in $[K+]_0$	yes	no
Geographic Location	Working and specialized atrial; infranodal specialized conduction system (Purkinje fibers); ventricular muscle.	SA and AV node; perhaps valves; coronary sinus; injured tissues in which i_{Na}-dependent converted to i_{si}-dependent phase 0

physiologic properties of fast- and slow-response tissues are summarized in table 6–1.

Fast-Response Tissues

Approximation 12: In the i_{Na}-dependent fiber, a V_m less negative than the normal resting potential will decrease i_{Na} by several mechanisms, including a decrease in driving force ($V_m - E_{Na}$ less than normal), a decrease in maximal sodium conductance, partial closure of the off-gate, and changes in other factors such as cable properties and the liminal length.

Fast-response or i_{Na}-dependent tissues are found in the atrium, the Purkinje fibers of the specialized infranodal conduction system, and ventricular muscle. The resting potential (V_r) is normally −80 to −95 mV. As mentioned, the Hodgkin–Huxley model, which includes time- and voltage-dependent activation and inactivation variables, rather well describes the behavior of the sodium current. A modification of equation 6.5 is useful in describing control of the sodium current in terms of conductance and driving force. In nerve, Hodgkin and Huxley [57] used the relationship:

$$i_{Na} = \overline{g_{Na}}\, m^3 h\, (V_m - E_{Na}) \qquad (6.27)$$

where i_{Na} is the sodium current per unit area; $\overline{g_{Na}}$ is the maximal sodium conductance; m and h are dimensionless activation and inactivation variables which, as will be discussed below, can

be conceptualized as on- and off-gates, respectively; and E_{Na} is the equilibrium potential for sodium. Several modifications of this equation have been used for heart muscle, such as that by Ebihara and Johnson [63].

As a first approximation, equation 6.27 describes the maximal sodium conductance as determined by two variables that change with voltage. The rapid activation variable *(m)* can be conceptualized as an on-gate and the slow inactivation variable *(h)* as an off-gate. During depolarization the on-gate opens and the off-gate closes, but the kinetics of the on-gate are faster than those of the off-gate. If the fiber is depolarized rapidly, at threshold the on-gate opens rapidly and sodium rushes into the cell, producing the rapid upstroke (phase 0) of the action potential. The maximal rate of rise of phase 0 is often termed $\dot{V}_{max}$ and has normal values of 200–1000^{+} V/s. V_m moves towards E_{Na} which is about +40 mV.

The off-gate is kinetically slow, so it closes very slowly following rapid depolarization and interferes little with the inrush of sodium ions at threshold. After the peak of the action potential and during the plateau, however, enough time has passed so that the off-gate closes completely. The sodium system, therefore, is *inactivated,* regardless of the state of the on-gate. Such inactivation is the basis of the refractory period and can be absolute or partial. If the tissue is depolarized by injury, hyperkalemia, or some other cause, the off-gate may maintain some degree of inactivation of the sodium system. If a constant or slowly increasing current makes V_m less negative, the off-gate will have sufficient time to close and partially or completely inactive the sodium system: a type of voltage-dependent inactivation of the sodium system that has been called "accommodation". Biologic equivalents of a constant or slowly increasing current would be injury currents and the currents responsible for slow diastolic depolarization in pacemaker cells. This, as will be discussed subsequently, will influence the conduction velocity. It has been difficult to measure i_{Na} directly in cardiac tissue, and often $\dot{V}_{max}$ upstroke has been used as an indirect measure of sodium conductance (to be discussed further in *The source).* More recently, however, the use of single-cell or small preparations has permitted direct measurement of the sodium current [64–67].

Approximation 13: Repolarization in fast-response tissues depends on the balance between several currents.

Repolarization in fast-response tissues is a regenerative process. Phase 1 depends on the inactivation of g_{Na} and, at least for Purkinje fibers, on inactivation of an inward negative current. During phase 2, the mixed Ca^{2+}-Na^{+} current, i_{si}, increases due to the positive voltage. Since i_{si} is an inward positive current, it has a depolarizing influence and helps to maintain the plateau. Potassium conductance decreases and becomes rectified in that K^{+} enters the cell more easily than it exits, a mechanism which also maintains the plateau. Phase-3 repolarization, which is the rapid return to the resting potential, results from inactivation of i_{si}, reversal of the process of inward rectification, and activation of repolarizing outward potassium currents. There seems to be a "threshold" at about −30 mV in Purkinje fibers at which phase 3 occurs. During phase 3, enough of the sodium system is normally reactivated, so that another action potential can be electrically induced. As will be considered below, failure of normal repolarization affects excitability and propagation.

Other characteristics of fast-response tissues are included in table 6–1.

Slow-Response Tissues

Approximation 14: Slow-response tissues depend on i_{si} *for phase 0 and as compared to fast-response tissues have a less negative resting potential, a slower* $\dot{V}_{max}$*, a slower conduction velocity, and reactivation that is time dependent (table 6–1).*

In the sinoatrial (SA) and atrioventricular (AV) nodes, phase-0 depolarization depends not on i_{Na}, but on the slow or secondary inward current i_{si}. As mentioned, this mixed Ca^{2+}-Na^{+} current uses a channel that is little influenced by blockers of the rapid sodium channel such as TTX, and this channel is kinetically slower than for i_{Na}. Slow-response fibers have a less negative resting potential of around −60

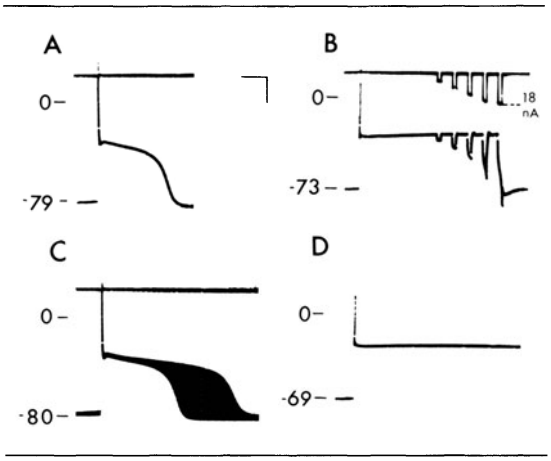

FIGURE 6–4. Two stable and quiescent steady states induced by LPC with normalization of the action potential by lidocaine. The calibration marks are 100 ms and 20 mV horizontally and vertically, respectively. *(A)* Control with an action potential duration of 290 ms. The resting potential (V_r) was −79 mV. *(B)* At 30 min after the application of LPC, two steady states were observed: one at a slightly less negative V_r of −73 mV and the other at the plateau potential. Intracellular hyperpolarizing constant currents ($t = 100$) were applied and with increasing strength at 18 nA finally caused attainment of the repolarization "threshold" and a return to V_r. If the current was not applied, V_m remained at the plateau indefinitely. *(C)* The application of lidocaine progressively shortened the action potential duration to a normal value of 300 ms and caused V_r to become more negative at −80 mV. The hyperpolarization was most likely due to an increase in membrane potassium conductance. *(D)* Washout of lidocaine during continued LPC superfusion resulted in the rapid reappearance of two stable steady states. Note the less negative V_r. From Sawicki and Arnsdorf (unpublished data).

mV. At this potential, the sodium system is essentially completely inactivated. Reactivation of i_{si} is time dependent and actually extends into electrical diastole. This characteristic is of importance in limiting the number of impulses that can traverse the AV node and protects the ventricles in atrial fibrillation and flutter.

If tissues that normally are i_{Na} dependent have their sodium system inactivated either by depolarization of the quiescent cell or by a failure of normal repolarization, the tissue may develop action potentials that are dependent on i_{si}. A striking example of this following the failure of normal repolarization is shown in figure 6–4 [49]. Other characteristics of slow-response tissues are included in table 6–1.

PRACTICAL CONSIDERATIONS

Approximation 15: In practical terms, a change in excitability may result from complex alterations in the passive and active determinants of excitability.

To continue our practice of demonstration techniques, figures 6–5 and 6–6 represent strength–duration relationships from our recent studies on LPC. This is the same experimental preparation depicted in earlier figures. Referring to figure 6–5A, three strength–duration curves are shown: control (open circles) and the situation after the application of LPC in concentrations of 20 μ*M* (closed triangles) and 45 μ*M* (closed squares). As compared to the control, the nonnormalized strength–duration curve was shifted downward after the lower concentration of LPC, indicating that less current was required to attain threshold for any current duration: that is, the cells were "more excitable" in the classic sense. The two curves began to converge at current durations of less than 60 ms. It is of note that $\dot{V}_{max}$ had decreased from 624 to 544 V/s without any significant change in the resting (V_r) or threshold (V_{th}) voltages (see inset in fig. 6–5). Excitability, therefore, increased despite a depressed sodium system as reflected by the reduction in $\dot{V}_{max}$, indicating that altered passive rather than active membrane properties were primarily responsible for the decrease in current requirements. Normalization of the strength–duration curves was accomplished by dividing the threshold current by the rheobasic current and the duration of the stimulus by the membrane time constant, and the normalized strength–duration curve is shown in panel B of figure 6–5. Note that the normalized curves for the control and the LPC of 20 μ*M* were essentially superimposable for the values of t/τ_m of 1.25 or more and diverged at lesser values. Normalization minimizes the differences in the shape of the curve caused by altered passive cable properties, but does not obscure and may even enhance those changes caused by altered active generator properties. These curves, then, also suggest that the increased excitability was due

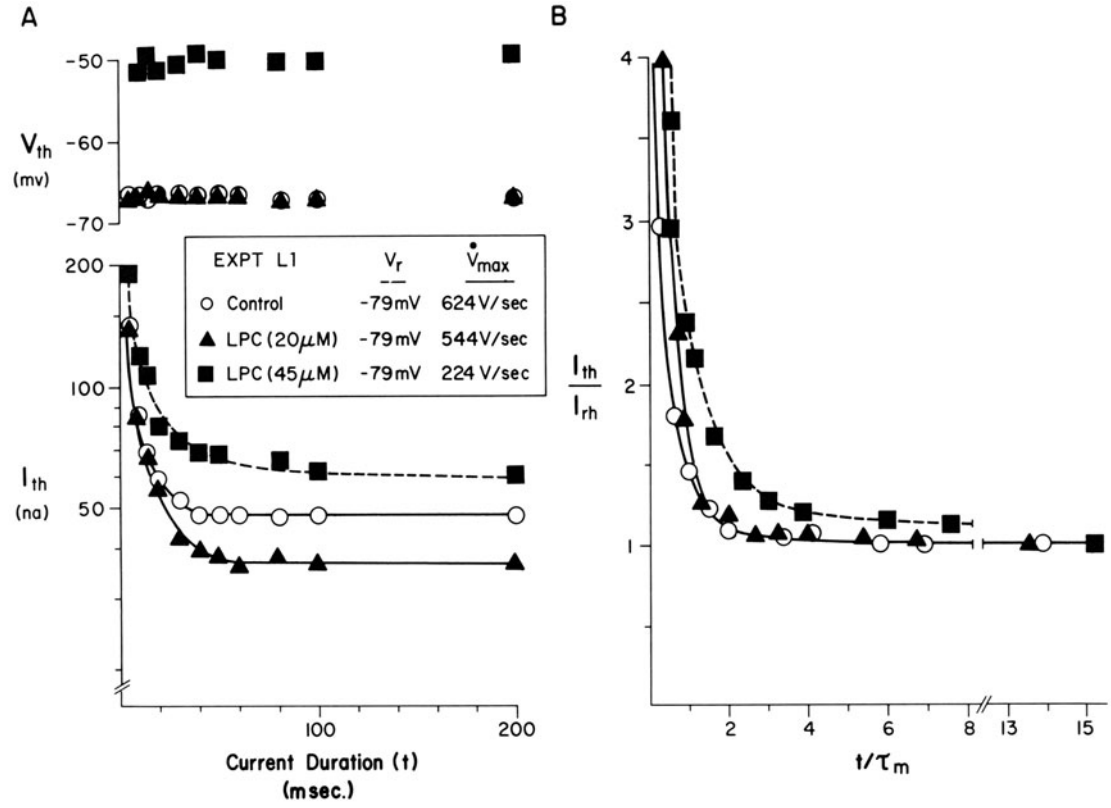

FIGURE 6–5. Nonnormalized *(A)* and normalized *(B)* strength–duration curves in the control period and after exposure of a Purkinje fiber to LPC. From Arnsdorf and Sawicki [48].

primarily to altered passive rather than active properties despite the reduction in $\dot{V}_{max}$ of the propagated action potential. Cable analysis and current–voltage relationships were performed in this preparation. In this experiment, R_m had increased, λ_m which initially had lengthened at an LPC of 10 μM now began to decrease due to an increase in R_i, and the current– voltage relationships demonstrated increased chord and slope conductances throughout the subthreshold range (fig. 6–3). All these changes resulted from altered passive properties and contributed to less current being required to attain threshold despite some depression of the sodium system.

At a higher concentration of LPC (closed squares in fig. 6–6A), the strength–duration curve was shifted upward, V_r remained unchanged, V_{th} became less negative, and $\dot{V}_{max}$ further decreased. The strength–duration curve indicated that the tissue was now "less excitable". The normalized strength–duration curve was not superimposable on the control of the lower LPC curve, indicating that active membrane generator properties were primarily responsible for the decreased excitability.

Propagation of the Action Potential

LOCAL CIRCUIT CURRENTS

Approximation 16: The influence of local circuit currents on excitability depends on the magnitude of the source and the characteristics of the sink. If liminal length requirements are fulfilled, a regenerative propagating action potential results; if the requirements are not fulfilled, only local electrotonic effects result.

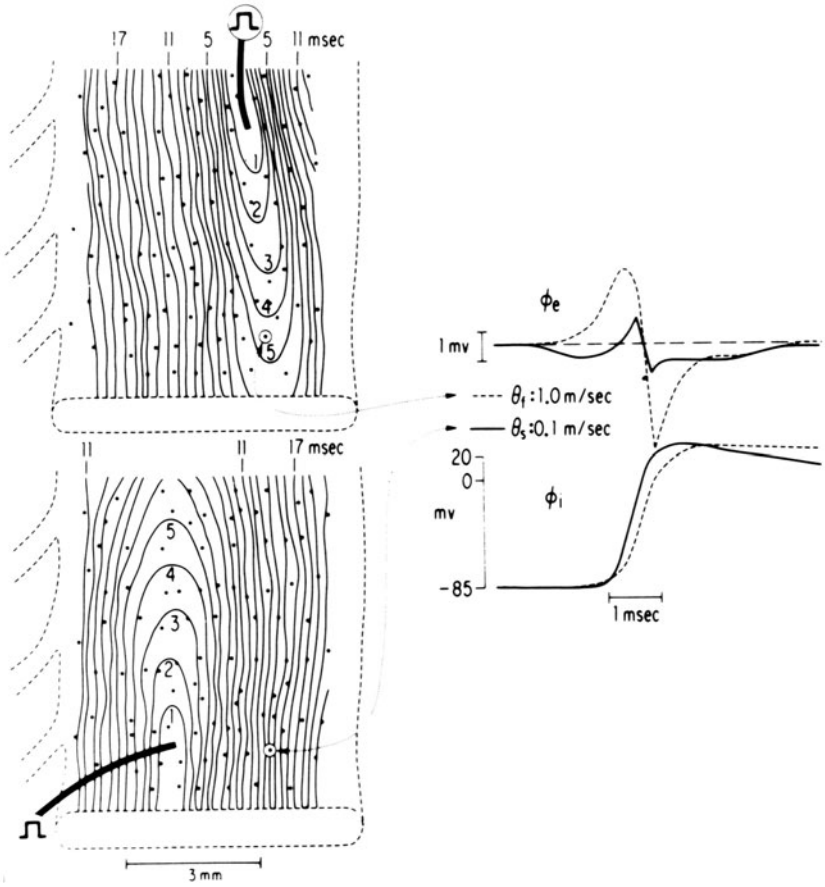

FIGURE 6–6. Directional effects on the action potential in the crista terminalis. The points of stimulation are indicated by the square wave and the sites of extracellular recording by the dots. The intracellular (ϕ_i) and extracellular (ϕ_e) potentials shown on the right were recorded at the site indicated when excitation proceeded in the longitudinal *(left, top)* and transverse *(left, bottom)* direction. Isochrone maps were constructed from the extracellular recordings and the peak negative derivative was used as the instant of excitation. Conduction velocity was calculated as the distance traveled normal to the isochrone per unit time. Note that when the velocity of propagation is low (θ_s for transverse propagation), $\dot{V}_{max}$ is higher and t_{foot} is lower as compared to the situation that pertains for the more rapid longitudinal propagation (θ_f). From Spach et al. [83].

When threshold in a fast-response fiber is attained, sodium rushes into the cell down the electrochemical gradient and renders the cellular element positive as compared to its neighbor. These positive charges displace the negative charges stored on the inside of the membrane, which results in depolarization. Since membrane sodium conductance (g_{Na}) increases as voltage becomes less negative, g_{Na} is further increased. The local V_m is now more positive than in neighboring parts of the cell, so a driving force for the longitudinal current in the myoplasm is established. The potassium ion is the major carrier of the longitudinal current within and between cells and its flow is regulated primarily by the resistance and capacitance at the gap junctions and, to a lesser extent, by impedances in the myoplasm. The longitudinal current displaces negative charge off the interior of the membrane, depolarizes adjacent elements toward threshold, and thereby increases membrane g_{Na}. The circuit is

completed by a capacitive current flow across the membrane and, finally, by current flow in the extracellular space. If the local electrontonic current established by and preceding the electrical stimulus or action potential is sufficient to meet the liminal length requirements for regenerative, g_{Na}-dependent regenerative depolarization, the next element is raised above threshold and propagation of the action potential results.

SOURCES, SINKS, AND PROPAGATION

Approximation 17: The fulfillment of liminal length requirements or the attainment of threshold can be considered a propagated event with the action potential a local membrane phenomenon. This approach emphasizes the importance of the source and sink.

Fozzard [6] has suggested that depolarization to threshold by the local circuit current can be considered the propagated event, with the action potential a local membrane response. If one views conduction in this way, the relationship between the active membrane generator properties (the source) and the passive membrane properties (the sink) becomes apparent.

The Source

Approximation 18: The relationship between the intensity of inward current and $\dot{V}_{max}$ as well as that between $\dot{V}_{max}$ and the conduction velocity is problematic. It is interesting that the proportional relationship between $\dot{V}_{max}$ and the conduction velocity holds as often as it does.

The development of a fast-response action potential in a unit of membrane (say unit A-B in fig. 6–1) was discussed in the section on *Fast-response tissues* and summarized in equation 6.25. This generator can be considered the source or battery which supplies current to neighboring units. If the unit is made very small, the pure-membrane case applies and the maximal rate of rise of phase 0 of the action potential ($\dot{V}_{max}$ or dV_m/dt_{max}) is proportional to the ionic current. As units are linked together, the relationship of $\dot{V}_{max}$ to the transmembrane current is less certain since it is now influenced by the state of neighboring membranes and the characteristics of longitudinal resistances.

Given the assumptions of a one-dimensional cable and assuming a propagated response along the uniform cable at a constant conduction velocity (θ in m/s), the distribution of the transmembrane voltage in space should be equivalent to its distribution in time, that is:

$$\frac{\partial^2 V_m}{\partial x^2} = \left(\frac{1}{\theta^2}\right)\frac{\partial^2 V_m}{\partial t^2} \tag{6.28}$$

If the basic cable equation (eq. 6.7) is combined with equation 6.28, we have:

$$\frac{1}{r_i\theta^2}\frac{d^2V_m}{dt^2} = c_m\frac{dV_m}{dt} + \frac{V_m}{r_m} \tag{6.29}$$

Remembering from equation 6.3 that V_m/r_m is the ionic current, equation 6.29 becomes:

$$\frac{1}{r_i\theta^2}\frac{d^2V_m}{dt^2} = c_m\frac{dV_m}{dt} + i_{ion} \tag{6.30}$$

In the case under discussion, the predominant ionic current is the inward sodium current, but in slow-response tissues it could be the so-called slow inward current.

As mentioned above, it has been difficult to measure sodium currents directly and $\dot{V}_{max}$ has been used as an indirect measure of this current. Since $\dot{V}_{max}$ is the maximal rate of rise of phase 0, that is, it is maximal dV_m/dt, the second derivative, d^2V_m/dt^2, at that instant becomes zero. Equation 6.30 then, becomes:

$$\dot{V}_{max} = \frac{i_{ion}}{c_m} \tag{6.31}$$

Assuming a constant c_m with i_{ion} being equivalent to the sodium current, $\dot{V}_{max}$ would be expected to correlate with the intensity of the sodium current.

It has been problematic to analytically describe the relationship between $\dot{V}_{max}$ and θ although it would be expected that an increased inward ionic current would be associated with an increased θ and, given equation 6.31, with an increased $\dot{V}_{max}$. Hunter et al. [68] found analytic solutions that suggested that conduction velocity did not depend greatly on the maximal sodium conductance and was approximately

equivalent to the square root of $\dot{V}_{max}$. Singer et al. [69] reported a correlation between $\dot{V}_{max}$ and θ in Purkinje fibers for depolarizations from different membrane-activating voltages.

Given all the assumptions of one-dimensional cable theory and the difficulty in extending linear theory to multidimensional systems, it is interesting that the proportional relationship between $\dot{V}_{max}$ and θ so frequently holds. Those conditions which affect driving force such as alterations in the transmembrane voltage and equilibrium potential *(The cell membrane: structure and function)* and which inactivate sodium channels *(Fast-response tissues)* or otherwise interfere with the proper function of the sodium channels such as drugs generally are associated with a decreased conduction velocity.

Slow-response tissues (as discussed previously) depend on the so-called slow inward current, a mixed calcium–sodium current that moves from a kinetically slow channel that is distinct from that of the fast-response tissues. The $\dot{V}_{max}$ of these tissues is very slow as is the conduction velocity. A very low $\dot{V}_{max}$, however, does not identify a slow-response tissue since depressed fast-response tissues can have similar rates of rise and conduction velocities.

The Sink: the Foot of the Action Potential

Approximation 19: Continuous cable theory predicts certain relationships between conduction velocity, the foot of the action potential, cable properties (see Fast-response tissues*) or otherwise interfere with the proper function of the sodium channels such as drugs generally are associated with a decreased conduction velocity.*

The local action potential, the source, influences the neighboring tissues by electrotonic interaction. The electrotonic spread of current first fills the capacitance of the adjacent quiescent segment, and this has the appearance of a slow exponentially rising increase in transmembrane voltage which precedes the rapid depolarization phase of the propagation action potential; this has been called the "foot" of the action potential [70]. Since the voltage has an exponential rise in time, it can be plotted on a semilogarithmic scale as a function of time and a time constant for the foot (τ_{foot}) can be determined. The solution for equation 6.29 is the sum of two exponentials, and solving for the positive root and simplifying we have:

$$\tau_{foot} = \left(\frac{\lambda m}{\theta}\right)^2 \frac{1}{\tau_m} \tag{6.32}$$

or, in terms of the cable equations,

$$\tau_{foot} = \frac{1}{\theta^2 r_i c_m} = \frac{a}{2\theta^2 R_i C m} \tag{6.33}$$

The fiber radius *(a)*, r_i, τ_{foot}, and θ can be determined experimentally, and the capacitance calculated. The error using this approach is less than 5% for a cable like Purkinje fiber. If this line of reasoning is correct, then conduction velocity should correlate *inversely* with τ_{foot}, and Dominguez and Fozzard [42] showed this to occur in sheep Purkinje fibers.

The Sink: Continuous Cable Theory and Propagation. We have already derived the equations that describe the effect of passive cable properties on conduction velocity in the one-dimensional cable. This can be easily appreciated by rearranging equation 6.33:

$$\theta^2 = \frac{1}{\tau_{foot} r_i c_m} = \frac{a}{2\tau_{foot} R_i C_m} \tag{6.34}$$

The topic of intercellular communication was considered in some detail previously in this chapter. As discussed, the gap junctions are the primary determinants of longitudinal resistance, and r_i may vary greatly, depending on the state of extracellular coupling. The direct experimental testing of the effect of r_i on θ has been limited. In nerve, Del Castillo and Moore [71] altered r_i by introducing wires into the axoplasm and found that θ could be varied over a wide range. A failure of the transmission of impulses has been observed in cardiac tissues when presumably r_i was manipulated by a variety of techniques [21, 26]. Lieberman et al. [72] thought that decreased electrical coupling caused decreased conduction velocity in cultured chick cells. Diaz et al. [73] and Joyner [74] have recently modeled the effects of elec-

trical coupling on propagation. Experimental alteration in extracellular conductivity has also been demonstrated in atrial tissue [75] and more recently in Purkinje tissues (see recent discussion in Antzelevitch and Moe [76]).

Equation 6.34 also suggests that θ should increase in proportion to the square root of the radius of the fiber. This, of course, assumes a constant internal conductivity, a large extracellular space, and unchanging membrane conductances and capacitances. Draper and Mya-Tu [77] found a rough relationship between diameter and conduction velocity. Schoenberg et al. [39] found no variation in the conduction velocity in sheep Purkinje fibers that were between 50 and 250 μm in diameter. Cable analysis in these studies showed that R_i was greater for Purkinje fibers with a large diameter which may have offset the influences of the diameter itself on conduction velocity. In the Purkinje fiber with a large diameter, the extracellular clefts are more important and it may be inaccurate to assume that r_o is negligible. It is interesting to speculate that the effects of $r_o + r_i$ counter the influence of diameter.

Goldstein and Rall [78] have modeled the change in conduction velocity in situations of changing fiber geometry and branching. They found that with a step reduction in diameter conduction velocity increases; with a step increase in diameter conduction velocity decreases. This follows from the amount of current lost downstream in the sink. When branching was considered, the impulse approaching the branching site first decreased since the branches provided a larger sink and, once past the junction and into a smaller branch, the conduction velocity increased. Critically slowed conduction at times resulted in the failure of propagation and at other times in an echo beat. Linear theory has been used in more complex two- and three-dimensional structural models which explained, in part, the rapid fall off in potential near the point of stimulation and the importance of longitudinal resistances and geometry on determining the conduction velocity, influences which seem more important than that of membrane conductances and driving forces.

The Sink: Discontinuous Propagation

Approximation 20: The continuous cable theory and the resultant predictions mentioned in approximation 19 do not always fit the experimental observations. Recent investigations suggest that discontinuous propagation may be important in cardiac tissue.

Models based on continuous cable theory do not fully consider structural complexities. Sommer and Dolber [79] describe "unit" bundles that contain 2 – 15 cells that have connections every 0.1 – 0.2 mm. These unit bundles form fascicles which are separated from each other by connective tissue and are connected at distances that Dolber [80] suggests are related to diameter. The fascicles, in turn, group into macroscopic bundles which have complex and varying interconnections. Intuitively, it is not surprising that there may be variation in the velocity of propagation with direction [81–84]. Spach et al. [83, 84] found that the propagation in atrial and ventricular muscle differed at different angles relative to the orientation of cells. Moreover, they observed in conditions where active and passive membrane properties could not have changed that not only was propagation in the direction of the long axis of the cellular structure relatively rapid as compared to conduction transverse to the long axis, but, rather unexpectedly, longitudinal conduction was associated with a slower $\dot{V}_{max}$ and longer τ_{foot} than was transverse propagation (for example, fig. 6–6). For the reasons discussed earlier and represented in equations 6.31 and 6.32, such findings could not be predicted from continuous cable theory. Spach et al. [84] also found a directional dependence of velocity and extracellular potentials at branch sites and at more complex muscular junctions (for example, fig. 6–7). Again, continuous cable theory would not predict such a dependency on angle and direction.

Spach et al. [83, 84] suggest that the discontinuous structure of cardiac muscle may be responsible for the observed discontinuities of propagation. This has been incorporated into what they term the "$\overline{R}_a$ Hypothesis". $\overline{R}_a$ is the "effective axial resistivity" which is the resistiv-

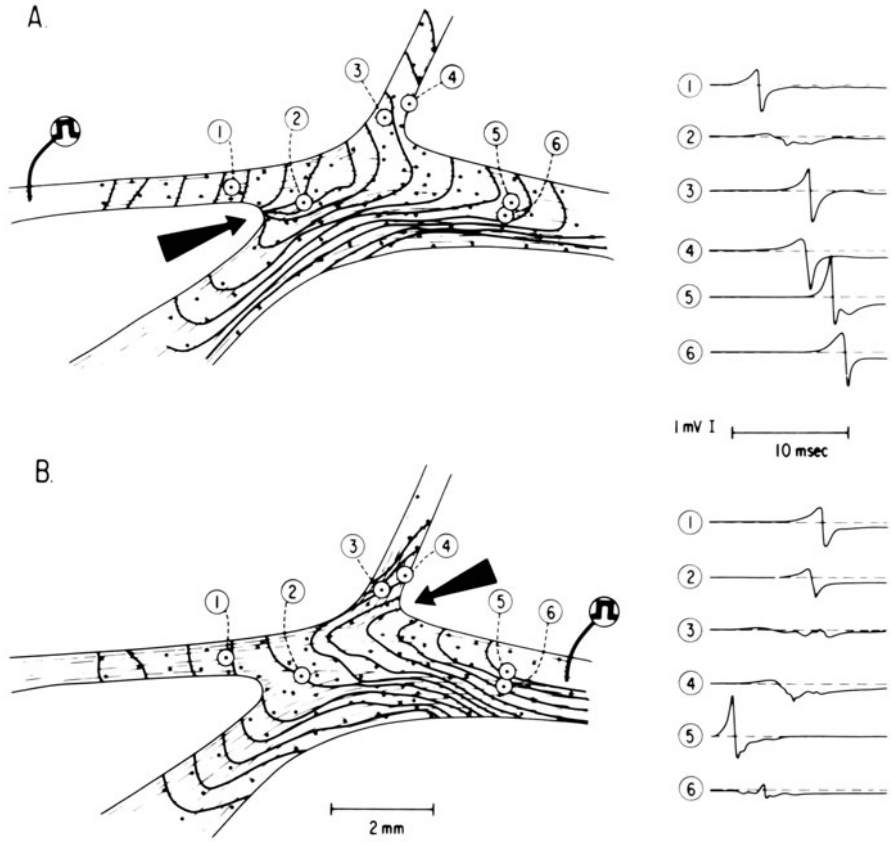

FIGURE 6–7. Directional dependence of velocity and extracellular potentials at branch sites. The drawings on the *left* show the activation sequences for the two stimulus sites (square wave) on the pectinate muscle bundles. The points on the outline of the preparation show the location of extracellular recording sites from which the activation maps were constructed. The extracellularly recorded waveforms at the numbered locations are shown on the *right*. From Spach et al. [84].

ity in the direction of propagation rather than the resistivity along the long axis of the fibers. This term includes the influences of cellular geometry, intracellular and extracellular resistivities, cellular packing, and the influences imparted by the resistances, extent, and distribution of couplings between cells and other structural units. If $\overline{R}_a$ is substituted for r_i in the cable equation and geometric terms included to consider membrane current per unit length, we have:

$$\frac{\pi a^2 \partial^2 V_m}{\overline{R}_a \partial x^2} = c_m \frac{\partial V_m}{\partial t} + i_{ion} \tag{6.35}$$

From modifications of this equation, axial currents and propagation velocities were calculated. Although the model is still somewhat crude, computed extracellular waveforms at the junction of two uniform cables of different $\overline{R}_a$ values did reproduce the type of results seen experimentally at tissue junctions.

Spach et al. speculate at length concerning the meaning of their findings to the so-called preferential atrial pathways and slow-response tissues and the interested reader is referred to their recent work [83, 84].

SAFETY FACTOR

The liminal length concept (discussed previously in this chapter) states that a certain amount of activating current (current in time

or charge) is required to overcome the repolarizing influences of adjacent tissues and produce a propagated action potential. The term "safety factor" is the excess in the activating current or charge over that just required to produce a regenerative propagated response: it is, then, the excess of source over sink. Clinicians are quite aware that certain tissues have a low safety factor, such as the AV node where propagation commonly fails; while others have a high safety factor, such as the Purkinje fibers of the specialized His–bundle branch system where conduction rarely fails. Let us consider the safety factor in terms of sources and sinks.

The Source. Hodgkin [85] calculated a relationship between the density of sodium channels and conduction velocity in the unmyelinated nerve. The sodium channels, it should be recalled, are opened by gating charges. An increase in the density of sodium channels will increase the maximal sodium current and favor propagation, but it will also require more gating charges which act as an extra capacitance and slow conduction velocity; the former would increase and the latter would decrease the safety factor. He calculated an optimal density of channels and arrived at a figure that corresponds to experimental studies. Analogous studies are not available in heart muscle, but it is reasonable to assume that the same general principles apply.

The driving force and resultant current flow are greater and reactivation is much faster in normal fast-response tissues which depend on the rapid inward sodium current such as the atria, the His–bundle branch–terminal Purkinje system, and ventricular muscle as compared to the slow-response tissues, which depend on the mixed Na^+-Ca^{2+} current (i_{si}) found in the SA and AV nodes as well as in some injured tissues. For the reasons discussed earlier, depolarization of the cell can partially inactivate the sodium system, an action which would tend to decrease the safety factor.

Intuitively, then, characteristics of the source are consistent with the commonly observed failure of propagation in the AV node and the relatively unusual failure of propagation in fast-response tissues such as the atrium, His–bundle branch–Purkinje system, and ventricles.

The Sink. Many of the characteristics of the sink that would increase or decrease the safety factor have already been discussed and are considered in equation 6.34 of classic cable theory and in the recent modification by Spach et al. [83, 84] expressed in equation 6.35. In some cases, such as the experimental studies by Antzelevitch, Jalife, Moe, and their collaborators (see, for example, Antzelevitch and Moe [76]), changes in extracellular resistivity can also decrease the safety factor. If the reader has an understanding of the principles discussed earlier in *Propagation of the action potential,* this should be apparent. Intuitively, two- and three-dimensional considerations suggest that the sink would be much greater in highly branched tissues such as the AV node as compared to cable-like Purkinje fibers, so the safety factor would be lower in the former and higher in the latter.

What is less intuitively obvious are some of the observations by Spach et al. [83, 84]. As mentioned, they observed in fast-response tissues that propagation velocity was high in the direction of the long axis of cells and low in the transverse direction: the difference thought due to electrical coupling. They found, using increasingly premature extrastimuli, that uniform propagation became first decremental and then ceased in the direction with the highest velocity originally, while propagation persisted in the direction which originally had the lower conduction velocity. In these experiments in "discontinuous" structures, the safety factor was higher when the conduction velocity was lower and vice versa, which contrasts to the opposite effects in "continuous" structures such as cables when the active and passive membrane properties are changed.

Arrhythmias and Antiarrhythmic Drugs

The topic of arrhythmogenesis and the mechanisms of antiarrhythmic drugs will be considered specifically elsewhere in this book (chapters 20 and 21) and will be related to

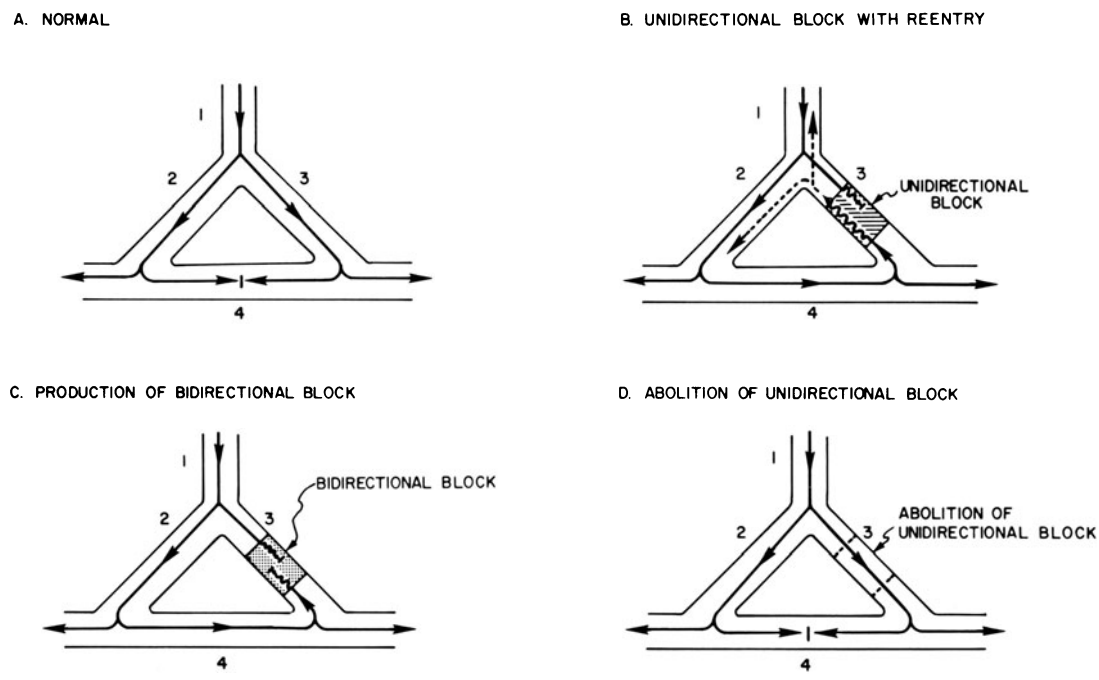

FIGURE 6–8. Diagrammatic scheme of unidirectional block with reentry. *(A)* An impulse propagates from a central Purkinje fiber (1) down two branches (2, 3) and activates the ventricle (4), producing a QRS complex. *(B)* Injury produces a depressed segment that unidirectionally blocks the impulse in branch 3. The impulse travels normally down branch 2, activates the ventricle, producing a normal QRS complex, and conducts very slowly in a retrograde manner through the depressed segment in branch 3. If the tissue at the bifurcation has recovered its excitability by the time the impulse emerges from the depressed segment, the tissue can be reentered and reexcited. As indicated by the dashed arrows, the impulse may travel both down branch 2 to the ventricle, producing a premature ventricular depolarization, or may conduct back up the central Purkinje fiber (1). If the reentrant circuit is sustained, a sustained ventricular tachycardia would result. The success or failure or reentry, then, depends on the conduction velocity in the normal and depressed tissues, the refractoriness of tissue that had previously been excited, and on other passive and active electrophysiologic properties of importance of cardiac excitability. The segment with unidirectional block may have as its source a depressed sodium current or a slow inward current. The latter is found normally in the SA and AV nodes. *(C)* The reentrant loop is abolished by the conversion of unidirectional to bidirectional block.

other chapters as well. It is useful, however, at this point to make a few observations that are relevant to the concepts regarding cable properties and propagation discussed in this chapter.

For many years, clinicians and physiologists have related arrhythmogenesis to altered impulse formation and abnormal propagation. New information suggests that automaticity must be considered part of a larger category of sustained rhythmic activity [62]. Recent studies of altered cardiac excitability fit uncomfortably into either category [16, 42–46, 86]. Often, these mechanisms coexist and interact.

REENTRY

Approximation 21: Conceptually, the success or failure of reentry depends on the relationships between anatomy, refractoriness, and conduction velocity. The electrophysiologic properties, in turn, depend on the active and passive determinants of excitability discussed in earlier sections of this chapter.

Although the term "reentry" has been criticized [62], it is retained since it is a useful concept and a familiar term. The Schmitt-Erlanger model of over a half-century ago remains a reasonable starting point for this discussion, and a modification of it is depicted in figure 6–8. Some segment blocks propagation in one direction as a result of local injury, altered refractoriness, or some other alteration in the source R sink. This segment must be functionally isolated from the surrounding tissues and the impulse must persist sufficiently to allow previously excited tissue to be reactivated and reentered. Conceptually, the simplest calculation of the length of the reentrant loop is:

$$L_c = \theta \times RP_r \qquad (6.36)$$

where L_c is the length of the reentrant circuit, θ is the slowest conduction velocity, and RP_r is the refractory period of the tissue to be reentered. For a normal fast-response Purkinje fiber, θ is about 3 m/s and RP_r is about a third of a second, so L_c would be a meter, a length that anatomically is not feasible. If θ is reduced to 0.01 m/s or less, then L_c enters the millimeter range which is appropriate. This circuit may involve supraventricular, junctional, and ventricular tissue. The circuit may be large as in bundle branch reentry or small such as reflection within a single strand of a Purkinje fiber.

As mentioned, the SA and AV nodes have slow responses and normally have slow conduction velocities. For this reason, reentrant beats and sustained reentrant rhythms commonly utilize the AV node. Clinically, reentrant paroxysmal supraventricular arrhythmias that utilize the AV node are the most common type of tachyarrhythmia in the patient with a normal heart. After all, we all have AV nodes. Less commonly reentrant arrhythmias utilize the SA node.

The conduction velocity in fast-response tissues has been discussed in detail above and depends both on the source and the sink. The maximal sodium conductance can be decreased by a loss of integrity of the channels, by blockade of the channels, by altered kinetics of the activation and inactivation variables, by inhibition of the ionic pumps, and by accommodation. Perhaps more important are the influences of the sink: particularly alterations in the r_o, r_i, and $\overline{R}_a$ discussed in *Propagation of the action potential.* The occurrence of reentry due to discontinuous propagation as reported by Spach et al. [84] is of particular interest. A failure of repolarization, as seen in figure 6–4, will also slow or abolish conduction since it influences the source and membrane conductances both locally and in adjacent tissues.

AUTOMATICITY

Approximation 22: Normal and abnormal automaticity may influence propagation by affecting the state of activation of the sodium system through electrotonic influences and, at times, may cause selective block in a certain type of tissue.

Normal automaticity and abnormal automaticity, including triggered rhythmic activity, may be arrhythmogenic in themselves, or may influence impulse propagation. A slowly rising pacemaker potential (phase 4) may close the off-gate to a slower or lesser extent (accommodation) and may result in a focal block for a conducted impulse. This is thought to be the mechanism of some bradycardia-dependent bundle branch blocks. Recent studies in the tissue bath indicate that slow conduction may be mediated by electrotonic transmission (see, for example, Antzelevitch and Moe [76]) and the source of the electrotonus could well be an automatic focus. Ferrier [87] has clearly demonstrated that, in the presence of digitalis excess, the propagation of an impulse from a papillary muscle via a Purkinje fiber to the free ventricular wall may be interupted by a rate-dependent oscillatory afterpotential in the connecting Purkinje strand.

ALTERED EXCITABILITY

Approximation 23: Certain interventions have been observed to alter the relationship between the charge requirements necessary for a regenerative action potential and the V_{max} of the action potential even though the activation voltage remains unchanged.

It was mentioned that some recent studies on excitability do not fit comfortably into the traditional categories of abnormal impulse formation or altered propagation. An example from

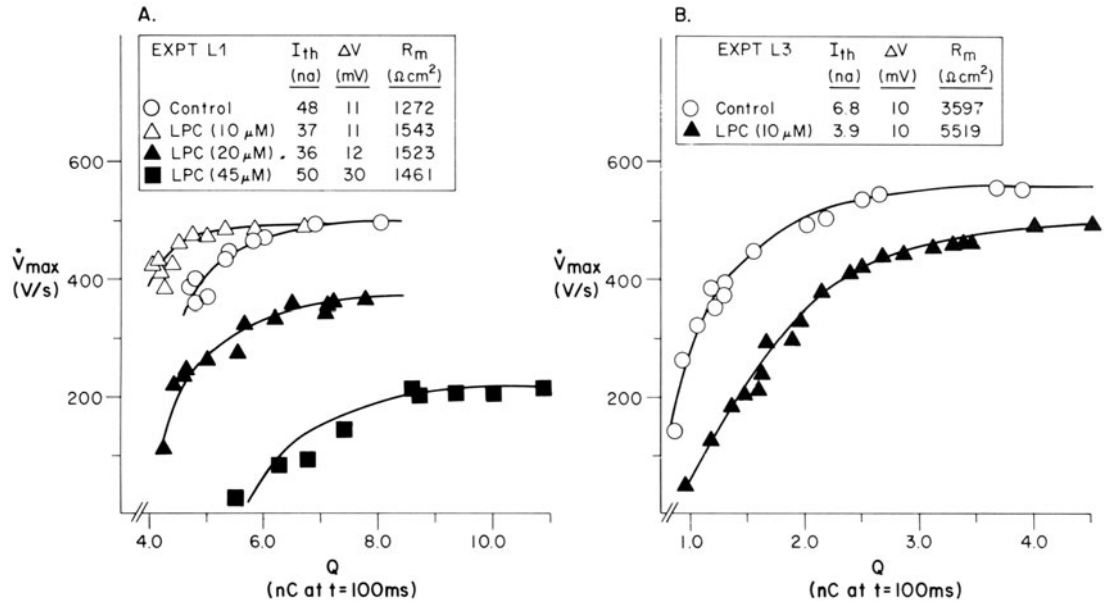

FIGURE 6–9. V_{max} vs charge (Q) relationships at $t = 100$ ms before and after LPC in two different experiments. From Arnsdorf and Sawicki [48].

our study on LPC is shown in figure 6–9 [49]. In this case $\dot{V}_{max}$ was assessed as a function of charge for intracellularly applied currents of 100 ms duration before and after LPC. The $\dot{V}_{max}$ in the control situation could be described as a smooth curve. The values for the current required to reach threshold (I_{th}), for the difference between the resting and threshold potentials (ΔV), and R_m are included in the insets. Note the altered relationship between $\dot{V}_{max}$ and charge after LPC. Such changes in the source would of necessity affect the conduction velocity in the tissue.

ANTIARRHYTHMIC DRUGS

Approximation 24: The effects of an antiarrhythmic drug on the electrophysiologic properties of normal tissues and tissues altered by an arrhythmogenic influence are complex. The net effect on cardiac excitability depends on the relative effect of arrhythmogenic influence and the antiarrhythmic drug on the active and passive determinants of excitability. The relationships between the intervention and the sources and sinks change in time. The use of multiple microelectrode techniques and rapid computer-based data analysis permits identification of such actions and interactions.

For a number of years, our view of the actions of antiarrhythmic drugs has been expressed in terms of the effects that these drugs have on fundamental electrophysiologic properties (see reviews by Arnsdorf and Hsieh [88] and Arnsdorf and Childers [61, 98]). Most antiarrhythmic drugs inhibit the sodium system. This has been termed a "local anesthetic" or "membrane-stabilizing" "direct membrane" action by many authors. At this point, it should be evident how terribly imprecise such terms are. Inhibition of the sodium system would decrease conduction velocity by acting on the source and could interrupt a reentrant circuit by producing bidirectional block. Calcium channel blockers would have the same type of action if the source in the area of unidirectional block was the slow inward current. Some consideration has been given to the effects that drugs have on repolarization and on autonomic influences. Very little attention, however, has been paid to the action of antiarrhythmic drugs on other determinants of cardiac excitability such as liminal length, current or charge threshold, passive membrane properties, and other properties of the "sink".

What is more important to antiarrhythmic drug action, the effects on the source, the sink,

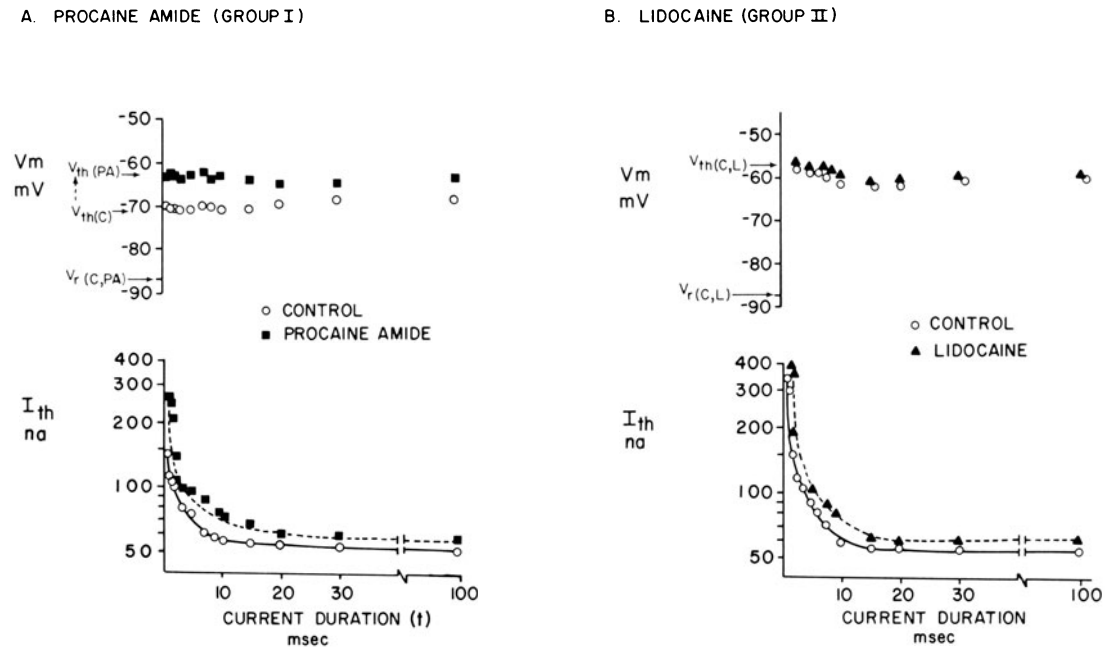

FIGURE 6–10. The effect of procainamide *(A)* and lidocaine *(B)* on the nonnormalized strength–duration curve. In the upper portion of each panel, the threshold voltage (V_{th}) is plotted as a function of current duration; in the lower portion of each panel, the strength–duration curve is shown with the current required to fulfill the liminal length requirements and produce a regenerative, propagating action potential, the so-called threshold current or I_{th}, plotted as a function of the current duration *(t)*. As compared to the control, both procainamide and lidocaine shifted the nonnormalized strength–duration curve upward, indicating that the threshold current requirement increased after the intervention, i.e., less excitable in classic terms. Note that neither drug affected the resting transmembrane voltage (V_r), but that procainamide made V_{th} less negative while lidocaine little influenced V_{th}. From Arnsdorf [86].

or some other component? We do not really know the answer to this question, but all are probably important and the relative importance may well depend on the state of the tissue. The one thing that we can say with certainty is that drugs influence much more than the source. Some time ago, we studied the effect of procainamide and lidocaine, in concentrations equivalent to clinical antiarrhythmic plasma levels, on the determinants of excitability in normal Purkinje fibers [44, 45]. Figure 6–10 shows strength–duration curves from these studies. Note that both drugs shifted the nonnormalized strength–duration curve upward, indicating that the tissue was less excitable in classic terms since more current, I_{th}, was required to attain threshold for any current duration after the drug had been applied. Although I_{th} was affected similarly by both drugs, the mechanisms differed in that procainamide decreased excitability by making V_{th} less negative (a term that depends on sodium conductance) while lidocaine little affected V_{th}, but decreased membrane resistance in the subthreshold range. Cable analysis showed that procainamide increased and lidocaine decreased the length constant, so that the sink would also be altered differently by the two drugs. Subsequently, studies have indicated that the effect of lidocaine on the sodium system depends greatly on the activation voltage, with the effect being much more intense in depolarized tissue.

A more complicated example of the interactions between an arrhythmogenic intervention and an antiarrhythmic drug was observed in our studies on LPC and lidocaine. As discussed in *Practical considerations,* LPC is thought to be

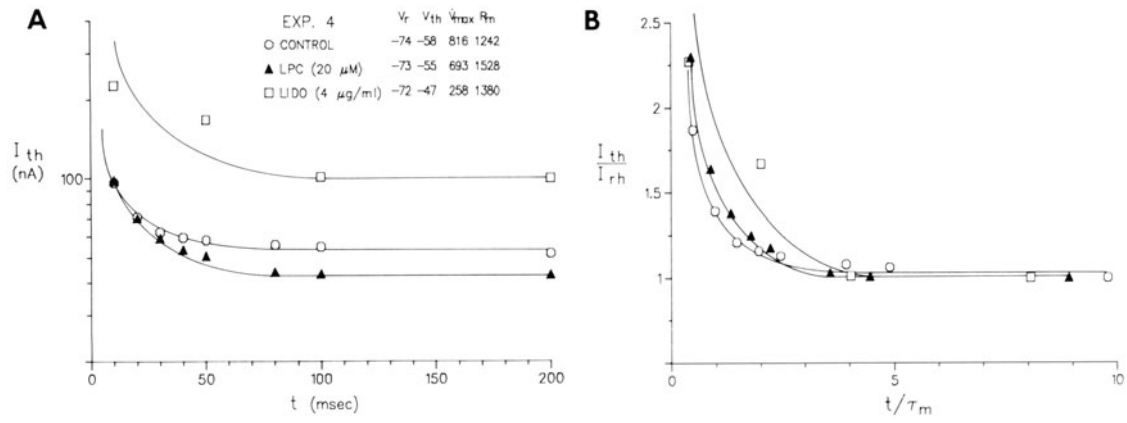

FIGURE 6–11. The effect of LPC and lidocaine during continued LPC superfusion on strength–duration curves in a Purkinje fiber. From Sawicki and Arnsdorf (unpublished data).

a metabolite of ischemia that is arrhythmogenic, and we discussed some of the complex effects that LPC has on active and passive membrane properties of the cell. In our studies on LPC and lidocaine, a computer-based data analysis system was critical since the changes induced by LPC and the interaction of the several effects of lidocaine needed to be defined rapidly so that the experimental conditions could be considered comparable from preparation to preparation. Nonnormalized and normalized strength–duration curves from a typical study are shown in figure 6–11. As seen in panel A of figure 6–11, LPC (triangles) caused the curve to shift downward, making it more excitable in the classic sense since less current (I_{th}) was required for any given duration to produce a propagated response. Note that this occurred despite a decrease in $\dot{V}_{max}$ from 816 to 693 V/s, that is, despite some depression of the sodium system. The increased excitability was mediated primarily by an increase in R_m and slope resistance throughout the subthreshold range as assessed by cable analysis and current–voltage relationships, respectively. R_m increased from 1242 to 1528 Ωm^2. During the phase of increased excitability after LPC, lidocaine decreased excitability as indicated by the upward shift in the nonnormalized strength–duration curve. Lidocaine acted by two distinct mechanisms: (a) a further depression in the sodium system that was additive to the depression caused by the LPC, and (b) a direct countering of LPC's effect on the membrane resistance at rest and in the subthreshold range as defined by cable analysis and current–voltage relationships. The additive suppression of the sodium system resulted in the drop in $\dot{V}_{max}$ from 693 to 258 V/s and in V_{th} becoming less negative (-55 to -47 mV); the countering effect on membrane properties was demonstrated by a decrease in R_m from 1528 to 1380 Ωcm^2. Both the arrhythmogenic intervention and the antiarrhythmic drug affected the source and the sink: the net effect on cardiac excitability depended on the relative effect of each on the active and passive properties.

Approximation 25: The literature has emphasized the effects of antiarrhythmic drugs on shortening and lengthening the action potential duration and refractory period. More complex effects have been described such as the "normalization" of action potentials having two stable steady states. Such action potentials will influence propagation and, at times, may be conducive to the development of abnormal automaticity. Normalization of the action potential will normalize conduction and abolish voltage-dependent abnormal automaticity.

The effects of antiarrhythmic drugs on repolarization are usually discussed in terms of the shortening or lengthening of the action potential duration and refractory periods. The action, however, may be much more complex. Referring once again to figure 6–5, lidocaine

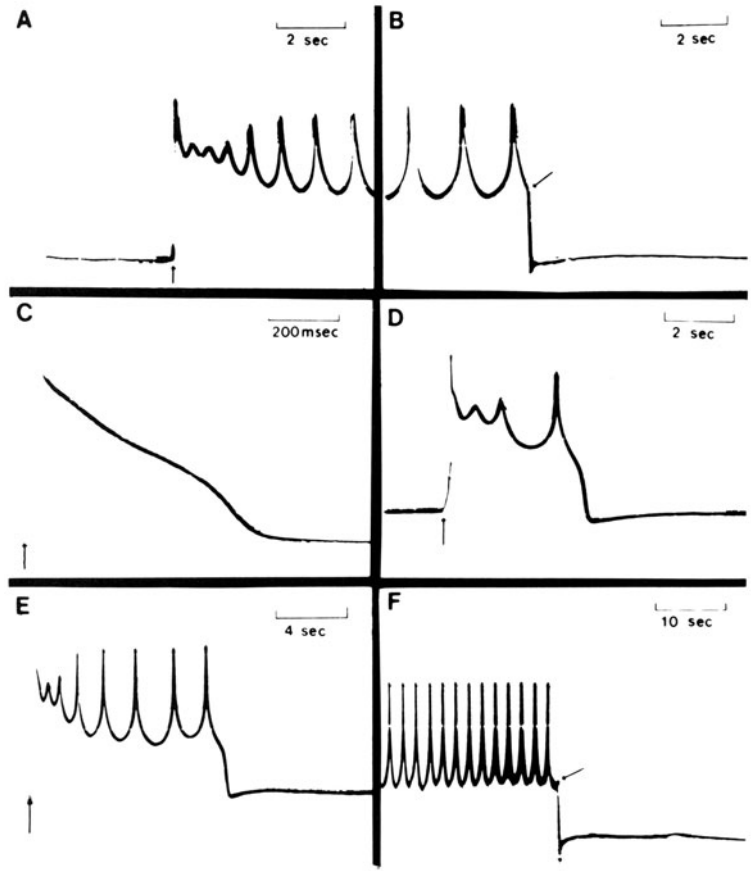

FIGURE 6–12. The effect of lidocaine on triggered sustained rhythmic activity (TRSA) in a Purkinje fiber. In the control situations (*A* and *B*), the electrically induced action potential triggered slow oscillatory activity that crescendoed into nondriven sustained action potentials. TSRA persisted indefinitely until terminated by a hyperpolarizing intracellular current that permitted attainment of the repolarization "threshold" and a return to V_r. The hyperpolarizing current (arrow in *B*) was applied 45 min after initiation of the TSRA. Lidocaine caused an almost immediate attainment of the repolarization threshold and a "normalization" of the action potential *(C)*. After lidocaine washout *(D–F)*, TSRA rapidly reappeared. From Arnsdorf [91].

in panel C converted an action potential with two stable steady states to an essentially normal action potential with normal parameters, and washout of the drug in panel D resulted in a return to two stable steady states. If depolarization of this type had created the segment of unidirectional block in a reentrant circuit, a drug-induced normalization of the action potential could interrupt the reentrant arrhythmia by abolishing the area of unidirectional block (panel D of figure 6–8). We have observed a number of drugs capable of "normalizing" such action potentials [90].

A failure of repolarization may also be conducive to the development of slow-response activity. For example, we observed [91] that the normal upstroke of the action potential could trigger sustained rhythmic activity during the plateau phase. This triggered activity conducted slowly. An example is shown in figure 6–12. In the control (panels A and B), an electrically induced action potential arising from V_r of -83 mV triggered slow oscillatory activity that developed into nondriven sustained action potentials. The triggered sustained rhythmic activity persisted until 45 min a hyperpolarizing intracellular current of 7 nA was applied (downward arrow) which allowed attainment of the repolarization "threshold" and

a return to the resting potential (panel B). This fiber also favored two stable steady states: the first at its quiescent V_r, the second at a low V_m which was sufficient to induce sustained abnormal automaticity of lidocaine. V_r had become more negative at -87 mV, repolarization threshold was normally attained with an action potential duration of 550 ms at a cycle length of 1200 ms, and the $\dot{V}_{max}$ of the action potential was 510 V/s. After lidocaine, then, there was only a single steady state at V_r. With washout of the lidocaine, the triggered sustained rhythmic activity rapidly appeared (E and F) and the preparation could be shifted from the steady state with the rhythmic activity to V_r by introduction of an intracellular hyperpolarizing current (arrow in panel F). The mechanisms of the repolarization are uncertain, but probably represent a combination of an increased outward current and a decreased inward background current.

The complex actions and interactions of arrhythmogenic influences and antiarrhythmic drugs on the active and passive properties of heart cells that are relevant to excitability and propagation have only begun to be investigated. Many such interactions would not have been appreciated except by using multiple-microelectrode techniques that allow controlled electrical perturbation of the cell and by employing a rapid data analysis system. To these influences must be added the effects of such influences and drugs on intracellular ionic activities.

The complexity of drug action makes the classification of antiarrhythmic drugs difficult. Any classification, including our own [61, 88, 89], must be considered an opinion and should be used as an intellectual framework for a rational approach to understanding drug action with the understanding that our knowledge of the alterations in the determinants of excitability caused by arrhythmogenic influences and antiarrhythmic drugs is very sketchy. Any dogmatic statements in the literature must be considered with skepticism.

Concluding Comments

Cardiac excitability depends on characteristics of the source and the sink which, in turn, are the determinants of impulse propagation. The source depends on active membrane generator properties; the sink depends on passive membrane properties as modified by tissue structure and geometry. Although the influence of the source on cardiac excitability and impulse propagation is important, recent investigations have shown that characteristics of the sink are of equal, or perhaps even greater, importance.

Consideration of biophysical theory can be tedious. Yet, some understanding of biophysical theory is required to appreciate whether experimental investigations are testing rational hypotheses and whether clinical extrapolations are reasonable. For the reasons discussed, we feel that much of the experimental work on cardiac excitability, impulse propagation, arrhythmogenesis, and the actions of antiarrhythmic drugs fails to consider adequately biophysical theory. Nevertheless, certain terms such as "membrane-stabilizing effects" and "local anesthetic action" have been used to describe drug actions and have become a regular part of the experimental and clinical literature despite their relative lack of meaning. Perhaps more seriously, these empty terms have a certain appeal because of their simplicity, and have been accepted by clinicians as a mechanism of drug action and a sufficient explanation for an antiarrhythmic effect. In a real sense, all effects of drugs on active and passive membrane properties may be arrhythmogenic as well as antiarrhythmic. This can be appreciated only through an understanding of fundamental electrophysiologic principles.

As stated in the *Introduction,* the purpose of this chapter was to create an intellectual framework for the reader based on biophysical theory which would allow him to appreciate what is known and what is unknown, to decide whether our current hypotheses are reasonable or unreasonable, and to critically assess extrapolations which have been made from the basic laboratory to the clinical situation. If this purpose has been achieved, the reader should be able to appreciate the interesting question posed by Plato in Book IV of the *Republic:* "For when a man knows not his own first principle and when the conclusion and intermediate steps are also constructed out of he knows not what, how can he imagine that such a fabric of

convention can ever become science?" We now know a few of the first principles, some of the intermediate steps, and can hazard a few conclusions.

References

1. Noble D: A modification of the Hodgkin–Huxley equations applicable to Purkinje fiber action and pacemaker potentials. J Physiol (Lond) 160:317–352, 1962.
2. Trautwein W: Membrane currents in cardiac muscle fibers. Physiol Rev 53: 793–835, 1973.
3. McAllister RE, Noble D, Tsien RW: Reconstruction of the electrical activity of cardiac Purkinje fibres. J Physiol (Lond) 251:1–59, 1975.
4. Fozzard HA, Beeler GW Jr: The voltage clamp and cardiac electrophysiology. Circ Res 37:403–413, 1975.
5. Fozzard HA: Cardiac muscle: excitability and passive electrical properties. Prog Cardiovasc Dis 19:343–359, 1977.
6. Fozzard HA: Conduction of the action potential. In: Berne RM (ed) The handbook of physiology. The cardiovascular system I. Baltimore: American Physiological Society, Williams and Wilkins, 1979, pp. 335–356.
7. Berne RM (ed): The cardiovascular system I. In: The handbook of physiology. Baltimore: American Physiological Society, Williams and Wilkins, 1979.
8. Jack JJB, Noble D, Tsien RW: Electric current flow in excitable cells. Oxford: Clarendon, 1975.
9. Sommer JR, Johnson EA: Ultrastructure of cardiac muscle. In: Berne RM (ed) The handbook of physiology. The cardiovascular system I, chap 5. Baltimore: American Physiological Society, Williams and Wilkins, 1979, pp 113–186.
10. Quinn PJ: The molecular biology of cell membranes. Baltimore: University Park, 1976.
11. Page E, Fozzard H: Capacitive, resistive, and syncytial properties of heart muscle: ultrastructural and physiological considerations. In: The structure and function of muscle, vol 2, 2nd edn. Structure, part 2. New York: Academic, 1973, pp 91–158.
12. Eisenberg RS: Structural complexity, circuit models and ion accumulation. Fed Proc 39:1540–1543, 1980.
13. January CT, Bump TE, Fozzard HA: Effects of membrane potential on the intracellular sodium activity of Purkinje and ventricular muscle [abstr]. Circulation 64:IV-49, 1981.
14. Lee CO: Ionic activities in cardiac muscle cells and application of ion-selective microelectrodes. Am J Physiol (Heart Circ, Physiol 10) 241:H459–H478, 1981.
15. Hodgkin AL, Rushton WAH: The electrical constants of a crustacean nerve fibre. Proc Soc [B] 133:444—479, 1946.
16. Fozzard HA, Schoenberg M: Strength–duration curves in cardiac Purkinje fibres: effects of liminal length and charge distribution. J Physiol (Lond) 226:593–618, 1972.
17. Heidenhain M: Ueber die Structur des menschlichen Herzmuskels. Anat Anz 20:3–79, 1901.
18. Sjöstrand FS, Andersson E: Electron microscopy of the intercalated discs of cardiac muscle tissue. Experientia 10:369–372, 1954.
19. Weidmann S: The electrical constants of Purkinje fibres. J Physiol (Lond) 188:348–360, 1952.
20. Weidmann S: The diffusion of radiopotassium across intercalated disks of mammalian cardiac muscle. J Physiol (Lond) 187:323–342, 1966.
21. De Mello WC (ed): Intercellular communication. New York: Plenum, 1977.
22. Lowenstein WR: Junctional intercellular communication: the cell-to-cell membrane channel. Physiol Rev 61:829–913, 1981.
23. Page E, Shibata Y: Permeable junctions between cardiac cells. Annu Rev Physiol 43:431–441, 1981.
24. Kensler RW, Goodenough DA: Isolation of mouse myocardial gap junctions. J Cell Biol 86:755–764, 1980.
25. Manjunath CK, Goings GE, Page E: Isolation and protein consumption of gap junctions from rabbit hearts [abstr]. J Cell Biol 91:100a, 1981.
26. Holland RP, Arnsdorf MF: Nonspatial determinants of electrograms in guinea pig ventricle. Am J Physiol (Cell Physiol 9) 240:C148–C160, 1981.
27. Dahl G, Isenberg G: Decoupling of heart muscle cells: correlation with increased cytoplasmic calcium activity and with changes of nexus ultrastructure. J Memr Biol 53:63–75, 1980.
28. Délèze J: The recovery of resting potential and input resistence in sheep heart injured by knife or laser. J Physiol (Lond) 208:547–562, 1970.
29. De Mello WC, Motta GE, Chapeau M: A study of the healing-over of myocardial cells of toads. Circ Res 24:475–487, 1969.
30. De Mello WC, Dexter D: Increased rate of sealing in beating heart muscle of the toad. Circ Res 26:481–489, 1970.
31. Baldwin KM: The fine structure of healing over in mammalian cardiac muscle. J Mol Cell Cardiol 9:959–966, 1977.
32. Ashraf M, Halverson C: Ultrastructural modifications of nexuses (gap junctions) during early myocardial ischemia. J Mol Cell Cardiol 10:263–269, 1978.
33. Freygang WH, Trautwein W: The structural implications of the linear electrical properties of cardiac Purkinje strands. J Gen Physiol 9:137–152, 1970.
34. Sperelakis N, Mann JE Jr: Evaluation of electric field charges in the cleft between excitable cells. J Theor Biol 64:71–96, 1977.
35. MacDonald RL, Hsu D, Mann JE Jr, Sperelakis N: An analysis of the problem of K^+ accumulation in the intercalcated disk clefts of cardiac muscle. J Theor Biol 51:455–473, 1975.
36. Mobley BA, Page E: The surface area of sheep cardiac Purkinje fibers. J Physiol 220:547–563, 1972.

37. Hellam DC, Studt JW: Linear analysis of membrane conductance and capacitance in cardiac Purkinje fibres. J Physiol (Lond) 243:661–694, 1974.
38. Fozzard HA: Membrane capacity of the cardiac Purkinje fibre. J Physiol 182:255–267, 1966.
39. Schoenberg M, Dominguez G, Fozzard HA: Effect of diameter on membrane capacity and conductance of sheep cardiac Purkinje fibers. J Gen Physiol 65:441–458, 1975.
40. Baumgarten CM, Isenberg G, McDonald T, Ten Eick RE: Depletion and accumulation of potassium in the extracellular clefts of cardiac Purkinje fibers during voltage clamp hyperpolarization and depolarization: experiments in sodium-free bathing media. J Gen Physiol 70:149–169, 1977.
41. Baumgarten CM, Isenberg G: Depletion and accumulation of potassium in the extracellular clefts of cardiac Purkinje fibers during voltage clamp hyperpolarization and depolarization. Pflugers Arch 368:19–31, 1977.
42. Dominguez G, Fozzard HA: Influence of extracellular K^+ concentration on cable properties and excitability of sheep cardiac Purkinje fibers. Circ Res 26:565–574, 1970.
43. Arnsdorf MF, Bigger JT Jr: Effect of lidocaine hydrochloride on membrane conductance in mammalian cardiac Purkinje fibers. J Clin Invest 51:2252–2263, 1972.
44. Arnsdorf MF, Bigger JT Jr: The effect of lidocaine on components of excitability in long mammalian cardiac Purkinje fibers. J Pharmacol Exp Ther 195:206–215, 1975.
45. Arnsdorf MF, Bigger JT Jr: The effect of procaine amide on components of excitability in long mammalian cardiac Purkinje fibers. Circ Res 38:115–122, 1976.
46. Arnsdorf MF, Friedlander I: The electrophysiologic effects of Tolamolol (UK-6558-01) on the passive membrane properties of mammalian cardiac Purkinje fibers. J Pharmacol Exp Ther 199:601–610, 1976.
47. Schmidt G, Sawicki GJ, Arnsdorf MF: Effects of encainide on components of excitability in cardiac Purkinje fibers. Circulation 64:IV-272, 1981.
48. Arnsdorf MF, Sawicki GJ: The effects of lysophosphatidylcholine, a toxic metabolite of ischemia, on the components of cardiac excitability in sheep Purkinje fibers. Circ Res 49:16–30, 1981.
49. Arnsdorf MF, Sawicki GJ: The effects of lidocaine on the electrophysiologic properties of cardiac Purkinje fibers exposed to lysophosphatidylcholine, a toxic metabolite of ischemia. Circulation 62:III-281, 1980.
50. Sobel BE, Corr PB, Robinson AK, Goldstein RA, Witkowski FX, Klein MS: Accumulation of lysophosphoglycerides with arrhythmogenic properties in ischemic myocardium. J Clin Invest 62:III-281, 1980.
51. Sobel BE, Corr PB, Cain ME, Witkowski FX, Price DA, Sobel BE: Potential arrhythmogenic electrophysiological derangements in canine Purkinje fibers induced by lysophosphoglycerides. Circ Res 44:822–832, 1979.
52. Katz AM, Messineo FC: Lipid–membrane interactions and pathogenesis of ischemic damage in the myocardium. Circ Res 48:1–16, 1981.
53. Cole KS, Curtis HJ: Membrane potential of the squid giant axon during current flow. J Gen Physiol 24:551–563, 1941.
54. Woodbury JW, Crill WE: On the problem of impulse conduction in the atrium. In: Florey L (ed) Nervous inhibition. New York: Plenum, 1961, pp 24–35.
55. Sperelakis N, MacDonald RL: Ratio of transverse to longitudinal resistivities of isolated cardiac muscle fiber bundles. J Electrocardiol 7:301–314, 1974.
56. Lapicque L: Recherches quantitative sur l'excitation electriques des nerfs traitee comme un popularisation. J Physiol (Paris) 9:620–635, 1907.
57. Hodgkin AL, Huxley AF: A quantitative description of membrane current and its application to conduction and excitation in nerve. J Physiol (Lond) 117:500–544, 1952.
58. Noble D, Stein RB: The threshold conditions for initiation of action potentials by excitable cells. J Physiol (Lond) 187:129–162, 1966.
59. Cooley JW, Dodge FA Jr: Digital computer solutions for excitation and propagation of the nerve impulse. Biophys J 6:583–599, 1966.
60. Rushton WA: Initiation of the propagated disturbance. Proc R Soc Lond [B] 124:210–243, 1937.
61. Arnsdorf MF, Childers R: Basic concepts of electrophysiology, In: Julian D, Resnekov (eds) Friedberg's diseases of the heart. New York: Churchill-Livingston, 1983 (in press).
62. Cranefield PF: The conduction of the cardiac impulse: the slow response and cardiac arrhythmias. Mt Kisco NY: Futura, 1975.
63. Ebihara L, Johnson EA: Fast sodium current in cardiac muscle: a quantitative description. Biophys J 32:779–790, 1980.
64. Colatsky TJ, Tsien RW: Sodium channels in rabbit cardiac Purkinje fibers. Nature 278:261–268, 1979.
65. Colatsky TJ: Voltage clamp measurements of sodium channel properties in rabbit cardiac Purkinje fibres. J Physiol (Lond) 305:215–243, 1980.
66. Brown AM, Lee KA, Powell T: Sodium current in single rat heart muscle cells. J Physiol (Lond) 318:479–500, 1981.
67. Cohen IR, Falk RP, Kline RP: Membrane currents following activity in canine cardiac Purkinje fibers. Biophys J 33:281–288, 1981.
68. Hunter PJ, McNaughton PA, Noble D: Analytical models of propagation in excitable cells. Prog Biophys Mol Biol 30:99–144, 1975.
69. Singer DH, Lazzara R, Hoffman BF: Interrelationships between automaticity and conduction in Purkinje fibers. Circ Res 21:537–558, 1967.
70. Tasaki I, Hagiwara S: Capacity of muscle fiber membrane. Am J Physiol 188:423–429, 1957.
71. Del Castillo J, Moore JW: On increasing the velocity

of a nerve impulse. J Physiol (Lond) 148:665–670, 1959.
72. Lieberman MM, Kootsey M, Johnson EA, Sawonobari T: Slow conduction in cardiac muscle. Biophys J 13:37–55, 1973.
73. Diaz PJ, Rudy Y, Plonsey R: The effects of the intercalated disc on the propagation of electrical activity in cardiac muscle. Fed Proc 40:393, 1981.
74. Joyner RW: Effects of the discrete pattern of electrical coupling on propagation through an electrical syncytium. Circ Res 50:192–200, 1982.
75. Barr LM, Dewey M, Berger W: Propagation of action potentials and the structure of the nexus in cardiac muscle. J Gen Physiol 48:797–823, 1965.
76. Antzelevitch C, Moe GK: Electrotonically mediated delayed conduction and reentry in relation to ventricular conducting tissue. Circ Res 49:1129–1139, 1981.
77. Draper MH, Mya-Tu M: A comparison of the conduction velocity in cardiac tissues of various mammals. Q J Exp Physiol 44:91–109, 1959.
78. Goldstein SS, Rall W: Changes in action potential shape and velocity for changing core conductor geometry. Biophys J 14:731–757, 1974.
79. Sommer JR, Dolber PC: Cardiac muscle: the ultrastructure of its cells and bundles. In: Paes de Carvalho A, Hoffman BF, Lieberman M (eds) Normal and abnormal conduction of the heart beat. Mt Kisco NY: Futura, 1983 (in press).
80. Dolber PC: A morphological approach to some problems of rabbit cardiac atrial physiology. PhD thesis, Department of Pathology, Duke University, 1980. Cited in Spach et al. [84].
81. Sano TN, Takayama N, Shimamoto T: Directional difference of conduction velocity in cardiac ventricular syncytium studied by microelectrodes. Circ Res 7:262–267, 1959.
82. Clerc L: Directional differences of impulse spread in trabecular muscle from mammalian heart. J Physiol (Lond) 255:335–346, 1976.
83. Spach MS, Miller WT, Geselowitz DB, Barr RC, Kootsey JM, Johnson EA: The discontinuous nature of propagation in normal canine cardiac muscle: evidence for recurrent discontinuities of intracellular resistance that affect membrane currents. Circ Res 48:39–54, 1981.
84. Spach MS, Miller WT, Dolber PC, Kootsey JM, Sommer JR, Mosher CE Jr: The functional role of structural complexities in the propagation of depolarization in the atrium of the dog: cardiac conduction disturbances due to discontinuities of effective axial resistivity. Circ Res 50:175–191, 1982.
85. Hodgkin AL: The optimum density of sodium channels in an unmyelinated nerve. Philos Trans T Soc Lond [B] 270:297–300, 1975.
86. Arnsdorf MF: Membrane factors in arrhythmogenesis: concepts and definitions. Prog Cardiovasc Dis 19:413–429, 1976.
87. Ferrier GR: Digitalis arrhythmias: role of oscillatory afterpotentials. Prog Cardiovasc Dis 19:459–474, 1977.
88. Arnsdorf MF, Hsieh Y: Antiarrhythmic agents. In: Hurst RW, Logue RB, Schlant RC, Wenger NK (eds) The heart. New York: McGraw Hill, 1978, pp 1943–1963.
89. Arnsdorf MF, Childers RW: The genesis, diagnosis, natural history and treatment of cardiac dysrhythmias. In: Julian D, Resnekov L (eds) Friedberg's diseases of the heart. New York: Churchill-Livingston, 1983 (in press).
90. Arnsdorf MF, Mehlman DJ: Observations on the effects of selected antiarrhythmic drugs on mammalian cardiac Purkinje fibers with two levels of steady-state potential: influences of lidocaine, phenytoin, propranolol, disopyramide, and procainamide on repolarization, action potential shape and conduction. J Pharmacol Exp Ther 207:983–991, 1977.
91. Arnsdorf MF: The effect of antiarrhythmmic drugs on sustained rhythmic activity in cardiac Purkinje fibers. J Pharmacol Exp Ther 201:689–700, 1977.

7. THE ELECTROCARDIOGRAM AND ITS RELATIONSHIP TO EXCITATION OF THE HEART

Roger C. Barr

Introduction

If voltage is recorded as a function of time between two electrodes separated on the body surface, a sufficiently sensitive amplifier will show that a changing voltage exists between the two electrodes that has the same periodicity as the heartbeat. A.D. Waller [1] and others demonstrated around 1900 that this voltage originates in the electrical activity of the heart. Accurate measurement of such electrocardiograms (ECGs) was greatly facilitated by the invention of the string galvanometer by Einhoven [2]. The string galvanometer, although bulky, was the first recording instrument capable of producing electrocardiograms comparable in fidelity to those observed today.

In a remarkable series of experiments, Sir Thomas Lewis [3] measured the sequence of electrical excitation of the atria and ventricles in dogs. Lewis simultaneously measured body surface electrocardiograms and waveforms from atrial and ventricular electrodes. Thereby, he established in some detail the temporal relationship between atrial and ventricular excitation and their manifestations in portions of the electrocardiogram.

Examples of ECG waveforms are shown in figure 7–1. By convention, deflections within the overall periodic waveform are referred to by the consecutive letters P, QRS, and T as shown (bottom, fig. 7–1). The P deflection originates from the electrical excitation of the atrium, the QRS deflections all originate from electrical excitation of the ventricles, and the T deflection originates in ventricular repolarization. The P, QRS, T nomenclature is a way of describing the observed electrocardiogram, not a method of interpretation. Waveforms of electrocardiograms vary widely from site to site on the body surface of a single individual (compare figure 7–1 top and bottom), or from individual to individual. As a result, a specialized nomenclature exists to describe different waveshapes [4].

The amplitude calibration of figure 7–1 indicates an order of magnitude of P waves of about 100 μV and of QRS and T of millivolts. Substantial variations in magnitude are seen on particular recordings. In comparison, noise levels of 30 μV peak to peak often are present even on recordings made with careful attention to the electrodes and the surroundings. Noise levels of 100 μV or more are (unfortunately) common under less-controlled circumstances. Because measured noise levels are significant in relation to the size of ECG deflections, the presence of noise is a theoretical and practical limitation on the amount of information that can be gained from interpreting ECG measurements.

If the noise were not present, it should be possible to observe a number of other deflections of cardiac origin on the body surface tracings that might prove of great value. For example, voltages from the ventricular

This work was supported in part by USPHS grant 11307.

N. Sperelakis (ed.), PHYSIOLOGY AND PATHOPHYSIOLOGY OF THE HEART.

Martinus Nijhoff Publishing, Boston/The Hague/ Dordrecht/Lancaster.

conduction system should be present. Recordings of such voltages have been reported from research laboratories where noise was reduced by averaging multiple beats or using multiple amplifiers [5]. Moreover, low-amplitude voltages not now observed from excitation of the ventricles during some types of arrhythmias might be observed.

Measurement of ECGs

Understanding of electrocardiograms has come about as an interplay between the development of careful methods for making more and higher-quality measurements and attempts to understand the origin of these observations. More extensive and better descriptions of the electrical events occurring on the body surface have provided the opportunity for more comprehensive understanding of their origin. Conversely, limitations in the number and quality of measurements posed by such considerations as electrodes' characteristics, external noise, or the number of leads available have made it impossible in practice to perform some kinds of ECG analysis that would be possible, at least in principle, were these limitations not present. It is therefore worthwhile to describe some aspects of how ECGs are measured, some conventions associated with their measurement, some of the characteristics associated with electrocardiographic waveforms as a group, and some aspects of how the resulting information is displayed to the investigator.

ELECTRODES AND AMPLIFIERS

A body surface ECG measurement in diagrammatic form is shown in figure 7–2. Three electrode sites, one each on the left arm (LA), left leg (LL), and right leg (RL), are portrayed. The function of the amplifier (Amp) is to amplify the voltage difference between electrodes LL and LA by a factor of about 500 so that the larger signal can be displayed on a screen (S) or recorder. Most real amplifiers achieve this result by taking the voltage difference between electrodes LL and RL, the difference between LA and RL, and subtracting the latter difference from the former. This plan is used to diminish the effects of external noise.

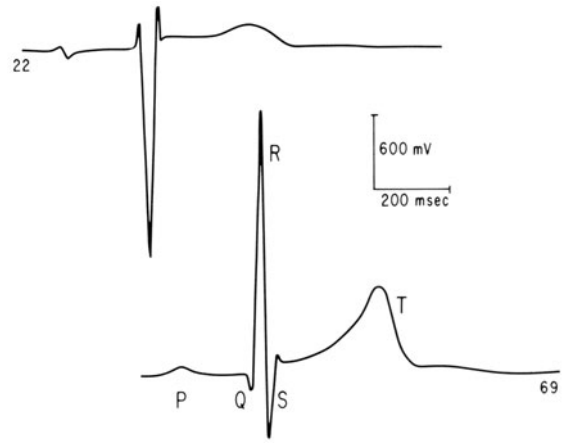

FIGURE 7–1. Electrocardiographic waveforms. The voltage and time calibration marks apply both to the *top* and *bottom* waveforms. Note the marked difference in waveshape.

There are a number of problems associated with making body surface ECG measurements that would exist even in the simple configuration of figure 7–2. Some of these are as follows. The electrical characteristics of each skin-electrode site can be modeled (imperfectly) as shown in figure 7–3. The electrochemical interface between the electrode and the skin tissue has the effect of generating a voltage, represented by battery B. The relatively resistive properties of the skin can be considered to be represented by a resistance R between the underlying body tissue and the amplifier. The contact impedance changes as the frequency considered increases, as indicated by capacitance C. One proposed standard for diagnostic ECG devices has set nominal values for R of 62 meg and for C of 47 nF [6].

Although the voltage of B is small in relation to common manmade batteries, it may be large in comparison with the magnitude of the ECG. The presence of the skin-electrode voltage has a number of important consequences. First, voltage B varies in magnitude up to about 100 mV and depends upon the specific composition and condition of the electrode, electrode paste, and skin. Furthermore, it will vary with time, for example, with changes in skin moisture. Finally, it may have significant

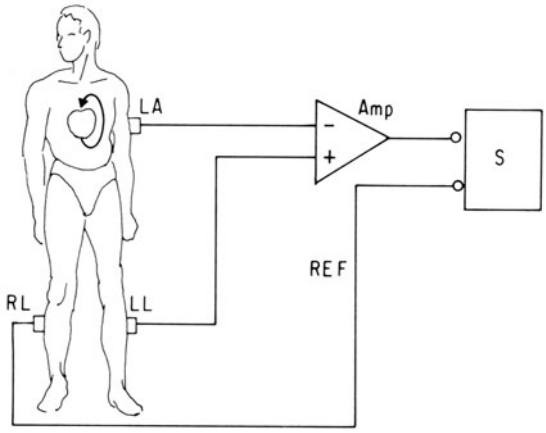

FIGURE 7–2. Idealized connections for making an ECG recording. The function of amplifier Amp is to amplify the voltage between the left arm (LA) and left leg (LL) electrodes by a factor of about 500. The right leg electrode (RL) is a voltage reference. Display of the waveform is on screen *A*. Real amplifiers usually vary from the connections drawn for safety, noise, and other reasons.

fluctuations due to physical movement of the electrode. The changing values of the skin-electrode voltage pose a limitation both in principle and practice to the precise comparison of voltages on a single lead at different times and particularly to the precise comparison of voltages from different leads. In principle, if two electrodes with precisely the same characteristics are connected, one to the positive and the other to the negative inputs of an amplifier, the two voltages should offset each other with no resulting effect. Such precision is not obtainable in practice, as can be seen by watching ECG monitors with good low-frequency response, where gross movement of the ECG baseline often is observed. To diminish the effect of the DC offset, ECG amplifiers are almost always AC coupled to the subject. The consequence of this AC coupling is that even in circumstances where DC currents might exist and be significant, perhaps with ischemia and infarction, it is not practical to measure them electrocardiographically.

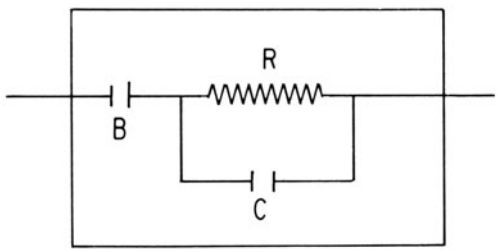

FIGURE 7–3. Equivalent circuit for the skin-electrode contact. As an approximation, the skin-electrode interface may be modeled electrically with a battery (B), resistance (R), and capacitance (C).

Measured values of resistance R of figure 7–3 at electrocardiographic frequencies have been reported from the range of a few thousand to a few hundred thousand ohms [7, 8]. These relatively high resistances also have many consequences. To compensate, amplifiers used to make electrocardiographic measurements have a high input resistance (that is, require a very small input current). With present-day technology such amplifiers are easily obtained. However, amplifiers of this kind are inherently highly sensitive to extraneous noise as well to the electrocardiographic signal. Specifically, they are highly sensitive to 60-Hz noise either capacitively or inductively coupled to the subject or to the leads from the amplifier. Coupling occurs from whatever power lines are in the vicinity, with the result that ECG traces often show 60-Hz noise. To decrease such noise, the leads from the amplifier to the subject generally are kept short and close together. An extensive discussion of the sources of 60-Hz noise in ECGs and measures that may be taken to deal with it has been presented by Huhta and Webster [9].

FILTERS

Electrocardiographic amplifiers often incorporate a high-pass filter because of the skin-electrode voltage, and a low-pass filter to remove high-frequency signals not of cardiac origin (such as radio broadcasts). Occasionally filters are used to remove 60-Hz interference. Filters may be included as analogue electrical circuits or as digital filters within ECG processing equipment. In either case, such filters must be used with considerable caution since they may affect the recorded wave *shape* in subtle but im-

portant ways. For example, Fourier series analysis of an ECG exactly repetitive at a heart rate of 1 beat per second would show no ECG components of frequency less than 1 Hz. Nonetheless, a high-pass filter with a cutoff of 1 Hz might significantly change the recorded ECG. Changes might occur because of small amplitude changes above 1 Hz, or because of phase shifts of frequencies in the 1- to 10-Hz range. Similar considerations apply to low-pass filters for removing high-frequency noise.

Filters of 60 Hz will change ECG waveforms to some extent, since components at 60 Hz also arise from cardiac sources. Moreover, all filters must be carefully examined for their tendency to cause an oscillatory baseline, called "ringing," for tens or hundreds of milliseconds after abrupt transitions (such as the QRS complex). In considering filter use with electrocardiographic signals, it is worth keeping in mind that most filters are designed for analyzing manmade signals; in these signals often only the components largest in amplitude are important. In contrast, the presence and timing of small features of cardiac electrocardiograms or body surface electrocardiograms often are highly significant.

SAFETY CONSIDERATIONS

Since the process of ECG recording requires that good electrical contact be obtained between the recording device and the subject, prudence requires that risk of shock be evaluated. Such consideration is particularly necessary where other electrical connections might be present directly to the heart, as in cardiac catheterization. The Committee on Electrocardiography of the American Heart Association has made a number of recommendations with respect to the standardization of electrocardiographic equipment, particularly with the question of patient safety as a consideration [10].

Lead Systems

STANDARD LEADS

Since ECG voltages occur between any two points on the body surface, with an arbitrarily selected polarity, comparison of results obtained from one laboratory with those from another or of recordings from one subject with those from another requires a common measurement protocol. This fact was recognized by early electrocardiographic investigators. Over time, a set of measurements called the "standard leads" has emerged. Included are the three limb leads of Einthoven: lead I is the voltage measured between the left arm (positive) with respect to the right arm, lead II is the voltage on the left leg (positive) with respect to the right arm, and lead III is the voltage on the left leg with respect to the left arm. The "precordial leads" are a set of six leads measured in standard anatomic locations located horizontally around the left chest [11]. The voltage at each of these sites is measured with respect to "Wilson's central terminal." Wilson's central terminal is formed by connecting electrodes on the right arm, left arm, and left leg to a common terminal through large-valued resistors. The precordial leads often are called "unipolar leads." In addition, three "augmented unipolar limb leads" [12] sometimes are measured. The augmented leads use the right arm, left arm, and the left leg, respectively, as the positive electrode and measure with respect to the average of the other two. They are referred to as aV_R, aV_L, and aV_F. Together the three limb leads, six precordial leads, and three augmented unipolar limb leads are referred to as the standard 12-lead ECG.

The nomenclature "standard 12-lead ECG" must not be taken as implying more standardization than exists, since in many contexts fewer electrodes are used, more electrodes are used, or different electrodes are used. For example, vectorcardiograms are a specialized form of electrocardiograms, based on the concept of an electrical dipole as equivalent to the electrical activity of cardiac sources (see below). Vectorcardiograms are made with special sets of leads. For example, the "Frank leads" [13] are used to record Frank vectorcardiograms.

COMPREHENSIVE LEAD SYSTEMS

A question of basic importance to ECG measurements is: how many different leads are required to record all the information available on the body surface about the cardiac state?

This question is not easy to answer, since every different site where an electrode is placed will yield a somewhat different trace. Conversely, two electrodes placed close together, particularly at body positions relatively far removed from the heart, will yield traces that are very similar.

One way of examining this question is to determine, for a possible new lead V_N, whether voltages measured from it are a linear combination of the voltages observed on other leads being recorded. Suppose two measured leads, V_1 and V_2, are compared to a new lead V_N. This test becomes whether constants a_1 and a_2 can be found so that

$$V_N(t) - [a_1 V_1(t) + a_2 V_2(t)] \leq N \qquad (7.1)$$

where N is the magnitude of the noise. If values for a_1 and a_2 can be found that cause equation 7.1 to be satisfied at all times t, then V_N can be computed from V_1 and V_2 within the noise level; therefore, V_N need not be measured. The same concept can be used to compare a new lead with the standard 12 leads. (It is interesting to note that if this test is used to inquire whether limb lead III need be added if limb leads I and II are measured, the conclusion is that it need *not* be. This redundancy between the limb leads is widely known but sometimes overlooked.)

If collections of 150–250 leads are compared to each other by a test similar to that of equation 7.1 the results show that 20–40 leads must be measured from a new subject to define the entire potential distribution on the body surface, depending on the noise level specified [14, 15]. (If constants a_1 . . . are chosen by retrospective analysis of a large number of leads from a single person, 3–10 leads may be all that are required.)

Temporal Characteristics

FREQUENCY CONTENT

Evaluation of the frequency content of ECG waveforms is useful as a guide to the equipment necessary for recording. More importantly, changes in frequency content might be used as an indicator of changes in the underlying cardiac state [16]. Evaluation of the frequency content of measured electrocardiograms shows that most of the signal power lies in frequencies under 100 Hz. There is a gradual decrease of power as frequency increases, in part due to noise in the measurements.

It is difficult (and risky) to specify a maximum frequency beyond which there are no signals of cardiac origin to be found. This difficulty occurs because small features of the electrocardiographic waveform, close to the noise level, may still be quite significant. For example, the entire P wave contributes relatively little to the overall ECG signal in terms of its "power," compared to the much larger QRS-T deflections generated by the ventricles. Nonetheless, as the manifestation of atrial electrical activity, accurate measurement of P waves obviously is significant. Moreover, more subtle features of the larger QRS waveform, such as notches and slurs, in some studies have been associated with hypertrophy or infarction.

SAMPLING RATES

The relative uncertainty of the frequency content is similarly reflected in digital measurements. Where ECG signals are recorded by digital sampling at a regular rate, commonly used sampling rates range from 200 to 1000 samples per second. Rates lower and higher than these are used in special circumstances. Some examples of waveforms reconstructed after sampling at different rates are shown in the report by Barr and Spach [17].

Origin of the Electrocardiogram

Determining body surface activity from cardiac electrical activity is called the "forward problem" of electrocardiography. Many fundamental elements of its solution are well established [18]. Some are summarized here briefly (more extensive consideration of cardiac electrophysiology is presented in other chapters).

The heart contains many electrically active cells. When these cells are electrically at rest, a potential difference of about 90 mV exists between the interior and exterior of each one, with the intracellular volume being more neg-

ative. In the course of a normal heartbeat, some cells in the region of the SA node spontaneously depolarize (that is, the interior becomes less negative with respect to the exterior). In a chain-reaction fashion there follows the depolarization of the atrium, the AV node, the ventricular conduction system, and the ventricular muscle. After a period of time the active cells spontaneously repolarize (that is, the interior of the cell again becomes relatively negative with respect to the exterior). The electrical characteristics of the total heart are determined to a major degree by the fact that the intracellular volume of adjacent cells apparently is electrically interconnected by relatively low-resistance connections [19]. As a result, the ventricular muscle often is said to behave as an "electrical syncytium."

Electrical depolarization is accompanied by current flow both within and outside each active cell. The extracellular current flow extends throughout the "volume conductor," the name given the resistive media between the cardiac and body surfaces. A major determinant of the relationships between cardiac excitation and body surface electrocardiograms is the geometric placement of the heart within the torso, since this placement determines the characteristics of the volume conductor between each region of the heart and each site on the body surface. Figure 7–4 shows a tracing of a photograph of a human cross section [20]. Among the features evident from this tracing are the lack of symmetry of the right and left ventricles with respect to the right and left sides of the body surface and the acentric location of the heart within the torso. Most of the volume conductor is constituted by the lungs, which have markedly lower conductivity than the heart, and skeletal muscle layers, which exhibit significantly anisotropic conductivities (i.e., conductivities differing in different directions).

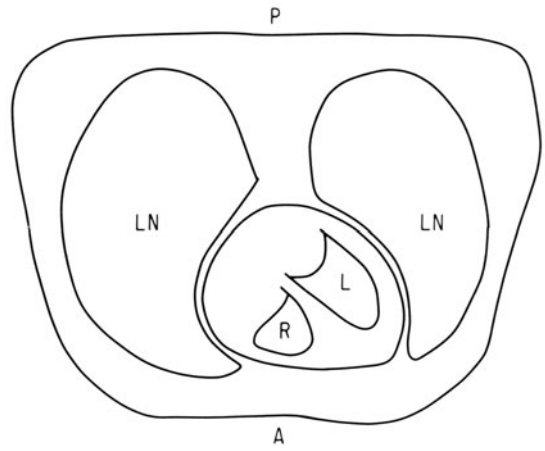

FIGURE 7–4. Tracing of a cross-sectional photograph from an adult male. This tracing was made from photographic section 26 in the book by Eycheshymer and Shoemaker [20]: A, anterior; P, posterior; LN, lung; R(L), right (left) ventricular cavity.

INTRACELLULAR–EXTRACELLULAR CURRENT FLOW

The way that excitation of cardiac cells leads to body surface electrocardiograms can be visualized by means of current flow diagrams. One such diagram is shown in figure 7–5. Two "cardiac strands" A and B are contained within a solution that conducts electrical current, the "volume conductor" of this example. On the surface of the volume conductor are attached two electrodes, E_1 and E_2. A similar pair of electrodes, C_1 and C_2, is within the volume conductor, and a final pair, I_1 and I_2, is within strand A. A meter M measures the potential

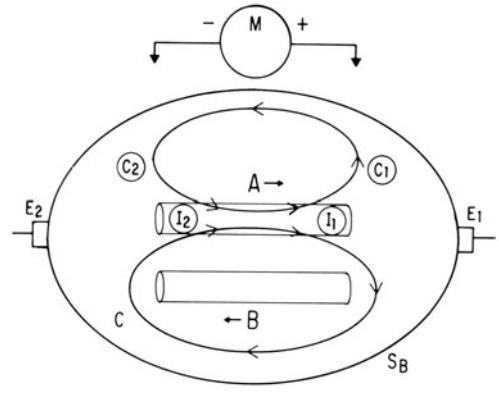

FIGURE 7–5. Current flow within and around idealized strands *A* and *B*. Propagation is assumed to the right in *A* and left in *B* (arrows). Electrodes I_1 and I_2, C_1 and C_2, and E_1 and E_2 are pairs located intracellularly, within volume conductor C, and on the surface S_B of the volume, respectively.

difference between any pair of these electrodes, with electrode 1 positive.

Suppose propagation occurs along strand A to the right, as shown by the arrow; thereafter, propagation occurs along strand B in the opposite direction. Suppose propagation along strand A has reached the midpoint. At this moment, consider the potential difference inside the strands between the two electrodes I_1 and I_2. A comparison of the *intracellular* potential between right and left ends of strand A (voltage difference between I_1 and I_2) would show that the right end is relatively negative with respect to the left end. That this potential difference exists can be understood as follows: The left side of strand A, through which propagation already has occurred, has become depolarized relative to the extracellular volume. The right side of strand A, not yet excited, remains polarized. Voltage differences within the extracellular volume are relatively small. Therefore a potential difference of about 90 mV exists intracellularly between the two ends of this strand.

As a consequence of this intracellular potential difference, ionic current will flow within the strand from the region of relatively high potential to the region of relatively low potential. Through the process of capacitive discharge across the membrane and ionic transport through the membrane, the intracellular current flow will be accompanied by current flow across the membrane walls between the intracellular and extracellular volumes. The gross geometric pattern of this current flow will be that of large loops, as shown diagrammatically in figure 7–5. The most intense current flow will be near the portion of the membrane undergoing depolarization at each moment; however, current flow of diminishing intensity will extend throughout the volume. (It is worth noting that these intracellular–extracellular current flow relationships can be analyzed in detail and demonstrated quantitatively, [e.g., 21].)

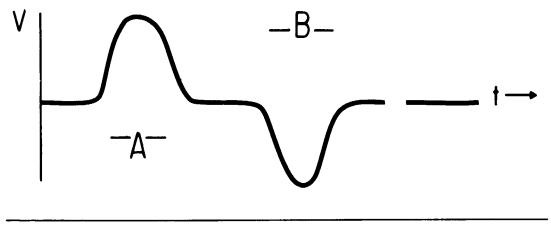

FIGURE 7–6. Hypothetical waveforms from excitation of strand *A*, then strand *B*, of figure 7–5, as might be recorded from electrodes E_1 and E_2: V, voltage; t, time; A(B), time of excitation of strand A(B).

If probes were inserted into the extracellular volume and the voltage measured at point C_1 with respect to C_2, then at the midpoint of depolarization of strand A, C_1 would be relatively positive. (Note the opposite polarity between the extracellular points C_1 and C_2 compared to the intracellular points I_1 and I_2.) That C_1 will be positive with respect to C_2 can be recognized from observing that current flows from the vicinity of C_1 to that of C_2, and that Ohm's law will apply in the resistive volume conductor.

Electrodes E_1 and E_2 are connected to the volume conductor at its surface. At the midpoint of depolarization of strand A, electrode E_1 will be positive with respect to electrode E_2, just as electrode C_1 was positive with respect to C_2; that is, electrical propagation toward E_1 (and therefore away from E_2) will make E_1 positive with respect to E_2.

Now consider a (hypothetical) record of voltage versus time that might be obtained if propagation occurred first in A to the right and then in B to the left (fig. 7–6). Voltage at E_1 with respect to E_2 is plotted on the vertical axis, with time is plotted on the horizontal axis. The waveform comprises a positive and then a negative deflection. The positive deflection is from propagation in strand A, as discussed above. The negative deflection is from propagation in strand B, in the opposite direction. The trace shows the composite effect of both strands. Information that could be deduced from such a record might include, for example, the time of propagation through A, corresponding to the width of the positive deflection.

Real electrocardiograms can be understood (qualitatively) in terms of the concepts of figures 7–5 and 7–6. The surface of the volume corresponds to the body surface, the electrically

active strands correspond to the electrical activity of the cardiac muscle, and the trace of figure 7–6 is an "electrocardiogram." It is obvious that conceiving of real electrocardiograms in such a way involves drastic simplifications, since the cardiac structure is geometrically and electrically complicated, with multiple different cardiac regions sometimes active simultaneously. Additionally, the real volume between the heart and body surface is inhomogeneous with respect to conductivity and anisotropic. Nonetheless, one of the most remarkable facts about the relationship of the electrocardiogram to excitation in the heart is that such simplified concepts frequently do provide a qualitative explanation for experimental and clinical observations.

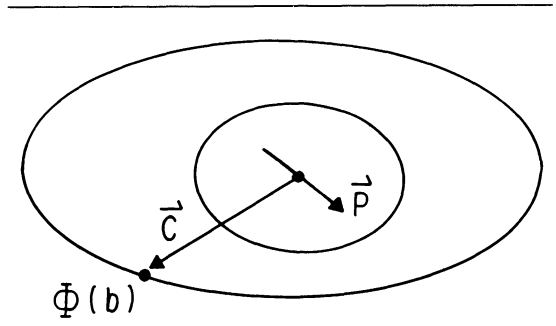

FIGURE 7–7. Equivalent dipole model. Vector $\vec{p}$ represents a dipole generating current flow "equivalent" to that of the heart, as observed on the body surface. Lead vector $\vec{c}$ represents the relationship between $\vec{p}$ and a particular point b on the body surface. Potential $\Phi(b)$ is measured at b.

SINGLE DIPOLE MODEL

A more mathematical viewpoint of the conceptually simply picture of the heart as a simple current source inside a uniform volume conductor is diagrammed in figure 7–7. In the figure, the electrical properties of the heart are represented by a "heart vector," $\vec{p}$. The geometric relationship between the current sources within the heart and a point on the body surface are represented by the "lead vector," $\vec{c}$[22]. In this model, the potential at a point b on the body surface, $\Phi(b)$, is computed as product of vectors $\vec{c}$ and $\vec{p}$:

$$\Phi(b) = \vec{c} \cdot \vec{p} = c_x p_x + c_y p_y + c_z p_z \qquad (7.2)$$

where

$\vec{p}$ = heart vector = (p_x, p_y, p_z)

and

$\vec{c}$ = lead vector = (c_x, c_y, c_z)

Changes in cardiac electrical sources correspond to changes in the heart vector, $\vec{p}$. The electrical and geometric relationships between the dipole source in the heart and a particular point on the body surface are represented by the lead vector, $\vec{c}$.

A special merit of this model is that it identifies and separates ECG changes that occur because of changes in the sequence of cardiac excitation or other cardiac electrophysiologic changes from changes that occur because of changes in the site of electrodes on the body surface or other changes in the volume conductor. Different sequences of cardiac excitation correspond to different sequences of changes in the vector $\vec{p}$, the lead vectors $\vec{c}$ all remaining the same. Conversely, the same sequence of cardiac electrical events observed at different positions on the body surface corresponds to changing the lead vector $\vec{c}$, without making changes in the sequence of heart vectors.

It is important to recognize that heart vector $\vec{p}$ represents the composite effect of all of the electrically active regions of the heart at any one moment. These will be of varying electrical intensity and distributed in position. Heart vector $\vec{p}$, as their composite effect, is not a physically real entity, so its value cannot be measured directly. Similarly, each lead vector represents the composite effect of the volume conductor between the site of the imaginary heart vector and a particular point on the body surface. As such, the lead vector is affected not only by the geometric distances from the observation site to the heart vector, but also by the electrical properties of the intervening volume conductor.

At one time some investigators thought that observations of cardiac electrical activity on the body surface might be described *quantitatively*

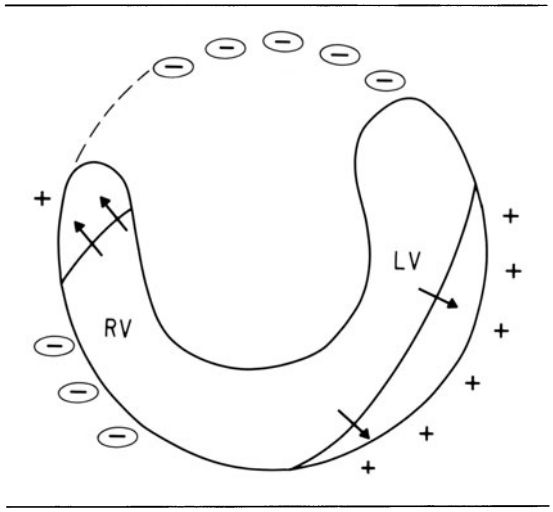

FIGURE 7–8. Cross-sectional diagram of right and left ventricular muscle, excluding the septum. The solid lines within the RV and LV might be isochrones, and the + and − signs the signs of the potentials observed around a closed surface surrounding the active muscle.

by the single dipole model. Several lines of experimental evidence now make it clear that this view is wrong. Body surface electrocardiographic events are too complicated to be explained by a model that is this simple. Moreover, the lack of the ability in principle to determine the heart vector from direct measurement of electrical potentials within and around the heart has diminished the utility of this model in recent years as direct heart measurements have been realized more often. Nonetheless, the single dipole model remains a useful way to summarize large quantities of diverse body surface electrocardiographic information in a simple way; it is sufficient for a first-order approximation of the major features of the observations. This model is the basis for vectorcardiography.

ISOCHRONES AND CARDIAC POTENTIAL DISTRIBUTIONS

The most comprehensive ways to measure cardiac electrical events, as they relate to body surface electrocardiograms, are measurements of cardiac excitation sequences using epicardial and plunge electrodes [23, 24], and measurements of potential distributions within and on the heart itself [25].

Figure 7–8 shows diagrammatically results that might be obtained from such measurements. Within the diagram of figure 7–8, the dark line in the LV and RV regions indicates a hypothetical excitation wavefront as it might exist at one moment. The complete sequence of excitation can be described by a series of such lines, often called "isochrones" since each line depicts the cardiac wavefront by joining all sites undergoing excitation simultaneously. In figure 7–8, it is assumed that a large wavefront of excitation is progressing through the left ventricular wall at the same time that a smaller wavefront is continuing excitation through the right ventricular wall.

Potential values measured ahead of the advancing wavefronts are usually positive, while those electrodes behind excitation waves are usually negative. These polarities are indicated by + and − signs around the borders of the figure. (Caution is necessary in estimating the potentials, however, both because the real excitation waves would be extending in all three dimensions and because of the fact that the potential at each site will be affected by both wavefronts.) Potentials measured on the epicardial surface of the heart have peak magnitudes ranging from a few millivolts to tens of millivolts.

Substantial advantages are associated with picturing cardiac excitation in terms of potentials. Among these is that information is gained from all recording sites during all phases of the cardiac cycle rather than being limited only to one moment of excitation. Potential distributions thereby are suitable for describing electrical events of repolarization, and the overlap of repolarization events with preceding excitation events. Moreover, they provide a means to measure the electrical events that occur when the cardiac muscle is abnormal and therefore not undergoing rapid and complete depolarization.

MATHEMATICAL MODELS RELATING CARDIAC TO BODY SURFACE POTENTIALS

If events in the heart are described in terms of cardiac potentials, their relationship with voltages recorded at points in the volume conductor or on the body surface can be specified

mathematically with moderate accuracy. Miller and Geselowitz [26] have developed computer models that work directly from intracellular potentials. Other calculations may be based on equation 7.3, an integral equation relating potentials at an observation point ϕ^b to the potential distributions existing on a closed surface around the heart, around the lungs, and around the body surface.

$$\phi^b = -\frac{\sigma_L}{4\pi\sigma_b}\int_{S_H}\phi_H\frac{\bar{r}_H\cdot\bar{n}_H}{r_H^2}\,dS_H - \frac{\sigma_L}{4\pi\sigma_b}\int_{S_H}\phi_H\frac{\nabla\phi_H\cdot\bar{n}_H}{r_H}\,dS_H + \frac{(\sigma_L-\sigma_m)}{4\pi\sigma_b}\int_{S_L}\phi_L\frac{\bar{r}_L\cdot\bar{n}_L}{r_L^2}\,dS_L + \frac{\sigma_m}{4\pi\sigma_b}\int_{S_B}\phi_B\frac{\bar{r}_B\cdot\bar{n}_B}{r_B^2}\,dS_B \qquad (7.3)$$

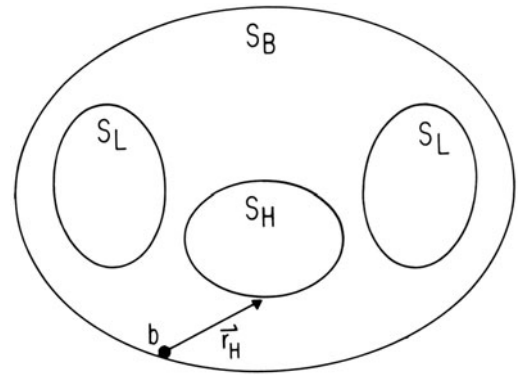

FIGURE 7–9. Schematic cross section of the torso identifying boundaries between major regions (see eq. 7.3 and compare with fig. 7–4): S_B, body surface-to-air boundary; S_H, surrounds the active sources within the heart; S_L, surrounds the lungs. As an approximation, tissue within each region is assumed to have uniform electrical properties.

Figure 7–9 shows each of these boundaries schematically. The point of observation, *b,* is drawn at the boundary of surface S_B, which represents the body surface. The cardiac electrical sources are contained within boundary S_H. It is assumed that bounding surfaces S_L can be drawn around "lungs" and separate uniform regions of different conductivity inside and outside the boundaries. Potentials on the heart, lung, and body surfaces are designated by ϕ_H, ϕ_L, and ϕ_B, respectively. The conductivity within lung regions, muscle regions, and at the observer's position are indicated by symbols σ_L, σ_m, and σ_b. Lines drawn from the position of the observer to points on the heart, lung, or body surface are designated as r_H, r_L, or r_B, respectively.

Active Cardiac Sources. Inspection of equation 7.3 shows how different quantities affect the potential at the observer's position *b.* The first two integrals of equation 7.3 are over surface S_H, surrounding the active cardiac sources. These two integrations are influenced by the potentials on surface S_H, ϕ_H, the gradients of potential on this surface (related to the current flow through the bounding surface), $\nabla\phi_H$, and by the distance r_H from the observer's location to each segment of the heart surface. Integrations are required since the potential for a single point on the surface of the torso is influenced by the potential distribution around the entire heart. Greater weight is given to potentials on S_H nearer position *b,* i.e., the integrals include a division by distance r_H.

Inhomogeneities such as the Lungs. The third integral is over the boundary separating the region of lung conductivity from the region of muscle conductivity. Notice that this integral has an influence on the value computed at the body surface position *b,* even though position *b* is not on or within the lungs, and even though the electrical sources that are active are contained entirely within S_H.

Body Surface Effects. Finally, the fourth integral is over the surface of the body. That this integral is needed indicates that the size and shape of the entire body-to-air boundary has an effect on the potential measured at any particular point on the body surface.

Computer Models. Although the integral operations of equation 7.3 are too complicated to be performed manually, especially in view of the irregular geometric shapes of all the structures involved, a number of studies that have

involved computer models have performed such calculations. In general such calculations require approximating the integrations as numerical summations, and approximating the potential distribution with a set of potential values for particular points on the surface under consideration.

Among the major results of such calculations have been the demonstration of the following points [27]: First, measured epicardial potential distributions may be used to calculate body surface potentials, based on the concepts of equation 7.3. If the calculated potentials are compared to potentials measured from the body surface, the same qualitative sequence of events is observed. Second, first-order quantitative approximation of computed with measured body surface potentials is achieved if (but only if) the effects of the body surface are included. Third, systematic quantitative discrepancies are observed between computed and measured body surface potentials if the calculation assumes a uniform homogeneous volume conductor of the correct size and shape. These discrepancies should diminish if internal inhomogeneities such as the lung boundary were incorporated [28], although conclusive simulations are yet to be performed. The interaction of the effects between lung and skeletal muscle may be especially important.

Comparison with Dipole Model. Some idea of the vastly different models used in evaluating the relationship between cardiac and body surface electrical events can be gained by comparison of figure 7–7 with figure 7–9 or comparison of equation 7.2 with equation 7.3. In the former case, a simple model, easily grasped intuitively, is satisfactory for separating the concept of changes in cardiac electrical events from changes in the way these are observed depending of the observer's site on the body surface. The simple model provides a way of bringing unity to the mass of body surface observations. However, it is insufficient to describe the body surface observations quantitatively, and grossly inaccurate in terms of its ability to describe electrical events within the heart occurring at multiple sites. Further, it assumes an unrealistically simple volume conductor.

In contrast, the model and mathetmatics of equation 7.3 are more realistic. Complex cardiac electrical events are allowed. Complex volume conductor properties can be taken into account, at least in principle. Further, a close association exists between what is described mathematically in the model and physically real, measurable quantities. However, a limitation of the more complicated model is that the increased complexity makes its manual or intuitive evaluation difficult; computer simulation methods must be used to cope with these complexities. Moreover, although equation 7.3 is more complicated than equation 7.2, it nonetheless incorporates numerous simplifying assumptions relative to actual hearts and volume conductors. For example, it assumes a simple boundary can be drawn separating uniform "lung" regions from uniform "muscle" regions.

Interpretation of Electrocardiograms

Determining cardiac electrical events from measurements on the body surface is called the "inverse problem" of electrocardiography.

OBJECTIVES AND FUNDAMENTAL LIMITATIONS

Characteristics of cardiac excitation are deduced from electrocardiograms for widely differing purposes: electrocardiograms are used to monitor normal cardiac function (astronauts), to detect and classify arrhythmias over periods of hours or days (arrhythmia monitors), to detect coronary atherosclerotic heart disease (electrocardiograms during exercise), as a means of classifying other types of heart disease, not necessarily of primarily electrophysiologic origin (the analysis of waveforms of resting ECGs), and to predict values of measurable cardiac electrical events within the heart, for research and clinical purposes (such as surgical treatment for WPW syndrome). As might be expected, the basis and specific procedures used in each different case vary markedly.

It may not be the case that "there are almost as many interpretations as there are electrocardiologists," as Meiler said [29], but there are certainly basic difficulties associated with electrocardiographic interpretation. The most basic

is that "while knowledge of the bioelectric sources, body shape, and conductivities specifies uniquely (at least in principle) the surface potentials, the reverse is not true . . ." [30]. This physical limitation means that the cardiac electrical sources generating electrocardiograms cannot be deduced from the electrocardiograms alone, even in principle. Instead, the electrocardiograms must be used with other information that limits the range of interpretations allowed. This other information may be a physical model of cardiac electrical sources, a collection of previously recorded electrocardiograms from patients with independently documented cardiac status, or information in some other form.

This fundamental difficulty is compounded by a related one: the theory of electrical current flow makes clear that as an observer moves away from any group of electrical sources, the pattern of electrical changes seen by moving around the sources becomes smoother. In electrocardiography, the consequence of this phenomenon is that different sequences of excitation producing distinctly different potentials on the epicardium might produce very similar potentials on the body surface, where, because of the noise present in the measurements, they could not be distinguished. (In multiple dipole heart models, for example, confusion for this reason of right ventricular with septal excitation has been reported.)

TYPES OF STATEMENTS

A variety of statements, fundamentally different in character, are called "interpretations" of electrocardiograms. Some statements simply identify features of the recorded electrocardiogram, such as identification of P or QRS complexes. Other statements give numerical values that are derived directly from the recorded data, for example, the interval between the P wave and QRS complex, QRS duration, etc.

Still other statements are inferences about the cardiac electrical sources probably causing the observed body surface electrical phenomena. Such statements involve a formal or informal model of the relationship between cardiac and body surface electrical events. Finally, there are statements associating new electrocardiograms with physiologic changes or types of heart disease. The underlying changes may or may not be primarily electrophysiologic but are hypothesized to lead to changes in cardiac electrophysiology; these electrophysiologic changes then cause changes in the electrocardiogram. For example, acute hyperkalemia is associated with electrocardiographic changes [31]. When changes in the ECG are associated with such underlying causes, considerable inference is required.

Recognizing that interpretations are made with different types of statements is significant particularly in relation to judging the validity of the interpretation. More specifically, the validity of statements of the first two kinds may be easily established, whereas the validity of statements about the electrical events within the heart or physiologic changes causing them may be very difficult to establish except from indirect evidence.

STATISTICAL CLASSIFICATION

The most widespread basis for the interpretation of electrocardiograms is systematic comparison of new recordings with collections of recordings previously obtained from populations of subjects with different kinds of heart disease. Such classification may be by means of a formal statistical procedure, or it may be a more informal process taking place in the mind of an experienced electrocardiographer. In either case, the reference population must be large enough that natural variability from individual to individual is observed, as emphasized by Pipberger [32] and others. Furthermore, objective, independent documentation of the classification of the reference population is required. That is, patients said to have "right bundle branch block" must be so classified by some means other than the electrocardiogram showing a "right bundle branch block pattern." The process of statistical classification has now become widely accomplished by means of computer programs, often offered commercially. (The IBM-Bonner program is a well-known example.) In general, the objectives of such programs are to accomplish rapidly and systematically an interpretation that would be the same as that given by a knowledgeable and

experienced individual. That is, the programs are not intended to bring to bear any fundamentally different principles of interpretation.

Statistical classification of ECGs usually is affected, either explicitly or implicitly, by the a priori probabilities of different outcomes. These values state that probability, prior to the time the ECG is recorded, of the "correct diagnosis" being in each one of the possible categories allowed as an outcome. A priori probabilities vary depending on the context: they are different for ECGs taken at random from the population as a whole than for ECGs recorded in the emergency room of a hospital; both are different than for a pediatric cardiology clinic. The way in which a priori probabilities are used, and how their values should be obtained has been a source of controversy.

PHYSICAL AND PHYSIOLOGIC ANALYSIS

ECGs may be analyzed based on an understanding of the electrical relationships that exist between cardiac electrical events and the ECGs measured on the body surface, taking into account the restricted scope of electrical events allowed by the nature of cardiac electrophysiology. There are several ways in which such interpretation is accomplished, often associated with a particular way of displaying body surface measurements.

Waveforms. ECG traces of voltage versus time are particularly useful for detecting and classifying temporal features of cardiac electrical events. The identification of deflections arising from ventricular excitation (QRS complexes) is relatively straightforward. Using this information alone, many cardiac arrhythmias can be detected and classified.

Interpretation of the source of each component of the deflections within a voltage-versus-time trace is not as easily accomplished. In part this is because electrical sources anywhere in the heart contribute to the voltage recorded on a single body surface trace. That is, there is no simple subdivision of the site of electrical activity within the heart as the source of events seen on a particular body surface tracing. (The subject of careful interpretation of electrocardiographic waveforms, particularly in a clinical context, is one about which there is an extensive literature in both journal and textbook form, and whose consideration is beyond the scope of this chapter.)

Vectorcardiograms. The conceptual basis of vectorcardiography is the use of a single dipole current source to represent cardiac electrical activity (fig. 7–6 and eq. 7.2). The dipole current source is thought of as "equivalent" to the real cardiac sources in the sense that such a dipole current source would produce potentials on the body surface approximating those potentials actually observed. The strength of vectorcardiography is the use of body surface information to determine and present explicitly information about the aggregate spatial orientation (and the changes in spatial orientation) of cardiac electrical events. (Such spatial information is not directly presented by waveforms of voltage versus time.) However, since electrical excitation and repolarization are phenomena that are spatially distributed throughout the electrically active tissue of the atria and ventricles, the single dipole current source is not "equivalent" as far as corresponding to the actual cardiac sources of electrical activity.

Vectorcardiographic lead systems measure and portray cardiac electrical activity in terms of geometric coordinates, e.g., along x, y, and z axes. Figure 7–10 shows a drawing of a vectorcardiographic origin, O, within an oval representing a horizontal cross section of the torso. At times T_1, T_2, and T_3, the equivalent dipole representation of the cardiac sources is represented by the three vectors P. The locus of the tips of the vectors forms a loop in the horizontal plane that is the vectorcardiogram in that plane. Often two or three vector loops are presented to show the trajectory of the equivalent dipole in all three geometric planes. Other systems for displaying vectorcardiographic information, such as polarcardiograms, also have received careful attention.

An important theoretical basis for vectorcardiography is the Gabor–Nelson equations [33], which show how to compute the x, y, and z components from body surface information, without knowledge of the site of the vector's position within the volume conductor.

Single Moving Dipole. Another type of physical inverse has emphasized those time instants when electrical activity is thought to be concentrated at one site. These models also have made use of a single dipole to represent cardiac events, but the dipole location also has been determined. The location chosen is the location that allows the dipole to best fit the measured body surface events, often using the multipole shift equations of Geselowitz [34]. These equations describe how to find the location within the volume conductor where a dipole might be located to account for the largest portion of the body source information. A comparison then can be made of the site computed for the location of the dipole, and independently measured sites of cardiac electrical activity. For example, the site of the dipole in early excitation can be compared to the site of earliest excitation as measured by epicardial or plunge electrodes [35, 36]. This strategy is oriented toward a relatively limited class of cardiac events, those that are concentrated spatially, and thereby is not generally applicable to much of either normal or abnormal cardiac excitation and depolarization sequences.

Potential Distributions and Body Surface Maps. A complete description of cardiac electrical events on the body surface may take the form of a series of potential distributions (often called "surface maps"). Each potential distribution ("map") shows the voltage as a function of position over the complete body surface, in concept, and over the chest and back in most real maps. For example, figure 7–11 shows how a surface map taken about 25 ms from the beginning of QRS might appear. The left two-thirds of the map portray the chest, and the right one-third the back. The lines connect points of equal voltage. The solid lines indicate voltages that are positive with respect to Wilson's central, and the dashed lines indicate negative voltages. At the moment shown, voltages over the right upper chest are negative, while those over the left chest and around the lower torso are positive. Maps for each of a series of times throughout the cardiac cycle must be present.

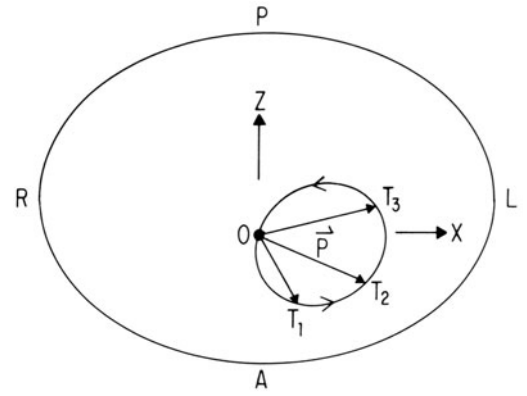

FIGURE 7–10. Idealized vectorcardiographic loop (horizontal plane). Three vectors are drawn from origin 0 for times T_1, T_2, and T_3. Each vector represents the equivalent dipole $\vec{p}$ for that time, as projected into the *x*-*z* plane. Joining the tips of these vectors plots a loop (the vectorcardiogram). The surrounding oval represents the body surface.

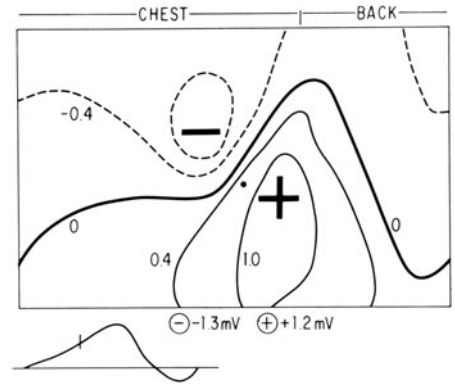

FIGURE 7–11. A body surface potential distribution (surface map). The left two-thirds of the map portrays the chest, the right one-third the back. The pattern of potentials is drawn for one time instant, identified by the vertical bar through the QRS portion of the reference trace below the figure. Solid lines are isopotential contours for the positive potentials (dashed for negative). The line for zero potential (same as Wilson's central terminal) is emphasized. The values of the highest and lowest voltages observed at this time are written below the map, and the positions of the maximum and minimum are indicated by the large + and − signs. As a gross approximation, the map can be understood by assuming that negative potential regions overlie regions of the ventricles that already have completed activation, while positive potentials overlie regions undergoing activation.

For the most part, collection and display of body surface electrocardiographic information in this form was too complicated to be achieved by manual methods, except with lengthy, painstaking procedures [37]. Therefore, development has occurred concurrently with the development of digital computer methods for storing, processing, and displaying this information [38].

Several significant advantages are associated with interpreting cardiac electrical activity from complete potential distributions. The first is the assurance that no significant data that might have been obtained from body surface measurements at other sites simply have been overlooked. The second is that inspection of the full potential distribution lends itself to an intuitive correlation between the pattern of potentials as observed on the body surface and the pattern of potentials that might be observed on the epicardium, or the pattern of current flow that might exist within the cardiac muscle and volume conductor. No reduction to an elementary model, such as that of a single dipole, is required. Thereby, maps lend themselves naturally to interpretations of regional cardiac electrical events distributed throughout the heart as they actually are. For example, in figure 7–11 the negative potentials overlying the right ventricular epicardium and the positive potentials overlying the left ventricular epicardium suggest that at the moment shown much of excitation of the right ventricle is complete, while left ventricular excitation is continuing.

Because obtaining complete potential distributions does require relatively elaborate equipment, it appears unlikely that such recordings will displace traditional methods for routine use. However, systems for map recording are now readily achieved with standard items of laboratory recording and computing equipment, so that the acquisition and display of potential maps is a straightforward technical process.

Substantial theoretical advantages are associated with using potential distributions to estimate cardiac electrical events based on the physical principles of electrical current flow through the volume conductor. For example, evaluation of equation 7.3 requires an integration over the body surface; performing the integration requires knowing the potential distribution everywhere. Just as significantly, the fundamental difficulties of estimating cardiac events from body surface measurement, and the fact that large changes within the heart may produce only small changes on the body surface, mean that the additional measured information gained from the full body surface potential distribution (as compared to the information in a vectorcardiogram or in the standard leads) may make an important quantitative difference in estimating cardiac potentials.

Body surface maps have been used to predict cardiac electrical events with several kinds of physical models of the heart. For example, Holt and co-workers performed inverse calculations using a multiple dipole model of the heart [39]. In that model, a number of dipoles were used to represent different regions of ventricular muscle. Activities were computed for each dipole as a function of time, and were interpreted as representing the electrical activity of a given portion of the muscle. Time integrals of the activity of each vector were used to evaluate the electrical activity near each dipole. For example, one test was to determine whether hypertrophy was present in that cardiac muscle region. Since the dipoles representing each muscle segment are not directly measurable entities, it remains difficult to verify the validity of the calculations through animal experiments.

Other mathematical procedures have been used to estimate the actual epicardial potential distributions from those on the body surface [40]. The epicardial potential distributions then were compared to potential distributions measured from the epicardial surface by means of implanted electrodes. The estimated potential distributions were found to be similar to those measured, in major features. Changes in the sequence of excitation produced by pacing the heart at different stimulus sites were easily recognized. However, the estimated and measured potential distributions differed in many important secondary features. In part these dif-

ferences must reflect the simplified basis for the results reported. For example, the calculations made use of simplified models of the volume conductor, assumed to be uniform and isotropic. At present, the degree to which quantitative estimates of cardiac epicardial events might be improved were better physical models to be used remains unknown.

Summary

The number of electrocardiograms recorded each year probably exceeds 50,000,000. Electrocardiographic waveforms have become so easily and widely measured, and their use so routine, that their very familiarity leads one to believe that their interpretation in terms of cardiac electrical events must have been fully and completely established long ago.

Such is far from true. While many relationships of fundamental importance have been deduced between body surface and cardiac electrical events, a marked lack of understanding of many aspects of body surface electrical events remains. In part, this limitation exists because of the remarkably small amount of experimental data recorded and reported about the electrical activity of the total heart. Particularly this limitation pertains to electrical events within the ventricular walls, not easily accessible to electrodes without significant tissue damage, and to human hearts, and in the presence of cardiac abnormalities. It is to be expected that an increasing understanding of cardiac electrical events will come about as newer and more extensive measurements are obtained of what happens, exactly, during such events as cardiac arrhythmias. Coupled with better models for current flow within the complex human volume conductor, this understanding may change altogether the way that body surface electrocardiograms are interpreted in terms of the events of cardiac excitation and repolarization.

References

1. Waller AD: On the electromotive changes connected with the beat of the mammalian heart and of the human heart in particular. Philos Trans R Soc [B] 180:169–94, 1889.
2. Einthoven W, Fahr G, De Waart A: Uber die Richtung und manifeste Grosse der Potentialschwankungen im menschlichen Herzen und uber den Einfluss der Herzlage auf die Form des Elektrocardiograms. Pflugers Arch ges Physiol 150:275–315, 1913. Translated: Am Heart J 40:163–211.
3. Lewis T, Rothschild MA: The excitatory process in the dog's heart. II. The ventricles. Philos Trans R Soc [B]206:181–226, 1915.
4. Goldman MJ: Principles of clinical electrocardiography, 10th edn. Los Altos CA: Lange Medical.
5. Flowers NC, Shvartsman V, Kennelly BM, Sohi GS, Horan LG: Surface recording of His–Purkinje activity on an every-beat basis without digital averaging. Circulation 63:948–952, 1981.
6. Association for the Advancement of Medical Instrumentation: Standard for diagnostic ECG devices. Arlington VA: AAMI (1901 North Fort Meyer Drive, Suite 602, Arlington VA 22209).
7. Spach MS, Barr RC, Havstad JW, Long EC: Skin electrode impedance and its effect on recording cardiac potentials. Circulation 34:649–656, 1966.
8. Schmitt OH, Almasi JJ: Electrode impedance and voltage offset as they affect efficacy and accuracy of VCG and ECG measurement. In: Proceedings of the 11th international vectorcardiography symposium. Amsterdam: North-Holland, 1970.
9. Huhta JC, Webster JG: 60-Hz interference in electrocardiography. IEEE Trans Biomed Eng 20:91–101, 1973.
10. American Heart Association Committee on Electrocardiography: Electrical safety standards for electrocardiographic apparatus. Circulation 61:669, 1980.
11. Wilson FN, Macleod AG, Barker PS: The order of ventricular excitation in bundle branch block. Am Heart J 7:305–330, 1932.
12. Goldberger E: Unipolar lead electrocardiography and vectorcardiography. Philadelphia: Lea and Febiger, 1953.
13. Frank E: An accurate clinically practical system for spatial vectorcardiography. Circulation 13:737–749, 1956.
14. Barr RC, Spach MS, Herman-Giddens GS: Selection of the number and positions of measuring locations for electrocardiography. IEEE Trans Biomed Eng 18:125–38, 1971.
15. Lux RL, Smith CR, Wyatt RF, Abildskov JA: A limited lead selection for estimation of body surface potential maps in electrocardiography. IEEE Trans Biomed Eng 25:270–276, 1978.
16. Goldberger AL, Bhargava V, Froelicher V, Covell J: Effect of myocardial infarction on high-frequency QRS potentials. Circulation 64:34–42, 1981.
17. Barr RC, Spach MS: Sampling rates required for digital recording of intracellular and extracellular cardiac potentials. Circ Res 55:40–48, 1977.
18. McFee R, Baule GM: Research in electrocardiography and magnetocardiography. Proc IEEE 60:290–322, 1972.

19. De Mello WC: Intracellular communication in cardiac muscle. Circ Res 51:1–9, 1982.
20. Eycleshymer AC, Schoemaker DM: A cross-section anatomy. New York: Appleton-Century-Crofts, 1911.
21. Spach MS, Barr RC, Johnson EA, Kootsey JM: Cardiac extracellular potentials: analysis of complex wave forms about the Purkinje network in dogs. Circ Res 33:465–473, 1973.
22. Burger HC, Van Milaan JB: Heart vector and leads. I, II, and III. Br Heart J 8:157, 1946; 9:154, 1947; 10:229, 1948.
23. Scher A, Young A: The pathway of ventricular depolarization in the dog. Circ Res 4:461–469, 1956.
24. Durrer D, Van Dam R, Freud MG, Janse MJ, Meijler FL, Arzbaecher RC: Total excitation of the heart. Circulation 41:899–912, 1970.
25. Spach MS, Barr RC, Lanning CF, Tucek PC: Origin of body surface QRS and T wave potentials from epicardial potential distributions in the intact chimpanzee. Circulation 55:268–278, 1977.
26. Miller WT III, Geselowitz DB: Simulation studies of the electrocardiogram II. Ischemia and infarction. Circ Res 43:315–23, 1978.
27. Ramsey M III, Barr RC, Spach MS: Comparison of measured torso potentials with those simulated from epicardial potentials for ventricular depolarization and repolarization in the intact dog. Circ Res. 41:660–672, 1977.
28. Rudy Y, Plonsey R: A comparison of volume conductor and source geometry effects on body surface and epicardial potentials. Circ Res 46:283–291, 1980.
29. Meiler FL: In: A new coding system for electrocardiography. Amsterdam: Excerpta Medica, EO Robles de Medina, 1972.
30. Plonsey R: Bioelectric phenomena. New York: McGraw-Hill, 1969, pp 202–275.
31. Hurst JW, Logue RB, Schlant, Wenger NK: The heart, 4th edn. New York: McGraw-Hill, 1978, p 309.
32. Pipberger HV, Schneiderman MA, Klingeman JD: The love-at-first-sight effect in research. Circulation 38:822–825, 1968.
33. Gabor D, Nelson CV: Determination of the resultant dipole of the heart from measurements on the body surface. J Appl Physiol 25:413–16, 1954.
34. Geselowitz DB: Two theorems concerning the quadrupole applicable to electrocardiography. IEEE Trans Biomed Eng 12:164–168, 1965.
35. Ideker RE, Bandura JP, Larsen RA, Cox JW, Keller FW, Brody DA: Localization of heart vectors produced by epicardial burns and ectopic stimuli. Circ Res 36:105–112, 1975.
36. Savard P, Roberge FA, Perry JB, Nadeau RA: Representation of cardiac electrical activity by a moving dipole for normal and ectopic beats in the intact dog. Circ Res 46:415–425, 1980.
37. Taccardi B: Distribution of heart potentials on the thoracic surface of normal human subjects. Circ Res 12:341–352, 1963.
38. Rush S, Lepeschkin: Body surface mapping of cardiac fields. Adv. Cardiol. 10, Karger, 1974.
39. Holt J, Barnard ACL, Lynn M: The study of the human heart as a multiple dipole source II. Diagnosis and quantization of left ventricular hypertrophy. Circ Res 40:697–710, 1969.
40. Barr RC, Spach MS: Inverse calculations of QRS-T epicardial potentials from body surface potential distributions for normal and ectopic beats in the intact dog. Circ Res 42:661–75, 1978.

8. THE SLOW ACTION POTENTIAL AND PROPERTIES OF THE MYOCARDIAL SLOW CHANNELS

Nicholas Sperelakis

Slow Channels and Their Role in Ca^{2+} Entry

Hormones and neurotransmitters play an important role in regulating the force of contraction of the heart. The force of contraction of the heart is controlled by the Ca^{2+} influx across the cell membrane during the action potential (AP) in the process of excitation–contraction coupling (fig. 8–1). This Ca^{2+} influx occurs through the voltage-dependent and time-dependent gated slow channels of the cell membrane. This chapter briefly reviews and summarizes some of the important properties of the myocardial slow channels, particularly their dependence on metabolism and their regulation by cyclic AMP. In addition, the slow action potentials and their possible role in cardiac arrhythmias will be briefly discussed.

Besides the slow channels, there are other types of voltage-dependent channels, including fast Na^+ channels and several types of K^+ channels. In addition, there are at least two types of voltage-independent Ca^{2+}-operated channels, one selective for K^+ ($g_{K(Ca)}$) and one mixed Na/K ($g_{Na,\ K(Ca)}$). Each type of ionic channel is a specific protein that floats in the lipid bilayer matrix of the cell membrane (fig. 8–2). Each channel has a water-filled central pore for ion passage. A cation passing through its ion-selective channel probably binds to two or three negatively charged sites on its journey through the channel down its electrochemical (electrical plus concentration) gradient. The voltage-dependent fast Na^+ channels and slow channels have a central activation (A, *m* or *d*) gate and an inactivation (I, *h* or *f*) gate at the inner surface of the membrane (fig. 8–3).

Compared to the fast Na^+ channels, the slow channels are kinetically slower, i.e., they behave as if their gates open, close, and recover more slowly. In addition, the slow-channel gates operate over a less-negative (more-depolarized) voltage range, i.e., their threshold potential and the inactivation voltage range are higher (less negative) (fig. 8–4). These two types of channels for carrying inward (depolarizing) current also are blocked by different drugs: tetrodotoxin (TTX) blocks fast Na^+ channels (by binding to the outer mouth of the channel and acting as a physical plug), but does not affect the slow channels; in contrast, calcium-antagonistic drugs, such as verapamil, nifedipine, and diltiazem, block the slow channels with relatively little or no effect on the fast Na^+ channels.

There are three types of slow channels with respect to ion selectivity: Ca^{2+}, Na^+, and Ca-Na (fig. 8–5). The Ca-Na type allows both Ca^{2+} ions and Na^+ ions to pass through, perhaps with competition between them. An example of a Ca-Na slow channel is in ventricular

The work of the author reviewed and summarized in this article was supported primarily by grant HL-18711 from the National Institutes of Health. The author wishes to acknowledge the collaborative efforts of his colleagues, particularly Drs. K. Shigenobu, J.A. Schneider, S. Vogel, I. Josephson, T. Li, D.C. Pang, P.-A. Molyvdas, G. Bkaily, and G. Wahler.

N. Sperelakis (ed.), PHYSIOLOGY AND PATHOPHYSIOLOGY OF THE HEART.

Martinus Nijhoff Publishing, Boston/The Hague/ Dordrecht/Lancaster.

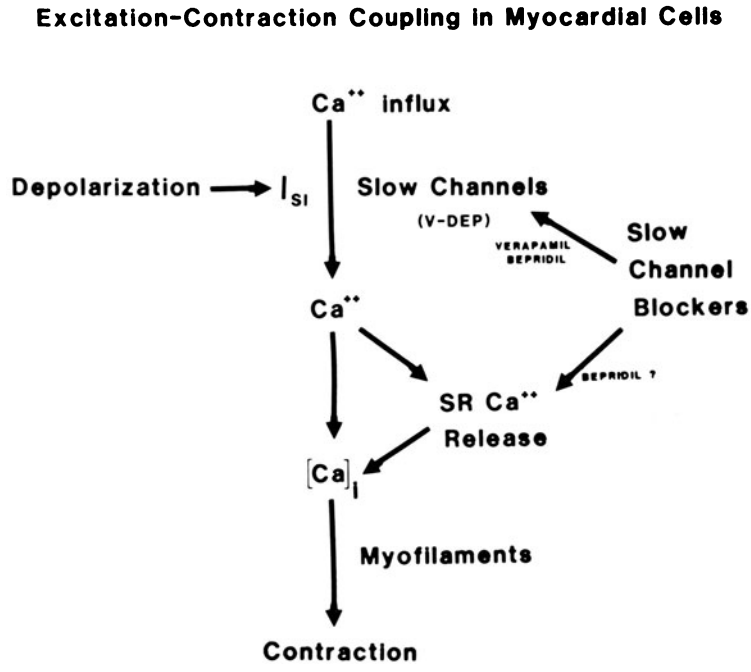

FIGURE 8–1. Summary diagram for excitation–contraction coupling in myocardial cells. Ca^{2+} influx during excitation occurs through the voltage-dependent and time-dependent gated slow channels. This entering Ca^{2+} helps to raise the myoplasmic Ca^{2+} concentration ($[Ca]_i$) to the level necessary to activate the contractile proteins (e.g., 10^{-5} *M*), and acts to bring about the release of additional Ca^{2+} from the SR by the mechanism of Fabiato and Fabiato [53].

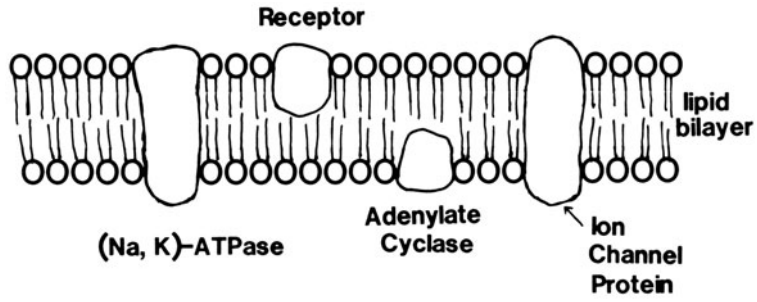

FIGURE 8–2. Diagrammatic illustration of the Singer–Nicolson model for the cell membrane as a lipid bilayer with proteins floating in the bilayer. Some protein molecules are inserted in only one leaflet of the bilayer, such as the autonomic receptors on the external surface and the adenylate cyclase complex on the inner surface. Some large protein molecules protrude through the entire thickness of the membrane, such as the ion channel proteins. Redrawn from Sperelakis [58].

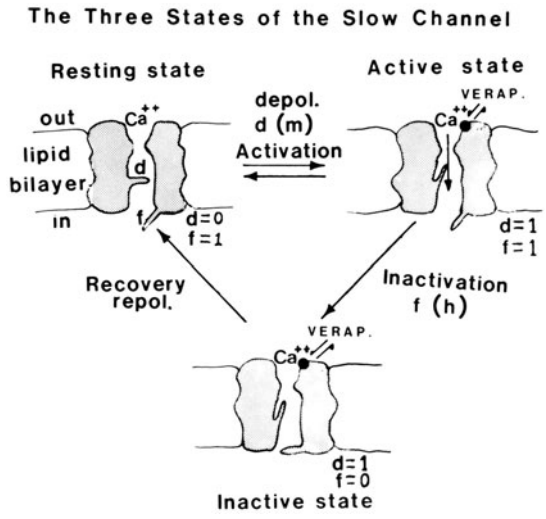

FIGURE 8–3. Cartoon model for the three hypothetical states of a slow channel, patterned after the Hodgkin–Huxley states for the fast Na^+ channel. In the resting state, the $d(m)$ gate is closed and the $f(h)$ gate is open ($d=0, f=1$). Depolarization to the threshold activates the slow channel to the active state, the d gate opening rapidly and the f fate still being open ($d=1$; $f=1$). The activated channel spontaneously inactivates to the inactive state due to closure of the f gate ($d=1$; $f=0$). The recovery process upon repolarization returns the channel from the inactive state back to the resting state, which is again available for reactivation. Ca^{2+} ion is depicted as being bound to the outer mouth of the channel and poised for entry down its electrochemical gradient when both gates are in the open position (active state of channel). Also depicted is the possible binding of verapamil to the outer mouth of the slow channel (solid circle) in the active state or inactive state, and thereby either blocking the activated channel or slowing the recovery process for converting from the inactive state back to the resting state. Modified from Sperelakis [2].

myocardial cells of adult guinea pig and chicken [1]. An example of a pure Ca-selective slow channel is found in arterial vascular smooth muscle (VSM) cells [2] or in guinea pig atrial cells [3]. An example of a nearly pure Na-selective slow channel is found in young (two- to three-day-old) embryonic chick hearts [4]. Since verapamil and D-600 (methoxy derivative of verapamil) block all three types of slow channels, such calcium-antagonistic drugs are more appropriately called "slow-channel blockers". Because Ca^{2+} ion entry into the cardiac cell during excitation is through the Ca or Ca-Na slow channels, the Ca antagonists are often called "calcium-entry blockers". Since Ca^{2+} influx into the cell controls the force of contraction, the calcium-antagonistic drugs partly or completely uncouple contraction from excitation. Slow channels are also found in nodal cells (SA and AV) and Purkinje fibers, as well as in working myocardial cells.

It was shown by Lee and Tsien [5], in voltage-clamp experiments on internally dialyzed isolated single adult heart cells (from guinea pig ventricle), that a reversal of the Ca slow-channel current occurs at large depolarizing clamps, and that the outward current is carried by K^+ ion through the slow channel. (An outward movement of Cs^+ can also occur through the slow channels.) D-600 blocked the current flow in either direction. This latter point must be remembered when considering all the actions of the calcium-antagonistic drugs.

Action of Neurotransmitters, Hormones, and Positive Inotropic Agents

A number of positive inotropic agents exert an effect to increase the number of available slow channels in the myocardial cell membrane. This action may be the predominant explanation for their increase in cardiac contractility, since the amount of Ca^{2+} ion entering the cell through the slow channels controls the force of contraction. The Ca^{2+} entering directly elevates $[Ca]_i$ (which activates the myofilaments) and indirectly elevates $[Ca]_i$ further by releasing Ca^{2+} from the intracellular sarcoplasmic reticulum (SR) stores. For example, the Ca^{2+} that entered the cell could bring about the release of more Ca^{2+} by the Ca-trigger-Ca release hypothesis of Fabiato and Fabiato [6]. Blockade of the slow channels, and hence Ca^{1+} influx, by Ca^{2+}-antagonistic agents (such as verapamil, nifedipine, diltiazem, Mn^{2+}, Co^{2+}, and La^{3+}) depresses or abolishes the contractions without greatly affecting the normal fast AP, i.e., contraction is uncoupled from excitation.

The positive inotropic agents that affect the number of available slow channels include: beta-adrenergic receptor agonists (such as isoproterenol and norepinephrine), histamine (H_2 receptor), and methylxanthines (such as caf-

feine, theophylline, and methylisobutylxanthine). The action of these agents is very rapid, the peak effect often occurring within 1–3 min. The effect of the catecholamines is blocked by beta-adrenergic blocking agents, and the effect of histamine is blocked by H_2-receptor blocking agents (but not by H_1-receptor antagonists [7]). The addition of exogenous dibutyryl cyclic AMP exerts a similar effect, but relatively slowly, the peak effect occurring in 15–30 min [8]. Angiotensin II also stimulates the myocardial slow channels [9].

It was recently demonstrated by Reuter et al. [10] that, in patch-clamp experiments on single Ca^{2+} slow channels of cultured neonatal rat heart cells, isoproterenol lengthened the mean open time of the channel and decreased the intervals between bursts (clustering of channel open states); the conductance of the single channel was not increased by isoproterenol. Therefore, the increase in the total maximal slow conductance ($\bar{g}_{si}$) produced by isoproterenol could be produced by the observed increase in mean open time of each channel as well as by an increase in number of channels participating in the conductance on a stochastic basis.

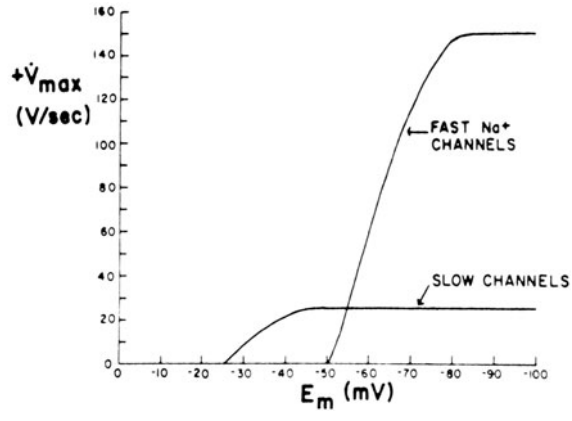

FIGURE 8–4. Graphic representation of differences in behavior, with respect to voltage inactivation, of the fast Na^+ channels and slow (Na^+ and Ca^{2+}) channels. Maximal rates of rise of the action potential ($+\dot{V}_{max}$) as a function of resting E_m for the normal cardiac action potential (dependent on inward current through the fast Na^+ channels) and for the slow action potential (dependent on inward current through the slow channels) elicited in cells whose fast Na^+ channels are blocked (by TTX or by depolarization to about -45 mV). $+V_{max}$ is a measure of the inward current intensity (everything else, such as membrane capacitance, held constant), which in turn is dependent on the number of channels available for activation. From Sperelakis [58].

Setup of the Slow Action Potentials

One method of detecting the effect of agents on the slow channels is to first block the fast Na^+ channels and excitability by tetrodotoxin (TTX) or to voltage inactivate them by partially depolarizing the cells (e.g., to -40 mV) in elevated $[K]_0$ (e.g., 25 m*M*). Then, addition of agents, such as catecholamines, which rapidly increase the number of slow channels available for activation upon stimulation, causes the appearance of slowly rising overshooting APs (the "slow responses"), which resemble the plateau component of the normal fast AP [3, 8] (fig. 8–6). Both Ca^{2+} and Na^+ inward currents participate in the slow APs (fig. 8–7), and they are accompanied by contractions that are nearly as large as the normal contractions [11]. The slow APs are blocked by agents which block inward slow current, including Mn^{2+}, La^{3+}, verapamil, D-600, nifedipine, and diltiazem [11, 12].

Special Properties of the Myocardial Slow Channels

CYCLIC-AMP DEPENDENCE

Cyclic AMP is somehow involved with functioning of the slow channels (table 8–1) [8, 11, 13–15]. The first evidence for this was provided in 1972 by Shigenobu and Sperelakis [8] and by Tsien et al. [16]. Histamine and beta-adrenergic agonists, subsequent to binding to their specific receptors, lead to rapid stimulation of adenylate cyclase with resultant elevation of cyclic-AMP levels. The methylxanthines enter into the myocardial cells and inhibit phosphodiesterase, the enzyme that destroys cyclic AMP, thus causing an elevation of cyclic AMP. These positive inotropic agents also rapidly induce the slow APs, along a parallel time course, presumably by making more slow channels available in the membrane and/or by increasing their mean open time. Dibu-

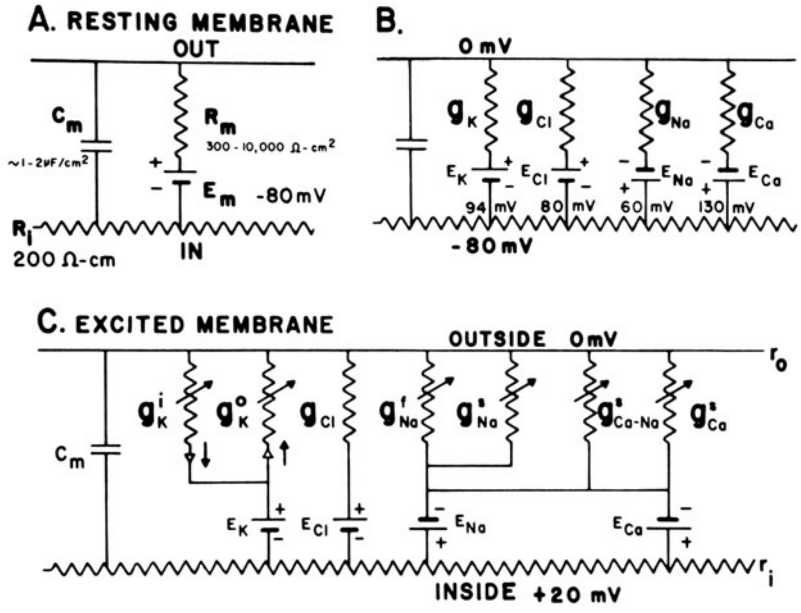

FIGURE 8–5. *(A–E)* Electrical equivalent circuits for a myocardial cell membrane at rest. *(C)* Electrical equivalent circuit for a myocardial cell membrane during excitation. *(A)* Membrane as a parallel resistance–capacitance network, the membrane resistance (R_m) being in parallel with the membrane capacitance (C_m). Resting potential (E_m) is represented by an 80-mV battery in series with the membrane resistance. *(B)* Membrane resistance is divided into its four component parts, one for each of the four major ions of importance: K^+, Cl^-, Na^+, and Ca^{2+}. These represent totally separate and independent pathways for permeation of each ion through the resting membrane. Equilibrium potential for each ion (e.g., E_K), determined solely by the ion distribution in the steady state and calculated from the Nernst equation, is shown in series with the conductance path for that ion. Resting potential of −80 mV is determined by the equilibrium potentials and by the relative conductances. *(C)* Equivalent circuit is further expanded to illustrate that for the voltage-dependent conductances there are at least two separate K^+-conductance pathways (labeled here g^o_K and g^i_K). Arrowheads in series with the K^+ conductances represent rectifiers, the arrowheads pointing in the direction of least resistance to current flow. There are two separate Na^+-conductance pathways, one a kinetically fast Na^+ conductance (g^f_{Na}) and the other a kinetically slow Na^+ conductance (g^s_{Na}). In addition, there is a nonspecific kinetically slow pathway that allows both Na^+ and Ca^{2+} to pass through, perhaps by competition with each other. Ca^{2+}-selective pathway (g^s_{Ca}) is also kinetically slow. Arrows drawn through the resistors represent that the conductances are variable, depending on membrane potential (and time). From Sperelakis [58].

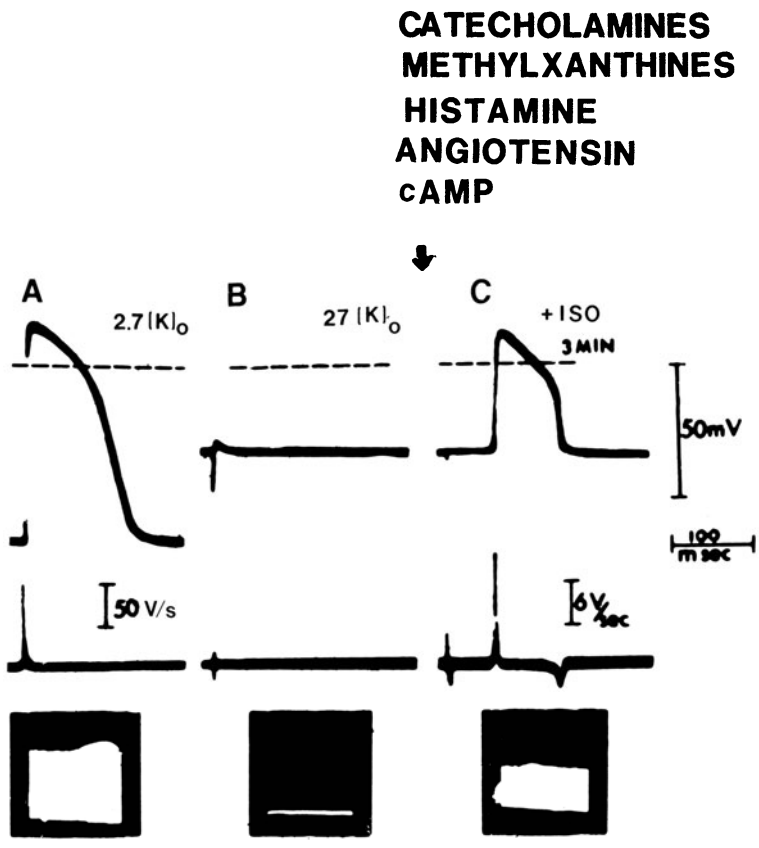

FIGURE 8–6. Characterization of the slow AP responses induced by catecholamines, methylxanthines, histamine, angiotensin II, or cyclic adenosine monophosphate (cAMP) in isolated perfused guinea pig hearts. The fast Na^+ channels were inactivated in elevated K^+. (Upper tracings) Intracellular potentials (V versus *t*) recorded from myocardial cells of the ventricular wall. (Lower tracings) The first time derivative of the action potential (dV/d*t*); the peak upward deflection of dV/d*t* gives the maximal rate of rise of the action potential ($\dot{V}_{max}$). The lower records in each panel are the contractions recorded on a penwriter at a slow speed. *(A)* The normal fast action potential (2.7 m*M* K^+–Ringer perfusate). *(B)* Perfusion with 27 m*M* K^+–Ringer solution depolarized the cells to −40 mV and inactivated the fast Na^+ channels; the heart was unresponsive to stimulation tenfold greater than the normal threshold. *(C)* Isoproterenol (10^{-7} *M*), caffeine (3 m*M*), histamine (10^{-6} *M*), and angiotensin II (10^{-7} *M*) rapidly restored electrical activity in the form of a slow AP response ($\dot{V}_{max}$ of 15 V/s), peak effect being attained within 1–3 min. Dibutyryl cAMP (10^{-4} *M*) slowly induced the slow APs with accompanying contractions, the peak effect occurring within 15–30 min. Contractions were always associated with these slow APs. Modified from Schneider and Sperelakis [55].

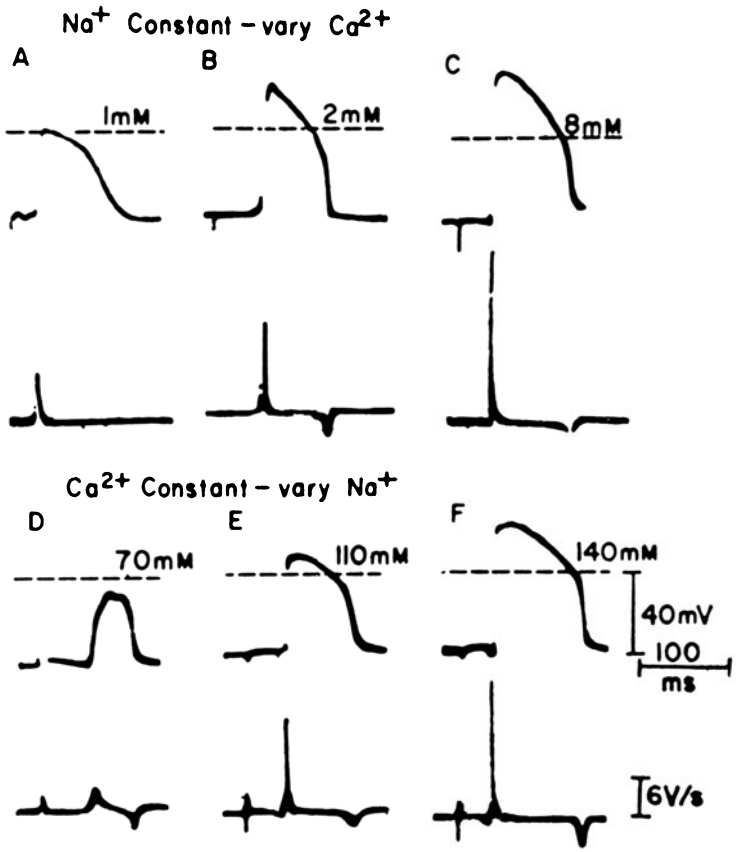

FIGURE 8–7. Demonstration of the dependence of the slow APs of guinea pig ventricular myocardium on $[Ca]_o$ and on $[Na]_o$. The fast Na^+ channels were voltage inactivated by perfusing the heart with 27 mM K^+–Ringer solution and slow APs were induced by isoproterenol (10^{-6} *M*). *(A–C)* Variation in $[Ca]_o$, with $[Na]_o$ held constant at 140 m*M*. Elevation of $[Ca]_o$ from 1 m*M (A)* to 2 m*M (B)* to 8 m*M (C)* increased the overshoot and maximal rate of rise ($\dot{V}_{max}$) of the slow APs. *(D–F)* Variation in $[Na]_o$, with $[Ca]_o$ held constant at 2 m*M*. Lowering of $[Na]_o$ from 140 m*M (F)* to 110 m*M (E)* to 70 m*M (D)* decreased the amplitude and $\dot{V}_{max}$ of the slow APs. Lower trace in each panel is dV/dt, the peak excursion of which gives $\dot{V}_{max}$. From Schneider and Sperelakis [55].

tyryl cyclic AMP also induces the slow APs after a long lag period of 15–30 min (fig. 8–8), as expected from either slow penetration through the membrane or from slow elevation of intracellular cyclic AMP.

Several tests of the cyclic-AMP hypothesis were done. Josephson and Sperelakis [17] showed that a GTP analogue (5' -guanylimidodiphosphate [GPP(NH)P], 10^{-5}–10^{-3} *M*) that directly activates adenylate cyclase induced the slow APs in cultured reaggregates of chick heart cells within 5–20 min (fig. 8–9). GPP(NH)P binds to the GTP site on the regulatory component of the adenylate cyclase complex, but cannot be hydrolyzed by the GTPase activity of the enzyme, and so causes an irreversible activation of adenylate cyclase and elevation of cyclic AMP. Forskolin, a highly potent activator of adenylate cyclase activity, was shown to be a strong positive inotropic agent in isolated guinea pig atrial muscle [18].

Vogel and Sperelakis [19] demonstrated that cyclic AMP iontophoretically microinjected intracellularly into dog Purkinje fibers and guinea pig ventricular muscle induced the slow APs in the injected cell for a transient period

TABLE 8–1. Summary of mechanisms for the control of Ca^{2+} influx by myocardial cells, and hence force of contraction of the heart; control is exerted by altering the fraction of the slow channels in the phosphorylated state, the dephosphorylated channel being electrically silent

I. Extrinsic control
Usually mediated by sarcolemmal receptors and adenylate cyclase activity
A. Autonomic nerves
1. Sympathetic nerves
Neurotransmitter: norepinephrine
2. Parasympathetic nerves
Neurotransmitter: acetylcholine
B. Circulating hormones and autacoids
1. Epinephrine and norepinephrine
2. Histamine
3. Angiotensin II
C. Drugs
1. Calcium antagonists (slow-channel blockers)
2. Beta-adrenergic receptor blockers
3. Histamine H_2-receptor blockers
4. Methylxanthines
5. Cardiac glycosides
II. Intrinsic control
Usually activated by ischemia
A. pH dependence of slow channels
B. Metabolic (ATP) dependence of slow channels
C. Cyclic-AMP dependence of slow channels
D. Protection hypothesis

of 1–2 min (fig. 8–10). A second injection of cyclic AMP again induced a slow AP, which again decayed within 1–2 min. The effect of the injected cyclic AMP was immediate, i.e., within seconds after the injection was stopped. The amplitude and duration of the induced slow APs were a function of the amount of cyclic AMP injected. Cyclic-AMP injections potentiated (increased their rate to rise and amplitude) slow APs induced by theophylline.

Li and Sperelakis [20] demonstrated that pressure injection of cyclic AMP, GPP(NH)P, and cholera toxin into single ventricular myocardial cells within guinea pig papillary muscles rapidly induced and potentiated slow APs (figs. 8–11 to 8–13). As illustrated in figure 8–11, pressure injection of cyclic AMP induced large slow APs within 15–25 s after injection was started. The effect persisted as long as the pressure was applied, and the slow APs decayed within 25 s after the injecting pressure was discontinued. Thus, these results confirm the data obtained by electrophoretic injection of cyclic AMP. Figure 8–12 illustrates that intracellular injection of GPP(NH)P (for 5 s only) produced a very rapid effect, i.e., large slow APs were induced within 40–50 s, in contrast to the relatively slow effect (5–20 min) of GPP(NH)P added to the bathing medium. The induced slow APs persisted for over 3 min after the injecting pressure was stopped, indicating the relatively long-acting effect of GPP(NH)P. Figure 8–13 illustrates that injection of cholera toxin rapidly potentiates an ongoing slow AP, the effect beginning within 30 s and reaching maximum within 3 min (during a 3-min injection period). The induced slow APs persisted for over 4 min after the injecting pressure was stopped, indicating the relatively long-acting effect of cholera toxin. (Cholera toxin has an effect on the adenylate cyclase complex that is similar to that of GPP[NH]P, namely, there is an irreversible activation of the regulatory component of the enzyme, by inhibiting the hydrolysis of the GTP.)

These results support the hypothesis that the intracellular level of cyclic AMP controls the availability of the slow channels in the myocardial sarcolemma (table 8–1).

METABOLIC DEPENDENCE

It was shown by Schneider and Sperelakis [1, 11, 14] that the induced slow APs are blocked by hypoxia, ischemia, and metabolic poisons (including cyanide, dinitrophenol, and valinomycin) within 5–15 min, accompanied by a lowering of the cellular ATP level. Only one example of the effect of metabolic interference will be given. Figure 8–14 shows that cyanide completely blocks the slow APs and contractions (A–C) at a time when the fast APs (D and E) are hardly affected; however, the contractions are nearly completely abolished, i.e., there is uncoupling of contraction from the fast AP. These data suggest that interference with metabolism leads to blockade of the slow channels. The fast APs are unaffected under these conditions, indicating that the fast Na^+ channels are essentially unaffected. However, the contractions accompanying the normal fast APs

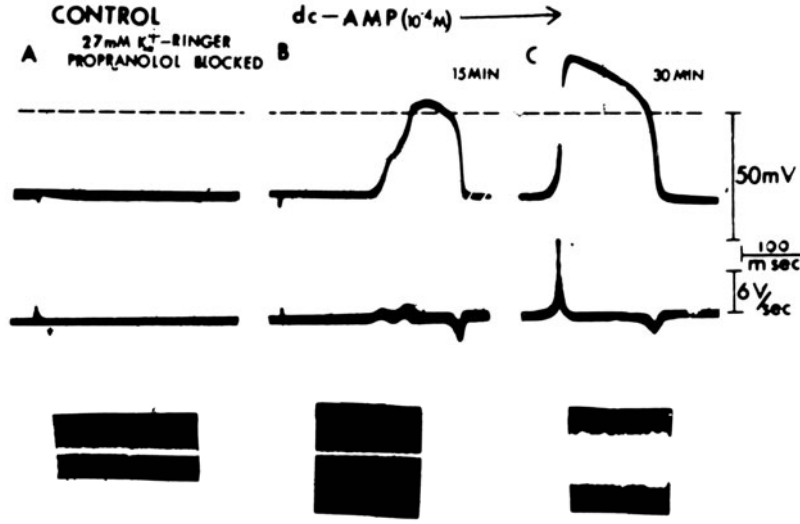

FIGURE 8–8. Induction of slow action potentials (APs) by perfusing a guinea pig heart with solution containing dibutyryl cyclic AMP. *(A)* Control condition with heart perfused with 27 m*M* K^+–Ringer solution to depolarize the cells to about −35 mV and thereby voltage inactivate the fast Na^+ channels. Propranolol (10^{-5} *M*) was also added to ensure that any observed effect was not mediated through the beta-adrenergic receptors. (*B* and *C*) Addition of 10^{-4} *M* db-cAMP produced large slow APs beginning at about 15 min *(B)*, and reaching a peak effect at about 30 min *(C)*. From Schneider and Sperelakis [55].

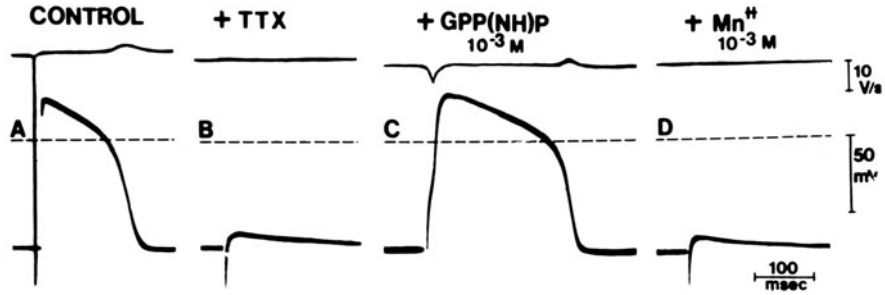

FIGURE 8–9. GPP(NH)P induction of a slow AP response in cultured chick heart cell reaggregates in the presence of propranolol. The preparation was paced at a rate of 1/s. All recordings are from one cell. *(A)* Control fast action potential recorded in normal Tyrode solution. *(B)* The addition of TTX (3.1×10^{-6} *M*) completely blocked excitability. Propranolol (10^{-6} *M*) was then added to ensure that any effect observed was not due to activation of the beta-adrenergic receptor. *(C)* Addition of GPP(NH)P (10^{-3} *M*) induced the slow APs in 15 min. *(D)* Addition of Mn^{2+} (1 m*M*) abolished the slow APs within 1 min. The upper traces give dV/d*t*. Modified from Josephson and Sperelakis [17].

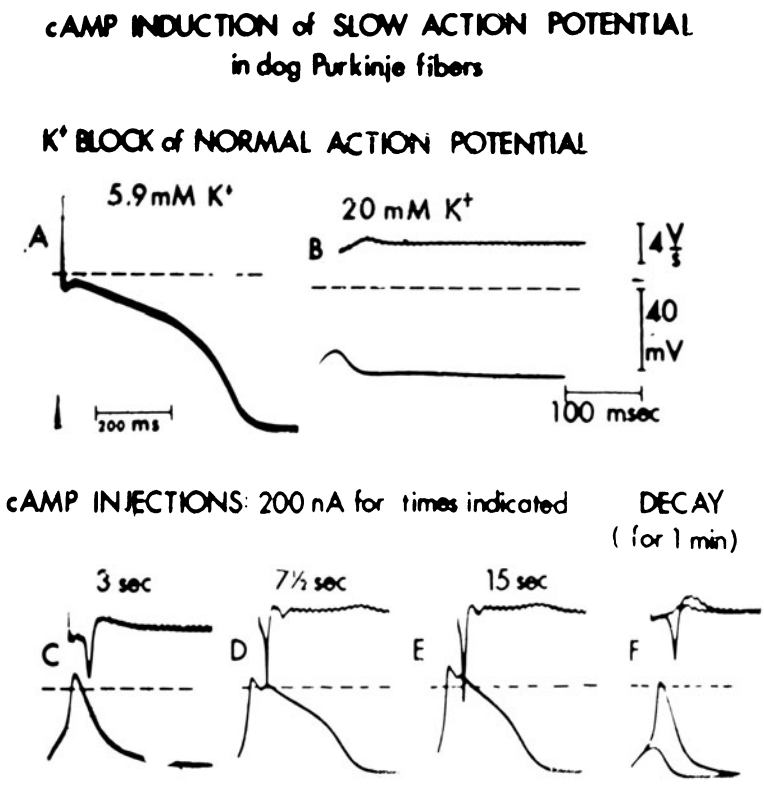

FIGURE 8–10. Cyclic-AMP induction of slow action potentials in short canine Purkinje fibers. *(A)* Normal fast action potential recorded from a fiber bathed in Krebs–Henseleit solution ($[K]_o$ = 5.9 m*M*). *(B)* Elevation of $[K]_o$ to 20 m*M* depolarized the fiber to about −40 mV and abolished excitability (field stimuli of tenfold the normal threshold intensity applied). *(C–E)* Induction of slow action potentials in a single fiber by cyclic-AMP injections of 200nA for 3 s *(C)*, 7.5 s *(D)*, and 15 s *(E)*. The induced responses were allowed to decay completely between injections (not illustrated for *C* and *D*). *(F)* Decay (for 1 min). At 1 min after the injection in *E*, the slow action potential had decreased markedly in $+\dot{V}_{max}$ and duration (first sweep) and then disappeared nearly completely (2nd sweep). Note graded effects of the cyclic-AMP injections on the maximal upstroke velocity ($+\dot{V}_{max}$, upper traces). Horizontal dashed lines give the zero potential level. Different time calibrations in *A* and *B–F*. Preparation paced at 0.3 Hz throughout. dV/d*t* trace arbitrarily shifted to the right, so as to not be obscured in the upstroke of the action potential. From Vogel and Sperelakis [19].

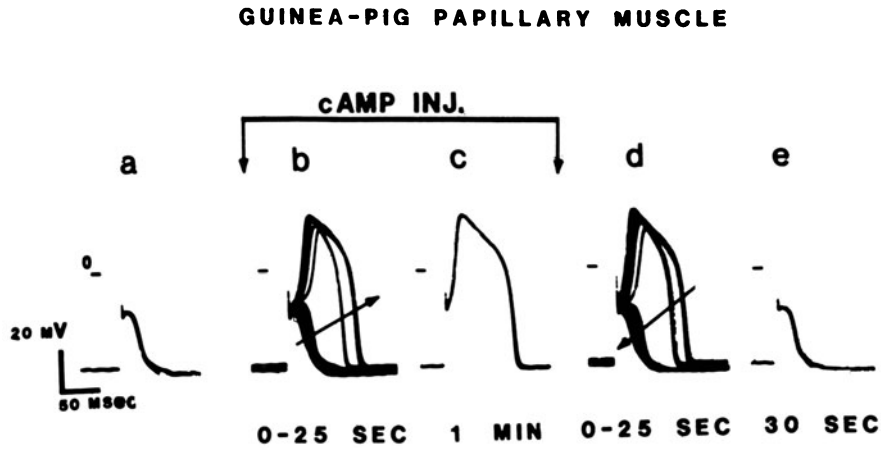

FIGURE 8–11. Induction of slow action potentials in guinea pig papillary muscle by intracellular pressure injection of cyclic AMP. The muscle was depolarized in 22 m*M* $[K]_o$ to voltage inactivate fast Na^+ channels. A microelectrode filled with 0.2 *M* Na^+-cAMP was used for both pressure injection and intracellular recording. *(A)* Small graded response (stimulation rate 30/min). *(B)* Superimposed records showing the gradual appearance of slow action potentials upon cyclic-AMP injection over a 25-s period. *(C)* Presence of stable slow action potential after injection for 1 min. *(D)* Gradual decrease of slow action potentials over a period of 25 s after stopping injection. *(E)* Complete decay of slow action potentials 30 s after cessation of cyclic-AMP injection. All records were obtained from one impaled cell. From Li and Sperelakis [20].

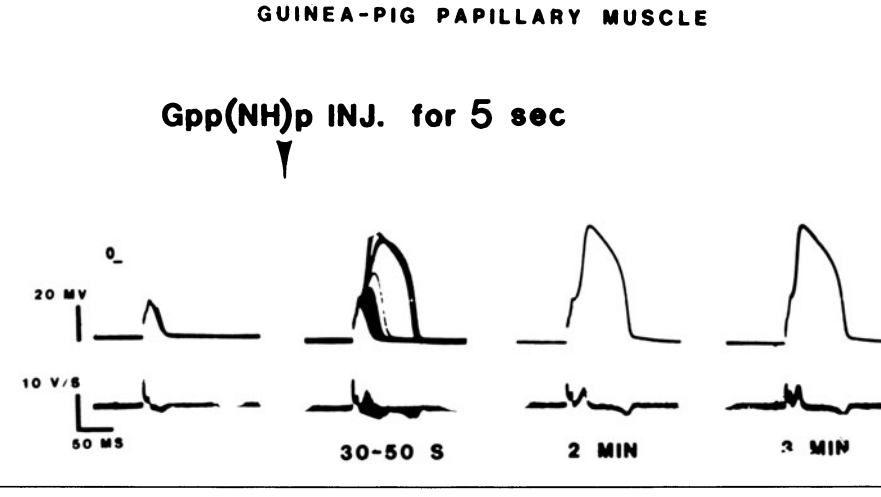

FIGURE 8–12. Induction of slow action potentials by intracellular injection of GPP(NH)P. *(A)* Small graded response induced by electrical stimulation (30/min) in 22 m*M* K–Ringer. *(B)* Induction of slow action potentials by intracellular injection of GPP(NH)P for 5 s. A microelectrode filled with 3×10^{-2} *M* GPP(NH)P in 0.2 *M* NaCl was used for injections and membrane potential recordings. Superimposed records show the gradual induction and enhancement of slow action potentials. (*C* and *D*) The induced slow action potentials were stable and persisted for more than 3 min after the injection was stopped. No slow action potentials were seen in a cell 50 μm away. Other experiments showed that the slow action potentials induced by GPP(NH)P injection were observed for at least 7 min after the injection was stopped. Modified from Li and Sperelakis [20].

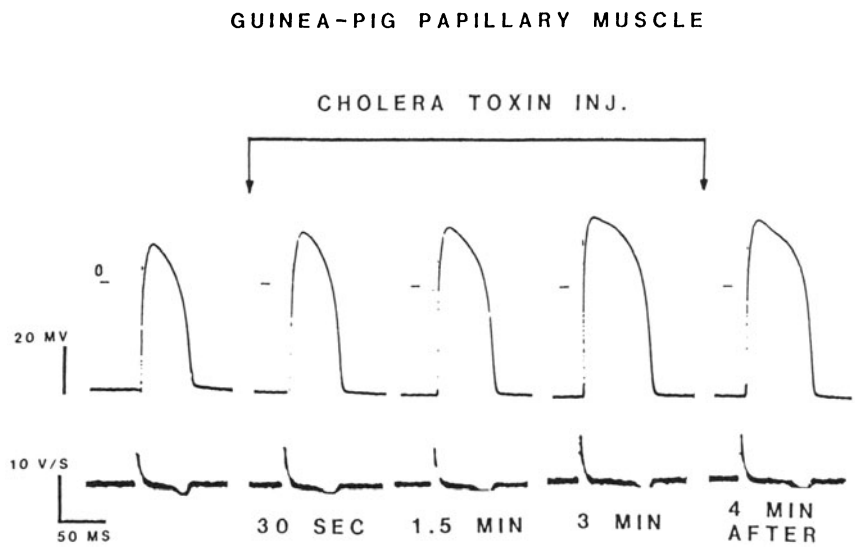

FIGURE 8–13. Stimulation of slow action potentials by intracellular injection of cholera toxin. *(A)* Slow action potential induced by electrical stimulation (30/min) in 22 m*M* $[K]_o$. *(B–D)* Effect of intracellular pressure injection of cholera toxin. A microelectrode filled with reconstituted cholera toxin (1 mg/ml) solution containing 0.2 *M* NaCl was used both for intracellular injections and membrane potential recordings. An enhancement of the slow action potential occurred within 30 s *(B)* of the commencement of the injection period. The amplitude and duration of the slow action potential continued to increase during the injection as seen at 1.5 min *(C)*, until about 3 min *(D)* when an apparent steady state was reached. *(E)* Persistent effect of cholera toxin after cessation of injection. The slow action potential remained enhanced 4 min after the injection had stopped. All records were obtained from one impaled cell. From Li and Sperelakis [20].

are depressed or abolished, indicating that contraction is uncoupled from excitation, as expected if the slow channels were blocked. The slow APs blocked by valinomycin or by hypoxia are restored by elevation of the glucose concentration [21], indicating that the effect of metabolic poisons or hypoxia is indeed mediated by metabolic interference. Thus, there is a specific dependence of the slow channels on metabolic energy.

With prolonged metabolic interference, e.g., 60–120 min of hypoxia or cyanide, there is a gradual shortening of the duration of the normal fast AP, until a relatively brief spike-like component only remains, but which is still rapidly rising (fig. 8–14F). Thus, metabolic interference exerts a second, but much slower, effect on the membrane. This effect is to increase the kinetics of K^+ conductance (g_K) turnon, thereby shortening the AP. The mechanism of this effect could be mediated by a gradual rise in $[Ca]_i$, which can cause an increase in the calcium-activated g_K (i.e., $g_{K(Ca)}$).

It was shown that the unstimulated ("native") and the stimulated ("induced") myocardial slow channels are similar with respect to their blockade by metabolic poisons [22].

PHOSPHORYLATION HYPOTHESIS

Because of the relationship between cyclic AMP and the number of available slow channels, and because of the dependence of the functioning of the slow channels on metabolic energy, Shigenobu and Sperelakis [8] and Sperelakis and Schneider [14] postulated that a membrane protein must be phosphorylated in order for the slow channel to become available for voltage activation (fig. 8–15). A similar hypothesis has been proposed by Tsien and colleagues, Watanabe and colleagues, and Rinaldi and colleagues [16, 23, 24]. Elevation of cyclic AMP by a positive inotropic agent activates a

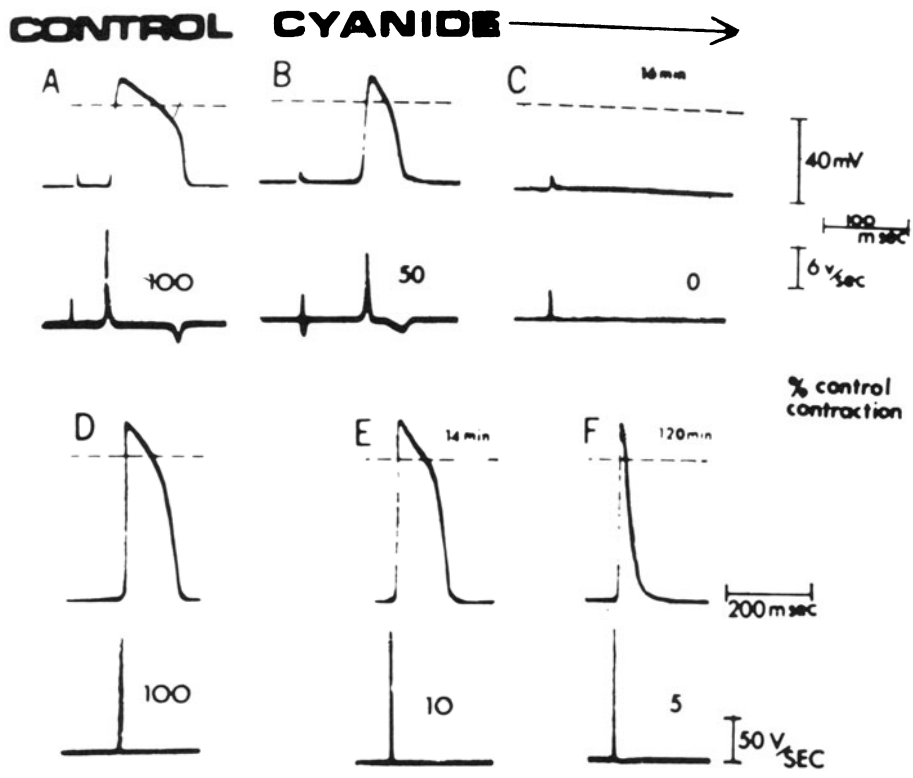

FIGURE 8–14. Inhibition by cyanide (10^{-3} *M*) of the inward Ca^{2+} current induced by catecholamines in hearts partially depolarized by 27 m*M* K^+ (fast Na^+ channels inactivated). Intracellular recordings shown in upper traces; first derivatives of the action potentials are shown in the lower traces. Percent of control contractile force is numerically indicated in each panel. *(A)* Control slow AP response induced by isoproterenol (10^{-7} *M*). (*B* and *C*) The slow AP was depressed at 13 min *(B)* and abolished by 16 min *(C)* following addition of KCN to the perfusate. Depression and loss of contractions followed a parallel time course. *(D)* Normal fast action potential in normal Ringer (2.7 m*M* K^+). *(E)* At 14 min after KCN addition. There was almost no effect on the fast AP ($\dot{V}_{max}$, amplitude or duration), at a time when the slow channels were blocked *(C)*. However, the contractions were greatly depressed. *(F)* After 120 min in cyanide, the fast APs became greatly shortened in duration, but retained fast rates of rise. Modified from Schneider and Sperelakis [1].

cyclic-AMP-dependent protein kinase (dimer split into two monomers), which phosphorylates a variety of proteins in the presence of ATP. Several myocardial membrane proteins become phosphorylated under these conditions.

The protein that is phosphorylated might be a protein constituent of the slow channel itself (fig. 8–15A). The phosphorylation required to make the slow channel functional need not be of the channel protein itself, but of a contiguous regulatory type (e.g., phospholambanlike) of protein associated with the myocardial slow channel. For example, Rinaldi et al. [23] suggested that the function of cardiac slow Ca^{2+} channels in isolated sarcolemmal vesicles is modulated by a cyclic-AMP-dependent phosphorylation of a 23,000 mol wt sarcolemmal protein ("calciductin").

Phosphorylation could make the slow channel available for activation by a conformational change that either allowed the activation gate to be opened upon depolarization or effectively increased the diameter of the water-filled pore (the "selectivity filter" portion) so that Ca^{2+} and Na^+ could pass through. The phosphorylated form of the slow channel would be the

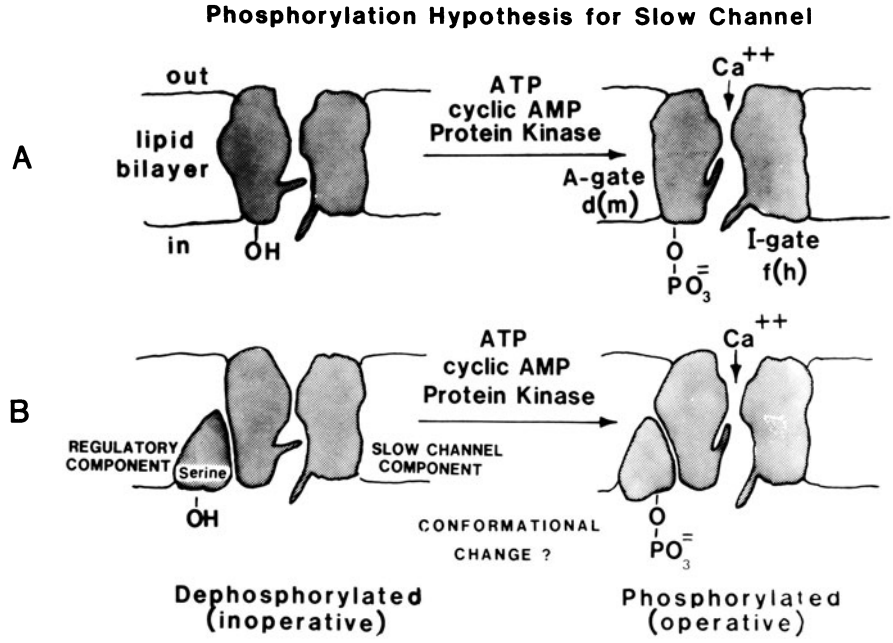

FIGURE 8–15. Cartoon model for a slow channel in myocardial cell membrane in two hypothetical forms: dephosphorylated (or electrically silent) form (*left* diagrams) and phosphorylated form (*right* diagrams). The two gates associated with the channel, an activation (A, *d*, or *m*) gate and an inactivation (I, *f* or *h*) gate, are kinetically much slower than those of the fast Na^+ channel. The hypothesis states that a protein constituent of the slow channel itself (part A) or a regulatory protein associated with the slow channel (part B) must be phosphorylated in order for the channel to be in a functional state available for voltage activation. Phosphorylation occurs by a cyclic-AMP-dependent protein kinase in the presence of ATP. Presumably, a serine or threonine residue in the protein becomes phosphorylated. Phosphorylation of the slow channel protein or of an associated regulatory protein may produce a conformation change that effectively allows the channel gates to operate or increases the diameter of the water-filled pore so that Ca^{2+} and Na^+ can pass through. Modified from Sperelakis and Schneider [14].

active (operational) form, and the dephosphorylated form would be the inactive (inoperative) form; that is, only the phosphorylated form would be available to become activated upon depolarization to threshold. The dephosphorylated channels would be electrically silent. An equilibrium would probably exist between the phosphorylated and dephosphorylated forms of the slow channels for a given set of conditions, including the level of cyclic AMP. Thus, agents that act to elevate the cyclic-AMP level would increase the fraction of the slow channels that are in the phosphorylated form, and hence available for voltage activation. Such agents would increase the force of contraction of the myocardium.

There are some positive inotropic agents that induce the slow channels, but do not elevate cyclic AMP, e.g., angiotensin II [25] and fluoride ion ($<$ 1 m*M*) [24, 26]. Flouride ion may act by inhibiting the phosphoprotein phosphatase which dephosphorylates the slow-channel protein, thereby resulting in a larger fraction of phosphorylated channels; that is, inhibition of the rate of dephosphorylation should have the same effect as stimulation of the rate of phosphorylation. Angiotensin may activate a non-cyclic-AMP-dependent protein kinase. Thus, the results with angiotensin and fluoride can be fitted within the framework of the phosphorylation hypothesis.

The role, if any, of cyclic GMP in the functioning of the slow channels is not known. However, in some cases, injection of cyclic GMP depresses ongoing slow APs (Bkaily and Sperelakis, unpublished observations). It is not

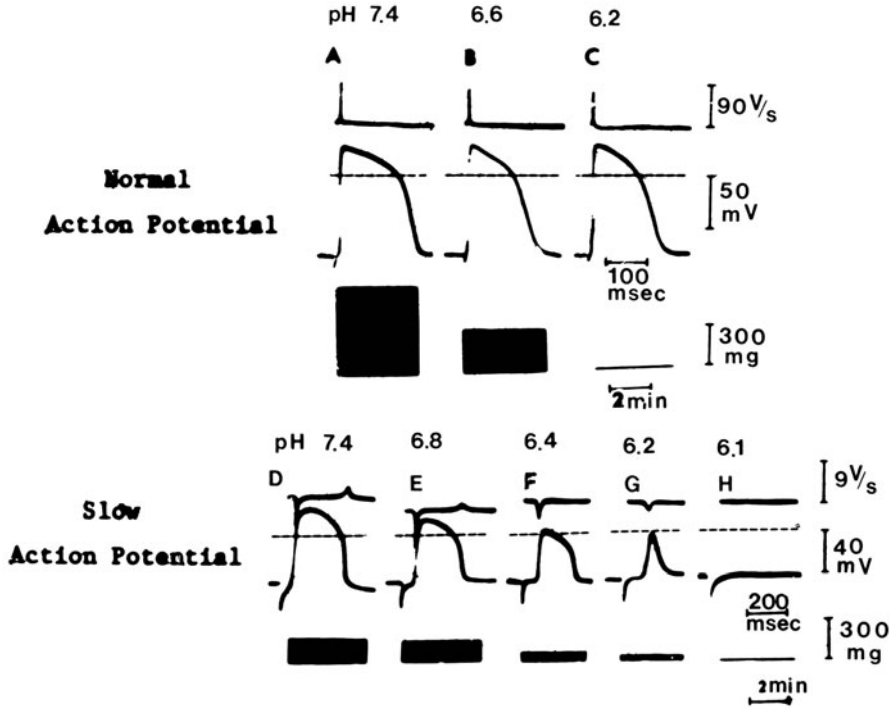

FIGURE 8–16. Selective blockade of the slow channels by acid pH. Bicarbonate–CO_2 buffer. A 20-day-old chick embryo heart was perfused with normal Ringer solution and paced at a rate of 0.5/s. *(A–C)* Normal fast APs. *(A)* Normal fast action potential and contractions at pH 7.4. *(B)* At pH 6.6, force of contraction was greatly reduced, whereas the action potentials were almost unaffected. *(C)* At pH 6.2, contractions were completely abolished, with almost no effect on the fast APs, i.e., excitation–contraction uncoupling was produced. *(D–H)* Blockade of isoproterenol (10^{-6} *M*)-induced slow AP responses at low pH (bicarbonate–CO_2 buffer system) (25 m*M* $[K]_0$). *(D)* Control slow AP response and mechanical record at pH 7.4. *(E–G)* Progressive blockade of slow AP responses and accompanying contractions as pH of perfusing solution was lowered. *(H)* At pH 6.1, complete blockade of slow APs and contractions occurred. Upper trace gives dV/dt, from which maximal rate rise of action potentials was obtained. Modified from Vogel and Sperelakis [29].

clear whether any of the effects of ACh are mediated through changes in cyclic-GMP level. It is also unknown what the role of Ca-calmodulin-activated protein kinase is in operation of the myocardial slow channels. However, trifluoperazine (TFP), an inhibitor of calmodulin, depresses the slow APs (Bkaily, Sperelakis, and Eldefrawi, unpublished observations).

In a test of the phosphorylation hypothesis, Bkaily and Sperelakis [27] demonstrated that intracellular injection (by the liposome method) of an inhibitor of protein kinase (cyclic AMP dependent) blocks the myocardial slow channels.

SELECTIVE BLOCKADE BY ACIDOSIS

The myocardial slow channels are selectively blocked by acidosis [28, 29]. Vogel and Sperelakis [29] showed that the slow APs induced by isoproterenol, for example, are depressed in rate of rise, amplitude, and duration as the pH of the perfusing solution is lowered below 7.0 (fig. 8–16). The slow AP is 50% inhibited at pH 6.6, and is completely abolished at pH 6.1. (The slow APs should be abolished before all the slow channels are blocked because of the requirement of a minimum density of slow channels for regenerative and propagating responses.) The contractions are depressed in parallel with the slow APs. Since two different

buffer systems, HCO_3^-–CO_2 and PIPES, gave similar results and about equally fast, and since the PIPES buffer system should only slowly change the intracellular pH, it appears that the blockade of the slow channels occurs with acidification of the outer surface of the cell membrane. This could change the surface charge of the membrane and/or the conformation of the slow-channel proteins.

Acidosis has little or no effect on the normal fast AP, i.e., the rate of rise remains fast and the overshoot and duration are only slightly affected. However, the contractions become depressed and abolished as a function of the degree of acidosis; that is, excitation–contraction uncoupling occurs, as expected from a selective blockade of the slow channels.

Since the myocardium becomes acidotic during hypoxia and ischemia (glycolysis is increased, and lactic acid diffuses into the interstitial fluid space), it is likely that part of the effect of these metabolic interventions on the slow channels is mediated by the accompanying acidosis and not solely by a decrease in ATP level. Consistent with this, the effects of hypoxia on the slow AP were almost immediately reversed, but only partially and transiently, by changing the pH of the perfusing solution to 8.0; the responses gradually diminished further during the hypoxia at the alkaline pH [30].

INTRINSIC CONTROL OVER Ca^{2+} INFLUX: PROTECTION HYPOTHESIS

The Ca^{2+} influx of the myocardial cell is controlled by extrinsic factors (table 8–1). For example, stimulation of the sympathetic nerves to the heart or circulating catecholamines or other hormones can have a positive inotropic action, whereas stimulation of the parasympathetic neurons has a negative inotropic effect. The mechanism for some of these effects is mediated by changes in the levels of the cyclic nucleotides. This extrinsic control of the Ca^{2+} influx is enabled by the peculiar properties of the slow channels, as, for example, the postulated requirement for phosphorylation.

However, in addition, there is intrinsic control by the myocardial cell itself over its Ca^{2+} influx (table 8–1). For example, under conditions of transient regional ischemia, many of the slow channels become unavailable (or silent). This effect may be mediated by lowering the ATP level of the affected cells and by the accompanying acidosis (since slow-channel blockade during hypoxia occurs faster at acid pH than at alkaline pH). Acidosis presumably blocks the slow channels directly, and metabolic interference causes indirect inactivation of the slow channels. Both effects are relatively selective for the slow channels.

Thus, the myocardial cell can partially or completely suppress its Ca^{2+} influx (which is part of the inward slow current, I_{si}) under adverse conditions. This causes the affected cells to contract weakly or not at all and, since most of the work done by the cell is mechanical, this conserves ATP. Such a mechanism may serve to protect the myocardial cells under adverse conditions, such as transient regional ischemia during coronary vasospasm. If the myocardial cell could not control its Ca^{2+} influx, then the ATP level might drop so low under such conditions that irreversible damage would be done, i.e., the cells would become necrotic. Because of the peculiar properties of the slow channels, they become inactivated, thus uncoupling contraction from excitation and conserving ATP. The cells could then recover fully when the blood flow returns to normal.

The almost normal resting potential and retention of fast APs in the ischemic zone would allow propagation through this area to be normal, thus minimizing the chances for the induction of arrhythmias. The effect of metabolic interference on shortening the AP after 30–120 min (due to enhanced kinetics for g_K turnon that terminates the AP) would also help to shut off I_{si} more quickly, thereby reducing the total Ca^{2+} influx per impulse and so helping to conserve ATP.

The AP in the ischemic region may be either a slow-channel AP or a depressed fast-channel AP. The depression of the rate of rise is caused by the partial depolarization of the cells due to K^+ accumulation in the interstitial space and perhaps to depression of electrogenic Na^+ pumping. (Progressive depolarization voltage inactivates a progressively larger fraction of the fast Na^+ channels due to closing of their inactivation [I] gates.) Many of the slow channels

also would be expected to be blocked because of the acidosis and lowered ATP level.

Blockade of the Slow Channels by Acetylcholine

The parasympathetic neurotransmitter, acetylcholine (ACh), exerts a negative inotropic effect on the heart, as well as a negative chronotropic effect by action on the SA nodal cells. Because of the positive treppe (staircase) phenomenon of cardiac muscle, the latter effect also produces a negative inotropic effect. ACh is well known to increase g_K, and thereby can hyperpolarize SA nodal cells (therefore depressing automaticity) and shorten the duration of the AP in atrial myocardial cells. This would also tend to suppress slow APs in atrial cells by increasing the overlapping outward K^+ current, and so diminishing the *net* inward (slow) current.

In ventricular myocardial cells, activation of the muscarinic receptor by ACh reverses the stimulation of the adenylate cyclase complex produced by beta-adrenergic agonists. Activation of the beta-adrenergic receptor activates the (stimulatory) regulatory component of the adenylate cyclase complex, whereas activation of the muscarinic receptor activates an inhibitory regulatory component of the enzyme (see fig. 8–21).

Josephson and Sperelakis [31] demonstrated, from voltage-clamp experiments on cultured chick ventricular cells, that ACh has a dual effect: it increases the outward K^+ current and depresses the inward slow current, I_{si} (figs. 8–17 to 8–19). Figure 8–17 illustrates a typical voltage-clamp experiment for measuring the intensity of inward I_{si} and outward I_K. A holding potential of -50 mV, as well as the addition of TTX in some cases, was used to inactivate the fast Na^+ channels. Progressively larger clamp steps between -30 mV and -10 mV increased I_{si} progressively; larger depolarizing clamp steps (e.g., to O mV and $+10$ mV) decreased I_{si} because of the diminished electrochemical driving force ($E_m - E_{si}$). The outward I_K increased with larger depolarizing clamp steps. These data are plotted as current–voltage curves in figure 8–18 (control curves). The peak inward I_{si} has a relatively broad peak (between about -15 mV and 0 mV), and the reversal potential for I_{si} is about $+20$ mV. Figure 8–18 also shows the dual effect of ACh to depress I_{si} and to potentiate the outward K^+ current.

Figure 8–19 illustrates control current–voltage curves from another experiment, and also illustrates the fact that verapamil greatly depresses I_{si}, with almost no effect on the outward I_K current, thus helping to identify the inward current as a slow inward Ca^{2+} current.

Blockade of Slow Channels by Drugs and Anesthetic Agents

The calcium-antagonistic drugs, such as verapamil, D-600, nifedipine, diltiazem, and bepridil, block the voltage-dependent slow channels (Ca^{2+} and Ca-Na types) found in myocardial cells, Purkinje fibers, nodal cells, and VSM cells. Some Ca antagonists, such as verapamil, D-600, and nifedipine (but not diltiazem, bepridil, and mesudipine), also block the slow Na^+ channels found in young (three-day-old) embryonic chick hearts [12, 35].

Figure 8–20 illustrates the effect of verapamil on blocking the slow APs in guinea pig papillary muscle and of nifedipine on blocking the isoproterenol-induced slow APs in guinea pig papillary muscle (A–D) and guinea pig Purkinje fibers (E–H) driven at a constant rate of 0.5 Hz. As indicated, nifedipine is more potent than verapamil in blocking the slow channels [32, 33]. The general order of potency of the calcium-antagonistic drugs in blocking the slow channels of various heart tissues is: nifedipine $>$ diltiazem $\geq$ verapamil $>$ bepridil [34].

By definition, to be a member of this class of compounds, a drug must block the slow channel by a direct action on the cell membrane channel itself (and not indirectly via metabolic depression or acidosis, for example), and this action must be relatively specific for the slow channel in contrast to the other types of voltage-dependent ion channels (e.g., fast Na^+ channel or delayed rectifier K^+ channel). Thus, this definition would distinguish Ca antagonists from local anesthetics or metabolic poisons, for example.

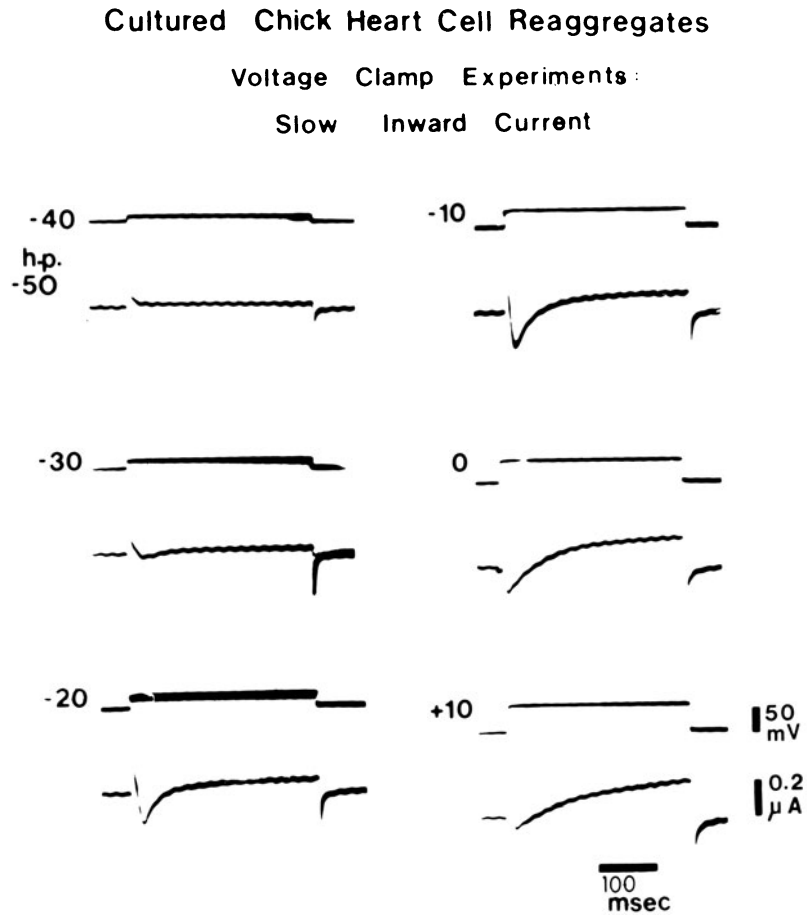

FIGURE 8–17. Membrane currents obtained during voltage clamp of a cultured chick heart cell reaggregate. TTX (10^{-6} *M*) and isoproterenol (10^{-6} *M*) were present in the superfusing solution. The holding potential was −50 mV. Therefore, the inward fast Na^+ current was prevented by block of the fast Na^+ channels with TTX and by their voltage inactivation. Depolarizing clamp steps of 300-ms duration were applied (at frequency of 0.3/s) to membrane potentials of −40, −30, −20, −10, 0, and +10 mV sequentially. A small inward slow current component (I_{si}) is visible at −30 mV, and increases to a maximum at −10 mV. Greater depolarizing clamps decrease I_{si} (due to a decreased electrochemical driving force [$E_m - E_{si}$]). The outward K^+ current (I_K) becomes progressively larger at the greater clamp steps. Capacity currents are not visible in some cases. From Josephson and Sperelakis [31].

Some Ca antagonists, such as bepridil, may exert, in addition, a second action, e.g., intracellularly to depress Ca^{2+} uptake into or release from the SR [36]. The evidence for a second effect of bepridil was the fact that this drug depressed cardiac contractile force more than could be accounted for by the depression of the inward slow Ca^{2+} current. Consistent with the possibility of a second intracellular effect, bepridil and verapamil were shown to enter the myocardial cells, the order of uptake being: bepridil > verapamil ≥ nitrendipine >> nifedipine > diltiazem [37, 38]. This order of uptakes followed the order of lipid solubilities [38]. In addition, those Ca antagonists that readily enter the cells have the possibility of exerting their effect on the slow channels from the inner surface of the cell membrane. For example, it was recently shown that a charged quaternary ammonium derivative of D-600 had

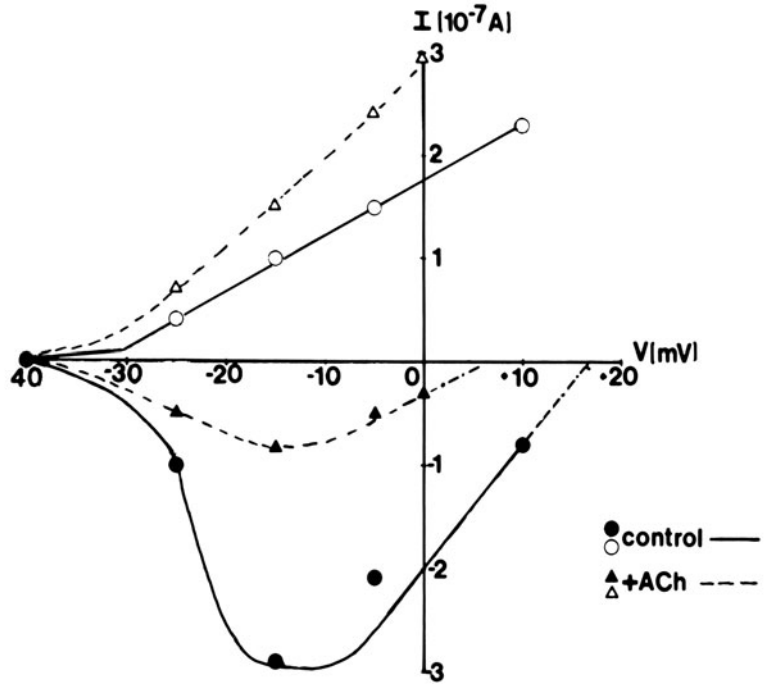

FIGURE 8–18. Effects of ACh on membrane currents in the presence of isoproterenol in a cultured chick heart (ventricular) cell reaggregate. Filled circles represent I_{si} obtained in the presence of TTX (10^{-6} *M*) and isoproterenol (10^{-6} *M*); outward currents (at 300 ms) are shown as unfilled circles. The triangles are currents recorded after 3-min exposure to ACh (10^{-6} *M*); outward currents are plotted as unfilled triangles, and the inward currents as filled triangles. These data demonstrate that ACh, not only increases the outward I_K, but also depresses the inward I_{si}. Modified from Josephson and Sperelakis [31].

no effect on the inward slow current of myocardial cells when added to the bathing solution, but did depress I_{si} when injected intracellularly [26].

Ca^{2+} binding to isolated sarcolemmal membranes (vesicles) was inhibited by verapamil and bepridil in a dose-dependent manner, verapamil being the more potent of the two, as it is in inhibition of slow APs [37]. Since Ca^{2+} binding to the outer mouth of the slow channel (as depicted in fig. 8–3) is probably the first step in ion permeation through the channel, Ca^{2+} displacement could be one possible mechanism for blockade of Ca^{2+} entry by verapamil and bepridil, although this would not readily account for the frequency dependency of the effect of these two drugs. On the other hand, the frequency-independent block of Ca^{2+} entry by Mn^{2+}, Co^{2+}, or La^{3+} ions could be by such a mechanism. Nifedipine and diltiazem did not inhibit Ca^{2+} binding [39]. Thus, there are great differences in properties of the calcium-antagonistic drugs, and they may block the slow channels by different molecular mechanisms, as might be predicted from their widely different chemical structures.

Apparent reversal of the block of the slow APs and contractions by the Ca antagonists by elevation of $[Ca]_o$ may result from either of two mechanisms: (a) competition between Ca^{2+} and drug for binding to the outer mouth of the channel, or (b) the increased electrochemical driving force for Ca^{2+} influx through the fraction of slow channels not blocked by the drug. The latter mechanism probably operates in all cases, whereas the former mechanism may be involved with some of the drugs, such as verapamil and bepridil.

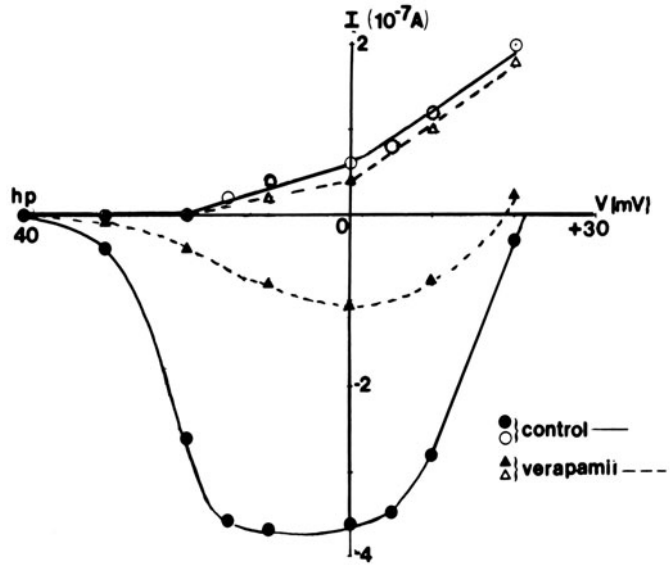

FIGURE 8–19. Effect of verapamil (10^{-6} *M*) on membrane currents recorded from a reaggregate cell culture. Solid circles are peak I_{si} recorded with TTX (10^{-6} *M*) and isoproterenol (10^{-6} *M*) present; open circles represent outward currents (at 300 ms). The triangles are values after 3-min exposure to verapamil (10^{-6} *M*); open triangles show outward currents and filled triangles the values for I_{si}. These data show that verapamil depresses I_{si} and has almost no effect on the outward I_K. From Josephson and Sperelakis [31].

The effect of most of the calcium-antagonistic drugs on depression of the slow APs and inward slow Ca^{2+} current (I_{si}) is frequency dependent; that is, the higher the frequency of stimulation, the greater the blocking effect on the slow channels. For example, a dose of drug that completely blocks the slow APs at a drive rate of 1 Hz may exhibit no effect at 0.1 Hz. This effect is prominent in the action of all this class of drugs, although nifedipine seems to have a lesser frequency dependence than the other drugs. In contrast, Ca^{2+}-entry blockers, such as Mn^{2+}, Co^{2+}, and La^{3+}, do not exhibit a frequency dependency; that is, the effect of Mn^{2+}, for example, is present even to the first stimulation after equilibration of the Mn^{2+} under resting conditions.

This frequency dependency of effect suggests that the calcium-antagonistic drugs do not act as simple plugs for the Ca^{2+} slow channels, as perhaps Mn^{2+} or La^{3+} might act. Rather, this property suggests that the drug might act to slow the recovery process of the slow channel from the inactive state back to the resting state (see fig. 8–3). If so, then a slow drive rate or a long quiescent period (e.g., 20–60 s) would allow complete recovery of the drugged slow channel before the next excitation occurred. To exert such an effect on the gate recovery kinetics, the drugs could bind anywhere on the channel protein. An alternative possibility is that the drug binds to the channel only in the active state or inactive state (membrane also depolarized) to block it, and then dissociates before conversion of the channel to the resting state. There is some evidence that binding of the drug is voltage dependent, depolarization favoring binding and hyperpolarization favoring unbinding.

Another possibility to be considered is that any drug which affected the phosphorylation of the slow channels by some direct means would also effectively block the slow channels selectively, and could account for the drug's frequency dependence. Consistent with this possibility, it was recently found that several of the calcium-antagonistic drugs, such as verapamil, inhibited the cyclic-AMP-dependent phosphorylation in vitro of three membrane

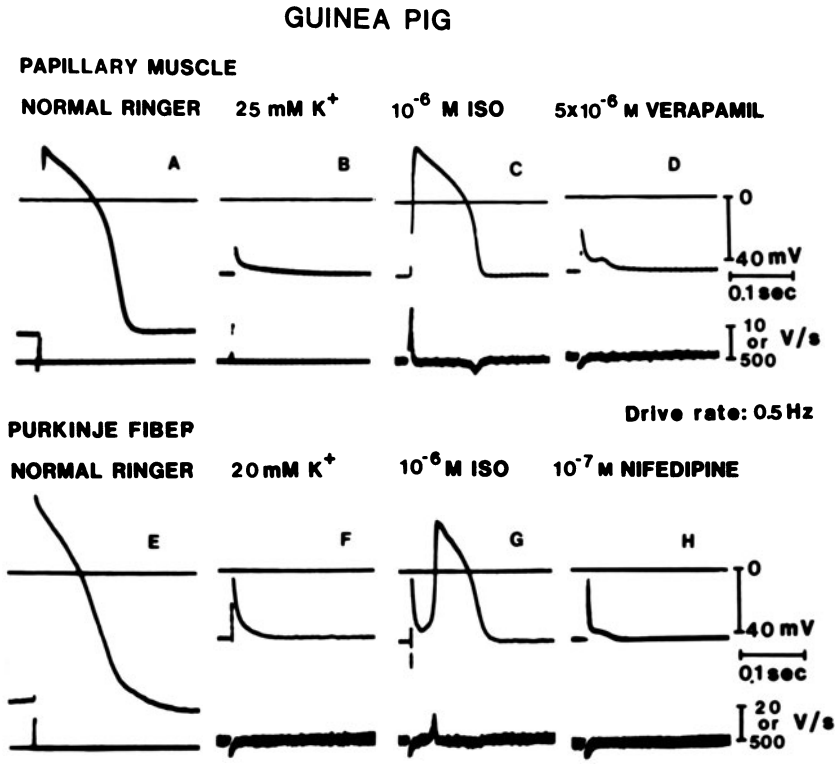

FIGURE 8–20. Induction of the slow action potentials (APs) and their block by calcium-antagonistic drugs. *(A–D)* Papillary muscle (guinea pig). *(E–H)* Purkinje fiber (guinea pig). *(A* and *E)* Normal fast APs. *(B* and *F)* Elevation of $[K]_o$ to 25 m*M* *(B)* or 20 m*M* *(F)* depolarized to about -45 mV and blocked excitability (shock artifacts only visible). *(C* and *G)* Addition of isoproterenol (10^{-6} *M*) rapidly induced slowly rising APs, and slow APs. *(D* and *H)* Addition of verapamil (5×10^{-6} *M*) *(D)* or nifedipine (10^{-7} *M*) *(H)* rapidly depressed and blocked the slow APs. The driving rate for the slow APs was 0.5 Hz. The upper straight line in each panel is the zero potential level, and the lower trace is d*V*/d*t*, the peak excursion of which gives $\dot{V}_{max}$. The voltage and time calibrations are the same throughout; the d*V*/d*t* calibration bars represent 500 V/s for *A* and *E*, and 10 V/s for *B–D* or 20 V/s for *F–H*. Modified from Molyvdas and Sperelakis [32, 33].

proteins (Carty, Sperelakis, and Villar-Palasi, unpublished observations).

A number of other chemicals and drugs also block the myocardial slow channels, including local anesthetics [40] and volatile general anesthetics [41]. The local anesthetics, lidocaine and procainamide, however, blocked the slow channels nonspecifically; that is, the dose–response curve for the slow APs were identical to that for the fast APs. In contrast, depressed fast APs, produced in 10 m*M* $[K]_o$, were about tenfold more sensitive to lidocaine [42]. Halothane and enflurane are more selective in inhibiting the slow channels of the heart than the fast Na^+ channels [43].

Excitation and Conduction of the Slow Action Potentials

The slow APs have a stimulation threshold nearly tenfold higher than that for the fast APs, i.e., slow APs have a lower excitability. The threshold potential (V_{th}) for the slow APs is at an E_m of about -35 mV, whereas that for the fast APs is about -55 mV, i.e., the critical depolarization required to excite is larger for the slow APs (assuming an unchanged resting potential of -80 mV). Chronaxie of the slow AP (0.9 ms) is about tenfold higher than that for the fast AP [43].

The slow APs propagate at a velocity of

about 4–10 cm/s [44]. In a simple cable, conduction velocity (θ) should vary directly with the $\sqrt{\dot{V}_{max}}$ [45]; that is, the faster the rate of rise of the AP, the faster the propagation. (There are exceptions to this in cardiac muscle when comparing transverse propagation versus longitudinal propagation, because the tissue is not a simple cable.) Thus, if the fast AP in cardiac muscle propagates at 0.40 m/s for a $\dot{V}_{max}$ of 150 V/s, then if $\dot{V}_{max}$ is reduced to 15 V/s for the slow AP, θ should be reduced by $\sqrt{10}$ times or to 0.127 m/s. However, propagation velocity is decreased more than the predicted amount in both myocardium (12.7 cm/s predicted vs 4–10 cm/s actual) and Purkinje fibers (0.2 m/s predicted vs <0.1 cm/s actual) [46]. The latter authors attributed the discrepancy to the slow AP, seeing a higher effective membrane capacitance (C_m) i.e., a higher capacitive reactance (X_o). It is not known to what degree decremental conduction may occur, i.e., decreasing propagation velocity and response amplitude as a function of the distance along the muscle.

Some studies have focused on the ability of propagating fast APs to trigger slow APs. In rabbit left atrial strips (composed of homogenous parallel bundles of fibers) compartmentalized into three functional segments, the left (test) segment being exposed to 12.7 m*M* $[K]_o$ and 1 m*M* $[Ba]_o$ to depolarize sufficiently to block the fast APs, Masuda et al. [44] found that high-frequency (0.63–2.5 Hz) stimulation caused 2:1 block due to fatigue of the slow AP (slowness of recovery of excitability). However, low-frequency (0.13–0.4 Hz) stimulation also produced complete block. Therefore, there was a limited frequency range in which a normal fast AP could stimulate slow APs at a sustained 1:1 ratio. The low-frequency block was attributed to the observed reduced amplitude and duration of the atrial fast AP, since ACh, which shortens the plateau of the atrial AP, also blocked the development of the slow AP in the test compartment when it was added to the middle compartment. Hence, the amplitude and duration and frequency of the fast APs determined whether they served as effective stimuli for the slow APs in the depolarized region.

Cukierman and Paes de Carvalho [43] studied the properties of "membrane" (nonpropagated) slow APs induced (stimulated with a suction electrode) in short (2–3 mm) atrial trabeculae from rabbit left atrium by 1 m*M* $[Ba]_0$ and 10 m*M* $[K]_0$. The resting potential in the high K^+-Ba^{2+} solution was −55 mV, the amplitude of the slow APs was 60 mV, and the APD_{50} was 84 ms. The slow AP upstroke was always initiated from a small subthreshold-depolarizing step. The slow AP was all-or-none. The slow AP fatigued at high pacing rates (>1 Hz), and a fully developed slow AP could only be obtained within a certain frequency range, as found in the long strip preparation of Masuda et al. [44].

Possible Role of Slow Action Potentials in Arrhythmias

Slow APs have been implicated in the genesis of arrhythmias [43, 47–49]. Propagating fast APs can trigger slow APs in depolarized regions [46]. Slow conduction in a pathway allows circus movement of excitation around that pathway, and may lead to reentrant type of arrhythmias. There is a requirement of one-way conduction through the depressed area, and the length of the reentry loop is critical, depending on velocity. In an ischemic or infarcted zone, and the surrounding border zone, there is a depressed area with slowed conduction. Partial depolarization of the cells in this area occurs because of a high $[K]_o$ due to the hypoxia/ischemia and consequent impaired metabolism. In addition, there is norepinephrine (NE) release from the sympathetic nerve terminals.

NE release should elevate cyclic AMP and increase the number of available slow channels, tending to increase I_{si} in the cells in the ischemic zone. However, the hypoxia/ischemia should tend to depress I_{si} because of the accompanying lowered ATP level and the metabolic dependence of the slow-channel functioning. Therefore, the ischemic AP can be either (a) a depressed fast AP (i.e., an AP whose inward current is carried through fewer fast Na^+ channels) due to the partial depolarization (and the h_∞ vs E_m relationship), or (b) a pure slow AP (i.e., an AP whose inward current is carried

only through slow channels) if the K^+ depolarization is great enough such that complete voltage inactivation of all (or most) fast Na^+ channels has occurred (at about -55 mV). There is some evidence for both possibilities [47].

Evidence that the ischemic AP is a depressed fast AP includes the fact that TTX blocks the AP whereas verapamil does not [50,51]. Additional points supporting the view that the ischemic AP is a depressed fast AP and not a slow AP are: (a) the metabolic dependence of the functioning of the slow channels, and (b) the dyskinesis or akinesis of the ischemic area. It is likely that the degree of K^+ accumulation, and hence depolarization, is one factor determining the nature of the AP in the ischemic zone; other factors may be the amount of the catecholamines released that persists in the interstitial fluid and the degree of ATP depletion and acidosis in the afflicted cells.

Although local anesthetics depress and block slow APs at the same concentrations that depress the normal fast APs [40], the depressed fast APs are nearly tenfold more sensitive to these drugs [42]. Thus, lidocaine and procainamide and related antiarrhythmic agents can relatively selectively suppress depressed fast APs in ischemic/infarcted regions, and thereby suppress dysrhythmias.

The APs in the ischemic area have slow upstroke velocities ($\dot{V}_{max}$), are conducted slowly (ca. 0.05 m/s), and about 35% of the APs have notched upstrokes or two peaks [48]. There are delays and possibly decremental conduction. The depressed area exhibits one-way block, frequency-dependent block, and the Wenckebach phenomenon. There is a low safety factor for conduction, causing the impulse to be prone to block at impediments. Structural inhomogeneities/asymmetries and pathologic changes can act as impediments to conduction [48]. In addition, premature excitation can unmask asymmetries, and so a premature impulse may travel more readily in one direction than the other. Such unidirectional block of a premature impulse sets up one condition necessary for circus movement, namely, one-way conduction. Increases in resistance of the cell-to-cell junctions (or in junctional cleft width) during hypoxia/ischemia were suggested as causes of conduction impediment [48].

Effect of $[Ca]_i$ on Membrane Channels

$[Ca]_i$ has profound effects on membrane electrical properties (fig. 8–21). A depolarizing afterpotential following a conventional hyperpolarizing afterpotential was first described in cultured embryonic chick heart cells by Lehmkuhl and Sperelakis [52], who turned trains of spontaneous APs on and off by applying hyperpolarizing current pulses of various intensities. They thereby demonstrated that each AP in a train was triggered by the preceding AP by means of the delayed depolarizing afterpotential. Ferrier and Moe [53], subsequently described this phenomenon in mammalian heart, and called it a delayed afterdepolarization (DAD). They showed that cardiac glycosides and elevated $[Ca]_0$ potentiated the DAD, that calcium-antagonistic drugs depress and abolish the DAD, and pointed out its possible importance in arrhythmogenesis.

Kass et al. [54] showed that the DAD is not directly produced by an inward Ca^{2+} current, but rather indirectly by release of Ca^{2+} from the SR, which, in turn, produces an increase in a nonspecific leakage-type conductance for a net inward depolarizing current, the transient inward current (I_{Ti}). The reversal potential (E_{rev}) for I_{Ti} is about -5 mV, and is sensitive to $[Na]_0$ but not to $[Ca]_0$. The increase in $[Ca]_i$ opens a nonspecific voltage-independent postsynaptic type of ion channel that allows both Na^+ and K^+ to pass through. This type of channel would be somewhat analogous to the Ca^{2+}-activated K^+ channel [$g_{K(Ca)}$] [26].

I_{Ti} and concomitant aftercontractions are enhanced by digitalis, K^+-free solution, catecholamine, and elevated $[Ca]_0$. The effects of digitalis and K-free solution can be explained by inhibition of the Na-K pump. For example, ouabain potentiates I_{Ti} by inhibiting the Na-K pump, thereby increasing $[Na]_i$, which increases $[Ca]_i$ via the Ca-Na exchange system. The elevated $[Ca]_i$, in turn, triggers Ca^{2+} release from the SR by the Ca-trigger-Ca mechanism of Fabiato and Fabiato [53]. An oscillatory release of Ca^{2+} can account for the

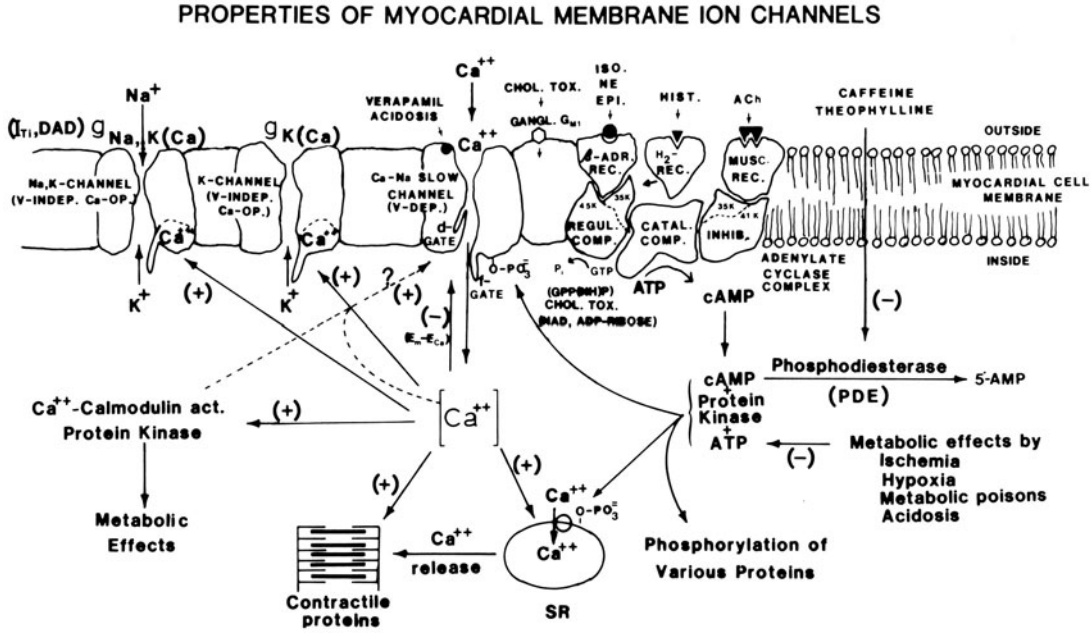

FIGURE 8–21. Diagrammatic summary of some of the properties of the ion channels in myocardial cell membrane. Included are the mechanism of action of some positive inotropic agents, such as beta-adrenergic agonists, histaminic H_2 agonists, and methylxanthines (phosphodiesterase inhibitors). The beta agonists and H_2 agonists act on the regulatory component (guanine nucleotide binding protein) of the adenylate cyclase complex to stimulate cyclic-AMP production. The voltage-dependent myocardial slow (Ca-Na) channels are dependent on cyclic AMP and on metabolism, presumably because a protein constituent (or regulatory component) of the slow channel must be phosphorylated in order for it to be in a form that is available for voltage activation. The sites of action of GPP(NH)P and cholera toxin on the regulatory component of adenylate cyclase are shown. Also depicted are the facts that the slow channels are selectively blocked by acidosis and by calcium-antagonistic drugs ("slow-channel blockers"). Also schematized are two types of ion channels that are voltage independent, but activated by internal Ca^{2+} ion: a K^+-selective channel ($g_{K(Ca)}$) and a nonselective Na-K channel ($g_{Na,\ K(Ca)}$). From Sperelakis [56].

damped oscillations in I_{Ti} (and in DADs and aftercontractions) sometimes observed. I_{Ti} is abolished by pretreatment with caffeine (10 m*M*) to deplete the SR stores of Ca^{2+}. The progressive potentiation of the DAD or I_{Ti} during a train of impulses can be explained by progressive loading of the SR with Ca^{2+}.

Thus, elevation in $[Ca]_i$ activates at least two different types of ion channels: (a) the nonspecific channel conductance ($g_{Na,\ K(Ca)}$) that underlies I_{Ti} and DAD, and which may be important in genesis of dysrhythmias and even in cardiac plateau formation; and (b) the Ca^{2+}-activated (Sr^{2+} and Ba^{2+} can substitute for Ca^{2+}) K^+ channel conductance ($g_{K(Ca)}$), which may be important in shortening of the cardiac AP. In addition, Marban and Tsien [49] provided evidence that elevation of $[Ca]_i$ (but not Sr^{2+}) increases the voltage-dependent I_{si} in Purkinje fibers, and that this might mediate some of the effects of cardiac glycosides. The mechanism for this effect of $[Ca]_i$ could involve the Ca-calmodulin-activated protein kinase and phosphorylation of the slow channels. This positive feedback effect of $[Ca]_i$ may not explode because higher $[Ca]_i$ could inhibit Ca^{2+} entry (negative feedback), either by somehow blocking the channels and/or decreasing the electrochemical gradient for Ca^{2+} entry.

Summary and Conclusions

Ca^{2+} ion influx through voltage-dependent and time-dependent slow channels during the cardiac action potential is the key step in excitation–contraction coupling and determines the

force of contraction of the heart. The model for slow channels is similar to that for fast Na^+ channels, except that the slow channels (a) have gates that open and close more slowly, (b) the gates operate over a different voltage range (less negative activation and inactivation voltages), and (c) are blocked by different agents (e.g., by calcium-antagonistic drugs such as verapamil and tetrodotoxin [TTX]). In addition, the slow channels have some special properties (in comparison with fast Na^+ channels and various types of K^+ channels) that enable the myocardial cell to exercise control over its Ca^{2+} influx in response to intrinsic and extrinsic factors and hormones/neurotransmitters. These peculiar properties include: (a) energy dependence, (b) pH dependence, and (c) cyclic-AMP dependence.

The sympathetic neurotransmitter, norepinephrine, catecholamine hormones, angiotensin II, histamine, and methylxanthines rapidly induce slow Ca-Na channels in myocardial cells. Following blockade of the fast Na^+ channels with TTX or by voltage inactivating them in 25 m*M* $[K]_o$, these agents rapidly allow the production of slowly rising APs by increasing the number of slow channels available for voltage activation and/or their mean open time. Concomitantly, these compounds rapidly elevate intracellular cyclic-AMP levels, suggesting that cyclic AMP is somehow related to the functioning of the slow channels. Exogenous cyclic AMP produces the same effect, but much more slowly.

Exposure of intact myocardial cells to the GTP analogue, GPP(NH)P, also induces slow APs within 10–20 min. This effect is presumably by activation of the adenylate cyclase complex. Intracellular injection of cyclic AMP, GPP(NH)P, and cholera toxin (also an activator of the adenylate cyclase complex) rapidly induces or potentiates ongoing slow APs in the injected cell. Thus, the time delay between exposure to the agent and an observed effect is greatly reduced by intracellular application of the agent. These results clearly indicate the key role played by cyclic AMP in regulation of the Ca^{2+} slow channels and hence Ca^{2+} influx and force of contraction.

The induced slow channels are very sensitive to blockade by metabolic poisons, hypoxia, and ischemia (fig. 8–21). The slow AP is blocked at a time when the rate of rise and duration of the normal fast AP is essentially unaffected. However, the contraction accompanying the fast AP is depressed or abolished, i.e., contraction is uncoupled from excitation, as expected from slow-channel blockade. The ATP level is greatly reduced by the metabolic poisons, e.g., by valinomycin and DNP, at the same time that the slow channels are blocked [55]. Therefore, the slow channels are metabolically dependent, presumably on ATP, whereas the fast Na^+ channels are not. A second, but much slower, effect of metabolism is to increase the kinetics of g_K turnon, perhaps mediated by an increase in steady-state $[Ca]_i$.

The dependence of the myocardial slow channels on cyclic-AMP level and on metabolism suggests that phosphorylation of a membrane protein constituent of the slow channel, or of an associated regulatory protein, by a cyclic-AMP-dependent protein kinase and ATP, may make it available for voltage activation (see Sperelakis [56, 57]). The dephosphorylated slow channel would be electrically silent, i.e., nonfunctional. Phosphorylation may produce a conformational change that allows the gates of the slow channel to operate in response to membrane potential.

The slow channels are also selectively sensitive to blockade by acid pH; that is, at pH 6.8–6.1, the slow AP is depressed or blocked. In contrast, the fast AP is not much affected, but excitation–contraction uncoupling occurs. Part of the rapid effect of ischemia in blocking the slow channels appears to be mediated by the concomitant acidosis.

By these special properties of the slow channels, Ca^{2+} influx into the myocardial cell can be controlled by extrinsic factors, such as by autonomic nerve stimulation or circulating hormones, and by intrinsic factors, such as cellular pH or ATP level. During transient regional ischemia, the selective blockade of the slow channels, which results in depression of the contraction and work of the afflicted cells, might serve to protect the cells against irreversible damage by helping to conserve their ATP content.

The parasympathetic neurotransmitter, ACh, depresses the inward slow current (I_{si})

stimulated by beta-adrenergic agonists, and potentiates the outward K^+ current.

The slow channels have a threshold potential at about −35 mV (compared to about −55 mV for the fast Na^+ channels). The $\dot{V}_{max}$ of the slow AP is about 10 V/s, and the propagation velocity (0.04–0.10 m/s) is about one-sixth to one-third that of the fast AP. The slow APs fatigue at frequencies above 1 Hz. Fast APs can trigger slow APs in K^+-depolarized regions. Slow APs have been implicated in the genesis of reentrant types of arrhythmias in ischemic zones, but there is also evidence that some ischemic APs are depressed fast APs rather than true slow APs; regardless, however, propagation velocity will be slow and there will be conduction disturbances that can predispose to dysrhythmias. Although local anesthetics depress and block slow APs and fast APs at the same concentrations, depressed fast APs are more sensitive to these drugs.

Delayed depolarizing afterpotentials have also been implicated in genesis of arrhythmias of the triggered automaticity type. These afterpotentials are due to an increase in $[Ca]_i$ opening up a voltage-independent nonspecific postsynaptic type of ion channel having an equilibrium (reversal) potential at about −5 mV. Any condition, such as hypoxia/ischemia or digitalis or catecholamines, that elevates $[Ca]_i$ potentiates the depolarizing afterpotential, and hence the possible triggering of AP trains from these ectopic foci and producing dysrhythmias. Calcium-antagonistic drugs, by their action to block the slow channels and thereby suppress Ca^{2+} influx and loading of the SR, suppress these afterpotentials and prevent such arrhythmogenesis.

References

1. Schneider JA, Sperelakis N: The demonstration of energy dependence of the isoproterenol-induced transcellular Ca^{++} current in isolated perfused guinea pig hearts: an explanation for mechanical failure in ischemic myocardium. J Surg Res 16:389–403, 1974.
2. Sperelakis N: Electrophysiology of vascular smooth muscle of coronary artery. In: Kalsner S (ed) The coronary artery. Croom Helm, 1982, pp 118–167.
3. Pappano AJ: Calcium-dependent action potentials produced by catecholamines in guinea pig atrial muscle fibers depolarized by potassium. Circ Res 27:379–390, 1970.
4. Sperelakis N: Changes in membrane electrical properties during development of the heart. In: Zipes DP, Bailey JC, Elharrar V (eds) The slow inward current and cardiac arrhythmias. The Hague: Martinus Nijhoff, 1980, pp 221–262.
5. Lee KS, Tsien RW: Reversal of current through calcium channels in dialysed single heart cells. Nature 297:498–501, 1982.
6. Fabiato A, Fabiato F: Calcium and cardiac excitation–contraction coupling. Annu Rev Physiol 41:473–484, 1979.
7. Josephson I, Renaud JF, Vogel S, McLean M, Sperelakis N: Mechanism of the histamine-induced positive inotropic action in cardiac muscle. Eur J Pharmacol 35:393–398, 1976.
8. Shigenobu K, Sperelakis N: Ca^{++} current channels induced by catecholamines in chick embryonic hearts whose fast Na^+ channels are blocked by tetrodotoxin or elevated K^+. Circ Res 31:932–952, 1972.
9. Freer RJ, Pappano AJ, Peach MJ, Bing KT, McLean MJ, Vogel SM, Sperelakis N Mechanism of the positive inotropic effect of angiotensin II on isolated cardiac muscle. Circ Res 39:178–183, 1976.
10. Reuter H, Stevens CF, Tsien RW, Yellen G: Properties of single calcium channels in cardiac cell culture. Nature 297:501–504, 1982.
11. Schneider JA, Sperelakis N: Valinomycin blockade of slow channels in guinea pig hearts perfused with elevated K^+ and isoproterenol. Eur J Pharmacol 27:349–354, 1974.
12. Shigenobu K, Schneider JA, Sperelakis N: Verapamil blockade of slow Na^+ and Ca^{++} responses in myocardial cells. J Pharmcol Exp Ther 190:280–288, 1974.
13. Reuter H, Scholz H: The regulation of the calcium conductance of cardiac muscle by adrenaline. J Physiol (Lond) 264:49–62, 1977.
14. Sperelakis N, Schneider JA: A metabolic control mechanism for calcium ion influx that may protect the ventricular myocardial cell. Am J Cardiol 37:1079–1085, 1976.
15. Watanabe AM, Besch HR Jr: Cyclic adenosine monophosphate modulation of slow calcium influx channels in guinea pig hearts. Circ Res 35:316–324, 1974.
16. Tsien RW, Giles W, Greengard P: Cyclic AMP mediates the effects of adrenaline on cardiac Purkinje fibers. Nature [New Biol] 240:181–183, 1972.
17. Josephson I, Sperelakis N: 5'-Guanylimidodiphosphate stimulation of slow Ca^{++} current in myocardial cells. J Mol Cell Cardiol 10:1157–1166, 1978.
18. Metzer H, Lindner E: The positive inotropic-acting forskolin, a potent adenylate cyclase activator. Arzneim Forsch 31:1248–1250, 1981.
19. Vogel S, Sperelakis N: Induction of slow action potentials by microiontophoresis of cyclic AMP into heart cells. J Mol Cell Cardiol 13:51–64, 1981.
20. Li T, Sperelakis N: Stimulation of slow action poten-

tials in guinea-pig papillary muscle cells by intracellular injection of cAMP, Gpp(NH)p, and cholera toxin. Circ Res 52:111–117, 1983.
21. Vogel S, Sperelakis N: Valinomycin blockade of myocardial slow channels is reversed by high glucose. Am J Physiol 235:H46–H51, 1978.
22. Wahler GM, Sperelakis N: Similar metabolic dependence of stimulated and unstimulated myocardial slow channels. Can J Physiol Pharmacol, 1983 (submitted for publication).
23. Rinaldi ML, Capony J-P, Demaille JG: The cyclic AMP-dependent modulation of cardiac sarcolemmal slow calcium channels. J Mol Cell Cardiol 14:279–289, 1982.
24. Vogel S, Sperelakis N, Josephson I, Brooker G: Fluoride stimulation of slow Ca^{++} current in cardiac muscle. J Mol Cell Cardiol 9:461–475, 1977.
25. Hescheler J, Pelzer D, Trube G, Trautwein W: Does the organic calcium channel blocker D-600 act from inside or outside on the cardiac cell membrane? Pflugers Arch 393:287–291, 1982.
26. Isenberg G: Cardiac Purkinje fibers: $[Ca^{2+}]_i$ controls the potassium permeability via the conductance components g_{k_1} and g_{k_2}. Pflugers Arch 371:77–85, 1977.
27. Bkaily G, Sperelakis N: Injection of protein kinase inhibitor into cultured heart cells blocks the calcium slow channels. Science, 1983 (submitted for publication).
28. Chesnais JM, Coraboeuf E, Sauvain MP, Vassas JM: Sensitivity to H, Li and Mg ions of the slow inward sodium current in frog atrial fibres. J Mol Cell Cardiol 7:627–642, 1975.
29. Vogel S, Sperelakis N: Blockade of myocardial slow inward current at low pH. Am J Physiol. 233: C99–C103, 1977.
30. Belardinelli L, Vogel SM, Sperelakis N, Rubio R, Berne RM: Restoration of inward slow current in hypoxic heart muscle by alkaline pH. J Mol Cell Cardiol 11:877–892, 1979.
31. Josephson I, Sperelakis N: On the ionic mechanism underlying adrenergic–cholinergic antagonism in ventricular muscle. J Gen Physiol 79:69–86, 1982.
32. Molyvdas P-A, Sperelakis N: Comparison of the effects of several calcium antagonistic drugs (slow-channel blockers) on the electrical and mechanical activities of guinea pig papillary muscle. J Cardiovasc Pharmacol 5:162–169, 1983.
33. Molyvdas P-A, Sperelakis N: Comparison of the effects of several calcium antagonistic drugs on the electrical activity of guinea pig Purkinje fibers. Eur J Pharmacol 88:205–214, 1983.
34. Li T, Sperelakis N: Calcium antagonist blockade of slow action potentials in cultured chick heart cells. Can J Physiol Pharmacol, 1983 (in press).
35. Kojima M, Sperelakis N: Calcium antagonistic drugs differ in blockade of slow Na^+ channels in young embryonic chick hearts. Eur J Pharmacol, 1983 (submitted for publication).
36. Vogel S, Crampton R, Sperelakis N: Blockade of myocardial slow channels by Bepridil (CERM-1978). J Pharmacol Exp Ther 210:378–385, 1979.
37. Pang DC, Sperelakis N: Nifedipine, diltiazem, verapamil and bepridil uptakes into cardiac and smooth muscles. Eur J Pharmacol 87:199–207, 1983.
38. Pang DC, Sperelakis N: Uptakes of calcium antagonists into mucles as related to their lipid solubilities. Biochem Pharmacol, 1983 (in press).
39. Pang DC, Sperelakis N: Differential actions of calcium antagonists on calcium binding to cardiac sarcolemma. Eur J Pharmacol 81:403–409, 1982.
40. Josephson I,, Sperelakis N: Local anesthetic blockade of Ca^{2+}-mediated action potentials in cardiac muscle. Eur J Pharmacol 40:201–208, 1976.
41. Lynch C, Vogel S, Sperelakis N: Halothane depression of myocardial slow action potentials. Anesthesiology 55:360–368, 1976.
42. Sperelakis N, Belardinelli L, Vogel SM: Electrophysiological aspects during myocardial ischemia. In: Hayase S, Murao S (eds) Proceedings of 8th world congress of cardiology. Amsterdam: Excerpta Medica, 1979, pp 229–236.
43. Cukierman S, Paes de Carvalho A: Slow response excitation: dependence on rate and rhythm. In: Paes de Carvalho A, Hoffman BF, Lieberman M (eds) Normal and abnormal conduction in the heart. Mt Kisco NY: Futura, 1982, pp 413–428.
44. Masuda MO, Paula-Carvalho M, Paes de Carvalho A: Excitability and propagation of slow responses in rabbit atrium partially depolarized by added K^+ and Ba^{2+}. In: Paes de Carvalho A, Hoffman BJ, Lieberman M (eds) Normal and abnormal conduction in the heart. Mt Kisco NY: Futura, 1982, pp 397–412.
45. Sperelakis, N, Mayer G, Macdonald R: Velocity of propagation in vertebrate cardiac muscles as functions of tonicity and $[K^+]_o$. Am J Physiol 219:952–963, 1970.
46. Dodge FA, Cranefield PF: Nonuniform conduction in cardiac Purkinje fibers. In: Paes de Carvelho A, Hoffman BF, Lieberman M (eds) Normal and abnormal conduction in the heart. Mt Kisco NY: Futura Publishing Company, p 379–396.
47. Cranefield PF: The conduction of the cardiac impulse. Mt Kisco NY, 1975.
48. Cranefield PF, Dodge FA: Slow conduction in the heart. In: Zipes DP, Bailey JC, Elharrar V (eds) The slow inward current and cardiac arrhythmias. The Hague: Martinus Nijhoff, 1980, pp 149–171.
49. Marban E, Tsien RW: Enhancement of calcium current during digitalis inotropy in mammalian heart: positive feed-back regulation by intracellular calcium? J Physiol 329:589–614, 1982.
50. Lazzara R, Scherlag B: Role of the slow current in the generation of arrhythmias in ischemic myocardium. In: Zipes DP, Bailey JC, Elharrar V (eds) The slow inward current and cardiac arrhythmias. The Hague: Martinus Nijhoff, 1980, pp 399–416.
51. Zipes DP, Rinkenberger RL, Heger JJ, Prystowsky EN: The role of the slow inward current in the genesis and maintenance of supraventricular tachyar-

rhythmias in man. In: Zipes DP, Bailey JC, Elharrar V (eds) The slow inward current and cardiac arrhythmias. The Hague: Martinus Nijhoff, 1980, 481–506.

52. Lehmkuhl D, Sperelakis N: Electrical activity of cultured heart cells. In: Tanz RD, Kavaler F, Roberts J (eds) Factors influencing myocardial contractility. New York: Academic, 1967, pp 245–278.
53. Ferrier GR, Moe GK: Effect of calcium on acetylstrophanthidin-induced transient depolarizations in canine Purkinje tissue. Circ Res 33:508–515, 1973.
54. Kass RS, Tsien RS, Weingart R: Ionic basis of transient inward current induced by strophanthidin in cardiac Purkinje fibres. J Physiol (Lond) 281:209–226, 1978.
55. Schneider JA, Sperelakis N: Slow Ca^{++} and Na^{+} responses induced by isoproterenol and methylxanthines in isolated perfused guinea pig hearts exposed to elevated K^{+}. J Mol Cell Cardiol 7:249–273, 1975.
56. Sperelakis N: Properties of calcium-dependent slow action potentials, and their possible role in arrhythmias. In: Opie LH, Krebs R (eds) Calcium antagonists and cardiovascular disease. New York: Raven, 1983.
57. Sperelakis N: Cyclic AMP and phosphorylation in regulation of Ca^{++} influx into myocardial cells, and blockade by calcium antagonistic drugs. Am Heart J, 1983.
58. Sperelakis N: Origin of the cardiac resting potential. In: Berne RM, Sperelakis N (eds) Handbook of physiology, the cardiovascular system, vol 1: the heart. Bethesda MD: American Physiological Society, 1979, pp 187–267.

9. EXCITATION–CONTRACTION COUPLING

Relationship of the Slow Inward Current to Contraction

Terence F. McDonald

Introduction

Although transient increases in Ca^{2+} concentration near the myofilaments underlie phasic contractile events, the source of this Ca^{2+} is not the same for all muscle cells. In skeletal muscle, the activator Ca^{2+} comes nearly exclusively from the cisternae of the sarcoplasmic reticulum (SR) whereas in the frog heart it appears to come from extracellular locations. Mammalian cardiac muscle lies between these two extremes in that contraction seems to be mainly dependent on Ca^{2+} released from the SR, but there is also a requirement for Ca^{2+} influx across the sarcolemma. This flux of Ca^{2+} occurs as part of the slow inward current (I_{si}) passing through Ca^{2+}-selective channels. Since these channels open at potentials positive to -50 mV, I_{si} flows during the plateau of the action potential and is therefore well placed to participate in the excitation–contraction coupling process. This chapter examines the role of I_{si}, with particular emphasis being given to voltage-clamp experiments on mammalian ventricular muscle.

The first section below contains brief descriptions of I_{si}, intracellular Ca^{2+} stores, and Ca^{2+} release by the SR. The subsequent sections highlight the key evidence in favor of I_{si} fulfilling at least three functions in the excitation–contraction process: (a) as a trigger for the release of activator Ca^{2+} from the internal SR stores, (b) as a modulator of the amount of Ca^{2+} released, and (c) as a source for the replenishment of the Ca^{2+} stores in the SR.

Needless to say, there are many important aspects of excitation–contraction coupling that cannot be covered here. Na^{+}-Ca^{2+} exchange fits into this category and, for a discussion of this topic, the reader is referred to recent reviews [1, 2] as well as to other chapters in this book. In addition, one should consult earlier reviews on excitation–contraction coupling [e.g., 3–7]; these offer a broad outlook on the subject and, in some cases, a different point of view than that expressed here.

Brief Overview of I_{si}, Internal Ca^{2+} Stores, and Ca^{2+} Release from the SR

I_{si} is thought to flow through voltage- and time-dependent Ca^{2+} channels in a manner analogous to Na^{+} flow through Na^{+} channels. Thus, a useful approach in the study of I_{si} has been the adoption of a Hodgkin–Huxley type formulation to describe the current [3]:

$$I_{si} = g_{si} (E - E_{si})$$

where g_{si} is the channel conductance, and $(E -$

I thank Lea Delbridge for assistance, and the Medical Research Council and Nova Scotia Heart Foundation for assistance.

N. Sperelakis (ed.), PHYSIOLOGY AND PATHOPHYSIOLOGY OF THE HEART.

Martinus Nijhoff Publishing, Boston/The Hague/ Dordrecht/Lancaster.

E_{si}) is the driving force for I_{si}. The time course of g_{si} is given by:

$$g_{si}(t) = \overline{g_{si}} \cdot d(t) \cdot f(t)$$

where $\overline{g_{si}}$ is the maximal conductance, d is an activation variable, and f an inactivation variable. The dimensionless variables d and f have steady-state values, d_∞ and f_∞, between 0 and 1. The steady-state values depend on voltage and are reached at a rate determined by the voltage-dependent time constants, τ_d and τ_f.

When step depolarizations are applied for the resting potential or negative holding potential, the threshold for I_{si} is between -50 and -35 mV. Depolarizations to more positive potentials trigger I_{si} whose peak amplitude increases sharply between threshold and 0 mV, and then declines to a small value at about $+50$ mV. The zero current potential, or reversal potential (E_{si}), is extremely difficult to measure. E_{si} is probably between $+50$ and $+80$ mV, depending on the species [8–10]; if I_{si} were solely a Ca^{2+} current, the reversal potential would be near $+120$ mV. Thus, the less positive E_{si} indicates that the movement of other ions, principally Na^+ and K^+ [9, 10], also contributes to I_{si}. Even though the selectivity of the channel for Ca^{2+} is at least 100 times greater than for Na^+ or K^+ [9], the fact that the current is not a pure Ca^{2+} current complicates the interpretation of experiments aimed at quantifying the relationship between current and contraction. The assumption usually made, and followed here, is that the amplitude of I_{si} is an indication of Ca^{2+} current amplitude. It should be borne in mind that this assumption becomes less tenable and even invalid at potentials near E_{si}. A final note on this description of I_{si} is that it is an operational one that may require modification as new information becomes available. More complete treatments of I_{si} and Ca^{2+} channel behavior can be found in the literature [11–16].

INTERNAL Ca^{2+} STORES AND CONTRACTION

Studies incorporating anodal and cathodal changes of the action potential duration in mammalian cardiac preparations provided the first suggestion of link between membrane Ca^{2+} current, intracellular stores of activator Ca^{2+}, and contraction. Antoni et al. [17], and Wood et al. [18] in particular, hypothesized that Ca^{2+} flowing into the cell during an action potential replenishes intracellular Ca^{2+} stores; subsequent depolarizations would release this bound Ca^{2+} and lead to myofibrillar activation. As reviewed by Fabiato and Baumgarten [19] in this book, evidence from experiments on isolated SR vesicles and skinned cardiac cells indicate that the site of internal Ca^{2+} store is almost certainly the SR.

The mechanism of Ca^{2+} release by the SR is unknown in both skeletal and cardiac muscle. A major hypothesis is that a small increase in the concentration of intracellular Ca^{2+} triggers the release of a large quantity of Ca^{2+} from the SR. This concept arose from pioneering work by Ford and Podolsky [20, 21] and Endo et al. [22] on skinned skeletal muscle fibers, and by Fabiato and Fabiato [23] on single skinned cardiac cells. While further studies on skinned skeletal muscle have led Endo [24] to reject this hypothesis, the imaginative and careful experiments of the Fabiatos over the past five years [25–28] have greatly increased the credibility of the hypothesis as applied to heart muscle cells. The reader is referred to the chapter by Fabiato and Baumgarten [19] for an extensive review of the evidence. A combination of Ca^{2+} uptake by the SR, Ca^{2+} efflux via Na^+-Ca^{2+} exchange, and Ca^{2+} efflux by active Ca^{2+} pumping, would seem to be quite capable of restoring intracellular Ca^{2+} concentration to its resting level within the appropriate time frame.

I_{si} and Contraction when I_{si} Amplitude Is Altered by Manipulation of the Membrane Voltage

Since I_{si} flows through channels whose gating is dependent on voltage and time, the amplitude of I_{si} can be varried over a wide range by the application of selected voltage-clamp sequences. A standard approach is to clamp the membrane potential to a negative holding potential and then to impose a series of voltage pulses to more positive potentials. The pulses usually have a duration approximating that of

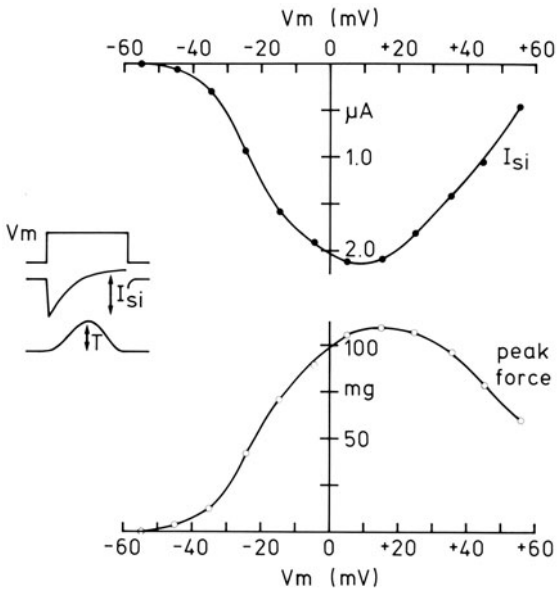

FIGURE 9–1. Steady-state dependencies of I_{si} and peak force on voltage in cat ventricular muscle. I_{si} and force were measured on 300-ms test pulses from −55 mV to potential V_m (see schematic). Each test pulse was applied after steady state had been attained with six pulses from −55 to −10 mV for 300 ms at a rate of 0.2 Hz (McDonald and Trautwein, unpublished).

the action potential, and an amplitude that is increased by 10–20 mV increments until the voltage range from −60 to +60 mV has been explored. The simultaneous measurements of I_{si} amplitude and force of contraction can then be plotted against the pulse voltage to yield current–voltage and tension–voltage curves. A second means of altering I_{si} amplitude is to keep the potential of the test pulses constant, but to apply the latter after voltage manipulations designed to vary the proportion of Ca^{2+} channels that can be activated. The results of these two types of experiments are presented in the next two sections.

CURRENT–VOLTAGE AND TENSION–VOLTAGE RELATIONS

Figure 9–1 illustrates the voltage dependencies of I_{si} amplitude and the force of contraction. The data were obtained from a cat papillary muscle and are similar in broad detail to published results on ventricular preparations from cat and other species. Three aspects which deserve attention are the threshold potential, the relation between I_{si} and the force of contraction at potentials up to +20 mV, and the relation at potentials positive to +20 mV.

Threshold potentials for the activation of I_{si} and the activation of contraction are very similar, if not identical, in ventricular muscle from dog [29], cat [8], sheep [30], and bull (McDonald and Trautwein, unpublished), as well as in sheep Purkinje fibers [31]. In fact, New and Trautwein [8] went so far as to state that they never saw I_{si} without tension, nor tension without I_{si}. In an earlier review of this topic [7], it has been suggested that I_{si} unaccompanied by contraction can be observed after depletion of presumed intracellular Ca^{2+} stores. In weighing up this statement, one should bear in mind that the study cited does not support the claim, and that, depending on techniques, there may be a problem in detecting very small forces in a voltage-clamped preparation.

There is a good correspondence between I_{si} amplitude and the force of contraction in ventricular muscle at potentials between threshold and about +20 mV; this has been a common finding in many species [e.g., 29, 32, 33]. However, a problem arises at more positive potentials where the decline in I_{si} amplitude is much steeper than that of peak tension. Again, this has been a common finding [8, 29] and has led to much agonizing over how a relatively large contraction can be triggered by small I_{si} at potentials near or even above E_{si}. In the light of recent studies by Reuter and Scholz [9] and Lee and Tsien [10] on the ionic nature of I_{si}, a plausible explanation is that while net I_{si} may reverse between +50 and +80 mV, an inward-directed Ca^{2+} component could be present at voltages up to +120 mV.

A final note with regard to the voltage dependencies of I_{si} and contraction is that they are affected by external Ca^{2+} in a predictable way, i.e., an increase in external Ca^{2+} increases both I_{si} and contraction [29, 32].

Ca^{2+} CHANNEL AVAILABILITY AND CONTRACTION

I_{si} amplitude can be manipulated over a wide range by taking advantage of the time- and

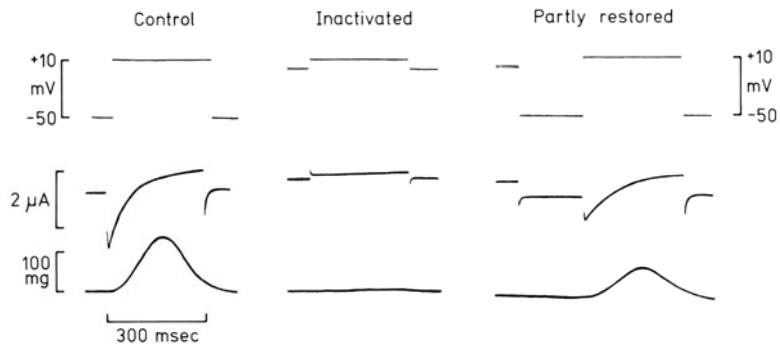

FIGURE 9–2. I_{ss} and contraction after inactivation and partial restoration of the Ca^{2+} channel system in cat ventricular muscle. After the control response *(left-hand panel)*, the Ca^{2+} channels were inactivated by moving the holding potential from −50 to 0 mV. Pulses to +10 mV now produced negligible I_{si} and tension *(middle panel)*. A 200-ms hyperpolarization to −50 mV results in partial removal of the inactivation as indicated by the partial restoration of I_{si} and tension on the subsequent test pulse to +10 mV *(right-hand panel)*.

voltage-dependent behavior of Ca^{2+} channel gating. For example, Ca^{2+} channels undergo inactivation when the membrane is depolarized for about 0.5 s to potentials positive to −50 mV. On the heels of such a depolarization, a channel-opening pulse now elicits I_{si} whose amplitude is only a fraction of that triggered by a similar pulse applied from potentials negative to −50 mV. After a depolarization to −20 mV, the channel-opening pulse elicits about 50% I_{si}, and after a depolarization to 0 mV, only about 5% of I_{si} is available [3, 12]. Hyperpolarization can restore inactivated channels to a state from which they can be opened again. The fraction of channels restored is dependent on the voltage achieved by the hyperpolarization, and the rate of restoration (removal of inactivation) is also a function of that voltage.

Our interest here is to examine how the force of contraction responds to changes in I_{si} amplitude produced by voltage sequences that alter the conductance state of the Ca^{2+} channels. Figure 9–2 compares a control response with those obtained when the Ca^{2+} channel system was either completely inactivated or partially restored. The control clamp pulse from −50 to +10 for 300 ms elicited large I_{si} and contraction (right-hand panel). The Ca^{2+} channels were then inactivated by moving the holding potential to 0 mV. An activating pulse to the same potential as before (+10 mV) now produced negligible I_{si} and contraction (middle panel). Inactivation can be removed by repolarizing the membrane to more negative potentials. When this was accomplished with a 200-ms prepulse to −50 mV, the test activation to +10 mV provoked I_{si} and contraction whose respective amplitudes were about 60% of control values (right-hand panel). This proportionality between I_{si} and contraction applies to the voltage range between full availability and full inactivation of Ca^{2+} channels (−60 to 10 mV; see fig. 9–3). In addition, the proportionality is also observed when the time course of I_{si} restoration is examined (fig. 9–4). As inactivation is removed during the hyperpolarization, I_{si}, and peak contraction recover along the same exponential time course.

From the information in figure 9–1, one could have argued that contraction is related to the level of depolarization, or to pulse amplitude, and that the resemblence of the tension–voltage curve to the I_{si}–voltage curve is purely coincidental. However, the results in figures 9–2 to 9–4 provide a strong argument against the possibility of a fortuitous relationship. The level of depolarization supposition is ruled out by the observations that pulses to the same potential can trigger contractions of greatly differing intensity (e.g., fig. 9–2). The pulse amplitude possibility is eliminated by the restoration experiment of figure 9–4; despite

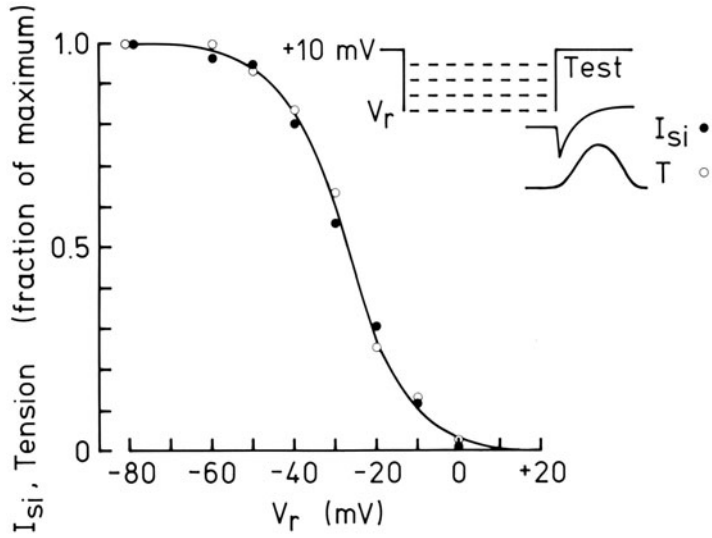

FIGURE 9–3. The correspondence between I_{si} and the force of contraction when I_{si} amplitude is altered by varying the availability of the Ca^{2+} channel system. From the holding potential of +10 mV (complete inactivation of I_{si}), the membrane potential of a cat papillary muscle was repolarized to potentials V_r for 1500 ms. I_{si} (filled circles) and tension (open circles) were triggered by the subsequent return of the potential to +10 mV (test). Pulses to V_r were applied at a rate of 0.1 Hz (McDonald and Trautwein, unpublished).

the constancy of the amplitude of the test pulse, the force of contraction varied widely.

A final note on conductance-type experiments concerns an observation made by Trautwein et al. [12]. They determined that there was a considerable overlap in the steady-state voltage relations of activation (d_∞) and inactivation (f_∞) in cat ventricular muscle (also see Bassingthwaite and Reuter [3]). These relations are almost mirror images of each other and cross over in the region between −40 to 0 mV with maximum overlap near −20 mV. At steady state, this implies a steady-state I_{si} (i.e., $g_{si} = \overline{g_{si}} \cdot d_\infty \cdot f_\infty$). Therefore, a slow voltage ramp sweeping the range −40 to 0 mV should create nearly steady-state conductance conditions, provoke a steady-state I_{si}, and a contractile response. The latter was expected to have an amplitude–voltage relation similar to a curve relating the product $d_\infty \cdot f_\infty$ to voltage. In fact, the experimental results were reasonably convincing (see fig. 6 in Trautwein et al. [12]).

Contraction in the Presence of Chemical Agents that Modify I_{si}

The space limitations dictate that this section be brief and limited to studies dealing with agents belonging to one of the following categories: catecholamines, cholinergic agonists, cardiac glycosides, and Ca^{2+} channel blockers. One should be aware that most chemical agents that have been shown to modify I_{si} are also known to have other cellular effects which could independently affect the force of contraction. Many of these actions are detailed elsewhere in the book; the objective here is to explore whether or not drug action on I_{si} affects contraction in the expected manner.

CATECHOLAMINES

An important study by Grossman and Furchgott [34] first established that catecholamines increase Ca^{2+} exchange in beating but not in quiescent cardiac preparations. The link between the extra Ca^{2+} influx and excitation was then determined by Reuter [35], who found that catecholamines augments I_{si} in cardiac Purkinje fibers. Reuter [36] has also measured

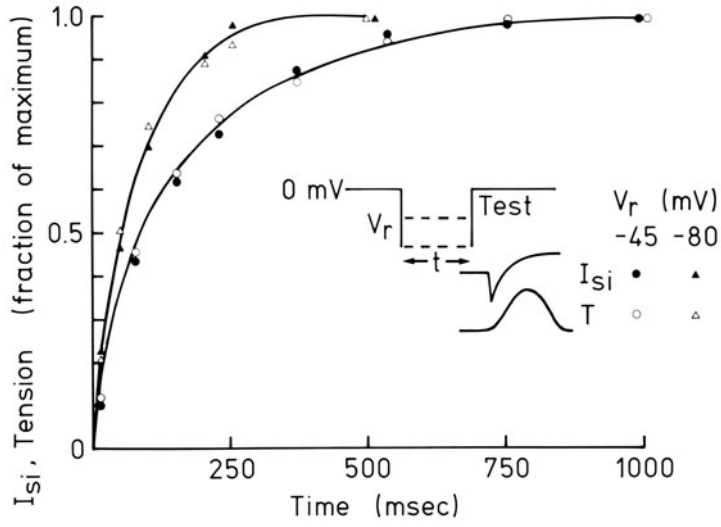

FIGURE 9–4. The correspondence between the time courses of restoration of I_{si} and tension. I_{si} (filled symbols) and tension (open symbols) recovered with a similar time constant as the duration of the pulse *(t)* to V_r was increased. V_r was set at either -45 mV or -80 mV. The -45-mV data were extracted from the results of Reuter [30] on sheep ventricular muscle; the -80 mV data were obtained from cat ventricular muscle by McDonald and Trautwein (unpublished).

I_{si} and the force of contraction in ventricular muscle treated with catecholamines. At a pulsing rate of 0.33 Hz, both I_{si} and tension increased to nearly 300% control within 1 min. In the same study, the cAMP analogue, db-cAMP, mimicked the catecholamine effect.

CHOLINERGIC AGONISTS

Acetylcholine reduces I_{si} in atrial trabeculae from amphibian [37, 38] and mammalian heart [39]. More recently, Hino and Ochi [40] have measured a sizeable block of I_{si} in guinea pig ventricular muscle treated with ACh. Prior to the experiments on mammalian atrial trabeculae by Ten Eick et al. [39], it had been difficult to pinpoint whether the well-known negative inotropic effect of the drug was related to a curtailment of the action potential plateau due to increased I_K, or whether a direct effect on Ca^{2+} permeability was also involved. Their study indicated that when membrane potential was under experimental control (i.e., voltage clamp), ACh-induced negative inotropy occurred only with concentrations of drug that suppressed I_{si}.

CARDIAC GLYCOSIDES

The relationship between I_{si} and the positive inotropic effect of cardiac glycosides is not yet fully resolved. A voltage-clamp study on cat ventricular muscle by McDonald et al. [33] indicated that the increase in contractility was independent of an effect on I_{si}. However, in recent work conducted by Marban and Tsien [41] on two different preparations, ferret ventricular muscle and calf Purkinje fibers, there was an enhancement of I_{si} with a time course similar to the development of the positive inotropic effect. The reason for the divergent results in the studies on cardiac glycosides is not clear. However, a regulation of Ca^{2+} entry by intracellular Ca^{2+} may be operative in ventricular muscle and, if so, it provides scope for a resolution of the problem (see McDonald [15] and Marbon and Tsien [41]).

Ca^{2+} CHANNEL BLOCKERS

Agents that block Ca^{2+} channels in the heart include the lanthanides, transition metals, and certain organic compounds. In voltage-clamp experiments, a concomitant reduction in I_{si} and the force of contraction has been observed with La^{3+} [42], Mn^{2+} [43] and Co^{2+} [44]. Among the organic blocking compounds, D600 and

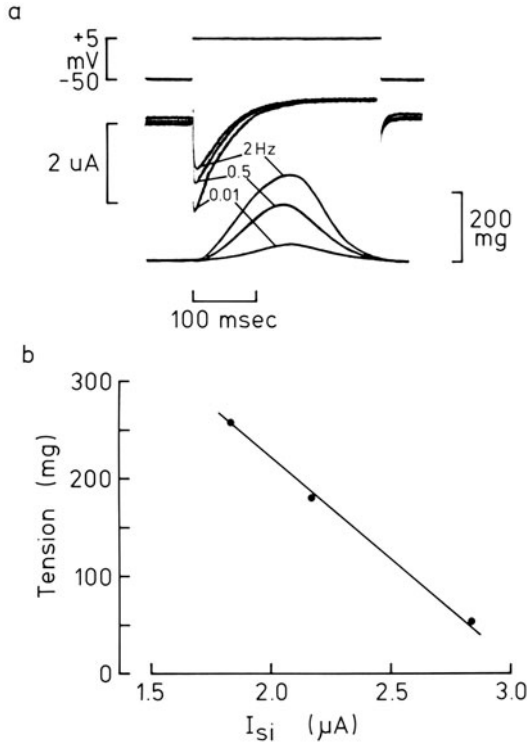

FIGURE 9–5. Effect of stimulus frequency on I_{si} and tension in cat ventricular muscle. Stimulation with 300-ms pulses from −50 to +5 mV was as folows: eight pulses at 0.01 Hz, eight at 0.5 Hz, and finally eight at 2 Hz. *(a)* Superimposed record of the eighth pulse at each frequency. *(b)* A plot of tension versus I_{si} amplitude, values from the eighth pulse at each frequency (McDonald and Trautwein, unpublished.)

AQA 39 suppress I_{si} and contraction in a dose-dependent manner [45, 46]. An interesting aspect of the D600 action is that after steady-state depression of tension has been reached, the amplitude of the first contraction following a rest period can be many times larger than the steady-state (drug) value during regular stimulation. The likely explanation is that drug unbinding from the Ca^{2+} channel receptor occurs during the rest period, and this results in a large I_{si} transient on the initial post-rest pulse [47].

Effects of Stimulus Frequency on I_{si} and Contraction

The effects of stimulus frequency on the action potential configuration and force of contraction are exceedingly complex. One reason is that there appear to be genuine differences related to tissue and species (for reviews see Boyett and Jewell [48] and Carmeliet [49]). The effects of stimulus frequency on I_{si} and contraction have been studied in dog, sheep, bovine, and cat ventricular preparations. The results form a reasonably coherent picture as discussed below. Note that an extensive series of experiments on sheep Purkinje fibers has been conducted by Gibbons and Fozzard [31, 50, 51] and reviewed recently by Fozzard [7].

A synopsis of the frequency-dependent changes in I_{si} and contraction is shown in figure 9–5. In this experiment on cat papillary muscle, eight voltage-clamp pulses were applied at a frequency of 0.01 Hz, eight at 0.5 Hz, and then eight at 2 Hz. The superimposed records of the membrane currents and contractions on the eighth pulse at each frequency indicate that I_{si} was largest, and force of contraction smallest, at the 0.01 Hz pulsing rate (fig. 9–5a). A plot of I_{si} amplitude versus tension illustrates the inverse relation between the two parameters (fig. 9–5b).

Earlier studies on dog canine preparations by Beeler and Reuter [29] and on cat fibers by New and Trautwein [8] did not detect any change in I_{si} associated with a frequency-induced positive staircase in tension. Technical improvements probably explain why an inverse relation has since been observed in dog and cat fibers by Šimurda et al. [52, 53]. An inverse relation has also been found by Isenberg [54] in isolated bovine ventricular myocytes.

In the earlier sections of this chapter, the results from several different types of experiments suggested that gradations in I_{si} can produce a corresponding grading of the force of contraction. Does the inverse relation in figure 9–5 contradict this view? The answer is no. In the experiments discussed earlier, the protocols were designed to minimize changes in the amount of intracellular Ca^{2+} stores available for release. In the frequency experiments, the amount of Ca^{2+} available from the SR is probably minimal after long rest periods, or with low-frequency pulsing. The reason is that the influx of Ca^{2+} per unit time available for charging up the SR stores is much greater with high-frequency pulsing, despite the relatively

smaller I_{si} per pulse. Thus, a comparison of I_{si} amplitude and tension under full-store condition versus empty-store condition provides little information on the ability of I_{si} to grade intracellular Ca^{2+} release. What one needs to know is whether I_{si} can grade tension independent of whether the stores are nearly empty, nearly full, or at some intermediate level. Recently acquired data from cat and bovine ventricular preparations suggest that the answer is in the affirmative (McDonald, Pelzer, and Trautwein, in preparation).

The decline in I_{si} with increasing frequency of stimulation is no doubt related to a reduction in Ca^{2+} channel conductance or to a reduction in the driving force for I_{si}. Although the latter has received the most support [e.g., 3, 30, 52, 53], the matter is by no means settled.

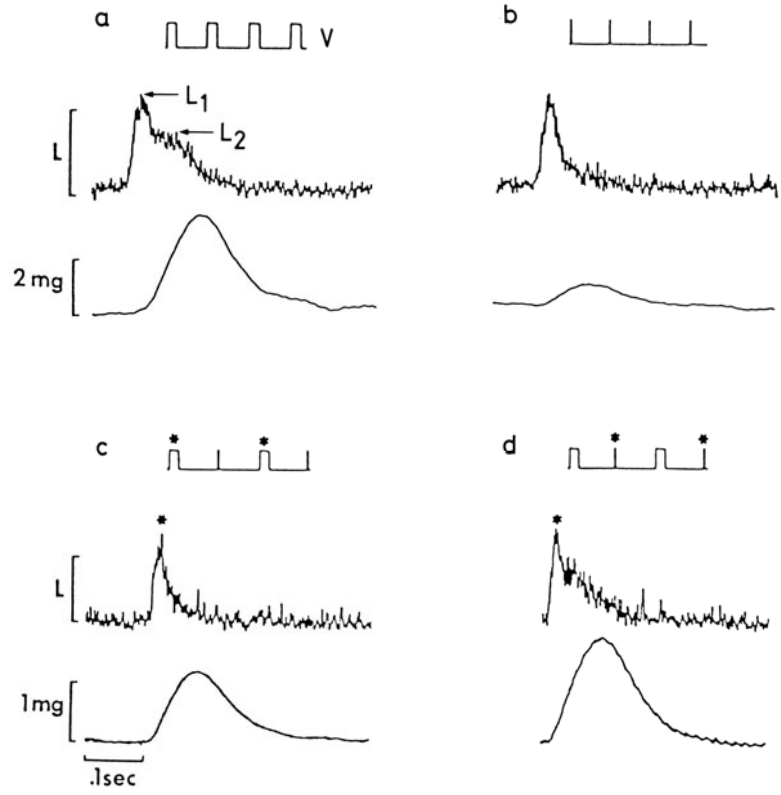

FIGURE 9–6. Voltage-clamp experiment on canine Purkinje fibers injected with aequorin. The traces in each panel are voltage *(top)*, light signal *(middle)*, and contraction *(bottom)*. The top two panels show the steady-state control responses to 0.4 Hz stimulation with 500-ms-long pulses *(a)* and 50-ms-long pulses *(b)*. The 500-ms pulses triggered large contractile events and the associated light signal had two components, L_1 and L_2. The contraction with 50-ms pulses was much smaller, and accompanied by a diminution of L_2 with no change of L_1. Since peak I_{si} amplitude was unchanged, and in other experiments was correlated with L_1, the L_2 component probably reflected the increase in intracellular Ca^{2+} concentration due to the release of activator Ca^{2+} from the SR. Thus, the 500-ms pulses filled the stores and produced a large release of Ca^{2+} from the SR, and thereby a large contraction; the 50-ms pulses produced less filling, a smaller release of Ca^{2+} from the SR, and a smaller force of contraction. These points are emphasized by the records in *c* and *d*. When 500-ms-long pulses were alternated with 50-ms pulses, the 50-ms pulse *(d)* was now accompanied by a larger contraction and L_2 than the 500-ms pulse *(c)*, i.e., the long pulse preceding the short one was more effective in replenishing the stores for release during the next activation.

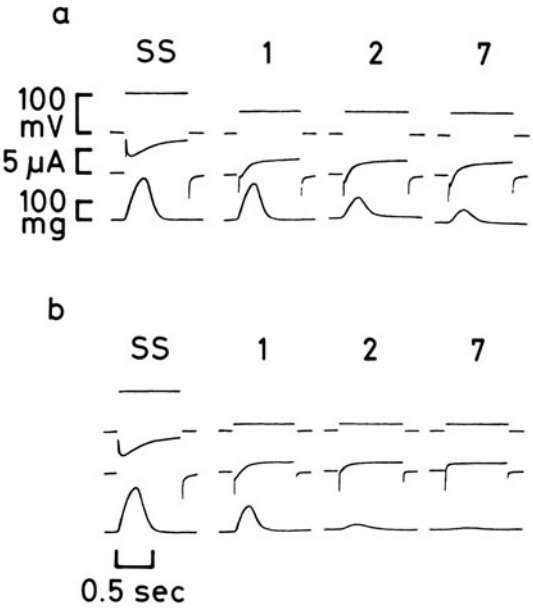

FIGURE 9–7. Dual behavior of I_{si} during descending tension staircases in cat papillary muscle. In *(a)* steady state pulsing with 110-mV steps was followed by a train of 65-mV steps; in *(b)* steady state was followed by a train of 18-mV steps. Both trains resulted in descending tension staircases. However, the 65-mV series produced an increase in I_{si} *(a)* whereas the 18-mV series was accompanied by the opposite effect *(b)*. Adapted from Simurda et al. [53].

Transient Changes in I_{si} and Contraction Induced by Alterations in the Clamp Stimulation Pattern

Most of the material presented in the preceding sections was concerned with steady-state relations between I_{si} and contraction. The purpose of this section is not to cover the numerous situations which could rightly be termed nonsteady state, but rather to focus on a few selected ones which address important areas of the overall topic. The transients which occur during changes in stimulation rate are straightforward. For example, increasing the frequency of stimulation applied to cat ventricular muscle results in a beat-to-beat decline in I_{si} and increase in tension; steady state (fig. 9–5) is approached within 6–8 pulses. The resumption of stimulation following a rest period produces an accentuated version of the above in cat [52] and sheep [30] ventricular muscle.

A particularly interesting set of results has emerged from experiments on canine Purkinje fibers injected with aequorin [55, 56]. Aequorin is a Ca^{2+}-activated luminescent phosphoprotein which, following its intracellular injection, has been successfully used for the detection of rapid intracellular Ca^{2+} transients in a variety of biologic preparations [57] including heart tissue [58, 59]. Wier [55] applied the aequorin technique to canine Purkinje fibers, and with Isenberg [56] obtained simultaneous recordings of luminescence, force of contraction, and I_{si} in voltage-clamped fibers. There were two components in the light signal, an early burst (L_1) that peaked at the same time as I_{si}, and a slower burst (L_2) (see fig. 9–6). In some fibers, L_1 was the predominant component, and they observed that peak force (very small in these "L_1 only" fibers), peak I_{si}, and L_1 were dependent on voltage in a similar way. On the other hand, L_2 had properties suggestive of Ca^{2+} release from a store and was related to normal contraction. Neither L_1 nor L_2 were linked to Ca^{2+} entry by Na^{+}-Ca^{2+} exchange, but both of these light components were suppressed by D600. The latter is expected if the L_1 burst depends on Ca^{2+} carried by I_{si}, and if the L_2 burst (Ca^{2+} release from the SR) also requires I_{si}.

Experimental records from one of the aequorin studies [56] illustrate the importance of I_{si} in filling the SR stores (fig. 9–6). On the control runs (top panels), regular pulsing at 0.4 Hz produced a much larger L_2 and twitch when the pulse duration was 500 ms (fig. 9–6a) rather than 50 ms (fig. 9–6b). However, L_1 and I_{si} (not shown) were unaffected by the pulse duration. If, instead, 500- and 50-ms-long pulses were alternated (bottom panels), L_1 and I_{si} (now shown) were unchanged, but L_2 and tension were greater with the 50-ms pulses (fig. 9–6c). The conclusions are that Ca^{2+} influx on a long pulse effectively fills the stores, and provides more Ca^{2+} for release on the subsequent pulse, regardless of whether that pulse has a long (500 ms) or short (50 ms) duration.

As stated earlier, an inverse relation between peak I_{si} and contraction during tension stair-

cases is the usual finding in mammalian ventricular muscle. However, Šimurda et al. [53] have reported that both an inverse relation and a direct relation can be observed in cat and dog ventricular preparations. Their recordings from a cat papillary muscle are duplicated in figure 9–7. The procedure was to fill the stores by imposing a series of large amplitude pulses at a rate of 0.5 Hz. When steady state was reached, a train of seven steps of either 65-mV amplitude (fig. 9–7, top) or 18-mV amplitude (fig. 9–7, bottom) resulted in a negative tension staircase. During the negative staircase, I_{si} increased in one case (65-mV pulses), but decreased in the other (18-mV pulses).

The latter result was all the more surprising because the 18-mV steps were to a potential negative to the threshold of I_{si} (assuming that the resting potential in these double-sucrose gap experiments was around -80 mV). The preferred explanation was that this inward current reflected an "escape" due to a regenerative depolarization of the SR membrane system [53]. This hypothesis incorporates earlier thinking on the possibility that there may be a loose electrical coupling between the sarcolemma and the SR, and that the SR might have voltage-dependent, Ca^{2+} conductance properties similar to the sarcolemma [3, 12]. What is intriguing is the recording of the escape current thought to be related to the large release of Ca^{2+} [53]. As pointed out by the authors, this "slow inward" current may have been due to an escape of a sarcolemmal current. A problem not mentioned is that all attempts to provoke Ca^{2+} release by presumed depolarization of the SR in skinned cardiac cells have been unsuccessful [19]. In addition, the notion of a continuity between the extracellular space and the interior of the SR has not been confirmed by microprobe experiments [60]. These objections aside, the experimental results are provacative and will no doubt spur other activity in this area.

Summary of the Role of I_{si} in Contraction

The evidence presented in this chapter points to I_{si} having three functions in the excitation–contraction process of mammalian ventricular muscle. First, it serves as the trigger for the release of activator Ca^{2+} from the internal SR stores. The supporting evidence is that phasic contraction is not seen in the absence of I_{si}, and the two processes share a common threshold. The mechanism by which Ca^{2+} is released from the SR is likely to involve the Ca^{2+}-activated Ca^{2+} release process detailed by the Fabiatos. The second role of I_{si} is the grading of the quantity of Ca^{2+} released from the SR. The supporting evidence is that, under conditions thought not to change the amount of Ca^{2+} available for release, grading of I_{si} amplitude by a variety of techniques results in a closely correlated grading of the force of contraction. Of importance here is that Ca^{2+}-activated Ca^{2+} release in skinned cardiac cells can be graded by grading the concentration of the trigger Ca^{2+} solution; the range of trigger Ca^{2+} concentrations required is not out of line with that expected from Ca^{2+} influx associated with I_{si} (see Fabiato and Baumgarten [19]). A third identified role of I_{si} is that of filling the internal SR stores. The supporting evidence is that an alteration in the charge carried by I_{si}, whether by modification of I_{si} amplitude, duration, or frequency of activation, has a predictable effect of contractility and aequorin light signals triggered by subsequent activations.

References

1. Langer GA: The role of calcium in the control of myocardial contractility: an update. J Mol Cell Cardiol 12:231–239, 1980.
2. Langer GA: Sodium–calcium exchange in the heart. Annu Rev Physiol 44:435–449, 1982.
3. Bassingthwaite G, Reuter H: Calcium movements and excitation–contraction coupling in cardiac cells. In: De Mello WC (ed) Electrical phenomena in the heart. New York: Academic, 1972, pp 353–393.
4. Morad M, Goldman Y: Excitation–contraction coupling in heart muscle: membrane control of development of tension. Prog Biophys Mol Biol 27:257–313, 1973.
5. Chapman RA: Excitation–contraction coupling in cardiac muscle. Prog Biophys Mol Biol 35:1–52, 1979.
6. Fabiato A, Fabiato F: Calcium and cardiac excitation–contraction coupling. Annu Rev Physiol 41:473–484, 1979.
7. Fozzard HA: Slow inward current and contraction. In: Zipes DP, Bailey JC, Elharrar V (eds) The slow inward current and cardiac arrhythmias. The Hague:

Martinus Nijhoff Medical Division, 1980, pp 173–203.
8. New W, Trautwein W: The ionic nature of slow inward current and its relation to contraction. Pflugers Arch 334:24–38, 1972.
9. Reuter H, Scholz H: A study of the ion selectivity and the kinetic properties of the calcium dependent slow inward current in mammalian cardiac muscle. J Physiol (Lond) 264:17–47, 1977.
10. Lee KS, Tsien RW: Reversal of current through calcium channels in dialysed single heart cells. *Nature* 297:498–501, 1982.
11. Reuter H: Divalent cations as charge carriers in excitable membranes. Prog Biophys Mol Biol 26:3–43, 1973.
12. Trautwein W, McDonald TF, Tripathi O: Calcium conductance and tension in mammalian ventricular muscle. Pflugers Arch 354:55–74, 1975.
13. Carmeliet E, Vereecke J: Electrogenesis of the action potential and automaticity. In: Berne RM, Sperelakis N, Geiger SR (eds) Handbook of physiology: the cardiovascular system I. Baltimore: Williams and Wilkins, 1979, pp 269–334.
14. Coraboeuf E: Voltage clamp studies of the slow inward current. In: Zipes DP, Bailey JC, Elharrar V (eds) The slow inward current and cardiac arrhythmias. The Hague: Martinus Nijhoff Medical Division, 1980, pp 25–95.
15. McDonald TF: The slow inward calcium current in the heart. Annu Rev Physiol 44:425–434, 1982.
16. Tsien RW: Calcium channels in excitable cell membranes. Annu Rev Physiol 45:341–358, 1983.
17. Antoni H, Jacob R, Kaufmann R: Mechanische Reaktionen des Frosch und Säugetiermyokards bei Veränderung der Aktionspotential-Dauer durch konstante Gleichstromimpulse. Pflugers Arch 306:33–57, 1969.
18. Wood E, Heppner RL, Weidmann S: Inotropic effects of electric currents. Circ Res 24:409–445, 1969.
19. Fabiato A, Baumgarten CM: Methods for detecting calcium release from the sarcoplasmic reticulum of skinned cardiac cells and the relationship between calculated transsarcolemmal calcium movements and calcium release. In: Sperelakis N (ed) Physiology and pathophysiology of the heart. The Hague: Martinus Nijhoff Medical Division, 1984.
20. Ford LE, Podolsky RJ: Regenerative calcium release within muscle cells. Science 167:58–59, 1970.
21. Ford LE, Podolsky RJ: Intracellular calcium movement in skinned muscle fibres. J Physiol (Lond) 223:21–32, 1972.
22. Endo M, Tanaka M, Ogawa Y: Calcium-induced release of calcium from the sarcoplasmic reticulum of skinned skeletal muscle fibres. Nature (Lond) 228:34–36, 1970.
23. Fabiato A, Fabiato F: Contractions induced by a calcium-triggered release of calcium from the sarcoplasmic reticulum of single skinned cardiac cells. J Physiol (Lond) 249:469–495, 1975.
24. Endo M: Calcium release from the sarcoplasmic reticulum. Physiol Rev 57:71–108, 1977.
25. Fabiato A, Fabiato F: Calcium release from the sarcoplasmic reticulum. Circ Res 40:119–129, 1977.
26. Fabiato A, Fabiato F: Calcium-induced release of calcium from the sarcoplasmic reticulum of skinned cells from adult human, dog, cat, rabbit, rat and frog hearts and from fetal and new-born rat ventricles. Ann NY Acad Sci 307:491–522, 1978.
27. Fabiato A, Fabiato F: Use of chlorotetracycline fluorescence to demonstrate Ca^{2+}-induced release of Ca^{2+} from the sarcoplasmic reticulum of skinned cardiac cells. Nature 281:146–148, 1979.
28. Fabiato A: Myoplasmic free calcium concentration reached during the twitch of an intact isolated cardiac cell and during calcium-induced release of calcium from the sarcoplasmic reticulum of a skinned cardiac cell from the adult rat or rabbit ventricle. J Gen Physiol 78:457–497, 1981.
29. Beeler GW, Reuter H: Relation between membrane potential, membrane currents, and activation of contraction in ventricular muscle fibres. J Physiol (Lond) 207:211–229, 1970.
30. Reuter H: Time and voltage-dependent contractile responses in mammalian cardiac muscle. Eur J Cardiol 112:177–181, 1973.
31. Gibbons WR, Fozzard HA: Voltage dependence and time dependence of contraction in sheep cardiac Purkinje fibers. Circ Res 28:446–460, 1971.
32. Trautwein W: The slow inward current in mammalian myocardium. Eur J Cardiol 112:169–175, 1973.
33. McDonald TF, Nawrath H, Trautwein W: Membrane currents and tension in cat ventricular muscle treated with cardiac glycosides. Circ Res 37:674–682, 1975.
34. Grossman A, Furchgott RF: The effect of various drugs on calcium exchange in the isolated guinea-pig left auricle. J Pharmacol Exp Ther 145:162–172, 1964.
35. Reuter H: The dependence of slow inward current in Purkinje fibers on the extracellular calcium-concentration. J Physiol (Lond) 192:479–492, 1967.
36. Reuter H: Localization of *beta* adrenergic receptors and effects of noradrenaline and cyclic nucleotides on action potentials, ionic currents and tension in mammalian cardiac muscle. J Physiol (Lond) 242:429–451, 1974.
37. Ikemato Y, Goto M: Nature of the negative inotropic effect of acetylcholine on the myocardium. Proc Jpn Acad 51:501–505, 1975.
38. Giles W, Noble SJ: Changes in membrane currents in bullfrog atrium produced by acetylcholine. J Physiol (Lond) 261:103–123, 1976.
39. Ten Eick R, Nawrath H, Trautwein W: On the mechanism of the negative inotropic effect of acetylcholine. Pflugers Arch 361:207–213, 1976.
40. Hino N, Ochi R: Effect of acetylcholine on membrane currents in guinea-pig papillary muscle. J Physiol (Lond) 307:183–197, 1980.

41. Marban E, Tsien RW: Enhancement of calcium during digitalis inotropy in mammalian heart: positive feed-back regulation by intracellular calcium? J Physiol (Lond) 329:589–614, 1982.
42. Katzung BG, Reuter H, Porzig H: Lanthanum inhibits Ca inward current but not Na-Ca exchange in cardiac muscle. Experientia 29:1073–1075, 1973.
43. Vassort G, Rougier O: Membrane potential and slow inward current dependence of frog cardiac mechanical activity. Pflugers Arch 331:191–203, 1972.
44. McDonald TF, Pelzer D, Trautwein W: Does the calcium current modulate the contraction of the accompanying beat? A study of E-C coupling in mammalian ventricular muscle using cobalt ions. Circ Res 49:576–583, 1981.
45. Nawrath H, Ten Eick RE, McDonald TF, Trautwein W: On the mechanism underlying the action of D600 on slow inward current and tension in mammalian myocardium. Circ Res 40:408–414, 1977.
46. Trautwein W, Pelzer D, McDonald TF, Osterrieder W: AQA 39, a new bradycardiac agent which blocks myocardial calcium channels in a frequency- and voltage-dependent manner. Naunyn Schmiedebergs Arch Pharmacol 317:228–232, 1981.
47. McDonald TF, Pelzer D, Trautwein W: On the mechanism of slow calcium channel block in heart. Pflugers Arch 385:175–179, 1980.
48. Boyett MR, Jewell BR: Analysis of the effects of changes in rate and rhythm upon electrical activity in the heart. Prog Biophys Mol Biol 36:1–52, 1980.
49. Carmeliet E: Repolarisation and frequency in cardiac cells. J Physiol (Paris) 73:903–923, 1977.
50. Gibbons WR, Fozzard HA: Relationships between voltage and tension in sheep cardiac Purkinje fibers. J Gen Physiol 65:345–365, 1975.
51. Gibbons WR, Fozzard HA: Slow inward current and contraction in sheep cardiac Purkinje fibers. J Gen Physiol 65:367–383, 1975.
52. Šimurda J, Šimurdova M, Braueny P, Sumbera J: Slow inward current and action potentials of papillary muscles under non-steady state conditions. Pflugers Arch 362:209–218, 1976.
53. Šimurda J, Šimurdova M, Braveny P, Sumbera J: Activity-dependent changes of slow inward current in ventricular heart muscle. Pflugers Arch 391:277–283, 1981.
54. Isenberg G: Ca entry and contraction as studied in isolated bovine ventricular myocytes. Z Naturforsch 37:502–512, 1982.
55. Wier WG: Calcium transients during excitation–contraction coupling in mammalian heart: aequorin signals of canine Purkinje fibers. Science 207:1085–1087, 1980.
56. Wier WG, Isenberg G: Intracellular [Ca^{2+}] transients in voltage clamped cardiac Purkinje fibers. Pflugers Arch 392:284–290, 1982.
57. Blinks JR, Wier WG, Hess P, Prendergast FG: Measurement of Ca^{2+} concentrations in living cells. Prog Biophys Mol Biol 40:1–114, 1982.
58. Allen DG, Blinks JR: Calcium transients in aequorin-injected frog cardiac muscle. Nature 273:509–513, 1978.
59. Allen DG, Kurihara S: Calcium transients in mammalian ventricular muscle. Eur Heart J (Suppl A) 1:5–15, 1980.
60. Somlyo AV, Gonzalez-Serratos H, Shuman H, McClellan G, Somlyo AP: Calcium release and ionic changes in the sarcoplasmic reticulum of tetanized muscle: an electron-probe study. J Cell Biol 90:577–594, 1981.

10. THE ROLE OF Na-Ca EXCHANGE IN HEART

Lorin J. Mullins

Introduction

Cardiac muscle cells differ from those of skeletal muscle in many respects; an important difference is that cardiac cells contract when placed in Na-free salines while skeletal muscle fibers do not. Since in many cardiac cells this sort of replacement does not change membrane potential, one must ask what is the signal for contraction produced by a reduction in external Na. It cannot be electrical since membrane potential does not change and, in spite of some rather exotic ideas that have been put forward, the most viable idea is that if Na_o is made low, Ca_o can exchange for Na_i and thus a flux of inward moving Ca is generated to provide for a contraction.

Another quite old observation is that, if heart muscle is treated with drugs such as ouabain or digitoxin, then quite small doses are capable of increasing the strength of contraction. Again, although many explanations have been advanced for this effect, the experimental evidence is clearly in favor of a change in internal Na concentration $[Na]_i$ of 2–3 m*M* as having a decisive effect on the quantity of Ca admitted to the cell during each depolarization, or heartbeat. This finding makes it necessary to suppose that the Na-Ca exchange process mentioned above is either voltage dependent or more simply electrogenic (i.e., moves more Na charges in one direction than Ca charges in the other). These new findings also make it unnecessary to invent new roles for cardiac glycosides—their well-known specificity in inhibiting the Na-K pump of all cell membranes suffices.

There are other sources of contractile Ca in heart muscle, specifically the Ca channel and the SR, and both of these sources of Ca are well documented by chapters in this book; hence, they will not be gone into any detail here. What is necessary to mention is that Na-Ca exchange is responsible not only for contributing Ca to the cardiac cell during depolarization, it also is responsible for removing Ca during diastole. An alternate view on Ca removal must consider an ATP-driven Ca pump; this point will be considered later. It must remove not only the Ca that itself contributed, but also that introduced by the Ca channel. Thus Na-Ca exchange Ca cannot be some small fraction of the total Ca economy involved in a contraction, otherwise cardiac glycosides would not have the effects they do.

The subject of Na-Ca exchange has been comprehensively reviewed most recently by Langer [1]. Highly relevant to this chapter are reviews by Fabiato and Fabiato [2], Chapman [3], Fozzard [4], and indeed a book has been published on the subject of Na-Ca exchange [5].

Ion Gradient Transport

Excitable cells, without exception, have a high concentration of K inside and a low concentration of Na; the reverse is true for external ion concentrations where Na is the dominant cation. This state of affairs is brought about be-

I am indebted to Dr. David Eisner for reading and commenting on this manuscript.

N. Sperelakis (ed.), PHYSIOLOGY AND PATHOPHYSIOLOGY OF THE HEART.

Martinus Nijhoff Publishing, Boston/The Hague/ Dordrecht/Lancaster.

cause there exists in the cell membrane an entity, the Na pump, that exchanges Na_i for K_o (although not in equal quantities). Since the outward movement of Na requires energy, it is understandable that the Na pump is dependent on a substrate, ATP, for its operation.

It is also clear that most of the ATP produced in cells results from the energy stored in proton gradients that develop across the mitochondrial membrane as a result of the chemical reactions taking place inside such structures. We have, therefore, this sequence: ion translocation produces ATP and the reverse reaction ATP produces ion translocation. What these generally accepted considerations suggest is that, in biologic systems, energy can be stored in the form of chemical bond energy or in the form of ion gradients and that means to interconvert these sources of energy exist within excitable cells. An extension of this idea of gradient–substrate interconversion is that the gradient of one ion across the cell membrane could be used as a source of energy to create a gradient of another ion (or molecule) across the membrane. The generic term for such energy conversion is "gradient transport," where the gradient in one ion can lead to the development of gradients of another. Gradient transport can be further subdivided into cotransport or countertransport, depending on whether the driving ion and the transported ion are on the same or on opposite sides of the membrane. The subject matter of this chapter, Na-Ca transport, is a case of countertransport whereby sodium ions moving in one direction bring about the movement of Ca in the opposite direction. This is gradient-driven transport since the general idea is that the gradient in Na concentration produced by the substrate-driven Na-K pump is dissipated while producing a gradient in [Ca].

The observations relating to Na-Ca exchange in heart are of much longer standing than the foregoing because it was observed quite early in the history of physiology that frog hearts would contract when exposed to Na-free solutions. This behavior was most reasonably interpreted as indicating the existence of a carrier that would combine either with Na or Ca as indicated in figure 10–1. This sort of model has a

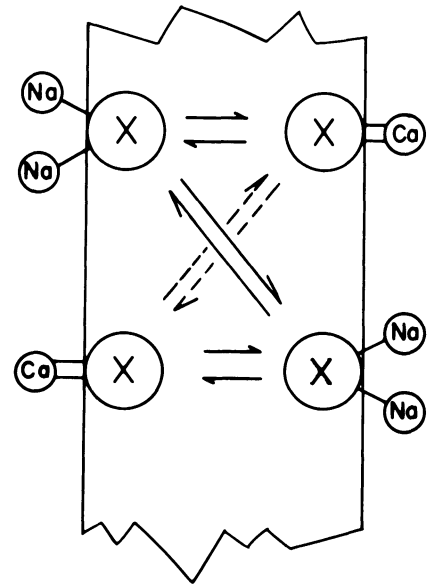

FIGURE 10–1. This is the classic Na-Ca exchange carrier moving either Na inward in exchange for Ca, or Ca inward in exchange for Na. Diagonal arrows indicate expected exchange fluxes.

number of properties that are not at first sight obvious; it should, according to assumptions, allow either the transfer of Na (left to right) in exchange for Ca in the opposite direction or the transfer of Ca (left to right) in exchange for Na in the opposite direction. If the carrier can only move when combined, then net ion movements are only Na gain at the expense of Ca exit and Ca gain at the expense of Na exit. There are ion exchange movements (shown as diagonal arrows) that represent Na-Na and Ca-Ca exchange; these will be important only if isotopic measurements are being considered.

Early investigators did not have any way of knowing what $[Ca]_i$ might be, but they considered it very low since, at least for muscle, this ion was recognized as being involved in contraction. With Ca_i close to zero, the *only* reaction of the carrier that produced net transport was $Ca_o + 2Na_i = Ca_i + 2Na_o$, that is, an entry of Ca in exchange for Na. Other models considered that perhaps the carrier, R, might return to the outer surface of the membrane

unloaded; if this were so, then the following reactions could be expected:

$$Ca_0 + R_0 \rightarrow Ca\,R_0 \rightarrow Ca\,R_i \rightarrow Ca_i + R_i \quad (1)$$

$$2Na_0 + R_0 \rightarrow Na_2R_0 \rightarrow Na_2R_i \rightarrow 2Na_i + R_i \quad (2)$$

$$R_i \rightarrow R_0 \quad (3)$$

We have, therefore, two reactions leading to R entry: The first is a reaction of Ca_O whose rate must be expected to be modified by the presence of Na_O since both these ions compete for attachment to the carrier on the outside. In the second case, there is a similar competition between Ca_O and Na_O when Na_O reacts with the carrier. It is important to notice that the predominant feature of these models is a competition between Na and Ca for the carrier as given by reactions 1 and 2 above. We can write the reactions for the combination of Na or Ca with the carrier as

$$\frac{([Na])^2\,[R]}{[Na_2R]} = K_{Na}$$

$$\frac{[Ca]\,[R]}{[CaR]} = K_{Ca}$$

so that if CaR/Na_2R is the fraction of the carrier moving Ca vs Na inward, this movement is described by [Ca] divided by $([Na])^2$ times a constant that represents the ratio of K_{Ca}/K_{Na}. Thus the idea that Ca entry was given by a ratio of the Ca and Na concentrations in the Ringer or Tyrode solution was initiated.

If only reactions 1 and 2 above are permitted, then the net ion movements possible are the entry of Ca in exchange for the exit of Na or the entry of Na in exchange for the exit of Ca since in each case the countertransport requires the return of carrier R from outside to in or the reverse. Isotopic measurements should show both a Na-Na exchange and a Ca-Ca exchange. If reaction 3 is also allowed, then in principle both the Na and Ca electrochemical gradients could run down via reactions 1 + 3 and 2 + 3, respectively. A rapid rundown of the ion gradients can be prevented by making the affinity of the carrier for Na high and the mobility of Na-loaded carrier small compared with when it is Ca loaded. It is worth noting that the idea that $[Na]_i$ might be involved in Ca entry has been lost in this analysis that puts all control of Ca entry on the reactions of Na and Ca with the carrier at the outside of the membrane. Apparent self-exchange Na_i N_0 has never been demonstrated.

As progress in understanding the contractile process both in cardiac and skeletal muscle advanced, it became clear that (a) $[Ca]_i$ while quite low was finite, and (b) that a rise in $[Ca]_i$ was the initiator of contraction. It was, therefore, a major advance for Reuter and Seitz [6] to suggest that not only was there a Ca entry by Na-Ca exchange if Na_0 were made low, but that this same process could provide for the removal of Ca from cardiac fibers that was essential if the reversal of Ca entry via Ca channels were to occur in a manner analogous to the well-known reversal of Na entry from Na channels that occurs via the Na pump. This suggestion posed some important difficulties because it was truly a Na-Ca exchange (or countertransport) process and the suggested stoichiometry of Na-Ca was 2:1. The first difficulty relates to the kinetic properties of the system. It is necessary to find dissociation constants K_{Na}, K_{Ca} that will lead to a reasonable rate of transport. The second difficulty is to address the thermodynamic requirements that enough energy be supplied by the Na gradient to pump Ca to the levels required for relaxation. The nature of the kinetic difficulty can be summarized by noting that in normal plasma the Na-Ca concentrations have a ratio of about 75 while inside relaxed muscle fibers the ratio is close to 10^6. This finding means that, if a significant fraction of the carrier is to bind Ca at the inside of the membrane, the presence of Na at the outside of the membrane is irrelevant since the affinity constant for Ca will have to be so high that no Na can be bound there. In turn, this result contradicts much experimental information that shows a large sensitivity of contraction to $[Na]_O$.

Another expectation of the model so far presented is that there should be Ca-Ca exchange fluxes as well as Na-Na exchange fluxes as measured with isotopes. Now experiments have shown a decrease in Ca efflux upon removing Ca_0 but they have not shown a corresponding decrease in Na efflux upon the removal of Na_o

so that a part of the exchange flux assumption is not supported by experiment. The Ca_0-free effect can have a quite different explanation that will be detailed below and the findings that no appropriate values for dissociation constants for Ca vs Na and the lack of Na-Na exchange via the Na-Ca carrier can be understood most simply by supposing that there are *separate sites* on the carrier for Na and Ca. Since Na^+ has substantial effects on both the kinetics and thermodynamics of Na-Ca exchange, it seems reasonable to suppose that the binding of Na to the carrier induces Ca-binding sites. It is also possible to construct a model where Ca binding induces Ca sites, but this arrangement is substantially more complicated. Much of the experimental information on the effects of Na on Na-Ca exchange can be most simply explained by supposing that the Na concentration on a particular side of the membrane determines the extent to which Ca can be bound on the opposite side. Quite separate from this purely kinetic effect, there is a thermodynamic determinant of the energy gradient that is to support the transport of Ca. If Na_0 is higher than Na_i, then the upper part of figure 10–2 may be appropriate; conversely, if Na_0 is reduced to low values and Na_i is higher than Na_0, the lower part of the figure may be valid. In the upper part, Na-Ca exchange removes Ca from the cell; in the lower part, this same process adds Ca to the cell.

One can make the system shown in figure 10–1 transport Ca inward in exchange for Na_i, but it is impossible for the carrier to develop significant power (i.e., ion flux) for the outward movement of Ca, given association constants for Na and Ca that will move Ca inward if Na_0 is reduced. It is, of course, possible to have differing values for K_{Ca} at the two surfaces (and for K_{Na}), but only at the expense of an energy supply from metabolism. We now consider a system such as that shown in figure 10–2 for a separate sited Na-Ca exchanger. There are several properties that are not entirely obvious. First, the exchange system must not be able to translocate ions when it is in *only* a Na- or Ca-loaded condition since this would allow a dissipation of these ion gradients, both of which are directed inward. A second requirement is that the unloaded carrier be free to move since otherwise a net movement in the absence of Ca ions on one side of the membrane and Na on the other would be impossible. It is known, however, that with $Na_i = 0$, $Ca_0 = 0$, there is a large Ca efflux in the presence of Na_0. With separate sites, the carrier moves Na_0 in by exchange for Ca_i moving out and then the carrier must return to its original position as an unloaded entity.

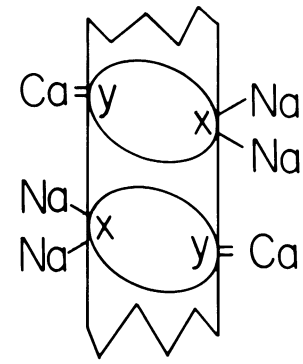

FIGURE 10–2. This shows a Na-Ca carrier with separate sites for the binding of Na and Ca designated, respectively, X and Y. Cell interior is on the left.

With a separate site carrier for Na and Ca, it will be noted that there cannot be competition for a site between Na and Ca, yet much of the literature suggests such competition. We may, therefore, ask the question of how Na-free conditions can lead to a large Ca entry in cells without the existence of competition between Na and Ca for a single site on a carrier. If we write the overall reaction between sites and ions we have the following:

$$2Na_0 + X_0 \rightleftharpoons Na_2X_0Y_i \quad (1)$$

$$Ca_i + Na_2X_0Y_i \rightleftharpoons Na_2X_0Y_iCa \quad (2)$$

$$Na_0Y_iCa \rightleftharpoons Na_2X_iY_0Ca \quad (3)$$

$$Na_2X_iY_0Ca \rightleftharpoons X_iY_0Ca + 2\,Na \quad (4)$$

$$X_iY_0Ca \rightleftharpoons X_i + Ca_0 \quad (5)$$

The scheme above envisages the formation of a Na_2X complex with the carrier, and thus a binding leading simultaneously to the development of a Ca-binding site Y. The binding of Ca to this complex then leads to the fully loaded carrier (reaction 2) that can translocate (3), dissociate Na (4), and thus lead to the dis-

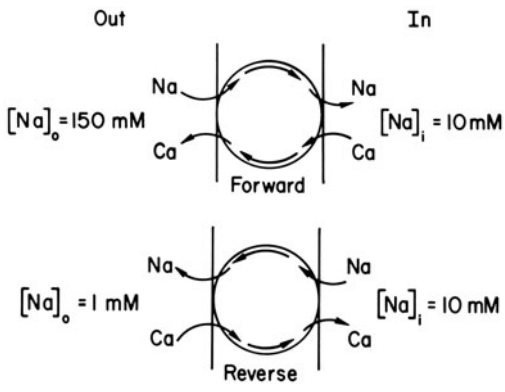

FIGURE 10–3. At *top*, $[Na]_0$ = 150 m*M* and separate sites move Na inward (down its concentration gradient) and Ca outward. *Lower diagram* is for $[Na]_0$ = 1 m*M* so Na gradient is outward and outward Na movement brings in Ca.

appearance of the Ca-binding site and the dissociation of Ca (5). Thus the translocation of Ca outward occurs because the low $[Na]_i$ allows the dissocation of carrier-bound Na inside. For Ca entry one expects that here it is the dissociation of $Na_0X_0Y_iCa$ that is important. Clearly this complex will release Na with much greater ease if $[Na]_0$ is low than if it is high. The separate site model thus has the property that Ca influx is facilitated if Na_o is low, not because Na and Ca compete for the same site, but because countertransport is itself sensitive to the Na concentration gradient. Figure 10–3 shows a separate site model for Na-Ca countertransport responding to changes in Na_0. In the upper part of the figure, where Na_0 is 150 m*M* and Na_i 10 m*M*, the inward flux of Na drives an outward flux of Ca; in the lower part of the figure, Na_0 has been made 1 m*M* so that the Na gradient is now directed outwardly and an outward flow of Na drives an inward flux of Ca. This is usually called a reverse mode of operation of Na-Ca exchange since it is the result of a lowering of Na_0 and results in a Ca gain for a tissue rather than a loss.

The Energetics of Na-Ca Exchange

The foregoing discussion argues for a dual-sited Na-Ca exchange carrier where Na^+ and Ca^{2+} combine, but no consideration has been given so far to the stoichiometry by which Na^+ combines with the carrier. It is simplest to consider that 2 Na move in one direction and 1 Ca in the other, and indeed this has been the usual assumption. We now consider the work that must be done in order to produce a $[Ca]_i$ that occurs in cells.

Actual values for $[Ca]_i$ have only recently become available as techniques for the estimation of this concentration have been developed. It has been clear from the use of CaEGTA–EGTA buffers and skinned muscle fibers that the process of relaxation requires values of the order of 0.1 μM for a Ca_i while actual measurements of $[Ca]_i$ in squid axons indicate values of 0.03 μM. This concentration is also close to the range where experiment indicates that $[Ca]_i$ has an effect on Ca_i-activated K channels so that a variety of quite different techniques indicate that resting values for $[Ca]_i$ in cells are less than 0.05 μM or 50 n*M*. (Recent measurements with Ca-sensitive electrodes suggest values of the order of 200 n*M*, a value that would, according to estimates of the interaction of Ca with the contractile machinery, suggest that substantial tension ought to be developed. The fact that cells are relaxed suggests that the estimate of $[Ca]_i$ is too high.) This means that the ratio of Ca_0/Ca_i is of the order of 10^5 in squid axons and is likely to have much the same value for mammalian cells. A ratio of this sort means that E_{Ca} is +145 and that with the usual values for membrane potential in cardiac cells there is both the chemical gradient of +145 mV and an additional electrical gradient of about −85 mV. Since the ion being affected by this gradient (Ca) is doubly changed, the force driving Ca inward is $(-85 - [145]) \times 2$ or −460 mV, as shown in figure 10–4. A corollary of this is that either the energy available from the Na electrochemical gradient must be greater than this if Ca extrusion is to take place or other methods of reducing $[Ca]_i$ to low levels must be in operation.

Figure 10–4 also shows that, given a value of E_{Na} of +50 mV, it will require more than three times the value $(E - E_{Na})$ to equal that for the Ca gradient. In the illustration, 4 Na are assumed to couple with the movement of 1 Ca so that the term $4(E - E_{Na}) = -2(e - E_{Ca}) = -80$. This measures the difference in the electrochemical gradients between Na and

Ca and is a measure of the driving force leading to Ca extrusion at the expense of Na entry. Such a gradient difference is necessary if Ca is to be actually extruded at the resting potential of a cardiac fiber. The sign of the gradient difference indicates an inward current of Na. The bottom part of figure 10–4 shows what happens if the cell is depolarized to a membrane potential of zero (a condition near the plateau in cardiac fibers). The chemical gradients for Na and Ca remain initially unchanged, but the electrical terms for both ions vanish. Now the difference in electrochemical gradients is given by $(-4E_{Na} - [-2E_{Ca}])$ or $+90$ mV. This condition therefore requires that Ca enter in exchange for Na inside and that we have an outward current generated by the exchange. It is apparent that, if at the normal membrane potential Ca extrusion occurs while at the plateau Ca entry is taking place, then there must be a potential where Ca entry and exit are both in balance, i.e., a reversal potential for the carrier exchange. This is simply obtained by making the gradient difference zero, i.e., $4(E - E_{Na}) - 2(E - E_{Ca}) = 0$; or $E = 2E_{NA} - E_{Ca}$. Thus the reversal potential in the example given above is -45 mV.

The assumption that there were 4 Na necessary to effect the extrusion of Ca at the resting potential was energetically necessary given $E_{Na} = +50$ mV and $E_{Ca} = +145$ mV, but these values are by no means unique. There is ample evidence that E_{Ca} changes greatly during the 200- to 300-ms duration of the action potential and that E_{Na} changes measurably over times of the order of seconds, depending on whether the cardiac fibers are beating or not and at what rate. Thus the value of $E_{Na} = 50$ corresponding to a Na ratio across the membrane of ~7 might be appropriate for a heart that is rapidly beating and hence subjected to a substantial Na load. At lighter loads or slower rates of contraction (or in resting fibers), the Na ratio across the membrane may approach 15 or an E_{Na} of $+70$ mV so that these two values $E_{Na} = +50$ and $+70$ may be convenient to use as extremes for the chemical part of the Na electrochemical gradient. For $[Ca]_i$ values for a ratio across the membrane of 10^5 have been measured and this may be regarded as the extreme.

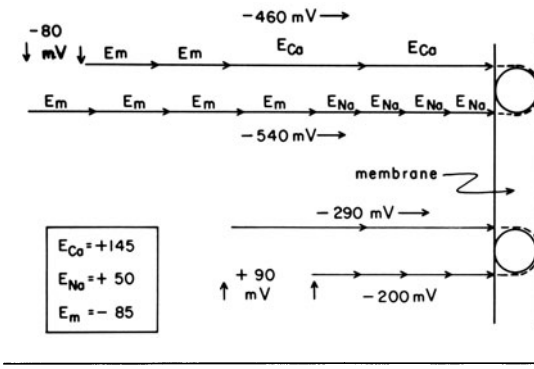

FIGURE 10–4. For the values given in the *box* (lower left), this shows the values of Ca and Na electrochemical gradients for 4Na-1Ca coupling with $E_m = -85$ mV *(top)* and $E_m = 0$ mV *(bottom)*. Note the reversal of direction of Ca movement.

Other measurements have suggested that the ratio is only 10^4 so that again we have two values for $E_{Ca} = +145$ or $+116$ (rounded to $+120$). Table 10–1 shows these extremes of ion equilibrium potentials for both ions and for a transport system where either 3 Na or 4 Na are coupled to the movement of 1 Ca. It also gives values for the gradient difference between the electrochemical gradients of Na and Ca since, on a purely empirical basis, it will be shown later that a large gradient difference means a large ion flux via Na-Ca exchange.

The table makes it clear that, except under circumstances where E_{Na} is very large ($+70$) and E_{Ca} rather small ($+120$), it is impossible for a 3Na-Ca stoichiometry to effect a reasonable gradient difference at the resting potential between the Na and Ca gradients. Our brief consideration of likely values for E_{Na} and E_{Ca} at the resting membrane potential indicates that it is impossible for an electroneutral exchange of 1 Ca for 2 Na to produce values for $[Ca]_i$ in the range where a cardiac fiber can be relaxed. It has been suggested that the addition of a substrate such as ATP might alter the Na-Ca exchange system in such a way that affinities for Na and Ca on the two sides of the membrane would be quite different and thus enable the exchanger to produce low values of $[Ca]_i$ by relying on energies partly derived from the Na gradient and partly from metabolism. Unfor-

tunately, from an experimental point of view there is no demonstration that ATP can produce Ca fluxes from a cell such as the squid giant axon that exceed values of 0.1 –0.2 pmol/cm^{2}s while real fluxes from cardiac fibers need to be 10–100 times larger than this. It would appear, therefore, that Na-Ca exchange needs to be nonelectroneutral (i.e., electrogenic) and that therefore 3 or more Na must move in one direction for 1 Ca in the other. Table 10–1 suggests, in fact, that 4 may be a minimum number for the Na-Ca coupling, giving the need for a brisk Ca efflux when the membrane potential reaches normal diastolic values.

During contraction, $[Ca]_i$ moves from a value of tens of nM to one of μM, hence the value for $[Ca]_0/[Ca]_i$ changes from $\sim 10^5$ to $\sim 10^3$ or E_{Ca} from +145 to +87. Since during the plateau with a membrane potential near zero, Na-Ca exchange is given by $(-4E_{Na} - [-2E_{Ca}])$ or $(-4 \times +50 + 2 \times +90)$, the gradient difference is now close to zero so that no further Ca entry or exit is to be expected. An equivalent statement is that Ca entry has inactivated.

Repolarization will now produce a large inward current and rapid Ca extrusion, E_{Ca} will rise toward normal diastolic values, and Ca extrusion will decline in magnitude.

It is usual to suppose that the Na-Ca exchange mechanism is at equilibrium during diastole, but this, in fact, may not always be the case. One may distinguish two cases: (a) Na-Ca exchange is the sole mechanism for Ca efflux, and (b) there is both an ATP-driven Ca efflux as well as Na-Ca exchange. Since in any real cardiac cell there are leaks of Ca inward via Na channels, Ca channels, and nonspecific leakage pathways, then a steady state is one where (Ca leakage influx + Ca influx via Na-Ca) = (Ca efflux). If (a) above is the case, then the Na-Ca system cannot be at equilibrium; while for (b), if the ATP-driven Ca efflux matches the leakage Ca influx, then the Na-Ca can be at equilibrium. The word "can" needs to be emphasized because, even if an ATP-driven pump takes care of resting Ca leaks, a reversal of Ca entry via channels and via Na-Ca exchange during depolarization requires time—if the beat interval is of insufficient duration, then Na-Ca exchange will not reach equilibrium even though $[Ca]_i$ may be below the threshold for contractile activation. This means that during the diastolic phase of the action potential there is always a net extrusion of Ca, and equilibrium can be reached only if a very long interval without a beat is allowed to take place. Similarly, a nonequilibrium of Na-Ca exchange will alter the extent to which Ca entry can take place by Na-Ca exchange during the systolic phase of the action potential.

TABLE 10–1. The reversal potential for the Na-Ca carrier and the electrochemical potential difference between Na and Ca if r = 3 or 4 and E_{Ca} and E_{Na} are as indicated

E_{Ca}	E_{Na}	E_R	Gradient at Resting E_m
$r=4$	$4(E_m - E_{Na}) - 2(E_m - E_{Ca}) =$ ⟶		
145	50	−45	−80
145	70	−5	−160
120	50	−20	−130
120	70	+20	−210
$r=3$	$3(E_m - E_{Na}) - 2(E_m - E_{Ca}) =$ ⟶		
145	50	−140	+55
145	70	−80	−5
120	50	−90	+5
120	70	−30	−55

The Kinetic Properties of Na-Ca Exchange

The thermodynamic analysis already presented has suggested that the difference between the Na and Ca electrochemical gradients might be a parameter that determines the magnitude of the net flux of the exchange system. Before accepting this conclusion, it is useful to examine the responses that can be observed in squid giant axons to the changes in the Na and Ca gradients as these affect Ca entry. In the first place, if Na_0 is made 1 mM and Na_i remains at about 20 mM, then E_{Na} is −75 mV as compared with a normal value of +70 mV when Na_0 is normal. This is a 145-mV change in E_{Na}, yet it produces a rather modest increase in Ca influx of about 33-fold (an increase from about 30 to 1000 fmol/cm^{2}s). If, instead of changing E_{Na}, we change E_m by 60 mV, the

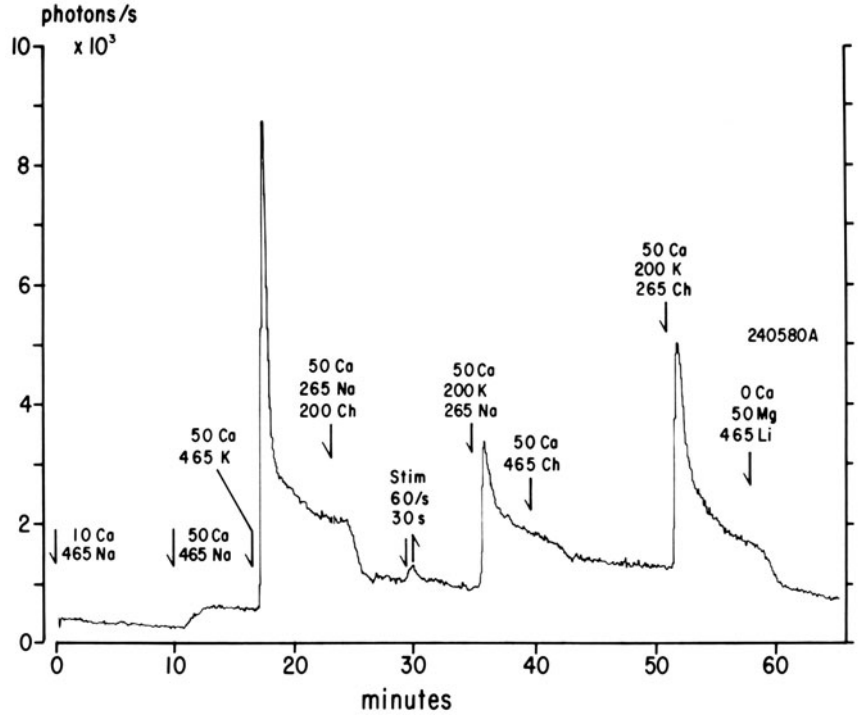

FIGURE 10–5. Aequorin light emission (as photon/s) is shown as a function of time for the changes in external solutions surrounding a squid axon as shown in the labels (Mullins and Requena, unpublished data).

result is a more than 300-fold change in Ca entry to levels that approach 50 pmol/cm^{2}s. How is it possible that a 60-mV change in membrane potential can produce a tenfold larger Ca entry than a 150-mV change in E_{Na}. To understand this result it is necessary to examine where the rate-limiting steps in the transport reaction occur under a variety of circumstances.

If $[Ca]_i$ is low, membrane potential normal, and there is a normal Na_0, then it seems likely that the rate-limiting step in the transport reaction for Ca efflux is the binding of Ca to the carrier at the inside of the membrane. Note that the other steps in the transport reaction (Ca transport outward, external Na binding, membrane potential) all would appear to be at saturating levels. By contrast, for the Ca influx reaction, $[Ca]_0$ would appear to be saturating, and $[Na]_i$ less than half-saturating while a high (negative) membrane potential would seem to be the principal barrier preventing carrier factor of 3–5 in more carrier for influx while a release of the electrical barrier to carrier translocation could in principle have a greatly increased role in bringing Ca into the cell.

Actual measurements with aequorin-injected squid axons show (fig. 10–5) that light emission is maximal if all Na_0 is replaced with K_0 (and E_m is therefore about +5 mV). If 265 m*M* Na is retained (and this is a saturating concentration for the Na-binding system), the response to 200 m*M* K is two-thirds that of total replacement of Na with choline. By way of calibration of these responses, a stimulation of the fiber for 1800 impulses in 30 s gives an extra Ca entry of stimulation (as measured with ^{45}Ca) of 90 pmol/cm^2 or 3 pmol/cm^{2}s. The results of this experiment are persuasive to the view that the rate-limiting step in Ca entry (with a fixed $[Na]_i$) is in overcoming the kinetic barrier posed by the membrane potential rather than E_{Na} since the responses at constant E_{Na} but differing E_m (first and last responses to

steady depolarization of fig. 10–5) differ only by a factor of 2, a result consistent with the greater depolarization produced by 450 vs 200 mM K^+. The results are opposed to the view that Na_0 and Ca_0 compete for a common site on a carrier.

The results in figure 10–5 also show that upon repolarization the rate of decline of light is highly dependent on whether or not Na is present in seawater (compare first repolarization [Na seawater] with second [choline seawater]). These observations suggest that Ca extrusion by Na-Ca exchange is important in reducing $[Ca]_i$.

The influx of Ca via Na-Ca exchange ought, according to the separate site model and the requirements for Na stoichiometry already discussed, be written as

$$4Na_i + X_i \rightleftarrows Na_4X_iY_0 \quad (1)$$

$$Ca_0 + Na_4X_iY_0 \rightleftarrows Na_4X_iY_0Ca \quad (2)$$

$$Na_4X_iY_0Ca \rightleftarrows Na_4X_0Y_0Ca \quad (3)$$

$$Na_4X_0Y_iCa \rightleftarrows X_0Y_iCa + 4Na_0 \quad (4)$$

$$X_0Y_iCa\ X_0 + Ca_i \quad (5)$$

$$X_0 \rightleftarrows X_i \quad (6)$$

where X is a Na-binding site and Y is a Ca-binding site that appears when sufficient Na is present for translocation. Reaction 1 emphasizes the essential nature of $[Na]_i$ in initiating the carrier reaction leading to Ca entry. An experiment is shown in figure 10–6 where using squid axons that are injected with aequorin we obtain (left-hand trace) the same response to depolarization as shown in figure 10–5. The axon was then stimulated in Li seawater, a treatment that has been shown to reduce $[Na]_i$ to about one-half its initial value. A retest of the response to depolarization now shows that the response is one-sixth of its former value while restimulating the axon in Na seawater to return $[Na]_i$ to its initial value leads to a recovery of the initial response.

In addition to $[Na]_i$, reaction 1 requires a supply of X_i. Now the total carrier X_T consists of $X_0 + X_i + Na_nX_0 + Na_nX_i$ where the symbol Na_nX refers to all the forms of X in combination with Na. Thus if Na_0 is at saturating concentrations, we have carrier in the forms of NaX_0, Na_2X_0, Na_3X_0, $Na_4X_0Y_i$ and all of this X_0 in its various combined states is unavailable as X_i. We conclude, therefore, that $[Na]_0$ is a parameter that can affect the concentration of X_i.

Reaction 2 is the binding of Ca_0 to the Na-carrier complex. Recent measurements on squid axons show that half-saturating concentration of Ca_0 is 0.5 mM and, since seawater is 10 mM in Ca, it is to be expected that at physiologic values of Ca_0 the Ca influx reaction is substantially saturated. The translocation of Na outward and Ca inward is reaction 3. Since two net charges move outward in this step, it is clear that the membrane potential will have a significant effect on this step in the transport reaction. Indeed, since depolarization of squid axons leads to the largest Ca influx of any experimental procedure, it is reasonable to suppose that with saturating $[Na]_i$, $[Ca]_0$ reaction 3 is the rate-limiting step for Ca influx. Reaction 4 is the dissociation of Na from the complex—it is difficult to tell whether this reaction or the increase of X_i (reaction 1) as a result of making $Na_0 = 0$ is the more important in producing the enhanced Ca influx known to occur under Na-free conditions. It is clear, however, that the Ca influx produced Na-free solutions is much less than the Ca influx induced by reducing E_m to zero. The reaction 5 ought not to be rate limiting while reaction 6 returns the carrier to recycle. If the empty carrier has a charge, then this reaction would also be potential sensitive. This reaction might be slower than if the carrier is returned by the efflux of Ca (i.e., conditions where Ca influx and efflux balance), but again there is insufficient information presently available to be certain about this point

The equation $2E_{Na} - E_{Ca} - E = 0$ is thermodynamic and defines the balance point between where the net flux of Ca is inward or outward. It says nothing about the magnitude of this flux and the point to be discussed now is how the value of the Ca flux is set both for conditions at equilibrium and for conditions far from equilibrium. It is useful to note that values of $[Na]_i/[Na]_0$ of 1:15 can be obtained by $[Na]_i = 1$ mM and $[Na]_0 = 15$ mM as well as by $[Na]_i = 10$ mM and $[Na]_0 = 150$ mM.

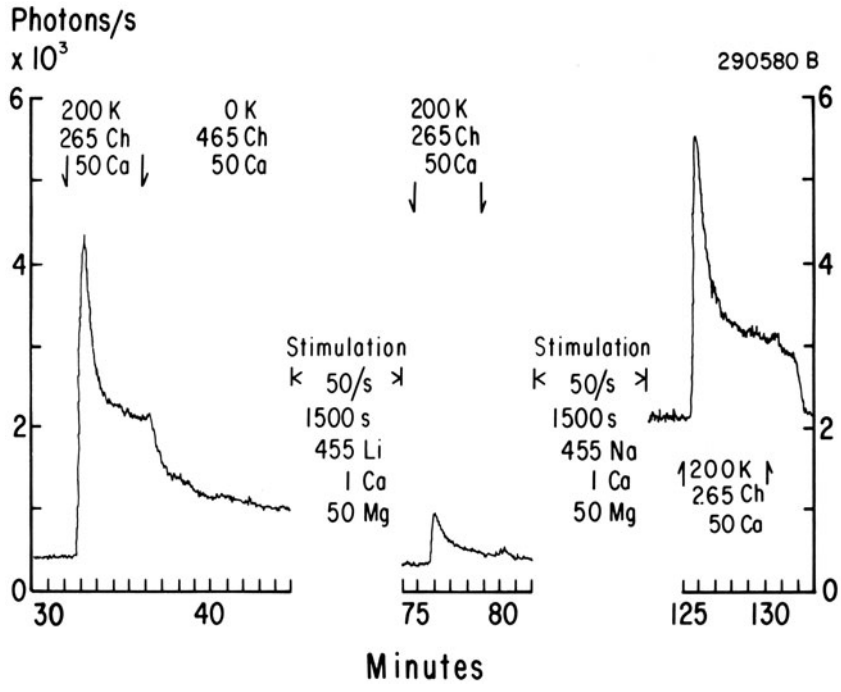

FIGURE 10–6. After a test depolarization with 200 m*M* K, 265 m*M* choline, 50 m*M* Ca seawater, an aequorin-injected axon was stimulated in Li seawater (1 m*M* Ca, 50 m*M* Mg), thus reducing $[Na]_i$ to half its initial value. The response of the axon was then one-eighth of its initial value. A restimulation of the axon in Na seawater (returning $[Na]_i$ to initial values) returned Ca entry to original values (Mullins and Requena, unpublished observations).

For both cases, E_{Na} is identical, but in the first case the fluxes of Ca by Na-Ca exchange will be very small while in the latter case they will be much larger. This is so because Na-Ca exchange involves a reaction between a carrier and Na such that NaX is formed—the first step in reaction 1 above. It has been argued earlier that it is the species Na_4X that is the likely exchanger for a Ca. This can be formed by NaX reacting with another Na to form Na_2X and so on to finally form Na_4X. The practical consequences of this arrangement are that, for high values of [Na], all of the X is combined with Na (and some of it in the form Na_4X); while, for low values of [Na], there is little NaX (and vanishingly little Na_4X)—most of the carrier X is free. Thus the flux of Ca will depend on [Na] and this will be a steep or power function since multiple Na are required to form the proper carrier complex.

A second property of the Na-Ca exchange system is that, with X having a finite value, there is the fact that X will be partitioned between the two membrane surfaces (outside, inside) in proportion to some function of the [Na] at those surfaces. It is clear that if $[Na]_0$ is saturating and $[Na]_i$ is gradually increased, carrier that was preempted by Na_0 is now made available for the carriage of Ca_0 inward by Na_i. The actual relation are relatively complex when both Na and Ca movements must be considered, but to see how the system works it is convenient to consider the carrier only in the presence of Na. Under these conditions, no actual transport is possible, but the effect of Na on carrier partitioning can be noted.

Condition	Carrier
$[Na]_0 = [Na]_i = 0$	$[X] = [X]_i = 0.5$
$[Na]_0 = [Na]_i$	$[X]_0 = [X]_i$
	$[Na_4X]_0 = [Na_4X]_i$

If Ca is being transported inward and outward at equal rates by the carrier, then the

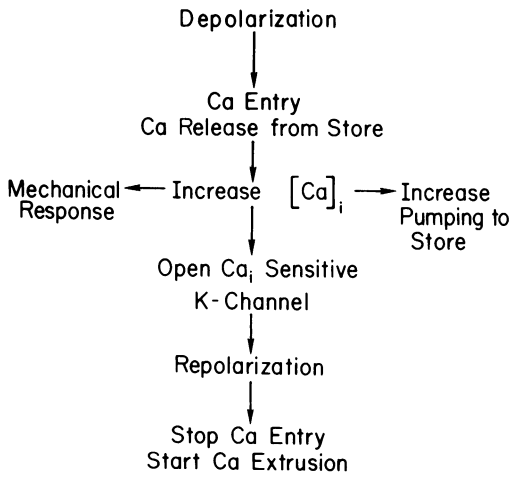

FIGURE 10–7. The sequence of events occurring when a cardiac cell is depolarized.

fluxes of both Na and X inward and outward are also equal. If, now, Ca is removed from the bathing solution so that Ca_0 falls to zero, the carrier reaction must shift to a new one.

$$Na_0 + 4X_0 \rightleftharpoons Na_4X_0Y_i \quad (1)$$
$$Na_4X_0Y_i + Ca_i \rightleftharpoons Na_4X_0Y_iCa \quad (2)$$
$$Na_4X_0Y_iCa \rightleftharpoons Na_4X_iY_0Ca \quad (3)$$
$$Na_4X_iY_0Ca \rightleftharpoons X_iY_0Ca + 4Na_i \quad (4)$$
$$X_iY_0Ca \rightleftharpoons Ca_0 + X_i \quad (5)$$
$$X_i \rightleftharpoons X_0 \quad (6)$$

If the last reaction—the translocation of X_i to X_0 which formerly occurred by an influx of Ca equal to its efflux—is slower than the Ca influx reaction, then a new rate-limiting step in the transport sequence will develop (a shortage of X_0) and Ca efflux will fall. Experimentally Ca_0-free conditions sometimes show such a reaction and it is usually thought of as providing evidence for a Ca-Ca exchange. The analysis above is an alternate explanation of such findings.

The Application of Na-Ca Exchange to Cardiac Contraction

Each sort of cardiac cell has an action-potential-generating system that has as a common feature the production of long duration (many hundred millisecond) depolarizations. Unlike nerve cells, cardiac cells have much higher than normal membrane resistances during depolarization and indeed the cells take extraordinary measures to protect themselves against K loss, which is the usual consequence of steady electrical depolarization in nerve fibers. As noted earlier in this chapter, if the reversal potential for Na-Ca exchange is around -40 mV, then at the resting potential the Na-Ca exchange mechanism is extruding previously accumulated Ca while during the plateau of the action potential the fiber should be gaining Ca. This gain can come about both by the entry of Ca via excitable Ca channels that open with depolarization and by the Na/Ca exchange operating such that it exchanges Ca_O for Na_i. The general arrangement for Ca movement in cardiac cells is shown in figure 10–7, where the initiating event is a depolarization generated by the action potential. In addition to the two sources of Ca entry mentioned above, there is also a release of internally stored Ca and these three sources of Ca go to increase the free internal Ca and this rise, in turn, has three effects: (a) it leads to the mechanical response of contraction, (b) it increases the rate of pumping of Ca back into the store (sarcoplasmic reticulum), and (c) it activates a Ca-sensitive K channel that is in part responsible for repolarization of the cell. The repolarization itself then stops all Ca entry by closing Ca channels and by reversing the direction of Na-Ca exchange which brings about Ca extrusion. Note that there are two processes that bring down $[Ca]_i$: the increase in pumping rate to the interal store and the Na-Ca exchange. There may well be an ATP-driven membrane pump as well that runs at a rate proportional to $[Ca]_i$, in addition, but given the large energy of ATP hydrolysis it cannot be expected to be a membrane-potential-sensitive mechanism. A consequence of this arrangement is, however, that virtually all the increased Ca that occurs in a fiber as a result of depolarization may be taken up by the store (sarcoplasmic reticulum, SR) so that relaxation occurs while the membrane is depolarized. The SR cannot continue to function in this way over many beats since it would rapidly accumulate Ca. Hence it is necessary to suppose that during membrane repolarization the Na-Ca exchange

which is reactivated to extrude Ca now pumps $[Ca]_i$ to very low values and that, at such low values, the Ca of the SR leaks out into the myoplasm and is pumped away by Ca pumps in the surface membrane.

The arrangement described above is not the only one possible; in frog cardiac cells the evidence is that relaxation follows membrane repolarization and that the rate of relaxation is quite dependent on $[Na]_0$; both of these findings are expected if Na-Ca exchange is the immediate mechanism in bringing about relaxation. Why does Ca extrusion depend on both $[Na]_0$ and membrane potential? The operation of the Na-Ca exchange carrier requires that Ca_i be exchanged for Na_0 (hence, the requirement for Na_0) and, if a 4 Na enter per 1 Ca extruded, then a large negative membrane potential will favor Na entry (and the coupled Ca exit).

To summarize the situation with respect to the relaxation of cardiac cells, one can distinguish two mechanisms for bringing this about: (a) a membrane-potential-independent movement of Ca from the myoplasm to the SR followed by a removal of a substantial part of this Ca by surface membrane pumps, and (b) a direct removal of Ca from the myoplasm via surface membrane pumps that are dependent on the Na electrochemical potential (i.e., Na-Ca exchange).

It may be useful at this juncture to make a statement regarding how cardiac excitation–contraction coupling was thought to occur five years ago, what changes in this viewpoint have occurred in this more recent period, and what the evidence is for Na-Ca exchange assuming a more dominant role. The general idea in 1978 was that Ca for contraction was derived from entry via slow channels and from the SR with the relative amounts from these two sources in some dispute [4]. Since these two sources of contractile Ca are fully presented in this volume in the chapters by McDonald and Fabiato, I can safely leave the resolution to them. It was also generally conceded that an electroneutral Na-Ca exchange played a role in (a) the contraction produced by Na-free soluions, and in (b) extruding Ca from the fiber when $[Ca]_i$ became high. Modification of ideas about Na-Ca exchange became necessary with the recognition that this process was sensitive to membrane potential and that, as noted earlier in this chapter, it could contribute Ca to the cardiac cell with depolarization. That Na-Ca exchange is electrogenic or at least voltage sensitive seems beyond reasonable doubt since studies in squid axons [7], in cardiac sarcolemmal vesicles [8], and in cardiac cells [9] all find this to be the case.

This single change from an electroneutral to an electrogenic Na-Ca exchange requires a substantial revision of many features of excitation–contraction coupling that had been thought to be settled. For example, an electroneutral exchange would result in one having maximal Ca entry by removing external Na with a normal membrane potential. Actually, there is a much larger entry in Na-free when the membrane potential is decreased below the reversal potential of Na-Ca exchange E_R. There is also a slow inward current with depolarization, subtracting from this an outward current produced by Ca entry in exchange for more Na charges moving outward than Ca charges moving inward. It is not strange, therefore, that it has proved difficult to relate slow inward current to contraction in all cases.

There are at present no inhibitors that will differentially act on either Na-Ca exchange or slow-channel current despite some claims to the contrary so that a separation of these oppositely directed currents by pharmacologic means is simply not possible. What can be done is to lower $[Na]_i$ by either speeding the rate of Na-K pumping or slowing the rate of inward leak of Na by lowering Na_o slightly; this change in Na_i will (as in fig. 10–6) virtually abolish Ca entry via Na-Ca. This finding is, itself, experimental evidence in support of an electrogenic Na-Ca exchange, as the following analysis will show. The expression for a coupling of 4 Na to 1 Ca ($E = 2E_{Na} - E_{Ca}$) can be rewritten by taking antilogarithms of both sides as

$$[Ca]_0 ([Na]_i)^4 k = [Ca]_i ([Na]_0)^4 k^{-1}$$

where k is $\exp E_m F/RT$ times a constant. Now the form of this expression is a product of Ca_0, Na_i which is the right sort to be related to Ca influx that is dependent on Na_i and the mem-

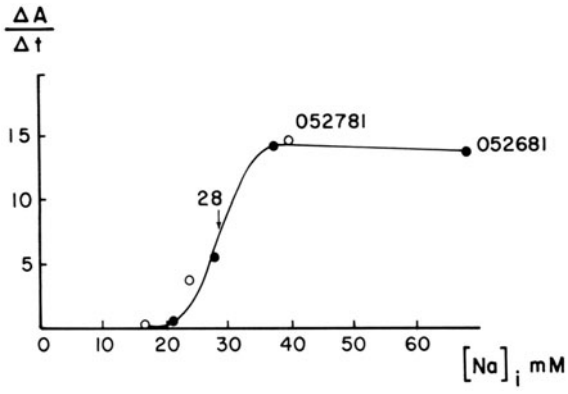

FIGURE 10–8. The rate of entry of Ca judged by a change in arsenazo-III absorbance in response to a depolarization of 65 mV is plotted against $[Na]_i$ in a squid axon. The data for two axons are shown. Note that entry is half-maximal when $[Na]_i$ = 28 m*M* and is not measurable at 20 m*M* (from ref. 11).

brane potential dependence is such that Ca influx will increase as depolarization proceeds. Since $[Ca]_0$ and $[Na]_0$ are well regulated in the animal body, we can rearrange the above expression as follows:

$$[Ca]_i = ([Na]_i)^4 a \exp 2E_mF/RT$$

Where *a* is $[Ca]_0/([Na]_0)^4$ times a constant. We conclude therefore that, at equilibrium, the internal Ca concentration is proportional to the power 4th of Na_i multiplied by a term in membrane potential. Note that this relationship required $[Ca]_i$ (and hence the contractile state) to be low if $[Na]_i$ is small or if membrane potential is large and negative. If $[Ca]_i$ is beyond some threshold value, then a steady tension will be developed in cardiac fibers that is (within limits) proportional to $[Ca]_i$. In a recent study [10] of cardiac Purkinje fibers that were impaled with Na_i-sensing electrodes and subjected to voltage clamp, it was found that steady tension was increased as $[Na]_i$ increased, but only if the membrane potential were low. At hyperpolarized values, changes in $[Na]_i$ had no effect on tension, thus leading to the conclusion that it was the product of $(Na_i)(E_m)$ that was controlling $[Ca]_i$. At constant E_m, tension was proportional to the 3.7 power of $[Na]_i$, while at constant $[Na]_i$ tension was proportional to exp $E_m/16.5$ mV. Note that this is close to $1.5E_mF/RT$.

Another finding [11] is shown as figure 10–8. Here, a squid axon was injected with arsenazo III, a dye that senses free Ca in the fiber. Spectrophotometry allows the experimenter to measure the fraction of the dye complexed with Ca and by suitable calibration to relate this to free Ca concentration in axoplasm. When this is done, the results of figure 10–8 show that it is possible to relate Ca influx during a depolarization to the internal [Na] as measured with a Na-sensitive electrode. The relationship between $[Na]_i$ and rate of Ca entry is very steep, as the coefficient in a Hill plot is 7, implying a high order of kinetic complexity of the carrier. Both the observations cited above strongly support the notion that Ca entry with depolarization that is Na_i dependent involves an interaction of more than 3 Na with a carrier and makes the entry both potential and delicately sensitive to $[Na]_i$.

The discussion so far has assumed that all of the Ca that enters a nerve or muscle fiber goes to increase $[Ca]_i$, whereas the usual situation is that most of the entering Ca is quickly sequestered by various intracellular Ca-binding entities such as mitochondria, sarcoplasmic reticulum in muscle or endoplasmic reticulum in nerve, and the contractile protein troponin C in muscle. The squid giant axon has an advantage for studies of this sort in that Ca entry over a time scale of 1 min can be shown to be solely the result of Na-Ca exchange if Na channels are blocked with tetrodotoxin (TTX). Part of the Ca entry is buffered by endoplasmic reticulum and part by mitochondria (if $[Ca]_i$ is high enough). The mitochondrial uptake of Ca can be totally blocked by CN (without affecting axoplasmic [ATP] if exposures to CN are limited to 100 min). An experiment with an aequorin-injected squid axon is shown in figure 10–9A. Here we are plotting photons/s emited by aequorin vs time for an axon in 50 m*M* Ca seawater (15 times normal) in CN seawater. There is known to be an increased entry of Ca over its exit, yet light emission with time is constant over periods of more than 1 h. A change from Na seawater to a choline-containing one leads to an abrupt increase in measured

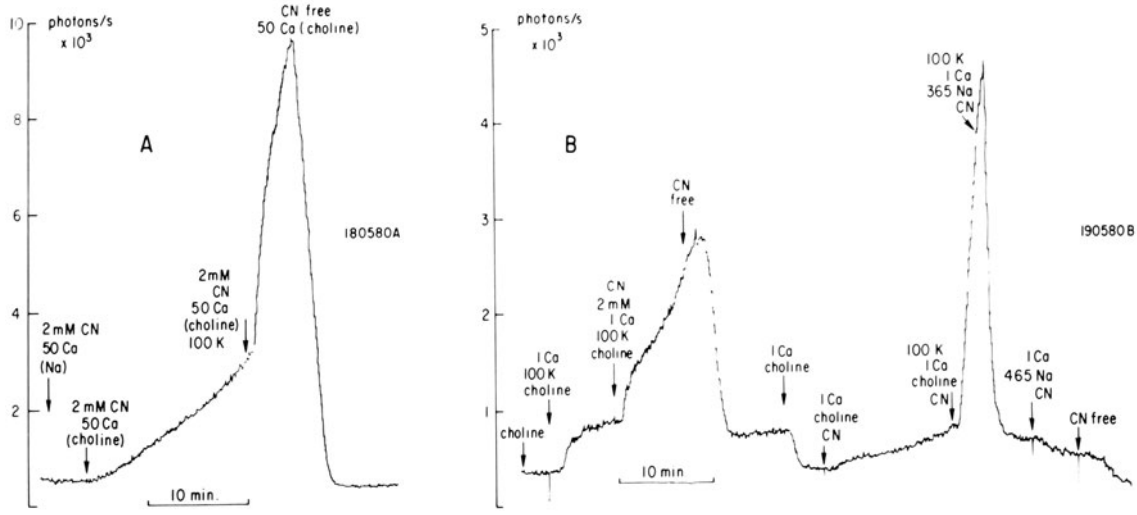

FIGURE 10–9. The light emission from aequorin-injected axons as a function of time is shown. *(A)* An axon in 50 mM Ca seawater with CN is treated with choline in exchange for Na and then depolarized with 100 m*M* K. *(B)* The Ca in seawater is only 1 m*M* (50 m*M* Mg) so that Ca entry by Na-Ca exchange will remain saturated ($K_{1/2}$ = 0.5 m*M*), but Ca entry via Na and K channels will be minimal. The extra Ca entry involved in making Na_0 zero can be buffered by mitochondria and a second finding is that an axon depolarized with 100 m*M* K in the presence of CN can have its Ca_i returned to normal by a simple change of the principal cation from choline in Na (Requena and Mullins, unpublished data).

$[Ca]_i$ that will continue indefinitely. Clearly the mitochondria were not involved in Ca buffering since they were blocked with CN before the change to choline, so we conclude that Ca is now entering faster than the endoplasmic reticulum can buffer it. A small (20 mV) depolarization occasioned by adding 100 m*M* K to the choline–CN seawater greatly enhances the rate of entry of Ca and the process is totally reversed by removing CN and 100 m*M* K. Since Ca extrusion from the nerve fiber is very small, it is clear that it is the removal of CN that allows the mitochondria to effect this rapid decline in $[Ca]_i$. In another axon, (fig. 10–9B), a treatment with 100 m*M* K–choline leads roughly to a doubling of the aequorin light signal when Ca_0 is 1 m*M* instead of 50 m*M* in the part A of the figure. Adding CN to the 100 m*M* K–choline–CN seawater leads to an increase in light that will continue indefinitely. The finding shows that the apparent plateau was the result of Ca entry and its sequestration by the mitochondria being in balance. Thus when mitochondrial uptake was eliminated by CN, ionized Ca increased. Note that the original threshold in 100 K–choline was recovered when CN was removed as was the initial glow when 100 m*M* K was removed. If the experiment is repeated without 100 m*M* K, but with CN, there is a small Ca entry from choline seawater that will continue indefinitely and an abrupt rise when CN is applied, showing the mitochondrial contribution to the control of $[Ca]_i$. To reverse this abrupt rise, a removal of CN is not necessary nor is repolarization necessary since a change from choline to Na in the seawater reduced Ca net flux sufficiently to bring down $[Ca]_i$ to control levels. The point of these observations is that $[Ca]_i$ cannot be predicted from the expected effects of a particular treatment on Ca influx or efflux without a detailed consideration of how the Ca-complexing entities in the cell will react. In a cardiac cell, electron-transport-blocking substances such as CN cannot be applied for very long without a total breakdown of ATP and hence a failure of both Na-K trans port and Ca pumping into the SR, but it must be expected that any tendency of conditions to

inhibit accumulation of Ca by internal Ca-sequestering mechanisms will affect the contractile process.

A Regulatory Role in Heart

There is every reason to believe that, in cardiac cells of a variety of types, Na-Ca exchange is the principal mode whereby Ca that enters with depolarization is removed from the cell during repolarization (diastole). Since, as we have seen above, Ca_0, Na_0, and E_m are likely to remain fixed during diastole, one must suppose that Ca efflux from cardiac cells is solely influenced by the $[Ca]_i$ that exists at any instant in time. Now, a rise in $[Ca]_i$ may also be expected to lead to an increase in Ca stored in the SR since the pump rate from myoplasm to SR may be expected to be influenced by the [Ca] in myoplasm, at least for values below saturation. The foregoing suggests that, if conditions are manipulated such that more Ca enters a cardiac fiber, then both the outward extrusion of this ion and its storage in the SR will be enhanced.

Since heart is subjected to greatly varying demands for cardiac output, it must have reliable mechanisms for increasing both the rate of beat and strength of contraction per beat in order to satisfy the highly variable demands of the circulation. What is to be discussed here is how Na-Ca exchange may contribute to the regulation of cardiac output. Since output is the product of rate $\times$ stroke volume, it is convenient to see whether Na-Ca exchange may be involved in controlling rate. The rate of beat is normally fixed by the SA node, whose cells have characteristics somewhat different from contractile cardiac tissues. First, the resting potential is low (perhaps -55 mV) and, second, the action potential is a slow or Ca-channel-mediated change. From the standpoint of Na-Ca exchange, the low resting potential may be expected to lead to an elevated $[Ca]_i$ from the relations given between $[Ca]_i$ and E_m earlier in this chapter. A second feature of such cells is that, if an agent such as epinephrine leads to an enhanced Ca entry via Ca channels and to an enhanced Ca release from the SR, then the resulting higher $[Ca]_i$ must be expected to lead to a larger inward current during diastole that is the result of Na-Ca exchange. Thus the relationship between rate of firing of pacemaking cells and Na-Ca exchange might be as follows: epinephrine $\rightarrow$ increased Ca-channel current $\rightarrow$ increased $[Ca]_i$ $\rightarrow$ increased Na-Ca exchange (inward current–diastole) $\rightarrow$ faster diastolic depolarization $\rightarrow$ more rapid firing rate. In parallel, there is an increase in $[Na]_i$ and hence in outward Na pump current.

In tension-developing cells, the increased rate of firing produced by more frequent discharge of pacemaking cells means that more Na enters cardiac fibers per unit time both from more frequent excitation of Na cells and, more importantly, from the need for more frequent extrusion of the Ca entering with each impulse. Thus: epinephrine $\rightarrow$ increased Ca-channel entry (systolic) $\rightarrow$ increased $[Ca]_i$ $\rightarrow$ increased $[Na]_i$ $\rightarrow$ increased Ca entry during depolarization (Na-Ca exchange) $\rightarrow$ increased tension with depolarization. The analysis presented above suggests therefore that Na-Ca exchange can exert a regulatory role both on the rate of firing of the heart and on the magnitude of the contraction produced by each beat.

It is to be emphasized that, with $[Na]_i$ determined by the summation of all Na leaks through channels or other mechanisms as well as by Na-Ca exchange during the depolarizing phase of the action potential, artificial interventions (such as ouabain) that might decrease the velocity of Na pumping via the Na-K pump will provide an additional way of increasing $[Na]_i$ and, hence, of increasing the contractile force per beat. The relationship between $[Na]_i$ and tension is very steep with a negligible effect at low values and a region of $[Na]_i$ where an increase of 1 m*M* produces a clear increase in tension. Such a result is understandable only if Ca influx is related to $[Na]_i$ as a power function where a power of 4 or greater is required [10].

Another way of influencing $[Na]_i$ is not to inhibit the Na-K pump, but to reduce the inward leak of Na, a procedure that will lead to a decrease in $[Na]_i$. For small changes in $[Na]_o$ around the normal value of 150 m*M*, Na influx will be linear with concentration so that, for example, a 5% decrease in plasma Na ought to be reflected in a 5% decrease in $[Na]_i$. This is

probably in the range where a detectable effect on Na-Ca exchange can be produced so that this change (of the order of 0.5 m*M* Na_i) may exert a significant effect on contractile force. Slowing of the heart rate will also produce a lowering of $[Na]_i$ not only because there are fewer depolarizations and, hence, less Na entry by Na channels, but also because fewer beats mean less Ca entry (from either channels or Na-Ca) per unit time and, hence, less Na entry is necessary to expel the entering Ca. A lower $[Na]_i$ means also a larger Na electrochemical gradient (E_{Na} is larger), hence a lower resting or diastolic value for $[Ca]_i$ which should lead to a lesser amount of Ca stored in the SR since SR storage ought to reflect the time average $[Ca]_i$. A review of the evidence for these points is given in Mullins [13].

Summary

Recent studies, especially with Na-sensing electrodes in cardiac cells, have revealed the critical role that $[Na]_i$ plays in determining not only the steady (tonic) tension that may be present, but also the magnitude of the transient (phasic) tension resulting from depolarization. A relatively simple explanation for these somewhat surprising findings is that an old and well-described process—Na-Ca exchange—is electrogenic and therefore is sensitive to membrane potential. This single assumption is able to explain why Na_o-free solutions are less effective in causing Ca entry in cells than is depolarization (in spite of the fact that depolarization also leads to other modes of Ca entry into the myoplasm). It also allows one to understand the mode of action of cardiac glycosides and to explain the differences in the way that cardiac cells relax. Throughout this analysis, the one principle that emerges is the extraordinary regulatory role that $[Na]_i$ plays in the control of cardiac contractility. Since the value of $[Na]_i$ is set by the Na-K pump and the external [Na], a role for the intake and excretion of Na by the whole organism is clearly connected to the regulation of cardiac contractility.

References

1. Langer GA: Sodium–calcium exchange in the heart. Annu Rev Physiol 44:389–400, 1982.
2. Fabiato A, Fabiato F: Calcium and cardiac excitation–contraction coupling. Annu Rev Physiol 41:473–484, 1979.
3. Chapman RA: Excitation–contraction coupling in cardiac muscle. Prog Biophys Mol Biol 35:1–52, 1979.
4. Fozzard HA: Heart: excitation–contraction coupling. Annu Rev Physiol 39:201–220, 1977.
5. Mullins LJ: Ion Transport in Heart. Raven Press, New York, 1981.
6. Reuter H, and Seitz N.: The dependence of Ca efflux from cardiac muscle on ion composition. J. Physiol 195:451–470, 1968.
7. Mullins LJ, Requena J: The "late" Ca channel in squid axons. J Gen Physiol 78:683–700, 1981.
8. Pitts BJR: Stoichiometry of sodium–calcium exchange in cardiac sarcolemmal vesicles. J Biol Chem 254:6232–6235, 1979.
9. Chapman RA, Tunstall J: The interaction of Na and Ca ions at the cell membrane and the control of contractile strength in frog atrial muscle. J Physiol 305:109–123, 1980.
10. Eisner D, Lederer WJ, Vaughan-Jones R: The control of tonic tension by membrane potential and intracellular Na activity in the sheep cardiac Purkinje fibre. J Physiol, 335:723–743, 1983.
11. Mullins LJ, Tiffert T, Vassort G, Whittembury J: The effects of internal Na^+ and H^+ and of external Ca^{++} and membrane potential on Ca entry in squid axons. J Physiol, 338:295–319, 1983.
12. Eisner DA, Lederer WJ, Vaughan-Jones R: The dependence of sodium pumping and tension on intracellular sodium activity in voltage-clamped sheep Purkinje fibres. J Physiol (Lond) 317:163–187, 1981.
13. Mullins LJ: The generation of electric currents in cardiac fibers by Na/Ca exchange. Am J Physiol 263:C103–C110, 1979.

11. METHODS FOR DETECTING CALCIUM RELEASE FROM THE SARCOPLASMIC RETICULUM OF SKINNED CARDIAC CELLS AND THE RELATIONSHIPS BETWEEN CALCULATED TRANSSARCOLEMMAL CALCIUM MOVEMENTS AND CALCIUM RELEASE

Alexandre Fabiato
and Clive Marc Baumgarten

Introduction

The mechanism of excitation–contraction coupling is not established for any type of muscle [1–3]. In cardiac muscle there is not even universal agreement on whether Ca^{2+} is released from the sarcoplasmic reticulum (SR) during excitation–contraction coupling. This will be the first question addressed in this chapter. In the discussion of this question, emphasis will be placed on the quantification of the Ca^{2+} fluxes across the sarcolemma and their possible relationships with the Ca^{2+} movements in and out of the SR. A detailed description of the simple calculations that permit this correlation will provide a tool for a critical analysis of the literature.

The second question addressed in this chapter will concern the mechanism of the possible Ca^{2+} release from the SR. To answer this question, it will be necessary to evaluate the different methods used for detecting Ca^{2+} release from skinned cardiac cells (preparations from which the sarcolemma has been removed). In this critical appraisal we found it appropriate to include previously unpublished data concerning the use of Ca^{2+} ion-selective electrodes for recording the transient Ca^{2+} release from the SR of skinned cardiac cells (fig. 11–6). Then, the arguments for and against the hypothesis of a Ca^{2+}-induced release of Ca^{2+} from the SR [1, 2] will be reviewed. The alternative hypotheses that have been proposed for the mechanism of Ca^{2+} release from the SR will not be discussed since they are reviewed in another article,[1] with the appraisal that all these alternative hypotheses, at least in their present form, can be eliminated on the basis of

The previously unpublished experimental studies and computations reported in this chapter were supported by grant HL19138 from the National Heart, Lung and Blood Institute to A.F., and by grants HL24847 from the National Heart, Lung and Blood Institute and 82–798 from the American Heart Association to C.M.B.

N. Sperelakis (ed.), PHYSIOLOGY AND PATHOPHYSIOLOGY OF THE HEART.

Martinus Nijhoff Publishing, Boston/The Hague/ Dordrecht/Lancaster.

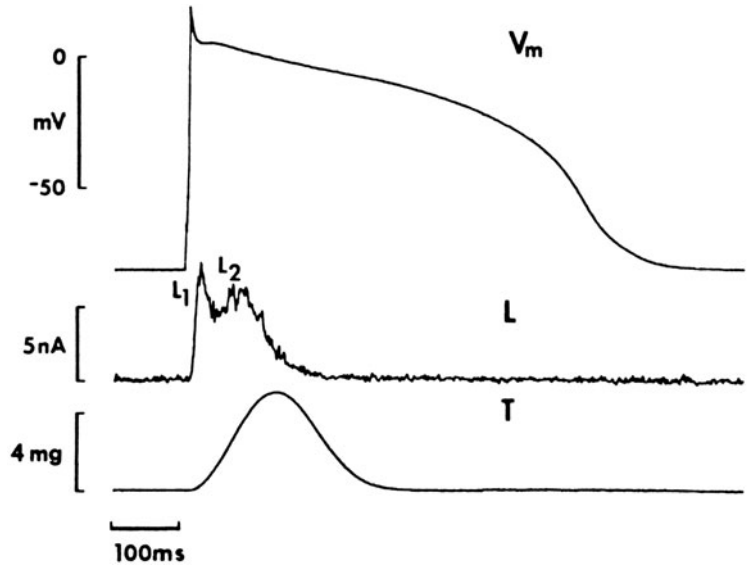

FIGURE 11–1. Fast (L_1) and slow (L_2) components of the aequorin bioluminescence signal in multicellular preparations from the dog Purkinje tissue. The membrane potential (V_m), aequorin bioluminescence (L), and tension (T) were simultaneously recorded from a 1.5-mm-long multicellular strand of Purkinje tissue from the dog. Aequorin had been injected by pressure microinjection into about 20 superficially located cells at the upper surface of the strand. The signals shown in this figure are the result of the averaging of about 100 signals. The aequorin bioluminescence was recorded with a photomultiplier tube to which light was transmitted by a lucite guide positioned beneath the transparent bottom of the recording chamber. The membrane potential was recorded with a conventional microelectrode and a high-impedance preamplifier. The resting potential was −82 mV. The action potential had an overshoot of +19 mV and a total duration of 680 ms. The stimulating currents were applied every 2 s through a second intracellular microelectrode. The action potential evokes a contraction which peaks within 130 ms and completely relaxes within about 250 ms. The onset of the aequorin signal precedes that of contraction, and its end also precedes the end of the relaxation. The differential response of the two components of the aequorin signal to the pattern of stimulation provides strong evidence that the initial component (L_1) corresponds to a Ca^{2+} influx across the sarcolemma while the second component (L_2) corresponds to Ca^{2+} release from an intracellular store. Reproduced from Figure 1 of Wier and Isenberg [9] with permission of the authors and of *Pflügers Archives*.

currently available data. This does not imply, however, that Ca^{2+}-induced Ca^{2+} release from the SR represents the physiologic mechanism of cardiac excitation–contraction coupling in the adult mammalian cardiac muscle. The conclusion that there is no compelling reason to eliminate this possibility is far from stating that it is the case.

The method for discussing the literature will consist of considering counterarguments and alternatives for each hypothesis presented [4] in order to emphasize how widely the field of cardiac excitation–contraction coupling is open to further experimental work. To maintain the discussion narrowly focused, some hypotheses or rationales will not be described in detail. Then, reference will be made to the most appropriate articles, generally selected because they present the points of view most strongly opposed to those taken in the present chapter.

Existence or Absence of Calcium Release from the Cardiac Sarcoplasmic Reticulum

EVIDENCE FOR A CALCIUM RELEASE FROM THE CARDIAC SARCOPLASMIC RETICULUM

Detailed analyses of the force–frequency relationship of the adult mammalian heart have generally been interpreted as evidence that the

Ca^{2+} influx across the sarcolemma during one action potential is not entirely used for activating the myofilaments during the corresponding contraction, but rather fills a store with Ca^{2+} that can be released during subsequent contractions [5–7]. These experiments do not, however, provide clues to the ultrastructural location of the Ca^{2+} store.

More direct evidence for a Ca^{2+} release from an internal store has been derived from experiments using the bioluminescence of aequorin to detect changes of myoplasmic free Ca^{2+} concentration ([free Ca^{2+}]) in multicellular preparations from the dog cardiac Purkinje tissue [8, 9]. In these preparations the aequorin signals present two components (fig. 11–1). The differential dependence of these two components upon the pattern of stimulation suggested that the first corresponds to a transsarcolemmal Ca^{2+} influx and the second to Ca^{2+} release from an internal store [8]. Voltage-clamp experiments showed that the transsarcolemmal Ca^{2+} influx had at least some characteristics expected for a Ca^{2+} current rather than for a carrier-mediated Ca^{2+} influx [9], but the location of the internal store from which Ca^{2+} would be released during the second component was not established.

Pharmacologic tools acting specifically on the SR would help in locating the Ca^{2+} store in the SR [10]. Caffeine has often been used for this purpose because it is well established that it specifically releases Ca^{2+} from the skeletal muscle SR. Unfortunately, the situation is more complex in cardiac muscle, where caffeine has multiple sites of action, including the sarcolemma [11]. The same type of criticism, a lack of specificity, can be made for the many other pharmacologic tools that have been used in an attempt to identify the SR as the Ca^{2+} storage site in cardiac muscle. Chapman's recent review [10] describes in detail the rationale for experiments using pharmacologic tools to dissect cardiac excitation–contraction coupling.

The evidence suggesting that the Ca^{2+} store is located in the SR comes mostly from experiments in preparations permitting direct access to the SR, including isolated SR vesicles and skinned cardiac cells. These studies demonstrate that the SR has the capacity to store the amount of Ca^{2+} necessary to activate the myofilaments sufficiently to produce the physiologic contraction [12–14]. In skinned cardiac cells it is possible to ascertain that the Ca^{2+} released by caffeine comes from the SR, since the sarcolemma has been removed [15]. It is also possible to destroy the ability of the SR to actively accumulate and release Ca^{2+} by detergent treatment; then the Ca^{2+} store disappears [15]. Some skinned cardiac cells, such as those from mammalian atrium [15], dog Purkinje tissue [16], and pigeon ventricle [16], do not contain transverse tubules. The observation of a Ca^{2+} release in these preparations demonstrates that the transverse tubules are not the Ca^{2+} storage site [15, 16]. Finally, the mitochondria do not appear to be able to accumulate Ca^{2+} when the myoplasmic [free Ca^{2+}] is in the physiologically relevant range, whereas they do accumulate Ca^{2+}, but extremely slowly, at unphysiologically high myoplasmic [free Ca^{2+}]. In addition, inhibitors and uncouplers of the mitochondrial respiration do not modify the Ca^{2+} release from the internal store at physiologically relevant myoplasmic [free Ca^{2+}] [15]. These findings demonstrate that the mitochondria cannot be the intracellular storage site. Therefore, the data from skinned cardiac cells permit the firm conclusion that Ca^{2+} can be released from the SR, at least in these preparations.

ARGUMENTS AGAINST A CALCIUM RELEASE FROM THE SARCOPLASMIC RETICULUM

Although the subcellular preparations permit a direct access to the SR, the techniques used to obtain them may damage this organelle and give it unphysiologic properties [2, 15]. This criticism is very difficult to answer in a definitive manner. Effort has been made to evaluate and correct some of the unphysiologic conditions of the skinned cardiac cells: unphysiologic level of myoplasmic [free Mg^{2+}] and of Ca^{2+} loading of the SR, swelling of the SR [15]. Nevertheless, it is obviously not possible to identify and correct all of the potentially unphysiologic conditions created by skinning of the membrane and substitution of computed solutions for the intracellular milieu. There-

fore, the conclusion that Ca^{2+} can be released from the SR is still widely open to alternative hypotheses. These hypotheses are of two types: (a) those admitting the presence of an intracellular Ca^{2+} store, but suggesting that its location is in structures other than the SR; and (b) those assuming that activation is possible by direct transsarcolemmal influx without the help of Ca^{2+} release from an internal store.

Among the first type of hypotheses suggesting an intracellular Ca^{2+} store different from the SR, it has been proposed that the mitochondria could be the storage site [17]. But this hypothesis has been almost completely abandoned because the affinity of the mitochondria for Ca^{2+} and their rate of Ca^{2+} accumulation and release are much too low with respect to the physiologic changes of myoplasmic [free Ca^{2+}] known to take place inside the cardiac cell [15, 18, 19].

Another hypothesis locates the store in high-affinity, "polarization-dependent" binding sites at the inner face of the sarcolemma [7, 20]. It has been proposed that these sites could be constituted of acidic lipids such as phosphatidylserine [20], which is observed in a high concentration in the isolated sarcolemmal preparation [21]. It is not possible to eliminate such a possibility, although it is not supported by any direct evidence. The concept of "polarization dependence" renders this hypothesis difficult to exclude. Otherwise, the Ca^{2+} binding sites studied in isolated sarcolemmal vesicles have a very low affinity (in the range of 10^4 M^{-1} at most) in the presence of the physiologic myoplasmic concentrations of K^+ and Mg^{2+} [22, 23]. Yet, even if this hypothesis were supported by data, the presence of binding sites inside the sarcolemma would not eliminate the possibility of additional Ca^{2+} storage in the SR.

The second type of hypotheses negates any intracellular release of Ca^{2+} [24, 25]. To raise this possibility appears legitimate in the view of the following unquestioned findings: the removal of Ca^{2+} from the bathing fluid results in the disappearance of cardiac contraction within a few tens of seconds [26] while the action potential remains present [27]. These observations support the conclusion that transsarcolemmal influx of Ca^{2+} is an essential step in excitation–contraction coupling of cardiac muscle, but they by no means exclude the possibility of an additional release of Ca^{2+} from an intracellular store [2, 22, 28]. The argument most often used to exclude the release of Ca^{2+} from the SR is a quantitative one: there is enough Ca^{2+} bound outside the sarcolemma to activate the myofilaments directly [24]. This argument can be challenged at two levels. First, even if it were demonstrated that there is enough Ca^{2+} influx across the sarcolemma to activate the myofilaments directly, this would not eliminate the possibility that an intracellular store of Ca^{2+}, such as the SR, could modify the transsarcolemmal Ca^{2+} before it reaches the myofilaments [15]. Thus, for instance, most of the transsarcolemmal Ca^{2+} influx could be accumulated into the SR, while an approximately equal amount would be released from the SR. Secondly, this quantitative argument is not yet supported by data. Neither the transsarcolemmal Ca^{2+} influx necessary to activate the myofilaments directly nor the actual value of the systolic transsarcolemmal Ca^{2+} influx has yet been established.

The amount of transsarcolemmal Ca^{2+} influx that would be necessary for activating the myofilaments directly has not yet been computed in the literature. A study by Solaro et al. [29] is often used for this purpose (e.g., see Langer [24]). In fact, the purpose of this study [29] was not to quantify the transsarcolemmal Ca^{2+} influx required for directly activating the myofilaments, but merely to establish the cytoplasmic level of [free Ca^{2+}] needed to achieve a certain level of contractile activation and to determine the amount of Ca^{2+} bound to the myofilaments at this level of activation. This study [29] takes into account only the Ca^{2+} binding to ATP and to troponin-C below the threshold for contractile activation, but ignores other cellular Ca^{2+} buffers which include: calmodulin [30], the superficial binding sites at the outer surface of the SR [31], and the binding sites at the inner face of the sarcolemma which have a low affinity but a very high capacity [21–23, 32].[2]

The systolic transsarcolemmal Ca^{2+} influx is not known either. Displacement of Ca^{2+} by

lanthanum [24], an ion that does not cross the sarcolemma, only establishes the presence of a pool of Ca^{2+} superficial to the surface membrane; this is, at least qualitatively, consistent with the large binding capacity of the isolated sarcolemmal vesicles [21–23, 32]. Compartmental analysis of the ionic flux data with ^{45}Ca [24] is difficult in the presence of multiple potential compartments [33]. This analysis confirms that the lanthanum-displaceable Ca^{2+} is superficially located [24]; but since it is done through the integration of many beats, the compartmental analysis does not indicate at what time during the cardiac cycle the superficial Ca^{2+} enters the cell and does not permit a quantification of what fraction of superficial Ca^{2+} enters the cell. Preliminary reports on attempts to measure the systolic Ca^{2+} influx with Ca^{2+} ion-selective electrodes [34, 35][3] or antipyrlazo III [36] are too premature to be evaluated and are open to many potential technical problems. Therefore, the only data currently available for quantifying the systolic transsarcolemmal influx of Ca^{2+} are those derived from voltage-clamp studies. The rationale for the calculation of the transsarcolemmal influx from these voltage-clamp studies will be explained in the section on *Calcium current.*

If one is to accept the hypothesis that transsarcolemmal Ca^{2+} influx could activate the myofilaments directly without Ca^{2+} release from the SR, then it is necessary to deal with the role of the SR in Ca^{2+} accumulation. One suggestion [24, 25] is that the SR is involved in Ca^{2+} reaccumulation, but not in Ca^{2+} release. Consequently one has to assume a unidirectional net flux of Ca^{2+} across the SR [24, 25]. Although this hypothesis cannot be eliminated and can indeed explain some data in an internally consistent manner [24, 25], it poses a difficult kinetics problem to explain how Ca^{2+} returns to the surface membrane to be reused during a subsequent beat [37]. In addition, this hypothesis is not compatible with any known properties of the cardiac SR [38].

An alternative hypothesis for direct activation of the myofilaments by the transsarcolemmal Ca^{2+} influx is conceptually simpler. This hypothesis assumes that the SR plays no role at all in the beat-to-beat Ca^{2+} regulation. The Ca^{2+} efflux would then be entirely accomplished by the surface membrane through Na^{+}-Ca^{2+} exchange and the Ca^{2+} pump of the sarcolemma. The rationale for the computation of the direction of the net Ca^{2+} flux carried by the Na^{+}-Ca^{2+} exchange and the possible role of the sarcolemmal Ca^{2+} pump will be discussed in the sections on *Sodium–calcium exchange* and *Sarcolemmal calcium pump.*

A direct activation of the myofilaments by transsarcolemmal Ca^{2+} influx and a Ca^{2+} extrusion entirely supported by Na^{+}-Ca^{2+} exchange and the sarcolemmal Ca^{2+} pump has been suggested for the cardiac cells which have the smallest diameter, particularly for the ventricular cell of the adult frog as first proposed in great detail by Morad and Goldman [39] and subsequently by others [e.g., 40, 41]. In the skinned single cardiac cells from the adult frog ventricle and in the fetal ventricular cells of mammalian species, there is no evidence of rapid Ca^{2+} release induced by Ca^{2+} or by caffeine [15, 16]. This lack of rapid release is also observed in pluricellular preparations, from the same tissues, in which the sarcolemma remains present but is disrupted, so that the superficial cisternae of the SR are preserved [15]. Yet even in frog heart, and especially in frog atrium,[4] it is not possible to exclude completely a participation of a Ca^{2+} release from the SR in excitation–contraction coupling [10, 42].

For the adult mammalian ventricle, a similar mechanism of direct activation and inactivation of the myofilaments by transsarcolemmal Ca^{2+} influx [24] and efflux is quantitatively neither supported nor excluded by any of the data on transsarcolemmal influx and efflux that will be discussed in the next section. Hypotheses suggesting a direct activation of the myofilaments in adult mammalian myocardium are challenged by experiments in skinned cardiac cells, however. These experiments indicate that the SR has the capability to accumulate Ca^{2+} and to modify, by a release, the transsarcolemmal Ca^{2+} influx irrespective of its magnitude [2, 13, 15]. Thus the hypothesis of the direct activation of the myofilaments by the transsarcolemmal influx of Ca^{2+} must disregard the results obtained from skinned cardiac cells on the grounds that these preparations may be in an

unphysiologic condition [24], which is certainly a legitimate concern. In contrast, it does not seem possible to attribute the properties of the SR of skinned cardiac cells to transverse tubules [20] which do not exist in several of the tissues used for preparing skinned cardiac cells [15, 16].

The Calcium Movements across the Sarcolemma and Their Possible Relationship with Those across the Sarcoplasmic Reticulum

CALCIUM CURRENT

Voltage-clamp studies demonstrate a slow inward current (I_{si}) which is distinguished from the fast Na^+ inward current by the fact that it is not inhibited by tetrodotoxin [43]. This current is largely attributable to Ca^{2+} influx [44]. In the past, the amplitude of the Ca^{2+} current has been difficult to estimate in part because of the superimposition of outward K^+ currents. If I_{si} can be isolated from other currents, it is possible to calculate the transsarcolemmal Ca^{2+} influx caused by the Ca^{2+} current and to consider whether the Ca^{2+} influx is of sufficient magnitude to directly activate the myofilaments. In a recent article, Marban and Tsien [43] measured the slow inward current in a multicellular strand of Purkinje fibers from the calf after blocking the superimposed currents. The experiments were done in the presence of tetrodotoxin to block the Na^+ current and after cesium loading to block the outward K^+ currents.

The following equation can be derived to calculate the Ca^{2+} influx by the slow inward current:

$$\frac{d[\text{total Ca}]}{dt} = \int_t^0 \left(\frac{J}{zF}\right) \times \left(\frac{S}{V}\right) \times \left(\frac{f_i}{f_v}\right) \qquad (11.1)$$

where

d[total Ca]	= change in myoplasmic total calcium concentration (no ionic charge is shown to emphasize that total rather than free calcium is meant).	mol/liter *(M)*
dt	= change in time, from 0 to t	s
J	= current density (current/surface area)	coul/s·cm^2
z	= valence, for Ca^{2+} = 2	dimensionless
F	= Faraday's constant, 9.65×10^4	coul/mol
S/V	= surface–volume ratio	cm^2/liter
f_i	= fraction of I_{si} carried by Ca^{2+}	dimensionless
f_v	= fraction of cell volume Ca^{2+} enters	dimensionless

The calcium current per surface area (variable J in eq. 11.1) can be calculated as follows: Upon depolarization from −60 to 0 mV (fig. 11–2A), an inward current rapidly turns on and reaches a peak (fig. 11–2B, solid curve) in about 5 ms. Then the current largely inactivates in about 20 ms to reach a plateau of remaining inward current while the depolarization is maintained. Upon repolarization the current returns to its original value. Exposure to a slow inward channel blocker (such as D-600) abolishes the transient inward current and shifts the current in an outward direction to a given level (fig. 11–2B, dotted curve). The difference between this level of current obtained with D-600 and the time-dependent current obtained without D-600 permits an inference [45] of the time course and magnitude of the slow inward current (fig. 11–2C). In the schematic drawing of figure 11–2C, the amplitude of the peak current was 5×10^{-6} A/cm^2 (from Marban and Tsien [43]). D-600 experiments revealed a noninactivating component of the slow inward current which was about 20% of peak current at 0 mV, whereas some noninactivating Ca^{2+} current remained after repolarization to −60 mV.

The level of noninactivating Ca^{2+} current shown in figure 11–2 was not directly derived from the data of Marban and Tsien [43], but was an average estimate derived from a critical review of the literature on the experiments with slow-channel blockers. Accurate measurements of noninactivating Ca^{2+} current require a highly selective blockade, which is unlikely

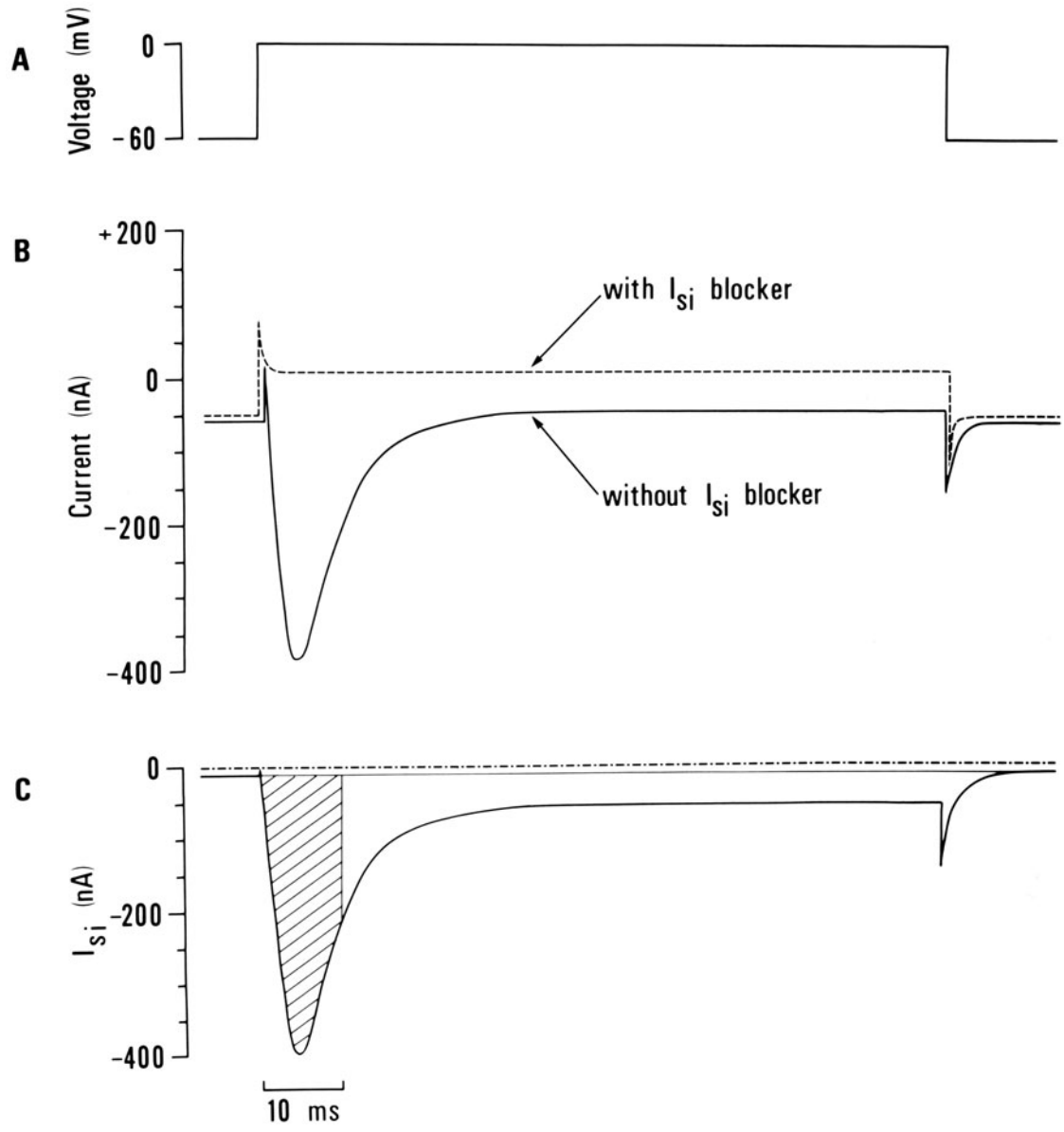

FIGURE 11–2. Schematic representation of the fast and slow components of the slow inward current derived from experiments by Marban and Tsien [43] and others (as referenced in the text). The fiber was treated with tetrodotoxin to block the fast sodium current and cesium loaded to block the outward K^+ current. *(A)* Voltage-clamp step. *(B)* Current with D-600 treatment (dotted curve) and without D-600 (solid curve). Note that the capacitance currents at the onset of the end of the clamp step have been modified to avoid superimposition. *(C)* Difference between solid and dotted curve, which represents the time course of the slow inward current (I_{si}). The area used for integrating the initial fast component of Ca^{2+} current is hatched. This integration over 10 ms yields an average value of 70% of peak I_{si}.

[46]. Estimates vary widely in different preparations [47] and also vary in the same preparation when different blocking agents are applied. For example, studies with D-600 in calf Purkinje fibers [45, 48] suggest that up to 50% of slow inward channels do not inactivate during depolarization to 0 mV. After calf Purkinje fibers have been loaded with cesium to block the outward current, however, the shift of the late current in an outward direction by D-600 suggests that about only 20% of the current does not inactivate at −10 mV (fig. 7C in Marban and Tsien [43]). Yet, exposure to manganese shifts the late current in an inward direction, a result that cannot be explained simply by a blockade of noninactivating slow inward channels (fig. 7B in Marban and Tsien [43]). In isolated cardiac cells, estimates also range from 15% in cow ventricular cells [49] to 50% in guinea pig ventricular cells [50]. On the other hand, there is no evidence for noninactivating slow inward current channels in guinea pig or cat ventricular muscle, rabbit sinoatrial node, and rat ventricular muscle treated with cobalt [51, 52], D-600 [49, 53, 54], or verapamil [55].

The percentage of slow inward channels which remain noninactivated near the resting potential is even more controversial. No steady-state calcium current was found at −40 mV in one study [48], while 20%–25% of the peak current was found at −60 mV in another study [50].

All of the current measured in the slow inward current is not carried by Ca^{2+}. The ions Na^+ and K^+ also pass through the slow channel [44]. The fraction of slow inward current carried by Ca^{2+} in Marban and Tsien's experiments [43] can be estimated by using the approach of Reuter and Scholz [44]. Assuming that the constant-field equation applies, permeability ratios can be calculated from the reversal potential for the slow inward current at different extracellular [Ca^{2+}] and from the intra- and extracellular ion activities. The data of Marban and Tsien [43] are reasonably fitted by a ratio of permeabilities to Ca^{2+} and Na^+, respectively, (P_{Ca2+}/P_{Na+}) of about 100 and a ratio P_{Ca2+}/P_{K+} of about 200. These ratios are independent of voltage [44], although the current carried by Ca^{2+} is dependent on voltage because the driving force is dependent on voltage. Then, at 0 mV, the fraction of slow inward current carried by Ca^{2+} is calculated to be 0.9 (variable f_i in eq. 11.1).

We were unable to find values for the surface–volume ratio for the calf Purkinje tissue. For Purkinje tissue of sheep, however, another ungulate, a value of 0.39×10^7 cm^2/liter has been reported [56]. This value will be used for the ratio, S/V, in equation 11.1.

Data on the fraction of the cell volume that Ca^{2+} enters are also lacking. As a first approximation, we will assume that Ca^{2+} is excluded from the volume of the mitochondria. The mitochondrial volume fraction, again from the sheep Purkinje tissue data, is 0.103 [56]. Thus the variable f_v in equation 11.1 is 0.897.

There is also uncertainty about how much of the Ca^{2+} current might be used for activating the corresponding contraction. Obviously, the late slow component of the Ca^{2+} influx, corresponding to noninactivated slow inward channels, cannot be responsible for the level of peak tension since this current continues after the tension has already reached its peak. Yet it is difficult to decide how much of the initial peak of relatively fast Ca^{2+} current is used for generating the peak tension. If one decides, as shown in figure 11–2 (hatched area), that the initial 10 ms of the Ca^{2+} current are responsible for the peak tension, then the integration of the current during this initial 10 ms gives an average current amplitude equal to 70% of the peak Ca^{2+} current. Since in the experiments of Marban and Tsien [43] the peak Ca^{2+} current was 5×10^{-6} A, the parameter $\int_t^0 J$ in equation 11.1 is $0.70 \times 5 \times 10^{-6}$.

Substituting these values in equation 11.1 gives a rate of Ca^{2+} influx of

$$\frac{d[\text{total Ca}]}{dt} = \frac{0.70 \times 5 \times 10^{-6}}{2 \times 9.65 \times 10^4} \times 0.39 \times 10^7 \times \frac{0.90}{0.897} = 71 \times 10^{-6}\ M/\text{s}$$

which gives an increase of [total Ca] in the myoplasm of 0.71 μM during the initial 10 ms.

If one decides instead that the initial 20 ms

are responsible for generating the peak tension, then the integration from 0 to 20 ms gives an average current amplitude of 50% of the peak current. It is just necessary to replace 0.70 by 0.50 to obtain:

$$\frac{d[\text{total Ca}]}{dt} = 51 \times 10^{-6}\ M/\text{s}$$

which gives an increase of [total Ca] in the myoplasm of 1.0 μM during the initial 20 ms. Considering what is known of the intracellular Ca^{2+} buffers, this increase of [total Ca] would produce an increase of [free Ca^{2+}] that would be unquestionably insufficient to induce any direct activation of the myofilaments.

Recent experiments in single cardiac cells permit the calculations of higher values of increase of [total Ca] during an action potential. The reason for these higher values is uncertain, although a partial explanation may be that series resistance in a multicellular preparation causes an underestimate of the slow inward current [49]. We have calculated the increase of [total Ca] during the peak slow inward current measured by Isenberg and Klöckner [49] in isolated adult rat ventricular cells. These investigators found a peak current of 2.8×10^{-9} A during voltage-clamp at 0 mV, but they did not relate the current to membrane surface area. The current density can be obtained as follows. An isolated adult rat cardiac cell has an average length of 93 μm, width of 19 μm, and thickness of 11 μm [13], which gives a volume of 19.4×10^{-12} liters. The surface–volume ratio of the rat ventricular cell is 0.44×10^{7} cm^2/liter [57]. Then,

$$S = S/V \times V = 0.44 \times 10^{7} \times 19.4 \times 10^{-12} = 8.54 \times 10^{-5}\ cm^2$$

Thus, the peak current is:

$$I/S = 2.8 \times 10^{-9}/8.54 \times 10^{-5} = 32.8 \times 10^{-6}\ A/cm^2.$$

The fraction of cell volume occupied by the mitochondria in rat ventricular cells is 0.34 [57]. Thus variable f_v in equation 11.1 is 0.66. One can estimate the fraction of slow inward current carried by Ca^{2+} (variable f) to be 0.90 as previously. Finally, we have assumed that the Ca^{2+} current in the study by Isenberg and Klöckner [49] had the same time course as that observed in the study by Marban and Tsien [43]. On the one hand, the time course of the slow inward current in single cells might be expected to be faster than in multicellular preparations because the series resistance is lower. On the other, the time course observed by Marban and Tsien [43] is already much more rapid than found in other multicellular preparations.

Substituting these values in equation 11.1 and integrating the current during the initial 10 ms gives a rate of increase of [total Ca] of 714×10^{-6} M/s, thus an increase of [total Ca] of 7.14 μM during the initial 10 ms. If the integration is done during the initial 20 ms, then the increase of myoplasmic [total Ca] is 10.2 μM. With such a change in [total Ca], precise calculations of the amount of Ca^{2+} buffering inside a cardiac cell are required to decide whether this Ca^{2+} influx is sufficient to partially activate the myofilaments. These computations are reported elsewhere with the conclusion that this Ca^{2+} influx would be insufficient to activate the myofilaments directly.[5]

Even if some direct activation of the myofilaments were possible with the large Ca^{2+} currents obtained in single cardiac cells, this would not prove that such a direct activation would take place. As previously emphasized, the SR could modify this Ca^{2+} influx before it reaches the myofilaments by active Ca^{2+} release and accumulation. How the SR could handle the slow and fast components of the Ca^{2+} current will be discussed in a subsequent section (*Evidence in favor of calcium-induced release of calcium. . . .*).

SODIUM–CALCIUM EXCHANGE

To infer the direction of the net flux of calcium across the sarcolemma during rest and during Ca^{2+} release from the SR shown in figure 11–3, the most recent information relative to the intracellular [free Ca^{2+}] and [free Na^{+}] and on the coupling ratio of the Na^{+}-Ca^{2+} exchange has been critically reviewed. The free ion values have been expressed in terms of activity. Trans-

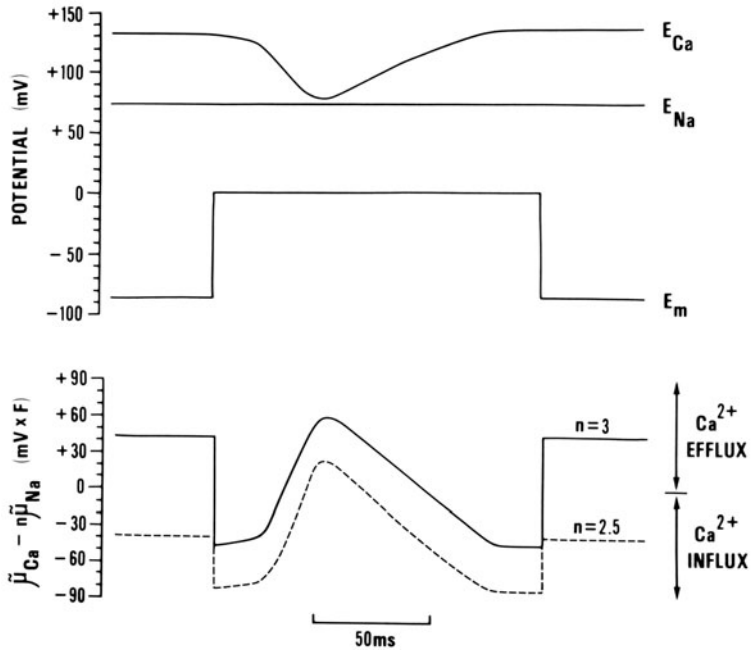

FIGURE 11–3. Direction of the net Ca^+ flux by Na^+-Ca^{2+} exchange during a voltage-clamp depolarization to the systolic potential and at resting potential in the mammalian myocardium. The computations are based on a critical review of the literature relative to the intracellular and extracellular Ca^{2+} and Na^+ activity. Two coupling ratios have been considered as extreme possibilities for the Na^+-Ca^{2+} exchange; $n = 3$ (solid curve) and $n = 2.5$ (dotted curve). E_m = membrane potential; E_{Na} = Nernst potential for Na^+; E_{Ca} = Nernst potential for Ca^{2+}; $\tilde{\mu}_{Na}$ = the electrochemical gradient for Na^+; $\tilde{\mu}_{Ca}$ = the electrochemical gradient for Ca^{2+}. The arrows on the right of the lowest panel indicate the direction of net Ca^{2+} movement by Na^+-Ca^{2+} exchange; the horizontal bar corresponds to equilibrium at which there is no net movement of Ca^{2+} or Na^+

lation to free concentrations can be obtained by dividing the values by the activity coefficients at 37°C: 0.74 for Na^+ and 0.32 for Ca^{2+} [58]. The activity coefficients are identified by the symbol *"a"* followed by a subscript indicating the ion and a superscript "o" for the external activity or "i" for the myoplasmic activity. The following values were selected: $a^o_{Na} = 115 \times 10^{-3}$ *M*; $a^i_{Na} = 6.4 \times 10^{-3}$ *M* [59]; $a^o_{Ca} = 0.58 \times 10^{-3}$ *M*; resting $a^i_{Ca} = 2.56 \times 10^{-8}$ *M* (from skinned cardiac cell experiments [13]; a critical review of the data from Ca^{2+} ion-selective electrodes [59–61] gives somewhat higher values, but potential errors in this method tend to cause overestimation of a^i_{Ca}). In the hypothesis of a Ca^{2+} release from the SR, the Ca^{2+} influx across the sarcolemma would result in an a^i_{Ca} of at least 6.4×10^{-8} *M* [13]. The maximum Ca^{2+} activity reached during Ca^{2+} release would be 1.28×10^{-6} *M* [13]. In the hypothesis of a direct activation of the myofilaments by the transsarcolemmal Ca^{2+} influx, the influx would cause a^i_{Ca} to increase to no more than 1.28×10^{-6} *M*. This myoplasmic activity would generate the maximum level of tension that an intact cardiac cell is able to develop [13]. This remains far from a full activation of the myofilaments, which is never obtained in an intact cell [13].

The electrochemical gradient for Na^+ ($\tilde{\mu}_{Na}$) is calculated according to equation 11.2:

$$\tilde{\mu}_{Na} = zFE_m - RT\ell n \frac{a^o_{Na}}{a^i_{Na}} \qquad (11.2)$$

where

$\tilde{\mu}_{Na}$ = electrochemical gradient for Na, in mV × F
R = gas constant, 8.3151 J/mol × °K

T = temperature in Kelvin degrees (°K)
z = valence
F = Faraday's constant, 9.65×10^4 coul/mol
E_m = membrane potential in mV

The Nernst equation permits the calculation of the Nernst equilibrium potential for Na^+ (E_{Na}, in mV):

$$E_{Na} = + \frac{RT}{zF} \ell n \frac{a^o_{Na}}{a^i_{Na}} \tag{11.3}$$

which gives a value of +77 mV for E_{Na}. Then,

$$\tilde{\mu}_{Na} = zF(E_m - E_{Na}) \tag{11.4}$$

where a negative value of $\tilde{\mu}_{Na}$ implies that the gradient favors an inward movement of Na^+. Assuming $E_m = -85$ mV at rest and 0 during depolarization, one can calculate $\tilde{\mu}_{Na}$ at the relevant times in the cardiac cycle.

Similar equations permit the calculation of E_{Ca}, which is found to be +134 mV at rest and +85 mV during Ca^{2+} release, and the computation of $\tilde{\mu}_{Ca}$ at rest, during the Ca^{2+} influx across the sarcolemma, and during Ca^{2+} release from the SR.

The energy available for ion transport by Na^+-Ca^{2+} exchange depends upon the electrochemical gradients ($\tilde{\mu}_{Na}$ and $\tilde{\mu}_{Ca}$) and the Na^+-Ca^{2+} coupling ratio *(n)* of the transport. There is still uncertainty about the coupling ratio (see Reuter [62] for a review), but a range between 2.5 and 3.0 seems reasonable, i.e., 2.5–3.0 Na^+ are transported for each Ca^{2+} ion (see Sheu and Fozzard [59] and Lado et al. [63]). Accordingly, the computation has been done for these two extreme values (fig. 11–3), yet the coupling ratio is likely to be closer to 3.0 than to 2.5 because a value of 2.6 has been computed [59, 63] with the assumption of an a^i_{Ca} higher than we have selected. Lowering the a^i_{Ca} to the level that we selected would increase the coupling ratio to 2.7.

At equilibrium, the energy available in the Na^+ and Ca^{2+} electrochemical gradients is equal, and no net transport occurs:

$$nzF(E_m - E_{Na}) = zF(E_m - E_{Ca}) \tag{11.5}$$

This is equivalent to:

$$n(E_m - E_{Na}) = 2(E_m - E_{Ca}) \tag{11.6}$$

If the Na^+ gradient multiplied by n is larger in magnitude than the Ca^{2+} gradient, Na^+ enters the cell via Na^+-Ca^{2+} exchange, causing Ca^{2+} efflux. If the magnitude of the Ca^{2+} gradient is larger, then there is Ca^{2+} influx coupled with Na^+ efflux.

This computation shows that during diastole the Na^+-Ca^{2+} exchange would cause either Ca^{2+} influx if the coupling ratio were 2.5, or Ca^{2+} efflux if the coupling ratio were 3.0. In fact, a Na^+-Ca^{2+} exchange near equilibrium with no significant net influx or efflux is perhaps the most likely possibility [59, 63].

To describe the systolic Ca^{2+} movements via Na^+-Ca^{2+} exchange, we shall consider first the hypothesis of a Ca^{2+} release from the SR and, secondly, the hypothesis of a direct activation of the myofilaments by the transsarcolemmal Ca^{2+} influx. In the first case, the Na^+-Ca^{2+} exchange would cause an additional Ca^{2+} influx during the initial part of the transsarcolemmal Ca^{2+} influx caused by the Ca^{2+} current. The velocity of the Na^+-Ca^{2+} exchange derived from experiments in isolated sarcolemmal vesicles [64, 65] seems to be sufficient to permit it to cause Ca^{2+} influx during the approximately 20 ms between the transsarcolemmal influx and the time when the Ca^{2+} release from the SR would cause the Na^+-Ca^{2+} exchange to reverse its direction. The amount of Ca^{2+} influx via Na^+-Ca^{2+} exchange during this time can be assumed to be small as compared to that brought by the Ca^{2+} current in the view of the high K_m of the Na^+-Ca^{2+} exchange [64]. If a significant Ca^{2+} influx occurs during this time, the resulting outward movement of Na^+ might somewhat complicate the measurement of the Ca^{2+} current. When Ca^{2+} release from the SR reaches its peak, permitting the activation of the myofilaments, the Na^+-Ca^{2+} exchange functions in the Ca^{2+} extrusion mode. Yet, this system will work efficiently only when the myoplasmic [free Ca^{2+}] is still high, since its K_m is high: 1.5×10^{-6} *M* [64]. At low myoplasmic [free Ca^{2+}] during diastole, the Ca^{2+} extrusion is probably done by the sarcolemmal Ca^{2+} pump.

With the hypothesis that the activation of the myofilaments results directly from transsarcolemmal Ca^{2+} influx [24], the Na^+-Ca^{2+} exchange would still be biphasic during systole. Initially it would transport Ca^{2+} inward at the beginning of the transsarcolemmal Ca^{2+} influx while the [free Ca^{2+}] is low, then Ca^{2+} would be transported outward when the transsarcolemmal Ca^{2+} influx has reached a level sufficient to activate the myofilaments. Thus, even in this case the Na^+-Ca^{2+} exchange would not function monophasically in the direction of a pure Ca^{2+} influx during the action potential, as was proposed by Mullins [66].

SARCOLEMMAL CALCIUM PUMP

Initial descriptions of a Ca^{2+}-ATPase in the sarcolemma sensitive to free Ca^{2+} in the micromolar range were by Sulakhe and St. Louis (see their recent review [67]). There was some question, however, of whether this sarcolemmal ATPase was in fact due to contamination of the preparation by SR vesicles [68]. However, Caroni and Carafoli [69, 70] have provided compelling evidence that this ATPase activity indeed takes place in the sarcolemma and that its affinity for Ca^{2+} is much lower than that of the Na^+-Ca^{2+} exchange with a K_m at 0.3×10^{-6} *M*. The rate of transport is also lower than that of Na^+-Ca^{2+} exchange.

Thus the sarcolemmal Ca^{2+} pump is likely to function at concentrations near or at the diastolic level. The computation shown in figure 11–3 suggests the possibility that with a coupling ratio of 2.5 and with the resting Ca^{2+} activity selected, the Na^+-Ca^{2+} exchange might function in the Ca^{2+} influx mode during diastole. It must be repeated that the diastolic Ca^{2+} influx shown in the case of a coupling ratio of 2.5 is an extreme and unlikely possibility. It is conceivable, however, that if there was some Ca^{2+} influx caused by Na^+-Ca^{2+} exchange during diastole, it would be balanced by the sarcolemmal Ca^{2+} pump.

The amount of total calcium that can be extruded from the cardiac cell by the sarcolemmal Ca^{2+} pump during a beat and between two beats could theoretically be calculated from the affinity of the pump for Ca^{2+}, its maximum rate of transport per milligram sarcolemmal protein as derived from experiments in isolated sarcolemma, and the concentration of sarcolemmal protein per milligram wet weight of tissue. The resulting change of myoplasmic [free Ca^{2+}] could then be derived by dividing the result of this calculation by the product of the tissue water expressed as percentage of wet weight multiplied by the intracellular water expressed as a percentage of the total water. There are still too many uncertainties about the degree of purity of the isolated sarcolemmal preparation and the percentage of vesicles inside-out versus right-side-out for such calculations to be meaningful at the present time.

If and when these calculations become reasonable, it may become possible to test quantitatively Langer's hypothesis [24] of an unidirectional route of calcium efflux through the SR. If such a route were to exist, then the total calcium influx per beat should be larger than the total calcium efflux through the Ca^{2+} pump and the Na^+-Ca^{2+} exchange by an amount equal to the calcium efflux through this specific route involving the SR. At the present time, however, the calcium efflux through Na^+-Ca^{2+} exchange and the sarcolemmal Ca^{2+} pump is not known. The total calcium influx during a beat is not known quantitatively either; there are uncertainties about the amount of total calcium carried by the Ca^{2+} current, no reliable information on the amount of total calcium entering by Na^+-Ca^{2+} exchange and, in addition, no knowledge about the passive Ca^{2+} leak through the membrane following the concentration gradient which is likely to bring additional Ca^{2+} into the cell during the rest between beats.

For dissecting the respective contributions of the different routes of Ca^{2+} influx and efflux across the sarcolemma, it would be useful to have specific pharmacologic tools inhibiting each of these routes but not the others. The Ca^{2+} blocking agents do not seem to affect the Na^+-Ca^{2+} exchange [71], but on the other hand they modify conductances other than the Ca^{2+} conductance [46]. Change of ATP concentration affects not only the Ca^{2+} pump, but also the Na^+-Ca^{2+} exchange [64]. Recently, doxorubicin, a cardiotoxic antibiotic, has been reported to block specifically the Na^+-Ca^{2+} exchange, but the results are too premature to be critically evaluated [72].

In conclusion, the currently available information with respect to the quantification of the Ca^{2+} influx and efflux during a cardiac beat does not provide any compelling reason to infer or eliminate a role of the SR in cardiac excitation–contraction coupling. Irrespective of the amplitude of these Ca^{2+} movements whenever they are established, and even if they were sufficient to activate or inactivate the myofilaments, this would not permit the elimination of a role for the SR. As previously emphasized, the Ca^{2+} accumulation in and release from the SR could modify the changes of myoplasmic [free Ca^{2+}] resulting from Ca^{2+} movements across the sarcolemma before and after the activation of the myofilaments.

In contrast, results obtained from subcellular preparations provide evidence for a beat-to-beat Ca^{2+} release and reaccumulation in the SR. Thus, it is justified now to deal with these results with the understanding that they can be criticized for being obtained from preparations placing the SR under unphysiologic conditions. Although a Ca^{2+} release from the SR has been demonstrated in isolated SR vesicles from cardiac [73, 74] and skeletal muscles (see Katz and Takenaka [75] for a recent review), the rate of Ca^{2+} release observed in these studies was much too low to directly correspond to a physiologically relevant phenomenon. In addition, the requirements in terms of [free Ca^{2+}] were unphysiologically high and those in terms of [free Mg^{2+}] unphysiologically low. Accordingly, and despite the interest in these data from isolated SR, the review will be focused on the results obtained from skinned cardiac cells. Before evaluating the arguments for and against the mechanism for Ca^{2+} release that has been inferred from these results, the methods used for detecting Ca^{2+} release from the SR of skinned cardiac cells will be critically appraised.

Appraisal of the Methods Used for Detecting Calcium Release from the Sarcoplasmic Reticulum in Skinned Cardiac Cells

Ca^{2+} release from the SR of skinned cardiac cells can be detected in two ways: by monitoring the resulting increase of [free Ca^{2+}] in the myoplasm or by monitoring the decrease of Ca^{2+} bound inside the SR. In addition, it is possible to detect changes of charge distribution on the SR membrane that accompany the Ca^{2+} release from the SR with potential-sensitive dyes.

The monitoring of changes of myoplasmic [free Ca^{2+}] has been accomplished by four different methods using respectively (a) tension developed by the myofilaments as a sensor of these changes of myoplasmic [free Ca^{2+}], (b) aequorin bioluminescence, (c) Ca^{2+} ion-selective microelectrodes, and (d) arsenazo III. Detection of changes in the amount of Ca^{2+} bound to the inner face of the SR has been accomplished by monitoring the fluorescence of the calcium–chlorotetracycline chelate. Finally, three potential-sensitive dyes have been used for experiments in skinned cardiac cells: merocyanine 540, merocyanine oxazolone (NK 2367), and di-S-C_3(5).

USE OF THE TENSION DEVELOPED BY THE MYOFILAMENTS AS A SENSOR OF THE CHANGES OF MYOPLASMIC FREE-CALCIUM CONCENTRATION

In all experiments using skinned cardiac cells, the [free Ca^{2+}] must be buffered with ethyleneglycol-bis (β-aminoethylether)-*N,N'*-tetraacetic acid (EGTA) at the low [free Ca^{2+}] levels (and with ATP at high [free Ca^{2+}]). The calculation of the composition of these solutions containing multiple metals and ligands requires a computer program [76].

The first method used for detecting Ca^{2+} release in skinned cardiac cells employed a low [total EGTA] [77]. An example of the results obtained with this protocol is shown in figure 11–4, which was obtained for a skinned cardiac cell from the rabbit atrium. A slight increase of the [free Ca^{2+}] in the bulk of the solution in the presence of a low [total EGTA] resulted in the induction of cyclic contractions (fig. 11–4A). When the same increase of [free Ca^{2+}] was applied in the presence of a higher [total EGTA], the amplitude of the cyclic contractions decreased so that eventually they became undetectable (fig. 11–4B and C). This indicates a competition for Ca^{2+} between the EGTA buffer and a Ca^{2+} store within the cell. Since the data were obtained from an atrial tissue

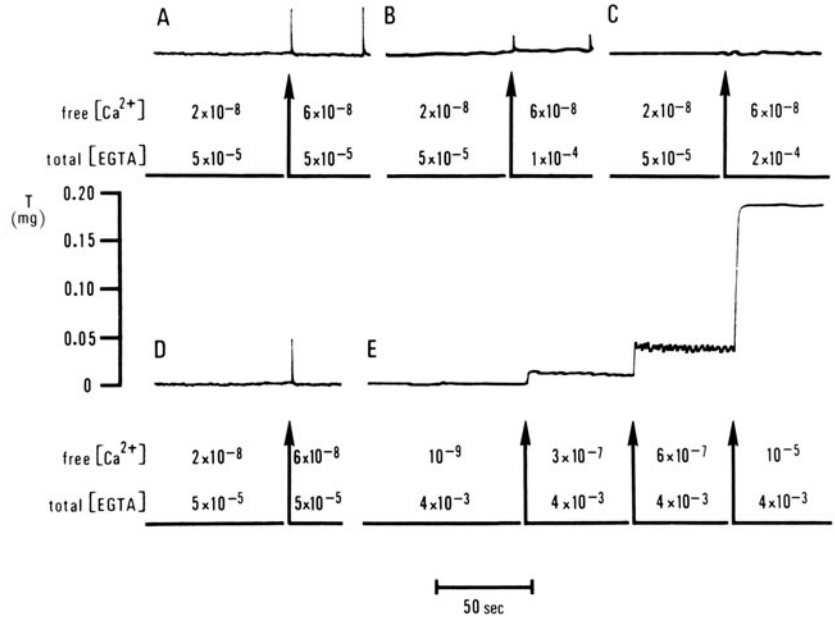

FIGURE 11–4. Methods using a tension recording in the presence of a low [total EGTA] to demonstrate Ca^{2+} release from the SR in skinned cardiac cells. The experiment was done on a 5-μm-wide and 25-μm-long skinned cardiac cell from the rabbit atrium. The [free Ca^{2+}] was calculated with an apparent stability constant for the CaEGTA complex which has now been demonstrated to be erroneously high [13]. Table IV of Fabiato and Fabiato [76] gives the correspondence between the [free Ca^{2+}] values obtained with this erroneous apparent stability constant and that currently used. The [free Mg^{2+}] was 3.16×10^{-4} *M*, which was believed at the time when these experiments were done [15] to be the physiologic [free Mg^{2+}]. Since then, a tenfold higher [free Mg^{2+}] has been used [76]. This modification only renders the Ca^{2+} release from the SR more obvious [13]. Finally, the pH was at 7.00 instead of the value of 7.10 which is currently used [76]. Again, the increase of pH enhances the Ca^{2+} release from the SR [79]. The ionic strength was 0.160 *M*, and the temperature was 22°C. The arrows indicate the time of solution change. The upper panels *(A–C)* demonstrate the presence of a Ca^{2+} store in this skinned cardiac cell as explained in the text (see *Use of the tension. . . .*). The lower panels *(D* and *E)* provide evidence for a Ca^{2+}-induced release of Ca^{2+} as explained in the text (see *Evidence in favor of a calcium-induced release. . . .* The amplitude of the phasic contraction induced by a small increase of [free Ca^{2+}] in the presence of a low [total EGTA] *(D)* is compared to the tension elicited by direct activation of the myofilaments with various levels of [free Ca^{2+}] in the presence of a high [total EGTA] *(E)* which prevents the SR from modifying the [free Ca^{2+}] significantly. Reproduced from the *Annals of the New York Academy of Sciences* [15] with permission of the publisher.

which does not contain transverse tubules, the Ca^{2+} sink could not be related to the transverse tubules. Experiments using inhibitors and uncouplers of the mitochondrial respiration permitted the exclusion of mitochondria as a Ca^{2+} store [77]. In contrast, inhibition of the ability of the SR to actively accumulate and release Ca^{2+} by detergent treatment suppressed the cyclic contractions. Thus, these cyclic contractions demonstrate that the SR is a storage site for Ca^{2+} in the skinned cardiac cell from which Ca^{2+} can be released and in which Ca^{2+} can be reaccumulated.

It must be emphasized that the assertion of the presence of a Ca^{2+} sink in the SR is the only conclusion that the observation of these cyclic contractions permits. This observation does not permit any inference of the mechanism whereby Ca^{2+} is released from the SR. A mechanism for Ca^{2+} release is suggested, however, by the experiment shown in figure 11–4D and E, which will be discussed later (see

Evidence in favor of calcium-induced release of calcium . . . .). Precisely because the principle of the method using a low [total EGTA] is a competition between the SR and the CaEGTA buffer, the [free Ca^{2+}] in the myoplasm between or during the cyclic contractions cannot be inferred from the [free Ca^{2+}] in the bulk of the solution [2, 77]. The myoplasmic [free Ca^{2+}] is likely to be lower in the vicinity of the outer surface of the SR than in other areas of the myoplasm because the SR binds and actively accumulates Ca^{2+}.

To permit precise definition of the [free Ca^{2+}] in the myoplasm, Endo [1, 78] has developed a method using a high [total EGTA] during the induction of the Ca^{2+} release. This method has been applied to skinned cardiac cells [15, 79], and an example is shown in figure 11–5. Since a high [total EGTA] is used, no change of tension is observed during the Ca^{2+} release induced by various manipulations (fig. 11-5A–D). The Ca^{2+} release can be detected afterward by estimating the amount of Ca^{2+} remaining in the SR. The estimate is obtained by measuring the amplitude of a contraction induced by caffeine in the presence of a low [total EGTA] [15, 79]. In skinned cardiac cells the amplitude of the caffeine-induced contraction is more reproducible than the area under the curve of this contraction. The area under the curve is used in studies of skinned fibers from skeletal muscle [1, 78], where there is no choice since the amplitude generally saturates at the level of the maximum tension that the myofilaments can develop. Thus, a caffeine-induced contraction smaller than control (fig. 11–5B and C compared to A and D) indicates that a Ca^{2+} release has taken place during the experimental interventions done in the presence of a high [total EGTA]. A larger difference from control (fig. 11–5C compared to B) indicates a larger Ca^{2+} release. For statistical analysis of the results obtained from different preparations, the amplitude of the caffeine-induced contractions can be expressed as a percentage of the maximum tension elicited by full activation of the myofilaments in the presence of a high [total EGTA] (fig. 11–5E).

This method gives only qualitative results with respect to the amount of Ca^{2+} released inasmuch as caffeine does not release all the Ca^{2+} contained in the cardiac SR (see fig. 9 in Fabiato and Fabiato [15]). In addition, caffeine increases the sensitivity of the myofilaments to Ca^{2+} [2, 15, 80]. If a high enough [total EGTA] is used in a small-diameter preparation, and the pH is strongly buffered, this method certainly ensures that the myoplasmic [free Ca^{2+}] is homogeneous throughout the preparation and equal to that set in the buffer. Accordingly, this method is very useful for comparative studies on the effect of various interventions on the Ca^{2+} release from the SR [1, 79], yet the exact values of the [free Ca^{2+}] are not directly physiologically relevant inasmuch as the principle of the method is precisely to set a homogeneous myoplasmic [free Ca^{2+}]. In contrast, the myoplasmic [free Ca^{2+}] of the intact cell is not homogeneous, but probably is lower at the outer surface of the SR than in other areas, as previously explained.

DIRECT DETECTION OF CHANGES OF MYOPLASMIC FREE-CALCIUM CONCENTRATION THROUGH THE BIOLUMINESCENCE OF AEQUORIN

The bioluminescence produced by the phosphoprotein, aequorin, in the presence of Ca^{2+} has been used in a number of systems to detect changes of [free Ca^{2+}] (see Blinks et al. [81] and Allen and Blinks [82] for reviews), including in skinned cardiac cells [13, 16]. At least with the batches of aequorin that have been used for the reported results [13, 16], this phosphoprotein does not appear to have any toxicity for the skinned cardiac cells (other batches did present a toxicity whose mechanism is under investigation). The fact that the product of the reaction is a bioluminescence renders the signal nonsensitive to contractions. As will be explained, this is a great advantage over methods using other types of optical recordings in which contractile artifacts are a major problem. The aequorin signal precedes tension development (figs. 11–6 and 11–7).

The aequorin signal can be calibrated in terms of [free Ca^{2+}] according to a method originally proposed by Allen and Blinks [82]. This is done by applying a solution at 3.16 m*M* free Ca^{2+}, which inactivates all the ae-

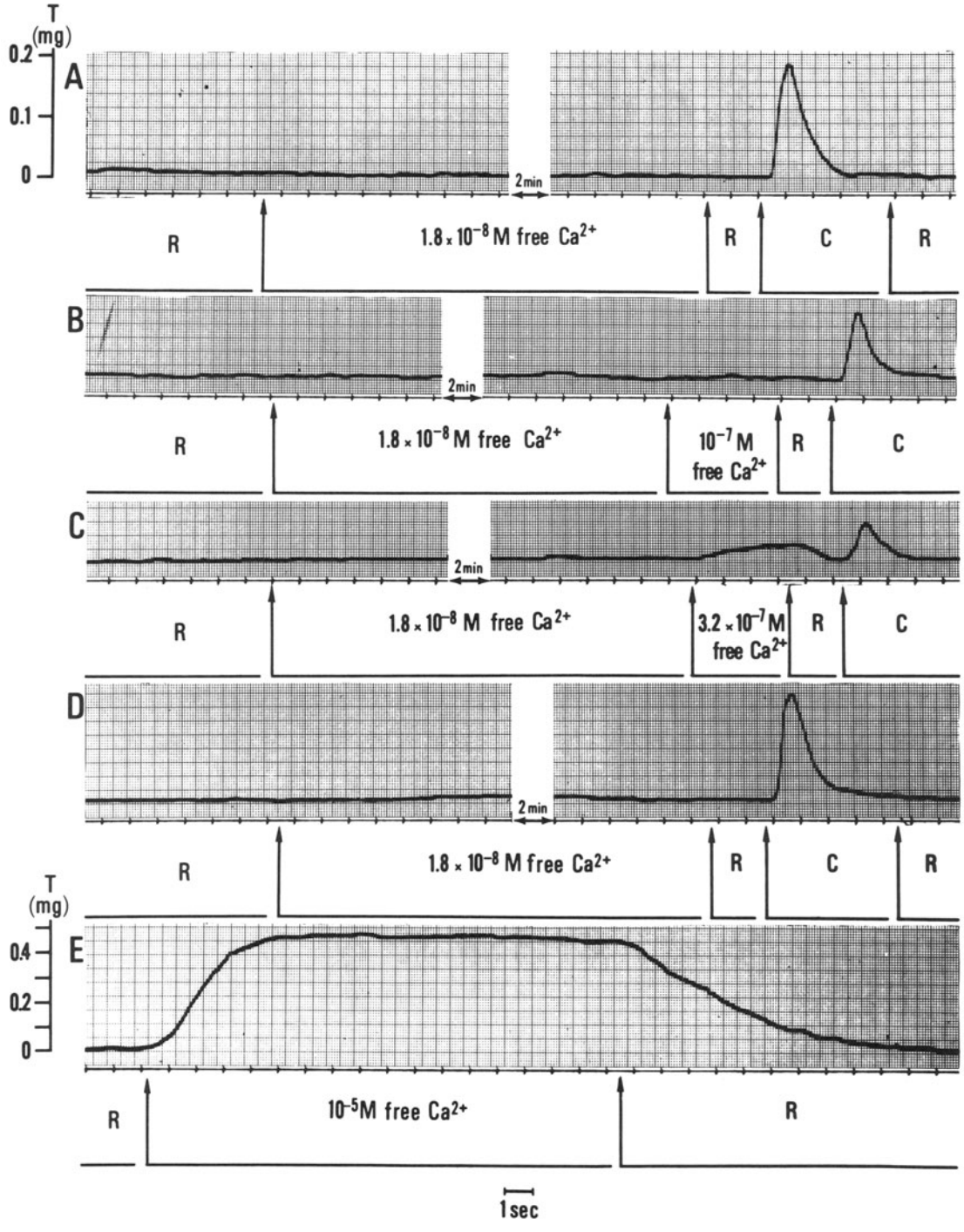
T
(mg)
0.2
0.1
0
A
2min
R
1.8 x 10⁻⁸ M free Ca²⁺
R
C
R
B
2min
R
1.8 x 10⁻⁸ M free Ca²⁺
10⁻⁷ M
free Ca²⁺
R
C
C
2min
R
1.8 x 10⁻⁸ M free Ca²⁺
3.2 x 10⁻⁷ M
free Ca²⁺
R
C
D
2min
R
1.8 x 10⁻⁸ M free Ca²⁺
R
C
R
T
(mg)
0.4
0.2
0
E
R
10⁻⁵M free Ca²⁺
R
1sec

quorin contained in the skinned cell. The result is an aequorin bioluminescence transient of large amplitude (see fig. 12 in Fabiato [13]). During this large transient, a microcomputer calculates the area under the curve and displays it on the recorder at a chart speed of 1 cm/s as a rectangular wave with a height equal to the time constant of decay of the aequorin bioluminescence as measured in a rapid-mixing chamber under the ionic conditions (especially the pMg) and at the temperature used for the experiment. As a first approximation, the light decay can be considered as purely exponential. It is a well-known property of an exponential function that the value of the intercept of the curve with the ordinate axis is equal to the area between the curve and the two axes divided by the time constant. Thus, the length of the rectangular wave generated by the computer directly gives the amplitude of the maximum light that would be produced by an instantaneous mixing of an excess of Ca^{2+} with all the aequorin contained in the skinned cell. The calibration curve [82] obtained by rapid mixing in cuvette of aequorin and various levels of [free Ca^{2+}] under the appropriate ionic conditions and temperature is used to infer the myoplasmic [free Ca^{2+}] reached during the Ca^{2+} release from the SR. This curve expresses the peak myoplasmic $-\log_{10}$ [free Ca^{2+}] (pCa) as a function of $-\log_{10} L/L_{max}$, where L is the amplitude of the aequorin light transient and L_{max} the maximum light given by the computer output (see fig. 13 in Fabiato [13]).

A major potential problem with the aequorin method is that localized areas where Ca^{2+} could reach a high concentration would contribute disproportionally to the signal because of the stoichiometry (2–3 Ca^{2+} ions per aequorin molecule) of the binding of aequorin to Ca^{2+} [81, 82]. Thus the calibration in terms of [free Ca^{2+}] may be misleading. This problem may be minimized in skinned cardiac cells because aequorin seems to diffuse homogeneously in the cell and, in particular, in the myofilament lattice. In intact cells, aequorin perhaps remains superficially distributed with respect to the myofilaments. Although there is no direct evidence for this assumption, it would help to explain that much larger signals are observed in skinned cardiac cells than could be inferred from the amplitude of the signals obtained in multicellular cardiac preparations and from the ratio of the respective volumes of aequorin-containing tissue [13]. In addition, it is possible, at least in skinned cardiac cells, that Ca^{2+} release takes place not only from the terminal cisternae, but from all the parts of the SR which tightly pack the myofilaments. Thus the diffusion of Ca^{2+} from the SR to the myofilaments could be over a very short distance. The aequorin molecule is large relative to the distance between the SR and the myofilaments. For these reasons, aequorin bioluminescence

FIGURE 11–5. Use of tension recording in the presence of a high [total EGTA] to demonstrate Ca^{2+} release from the SR with the help of a subsequent application of caffeine in the presence of a low [total EGTA]. The experiment was done in a 9-μm-wide, 32-μm-long skinned cardiac cell from the adult rat ventricle. Except for the caffeine solution (C), all solutions contained 4×10^{-3} *M* total EGTA. The caffeine solution contained 2×10^{-4} *M* total EGTA, 5×10^{-9} *M* free Ca^{2+}, and 10 m*M* caffeine. The relaxing solution (R) was at 10^{-8} *M* free Ca^{2+}. The other characteristics of the solutions and the stability constants were the same as those described in Figure 11–4. The tonic tension observed in panel *C* during the brief perfusion with 3.2×10^{-7} *M* free Ca^{2+} was caused by the direct effect of this [free Ca^{2+}] on the myofilaments. The experiments started in relaxing solution. Then the SR was loaded during about 2½ min in the presence of 1.8×10^{-8} *M* free Ca^{2+}, which has been shown to correspond to the optimum loading in this preparation. This [free Ca^{2+}] in the loading solution does not permit any inference of the [free Ca^{2+}] reached in the lumen of the SR. Subsequently a higher [free Ca^{2+}] was applied which was demonstrated to induce Ca^{2+} release *(B* and *C)*. This step was omitted in the control recordings *(A* and *D)*. The Ca^{2+} release did not produce any tension transient, except in panel *C* as previously explained, because it occurred in the presence of a high [total EGTA]. Then in both panels *B* and *C* and in the controls *(A* and *D)*, the skinned cell was washed with the relaxing solution for about 2 s. The experiment was terminated by the application of caffeine. The amplitude of the caffeine-induced contraction was used to estimate the amount of Ca^{2+} remaining in the SR. For statistical analysis of the results obtained from different preparations, the amplitude of the caffeine-induced contraction was normalized as a percentage of the maximum tension developed by activation of the myofilaments *(E)*. Note that the tension scale in panel *E* is one-half of that used for panels *A–D*. Reproduced from the *Annals of the New York Academy of Sciences* [15] with permission of the publisher.

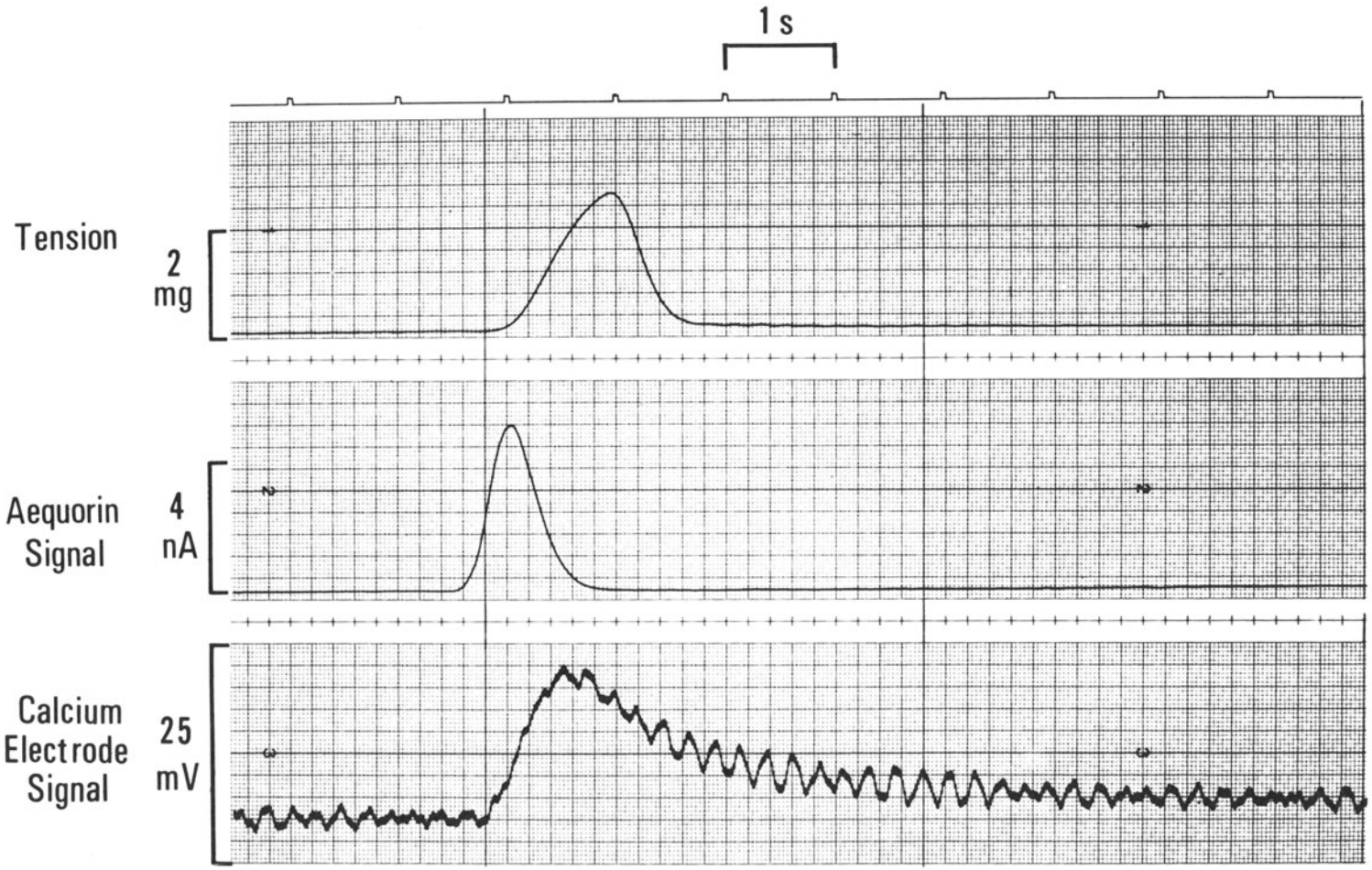
1 s
Tension
2
mg
Aequorin
Signal
4
nA
Calcium
Electrode
Signal
25
mV

may integrate [free Ca^{2+}] changes during the circulation of Ca^{2+} over the very short distance between the SR and the myofilaments. This would explain the surprisingly good consistency that was observed when the myoplasmic [free Ca^{2+}] reached during Ca^{2+} release was inferred comparatively from the calibration of the aequorin transient and from the use of tension developed by the myofilaments to measure changes of myoplasmic [free Ca^{2+}] [13]. Although aequorin may provide reliable information on the maximum myoplasmic [free Ca^{2+}] reached during Ca^{2+} release in skinned cardiac cells, it does not seem to be usable to define the level of resting myoplasmic [free Ca^{2+}] in skinned cardiac cells [13].

MEASUREMENT OF MYOPLASMIC FREE-CALCIUM CONCENTRATION WITH CALCIUM ION-SELECTIVE ELECTRODES

The resting level of myoplasmic [free Ca^{2+}] can be measured accurately with ion-selective electrodes. The combination of this method with the use of aequorin would help to accurately determine the amplitude of the change of [free Ca^{2+}] taking place during Ca^{2+} release. Then an accurate interpretation of the resting glow of aequorin bioluminescence would be possible. In fact this should be required for a fully warranted calibration of the amplitude of the aequorin transient in terms of [free Ca^{2+}]. In addition, ion-selective electrodes give a signal which is detected with a high-input impedance preamplifier. Accordingly, this recording can be made simultaneously with an optical recording. This is very valuable for calibrating the change of [free Ca^{2+}] in conjunction with the recording of aequorin bioluminescence. As will be explained, this would be even more important for interpreting the preliminary results obtained with potential-sensitive dyes (see *Evidence in favor of calcium-induced release of calcium . . . .*).

Ion-selective electrodes of 2- to 5-μm-tip diameter were prepared using the ETH 1001 neutral ligand cocktail of Simon [83]. In order to retain the neutral ligand in the tip of the electrodes, it was necessary to make the glass of the micropipette hydrophobic (silanization). This was done by dipping the tips of the microelectrodes into a freshly made solution of 10% tri-*n*-butylcholorosilane (obtained from Columbia Organic Chemicals Co., Columbia, SC) in xylene. Then the silane reaction was performed at 200°C for 1 h. A column of the ETH 1001 resin at least 5 mm long was introduced into the tip of the microelectrode by aspiration. The rest of the barrel of the microelectrode was filled from the back with 100 m*M* $CaCl_2$ to make electrical contact with a chlorided silver wire. After storage in this 100-m*M* $CaCl_2$ solution for several hours, the electrodes were calibrated with a series of buffered Ca^{2+} solutions at pCa values from 5.00 to 8.00 in 0.5 steps. These solutions contained 140 m*M* KCl, 10 m*M* EGTA, 10 m*M* *N*-tris(hydroxymethyl)-methyl-2-aminoethane sulfonic acid (TES) at pH 7.10. The most recently updated stability constants [13] and the previously reported calculator program [76] were used for making these solutions. Standard methods for calculating activity from the calibration parameters were used (see Lee [61] and Tsien and Rink [85], for details). At the time of their use, the Ca^{2+} ion-selective electrodes had a resistance of $2–9 \times 10^9\ \Omega$.

The ion-selective electrodes were impaled into skinned cardiac cells from the dog Purkinje tissue. The impalement was longitudinal with respect to the axis of the myofibrils to en-

FIGURE 11–6. Simultaneous monitoring of the Ca^{2+} release from the SR with Ca^{2+} ion-selective electrode, aequorin bioluminescence, and tension recording. The experiment was done in a 21-μm-wide, 18-μm-thick, and about 60-μm-long skinned cardiac cell from the dog Purkinje tissue. A 3-μm-tip Ca^{2+} ion-selective electrode was inserted within the myofibrils longitudinally with respect to the axis of the myofibrils. The indifferent electrode was placed in the solution close to the skinned cell. Aequorin bioluminescence was recorded according to the previously described method [13]. The solution contained 50 μm EGTA, 3.12×10^{-7} *M* free Ca^{2+}, 3.12×10^{-3} *M* Mg^{2+}, 1.0×10^{-4} *M* MgATP, ionic strength 0.160 *M* with K^+ and Cl^- as the major ionic species, at pH 7.10, buffered with 30 m*M* TES, and at 22°C. At this [free Ca^{2+}], the preparation presented cyclic Ca^{2+} releases resulting in cyclic contractions of an amplitude equal to about 10% of maximum tension. An unphysiologically low [MgATP] was used to increase the delay between Ca^{2+} release and contraction. The stability constants were those most recently updated [13].

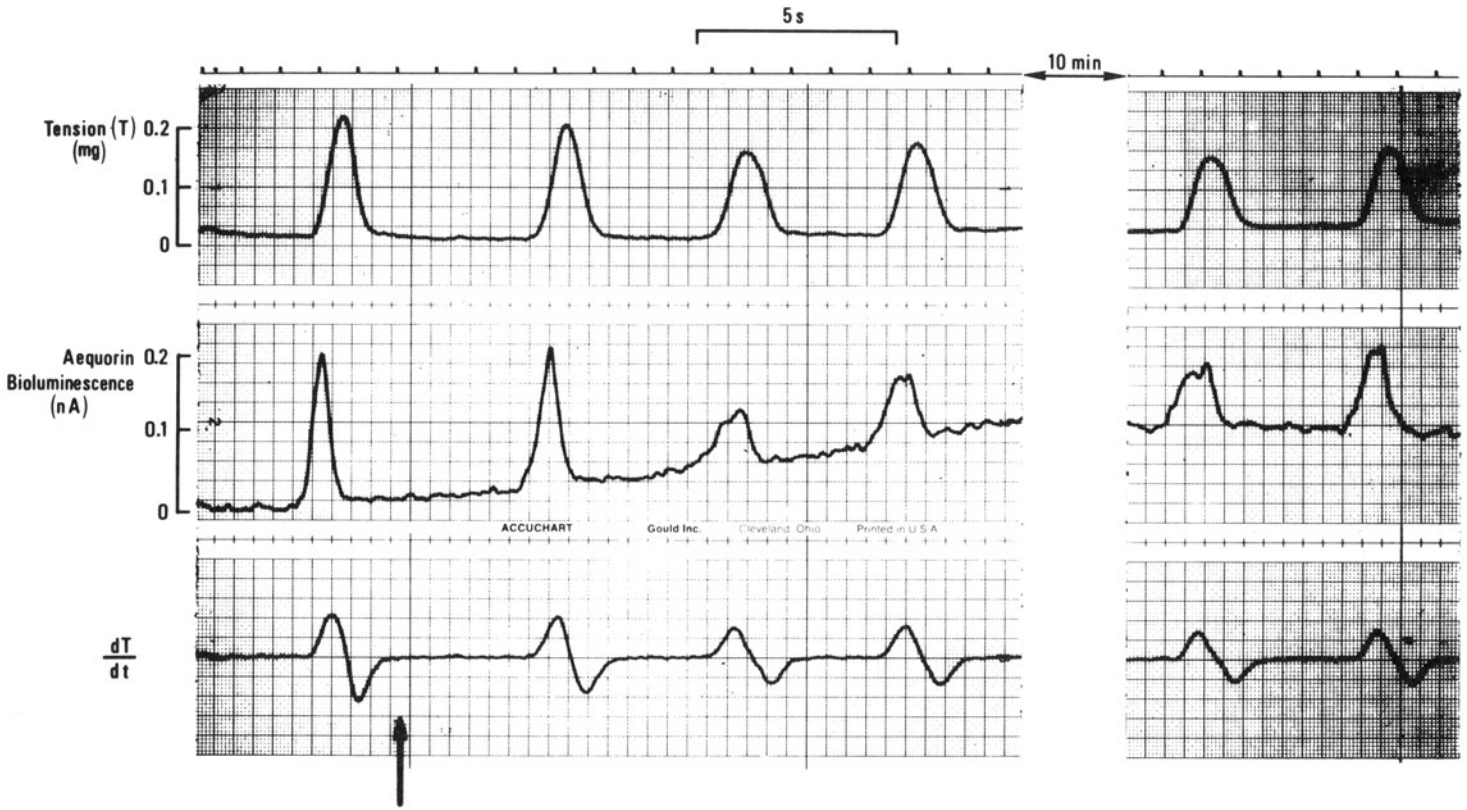

FIGURE 11–7. Effect of 5.0×10^{-5} *M* arsenazo III on the transients of Ca^{2+} release from the SR detected through tension transients (scale in milligrams) and through transients of aequorin bioluminescence (scale in nanoamperes) in a skinned cardiac cell from the adult rat ventricle. The initial solution contained aequorin, 5.0×10^{-3} *M* total EGTA, a free Ca^{2+} of 5.6×10^{-7} *M*, free Mg^{2+} 3.2×10^{-3} *M*, MgATP 3.2×10^{-3} *M*, at pH 7.10, ionic strength 0.160 *M*, and temperature 22°C. The stability constants were those most recently updated [13]. At the time indicated by the arrow, the solution was replaced by a solution of the same composition except that it also contained 5.0×10^{-5} *M* arsenazo III. As explained in detail elsewhere [13], the zero for the aequorin bioluminescence is set at the beginning of the experiment with the tips of all the microinjection pipettes containing aequorin in the field of the photomultiplier tube. Thus the changes of baseline on the bioluminescence recording correspond to physiologic modifications rather than to the mere change of the solution. The photomultiplier tube "sees" all the solutions permanently, when they are around the cell as well as when they are in the tip of the perfusion pipettes. Detailed arguments have been presented to demonstrate that the deterioration of the Ca^{2+} transient detected with aequorin and with tension was not caused by any decrease of [free Ca^{2+}] due to the binding of Ca^{2+} to arsenazo III [87]. Reproduced from the *Canadian Journal of Physiology and Pharmacology* [87] with permission of the publisher.

sure that the electrode tip was in the middle of the myofilament bundle and remained there during contraction. The Purkinje tissue of the dog was selected because larger skinned cells can be obtained from this preparation inasmuch as the original intact cells are of larger diameter than those obtained from other mammalian cardiac tissues. In addition, aequorin bioluminescence recordings have demonstrated that the Ca^{2+} transient reaches a higher level of [free Ca^{2+}] in this preparation than in the ventricular skinned cells from the dog or other mammalian species [16].

The recording was made, with a 10^{13}-Ω-input impedance preamplifier, between the ion-selective electrode and an indifferent electrode which were placed very close to each other. The indifferent electrode was filled with the same solution as that bathing the skinned cardiac cell containing 5×10^{-5} *M* total EGTA, 8×10^{-8} *M* free Ca^{2+}, 3.16×10^{-3} *M* free Mg^{2+}, 3.16×10^{-3} *M* MgATP, and 0.160 *M* ionic strength, at pH 7.10, buffered with 30 m*M* TES, and at 22°C. The Ca^{2+} ion-selective electrode signal was recorded simultaneously with the tension and aequorin bioluminescence (fig. 11–6). All three signals were filtered above 5 Hz, so that the delays between them could not be attributed to a higher degree of filtration of some of the signals. A filtration at as low a frequency as 5 Hz was imposed by the tension transducer and has been demonstrated not to result in any loss in the amplitude of the aequorin bioluminescence transient in skinned cardiac cells. The low-frequency noise on the Ca^{2+} ion-selective electrode recording (fig. 11–6) was caused by the close proximity (less than 1 mm) of the tip of this electrode to the cathode of the photomultiplier tube.

Cyclic Ca^{2+} releases were induced by increasing the [free Ca^{2+}] in the solution from 8.00×10^{-8} *M* to 3.12×10^{-7} *M*. Under these optimum conditions (large size of the pipette tip and large skinned cardiac cell from a tissue in which a high level of myoplasmic [free Ca^{2+}] is reached), it was possible to detect a Ca^{2+} transient with the Ca^{2+} ion-selective electrode during the Ca^{2+} release from the SR (fig. 11–6). The peak of this transient obtained with Ca^{2+} ion-selective electrode preceded the tension peak, yet the Ca^{2+} ion-selective electrode signal lagged behind the aequorin signal. This indicates that this method is not yet able to record accurately the rate of Ca^{2+} release. Comparison between the estimate of change of myoplasmic [free Ca^{2+}] inferred from the calibration of the ion-selective electrode and the aequorin signal (according to the method described in *Direct detection of changes of myoplasmic free-calcium concentration. . . .*). showed lower values with the former method. The data were deemed too preliminary to be published at this point, yet they showed that the ion-selective electrode underestimated the change of Ca^{2+} activity because its response was too slow to faithfully follow the ascending phase of the Ca^{2+} transient, as already suggested by the lag of the ion-selective electrode signal behind the aequorin signal (fig. 11–6). The lag of the ion-selective electrode response was considerably greater during its falling phase, probably because of the hysteresis previously observed by others [85]: a slower response is usually obtained with decreasing the [free Ca^{2+}] rather than increasing it.

RECORDING OF CHANGE OF THE MYOPLASMIC FREE-CALCIUM CONCENTRATION BY DIFFERENTIAL SPECTROPHOTOMETRY WITH ARSENAZO III

Arsenazo III is a very sensitive probe for changes of myoplasmic [free Ca^{2+}] in the μ*M* and even n*M* range [86]. It has been used to detect the increase of myoplasmic [free Ca^{2+}] caused by Ca^{2+} release from the SR in skinned cardiac cells [87]. A differential microspectrophotometry between 660 and 685 nm was not sufficient to avoid contractile artifacts much larger than the Ca^{2+} signals. Accordingly, it was necessary to use skinned cardiac cells in which the myosin had been extracted by an exposure to high ionic strength [87]. Under these conditions, a good signal–noise ratio was obtained (see fig. 11–9*c*), yet it was not possible to calibrate the signal obtained during Ca^{2+} release from the SR in terms of myoplasmic [free Ca^{2+}] because of the short length of the light path in these very thin skinned cardiac cells (less than 8 μm thick).

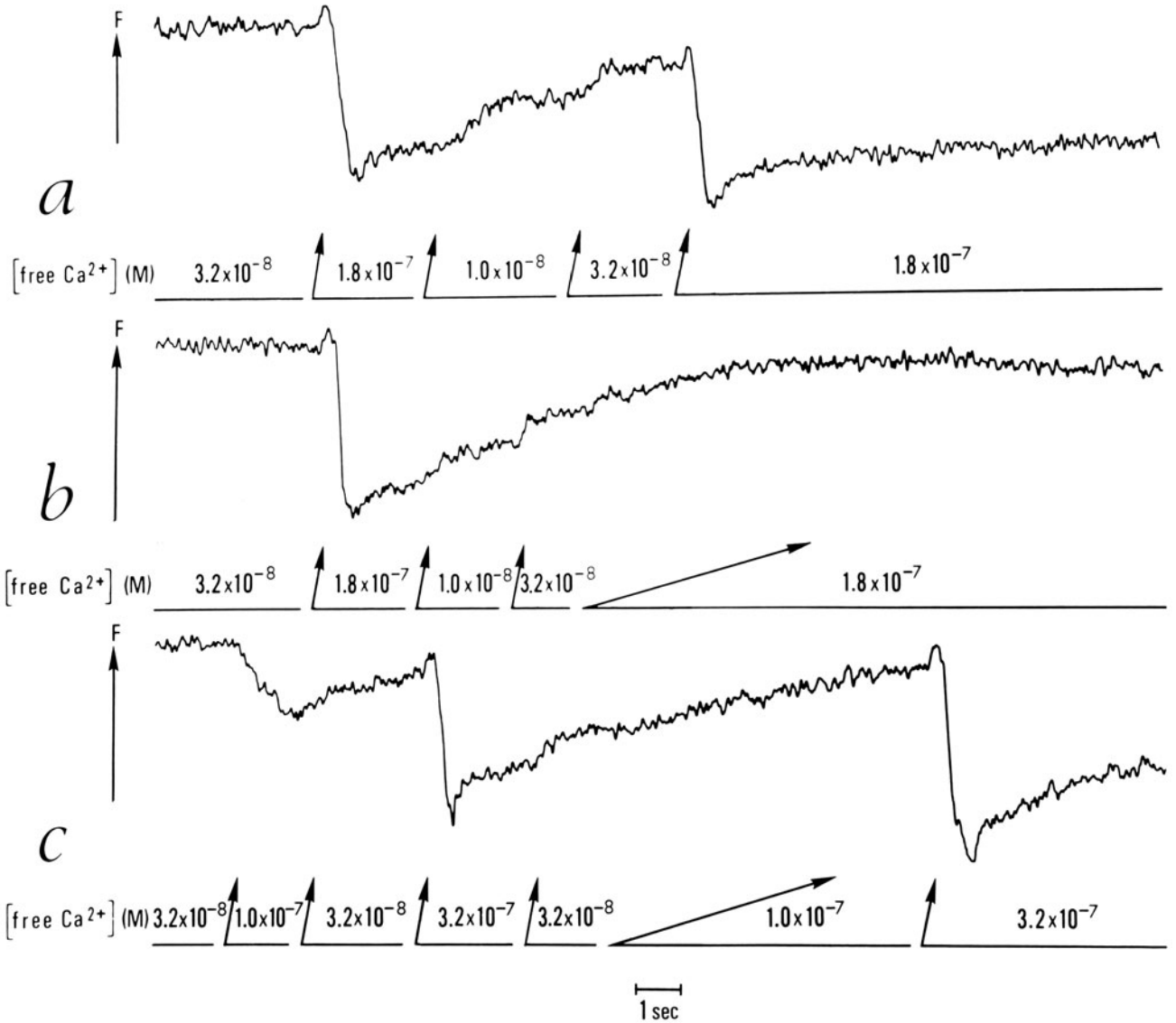
F
a
[free Ca2+] (M)
3.2x10−8
1.8x10−7
1.0x10−8
3.2x10−8
1.8x10−7
F
b
[free Ca2+] (M)
3.2x10−8
1.8x10−7
1.0x10−8
3.2x10−8
1.8x10−7
F
c
[free Ca2+] (M)
3.2x10−8
1.0x10−7
3.2x10−8
3.2x10−7
3.2x10−8
1.0x10−7
3.2x10−7
1 sec

The disadvantages of arsenazo III over aequorin are the following: (a) It is not possible to record contractions simultaneously with the Ca^{2+} signal, at least in skinned cardiac cells. This has been possible, however, for Scarpa in the much larger barnacle muscle fibers [88]. (b) It does not seem possible to calibrate the signal in terms of [free Ca^{2+}] in skinned cardiac cells, while this is obviously possible in preparations of larger dimensions [86, 88]. (c) Arsenazo III at a concentration of 50 μM, which is necessary to obtain satisfactory signals, depresses the ability of the SR to actively accumulate and release Ca^{2+} (fig. 11–7), while it does not affect the sensitivity of the myofilaments to Ca^{2+} [87]. This effect on the cardiac SR is not observed in other tissues [86, 88], but may correspond to a binding of arsenazo III to the cardiac SR similar to the binding which has been described in rabbit skeletal muscle by Beeler et al. [89]. An intracellular binding of arsenazo III seems to exist only in some tissues since Scarpa [86], who has the most extensive experience with arsenazo III, found that its binding to various cellular organelles was negligible in most tissues, including the barnacle muscle [86, 88].

FIGURE 11–8. Demonstration of Ca^{2+} release from the SR by monitoring the changes in the amount of Ca^{2+} bound inside the SR membrane through the detection of the fluorescence of the calcium–chlorotetracycline chelate. The arrow labelled "F" at the left of each tracing indicates an increase of fluorescence, and the size of the arrow corresponds to 5% of the fluorescence measured during the initial perfusion with 3.2×10^{-8} *M* free Ca^{2+}. An increase of fluorescence indicates Ca^{2+} accumulation into the SR, and a decrease of fluorescence indicates Ca^{2+} release. The arrows below each tracing indicate the time of solution change. The degree of obliquity of each arrow indicates the rate of solution change. Three different skinned cardiac cells were used for this experiment with a width between 9 and 10 μm and a length between 55 and 60 μm. The [total EGTA] was 1.0 m*M*, [free Mg^{2+}] 3.16×10^{-4} *M*, [MgATP] 3.16×10^{-3} *M*, pH 7.10, ionic strength 0.160 *M*, and temperature 22°C. The stability constant for the CaEGTA complex was that still considered as correct [13], but the [free Mg^{2+}] was ten times lower than that currently used. Panel *a* demonstrates the reproducibility of the Ca^{2+} release from and subsequent Ca^{2+} reaccumulation into the SR. Note, however, a progressive shift of the baseline due to various factors explained in the text (see *Recording of changes in the amount of calcium. . . .*). Panels *b* and *c* are discussed in the text (see *Evidence in favor of a calcium-induced release. . . .*). Panel *b* demonstrate that the same increase of [free Ca^{2+}] induced Ca^{2+} release when it is applied rapidly (in 0.2 s) whereas it induced Ca^{2+} loading of the SR when it is applied slowly (in 5.4 s). Panel *c* demonstrates that the Ca^{2+}-induced release of Ca^{2+} is graded with the level of [free Ca^{2+}] used as a trigger (compare first and second transients) and with the degree of preload of the SR with Ca^{2+} (compare second and last transients). The preloading has been accomplished by a slow increase of [free Ca^{2+}]. Thus all together this figure demonstrates three factors causing the gradation of the Ca^{2+}-induced release of Ca^{2+}: rate of change of [free Ca^{2+}] outside the SR, level of [free Ca^{2+}] used as a trigger, and degree of preload of the SR with Ca^{2+}. Reproduced from *Nature* [92] with permission of Macmillan Journals Limited.

RECORDING OF CHANGES IN THE AMOUNT OF CALCIUM BOUND TO THE INNER FACE OF THE SARCOPLASMIC RETICULUM MEMBRANE BY MONITORING THE FLUORESCENCE OF CHLOROTETRACYCLINE

Chlorotetracycline has been used for monitoring the amount of Ca^{2+} bound to a variety of biologic membranes or micelles [90, 91]. To circumvent the problem presented by the low permeability of chlorotetracycline across the SR membrane, the SR had to be loaded with the calcium–chlorotetracycline chelate prior to inducing Ca^{2+} release [92]. Then changes of the [free Ca^{2+}] in the lumen of the SR caused by Ca^{2+} movements in and out of the SR resulted in changes in the amount of Ca^{2+} bound to the SR membrane, while chlorotetracycline remained trapped inside the SR. This resulted, in turn, in changes in the amount of calcium–chlorotetracycline chelate bound at the inner face of the SR membrane. In order to eliminate contractions that would cause artifacts on the fluorescence recording, the experiments had to be done either in the presence of a high [total EGTA] [92] or in skinned cardiac cell preparations from which the myosin had been extracted [87]. The fluorescence caused by the calcium–chlorotetracycline chelate can be distinguished from that caused by the magnesium–chlorotetracycline chelate by the use of an appropriate wavelength for excitation (400 nm). The fluorescence emission was recorded at 530 nm. A decrease of fluorescence indicated Ca^{2+} release from the SR whereas an increase of flu-

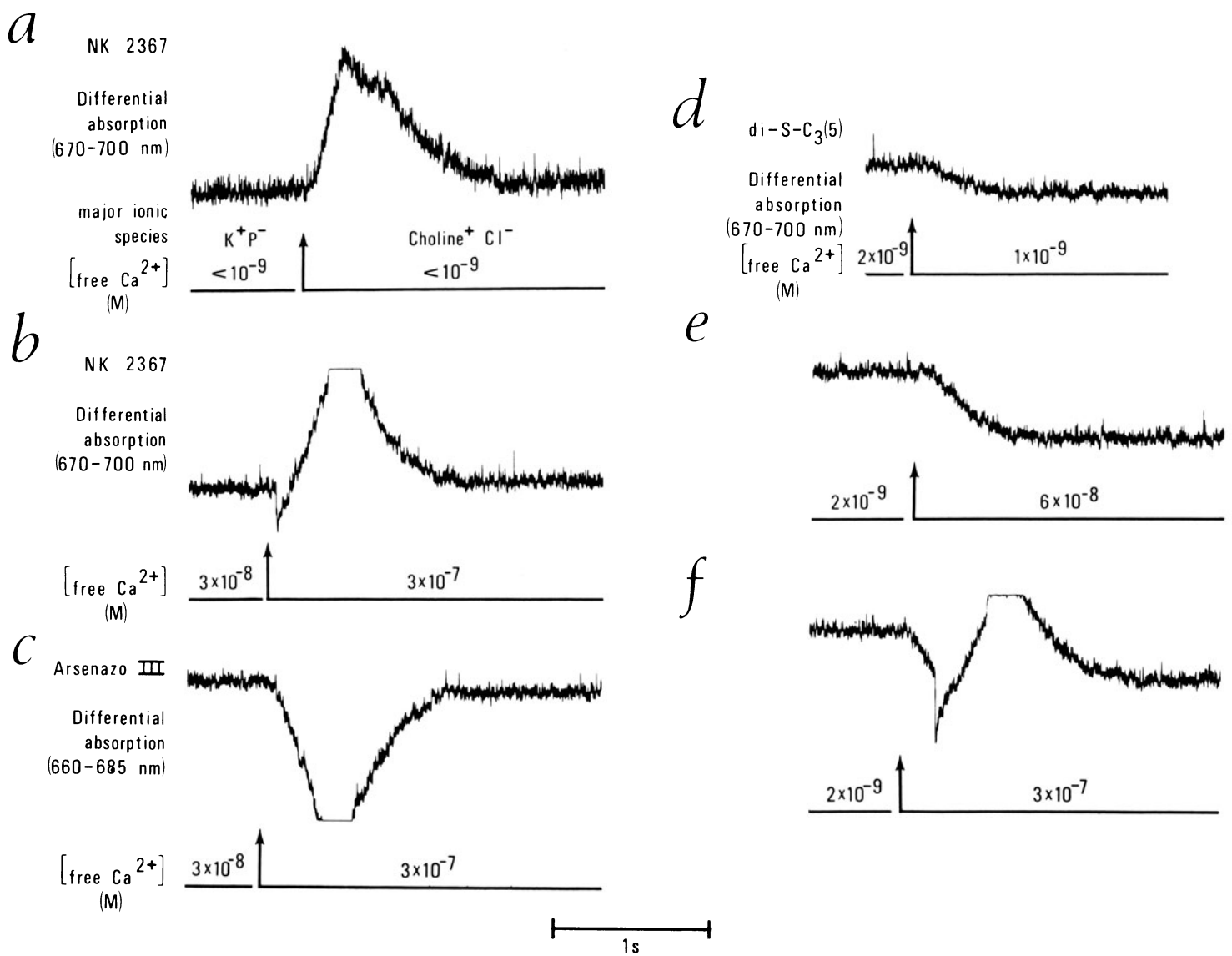
a
NK 2367
Differential absorption (670–700 nm)
major ionic species
$[\text{free } Ca^{2+}]$ (M)
K^+P^-
$<10^{-9}$
$Choline^+ Cl^-$
$<10^{-9}$
b
NK 2367
Differential absorption (670–700 nm)
$[\text{free } Ca^{2+}]$ (M)
3×10^{-8}
3×10^{-7}
c
Arsenazo III
Differential absorption (660–685 nm)
$[\text{free } Ca^{2+}]$ (M)
3×10^{-8}
3×10^{-7}
1s
d
di-S-C_3(5)
Differential absorption (670–700 nm)
$[\text{free } Ca^{2+}]$ (M)
2×10^{-9}
1×10^{-9}
e
2×10^{-9}
6×10^{-8}
f
2×10^{-9}
3×10^{-7}

orescence corresponded to a Ca^{2+} accumulation in the SR (fig. 11–8).

The limitations of this method are the following: (a) It is not possible to record contraction simultaneously with the Ca^{2+} transient. (b) The measurement cannot be quantitative in terms of change of [free Ca^{2+}] inside the lumen of the SR. The change of [free Ca^{2+}] inside the lumen of the SR can be safely assumed to result in a change in the amount of Ca^{2+} bound to the inner face of the SR membrane because this bound Ca^{2+} is likely to be in rapid equilibrium with the free Ca^{2+} inside the lumen of the SR, yet the relation between the [free Ca^{2+}] inside the lumen of the SR and the amount of Ca^{2+} bound to the inner face of the membrane is unknown and is unlikely to be linear [87]. (c) The experiments have to be done within a few seconds because of a photodynamic damage to the SR induced by the illumination of the preparation in the presence of chlorotetracycline and because chlorotetracycline has a weak Ca^{2+} iontophoretic effect [92]; in addition, despite its low permeability, chlorotetracycline slowly leaks through the SR membrane, which results in a progressive shift of the baseline (fig. 11–8). Despite these disadvantages, the chlorotetracycline method has a unique value because it is the only one available to monitor change of Ca^{2+} content of the SR as opposed to change of myoplasmic [free Ca^{2+}] resulting from Ca^{2+} release from the SR.

RECORDING OF CHANGES OF CHARGE DISTRIBUTION ON THE SARCOPLASMIC RETICULUM MEMBRANE WITH POTENTIAL-SENSITIVE DYES

A number of dyes are used to record change of membrane potential from various tissues and organelles [93]. In skinned cardiac cells, three potential-sensitive dyes were used: merocyanine 540 with fluorescence measurements, merocyanine oxazolone (NK 2367) with light absorption measurements, and di-S-C_3(5) with both fluorescence and absorption measurements [87, 94]. Again for this optical recording it is necessary to eliminate the contraction by the use of a high [total EGTA] or by extraction of the myosin. This is the case, at least for the 8- to 10-μm-thick skinned preparations from both cardiac and skeletal muscle, even when the preparations are stretched at a sarcomere length beyond the overlap between thick and thin filaments [94]. In contrast, according to Best et al. [95], a differential recording entirely eliminates the contractile artifacts in about 70-μm-diameter skinned fibers from skeletal muscle.

In a first series of experiments (fig. 11–9A), it was demonstrated that change of charge distribution on the SR membrane can be detected with these dyes. This change of charge distribution was generally elicited after equilibrating the preparation during more than 10 min in the presence of a medium containing potassium (K^+) as the major cation and propionate (P^-) as the major anion. Then the solution was rapidly replaced by a solution containing choline (Ch^+) as the major cation and chloride (Cl^-) as the major anion. Since Ch^+ diffuses more slowly into the SR than K^+ diffuses out, there should be a transient increase of cation concentration, and thus positive charge, outside the SR membrane. Simultaneously there should be a transient increase of anion concentration, and thus negative charge, inside the SR membrane because Cl^- diffuses more rapidly into the SR than P^- diffuses out. Both cationic and anionic changes should, therefore, result in the outside

FIGURE 11–9. Recording of change of charge distribution on the SR membrane of skinned cardiac cells from the adult rat ventricle stained with 0.3 mg/ml of the potential-sensitive dye NK 2367 *(a* and *b)* or with 5.0×10^{-6} *M* of the potential-sensitive dye di-S-C_3(5) *(d–f)*. For comparison, phasic changes of myoplasmic [free Ca^{2+}] are also recorded in the presence of 5×10^{-5} *M* arsenazo III *(c)*. For these experiments, different skinned cardiac cells, which all had a width of 9–10 μm and a length of 57–61 μm, were used. In all cases, the skinned cells had the myosin extracted by prior exposure to 0.510 *M* ionic strength, and the recording was done with differential absorption microspectrophotometry. The [total EGTA] was 4×10^{-4} *M*, the [free Mg^{2+}] 3.2×10^{-3} *M*, [MgATP] 3.2×10^{-3} *M*, pH 7.10, ionic strength 0.160 *M*, and temperature 22°C. The stability constants were those currently employed [13]. Azide (1×10^{-2} *M*) was present in all cases to dissipate the membrane potential of the mitochondria (see Fabiato [94]). Note that in panels *b*, *c*, and *f* the signals exceeded the full-scale amplitude of the recorder channel. Reproduced from the *Canadian Journal of Physiology and Pharmacology* [87] with permission of the publisher.

of the SR membrane becoming relatively more positive (or less negative) with respect to the inside. This will be subsequently referred to as a net increase of positive charge outside the SR membrane. The solution change from K^+P^- to Ch^+Cl^- resulted in a transient signal on the light absorption or fluorescence recording (fig. 11–9*a*), while the return to the initial solution caused the recording to return to its initial baseline (fig. 11–9*a*).

A number of artifactual possibilities for explaining this type of signal have been eliminated [94]: (1) The signal appeared to be dye related since it was not observed in the absence of the dye. (2) The signal was not a particular property of a given dye or an artifact of a particular optical recording method since light absorption and fluorescence recordings done with three different dyes gave qualitatively the same results. (3) The signal was not caused by a contraction artifact since all contraction had been eliminated. (4) The signal was not influenced by the polarization of the light at 0° or 90°. (5) The signal was related to the presence of the SR since no signal was observed in preparations in which the SR had been destroyed by detergent treatment. (6) The signal was not caused by a change of potential across the membrane of the mitochondria since azide (10 m*M*) was added to all the solutions in order to dissipate the membrane potential of the mitochondria. Comparative experiments in practically mitochondria-free, 10-μm-wide skinned fibers from a fast skeletal muscle also eliminated a role of the mitochondria in the generation of the transient signal. (7) The signal was not caused by the osmotic effect on the SR of the ionic substitution. The change from K^+P^- to K^+Cl^- and the change from K^+P^- to Ch^+P^- both produced a signal in the same direction, the one presumed to correspond to an increase of the net positive charge outside the SR membrane. These ionic substitutions should have had opposite osmotic effects: swelling for the change from K^+P^- to K^+Cl^-, shrinkage for the change from K^+P^- to Ch^+P^-. (8) The signal was not caused by the translocation of Ca^{2+} across the SR membrane, since it could be observed when the SR had been unloaded of Ca^{2+} and in the virtual absence of free Ca^{2+} in the solution (fig. 11–9*a*). It must be noted, however, that such signals, induced by changes of charge distribution on the SR membrane that are not related to Ca^{2+} movement, have not been observed in large preparations of skinned fibers from skeletal muscles [95]. In these preparations and with the methods used by Best et al. [95], Ca^{2+} movements across the SR membrane were a requirement for the obtaining of signals (see the discussion following this symposium paper [95]).

These experiments did not permit, however, a decision as to whether the signals recorded with potential-sensitive dyes corresponded truly to a change of transmembrane potential rather than to a change of surface potential (see Russell et al. [96, 97] for a discussion of this problem).

A second series of experiments demonstrated that a signal in the direction of a decrease of net positive charge outside the SR membrane was observed during Ca^{2+} accumulation (fig. 11–9*d–e*), whereas a signal in the direction of an increase of net positive charge was observed during Ca^{2+} release (fig. 11–9*b* and *f*, and Fabiato [87, 94] and Fabiato and Fabiato [98]). These results will be discussed in the following section of the chapter.

The major problem with respect to these potential-sensitive dye experiments is that they do not either support or eliminate the presence of a potential change across the SR membrane during Ca^{2+} accumulation and release. In addition, the experiments cannot be done in the presence of a contraction.

Mechanism of the Calcium Release from the Sarcoplasmic Reticulum

EVIDENCE IN FAVOR OF A CALCIUM-INDUCED RELEASE OF CALCIUM FROM THE CARDIAC SARCOPLASMIC RETICULUM

The hypothesis of a Ca^{2+}-induced release of Ca^{2+} was proposed initially for skeletal muscle [99] (see Frank [100] for a recent review). Direct tests of this hypothesis have been provided by experiments on skinned fibers of skeletal muscle [101, 102], cardiac muscle [103], and even smooth muscle [104]. For cardiac muscle, the hypothesis is that the transsarcolemmal in-

flux of Ca^{2+} would not activate the myofilaments directly, but would induce a Ca^{2+} release from the SR that would then activate the myofilaments.

In skinned cardiac cells of all adult mammalian cardiac tissues, it is possible to induce a Ca^{2+} release from the SR with a [free Ca^{2+}] much lower than that required for directly activating the myofilaments. This can be quantitatively demonstrated by experiments done in the presence of a high [total EGTA] and using caffeine for the detection of the Ca^{2+} release as shown in figure 11–5 [2, 15, 79]. In contrast to the results reported for skinned fibers of skeletal muscle [1, 78], a high, probably physiologic [free Mg^{2+}] such as 3.16 m*M* free Mg^{2+}, does not inhibit the Ca^{2+} release, but instead increases the amount of Ca^{2+} released [13, 105]. The increase of [free Mg^{2+}] results in an increase of [free Ca^{2+}] required for triggering Ca^{2+} release, but it also decreases the sensitivity of the myofilaments to Ca^{2+}. Consequently the [free Ca^{2+}] requirement for Ca^{2+}-induced release of Ca^{2+} remains much lower than that needed for directly activating the myofilaments [13, 105].

The experiments done in the presence of a high [total EGTA], however, place the cell under an unphysiologic condition, in that myoplasmic [free Ca^{2+}] is homogeneous. In addition, EGTA, at concentrations higher than 1 m*M*, tends to modify the charge distribution on the SR membrane as detected with potential-sensitive dyes [16, 87, 94]. The experiments done in the presence of a low [total EGTA], as shown in figure 11–4D and E, demonstrate a Ca^{2+}-induced release of Ca^{2+} under conditions more closely approaching the physiologic Ca^{2+} buffering present in the intact cardiac cells. Unfortunately, these experiments do not permit an assessment of the [free Ca^{2+}] required to induce this Ca^{2+} release.

Thus, it has not yet been possible to provide quantitative information on the Ca^{2+} flux required to trigger Ca^{2+} release, information that could be compared with the measurement of Ca^{2+} influx across the sarcolemma of an intact cell. Yet, some experiments suggest that no transsarcolemmal Ca^{2+} influx, irrespective of its magnitude, could activate the myofilaments without first triggering a Ca^{2+} release from the SR. Such an experiment is shown in figure 11–10. In this experiment, the [free Ca^{2+}] requirement for tension development and the rate of tension development of the same skinned cardiac cell were evaluated before and after the disruption of the SR with a nonionic detergent. Controls confirmed that the detergent does not significantly modify the sensitivity of the myofilaments to Ca^{2+} (fig. 11–10A and C). The experiment itself was done in the presence of a constant low [total EGTA] of 5×10^{-5} *M* (fig. 11–10B). The widest skinned cardiac cell possible (14 μm) was chosen to accentuate the diffusion delays of externally applied solutions. It was observed that (a) contraction could be elicited by a much lower [free Ca^{2+}] (or, if one prefers, much less total calcium with the same [total EGTA]) when the SR was present than after its destruction; and (b) tension induced in the absence of the SR even by a high [free Ca^{2+}] had a much lower rate of development than when the SR was present.

Because these data were obtained in the presence of a low [total EGTA], they do not permit a precise definition of the [free Ca^{2+}] required for the induction of a Ca^{2+} release. Nevertheless, these data suggest that no transsarcolemmal influx of Ca^{2+} of any magnitude could directly activate the myofilaments without producing a Ca^{2+}-induced release of Ca^{2+} from the SR unless unphysiologic experimental conditions give to the SR of skinned cardiac cells properties that they do not have in the intact cells.

The calcium "trigger" is not a simple change of [free Ca^{2+}] at the external surface of the SR, $d[Ca^{2+}]_{ext}$, but also a function of the rate of this change, $d[Ca^{2+}]_{ext}/dt$. Thus a fast change of [free Ca^{2+}] induces Ca^{2+} release from the SR whereas a slow change of [free Ca^{2+}] results in a loading of the SR with Ca^{2+} (fig. 11–8*b*). Thus, it was proposed [92] that the initial relatively fast burst of Ca^{2+} influx across the sarcolemma (fig. 11–2, hatched area) could trigger Ca^{2+} release from the SR. The subsequent slow component of Ca^{2+} influx, corresponding to current flow through noninactivating Ca^{2+} channels (fig. 11–2), would load the SR with

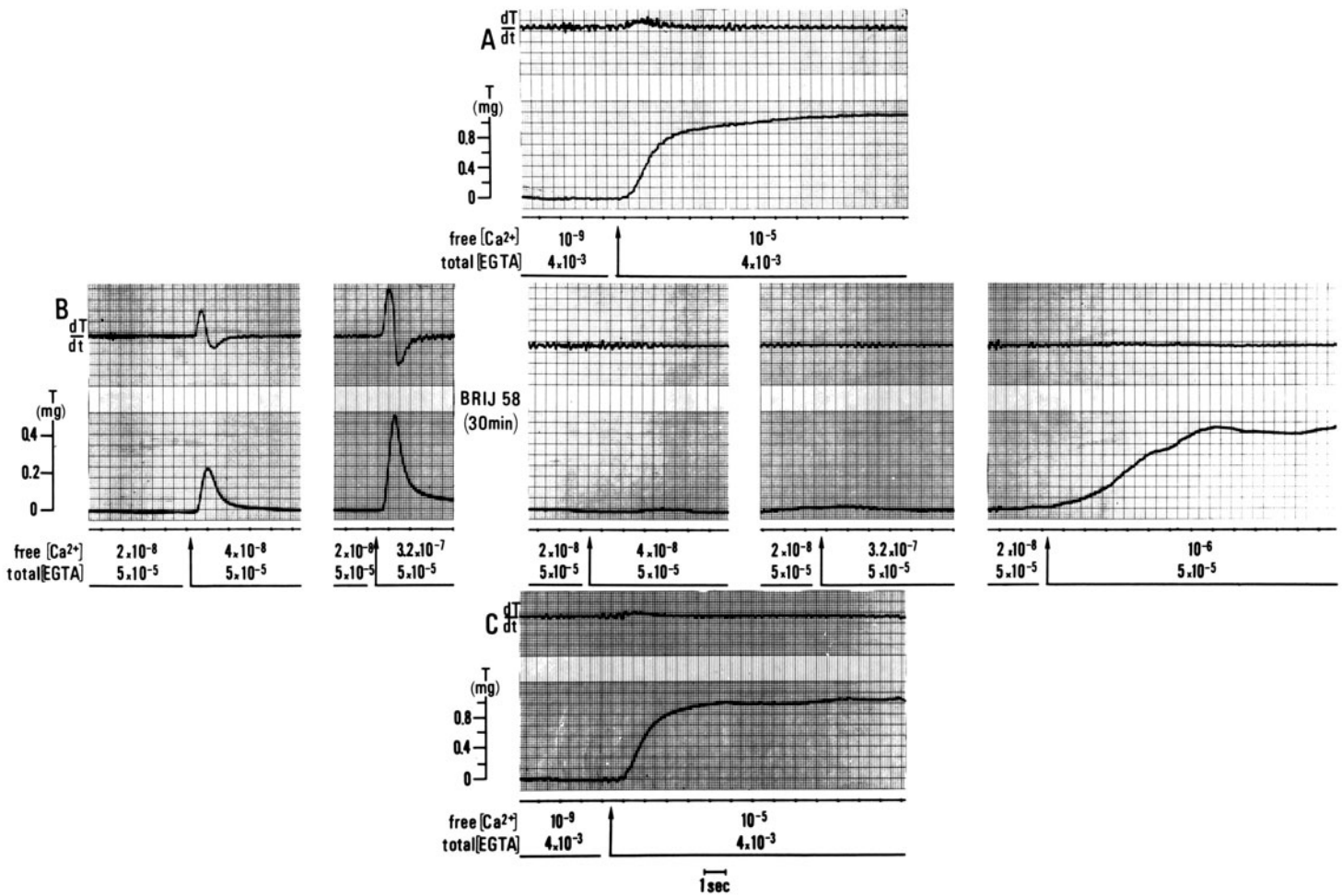
A
dT/dt
T (mg)
0.8
0.4
0
free [Ca2+] 10-9 10-5
total [EGTA] 4.10-3 4.10-3
B
dT/dt
T (mg)
0.4
0.2
0
BRIJ 58
(30min)
free [Ca2+] 2.10-8 4.10-8 2.10-8 3.2.10-7 2.10-8 4.10-8 2.10-8 3.2.10-7 2.10-8 10-6
total [EGTA] 5.10-5 5.10-5 5.10-5 5.10-5 5.10-5 5.10-5 5.10-5 5.10-5 5.10-5 5.10-5
C
dT/dt
T (mg)
0.8
0.4
0
free [Ca2+] 10-9 10-5
total [EGTA] 4.10-3 4.10-3
1 sec

an amount of Ca^{2+} available for release during subsequent beats [92].

The Ca^{2+}-induced release of Ca^{2+} is not an all-or-none process. Three factors of gradation have been described: the level of preload of the SR with Ca^{2+}, the rate of change of [free Ca^{2+}], and the level of [free Ca^{2+}] used as a trigger (fig. 11–8). The gradation as a function of the [free Ca^{2+}] used as a trigger has been observed in experiments detecting Ca^{2+} release through (a) tension transients in the presence of a low [total EGTA] [77], (b) tension recording in the presence of a high [total EGTA] (fig. 11–5B and C), (c) aequorin bioluminescence [13], and (d) chlorotetracycline fluorescence (fig. 11–8). This tight gradation of the Ca^{2+}-induced release of Ca^{2+} with both the rate and amplitude of the [free Ca^{2+}] change triggering it is qualitatively consistent with the gradation of the contraction of the mammalian ventricle with the transsarcolemmal Ca^{2+} current [28, 106, 107]. When the [free Ca^{2+}] becomes supraoptimum, the amount of Ca^{2+} released is decreased, suggesting an inactivation of the Ca^{2+} release caused by the excessive increase of [free Ca^{2+}] outside the SR [13]. This finding is also consistent with the observation that the amplitude of the contraction of intact cardiac muscle from the rat ventricle is decreased in the presence of a supraoptimum extracellular [Ca^{2+}] [108, 109].

Comparative studies between different animal species and between different developmental stages in the same cardiac tissue show a good correlation between a highly developed Ca^{2+}-induced release of Ca^{2+} from the SR and a short plateau of the action potential [16]. In the skinned cell of the dog Purkinje tissue the [free Ca^{2+}] required to trigger Ca^{2+} release is higher than in the dog ventricular tissue, but a larger Ca^{2+} release is obtained. In addition, the myofilaments are less sensitive to Ca^{2+} in the dog Purkinje tissue than in the dog ventricular tissue or in any other adult mammalian cardiac tissue [16].

As previously indicated, the observation of cyclic contractions (fig. 11–4) does not demonstrate in itself a Ca^{2+}-induced release of Ca^{2+}; yet, after a Ca^{2+} release has been induced by a rapid increase of [free Ca^{2+}] in the myoplasm, the Ca^{2+} release repeats itself cyclically. This is clearly an unphysiologic phenomenon. However, the repetition of the Ca^{2+} release can be prevented by a decrease of the myoplasmic [free Ca^{2+}] by the same small amount that has been used to induce Ca^{2+} release (fig. 11–11A as compared to B). This

FIGURE 11–10. Comparison of the amplitude and rate of tension development induced by application of Ca^{2+} before and after the destruction of the SR. The experiment was done in a particularly large skinned cardiac cell from the rat ventricle (14 μm wide and 50 μm long). Such a large preparation was done in order to render more obvious the difference in rate of tension development caused by the Ca^{2+} release from the SR. Much shorter diffusion delays are obtained when directly activating the myofilaments in the less than 10-μm-wide preparations that are usually employed. The recordings were done in the order in which they are shown. The destruction of the ability of the SR to actively accumulate and release Ca^{2+} was accomplished by a 30-min treatment with 0.5% of the nonionic detergent polyoxyethylene cetyl ether 20 (Brij 58). Note that the tension scale in panels *A* and *C* is half of that used in panel *B*. Arrows indicate the time of solution change. *(A* and *C)* Controls demonstrating that the detergent treatment did not modify the sensitivity of the myofilaments to Ca^{2+}, as previously demonstrated [77]. *(B)* The experiment itself comparing the contractile activation before and after detergent treatment in the presence of a constant [total EGTA] of 5.10×10^{-5} *M*. If it could be ascertained that the procedure used for removing the membrane and the artificial solutions used for superfusing the skinned cell do not give unphysiologic properties to the SR, then this experiment would demonstrate that no transsarcolemmal Ca^{2+} influx, irrespective of its magnitude, could activate the myofilaments without first triggering a Ca^{2+} release from the SR. Similar experiments have been done in skinned cells from the rabbit ventricle which is the adult cardiac tissue in which Ca^{2+}-induced release of Ca^{2+} from the SR is the least developed [15]. Even in the rabbit ventricular skinned cardiac cells, the results were qualitatively similar to those shown in the present figure which were obtained from the rat ventricular skinned cell in which the Ca^{2+}-induced release of Ca^{2+} from the SR is the most highly developed. Thus, the conclusion derived from these experiments seems to apply to all mammalian cardiac tissues. It must be repeated, however, that this conclusion is qualified by the possibility that the SR of skinned cardiac cells may be in an unphysiologic condition, a possibility that cannot be definitely discounted. (Reproduced from the *Annals of the New York Academy of Sciences* [15] with permission of the publisher.)

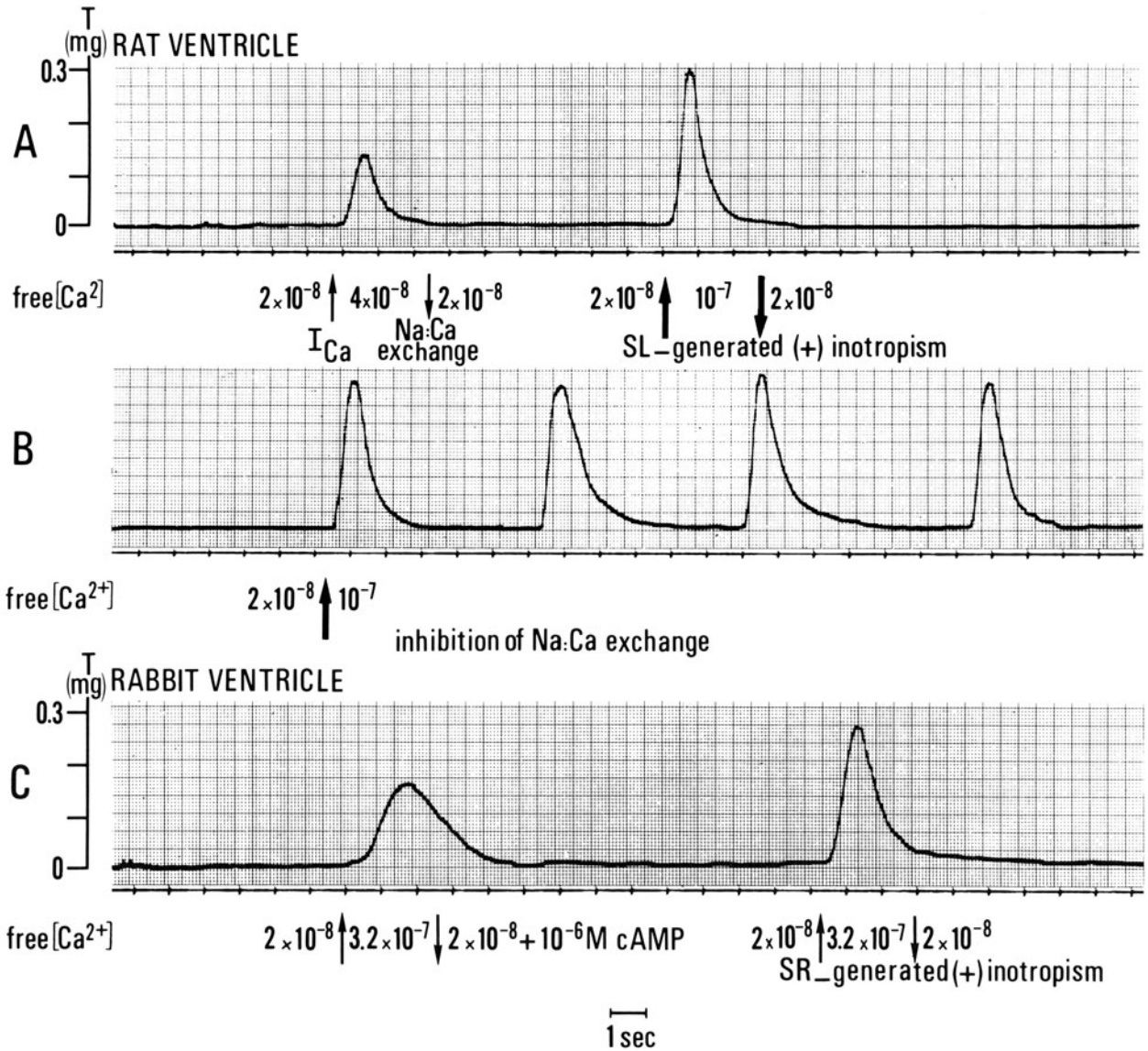
T
(mg) RAT VENTRICLE
0.3
0
A
free[Ca2]
2×10-8 4×10-8 2×10-8
ICa
Na:Ca exchange
2×10-8 10-7 2×10-8
SL–generated (+) inotropism
B
free[Ca2+]
2×10-8 10-7
inhibition of Na:Ca exchange
T
(mg) RABBIT VENTRICLE
0.3
0
C
free[Ca2+]
2×10-8 3.2×10-7 2×10-8+10-6M cAMP
2×10-8 3.2×10-7 2×10-8
SR–generated (+) inotropism
1 sec

suggests that reaccumulation of Ca^{2+} by the SR is not sufficient to lower the myoplasmic [free Ca^{2+}] to a level low enough to prevent repetition of the Ca^{2+} release. Thus the Ca^{2+} reaccumulation into the SR must be backed up by another process which is likely to take place in the sarcolemma. As discussed in *Sodium–calcium exchange,* this process is not likely to be limited by the Na^{+}–Ca^{2+} exchange which would function in the direction of an extrusion of Ca^{2+} after the Ca^{2+} release from the SR has caused an increase of myoplasmic [free Ca^{2+}]. Instead the Ca^{2+} pump across the sarcolemma would function during diastole to maintain the myoplasmic [free Ca^{2+}] at a low level and prevent the reinduction of a Ca^{2+} release (see *Sarcolemmal calcium pump*). If the hypothesis that the cyclic repetition of Ca^{2+}-induced release of Ca^{2+} from the SR is prevented by the Ca^{2+} extrusion through the sarcolemma is correct, then it should be possible to induce repetitive Ca^{2+} release in intact preparations by inhibiting the extrusion of Ca^{2+} across the sarcolemma. This seems indeed to be the case under conditions causing an increase of myoplasmic [free Ca^{2+}]. Thus, for instance, aftercontractions are observed during digitalis intoxication [112, 113] that may depress Ca^{2+} extrusion by both Na^{+}-Ca^{2+} exchange and sarcolemmal Ca^{2+} pump.

The Ca^{2+}-induced release of Ca^{2+} is influenced by a number of factors that are known to influence the contraction in intact cardiac muscle. Many ionic or pharmacologic interventions which enhance Ca^{2+} accumulation into the SR also facilitate Ca^{2+} release. Consequently a lower [free Ca^{2+}] is required to induce Ca^{2+} release, and a larger amplitude Ca^{2+} transient is detected by tension or aequorin bioluminescence. Figure 11–11C shows this type of effect

---

FIGURE 11–11. Examples of experiments suggesting that the Ca^{2+}-induced release of Ca^{2+} from the SR demonstrated in skinned cardiac cells is compatible with known properties of the physiologic excitation–contraction coupling. The skinned cardiac cell from the rat ventricle *(A* and *B)* was 10 μm wide and 48 μm long. The skinned cardiac cell from the rabbit was 11 μm wide and 42 μm long. SL, sarcolemma; SR, sarcoplasmic reticulum. The arrows indicate the time of solution change. The [free Mg^{2+}], pH, and apparent stability constant for the CaEGTA complex were the same as used for Figures 11–4 and 11–5. Comparison between the first and the second tension transients in panel *A* demonstrates that the amount of Ca^{2+} release resulting from the Ca^{2+}-induced release of Ca^{2+} from the SR increases when the [free Ca^{2+}] used as a trigger is increased. This mechanism of gradation of the Ca^{2+} release could be produced physiologically by an increase in the Ca^{2+} influx across the sarcolemma, such as that caused by catecholamines [114], or by a decrease of the Ca^{2+} extrusion from the cell by Na^{+}-Ca^{2+} exchange, which is a possible mechanism for the positive inotropic effect of digitalis. Comparison between panels *A* and *B* demonstrates that the cyclic repetition of the Ca^{2+}-induced release of Ca^{2+} can be prevented by a decrease of the [free Ca^{2+}] in the bulk of the solution by an amount whose absolute value is equal to the increase of [free Ca^{2+}] that has been used to induce Ca^{2+} release. This suggests that the physiologic excitation–contraction coupling requires that a mechanism of Ca^{2+} extrusion across the SL back up the Ca^{2+} accumulation in the SR. When these results were initially presented [15], it was thought that the arguments for a Ca^{2+} pump in the SL were insufficient. Thus the backup mechanism was entirely attributed to the Na^{+}-Ca^{2+} exchange. In fact, recent evidence reviewed in the text (see *Sodium–calcium exchange*) suggests that, although the Na^{+}-Ca^{2+} exchange helps in removing Ca^{2+} at the peak of the Ca^{2+} release from the SR, the Ca^{2+} pump of the SL is the likely mechanism for maintaining the diastolic myoplasmic [free Ca^{2+}] low and preventing the repetitive reinduction of the Ca^{2+} release from the SR. Abnormal conditions indirectly depressing the Ca^{2+} extrusion mechanisms across the SL in the intact cardiac cells would result in a cyclic repetition of the Ca^{2+}-induced release of Ca^{2+} from the SR causing after contractions, as is observed during digitalis intoxication [112, 113]. The experiment in panel *C* demonstrates that cyclic AMP, one of the effects of which is directly on the SR [114], causes an increase of the amount of Ca^{2+} released together with an increase of the rate of relaxation. This is an example of positive inotropic effect generated by action of a pharmacologic mediator on the SR. This experiment has been done in a skinned cardiac cell from the rabbit ventricle in which the Ca^{2+}-induced release of Ca^{2+} is poorly developed and the rate of relaxation slow under control conditions. Comparison between panels *C* and *A* and *B* shows that the application of cyclic AMP gives to the SR of the rabbit ventricular skinned cell properties similar to those observed in the skinned cell from the rat ventricle, which is the mammalian ventricular tissue in which the Ca^{2+}-induced release of Ca^{2+} is the most highly developed [15, 16]. Reproduced from the *Annals of the New York Academy of Sciences* [15] with permission of the publisher.

with cyclic AMP. A skinned cardiac cell from the rabbit ventricle has been selected for this experiment because the skinned cells from this tissue have a poorly developed Ca^{2+}-induced release of Ca^{2+} and a low rate of relaxation under control conditions. The results of this type of experiment have suggested some interaction between the mechanism of the Ca^{2+}-induced release of Ca^{2+} and the Ca^{2+} pump of the SR [15, 74, 75, 79], but the effect of Mg^{2+} is an exception inasmuch as it enhances Ca^{2+} accumulation in the SR while increasing the [free Ca^{2+}] required to trigger Ca^{2+} release. Thus it seems that the hypothesis of a direct participation of the mechanism of Ca^{2+} accumulation to the Ca^{2+}-induced release process should be rejected.[6] One possibility, which has been suggested by Chiesi et al. [110], is that the occupancy of the high-affinity sites of the Ca^{2+} pump of the sarcolemma plays a permissive role for the Ca^{2+} release from the SR.

Experiments with potential-sensitive dyes [87, 94] might provide a first test of the hypothesis proposed by Chiesi et al. [110]. When Ca^{2+} release is induced by an increase of myoplasmic [free Ca^{2+}], a small, brief signal in the direction of a decrease of net positive charge outside the SR membrane is observed before the large, long signal in the direction of an increase of positive charge outside the SR membrane. The latter signal corresponds to the Ca^{2+} release from the SR (fig. 11–9*b*), while the former is much faster than any signals in the same direction that are observed during Ca^{2+} accumulation. This is demonstrated by the experiments shown in figure 11–9*d–f*. To clearly show the phase of Ca^{2+} accumulation, the skinned cell was initially placed in a low [free Ca^{2+}] in all the three runs. Thus the SR was empty, and a phase of Ca^{2+} accumulation of long duration was observed when the [free Ca^{2+}] in the bathing solution was increased. A larger increase of [free Ca^{2+}] resulted in a larger signal in the direction of a decrease of net positive charge outside the SR membrane (fig. 11–9*d* and *e*). When the [free Ca^{2+}] reached a level sufficient to induce Ca^{2+} release, the signal caused by Ca^{2+} accumulation was followed by a more than 50-fold faster signal in the direction of a decrease of positive charge outside the SR membrane. This was, in turn, followed by a reversal of the signal during the phase of Ca^{2+} release.

It was tentatively suggested [87, 94] that this rapid, small signal might give a first hint to the Ca^{2+} binding to the high-affinity sites of the Ca^{2+} pump proposed in the hypothesis of Chiesi et al. [110]. Many problems remain to be solved before the testing of this hypothesis may be pursued. The fact that a similar signal preceding Ca^{2+} release is observed with chlorotetracycline (see fig. 11–8 and Fabiato [87]) may suggest that it corresponds to an event taking place inside the SR. On the other hand, it may also suggest that chlorotetracycline and potential-sensitive dyes record, in fact, the same basic transmembrane ionic pertubation, or change of charge distribution, or undefined conformational change. For instance, Cohen et al. [111] briefly mentioned that the fluorescence signal recorded with chlorotetracycline is sensitive to membrane potential in squid axons. In the case of the cardiac SR there may be no membrane potential at all, but both chlorotetracycline and the three potential-sensitive dyes used may record the same type of altered charge distribution related to Ca^{2+} movement across the SR membrane. Yet, control experiments have demonstrated that ionic switch from K^+P^- to Ch^+Cl^- does not induce any signal in skinned cardiac cells stained with chlorotetracycline (Fabiato, unpublished observations). It must be noted that although this ionic switch induced a signal with potential-sensitive dyes, it does not produce a Ca^{2+} release from cardiac SR even when the SR has been loaded with Ca^{2+} [2, 80, 123] as opposed to the results obtained from skinned fibers of skeletal muscle [1].

Another potential problem with the experiment shown in figure 11–9*b* and *d–f* is that the brief signal in the direction of a decrease of net positive charge outside the SR membrane might correspond to a redistribution of the dye with respect to the SR membrane during the beginning of the Ca^{2+} release. Such oscillations of the signal are observed with potential-sensitive dyes during the recording of change

of transmembrane potential in squid axon when the preparations are damaged, for instance, by microelectrode impalement. Thus, it would be very interesting to be able to ascertain that this brief signal in the direction of a decrease of positive charge outside the SR membrane indeed precede the Ca^{2+} release. Since two optical recordings cannot be done simultaneously, a Ca^{2+} recording with ion-selective electrodes would theoretically be the best approach. This is why we have done the collaborative work which is illustrated in figure 11–6. Unfortunately, the result indicates that the recordings with Ca^{2+} ion-selective electrodes are too slow to answer the question of whether the very rapid signal recorded with potential-sensitive dyes precedes the Ca^{2+} release from the SR.

ARGUMENTS AGAINST A CALCIUM-INDUCED RELEASE OF CALCIUM FROM THE SARCOPLASMIC RETICULUM

Perhaps the most important argument against the hypothesis of a Ca^{2+}-induced release of Ca^{2+} from the SR is that no satisfactory mechanism has yet been proposed to explain how an increase of [free Ca^{2+}] outside the SR membrane induces a release of Ca^{2+} from the lumen of the SR and why this phenomenon is graded rather than all-or-none.[7] However major this problem may be, it does not represent in itself a compelling argument against the hypothesis. It simply indicates that much more work is needed before the hypothesis can be thoroughly tested.

Another major argument against the acceptance of a physiologic role for Ca^{2+}-induced release of Ca^{2+} from the SR is the possibility, stated many times in this chapter, that unphysiologic conditions may give the SR properties that it does not have in the intact cells. These potential unphysiologic conditions are of two types: structural modifications and superfusing solutions which do not accurately mimic the physiologic intracellular milieu.

Among the structural modifications, a dilation of the SR has been shown in skinned cardiac cells (see fig. 6 in Fabiato and Fabiato [15]). The addition of 100 m*M* sucrose to the solution in order to reduce the swelling of the SR [115, 116] did not inhibit the Ca^{2+}-induced release of Ca^{2+} from skinned cells but, to the contrary, facilitated it [15]. Alternatively it has been suggested that the swelling of the SR could be passive and caused by the swelling of the myofilament lattice observed in skinned fiber preparations [117]. Shrinkage of the myofilament lattice by adding polyvinylpyrrolidone to the solution did not modify the Ca^{2+}-induced release of Ca^{2+} [15, 77].

Another possibility is that the skinning procedure may remove important structures participating in excitation–contraction coupling such as the junction between the sarcolemma and superficial cisternae of the SR[118]. This possibility has been explored by comparing results in skinned single cardiac cells with those obtained in groups of cardiac cells with disrupted, but not removed, sarcolemma. Some results from preparations with disrupted sarcolemma made from frog ventricle have been reviewed in this chapter (see *Arguments against a calcium release. . . .*). Results obtained with similar preparations from the mammalian cardiac tissue have been previously discussed [16, 80, 123] with the conclusion that these data are very difficult to interpret. Nevertheless, even in these preparations, phasic contractions are induced by a small increase of [free Ca^{2+}] in the solution [16, 80].

With respect to imperfections in simulating the intracellular milieu, two types of problems are encountered. The first concerns the ionic composition of the intracellular milieu. As knowledge of the intracellular ionic concentrations has progressed, the solutions used for experiments in skinned cardiac cells have been modified [76]. Unphysiologic constituents in the solution, such as glucose[8] which was used in early experiments [77] have been removed [76], while intracellular metabolites, such as pyruvate and malate, have been introduced in the experiments in which the function of the mitochondria was evaluated [76]. The results reported up to now did not include the systematic addition of metabolites and mediators such as cyclic-AMP-dependent protein kinase and calmodulin to the solutions.

The improvement in the accuracy in which

the solution used in skinned cardiac cells mimics the intracellular milieu is apparent when comparing the methods section of the successive publications. This improvement is slow for two reasons. First, the composition of the intracellular milieu, the concentration of metabolites and mediators, and the stability constants for these compounds such as calmodulin that bind Ca^{2+} are only slowly established. Secondly, when the concentration and stability constants of an ion, metabolite, or pharmacologic mediator become known, then it is needed to thoroughly test the effects of its addition to the solution on the properties of skinned cardiac cells. At this point, comparisons between the results obtained before and after the additions and modifications are published so that the earlier results can be reinterpreted.

An example of this slow improvement has been the successive changes of the pH buffer used for the experiments. Initially [103], imidazole was used because this was the pH buffer employed by most investigators in skeletal muscle skinned fiber experiments [101]. Then it was observed that imidazole, a phosphodiesterase stimulator, depressed the contraction elicited by Ca^{2+}-induced release of Ca^{2+} from the SR [119]. Accordingly, imidazole was replaced by tris-(hydroxymethyl) aminomethane (Tris) which had been thoroughly tested by Endo [102] for its absence of deleterious effect in skinned skeletal muscle fibers. But Tris is a poor buffer at a pH of around 7.00. This problem became a major one when Endo's method [1, 78] using a high [total EGTA] to induce Ca^{2+} release was employed. The release of Ca^{2+} from the SR causes a displacement of H^+ from EGTA. The resulting decrease of pH causes a decrease of the apparent stability constant of the CaEGTA complexes. This may explain why Endo observed a phasic contraction induced by caffeine even in the presence of 10 m*M* total EGTA. The effective Ca^{2+} buffering capacity of CaEGTA was considerably reduced during Ca^{2+} release. Accordingly, when this method had been employed in skinned cardiac cells, it was necessary to return to the use of imidazole, especially when the effect of lowering the pH was studied; yet, for the experiments at acidic pH, controls were done [79] with (bis[2-hydroxyethyl]amino)-tris(hydroxymethyl)methane (Bis-Tris, pK_a 6.46). Then Ashley and Moisescu [120] demonstrated that TES is devoid of any deleterious effect on skinned fibers of skeletal muscle while it has a better buffering capacity at physiologic pH than Tris. Accordingly, TES was used in all subsequent experiments in skinned cardiac cells [13, 16, 76, 87, 92, 94]. This was reasonable because at that time it was established that the intracellular physiologic pH was probably slightly more alkaline than 7.00 [76], yet TES has a too alkaline pK_a (7.44 at 22°C) to be ideal. More recently, thorough tests done by A. Fabiato and by J.C. Kentish, in the Department of Physiology of Leeds University (personal communication 1980), have demonstrated that *N,N*-bis(2-hydroxyethyl)-2-aminoethane sulfonic acid (BES) which has a pK_a of 7.14 has no toxic effect on skinned cardiac cells. Thus its use is recommended for further experiments in these preparations.

In conclusion, with respect to the successive corrections of the artificial intracellular milieu, none of these corrections has resulted in an inhibition of the Ca^{2+}-induced release of Ca^{2+} from the SR, whereas some of them have resulted in the enhancement of this process. There is no doubt, however, that more corrections will have to be done.

To these arguments against the hypothesis of a Ca^{2+}-induced release of Ca^{2+} from the SR, Chapman [10] adds some others which deserve careful consideration inasmuch as they led him to the firm conclusion that the hypothesis should be rejected. Before considering these arguments in detail, it must be stated that they are only minor considerations in this excellent article, whose reading is encouraged as this is probably the most comprehensive and thought-provoking recent review on cardiac excitation–contraction coupling.[9]

When evaluating the method using a low [total EGTA] (see p. 18 in Chapman [10]), Chapman finds it puzzling that the sustained tension levels in the presence of a low [total EGTA] are lower than those in the presence of a high [total EGTA]. In fact, this is the very principle of the method since this finding sug-

gests a competition between a Ca^{2+} store inside the cell and the CaEGTA buffer, as had been thoroughly explained in the article that he reviews [77]. Chapman rightly emphasizes that the [free Ca^{2+}] in the solution containing a low [total EGTA] does not permit an inference of the [free Ca^{2+}] in the vicinity of the SR. But this had been stated in all the articles in which this method has been used (see pp. 477 and 483 and fig. 3 in ref. 77; p. 121 and fig. 1A in ref. 2; pp. 501–508 and fig. 1 in ref. 15; and pp. 469 and 492 in ref. 13). As explained in detail (for instance in refs. 2, 13, and 15), the arguments for demonstrating a Ca^{2+}-induced release of Ca^{2+} do not make any use of the actual value of the [free Ca^{2+}] in the vicinity of the SR. One example of such an argument is shown by the experiment in figure 11–10. Although Chapman seems to prefer the method using a [high EGTA] and caffeine [10] to demonstrate Ca^{2+} release, he does not discuss the results obtained with this method in skinned cardiac cells which were reported in the articles that he reviewed.

Chapman is correct in emphasizing that imidazole has depressive effects on the cardiac SR [119], yet he may be inaccurate in using this fact as an argument (see p. 19 in Chapman [10]) for rejecting the results obtained in a study [77] in which imidazole was not used as a pH buffer, while on the other hand not criticizing another study [121] in which the concentration of imidazole was not only very high but also was varied to adjust the ionic strength at different [free Ca^{2+}] values. Since imidazole is only partially ionized, a large concentration is needed to compensate for a relatively small change in ionic strength.

Even if all his preceding arguments against the hypothesis of Ca^{2+}-induced release of Ca^{2+} are not compelling, Chapman's review offers the following very interesting argument: the hypothesis should be rejected for the cardiac SR because Endo [102], who originally proposed this hypothesis for skeletal muscle, has now rejected it [1]. Indeed, the similarity between cardiac and skeletal muscle suggests that a process present in one of the tissues is unlikely to be absent in the other. Accordingly, one of the most productive approaches for cardiac muscle physiology has been to extend to this muscle type the conclusions derived from experiments in skeletal muscle fibers, as is very nicely explained by Chapman [10].

Yet, it may also be productive to use the reverse approach, at least for the excitation–contraction coupling process. The mechanism of excitation–contraction coupling may be simpler, more rudimentary, in cardiac than in skeletal muscle because the cardiac cell offers a shorter pathway for the diffusion of Ca^{2+}. Thus, the following working hypothesis has been developed [16, 87, 122]: the complexity of excitation–contraction coupling may increase with the diameter of the striated muscle cell. The simplest process would be present in frog ventricular cells in which the 3- to 5-μm diameter could permit a direct activation of the myofilaments by the transsarcolemmal Ca^{2+} influx. In mammalian cardiac cells, which have a fivefold larger diameter than the frog cardiac cells, the transsarcolemmal Ca^{2+} influx might be amplified by the Ca^{2+}-induced release of Ca^{2+} from the SR. In skeletal muscle fibers, with a diameter about five times that of mammalian ventricular cells, an unknown process would precede the Ca^{2+}-induced release of Ca^{2+}. This process is likely to involve the transverse tubules, but not the extracellular Ca^{2+} (see, for instance, Frank [100] for a review).

This working hypothesis has led to a reconsideration of the arguments against a Ca^{2+}-induced release of Ca^{2+} in skinned fibers of skeletal muscle based on the experience gained from skinned cardiac cells in which the Ca^{2+}-induced release of Ca^{2+} is easier to demonstrate [1, 2]. As previously indicated, the experiments in skinned cardiac cells showed that the [free Ca^{2+}] trigger is dependent upon the time required for the change of [free Ca^{2+}] outside the SR (see *Evidence in favor of a calcium-induced release. . . .*). In the approximately 100-μm-wide skeletal muscle skinned fibers, the changes of myoplasmic [free Ca^{2+}] are extremely slow. This may explain the very high [free Ca^{2+}] changes in 200 ms resulted in a [free Ca^{2+}] requirement for inducing Ca^{2+} re- μm-wide bundles of myofibrils with attached SR from a fast mammalian skeletal muscle,

[free Ca^{2+}] changes in 200 ms resulted in a [free Ca^{2+}] requirement for inducing Ca^{2+} release 2–3 orders of magnitude lower than that observed by Endo [1, 78]. In addition, this Ca^{2+}-induced release of Ca^{2+} [16, 87] did not require a heavy preload of the SR and was obtained in the presence of a high [free Mg^{2+}] (3.16×10^{-3} *M*) which inhibits Ca^{2+}-induced release of Ca^{2+} in the usual large skinned fibers [1, 78]. Yet, it must be emphasized that these experiments have not yet been done in the amphibian skeletal muscle in which Endo [1, 78] has done other experiments, permitting him to exclude any role of the Ca^{2+}-induced release of Ca^{2+}. His conclusion remains unchallenged, at least in this particular type of skeletal muscle.

In this comparison between cardiac and skeletal muscles, the reverse working hypothesis supported by Chapman [10] should continue to be considered simultaneously [4]. Until the mechanism initiating the Ca^{2+} release from the SR of skeletal muscle is established, some doubt should remain about the possible role of such a still-unknown mechanism in intact cardiac muscle in addition to, or instead of, the Ca^{2+}-induced release of Ca^{2+}. Several hypotheses have been proposed for such a mechanism. As indicated in the *Introduction,* they will be reviewed in another article. Accordingly, the present chapter must end with no conclusion on whether there is Ca^{2+} release from the SR during the physiologic cardiac excitation–contraction coupling or on whether the mechanism of this possible Ca^{2+} release is that described as Ca^{2+}-induced release of Ca^{2+} from the SR.

Notes

1. Reference 123, published after the original submission of this chapter.

2. These cellular fixed and soluble Ca^{2+} buffers are taken into account in computations of the relationship between tension and increase of [total calcium] resulting from transsarcolemmal Ca^{2+} influx which are reported in another article that was published after the original submission of this chapter [124].

3. Since the submission of this chapter, reference 35 has been written as an excellent and challenging full article [125]. The quantitative inference of the increase of myoplasmic [free Ca^{2+}] resulting from the extracellular total calcium depletion measured in this article is discussed in reference 124.

4. See Fabiato [124].

5. These computations are reported in reference 124, which also includes a discussion of the highly pertinent estimates of the increase of [total Ca] caused by the Ca^{2+} current in isolated bovine myocytes done by Isenberg [126], which were not available when this chapter was initially written. In addition, a recent series of articles by Isenberg and Klöckner [127–129] describes in detail the Ca^{2+} tolerance and electrical properties of the excellent preparation of intact isolated adult cardiac myocytes that these investigators have developed.

6. This process is further discussed in reference 124, in which the current working hypothesis for the mechanism of Ca^{2+}-induced release of calcium is described in detail.

7. Reference 124, however, proposes a mechanism for the Ca^{2+}-induced release of Ca^{2+} from the SR and explains that it is not all-or-none because of the presence of the negative feedback: increase of [free Ca^{2+}] to the level reached during the peak of the Ca^{2+} transient inactivates the Ca^{2+}-induced release of Ca^{2+}.

8. Credit should be given to Dr. H.J. Mensing from Tübingen University for wondering in a personal letter why glucose was present in the solutions used. This question, however, came at a time when glucose had already been deleted from the solutions. Glucose was included because the first experiments were done in homogenate of disrupted, but not skinned, cells [103]. It was wrong, however, to maintain glucose in the subsequent early experiments in which one skinned single cardiac cell was studied. However, the 7 m*M* glucose did not appear to have any effect since its deletion did not cause any significant modification of the results.

9. Since the submission of this chapter, Chapman's work has led him to a much less negative view of the possible physiologic role of the Ca^{2+}-induced release of Ca^{2+} from the SR in cardiac excitation–contraction coupling [130]. Therefore, most of what is said in this section of the chapter is no longer relevant, and we apologize for it.

References

1. Endo M: Calcium release from the sarcoplasmic reticulum. Physiol Rev 57:71–108, 1977.
2. Fabiato A, Fabiato F: Calcium release from the sarcoplasmic reticulum. Circ Res 40:119–129, 1977.
3. Oetliker H: An appraisal of the evidence for a sarcoplasmic reticulum membrane potential and its relation to calcium release in skeletal muscle. J Muscle Res Cell Motil 3:247–272, 1982.
4. Platt JR: Strong inference: certain systematic methods of scientific thinking may produce much more rapid progress than others. Science 146:347–353, 1964.
5. Antoni H, Jacob R, Kaufmann R: Mechanische Reaktionen des Frosch- und Säugetiermyokards bei

Veränderung der Aktionspotential-Dauer durch konstante Gleichstromimpulse. Pflugers Arch 306:33–57, 1969.
6. Boyett MR, Jewell BR: Analysis of the effects of changes in rate and rhythm upon electrical activity in the heart. Prog Biophys Mol Biol 36:1–52, 1980.
7. Wohlfart B, Noble MIM: The cardiac excitation–contraction cycle. Pharmacol Ther 16:1–43, 1982.
8. Wier WG: Calcium transients during excitation–contraction coupling in mammalian heart: aequorin signals of canine Purkinje fibers. Science 207:1085–1087, 1980.
9. Wier WG, Isenberg G: Intracellular [Ca^{2+}] transients in voltage clamped cardiac Purkinje fibers. Pflugers Arch 392:284–290, 1982.
10. Chapman RA: Excitation–contraction coupling in cardiac muscle. Prog Biophys Mol Biol 35:1–52, 1979.
11. Blinks JR, Olson CB, Jewell BR, Braveny P: Influence of caffeine and other methylxanthines on mechanical properties of isolated mammalian heart muscle: evidence for a dual mechanism of action. Circ Res 30:367–392, 1972.
12. Solaro RJ, Briggs FN: Estimating the functional capabilities of the sarcoplasmic reticulum in cardiac muscle: calcium binding. Circ Res 34:531–540, 1974.
13. Fabiato A: Myoplasmic free calcium concentration reached during the twitch of an intact isolated cardiac cell and during calcium-induced release of calcium from the sarcoplasmic reticulum of a skinned cardiac cell from the adult rat or rabbit ventricle. J Gen Physiol 78:457–497, 1981.
14. Levitsky DO, Benevolensky DS, Levchenko TS, Smirnov VN, Chazov EI: Calcium-binding rate and capacity of cardiac sarcoplasmic reticulum. J Mol Cell Cardiol 13:785–796, 1981.
15. Fabiato A, Fabiato F: Calcium-induced release of calcium from the sarcoplasmic reticulum of skinned cells from adult human, dog, cat, rabbit, rat, and frog hearts and from fetal and new-born rat ventricles. Ann NY Acad Sci 307:491–522, 1978.
16. Fabiato A: Calcium release in skinned cardiac cells: variations with species, tissues, and development. Fed Proc 41:2238–2244, 1982.
17. Affolter H, Chiesi M, Dabrowska R, Carafoli E: Calcium regulation in heart cells: the interaction of mitochondrial and sarcoplasmic reticulum with troponin-bound calcium. Eur J Biochem 67:389–396, 1976.
18. Scarpa A, Graziotti P: Mechanisms for intracellular calcium regulation in heart. I. Stopped-flow measurements of Ca^{++} uptake by cardiac mitochondria. J Gen Physiol 62:756–772, 1973.
19. Somlyo AP, Somlyo AV, Shuman H, Scarpa A, Endo M, Inesi G: Mitochondria do not accumulate significant Ca concentrations in normal cells. In: Bronner F, Peterlik M (eds) Calcium and phosphate transport across biomembranes. New York: Academic, 1981, pp 87–93.
20. Lüllman H, Peters T, Preuner J: Role of the plasmalemma in calcium-homeostasis and for excitation-contraction coupling in cardiac muscle. In: Noble MIM, Drake A (eds) Cardiac metabolism. London: Wiley and Sons, 1983, pp. 1–18.
21. Philipson KD, Bers DM, Nishimoto AY: The role of phospholipids in the Ca^{2+} binding of isolated cardiac sarcolemma. J Mol Cell Cardiol 12:1159–1173, 1980.
22. Bers DM, Philipson KD, Langer GA: Cardiac contractility and sarcolemmal calcium binding in several cardiac muscle preparations. Am J Physiol 240:H576–H583, 1981.
23. Bers DM: A correlation of the effects of cationic uncouplers on intact cardiac muscle and on Ca^{2+} bound to isolated cardiac muscle plasma membranes. UCLA PhD, 1978. Ann Arbor MI: University Microfilms.
24. Langer GA: Events at the cardiac sarcolemma: localization and movement of contractile-dependent calcium. Fed Proc 35:1274–1278, 1976.
25. Mensing HJ, Hilgemann DW: Inotropic effects of activation and pharmacological mechanisms in cardiac muscle. Trends Pharmacol Sci 2:303–307, 1981.
26. Ringer S: A further contribution regarding the influence of the different constituents of the blood on the contraction of the heart. J Physiol (Lond) 4:29–42, 1883.
27. Mines GR: On functional analysis by the action of electrolytes. J Physiol (Lond) 46:188–235, 1913.
28. Langer GA: The role of calcium in the control of myocardial contractility: an update. J Mol Cell Cardiol 12:231–239, 1980.
29. Solaro RJ, Wise RM, Shiner JS, Briggs FN: Calcium requirements for cardiac myofibrillar activation. Circ Res 34:525–530, 1974.
30. Klee CB, Vanaman TC: Calmodulin. In: Anfinsen CB, Edsall JT, Richards RM (eds) Advances in protein chemistry, vol 35. New York: Academic, 1982, pp. 213–321.
31. Feher JJ, Briggs FN: The effect of calcium load on the calcium permeability of sarcoplasmic reticulum. J Biol Chem 257:10191–10199, 1982.
32. Philipson KD, Bers DM, Nishimoto AY, Langer GA: Binding of Ca^{2+} and Na^{+} to sarcolemmal membranes: relation to control of myocardial contractility. Am J Physiol 238:H373–H378, 1980.
33. Solomon AK: Compartmental methods of kinetic analysis. In: Comar CL, Bronner F (eds) Mineral metabolism: an advanced treatise. Vol 1: Principles, processes, and systems, part A. New York: Academic, 1960, pp 119–167.
34. Dresdner K, Kline RP, Kupersmith J: Extracellular calcium ion depletion in frog ventricle. Biophys J 37:239a, 1982.
35. Bers DM: Early transient depletion of $[Ca]_0$ during single beats of rabbit ventricular muscle measured with Ca selective microelectrodes. Physiologist 25:286, 1982.

36. Hilgemann D, Delay M, Vergara J, Langer G: Measurement of activation-related extracellular Ca^{++} concentration changes in atrial muscle with antipyrlazo III. Physiologist 25:286, 1982.
37. Solaro RJ, Briggs FN: Calcium conservation and the regulation of myocardial contraction. In: Dhalla NS (ed) Recent advances in studies on cardiac structure and metabolism. Myocardial biology, vol 4. Baltimore: University Park, 1974, pp 359–374.
38. Van Winkle WB, Schwartz A: Ions and inotropy. Annu Rev Physiol 38:247–272, 1976.
39. Morad M, Goldman Y: Excitation–contraction coupling in heart muscle: membrane control of development of tension. Prog Biophys Mol Biol 27:257–313, 1973.
40. Kavaler F, Anderson TW: Indirect evidence that calcium extrusion causes relaxation of frog ventricular muscle. Fed Proc 37:300, 1978.
41. Kavaler F, Anderson TW, Fisher, VJ: Sarcolemmal site of caffeine's inotropic action on ventricular muscle of the frog. Circ Res 42:285–290, 1978.
42. Niedergerke R, Page S: Analysis of caffeine action in single trabeculae of the frog heart. Proc R Soc Lond [B]213:303–324, 1981.
43. Marban E, Tsien RW: Effects of nystatin-mediated intracellular ion substitution on membrane currents in calf Purkinje fibres. J Physiol (Lond) 329:569–587, 1982.
44. Reuter H, Scholz H: A study of the ion selectivity and the kinetic properties of the calcium dependent slow inward current in mammalian cardiac muscle. J Physiol (Lond) 264:17–47, 1977.
45. Siegelbaum SA, Tsien RW: Calcium-activated transient outward current in calf cardiac Purkinje fibres. J Physiol (Lond) 299:485–506, 1980.
46. Kass RS, Tsien RW: Multiple effects of calcium antagonists on plateau currents in cardiac Purkinje fibers. J Gen Physiol 66:169–192, 1975.
47. McDonald TF: The slow inward calcium current in the heart. Annu Rev Physiol 44:425–434, 1982.
48. Kass RS, Siegelbaum S, Tsien RW: Incomplete inactivation of the slow inward current in cardiac Purkinje fibres. J Physiol (Lond) 263:127P–128P, 1976.
49. Isenberg G, Klöckner U: Glycocalyx is not required for slow inward calcium current in isolated rat heart myocytes. Nature 284:358–360, 1980.
50. Lee KS, Tsien RW: Reversal of current through calcium channels in dialysed single heart cells. Nature 297:498–501, 1982.
51. Hino N, Ochi R: Effect of acetylcholine on membrane currents in guinea-pig papillary muscle. J Physiol (Lond) 307:183–197, 1980.
52. McDonald TF, Pelzer D, Trautwein W: Does the calcium current modulate the contraction of the accompanying beat? A study of E-C coupling in mammalian ventricular muscle using cobalt ions. Circ Res 49:576–583, 1981.
53. Nawrath H, Ten Eick RE, McDonald TF, Trautwein W: On the mechanism underlying the action of D-600 on slow inward current and tension in mammalian myocardium. Circ Res 40:408–414, 1977.
54. Noma A, Kotake H, Irisawa H: Slow inward current and its role mediating the chronotropic effect of epinephrine in the rabbit sinoatrial node. Pflügers Arch 388:1–9, 1980.
55. Ehara T, Kaufmann R: The voltage- and time-dependent effects of (-)-verapamil on the slow inward current in isolated cat ventricular myocardium. J Pharmacol Exp Ther 207:49–55, 1978.
56. Mobley BA, Page E: The surface area of sheep cardiac Purkinje fibres. J Physiol (Lond) 220:547–563, 1972.
57. Stewart JM, Page E: Improved stereological techniques for studying myocardial cell growth: application to external sarcolemma, T system, and intercalated disks of rabbit and rat hearts. J Ultrastruct Res 65:119–134, 1978.
58. Baumgarten CM: A program for calculation of activity coefficients at selected concentrations and temperatures. Comput Biol Med 11:189–196, 1981.
59. Sheu S-S, Fozzard HA: Transmembrane Na^+ and Ca^{2+} electrochemical gradients in cardiac muscle and their relationship to force development. J Gen Physiol 80:325–351, 1982.
60. Marban E, Rink TJ, Tsien RW, Tsien RY: Free calcium in heart muscle at rest and during contraction measured with Ca^{2+}-sensitive microelectrodes. Nature 286:845–850, 1980.
61. Lee CO: Ionic activities in cardiac muscle cells and application of ion-selective microelectrodes. Am J Physiol 241:H459–H478, 1981.
62. Reuter H: Na-Ca countertransport in cardiac muscle. In: Martonosi AN (ed) Membranes and transport, vol 1. New York: Plenum, 1982, pp 623–631.
63. Lado MG, Sheu S-S, Fozzard HA: Changes in intracellular Ca^{2+} activity with stimulation in sheep cardiac Purkinje strands. Am J Physiol 243:H133–H137, 1982.
64. Caroni P, Reinlib L, Carafoli E: Charge movements during the Na^+-Ca^{2+} exchange in heart sarcolemmal vesicles. Proc Natl Acad Sci USA 77:6354–6358, 1980.
65. Kadoma M, Froehlich J, Reeves J, Sutko J: Kinetics of sodium ion induced calcium ion release in calcium ion loaded cardiac sarcolemmal vesicles: determination of initial velocities by stopped-flow spectrophotometry. Biochemistry 21:1914–1918, 1982.
66. Mullins LJ: Ion transport in heart. New York: Raven, 1981, pp 1–136.
67. Sulakhe PV, St. Louis PJ: Passive and active calcium fluxes across plasma membranes. Prog Biophys Mol Biol 35:135–195, 1980.
68. Jones LR, Besch HR Jr, Fleming JW, McConnaughey MM, Watanabe AM: Separation of vesicles of cardiac sarcolemma from vesicles of cardiac sarcoplasmic reticulum: comparative biochem-

ical analysis of component activities. J Biol Chem 254:530–539, 1979.
69. Caroni P, Carafoli E: An ATP-dependent Ca^{2+}-pumping system in dog heart sarcolemma. Nature 283:765–767, 1980.
70. Caroni P, Carafoli E: The Ca^{2+}-pumping ATPase of heart sarcolemma. J Biol Chem 256:3263–3270, 1981.
71. Baker PF: Transport and metabolism of calcium ions in nerve. Prog Biophys Mol Biol 24:177–223, 1972.
72. Carafoli E: Calcium transport systems of heart sarcolemma vesicles. Naunyn Schmiedebergs Arch Pharmacol 321:R7, 1982.
73. Dunnett J, Nayler WG: Calcium efflux from cardiac sarcoplasmic reticulum: effects of calcium and magnesium. J Mol Cell Cardiol 10:487–498, 1978.
74. Kirchberger MA, Wong D: Calcium efflux from isolated cardiac sarcoplasmic reticulum. J Biol Chem 253:6941–6945, 1978.
75. Katz AM, Takenaka H: Calcium transport across the sarcoplasmic reticulum. In: Bronner F, Peterlik M (eds) Calcium and phosphate transport across biomembranes. New York: Academic, 1981, pp 59–66.
76. Fabiato A, Fabiato F: Calculator programs for computing the composition of the solutions containing multiple metals and ligands used for experiments in skinned muscle cells. J Physiol (Paris) 75:463–505, 1979.
77. Fabiato A, Fabiato F: Contractions induced by a calcium-triggered release of calcium from the sarcoplasmic reticulum of single skinned cardiac cells. J Physiol (Lond) 249:469–495, 1975.
78. Endo M: Conditions required for calcium-induced release of calcium from the sarcoplasmic reticulum. Proc Jpn Acad 51:467–472, 1975.
79. Fabiato A, Fabiato F: Effects of pH on the myofilaments and the sarcoplasmic reticulum of skinned cells from cardiac and skeletal muscles. J Physiol (Lond) 276:233–255, 1978.
80. Fabiato A, Fabiato F: Techniques of skinned cardiac cells and of isolated cardiac fibers with disrupted sarcolemmas with reference to the effects of catecholamines and of caffeine. In: Roy P-E, Dhalla NS (eds) Recent advances in studies on cardiac structure and metabolism. Vol 9: The sarcolemma. Baltimore: University Park, 1976, pp 71–94.
81. Blinks JR, Prendergast FG, Allen DG: Photoproteins as biological calcium indicators. Pharmacol Rev 28:1–93, 1976.
82. Allen DG, Blinks JR: The interpretation of light signals from aequorin-injected skeletal and cardiac muscle cells: a new method of calibration. In Ashley CC, Campbell AK (eds) Detection and measurement of free Ca^{2+} in cells. Amsterdam: Elsevier/North Holland Biomedical, 1979, pp 159–174.
83. Oehme M, Kessler M, Simon W: Neutral carrier Ca^{2+}-microelectrode. Chimia 30:204–206, 1976.
84. Walker JL, Brown HM: Intracellular ionic activity measurements in nerve and muscle. Physiol Rev 57:729–778, 1977.
85. Tsien RY, Rink TJ: Neutral carrier ion-selective microelectrodes for measurement of intracellular free calcium. Biochim Biophys Acta 599:623–638, 1980.
86. Scarpa A: Measurement of calcium ion concentrations with metallochromic indicators. In: Ashley CC, Campbell AK (eds) Detection and measurement of free Ca^{2+} in cells. Amsterdam: Elsevier/North Holland Biomedical, 1979, pp 85–115.
87. Fabiato A: Fluorescence and differential light absorption recordings with calcium probes and potential-sensitive dyes in skinned cardiac cells. Can J Physiol Pharmacol 60:556–567, 1982.
88. Dubyak GR, Scarpa A: Sarcoplasmic Ca^{2+} transients during the contractile cycle of single barnacle muscle fibres: measurements with arsenazo III-injected fibres. J Muscle Res Cell Motil 3:87–112, 1982.
89. Beeler TJ, Schibeci A, Martonosi A: The binding of arsenazo III to cell components. Biochim Biophys Acta 629:317–327, 1980
90. Caswell AH, Hutchison JD: Selectivity of cation chelation to tetracyclines: evidence for special conformation of calcium chelate. Biochem Biophys Res Commun 43:625–630, 1971.
91. Jilka RL, Martonosi AN: The effect of calcium ion transport ATPase upon the passive calcium ion permeability of phospholipid vesicles. Biochim Biophys Acta 466:57–67, 1977.
92. Fabiato A, Fabiato F: Use of chlorotetracycline fluorescence to demonstrate Ca^{2+}-induced release of Ca^{2+} from the sarcoplasmic reticulum of skinned cardiac cells. Nature 281:146–148, 1979.
93. Freedman JC, Laris PC: Electrophysiology of cells and organelles: studies with optical potentiometric indicators. Int Rev Cytol Suppl 12:177–246, 1981.
94. Fabiato A: Mechansim of calcium-induced release of calcium from the sarcoplasmic reticulum of skinned cardiac cells studied with potential-sensitive dyes. In: Ohnishi ST, Endo M (eds) The mechanism of gated calcium transport across biological membranes. New York: Academic, 1981, pp 237–255.
95. Best PM, Asayama J, Ford LE: Membrane voltage changes associated with calcium movement in skinned muscle fibers. In: Grinnell AD, Brazier MAB (eds) The regulation of muscle contraction: excitation–contraction coupling. New York: Academic, 1981, pp 161–173.
96. Russell JT, Beeler T, Martonosi A: Optical probe responses on sarcoplasmic reticulum: oxacarbocyanines. J Biol Chem 254:2040–2046, 1979.
97. Russell JT, Beeler T, Martonosi A: Optical probe responses on sarcolasmic reticulum: merocyanine and oxonol dyes. J Biol Chem 254:2047–2052, 1979.
98. Fabiato A, Fabiato F: Variations of the membrane potential of the sarcoplasmic reticulum of skinned cells from cardiac and skeletal muscle detected with

a potential-sensitive dye. J Gen Physiol 70:6a, 1977.
99. Bianchi CP, Shanes AM: Calcium influx in skeletal muscle at rest, during activity, and during potassium contracture. J Gen Physiol 42:803–815, 1959.
100. Frank GB: The current view of the source of trigger calcium in excitation–contraction coupling in vertebrate skeletal muscle. Biochem Pharmacol 29: 2399–2406, 1980.
101. Ford LE, Podolsky RJ: Regenerative calcium release within muscle cells. Science 167:58–59, 1970.
102. Endo M, Tanaka M, Ogawa Y: Calcium induced release of calcium from the sarcoplasmic reticulum of skinned skeletal muscle fibres. Nature 228:34–36, 1970.
103. Fabiato A, Fabiato F: Excitation–contraction coupling of isolated cardiac fibers with disrupted or closed sarcolemmas: calcium-dependent cyclic and tonic contractions. Circ Res 31:293–307, 1972.
104. Saida K: Ca^{2+}- and 'depolarization'-induced Ca^{2+} release in skinned smooth muscle fibers. Biomed Res 2:453–455, 1981.
105. Fabiato A, Fabiato F: Effects of magnesium on contractile activation of skinned cardiac cells. J Physiol (Lond) 249:497–517, 1975.
106. McDonald TF, Nawrath H, Trautwein W: Membrane currents and tension in cat ventricular muscle treated with cardiac glycosides. Circ Res 37:674–682, 1975.
107. Trautwein W, McDonald TF, Tripathi O: Calcium conductance and tension in mammalian ventricular muscle. Pflügers Arch 354:55–74, 1975.
108. Aronson RS, Capasso JM: Negative inotropic effect of elevated extracellular calcium in rat myocardium. J Mol Cell Cardiol 12:1305–1309, 1980.
109. Li T, Vassalle M: The negative inotropic effect of calcium overload in cardiac Purkinje fibers. J Mol Cell Cardiol 16:65–77, 1984.
110. Chiesi M, Ho MM, Inesi G, Somlyo AV, Somlyo AP: Primary role of sarcoplasmic reticulum in phasic contractile activation of cardiac myocytes with shunted myolemma. J Cell Biol 91:728–742, 1981.
111. Cohen LB, Salzberg BM, Davila HV, Ross WN, Landowne D, Waggoner AS, Wang CH: Changes in axon fluorescence during activity: molecular probes of membrane potential. J Membr Biol 19:1–36, 1974.
112. Kass RS, Lederer WJ, Tsien RW, Weingart R: Role of calcium ions in transient inward currents and aftercontractions induced by strophanthidin in cardiac Purkinje fibres. J Physiol (Lond) 281:187–208, 1978.
113. Kass RS, Tsien RW: Fluctuations in membrane current driven by intracellular calcium in cardiac Purkinje fibers. Biophys J 38:259–269, 1982.
114. Tsien RW: Cyclic AMP and contractile activity in heart. In Greengard P, Robison GA (eds) Advances in cyclic nucleotide research, vol 8. New York: Raven, 1977, pp 363–420.
115. Page E, Upshaw-Earley J: Volume changes in sarcoplasmic reticulum of rat hearts perfused with hypertonic solutions. Circ Res 40:355–366, 1977.
116. Ford LE, Surdyk MF: Electronmicroscopy of skinned muscle cells. J Gen Physiol 72:5a, 1978.
117. Taylor SR, Godt RE: Calcium release and contraction in vertebrate skeletal muscle. In: Symposia of the society for experimental biology. No. 30: Calcium in biological systems. Cambridge: University Press, 1976, pp 361–380.
118. Page E, Surdyk-Droske M: Distribution, surface density, and membrane area of diadic junctional contacts between plasma membrane and terminal cisterns in mammalian ventricle. Circ Res 45:260–267, 1979.
119. Fabiato A, Fabiato F: Activation of skinned cardiac cells: Subcellular effects of cardioactive drugs. Eur J Cardiol 1:143–155, 1973.
120. Ashley CC, Moisescu DG: Effect of changing the composition of the bathing solutions upon the isometric tension–pCa relationship in bundles of crustacean myofibrils. J Physiol (Lond) 270:627–652, 1977.
121. Kerrick WGL, Best PM: Calcium ion release in mechanically disrupted heart cells. Science 183:435–437, 1974.
122. Fabiato A, Fabiato F: Calcium and cardiac excitation–contraction coupling. Annu Rev Physiol 41:473–484, 1979.
123. Fabiato A: Appraisal of the hypothesis of the "depolarization-induced" release of calcium from the sarcoplasmic reticulum in skinned cardiac cells from the rat or pigeon ventricle. In: Fleischer S, Tonomura Y (eds) Structure and function of the sarcoplasmic reticulum. New York: Academic, 1984 (in press).
124. Fabiato A: Calcium-induced release of calcium from the cardiac sarcoplasmic reticulum. Am J Physiol 245:C1–C14, 1983.
125. Bers DM: Early transient depletion of extracellular Ca during individual cardiac muscle contractions. Am J Physiol 244:H462–H468, 1983.
126. Isenberg G: Ca entry and contraction as studied in isolated bovine ventricular myocytes. Z Naturforsch 37c:502–512, 1982.
127. Isenberg G, Klöckner U: Calcium tolerant ventricular myocytes prepared by preincubation in a "KB medium". Pflugers Arch 395:6–18, 1982.
128. Isenberg G, Klöckner U: Isolated bovine ventricular myocytes: characterization of the action potential. Pflügers Arch 395:19–29, 1982.
129. Isenberg G, Klöckner U: Calcium currents of isolated bovine ventricular myocytes are fast and of large amplitude. Pflügers Arch 395:30–41, 1982.
130. Chapman RA: Control of cardiac contractility at the cellular level. Am J Physiol 245:H535–H552, 1983.

12. UPTAKE OF CALCIUM BY THE SARCOPLASMIC RETICULUM AND ITS REGULATION AND FUNCTIONAL CONSEQUENCES

Michihiko Tada,
Munekazu Shigekawa,
and Yasuharu Nimura

Introduction

The contraction–relaxation cycle of the myocardium is physiologically regulated by a change in the intracellular Ca^{2+} concentration [1–3]. The cardiac contractile system, like that of skeletal muscle, is activated maximally when the ionized Ca^{2+} concentration reaches the value of $\sim 10^{-5}$ *M* while the active state can be converted to the resting one when the ionized Ca^{2+} falls below 10^{-7} *M*. In the fast skeletal muscle, this change in the intracellular Ca^{2+} is regulated solely by the sarcoplasmic reticulum (SR). Release and subsequent accumulation of Ca^{2+} by this organelle induce contraction and relaxation of the contractile system. In the cardiac muscle, however, the intracellular Ca^{2+} concentration during the contraction–relaxation cycle is controlled not only by the SR but also by other cellular organelles such as the sarcolemma [4–8]. The extent to which the SR participates in the regulation of the beat-to-beat Ca^{2+} movement varies among different animal species [5, 6]. In the mammalian ventricle, the SR is fairly well developed [9] and there is evidence that the SR plays a major role in initiating contraction and relaxation [5–7]. In contrast, in the cardiac muscle of lower vertebrates such as frog ventricle, the SR appears to be less developed and available data indicate that the sarcolemma plays a more important role [5, 6]. Although mitochondria have long been implicated in the control of cardiac relaxation, recent experiments indicate that they do not play a significant role both in amphibian and mammalian cardiac muscle under physiologic conditions [5, 7].

Accumulation by and release of Ca^{2+} from the SR have been studied using various experimental systems ranging from the preparations of isolated SR vesicles to the intact fiber, obtained mainly from the mammalian cardiac muscle. The mechanism by which the SR accumulates Ca^{2+} to induce relaxation, and its regulation, which is physiologically and pharmacologically important, have been elucidated fairly well. In contrast, the mechanism by which the SR releases Ca^{2+} to initiate contraction has not been clarified. As the latter subject is discussed elsewhere in this book (chapter 11), this chapter summarizes the present knowledge of Ca transport across the SR membranes and its regulation, with an emphasis on the molecular mode by which Ca^{2+} is accumulated by the Ca pump of the cardiac SR.

We wish to thank Dr. M. Kadoma for his help in writing this chapter. This work was supported by grants from the Ministry of Education, Science, and Culture, the Ministry of Welfare, and the Muscular Dystrophy Association.

N. Sperelakis (ed.), PHYSIOLOGY AND PATHOPHYSIOLOGY OF THE HEART.

Martinus Nijhoff Publishing, Boston/The Hague/ Dordrecht/Lancaster.

Structure and Composition of SR Membranes

The SR of the mammalian myocardium consists of a membrane-limited structure that forms a network surrounding the bundles of myofilaments [9]. The lumen of the SR forms a closed intracellular system that is not continuous with the extracellular space. The transverse tubular system (T system), another tubular structure running mainly perpendicular to the long axis of the myocardial cell and thus segmenting the SR at the Z lines, is continuous with the surface membrane, its lumen communicating with the extracellular space. The SR can be divided into two components: the free SR and the junctional SR [9, 10]. The former does not participate in the formation of any junction with other membranes, but surrounds the myofilaments mainly in the center of the sarcomere. The latter is located beneath the cell surface membrane to form a peripheral coupling with the sarcolemma or situated alongside the T system to form an interior coupling with the membranes of the T system. The interior couplings occur in the forms of the dyads or triads in which one or two elements of junctional SR form couplings on one or either side of the T tubules, respectively. The junctional SR that forms peripheral and interior couplings is often referred to as the subsarcolemmal cisternae and the terminal cisternae, respectively. The junction between the junctional SR and either the cell surface membrane or the membrane of the T system is characterized by the presence of "feet", regular periodic projections extended from the membrane of the junctional SR [9, 10]. These structures may provide the basis for transmission of a signal from the sarcolemma to the SR. In addition to "feet", the junctional SR is further characterized by the presence of dense granular material inside its lumen. These dense materials are negatively charged and are considered to represent a Ca-binding protein which is similar to calsequestrin of skeletal SR. In addition to these portions of SR, specialized form of junctional SR, which differ from ordinary junctional SR in geometry and in topographic aspect, can be identified in the cardiac muscle [9]. In contrast, the free SR is devoid of these features of the junctional SR. Therefore, different portions of the SR have special structural features, suggesting that different functions may be assigned to these portions of the SR. In accord with this notion, storage and release of Ca^{2+} occur primarily at the terminal cisternae in the skeletal muscle fiber [11, 12], while Ca uptake appears to occur alongside the entire surface of the SR membrane.

The ionic composition of the SR in situ has been studied with electron-probe analysis of skeletal muscle [12]. The contents of K^+, Na^+, and Cl^- in the SR in the resting muscle are not very different from those in the cytoplasm, but are quite different from those of the extracellular space. Such observations indicate that the SR is an intracellular compartment and argue against the existence of a resting potential across the SR membranes if the in situ SR membranes are permeable to K^+, Na^+, and Cl^- as in the isolated SR vesicles. When a short tetanus is induced in frog muscle, it has been shown that the terminal cisternae release more than half of their Ca^{2+} content into the cytoplasm [12]. This Ca^{2+} release is associated with a significant uptake of Mg^{2+} and K^+ into the terminal cisternae. As Ca^{2+} released significantly exceeds the total measured cation accumulation, it was suggested that protons and/or organic ions are also taken up by the terminal cisternae to compensate for a large charge deficit. These results thus indicate that various ions are moving into or out of the SR coupled to the Ca movement during activation and relaxation of the muscle fiber.

PREPARATION OF FRAGMENTED SR

When cardiac muscle is homogenized, the SR membranes are fragmented and then reseal spontaneously into small vesicles. These vesicles can be isolated in microsomal fractions by differential centrifugation of homogenized cardiac muscle [13–17]. The microsomes sedimented between 8000–10,000 and 37,000–40,000 *g* are usually further treated with 0.6 *M* KCl to remove contaminating contractile proteins. The resultant preparations, which are used commonly in most laboratories, are highly enriched in the SR membranes, as judged on

the basis of the marker enzyme activities (Ca uptake and Ca^{2+}-dependent ATPase activities, and Ca^{2+}-dependent acylphosphoenzyme formation; see below). The yield of this preparation from dog heart is about 0.63 mg/g wet muscle, which is approximately 10% of the SR membranes present in the muscle homogenate [16]. These preparations are contaminated with mitochondrial fragments so that their ATPase activity is inhibited significantly by sodium azide, a mitochondrial inhibitor [13, 18–20]. Their Ca-uptake activity, however, is not affected by this reagent [13, 16]. These preparations are also significantly contaminated with the sarcolemmal membranes, the latter content being estimated to be up to 15% [21]. The SR and the contaminating membrane fractions can be separated by sucrose density gradient centrifugation after the microsomal fraction is subjected to Ca oxalate loading in the presence of ATP prior to centrifugation [17, 21, 22]. The sarcolemmal membranes are concentrated in the light fraction but are practically absent in the densest fraction which contains Ca oxalate. As can be predicted from the finding that the SR in situ is composed of different regions within the sarcomere, the isolated fragmented SR membranes are not homogenous. Meissner [23] separated the fragmented SR membranes isolated from skeletal muscle into subfractions of different density by centrifugation through sucrose gradient. The light and heavy fractions show some difference in protein composition [23] and Ca-release activity [24]. The biochemical and morphologic data indicate that light and heavy fractions are derived from the longitudinal SR (free SR) and the terminal cisternae (junctional SR), respectively [23, 25]. Similar studies have not been carried out with cardiac fragmented SR membranes, but Jones and Cala [26] have recently shown that cardiac SR membranes also consist of heterogeneous subpopulations. They observed that ryanodine, an alkaloid, could selectively enhance Ca uptake by a subpopulation of cardiac SR membranes and that this ryanodine-sensitive SR fraction could be differentiated from the remainder of the SR membranes by other biochemical properities including protein composition. At present, however, the physiologic relevance of this observation is not clear.

The isolated cardiac SR membrane vesicles are largely spherical with a diameter of about 0.1–0.2 μ when examined in an electron microscope [27]. These vesicles are considered to be sealed and retain the original right-side-out orientation, Ca^{2+} thus being transported into their lumen.

PROTEIN AND LIPID COMPOSITION

When cardiac SR vesicles are subjected to polyacrylamide gel electrophoresis in the presence of sodium dodecylsulfate, a considerable number of protein bands can be observed (fig. 12–1). The major component is a polypeptide with a molecular weight of approximately 100,000 daltons. This polypeptide represents the ATPase protein of the SR which plays a central role in the Ca transport by the SR. The ATPase protein has recently been partially purified from pigeon heart [17] and dog heart [28, 29] SR membranes after solubilizing the membrane proteins by deoxycholate. The cardiac ATPase protein is immunologically different from that of fast skeletal muscle [27]. Electrophoresis of cardiac SR membranes also demonstrates protein bands with molecular weights ranging from 50,000 to 60,000 daltons. These components may correspond to calsequestrin, the high-affinity Ca-binding protein and/or the glycoprotein of the skeletal muscle SR (see below). However, the properties and functional roles of these and other protein components of cardiac SR membranes have not been well defined except for the ATPase protein, calsequestrin, and phospholamban, a 22,000-dalton protein which serves as the substrate for protein kinase and controls the function of the Ca pump of the SR (see below and Tada and Katz [30]). Phospholamban appears to be an acidic proteolipid and partially exposed on the cytoplasmic surface of the SR vesicles. Its content in the cardiac SR membranes was estimated to be 4%–6% of the total protein [30].

In contrast to the cardiac SR, the protein composition of SR membranes isolated from fast skeletal muscle has been studied extensively and five major protein components—namely, the ATPase protein (Mr ~ 100,000), the 12,000-dalton proteolipid, the 53,000-dal-

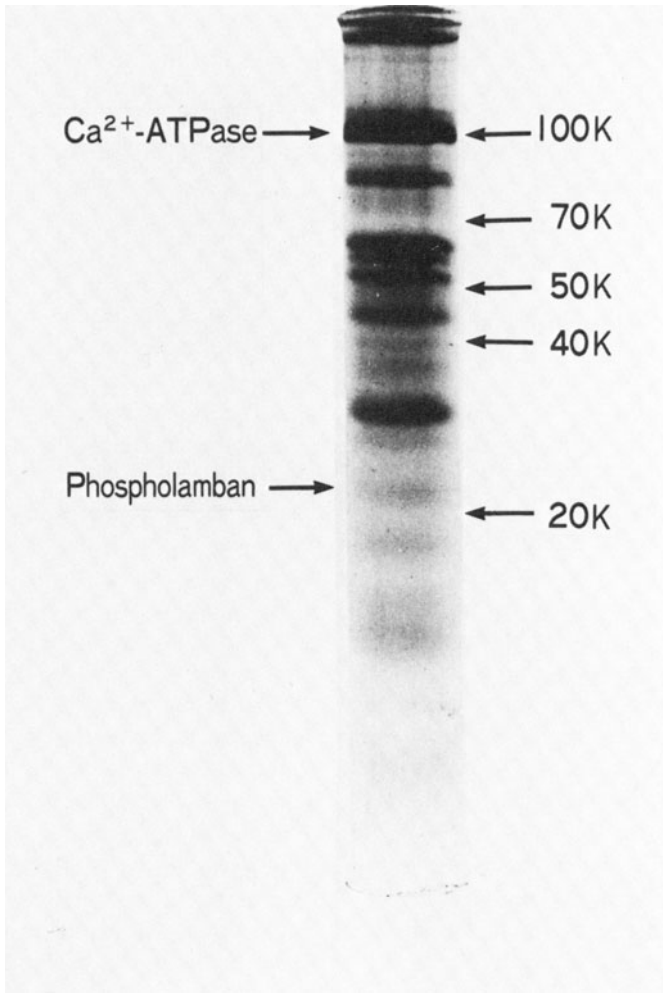

FIGURE 12–1. Sodium dodecylsulfate polyacrylamide gel electrophoresis of dog cardiac SR preparation.

ton glycoprotein, calsequestrin (Mr ~ 44,000), and the high-affinity Ca-binding protein (Mr ~ 55,000)—have been identified and characterized [31, 32]. The ATPase protein constitutes 60%–90% of the total protein; 1 mol of the ATPase protein contains approximately 2 mol of high-affinity Ca-binding sites (K_d, ~ 0.3 μM) and 1 mol of high-affinity ATP-binding site (K_d, 0.5–3.0 μM) [33–35].

The ATPase protein is an amphipathic single-chain polypeptide. Its molecular weight determined by sedimentation equilibrium in the analytic ultracentrifuge in the presence of detergents is 115,000–119,000 [36]. The hydrophobic region of the ATPase polypeptide is intimately associated with the membrane lipid phase while its hydrophilic portion appears to be exposed on the cytoplasmic side of the SR membrane (fig. 12–2). Five major water-soluble peptides (segments I–V in fig. 12–2), which constitute about 60% of the total amino acid residues, have been sequenced [37–39]. These include the NH_2-terminal peptide (segment I) and the COOH-terminal peptide (segment V). Limited trypsin digestion of the intact closed SR vesicles cleaves the ATPase polypeptide first into two fragments: fragment A (Mr ~ 55,000) and fragment B (Mr ~ 45,000). By further trypsin digestion, fragment A is cleaved into two fragments: fragment A_1 (Mr ~ 30,000) and fragment A_2 (Mr ~ 25,000) [31, 37, 38]. These tryptic fragments contain both the hydrophilic and hydrophobic portions, and remain firmly bound to

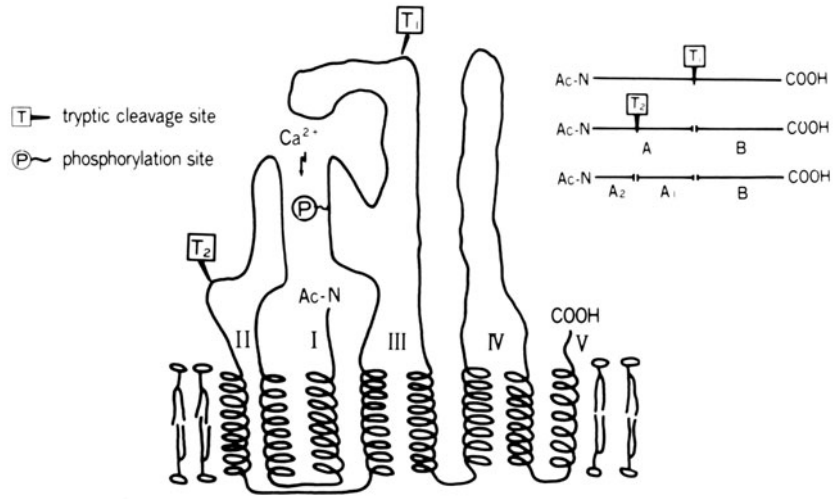

FIGURE 12–2. Diagrammatic representation of the alignment and location of various segments of the ATPase polypeptide: T_1, T_2, tryptic cleavage site; Ⓟ~, phosphorylation site; Ac-N, amino terminus of peptide; COOH, carboxyl terminus of peptide. Modified from MacLennan et al. [38].

the membrane (fig. 12–2). Based on the sequence data, these tryptic fragments could be aligned in the following order: fragment A_2–fragment A_1–fragment B [37–39]. Fragment A_2 contains the NH_2 terminus which is acetylated, whereas fragment B contains the COOH terminus. Figure 12–2 illustrates the alignment and location of the tryptic and the sequenced fragments of the ATPase polypeptide. Water-soluble sequenced fragments (segments I–V) of the ATPase are considered to be exposed on the cytoplasmic surface of the SR vesicles because little of the ATPase is located at the inner surface of the vesicles (see below). In contrast, water-insoluble peptide regions are presumably embedded in the membrane. Therefore, the ATPase appears to fold in a complex way in the membrane (see fig. 12–2). Localization of segments I–III on the cytoplasmic surface is consistent with the following observations [37–40]: (a) The tryptic cleavage sites (T_1 and T_2), which should be exposed on the cytoplasmic surface, are located on segments II and III, respectively. (b) The active site of the ATPase, which is phosphorylated by the terminal phosphate of ATP during the enzyme catalysis (see below), is located on the tryptic fragment A_1, the aspartate residue in segment III being phosphorylated. (c) A specific cysteinyl residue of segment I is labeled by membrane-impermeant SH reagents.

It should be noted that the phosphorylation site and the Ca-transporting site appear to be located in the different regions of the polypeptide. The Ca-transporting site appears to be associated with the tryptic fragment A_2 since this fragment possesses Ca ionophore activity when incorporated into lipid bilayer [38], and is covalently labeled with dicyclohexylcarbodiimide (DCCD) under conditions in which high-affinity Ca binding to the ATPase is inhibited by this reagent [41].

The proteolipid is also an intrinsic protein of the SR membranes. Although it was suggested that this proteolipid is necessary for reconstitution of the efficient Ca pump with purified ATPase and phospholipids [42], its physiologic role has yet to be clarified [38].

Calsequestrin and the high-affinity Ca-binding protein are loosely bound to the membrane and are easily extracted by mild treatment with detergents [31, 32]. Calsequestrin is a protein of strong negative charge, its molecular weight varying between 44,000 and 65,000, depending on the conditions used for gel electrophoresis. This protein, presumably localized inside the SR vesicles, has a low affinity but a large

binding capacity for Ca^{2+}. It binds an appreciable amount of Ca^{2+} when intravesicular Ca^{2+} concentration exceeds millimolar ranges. This protein varies greatly in its content, being very low in the light fraction and greatly enriched in the heavy fraction (up to 25% of total protein) [23, 25]. It is suggested that this protein primarily serves as a storage site of accumulated Ca. Recently purified cardiac calsequestrin has been shown to have properties similar to those of skeletal calsequestrin [141]. The high-affinity Ca-binding protein is also suggested to be localized inside SR vesicles [43]. Its physiologic role is not known at present.

The 53,000-dalton glycoprotein is, like the ATPase and the proteolipid, an intrinsic membrane protein of the SR [43, 44]. It is exposed on both outside and inside surfaces of the SR vesicles. Interestingly, this glycoprotein has molecular weight and amino acid and sugar compositions very similar to the glycoprotein subunit of Na^+, K^+ ATPase. Therefore this glycoprotein may have some role in the Ca transport by the SR membranes.

The lipids of cardiac SR membranes are not well defined because the purity of cardiac SR preparations has not been established. In the SR preparations isolated from fast skeletal muscle, phospholipids make up about 80% of the total lipids on a molar basis, phosphatidylcholine being the most prominent molecular species (65%–73%) [32]. The low cholesterol content and the relatively high degree of unsaturation of the fatty acid component of the major phospholipids are characteristics of the SR membranes of rabbit fast skeletal muscle. The purified ATPase protein contains phospholipid, the composition of which is similar to that of the intact SR membrane [31]. Phospholipid molecules intimately associated with the ATPase protein are required for its enzymic activity. Thus, phospholipase treatment of the purified ATPase protein or the native SR membranes results in inhibition of ATP hydrolysis and/or Ca transport by the membranes [45].

STRUCTURAL ORGANIZATION OF SR MEMBRANES

The structural organization of the SR membranes of skeletal and cardiac muscles, either isolated or in situ, has been studied using various electron-microscopic preparations [9, 10, 15, 27, 31, 46, 47]. The thin-sectioned SR membranes demonstrate a trilamellar structure which is characteristic of biologic membranes. Electron-microscopic pictures of freeze-fractured SR membranes indicate that the hydrophobic interior of the membranes is filled with globular particles about 90 Å in diameter. The majority of these particles are concentrated in the outer leaflet of the membrane bilayer. Negative staining of the SR membrane vesicles reveals the presence of smaller particles (about 40 Å in diameter) with stalks projecting from the surface of the membranes. These surface and intramembranous particles have been shown to represent the structural features of the ATPase protein. It is thus thought that a large part of the ATPase protein is localized in the cytoplasmic leaflet of the bilayer membrane of the SR and that this protein extends into the cytoplasm to form 40-Å particles. The density of 90-Å particles in cardiac muscle SR is about half that in skeletal muscle SR [9]. Therefore, the density of the ATPase protein in the membrane would be correspondingly lower in the cardiac SR. Although the nonpolar portion of the ATPase polypeptide penetrates the membrane interior (fig. 12–2), there is no direct experimental evidence to support the view that the ATPase polypeptide spans the entire SR membrane and is exposed at the inner surface. However, the exposure of the polypeptide at the inner surface is presumably required for Ca^{2+} to be transported through the membrane.

The ATPase peptide appears to be self-associated in the membrane [32, 36, 46, 48]. The number of the smaller surface particles on the outer surface of the vesicles is 3–4 times more than that of the intramembranous particles, suggesting that the ATPase forms oligomers within the membrane. Some recent kinetic, spectroscopic, and labeling experiments also support this conclusion [36, 48]. Although it was shown that the monomeric form of the ATPase obtained in the presence of detergents still maintains full enzymic activity [36], these results may suggest that an oligomer of ATPase peptide is the functional unit for Ca transport in the native SR membrane.

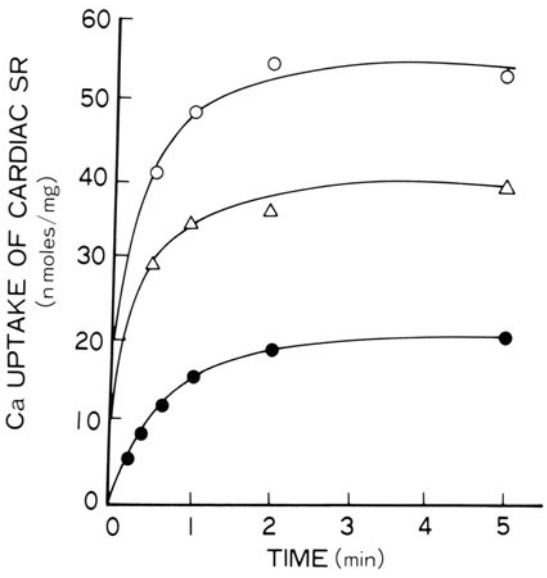

FIGURE 12–3. Ca uptake by cardiac SR vesicles in the absence of Ca-precipitating anion. Ca uptake was measured with 0.2 mg/ml of chicken cardiac SR preparation in 0.1 *M* KCl, 20 m*M* Tris-maleate (pH 6.8), 5 m*M* $MgCl_2$, 2 m*M* ATP, 0.1 m*M* $^{45}CaCl_2$, and various concentrations of EGTA. Ionized Ca^{2+} concentrations were ○, 3.0 μ*M*,; △, 1.1 μ*M*; ●, 0.35 μ*M*. Membrane filtration method was used. From Kitazawa [51].

Ca Uptake by the Fragmented SR

Ca UPTAKE AND ATP HYDROLYSIS

Isolated cardiac SR vesicles can take up Ca^{2+} in the presence of Mg^{2+} and ATP, thereby reducing markedly Ca^{2+} concentration in the reaction medium [1, 45]. At relatively low ionized Ca^{2+} (3–50 μ*M*) and in the absence of Ca^{2+}-precipitating anions such as oxalate or phosphate, SR vesicles rapidly accumulate up to 70 nmol Ca^{2+}/mg protein (fig. 12–3) [14–16, 49–51]. This Ca^{2+} flows out of the vesicles at a slow rate in the presence of EGTA, a membrane-impermeable Ca-chelating agent. This Ca^{2+}, however, is rapidly and completely released when the SR membrane is made leaky with detergents or Ca ionophores [52]. These observations indicate that Ca^{2+} is transported across the SR membranes and stored within their lumen. If the internal space of the cardiac SR vesicles is assumed to be 4–5 μl/mg protein, which is the value reported for the skeletal SR vesicles [45], the intravesicular Ca^{2+} concentration could be as high as 17 m*M*. Although a significant portion of this Ca^{2+} may be bound to the intravesicular structures such as Ca-binding proteins and membrane phospholipids, the intravesicular ionized Ca^{2+} would still be at the millimolar range, indicating that Ca^{2+} is transported against the concentration gradient under these conditions.

After a steady-state level of up to 70 nmol Ca^{2+}/mg protein is reached, further Ca accumulation is not observed even when the Ca^{2+} and ATP concentrations in the medium are sufficient to activate the Ca pump. The constant level of Ca accumulation indicates that both the rates of active Ca influx by the pump and passive Ca efflux are equal. The influx depends on the degree of activation of the Ca pump and the concentration of intravesicular Ca^{2+} while the efflux depends on the intravesicular Ca^{2+} concentration and the Ca permeability of the SR membranes. As noted below, intravesicular Ca^{2+} at millimolar ranges inhibits the Ca pump by interfering with an intermediary step of ATP hydrolysis. The passive permeability of the SR membranes to Ca^{2+} in the absence of ATP is relatively low, about 50–100 times slower than the maximal initial rate of Ca uptake in skeletal muscle SR [45]. This low permeability to Ca^{2+} primarily reflects the intrinsic property of the lipid bilayer matrix on which SR membranes are built. It was found, however, that the SR permeability to Ca^{2+} increases markedly during ATP-supported Ca uptake when Ca^{2+} concentrations outside the SR vesicles increase [53].

When oxalate is included in the reaction medium, cardiac SR vesicles take up as much as 6–10 μmol Ca^{2+}/mg protein [16, 17]. An equimolar amount of Ca^{2+} and oxalate is taken up under these conditions and Ca oxalate crystal is formed inside the SR vesicles [1, 13, 22, 54], indicating that the intravesicular concentration of Ca oxalate is higher than its solubility product. Ca uptake observed under these conditions proceeds linearly over a considerable period of time until Ca^{2+} concentrations in the medium become too low to activate the Ca pump or until Ca uptake is limited by the Ca oxalate storing capacity of the vesicles. Therefore, oxalate, which is freely permeable to the

SR membranes and forms crystal with Ca^{2+}, appears to sustain Ca uptake by maintaining the intravesicular Ca^{2+} concentrations at a low level, thereby removing an inhibitory effect of intravesicular high Ca^{2+} on Ca transport [55].

Ca uptake by SR vesicles is usually measured using radioactive $^{45}Ca^{2+}$ by the membrane filtration method, which allows rapid separation of $^{45}Ca^{2+}$-loaded vesicles from the reaction medium. This technique is appropriate for following the time course of Ca uptake in a time scale of minutes. The reported maximal rates of Ca uptake by cardiac SR vesicles measured with this techique in the presence of oxalate range from 0.2 μmol/mg protein/min at 25°C [56] to 1.5 μmol/mg protein/min at 37°C [16]. In the absence of Ca-precipitating anion, this technique does not allow accurate determination of the rate of Ca uptake because Ca uptake proceeds linearly only for a short time (fig. 12–3). Ca uptake in time scales of milliseconds to seconds can be followed with stopped-flow techniques or quench-flow method. In the former, a rapid time-dependent spectral change of Ca indicator dyes such as murexide or arsenazo III, which reflects variation of the Ca^{2+} concentration in the medium, is monitored spectrophotometrically; while, in the latter, fast ^{45}Ca uptake by the vesicles is measured after quenching the uptake reaction with EGTA or La^{3+} using a rapid-quenching apparatus. The initial rate of ATP-supported Ca uptake by cardiac SR vesicles measured with murexide through the stopped-flow technique was reported to be 16 ~ 21 nmol Ca^{2+}/mg protein / 150 ms at 25°C [49]. In contrast, an initial uptake rate of 33.4 nmol Ca^{2+}/mg protein/s was measured at 22°C in the presence of 18.9 μM Ca^{2+} with a rapid-quenching apparatus and EGTA [57]. It should be noted that these values of Ca-uptake rate are much greater than those obtained at the steady state in the presence of oxalate (see above).

Ca transport across cardiac SR membranes is an energy-requiring process [1, 54]. SR vesicles exhibit Ca^{2+}-dependent and Ca^{2+}-independent ATP hydrolysis. In the usual preparations of cardiac SR membranes, a large portion of Ca^{2+}-independent ATPase activity appears to be derived from the activity associated with the contaminating mitochondrial fragments [13, 18–20]. In contrast, the Ca^{2+}-dependent portion of ATP hydrolysis is catalyzed by the ATPase protein of the SR. In skeletal muscle SR, the Ca^{2+}-dependent ATP hydrolysis and Ca uptake parallel each other under a variety of conditions [1, 54], indicating that the former represents an energy source for the latter. Ca^{2+}-dependent ATP hydrolysis and Ca uptake are tightly coupled, 2 mol Ca^{2+} being transported for 1 mol ATP hydrolyzed both in the presence and absence of oxalate [1, 46, 54]. In accord with this coupling ratio, 1 mol of ATPase protein was shown to contain 2 mol of high-affinity Ca-binding sites and 1 mol of high-affinity ATP-binding site (see above). A coupling ratio of 2 mol Ca^{2+} taken up per mole ATP hydrolyzed is also observed in the intact cardiac SR vesicles [19]. The coupling ratio, however, decreases when the passive permeability of SR membranes to Ca^{2+} is increased by various means. Treatment of SR vesicles with detergents or ionophores, for example, renders the SR membranes leaky and prevents net uptake of Ca^{2+} while a high rate of ATP hydrolysis is maintained for a prolonged period of time. Low coupling ratios have often been reported even in intact SR vesicles [26]. This may indicate that a significant fraction of the SR vesicles in these preparations is open membrane fragments or that some unknown mechanisms may be operating to maintain the increased permeability of the SR membranes under certain experimental conditions.

Ca uptake and Ca^{2+}-dependent ATP hydrolysis by cardiac SR vesicles are activated by very low Ca^{2+} concentrations in the medium outside SR vesicles [1, 45]. The rates of both activities rise with increasing Ca^{2+} concentrations, reaching a maximum at 3–10 μM Ca^{2+}. Half-maximal activation is seen at 0.3–4.7 μM Ca^{2+} (K_{Ca}) at pH 6.8–7.0 [14–16, 20, 50, 51, 56, 58]. This rather large variation of the optimal range of Ca^{2+} for activation arises partly from the different binding constants for the Ca-EGTA complex employed by different investigators. It should be noted that the optimal range of Ca^{2+} (K_{Ca}) for Ca uptake and ATP hydrolysis measured in the presence of oxalate is approximately fivefold greater than that

for the steady-state Ca accumulation obtained in the absence of Ca-precipitating anions [16]. The former, being in agreement with that for formation of a phosphoenzyme intermediate of ATP hydrolysis (see below), appears likely to reflect Ca^{2+} dependence of Ca influx effected by the Ca pump. The latter, however, may not give true Ca^{2+} dependence of the pump activity because a steady-state Ca accumulation is determined by the dynamic equilibrium between Ca influx into and Ca efflux from the SR vesicles. Because the permeability of the SR membrane to Ca^{2+} increases with increasing Ca^{2+} outside the SR vesicles [53], the high intravesicular Ca^{2+}, which is the result of the pump activity, would increase Ca efflux significantly at higher Ca^{2+} in the medium. This, together with the decreased turnover of the Ca pump caused by high intravesicular Ca^{2+} (see below), could lower Ca^{2+} concentrations at which Ca^{2+} dependence of the steady-state accumulation exhibits a saturation. The activating effect of Ca^{2+} can be mimicked by Sr^{2+} or Mn^{2+} [1, 59]. La^{3+} at relatively high concentrations inhibits both Ca uptake and ATP hydrolysis [32]. Both activities are inhibited by high Ca^{2+} inside SR vesicles, as mentioned above.

In cardiac SR, like in skeletal SR [32], an equimolar complex of Mg^{2+} and ATP appears to serve as the substrate for Ca uptake and Ca^{2+}-dependent ATP hydrolysis. The Ca^{2+}-dependent ATP hydrolysis exhibits a complex MgATP dependence: in the presence of an ATP-regenerating system, the ATPase activity shows saturation at about 10 μM MgATP (K_m, 1–2 μM) while a further increase in activity is observed at higher MgATP concentrations (K_m ~ 0.18 mM) [20, 60]. The K_m value obtained at low ATP is similar to that for formation of phosphoenzyme intermediate of the ATPase (see below), indicating that this low K_m site corresponds to a high-affinity catalytic site. The stimulatory effect of high ATP is considered to arise from the regulatory action of the nucleotide on the turnover of the Ca pump because high concentrations of ATP exert an activating effect on the intermediary steps of ATP hydrolysis (see below). In addition, the analogues of ATP, which are not hydrolyzed or hydrolyzed little by the enzyme, mimic the effect of high ATP [35, 61]. Therefore, the ATPase appears to have a high-affinity catalytic site and low-affinity regulatory site. Besides ATP, the Ca pump of SR utilizes other natural nucleotide triphosphates [1, 32, 62]. The rates of utilization at 5 mM by the cardiac Ca pump are in the following order; ATP > CTP > ITP > GTP > UTP [13]. Other phosphate compounds such as acetylphosphate and *p*-nitrophenylphosphate also serve as substrates although the rates of utilization are very slow [63].

Mg^{2+}, in addition to serving as the component of the true substrate MgATP, accelerates an intermediary step of ATP hydrolysis (see below). The possibility that Ca uptake is obligatorily coupled to countertransport of Mg^{2+} has been excluded by recent experiments with skeletal SR vesicles [59, 64.].

Monovalent cations such as K^+ are required for the full activation of the Ca-pump activity [65–67]. Removal of monovalent salts from reaction medium reduces the rates of Ca uptake and Ca^{2+}-dependent ATP hydrolysis to approximately one-fourth of those observed in the presence of optimal concentrations of these salts. The effectiveness of these salts at 100 mM is graded in the following order: $K^+ > Na^+ \gtrsim NH_3^+ \gtrsim Rb^+ > Cs^+ > Li^+$ [65–67]. As discussed later, these monovalent salts also accelerate one of the intermediary steps of ATP hydrolysis.

pH dependence of the rates of Ca uptake and Ca^{2+}-dependent ATP hydrolysis by the cardiac SR vesicles exhibits a bell-shaped profile with the optimum at pH 6.2–6.5 for Ca uptake and at pH 7.5–8.0 for ATP hydrolysis [20, 68].

Effects of ion fluxes and the membrane potential on Ca uptake have been studied using native skeletal SR vesicles [69] or purified skeletal SR ATPase protein incorporated into phospholipid bilayer vesicles [70]. The rate of ATP-dependent Ca uptake is stimulated when a membrane potential, negative inside, is imposed across the reconstituted SR membranes with a K^+ concentration gradient and valinomycin. This observation suggests that the Ca pump of the SR is electrogenic. pH gradient (inside acidic) was also shown to increase the

initial rate of Ca uptake [69, 71]. H^+ was found to be ejected from the SR vesicles during the initial phase of Ca uptake [59, 72]. This H^+ ejection and Ca uptake may be tightly coupled in such a way that H^+ is exchanged for Ca^{2+} in an antiport system [59, 71]. On the other hand, the native membranes of skeletal SR have been shown to be highly permeable to ions such as K^+, Na^+, H^+, and Cl^-, although they are relatively impermeable to Ca^{2+}, Mg^{2+}, and larger ions such as $Tris^+$, $choline^+$, or $gluconate^-$ [73, 74]. A specific K^+ channel has been identified and extensively characterized in the skeletal SR membranes [75, 76]. An anion channel which is blocked by anion-transport inhibitors was also identified in the skeletal SR membranes [77]. It is, therefore, also possible that charge displacement caused by the activity of the electrogenic Ca pump may be counterbalanced by fluxes of these highly permeable ions which are not directly coupled to the Ca-pump activity.

MECHANISM OF ATP HYDROLYSIS

As mentioned earlier, Ca uptake by cardiac SR is an energy-requiring process and is stoichiometrically linked to ATP hydrolysis. As Ca uptake can be reconstituted from the ATPase protein purified from skeletal SR and phospholipids [38, 78], the ATPase protein is considered to serve not only as a Ca transporter but also as a transducer of chemical energy into the osmotic energy. To elucidate the mechanism by which Ca^{2+} is transported across SR membranes, analysis of the elementary steps of Ca^{2+}-dependent ATP hydrolysis and comparison of these with those of Ca transport must be carried out. A current view of the mechanism of ATP hydrolysis by the Ca-pump ATPase is summarized below.

During Ca^{2+}-dependent ATP hydrolysis by cardiac SR vesicles, the terminal phosphate of ATP is incorporated into the ATPase protein [18, 20, 58, 79–82]. The phosphoenzyme formation requires micromolar ranges of Ca^{2+} and ATP, indicating that high-affinity sites for Ca^{2+} and ATP, which are responsible for activation of ATP hydrolysis (see above), are involved in phosphorylation of the ATPase [20, 58, 80]. When concentrations of Ca^{2+} and ATP are varied at a relatively low concentration range, complete parallelism can be observed between the steady-state level of phosphoenzyme and the rate of ATP hydrolysis [20], supporting the view that the phosphoenzyme is an intermediate of ATP hydrolysis. The chemical characteristics of the phosphoenzyme isolated by the addition of acid are those of an acylphosphoprotein [20, 80]. In skeletal SR, the phosphoryl group was shown to be covalently bound to the β-carboxyl group of aspartic acid residue [83]. The maximum amount of phosphoenzyme formed in the ordinary preparations of cardiac SR, which could reflect the amount of the ATPase protein in the preparations, varies significantly from one animal species to the other, the SR preparation from dog heart giving the highest value of up to 1.3 nmol/mg protein [18, 20, 80]. When the SR preparations from pigeon heart are further purified by sucrose density gradient after Ca oxalate loading, a phosphoenzyme level as high as 2.45 nmol/mg protein can be obtained [17].

Steady-state and transient kinetic studies of ATP hydrolysis by cardiac and skeletal SR membranes and the extensive use of various conformational probes revealed that the ATPase enzyme undergoes successive conformational transitions during catalysis [32, 46, 48, 62, 81, 84–86]. The results may be summarized as shown in the following scheme (scheme 1):

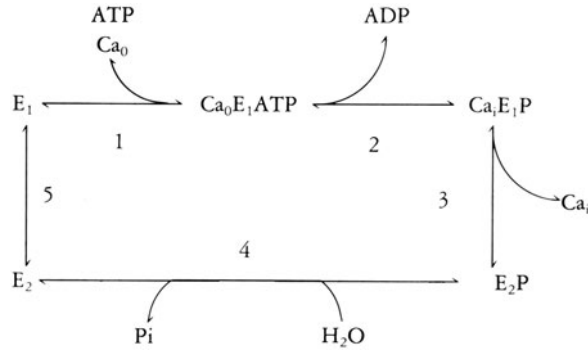

where Ca_0 and Ca_i refer to Ca^{2+} located outside and inside the SR vesicles, respectively. Ca occluded within the membrane is also referred to as Ca_i. The ATPase is considered to assume two

major conformations E_1 and E_2, the former (E_1 or E_1P) having high Ca affinity and the latter (E_2 or E_2P) having low Ca affinity. The micromolar range of Ca^{2+} stabilized the E_1 conformation of the free enzyme whereas removal of Ca^{2+} from the medium at low pH and high temperature or addition of vanadate stabilized the E_2 type of the free enzyme [86, 87]. Under physiologic conditions, 2 mol Ca^{2+} and 1 mol of MgATP react with 1 mol of the ATPase (E_1) on the outside surface of the SR membranes to form a Michaelis complex (step 1). Formation of the E_1-type phosphoenzyme (E_1P) (step 2) is accompanied by the transient occlusion of Ca bound to the Ca-transport site [88]. Metal-free ADP is released on the outside surface of the membranes [89]. Mg^{2+} thus remains bound to the enzyme at this stage [93]. Ca^{2+} is then released into the vesicular lumen when E_1P is converted to the E_2 type of phosphoenzyme (E_2P) (step 3). E_1P is a "high energy" type of phosphoenzyme as it donates its phosphate group to added ADP to form ATP, while E_2P is a "low energy" type because it does not react with added ADP. Therefore, decrease of the affinity for Ca^{2+} is coupled to the conversion of the "high energy" to "low energy" state of the phosphoenzyme. In step 4, E_2P decomposes to yield inorganic phosphate (P_i) and the free enzyme E_2 on the outside surface of the SR vesicles. Mg^{2+} appears to be released from the ATPase at this step. Then, E_2 is transformed to E_1, the enzyme thus completing a catalytic cycle.

Enzyme phosphorylation in cardiac SR vesicles is very rapid (fig. 12–4) [81, 90, 91]. It reaches a maximum level at 30 ms at 20°–22°C when ATP (10 μM) is added to cardiac SR vesicles in a Ca^{2+}-containing medium. After reaching a maximum level, phosphoenzyme decreases slightly to the steady-state level ("overshoot"). In contrast, P_i liberation exhibits a distinct lag phase during accumulation of phosphoenzyme, indicating that P_i is derived from the turnover of phosphoenzyme. When enzyme phosphorylation is started by the addition of ATP and Ca^{2+} to the reaction medium containing the enzyme and EGTA, phosphorylation proceeds at a much slower rate and the "overshoot" cannot be observed (fig. 12–4). These observations are taken to indicate that the E_2 to E_1 transition (step 5), which is induced by Ca^{2+} addition, is slow and controls the rate of enzyme phosphorylation. The slow transition of E_2 to E_1 (step 5) can also be followed by monitoring changes of intrinsic fluorescence of the enzyme or the fluorescence of fluorescein bound to the enzyme [86, 87, 92].

Phosphoenzyme decomposition is accelerated by Mg^{2+} or K^+, but inhibited by high Ca^{2+} [18, 20, 32, 46, 65, 82]. At high Ca^{2+} (> 1.0 mM), the E_1P to E_2P conversion is inhibited because Ca binding to the low-affinity Ca-binding site on E_2P accelerates reversal of this reaction step, thereby decreasing the concentration of E_2P. Mg^{2+} accelerates the E_1P to E_2P conversion and E_2P hydrolysis [84, 94]. A recent report [93] has shown that Mg^{2+}, which is derived from the metal component of the MgATP complex bound to the substrate site of the enzyme, is responsible for acceleration of phosphoenzyme decomposition.

Monovalent cations such as K^+ accelerate E_2P hydrolysis [94], thus shifting the equilibrium of step 4 markedly to E_2 plus P_i. In the absence of K^+, E_2P hydrolysis is very slow and limits the overall rate of ATP hydrolysis. In the presence of 100 mM KCl, which is usually included in the reaction medium for the measurement of Ca uptake and ATP hydrolysis by the SR, E_2P hydrolysis is much faster than the rate of the E_1P to E_2P conversion [94, 95].

High concentrations of ATP exert stimulatory effects on the intermediary steps of ATP hydrolysis [96]. High ATP accelerates E_2P hydrolysis and the conformational transition of E_2 to E_1 (step 5) [85, 94], suggesting that high ATP unstabilizes the E_2 conformation of the enzyme. A low-affinity regulatory site for ATP (see above) appears to be involved in this effect of high ATP [35, 61, 85, 87, 94]. Therefore, in the physiologic conditions where high concentrations of Mg^{2+}, ATP, and KCl are present, E_2P hydrolysis and the E_2 to E_1 transition become faster, and may not limit the overall reaction rate. Instead, the rate of the E_1P to E_2P conversion (step 3) may control the overall reaction rate under these conditions. In addition to the effects described above, high ATP

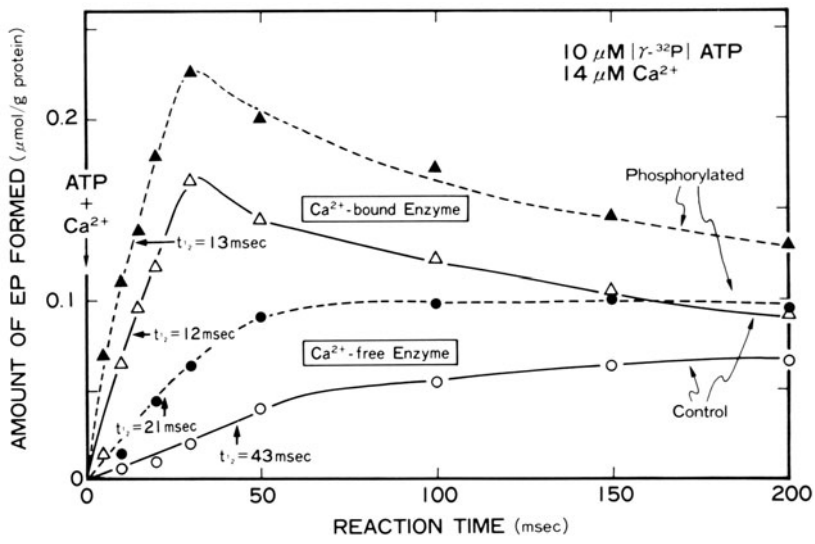

FIGURE 12–4. Time courses of formation of phosphoenzyme intermediate before (○ △) or after (● ▲) the treatment with cyclic-AMP-dependent protein kinase: △, ▲, ATPase reaction started with SR plus Ca^{2+}; ○, ●, ATPase reaction started with Ca^{2+}-free SR. The final reaction medium contained 10 μ*M* [γ-^{32}P]ATP and 14 μ*M* ionized Ca^{2+}. Temperature and pH used were 22°C and 6.8, respectively. From Tada et al. [90].

was shown to accelerate the formation of the phosphoenzyme intermediate [32].

It was shown in skeletal SR vesicles that the reaction sequence outlined above is completely reversible [32, 62, 85, 97]. Lowering Ca^{2+} in the medium outside the Ca-loaded intact SR vesicles by a Ca-chelating agent leads to ATP synthesis from ADP and P_i, which is coupled with Ca efflux. Synthesis of 1 mol ATP is coupled to the outflow of 2 mol Ca^{2+} [98]. Reversal of Ca transport requires that ADP, P_i, and Mg^{2+} are present in the medium outside the SR vesicles. The free enzyme should be in the E_2 conformation for the reversal of the Ca pump to occur. Therefore, high ATP or the micromolar range of Ca^{2+}, which stabilizes the E_1 conformation, inhibits the pump reversal. During the pump reversal, the ATPase is phosphorylated by P_i. The resultant phosphoenzyme reacts with added ADP to form ATP, which is coupled to Ca efflux. Phosphorylation of the ATPase by P_i also occurs even when the SR vesicles are rendered leaky or solubilized so that Ca gradient across the SR membranes cannot be developed [62, 85, 99]. The resultant phosphoenzyme, however, does not react with added ADP to form ATP. Under these conditions, simultaneous addition of high Ca^{2+} and ADP to the phosphoenzyme leads to the net synthesis of ATP [85, 100]. The Ca^{2+} concentration required for the synthesis of ATP is in the millimolar range, which presumably reacts with the low-affinity Ca-binding site on the enzyme. Therefore, reversal of ATP hydrolysis can be achieved without using the osmotic energy that might be derived from the concentration graident of Ca^{2+} across the SR membrane. For the synthesis of ATP in the intact SR vesicles, therefore, the concentration gradient of Ca^{2+} appears to be required only to provide high intravesicular Ca^{2+} concentrations and to saturate the internal low-affinity Ca-binding site [85].

COMPARISON OF Ca PUMPS OF CARDIAC AND SKELETAL MUSCLE SR

As described in the preceding section, the mechanism of Ca uptake and ATP hydrolysis by cardiac SR vesicles is generally similar to that by skeletal SR vesicles. However, significant differences are noted in the two types of SR preparations. (a) Ca uptake and ATP hy-

drolysis are considerably slower in cardiac than in skeletal SR preparations [1, 45]. (b) In the cardiac SR membranes, a specific regulatory mechanism, which is physiologically and pharmacologically important, controls Ca transport and ATP hydrolysis (see below) [30]. (c) The cardiac SR ATPase protein is immunologically different from that of fast skeletal muscle [27], suggesting that there may be some structural difference in the two types of ATPase protein.

To define the basis for the slower Ca uptake by the cardiac SR preparations, the steady-state ATPase reactions by dog cardiac and rabbit fast skeletal SR preparations were compared under the identical experimental conditions [20]. ATP hydrolysis by cardiac preparations at saturating Ca^{2+} is 3–6 times slower than that by skeletal preparations, whereas, at low Ca^{2+} (1–2 μM), the former is more than ten times slower than the latter. A study on ATP dependence of the rate of ATP hydrolysis revealed that the K_m value for ATP is similar in both types of SR preparation while the maximum rate of ATP hydrolysis is about fourfold less in cardiac preparations. The maximum level of enzyme phosphorylation, which reflects the density of the ATPase protein in each SR preparation was also found to be about fourfold less in dog cardiac preparations. In addition, the concentration of ionized Ca^{2+} that elicits half-maximal activation of the ATPase of dog cardiac preparation (K_{Ca}) is 3–4 times higher than that of the corresponding value for K_{Ca} in rabbit skeletal preparations. These results therefore indicate that the relatively slow rate of Ca uptake by dog cardiac preparations primarily reflects a low density of Ca-pumping sites and lower Ca affinity for these sites, rather than a low turnover rate. It may be added that the pH optimum for ATP hydrolysis is at a slightly more alkaline level in cardiac SR preparations.

In addition to these results obtained in the steady-state analysis of ATP hydrolysis, the recent transient-state kinetic data indicate that there are quantitative differences in the rate constants of some of the partial reactions of the ATPase of both types of SR [81, 101]. When the ATPase reaction is started by the addition of ATP and Ca^{2+} to the reaction medium containing EGTA and enzyme, enzyme phosphorylation is slow, reflecting the slow conformational transition of E_2 to E_1 (step 5 of scheme 1). In dog cardiac preparations, the estimated rate constant of the E_2 to E_1 transition in the presence of 10 μM ATP is approximately five times smaller than that in rabbit skeletal preparations. The rate of phosphorylation, however, is the same for both types of SR preparation when the reaciton is started by the addition of ATP (10–50 μM) to SR vesicles in a Ca^{2+}-containing medium, indicating that steps 1 and 2 of Scheme 1 occur at similar rates in the two types of SR preparation.

It was shown that dissociation of Ca^{2+}, which is bound to the ATPase protein during the initial phase of enzyme activation, is 1.5-fold slower in the dog cardiac preparations. Phosphoenzyme decomposition, as measured after the new formation of phosphoenzyme is prevented by chelation of Ca^{2+} by EGTA in the presence of 3 mM $MgCl_2$ and 100 mM KCl, exhibits complex time courses but appears to be slightly slower in the dog cardiac SR preparations. These transient-state kinetic data collectively indicate that the slower conformational transition of the E_2 to E_1 (step 5) in the dog cardiac preparations is the most prominent difference observed. The difference in the rate of this reaction step could be responsible for the lower rates of ATP hydrolysis and Ca uptake by cardiac SR preparations at low ATP. At high ATP concentrations, however, the E_2 to E_1 transition may not control the overall rate of reaction because high ATP appears to enhance this reaction step [85]. It should be added that enzyme phosphorylation (steps 1 and 2), when started by the addition of ATP to the enzyme in a Ca^{2+}-containing medium, is significantly slower in the absence of added KCl than in the presence of this salt at 100 mM in the dog cardiac SR preparations [91]. This effect of KCl was not observed in the rabbit skeletal preparations [89, 102].

Regulation of Ca Uptake by Fragmented SR

In cardiac SR membranes, a regulatory mechanism exists in which a specific protein component of the SR membranes (phospholamban)

serves as a regulator controlling the Ca-pump activity and presumably plays a key role in mediating the actions of hormones and drugs on heart muscle.

CYCLIC-AMP REGULATION OF Ca UPTAKE

Phospholamban Phosphorylation. When cardiac SR membranes are incubated with [γ-^{32}P]ATP and cyclic AMP in the presence or absence of cyclic-AMP-dependent protein kinase, ^{32}P is incorporated into SR membranes [103–105]. Formation of this phosphoprotein is independent of Ca^{2+} up to 0.1 m*M*, but is markedly dependent on cyclic AMP between 0.1 and 10 μM with the half-maximal activation occurring at about 0.2 μM [104]. The phosphoprotein, unlike the phosphorylated intermediate of the ATPase of the SR (see above), exhibits stability characteristics of a phosphoester in which the phosphate is largely incorporated into serine residue [104–106]. On gel electrophoresis in the presence of sodium dodecylsulfate, most of the ^{32}P label is associated with a protein of approximately 22,000 daltons [105, 107]. Phosphorylation of the 22,000-dalton protein also occurs in cardiac SR preparations that were virtually freed from sarcolemmal membranes through sucrose density gradient centrifugation after Ca oxalate loading [21]. Since this 22,000-dalton protein is specifically associated with functional alterations in the SR (see below), it was termed "phospholamban" in view of its ability to receive phosphate from ATP [107, 108]. Under the conditions in which phospholamban is phosphorylated, several other lower-molecular-weight proteins are also phosphorylated [30].

Phospholamban, which is an acidic proteolipid and contains 40%–45% hydrophobic amino acid residues [29, 109, 110], is intimately associated with the SR membrane. A portion of phospholamban is exposed at the outer surface of SR vesicles because it is labeled with [γ-^{32}P]ATP in the presence of cyclic-AMP-dependent protein kinase and because proteolytic digestion results in the disappearance of the 22,000-dalton protein when the latter is not phosphorylated [107]. Upon phosphorylation, the phosphorylation site of phospholamban may be transposed within the membrane because tryptic digestion becomes much less effective [107]. The lack of iodination of phospholamban, which contains tyrosine, may reflect the location of these residues within the membrane interior [111].

Although phospholamban is originally thought to represent a single peptide that electrophoretically migrates as a 22,000-dalton component in the presence of sodium dodecylsulfate, addition of Triton X-100 or boiling of the phosphorylated SR membranes in sodium dodecylsulfate solution results in the complete disappearance of the 22,000-dalton phosphoprotein with the concomitant appearance of 11,000-dalton and, even lower, 5000- to 7000-dalton phosphoproteins [112, 113]. While the possible existence of oligomer–monomer transition should be further sought, these results may be related to the observation that phospholamban contains two kinds of phosphorylatable sites that are phosphorylated by two different protein kinases (see below).

A protein–protein interaction appears to exist between phospholamban and the ATPase protein, which is dependent on the phosphorylation state of the former [109, 114]. When phospholamban is phosphorylated, the two proteins remain associated even after solubilization of the SR membranes with detergents. In contrast, phospholamban appears to be separated easily from the ATPase protein by mild treatment with detergents when it is not phosphorylated. The stoichiometric relation between the amounts of phospholamban and the ATPase protein in the membranes may be 1:1 as the amount of phospholamban phosphorylation is similar to the maximum amount of the phosphorylated intermediate of the ATPase [58].

Stimulation of Ca Uptake. The rate of Ca uptake by cardiac SR vesicles in the presence of oxalate is more than doubled when the SR vesicles are previously phosphorylated by incubation with an optimum concentration of cyclic AMP and cyclic-AMP-dependent protein kinase [19]. In contrast, Ca uptake by the SR vesicles isolated from fast skeletal muscle does not exhibit such stimulation, nor is there any

significant phosphorylation of similar protein [115]. The extent to which Ca uptake by cardiac SR vesicles is stimulated is correlated well with the increase in phospholamban phosphorylation, but not with other phosphoproteins [116]. Protein kinase obtained from cardiac muscle (type-II kinase) produces such stimulation, while that obtained from skeletal muscle (type-I kinase) is also functional but to a much lesser extent [104]. When the rate of Ca uptake by cardiac SR vesicles is examined at different Ca^{2+} concentrations, cyclic-AMP-dependent phosphorylation of phospholamban reduces by approximately threefold the Ca^{2+} concentration at which a half-maximal activation of Ca uptake is observed [19, 117]. When the phosphorylated SR membranes are incubated with phosphoprotein phosphatase obtained from bovine heart, most of the phosphorylated phospholamban is dephosphorylated [118, 119]. Dephosphorylation leads to a complete reversal of the effect produced by protein kinase. When Ca uptake and phospholamban phosphorylation are compared in the presence of a fixed amount of protein kinase and different amounts of protein kinase inhibitor (modulator), a linear relationship is observed between the decrease in Ca uptake and the inhibition of phosphorylation of the SR membranes [120].

Protein-kinase-catalyzed phosphorylation is capable of stimulating Ca transport also in the absence of oxalate [57, 90]. Under these conditions, the effect is evident only at the initial phase (up to 300 ms) after the start of the reaction.

Effect of Phospholamban on Partial Reactions of ATP Hydrolysis. Ca uptake by SR vesicles is coupled with Ca^{2+}-dependent ATP hydrolysis. The observed stimulation of Ca uptake by phospholamban phosphorylation could be derived either from the enhanced turnover of the ATPase or from the increased efficiency of the Ca pump, namely, the increased coupling ratio between Ca uptake and ATP hydrolysis. In fact, acceleration of Ca uptake is accompanied by the enhanced rate of concomitant ATP hydrolysis, the stoichiometry between Ca^{2+} taken up and ATP hydrolyzed being maintained at about 2 after phospholamban is phosphorylated [19]. The observed alteration in kinetic properties of Ca^{2+}-dependent ATPase induced by phospholamban phosphorylation can be discussed using the reaction sequence described in scheme 1. When phospholamban is phosphorylated, the ATPase activity in the presence of saturating concentrations of Ca^{2+} and ATP increases without alteration of a phosphoenzyme intermediate level [58], suggesting that the increased rate of ATP hydrolysis may be due to the enhanced turnover of the phosphoenzyme intermediate. In accord with this view, the ratios between rates of ATP hydrolysis and steady-state levels of phosphoenzyme intermediate obtained at different Ca^{2+} concentrations (0.1–10.0 μM), and the hydrolysis rates of phosphoenzyme intermediate which are measured directly after preventing the new formation of phosphoenzyme by the addition of Ca-chelating agent, are doubled when phospholamban is phosphorylated [58]. In light of the presently available reaction scheme of Ca^{2+}-dependent ATPase as seen in scheme 1, enhancement of phosphoenzyme hydrolysis can be derived from acceleration of either step 3 or step 4 and 5. Step 3 is probably accelerated since it is the rate-limiting step during phosphoenzyme decomposition under conditions where saturating concentrations of Ca^{2+}, Mg^{2+}, and K^+ are present (see above). Thus, phospholamban phosphorylation may stimulate the conversion of E_1P to E_2P (step 3 of scheme 1).

The rate of formation of phosphoenzyme intermediate is significantly accelerated by phospholamban phosphorylation when reaction is initiated by the addition of ATP and Ca^{2+} to the reaction medium containing EGTA and the enzyme (fig. 12–4) [90]. However, the rate of phosphoenzyme formation is not affected significantly when ATP is added to cardiac SR vesicles in a Ca^{2+}-containing medium. In the former experiment, the rate of phosphoenzyme formation is limited by the E_2 to E_1 transition (step 5 of scheme 1, see above). Phospholamban phosphorylation, therefore, enhances this slow reaction step. It is of interest to note that phospholamban phosphorylation enhances two slow steps (steps 3 and 5) in the reaction se-

quence of ATP hydrolysis. These are the steps at which a significant conformational change of the ATPase enzyme occurs and the affinity of enzyme for Ca^{2+} is greatly altered (see above). As mentioned earlier, ATP phosphorylates the 30,000-dalton moiety of the ATPase protein while Ca^{2+} appears to interact with the 25,000-dalton portion of the enzyme. Phospholamban phosphorylation may exert a direct effect on the conformational state of the 30,000-dalton moiety, allowing the rate of translocation of Ca^{2+} through the 25,000-dalton moiety of the enzyme to be stimulated [30]. The molecular mechanism by which phospholamban phosphorylation controls Ca uptake by the cardiac SR vesicles remains to be found.

CALMODULIN-DEPENDENT REGULATION OF Ca UPTAKE

It has recently been shown that phosphate can be incorporated into phospholamban in the presence of Ca^{2+} and calmodulin [112, 121–123]. It is postulated that phosphorylation is catalyzed by an endogenous protein kinase associated with cardiac SR membranes which is activated by calmodulin and Ca^{2+}. The phosphorylation of phospholamban by calmodulin-stimulated protein kinase occurs at a serine residue which is different from that phosphorylated by cyclic-AMP-dependent protein kinase [110, 112]. The maximal amount of phospholamban phosphorylation catalyzed by calmodulin-dependent protein kinase at the optimal Ca^{2+} concentration of 5–10 μM is about the same as that found with cyclic-AMP-dependent protein kinase [122]. Since phosphorylation catalyzed by the two kinases occurs independently, an additive elevation of the amount of phosphorylation is observed when the cardiac SR vesicles are incubated under conditions favorable for both types of kinases [112, 121, 122].

In accord with the reports that phospholamban is phosphorylated by Ca^{2+} and calmodulin-dependent protein kinase, preincubation of the SR membranes with calmodulin results in an enhanced rate of Ca uptake [112, 121–124]. It was reported that, in the absence of calmodulin-dependent phosphorylation of phospholamban, Ca uptake is not enhanced by cyclic-AMP-dependent protein kinase [112]. Others found, however, that cyclic-AMP-mediated enhancement of Ca uptake can be observed even when calmodulin-dependent phosphorylation does not occur [121, 122]. Ca uptake is enhanced when either of the systems is operational and the effects are additive in accord with the finding that phosphorylation by the two kinases occurs in the independent and additive manners [121, 122]. It is possible that the Ca^{2+} concentrations employed in the former report are far too high (0.1 mM) to see the physiologic effect of Ca control in the cardiac SR. The stimulatory effects could be seen only when the Ca^{2+} concentrations are within the physiologic range (0.1–10 μM) [121, 122]. One group claims that calmodulin does not affect ATPase activity [112]. Others, however, indicate that at physiologic concentrations of Ca^{2+} (0.1–50.0 μM), calmodulin-dependent phosphorylation of phospholamban results in stimulation of the rate of ATP hydrolysis [122, 123, 125]. The stoichiometry of Ca^{2+} taken up per mole of ATP hydrolyzed remains the same before and after phospholamban phosphorylation by Ca^{2+} and calmodulin-dependent protein kinase [122, 123]. At present it is not clear how the stimulatory effects produced by calmodulin are related to cyclic-AMP-mediated enhancement of the Ca uptake and ATP hydrolysis by the cardiac SR membranes.

Physiologic Relevance

In the mammalian myocardium, the SR is considered to be the major system involved in bringing about relaxation [5–8]. The SR is also implicated as the major source of Ca^{2+} for activation of contraction (see chapter 11). The molecular mechanism of the Ca pump of the SR, which effects cardiac relaxation, is fairly well understood as described in the preceding sections. In the following, the physiologic relevance of the Ca-pump activity of the isolated cardiac SR membranes is discussed briefly.

Ca UPTAKE BY THE SR AND CARDIAC RELAXATION

In the isolated cardiac contractile system, full activity occurs when 50–100 nmol Ca^{2+}/g wet

muscle are available for binding to the contractile proteins [3, 126]. In the intact mammalian heart cells, however, the myoplasmic free Ca^{2+} reached during the physiologic contraction appears to be significantly lower than that necessary for the full activation of the contractile system [127, 128]. In heart cells from adult rat or rabbit, the tension developed during the maximum twitch was estimated to be about 70% of the maximum tension [128]. In addition, in intact rabbit ventricular cells the tension developed during regular single-pulse stimulation at 12/min was only 20% of the maximum [128]. According to the estimate by Solaro et al. [126], 70% and 20% maximal force development require that 25.8 and 17.1 nmol Ca^{2+}/g wet muscle are delivered to the dog cardiac myofibrils, respectively, suggesting that this range of Ca^{2+} must bind to and be removed from the contractile system in vivo during each cardiac cycle under physiologic conditions.

ATP-supported Ca accumulation by the isolated cardiac SR vesicles has been studied in the presence and absence of Ca-precipitating anions. Ca accumulation in the absence of Ca-precipitating anions is clearly the one that is more physiologically relevant because a Ca^{2+}-trapping mechanism like that provided by oxalate has not been defined in vivo. The steady-state levels of Ca accumulation by the isolated cardiac vesicles, obtained at the physiologic ranges of Ca^{2+} in the absence of Ca-precipitating anions, and the maximum yield of the SR vesicles isolated from the heart muscle, can give an estimate of the maximum capacity of the SR in vivo to accumulate Ca^{2+} at corresponding Ca^{2+} concentrations. The estimate given by Solaro and Briggs [16] indicates that the SR in dog heart can accumulate Ca^{2+} in amounts well in excess of those necessary to activate the contractile proteins under the comparable conditions. Therefore, the Ca-accumulating capacity of the isolated SR vesicles can adequately explain the relaxed state of cardiac muscle at the steady state.

There have been some uncertainties, however, regarding the relationship between the quantitative aspects of the rate of Ca uptake by the isolated SR vesicles and of relaxation in the intact heart. The rate of Ca uptake by cardiac SR vesicles in vitro, as measured in the presence of oxalate over a time scale of minutes, is about 5–20 times less than the physiologic requirement [45]. Recent experiments in which fast Ca accumulation by the SR vesicles is followed with stopped-flow or quench-flow techniques, however, provide different results. One group reported that the amount of Ca^{2+} taken up by the cardiac SR vesicles during an interval of 0–150 ms, when measured with stopped-flow techniques in the presence of murexide, was 37 nmol/mg protein at 37°C [49]. If adjustment is made for the SR content in the heart muscle (~6.3 mg/g wet muscle [16]), the SR vesicles could remove as much as 250 nmol/g wet muscle during times required for heart relaxation (~200 ms). This amount of Ca^{2+} is significantly greater than that which must be removed from the fully activated contractile system to effect complete relaxation. In contrast to this report, 1–2 orders of magnitude smaller rate of Ca uptake was measured by another group using a similar experimental method [129]. It should be pointed out, however, that the experimental conditions employed by the latter group are likely to be the reason for the very low rate of Ca uptake observed. The reaction mixture used as described in the figure legends does not contain Mg^{2+}, which is essential for the optimum activity of the Ca pump of the SR (see above).

The fast rate of Ca uptake by the cardiac SR vesicles was also measured with a rapid-quenching apparatus using Ca^{2+} chelator as a quencher of the uptake reaction [57]. The amount of Ca^{2+} accumulated by the cardiac SR vesicles at 0.2–18.9 μM Ca^{2+} during the first 200 ms of the uptake reaction was found to be comparable to that which is necessary to activate the isolated contractile system at corresponding Ca^{2+} concentrations. Although the data described above do not provide an adequate quantitative description of Ca uptake by the SR in vivo during cardiac relaxation, they are consistent with the view that the SR plays the major role in the relaxation of the mammalian myocardium, especially since it is known that mitochondria do not take up Ca^{2+} significantly under physiologic conditions [5, 7, 51].

PHYSIOLOGIC RELEVANCE OF PHOSPHOLAMBAN PHOSPHORYLATION

Tada et al. [19, 107, 108] first proposed that cyclic-AMP-mediated acceleration of Ca uptake by cardiac SR may explain the two principal mechanical effects of catecholamines on heart muscle: abbreviation of systole and increased contractility. Cyclic-AMP-mediated stimulation of the rate of Ca uptake by the SR could explain abbreviation of systole because Ca^{2+} would be removed from troponin at an increased rate. The increased rate of Ca uptake following phospholamban phosphorylation could increase the amount of Ca^{2+} stored inside the SR membranes, allowing the cell to retain some of the Ca^{2+} which would otherwise be lost during diastole. This Ca^{2+} could add to the amount of Ca^{2+} available for delivery to the contractile proteins in subsequent contractions, thus promoting augmentation of myocardial contractility [142].

The proposed sequence of events appears to find support from experiments in skinned and intact heart cells. Catecholamines produce relaxation at the very early phase, followed by augmentation of contraction [130]. The onset of increased tension development after exposure of the heart to catecholamines is gradual, reaching the steady state after about 20 beats [131]. A recent experiment in which the Ca transient in the intact heart cell is studied with the use of aequorin, a Ca-sensitive bioluminescent protein, indicates that catecholamines augment the initial rate of Ca release into the cytoplasm during the early phase of contraction as well as the rate of reduction of Ca^{2+} during relaxation [132]. Employing a skinned cardiac cell, which exhibits cycles of phasic contractions upon addition of an appropriate amount of Ca^{2+}, Fabiato and Fabiato [133] demonstrated that a brief preincubation with cyclic AMP results in an increased amplitude of contraction and faster rates of tension development and relaxation.

The intracellular level of cyclic AMP appears to increase prior to the development of increased contractility after exposure of the heart cell to catecholamines [134, 135]. Others found, however, that there is no detectable increase in cyclic AMP when catecholamines covalently attached to glass beads augment contraction [136, 137]. It is not known at present whether a subtle increase in cyclic AMP, which might have been too low to detect, could have given rise to significant mechanical changes. Alternatively, dissociation of inotropic responses from cyclic-AMP formation may reflect some other effect of catecholamines on sarcolemmal systems such as calcium channels.

Phospholamban phosphorylation was demonstrated to occur in the intact heart. The addition of the isoproterenol to the heart perfused with $^{32}P_i$ results in increased ^{32}P incorporation into the 22,000-dalton microsomal protein (phospholamban) with simultaneous increase in the rates of tension development and relaxation [138, 143]. It is of interest to note that the extent of phospholamban phosphorylation and the rate of Ca uptake are significantly increased in the cardiac SR preparations of the hyperthyroid rat [139]. Aging does not affect the extent to which Ca uptake by the SR is accelerated by the cyclic-AMP–phospholamban system [140].

In addition to the cyclic-AMP-mediated phosphorylation of phospholamban, additional phosphorylation is catalyzed by Ca^{2+} and calmodulin-dependent protein kinase (see above). Phospholamban phosphorylation by the latter system appears to function in the intact heart cell because calmodulin inhibitor (fluphenazine) significantly reduced phospholamban phosphorylation in vivo [138]. As Ca uptake by the isolated cardiac SR vesicles is enhanced when either of the cyclic-AMP-mediated or calmodulin-dependent systems is operational, and effects are additive, Ca uptake by the SR in vivo may be regulated by these two systems in separate manners. Calmodulin-mediated phosphorylation of phospholamban would occur when the intracellular Ca^{2+} concentration increases during contraction, thus enhancing Ca uptake by the SR. It is possible, therefore, that the calmodulin system could regulate the function of the SR at least on a beat-to-beat basis.

References

1. Weber A: Energized calcium transport and relaxing factors. Curr Top Bioenerg 1:203–254, 1966.
2. Ebashi S, Endo M: Calcium ion and muscle con-

traction. Prog Biophys Mol Biol 18: 123–183, 1968.
3. Katz AM: Contractile proteins of the heart. Physiol Rev 50:63–158, 1970.
4. Langer GA: Heart: excitation–contraction coupling. Annu Rev Physiol 35:55–86, 1973.
5. Chapman RA: Excitation–contraction coupling in cardiac muscle. Prog Biophys Mol Biol 35:1–52, 1979.
6. Fabiato A, Fabiato F: Calcium and cardiac excitation–contraction coupling. Annu Rev Physiol 41:473–484, 1979.
7. Winegrad S: Electromechanical coupling in heart muscle. In: Berne RM, Sperelakis N, Geiger SR (eds) Handbook of physiology. Sect 2: The cardiovascular system Vol 1: The heart. Bethesda MD: American Physiological Society, 1979, pp. 393–428.
8. Katz AM: Congestive heart failure: role of altered myocardial cellular control. N Engl J Med 293:1184–1191, 1975.
9. Sommer JR, Johnson EA: Ultrastructure of cardiac muscle. In: Berne RM, Sperelakis N, Geiger SR (eds) Handbook of physiology. Sect 2: The cardiovascular system. Vol 1: The heart. Bethesda MD: American Physiological Society, 1979, pp. 113–186.
10. Franzini-Armstrong C: Structure of sarcoplasmic reticulum. Fed Proc 39:2403–2409, 1980.
11. Winegrad S: Intracellular calcium movements of frog skeletal muscle during recovery from tetanus. J Gen Physiol 51:65–83, 1968.
12. Somlyo AV, Gonzalez-Serratos H, Shuman H, McClellan G, Somlyo AP: Calcium release and ionic changes in the sarcoplasmic reticulum of tetanized muscle: an electron-probe study. J Cell Biol 90:577–594, 1981.
13. Fanburg B, Gergely J: Studies on adenosine triphosphate-supported calcium accumulation by cardiac subcellular particles. J Biol Chem 240:2721–2728, 1965.
14. Harigaya S, Schwartz A: Rate of calcium binding and uptake in normal animal and failing human cardiac muscle. Circ Res 25:781–794, 1969.
15. Pretorius PJ, Pohl WG, Smithen CS, Inesi G: Structural and functional characterization of dog heart microsomes. Circ Res 25:487–499, 1969.
16. Solaro RJ, Briggs FN: Estimating the functional capabilities of sarcoplasmic reticulum in cardiac muscle: calcium binding. Circ Res 34:531–540, 1974.
17. Levitsky DO, Aliev MK, Kuzmin AV, Levchenko TS, Smirnov VN, Chazov EI: Isolation of calcium pump system and purification of calcium ion-dependent ATPase from heart muscle. Biochim Biophys Acta 443:468–484, 1976.
18. Pang DC, Briggs FN: Reaction mechanism of the cardiac sarcotubule calcium (II) dependent adenosine triphosphatase. Biochemistry 12:4905–4911, 1973.
19. Tada M, Kirchberger MA, Repke DI, Katz AM: The stimulation of calcium transport in cardiac sarcoplasmic reticulum by adenosine 3′:5′-monophosphate-dependent protein kinase. J Biol Chem 249:6174–6180, 1974.
20. Shigekawa M, Finegan JM, Katz AM: Calcium transport ATPase of canine cardiac sarcoplasmic reticulum. J Biol Chem 251:6894–6900, 1976.
21. Jones LR, Besch HR Jr, Fleming JW, McConnaughey MM, Watanabe AM: Separation of vesicles of cardiac sarcolemma from vesicles of cardiac sarcoplasmic reticulum: comparative biochemical analysis of component activities. J Biol Chem 254:530–539, 1979.
22. Carsten ME, Reedy MK: Cardiac sarcoplasmic retiulum: chemical and electron microscope studies of calcium accumulation. J Ultrastruct Res 35:554–574, 1971.
23. Meissner G: Isolation and characterization of two types of sarcoplasmic reticulum vesicles. Biochim Biophys Acta 389:51–68, 1975.
24. Miyamoto H, Racker E: Calcium-induced calcium release at terminal cisternae of skeletal sarcoplasmic reticulum. FEBS Lett 133:235–238, 1981.
25. Campbell KP, Franzini-Armstrong C, Shamoo AE; Further characterization of light and heavy sarcoplasmic reticulum vesicles: identification of the "sarcoplasmic reticulum feet" associated with heavy sarcoplasmic reticulum vesicles. Biochim Biophys Acta 602:97–116, 1980.
26. Jones LR, Cala SE: Biochemical evidence for functional heterogeneity of cardiac sarcoplasmic reticulum vesicles. J Biol Chem 256:11809–11818, 1981.
27. De Foor PH, Levitsky D, Biryukova T, Fleischer S: Immunological dissimilarity of the calcium pump protein of skeletal and cardiac muscle sarcoplasmic reticulum. Arch Biochem Biophys 200:196–205, 1980.
28. Van Winkle WB, Pitts BJR, Entman ML: Rapid purification of canine cardiac sarcoplasmic reticulum Ca^{2+}-ATPase. J Biol Chem 253:8671–8673, 1978.
29. Bidlack JM, Ambudkar IS, Shamoo AE: Purification of phospholamban, a 22,000-dalton protein from cardiac sarcoplasmic reticulum that is specifically phosphorylated by cyclic AMP-dependent protein kinase. J Biol Chem 257:4501–4506, 1982.
30. Tada M, Katz AM: Phosphorylation of the sarcoplasmic reticulum and sarcolemma. Annu Rev Physiol 44:401–423, 1982.
31. MacLennan DH, Holland PC: Calcium transport in sarcoplasmic reticulum. Annu Rev Biophys Bioeng 4:377–404, 1975.
32. Tada M, Yamamoto T, Tonomura Y: Molecular mechanism of active calcium transport by sarcoplasmic reticulum. Physiol Rev 58:1–79, 1978.
33. Meissner G: ATP and Ca^{2+} binding by the Ca^{2+} pump protein of sarcoplasmic reticulum. Biochim Biophys Acta 298:906–926, 1973.
34. Ikemoto N: The calcium binding sites involved in the regulation of the purified adenosine triphospha-

tase of the sarcoplasmic reticulum. J Biol Chem 249:649–651, 1974.
35. Dupont Y: Kinetics and regulation of sarcoplasmic reticulum ATPase. Eur J Biochem 72:185–190, 1977.
36. Møller JV, Andersen JP, Le Maire M: The sarcoplasmic reticulum Ca^{2+}-ATPase. Mol Cell Biochem 42:83–107, 1982.
37. Green NM, Allen G, Hebdon GM: Structural relationship between the calcium- and magnesium-transporting ATPase of sarcoplasmic reticulum and the membrane. Ann NY Acad Sci 358:149–158, 1980.
38. MacLennan DH, Reithmeier RAF, Shoshan V, Campbell KP, Le Bel D, Herrmann TR, Shamoo AE: Ion pathways in proteins of the sarcoplasmic reticulum. Ann NY Acad Sci 358:138–148, 1980.
39. Tong SW: Studies on the structure of the calcium-dependent adenosine triphosphatase from rabbit skeletal muscle sarcoplasmic reticulum. Arch Biochem Biophys 203:780–791, 1980.
40. Reithmeier RAF, MacLennan DH: The NH_2 terminus of the (Ca^{2+} + Mg^{2+})-adenosine triphosphatase is located on the cytoplasmic surface of the sarcoplasmic reticulum membrane. J Biol Chem 256:5957–5960, 1981.
41. Pick U, Racker E: Inhibition of the (Ca^{2+}) ATPase from sarcoplasmic reticulum by dicyclohexycarbodiimide: evidence for location of the Ca^{2+} binding site in a hydrophobic region. Biochemistry 18:108–113, 1979.
42. Racker E, Eytan E: A coupling factor from sarcoplasmic reticulum required for the translocation of Ca^{2+} ions in a reconstituted Ca^{2+} ATPase pump. J Biol Chem 250:7533–7534, 1975.
43. Michalak M, Campbell KP, MacLennan DH: Localization of the high affinity calcium binding protein and an intrinsic glycoprotein in sarcoplasmic reticulum membranes. J Biol Chem 255:1317–1326, 1980.
44. Campbell KP, MacLennan DH: Purification and characterization of the 53,000-dalton glycoprotein from the sarcoplasmic reticulum. J Biol Chem 256:4626–4632, 1981.
45. Martonosi A: Biochemical and clinical aspects of sarcoplasmic reticulum function. Curr Top Membr Transp 3:83–197, 1972.
46. Inesi G: Transport across sarcoplasmic reticulum in skeletal and cardiac muscle. In: Giebish G, Tosteson DC, Ussing HH (eds) Membrane transport in biology. Berlin: Springer, 1979, pp 357–393.
47. Martonosi A: The structure and function of sarcoplasmic reticulum membranes. In: Mason LA (ed) Biomembranes, vol 1. New York: Plenum, 1971, pp 191–256.
48. Ikemoto N: Structure and function of the calcium pump protein of sarcoplasmic reticulum. Annu Rev Physiol 44:297–317, 1982.
49. Besch HR, Schwartz A: Initial calcium binding rates of canine cardiac relaxing system (sarcoplasmic reticulum fragments) determined by stopped-flow spectrophotometry. Biochem Biophys Res Commun 45:286–292, 1971.
50. Repke DI, Katz AM: Calcium-binding and calcium-uptake by cardiac microsomes: a kinetic analysis. J Mol Cell Cardiol 4:401–416, 1972.
51. Kitazawa T: Physiological significance of Ca uptake by mitochondria in the heart in comparison with that by cardiac sarcoplasmic reticulum. J Biochem 80:1129–1147, 1976.
52. Entman ML, Gillette PC, Wallick ET, Pressman BC, Schwartz A: A study of calcium binding and uptake by isolated cardiac sarcoplasmic reticulum: the use of a new ionophore (X537A). Biochem Biophys Res Commun 48:847–853, 1972.
53. Katz AM, Repke DI, Fudyma G, Shigekawa M: Control of calcium efflux from sarcoplasmic reticulum vesicles by external calcium. J Biol Chem 252:4210–4214, 1977.
54. Hasselbach W: Relaxing factor and the relaxation of muscle. Prog Biophys Mol Biol 14:167–222, 1964.
55. Weber A: Regulatory mechanisms of the calcium transport system of fragmented rabbit sarcoplasmic reticulum. I. The effect of accumulated calcium on transport and adenosine triphosphate hydrolysis. J Gen Physiol 57:50–70, 1971.
56. Suko J: The calcium pump of cardiac sarcoplasmic reticulum: functional alterations at different levels of thyroid state in rabbits. J Physiol 228:563–582, 1973.
57. Will H, Blanck J, Smettan G, Wollenberger A: A quench-flow kinetic investigation of calcium ion accumulation by isolated cardiac sarcoplasmic reticulum: dependence of initial velocity on free calcium ion concentration and influence of preincubation with a protein kinase, MgATP, and cyclic AMP. Biochim Biophys Acta 449:295–303, 1976.
58. Tada M, Ohmori F, Yamada M, Abe H: Mechanism of the stimulation of Ca^{2+}-dependent ATPase of cardiac sarcoplasmic reticulum by adenosine 3′:5′-monophosphate-dependent protein kinase: role of the 22,000-dalton protein. J Biol Chem 254:319–326, 1979.
59. Chiesi M, Inesi G: Andenosine 5′-triphosphate dependent fluxes of manganese and hydrogen ions in sarcoplasmic reticulum vesicles. Biochemistry 19:2912–2918, 1980.
60. Van Winkle WB, Tate CA, Bick RJ, Entman ML: Nucleotide triphosphate utilization by cardiac and skeletal muscle sarcoplasmic reticulum: evidence for a hydrolysis cycle not coupled to intermediate acyl phosphate formation and calcium translocation. J Biol Chem 256:2268–2274, 1981.
61. Shigekawa M, Akowitz AA, Katz AM: Stimulation of adenosine triphosphatase activity of sarcoplasmic reticulum by adenylyl methylene diphosphate. Biochim Biophys Acta 526:591–596, 1978.

62. Hasselbach W: The reversibility of the sarcoplasmic calcium pump. Biochim Biopnys Acta 515:23–53, 1978.
63. Trumble WR, Sutko JL, Reeves JP: ATP-dependent calcium transport in cardiac sarcolemmal membrane vesicles. Life Sci 27:207–214, 1980.
64. Ueno T, Sekine T: Study on calcium transport by sarcoplasmic reticulum vesicles using fluorescence probes. J Biochem 84:787–794, 1978.
65. Shigekawa M, Pearl LJ: Activation of calcium transport in skeletal muscle sarcoplasmic reticulum by monovalent cations. J Biol Chem 251:6947–6952, 1976.
66. Jones LR, Besch HR Jr, Watanabe AM: Monovalent cation stimulation of Ca^{2+} uptake by cardiac membrane vesicles: correlation with stimulation of Ca^{2+}-ATPase activity. J Biol Chem 252:3315–3323, 1977.
67. Duggan PF: Calcium uptake and associated adenosine triphosphatase activity in fragmented sarcoplasmic reticulum: requirement for potassium ions. J Biol Chem 252:1620–1627, 1977.
68. Tate CA, Van Winkle WB, Entman ML: Time-dependent resistance to alkaline pH of oxalate-supported calcium uptake by sarcoplasmic reticulum. Life Sci 27:1453–1464, 1980.
69. Meissner G: Calcium transport and monovalent cation and proton fluxes in sarcoplasmic reticulum vesicles. J Biol Chem 256:636–643, 1981.
70. Zimniak P, Racker E: Electrogenicity of Ca^{2+} transport catalyzed by the Ca^{2+}-ATPase from sarcoplasmic reticulum. J Biol Chem 253:4631–4637, 1978.
71. Ueno T, Sekine T: A role of H^+ flux in active Ca^{2+} transport into sarcoplasmic reticulum vesicles. I. Effect of an artificially imposed H^+ gradient on Ca^{2+} uptake. J Biochem 89:1239–1246, 1981.
72. Madeira VMC: Proton movements across the membranes of sarcoplasmic reticulum during the uptake of calcium ions. Arch Biochem Biophys 200:319–325, 1980.
73. Meissner G, McKinley D: Permeability of sarcoplasmic reticulum membrane: the effect of changed ionic environments on Ca^{2+} release. J Membr Biol 30:79–98, 1976.
74. Meissner G, Young RC: Proton permeability of sarcoplasmic reticulum vesicles. J Biol Chem 255: 6814–6819, 1980.
75. McKinley D, Meissner G: Evidence for a K^+, Na^+ permeable channel in sarcoplasmic reticulum. J Membr Biol 44:159–186, 1978.
76. Miller C: Voltage-gated cation conductance channel from fragmented sarcoplasmic reticulum: steady-state electrical properties. J Membr Biol 40:1–23, 1978.
77. Kasai M, Kometani T: Inhibition of anion permeability of sarcoplasmic reticulum vesicles by 4-acetoamido-4′-isothiocyano-stilbene-2, 2′-disulfonate. Biochim Biophys Acta 557:243–247, 1979.
78. Racker E: Reconstitution of a calcium pump with phospholipids and a purified Ca^{++}-adenosine triphosphatase from sarcoplasmic reticulum. J Biol Chem 247:8198–8200, 1972.
79. Fanburg BL, Matsushita S: Phosphorylated intermediate of ATPase of isolated cardiac sarcoplasmic reticulum. J Mol Cell Cardiol 5:111–115, 1973.
80. Suko J, Hasselbach W: Characterization of cardiac sarcoplasmic reticulum ATP–ADP phosphate exchange and phosphorylation of the calcium transport adenosine triphosphatase. Eur J Biochem 64:123–130, 1976.
81. Sumida M, Wang T, Mandel F, Froehlich JP, Schwartz A: Transient kinetics of Ca^{2+} transport of sarcoplasmic reticulum: a comparison of cardiac and skeletal muscle. J Biol Chem 253:8772–8777, 1978.
82. Jones LR, Besch HR Jr, Watanabe AM: Regulation of the calcium pump of cardiac sarcoplasmic reticulum: interactive roles of potassium and ATP on the phosphoprotein intermediate of the (K^+, Ca^{2+})-ATPase. J Biol Chem 253:1643–1653, 1978.
83. Degani C, Boyer PD: A borohydride reduction method for characterization of the acyl phosphate linkage in proteins and its application to sarcoplasmic reticulum adenosine triphosphatase. J Biol Chem 248:8222–8226, 1973.
84. Shigekawa M, Dougherty JP: Reaction mechanism of Ca^{2+}-dependent ATP hydrolysis by skeletal muscle sarcoplasmic reticulum in the absence of added alkali metal salts. III. Sequential occurrence of ADP-sensitive and ADP-insensitive phosphoenzymes. J Biol Chem 253:1458–1464, 1978.
85. De Meis L, Vianna AL: Energy interconversion by the Ca^{2+}-dependent ATPase of the sarcoplasmic reticulum. Annu Rev Biochem 48:275–292, 1979.
86. Pick U, Karlish SJD: Regulation of the conformational transition in the Ca-ATPase from sarcoplasmic reticulum by pH, temperature, and calcium ions. J Biol Chem 257:6120–6126, 1982.
87. Pick U: The interaction of vanadate ions with the Ca-ATPase from sarcoplasmic reticulum. J Biol Chem 257:6111–6119, 1982.
88. Dupont Y: Occlusion of divalent cation in the phosphorylated calcium pump of sarcoplasmic reticulum. Eur J Biochem 109:231–238, 1980.
89. Yamada S, Ikemoto N: Reaction mechanism of calcium-ATPase of sarcoplasmic reticulum: substrates for phosphorylation reaction and back reaction, and further resolution of phosphorylated intermediates. J Biol Chem 255:3108–3119, 1980.
90. Tada M, Yamada M, Ohmori F, Kuzuya T, Inui M, Abe H: Transient state kinetic studies of Ca^{2+}-dependent ATPase and calcium transport by cardiac sarcoplasmic reticulum: effect of cyclic AMP-dependent protein kinase-catalyzed phosphorylation of phospholamban. J Biol Chem 255:1985–1992, 1980.
91. Briggs FN, Wise RM, Hearn JA: The effect of lith-

ium and potassium on the transient state kinetics of the (Ca + Mg)-ATPase of cardiac sarcoplasmic reticulum. J Biol Chem 253:5884–5885, 1978.
92. Dupont Y: Fluorescence studies of the sarcoplasmic reticulum calcium pump. Biochem Biophys Res Commun 71:544–550, 1976.
93. Shigekawa M, Wakabayashi S, Nakamura H: Effect of divalent cation bound to the ATPase of sarcoplasmic reticulum: activation of phosphoenzyme hydrolysis by Mg^{2+}. J Biol Chem 258:14157–14161, 1983.
94. Shigekawa M, Dougherty JP: Reaction mechanism of Ca^{2+}-dependent ATP hydrolysis by skeletal muscle sarcoplasmic reticulum in the absence of added alkali metal salts. II. Kinetic properties of the phosphoenzyme formed at the steady state in high Mg^{2+} and low Ca^{2+} concentrations. J Biol Chem 253:1451–1457, 1978.
95. Shigekawa M, Akowitz AA: On the mechanism of Ca^{2+}-dependent adenosine triphosphatase of sarcoplasmic reticulum: occurrence of two types of phosphoenzyme intermediates in the presence of KCl. J Biol Chem 254:4726–4730, 1979.
96. Froehlich JP, Taylor EW: Transient state kinetic studies of sarcoplasmic reticulum adenosine triphosphatase. J Biol Chem 250:2013–2021, 1975.
97. Panet R, Selinger Z: Synthesis of ATP coupled to Ca^{2+} release from sarcoplasmic reticulum vesicles. Biochim Biophys Acta 255:34–42, 1972.
98. Makinose M, Hasselbach W: ATP synthesis by the reverse of the sarcoplasmic calcium pump. FEBS Lett 12:271–272, 1971.
99. Kanazawa T: Phosphorylation of solubilized sarcoplasmic reticulum by orthophosphate and its thermodynamic characteristics. J Biol Chem 250:113–119, 1975.
100. Knowles AF, Racker E: Formation of adenosine triphosphate from P_i and adenosine diphosphate by purified Ca^{2+}-adenosine triphosphatase. J Biol Chem 250:1949–1951, 1975.
101. Sumida M, Wang T, Schwartz A, Younkin C, Froehlich JP: The Ca^{2+}-ATPase partial reactions in cardiac and skeletal sarcoplasmic reticulum: a comparison of transient state kinetic data. J Biol Chem 255:1497–1503, 1980.
102. Shigekawa M, Kanazawa T: Phosphoenzyme formation from ATP in the ATPase of sarcoplasmic reticulum: effect of KCl or ATP and slow dissociation of ATP from precursor enzyme–ATP complex. J Biol Chem 257:7657–7665, 1982.
103. Wray HL, Gray RR, Olsson RA: Cyclic adenosine 3′,5′-monophosphate-stimulated protein kinase and a substrate associated with cardiac sarcoplasmic reticulum. J Biol Chem 248:1496–1498, 1973.
104. Kirchberger MA, Tada M, Katz AM: Adenosine 3′:5′-monophosphate-dependent protein kinase-catalyzed phosphorylation reaction and its relationship to calcium transport in cardiac sarcoplasmic reticulum. J Biol Chem 249:6166–6173, 1974.
105. La Raia PJ, Morkin E: Adenosine 3′,5′-monophosphate-dependent membrane phosphorylation: a possible mechanism for the control of microsomal calcium transport in heart muscle. Circ Res 35:298–306, 1974.
106. Will H, Levchenko TS, Levitsky DO, Smirnov VN, Wollenberger A: Partial characterization of protein kinase-catalyzed phosphorylation of low molecular weight proteins in purified preparations of pigeon heart sarcolemma and sarcoplasmic reticulum. Biochim Biophys Acta 543:175–193, 1978.
107. Tada M, Kirchberger MA, Katz AM: Phosphorylation of a 22,000-dalton component of the cardiac sarcoplasmic reticulum by adenosine 3′:5′-monophosphate-dependent protein kinase. J Biol Chem 250:2640–2647, 1975.
108. Katz AM, Tada M, Kirchberger MA: Control of calcium transport in the myocardium by the cyclic AMP-protein kinase system. Adv Cyclic Nucleotide Res 5:453–472, 1975.
109. Bidlack JM, Shamoo AE: Adenosine 3′,5′-monophosphate-dependent phosphorylation of a 6000 and a 22,000 dalton protein from cardiac sarcoplasmic reticulum. Biochim Biophys Acta 632:310–325, 1980.
110. Le Peuch CJ, Le Peuch DAM, Damaille JG: Phospholamban, activator of the cardiac sarcoplasmic reticulum calcium pump: physicochemical properties and diagonal purification. Biochemistry 19:3368–3373, 1980.
111. Louis CF, Katz AM: Lactoperoxidase-coupled iodination of cardiac sarcoplasmic reticulum proteins. Biochim Biophys Acta 494:255–265, 1977.
112. Le Peuch CJ, Haiech J, Demaille JG: Concerted regulation of cardiac sarcoplasmic reticulum calcium transport by cyclic adenosine monophospate dependent and calcium–calmodulin-dependent phosphorylations. Biochemistry 18:5150–5157, 1979.
113. Kirchberger MA, Antonetz T: Phospholamban: dissociation of the 22,000 molecular weight protein of cardiac sarcoplasmic reticulum into 11,000 and 5,500 molecular weight forms. Biochem Biophys Res Commun 105:152–156, 1982.
114. Tada M, Yamada M, Ohmori F, Kuzuya T, Abe H: Mechanism of cyclic AMP regulation of active calcium transport by cardiac sarcoplasmic reticulum. In: Mukohata Y, Packer L (eds) Cation flux across biomembranes. New York: Academic, 1979, pp 179–190.
115. Kirchberger MA, Tada M: Effects of adenosine 3′:5′-monophosphate-dependent protein kinase on sarcoplasmic reticulum isolated from cardiac and slow and fast contracting skeletal muscles. J Biol Chem 251:725–729, 1976.
116. Kirchberger MA, Chu G: Correlation between protein kinase-mediated stimulation of calcium transport by cardiac sarcoplasmic reticulum and phosphorylation of a 22,000 dalton protein. Biochim Biophys Acta 419:559–562, 1976.
117. Hicks MJ, Shigekawa M, Katz AM: Mechanism by which cyclic adenosine 3′:5′-monophosphate-

dependent protein kinase stimulates calcium transport in cardiac sarcoplasmic reticulum. Circ Res 44:384–391, 1979.
118. Tada M, Kirchberger MA, Li HC: Phosphoprotein phosphatase-catalyzed dephosphorylation of the 22,000 dalton phosphoprotein of cardiac sarcoplasmic reticulum. J Cyclic Nucleotide Res 1:329–338, 1975.
119. Kirchberger MA, Raffo A: Decrease in calcium transport associated with phosphoprotein phosphatase-catalyzed dephosphorylation of cardiac sarcoplasmic reticulum. J Cyclic Nucleotide Res 3:45–53, 1977.
120. Tada M, Ohmori F, Nimura Y, Abe H: Effect of myocardial protein kinase modulator on adenosine 3′:5′-monophosphate-dependent protein kinase-induced stimulation of calcium transport by cardiac sarcoplasmic reticulum. J Biochem (Tokyo) 82:885–892, 1977.
121. Kranias EG, Bilezikjian LM, Potter JD, Piascik MT, Schwartz A: The role of calmodulin in regulation of cardiac sarcoplasmic reticulum phosphorylation. Ann NY Acad Sci 356:279–291, 1980.
122. Tada M, Inui M, Yamada M, Kadoma M, Kuzuya T, Abe H, Kakiuchi S: Effects of phospholamban phosphorylation catalyzed by adenosine 3′:5′-monophosphate- and calmodulin-dependent protein kinases on calcium transport ATPase of cardiac sarcoplasmic reticulum. J Mol Cell Cardiol 15:335–346, 1983.
123. Kirchberger MA, Antonetz T: Calmodulin-mediated regulation of calcium transport and (Ca^{2+} + Mg^{2+})-activated ATPase activity in isolated cardiac sarcoplasmic reticulum. J Biol Chem 257:5685–5691, 1982.
124. Katz S, Remtulla MA: Phosphodiesterase protein activator stimulates calcium transport in cardiac microsomal preparations enriched in sarcoplasmic reticulum. Biochem Biophys Res Commun 83:1373–1379, 1978.
125. Lopaschuk G, Richter B, Katz S: Characterization of calmodulin effects on calcium transport in cardiac microsomes enriched in sarcoplasmic reticulum. Biochemistry 19:5603–5607, 1980.
126. Solaro RJ, Wise RM, Shiner JS, Briggs FN: Calcium requirements for cardiac myofibrillar activation. Circ Res 34:525–530, 1974.
127. Winegrad S: Studies of cardiac muscle with a high permeability to calcium produced by treatment with ethylenediaminetetraacetic acid. J Gen Physiol 58:71–93, 1971.
128. Fabiato A: Myoplasmic free calcium concentration reached during the twitch of an intact isolated cardiac cell and during calcium-induced release of calcium from the sarcoplasmic reticulum of a skinned cardiac cell from the adult rat or rabbit ventricle. J Gen Physiol 78:457–497, 1981.
129. Scarpa A, Williamson JR: Calcium binding and calcium transport by subcellular fractions of heart. In: Drabikowski W, Strzelecka-Gotaszewska H, Carafoli E (eds) Calcium binding proteins. Amsterdam: Elsevier, 1974, pp 547–585.
130. Morad M, Rolett EL: Relaxing effects of catecholamines on mammalian heart. J Physiol (Lond) 224:537–558, 1972.
131. Reuter H: Localization of beta adrenergic receptors, and effects of noradrenaline and cyclic nucleotides on action potentials, ionic currents and tension in mammalian cardiac muscle. J Physiol (Lond) 242:429–451, 1974.
132. Allen DG, Blinks JR: Calcium transients in aequorin-injected frog cardiac muscle. Nature 273:509–513, 1978.
133. Fabiato A, Fabiato F: Relaxing and inotropic effects of cyclic AMP on skinned cardiac cells. Nature 253:556–558, 1975.
134. Tsien RW: Cyclic AMP and contractile activity in heart. Adv Cyclic Nucleotides Res 8:363–420, 1977.
135. Schümann HJ, Endoh M, Brodde OE: The time course of the effects of β- and α-adrenoceptor stimulation by isoprenaline and methoxamine on the contractile force and cAMP level of the isolated rabbit papillary muscle. Naunyn Schmiedebergs Arch Pharmacol 289:291–302, 1975.
136. Ingebretsen WR Jr, Becker E, Friedman WF, Mayer SE: Contractile and biochemical responses of cardiac and skeletal muscle to isoproterenol covalently linked to glass beads. Circ Res 40:474–484, 1977.
137. Venter JC, Ross J Jr, Kaplan NO: Lack of detectable change in cyclic AMP during the cardiac inotropic response to isoproterenol immobilized on glass beads. Proc Natl Acad Sci USA 72:824–828, 1975.
138. Le Peuch CJ, Guilleux JC, Demaille JG: Phospholamban phosphorylation in the perfused rat heart is not solely dependent on β-adrenergic stimulation FEBS Lett 114:165–168, 1980.
139. Limas CJ: Enhanced phosphorylation of myocardial sarcoplasmic reticulum in experimental hyperthyroidism. Am J Physiol 234:H426–431, 1978.
140. Kadoma M, Sacktor B, Froehlich JP: Stimulation by cAMP and protein kinase of calcium transport in sarcoplasmic reticulum from senescent rat myocardium [abstr]. Fed Proc 39:2040, 1980.
141. Campbell KP, McLennan DH, Jorgensen AO, Mintzer MC: Purification and characterization of calsequestrin from canine cardiac sarcoplasmic reticulum and identification of the 53,000 dalton glycoprotein. J Biol Chem 258:1197–1204, 1983.
142. Tada M, Inui M: Regulation of calcium transport by the ATPase-phospholamban system. J Mol Cell Cardiol 15:565–575, 1983.
143. Lindemann JP, Jones LR, Hathaway DR, Henry BG, Watanabe AM: β-adrenergic stimulation of phospholamban phosphorylation and Ca^{2+}-ATPase activity in guinea pig ventricles. J Biol Chem 258:464–471, 1983.

13. CONTRACTILE AND MECHANICAL PROPERTIES OF THE MYOCARDIUM

Allan J. Brady

Introduction

One of the principal concerns of cardiac muscle mechanics is the understanding of the relation between the contractile properties of the whole heart and the myofilaments. In its most superficial sense this relation is one of geometry. Dimensionally, a measure of whole heart performance should be understandable from studies of the mechanical properties of long thin papillary muscles or trabeculae. From such one-dimensional analyses, one could surmise that the three-dimensional complexity of the whole heart could be approximated. Indeed, there have been numerous attempts to formulate ventricular performance in terms of "constitutive" parameters, i.e., in terms of parameters that are independent of external influences, which are based on the mechanical characteristics of papillary muscles. However, these approaches generally prove inadequate where functional differences in organ contractility are of interest. These deficiencies, in the large part, arise from the geometric approximations required to describe the thick-walled asymmetric ventricle and from an inappropriate characterization of the one-dimensional mechanical properties of papillary muscle or trabecular preparations. This chapter primarily discusses the characterization of the functional relations between force and length that may be used as the basis for the formulation of constitutive relations.

Specifically, force–length relations are discussed relating sarcomere length and muscle length to force development. Particular emphasis is given to those parameters which affect force development such as nonuniform sarcomere length, length-dependent activation, restoring forces, and shortening. Also, the status of the force–velocity relation in heart muscle is discussed as it relates to earlier concepts of its use as an index of contractility. Finally, stepwise and cyclic perturbation analysis is mentioned as this approach promises insight into muscle contractile properties of crossbridge kinetics and their relation to known biochemical steps of the cardiac contractile process.

N. Sperelakis (ed.), PHYSIOLOGY AND PATHOPHYSIOLOGY OF THE HEART.

Martinus Nijhoff Publishing, Boston/The Hague/Dordrecht/Lancaster.

Force Development

The sliding filament mechanism of contraction proposed for skeletal muscle by Huxley and Hansen [1] and Huxley and Niedergerke [2] has gained wide acceptance. However, some controversy exists as to whether there is attachment of the myosin crossbridges to actin or only an electrostatic interaction between the myofilaments (discussed in Noble and Pollack [3]). Presumably, the attachment concept, as modified by Huxley and Simmons [4], in general, must apply to heart muscle as well. For example, the kinetics of myofilament interaction of skeletal and cardiac muscle are obviously different, but the myofilament structures are similar, calcium is an essential element in the initiation of contraction, and many of the contractile properties of force generation and of shortening are related. Based on these common factors it is prudent to look for similarities in myofilament interaction processes in these two systems.

Briefly, as summarized in various accounts by Ingels [5], the sliding filament crossbridge

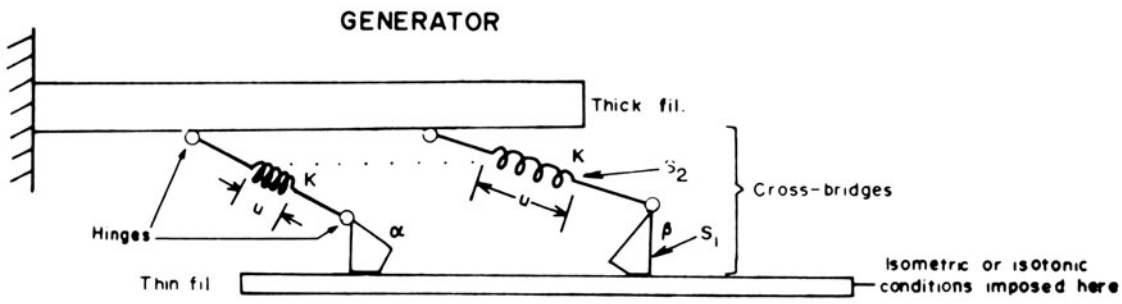

FIGURE 13–1. Sketch of crossbridge (CB) attachment mechanism showing two attached states: (α) before head rotation and (β) after head rotation. S_1 and S_2 denote CB head and extensible connecting element, respectively. K is the elastic constant of S_2 and u is the extension of S_2 from its zero force position. From Julian [7].

attachment concept of force development is the following: Calcium released from the sarcoplasmic reticulum (SR) by sarcolemmal excitation reacts with sites on tropomyosin (summarized in Murray and Weber [6]). A translation then occurs in the relation of tropomyosin to actin in the thin filaments such that a head (or heads) of the myosin thick filament crossbridge (CB) attaches to an actin site (fig. 13–1). This attachment is manifested as an increase in muscle stiffness (resistance to stretch) although not necessarily as an increase in active force development (see Julian [7] for a résumé of the steps of the CB mechanical cycle). Presumably, force development occurs following CB attachment as the head undergoes a rotation about a flexible "joint" between the S-1 and S-2 segments of the crossbridge (fig. 13–1). During the process of this rotation, two events are hypothesized to occur as force is developed and longitudinal translation begins to occur: (a) a spatial sequence of interactions of a CB head with actin sites occurs [4], and (b) the rotation results in an elongation of the S-2 segment of the CB. For the present a highly extensible S-2 segment (composed of a coiled-coil, alpha-helix element) should be considered more hypothetical than real as discussed by Julian [7]. In this manner the CB head rotation and consequent S-2 elongation is presumed to create a translational force between the two sets of filaments.

For the sake of analytic simplicity in some considerations [8] (and as also depicted in fig. 13–1) this rotational event is assumed to be a two-step process for each CB, i.e., attachment and rotation; however, from energetic considerations [9, 10] the rotation needs to be continuous, perhaps with many steps, but is presumably limited to a specific maximum rotational angle.

These concepts of CB attachment and rotation lead to the prediction that total active force and stiffness in a muscle should be directly proportional to the number of attached CB. It must be kept in mind, however, that an attached CB may not be in a force-developing mode (i.e., the CB head may not have rotated to a force-developing position but, if attached to actin, would still contribute to a resistance to stretch or compression). In any case, the current most widely accepted operating hypothesis of muscle force development relates active force development directly to the number of attached crossbridges.

Force–Length Relations

INTERMEDIATE AND LONG SARCOMERE LENGTHS

At the next level of structural organization, i.e., the sarcomere, force development should be directly related to sarcomere length if force development is assumed to be directly related to the number of attached crossbridges. More specifically, force development should be related to the volume of overlap or interfilament surface between the sets of thick and thin filaments. In fully activated fibers this expectation

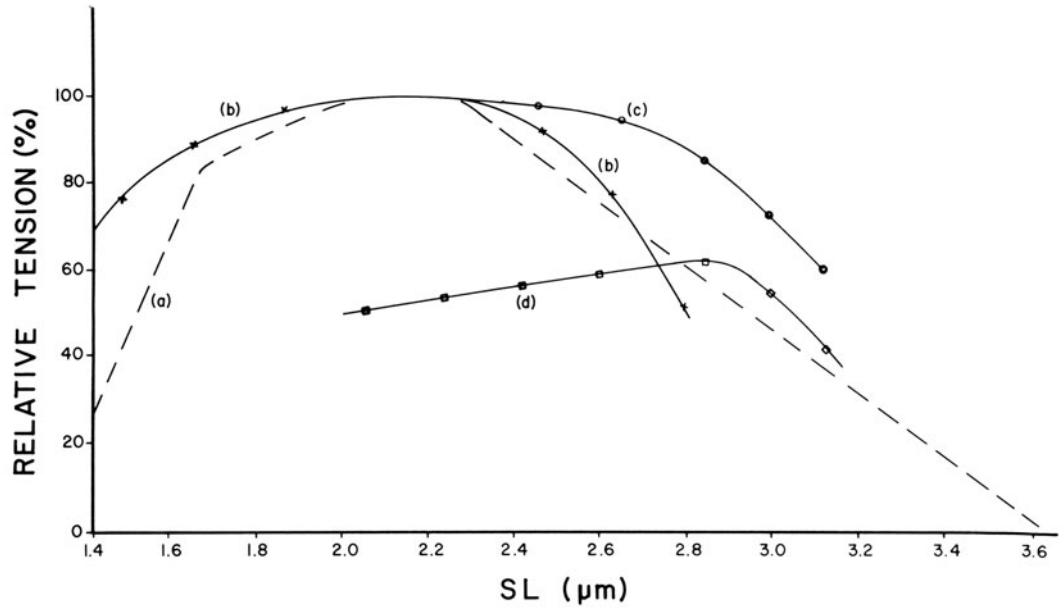

FIGURE 13–2. Tension–sarcomere-length (SL) plots of normalized data from various muscle preparations. *(a)* Skeletal muscle [11]. *(b)* Tonically activated mechanically skinned rat ventricular fiber: data at short SL from Fabiato and Fabiato [105]; data at long SL from Fabiato and Fabiato [13]. (C) Similar data for dog mechanically skinned ventricular fiber. *(d)* Partially activated mechanically skinned rat ventricular fiber. Tensions are relative to peak active tension (P_0) in respective muscle preparations.

appears to be realized (fig. 13–2, dashed curve a) in skeletal muscle [11, 12] over the range of sarcomere lengths (SL) 2.2–3.6 μm and, in cardiac muscle as well [13], to the extent that long sarcomere lengths can be obtained without undue constraints from other structural elements (fig. 13–2, curves b and c). Measurement of active force in intact cardiac fibers is severely limited by the rapid rise in rest tension above SL = 2.2 μm (fig. 13–3, curve h) and no plateau in total tension appears. However, the plateau of active tension can be very broad in tonically activated skinned cardiac fibers (fig. 13–2, curve b).

A simple relation between myofilament overlap and force development is challenged by some investigators [14] who, using laser diffraction to measure SL, found a positive slope for the length–tension relation of "conditioned" skinned rabbit soleus fibers at all sarcomere lengths up to 3.0 μm (similar to curve d). In contrast, Julian and Moss [15], noting sarcomere uniformity by direct photomicrography of skinned frog anterior tibial fibers, found a linear decline in force from SL = 2.2 to 3.6 μm similar to previous studies in intact frog semitendinosus (curve a) [11].

Deviations from a simple relation between overlap and tension in this range of SL are apparent in partially activated cardiac muscle (fig. 13–2, curve d) [13, 16, 17] and in skeletal muscle [14, 18–20]. In these responses, active force development continues to increase with extension of SL up to 3.0 μm before beginning to decline. This observation that peak active force development in partially activated fibers occurs at less than optimum overlap challenges the simplicity of the overlap model and compels us to be concerned about other parameters of CB attachment or force development. Fabiato and Fabiato [13] discuss the possibility that myofilament sensitivity to Ca^{2+} may be increased at longer sarcomere lengths. Some indication of this possibility is found in recent observations in intact skeletal muscle [21] in that maximum Ca^{2+} activation in skeletal muscle does indeed occur on the descending limb of the force–length relation.

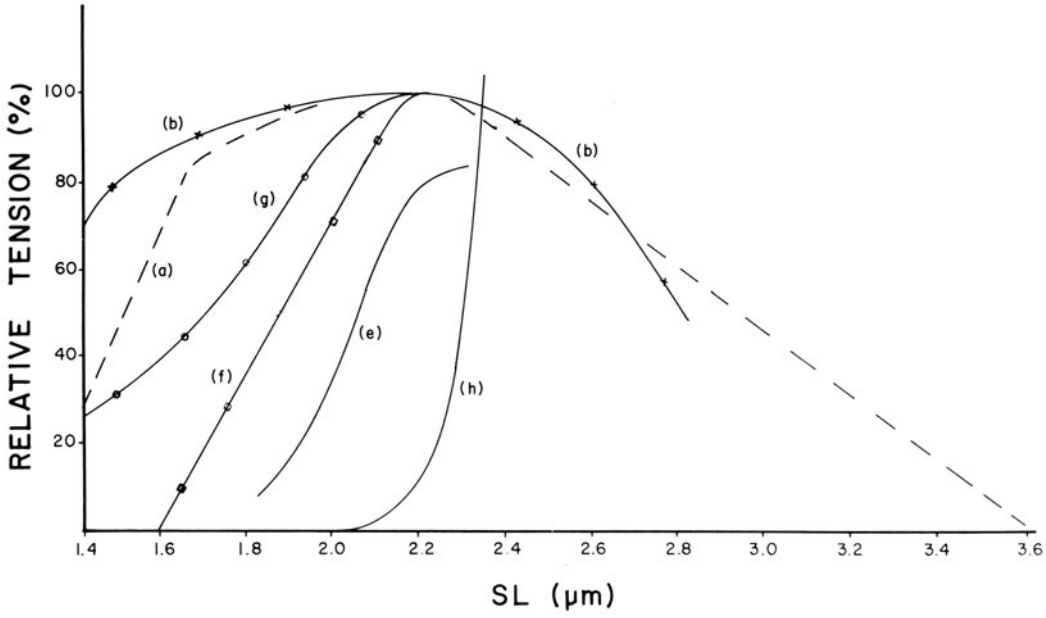

FIGURE 13–3. Tension–SL plots of normalized data from various muscle preparations. *(a)* Skeletal muscle [11]. *(b)* Mechanically skinned rat ventricular fiber, as in figure 13–2. *(e)* Data from thin intact papillary muscle with SL measured at peak of isometric muscle contraction [22]. *(f)* Same reference as *e*, but SL maintained constant by controlled stretch during contraction. *(g)* Phasic contractions of mechanically skinned rat ventricular fiber induced by Ca^{2+}-induced Ca^{2+} release [105]. *(h)* Resting tension data from thin rat papillary muscle [54]. Tensions are relative to peak active tension (P_0) in respective muscle preparations.

In fully activated muscle, including heart muscle (fig. 13–2, curves b and c), a plateau of active force development occurs over the range of sarcomere lengths 1.8–2.2 μm (or −2.4 μm in mechanically skinned skeletal and cardiac fibers [13, 15]). In fact, the force–SL relation in mechanically skinned muscle appears to lie above that of intact fibers at SL > 2.2 μm (fig. 13–2).

Maximum tension (stress) is about 12 N/m^2 (1.2 kg/cm^2) for papillary muscle [22] compared to 30–40 N/m^2 in single skeletal muscle fibers [11]. However, if allowance is made for the lower fractional cross–sectional area of myofilaments in heart muscle [23] the maximal force-generating capabilities of the two types of muscle myofilaments are similar.

FORCE–LENGTH RELATIONS AT SHORT SARCOMERE LENGTHS (FRANK–STARLING RELATION)

A remarkable variation in the force–length relation occurs in heart muscle below SL = 2.2 μm (fig. 13–3), depending on the mode of activation and the amount of shortening that occurs during contraction. Comparison of curve e (force plotted vs initial muscle length in an intact papillary muscle) with f (the same muscle force developed at constant controlled SL) shows the reduction in force development that can occur in a so-called "isometric" contraction (curve e) [22]. Curve g is a plot of the same parameters in a mechanically skinned rat ventricular fiber activated by phasic Ca^{2+}-induced Ca^{2+} release and curve b shows the response of a similar preparation with tonic Ca^{2+} activation. Curve a, as in figure 13–2, gives the force–length relation of a tetanized single skeletal muscle fiber preparation. Comparison of the four curves for rat cardiac muscle emphasizes the fact that the full contractile potential of a fiber far excels the performance seen in an isometric muscle contraction (curve e).

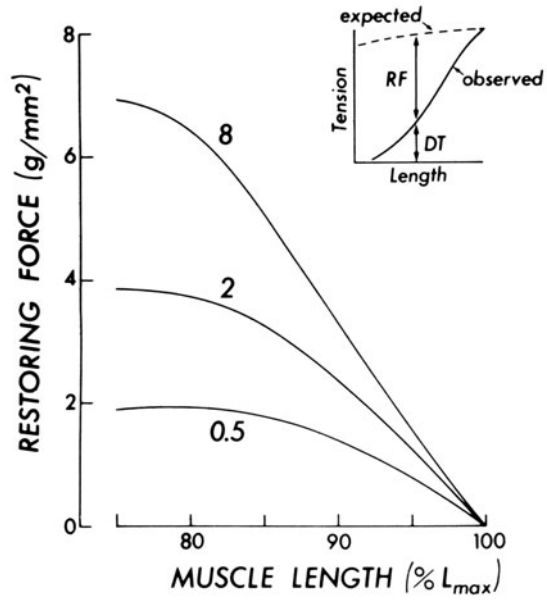

FIGURE 13–4. Plot of restoring force (RF, see inset) necessary to account for the decline in developed tension (DT) at short muscle lengths. Curves show the Ca^{2+} dependence of this restoring force factor. Numbers on curves give $[Ca^{2+}]_0$ in m*M*. From Jewell [27] and by permission of the American Heart Association.

At least three factors are presumed to be responsible for this disparity of force–length relations at sarcomere lengths below 2.0 μm (a) the possible limitation of force development by external and internal elastic structures that are distorted by muscle shortening, (b) shortening deactivation in which active shortening per se tends to reduce the ability of muscle to develop tension [24], and (c) length-dependent activation as exemplified by the reduction in Ca^{2+}-induced Ca^{2+} release at short sarcomere lengths in mechanically skinned single cardiac myocytes in phasic contraction [25].

All three factors would be expected to significantly influence the shape of the ascending limb of the Frank–Starling force–length relation. However, their relative contributions have yet to be quantified. Since, in any case, each factor is likely to play a role in contractile responses of cardiac muscle along the ascending limb, each phenomenon will be discussed in some detail.

Restoring Forces (Extracellular) Actively shortened muscle fibers (even single mechanically skinned fibers) will not remain at short sarcomere lengths (<1.9 μm) during relaxation. Hence some restoring force must exist in the structural network of the muscle or within the cells themselves. In this regard it might be expected that as the muscle fibers increase in diameter with active shortening at constant volume the extracellular structures would offer some elastic resistance and this constraint would limit the amount of force that the fibers could develop in the longitudinal direction. Additionally, compression of the extracellular collagen in the longitudinal direction with fiber shortening might also tend to reduce active force development external to the cells. Also Robinson and Winegrad [26] described a network of microfibrils and microthreads as well as collagen fibrils which link cells of the rat myocardium together. They suggested that this network might influence fiber motion.

However, if contraction against restoring forces were solely responsible for the decline in tension at short sarcomere lengths, then the difference between peak tension at L_{max} and isometric tension at shorter SL should be a measure of the restoring force (assuming that the same number of CB attach between SL = 1.6 and 2.2 μm). Since the restoring force then should be strictly length dependent, the same restoring force–length correction should apply at all sarcomere lengths along the ascending limb of the Frank–Starling curve. Jewell [27] and Bodem et al. [28] tested this hypothesis (fig. 13–4) by noting, in varied external Ca^{2+}, the difference between peak tension at L_{max} and peak tension along the ascending limb. They found that the difference factor (i.e., the restoring force component) must also be Ca^{2+} dependent.

With respect to shortening capabilities in rat papillary muscle and frog atrial cells, a comparison of the minimum sarcomere length to which unloaded multicellular and isolated single-cell preparations can shorten indicates little difference in their minimal sarcomere lengths. For example, rat papillary muscle [22, 29, 30] and mechanically skinned single rat ventricular fibers [25] will contract to a minimum sarco-

mere length of about 1.6 μm in unloaded shortening. In intact frog atrial trabeculae, Winegrad [31] reported a minimum sarcomere length of 1.5–1.6 μm in freely shortening preparations, while Tarr et al. [32] showed shortening to about 1.45 μm in very lightly loaded single atrial fibers. Contrasting the single-fiber and multifiber preparations, these observations would suggest that the limitation to shortening probably lies within the cells rather than in external constraints to diameter change or longitudinal resistance to shortening. Similar conclusions were reached by Parsons and Porter [33], who observed, in cultured chick heart cells, some kinked fibrils at rest which straightened during contraction, indicating that an internal restoring force exists which reestablishes the rest length during relaxation.

In skeletal muscle, Brown et al. [34] and Gonzales-Serratos [35] observed that the myofibrils of contracted fibers imbedded in gelatin became wavy during relaxation but straightened again during activation. Similar responses occurred in skinned cardiac cells [25, 36]. Thus, restoring forces do appear to exist in contracted muscle, but the major component must lie within the cell at short sarcomere lengths.

These conclusions are not surprising when considering the fact that the collagen fiber direction appears to be predominantly parallel to the fiber direction. However, an absence of elastic constraints oriented radially to the muscle fibers indicates that the collagen probably is not rigidly linked in the transverse direction.

Intracellular Restoring Forces. One consideration for a restoring force in intact heart muscle is a compression, during muscle shortening, of the sarcolemma, the SR, or mitochondria. However, this seems unlikely in view of the observation in the above study that relaxation to initial rest length still occurs in skinned preparations after Brij-58 treatment to remove all membrane structures [25].

Fabiato and Fabiato [25] reported that relaxation in highly activated (pCa = 6), mechanically skinned rat ventricular fibers occurred in two phases, i.e., a fast component of relaxation from SL = 1.1 to 1.57 μm occurring in about 0.6 s and a slow component of further relaxation to 1.91 μm occurring in about 43 s. Since there were no external forces on these fibers, the restoring forces must all lie within the skinned fiber.

Fabiato and Fabiato [25] also attempted to measure this restoring force by letting a contracted cell relax against the force transducer. A restoring force of only 4% P_0 was measured; however, this observation may be somewhat inaccurate because it was not clear whether some myofilament buckling occurred in the relaxation process so that the full restoring force was not measured by the transducer.

Krueger et al. [37] considered internal elastic restoring forces as the basis for the spontaneous and rapid relation that occurs in intact cardiac myocyte twitches. However, they concluded that, since the velocity of shortening in highly activated fibers was constant over the range SL = 2.0–1.7 μm, no simple or appreciable elastic restoring force could be responsible for the constant shortening velocity.

In any case the restoring force in these skinned cells seems insufficient to account for the major portion of the slope of the ascending limb of the Frank–Starling relation. On the other hand, skinned fibers have a swollen lattice [25] so that a true measure of normal restoring forces probably cannot be made in these preparations. We must wait for a more adequate quantification of the radial and longitudinal forces within heart cells before the magnitude of this component of the Frank–Starling force–length relation can be evaluated.

Shortening Deactivation. One of the proposed factors that may influence the shape of the length–tension relation is the observation that shortening tends to reduce the ability of muscle to develop tension (in skeletal muscle [38–40]; in heart muscle [24, 41–43]). Figure 13–5 shows one of several possible manifestions of the influence of shortening on the ability of a muscle to develop force. In these responses, releases to a light load are given at various times during contraction. These responses show that shortening following early releases reduces the later force generation capacity of the muscle relative to its capability when it remains iso-

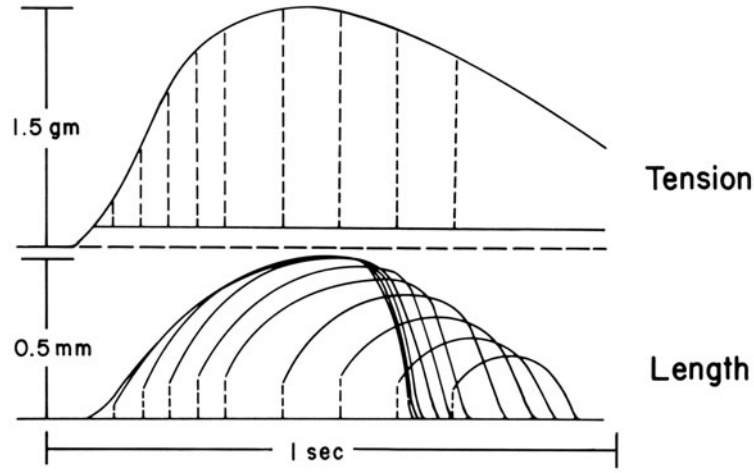

FIGURE 13–5. Tension (upper curves) and length change (lower curves) showing releases of a rabbit papillary muscle to a small load at various times during contraction. Note the reduced ability of the muscle to shorten or bear the load (deactivation) following the releases, i.e., early releases reduce the period of shortening or force-generating capability. Modified from Brady [106].

metric until the later period. This deactivation is apparent immediately upon the onset of shortening since only brief transient shortening intervals (<20 ms) initiate deactivation and the effect can last beyond a given contraction. Shortening deactivation is more prominent the later in a contraction the perturbation occurs. Shortening during the first ¼–⅓ of a twitch has little effect on subsequent tension generation or shortening capacity, but shortening during the relaxing phase of contraction may abruptly terminate the contraction and also reduce the force generation or shortening capacity of a subsequent contraction. Shortening deactivation appears to be a result of shortening per se because the velocity of the shortening does not appear to influence subsequent contractile capability. The magnitude and time of occurrence of shortening during a contraction seem to be the primary factors that influence this negative inotropic effect. Edman [40] reports that in skeletal muscle the deactivation effect has a Q_{10} of around 1 and therefore probably has a basis in the myofilament protein structures.

Shortening deactivation may play a significant role in the determination of the shape of the force–length relation, particularly in heart muscle. Considerable series compliance is evident in most cardiac multicellular preparations and sarcomeric nonuniformity is evident in both multicellular and loaded single-cell preparations. Thus, even during an isometric contraction, some degree of sarcomere shortening (and/or lengthening) probably occurs so that it is likely that sarcomeric shortening which occurs during these "isometric" muscle contractions reduces the peak developed force. Resting sarcomere length in most multicellular preparations (i.e., slack length) is between 1.9 and 2.2 μm. Therefore, the force developed at a mean sarcomere length of, say, 1.6 μm requires extensive sarcomere shortening, and probably deactivation, before the contraction becomes isometric at 1.6 μm. The magnitude of this deactivation is difficult to evaluate because of the above-mentioned factors of internal loading with shortening and length-dependent activation (next section).

Some evidence for the magnitude of shortening deactivation was obtained by Pollack and Krueger [22], who measured force development at short sarcomere lengths using an exponential controlled stretch to compensate for SL shortening (similar to the method proposed by Brady [44]). They found that this method reduces series compliance to 1%–2% (from

about 5%), but that peak tension still fell at reduced SL even with this minimal shortening; hence, they concluded that the ascending limb of the length–tension relation is not primarily due to shortening deactivation.

Again, we do not have good quantitative data to provide a measure of the contribution of shortening deactivation to the slope of the Frank–Starling relation, but shortening deactivation is probably a significant factor.

Length-Dependent Activation. In the operational range for heart muscle, i.e., 1.6–2.2 μm, our concept of the relation between myofilament overlap and active force development is extremely unclear in both cardiac and skeletal muscle. It is readily apparent that in all kinds of preparations (from intact multicellular preparations to length-clamped glycerinated myofibrils) active force development declines at sarcomere lengths below 2.0 μm. In the early proposals of the sliding filament hypothesis [11], and as proposed still by Julian and Moss [15], the fall in developed tension at short sarcomere lengths (1.6–2.0 μm) was related to a resistive elastic interaction between overlapping thin filaments and to a distortion of thick filaments abutting against the Z bands at less than 1.6 μm SL. In this scheme, total CB force would decline very little, but sarcomere force would be reduced by the magnitude of the elastic interaction between thin filament regions of the sarcomere. This interpretation was called into question when it was observed that the deeper sarcomeres of myofibrils in a whole muscle fiber at short SL became wavy during twitch responses and that this waviness disappeared with tetanic stimulation or in the presence of caffeine [45, 46]. These observations suggested that perhaps activation was graded at short SL and that a reduction in CB force development (i.e., a reduction in the number of CB attachments) might be responsible for the decline in active force development at short SL. This interpretation has gained further support both in skeletal muscle [21] and cardiac muscle preparations by the observation that less Ca^{2+} is released from the SR at short sarcomere lengths [25].

In further support of the length-dependent activation concept, Hibbard and Jewell [47] found that the pCa–tension curve in chemically skinned rat trabeculae was shifted to the right by 0.2 pCa units at sarcomere length 1.9–2.04 μm compared to the range 2.3–2.5 μm. Also in skinned cardiac cells Fabiato [48] found an increasing relation between Ca^{2+}-induced Ca^{2+} release (determined with arsenaza III) and SL over the range of 1.8–2.3 μm SL. These two observations suggest both a reduction in released Ca^{2+} and a reduction in Ca^{2+} sensitivity at short sarcomere lengths.

However, the picture is not yet clear. Moss [49] found a similar shape of the ascending limb in unskinned (tetanized) and skinned skeletal muscle fibers in fixed Ca^{2+} concentrations and concluded that length-dependent variation in activator Ca^{2+} did not play a major role in determining the shape of the ascending limb. In support of this interpretation, he cites the observation of Blinks et al. [17] that peak light responses of aequorin declined only gradually with sarcomere length from SL = 2.4 to 1.4 μm. But Lopez et al. [21] indicate that Ca^{2+}-induced activation (measured by aequorin fluorescence) in skeletal muscle is in fact decreased at short lengths and reaches its maximum on the descending limb of the length–tension relation (SL = 3.0–3.2 μm).

Perhaps the most novel concept suggesting a basis for an apparent dependence of force development on length comes from the recent report by Allen and Kurihara [50], who showed a reduced duration of aequorin fluorescence in twitches at increasing length (80%–100% L_{max}) in mammalian myocardium. These observations led them to the proposal that Ca^{2+} binding to troponin is increased with increasing force development. They point out that a force-dependent increase in the binding constant of troponin for Ca^{2+} predicts a steepening relation between pCa and tension [51] and also accounts for the shift in pCa–tension relation noted by Hibbard and Jewell [47]. This mechanism offers an alternative to the concept of a length dependence of Ca^{2+}-induced Ca^{2+} release [25] which does not well explain either the relative constancy of the peak aequorin sig-

nal with muscle length noted by Allen and Kurihara [50] in the above report or the shallow slope of the tension–length relation in tonically activated skinned heart cells (curve b, fig. 13–3). An increase in Ca^{2+} release from SR has also been questioned by Chuck and Parmley [52] as a basis for the slow caffeine-reversible increase in tension following a length change in cat papillary muscle.

Obviously, the data are controversial and, furthermore, a detailed mechanism for the length dependence of activation has not been substantiated so that we have little direct insight into the details of this phenomenon. At this point we can only recognize that a length dependence of activation of contraction must be a consideration in any evaluation of cardiac performance.

RELATION BETWEEN SARCOMERIC AND MUSCLE FORCE–LENGTH RELATIONS

As an example of the problem of relating muscle length to sarcomere length, consider the following data. Julian and Sollins [53] measured sarcomere lengths in thin rat papillary muscles by direct photomicrography of the sarcomeres. Resting sarcomere length averaged 2.23 μm at L_{max}. Although the muscle was restrained at L_{max}, sarcomere shortening occurred in the body of the muscle to a mean length of 1.98 μm (i.e., about 11%) during "isometric" contraction. At 0.75 L_{max}, 3%–6% sarcomere shortening occurred with isometric muscle contraction. At some points between these two muscle lengths, sarcomere shortening up to 15% was noted at constant muscle length. Similar results were obtained by Pollack and Huntsman [54], who found that about 40% of this length change could be attributed to end compliance, but the rest occurred as nonuniformity within the body of the muscle.

Thus it is evident that an isometric "muscle" contraction cannot be assumed to occur at constant sarcomere length or constant myofilament overlap. Furthermore, whether we attempt to deduce myofilament interactions from measurements in multifiber preparations or whether we try to predict papillary muscle or whole heart function from myofilament properties, we must contend with the complex structural organization and variability of this tissue.

Sarcomeric and Segmental Nonuniformity. Since nearly all force measurements in heart muscle have been made in multicellular preparations, it has generally been presumed that muscle length was synonymous with sarcomere length. Only in the last few years have investigators become concerned with the now established observation that, particularly in heart muscle, sarcomere lengths can vary considerably from segment to segment and even from cell to cell within the preparations. Thus, measured force–length relations in these preparations give only force–mean-sarcomere-length relations and cannot be interpreted in terms of myofilament overlap directly. The degree to which sarcomere nonuniformity exists in heart muscle has been documented in several recent studies [53–58]. In these studies, sarcomere uniformity existed only in segments of varied length. A compliance of as much as 7% occurred in the end regions of these preparations, but significant nonuniformity also existed within the body of the muscle.

Several techniques have been recently introduced to reduce the nonuniformity problem so that a relation between contractile force and myofilament overlap could be determined. As a measure of segment length, Pollack and Krueger [22] used the first-order laser diffraction line generated by the sarcomeres in a selected uniformly responding segment of a thin papillary muscle of the rat. This diffraction line served as the sensing element for segment control in a servo system. Donald et al. [59] inserted transverse pins through a papillary muscle and used the image of these pins projected onto a light-sensing device (CCD) to control segment length. Brady [44] attempted to determine the series elastic component of papillary muscles (including end compliance) by quick-stretch techniques and then use the force–extension relation of this SE to control a linear motor device attached to the muscle. All these approaches led to a large reduction in SE (to about 1.5%–2.0%) and to a broader plateau of the active force–length relation. While

these studies offered better control of sarcomere length during force–length evaluations, however, they did not overcome the problem that sarcomeres must actively shorten (and therefore deactivate to some extent) in order to measure contractile force at short sarcomere lengths. Thus these techniques do not provide the clear–cut approach we need to resolve the basis of the ascending limb of the Frank–Starling force–length relation.

On the other hand, sarcomere lengths in unrestrained single isolated cardiac cells display a remarkable uniformity even during contraction [25, 37, 60–62]. These latter observations indicate that either the collagen matrix within which the cells exist in multicellular preparations or the application of mechanical constraints (i.e., ties, clamps), or both, leads to a nonuniform distribution of stress during contraction. Actually, Pinto and Win [55] report a high degree of nonuniformity in sarcomere lengths in resting papillary muscle as well. Therefore, it appears that the extracellular structures of cardiac muscle may impose a nonuniformity on both the active and passive muscle.

Viscoelastic Properties of Heart Muscle

The interpretation of the contractile properties of heart muscle, including its many inotropic states, requires an appreciation of the viscoelastic character of both resting and active muscle. Resting muscle length presages the subsequent contractile response, but resting length in multicellular and whole heart preparations is determined by both internal and external viscoelastic properties.

The passive time- and velocity-dependent stress components of heart muscle responses are complex and play a significant role in the determination of sarcomere length and in the manifestation of muscle force. The more dramatic viscoelastic component of active muscle is stress relaxation, which is multiexponential in its decay. However, it is most pertinent to rapid-perturbation studies and will be discussed in that section. In resting muscle, stress relaxation is less dramatic since the forces involved are usually of lower magnitude; however, it is present and usually displays different decay factors than that of active muscle. Creep is another long-term phenomenon that must be dealt with when sarcomere length over an extended time period is of interest. These phenomena have been quantified in various preparations [63], but we have little information regarding their structural or molecular basis. Consequently, we can do little more than describe their appearance and discuss how they relate to contractile responses. In the case of viscoelasticity and creep of passive heart muscle, this will be mentioned in the section on *Resting tension.*

MECHANICAL ANALOGUES

When considering the relation between passive resting tension and active force development it is not clear that resting tension can be simply subtracted from total tension in order to obtain active tension. Such an operation presumes that these two forces are arranged in parallel. In general we do not know that this is the case. Indeed, if compliance at the ends of the muscle preparation is appreciable, as is apparent in the work of Pollack and Huntsman [54] and Julian and Sollins [53] above, the simple additive relation of resting and active tension is invalid because passive parallel elastic elements in the body of the muscle will be unloaded during active contraction while their counterparts at the ends of the muscle become more loaded. For a meaningful measurement of active force, the mechanical relation between these two passive components must be known. Similarly, since it is well established that active force development is highly dependent upon sarcomere length over much of the operating length of the sarcomeres, sarcomere length must be known in order to establish the relation between active force and sarcomere length. With the presence of end compliance and with the possibility of nonuniformity of stress distribution in the muscle during contraction, however, sarcomere length variations within the preparation are likely to occur. Additionally, as mentioned above, there is evidence that shortening or extension of a sarcomere during active contraction alters its subsequent contractility. All these factors will influence the transform

(or constitutive relation) which we must develop in order to relate myofilament mechanics to, say, papillary muscle behavior or whole heart performance.

A good deal of information has been obtained in the past two decades in regard to these problems. While we cannot say that the ideal and unique transform has been derived for heart muscle, many previous simplifying assumptions in model analysis are now invalidated and the types of experiments that must be done are more clearly defined.

In recent years a large number of mechanical analogues have been evaluated in an attempt to define a unique analytic relation which would make possible an interpretation of myofilament force and length interactions in terms of mechanical parameters measurable at the ends of the muscle. These models generally have tended to ignore viscous properties and have mostly dealt with undamped elastic responses of the preparation. To this extent these models only relate to instantaneous elastic properties of the muscle. Some more complex models include dampers, but the inclusion of these additional elements results in a model with so many parameters that unique characterization of a preparation is beyond experimental verification. While muscle viscosity cannot be ignored, there is little advantage in phenomenologic attempts to model it until the structures with which it is associated can be identified. In any case the following models are based on rapid-perturbation data (quick stretch and releases) and do not include viscous components.

The models in question include first a discussion of the classic three-element model of A.V. Hill [64] (i.e., the so-called Maxwell model) in which resting tension was assumed to be attributable to passive elastic elements (PE) that solely bore rest tension and thus determined initial sarcomere length. Additional passive elastic elements (SE) that became evident in an active muscle were presumed to be in series with the force-generating elements of the muscle. This series elastic component was most vividly demonstrated by releasing an active muscle to zero load during a contraction [65]. In multicellular heart preparations, SE compliance thus defined is of the order of 5% L_0 [22, 66]. PE varies widely with species from a relatively small stiffness at sarcomere lengths of 3.0–3.6 μm in frog heart [13] to an exceedingly stiff PE in rat ventricle such that rest tension at SL = 2.8 μm can be as large as active tension [13].

The Hill model has been very popular because resting tension–length relations could be algebraically subtracted from total length–tension relations in order to calculate active tension. However, it is obvious that this simple analogue has serious limitations particularly in preparations in which considerable compliance exists at the ends of or in the attachments to the muscle.

Recognition of this end compliance suggests an alternate three-element model, i.e., the so-called Voigt arrangement in which the series elasticity (SE) bears both resting and active contractile force. The interpretation of myofilament force–length relations in terms of this analogue gives different characteristics for myofilament interactions than the Maxwell arrangement if short-term myofilament interaction is assumed to be stiff, i.e., if the contractile element is assumed to be rigid to short, fast perturbations [44, 67, 68]. Fung [69] did not accept this assumption and claimed that the two models were indistinguishable. However, neither of these two analogues includes the additional elastic component of the crossbridges.

Brady et al. [70] considered a large number of mechanical analogues and attempted to describe a unique arrangement of elastic elements, including parallel, series, and CB elasticity, which would be applicable to a given cardiac preparation. He used the stiffness–force relation at varied initial muscle lengths to describe elastic responses of rabbit papillary muscle (see also Fung [71]). Perturbations of 1- to 2-ms duration were employed in order to obtain some limited measure of CB elasticity as well as to characterize passive elasticity of the muscle. In some preparations a three-elastic-element lumped parameter model appeared to be adequate to fully describe the elastic properties of papillary muscle over the functional range of muscle lengths (0.75–1.05 L_{max}). However, it was recognized that considerable segmental inhomogeneity existed in these prep-

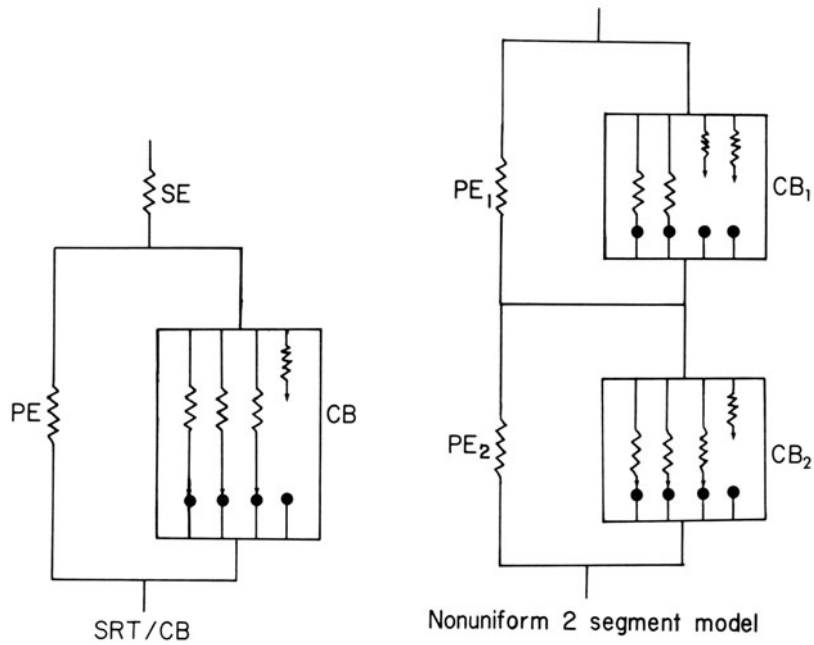

FIGURE 13–6. Lumped three-element mechanical analogue *(left)* and two-segment four-element distributed analogue *(right)* of papillary muscle: PE, parallel elastic element; SE, series elastic element; CB, crossbridge elastic and force-generating element; numerical subscripts on distributed analogue denote the two populations which may have different characteristics. Modified from Brady et al. [70].

arations as indicated by the movement of opaque microspheres placed in the vasculature of the papillary muscle prior to excision of the muscle.

Furthermore, consideration of these stiffness–force data as a two-segment distributed system made up of two populations of sarcomeres with different stiffness–force characteristics (right diagram, fig. 13–6) led to an analogue analytically indistinguishable from the lumped three-element system (SRT/CB model, fig. 13–6). In other words, the elastic constants for the PE, SE, and crossbridges for either model (lumped or distributed parameters) could be derived from the stiffness–force data. Thus, without an independent measurement of segmental motion during contraction, it was impossible to determine which analogue applied to a given preparation. It is clear then that this ambiguity makes it impossible to interpret myofilament interactions from measurements of whole muscle preparations where sarcomere nonuniformity is present.

RESTING TENSION

Extracellular Origins. Since the collagen matrix in which heart cells are imbedded form a three-dimensional system around the cells, these elastic structures may contribute to resting tension by resisting longitudinal extension of the muscle fibers. As with restoring forces that may occur with muscle shortening, other candidates for elements bearing resting tension with muscle extension are the membrane structures (sarcolemma, SR, mitochondria) and intermediate filaments. The availability of single intact myocytes of several species and procedures for partial extraction of cellular components makes possible a comparison of length–tension relations in single, multicellular, and partially extracted preparations of the same species. These components are discussed below.

The contribution of extracellular elastic structures to muscle force has received considerable attention in the past two decades. Cardiac muscle exhibits substantial rest tension at much shorter lengths than skeletal muscle so

that the meshwork of collagen around the cells is a prime candidate for the higher rest tension. For example, Winegrad [31] concluded that connective tissue must limit the extension of frog atrial trabeculae because locally contracting cells could stretch the sarcomeres of quiescent cells which were in series with the active cells more effectively than did a simple extension of the whole trabecular preparation. Adjacent cells were not influenced by these local contractions.

The contribution of extracellular structures to rest tension at long sarcomere lengths was more clearly shown in this preparation by Tarr et al. [72], who found that resting stress in the range of SL = 2.35–3.45 μm was 8- to 30-fold greater in intact frog atrial trabeculae than in the same isolated single cells.

However, several studies show that, in the operating range of heart muscle, extracellular structures may not be the major components of resting tension. A particularly definitive study was conducted by Grimm and Whitehorn [73] which showed that the extraction of the myofilaments of a rat papillary muscle with high salt (0.6 *M* KCl) destroyed the high rest tension of this muscle while the collagen and other cellular structures were left intact. On the other hand, enzymatic disruption of the cellular integrity (presumably the intercalated discs) reduced both active and passive rest tension, again suggesting that some structure within the cells, as well as cell-to-cell contact, was responsible for rest tension.

Cellular Components of Resting Tension. As indicated above, cellular components that might be sources of resting tension are the sarcolemma, intracellular membrane structures, and intermediate filaments [74]. However, studies in mechanically skinned skeletal muscle by Natori [75] and Podolsky [76] all show that the sarcolemma does not contribute to rest tension until SL = 3 μm.

On the other hand, there is evidence in mammalian heart tissue that some detergent-soluble structures may be involved, at least to a limited extent, in the development of resting tension. For example, Fabiato and Fabiato [13] found that mechanically skinned dog ventricular fibers had a high resting tension until detergent treatment, whereupon they exhibited a resting tension less than one-quarter P_0 at SL = 3 μm (fig. 13–7, curve j). In contrast, skinned frog ventricular cells had a low resting tension (10% P_0 at SL = 3.0 μm) which was not significantly affected by the detergent Brij [58] and these fibers could be extended to SL = 8 μm. However, they also noted that these ventricular cells had a higher resting tension than similarly prepared frog semitendinosus fibers.

In mechanically skinned rat ventricular fibers [13], detergent treatment reduced resting tension in the range of sarcomere lengths 2.1–2.4 μm, but not beyond (fig. 13–7, curve i). Only treatment of the preparation with elastase reduced resting tension at the longer sarcomere lengths. This treatment also tended to disrupt lateral connections between myofibrils.

Collectively, these findings indicate that the structural source of resting tension in heart muscle at SL below 3 μm probably is not related to extracellular collagen, but must be a property of the muscle fibers themselves. In the range of SL = 2.0–2.4 μm, the sarcolemma or other detergent-soluble structures probably bear a substantial portion of resting tension (depending on species), but in preparations such as the rat ventricle other intracellular elastic structures must bear a major portion of the rest tension.

Other candidates for rest tension are the longitudinal distributions of intermediate filaments of heart cells (Lazarides, personal communication). The mechanical properties of these elements are not established yet, but preliminary studies indicate that little stiffness remains in the observable residue of single rat heart myocytes after detergent (0.5% Triton X-100) and high-salt (0.6 *M* KI) treatment (Brady, unpublished observations). These results and those of Grimm and Whitehorn [73] already cited indicate that the thin myofilaments must be intact in order for heart cells to bear resting tension.

VISCOSITY AND CREEP

It has long been appreciated that muscle, particularly cardiac muscle, undergoes a continuous increase in length when subjected to a constant load. This phenomenon has been de-

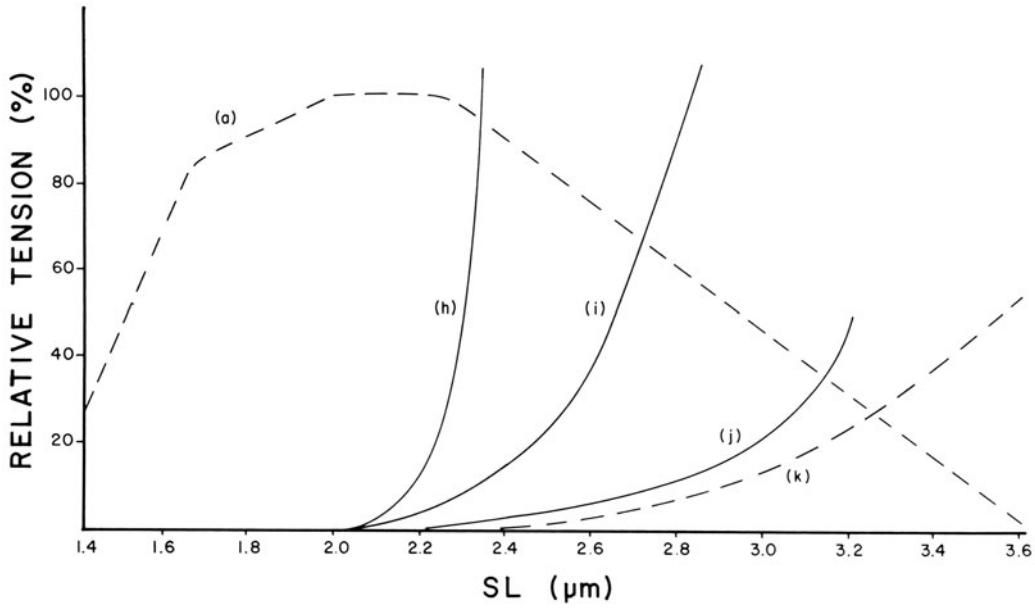

FIGURE 13–7. Tension–SL plots similar to figures 13–2 and 13–3. *(a)* Data from skeletal muscle [11]. *(h)* Resting tension data from thin rat papillary muscle [54]. *(i)* Resting tension data from mechanically skinned rat ventricular fiber [13]. *(j)* Resting tension data from mechanically skinned dog ventricular fiber [13]. *(k)* Resting tension data from chemically or mechanically skinned frog anterior tibial muscle [15]. Tensions are relative to peak active tension (P_0) in respective muscle preparations.

scribed as creep and is characteristic of many long-chain highly cross-linked substances. In papillary muscle, creep has been characterized phenomenologically by Pinto and Patitucci [77]. They showed that at a load corresponding to the peak stress–strain ratio (0.2–1.0 g/mm^2, depending on species) an extension of 2%–3% occurred (logarithmically in time) over a 100-s period. Large initial extensions (>15%) resulted in less creep in this interval. Creep was not strongly dependent on temperature.

A most critical observation in these studies was that in conditioned preparations (i.e., following cyclic perturbations for a given period of time) creep deformation was symmetrically reversible in time. The initial creep rate was about 1%/s following an applied stress equal to the peak stress–strain ratio. Based on these observations we would expect creep extensions of less than 1% during the normal cardiac cycle (60 beats/min). Also, since creep is symmetrically reversible, in the normal heart cycle, creep occurring during systole should be reversed during diastole. Only with sustained changes in diastolic tension (or pressure) would the creep phenomenon affect successive contractions differently.

In this study [77], some attention was given to the tied ends of the preparation, but no consistent relation between creep and end effects was noted. They concluded that the creep effect was not specifically related to the end regions although the distribution of the creep deformation between the ends and the body of the muscle was not clear in their study. However, the relative creep rate in a 14-mm cat ventricular strip was almost identical to that in a 4-mm cat papillary muscle so that these creep rate values are probably indicative of the changes in mean sarcomere length under these loading conditions. In the worst case, it appears that changes in force development, expected from SL changes of 1%, should be anticipated during short-term changes in resting tension. Long-term changes (>100 s) may correspond to SL changes of 2%–3%.

Force–Velocity–Length Relations

In cardiac muscle the interest in the force–velocity (P-V) relation has been twofold. First, there is the common interest with skeletal muscle that P-V relation might provide a relation between the mechanical and energetic relations of the contracting muscle. Second, the fact that heart muscle functions on the ascending limb of the force–length relation makes difficult the separation of inotropic contractile changes from length-dependent changes. Previous work with mammalian papillary muscle indicated that shortening velocity reached its maximum early in contraction [78] and also suggested that V_{max} (maximum shortening velocity) might be independent of initial muscle length so that this factor may serve as an index of contractility which related only to changes in the nongeometric aspects of the muscle [79, 80]. More detailed studies show, however, that problems with the extrapolation of force–velocity curves, the complicated interactions of contractile parameters such as length-dependent force changes, nonlinear elastic elements, shortening inactivation, nonuniformity of sarcomeres, and the time dependence of force generation [22, 24, 81–86], leave serious doubts of the utility of finding such a simple index of contractility in multicellular preparations.

Parmley et al. [86] surveyed a number of possible indices of contractility and found that indices which were sensitive to the contractile state were also sensitive to preload (initial length) while indices that were less preload sensitive were also less reflective of contractile-state changes. In their analysis the maximum rate of isometric tension development (dP/dt) seemed most sensitive to the state of contractility.

Edman and Hwang [87] and Edman [88] introduced a measure of unloaded shortening velocity (V_0) whereby velocity is measured as the length change of a quick release to zero force divided by the time interval to take up the slack of the release. He showed that, in skeletal muscle, V_0 compared favorably with V_{max} in single fibers. Each had a similar Q_{10} (2.67) between 2° and 12°; V_0 was independent of sarcomere length from 1.65 to 2.7 μm and was similar for both twitch and tetanus. Tarr et al. [32] also found shortening velocity in single intact frog atrial fibers to be constant down to SL = 1.6 μm. In contrast, Pollack and Krueger [22] used this technique along with a measurement of sarcomere length with laser diffraction in a servo loop and showed that, in thin rat papillary muscles, P_0 and V_0 varied in parallel with changes in sarcomere length in the range SL = 1.6–2.1 μm, but was constant only between SL = 2.1 and 2.3 μm. In view of the latter observation in heart muscle, the possibility of obtaining a length-independent measure of contractility in terms of shortening velocity seems to be ruled out at the sarcomere level also.

By way of comparison of shortening velocities in intact and isolated cells, Pollack and Krueger [22] measured V_0 at 10 μm/s at 26°C at SL = 2.0 μm. At the next level of structural simplicity, Fabiato and Fabiato [13] calculated a maximum shortening velocity of 20 μm/s in maximally activated, mechanically skinned rat myocytes.

These values compare with an extrapolated V_{max} in cat papillary muscle in the range of 0.5–2.0 muscle lengths/s at comparable temperatures [82, 85, 89]. Obviously, the shortening velocity in isolated cells can be much higher than in the larger multicellular preparations. These comparisons suggest that intercellular interactions considerably impede shortening rate capabilities of the fibers, although the same ultimate sarcomere length may be achieved if force generation is sustained.

Velocity–length relations have been considered in cardiac muscle [78] and show an early maximum shortening rate followed by a constancy in the velocity–length profile of contraction which is independent of initial muscle length and time. These results were interpreted to indicate that during the twitch the effects of shortening, i.e., internal forces, length-dependent activation, and shortening inactivation, exactly balance the rising activation from Ca^{2+} release. While this balance of interactions seems rather fortuitous, it demonstrates the complexity and reinforces the reservations that must be considered in the interpretation of the measured parameters of cardiac contraction.

P-V relations in heart muscle are (a) short-

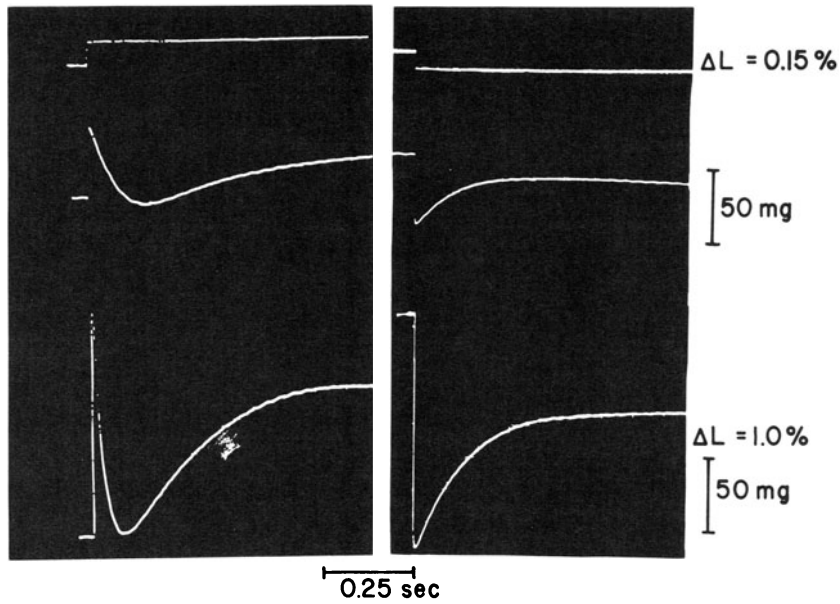

FIGURE 13–8. Delayed tension responses of glycerol-extracted rabbit papillary muscle to quick stretch *(left panel)* and quick release *(right panel). (Upper traces)* Imposed length change (stretch or release). *(Middle traces)* Tension responses following 0.15% length step. *(Lower traces)* Tension responses following 1.0% length step. Active tension (T_0) prior to each step is about 250 mg. From Steiger [91].

ening velocity, because of the many contractile parameters that influence its measurement, cannot serve as a useful index of cardiac contractility independent of length factors, but (b) the high constant velocity of shortening in isolated cardiac cell systems, perhaps only minimally complicated by internal loading, may indicate more directly the shortening kinetics of CB turnover. This shortening rate may reflect the net effect of length-dependent activation and shortening deactivation, but these processes now seem more amenable to experimental control, particularly if force measurements and SL can be simultaneously determined in intact isolated cells.

Perturbation Analysis

As mentioned in the *Introduction,* a primary objective of the study of muscle function is to understand the mechanism whereby metabolic energy is transformed into mechanical work. Considerable advances have been made in muscle physiology at the biochemical level which relate the splitting of ATP to actomyosin interactions. Understandably, the most detailed information on this energy transduction process comes from the most isolated or more completely extracted muscle systems. From these structurally and chemically simplified systems we now have a large number of rate constants of reaction kinetics that pertain to the CB cycle. However, the effect of structural order and mechanical stress in these reaction kinetics is more difficult to obtain.

In an attempt to derive this information from structured and mechanically stressed muscle preparations, a number of laboratories have introduced perturbation techniques (both stepwise and sinusoidal) to analyze the force or length response of intact muscle preparations to changes in applied strain or stress. The rationale for this approach in terms of stepwise perturbations is that, when an actively contracting muscle in a steadstate of activation is subjected to an abrupt change in stress or strain, the time course of the subsequent response should reveal kinetic properties of myofilament interactions.

In the case of sinusoidal perturbations, this approach is prompted by observations in asyn-

chronus muscle systems (e.g., insect fibrillar flight muscle) that an optimal range of frequencies exist over which an oscillatory perturbation leads to a phase shift between muscle force and length such that the muscle does work against the system rather than simply dissipating the applied energy as would a viscoelastic body. The frequency and amplitude characteristics of these critical oscillations should also reflect the interaction of chemical and mechanical kinetics of the active contractile system.

Steiger [90, 91] and Herzig and Ruegg [92] found that, as in insect fibrillar flight muscle [93, 94] and glycerinated rabbit psoas muscle [95, 96], glycerol-extracted rabbit ventricular muscle activated with Ca^{2+} responded to a quick stretch or release with a delayed tension change (at constant length). Figure 13–8 shows typical tension responses of glycerol-extracted heart muscle to two levels of step-length perturbations (middle and lower curves, respectively; top trace is length change). The first phase of the response following the step (stretch or release) is a rapid, temperature-insensitive return of tension toward T_0. Phase 2 is an order of magnitude slower and, in figure 13–8, appears as the slow tail on the first phase before reversing direction (stretch response) to redevelop delayed tension (phase 3). Delayed tension with releases is not as dramatic as with stretches. Phase 2 is Ca^{2+} sensitive and reflects inotropic states of the muscle. Phase-3 rate constants correspond with the normal heart rate of a wide variety of animals from frog and pig (30–50 beats/min) to hummingbird (2000 beats/min) [97].

While the responses in heart muscle are an order of magnitude slower than in insect and skeletal muscle preparations, they display the same mechanical features that are responsible for the oscillatory behavior of asynchronus insect fibrillar flight muscle.

Superimposed high-frequency length perturbations (100 Hz) also show that muscle stiffness parallels the force changes during delayed tension responses, indicating that these induced force changes involve CB attachments [98].

Further studies in living cardiac muscle [98] in which steady-state activation was achieved by a short period of caffeine or Ba^{2+} contracture also showed the delayed tension effect in response to step perturbations and further identified a range of oscillatory frequencies (0.05–1.20 Hz) in which muscle force lagged the imposed length change so as to do work on the system.

A further elaboration of these studies [99, 100] suggests that the rate constants fitted to the transient mechanical responses should correspond to the following chemical rate constants: k_1, the fast temperature-insensitive phase may correspond to actomyosin dissociation; k_2, which is strongly temperature and perturbation amplitude dependent, to recombination and dissociation of the [myosin products] component of the CB with actin; and k_3, which characterizes the delayed tension, to V_{max}, i.e., the maximum ATPase and attachment of new crossbridges. In a four-state CB cycle model, Steiger and Abbott [100] have matched these rate constants obtained in several muscle types to known biochemical rate constants. Rate constants for some of these processes have also been derived by Kawai and Brandt [96] from Nyquist plots of complex stiffness of several species' skeletal muscle using sinusoidal perturbation analysis. Although the correspondences of the mechanical and biochemical rate constants are somewhat arbitrary, and they give only a measure of net reaction rates rather than specific forward and backward rate constants, nevertheless they look promising in terms of developing useful relations between mechanical and chemical muscle contractile processes.

At this stage these correspondences can only be considered speculative because (a) the data were not obtained in muscle systems with controlled sarcomere lengths, i.e., series compliance and sarcomere uniformity are not controlled; and (b) the identification of specific mechanical rate constants with a certain biochemical reaction process is presumptive. But, in any case, some correlations between mechanical and chemical events are now plausible.

Active State

The concept of the active state was originally defined as the ability of a muscle to develop force at constant length [101]. In this respect

the onset of the active state is slow, particularly in heart muscle, since force development requires considerable time to reach its maximum. In contrast, in terms of shortening capability, the maximum velocity of shortening occurs very early (in skeletal muscle [102]; in heart muscle [78]). The question then arises of which parameter should be the measure of activation.

The active-state concept has been critically evaluated in several discussions [65, 67, 103, 104], with the recommendation in the latter review that the concept be abandoned. For example, Pollack and co-workers [67] could not determine a unique elastic modulus for series elasticity in heart muscle. Julian and Moss [104] considered force development and shortening in terms of a crossbridge model and series elasticity, and concluded that such a model predicted both a slow development of force and an early maximum shortening capability as observed experimentally. But, since muscle activation is now recognized to be regulated by myoplasmic Ca^{2+} and both shortening velocity and force development are strongly dependent on myoplasmic Ca^{2+}, the uniqueness of the classic active-state concept in terms of force development alone is lost. Indeed, the concept has little definitive value and should be abandoned.

Implications for Whole Heart Function

From this discussion it is apparent that the formulation of a fundamental constitutive relation that would describe heart muscle contractility in an effective manner is still premature. The complex dependence of contractile force on such factors as shortening deactivation, restoring forces, length-dependent activation, and sarcomere nonuniformity and, in addition, our inability to quantitatively represent these factors leaves possible only an empirical formulation of contractile parameters. Also, even empirical relations will have to be prescribed for very specific operational situations and these will likely apply only to a narrow range of cardiac function.

Similar concerns are expressed by Elzinga and Westerhof [107], who have considered the merits of isolated myocardium variables as they might serve as a means to quantify the pump function of the heart. Their conclusion is that force–length relations of isolated heart tissue are not necessarily related to the shape of the left ventricular function curve. For example, end-systolic volume can be larger when stroke volume is increased by an increase in end-diastolic volume, as might be predicted from the above discussion of shortening deactivation. Their suggestion is that an understanding of the basis of the cardiac pump function curve should come from the consideration of muscle fibers as they operate in the wall of the heart rather than in terms of parameters which are under rigidly controlled length and force conditions.

The complexity and ambiguity of the cardiac contractile process at short muscle lengths emphasize these recommendations in so far as the search goes for a unique index of cardiac contractility. Thus it seems unlikely that a simple constitutive relation [108] will be found which can be related to pump function with only a three-dimensional geometric transfer function. It is possible that empirical constitutive relations may be determined which may be useful, but these relations will likely need to be separately prescribed for each contractile state.

Therefore, it becomes critical to understand the functional basis for the ascending limb of the Frank–Starling relation so that the relative contributions of more of the underlying factors, i.e., external and internal loading, shortening deactivation, nonuniformity, and length-dependent activation, can be included in the constitutive relation. Additionally, there must also be a consideration of the contribution of the three-dimensional geometry of the heart to these intrinsic factors. Certainly, the shape, structure, and strain and stress distribution of the wall, as well as complex pressure loading, will have an effect on these interactions between contractile parameters.

From these considerations we must conclude that further mechanical studies at the level of the myocyte and further insight into myocyte integration into whole heart structure and function are as essential now as they were when the Frank–Starling relation was originally proposed.

References

1. Huxley HE, Hanson J: Changes in the cross-striations of muscle during contraction and stretch and their structural interpretation. Nature 173:973–976, 1954.
2. Huxley AF, Niedergerke R: Interference microscopy of living muscle fibers. Nature 173:971–973, 1954.
3. Noble MIM, Pollack GH: Molecular mechanisms of contraction. Circ Res 40:333–342, 1977.
4. Huxley AF, Simmons RM: Proposed mechanism of force generation in striated muscle. Nature 233:533–538, 1971.
5. Ingels NB Jr (ed): The molecular basis of force development. Palo Alto CA: Palo Alto Medical Research Foundation, 1979.
6. Murray JM, Weber A: A cooperative action of muscle proteins. Science 230:58–71, 1974.
7. Julian FJ: Some theories for muscle contraction based on cyclic, short-range interactions between actin and myosin. In: Ingels NB Jr (ed) The molecular basis of force development. Palo Alto CA: Palo Alto Medical Research Foundation, 1979.
8. Julian FJ, Sollins KR, Sollins MR: A model for the transient and steady-state mechanical behavior of contracting muscle. Biophys J 14:546–562, 1974.
9. Hill TL: Theoretical formalism for the sliding filament model of contraction of striated muscle. Part I. Prog Biophys Mol Biol 28:267–340, 1974.
10. Hill TL: Theoretical formalism for the sliding filament model of contraction of striated muscle. Part II. Prog Biophys Mol Biol 29:105–159, 1975.
11. Gordon AM, Huxley AF, Julian FJ: The variation in isometric tension with sarcomere length in vertebrate muscle fibers. J Physiol 184:170–192, 1966.
12. Julian FJ, Sollins MR, Moss RL: Sarcomere length nonuniformity in relation to tetanic responses of stretched skeletal muscle fibers. Proc R Soc Lond [B] 200:109–116, 1978.
13. Fabiato A, Fabiato F: Myofilament-generated tension oscillations during partial calcium activation and activation dependence of the sarcomere length–tension relation of skinned cardiac muscle. J Gen Physiol 72:667–699, 1978.
14. Iwazumi T, Pollack GH: The effect of sarcomere nonuniformity on the sarcomere length–tension relationship of skinned fibers. J Cell Physiol 106:321–337, 1981.
15. Julian FJ, Moss RL: Sarcomere length–tension relations of frog skinned muscle fibers at lengths above the optimum. J Physiol 304:529–539, 1980.
16. Winegrad S, McClellan G, Robinson T, Lai N-P: Variable diastolic compliance and variable Ca^{++} sensitivity of the contractile system in cardiac muscle. Eur J Cardiol (Suppl)4:41–46, 1976.
17. Blinks JR, Rudel R, Taylor SR: Calcium transients in isolated amphibian skeletal muscle fibres: detection with aequorin. J Physiol 277:291–323, 1978.
18. Rack PMH, Westbury DR: The effects of length and stimulus rate on tension in isometric cat soleus muscle. J Physiol 204:443–460, 1969.
19. Endo M: Stretch-induced increase in activation of skinned fibers by calcium. Nature 237:211–213, 1972.
20. Close RI: The relations between sarcomere length and characteristics of isometric twitch contractions of frog sartorius muscle. J Physiol 220:745–762, 1972.
21. Lopez JR, Wanek LA, Taylor SR: Skeletal muscle: length-dependent effects of potentiating agents. Science 214:79–82, 1981.
22. Pollack GH, Krueger JW: Sarcomere dynamics in intact cardiac muscle. Eur J Cardiol (Suppl)4:53–65, 1976.
23. Page E, McCallister LP, Power B: Stereological measurements of cardiac ultrastructure implicated in excitation–contraction coupling. Proc Natl Acad Sci 68:1465–1466, 1971.
24. Edman KAP, Nilsson E: Time course of the active state in relation to muscle length and movement: a comparative study on skeletal muscle and myocardium. Cardiovasc Res Suppl 1:3–10, 1971.
25. Fabiato A, Fabiato F: Dependence of calcium release, tension generation and restoring forces on sarcomere length in skinned cardiac cells. Eur J Cardiol (Suppl)4:13–27, 1976.
26. Robinson TF, Winegrad S: A variety of intercellular connections in heart muscle. J Mol Cell Cardiol 13:185–195, 1981.
27. Jewell BR: A reexamination of the influence of muscle length on myocardial performance. Circ Res 40:221–226, 1977.
28. Bodem R, Skelton CL, Sonnenblick EH: Inactivation of contraction as a determinant of the length–active tension relation in heart muscle of the cat. Res Exp Med 168:1–13, 1976.
29. Grimm AF, Whitehorn WV: Myocardial length–tension sarcomere relationships. Am J Physiol 214:1378–1387, 1968.
30. Gordon AM, Pollack GH: Effects of calcium on the sarcomere length–tension relation in rat cardiac muscle: implications for the Frank–Starling mechanism. Circ Res 47:610–619, 1980.
31. Winegard S: Resting sarcomere length–tension relation in living frog heart. J Gen Physiol 64:343–355, 1974.
32. Tarr M, Trank JW, Goertz KK, Leiffer P: Effect of initial sarcomere length on sarcomere kinetics and force development in single frog atrial cardiac cells. Circ Res 49:767–774, 1981.
33. Parsons C, Porter KR: Muscle relaxation: evidence for an intrafibrillar restoring force in vertebrate striated muscle. Science 153:426–427, 1966.
34. Brown LM, Gonzales-Serratos H, Huxley AF: Electron microscopy of frog muscle fibers in extreme passive shortening. J Physiol 208:86P, 1970.
35. Gonzales-Serratos H: Inward spread of activation in vertebrate muscle fibers. J Physiol 211:777–799, 1971.

36. Fabiato A, Fabiato F: Activation of skinned cardiac cells: subcellular effects of cardioactive drugs. Eur J Cardiol 1:143–155, 1973.
37. Krueger JW, Forletti D, Wittenberg BA: Uniform sarcomere shortening behavior in isolated cardiac muscle cells. J Gen Physiol 76:587–607, 1980.
38. Jewell BR, Wilkie DR: The mechanical properties of relaxing muscle. J Physiol 152:30–47, 1960.
39. Edman KAP: Mechanical deactivation induced by active shortening in isolated fibres of the frog. J Physiol 246:255–275, 1975.
40. Edman KAP: Depression of mechanical performance by active shortening during twitch and tetanus of vertebrate muscle fibers. Acta Physiol Scand 109:15–26, 1980.
41. Brady AJ: Onset of contractility in cardiac muscle. J Physiol 184:560–580, 1966.
42. Bodem R, Sonnenblick EH: Deactivation of contraction by quick releases in the isolated papillary muscle of the cat: effects of lever damping, caffeine, and tetanization. Circ Res 34:214–225, 1974.
43. Leach JK, Brady AJ, Skipper BJ, Millis DL: Effects of active shortening on tension development of rabbit papillary muscle. Am J Physiol 238:H8–H13, 1980.
44. Brady AJ: Active state in cardiac muscle. Physiol Rev 48:570–600, 1968.
45. Taylor SR, Rudel R: Striated muscle fibers: inactivation of contraction induced by shortening. Science 167:882–884, 1970.
46. Taylor SR: Decreased activation in skeletal muscle fibres at short lengths. In: The physiological basis of Starling's law of the heart. London: Ciba Foundation symposium 24, 1974.
47. Hibbard MG, Jewell BR: Length dependence of the sensitivity of the contractile system to calcium in rat ventricular muscle. J Physiol 290:30P, 1979.
48. Fatiato A: Sarcomere length dependence of calcium release from the sarcoplasmic reticulum of skinned cardiac cell demonstrated by differential microspectrophotometry with arsenazo III. J Gen Physiol 76:15a, 1980.
49. Moss RL: Sarcomere length–tension relations of frog skinned muscle fibers during calcium activation at short lengths. J Physiol 292:177–192, 1979.
50. Allen DG, Kurihara S: The effects of muscle length on intracellular calcium transients in mammalian cardiac muscle. J Physiol 327:79–94, 1982.
51. Chapman RA: Excitation–contraction coupling in cardiac muscle. Prog Biophys Mol Biol 35:1–52, 1979.
52. Chuck LHS, Parmley WW: Caffeine reversal of length-dependent changes in myocardial contractile state in the cat. Circ Res 47:592–598, 1980.
53. Julian FJ, Sollins MR: Sarcomere length–tension relations in living rat papillary muscle. Circ Res 37:299–308, 1975.
54. Pollack GH, Huntsman LL: Sarcomere length–active force relations in living mammalian cardiac muscle. Am J Physiol 227:383–389, 1974.
55. Pinto JG, Win R: Non-uniform strain distribution in papillary muscle. Am J Physiol 233:H410–H416, 1977.
56. Pinto JG: Macroscopic inhomogeneities in the mechanical response of papillary muscles. Biorheology 15:511–522, 1978.
57. Krueger JW, Farber S: Sarcomere length "orders" relaxation in cardiac muscle. Eur Heart J (Suppl A)1:37–47, 1980.
58. Huntsman LL, Joseph DS, Oiye MY, Nichols GL: Auxotonic contractions in cardiac muscle segments. Am J Physiol 237:H131–138, 1979.
59. Donald TC, Reeves DNS, Reeves RC, Walker AA, Hefner LL: Effects of damaged ends in papillary muscle preparations. Am J Physiol 238:H14–H23, 1980.
60. Brady AJ, Tan ST, Ricchiuti NV: Contractile force measured in unskinned isolated adult rat heart fibers. Nature 282:728–729, 1979.
61. De Clerck NM, Claes VA, Van Ocken ER, Brutsaert DL: Sarcomere distribution patterns in single cardiac cells. Biophys J 35:237–242, 1981.
62. Roos KP, Brady AJ, Tan ST: Direct measurement of sarcomere length from isolated cardiac cells. Am J Physiol 242:H68–H78, 1982.
63. Pinto JG, Fung YC: Mechanical properties of the heart muscle in the passive state. J Biomechanics 6:597–616, 1973.
64. Hill AV: The heat of shortening and the dynamic constants of muscle. Proc Roy Soc Lond [B] 126:136–195, 1938.
65. Jewell BR, Wilkie DR: An analysis of the mechanical components in muscle. J Physiol 143:515–540, 1958.
66. McLaughlin RJ, Sonnenblick EH: Time behavior of series elasticity in cardiac muscle: real-time measurements by controlled-length techniques. Circ Res 34:798–811, 1974.
67. Pollack GH, Huntsman LL, Verdugo P: Cardiac muscle models: an overextension of series elasticity. Circ Res 31:569–579, 1972.
68. Hefner LL, Bowen TE Jr: Elastic components of cat papillary muscle. Am J Physiol 212:1221–1227, 1967.
69. Fung YC: Comparison of different models of the heart muscle. J Biomechanics 4:289–295, 1971.
70. Brady AJ, Tan ST, Ricchiuti NV: Perturbation measurements of papillary muscle elasticity. Am J Physiol 241:H155–H173, 1981.
71. Fung YC: Elasticity of soft tissues in simple elongation. Am J Physiol 213:1532–1544, 1967.
72. Tarr M, Trank JW, Leiffer P, Shepherd N: Sarcomere length–resting tension relation in single frog atrial cardiac cells. Circ Res 45:554–559, 1979.
73. Grimm AF, Whitehorn WV: Characteristics of resting tension of myocardium and localization of its elements. Am J Physiol 210:1362–1368, 1966.
74. Lazarides E: Intermediate filaments as mechanical integrators of cellular space. Nature 283:249–256, 1980.

75. Natori R: The property and contractile process of isolated myofibrils. Jikeikai Med J 1:119–126, 1954.
76. Podolsky RJ: The maximum sarcomere length for contraction of isolated myofibrils. J Physiol 170:110–123, 1964.
77. Pinto JG, Patitucci PJ: Creep in cardiac muscle. Am J Physiol 232:H553–H563, 1977.
78. Brutsaert DL: The force–velocity–length–time interaction of cardiac muscle. In: The physiological basis of Starling's law of the heart. London: Ciba Foundation, 1974.
79. Sonnenblick EH: Implications of muscle mechanics in the heart. Fed Proc 21:975–990, 1962.
80. Sonnenblick EH, Parmley WW, Parmley CW: The contractile state of the heart as expressed by force–velocity relations. Am J Cardiol 23:488–503, 1969.
81. Yeatman LA Jr, Parmley WW, Sonnenblick EH: Effects of temperature on series elasticity and contractile element motion in heart muscle. Am J Physiol 217:1030–1034, 1969.
82. Noble MIM, Bowen TE, Hefner LL: Force–velocity relationship of cat cardiac muscle, studied by isotonic and quick-release techniques. Circ Res 24:821–833, 1969.
83. Parmley WW, Yeatmean L, Sonnenblick EH: Differences between isotonic and isometric force–velocity relations in cardiac and skeletal muscle. Am J Physiol 219:546–550, 1970.
84. Pollack GH: Maximum velocity as an index of contractility in cardiac muscle. Circ Res 26:111–127, 1970.
85. Donald TC, Unnoppetchara K, Peterson D, Hefner LL: Effect of initial muscle length on V_{max} in isotonic contraction of cardiac muscle. Am J Physiol 223:262–267, 1972.
86. Parmley WW, Chuck L, Yeatman L: Comparative evaluation of the specificity and sensitivity of isometric indices of contractility. Am J Physiol 228:506–510, 1975.
87. Edman KAP, Hwang JC: The force–velocity relationship in vertebrate muscle fibers at varied tonicity of the extracellular medium. J Physiol 269:255–272, 1977.
88. Edman KAP: The velocity of unloaded shortening and its relation to sarcomere length and isometric force in vertebrate muscle fibers. J Physiol 291:143–159, 1979.
89. Sonnenblick EH: Determinants of active state in heart muscle: force, velocity, instantaneous muscle length, time. Fed Proc 24:1396–1409, 1965.
90. Steiger GJ: Stretch activation and myogenic oscillation of isolated contractile structures of heart muscle. Pflugers Arch 330:347–361, 1971.
91. Steiger GJ: Tension transients in extracted rabbit heart muscle preparations. J Mol Cell Cardiol 9:671–685, 1977.
92. Herzig JW, Ruegg JC: Myocardial cross-bridge activity and its regulation by Ca^{++}, phosphate and stretch. In: Riecher G, Weber A, Goodwin J (eds) Myocardial failure. New York: Springer-Verlag, 1977.
93. Goodall MC: Autooscillations of extracted muscle fibers. Nature 177:1238–1239, 1956.
94. Lorand L, Moos C: Autooscillations of extracted muscle fibers. Nature 177:1239–1240, 1956.
95. Ruegg JC, Steiger GJ, Schadler M: Mechanical activation of the contractile system. Pflugers Arch 319:139–145, 1970.
96. Kawai M, Brandt PW: Sinusoidal analysis: a high resolution method of correlating biochemical reactions with physiological processes in activated skeletal muscles of rabbit, frog and crayfish. J Muscle Res Cell Motil 1:279–303, 1980.
97. Steiger GJ: Stretch activation and tension transients in cardiac, skeletal and insect flight muscle. In: Tregear RT (ed) Insect flight muscle. Amsterdam: Elsevier/North-Holland Biomedical, 1977.
98. Steiger GJ, Brady AJ, Tan ST: Intrinsic regulatory properties of contractility in the myocardium. Circ Res 42:339–350, 1978.
99. Steiger GJ: Kinetic analysis of isometric tension transients in cardiac muscle. In: Sugi H, Pollack GH (eds) Cross-bridge mechanism in muscle contraction. Tokyo: University of Tokyo, 1979.
100. Steiger GJ, Abbott RH: Biochemical interpretation of tension transients produced by a four-state mechanical model. J Muscle Res Cell Motil 2:245–260, 1981.
101. Hill AV: The onset of contraction. Proc Roy Soc Lond [B] 136:242–254, 1949.
102. Hill AV: The transition from rest to full activity in muscle: the velocity of shortening. Proc Roy Soc Lond [B] 138:329–338, 1951.
103. Pringle JWS: Models of muscle. Symp Soc Exp Biol 14:41–68, 1960.
104. Julian FJ, Moss RL: The concept of active state in striated muscle. Circ Res 38:53–59, 1976.
105. Fabiato A, Fabiato F: Dependence of the contractile activation of skinned cardiac cells on the sarcomere length. Nature 256:54–56, 1975.
106. Brady AJ: Length–tension relations in cardiac muscle. Am Zool 7:603–610, 1967.
107. Elzinga G, Westerhof N: How to quantify pump function of the heart: the value of variables derived from measurements on isolated muscle. Circ Res 44:303–308, 1979.
108. Ghista DN, Brady AJ, Radhakrishnan S: A three-dimensional analytical (rheological) model of the human left ventricle in passive–active states: non-traumatic determination of the in vivo values of the rheological parameters. Biophys J 13:832–854, 1973.

14. SUBSTRATE AND ENERGY METABOLISM OF THE HEART

L.H. Opie

Introduction

The purpose of the energy metabolism of the heart is to provide an adequate supply of high-energy phosphate compounds to replace the continuous use of ATP in contraction, in ionic exchange processes, and to a lesser extent in other energy-demanding processes. Because of the very high turnover rate of ATP in the myocardium, a correspondingly high rate of mitochondrial production of ATP is required. Within the mitochondria, the citrate cycle of Krebs breaks down the critical compound acetyl CoA to CO_2 and hydrogen atoms; the latter in turn yield electrons which are conveyed along the electron transmitter chain to yield ATP by oxidative phosphorylation, before finally combining with oxygen to form water.

Acetyl CoA is an activated 2-carbon fragment eventually derived from one of the three major substrates of the myocardium: glucose, lactate, or free fatty acid. Strictly speaking, a substrate is a chemical compound which an enzyme converts by its catalytic function to the production of that reaction. As each energy source needs a series of catalytic reactions before it can be converted to acetyl CoA, the term "substrate" is used in studies of myocardial metabolism to indicate a fuel for the myocardium.

This chapter discusses the pathways whereby each of the major substrates is broken down to acetyl CoA, and the role of each substrate in myocardial energy production.

The original work referred to was supported by the Medical Research Council of South Africa and the Chris Barnard Fund. Members of my laboratory are thanked for many critical discussions.

N. Sperelakis (ed.), PHYSIOLOGY AND PATHOPHYSIOLOGY OF THE HEART.

Glucose

IMPORTANCE OF GLUCOSE FOR METABOLISM OF THE HEART

Glucose is a myocardial fuel of special historical and evolutionary interest, although it is now known to be the major fuel only after a carbohydrate meal (table 14–1). Historically, interest in glucose metabolism dates back to at least 1907 when Locke and Rosenheim [1] found glucose uptake in the isolated heart preparation of Langendorff. In 1912, Knowlton and Starling [2] found that sugar was used by the dog heart and that pancreatectomy impaired this power of "consuming sugar". Evans [3], in 1914, suggested that only one-third of the heart's energy is supplied by carbohydrate oxidation. Cruickshank and his associates suggested that "direct combustion" of fat, probably the blood fatty acids, met the rest of the heart's energy requirements. Thus, these early workers delineated carbohydrate and fatty acids as two of the most important myocardial fuels. From the biochemical point of view, glucose is of interest because factors controlling its uptake and utilization by glycolysis or glycogen synthesis have been extensively studied and an integrated scheme of the control of these processes has now been established (fig. 14–1). Therapeutically, glucose is of interest because of the possible use of glycolysis in maintaining anaerobic metabolism. Thus glucose is a component of the glucose–insulin–potassium solu-

TABLE 14–1. Effect of nutritional state on fuel for oxidative metabolism of the human heart: percentage of oxygen uptake accounted for, if various substrates are fully oxidized[a]

Conditions	Authors[b]	Glucose	Pyruvate	Lactate	Total CHO	FFA	TG	Ketones	Amino acids	Respiratory quotient
Glucose and insulin	Gordon & Cherkes[1]	—	—	—	—	none	—	—	—	—
"Feeding"	Olson & Piatnek[2]	—	—		92	5	—	—	—	Approaches 1.0
Postprandial CHO	[c]Goodale et al.[3]	68	4	28	100	—	—	—	—	0.94
-do- lipid	Carlson et al.[12]	10	—	?10	?20	30	50	—	—	—
Fasting, few hours	[d]Keul et al.[4]	31	2	28	61	34	—	5	0	—
Same during exercise	-do-	16	0	61	77	21	—	2	0	—
Same with recovery	-do-	21	2	36	59	36	—	3	0	—
Fasting overnight	[e]Bing[1]	18	1	16	35	(67)[f]	?	5	6	—
	Gordon & Cherkes[5]	—	—	—	—	50	—	—	—	—
	Goodale et al.[6]	23	3	8	34	—	—	—	—	0.74
	[e]Olson & Piatnek[7]	—	—	—	30	58	—	—	—	—
	Harris et al.[8]	56	1	10	67	66	—	—	—	—
	Rudolph et al.[9]	15	1	13	29	70	—	9	—	—
	Willebrands[10]	30	0	8	38	58	—	—	—	—
	Lassers et al.[11]	22	1	8	31	53	14	—	—	—
	Mean values	27	1	11	38	59	14	7		

[a]CHO, carbohydrate; FFA, free fatty acids; TG, triglyceride; — absence of data.
[b]References 1–10, see Opie [38]; 11, Lassers et al. [56]; 12, Carlson et al., *Acta Med Scand* 193:233, 1973.
[c]Subjects studied 2–3 h after a light low-fat breakfast.
[d]Subjects studied in the early afternoon after a light breakfast.
[e]Exact conditions not specified; overnight fast assumed.
[f]Total fatty acid, includes triglyceride.

tion now being evaluated as possible therapy in acute myocardial infarction.

REGULATION OF GLUCOSE UPTAKE

The rate of glucose uptake from the extracellular space into the heart cells is normally limited by the rate of transport of glucose across the cell membrane [5], a process thought to involve a stereoscopic glucose carrier [6–9]. Three major factors which increase glucose uptake by the heart are insulin, hypoxia, and increased heart work (fig. 14–1). When insulin is added to the medium, there is acceleration of membrane transport by an unknown mechanism; in these circumstances the rate of membrane transport exceeds the rate of the next step in the metabolism of glucose (phosphorylation of glucose to glucose 6-phosphate), so that glucose 6-phosphate accumulates and glucose uptake fails to increase further after a certain point. Acceleration of the rate of transsarcolemmal transport of glucose also occurs during the anoxic perfusion [4] or when the heart work is increased [10]; in either case, the rate of transport of glucose across the sarcolemma remains rate limiting [5, 11].

The stimulation of glucose transport by hypoxia or increased heart work is ill-understood, but could be explained by the original suggestion of Randle and Smith [12] that the "entry of glucose . . . is restrained . . . by a process dependent on a supply of energy-rich phosphate". This mechanism is presumably different from the acceleration achieved by insulin, which does not involve changes in high-energy phosphate contents.

GLYCOLYSIS

By glycolysis is generally meant a pathway common to glucose and glycogen breakdown, which produces lactate in anaerobic conditions. In normal oxidative metabolism, glycolysis yields pyruvate which is then aerobically broken down in the citrate or Krebs cycle; conver-

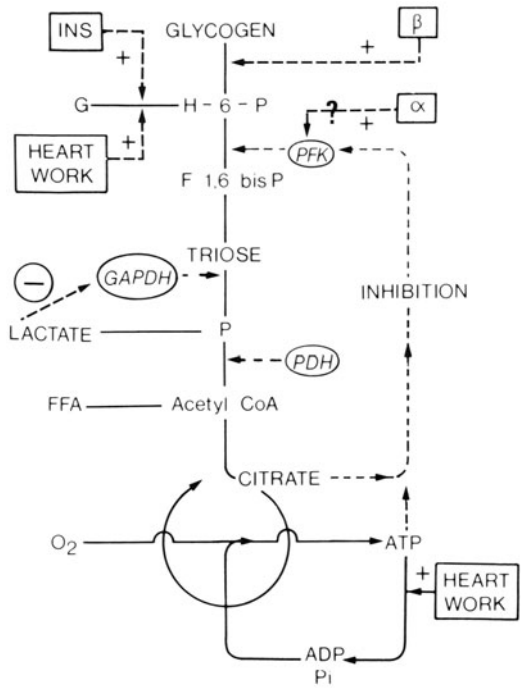

FIGURE 14–1. Overall control of pathways of glycolysis which is taken as the conversion of glucose 6-phosphate (G6P) to pyruvate (P): Ins, insulin; β, beta-adrenergic stimulation; α, alpha-adrenergic stimulation; PFK, phosphofructokinase; F 1,6bisP, fructose 1,6-diphosphate or fructose 1,6-bisphosphate; GAPDH, glyceraldehyde phosphate dehydrogenase. The basal inhibition of glycolysis at the level of phosphofructokinase is overcome by heart work (via changes in ATP/ADP and citrate) or by anoxia or mild ischemia (similar metabolic changes). During severe ischemia, when lactate accumulates in the tissue, glyceraldehyde 3-phosphate dehydrogenase is inhibited and the rate of glycolysis falls.

sion of glucose or glycogen to pyruvate in these circumstances may be termed aerobic glycolysis. The critical function of glycolysis is to produce ATP independently of oxygen. This will happen whether the ultimate end-point of glycolysis is the aerobic conversion of pyruvate to acetyl CoA or whether this is anaerobic glycolysis with production of anaerobic ATP. In aerobic circumstances, mitochondrial metabolism is the chief source of ATP and the rate of oxygen-independent production of ATP has not been shown to be critical. In contrast, in anaerobic circumstances, glycolysis is the sole source of ATP and therefore becomes a critical reaction. In response to anaerobiosis, glycolysis can be accelerated severalfold by the Pasteur reaction.

PASTEUR EFFECT

Pasteur [13], working in Paris in 1876, discovered the principles involved in the reactions of living organisms to deprivation of oxygen by showing that unicellular microorganisms accelerated their rate of "fermentation" when deprived of oxygen. By "fermentation" he meant those processes able to sustain life in the absence of oxygen. In modern terms, the Pasteur effect can be paraphrased to indicate that during anaerobiosis lactate production is accelerated (fig. 14–2). The first experimental evidence for the application of this hypothesis to the heart was the demonstration by Lovatt Evans [3] that respiration of a dog heart–lung preparation by a low oxygen mixture led to increased glucose uptake while lactate output replaced the normal uptake of lactate.

PHOSPHOFRUCTOKINASE ACTIVITY

Much later the biochemical basis for these observations was laid by Randle et al. in Cambridge and Morgan's group in Nashville, Tennessee. They induced anoxia in isolated perfused hearts and established that the increased glycolytic flux was governed by a series of reactions including acceleration of glucose transport into the cell, and increased activity of the rate-limiting enzyme phosphofructokinase (which converts fructose 6-phosphate to fructose 1,6-bisphosphate). Fructose 6-phosphate is in turn derived by an equilibrium reaction from glucose 6-phosphate, the common meeting point of the pathways of glucose uptake and glycogen breakdown. In simplified form the equations from glucose uptake are:

$$\text{glucose} + \text{ATP} \rightarrow \text{glucose 6-phosphate} + \text{ADP} \quad (14.1)$$

$$\text{glucose 6-phosphate} \leftrightarrows \text{fructose 6-phosphate} \quad (14.2)$$

$$\text{fructose 6-phosphate} + \text{ATP} \rightarrow \text{fructose 1,6-bisphosphate} + \text{ADP} \quad (14.3)$$

$$\text{fructose 1,6-bisphosphate} \rightleftarrows \text{glyceraldehyde 3-phosphate} + \text{dihydroxyacetone-P} \quad (14.4)$$

$$\text{dihydroxyacetone P} \leftrightarrows \text{glyceraldehyde 3-phosphate} \quad (14.5)$$

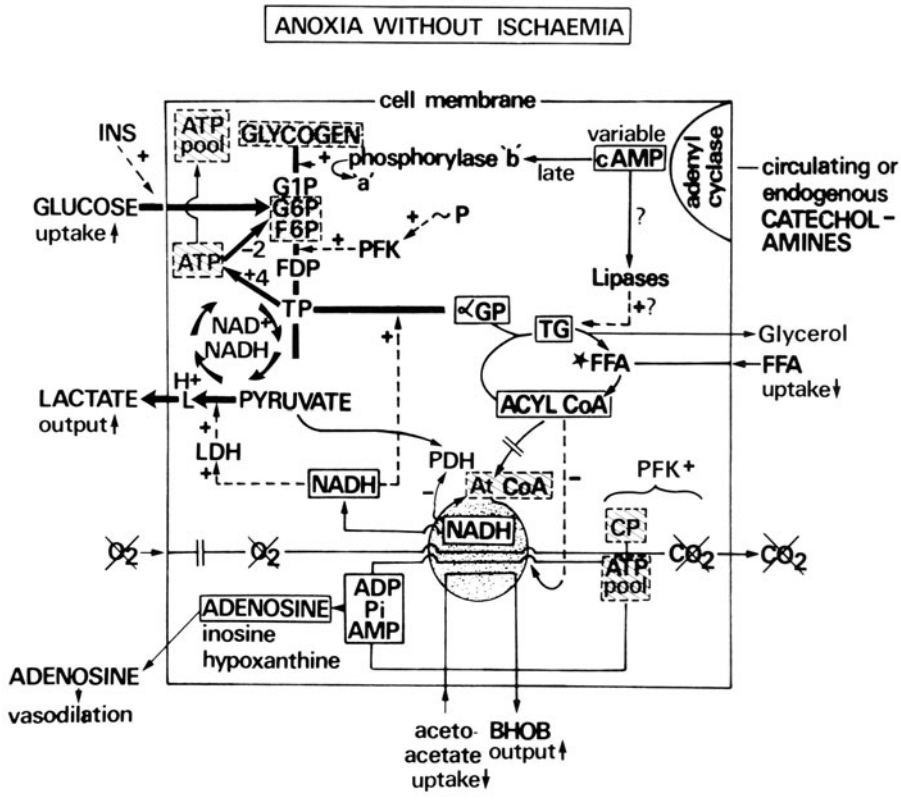

FIGURE 14–2. Anoxia without ischemia. Note accelerated pathways of anaerobic glycolysis, indicated by thickened arrows. ATP produced glycolytically (−2 ATP used up, +4 produced per glucose molecule) may enter the same ATP pool into which oxidatively produced ATP would be received; alternatively, there may be a special glycolytic ATP pool with a special function in relation to the membrane. In anoxia, oxygen uptake ceases; no CO_2 is produced by respiration but could form from tissue bicarbonate during buffering of H^+ formation. Total ATP and CP fall, ADP, AMP, and P_i rise; there is increased formation of adenosine in anoxic tissue which is thought to help in the compensatory vasodilation. The H^+ produced by anaerobic glycolysis via ATP breakdown is insufficient to cause a severe intracellular acidosis (see text) and the activity of phosphofructokinase is accelerated (PFK+). Citrate cycle activity is severely compromised by: cessation of oxygen uptake, increased formation of mitochondrial NADH (as judged by reduced uptake of acetoacetate and output of β-hydroxybutyrate), inhibition of pyruvate dehydrogenase (PDH), and decreased acetyl CoA (At CoA). Note areas of ignorance in relation to lipid metabolism. Note the increased incorporation of exogenous ^{14}C-FFA into ^{14}C-tissue FFA indicated as *FFA; there is no adequate information on tissue FFA contents. The role of cyclic AMP in stimulating lipase and phosphorylase activity is not yet clarified. Glycogenolysis may occur without phosphorylase activation. Because of continued coronary flow, CO_2, H^+ and lactate rise much less than in ischemia (see fig. 14–3).

Key to Figures 14–2 and 14–3: □ increased tissue content of metabolite; ▨ decreased tissue content of metabolite; × absence of metabolite; → pathways of metabolism; ➡ accelerated pathways; ----> factors altering rates of enzyme activity; ⊛ citrate cycle activities.

INS, insulin activity; PFK, phosphofructokinase; TP, triose phosphates, including dihydroxyacetone phosphate; αGP, α-glycerophosphate; L, lactate; LDH, lactate dehydrogenase; PDH, pyruvate dehydrogenase; cAMP, cyclic AMP; TG, triglyeride; BHOB, β-hydroxybutyrate; GIP, glucose 1-phosphate; G6P, glucose 6-phosphate; F6P, fructose 6-phosphate; FDP, fructose 1,6-diphosphate; FFA free fatty acid.

Modified from Opie [138] by permission of *Circ Res* and the American Heart Association.

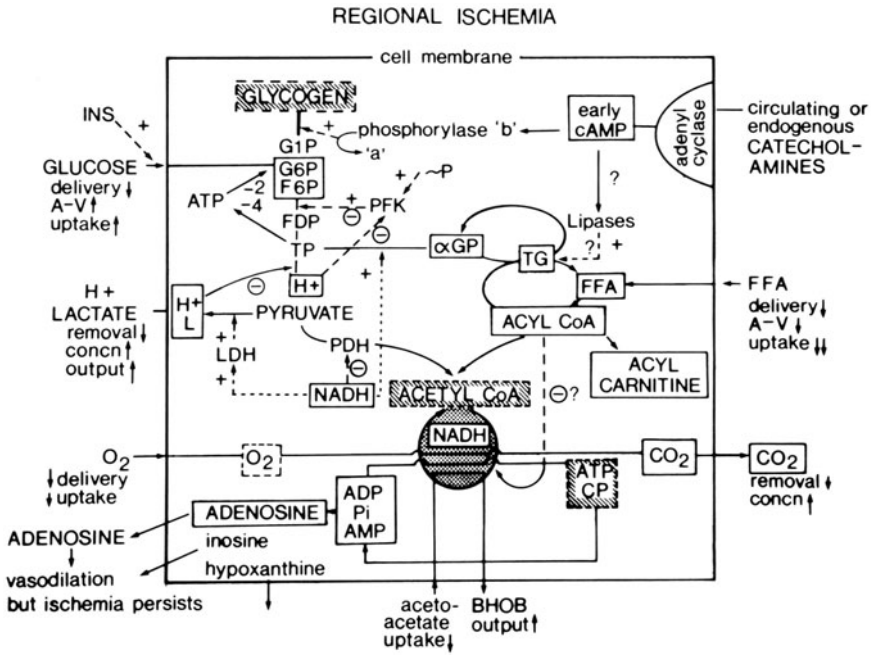

FIGURE 14–3. Regional ischemia without total anoxia (developing myocardial infarction). The major differences from anoxia without ischemia are: a residual oxidative metabolism resulting from a decreased but not absent tissue O_2, increased tissue CO_2, definite intracellular acidosis, a much increased tissue lactate, and a definite increase in acyl CoA. Decreased blood flow results in decreased blood flow results in decreased delivery of oxygen, glucose, and FFA; at circulating FFA levels of about 500–700 μEq/liter, the glucose arteriovenous (AV) difference is increased relative to that of FFA. PFK activity is relatively inhibited (compare anoxia) and tissue contents of hexose monophosphates (G6P and F6P) rise rather than fall as in anoxia. Glycolytic flux is not stimulated to the same extent as in anoxia (thinner arrows compared with fig. 14–2). Glycolytic H^+ is produced via ATP breakdown (bottom right corner of figure) and intracellular acidosis may both contribute to and be caused by the increased tissue P_{CO_2}. The intracellular (IC) acidosis inhibits PFK (−), which receives conflicting stimuli from changes in high energy phosphate (~P) and from H^+ accumulation. αGP and acyl CoA increase; the latter inhibits the adenine translocase transferring ATP across the mitochondrial membrane. Values of acetyl CoA are not known in regional ischemia but tend to fall in uniform ischemia. Values of TG are not reported, and the roles of cAMP and catecholamine activity need clarification. In global ischemia, catecholamine release may stimulate lipase activity. There is evidence for an increased turnover of a "triglyceride cycle" which would "waste" ATP and produce H^+. Abbreviations and symbols are identified in the legend for figure 14–2. Modified from Opie [138] by permission of *Circ Res* and the American Heart Association.

The enzymes concerned are, respectively: hexokinase, hexosephosphate isomerase (= phosphoglucose isomerase), phosphofructokinase, aldolase, and triose phosphate isomerase. Only equations 14.1 and 14.3 are thought to have regulatory properties.

Evidence for control at the level of phosphofructokinase is briefly summarized as follows. First, the activity of the enzyme is low among the enzymes of glycolysis. Secondly, the mass action ratio of the reactants is far removed from the apparent equilibrium constant; hence some factor is keeping the reactants from reaching equilibrium and that factor is probably the activity of the enzyme. Thirdly, flow through the enzyme can increase even when the tissue content of its substrate (fructose 6-phosphate) falls as in anoxia. Fourthly, the enzyme has been isolated and has complex allosteric properties including inhibition by ATP (and probably creatine phosphate), by citrate, and by a low pH; on the other hand, there is relief of inhibition by products of ATP (such as ADP, Pi, and AMP) or by a decreased citrate concen-

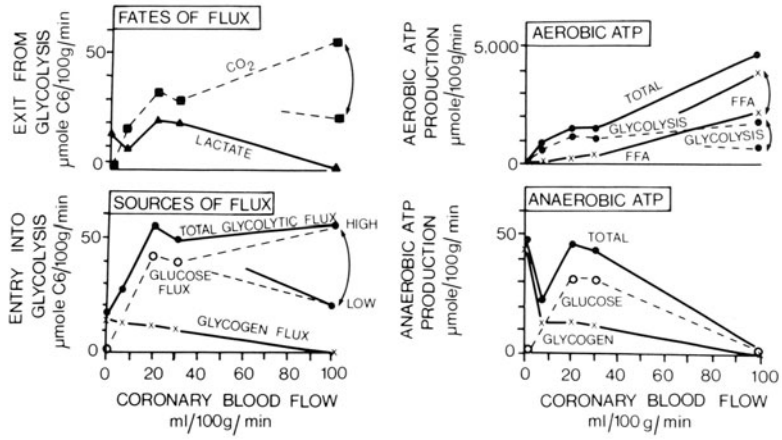

FIGURE 14–4. Glycolytic flux *(a)* and ATP production *(b)*. Schematic representation of sources of glycolytic flux (glucose, glycogen, and total flux), fates of glycolytic flux (lactate or CO_2 formation), relative contributions of glucose and glycogen to anaerobic ATP formation, and glycolysis and exogenous free fatty acid (FFA) to aerobic ATP formation. For details of calculations, see Opie [138]. Reproduced by permission of *Circ Res* and American Heart Association.

tration or by alkalosis. Situations have been found where all these in vitro properties can be mimicked in the whole perfused heart, thus strongly supporting the controlling role of phosphofructokinase [14].

GLYCERALDEHYDE 3-PHOSPHATE DEHYDROGENASE

It has long been appreciated that control of glycolysis could pass from phosphofructokinase to other points down the line of glycolysis during extreme conditions such as severe total ischemia [15] or an abrupt normoxic–anoxic transition [16]. It is now known that glyceraldehyde phosphate dehydrogenase (GAPDH) is the most important of these in explaining the ischemic inhibition of glycolysis (fig. 14–3).

During severe ischemia, glycolysis is inhibited rather than stimulated (fig. 14–4). In mild ischemia, the Pasteur effect accelerates glucose uptake and glycolytic flux through stimulation of glucose uptake and of phosphofructokinase; in severe ischemia, phosphofructokinase is inhibited by acidosis while glyceraldehyde 3-phosphate dehydrogenase is inhibited by several products of glycolysis [17, 18]. The molecular mechanisms involved are as yet unknown. The inhibitory powers of lactate are found on the crude enzyme preparation, but not on the purified enzyme [18]. The inhibitory effect of lactate is independent of any pH effect although protons also inhibit glyceraldehyde phosphate dehydrogenase [19]. High concentrations of NADH and ATP strongly inhibit the enzyme [18].

Anaerobic glycolysis will tend to slow down as tissue NADH rises, pH falls, ATP declines, and lactate rises. The tissue pH falls with increasing severity of ischemia [20], which could explain greater glycolytic inhibition with increasing ischemia (fig. 14–4). This deceleration of glycolysis will slow down the rate of formation of protons, which are derived from ATP turnover (next section). Hence there appears to be a self-protective mechanism:

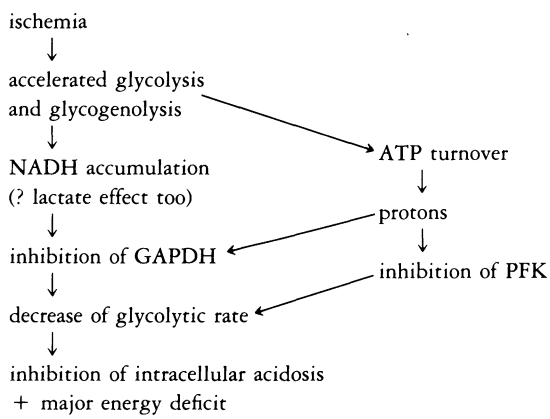

PROTON PRODUCTION BY
ANAEROBIC GLYCOLYSIS

glyceraldehyde 3-phosphate + NAD^+ + Pi	→	1,3-diphosphoglycerate + NADH + H^+
1,3-diphosphoglycerate + ADP	→	3-phosphoglycerate + ATP
3-phosphoglycerate	→	2-phosphoglycerate
2-phosphoglycerate	→	phosphoenolpyruvate + H_2O
phosphoenolpyruvate + ADP	→	pyruvate + ATP
pyruvate + NADH + H^+	→	lactate + NAD^+
glyceraldehyde 3-phosphate + Pi + 2 ADP	→	lactate + 2 ATP

During anaerobic glycolysis, the reduced cofactor (NADH + H^+, which equals $NADH_2$) formed by the enzyme glyceraldehyde 3-phosphate dehydrogenase is reconverted to NAD during the formation of lactate. The overall reaction produces two molecules of ATP, independently of oxygen (see above).

Thus during anaerobic glycolysis, no protons are formed. Why then is anaerobic glycolysis usually held to be proton producing and a potential source of acidosis?

Gevers [21] has examined this question in detail. When all the charges are written into the individual glycolytic reactions, and allowance is made for the probable degree of complex formation of ADP and ATP with Mg^{2+}, the following equations are derived:

$$\text{glucose} + 2\ MgADP^{1-} + 2\ Pi^{2-} \rightarrow 2\ \text{lactate}^{1-} + 2\ MgATP^{2-} \quad (14.6)$$

In anaerobic conditions, all ATP produced will be broken down so that protons are produced:

$$2\ MgATP^{2-} \rightarrow 2\ MgADP^{1-} + 2\ Pi^{2-} + 2\ H^+ \quad (14.7)$$

These equations are only approximations and depend on a number of assumptions including the free Mg^{2+} in the cytosol and intracellular pH (the latter influencing the phosphate charge). Normally anaerobiosis will not only cause pyruvate to form lactate, but will break down the newly formed glycolytic ATP to ADP (eq. 14.7), thereby liberating inorganic phosphate and protons. Thus glycolytically made ATP (and not lactate) is the "source" of the protons produced during anaerobic glycolysis.

GLUCOSE METABOLISM: CRITICAL FEATURES

1. The rate of transport of glucose across the sarcolemma by the stereospecific glucose carrier is of major importance in controlling the rate of glucose uptake by the heart.
2. Glucose transport is accelerated by insulin, hypoxia, and increased heart work, which also increase the rate of flow through glycolysis by increasing the activity of the rate-limiting enzyme, phosphofructokinase. Insulin acts by increased provision of substrate (fructose 6-phosphate derived from the uptake of glucose), while anoxia and increased heart work act by breakdown of high-energy phosphate compounds which relieve the inhibition that high levels of ATP exert on phosphofructokinase.
3. In aerobic conditions (normal oxygenation), the end-point of glycolysis is pyruvate, which enters the citrate cycle of Krebs for further aerobic metabolism.
4. In anaerobic conditions, the end-point of glycolysis is lactate; the rates of anaerobic glycolysis are not high enough to provide sufficient energy for the contracting heart, but can provide for the needs of the potassium-arrested heart.
5. In mild ischemia, glycolysis is accelerated.
6. In severe ischemia, both the supply of oxygen and the blood flow are restricted so that products of glycolysis accumulate to inhibit glycolytic flux at the level of glyceraldehyde 3-phosphate dehydrogenase; simultaneously the accumulation of protons (derived from the turnover of ATP which is broken down as rapidly as it is made by anaerobic glycolysis) inhibits both phosphofructokinase and glyceraldehyde 3-phosphate dehydrogenation. Hence, in severe ischemia, the ability

of glycolytic flux to provide anaerobic energy is very limited and a major deficit of energy develops.

Thus far the input into glycolysis from the uptake of glucose from the circulation has been discussed. Another source of glycolysis is the breakdown of glycogen.

Glycogen

BASIC CONCEPTS

Glycogen is a polysaccharide (i.e. a combination of many molecules of glucose) which forms large storage granules in the cytoplasm of the heart. Chemically, it resembles glycogen found in other organs such as the liver. Although frequently thought of as a "storage" carbohydrate, the glycogen molecule is in a constant state of turnover as a result of variable rates of synthesis and degradation. In contrast to the very detailed understanding of the complex chemical signals controlling glycogen synthesis and breakdown, the physiologic function of cardiac glycogen is poorly understood. Glycogen is not a reserve carbohydrate fuel for the heart during fasting, because the glycogen content of the heart rises during fasting and falls in the fed state. These changes in the glycogen content can be related to changes in blood free fatty acids. When blood free fatty acid concentration is high as during fasting, then glycolysis is inhibited and the content of cardiac glycogen is also high and increases in response to an increased tissue content of glucose 6-phosphate. In the fed state, blood free fatty acid concentration is low and so is cardiac glycogen, despite the high rates of glucose uptake and the activity of insulin which stimulates glycogen synthesis. The probable explanation is that in the fed state a high rate of glycogen turnover is accompanied by high rates of synthesis and breakdown of glycogen, so that the overall content of glycogen is low. During prolonged fasting, on the other hand, the high cardiac glycogen content probably consists largely of low-turnover glycogen.

GLYCOGEN SYNTHESIS

The pathways of glycogen synthesis function separately from those of glycogen breakdown because two different enzyme systems are involved (fig. 14–5). The major factors stimulating glycogen synthesis are a high circulating insulin level or high blood free fatty acid levels. Glycogen synthesis starts with conversion of glucose 6-phosphate to glucose 1-phosphate. The critical step in glycogen synthesis is the transfer of glucose 1-phosphate to the end of a preexisting glycogen chain. The chief enzyme regulating this process is glycogen synthase (= glycogen synthetase = glycogen transferase), which exists in the more active *a* form and the less active *b* form. Glycogen synthesis requires the presence of high-energy phosphate—not as ATP, but as uridine triphosphate (UTP is derived from ATP). Hence glycogen synthesis cannot take place in a state of energy depletion.

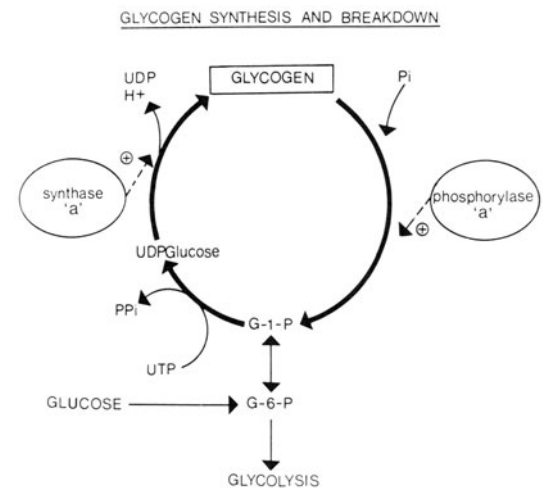

FIGURE 14–5. Control of glycogen metabolism. Note different pathways for synthesis which is controlled by glycogen synthase (= synthetase) when compared with glucose breakdown which is controlled by glycogen phosphorylase.

The mode of action of insulin in stimulating glycogen synthesis is very complex and not fully understood. Insulin increases the percentage of glycogen synthase in the *a* form possibly by controlling the phosphatase enzyme which converts the synthase *b* to *a* form; in experimental ketotic diabetes, glycogen synthesis is diminished as the activity of the synthase phosphatase falls [22].

Besides the presence of insulin, the other

major factor stimulating glycogen synthesis is a high cellular content of glucose 6-phosphate. Conditions increasing the cardiac contents of glucose 6-phosphate are: (a) a high circulating insulin and glucose as after a meal, (b) inhibition of glycolysis as when the heart is using fatty acids, or (c) ketotic diabetes, when glycolysis is inhibited by a combination of high fatty acids and high blood ketones. In the latter two situations, the continued buildup of cardiac glycogen will eventually inhibit its own synthesis, to explain why a high level of glycogen is accompanied by a low rate of turnover.

Thus there are multiple mechanisms for glycogen synthesis, which proceeds at a high rate in the fed state under the influence of insulin and at a lower rate in the fasted state despite the deficit of insulin, because of the influence of high myocardial levels of glucose 6-phosphate.

GLYCOGEN BREAKDOWN

The two major mechanisms for stimulating glycogen breakdown are mediated either by cyclic AMP or, in anoxia, by a fall in high-energy phosphate levels. Cyclic AMP promotes the well-known cascade of events which eventually converts the inactive glycogen phosphorylase *b* to the highly active phosphorylase *a*. Thus:

catecholamine stimlus → beta-receptor → adenyl cyclase → cyclic-AMP activation of protein kinase → activation of phosphorylase *b* kinase → change of phosphorylase *b* to *a* → breakdown of glycogen

Calmodulin, the intracellular calcium-binding receptor protein, is one of the subunits of phosphorylase *b* kinase; hence calcium ions are required for the activity of the latter enzyme and for formation of phosphorylase *b*.

Another mechanism for promotion of glycogenolysis is by enhancing the activity of phosphorylase *b*, that is, without interconversion of the two forms. This process, which therefore occurs independently of adrenergic stimulation, is set in motion by the breakdown of ATP to AMP and inorganic phosphate [23]. Hence, in ischemia, glycogenolysis is enhanced both by the cyclic-AMP-dependent formation of phosphorylase *a* and the enhanced activity of phosphorylase *b* as ATP breakdown. Eventually, if ischemia is severe enough, the rate of glycogenolysis will slow down; the mechanism is inhibition of glycolysis (discussed in the preceding section) with accumulation of glucose 6-phosphate which in turn inhibits the activity of phosphorylase *b*. Such regulation by phosphorylase *b* could be important after the early rise of tissue cyclic AMP in ischemia has returned to normal.

FUNCTION OF CARDIAC GLYCOGEN

By its breakdown to glucose compounds (glycogenolysis), cardiac glycogen is a potential source of myocardial energy; yet the oxygen uptake of the heart is so avid that the cardiac glycogen content would have to be extremely high and glycogenolysis extremely rapid for glycogen to be the major fuel of the heart over a long period. For short periods (for example, in experimental anoxia or right at the start of ischemia or when there is a severe work load), enough glycogen can (theoretically) be broken down rapidly enough to become a very transient and temporary source of energy. When cardiac glycogen breaks down, such glycogenolysis yields glucose 6-phosphate—also formed from glucose uptake. Whether glucose 6-phosphate is formed from glycogenolysis or from glucose uptake, its fate is either resynthesis to glycogen, or breakdown by glycolysis to pyruvate.

Many workers have thought that a measure of glycogen breakdown occurs with each cardiac cycle, but there is as yet no proof for this hypothesis. There is little advance beyond the view of Evans et al. [24] that glycogen is reserved for anoxemic emergencies such as the "fight or flight" reaction, which includes the abrupt onset of much increased heart work. Apart from these specific situations, the sequential cascades for glycogen breakdown (controlled chiefly by adrenergic stimulation) and glycogen synthesis (controlled chiefly by insulin) are far more complex than the limited physiologic use of glycogen appears to warrant. Possibly such complex mechanisms merely reflect the evolutionary inheritance of red heart muscle from the more primitive white skeletal muscle. It is equally possible that the complex mechanisms controlling glycogen synthesis and

breakdown might have a function as yet unknown. In skeletal muscle, glycogen undoubtedly plays a vital role by allowing skeletal muscle to function despite a minimal blood supply as may occur during intense isometric muscular activity. In the heart, such situations occur much more rarely because the heart muscle is so well oxygenated. Nevertheless, it seems that when there is a sudden severe spurt of work, very rapid glycogen breakdown within seconds may protect from an acute lack of fuel for the heart [25].

Lactate

COMPETITION OF LACTATE WITH OTHER SUBSTRATES FOR MYOCARDIAL OXYGEN UPTAKE

The uptake of lactate by the well-oxygenated heart can account for about 10% of the oxygen uptake of the heart of a resting, fasting person (table 14–1) and about 60% of the oxygen uptake during vigorous exercise. When lactate is infused into dogs, then lactate becomes a progressively more important fuel until, at 4.5 m*M* or more (levels reached during exercise), lactate can account for over 80% of the oxygen uptake of the heart [26].

There is some competition between lactate and free fatty acid for the myocardial oxygen uptake [27]; either can be a major fuel, depending on the blood levels (table 14–1). The probable mechanism whereby lactate decreases free fatty acid metabolism is by inhibition of activation by thiokinase [28]; the probable mechanism whereby free fatty acid inhibits lactate metabolism is by inhibition of the enzyme complex pyruvate dehydrogenase [29, 20].

PATHWAYS OF LACTATE

The uptake of lactate by the heart depends on a stereospecific transport mechanism [31]. The sarcolemma is not entirely freely permeable to lactate, and a "permease" has been postulated [32]. Once taken up, intracellular lactate is converted by lactate dehydrogenase to pyruvate, thereby joining the pyruvate derived from glycolysis.

LACTATE DEHYDROGENASE

The following reaction is freely reversible:

$$\text{lactate} + NAD^+ \rightleftarrows \text{pyruvate} + NADH + H^+$$

Thus, in conditions of adequate oxygenation and a high rate of lactate uptake, the equation proceeds toward pyruvate. In hypoxia, when NAD and H^+ accumulate and pyruvate cannot undergo dehydrogenation, the reaction proceeds toward lactate.

The myocardial activity of lactate dehydrogenase is high enough to make it unlikely that it could be a rate-limiting enzyme. There are five LDH isoenzymes, named in order of rapidity of electrophoretic migration; each isoenzyme is a tetrameric unit composed of four subunits of the H or M type, where H is the form predominating in the heart and M in skeletal muscle. The major interest in the isoenzymes stems from their liberation into the blood stream in patients with acute myocardial infarction. In clinical practice, the H isoenzyme is also known as alpha-hydroxybutyrate dehydrogenase because alpha-oxybutyrate can replace pyruvate as substrate to form alpha-hydroxybutyrate.

LACTATE DISCHARGE IN ISCHEMIA

The normal dog heart takes up lactate to the extent of about 30% of the arterial value [10]. When the heart is rendered ischemic, about 25% by mass must be ischemic before there is lactate discharge into the coronary sinus [10]. Such discharge is traditionally regarded as a good sign of myocardial hypoxia or ischemia [33]. Decreased lactate extraction (without actual discharge) is not a reliable indicator of ischemia because lactate uptake can be inhibited by free fatty acids [34].

There are unusual circumstances in which lactate discharge occurs from the heart in the absence of oxygen limitation: (a) the neonatal heart in situ, (b) states in which the extracellular fluid contains little or no lactate as in the isolated heart perfused with glucose as the only substrate, (c) the transplanted heart, (d) intermittently in some apparently normal awake dogs with chronically implanted coronary sinus catheters, and (e) in some apparently normal

patients (for references, see Opie [35]). Also, the burst of glycogenolysis, when mechanical work is suddenly increased, may liberate lactate [25]. In patients with thyrotoxicosis, lactate-producing angina can occur even in the presence of normal coronary arteries [36].

Pyruvate

The circulating concentration of pyruvate is usually very low, so that it only accounts for a small part of the myocardial oxygen uptake of the normal heart (table 14–1). There are no known physiologic conditions in which pyruvate becomes a major fuel of the heart. When, however, pyruvate is presented to the isolated heart in unphysiologically high concentrations, pyruvate can account for 42%–60% of the myocardial oxygen uptake [37] (for summary, see Opie [38]). The addition of free fatty acids decreases the decarboxylation and oxidation of pyruvate [37, 39].

FATES OF PYRUVATE

The major pathways of pyruvate are either aerobic oxidation via pyruvate dehydrogenase and the citrate cycle, or anaerobic conversion to lactate. Anaerobic conversion to lactate helps to convert back to NAD^+ the $NADH + H^+$ accumulating during anaerobic glycolysis (fig. 14–2) and is therefore an essential part of the anaerobic pathway. There is also a small anaerobic conversion to alanine by the transamination pathway. Aerobic oxidation of pyruvate requires first the activity of pyruvate dehydrogenase.

PYRUVATE DEHYDROGENASE

Pyruvate dehydrogenase is a multienzyme compound with a very high molecular weight (about four million) situated on the inner mitochondrial membrane; pyruvate reaches the enzyme from the cytosol probably by simple diffusion to be adsorbed to the mitochondrial membrane [40]. Pyruvate dehydrogenase can exist in either active or inactive form. Normally in the fed state only about 20% of the enzyme is in the active form, but increased provision of pyruvate from increased glycolytic flux can increase the activity up to 60%–90% [30]. Increased heart work increases the percentage of the active form, acting at least in part through changes in the redox state of the mitochondria (fall of NAD^+–NADH ratio, see Kobayashi and Neely [41]). Increased intramitochondrial calcium, as occurs with increased heart work, may also activate the enzyme [42] (for reservations, see Kobayashi and Neely [41]). Alteration of the activity of pyruvate dehydrogenase results from a phosphorylation–dephosphorylation cycle, which is similar to the cycle controlling glycogen phosphorylase *b* → *a* interconversion, but acts independently of cyclic AMP. Phosphorylation causes the enzyme to assume the inactive form; activity is restored only by dephosphorylation (and not by allosteric effectors as in the case of most other enzymes subject to phosphorylation–dephosphorylation). A kinase (pyruvate dehydrogenase kinase) phosphorylates and inactivates the enzyme. The kinase is activated by acetyl CoA and NADH which, therefore, inactivates pyruvate dehydrogenase; ADP, NAD^+, CoA, and pyruvate have the opposite effects, and activate.

Another regulatory mechanism is that the active form is subject to end-product inhibition by acetyl CoA and NADH. Thus when NADH falls, as with increased heart work, then flux through pyruvate dehydrogenase is accelerated [41]. Thus increased heart work has two effects. First, pyruvate dehydrogenase is activated. Secondly, active pyruvate dehydrogenase is stimulated by removal of end-product inhibition as NADH falls. Although changes in the mitochondrial ATP–ADP ratio might be expected during increased heart work, it is the cytosolic ATP–ADP ratio rather than the mitochondrial ratio which changes with increased heart work [43].

When the heart is provided with noncarbohydrate fuels (free fatty acids, ketones), pyruvate dehydrogenase is inactivated [30]. An important factor is that pyruvate dehydrogenase is strongly inhibited by NADH [44] which accumulates during the metabolism of fatty acids and ketones. In addition, noncarbohydrate fuels also inhibit the enzyme because they increase myocardial acetyl CoA and the ratio acetyl CoA–CoA [45]. NADH and acetyl

CoA in turn activate the kinase which phosphorylates and inactivates pyruvate dehydrogenase.

It might be supposed that pyruvate dehydrogenase would be inactivated during ischemia because of the accumulation of NADH. However, the concurrent fall of mitochondrial ATP and rise of ADP keep the enzyme active [46]. Hence the decreased flux through pyruvate dehydrogenase in anoxia and ischemia (figs. 14–2 and 14–3) probably represents inhibition of the active form of the enzyme.

Coordinated Control of Glycolysis

The idea that there is a coordinated control of flow through glycolysis and through pyruvate dehydrogenase receives support from the many conjoint metabolic signals which act both on phosphofructokinase and on pyruvate dehydrogenase. Closest coordination of control of glycolysis is possible when the same closely related signals enhance the activities of these two major enzymes, as at the acute onset of increased heart work. Then glycolysis is accelerated by changes in high-energy phosphate compounds and pyruvate dehydrogenase activity is accelerated by the decreased cellular NADH, by a fall in acetyl CoA, and possibly by an influx of Ca^{2+} into the mitochondria. Increased heart work also directly stimulates transfer of glucose across the cell membrane, possibly acting by the changes in energy status. A third effect of increased heart work is suggested by computer-calculated data [25]. It is proposed that the cytosolic free magnesium ion concentration increases as cytosolic Ca^{2+} rises and that glycolysis is stimulated at the level of phosphofructokinase and other enzymes.

In the case of addition of insulin, glucose uptake is stimulated to increase formation of the substrates of phosphofructokinase and hence to increase flow through glycolysis. If the consequences include an increased tissue pyruvate dehydrogenase may be activated [47]. If mitochondrial NADH–NAD^+ rises, as may occur from high rates of glycolytic flux in the absence of competing substrates, then pyruvate dehydrogenase may even be inactivated [41]. In contrast, insulin has little or no direct effects on pyruvate dehydrogenase except in severe experimental diabetes [48].

A third example of coordinated control is when the heart uses noncarbohydrate fuels such as fatty acids and ketone bodies; then phosphofructokinase is inhibited by a high level of citrate as result of high rates of citrate-cycle activity, while pyruvate dehydrogenase is both inhibited and inactivated probably by the increased NADH and the rising level of acetyl CoA. Thus the whole flux through glycolysis is much decreased.

There is one important stimulus, hypoxia, which accelerates glycolysis, but inhibits pyruvate entry into the citrate cycle. Hypoxia increases the activity of phosphofructokianse by changes in high-energy phosphates and by decreasing tissue citrate, whereas hypoxia allows the accumulation of NADH which inhibits active pyruvate dehydrogenase (see preceding section).

Free Fatty Acids

The importance of free fatty acids (FFA = nonesterified fatty acids = NEFA) as fuel for the human heart was originally stressed by the studies of Bing [49–51], who found that carbohydrate only accounted for a minor part of the oxygen taken up by the heart, with the rest coming from fatty acid. In 1961, Shipp et al. [52] found that free fatty acids inhibited the myocardial oxygenation of glucose. There has since been increasing emphasis on the role of free fatty acids as the major myocardial fuel [38, 53]. FFA inhibit the metabolism of glucose at several sites [30] and are the dominant fuel for the human heart especially in the fasted state. Clinical interest in the metabolism of FFA has been stimulated by recent evidence that FFA can in certain circumstances be toxic to the heart, and that FFA can promote the severity of ischemia in some experiments.

FREE FATTY ACID UPTAKE BY THE HEART: GENERAL FACTORS

The general factors determining the rate of uptake by the heart of FFA include: (a) the circulating concentration of FFA, (b) the circulating FFA–albumin molar ratio, (c) the barriers

at the level of the capillary wall, (d) the rate of transport across the cell membrane, (e) the rate of formation of acyl carnitine and the availability of carnitine, and (f) the rate of intracellular oxidation.

That the rate of removal of products of FFA metabolism by oxidation can influence the uptake of FFA by the isolated rat heart is suggested because: (a) there is a correlation between the rates of uptake and oxidation of FFA, and (b) intracellular FFA and intermediates such as acyl CoA accumulate when fatty acid oxidation is blocked by the addition of acetoacetate (see Menahan and Hron [54]) or by an alteration in the structure of the chain, and (c) there is accumulation of intracellular FFA when the circulating concentration is high and the oxidative capacity of the system is blocked (for references, see Opie [55]).

That there is release as well as uptake of FFA by the heart is shown by the release of FFA into the perfusate of the isolated heart when the external FFA concentration is low, by studies in normal man [56]. and by the kinetics of FFA uptake and release from the perfused dog heart in situ [28]. There is, however, no simple equilibrium because in vivo the pattern of fatty acid in the intracellular and extracellular spaces is not the same [57].

When the heart is perfused with equimolar mixtures of fatty acids, the molecular structure of fatty acid chain may regulate FFA uptake [58]. Differences between the various fatty acids may be explained by the varying affinity of the carrier albumin for the fatty acid, and by the different intracellular rates of disposal. But only in the case of erucic acid (see later) does the structure of the fatty acid appear to play a dominant role in regulating the metabolic patterns.

TRANSPORT OF FFA ACROSS THE CELL MEMBRANE

Contrary to the case of glucose, transport across the cell wall does not involve any hormonal-sensitive step, nor is it accelerated by anoxia [58]. The rate of transport of labeled FFA across the sarcolemmal membrane is rather similar to the rate across the capillary membrane, suggesting that transport across each membrane is simply a physical process [28]. Possibly the transport process involves the dissolution of the undissociated molecule in the capillary or cell wall membrane.

INTRACELLULAR FFA AND INTRACELLULAR BINDING PROTEIN

The measured FFA values in the heart cell are very much lower than those in the circulation [59]. There is an intracellular protein which binds free fatty acid and has a high affinity for FFA [58]. At the onset of increased heart work, the tissue content of FFA falls abruptly together with increased FFA uptake, suggesting that it is the lower levels of intracellular FFA which establish a concentration gradient for diffusion into the cell. The sequence appears to be:

albumin-bound FFA → free circulating FFA → unionized form crosses capillary and sarcolemmal membranes → intracellular free FFA → some activated and metabolized; some remains bound to intracellular binding protein.

SUMMARY OF INTRACELLULAR PATHWAYS

The intracellular processes involved in fatty acid oxidation are complex (fig. 14–8) and include the activation of FFA to acyl CoA, the transfer of extramitochondrial acyl CoA to intramitochondrial acyl CoA with the participation of the carnitine system, and subsequent liberation of acyl CoA within the intramitochondrial space with beta-oxidation to acetyl CoA which can then enter the citrate cycle for further oxidation. ATP, synthesized in the mitochondria, is transported to the cytoplasm by a translocase enzyme which is inhibited by an accumulation of acyl CoA, as occurs during ischemia. Activated intracellular FFA (acyl CoA), which is not oxidized, can form triglyceride.

ACTIVATION OF INTRACELLULAR FFA

Intracellular FFA can be activated by a reaction requiring ATP, reduced CoA, and Mg^{2+} (fig. 14–6). Using palmitate as an example:

$$\text{palmitate} + \text{CoA} + \text{ATP} \xrightarrow{Mg^{2+}} \text{palmityl CoA} + \text{AMP} + \text{PPi}$$

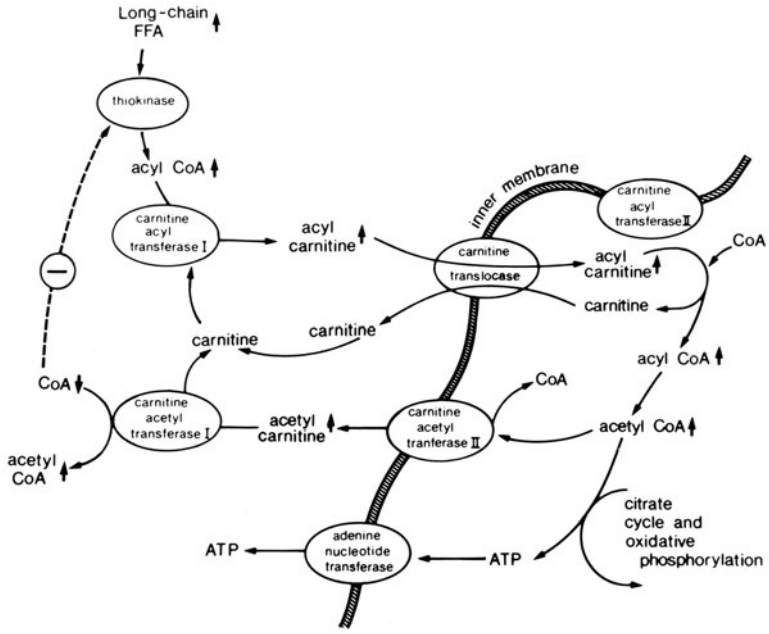

FIGURE 14–6. Scheme to show steps thought to be required to transport extramitochondrial acyl CoA to within the mitochondrion. The inner membrane represents the permeability barrier. The inner-mitochondrial enzymes are carnitine acyl transferase II, carnitine translocase (= carnitine acyl carnitine translocase,), carnitine acetyl transferase II, and adenine nucleotide transferase. Such enzymes are required in transporting acyl carnitine inward and carnitine, acetyl carnitine, and ATP outward. The enzymes canitine acyl transferase I and carnitine acetyl transferase I are held to be located on the outer part of the inner-mitochondrial membrane. The two carnitine acyl transferases may be in close physical opposition to the carnitine translocase. Note that the evidence for two carnitine acetyl transferases is disputed. The proposed reactions to an increased supply of blood free fatty acids are shown as an increase (↑) or decrease (↓) of intermediates. Modified from Opie [85] with permission of the *Am Heart J.* For details, see Opie [85].

Thus long-chain fatty acid is converted to long-chain acyl CoA. Theoretically reversible, the presence of the enzyme pyrophosphatase breaks down the pyrophosphate and effectively makes the reaction irreversible:

$$PPi + H_2O \rightarrow 2\ Pi$$

Thus, "once the molecule has entered this reaction, it must proceed to be either esterified or oxidized" [28]. The reaction rate is decreased by accumulation of acyl CoA and AMP, which may be limiting in, respectively, ischemia and anoxia. During provision of excess circulating FFA, cytosolic CoA falls through a series of reactions involving carnitine. During increased heart work, activation of citrate synthase [60] converts acetyl CoA to citrate and CoA. The increased CoA would help increase the rate of the fatty acid activation to help increase uptake of FFA required as fuel [61].

ACYL CoA AND CARNITINE

Acyl CoA has two possible fates: (a) transport into the mitochondria and (b) formation of triglyceride and other glycerides. The former mechanism depends on carnitine, which is a relatively simple compound of widespread distribution with some properties resembling those of a vitamin. The structure is:

$$(CH_3)_3\ N^+\ CH_2\ CH\ (OH).\ CH_2.\ COO^-$$

Thus carnitine is betaine gamma-amino, beta-hydroxybutyric acid, and the naturally occurring form is (−). How does carnitine act? Fritz

[62] made the fundamental suggestion that the "presence of carnitine in muscle and other tissue may facilitate the transfer of long-chain fatty acids to the enzymatically active intramitochondrial sites for fatty acid oxidation." Thereafter it was found that carnitine could be incorporated into the compound palmityl carnitine (the C16 acyl carnitine compound) and the requirements for the reaction did not include ATP nor CoA (i.e., the reaction differed fundamentally from fatty acid activation). Carnitine reacted with acyl CoA in a reaction catalyzed by the enzyme acyl carnitine transferase. Taking palmityl CoA as an example:

$$\text{carnitine} + \text{palmityl CoA} \xrightarrow{\text{carnitine acyl transferase}} \text{palmityl carnitine} + \text{CoA}$$

Fritz and Yue [63] made the further proposal that "palmityl carnitine may function as a carrier to transport the acyl group from acyl CoA past mitochondrial barriers to the fatty acid oxidase system." They proposed that acyl CoA existed in two pools, one within the mitochondria and one in the cytoplasm. These pools were separated by a barrier (which was later established as the inner-mitochondrial membrane) and that acyl carnitine, but not acyl CoA, could cross that barrier. Those predictions were remarkably accurate. They also predicted that there would have to be two carnitine acyl transferase enzymes, the one accessible to the cytoplasmic pool of acyl CoA which would regulate the reaction just described. The other enzyme would be accessible to the intramitochondrial pool of acyl CoA to regulate the reaction:

$$\text{acyl carnitine} + \text{CoA} \rightarrow \text{intramitochondrial acyl CoA} + \text{carnitine}$$

or taking palmitate as an example:

$$\text{palmityl carnitine} + \text{CoA} \rightarrow \text{palmityl CoA} + \text{carnitine}$$

Later the use of specific antibodies showed the existence of carnitine transferases localized respectively to the outer portion of the inner-mitochondrial membrane (carnitine acyl transferase I) and to the inner portion of the membrane (carnitine acyl transferase II; for references see Hoppel and Tomec [64] and Kopec and Fritz [65]). The activity of the above pathways would lead to liberation of carnitine within the mitochondria.

Ramsay and Tubbs [66] used double-labeled carnitine and measured the rates of carnitine uptake and export into and out of the heart mitochondria. They found a 1:1 ratio and suggested a carnitine–acyl-carnitine exchange mechanism across the inner mitochondrial membrane. Pande [67] and Pande and Parvin [68] described a carnitine–acyl-carnitine translocase system, located on the inner-mitochondrial membrane, and with properties different from those of the acyl transferase.

Thus the vital steps can be summarized as follows, using figure 14–6 as a guide:

1. Thiokinase activity results in fatty acid activation with formation of extramitochondrial acyl CoA.
2. Carnitine acyl transferase-I activity results in formation of extramitochondrial acyl carnitine from extramitochondrial acyl CoA.
3. The activity of the carnitine–acyl-carnitine translocase transfers extramitochondrial acyl carnitine to within the mitochondrial space.
4. The activity of carnitine acyl transferase II allows intramitochondrial acyl carnitine to react with CoA, to liberate intramitochondrial acyl CoA and carnitine.
5. Intramitochondrial acyl CoA enters the fatty acid oxidation spiral.
6. The activity of the carnitine–acyl-carnitine translocase system transfers intramitochondrial carnitine to without the mitochondria.

The above scheme explains how extramitochondrial FFA are transferred to acyl CoA within the mitochondria. The next step is beta-oxidation with the ultimate production of acetyl CoA which enters the citrate cycle. At this level, carnitine plays an additional, more subtle, and less immediately obvious role.

ACETYL CoA AND CARNITINE

The proposal is that transfer of acetyl carnitine across the mitochondrial membrane in either

direction can help to couple rates of cytosolic fatty acid activation to mitochondrial oxidation rates [69]. Thus when excess fatty acids are provided, mitochondrial acetyl CoA rises so that cytosolic acetyl carnitine increases and more cytosolic acetyl CoA is formed with a fall in cytosolic CoA; the rate of fatty acid activation, therefore, falls (this sequence is shown in fig. 14–6). When mitochondrial oxidation increases, as during increased heart work, this series of reactions is thought to be reversed so that fatty acid activation is now enhanced.

ACYL CoA INHIBITION OF ADENINE NUCLEOTIDE TRANSLOCASE

Pande and Blanchaer [70] made the fundamental discovery that acyl CoA could instantly and reversibly inhibit heart mitochondria from using external ADP, which is required for oxidative phosphorylation to proceed. Concentrations of long-chain acyl CoA as low as 2-4 μmol/l caused these effects, which could be distinguished from the many other inhibitions also caused by long-chain acyl CoA, but more probably due to a detergent effect. The inhibitory effect of acyl CoA resembled that of atractyloside, a known inhibitor of the adenine nucleotide translocase [71]. Klingenberg's group described how adenine nucleotide translocase acts by a "swing-door" mechanism to permit entry of ADP and exit of ATP from the mitochondria ("ping-pong" model). Continued operation of this translocase mechanism is essential for the maintenance of normal myocardial energy metabolism.

In 1975, Shug et al. [72] showed that myocardial ischemia, produced by coronary artery ligation in the dog, caused the twin changes of accumulation of long-chain acyl CoA and decreased activity of the adenine nucleotide translocase. A physiologic increase in myocardial acyl CoA could be achieved by perfusion of the heart with FFA alone [73, 74], or by provision of ketone bodies, or by prolonged starvation, or by alloxan diabetes; conversely, provision of carbohydrate in the form of glucose plus insulin could decrease myocardial acyl CoA [73].

Currently the outstanding question is whether the inhibition of the translocase induced by acyl CoA has pathophysiologic significance as questioned by the recent studies of Lochner et al. [75] and La Noue et al. [76]. A further question is whether the Klingenberger translocase model needs modification, because recent evidence suggests the formation of a carrier–nucleotide–ternary complex [77] which is inconsistent with the earlier ping-pong model (ATP in, ADP out).

BETA-OXIDATION

Beta-oxidation converts acyl CoA to acetyl CoA, passing through the fatty acid oxidation spiral which removes two carbon fragments as acetyl CoA from the carboxyl ($-COOH$) end of the chain. The fatty acid oxidation spiral is the basic mechanism of beta-oxidation. The enzymes of beta-oxidation are loosely organized into a multienzyme complex in which the intermediates never leave the complex except for entering and departing. Thus the products of each reaction do not leave the microenvironment of the enzyme complex, but are simply displaced by the arrival of fresh substrates for that reaction, and then in turn move on to the next enzyme in the spiral [61]. The basic reactions are:

1. Removal of two hydrogens from acyl CoA, with the conversion of FAD to $FADH_2$ and to yield the alpha-beta-unsaturated acyl CoA.
2. Regaining of a hydroxyl group, derived from water, to give beta-hydroxyacyl CoA.
3. Then follows an important dehydrogenase reaction, converting NAD^+ to NADH, and also converting the hydroxyl group to a ketone group (similar to the formation of pyruvate from lactate):

$$\text{beta-hydroxyacyl CoA} + NAD^+ \rightarrow \text{beta-ketoacyl Co} \pm NADH + H^+$$

4. Finally, the beta-ketoacyl compound reacts with CoA to split off two carbons as acetyl CoA:

$$\text{beta-ketoacyl CoA} + \text{CoA} \rightarrow \text{acetyl CoA} + (\text{an acyl CoA chain shortened by 2 carbons})$$

5. The shortened acyl CoA chain enters step 1 for a further turn of the spiral.

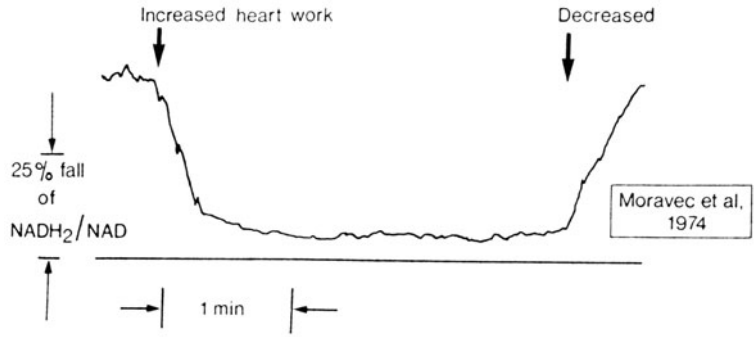

FIGURE 14–7. Effect of increased heart work in isolated rat heart in increasing the fluorescence emission in the direction of NAD so that the ratio NAD/$NADH_2$ rises. The conditions selected are such that the fluorescence changes reflect chiefly the mitochondrial NAD/$NADH_2$ ratio. $NADH_2/NAD = (NAD^+)/(NADH)(H^+)$. Modified from Moravec et al. (1974) by permission of Academic Press.

During *increased heart work,* the mitochondria become more oxidized (fig. 14–7) [60] and intramitochondrial levels of $NADH_2$ and presumably of $FADH_2$ fall, and reactions 1 and 3 are accelerated; there is an increased turnover of the whole fatty acid oxidation spiral [74]. The following events are thought to occur: Mitochondrial acetyl CoA falls, acetyl carnitine falls (probably to replace the mitochondrial acetyl CoA), carnitine rises (as acetyl carnitine forms acetyl CoA), and acyl carnitine increases (as cytosolic carnitine forms), to help transport acyl CoA across the mitochondrial membrane. As cytosolic acetyl carnitine is formed from cytosolic acetyl CoA, cytosolic CoA forms and the rate of fatty acid activation is enhanced.

Conversely, *during deprivation of oxygen,* intramitochondrial NADH rises [60] and so probably does $FADH_2$. The basic defect is probably impaired beta-oxidation due to decreased electron transport rather than diminished fatty acid uptake, fatty acid activation, or transfer to within the mitochondria [78]. Hence it may be inferred that, during hypoxia or ischemia, $NADH_2$ rises more rapidly than $FADH_2$ so that the rate of the FAD-dependent step of the cycle (reaction 1 above) exceeds the rate of the NAD-dependent step (reaction 3). Intermediates of fatty acid metabolism accumulate, including the hydrogen-containing beta-hydoxy–fatty-acid compounds [78] and acyl CoA itself. These observations suggest that oxidation of beta-hydroxyacyl CoA (reaction 3 above) is the rate-limiting step in fatty acid beta-oxidation by the oxygen-deficient heart.

FORMATION OF TRIGLYCERIDE AND GLYCERIDE

Triglyceride can be formed from acyl CoA and alpha-glycerophosphate, the latter derived from glycolysis, by the process of *esterification,* as follows:

(a) acyl CoA + alpha-glycerol-P
$\rightarrow$ acyl glycerol-P + CoA

(b) acyl glycerol-P + CoA
$\rightarrow$ diacylglycerol-P (phosphatidic acid) + CoA

(c) diacylglycerol-P
$\rightarrow$ diacylglycerol (i.e., diglyceride) + Pi

(d) diglyceride + acyl CoA $\rightarrow$ triglyceride + CoA

When the overall equation for triglyceride formation from FFA is written out, and allowance is made for the changes, we have [21]:

$$3\ \text{palmitate}^{1-} + 3\ MgATP^{2+} + 3\ CoA^{4-} \rightarrow 3\ \text{palmityl-CoA}^{4-} + 3\ AMP^{2-} + 6\ Pi^{2-} + 3\ H^+ + 3\ Mg^{2+}$$

$$\text{alpha-glycerol-3-phosphate}^{2-} + 3\ \text{palmityl-CoA}^{4+} \rightarrow \text{triglyceride} + 3\ CoA^{4-} + Pi^{2-}$$

Details of the enzymes of esterification are given by Monroy et al. [79]. For every mole of triglyceride synthesized, there is the production of three protons, occurring at the stage of fatty acid activation. Continued triglyceride

turnover in ischemia may, theoretically, be proton generating and be potentially harmful (see next section). Increased myocardial triglyceride found in severe experimental diabetes mellitus is probably accounted for by increased uptake of circulating ketone bodies with inhibition of fatty acid oxidation [54].

CARDIAC LIPOLYSIS

Lipolysis in the heart is under the influence of a hormonally sensitive lipase (fig. 14–3). When the heart is deprived of external fuels, there is lipolysis of endogenous triglycerides to provide energy [57]. However, not all the triglyceride is available for such energetic purposes because about one-fifth remains even when the heart is exhausted by substrate depletion. For the normal heart in situ, receiving an adequate substrate supply, there is no evidence at all to suggest that endogenous lipid is an energy source with the possible exception of very intense exercise or prolonged fasting. There is indirect evidence for the existence of a "triglyceride–FFA cycle" (see Opie [80] and Gevers [21]), the turnover of which is thought to be increased in alloxan diabetes and in ischemia (fig. 14–3). The proposed metabolic pathways can be summarized as:

intracardiac FFA → intracardiac acyl CoA → acyl CoA combines with alpha-glyerophosphate → glyceride chiefly triglyceride is formed → triglyceride breaks down under the stimulus of a catecholamine-sensitive lipase → intracardiac glycerol and FFA form → extra cardiac glycerol and FFA form → but intracardiac FFA recombines with intracardiac alpha-glycerophosphate derived from glycolysis to remove triglyceride

There are several lipases in the heart [81] which are cyclic-AMP sensitive [82], which explains the dose-dependent enhancement of lipolysis in the heart by catecholamines [83]. However, insulin does not block catecholamine-induced lipolysis in the heart, unlike the situation in adipose tissue [82]. The neutral lipase is inhibited by free fatty acids and acyl CoA [84]; the inhibitory concentration of the former is close to normal myocardial values [59] so that physiologic regulation by end-product inhibition is possible. The significance of inhibition of lipolysis by acyl CoA is hard to assess, because of the rather high concentration needed (see Opie [85]). Increased activity of the lipase in alloxan diabetes or ischemia could be accounted for by stimulation by the increased levels of acyl carnitine [84].

That lipolysis could give rise to FFA within the heart with the same effects of external FFA is suggested because stimulation of endogenous lipolysis by adrenaline increases the myocardial oxygen consumption in a way similar to the effects of exogenous FFA [86]. That the lipase system is sensitive to cholinergic stimulation is suggested because triglyceride accumulates after such stimulation [87].

"FATTY ACID TOXICITY", ACYL CARNITINE, AND LYSOPHOSPHOGLYCERIDES

Oliver and his colleagues [88] made the important observation that patients with acute myocardial infarction with complications were more likely to have high blood FFA levels than other patients and that the mortality appeared to be related to the FFA level. In experimental developing myocardial infarction, there is still some continued uptake of FFA, albeit at a reduced rate [89]. The significance of this continued uptake of FFA lies in the possibility of accumulation of FFA intermediates "driving" the oxygen consumption of those mitochondria still receiving oxygen [90, 91], thereby aggravating ischemia.

Further evidence for "fatty acid toxicity" is provided by the causation of arrhythmias [92], depression of contractility [93], and the aggravation of enzyme release (fig. 14–8) [94]. In some preparations, excess FFA can have toxic effects even in the absence of oxygen deprivation [35]. The observations on arrhythmias have been contested (e.g., Opie et al [10]), and many of the observations were made at highly unphysiological FFA levels with extremely high FFA–albumin molar ratios (see Opie [80]). In other systems, "toxic" effects can be found with physiologic fatty acid levels (fig. 14–11). The earlier biochemical evidence on the effects of accumulation of acyl CoA (as already discussed) provided a reasonable basis for "fatty acid toxicity", although recently doubt has been cast on the significance of inhibition

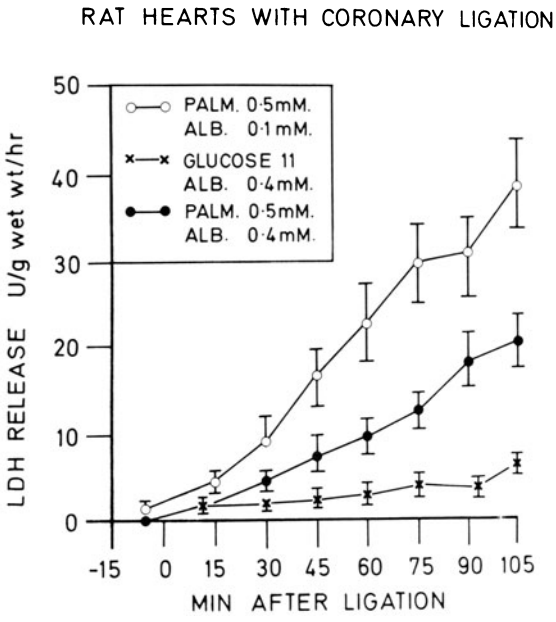

FIGURE 14–8. Rates of release of lactate dehydrogenase (LD) in isolated pumping rat heart with coronary artery ligation 15 min after the onset of recirculation perfusion. Note that (a) palmitate-perfused hearts have higher rates of LD release than do glucose-perfused hearts, (b) an increased albumin concentration decreases lactate dehydrogenase release in palmitate-perfused hearts, and (c) lactate dehydrogenase release is approximately linear. Data based on De Leiris and Opie [94].

of the mitochondrial translocase by acyl CoA (see earlier) so that attention is turning to the possible role of acyl carnitine. Whether *carnitine* itself may modify myocardial ischemic injury probably depends on whether or not circulating FFA are high, because L-carnitine is able to reduce FFA uptake by the mildly ischemic myocardium and to reduce levels of acyl CoA [95].

Acyl carnitine may be involved. In the normal heart, the cytosolic concentration of this intermediate is very low, being estimated at 25 μmol/l [96] with none in the mitochondria. During ischemia the concentration in both cytosol and mitochondria rises to about 2000 μmol/l. Such increases are very much more than those undergone by acyl CoA. Similarly, during perfusions with high exogenous FFA, long-chain acyl CoA increases only by 1½ times, but acyl carnitine nearly four times [74]. Long-chain acyl carnitine inhibits Na^+–K^+ ATPase activity at concentrations likely to be present in the ischemic tissue and the inhibition is much more marked than in the case of equimolar acyl CoA [97]. However, acyl carnitine does not inhibit the adenine translocase [70].

Lysophosphoglycerides are membrane-active fatty acids that are released from the phospholipids of the sarcolemma and other membranes during ischemia. The metabolic pathways and proposed regulatory signals in ischemia are shown in figure 14–9. Especially accumulated lysophosphatidyl choline (LPC) has arrhythmogenic properties [98, 99]. These proposals are controversial, although well argued [99]. If correct, there would be a lipid vicious circle in ischemia:

ischemia → membrane phospholipids
→ lysophosphoglycerides → increasing membrane damage
→ increasing ischemia

FREE FATTY ACIDS: CRITICAL FEATURES

Free fatty acids (FFA) are the major myocardial fuel of the normal heart, especially in the fasted state, and are able to inhibit the metabolism of glucose. FFA metabolism can in turn be inhibited by a high blood lactate, as occurs during exercise. That part of the FFA taken up which is not oxidized can form triglyceride and myocardial structural lipids, the latter by changes in the degree of saturation and chain length. Generally the heart does not synthesize lipid from glucose, nor from other nonlipid sources.

In ischemia the position is very complex. For example, in the first hours of an acute myocardial infarction, circulating FFA may be very high [100]. When such excess FFA is provided to the myocardium, the rate of uptake exceeds the rate of disposal (fig. 14–7) and intermediates of lipid metabolism such as intracellular FFA, acyl CoA, and acyl carnitine accumulate; these changes occur despite the effect of ischemia itself in decreasing FFA uptake (fig. 14–3) and in decreasing the oxidative contribution of FFA relative to that of glucose in the ischemic tissue. At least some of the lipid intermediates might be derived from endogenous li-

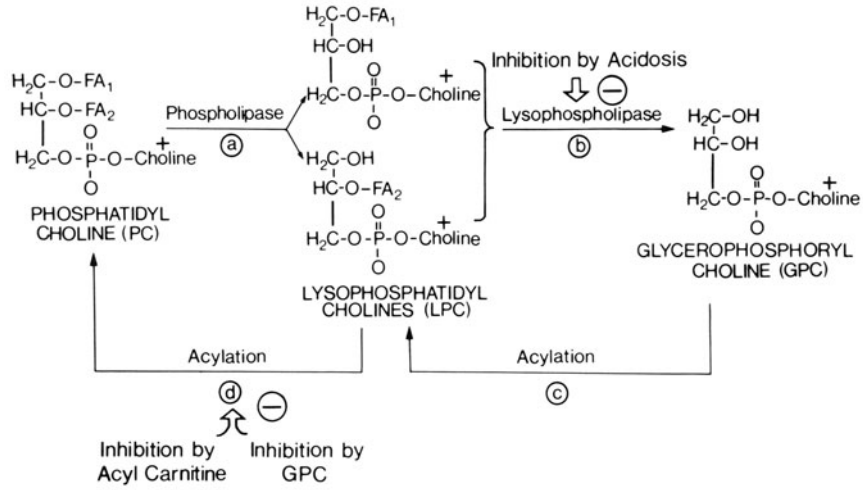

FIGURE 14–9. Pathways of synthesis of major phospholipid compounds. In ischemia, lysophosphatidyl cholines may accumulate because of inhibition of lysophospholipase by acidosis (*b* on figure) and because pathway *d* is inhibited by accumulated acyl carnitine and glycerophosphoryl choline. Modified from Corr et al [99] with permission.

polysis (fig. 14–3). The exact mechanism whereby these lipid intermediates exert their "toxic" effect still remains to be clarified. In the case of accumulated lysophosphoglycerides (derived from membrane phospholipids), an arrhythmogenic potential has been found [98, 101]. Derangements of fatty acid metabolism could, therefore, make a substantial contribution to myocardial ischemic injury (for review, see Katz and Messineo [102]).

Ketone Bodies

There is no evidence that ketone bodies are ever a major substrate of the normal heart human. In the postabsorptive or after an overnight fast, when the circulating ketone concentration is about 0.1–0.3 m*M*, the uptake of ketones can account for only 2%–9% of the total myocardial oxygen uptake during rest, and for even less during exercise [51, 103]. Even in fasting adult diabetic patients deprived of insulin for 24 h or more, ketones can account for only 10% of the total oxidative metabolism of the heart [104]. It is, however, anticipated that ketones may contribute significantly to the energy metabolism of the heart in severe diabetic ketosis. Furthermore, when the isolated heart is perfused with both ketone bodies and FFA, then the FFA taken is diverted away from oxidation toward formation of triglyceride [54].

In anoxia, the uptake of acetoacetate is converted to beta-hydroxybutyrate (fig. 14–2) [60]; this, however, has not proved a practical way of indirectly assessing the rate of formation of mitochondrial NADH in coronary sinus studies.

Energetics of the Normal Heart

Current knowledge of myocardial metabolism is a direct result of the pioneering work of Bing [49, 50], who introduced coronary sinus catheterization in man. In general, the isolated heart can use virtually any exogenous substrate for its energy metabolism. However, the uptake of amino acids and of ketone bodies in vivo is generally limited by low circulating concentrations, and there is a "threshold" below which glucose will not be taken up. The uptake of glucose is increased by hyperglycemia and/or insulin. Thus, when there is forced feeding of glucose plus insulin, the myocardial respiratory quotient approaches 1, and carbohydrate is the major fuel. After fasting, free fatty acids are the major fuel. During exercise, when

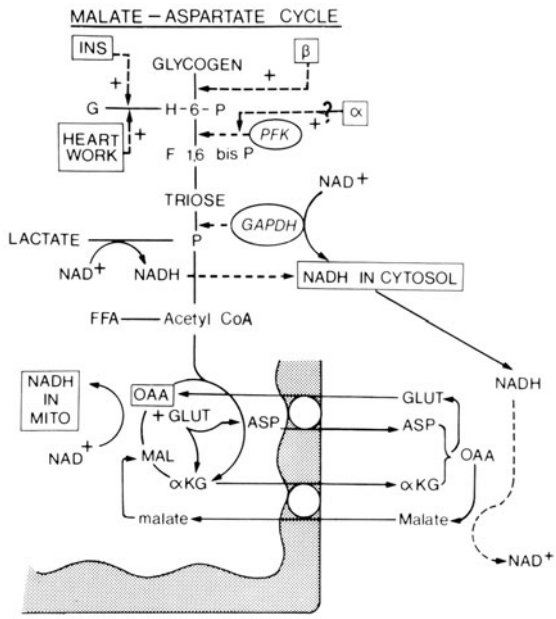

FIGURE 14–10. The malate–aspartate cycle: OAA, oxaloacetate; Glut, glutamate ASP, aspartate; Mal, malate; αKG, alpha-ketoglutarate. For other abbreviations see figure 14–1 legend. From Opie [140] by permission of Grune and Stratton.

circulating lactate levels are high, lactate extraction is increased and lactate becomes the most important fuel. In addition, Lassers et al. [56] have shown by very careful measurements that triglyceride can account for about 14% of the basal oxygen uptake of the human heart.

Some of the major factors influencing variations in the substrate uptake are shown in table 14–1. First, the spontaneous elevation of free fatty acids (FFA) in the blood, which occurs during fasting, leads to inhibition of glucose uptake and oxidation. Conversely, the decrease in blood levels of FFA during glucose and insulin administration leads to decreased oxidation of FFA and increased oxidation of glucose. The inhibitory effect of fatty acids on glucose uptake and glycolysis constitutes the basis for part of the "fatty acid–glucose cycle", first described by Randle et al. [105]; the cycle is completed by the effect of the administration of glucose and insulin in reducing the blood concentration of free fatty acid and thereby decreasing the uptake of free fatty acids by the heart

PRODUCTION OF NADH

Whatever the original substrate taken up from the coronary circulation, in each case there are pathways of substrate "simplification" to convert the original substrate ultimately to acetyl CoA which can then enter the citrate cycle. In the process there are a variable number of dehydrogenations, which split off 2 H units from the substrate and reduce NAD^+ to ($NADH + H^+$), i.e., NAD to $NADH_2$; further dehydrogenations in the citrate cycle produce more NADH. The reduction of FAD to $FADH_2$ also occurs, but is of much less quantitative importance. From $NADH_2$ ($NADH + H^+$), the reducing equivalents can pass through the electron transmitter chain to produce ATP and, ultimately, to link with oxygen atoms to form water.

When $NADH + H^+$ (or $FADH_2$) is produced within the mitochondrial space, then there is ready access to the electron transmitter chain (located within the mitochondrial space); when $NADH + H^+$ is produced extramitochondrially, then there must be provision for such $NADH + H^+$ to be transported into the mitochondria, or else accumulation of $NADH + H^+$ in the cytosol will inhibit the pathways of glycolysis (at the level of glyceraldehyde 3-phosphate dehydrogenase activity), and the uptake of lactate (which requires NAD^+ for conversion to pyruvate), so that only free fatty acids could act as fuel for the heart. Such cytosolic NADH is formed either by (a) glycolysis at the stage of glyceraldehyde 3-phosphate dehydrogenase, or by (b) conversion of lactate taken up from the circulation to pyruvate before oxidation.

MALATE–ASPARTATE SHUTTLE

During oxidative conditions, the chief mechanism for transfer of extramitochondrial NADH to intramitochondrial NADH is by the malate–aspartate shuttle (fig. 14–10). (During anaerobic conditions, lactate cannot be taken up and conversion of cytosolic pyruvate to lactate disposes of glycolytically produced NADH.) Malate and oxaloacetate occur both in cytosol and

in the mitochondrial space, as does the enzyme malate dehydrogenase which interconverts the two compounds:

$$\text{oxaloacetate} + \text{NADH} + \text{H}^+ \rightleftarrows \text{malate} + \text{NAD}^+ \quad (14.8)$$

During production of NADH + H^+ by glycolysis, oxaloacetate in the cytosol is converted to malate with the utilization of NADH + H^+ (the re-formation of NAD^+ allows glycolysis to proceed). Malate can pass into the mitochondrial space as part of a complex transport system which "exports" alpha-ketoglutarate [106]. Once within the mitochondrial space, malate will re-form oxaloacetate to enter the *citrate cycle;* $NADH_2$ (NADH + H^+) also re-forms and is accessible to the electron transmitter chain so that 3 ATP are formed for every 2 H entering.

$$\text{malate} + \text{NAD} \rightarrow \text{oxaloacetate} + \text{NADH} + \text{H}^+ \quad (14.9)$$

$$\text{NADH} + \text{H}^+ \rightarrow \text{electron transmitter chain} \rightarrow 3\ \text{ATP} \quad (14.10)$$

The mitochondrial oxaloacetate formed from malate forms alpha-ketoglutarate and aspartate, via aspartate aminotransferase; the alpha-ketoglutarate leaves the mitochondrial space in exchange for malate, while the aspartate is transported to the extramitochondrial space [107] in exchange for uptake of glutamate. A recent model for glutamate–aspartate exchange proposes that the rate-limiting step is the rate of transport of a negatively charged aspartate-carrier complex across the mitochondrial membrane while glutamate is released from its binding site to the carrier; a simple "ping-pong" mechanism seems unlikely [108]. Thus the earlier idea of a glutamate–aspartate "antiporter" [109] is supplanted by a "translocator". Once in the cytosol, aspartate reacts with alpha-ketoglutarate to re-form oxaloacetate and glutamate. The oxaloacetate reenters equation 14.8 above, and the glutamate enters the mitochondrial space in exchange for aspartate; here too an "antiport" system is proposed.

Maximal possible rates of malate transport are about 40–45 nmol/min/mg mitochondrial protein, or about 4 μmol/min/g wet weight of heart [107, 110] and about double those required to cope with maximal rates of glucose oxidation even of the "working" isolated rat heart, even in the presence of insulin (compare data of Opie et al. [10] with those of Puckett and Reddy [110]). Kobayashi and Neely [111] found similar rates of peak glycolytic flux in their model, which also means that the maximal capacity of the malate–aspartate system is not limiting for disposal of cytosolic NADH (fig. 14–12). Noakes [112] changed the mechanics of the perfusion system and found peak rates of glycolysis of 5.5 μmol/g wet weight/min compared with the 3.3 μmol/g/min of Kobayashi and Neely [111]. Peak rates of glycolysis in isolated hearts at peak rates of work, therefore, exceed the peak capacity of the malate–aspartate system, and alternate means of disposal of cytosolic NADH are required. First, some glycolytic flux can form lactate even in aerobic conditions during such very high rates of heart work; secondly, the alpha-glycerophosphate shuttle may play a role.

GLYCEROPHOSPHATE SHUTTLE

The route of disposal of cytosolic NADH in many tissues is entry into mitochondria by way of the alpha-glycerophosphate (alpha-GP) shuttle:

$$\text{NADH} + \text{H}^+ + \text{DHAP} \rightleftarrows \text{NAD}^+ + \text{alpha-GP}$$

under the influence of alpha-GP dehydrogenase and where DHAP = dihydroxyacetone phosphate. The alpha-GP enters the mitochondria to be oxidized by alpha-GP oxidase. DHAP re-forms as does $FADH_2$; the former is transported outward, the latter enters the respiratory chain (fig. 14–11). It has been difficult to assess the capacity of this system for transport of $NADH_2$ in the heart and it is generally thought that the malate–aspartate system is dominant in transport of NADH. The chief reason for this conclusion is the relatively low rates of activities of the enzyme alpha-GP dehydrogenase [113].

ENERGY PRODUCTION FROM VARIOUS SUBSTRATES

When *glucose* is the source of glycolysis, the whole glycolytic path uses 2 ATP and produces 4 ATP, i.e., the net production is 2. When

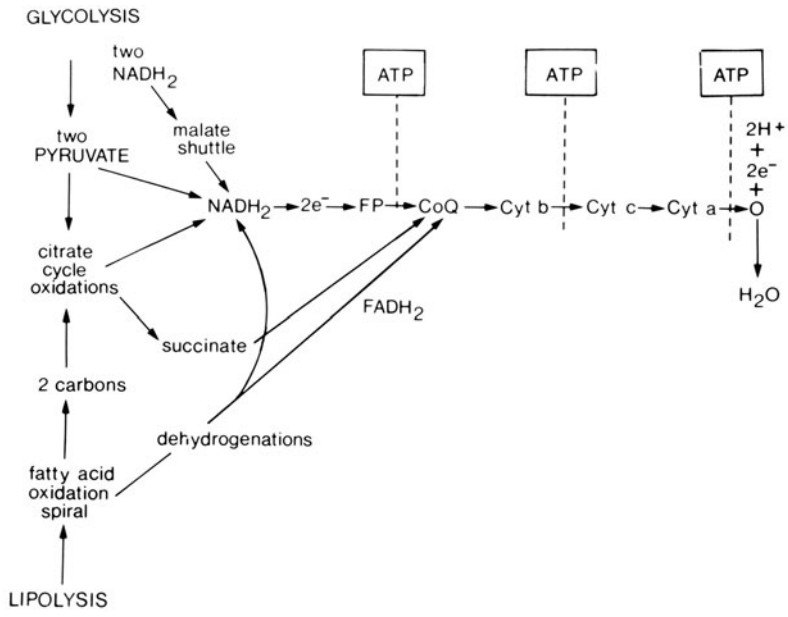

FIGURE 14–11. Patterns of aerobic metabolism with intramitochondrial production of ATP.

glycogen is the source, ATP production is 3 per glucose molecular passing through glycolysis. An important point is that glycolytic ATP will be made whenever hexosephosphates are converted to pyruvate even during oxidative metabolism when pyruvate enters the citrate cycle via acetyl CoA. The major source of energy from either glucose or glycogen lies in the citrate cycle with ultimate conversion of pyruvate to Co_2 with the formation of intramitochondrial NADH.

Each molecule of *lactate* fully oxidized yields 18 molecules of ATP, of which 3 molecules result from the extramitochondrial production of NADH as lactate is converted to pyruvate; the further 15 ATP are the standard result of the further oxidation of pyruvate.

Although *pyruvate* is an insignificant fuel in absolute terms, both glucose and lactate only produce the major part of their energy after conversion to pyruvate. Pyruvate dehydrogenation produces 1 molecule of NADH which will give rise to 3 ATP molecules; the further 12 molecules are produced by one turn of the citrate cycle.

Fatty acid activation uses up 1 ATP per molecule. Taking the example of palmitate, seven turns of the fatty acid oxidation spiral will produce 7 $NADH_2$ = (NADH + H^+) and 7 $FADH_2$, all of these being intramitochondrial. The former will produce 21 ATP, the latter 14 ATP. Finally, 8 acetyl CoA will produce 96 ATP (12 ATP per acetyl CoA passing through the citrate cycle), with an overall energy yield of 129 ATP per palmitate molecule.

Acetoacetate, when ultimately converted to 2 acetyl CoA, will have the usual yield of 24 ATP when ultimately oxidized. However, the simultaneous conversion of succinyl CoA to succinate when acetoacetyl CoA is formed will deprive the heart of one substrate-level phosphorylation per two acetyl CoA units oxidized, with a net energy yield of 23 ATP per molecule of acetoacetate. When beta-hydroxybutyrate is being utilized, an additional $NADH_2$ (= NADH + H^+) will be formed during the initial dehydrogenation to acetoacetate, and a further 3 ATP will be formed with a total energy yield of 26 ATP per molecule of beta-hydroxybutyrate.

PHOSPHORYLATION–OXIDATION RATIO

Each of the myocardial fuels yields a different amount of ATP per molecule. The highest

yield of ATP per molecule is from a fatty acid such as palmitate. The fatty acid molecules contain little oxygen and therefore can yield more ATP per carbon atom. The disadvantage of fatty acids as fuel is that, for each molecule of ATP produced, they need relatively more oxygen. Experimentally, a heart using fatty acid alone would need about 17% more oxygen to produce the same amount of ATP than when using glucose.

The molecular explanation for the relatively poor ATP yield of fatty acids per oxygen taken up is that each turn of the fatty acid spiral yields equal amounts of $FADH_2$ and $NADH_2$. $FADH_2$ enters the respiratory chain further along than $NADH_2$ and yields less ATP. Such processes account for part of the "oxygen-wasting" capacity of fatty acids; in addition, when fatty acids are presented in excess to the heart or when fatty acids cannot be fully oxidized as in ischemia, then fatty acids can "waste" even more oxygen through mechanisms which are still obscure [91].

Effect of Increased Heart Work on Substrates

Of the three major types of substrate, glucose (or glycogen), lactate, and free fatty acid, there are basically only two types of response to increased mechanical work of the heart: first, glycolysis and glycogenolysis basically respond to the breakdown of ATP and creatine phosphate during increased work; secondly, the uptake and metabolism of lactate and the rate of turnover of the fatty acid oxidation spiral respond to an increased mitochondrial ratio of NAD/$NADH_2$ ($NAD^+/NADH + H^+$) resulting in turn from the formation of ADP from ATP. Thus basic to both mechanisms is the response of cardiac high-energy phosphate compounds to increased mechanical work. In response to exercise, there are also the effects of increased catecholamine stimulation.

LACTATE UPTAKE

The molecular mechanisms whereby the uptake of lactate increases during increased heart work have not been well studied. The increased uptake of lactate during exercise is probably the direct result of an increased circulating lactate concentration. Another possible mechanism is that increased heart work stimulates pyruvate dehydrogenase activity, thereby removing the product of the lactate dehydrogenase reaction and stimulating conversion of intracellular lactate to pyruvate. Increased extraction of free fatty acids by the heart will decrease the extraction of lactate by inhibition of pyruvate dehydrogenase. Conversely, a decreased circulating free fatty acid level, as found during acute exercise, should release the inhibition of pyruvate dehydrogenase and increase uptake of lactate.

FATTY ACID UPTAKE AND OXIDATION

The increased formation of NAD^+ from $NADH_2$ ($NADH + H^+$) during heart work stimulates the fatty acid oxidation spiral, which in turn promotes fatty acid uptake. To keep up a supply of acetyl CoA requires continued activity of the carnitine carrier for acyl CoA. One possible mechanism is the removal of acyl CoA within the mitochondrial space by increased activity of the fatty acid oxidation spiral [61]. At the same time, an increase in the rate of fatty acid activation requires CoA, derived from acetyl CoA in the cytosol, and the acetyl group formed is free to form acetyl carnitine, and thereby to enter the mitochondrial space to help replenish acetyl CoA. The thiokinase reaction is basically stimulated by removal of acyl CoA from the cytosol to the mitochondrial space and by provision of CoA [69].

GLUCOSE AND GLYCOLYSIS

Glycolysis is accelerated as increased heart work breaks down ATP and creatine phosphate to stimulate glycolysis. Glucose transport into the heart cell is increased by three possible mechanisms: (a) the activity of the glucose carrier is stimulated by increased heart work in an unknown way, possibly involving the acute fall in high-energy phosphate compounds; (b) after glucose is taken up, its phosphorylation by hexokinase to glucose 6-phosphate is enhanced by more rapid removal of glucose 6-phosphate by the enhanced activity of the glycolytic pathway; and (c) possibly as a result of alpha-stimulation [114]. Glycogen breakdown is en-

hanced by the breakdown of ATP and creatine phosphate; products such as AMP and inorganic phosphate directly stimulate phosphorylase-*b* activity (without requiring a catecholamine-mediated change into the *a* form). Glycolysis itself is stimulated because high levels of ATP and creatine phosphate normally inhibit phosphofructokinase, and their breakdown products (AMP and inorganic phosphate) stimulate the activity of phosphofructokinase.

The generalized statement can be made that the whole of glycolysis, including entry into glycolysis from glucose or glycogen, and the exit from glycolysis by pyruvate dehydrogenase, is responsive to the effects of acute work. In many instances the metabolic signal is the formation of products of ATP and creatine phosphate. In vivo, the effects of catecholamine stimulation also accelerate glycolysis.

CATECHOLAMINE STIMULATION

Stimulation of beta-adrenergic receptors produces two predictable effects on glycolysis in the heart. First, the well-known "cyclic-AMP cascade" will accelerate glycogenolysis to feed in more units of glucose 6-phosphate which in turn will be transformed to fructose 6-phosphate to provide more substrate for phosphofructokinase so that glycolysis increases. Simultaneously, the beta-adrenoceptor-mediated inotropic effect of catecholamines will enhance mechanical work to break down high-energy phosphate compounds, so that the activity of phosphofructokinase increases further. Recently a role of alpha-adrenoceptor stimulation has been proposed by Clark et al. [114]. On the basis of studies with alpha-agonists (such as naphazoline) and antagonists, they propose that phosphofructokinase exists in a less active "b" form, which is converted to the "a" form by a calcium-dependent mechanism during alpha-stimulation. Glucose entry is also enhanced by alpha-adrenoceptor stimulation. The overall proposal is that these effects mediated by beta-adrenoceptor stimulation occur very rapidly and the alpha-adrenoceptor effects occur later. These novel proposals require further evaluation, but provide a mechanism for a sustained enhancement of glycolysis during catecholamine stimulation. It is now appropriate to examine evidence that maintenance of glycolysis is an important aspect of myocardial metabolism.

Functional Correlates of Glycolysis

The amount of ATP generated by glycolysis in the normally oxygenated heart is negligible from the point of view of the normal energy requirements of the heart. In the ischemic myocardium, glycolysis from glucose is accelerated by the Pasteur effect in zones of moderate ischemia; even then the rate of production of anaerobic ATP is negligible when compared with the rate of ATP produced by the residual oxygen uptake (fig. 14–4). Yet sustenance of glycolysis in ischemic hearts can (a) reduce the rate of enzyme release [115, 116], (b) help prevent reperfusion arrhythmias [115], (c) maintain the action potential duration [117], and (d) prevent ischemic contracture [118]. In the hypoxic heart, glycolytic inhibition increased the severity of ultrastructural damage [119] in agreement with the previous findings.

In the well-oxygenated heart, there is recent evidence favoring the view that glycolysis may play a role over and above that of provision of energy by glycolytic ATP. Noakes [112] established the exact perfusion conditions for maximal mechanical work of the heart, achieving higher rates of work (power production) than previously reported (fig. 14–12). Of the wide variety of different substrates tested, including combinations of glucose with insulin or lactate or ketone bodies or fatty acids, or single substrates, it emerged that the rate of glycolytic flux could be related to the peak rate of relaxation (max neg dP/dt) which in turn limited cardiac work. Hence the proposal is that glycolysis can be linked to the rate of relaxation of the heart in diastole. Because the associated molecular event is thought to be the rate of uptake of Ca^{2+} by the sarcoplasmic reticulum, it may be that glycolysis plays a role in provision of ATP to an appropriate microcompartment. A link between glycolysis and the uptake of Ca^{2+} by the sarcoplasmic reticulum has already been proposed in the case of the ischemic myocardium [115]. Entman et al. [120] have described a glycogenolytic–sarcoplasmic-

reticulum complex. They found that fragments of the sarcoplasmic reticulum possess their characteristic calcium-accumulating system in physical association with a series of glycogenolytic enzymes. Speculatively, they proposed that the membrane of the sarcoplasmic reticulum normally protects the glycogenolytic complex against the effects of external calcium ions, but a membrane perturbation such as depolarization could allow access of the calcium ion to the complex, so as to accelerate glycogenolysis. Their proposal means that the arrival of Ca^{2+} would stimulate glycogenolysis and glycolysis and, hence, produce more glycolytic ATP. Our tentative proposal is that glycolysis limits the rate of uptake of Ca^{2+} and hence the rate of relaxation.

Several of the above observations can be interpreted in terms of cytosolic compartmentation of ATP. It is, therefore, appropriate to examine some aspects of the metabolism of high-energy phosphate compounds in the myocardium.

ATP and Phosphocreatine

The initial picture that emerged was that ATP was the immediate source of energy for contraction and other energy-consuming processes, with phosphocreatine as the reserve energy. More recently, phosphocreatine has come to play a "transport" role. As ATP is exported from the mitochondria by the translocator (as already discussed in section on free fatty acids), the proposal is that ATP is immediately converted to phosphocreatine by a mitochondrial creatine kinase (= creatine phosphokinase) isoenzyme [121, 122]. Phosphocreatine may then be transported throughout the cytosol presumably following a downhill gradient to a cytosolic site of utilization of energy, where another creatine kinase isoenzyme liberates the high-energy phosphate required for energetic purposes:

$$PC + ADP \rightarrow ATP + \text{creatine}$$

An assessment of the data favoring the existence of creatine kinase isoenzymes is given elsewhere [123].

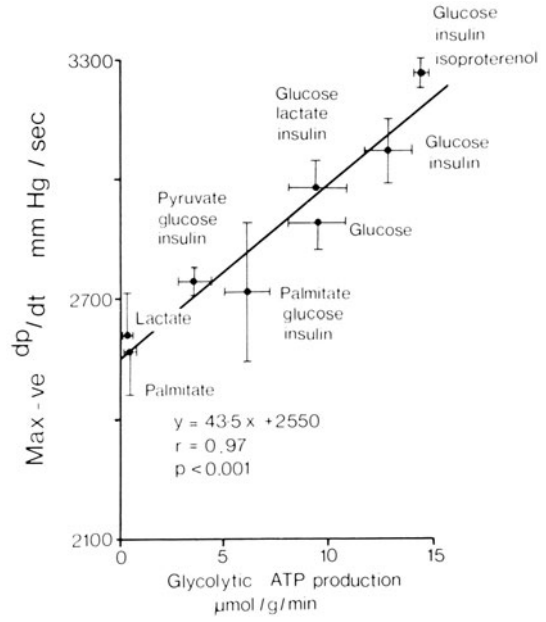

FIGURE 14–12. Graph showing significant correlation between the mean rates of myocardial glycolytic ATP production and the mean maximum rates of left ventricular relaxation (max -ve d*P*/d*t*) for hearts perfused with eight different substrate combinations. Noakes and Opie, unpublished data.

This 'transport role' of phosphocreatine does not eliminate its alternate role as an energy reservoir, especially because the equilibrium constant of the above reaction favors formation of ATP. During a sustained hypoxic stimulus both ATP and phosphocreatine will fall; while ATP may fall before phosphocreatine, in the next phase phosphocreatine falls more as it is the energy reservoir.

BREAKDOWN PRODUCTS OF PHOSPHOCREATINE

Creatine may help stimulate the production of high-energy phosphate by the mitochondria [124], probably by providing ADP by the action of the mitochondrial creatine kinase isoenzyme.

Inorganic phosphate may stimulate glycolysis at the level of phosphofructokinase, because this regulatory enzyme is inhibited by phosphocreatine (as well as by ATP) and the inhi-

bition is relieved by inorganic phosphate [125]. Inorganic phosphate may also play a complex role in regulation of Ca^{2+} transport into myocardial cells [126]. In acidotic conditions, inorganic phosphate helps the mitochondria to take up calcium, thereby accelerating calcium influx and presumably contributing to myocardial damage. In normal conditions, inorganic phosphate will inhibit the sodium pump, thereby increasing intracellular sodium and accelerating the sodium–calcium exchange pump. Hence during increased heart work, when inorganic phosphate rises as phosphocreatine falls, then calcium efflux may be stimulated to balance the enhanced calcium influx.

These observations focus attention on the changes in high-energy phosphate compounds induced by increased heart work.

HEART WORK AND HIGH-ENERGY PHOSPHATES

Earlier confusion about the effects of mechanical heart work on high-energy phosphate compounds (discussed by Opie [123]) has been resolved by the general agreement that it is the cytosolic phosphate potential, defined by the ratio of cytosolic (ATP)/(ADP)(Pi), that drives respiration [43]; 90% or more of ATP is found in the cytosol, whereas cytosolic ADP is very low. Hence the ratio ATP/ADP in the cytosol is 200–300 times greater than in the mitochondria. During acute heart work, it is the cytosolic ATP which is utilized; cytosolic ADP rises to drive mitochondrial respiration according to classic concepts. Phosphocreatine functions as a reserve energy at the acute onset of heart work [10, 25]. As the oxygen uptake rises, so will phosphocreatine tend to be restored, so that a high work loads overall values of tissue high-energy phosphates are little changed despite a doubling of the cytosolic ratio of ATP/ADP (for details see Opie [123]). The above concepts, based on theoretical calculations, are largely validated by direct measurements of mitochondrial and cytosolic adenine nucleotides in the isolated working guinea-pig heart [127], using density-gradient centrifugation of lyophilized myocardial homogenates.

BEAT-TO-BEAT CONTROL

Another explanation for failure to find changes in overall tissue values of high-energy phosphate compounds in some preparations is the possibility of beat-to-beat control. Wollenberger et al. [128] first proposed that the tissue contents of high-energy phosphates could vary within the cardiac cycle, with the phosphate potential falling at the start of systole as ATP is used; these data on the frog heart may not be applicable to the mammalian myocardium. More recently Morgan's group [129] found that there are small changes in the isolated rat heart, detectable by nuclear magnetic resonance techniques. Small overall changes can be translated into large changes in the cytosolic phosphate potential, as already discussed. Hence there may be cyclical variations in the mitochondrial oxygen uptake.

HYPOXIA VERSUS EFFECTS OF HEART WORK

Both hypoxia and increased heart work break down high-energy phosphate compounds. Because the isolated saline-perfused rat heart model of Neely et al. [11] has been extensively used to study the metabolic effects of heart work, it is appropriate to question tissue oxygenation. Production of lactate by such hearts is probably a result of the absence of lactate in the perfusate. The mitochondrial NAD^+/NADH ratio changes in favor of NAD^+ with work and NADH with hypoxia [25, 60]. With hypoxia, hexosemonophosphates accumulate; with heart work, they fall [10]. Computer simulation techniques cannot equate the metabolic effects of hypoxia with heart work [25]. Other substantial arguments eliminating the possibility of hypoxia are given elsewhere [10].

COMPARTMENTATION OF ENERGY

That ATP and ADP as well as phosphocreatine exist in at least two physical compartments (mitochondria and cytosol) is well established. Evidence favoring cytosolic subcompartmentation hinges on the discrepancy between changes in overall tissue ATP (largely cytosolic) and physiologic events that should be regulated by a uniform cytosolic level. Thus a pool of "contractile ATP" may exist, not in equilibrium

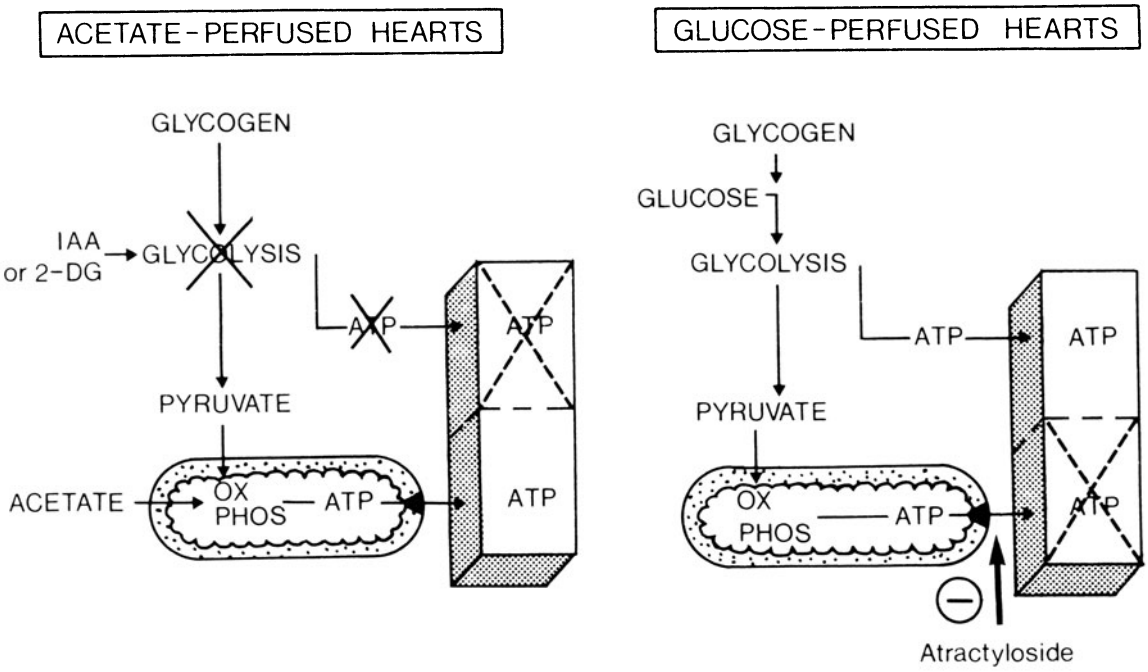

FIGURE 14–13. A simplified scheme of the energy-producing metabolic pathways and the points where the inhibitors are thought to act: IAA, iodoacetic acid, sodium salt; 2-DG, = 2-deoxy-glucose; ATP, = adenosine triphosphate; OX PHOS, = oxidative phosphorylation (intramitochondrial). The "box" represents the cytosolic ATP while the division represents the hypothetical compartmentalization. Total tissue ATP is the sum of the cytosolic ATP and the mitochondrial ATP. *(a)* Acetate-perfused hearts; *(b)* glucose-perfused hearts. It is proposed that inhibited glycolysis in hearts perfused with acetate and iodoacetate or deoxyglucose promotes the development of ischemic contracture, while continued glycolysis in glucose-perfused hearts with inhibited mitochondrial metabolism inhibits the development of ischemic contracture. From Bricknell et al. [118] with permission of Academic Press.

with the overall tissue (cytosolic) phosphocreatine values [55, 123]. Presumably unequal distribution of creatine kinase isoenzymes throughout the cytosol (as found by some but not all workers) would allow local liberation of ATP from phosphocreatine, thereby permitting functional subcompartments of high-energy phosphate. Also favoring the concept of compartments are the links between enhanced glycolysis and events such as decreased enzyme release and decreased ischemic contracture. Bricknell et al. [118] could show that, at equal overall levels of ATP and phosphocreatine, glycolytic flux prevented ischemic contracture more effectively than did residual mitochondrial respiration (fig. 14–13).

None of the above arguments conclusively prove the existence of subcompartments of ATP in the cytosol. A viable alternate hypothesis is that there is no "privileged" communication of mitochondrial ATP to a mitochondrial creatine kinase (as postulated by Saks et al. [122]), so that all the creatine kinases keep the mitochondrial pool of ATP in equilibrium with phosphocreatine [130]. This view requires the classic "reservoir" function of phosphocreatine, and also requires that phosphocreatine–creatine ratios and inorganic phosphate should communicate changes in contractile activity to the mitochondria. This view is currently less favored than that of ATP subcompartments.

ATP AND ISCHEMIC INJURY

When studying a variety of injuries to the cell, various other workers have concluded that the degree of fall of the total ATP level may help indicate whether or not the cell could recover. Thus Kübler and Spieckermann [15] found that as myocardial ATP fell below 3.5 μmol/g wet weight in hearts arrested by ischemia at 15°C, lactate production ceased because of ATP lack for the conversion of fructose 6-phosphate to fructose 1,6-diphosphate (phosphofructokinase reaction), and that ATP level was also the theoretical limit of myocardial ischemia that could be tolerated. (By toleration they mean recovery of adequate cardiac function after rewarming the heart.)

Hearse [131] has claimed a similar limit for recovery from whole heart ischemia induced by aortic clamping. And Trump [132, 133] has shown that the decline in the level of ATP during cell injury could be correlated with the development of mitochondrial swelling. However, Gudbjarnason et al. [134] found that, in the noninfarcted zone after coronary ligation in the dog, ATP could drop as low as 1.5–2.0 $\mu mol.g^{-1}$ and the heart could contract and survive. It may be that the studies by Trump et al. [133] on Ehrlich tumor cells are not directly applicable to the heart.

The studies on ischemia clearly show that creatine phosphate is depleted before ATP and it is not unreasonable to suppose that there must be some overall correlation between life and death of the cell and the presence or absence of ATP (taking extremes) and hence some correlation of ATP decrease with irreversibility. Also it is easy to see that when the heart cells are deprived of glycolysis, as in the data of Haworth et al. [135], it will be total ATP and not glycolytic ATP production that is of prime importance. Thus the evidence from studies on ischemic cells does not disprove the concept of compartmentalization of ATP.

Mitochondrial Reactions in Response to Heart Work

The effect of increased cytosolic breakdown of ATP is to accelerate (a) the transfer of ADP into the mitochondria, (b) oxidative phosphorylation, (c) the conversion of $NADH_2$ ($NADH + H^+$) to NAD^+, and thus (d) the citrate cycle. Changes in adenine nucleotides and cytosolic Mg^{2+} simultaneously accelerate glycolysis, so that the rate of the malate–aspartate cycle increases by a corresponding amount (fig. 14–14). Two other reactions are thought to occur: (a) unspanning of the citrate cycle, and (b) anaploretic reactions.

UNSPANNING OF THE CITRATE CYCLE

The activity of the citrate cycle in the rat heart can suddenly be accelerated by a surge of metabolic activity as when glucose is replaced by acetate as the major fuel [136] when a substrate-free heart is perfused with glucose and insulin [43]. Using these instructive (but unphysiologic) situations, it appears that the citrate cycle can operate in two spans. The first span from the acetyl CoA to alpha-keotglutarate is held to be regulated by citrate synthase, and the second span from alpha-ketoglutarate to oxaloacetate is regulated by alpha-ketoglutarate dehydrogenase. When acetyl CoA is suddenly formed by excess provision of glucose and insulin, the second part of the cycle is bypassed and the cycle is "unspanned". Such unspanning may seem unlikely to occur during increased heart work, when the primary event driving the cycle is the removal of $NADH_2$ rather than the arrival of acetyl CoA. However, Garfinkel's computer calculations [32] show that alpha-ketoglutarate (and isocitrate dehydrogenase) increase in activity more than citrate synthase at the start of increased heart work—probably because the inhibition on alpha-ketoglutarate dehydrogenase is removed as $NADH_2$ falls abruptly. Hence unspanning of the cycle is possible at the start of increased heart work.

TRANSAMINATION TO REPLENISH THE CITRATE CYCLE

If the citrate cycle suddenly speeds up due to a work jump, and glycolysis or lipolysis fails to deliver the required amount of acetyl CoA, the cardiac stores of amino acids can be used to form citrate-cycle intermediates by transamination [137]. Such reactions, "filling up" the

citrate cycle, are anaplerotic reactions (fig. 14–14). The potential effectiveness of this mechanism is seen by comparing the tissue value of aspartate (about 5 μmol fresh weight [43]) with the mitochondrial oxaloacetate concentration, thought to be about 100 pmol/g in the working heart [60]. Thus only a very little aspartate is required to "top up" mitochondrial oxaloacetate. On the other hand, the maximum turnover of the citrate cycle is about 10 μmol/g fresh weight/min and tissue aspartate can only fall at the rate of 1.7 μmol/g fresh weight/min [43]. Aspartate could not make a sustained contribution to maintenance of sustained high rates of citrate-cycle activity which require input from acetyl CoA from glycolysis or fatty acid metabolism.

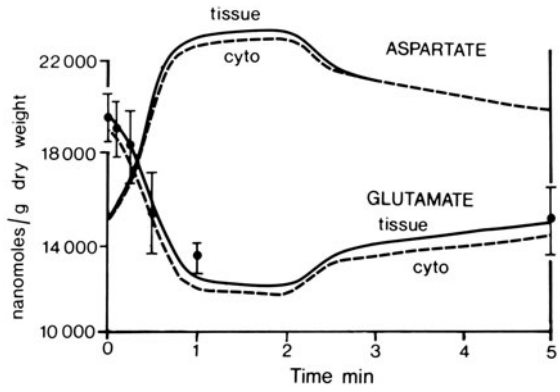

FIGURE 14–14. Rate of change of tissue glutamate and aspartate at onset of a work jump, probably reflecting use of glutamate in anaplerotic reactions which can "fill up" the mitochondrial oxaloacetate (see fig. 14–10). Means ± SEM of measured points, with computer-calculated patterns of flux. From Achs et al. [25] by permission.

Concluding Comments

High rates of myocardial energy production are required to maintain the constant demand for ATP, required largely for contractile purposes, but also for maintenance of ion gradients and other metabolic functions. A constant supply of oxygen to the myocardial cell is assured by the regulation of the coronary blood flow, which only fails when coronary arterial disease or spasm develops. The coronary flow also provides a more than adequate supply of external substrates: glucose, lactate, and free fatty acids. In the case of glucose, the complex uptake mechanism is sensitive to hormonal regulation by insulin and alpha-adrenoceptor stimulation, and responds to the state of oxygenation of the myocardium, as reflected in the high-energy phosphate compounds. During anoxia, tissue levels of ATP and phosphocreatine fall, while glucose uptake, glycogen breakdown, and anaerobic glycolysis are accelerated.

The pathways for fatty acid oxidation are complex apart from the transsarcolemmal uptake of FFA which proceeds along a concentration gradient. Thereafter fatty acid activation is followed by formation of acyl carnitine which is transported by a complex mechanism into the intramitochondrial space where acyl CoA is reformed. The latter compound enters the fatty acid oxidation spiral to form acetyl CoA units while shedding 2 H units to FAD and NAD, to form $FADH_2$ and $NADH_2$ (i.e., NADH + H^+). The acetyl CoA is oxidized via the citrate cycle of Krebs to yield more $NADH_2$. $NADH_2$ and $FADH_2$ are reoxidized by the electron transport chain to yield, respectively per molecule, 3 and 2 molecules of ATP. The overall energy yield of free fatty acid is 129 ATP per C16 molecule. This value seems substantially higher than that of glucose (3 ATP per molecule anaerobically oxidized), but the advantage is bought at the cost of a lower P/O (phosphorylation–oxidation) ratio. Therefore, oxidation of free fatty acid is relatively "oxygen-wasting". With the very high circulating FFA values and high rates of uptake, another as yet ill-understood mechanism of oxygen-wasting comes into play.

During myocardial ischemia, free fatty acid uptake is decreased as the rate of mitochondrial oxidation falls. Probably an early step in this sequence is the accumulation of intramitochondrial $NADH_2$ which inhibits the oxidation of one of the intermediates of the fatty acid oxidation spiral (beta-hydroxyacyl CoA), thus explaining the accumulation of acyl CoA, acyl carnitine, and intracellular FFA in ischemia.

Each of these metabolites has been postulated to have adverse effects in the setting of myocardial ischemia. A further potentially adverse change in lipid metabolism in ischemia is the formation of membrane-derived phospholipids, which may have arrhythmogenic potential.

During increased heart work, glycolysis is also accelerated, but now the mitochondrial ratio of $NADH_2/NAD$ falls (i.e., NAD^+ rises), which is the converse of what happens in anoxia of ischemia. The increase in mitochondrial $NAD/NADH_2$ increases citrate-cycle turnover, the activity of pyruvate dehydrogenase, and the activity of the fatty acid oxidation spiral and, eventually, fatty acid activation. The acceleration of glycolysis produced increased cytosolic $NADH_2$ which requires the activity of the malate–aspartate cycle. Through additional regulatory mechanisms, the uptake of three "primary substrates" (glucose, lactate, FFA) can be accelerated. Which substrate becomes the major one for the working heart depends on the physiologic conditions.

The stimulus to increased production of increased mitochondrial NAD^+ during increased heart work is probably increased formation of ADP from ATP in the cytosol, which drives mitochondrial respiration. The currently favored view is that ATP is not only compartmentalized between the mitochondria and cytosol, with most in the cytosol, but that subcompartments of ATP in the cytosol exist as a result of cytosolic creatine kinase isoenzymes. According to this view, ATP produced in the mitochondria leaves by the ATP translocase and is then rapidly converted to phosphocreatine; the latter acts as a barrier of high-energy phosphates to the local cytosolic site where ATP is used and replenishes ATP. Further evidence favoring the existence of cytosolic compartments of ATP is the apparent role of glycolysis in protecting from ischemic injury and ischemic contracture. Alternate points of view also merit attention. In ischemic injury, a relationship is claimed between the severity of loss of total tissue ATP and irreversibility; however, much data can also be interpreted within the view favoring ATP subcompartmentation.

References

1. Locke FS, Rosenheim O: Contributions to the physiology of the isolated heart: the consumption of dextrose by mammalian cardiac muscle. Physiol (Lond) 36:205–220, 1907.
2. Knowlton FP, Starling EH: The influence of variations of temperature and blood-pressure on the performance of the isolated mammalian heart. J Physiol 45:146–163, 1912.
3. Evans CL: The effect of glucose on the gaseous metabolism of the isolated mammalian heart. J Physiol 47:407–418, 1914.
4. Cruickshank EWH, Kosterlitz HW: Utilization of fat by aglycaemic mammalian heart. J Physiol 99:208, 1941.
5. Morgan HE, Neely JR, Brineaux JP, Park CR: Regulation of glucose transport. In: Chance B, Estabrook RW, Williamson JR (eds) Control of energy metabolism. New York: Academic, 1965, pp 347–355.
6. Fisher RB, Zacchariah P: The mechanism of the uptake of sugar by the rat heart and the action of insulin on this mechanism. J Physiol 158:73–85, 1961.
7. Park CR, Reinwein D, Henderson MJ, Cadenas E, Morgan HE: The action of insulin on the transport of glucose through the cell membrane. Am J Med 26:674–684, 1959.
8. Randle PJ, Morgan HE: Regulation of glucose uptake by muscle. Vitam Horm 20:199–243, 1962.
9. Gerards P, Graf W, Kammermeier H: Glucose transfer studies in isolated cardiocytes of adult rats. J Mol Cell Cardiol 14:141–149, 1982.
10. Opie LH, Norris RM, Thomas M, Holland AJ, Owen P, Van Noorden S: Failure of high concentrations of free fatty acids to provoke arrhythmias in experimental myocardial infarction. Lancet 1:818–822, 1971.
11. Neely JR, Liebermeister H, Battersby EJ, Morgan HE: Effect of pressure development of oxygen consumption by isolated rat heart. Am J Physiol 212:804–814, 1967.
12. Randle PJ, Smith GH: Regulation of glucose uptake by muscle. I. The effects of insulin, anaerobiosis and cell poisons on the uptake of glucose and release of potassium by isolated rat diaphragm. Biochem J 70:490–500, 1958.
13. Pasteur L: Etudes sur la Biere. Paris: Gauthier-Villars, 1876.
14. Hofmann E: The significance of phosphofructokinase in the regulation of carbohydrate metabolism. Rev Physiol Biochemistry Pharmacol 75:2–68, 1976.
15. Kübler W, Spieckermann PG: Regulation of glycolysis in the ischemic and the anoxic myocardium. J Mol Cell Cardiol 1:351–357, 1970.
16. Williamson JR: Glycolytic control mechanisms. II. Kinetics of intermediate changes during the aero-

bic–anoxic transition in perfused rat heart. J Biol Chem 241:5026–5036, 1966.
17. Neely JR, Whitmer JT, Rovetto MJ: Inhibition of glycolysis in hearts during ischemic perfusion. In: Recent advances in studies on cardiac structure and metabolism, vol 1, 1976, pp 243–248 University Park Press, Baltimore, Maryland.
18. Mochizuki S, Neely JR: Control of glyceraldehyde-3-phosphate dehydrogenase in cardiac muscle. J Mol Cell Cardiol 11:221–236, 1979.
19. Rovetto MJ, Lamberton WF, Neely JR: Mechanism of glycolytic inhibition in ischemic rat hearts. Circ Res 37:742–751, 1975.
20. Apstein CS, Deckelbaum L, Mueller M, Hagopian L, Hood WB Jr: Graded global ischemia and reperfusion: cardiac function and lactate metabolism. Circulation 55:864–872, 1977.
21. Gevers W: Generation of protons by metabolic processes in heart cells. J Mol Cell Cardiol 9:867–874, 1977.
22. Miller TB: A dual role for insulin in the regulation of cardiac glycogen synthase. J Biol Chem 253:5389–5394, 1978.
23. Morgan HE, Parmeggiani A: Regulation of glycogenolysis in muscle. III. Control of muscle glycogen phosphorylase activity. J Biol Chem 239:2440–2445, 1964.
24. Evans CL, Grande F, Hsu FY: Two simple heart-oxygenator circuits for blood-fed hearts. Q J Exp Physiol 24:283–287, 1934.
25. Achs MJ, Garfinkel D, Opie LH: Computer simulation of metabolism of glucose-perfused rat heart in a work-jump. Am J Physiol 243:R389–R399, 1982.
26. Drake AJ, Papadoyannis DE, Butcher RG, Stubbs J, Noble MIM: Inhibition of glycolysis in denervated dog heart. Circ Res 47:338–345, 1980.
27. Hirche HJ, Langohr HD: Hemmung der Milchsäureaufnahme im Herzmuskel narkotisierter Hunde durch hohe arterielle Konzentration der freien Fettsäuren. Pflugers Archiv 293:208–214, 1967.
28. Rose CP, Goresky CA: Constraints on the uptake of labeled palmitate by the heart: the barriers at the capillary and sarcolemmal surfaces and the control of intracellular sequestration. Circ Res 41:534–545, 1979.
29. Lassers BW, Kaijser L, Wahlqvist ML, Carlson LA: Relationship in man between plasma free fatty acids and myocardial metabolism of carbohydrate substrates. Lancet 2:448–450, 1971.
30. Randle PJ: Regulation of glycolysis and pyruvate oxidation in cardiac muscle. Circ Res (Suppl 1)38:8–12, 1976.
31. Brin M, Olson RE, Stare FJ: Metabolism of cardiac muscle. V. Comparative studies with L(+) and D(−) C^{14} in duck and rat tissues. J Biol Chem 199:467–473, 1952.
32. Garfinkel D: Lactate permeation. In: Discussion of regulation of glycolysis and pyruvate oxidation in cardiac muscle, by Randle PJ. Circ Res (Suppl 1):38:13–15, 1976.
33. Krasnow N, Neill WA, Messer JV: Myocardial lactate and pyruvate metabolism. J Clin Invest 41:2075–2085, 1962.
34. Gertz EW, Wisneski JA, Neese R, Houser A, Korte R, Bristow JD: Myocardial lactate extraction: multi-determined metabolic function. Circulation 61:256–261, 1980.
35. Opie LH, Owen P, Thomas M, Samson R: Coronary sinus lactate measurements in the assessment of myocardial ischemia. Am J Cardiol 32:295–305, 1973.
36. Resnekov L, Falicov RE: Thyrotoxicosis and lactate-producing angina pectoris with normal coronary arteries. Br Heart J 39:1051–1057, 1977.
37. Willebrands AF: The metabolism of elaidic acid in the perfused rat heart. Biochim Biophys Acta 116:583–585, 1966.
38. Opie LH, Metabolism of the heart. I. Metabolism of glucose, glycogen, free-fatty acids and ketone bodies. Am Heart J 76:685–698, 1968.
39. Evans JR, Opie LH, Renold AE: Pyruvate metabolism in the perfused rat heart. Am J Physiol 205:971–976, 1963.
40. Zahlten RN, Hochberg AA, Stratman HW, Lardy HA: Pyruvate uptake in rat liver mitochondria: transport or adsorption. FEBS Lett 21:11–13, 1972.
41. Kobayashi K, Neely JR: Mechanism of pyruvate dehydrogenase activation by increased heart work. J Mol Cell Cardiol 15:369–382, 1983.
42. Kohn MC, Achs MJ, Garfinkel D: Computer simulation of metabolism in pyruvate-perfused rat heart. III. Pyruvate dehydrogenase. Am J Physiol 237:R167–R173, 1979.
43. Williamson JR, Ford C, Illingworth J, Safer B: Coordination of citric acid cycle activity with electron transport flux. Circ Res (Suppl 1)38:39–48, 1976.
44. Bremer J: Pyruvate dehydrogenase, substrate specificity and product inhibition. Eur J Biochem 8:535–540, 1969.
45. Kerbey AL, Randle PJ, Cooper RH, Whitehouse S, Pask HT, Denton RM: Regulation of pyruvate dehydrogenase in rat heart. Mechanism of regulation of proportions of dephosphorylated and phosphorylated enzyme by oxidation of fatty acids and ketone bodies and of effects of diabetes: role of coenzyme A, acetyl–coenzyme A and reduced and oxidized nicotinamide–adenine dinucleotide. Biochem J 154:327–348, 1976.
46. Kobayashi K, Neely JR: Effects of ischemia and reperfusion on pyruvate dehydrogenase activity in isolated rat hearts. J Mol Cell Cardiol 15:359–367, 1983.
47. Mowbray J, Ottaway JH: The effect of insulin and growth hormone on the flux of tracer from labelled lactate in the perfused rat heart. Eur J Biochem 36:369–379, 1973.

48. Ohlen J, Siess EA, Löffler G, Wieland OH: The effect of insulin on pyruvate dehydrogenase interconversion in heart muscle of alloxan-diabetic rats. Diabetologia 14:135–139, 1978.
49. Bing RJ: Cardiac metabolism. Physiol Rev 45:171–213, 1965.
50. Bing RJ, Siegel A, Vitale A, Balbano F, Sparks E, Taeschler M, Klapper M, Edwards S: Metabolic studies on the human heart in vivo. I. Studies on carbohydrate metabolism of the human heart. Am J Med 15:284–296, 1953.
51. Bing RJ, Siegel A, Ungar I, Gilbert M: Metabolism of the human heart. II. Studies on fat, ketone and amino acid metabolism. Am J Med 16:504–515, 1954.
52. Shipp JC, Opie LH, Challoner D: Fatty acid and glucose metabolism in the perfused heart. Nature (Lond) 189:1018–1019, 1961.
53. Neely JR, Morgan HE: Relationship between carbohydrate and lipid metabolism and the energy balance of heart muscle. Annu Rev Physiol 36:413–459, 1974.
54. Menahan LA, Hron WT: Regulation of acetoacetyl-CoA in isolated perfused rat hearts. Eur J Biochem 119:295–299, 1981.
55. Opie LH: Metabolism of the heart in health and disease. II. Metabolism of triglycerides. Substrates for oxidative metabolism. Mitochondrial metabolism. Synthetic reactions. Excitation coupling. Am Heart J 77:100–122, 1969.
56. Lassers BW, Kaijser L, Carlson LA: Myocardial lipid and carbohydrate metabolism in healthy, fasting men at rest: studies during continuous infusion of ^{3}H-palmitate. Eur J Clin Invest 2:348–358, 1972.
57. Olson RE, Hoeschen RJ: Utilization of endogenous lipid by the isolated perfused rat heart. Biochem J 103:796, 1967.
58. Evans JR: Structure and function of heart muscle. Circ Res 15:1–224, 1964.
59. Van der Vusse GJ, Roemen THM, Prinzen FW, Coumans WA, Reneman RS: Uptake and tissue content of fatty acids in dog myocardium under normoxic and ischemic conditions. Circ Res 50:538–546, 1982.
60. Opie LH, Owen P: Assessment of mitochondrial free NAD^{+}/NADH ratios and oxaloacetate concentrations during increased mechanical work in isolated perfused rat heart during production or uptake of ketone bodies. Biochem J 148:403–415, 1975.
61. Hochachka DW. Neely JR, Driedzic WR: Integration of lipid utilization with Krebs cycle activity in muscle. Fed Proc 36:2009–2014, 1977.
62. Fritz IB: Action of carnitine on long chain fatty acid oxidation by liver. Am J Physiol 197:297–304, 1959.
63. Fritz IB, Yue KTN: Long-chain carnitine acyltransferase and the role of acylcarnitine derivatives in the catalytic increase of fatty acid oxidation induced by carnitine. J Lipid Res 4:279–288, 1963.
64. Hoppel CL, Tomec RJ: Carnitine palmityl transferase. J Biol Chem 247:832–841, 1972.
65. Kopec B, Fritz IB: Comparison of properties of carnitine palmitoyltransferase I with those of carnitine palmitoyltransferase II and preparation of antibodies to carnitine palmitoyltransferases. J Biol Chem 248:4069–4074, 1973.
66. Ramsay RR, Tubbs PK: The mechanism of fatty acid uptake by heart mitochondria: an acylcarnitine–carnitine exchange. FEBS Lett 54:21–25, 1975.
67. Pande SV: A mitochondrial carnitine acylcarnitine translocase system. Proc Natl Acad Sci USA 72:883–887, 1975.
68. Pande SV, Parvin R: Characterization of carnitine acylcarnitine translocase system of heart mitochondria. J Biol Chem 251:6683–6691, 1976.
69. Idell-Wenger JA, Grotyohann LW, Neely JR: Regulation of fatty acid utilization in heart: role of the carnitine–acetyl CoA–transferase and carnitine–acetyl carnitine translocase system. J Mol Cell Cardiol 14:413–417, 1982.
70. Pande SV, Blanchaer MC: Reversible inhibition of mitochondrial adenosine diphosphate phosphorylation by long chain acyl CoA esters. J Biol Chem 246:402–411, 1971.
71. Heldt HW, Jacobs H, Klingenberg M: Endogenous ADP of mitochondria, an early phosphate acceptor of oxidative phosphorylation as disclosed by kinetic studies with C^{14} labelled ADP and ATP and with atractyloside. Biochem Biophys Res Commun 18:174–178, 1965.
72. Shug AL, Shrago E, Bittar N, Folts JD, Kokes JR: Long chain fatty acyl CoA inhibition of adenine nucleotide translocase in the ischemic myocardium. Am J Physiol 228:689–692, 1975.
73. Garland PB, Randle PJ: Regulation of glucose uptake by muscle: effects of fatty acids and ketone bodies, and of alloxan-diabetes and starvation on pyruvate metabolism and on lactate/pyruvate and 1-glycerol 3-phosphate/dihydroxyacetone phosphate concentration ratios in rat heart and rat diaphragm muscles. Biochem J 93:678–687, 1964.
74. Oram JF, Bennetch SL, Neely JR: Regulation of fatty acid utilization in isolated perfused rat hearts. J Biol Chem 248:5299–5309, 1973.
75. Lochner A, Van Niekerk I, Kotze JCN: Mitochondrial acyl CoA, adenine nucleotide translocase activity and oxidative phosphorylation in myocardial ischaemia. J Mol Cell Cardiol 13:991–997, 1981.
76. La Noue KF, Watts JA, Koch CD: Adenine nucleotide transport during cardiac ischemia. Am J Physiol 241:H663–H677, 1981.
77. Barbour RL, Chan SHP: Characterization of the kinetics and mechanism of the mitochondrial ADP–ATP carrier. J Biol Chem 256:1940–1948, 1981.
78. Moore KH, Radloff JF, Koen AE, Hull PE: Incom-

plete fatty acid oxidation by heart mitochondria: beta-hydroxy fatty acid production. J Mol Cell Cardiol 14:451–459, 1982.
79. Monroy G, Kelker HC, Pullman ME: Partial purification and properties of an acyl coenzyme A: synglycerol 3-phosphate acyltransferase from rat liver mitochondria. J Biol Chem 248:2845–2852, 1973.
80. Opie LH: Metabolism of free fatty acids, glucose and catecholamines in acute myocardial infarction. Am J Cardiol 36:938–953, 1975.
81. Hough FS, Gevers W: Catecholamine release as a mediator of intracellular enzyme activation in ischaemic perfused heart. S Afr Med J 49:538–543, 1975.
82. Christian DR, Kilsheimer GS, Pettett G, Paradise R, Ashmore J: Regulation of lipolysis in cardiac muscle: a system similar to the hormone-sensitive lipase of adipose tissue. Adv Enzyme Regul 7:71–81, 1969.
83. Crass MF III, Shipp JC, Pieper GM: Effects of catecholamines on myocardial endogenous substrates and contractility. Am J Physiol 228:618–627, 1975.
84. Severson DL, Hurley B: Regulation of rat heart triacylglycerol ester hydrolases by free fatty acids, fatty acyl CoA and fatty acyl carnitine. J Mol Cell Cardiol 14:467–474, 1982.
85. Opie LH: Role of carnitine in fatty acid metabolism of normal and ischemic myocardium. Am Heart J 97:375–388, 1979.
86. Challoner DR, Steinberg D: Metabolic effect of epinephrine on the oxygen consumption of the perfused rat heart. Nature 205:602–663, 1965.
87. Glaviano VV, Goldberg JM, Pindok M, Wallick D, Aranis C: Cholinergic intervention on myocardial dynamics and metabolism in the nonworking dog heart. Circ Res 41:508–514, 1977.
88. Oliver MF, Kurien VA, Greenwood TW: Relation between serum free fatty acids and arrhythmias and death after acute myocardial infarction. Lancet 1:710–715, 1968.
89. Opie LH, Owen P, Riemersma RA: Relative rates of oxidation of glucose and free fatty acids by ischemic and non-ischaemic myocardium after coronary artery ligation in the dog. Eur J Clin Invest 3:419–435, 1973.
90. Challoner DR, Steinberg D: Oxidative metabolism of myocardium as influenced by fatty acids and epinephrine. Am J Physiol 211:897–892, 1966.
91. Pearce FJ, Forster J, De Leeuw G, Williamson JR, Tutwiler GF: Inhibition of fatty acid oxidation in normal and hypoxic perfused rat hearts by 2-tetradecylglycidic acid. J Mol Cell Cardiol 11:893–915, 1979.
92. Kurien VA, Yates PA, Oliver MF: The role of free fatty acids in the production of ventricular arrhythmias after acute coronary artery occlusion. Eur J Clin Invest 1:225–241, 1971.
93. Henderson AH, Craig RJ, Gorlin R, Sonnenblick EH: Free fatty acids and myocardial function in perfused rat hearts. Cardiovasc Res 4:466–472, 1970.
94. De Leiris J, Opie LH: Effect of substrates and of coronary artery ligation on mechanical performance and on release of lactate dehydrogenase and creatine phosphokinase in isolated working rat hearts. Cardiovasc Res 12:585–596, 1978.
95. Liedtke AJ, Nellis SH, Whitesell LF: Effects of carnitine isomers on fatty acid metabolism in ischemic swine hearts. Circ Res 48:859–866, 1981.
96. Idell-Wenger JA, Grotyohann LW, Neely JR: Coenzyme A and carnitine distribution in normal and ischemic hearts. J Biol Chem 253:4310–4318, 1978.
97. Wood JM, Rush B, Pitts BJR, Schwartz A: Inhibition of bovine heart Na^+, K^+-ATPase by palmitylcarnitine and palmityl CoA. Biochem Biophys Res Commun 74:677–683, 1977.
98. Sobel BE, Corr PB, Robison AK: Accumulation of lysophosphoglyceride with arrhythmogenic properties in ischemic myocardium. J Clin Invest 62:546–553, 1978.
99. Corr PB, Gross RW, Sobel BE: Arrhythmogenic amphiphilic lipids and the myocardial cell membrane. J Mol Cell Cardiol 14:619–626, 1982.
100. Opie LH, Tansey MJ, Kennelly BM: Proposed metabolic vicious circle in patients with large myocardial infarcts and high plasma free fatty acid concentrations. Lancet 2:890–892, 1977.
101. Man RYK, Choy PC: Lysophosphatidylcholine causes cardiac arrhythmia. J Mol Cell Cardiol 14:173–175, 1982.
102. Katz AM, Messineo FC: Lipid–membrane interactions and the pathogenesis of ischemic damage in the myocardium. Circ Res 48:1–16, 1981.
103. Rudolph W, Maas D, Richter J, Hasinger F, Hofmann H, Dohrn P: Uber die Bedeutung von acetoacetat und beta-hydroxybutyrat im stoffwechsel des menslichen Herzens. Klin Wochenschr 43:445–451, 1965.
104. Ungar I, Gilbert M, Siegel A, Blain JM, Bing RJ: Studies on myocardial metabolism. IV. Myocardial metabolism in diabetes. Am J Med 18:385–396, 1955.
105. Randle PJ, Garland PB, Hales CN, Newsholme EA: The glucose fatty-acid cycle: its role in insulin sensitivity and the metabolic disturbances of diabetes mellitus. Lancet 1:785–789, 1963.
106. La Noue KF, Walajtys EI, Williamson JR: Regulation of glutamate metabolism and interactions with the citric acid cycle in rat heart mitochondria. J Biol Chem 248:7171–7183, 1973.
107. Digerness SB, Reddy WJ: The malate–aspartate shuttle in heart mitochondria. J Mol Cell Cardiol 8:779–785, 1976.
108. Murphy E, Coll KE, Viale RO, Tischler ME, Williamson JR: Kinetics and regulation of the glutamate–aspartate translocator in rat liver mitochondria. J Biol Chem 254:8369–8376, 1979.

109. La Noue KF, Tischler ME: Electrogenic characteristics of mitochondrial glutamate–aspartate antiporters. J Biol Chem 249:7522–7528, 1974.
110. Puckett SW, Reddy WJ: A decrease in the malate–aspartate shuttle and glutamate translocase activity in heart mitochondria from alloxan-diabetic rats. J Mol Cell Cardiol 11:173–187, 1979.
111. Kobayashi K, Neely JR: Control of maximum rates of glycolysis in rat cardiac muscle. Circ Res 44:166–175, 1979.
112. Noakes TD: Exercise and the heart. MD thesis, University of Cape Town, 1981.
113. McGinnis JF, De Vellis J: Glycerol-3-phosphate dehydrogenase isoenzymes in human tissues: evidence for a heart specific form. J Mol Cell Cardiol 11:795–802, 1979.
114. Clark MG, Patten GS, Filsell OH: Evidence for an alpha-adrenergic receptor-mediated control of energy production in hearts. J Mol Cell Cardiol 14:313–321, 1982.
115. Bricknell OL, Opie LH: Glycolytic ATP and its products during ischaemia in isolated Langendorff-perfused rat hearts. In: Kobayashi T, Sano T, Dhalla NS (eds) Recent advances in studies on cardiac structure and metabolism. Vol. 2: Heart function and metabolism. Baltimore: University Park Press, 1978, pp 509–519.
116. Opie LH, Bricknell OL: Role of glycolytic flux in effect of glucose in decreasing fatty acid-induced release of lactate dehydrogenase from isolated coronary ligated rat heart. Cardiovasc Res 13:693–702, 1979.
117. Cowan JC, Vaughan Williams EM: The effects of palmitate on intracellular potentials recorded from Langendorff-perfused guinea–pig hearts in normoxia and hypoxia and during perfusion at reduced rate of flow. J Mol Cell Cardiol 9:327–342, 1977.
118. Bricknell OL, Daries PS, Opie LH: A relationship between adenosine triphosphate, glycolysis and ischaemic contracture in the isolated rat heart. J Mol Cell Cardiol 13:941–945, 1981.
119. Bing OHL, Fishbein MC: Mechanical and structural correlates of contracture induced by metabolic blockade in cardiac muscle from the rat. Circ Res 45:298–308, 1979.
120. Entman ML, Bornet EP, Van Winkle WB, Goldstein MA, Schwartz A: Association of glycogenolysis with cardiac sarcoplasmic reticulum. II. Effect of glycogen depletion, deoxycholate solubilization and cardiac ischemia: evidence for a phosphorylase kinase membrane complex. J Mol Cell Cardiol 9:515–528, 1977.
121. Saks VA, Chernousova GB, Gukovsky DE, Smirnov VN, Chazov EI: Studies of energy transport in heart cells. Mitochondrial isoenzymes of creatine phosphokinase: kinetic properties and regulatory action of Mg^{2+} ions. Eur J Biochem 57:273–290, 1975.
122. Saks VA, Lipina NV, Smirnov VN, Chazov EI: Studies of energy transport in heart cells. The functional coupling between mitochondrial creatine phosphokinase and ATP–ADP translocase: kinetic evidence. Arch Biochem Biophysiol 173:34–41, 1976.
123. Opie LH: High energy phosphate compounds. In: Drake-Holland AJ, Noble MIM (eds) Cardiac metabolism. London: Wiley, 1983, pp 279–307.
124. Seraydarian MW, Artaza L: Regulation of energy metabolism by creatine in cardiac and skeletal muscle cells in culture. J Mol Cell Cardiol 8:669–678, 1976.
125. Krzanowski J, Matchinsky FM: Regulation of phosphofructokinase by phosphocreatine and phosphorylated glycolytic intermediates. Biochem Biophys Res Commun 34:816–823, 1969.
126. Ponce-Hornos JE, Langer GA, Nudd LM: Inorganic phosphate: its effects on Ca exchange and compartmentalization in cultured heart cells. J Mol Cell Cardiol 14:41–51, 1982.
127. Soboll S, Bünger R: Compartmentation of adenine nucleotides in the isolated working guinea pig heart stimulated by adrenaline. Hoppe Seylers Z Physiol Chem 362:125–132, 1981.
128. Wollenberger A, Babskii EB, Krause E-G, Genz S, Blohm D, Bogdanova EV: Cyclic changes in levels of cyclic AMP in frog myocardium during the cardiac cycle. Biochem Biophys Res Commun 55:446–452, 1973.
129. Fossel ET, Morgan HE, Ingwall JS: Measurement of changes in high-energy phosphates in the cardiac cycle by using gated ^{31}P nuclear magnetic resonance. Proc Natl Acad Sci USA 77:3654–3658, 1980.
130. Altschuld RA, Brierley GP: Interaction between the creatine kinase of heart mitochondria and oxidative phosphorylation. J Mol Cell Cardiol 9:875–896, 1977.
131. Hearse DJ: Oxygen deprivation and early myocardial contractile failure: a reassessment of the possible role of adenosine triphosphate. Am J Cardiol 44:1115–1121, 1979.
132. Laiho KU, Trump BF: Studies on the pathogenesis of cell injury—effects of inhibitors of metabolism and membrane function on the mitochondria of Ehrlich ascites tumor cells. Lab Invest 32:163–182, 1975.
133. Trump BF, Mergner WJ, Kahng MW, Saladino AJ: Studies on the subcellular pathophysiology of ischemia. Circulation 53:17–26, 1976.
134. Gudbjarnason S, Mathes R, Ravens KG: Functional compartmentation of ATP and creatine phosphate in heart muscle. J Mol Cell Cardiol 1:325–339, 1970.
135. Haworth RA, Hunter DR, Berkoff HA: Contracture in isolated adult rat heart cells: role of Ca^{2+}, ATP and compartmentation. Circ Res 49:1119–1128, 1981.
136. Randle PJ, England PJ, Denton RM: Control of the

tricarboxylic acid cycle and its interactions with glycolysis during acetate utilization in rat heart. Biochem J 117:677–695, 1970.
137. Bowman RH: Effects of diabetes, fatty acids, and ketone bodies on tricarboxylic acid cycle metabolism in the perfused rat heart. J Biol Chem 241:3041–3048, 1966.
138. Opie LH: Effects of regional ischemia on metabolism of glucose and fatty acids. Circ Res 38, suppl 1:52–74, 1975.
139. Moravec J, Corsin A, Owen P, Opie LH: Effect of increased aortic perfusion pressure on fluorescent emission of the isolated rat heart. J Mol Cell Cardiol 6:187–200, 1974.
140. Opie LH: The Heart. Physiology, Metabolism, Pharmacology and Therapy. Grune and Stratton, Lonwon & New York, 1984. In press.

15. NEURAL CONTROL OF THE HEART

Matthew N. Levy
and Paul J. Martin

Introduction

The various structures in the heart are regulated by both divisions of the autonomic nervous system. The sympathetic division exerts facilitatory effects, whereas the parasympathetic has an inhibitory influence. The central nervous system controls the relative levels of sympathetic and vagal activity, usually in a reciprocal fashion; that is, as sympathetic activity is increased, parasympathetic activity is usually diminished, and vice versa. In certain regions of the heart, such as the nodal tissues, parasympathetic effects tend to predominate over sympathetic influences. In other regions, however, such as the ventricular myocardium, the effects of the sympathetic division are usually much greater than those of the parasympathetic division. When both divisions are active simultaneously, the sympathetic and vagal effects are usually not additive in a simple, algebraic fashion, but the sympathetic–parasympathetic interactions tend to be highly nonlinear.

These and other features of the neural control of the heart are described in greater detail in this chapter. Several detailed reviews of this subject have been published during the past decade [1–7].

Anatomy of the Cardiac Innervation

There are pronounced species differences in the details of the distribution of the efferent autonomic fibers to the heart. The anatomy of the cardiac innervation has been studied most extensively in the dog, and a representation of that anatomy is illustrated in figure 15–1.

The preganglionic cell bodies of the sympathetic fibers to the heart lie in the intermediolateral columns of the first five or six thoracic segments of the spinal cord [8]. The preganglionic neurons pass out through the white rami communicantes to the paravertebral chains. Most of the preganglionic fibers funnel through the stellate ganglia at the superior ends of the paravertebral chains in the dog. They continue on through the limbs of the ansae subclaviae, and synapse with postganglionic neurons in the caudal cervical ganglion. In other species, such as the cat, most of the synapses between pre- and postganglionic neurons occur in the stellate ganglia. The postganglionic sympathetic fibers travel to the heart as a complex plexus of small nerve bundles [1]. The individual bundles contain both sympathetic and parasympathetic fibers.

The details of the parasympathetic innervation of the heart also vary among the different mammalian species. In certain species, such as the cat, the cell bodies of the preganglionic vagal neurons are located almost entirely in the nucleus ambiguus [9]. Most of the preganglionic vagal neurons in the dog are also located in that same nucleus, but some also arise from the dorsal motor nucleus. The preganglionic fibers exit from the skull, travel down the neck in the carotid sheaths, and enter the thorax. In the dog (fig. 15–1), as they pass near the caudal cervical ganglia, the preganglionic vagal fibers become part of the cardiac plexus by forming a number of mixed nerve

This work was supported by USPHS grants HL 10951, HL 15658, and HL 22484.

N. Sperelakis (ed.), PHYSIOLOGY AND PATHOPHYSIOLOGY OF THE HEART.

Martinus Nijhoff Publishing, Boston/The Hague/Dordrecht/Lancaster.

trunks along with postganglionic sympathetic fibers [10]. The synapses between pre- and postganglionic vagal fibers occur in ganglia within the walls of the heart itself. Such ganglia are most abundant near the sinoatrial (SA) and atrioventricular (AV) nodes.

Neural Control of Heart Rate

SYMPATHETIC CONTROL

Increased sympathetic activity acts to increase the heart rate. The norepinephrine (NE) released from the sympathetic nerve endings in the SA node increases the firing rate of the automatic cells in the node. This is accomplished by increasing the rate of slow diastolic depolarization, probably by increasing the influx of calcium during phase 4 [11]. When a long train of pulses is used to stimulate the cardiac sympathetic nerves, the heart rate begins to increase after a latent period of 1–3 s [12]. The steady-state level of heart rate is not reached until about 30–60 s after the beginning of sympathetic stimulation (fig. 15–2).

After cessation of sympathetic stimulation, the chronotropic response gradually returns to the control level (fig. 15–2). The principal mechanisms for dissipating the NE released by the sympathetic nerve endings in the heart are (a) the uptake of neurotransmitter by those same nerve endings and by the cardiac cells, and (b) diffusion of neurotransmitter away from the site of release and into the coronary bloodstream [13]. When the neuronal reuptake mechanism is suppressed by specific blocking agents, such as cocaine, the decay of the chronotropic response is markedly prolonged [14, 15].

The magnitude of the positive chronotropic response to sympathetic stimulation varies with the stimulation frequency. The maximum response occurs with stimulation frequencies of about 20–30 Hz [16]. The spontaneous discharge frequencies in sympathetic nerves ordinarily do not exceed 10 Hz, however.

The distribution of sympathetic fibers to the various structures in the heart is very asymmetric [2, 8, 17–19]. The sympathetic nerves from the right side of the body have a much greater effect on heart rate than do those from the left side.

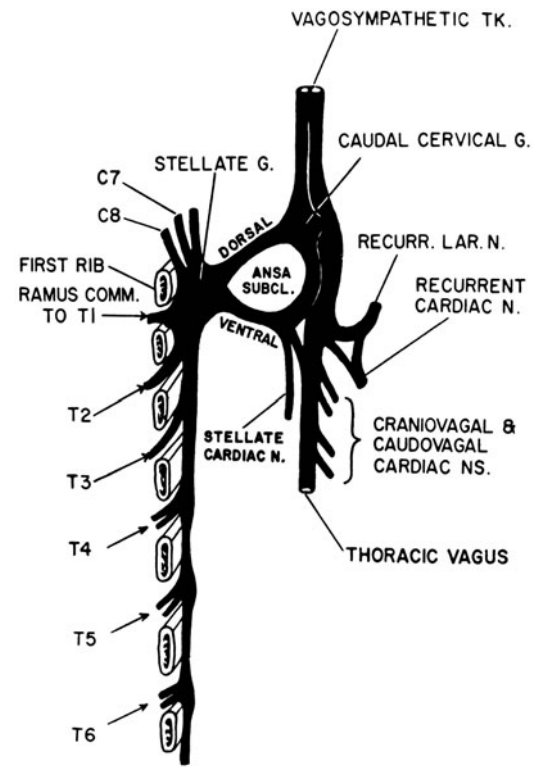

FIGURE 15–1. Upper thoracic sympathetic chain and the cardiac autonomic nerves on the right side in the dog. Modified from Mizeres [8].

PARASYMPATHETIC CONTROL

Steady-state Control. In contrast to the rather slow chronotropic response to sympathetic stimulation (fig. 15–2), the latent period of the response to a train of vagal stimuli is only about 200 ms, and the steady-state heart rate is achieved within a few heartbeats (fig. 15–3). Furthermore, when stimulation is discontinued, the response decays very rapidly back to the control level [12]. There are large quantities of acetylcholinesterase present in the nodal regions of the heart [20], and this undoubtedly accounts for the rapid decay of the chronotropic response.

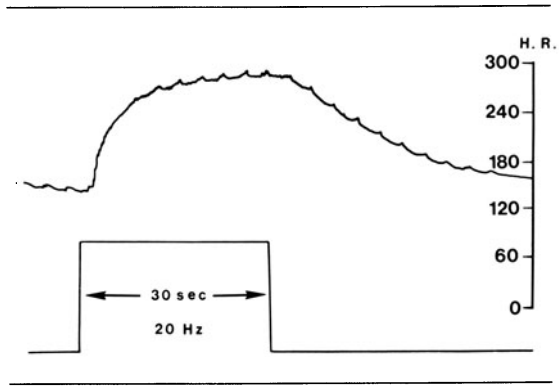

FIGURE 15–2. Heart rate (H.R.) Response of an anesthetized dog to steady stimulation of the cardiac sympathetic nerves at a frequency of 20 Hz for 30 s. Modified from Warner and Cox [12].

Effects of Brief Vagal Stimuli. It has been recognized for about 50 years that a single stimulus or a brief burst of stimuli delivered to the vagus nerves influences the heart rate for the next 10–15 s [21–25]. The negative chronotropic response is typically triphasic (fig. 15–4). There is a brief but pronounced decelerator phase (ABC), then a short phase of relative or absolute cardiac acceleration (CDE), and then a final small, but more prolonged, secondary phase of deceleration (EFG).

Some of the mechanisms underlying this triphasic response have only recently been elucidated. Eletrophysiologic studies have shown that the initial deceleration (the beginning of the first upstroke, AB) reflects a prolongation of the sinoatrial conduction time rather than a true reduction in firing rate of the automatic cells in the SA node [25]. The remainder of the primary phase of deceleration (ABC) is associated with a hyperpolarization of the automatic cells [24, 25], as shown in figure 15–5. The acetylcholine (ACh) released at the vagal endings undoubtedly diminishes the potassium conductance of the automatic cells [26], thereby evoking the hyperpolarization. This hyperpolarization is transient, however, and it disappears within one or two heartbeats.

Electrophysiologically, the secondary phase of cardiac deceleration (EFG, fig. 15–4) is characterized by a reduction in the slope of the pacemaker potential [24, 25], as demonstrated by the last three cardiac cycles in figure 15–5. Measurements made with a potassium-sensitive electrode indicate that the changes in cycle length during the secondary phase (EFG) are paralleled by changes in the extracellular potassium concentration [25]. These changes in potassium concentration may be responsible for this secondary increase in cardiac cycle length [25].

The two deceleratory phases are characteristically separated by a brief phase of relative or absolute cardiac acceleration (CDE, fig. 15–4); that is, the dip in the curve may or may not extend below the prestimulation level of cardiac cycle length. During this acceleratory phase, the maximum diastolic potential of the pacemaker cells becomes slightly less negative [25]. This transient acceleration might therefore be ascribable to an evanescent increase in sodium conductance.

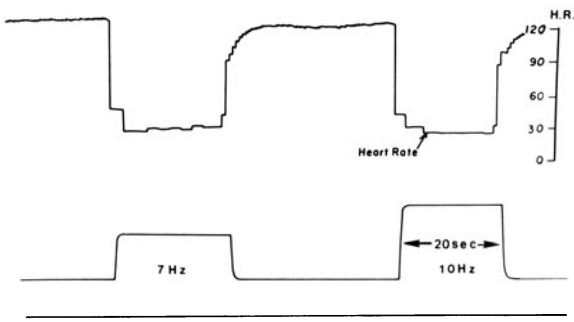

FIGURE 15–3. The changes in heart rate evoked by trains of right vagal stimulation at frequencies of 7 and 10 Hz in a dog. Modified from Warner and Cox [12].

Effect of Repetitive Vagal Stimuli. If the vagus nerves are stimulated once each cardiac cycle, the change in heart rate will depend on the phase of the cardiac cycle in which the stimulus is given [27, 28]. In the experiment illustrated in figure 15–6, one supramaximal stimulus was delivered to the cervical vagi of an anesthetized dog each cardiac cycle [28]. The control value of the cardiac cycle length (P-P interval), prior to vagal stimulation, was 390 ms. It is evident that the increase in cardiac cycle length evoked

by one vagal stimulus each cardiac cycle depended on the timing of those stimuli. When each stimulus (St) was given 225 ms after the beginning of atrial depolarization (P wave), the maximum increase in cardiac cycle length (P-P interval) was achieved. On the other hand, when each stimulus was given 390 ms after the beginning of atrial depolarization (i.e., at P-St = 390), the stimuli were only minimally effective in prolonging the cardiac cycle length. Such a curve of P-P intervals, plotted as a function of the P-St interval, constitutes a "phase–response curve" for the SA nodal pacemaker cells.

The phase dependency of the chronotropic response to repetitive vagal stimulation confers a peculiar characteristic to such stimulation; namely, such stimuli tend to synchronize the SA nodal pacemaker cells [27, 28]. As a consequence of such synchronization, the heart rate tends to assume the same frequency as the vagal stimulation, within a critical range of frequencies. Thus, within this range, a given increase in the frequency of vagal stimulation will cause an equal change in heart rate. This is a paradoxical response, considering that a greater stimulation of the inhibitory vagus nerves is actually causing the heart rate to increase!

When repetitive, brief bursts of pulses, rather than single, equally spaced pulses, are used to stimulate the vagi, the tendency for the SA nodal cells to be synchronized by the vagal activity is exaggerated [29, 30]. The spontaneous activity recorded from efferent vagal fibers to the heart consists of such repetitive bursts of action potentials clustered within a discrete portion of each cardiac cycle.

The chronotropic effects of a progressive increase in the frequency of repetitive bursts of vagal stimuli are shown in figure 15–7. As the stimulation frequency was increased, an overall increase in cardiac cycle length (P-P interval) was evident [29]. This conforms to the well-established tenet that the vagus exerts a negative chronotropic effect on the heart.

It is obvious, however, that the change in cycle length evoked by the vagal stimulation is not a continuous, monotonic function of the stimulation frequency. Instead, the P-P interval tracing in figure 15–7 displays several discontinuities, such that a small change in stimulation frequency may evoke a pronounced change in cycle length. Between each of the discontinuities (indicated by the arrows), the cardiac rate undergoes a paradoxical response; i.e., the cardiac cycle length decreases with an increase in the frequency of stimulation. The ratios of the number of stimulus bursts (St) to the number of atrial depolarizations (P waves) are denoted by the ratios (St:P) between the arrows. Between the arrows that signify an

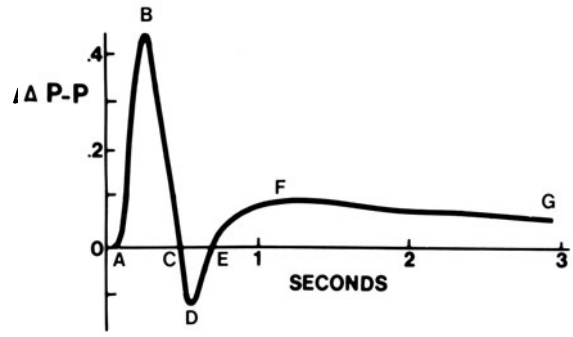

FIGURE 15–4. Time course of the changes in P-P interval evoked by a brief burst of vagal stimuli in a dog. Adapted from Iano et al. [23].

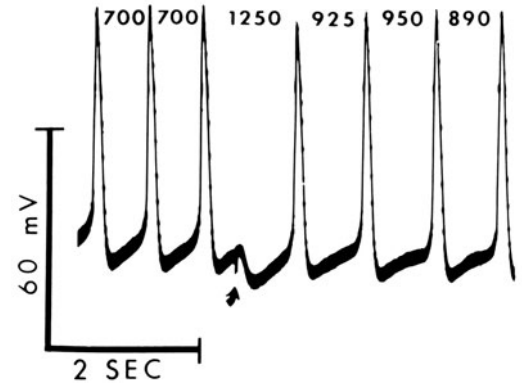

FIGURE 15–5. Transmembrane action potentials recorded from the SA node of a cat. A brief burst of vagal stimuli was given at the arrow. The numbers between the peaks of the action potentials indicate the cardiac cycle lengths, in ms. Adapted from Jalife and Moe [24] with permission of the American Heart Association.

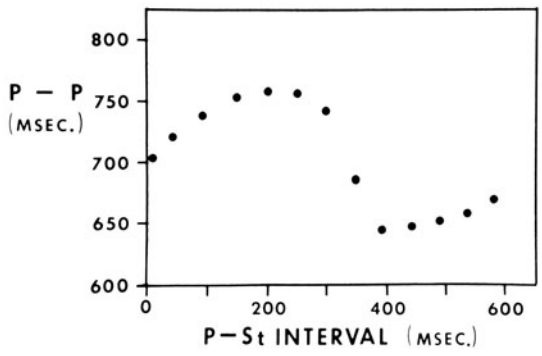

FIGURE 15–6. The effects of vagal stimuli, delivered once each cardiac cycle, on the cardiac cycle length (P-P interval) in the dog. The effect varied, depending on the P-St inverval, which is the time after the onset of atrial depolarization (P wave). From Levy et al. [28] with permission of the American Heart Association.

St:P ratio of 1:1, as the burst frequency had been increased from 0.76 to 1.33 bursts/s, the frequency of cardiac contractions (computed from the observed P-P intervals) had similarly increased from 0.76 to 1.33 beats/s, or from 46 to 80 beats/min. The contraction frequency was identical to the stimulation frequency, indicating that the heart had been beating once for each vagal stimulus burst over the frequency range from 0.76 to 1.33 Hz. Over other frequency ranges, synchronization had also prevailed, but in other St:P ratios (fig. 15–7).

In the SA node, conduction velocity is very slow from one cluster to the next [31, 32]. Hence, the clusters of automatic cells are in poor communication with each other. The pronounced synchronizing tendency of repetitive vagal activity probably serves to coordinate the automatic activity of such diverse cell clusters [31].

SYMPATHETIC–PARASYMPATHETIC INTERACTIONS

Many of the postganglionic sympathetic and vagal nerve endings within the walls of the heart lie very close to one another. This permits complex interactions to take place between the components of the two subdivisions of the autonomic nervous system [2, 4–7, 33]. Many complex interactions have been described, but the principal type has been called *accentuated antagonism* [33]. The manifestation of this interaction is such that the inhibitory effect of a given level of vagal activity becomes more pronounced the greater the prevailing level of sympathetic activity.

Accentuated antagonism is mediated at both prejunctional and postjunctional levels, the junction in question being that between the postganglionic sympathetic nerve ending and the cardiac effector cell. The prejunctional mechanism involves a cholinergically mediated inhibition of norepinephrine release from the postganglionic sympathetic nerve terminals. The postjunctional mechanisms involve interactions at the level of the effector cell itself, and are probably mediated by the cyclic nucleotides, cAMP and cGMP. This section will deal with the manifestations of accentuated antagonism in the control of heart rate and myocardial contractility, and with the prejunctional mechanisms that are involved in the process. The postjunctional aspects of this interaction are described in chapter 17.

Manifestations of Accentuated Antagonism. The accentuated antagonism involved in the autonomic control of heart rate is illustrated in figure 15–8. In this experiment [34], supramaximal vagal stimulation at a frequency of 8 Hz (left panel) caused a reduction in heart rate of 80 beats/min (closed circles) in the absence of sympathetic stimulation (S = O). Stimulation of the cardiac sympathetic nerves alone at a frequency of 4 Hz (S = 4) increased the heart rate by 80 beats/min (closed triangles). When vagal stimulation at 8 Hz was then added to this level of sympathetic stimulation (S = 4), the heart rate decreased by 170 beats/min (closed triangles). Hence, the negative chronotropic effect of a given level of vagal activity was much more pronounced in the presence than in the absence of concomitant sympathetic activity.

The inhibitory effects of vagal activity on the atrial [35] and ventricular [36–38] myocardium are also accentuated as the level of sympathetic activity is progressively raised. In the experiment shown in figure 15–9, vagal stimulation (event marks A and C) had virtually no effect on ventricular contractility when there

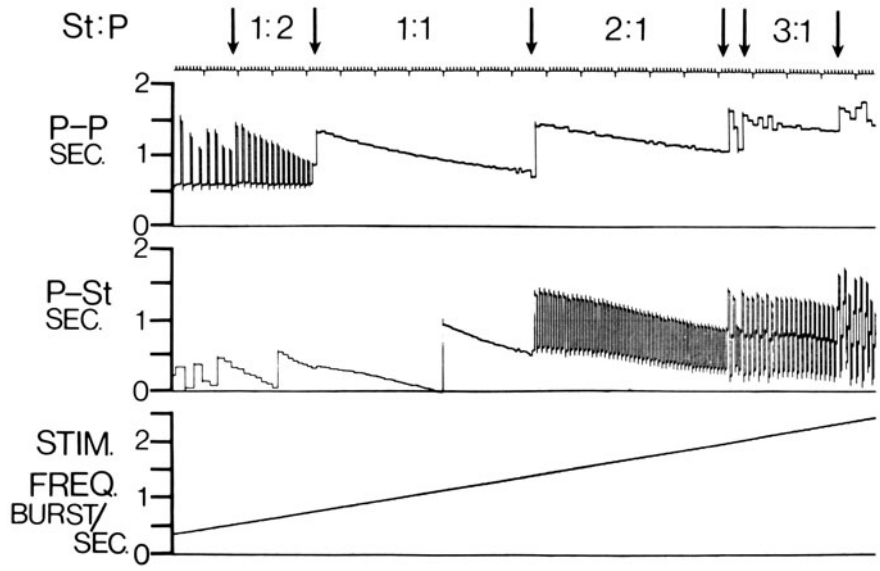

FIGURE 15–7. Changes in P-P interval as the frequency of vagal stimulation was progressively increased in a dog. The P-St interval denoted the time after the beginning of atrial depolarization (P wave) that the vagal stimulus (St) happened to be given. The numbers between the arrows denote the ratio of vagal stimulus bursts to heartbeats. Adapted from Levy et al. [29] with permission of the American Heart Association.

was no concurrent sympathetic activity [38]. However, during a train of sympathetic stimulation (between marks 1 and 2), the same vagal stimulus (event mark B) depressed ventricular contractility substantially. These results suggest that the inhibitory effect of vagal activity on the ventricles is achieved in large part by antagonizing the prevailing level of sympathetic activity.

Prejunctional Mechanism Responsible for Accentuated Antagonism. Various receptors involved in the regulation of norepinephrine (NE) release appear to be located on the postganglionic sympathetic nerve endings in the heart. One such receptor is the muscarinic cholinergic receptor, the action of which is to inhibit the release of NE during sympathetic neural activity [39].

This prejunctional inhibition of NE release is illustrated by the experiments shown in figure 15–10. When a standard stimulus was applied to the cardiac sympathetic nerves of an anesthetized dog, the overflow of catecholamines (CA) into the coronary sinus blood amounted to 12 mg/min [40]. Concurrent vagal stimulation caused a frequency-dependent reduction in the CA overflow. Stimulation at a frequency of only 1 Hz (Vg 1) caused a 25% reduction in a CA overflow. When the stimulation frequency was increased to 16 Hz, the CA output was diminished to about 30% of that obtained in the absence of vagal stimulation. Such a marked suppression of NE release explains in part the pronounced vagally induced attenuation of the inotropic response to sympathetic stimulation, and the occurrence of a relatively weak negative inotropic effect of vagal stimulation when there is no background level of sympathetic activity (fig. 15–9).

Neural Control of Atrioventricular Conduction

STEADY-STATE CONTROL

Studies of the direct effect of vagal activity on AV conduction are best done with the heart paced at a constant rate. This is because a change in cardiac cycle length will, of itself, alter AV conduction time. An increase in cycle

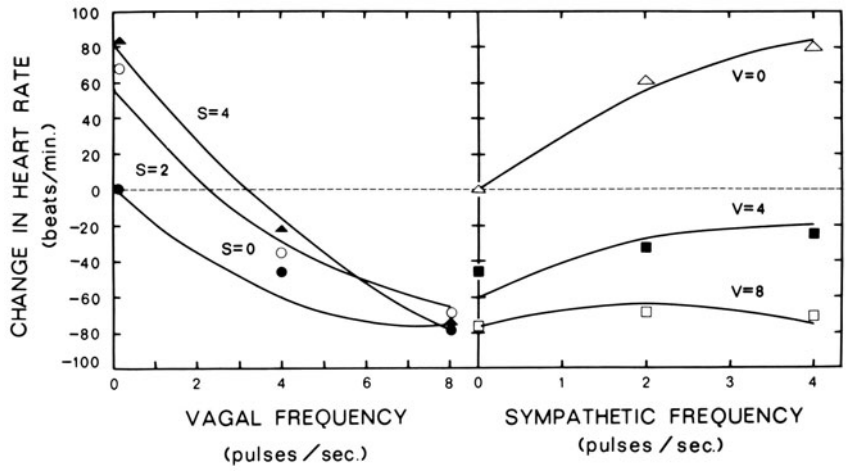

FIGURE 15–8. Changes in heart rate elicited by simultaneous left vagal and right stellate stimulation in a dog. Symbols represent actual data, and the curves were derived by regression analysis. Numbers along the curves represent the frequencies (in Hz) of sympathetic (S) and vagal (V) stimulation. From Levy and Zieske [34].

length can cause an appreciable decrease in AV conduction time, and a reduction in cycle length will have the opposite effect. Thus, in the unpaced heart, vagal activity will increase the cardiac cycle length, and this will indirectly decrease AV conduction time, but the direct vagal effect on the AV conducting fibers will tend to prolong AV conduction. Because these direct and indirect influences are oppositely directed, their effects tend to cancel. Hence, during vagal stimulation, the simultaneous changes in cycle length mask the direct neural effects on AV conduction. Thus, studies of the effects of vagal stimulation on AV conduction in the unpaced heart are liable to be misinterpreted. Parallel studies of the sympathetic control of AV conduction and its interaction with cardiac cycle length have not yet been reported, but such studies would also require cautious interpretation.

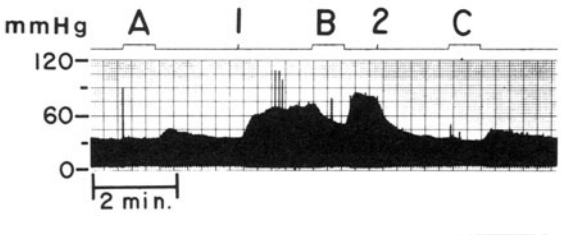

FIGURE 15–9. Changes in left ventricular pressure in a canine, isovolumetric left ventricle preparation evoked by supramaximal vagal stimulation (20 Hz) before (A), during (B), and after (C) left stellate ganglion stimulation (2 Hz, between marks 1 and 2). From Levy [38].

It has been long appreciated that vagal activity may depress AV conduction in anesthetized animals. It is now also clear that the vagi are an important determinant of normal AV conduction in conscious humans as well. A significant prolongation of AV conduction time in trained athletes is ascribable to their elevated vagal tone. When the heart was paced at a constant rate in human subjects, an increase in blood pressure reflexly caused a significant increase in the A-H interval (but not the H-V interval); a fall in blood pressure had the opposite effect [41]. These changes were blocked by atropine. Direct stimulation of the carotid sinus nerves in patients significantly prolonged the AV interval when the heart was paced [42]. This response appeared after a latency of about a second, reached a maximum in about 5 s, and then it declined gradually to attain a steady-state level after about 20 s. Again, the vagus played a major role in this response, with only a minor contribution from the sympathetic system.

In experimental animals, continuous supramaximal trains of vagal stimulation prolonged the AV conduction time after a latency of less than 1 s, and they induced bradydysrhythmias with fixed or variable degrees of AV block [43]. The prolongation of AV conduction time was a monotonically increasing function of stimulus intensity. Complete AV block usually did not appear until the AV conduction time had been prolonged by 50%–70% of control. The degree of prolongation depended strongly on the concomitant degree of SA nodal slowing; that is, there was a strong interaction between the direct vagal inhibitory effect on the AV node and the indirect facilitative effect on AV conduction ascribable to the concomitant decrease in heart rate.

In a study on dogs with atrial fibrillation, the opposing effects of simultaneous activity in the two autonomic divisions on AV conduction were found to be algebraically additive. We confirmed this result in dogs whose hearts were in normal sinus rhythm [34.]. The change in conduction time in response to activity in one autonomic division was independent of the level of activity in the other; i.e., there was no significant vagal–sympathetic interaction with respect to AV conduction. This is in sharp contrast to the autonomic control of SA nodal function and of myocardial contractility, where such an interaction is pronounced [33].

Autonomic blockade experiments in man have revealed that, when both divisions were blocked and the heart rate was not controlled artificially, there was little change of AV conduction time [44]. The authors concluded that the effects of the two autonomic divisions were balanced in the control of AV conduction. The problem with this interpretation, of course, is that the concomitant changes in rate also influenced AV conduction. Thus, the lack of change in AV conduction may have been due to the balance of the direct vagal inhibition of the conducting fibers and indirect vagal effects on heart rate, as discussed above.

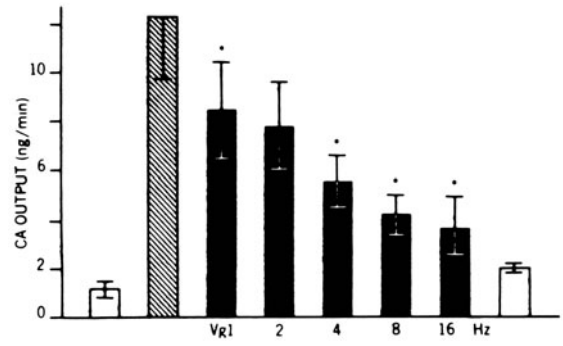

FIGURE 15–10. The overflow of catecholamines (CA) into the coronary sinus blood in a dog in the absence of sympathetic stimulation (open bars), in response to cardiac sympathetic nerve stimulation alone (10 Hz, hatched bar) and during concurrent sympathetic (10 Hz) and vagal stimulation (solid bars). Adapted from Lavallée et al. [40].

DYNAMIC CONTROL

Virtually all work on the dynamic or transient responses of AV conduction to autonomic stimulation have been focused on the vagal effects. A single vagal stimulus burst given in one cardiac cycle can prolong AV conduction on the very next cardiac cycle [45], and the effect quickly decays over the next few cycles (fig. 15–11). The response to a single sympathetic stimulus burst has a longer latency, takes several cycles to become fully manifest, and many more cycles to decay. Thus, dynamic responses to vagal stimulation have received more attention, since they may participate in arrhythmias on a beat-to-beat basis, whereas sympathetic responses are inherently too slow for such a role.

When we studied the dynamic responses of the SA and AV nodes to vagal stimulation simultaneously, we found the AV nodal responses to be extremely variable [22]. When identical stimulus bursts were given at different phases of the cardiac cycle, the AV responses varied in magnitude and direction (fig. 15–12). The change in AV conduction elicited by the vagal stimulus depended on the degree of the increase of the cardiac cycle length [22]. When the cycle length was held constant by pacing, vagal stimuli always prolonged the AV conduction time.

The phase of the cardiac cycle at which a vagal impulse arrives at the AV junction is also

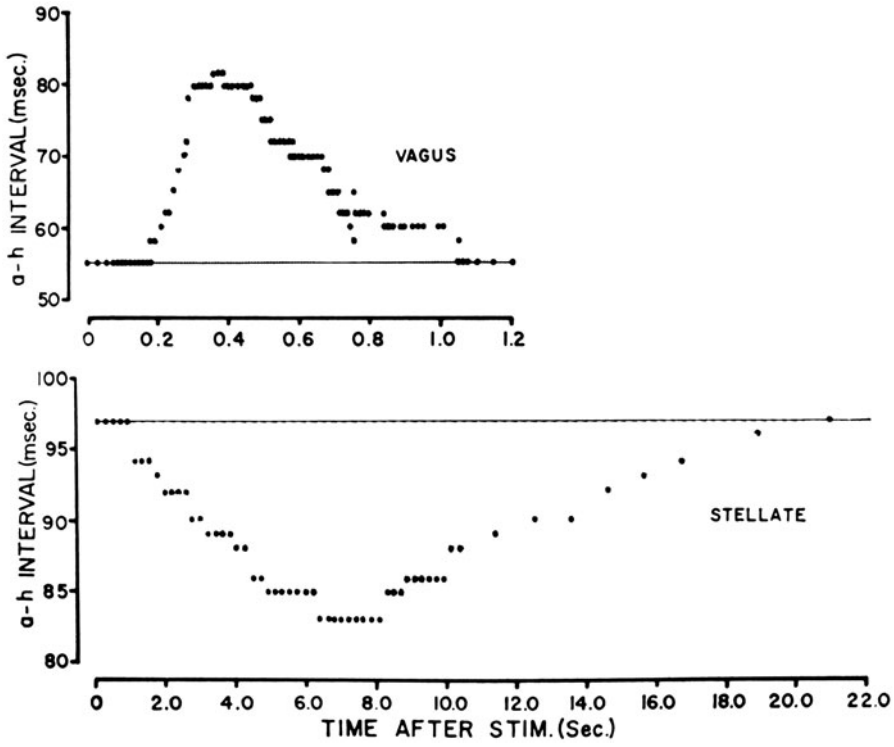

FIGURE 15–11. The effects of vagal and stellate stimulation on AV nodal conduction are compared. Each graph is a representative experiment. The interval from the atrial septal activation to the His bundle activation (the a-h interval in the His bundle electrogram) was used as the index of AV nodal conduction time. In the examples shown in this figure, 100-ms trains of stimuli were delivered to the left vagus *(top)* and the right stellate ganglion *(bottom)*. Notice the tenfold differencee in the scaling factor of the abscissae for the vagal and the stellate effects. From Spear and Moore [45] with permission of the American Heart Association.

an important determinant of its efficacy, just as it is for the vagal control of the SA node. To quantify the effects of stimulus timing on AV conduction, we constructed *vagal effect curves* that were analogous to those employed for the SA nodal responses to vagal stimulation [46]. The phase of the stimulus burst relative to the cardiac cycle was the primary independent variable. A second independent variable was the constant rate at which the heart was paced. Figure 15–13 shows that the vagal effect was more pronounced when the pacing rate was increased.

The probable mechanism responsible for this effect is that the relative refractory periods of the AV conduction system are longer than tne durations of the associated action potentials. As the AV conduction time is prolonged (by vagal activity or otherwise), the action potential duration in the critical conducting fibers in the AV node is increased, due to electrotonic effects. The relative refractory periods are also increased. This may lead to the following sequence of events when the heart is paced at a constant rate: (a) vagal stimulus given early in the cardiac cycle prolongs the AV conduction time and AV nodal refractory period during the first beat after the stimulus, (b) the second atrial impulse after the stimulus will arrive at the AV node when the conducting fibers are relatively more refractory, and (c) this will evoke an additional increment in AV conduction time on this second beat, just as indicated in figure 15–13. This mechanism may also be involved in the genesis of the AV nodal Wenckebach phenomenon.

Neural Control of Myocardial Excitability

Vagal stimulation significantly reduces the atrial refractory period [47]. This effect is undoubtedly due to the significant shortening of the atrial action potential induced by acetylcholine [48].

The effects of acetylcholine and vagal stimulation on ventricular refractory periods are not so clear, however. In both the dog [49] and in man [50], blockade of muscarinic receptors decreased the ventricular refractory periods. However, blockade of both autonomic divisions evoked negligible changes in refractory periods. Also, in the dog, vagal stimulation significantly prolonged ventricular refractory periods, but not after sympathectomy [51]. These findings suggest that the ACh released from vagal nerve endings acted indirectly by antagonizing the sympathetic effects, rather than by a direct action [49, 51, 52]. Autonomic blockade experiments in man, however, indicate that resting vagal tone significantly increases ventricular refractoriness, and that the effect can occur in the absence of sympathetic influences [44]. The vagi appear to constitute the dominant pathway for the reflex control of ventricular refractoriness in cats, and the vagal effect is prominent even when sympathetic activity is negligible [53]. Thus, these latter two studies are in conflict with the view that ACh acts only or primarily by antagonizing the effects of sympathetic activity. No obvious differences in experimental methodologies are evident that might resolve the dispute concerning how much the vagi affect refractoriness independently of sympathetic antagonism.

Prolongation of AV junctional and ventricular refractory periods may prove beneficial in terminating certain arrhythmias. Many arrhythmias are sustained by a reentrant circuit. Prolongation of the refractory periods locally may slow conduction sufficiently to interrupt the reentrant loop. This mechanism may explain the effect of vagal activity in suppressing ventricular tachycardias [54].

Neural Control of Myocardial Contractility

SYMPATHETIC EFFECTS

The adrenergic innervation of the atria is abundant, but not uniform. Stellate stimulation produces profound effects on the heart. It decreases the duration and increases the amplitude of the a wave of the atrial pressure pulse. The increase in atrial contractility evoked by sympathetic activity augments ventricular filling. The consequent rise in left ventricular

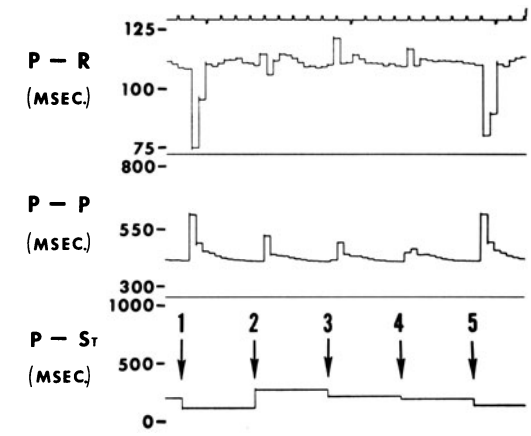

FIGURE 15–12. Changes in AV conduction *(top panel)*, cardiac cycle length *(middle panel)*, and P-St interval *(bottom panel)* in response to five single bursts of vagal stimulation in an anesthetized dog. From Levy et al. [22].

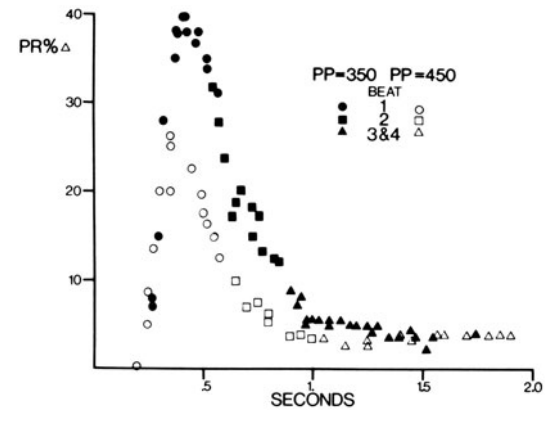

FIGURE 15–13. Vagal effect curves recorded from an anesthetized dog at two different atrial pacing intervals. The abscissa indicates the elasped time from a single vagal stimulus burst given at $t = 0$. The ordinates are the percent changes in AV conduction time over a sequence of consecutive cardiac cycles. The circles, squares, and triangles represent the changes that occurred in the first, second, and subsequent beats after the beat during which the stimulus was given.

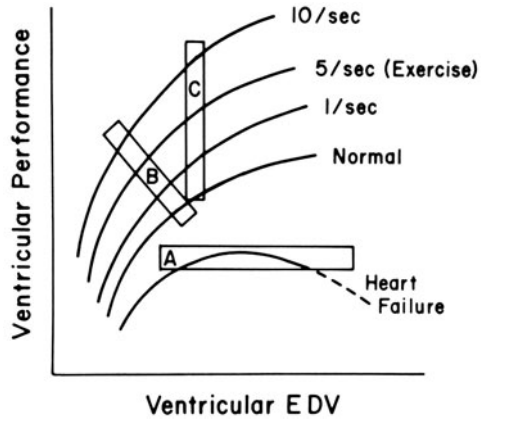

FIGURE 15–14. A family of ventricular function curves. Curve A shows the heart failure that tends to occur in a heart–lung preparation. The remaining curves (B and C) show the response to sympathetic stimulation at 1, 5, and 10 Hz. From Randall [1].

end-diastolic pressure thus produces a greater increment in ventricular end-diastolic volume and in stroke volume. Sympathetic activity can significantly alter ventricular filling not only by changing the duration of the filling period, but also by altering the strength and timing of atrial systole.

The sympathetic nervous system also richly innervates ventricular tissue. Stimulation of the right stellate ganglion in the dog usually increases heart rate more than does left-sided stimulation [2]. Left stellate stimulation enhances ventricular contractility, causing increases in left ventricular systolic pressure, the rate of change of ventricular pressure, and in the mean arterial pressure and pulse pressure. Sympathetic stimulation also increases coronary blood flow, myocardial oxygen consumption, stroke volume, stroke work, and cardiac output. Furthermore, these effects are produced independently of changes in preload and afterload; i.e., they obtain even when preload and afterload are held constant.

Various types of *ventricular function curves* have been used to characterize ventricular performance. These curves are plots of stroke work, stroke volume, or cardiac output versus some measure of initial fiber length, such as mean atrial pressure or ventricular volume or pressure at end-diastole (fig. 15–14). Such curves represent the classic Frank–Starling mechanism, whereby the performance of the heart increases with initial fiber length up to some optimal fiber length. Sympathetic activity shifts these curves upward and to the left (fig. 15–14); that is, an adrenergic influence increases cardiac output, and this change may be accompanied by a decrease in end-diastolic volume or pressure. The cardiac output is additionally augmented by the increase in heart rate induced by the increased sympathetic activity.

Sympathetic activity profoundly affects ventricular ejection dynamics. The peak ventricular pressure and the maximal positive rates of change of the ventricular volume and the ventricular pressures are significantly increased by sympathetic activity. These increases are usually interpreted to indicate that the myocardial fibers have contracted with greater force and at a higher velocity. An increase in velocity may be due in part to a greater synchrony of contraction, although this is considered by most to be a relatively minor factor. Also, the duration of systole is reduced; in the intact circulation this would help to preserve diastolic filling time despite the reduction of the cardiac cycle duration. Another important factor that helps to maintain ventricular filling at higher heart rates is the adrenergic augmentation of atrial contractility.

VAGAL EFFECTS

Until about two decades ago, it was commonly considered that the vagi had a negligible influence on ventricular function in mammals [2]. The neural control of myocardial contractility is difficult to study because contractility is influenced by so many variables in addition to the neural factors. Our laboratory has employed three different experimental canine preparations to control rigorously these other experimental variables; i.e., heart rate, preload, afterload, atrial transport function, and coronary perfusion pressure [55]. Trains of vagal stimuli caused reductions in ventricular contractility that varied inversely as the frequency of vagal stimulation. When the vagi were maximally stimulated, ventricular contractility was depressed by 15%–25%.

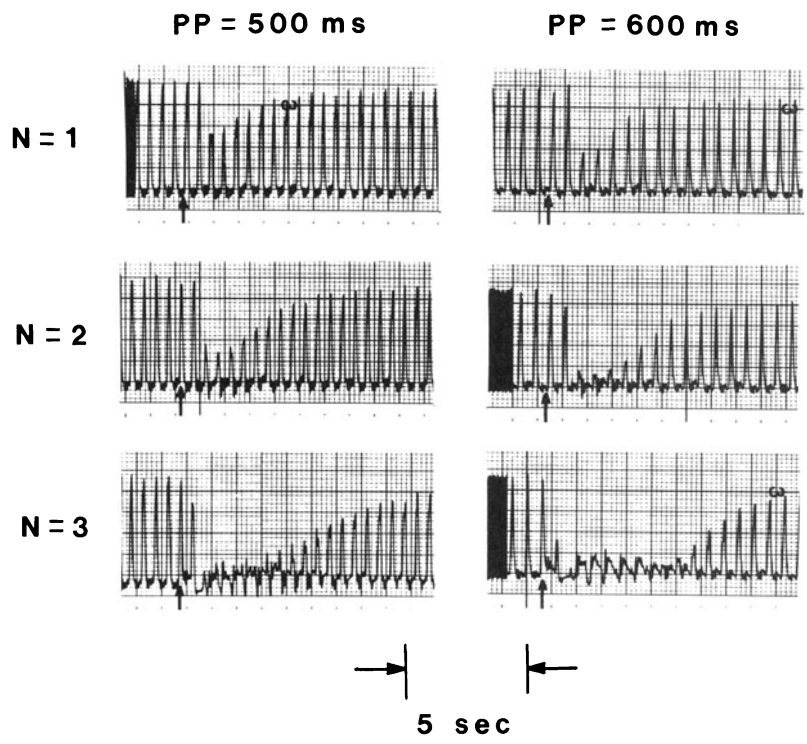

FIGURE 15–15. The changes in pressure in an atrial balloon in response to one, two, or three stimuli (N) per vagal burst, given at the time marked by the arrows, at cycle lengths (PP) of 500 and 600 ms. From Martin [60].

These findings have been confirmed in a variety of canine preparations and in other mammals, including humans. Vagal stimulation caused the ventricular function curves to be shifted to the right, it significantly reduced the maximum rate of rise of intraventricular pressure, and it diminished the ventricular contractile force [56].

Many decades ago, Wiggers [57] showed that the atria are very responsive to vagal influences, and his findings have been amply confirmed [58, 59]. The atria have a much richer parasympathetic innervation and a higher cholinesterase concentration than the ventricles [4, 5]. Thus, ACh has much shorter diffusion distances in the atria than in the ventricles, and the response is terminated more rapidly due to the higher concentrations of cholinesterase. This accounts in part for the faster time constants of the atrial than of the ventricular responses to vagal stimulation.

In the early studies of the atrial responses to vagal activity in mammals, long trains of stimuli were used and steady-state responses were measured. We recently studied the transient inotropic responses of canine atria to single or brief vagal stimuli [60]. Figure 15–15 shows the typical results of applying a single burst of one, two, or three pulses to the vagi while the heart was paced at one of two different cycle lengths. Note that a single vagal stimulus pulse reduced atrial contractile amplitude by 62% when the cycle length was 600 ms. One burst of two or three pulses eliminated effective atrial contractions entirely for 2–8 s. The depression of the inotropic response was less when the cycle length was diminished to 500 ms.

The inotropic responses were quantified by means of vagal effect curves. Figure 15–16 shows the vagal effect curves for the simultaneous changes in cardiac cycle length (A-A) and atrial contractility. The time course of the

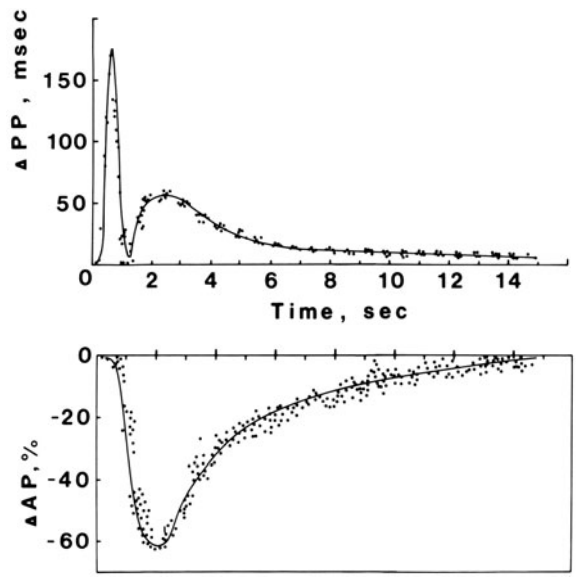

FIGURE 15–16. Vagal effect curves for cardiac cycle length (PP) in an unpaced-heart preparation and for atrial balloon pressure (AP) in a paced-heart preparation. The data were obtained from a sequence of vagal stimulus bursts given at various P-St intervals in the same dog. From Martin [60].

inotropic response was similar to that of the secondary peak of the chronotropic response. The similar time course suggests that the physiologic mechanisms of these two responses may share a common component.

The response of the atrial myocardium to vagal stimulation also depends on the phase of the cardiac cycle at which the stimulus burst is given [60], just as do the SA and AV nodes. A burst of vagal activity that occurs during one phase of the cardiac cycle may depress the next atrial contraction completely whereas, at a different phase of the cycle, the same burst of vagal activity may have relatively little effect. Such effects of timing would influence the atrial contribution to ventricular filling.

The inotropic responses of the atria to vagal stimulation were greater when the heart rate was held constant than when it was allowed to vary [60]. This difference could not be explained by changes of preload. The explanation may involve the dynamic frequency–force relationship, which is probably quite different from the traditional steady-state characterization of this relationship.

When a constant train of vagal stimuli was given over several minutes [61], heart rate initially increased to some maximum value and contractile force initially declined to some minimum value (fig. 15–17). However, both responses then began to "fade" back toward their control levels. The decline in heart rate back toward control reached a steady state in about 15–20 s, whereas the increase of contractile force back toward control required 1–2 min. However, AV conduction responses do not fade during continuous vagal stimulation [62]. Thus different mechanisms appear to be responsible for the fade of different types of cardiac responses. Although a progressive reduction in the neuronal release of ACh during the stimulus train cannot be entirely ruled out, the available evidence suggests that desensitization of the muscarinic receptors plays a significant role [63]; that is, the receptors seem gradually to lose their ability to bind the agonist.

Reflex Control of the Heart

The reflex control of the heart has been studied extensively, and several comprehensive reviews have recently been published [64–68]. Only a brief description of three important reflexes will be presented here; namely, the baroreceptor, Bainbridge, and chemoreceptor reflexes.

BARORECEPTOR REFLEX

Baroreceptors are arterial stretch receptors that are located in the carotid sinuses and aortic arch [65, 68]. Afferent impulses from the carotid sinus receptors travel to the brain in the carotid sinus nerves, which are branches of the glossopharyngeal, or ninth cranial nerves. Impulses from the aortic baroreceptors ascend to the brain via the aortic nerves, which are branches of the vagus, or tenth cranial nerves. Sympathetic and parasympathetic (vagal) fibers constitute the efferent limbs of the baroreceptor reflex.

The arterial baroreceptors discharge impulses at an increasing frequency as the mean arterial pressure rises in the carotid sinuses and aortic arch. An increased frequency of impulses in the

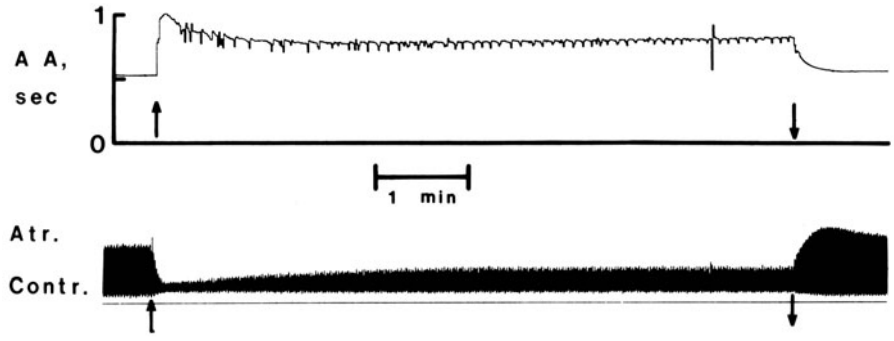

FIGURE 15–17. Changes in cardiac cycle length *(top panel)* and atrial contractility *(bottom panel)* in response to a continuous train of vagal stimuli (between the arrows). Note that both the chronotropic and inotropic responses return toward control from some initial maximal value, despite the continued vagal stimulation. From Martin et al. [61].

carotid sinus and aortic nerves diminishes the neural activity in efferent sympathetic fibers and augments the activity in efferent vagal fibers. The decreased sympathetic activity diminishes the vasomotor tone in resistance and capacitance vessels throughout the body, and tends to reduce heart rate, prolong AV conduction, and diminish atrial and ventricular contractility. The augmented vagal activity has effects on the heart that are similar directionally to those induced by the diminished sympathetic activity.

The reciprocal changes in efferent sympathetic and vagal activity in response to a blood pressure change take place only at arterial pressures within or near the normal range of pressures. If the arterial blood pressure is acutely reduced to abnormally low levels, vagal tone virtually disappears; the gradation of reflex control is then achieved solely by variations in efferent sympathetic activity. Conversely, if the arterial blood pressure is acutely elevated to abnormally high levels, sympathetic tone is completely suppressed; the gradation of reflex control is then accomplished by alterations in efferent vagal activity.

BAINBRIDGE REFLEX

Bainbridge noted in 1915 that, when he infused blood or saline into anesthetized animals, the heart rate increased, despite a concomitant rise in the arterial blood pressure [69]. Cardiac acceleration was correlated with an increase in central venous pressure, and it was abolished by bilateral vagotomy. Bainbridge postulated

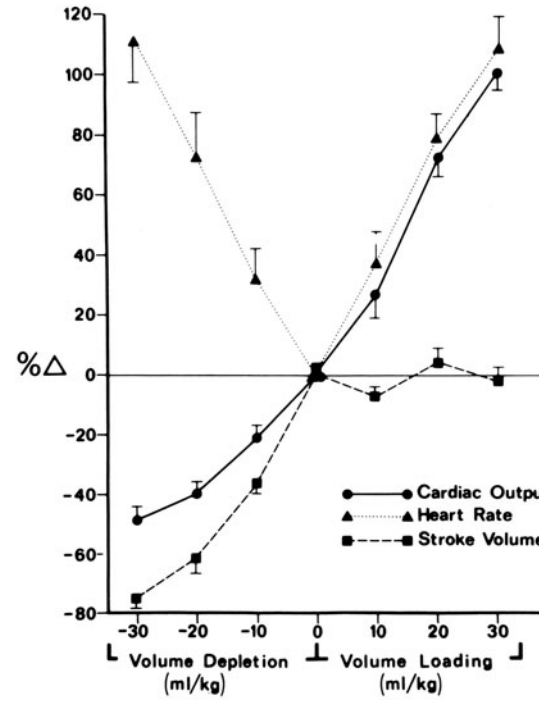

FIGURE 15–18. Effects of blood transfusion and of bleeding on cardiac output, heart rate, and stroke volume in unanesthetized dogs. From Vatner and Boettcher [70] with permission of the American Heart Association.

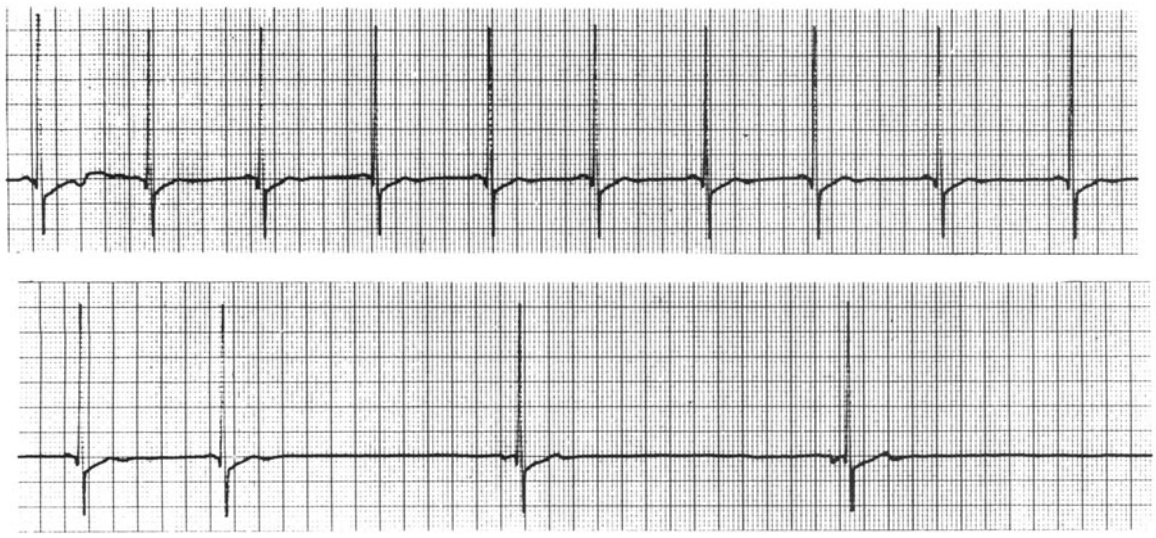

FIGURE 15–19. Electrocardiogram of a quadriplegic patient who required tracheal intubation and artificial respiration; the two strips are continuous. At the beginning of the top strip, the tracheal catheter was disconnected to permit nursing care. In less than 10 s, the patient's heart rate decreased from 65 to about 20 beats/min. Adapted from Berk and Levy [72].

that the reflex was initiated by distension of the right side of the heart, and that the afferent impulses were carried in the vagi.

The importance, and even the presence, of a Bainbridge reflex have been controversial since its original description. Other reflexes, notably the baroreceptor reflex, are also induced by a change in blood volume. Hence, the directional change in heart rate elicited by an alteration of blood volume will be the resultant of opposing reflex influences. Frequently, infusions of fluid cause cardiac acceleration when the prevailing basal heart rate is slow, but they induce a diminished heart rate when the basal rate is rapid.

In a recent study in unanesthetized dogs [70], infusions of blood increased the cardiac output and arterial blood pressure substantially. The heart rate increased in proportion to the cardiac output (fig. 15–18), despite the elevation of blood pressure. Hence, the Bainbridge reflex must have predominated over the baroreceptor reflex during volume expansion. Conversely, volume depletion reduced the cardiac output and arterial blood pressure. Heart rate rose as the blood pressure and cardiac output diminished (fig. 15–18). Therefore, the baroreceptor reflex must have predominated over the Bainbridge reflex during volume depletion.

CHEMORECEPTOR REFLEX

The peripheral arterial chemoreceptors respond to reductions in arterial P_{O_2} and pH and to elevations in arterial P_{CO_2}. The chemoreceptors are located in the aortic arch and in the carotid bodies, which are adjacent to the carotid sinuses. Arterial chemoreceptor stimulation induces pulmonary hyperventilation, vasoconstriction, and bradycardia. The magnitude of these cardiovascular responses, however, depends on the extent of the concomitant change in pulmonary ventilation [67, 71]. For example, if the chemoreceptor stimulus elicits only a mild degree of hyperventilation, the cardiac response tends to be bradycardia. Conversely, if the chemoreceptor stimulus leads to intense hyperventilation, the heart rate is likely to increase.

An extreme example of this reflex interaction is the dramatic cardiac response that may ensue when hyperventilation fails to occur in response

to chemoreceptor stimulation. In experimental animals, when ventilation is controlled by an artificial respirator, carotid chemoreceptor stimulation evokes an intense vagal discharge, which induces a pronounced bradycardia and an impairment of AV conduction [67, 71]. Similar changes have been reported in quadriplegic patients who are dependent on mechanical respirators [71, 72]. Profound bradycardia (fig. 15–19) promptly occurred in a quadriplegic patient when his tracheal catheter was briefly disconnected from the respirator in order to permit tracheal aspiration [72]. His heart rate dropped precipitously within 10 s after cessation of artificial respiration. This bradycardia could be retarded by hyperventilating the patient prior to disconnecting the tracheal catheter, and it could be prevented by administering atropine. The abrupt reduction in heart rate undoubtedly reflects the primary reflex cardiac response to arterial chemoreceptor excitation in a patient in whom the secondary effects of hyperventilation could not develop.

References

1. Randall WC: Neural regulation of the heart. New York: Oxford University, 1977.
2. Levy MN, Martin PJ: Neural control of the heart. In: Berne RM (ed) Handbook of physiology. Sect 2: Cardiovascular system. Vol 1: The heart. Bethesda MD: American Physiological Society, 1979, pp 581–620.
3. Levy MN, Martin PJ: Neural control of heart rate and atrioventricular conduction. In: Abboud FM, Fozzard HA, Gilmore JP, Reis DJ (eds) Disturbances in neurogenic control of the circulation. Bethesda MD: American Physiological Society, 1981, pp 205–216.
4. Higgins CB, Vatner SF, Braunwald E: Parasympathetic control of the heart. Pharmacol Rev 25:120–155, 1973.
5. Duchêne-Marullaz P, Arnould P, Schaff G, Lavarenne J, Billaud J: Comparaison des effets chronotrope, inotrope et dromotrope de l'excitation du stellaire droit chez le chien chloralosé. C R Soc Biol (Paris) 160:1586–1589, 1966.
6. Loffelholz K: Release of acetylcholine in the isolated heart. Am J Physiol 240:H431–H440, 1981.
7. Watanabe AM, Jones LR, Manalan AS, Besch HR Jr: Cardiac autonomic receptors: recent concepts from radiolabeled ligand-binding studies. Circ Res 50: 161–174, 1982.
8. Mizeres MJ: The origin and course of the cardioaccelerator fibers in the dog. Anat Rec 132:261–279, 1958.
9. Spyer KM: Baroreceptor control of vagal preganglionic activity. In: Brooks CM, Koizimi K, Sato A (eds) Integrative functions of the autonomic nervous system. Tokyo: University of Tokyo, 1979, pp 283–292.
10. Weiss GK, Priola DV: Brainstem sites for activation of vagal cardioaccelerator fibers in the dog. Am J Physiol 223:300–304, 1972.
11. Noble D: The initiation of the heartbeat. Oxford: Clarendon, 1979.
12. Warner HR, Cox A: A mathematical model of heart rate control by sympathetic and vagus efferent information. J Appl Physiol 17:349–355, 1962.
13. Axelrod J, Weinshilboum R: Catecholamines. N Engl J Med 287:237–242, 1972.
14. Matsuda Y, Masuda Y, Levy MN: The effects of cocaine and metanephrine on the cardiac responses to sympathetic nerve stimulation in dogs. Circ Res 45:180–187, 1979.
15. Matsuda Y, Masuda Y, Blattberg B, Levy MN: The effects of cocaine, chlorpheniramine and tripelennamine on the cardiac responses to sympathetic nerve stimulation. Eur J Pharmacol 63:25–33, 1980.
16. Rosenblueth A: The chemical mediation of autonomic nervous impulses as evidenced by summation of responses. Am J Physiol 102:12–38, 1932.
17. Levy MN, Ng ML, Zieske H: Functional distribution of the peripheral cardiac sympathetic pathways. Circ Res 19:650–661, 1966.
18. Randall WC, McNally H, Cowan J, Caliguiri L, Rohse WG: Functional analysis of the cardioaugmentor and cardioaccelerator pathways in the dog. Am J Physiol 191:213–217, 1957.
19. Randall WC, Priola DV, Ulmer RH: A functional study of the distribution of cardiac sympathetic nerves. Am J Physiol 205:1227–1231, 1963.
20. James TN, Spence CA: Distribution of cholinesterase within the sinus node and AV node of the human heart. Anat Rec 155:151–162, 1966.
21. Brown GL, Eccles JE: The action of a single vagal volley on the rhythm of the heart beat. J Physiol (Lond) 82:211–240, 1934.
22. Levy MN, Martin PJ, Iano T, Zieske H: Effects of single vagal stimuli on heart rate and atrioventricular conduction. Am J Physiol 218:1256–1262, 1970.
23. Iano TL, Levy MN, Lee MH: An acceleratory component of the parasympathetic control of heart rate. Am J Physiol 224:997–1005, 1973.
24. Jalife J, Moe GK: Phasic effects of vagal stimulation on pacemaker activity of the isolated sinus node of the young cat. Circ Res 45:595–608, 1979.
25. Spear JF, Kronhaus KD, Moore EN, Kline RP: The effect of brief vagal stimulation on the isolated rabbit sinus node. Circ Res 44:75–88, 1979.
26. Hutter OF: Mode of action of autonomic transmitters on the heart. Br Med Bull 13:176–180, 1957.
27. Reid JVO: The cardiac pacemaker: effects of regu-

larly spaced nervous input. Am Heart J 78:58–64, 1969.
28. Levy MN, Martin PJ, Iano T, Zieske H: Paradoxical effect of vagus nerve stimulation on heart rate in dogs. Circ Res 25:303–314, 1969.
29. Levy MN, Iano T, Zieske H: Effects of repetitive bursts of vagal activity on heart rate. Circ Res 30:186–195, 1972.
30. Dong E Jr, Reitz BA: Effect of timing of vagal stimulation on heart rate in the dog. Circ Res 27:635–646, 1970.
31. James TN: The sinus node as a servomechanism. Circ Res 32:307–313, 1973.
32. Hariman RJ, Hoffman RB, Naylor RE: Electrical activity from the sinus node region in conscious dogs. Circ Res 47:755–791, 1980.
33. Levy MN: Sympathetic–parasympathetic interactions in the heart. Circ Res 29:437–445, 1971.
34. Levy MN, Zieske H: Autonomic control of cardiac pacemaker activity and atrioventricular transmission. J Appl Physiol 27:465–470, 1969.
35. Stuesse SL, Wallick DW, Levy MN: Autonomic control of right atrial contractile strength in the dog. Am J Physiol 236:H860–H865, 1979.
36. Levy MN, Ng M, Martin P, Zieske H: Sympathetic and parasympathetic interactions upon the left ventricle of the dog. Circ Res 19:5–10, 1966.
37. Levy MN, Blattberg B: Effect of vagal stimulation on the overflow of norepinephrine into the coronary sinus during cardiac sympathetic nerve stimulation in the dog. Cir Res 38:81–85, 1976.
38. Levy MN: Neural control of the heart: sympathetic–vagal interactions. In: Baan J, Noordergraaf A, Raines J (eds) Cardiovascular system dynamics. Cambridge: MIT, 1978, pp 365–370.
39. Muscholl E: Peripheral muscarinic control of norepinephrine release in the cardiovascular system. Am J Physiol 239:H713–H720, 1980.
40. Lavallée M, De Champlain J, Nadeau RA, Yamaguchi N: Muscarinic inhibition of endogenous myocardial catecholamine liberation in the dog. Can J Physiol Pharmacol 56:642–649, 1978.
41. Mancia G, Bonazzi O, Pozzoni L, Ferrari A, Gardumi M, Gregorini L, Perondi R: Baroreceptor control of atrioventricular conduction in man. Circ Res 44:752–758, 1979.
42. Borst C, Karemaker JM, Danning AJ: Prolongation of atrioventricular conduction time by electrical stimulation of the carotid sinus nerves in man. Circulation 65:432–434, 1982.
43. Hageman GR, Randall WC, Armour JA: Direct and reflex cardiac bradydysrhythmias from small vagal nerve stimulations. Am Heart J 89:338–348, 1975.
44. Prystowsky EN, Jackman WM, Rinkenberger RL, Heger JJ, Zipes DP: Effect of autonomic blockade on ventricular refractoriness and atrioventricular nodal conduction in humans. Circ Res 49:511–518, 1981.
45. Spear JF, Moore EN: Influence of brief vagal and stellate nerve stimulation on pacemaker activity and conduction within the atrioventricular conduction system of the dog. Circ Res 32:27–41, 1973.
46. Martin PJ: Dynamic vagal control of atrial–ventricular conduction: theoretical and experimental studies. Ann Biomed Eng 3:275–295, 1975.
47. Zipes DP, Mihalick MJ, Robbins GT: Effects of selective vagal and stellate ganglion stimulation on atrial refractoriness. Cardiovasc Res 8:647–655, 1974.
48. Cagin NA, Kunstadt D, Wolfish P, Levitt B: The influence of heart rate on the refractory period of the atrium and A-V conducting system. Am Heart J 85:358–366, 1973.
49. Schwartz PJ, Verrier RL, Lown B: Effect of stellectomy and vagotomy on ventricular refractoriness in dogs. Circ Res 40:536–540, 1977.
50. Vallin HO: Autonomous influence on sinus node and AV node function in the elderly without significant heart disease: assessment with electrophysiological and autonomic tests. Cardiovasc Res 14:206–216, 1980.
51. Martins JB, Zipes DP: Effects of sympathetic and vagal nerves on recovery properties of the endocardium and epicardium of the canine left ventricle. Circ Res 46:100–110, 1980.
52. Kolman BS, Verrier RL, Lown B: Effect of vagus nerve stimulation upon excitability of the canine ventricle: role of sympathetic–parasympathetic interactions. Am J Cardiol 37:1041–1045, 1976.
53. Blair RW, Shimizu T, Bishop VS: The role of vagal afferents in the reflex control of the left ventricular refractory period in the cat. Circ Res 46:378–386, 1980.
54. Waxman MB, Wald RW: Termination of ventricular tachycardia by an increase in cardiac vagal drive. Circulation 56:385–391, 1977.
55. De Geest H, Levy MN, Zieske H, Lipman RI: Depression of ventricular contractility by stimulation of the vagus nerves. Circ Res 17:222–235, 1965.
56. Randall WC, Wechsler JB, Pace JB, Szentivanyi M: Alterations in myocardial contractility during stimulation of the cardiac nerves. Am J Physiol 214:1205–1212, 1968.
57. Wiggers CJ: The physiology of the mammalian auricle. II. The influence of the vagus nerves on the fractionate contraction of the right auricle. Am J Physiol 42:133–140, 1917.
58. Sarnoff SJ, Brockman SK, Gilmore JP, Linden RJ, Mitchell JH: Regulation of ventricular contraction: influence of cardiac sympathetic and vagal nerve stimulation on atrial and ventricular dynamics. Circ Res 8:1108–1122, 1960.
59. Randall WC, Armour JA: Complex cardiovascular responses to vagosympathetic stimulation. Proc Soc Exp Biol Med 145:493–499, 1974.
60. Martin P: Atrial inotropic responses to brief vagal stimuli: frequency–force interactions. Am J Physiol 239:H333–H341, 1980.

61. Martin P, Levy MN, Matsuda Y: Fade of the cardiac responses during tonic vagal stimulation. Am J Physiol 243:H219–H225, 1982.
62. Loeb JM, Dalton DP, Moran JM: Sensitivity differences of SA and AV node to vagal stimulation: attenuation of vagal effects at SA node. Am J Physiol 241:H684–H690, 1981.
63. Jalife J, Hamilton AJ, Moe GK: Desensitization of the cholinergic receptor at the sinoatrial cell of the kitten. Am J Physiol 238:H439–H448, 1980.
64. Korner PI: Central nervous control of autonomic cardiovascular function. In: Berne RM (ed) Handbook of physiology. Sect 2: The cardiovascular system. Vol 1: The heart. Bethesda MD: American Physiological Society, 1979, pp 691–739.
65. Kirchheim HR: Systemic arterial baroreceptor reflexes. Physiol Rev 56:100–176, 1976.
66. Brown AM: Cardiac reflexes. In: Berne, RM (ed) Handbook of physiology. Sect 2: Cardiovascular system. Vol 1. Washington DC: American Physiological Society, 1979, pp 677–690.
67. Coleridge JCG, Coleridge HM: Chemoreflex regulation of the heart. In: Berne, RM (ed) Handbook of physiology. Sect 2: Cardiovascular system. Vol 1. Washington DC: American Physiological Society, 1979, pp 653–676.
68. Downing SE: Baroreceptor regulation of the heart. In: Berne, RM (ed) Handbook of physiology. Sect 2: Cardiovascular system. Vol 1. Washington DC: American Physiological Society, 1979, pp 621–652.
69. Bainbridge FA: The influence of venous filling upon the rate of the heart. J Physiol (Lond) 50:65–84, 1915.
70. Vatner SF, Boettcher DH: Regulation of cardiac output by stroke volume and heart rate in conscious dogs. Circ Res 42:557–561, 1978.
71. Daly MB, Angell-James JE, Elsner R: Role of carotid-body chemoreceptors and their reflex interactions in bradycardia and cardiac arrest. Lancet 1:764–767, 1979.
72. Berk JL, Levy MN: Profound reflex bradycardia produced by transient hypoxia or hypercapnia in man. Eur Surg Res 9:75–84, 1977.

16. THE DEVELOPMENT OF POSTSYNAPTIC CARDIAC AUTONOMIC RECEPTORS AND THEIR REGULATION OF CARDIAC FUNCTION DURING EMBRYONIC, FETAL, AND NEONATAL LIFE

Achilles J. Pappano

Introduction

The appearance and development of autonomic receptors and of the mechanisms by which these receptors permit extrinsic regulation of cardiac performance are the object of much research. Interest in this subject has been stimulated because of the fundamental importance that a knowledge of receptor properties and receptor mechanisms has for an understanding of the biochemical, physiologic, pharmacologic, and pathologic features of cardiac function [1, 2]. Furthermore, a systematic examination of the ontogenetic sequence for incorporation of autonomic receptors, the inception of receptor-initiated reactions, and the modifications in receptor-dependent functions is essential for our understanding of how autonomic transmitters regulate the heartbeat.

The development of postsynaptic autonomic receptors and their reaction mechanisms for modulating cardiac function are reviewed in this chapter. Particular attention is given to biochemical studies of receptor properties and how cyclic AMP (cAMP) may connect activated receptors with physiologic and pharmacologic responses. Although some aspects of autonomic innervation of the embryonic heart are considered, the reader may wish to consult recent reviews for a more detailed account of neurogenesis [3–6]. This chapter does not deal with changes of autonomic mechanisms in the hearts of adult and old animals. The reader is referred to a stimulating review for analysis of alterations in adrenergic function in senescent animals [7].

Research done in the author's laboratory was supported by USPHS grant HL-13339. Thanks are due to my colleagues, Dr. D. Inoue, Dr. M. Hachisu, L. Adam, D. Black, C. Smith, and C. Zotter, for their contributions to this research.

N. Sperelakis (ed.), PHYSIOLOGY AND PATHOPHYSIOLOGY OF THE HEART.

Martinus Nijhoff Publishing, Boston/The Hague/ Dordrecht/Lancaster.

Muscarinic Cholinergic Receptor

RECEPTOR BINDING STUDIES

The chemical properties of the muscarinic cholinergic receptor have been examined with ^{3}H-3-quiniclidynyl benzilate ([^{3}H]-QNB) a muscarinic receptor antagonist. The specific binding of ^{3}H-QNB to homogenates of embryonic and neonatal heart tissue is saturable and accounts for $\geq$ 90% of total binding [8–11]. Antagonists of muscarinic receptors displace ^{3}H-QNB from specific binding sites at concentrations 1000 times lower than those observed

TABLE 16–1. Muscarinic cholinergic receptor binding[a]

Heart tissue			IC_{50}	Reference
	B_{max} (10^{-12} mol/mg protein)			
Chick, newborn		Atropine	$3–4 \times 10^{-9}$ M	8
		ACh	3×10^{-6} M	
		Carb	$1–2 \times 10^{-5}$ M	
Chick, 3-day embryo	0.4			
7-day embryo	0.7			
12-day embryo	1.5–2.0			
17-day embryo	2–3			
21-day embryo	~5			
Chick, 9-day embryo	~0.25[b]	QNB	1×10^{-9} M	9
		Atropine	2.2×10^{-9} M	
		Carb (3E)	3.7×10^{-6} M	
		Carb (9E)	0.8×10^{-6} M	
Chick, 11-day embryo	~0.17[b]	Atropine	25×10^{-9} M	10
		Oxtremorine	4.8×10^{-6} M	
Chick, 10-day embryo[c]	0.28	Atropine (10E)	6×10^{-9} M	11
		Atropine (H)	6.2×10^{-9} M	
21-day[c]	0.59	Carb (10E)	3.3×10^{-6} M	
		Carb (H)	30×10^{-6} M	
		ACh (10E)	1.5×10^{-7} M	
		ACh (H)	40×10^{-7} M	
	B_{max} (^{3}H-QNB sites/μm^2)[d]			
Mouse, 9-day embryo	452		—	27
14-day embryo	844		—	
17-day embryo	784		—	
1-day neonate	407		—	
	B_{max} (10^{-15} mol/mg tissue)			
Mouse, 13–14-day embryo	Not detected			12
15–16-day embryo	~1.5			
17–18-day embryo	~3.1			
19–20-day embryo	~2.9			
21–22-day embryo	~5.3			
Adult	12	Atropine	6.7×10^{-9} M	

[a]^{3}H-QNB (tritium-labeled quiniclidynyl benzilate) was used in all experiments to identify muscarinic cholinergic receptors.
[b]No change in maximum specific binding was observed between the third and 18th embryonic days.
[c]Values obtained from homogenate (B_{max}) and from membrane fraction of homogenates (IC_{50}).
[d]Number of binding sites approximately doubled within one week in culture.

with agonists (table 16–1). Moreover, the binding of muscarinic antagonists (QNB, atropine, scopolamine) is characterized by a Hill coefficient of 1.0, whereas agonist binding displays a Hill coefficient of about 0.5 [9–11]. Kinetic analysis indicated that the binding of ^{3}H-QNB is consistent with a two-step sequential reaction in which a rapidly reversible complex of ^{3}H-QNB with receptor is transformed to a slowly reversible complex during long (1 h) exposure to the ligand [9].

Binding of ^{3}H-QNB with high affinity was also observed in homogenates of heart muscle prepared from embryonic, neonatal, and adult mice (table 16–1). The concentration of atropine required to displace 50% of ^{3}H-QNB specifically bound to mouse heart homogenate did not change during development [12]. Similarly, neither the K_D (dissociation constant) for QNB [10] nor the IC_{50} for atropine [9] was reported to change during embryonic development of the chick heart. Finally, in both chick

and mouse hearts, nicotinic cholinergic antagonists (*d*-tubocurarine, hexamethonium, Naja mossambica neurotoxin, α-bungarotoxin) displaced ^{3}H-QNB only at high concentrations ($IC_{50} \geq 10^{-4}$ *M*). Therefore, it has been concluded that the determination of the K_D and number of specific ^{3}H-QNB binding sites provides a quantitative estimation of the properties of muscarinic cholinergic receptors in embryonic heart tissue. This conclusion agrees with that drawn from experiments done with the hearts of adult animals [1, 2, 13].

The number of specific ^{3}H-QNB binding sites increased during development of the embryonic chick heart according to Sastre et al. [8] and Hosey and Fields [11]. This observation differs from that of others [9, 10] who reported no change in the number of such sites. Protein content was determined by the method of Lowry in the experiments of Sastre et al. [8] and in those of Galper et al. [9] so that the estimation of specific ^{3}-QNB binding sites was probably not made discrepant by this aspect of the experimental procedure. Binding of ^{3}H-QNB can be modulated by cations and by guanine nucleotides in adult mammalian hearts [1] and in embryonic avian hearts [14, 15]. However, the possibility that different concentrations of these substances might influence the number as well as the affinity of specific ^{3}H-QNB binding sites detected is not a convincing explanation for the discrepancy in results. Muscarinic cholinergic receptors are present in sympathetic adrenergic nerves and could contribute to estimates of B_{max} in homogenates of embryonic cardiac cells. Homogenates were used in the experiments of Galper et al. [9] and of Hosey and Fields [11] and it is unlikely that neuronal binding sites for ^{3}H-QNB were absent in the preparations used by Galper et al. [9]. In this regard, Galper et al. [9] noted that there was no difference between atrial and ventricular tissue in either the number of ^{3}H-QNB binding sites per milligram protein or in their distribution as a function of developmental age. In cell culture experiments with eight-day embryonic chick heart tissues, B_{max} was 200 fmol/mg protein and 150 fmol/mg protein in atria and ventricles, respectively [16]. The distribution of specific ^{3}H-QNB binding sites (K_D = 30 p*M*) appeared diffuse in autoradiographs and the estimated density of muscarinic cholinergic receptors (sites/μm^2) was 83 ± 5 in atria and 81 ± 4 in ventricles [16].

The concentration–effect relationship for displacement of ^{3}H-QNB by agonists from binding sites in embryonic chick heart had Hill coefficients of around 0.5 in contrast to values of about 1.0 for antagonists. On the basis of similar results obtained in adult mammalian hearts, it has been concluded that muscarinic receptor sites are heterogeneous and that the agonist (but not antagonist) can "induce or stabilize an active conformational state of the receptor" (p. 24 in Hulme et al. [1]). It is noteworthy that the concentration of agonist required to displace 50% of specifically bound ^{3}H-QNB changed as a function of embryonic age. Galper et al. [9] found that 50% inhibition of ^{3}H-QNB binding required 3.7×10^{-6} *M* carbachol (Carb) in hearts from three-day embryos and 8×10^{-7} *M* in those from nine-day embryos. Hosey and Fields [11] reported that the IC_{50}s for displacement of ^{3}H-QNB binding by acetylcholine (ACh) were 0.16×10^{-6} *M* and 3.98×10^{-6} *M* in ten-day embryos and hatched chick hearts, respectively. Similar results were obtained in experiments with Carb. Because of the different and noninclusive ages of the animals used in these two studies, no satisfactory explanation can be given for these seemingly divergent results. The IC_{50} for Carb was 3.28×10^{-6} *M* in ten-day embryos [11] and 0.8×10^{-6} *M* in nine-day embryos [9]. However, the experimental preparations were sufficiently different (cell membrane fraction in the report by Hosey and Fields [11] as contrasted with homogenate in the report by Galper et al. [9]) to preclude a systematic comparison.

Another difference in experimental results has been addressed by Hosey and Fields [11], who reported that ^{3}H-QNB binding was more rapidly reversed by addition of atropine than reported by others [9, 10]. This discrepancy was not solved by an experiment by Hosey and Fields in which these investigators used the same incubation and assay media described by Galper et al. [9].

The presence of a heterogeneous population of muscarinic receptors in the embryonic heart has been evaluated in experiments in which the

pharmacologic effect of Carb displayed desensitization in cultured heart cells [14] and in intact embryonic atria [17]. The results from both laboratories are similar insofar as a 3- to 6-h treatment of heart cells with Carb reduced the number of ^{3}H-QNB binding sites without changing the affinity of these sites for ^{3}H-QNB. Galper and Smith [14] reported that a rapid ($\leq$1 min) loss of 26% of the ^{3}H-QNB binding sites occurred in the presence of Carb and that this fraction of sites was insensitive to colchicine, which disrupts microtubules. Moreover, this reduction in the number of binding sites was accompanied by a decrease in the affinity of Carb for all remaining ^{3}H-QNB binding sites. A similar shift in IC_{50} for Carb-induced displacement of ^{3}H-QNB from binding sites occurred in the presence of guanylylimidodiphosphate (Gpp[NH]p) [14]. By contrast, the slower loss of ^{3}H-QNB binding sites induced by Carb was partially inhibited by treatment with colchicine and recovery of ^{3}H-QNB binding sites was not affected by treatment with Gpp(NH)p. Similar results were obtained when desensitization was produced by treatment of intact embryonic heart cell with Carb [17]. Chronic treatment with Carb reduced the fraction of receptors in the high-affinity (R_H) state without changing the affinity for Carb in either R_H or low-affinity (R_L) states of the receptor. Finally, Halvorsen and Nathanson [17] concluded that the R_H state of the receptor is not necessarily required for the negative chronotropic effect of Carb, a view that does not disagree with the proposal (reviewed by Hulme et al. [1]) that R_L is the physiologically active form of the muscarinic receptor.

RECEPTOR ACTIVATION

Electrophysiologic and Contractile Effects. In general, the parasympathetic neurotransmitter, ACh, and muscarinic agonists inhibit the embryonic heart. The relationship between the sensitivity of the sinoatrial node to inhibition by muscarinic agonists and the onset of parasympathetic neuroeffector transmission has been reviewed [3]. Inhibition of sinoatrial pacemaker activity in hearts from three- and four-day embryos was associated with membrane depolarization in contrast to the hyperpolarization observed in hearts taken from animals at and after the sixth embryonic day [18]. It was concluded that ACh increased Na^+ conductance (g_{Na}) when it depolarized the sinoatrial membrane and that this conductance change masked an increase of g_K and membrane hyperpolarization that could be observed when Na^+ was omitted from the fluid bathing four-day embryonic hearts. The ability of ACh to increase g_K and thereby hyperpolarize the sinoatrial membrane increased during embryogenesis in parallel with an increase in g_K of atrial membranes. A gradual reduction in g_{Na}/g_K has also been observed in ventricular membranes of the chick during embryogenesis [19]. That membrane g_K increases during embryonic development of the chick ventricle has been corroborated by measurements of membrane permeability to K^+ [20].

Sensitivity of the sinoatrial node to inhibition by ACh increased during ontogenesis [21, 22]. These results have been confirmed by others who have also examined the properties of the muscarinic receptor with ^{3}H-QNB [9, 10]. Two aspects of the ^{3}H-QNB binding studies require additional consideration. First, muscarinic cholinergic receptors are present in ventricles of three-day embryos, a time when the authors concluded that muscarinic agonists had no inhibitory effect on the rate of beating [9, 10]. However, these results were obtained in cultures or in whole hearts containing a mixture of atrial and ventricular cells. Therefore, it may not be appropriate to relate a 20%–60% reduction in beating rate by muscarinic agonists to muscarinic cholinergic receptor properties in atrial and ventricular cells because the former can arise from drug action on the sinoatrial node whereas the latter derives from the receptor population in atria and ventricles. In this connection, it has been reported that specific ^{3}H-QNB binding sites are undetectable in hearts obtained from mice on days 13–14 of gestation [12]. At this age, 10^{-6} *M* ACh reduced heart rate by 44%. The failure to detect specific ^{3}H-QNB binding sites when a pharmacologic effect of ACh through muscarinic receptors is demonstrable might be due to dilution of ^{3}H-QNB binding sites in the sinoatrial

node by membranes derived from the whole heart [23]. Second, Galper et al. [9] concluded that the embryonic chick heart was practically insensitive to Carb in two- to four-day embryos and completely sensitive in seven-day embryos. These results were obtained in the presence of isoproterenol, a β-adrenergic agonist that increases heart rate. It was subsequently demonstrated that inhibition of Ca^{2+}-dependent action potentials by ACh in the embryonic chick ventricle was not consistently observed until the seventh embryonic day and required the presence of β-adrenergic agonist for inhibition thereafter during embryogenesis [24]. Perhaps the discrepancy between the results of Renaud et al. [10], who detected muscarinic inhibition at an earlier time than Galper et al. [9], is due to a greater proportion of atrial cells which are directly inhibited by ACh in the preparations used by Renaud et al.

Because the number of specific ^{3}H-QNB binding sites did not increase with age in embryonic chicks, the increased sensitivity to muscarinic agonists during development was attributed to a more efficient coupling of muscarinic receptor to the membrane conductance thought responsible for effecting inhibition, namely, P_K [9, 10]. This conclusion is essentially the same as that drawn earlier from electrophysiologic experiments [18]. However, none of these studies considered the possibility that muscarinic agonists inhibited cardiac function, specifically in the sinoatrial node, by reducing the slow inward current (i_{si}) carried by Ca^{2+} and that this current system became more sensitive to inhibition by ACh. The fact that ACh can inhibit atrial cells by an action on both i_{si} and i_K has been demonstrated in adult mammalian hearts (reviewed by Reuter [25]) and observed in the chick heart [26].

Results obtained in the mouse heart indicate that this preparation becomes more sensitive to inhibition by ACh as the number of muscarinic cholinergic receptors increases (reviewed by Roeske and Wildenthal [23]). Although there is agreement that there is an ontogenetic increase in sensitivity to muscarinic inhibition and in muscarinic cholinergic binding sites in the embryonic mouse heart, it is noteworthy that both aspects of the muscarinic system were demonstrable at an earlier time (nine-day embryonic heart in culture for two days) in the experiments of others [27]. There is no information available on the role of changes in membrane conductance, particularly g_K, in the increased sensitivity of the embryonic mouse heart to muscarinic inhibition of pacemaker function. In the embryonic rat heart, atrial sensitivity to ACh increased in parallel with an increase of membrane g_K [28] and the sensitivity of the sinoatrial pacemaker to the negative chronotropic effect of ACh and Carb did not change after birth [29]. If one assumes that the rat heart displays the same ontogenetic increase in specific ^{3}H-QNB binding sites as the mouse heart, it may be speculated that there is a coordinate development of muscarinic receptors and associated K^+ channels responsible for muscarinic inhibition. This model would not apply to the embryonic chick heart if there is no ontogenetic change in muscarinic receptor density, as proposed by some investigators [9, 10].

Muscarinic inhibition of the embryonic chick ventricle can be attributed to a decrease of g_{si} that has been augmented by substances that increase cellular content of cyclic AMP (reviewed by Pappano [4] and Pappano and Biegon [30]; see the next section of this chapter). Inhibition of Ca^{2+}-dependent action potentials in ventricles from embryonic [24, 31] and hatched chicks [26] can be explained by a reduction of g_{si} alone. This differs from muscarinic inhibition in the chick atrium where g_K is increased during suppression of the Ca^{2+}-dependent action potential [26]. Inhibition of the maximum rate of rise ($\dot{V}_{max}$) of the Ca^{2+}-dependent action potential (an index of inward i_{Ca}) by ACh in the ventricle was noncompetitive [26] in contrast to the competitive interaction between ACh and $[Ca^{2+}]_0$ in the atrium [32]. Calcium channel blockers (verapamil, nifedipine, and nimodipine), at concentrations $\leq 10^{-6}$ *M*, inhibited $\dot{V}_{max}$ of the ventricular Ca^{2+}-dependent action potential competitively [33]. Therefore, there seems to be no qualitative change in the ionic mechanism (g_{si}) for muscarinic inhibition of the avian ventricle during ontogenesis [26] in contrast to that reported for muscarinic inhibition of the sinoatrial node [18].

Are muscarinic receptors in atrial cells different from those in ventricular cells? It was mentioned previously in this chapter that the density of muscarinic receptor sites is the same in chick atrial and ventricular cells. Receptor affinity for atropine, estimated by Schild analysis, is also the same ($1–4 \times 10^{-9}$ *M*) in atria and ventricles (Adam and Pappano, unpublished observations). The differences in ionic currents modified by ACh in atria and ventricles cannot be explained by systematic differences in the density or antagonist affinity of muscarinic cholinergic receptors. Nevertheless, it is essential to determine the affinity of muscarinic receptors for agonist in the two cell types before one can reach a definitive conclusion about the role of muscarinic receptor properties in regulating ionic conductances.

Role of Cyclic Nucleotides in Muscarinic Inhibition. The role of adenosine-3′,5′-cyclic monophosphoric acid (cyclic AMP, or cAMP) in the action of parasympathetic and sympathetic neurotransmitters on embryonic heart function has been recently reviewed [4, 23]. Additional evidence in support of the cAMP hypothesis for sympathetic transmitter action on the embryonic heart is given later in this chapter.

There is considerable support for the participation of the adenylate-cyclase–cAMP system in the inhibition of the chick heart caused by activation of muscarinic receptors. Acetylcholine has little effect on adenylate cyclase activity, cAMP content, Ca^{2+}-dependent action potentials, and contractions in embryonic chick ventricle. However, ACh inhibits the activation of adenylate cyclase, the accumulation of cAMP, the augmentation of Ca^{2+}-dependent action potentials, and the positive inotropic effect of isoproterenol (ISO) in embryonic chick ventricle (reviewd by Pappano and Biegon [30]). This effect, termed *indirect* muscarinic inhibition, was not detected until the seventh incubation day, a finding consistent with the results of others [9]. Because muscarinic cholinergic receptors are present on the third incubation day, it was speculated that inhibition by ACh required the synthesis or incorporation of a nucleotide regulatory component (termed N_i in the hypothesis of Rodbell [34]) that permits inhibition of adenylate cyclase activation by the β-adrenergic receptor [30]. After hatching, ACh inhibits *directly* the activation of adenylate cyclase, the accumulation of cAMP, Ca^{2+}-dependent action potentials, and contractility, even in the absence of adrenergic nerves and β-adrenergic agonist. The mechanism for the transition from indirect to direct muscarinic inhibition could involve a change in regulation of catalytic unit activity by N_i because it has been demonstrated that ACh inhibits GTP-stimulated adenylate cyclase in adult mammalian ventricle [35]. The transition from indirect to direct muscarinic inhibition in the avian ventricle may reside in a change of the regulation of adenylate cyclase activity by muscarinic receptor because there is no qualitative change in the ionic conductance (g_{si}) acted upon by muscarinic agonists [26, 31].

The reaction mechanism for muscarinic inhibition is complex because it may also include an inhibition of the effect of accumulated cAMP. The phosphodiesterase inhibitor, isobutylmethylxanthine (IBMX), causes cAMP to accumulate in the embryonic avian heart and thereby augments the Ca^{2+}-dependent action potential and the force of contraction. Low concentrations of ACh inhibit the effects of IBMX on the Ca^{2+}-dependent action potential and reverse the positive inotropic effect without reducing the accumulated cAMP AMP [36]. That activation of muscarinic receptors can inhibit the effect of accumulated cAMP in the embryonic heart is strengthened by experiments done with cholera toxin. Within 3 min, acetylcholine reversed the positive inotropic effect of cholera toxin without changing the stimulation of adenylate cyclase activity nor the 2.5-fold accumulation of cAMP produced by a 3-h exposure to the toxin [37]. It is not known whether this form of muscarinic inhibition involves an effect on the activation of cAMP-dependent protein kinases or on phosphorylation of membrane proteins. It has been suggested that the stimulatory effect of IBMX may occur by inhibition of the inhibitory actions of endogenous adenosine on adenylate cyclase and that ACh facilitates the inhibitory action of adenosine [36], but this view has been challenged by Linden et al. [38]. Although these

investigators confirmed the observation that activation of muscarinic receptors inhibited the effects of IBMX on Ca^{2+}-dependent action potentials, they concluded that endogenous adenosine was not an essential component for either the stimulatory effect of IBMX or the inhibitory effect of acetyl-β-methylcholine (MCh). This conclusion was prompted by their finding that nonmethylxanthine inhibitors of phosphodiesterase, which do not act on adenosine receptors, permitted muscarinic inhibition that was attributed to reduced accumulation of cAMP. Solution of the discrepancy requires more careful study. Whatever the outcome in the experiments with IBMX, the results of experiments with ACh and cholera toxin are most reasonably explained by an effect of muscarinic receptors that inhibits the activation of cAMP-dependent cell functions without changing the cellular content of cAMP. A similar conclusion has been drawn from experiments with adult mammalian hearts where ACh inhibited the positive inotropic effect but not the accumulation of cAMP caused by epinephrine. Muscarinic inhibition was attributed either to a diminished activation of cAMP-dependent protein kinase [39] or to diminished phosphorylation in the presence of an unchanged protein kinase activity ratio [40].

The possibility that cyclic-3′,5′-guanosine monophosphate (cyclic GMP, or cGMP) mediates the inhibition caused by activation of muscarinic receptors in the adult heart has been examined and has not received consistent experimental support (reviewed by Linden and Brooker [41]). Renaud et al. [10] found that cGMP content of embryonic heart muscle strips increased in association with the negative chronotropic effect of muscarinic agonists, but these investigators also found that muscarinic agonists had no effect on cGMP content of heart cell reaggregates when these drugs inhibited automaticity [10]. More recently, muscarinic inhibition of the positive inotropic effect of cholera toxin was reported to be unaccompanied by changes in cGMP content of embryonic chick ventricles [37]. Neither of these reports excludes the possibility that muscarinic drugs increase cGMP content in a small cellular pool and thereby activate a protein kinase associated with inhibition. This mechanism has been proposed as a result of experiments that support the validity of the cGMP hypothesis for muscarinic inhibition [42].

Consideration must also be given to the possibility that muscarinic cholinergic receptors are connected to reaction pathways completely independent of cyclic nucleotides. Results from several laboratories (reviewed by Pappano [3]) and more recent data obtained by others [10] and ourselves [36] indicate that muscarinic agonists have stimulatory effects in the avian heart. At high concentrations ($>10^{-6}$ *M*), ACh increases the force of contraction in embryonic [36] and hatched chick ventricles (L.P. Adam, D. Black, and A.J. Pappano, unpublished observations). The positive inotropic effect of ACh (or reversal of negative inotropic effect in hatched chicks) is not prevented by propranolol, a β-adrenergic antagonist, nor associated with an increase of cAMP [36]. Atropine antagonizes the positive inotropic effect of high concentrations of ACh and Carb in the embryonic chick ventricle. The mechanism for this apparently stimulatory effect of muscarinic receptor activation is unknown. It may be speculated that the positive inotropic effect of ACh is related to increased synthesis of prostaglandin-like substances. Prostaglandin E has a positive inotropic effect in the embryonic chick ventricle (Black and Pappano, unpublished observations) and it has been established that ACh can increase prostaglandin synthesis in endothelial cells of vascular smooth muscle [43, 44]. The fact that the embryonic heart is formed by the fusion of blood vessels adds an intriguing aspect to this speculation.

β-*Adrenergic Receptor*

BINDING STUDIES

Recent reports for the binding of radioactively labeled ligands for the β-adrenegic receptor in embryonic and fetal hearts have been summarized in table 16–2; ^{3}H-dihydroalprenolol (^{3}H-DHA) is the labeled antagonist used in these studies. Criteria for identification of specific ^{3}H-DHA binding sites as β-adrenergic receptors have been rigorously applied in experi-

TABLE 16–2. β-Adrenergic receptor binding[a]

Heart tissue			Reference
	B_{max} (pmol/mg protein)	K_D ($\times 10^{-9}$ *M*)	
Chick heart			
5-day embryo	0.36 ± 0.03	13.3 ± 3.0	48
7-day embryo	0.36 ± 0.03	—	
9-day embryo	0.22 ± 0.02	—	
13-day embryo	0.14 ± 0.01	10.5 ± 0.5	
17-day embryo	0.16 ± 0.01	—	
Chick erythrocyte			
8-day embryo	7.3	21.0	53
9-day embryo	7.4	16.3	
13-day embryo	7.4	22.5	
17-day embryo	6.9	15.9	
18-day embryo	4.9	13.2	
Hatched	4.3	21.2	
Adult	4.5	19.5	
	B_{max} (fmol/mg membrane protein)		
Rat heart			
5 days after birth	50.2	1.65	47
15 days after birth	49.0 ± 1.8	1.73	
28 days after birth	45.8 ± 6.8	2.21 ± 0.39	
	B_{max} (fmol/mg protein)		
3 weeks after birth	138	10.5	56
6 weeks after birth	67 ± 8	5 ± 1.0	
12 weeks after birth	42 ± 7	2 ± 0.4	
Mouse heart			
	B_{max} (fmol/mg tissue)		
17–18-day fetus	1.04 ± 0.20	0.24 ± 0.04	23
19–20-day fetus	1.85 ± 0.13	0.31 ± 0.04	
21–22-day fetus	1.89 ± 0.09	0.26 ± 0.02	
1-day neonate	2.41 ± 0.10	0.32 ± 0.03	
3-day neonate	4.00 ± 0.31	0.30 ± 0.03	
14-day neonate	3.92 ± 0.31	0.36 ± 0.02	
3–5 months (adult)	2.24 ± 0.10	0.32 ± 0.06	
		IC_{50} ($\times 10^{-9}$ *M*)	
Adult	2.24 ± 0.10	(±)-DHA 0.33 ± 0.03	
		(−)Propranolol 0.38 ± 0.07	
		(−)Isoproterenol 38 ± 4	
		(−)Epinephrine 330 ± 30	
		(−)Norepinephrine 350 ± 50	

[a]^{3}H-DHA (tritium-labeled dihydroalprenolol) was used in all experiments to identify β-adrenergic receptors.

ments with the mouse heart [45]. Specific binding of ^{3}H-DHA was saturable, reversible, and displayed high affinity and steric specificity. The apparent K_D for specific ^{3}H-DHA binding was 0.32 n*M* in equilibrium experiments and 0.30 ± 0.05 n*M* in kinetic experiments done with homogenates from adult mouse hearts [45]. In the adult mouse heart, the IC_{50} for displacement of specifically bound ^{3}H-DHA displayed steric specificity and the expected difference between agonists and antagonists (table 16–2). Specific ^{3}H-DHA binding sites may be identified as β_1-adrenergic receptors because of the similar IC_{50}s for epinephrine and norepinephrine, which are about ninefold greater than that for ISO. It is

noteworthy that 10^{-4} *M* ACh had no effect on specific ^{3}H-DHA binding. The Hill coefficient for ^{3}H-DHA binding was 1.0, a result consistent with the presence of a single class binding sites. The observation that the Hill coefficients for other agonists and antagonists was 0.7 is puzzling because the Hill coefficient is usually 1.0 for antagonists and about 0.5 for agonists [46]. Similar results for saturability and for reversibility of ^{3}H-DHA binding and displacement of ^{3}H-DHA by agonists and antagonists have been reported for a 30,000 *g* particulate preparation from the neonatal rat heart [47] and for a 50,000 *g* particulate preparation from the embryonic chick heart [48]. Specific binding of ^{3}H-DHA, ranged from 50% [45] to 80% [47, 48]. Experiments with rat heart membranes also examined the specific binding of (±)-[^{125}I] iodohydroxybenzylpindolol, [(±)^{125}I-HYP], a β-adrenergic antagonist that can be labeled to very high specific activity [49]. The results of these experiments confirmed those obtained with ^{3}H-DHA regarding the identification of β-adrenergic receptors. Estimates of B_{max} with ^{3}H-DHA were 64 and 36 fmol/mg protein in fetal and adult hearts; corresponding values of B_{max} with ^{125}I-HYP were 42 and 16 fmol/mg protein, respectively [49]. However, the authors noted that the relative difference in number of β-adrenergic binding sites between fetal and adult hearts was maintained with each of the radioactive ligands. It is noteworthy that β_1-adrenergic receptors and β_2-adrenergic receptors accounted for 75% and 25%, respectively, of the total population of specific binding sites [49] and 10^{-5} *M* phentolamine did not alter binding of ^{3} H-DHA [47]. The presence of 10^{-4} *M* Gpp(NH)p did not alter the maximum number of specific ^{3}H-DHA binding sites in embryonic chick hearts isolated on the fifth and 13th incubation days [48]. It is not known whether the displacement–concentration curves for antagonist are unchanged in the presence of Gpp(NH)p, but the presence of GTP reduced the apparent affinity of agonists for ^{125}I-HYP binding sites and increased the Hill coefficient to 1.0 in fetal rat hearts [49]. This result is similar to that described in adult hearts [2] and it seems appropriate to conclude that the radioactive ligand binding studies in embryonic and fetal avian and mammalian hearts describe the properties of β-adrenergic receptors.

Modulation of specific ^{3}H-DHA binding sites during ontogenesis is expressed in strikingly different patterns in the systematic studies of the β-adrenergic receptor. In the mouse, there is no significant change in the K_D for ^{3}H-DHA binding between fetal and adult hearts [45]. The maximum number of binding sites increased significantly during late fetal stages, attained adult levels (100%) one day after birth, and then rose sharply to 178% in three- to 14-day neonates before declining in the adult (2.24 ± 0.1 fmol/mg tissue) [23]. This pattern was replicated in a second series of experiments [50]. It was concluded that the number of β-adrenergic receptor sites decreased after weaning in the mouse because of the development of sympathetic adrenergic innervation that was associated with increased norepinephrine content of the heart [23]. These results would be consistent with the occurrence of down-regulation of β-adrenergic receptors caused by increased transmitter availability [2, 46].

A similar conclusion has been drawn from measurements of the changes in β-adrenergic receptor in the embryonic chick heart from incubation days 5 to 17 [48]. The authors speculate that the marked decrease in specific ^{3}H-DHA binding sites may be determined by the presence of noradrenergic neurons that are establishing neuroeffector relationships in the heart at this time. This proposal is supported by the finding that cardiac content of norepinephrine (NE) increased markedly between incubation days 7 and 10 [51]. Experiments in our laboratory indicated that cocaine-sensitive uptake of NE is first detected at incubation day 12 when the few adrenergic axons present are first able to release NE by a calcium-dependent process initiated by K^{+}-induced depolarization [52]. Therefore, it is possible that development of secretory mechanisms by adrenergic neurons is sufficiently well developed by incubation day 13 to induce down-regulation of a β-adrenergic receptors. However, secretion of NE by electri-

cal stimuli and K^+ increases dramatically (20-fold) between incubation days 12 and 16 [52]. During this interval, there is no change in the number of β-adrenergic receptors in the chick heart (see table 16–2). In embryonic chick red cells, the number of specific ^{3}H-DHA binding sites was rather constant between incubation days 8 and 17, decreased markedly on incubation day 18, and remained low in hatched chicks and adult chickens (table 16–2) [53]. Perhaps the diminution of β-adrenergic receptor density in erythrocytes is the result of down-regulation due to increased levels and secretion of catecholamines in neurons which develop at this time (see above). The decrease of β-adrenergic receptors reported by Alexander et al. [48] was larger between incubation days 7 and 9 than between days 9 and 13. There is little evidence to support the suggestion that structures having the properties of sympathetic adrenergic axons are present by incubation day 9 [52]. Finally, Ignarro and Shideman [51] reported that cardiac NE content increased twice during embryogenesis in the chick, once between incubations day 7 and 10 and later between incubation days 14 and 18. The peak NE content was essentially the same on incubation days 10 and 18, and it is noteworthy that the second increase in NE content observed coincided with the development of adrenergic neuroeffector transmission in the ventricle [54]. Before it can be accepted that the results obtained by Alexander et al. [48] are due to a sympathetic adrenergic innervation-dependent down-regulation of β-adrenergic receptors, it is essential to ascertain that the number of β-adrenergic receptors remains low at times after adrenergic neuroeffector relationships have been established and that β-adrenergic receptor density increases following sympathetic adrenergic denervation.

Ontogenetic regulation of the β-adrenergic receptor has also been examined in the rat heart. The maximum binding of ^{3}H-DHA per milligram of protein decreased from 58.3 ± 6.3 fmol in fetal heart to 36.8 ± 4.1 fmol in adult rat heart [49]. This observation was confirmed in a study that examined the role of thyroid hormone in regulation of β-adrenergic receptors [47] and this result extends that originally described by others [55]. Bhalla et al. [56] reported that the number of β-adrenergic receptors per milligram of protein decreased with age in rats from three to 12 weeks after birth (table 16–2). The decline in B_{max} is greater than in the study by others [47] although the results are qualitatively similar. Unlike Whitsett et al. [47], Bhalla and coinvestigators observed an increased affinity of the β-adrenergic receptor for ^{3}H-DHA during the experimental period. An explanation for this discrepancy is lacking. Although the number of specific ^{3}H-DHA binding sites per heart increased as heart weight increased [49, 55], protein content and the activity of Na,K-ATPase, 5′-nucleotidase, and adenylate cyclase increased more rapidly than did ventricular weight [49]. These results, together with stereologic estimates of cell surface–volume ratio, indicated that the number of β-adrenergic receptors per area of sarcolemmal membrane remained constant and that sarcolemmal surface area decreased during development in the rat heart [49, 55]. It was speculated that male and female sex hormones did not exert a detectable regulation of β-adrenergic receptors [55], but thyroid hormone deficiency and excess were associated with a decrease and increase, respectively, in the B_{max} for specific ^{3}H-DHA binding in young rat hearts [47, 57–59]. It was concluded that thyroid hormone or factors dependent on it could regulate the β-adrenergic receptor as well as hypertrophic growth of the postnatal rat heart.

EFFECTS ON ELECTROPHYSIOLOGIC AND CONTRACTILE ACTIVITY

Isoproterenol (ISO), epinephrine (EPI), and norepinephrine (NE) stimulate the rate and force of myocardial contractions by interaction with β-adrenergic receptors in embryonic avian and mammalian hearts (reviewed by Pappano [3, 4], Roeske and Wildenthal [23], and Sperelakis [60]). The role of adenylate cyclase stimulation and cAMP accumulation in the positive chronotropic and positive inotropic effects of catecholamines is discussed below.

Activation of β-adrenergic receptors increases the amplitude, duration, and rate of rise ($\dot{V}_{max}$) of Ca^{2+}-dependent action potentials in

the embryonic chick heart [24, 61]; this effect is a reflection of an increased membrane conductance to Ca^{2+} in slow, inward current channels (g_{si}). When $(\dot{V}_{max})^{-1}$ is plotted against $[Ca^{2+}]_0^{-1}$, there is a rectilinear relation observed [33] that is consistent with the surface-density hypothesis for Ca^{2+} entry first described in barnacle muscle fibers [62]. Isoproterenol increases the limiting value of $\dot{V}_{max}$ without changing the apparent dissociation constant for Ca^{2+} with the membrane sites associated with Ca^{2+} current regulation [26]. This result indicates that the catecholamine-induced increase of g_{si}, as in adult ventricular muscle, is referable to an increase in the number of g_{si} channels activated by a given voltage without a change in the selectivity of g_{si} channels for Ca^{2+} (reviewed by Reuter [25]). Measurements of i_{si} in voltage-clamp experiments with embryonic chick ventricle reaggregates in the presence of ISO are in accordance with this hypothesis [31]. No change in outward K^+ current (i_x) occurred in embryonic ventricular cells treated with ISO [31]. This result contrasts with those obtained in atrial [63] and Purkinje fibers [64, 65] where activation of β-adrenergic receptors increases i_x.

The relationship between ontogenetic changes in the number of β-adrenergic receptors and pharmacologic effect has been examined in several species. In the fetal mouse heart, the increase of β-adrenergic receptors in fetal life (table 16–2) was associated with an increased sensitivity of the sinoatrial pacemaker to ISO [45]. These investigators also reported that ISO had no positive chronotropic effect in 13-day fetal mouse hearts when specific ^{3}H-DHA binding amounted to 14% of adult values. At variance with these results is the observation that ISO increased beating rate in mouse heart cells isolated from embryos on ninth day in utero and maintained in cell culture for two days [27]. Although estimates of β-adrenergic receptor number were not obtained because of the large fraction of nonspecific binding of ^{3}H-DHA, the presence of specific ^{3}H-DHA binding sites was reported in these heart cells by autoradiography. An increase in sensitivity to β-adrenergic agonist occurred during cardiac development, but could not be compared to the density of β-adrenergic receptor sites [27]. The rapid increase in β-adrenergic receptor number and sensitivity to ISO that occurred in late fetal life was not associated with alterations of the K_D for antagonist [45]. (The relationship between the postnatal increase of β-receptor number [table 16–2] and sensitivity of the mouse heart to β-adrenergic agonists has not been examined.) It would be of interest to know whether changes in affinity for β-adrenergic agonist can also be excluded as an explanation for the increased sensitivity to ISO. Finally, these studies have not excluded the possibility that changes in coupling mechanisms, which can have a significant effect on β-adrenergic sensitivity in the chick heart (see the following section), occur during development in the mouse heart [45].

In the embryonic chick heart, sensitivity of the sinoatrial pacemaker [22] and of ventricular muscle [54] to the positive chronotropic and positive inotropic effects of catecholamines decreased during the last five days in ovo and then increased after hatching. This subsensitivity to β-adrenergic agonists, which seems temporally but not casually related to the onset of adrenergic neuroeffector transmission, may be explained by a modification of the β-adrenergic receptor, the catalytic unit of adenylate cyclase, or the GTP-dependent regulatory protein that couples receptor to catalytic unit (see the following section). A reduction in the number of β-adrenergic receptors may be insufficient to explain this form of β-adrenergic subsensitivity. According to Alexander et al. [48], the density of β-adrenergic receptors is unchanged between incubation days 13 and 17 when sensitivity to ISO is high (day 13) and low (day 17) [54]. A further reduction of the number of β-adrenergic receptors would be expected at one week after hatching when adrenergic transmitter release and transmission are well established [52, 54] and one would expect greater manifestation of down-regulation. This problem can be resolved when measurements of specific ^{3}H-DHA binding are done in hatched chicks.

Experiments in the chick heart indicate that sensitivity of β-adrenergic receptors to agonists undergoes similar changes at the same time

during development of atria and ventricles (reviewed by Pappano and Higgins [5] and Higgins [6]). In the rat heart, the sensitivity of the sinoatrial pacemaker to NE did not change between birth and 6–8 weeks later while the sensitivity of the left atrium [66] and of papillary muscle [67] decreased. The sensitivity to ISO did not change in any of these preparations over the same experimental period. (These results conflict with those reported by others who found that the sensitivity of rat heart sinoatrial pacemaker to ISO, determined in vivo, decreased significantly 4–11 days after birth and then increased by the 16th day to a level that was not different from that in the adult rat [68]. An additional discrepancy is found in the experiments of Nukari-Siltovuori [29], who observed a decreased maximum effect of ISO in the isolated rat sinoatrial node with no change in sensitivity [ED_{50} was constant].) Because ISO is not taken up by adrenergic nerves and adrenergic transmission was established in the sinoatrial node at birth in contrast to its later development in left atrium and papillary muscle, it was concluded that the diminished sensitivity to NE in the latter two preparations was caused by a neuronally dependent uptake of NE that effectively reduced its concentration at postsynaptic β-adrenergic receptors [66, 67]. This hypothesis was supported by the results of Ishii et al. [69], who showed that chemical sympathetic denervation (6-hydroxydopamine) and immunologic sympathetic denervation (anti-nerve-growth factor) in neonatal rat atria increased sensitivity to NE. The observation that sensitivity of postsynaptic β-adrenergic receptors to ISO did not change from birth to eight weeks [67] appears at odds with the observation that the number of these receptors per cell is reported to increase [49]. Ishii et al. [69] did not confirm the results of Mackenzie and Standen [67] in ventricular muscle insofar as there was no developmental change in sensitivity to NE during the time when both laboratories agree that adrenergic innervation of this tissue is established. It may be speculated that a postjunctional increase in sensitivity to β-adrenergic agonists is masked by neuronal transport which takes up NE but not ISO. Adrenergic denervation also increased papillary muscle sensitivity to ISO and therefore there is a postjunctional contribution to β-adrenergic supersensitivity in this condition [69]. The hypothesis of Ishii et al. [69] for a postjunctional component of supersensitivity is in accordance with the finding that the maximal catalytic activity of adenylate cyclase (epinephrine plus guanylylimidodiphosphate) was greater in adults as compared to neonates [49].

THE ROLE OF CYCLIC NUCLEOTIDES IN THE ACTION OF β-ADRENERGIC AGONISTS

The cAMP hypothesis for β-adrenergic agonist action on embryonic heart cells has been reviewed [4, 23, 60]. Additional support for this hypothesis is the finding of a close correlation between the increase of $\dot{V}_{max}$ (which is proportional to i_{si}) and the increase of cAMP in embryonic chick ventriculr cells exposed to several β-adrenergic agonists [70]. These results are consistent with the hypothesis that the amount of Ca^{2+} entry through i_{si} channels is controlled by the intracellular level of cAMP. Additional support for the hypothesis is that propranolol antagonized the effects of catecholamines on cAMP accumulation and on $\dot{V}_{max}$ of the Ca^{2+}-dependent action potential while verapamil, a Ca^{2+} channel blocking agent, prevented only the stimulatory action of catecholamines on the Ca^{2+}-dependent action potential [70].

The relationship between β-adrenergic receptors and adenylate cyclase activity has been examined in several ways with embryonic hearts. The number of β-adrenergic receptor sites decreased between incubation days and 7 and 13 in the embryonic chick heart (table 16–2) [48]. During this period, there was no change either in basal adenylate cyclase activity (pmol cAMP/10 min·mg protein) or in the stimulation of enzyme activity by ISO, Gpp(NH)p, and a combination of ISO plus Gpp(NH)p. It was concluded that the β-adrenergic receptor and adenylate cyclase were not coordinately regulated during this stage of chick heart development [48]. The possibility that β-adrenergic receptor density is regulated by sympathetic adrenergic innervation has been mentioned previously in this chapter. Because the ontogenetic decrease in number of β-adrenergic receptors was not associated with a de-

crease in ISO-induced stimulation of adenylate cyclase, the diminished accumulation of cAMP caused by ISO in intact cells [71, 72] may not be related to a reduction in adenylate cyclase responsiveness to β-adrenergic agonist [48].

Experiments with neonatal rat hearts illustrate the importance of changes in the number of β-adrenergic receptors in determining the pharmacologic response to agonist. Treatment of neonatal rats with triiodothyronine (T_3) accelerated the development of adrenergic transmission to the heart [57]. Triiodothyronine also permitted enhanced sensitivity to the positive chronotropic effect of ISO at four days after birth. This result confirmed the finding, obtained with neonatal rat heart cells in culture, of a significant postjunctional effect of T_3 to increase the number of β-adrenergic receptors and the sensitivity to the stimulatory effect of EPI on adenylate cyclase [59]. Sensitivity to ISO in T_3-treated animals eventually became less than that in untreated animals by 11 days after birth [57]. The periods of enhanced sensitivity (4–8 days) and subsensitivity (14–18 days) to the positive chronotropic effect of ISO in T_3-treated animals were directly associated with increased and decreased B_{max} of ^{3}H-DHA binding sites when compared to control animals [57]. No appreciable difference of the K_D for ^{3}H-DHA (7–11 n*M*) was detected between control and T_3-treated animals. In rats rendered hypothyroid by treatment with propylthiouracil, both the B_{max} for ^{3}H-DHA binding and the sensitivity of the sinoatrial node to ISO decreased [58]. Whereas there is qualitative agreement between this report and the work of others [47] regarding the B_{max} for ^{3}H-DHA binding in control and hypothyroid rat hearts, Lau and Slotkin [58] observed a significant increase of K_D for ^{3}H-DHA in three-day and 15-day animals treated with propylthiouracil. The significance of this finding is not known.

The effect of β-adrenergic agonist on adenylate cyclase activity can be regulated in a manner that is independent of the number of β-adrenergic receptors. Incubation of ten-day embryonic chick ventricles in the presence of 10^{-6} *M* ISO for 30 min decreased the stimulation of adenylate cyclase activity caused by a subsequent addition of the same concentration of ISO to 35 ± 8% of the initial response [73]. The effect of ISO on contractility was also diminished by this procedure. This desensitization, which seemed specific for the β-adrenergic agonist, was not associated with a change in the number of specific ^{3}H-DHA binding sites, a small (5.2 ± 0.3 n*M* vs 7.0 ± 0.3 n*M*) but significant change in receptor affinity for ^{3}H-DHA and no apparent change in receptor affinity or ISO [73]. The desensitized state could be overcome by the addition of Gpp(NH)p to the isolated membrane fraction. Therefore, the desensitization of the β-adrenergic-receptor–adenylate-cyclase system was attributed to an uncoupling of these components that is prevented by an action of guanine nucleotide on the regulatory protein that links receptor with the catalytic unit.

Experiments done with 10½-day embryonic chick ventricular cells in culture indicated that desensitization of the β-adrenergic-receptor–adenylate-cyclase system may involve a reduction in receptor–cyclase coupling and a decrease in the number of receptors [74]. A 1-h exposure to ISO, even at a nonstimulatory concentration of 10^{-7} *M*, diminished the stimulation of adenylate cyclase activity in a broken cell preparation and the accumulation of cAMP in intact cells caused by 5×10^{-5} *M* ISO. The number of β-adrenergic receptors (^{125}I-HYP specific binding sites) was unchanged after a 1-h exposure to ISO, a result similar to that reported by Marsh et al. [73]. This manifestation of short-term desensitization was attributed by Bobik et al. [74] to an uncoupling of β-adrenergic receptor from the catalytic unit of adenylate cyclase as in the experiments of Marsh et al. [73]. The short-term desensitization to ISO was not accompanied by a change in cAMP phosphodiesterase activity [74]. However, Gpp(NH)p did not prevent the short-term desensitization caused by ISO [74] in contrast to the results of others [73]. Desensitization caused by long-term (16-h) exposure to ISO, was accompanied by a reduction of the number of specific ^{125}I-HYP binding sites, and it was concluded that down-regulation of β-adrenergic receptors contributed to this form of desensitization [74]. Recovery of cells from desensitization was about 50% and 100% com-

plete at 6 h and 24 h, respectively, after removal of ISO. This result is consistent with the possibility, as yet untested, that protein synthesis is required to regenerate β-adrenergic receptors and thereby restore β-adrenergic responsiveness [74].

Another form of diminished sensitivity to β-adrenergic agonists has been described in the chick ventricle. A transient subsensitivity to the positive inotropic effect of ISO occurred between (hatching) incubation days 16 and 21 [54]. This subsensitivity was associated with an increase of the ED_{50} for the positive inotropic effect of ISO without a change in the maximum effect [36]. Therefore, this form of β-adrenergic subsensitivity is unlike the short-term desensitization reported by others in which the ED_{50} for the positive inotropic effect of ISO was not changed while the maximum positive inotropic effect was significantly reduced [73]. Additional evidence that the subsensitivity to ISO observed late in embryonic life in our laboratory may not be the short-term desensitization is provided by measurements of adenylate cyclase activity in particulate preparations from chick ventricles (figure 16–1). Basal activity of adenylate cyclase increased with age and ISO had little stimulatory effect on enzyme activity, presumably because of the lack of GTP that occurred during washing of the 12,000 *g* pellet. In the presence of Gpp(NH)p, adenylate cyclase activity attained similar levels in all three age groups examined. However, the stimulatory effect of ISO in the presence of Gpp(NH)p was greater in ten- to 11-day embryonic and five-to eight-day chick ventricles than in those from the 17- to 18-day embryos. Therefore, the subsensitivity to ISO observed in intact embryonic ventricular muscle at 17–18 days is also displayed with an assay of adenylate cyclase activity. The inability of Gpp(NH)p to restore stimulation of adenylate cyclase by ISO in the 17- to 18-day group to values as great as in the other preparations indicates that the subsensitivity is not a manifestation of short-term desensitization described by Marsh et al. [73]. An understanding of the mechanism for subsensitivity to ISO that occurs late in embryonic life may provide additional clues for the ontogenetic regulation of

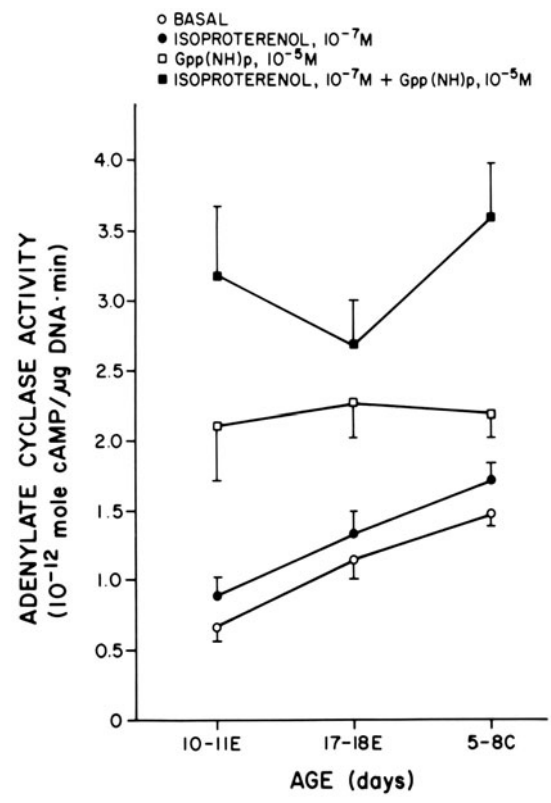

FIGURE 16–1. Adenylate cyclase activity was determined in 12,000 *g* particulate preparations obtained from chick ventricles on the 10th–11th embryonic days ($N = 8$), the 17th–18th embryonic days ($N = 8$), and the 5th–8th days after hatching ($N = 6$). Additional details of the assay procedure are given in Pappano et al. [37]. Ordinate: adenylate cyclase activity (10^{-12} mol/μg DNA · min); abscissa: age of chicks. Enzyme activity is shown in basal conditions (○) and in the presence of 10^{-7} *M* ISO (●), 10^{-5} *M* Gpp(NH)p (□), and 10^{-7} *M* ISO plus 10^{-5} *M* Gpp(NH)p (■).

adenylate cyclase activity that can modify the sensitivity to β-adrenergic agonists.

Intracellular regulation of the response to β-adrenergic agonists includes the operation of cAMP-dependent processes, a feature also displayed for cardiac cell responses to muscarinic agonists. There are several examples for the role of cAMP-dependent protein kinases in the regulation of β-adrenergic reactivity of embryonic and neonatal hearts.

The cAMP content of the embryonic chick heart decreases during ontogenesis (reviewed by

Sperelakis [60]). Measurements of cAMP-dependent protein kinase activity in the chick revealed the presence of a single isozyme (type I) isolated by DEAE–cellulose chromatography [75]. Basal cAMP-dependent protein kinase activity ratio decreased from 0.56 ± 0.05 to 0.25 ± 0.004 in parallel with a decrease of cAMP content (pmol/mg protein) from 39.0 ± 2.5 to 9.1 ± 0.6 in seven-day embryos and hatched chicks, respectively. The increase of cAMP content produced by 10^{-5} *M* ISO also diminished with age (see also Renaud et al. [72]); however, this effect could not be explained by an appropriate reduction of the stimulant action of ISO on adenylate cyclase activity. Therefore, a diminished inotropic response to β-adrenergic agonist during ontogenesis of the chick may arise not only from alterations in the number of β-adrenergic receptors and coupling to the catalytic unit of adenylate cyclase, but also from a reduction in an intracellular effector, cAMP-dependent protein kinase [75]. Whereas there was no difference in the basal cAMP phosphodiesterase activity of the seven- to nine-day embryonic and hatched chick hearts, addition of the phosphodiesterase inhibitor, RO-20-1724, permitted the response of the hatched chick heart (cAMP accumulation) to ISO to reach levels comparable to those observed in similarly treated embryonic hearts [75]. Therefore, an important role of cAMP-dependent phosphodiesterase activity was proposed to account for the diminished response to β-adrenergic agonist in the hatched chick ventricle.

The murine heart displays type-I and type-II cAMP-dependent protein kinases as determined in the same manner as in the chick heart by DEAE–cellulose chromatography [76]. Total cAMP-dependent protein kinase activity (nmol ^{32}P/min·mg protein) was 1.95 ± 0.01 in 15- to 16-day embryonic mouse hearts, rose progressively to 7.0 ± 0.89 in hearts isolated seven days after birth, and then declined to 2.5 ± 0.14 in adult mouse hearts. The ratio (type I/type II) increases from 1.10 ± 0.19 (15- to 16-day embryos) to 3.00 ± 0.16 (seven-day neonates) and then decreases to 0.94 ± 0.12 (adult mouse). Changes in the ratio of type-I to type-II cAMP-dependent protein kinase are largely due to changes in activity of the type-I isozyme [76]. Participation of the isozymes in the response to β-adrenergic agonists has not been reported although it has been suggested that the isozymes have different functions in the regulation of growth and differentiation. In this regard, Claycomb [77] proposed that the progressive decline in DNA synthesis and cellular differentiation in the neonatal rat heart was related to the development of adrenergic innervation and the eventual regulation of cardiac cAMP by the transmitter, NE. However, it is not known whether type-I and/or type-II cAMP-dependent protein kinases participate in the regulation of DNA synthesis and cell differentiation.

The cAMP content of rat hearts decreased from 0.82 ± 0.08 pmol/mg wet weight in two-day-old animals to 0.51 ± 0.07 in 20-day animals [78]. The two-day-old heart was more sensitive than the 20-day-old preparation to EPI, which increased cAMP content by 100% and 40%, respectively, in the two age groups. However, EPI had no positive inotropic effects in ventricles from two-day–old rats whereas a linear relationship between the increase in cAMP content and an increase of the force of contraction occurred in ventricles from 20-day animals. The results in two-day neonatal hearts could be explained by a lack of cAMP receptors (? protein kinases) although compartmentalization of β-adrenergic receptors and/or cAMP could not be excluded [78]. The β-adrenergic receptor, the GTP-dependent regulatory protein, and the catalytic unit of adenylate cyclase are present before birth in homogenates prepared from whole rat hearts [79]. Because basal adenylate cyclase activity increased continuously from the 16th day in utero to adult [79], the decline of basal cAMP content reported by other [78] could be related to increased hydrolysis by phosphodiesterase. The stimulant effect of EPI increased at birth, declined during the first week after birth, and then increased thereafter. However, the response of adult hearts to EPI plus Gpp(NH)p was not as great as that observed just before birth [79]. This observation is not inconsistent with the mechanism proposed by others [78] for the delayed appearance of the positive inotropic effect of EPI, but

the ontogenetic pattern of adenylate cyclase stimulation by EPI + Gpp(NH)p reported by Clark et al. [79] differs qualitatively from that found by others [49]. Therefore, it is difficult to resolve the relative importance of changes in adenylate cyclase activation from changes in cAMP-dependent processes in the development of the positive inotropic effect of EPI in the rat heart.

The regulation of β-adrenergic reactivity by processes dependent upon cAMP is provided by experiments in the neonatal dog heart [80]. The maximum positive inotropic effect of ISO was significantly less in newborn than in adult dogs. The ED_{50} for the positive inotropic effect was lower in newborn dogs, however, and this was paralleled by a lower ED_{50} for activation of adenylate cyclase in the newborn (0.02 μ*M*), which was significantly less than in the adult (0.15 μ*M*). Moreover, the density of β-adrenergic receptors decreased from 147 ± fmol/mg protein in the newborn to 60 ± 19 in the adult. No difference in the K_D of ^{3}H-DHA was detected as a function of age nor did the IC_{50} for displacement of ^{3}H-DHA from specific binding sites change [80]. Because 50% of maximum activation of adenylate cyclase by ISO occurred at concentrations corresponding to much less than 50% occupancy of β-adrenergic receptors in newborn animals, it was concluded that receptor–cyclase coupling was more efficient in hearts from these animals. The mechanism that impeded the β-adrenergic response in hearts from newborn dogs is not known. In view of the close coupling between β-adrenergic receptors and the catalytic unit of adenylate cyclase, it was suggested that activation of cAMP-dependent protein kinases, phosphorylation of specific cytoplasmic proteins, or the reactivity of contractile proteins themselves should be explored as mechanisms for the subsensitive response of the neonatal dog heart to β-adrenergic agonists [80].

A role for β-adrenergic receptor-mediated increases of cAMP in regulating growth and differentiation in the neonatal rat heart has been suggested [77]. Evidence has also been presented for the β-adrenergic receptor in the pathogenesis of cardiovascular disorders in the embryonic chick [81]. The incidence of aortic arch defects and cardiac defects (ventricular septal defect, dual-outlet right ventricle) increased in the presence of catecholamines whose deleterious effects were prevented by administration of propranolol [81]. Support for the role of β-adrenergic receptors in mediating pathologic changes in the heart and vasculature of chick embryos was provided by Oštádal et al. [82], who noted that the pathologic lesions produced by ISO occurred at critical times during development. Subsequently, Janatová et al. [83] confirmed the results that revealed a marked increase of cardiac cAMP content caused by intra-amnial administration of ISO [84]. The basal level of cAMP and the increase in cAMP content caused by ISO were significantly greater in seven-day than in 15-day embryonic chick hearts [84]. The cardiotoxicity of ISO may be related to an increased cAMP con tent and it has been noted that the intra-amnial administration of dibutyryl cAMP also caused pathologic changes in the structure of the embryonic chick heart [83]. However, the incidence of mortality due to derangements of cardiovascular development was not related to the dose of dibutyryl cAMP and was lower than that observed with ISO. Therefore, the role of cAMP in the pathologic effects of β-adrenergic agonists on embryonic heart muscle is less well defined than for its participation in the pharmacologic effects.

α-*Adrenergic Receptor*

RECEPTOR BINDING STUDIES

The biochemical properties of the α-adrenergic receptor have been studied in the mouse (reviewed by Roeske and Wildenthal [23]). A specific α_1-adrenergic antagonist, ^{3}H-WB4101 (2-N-[2,6-dimethoxyphenoxyethyl]aminomethyl-1,4-benzodioxane), has been used to identify α_1-adrenergic receptor sites; more than 50% of the binding of ^{3}H-WB4101 was specific at a concentration of 4×10^{-10} *M*. The density (B_{max}, fmol/mg tissue) increased from the 13th embryonic day, reached a peak at two weeks after birth (2 fmol/mg tissue), and then declined to a level characteristic of the adult (~1 fmol/mg tissue) [85]. Determination of myocardial NE content, taken as an index of sympathetic adrenergic innervation of the mouse

heart, indicated that NE levels increased progressively beginning at seven days after birth to reach adult levels (~0.6 μg/g wet weight) at 21 days after birth. The decrease in specific binding of ^{3}H-WB4101, which began between the 14th and 21st days after birth, was attributed to a down-regulation of α_1-adrenergic receptors by the sympathetic adrenergic transmitter, NE (see Roeske and Wildenthal [23]). It was concluded that the α-adrenergic receptor matured earlier than the β-adrenergic receptor in the mouse heart; however, both receptors were reported to decline in density at the time of sympathetic adrenergic innervation. Treatment with 6-hydroxydropamine, which destroys adrenergic nerve terminals, was associated with an increased density of α- and β-adrenergic receptors (reviewed by Roeske and Wildenthal [23]). The concentration of EPI needed to displace ^{3}H-WB4101 from specific binding sites was increased by Gpp(NH)p whereas the guanine nucleotide did not modify the affinity of antagonist for these sites [86]. It is noteworthy that the muscarinic agonist, carbachol, increased α_1-adrenergic receptor affinity for EPI but not for WB4101 in the presence of Gpp(NH)p [86]; this is similar to that described for the interaction between β-adrenergic and muscarinic cholinergic receptors in the adult heart [35].

RECEPTOR ACTIVATION

The pharmacologic properties of α-adrenergic receptor activation in the adult heart have been critically reviewed [87]. There are only a few reports on the pharmacologic effects of α-adrenergic agonists in embryonic and neonatal hearts. In embryonic mouse heart cells maintained in culture, EPI and NE increased beating rate by an action on α- and β-adrenergic receptors because their positive chronotropic effects were completely prevented by a combination of propranolol and phentolamine, but not by either agent alone [27]. Experiments with ISO and with phenylephrine, which presumably act selectively on β- and α-adrenergic receptors, respectively, indicated that both adrenergic receptor types were present on cardiac muscle cells.

Although less potent than NE, phenylephrine has a positive inotropic effect in adult chicken hearts [88]. However, it is not known whether phenylephrine acts exclusively on α-adrenergic receptors in the adult avian heart or when such receptors appear postjunctionally and begin to regulate muscle cell function. Prejunctional α-adrenergic receptors, which inhibit the release of NE from adrenergic nerves in the chick ventricle, have been demonstrated at three days after hatching [89].

The operation of α-adrenergic receptors has been demonstrated in cardiac Purkinje fibers obtained from neonatal dogs [90]. At low concentrations (10^{-9}–10^{-7} *M*), phenylephrine decreased the rate of spontaneous impulse generation; this effect was prevented by the α-adrenergic antagonist, phentolamine. At high concentrations ($\geq 10^{-5}$ *M*), phenylephrine increased the rate of spontaneous impulse generation by an action on propranolol-sensitive β-adrenergic receptors [90]. There was no difference in the concentration–effect relationships for these actions of phenylephrine in neonatal (0–7 days after birth) and adult dogs. It is noteworthy that ISO, which is usually regarded as a selective agonist of β-adrenergic receptors, decreased the rate of spontaneous impulse generation at low concentrations ($\sim 10^{-10}$ *M*) in neonatal and adult dogs and this effect was prevented by phentolamine. This result is puzzling in view of the suggestion that β- but not α-adrenergic receptors mediate changes in automaticity of adult cardiac Purkinje fibers at negative (−60 to −100 mV) potentials [91]. It is conceivable that the α-adrenergic receptor could regulate automaticity by an action on membrane currents at plateau potentials (0 to −50 mV), but this has not been reported.

Role of Cyclic Nucleotides in α-Adrenergic Stimulation. Experiments in hearts from adult animals indicate that the stimulatory effects of α-adrenergic agonists are not mediated by stimulation of adenylate cyclase or by the accumulation of cAMP [87]. There is no information from embryonic hearts concerning this possibility.

Summary

The physiochemical properties of muscarinic cholinergic and of α- and β-adrenergic recep-

tors and the regulation of receptor properties during ontogenesis have been reviewed. In turn, the consequences of autonomic receptor activation on the electrical and mechanical properties of embryonic, fetal, and neonatal hearts have been evaluated in light of a cyclic nucleotide hypothesis. There is much evidence consistent with the cAMP hypothesis for muscarinic inhibition and β-adrenergic stimulation of the embryonic heart. By contrast, there is little support for a role of cGMP in muscarinic inhibition. The mechanism of action of α-adrenergic agonists on embryonic heart muscle is less clear because of a paucity of experimental investigations of this important topic. A systematic study of the actions of α-adrenergic agonists and antagonists will not only remove this deficit, but also provide additional clues for the regulation of cardiac function by the sympathetic adrenergic nervous system.

References

1. Hulme EC, Berrie CP, Birdsall NJM, Burgen ASV: Interactions of muscarinic receptors with guanine nucleotides and adenylate cyclase. In: Birdsall NJM (ed) Drug receptors and their effectors. London: MacMillan, 1981, pp 23–24.
2. Watanabe AM, Jones LR, Manalan AS, Besch HR Jr: Cardiac autonomic receptors: recent concepts from radiolabeled ligand-binding studies. Circ Res 50:161–174, 1982.
3. Pappano AJ: Ontogenetic development of autonomic neuroeffector transmission and transmitter reactivity in embryonic and fetal hearts. Pharmacol Rev 29:3–33, 1977.
4. Pappano AJ: Adrenergic receptors and adrenergic mechanisms in the embryonic and fetal heart. In: Kunos G (ed) Adrenoceptors and catecholamine action. New York: John Wiley and Sons, 1981, pp 69–97.
5. Pappano AJ, Higgins D: Initiation of transmitter secretion by adrenergic neurons and its relation to morphological and functional innervation of the embryonic chick heart. In: Bouman LN, Jongsma HJ (eds) Cardiac rate and rhythm. Vol 17: Developments in cardiovascular medicine. Boston: Martinus Nijhoff, 1982, pp 631–651.
6. Higgins D: The ontogeny of the response of the chick embryo heart to autonomic transmitters and to neurotransmitter-like drugs. Pharmacol Ther 20:53–77, 1983.
7. Lakatta EG: Age-related alterations in the cardiovascular response to adrenergic mediated stress. Fed Proc 39:3173–3177, 1980.
8. Sastre A, Gray DB, Lane MA: Muscarinic cholinergic binding sites in the developing avian heart. Dev Biol 55:201–205, 1977.
9. Galper JR, Klein W, Catterall WA: Muscarinic acetylcholine receptors in developing chick heart. J Biol Chem 252:8692–8699, 1977.
10. Renaud JF, Barhanin J, Cavey D, Fosset M, Lazdunski M: Comparative properties of the in ovo and in vitro differentiation of the muscarinic cholinergic receptor in embryonic heart cells. Dev Biol 78:184–200, 1980.
11. Hosey MM, Fields JZ: Quantitative and qualitative differences in muscarinic cholinergic receptors in embryonic and newborn chick hearts. J Biol Chem 256:6395–6399, 1981.
12. Roeske WR, Yamamura HI: Maturation of mammalian myocardial muscarinic cholinergic receptors. Life Sci 23:127–132, 1978.
13. Fields JZ, Roeske WR, Morkin E, Yamamura HI: Cardiac muscarinic cholinergic receptors: biochemical identification and characterization. J Biol Chem 253:3251–3258, 1978.
14. Galper JB, Smith TW: Agonist and guanine nucleotide modulation of muscarinic cholinergic receptors in cultured heart cells. J Biol Chem 255:9571–9579, 1980.
15. Hosey MM: Regulation of antagonist binding to cardiac muscarinic receptors. Biochem Biophys Res Commun 107:314–321, 1982.
16. Siegel RE, Fischbach GD: Muscarinic receptors in intact chick heart cells in culture. Soc Neurosci 6:358, 1980.
17. Halvorsen SW, Nathanson NM: In vivo regulation of muscarinic acetylcholine receptor number and function in embryonic chick heart. J Biol Chem 256:7941–7948, 1981.
18. Pappano AJ: Sodium-dependent depolarization of non-innervated embryonic chick heart by acetylcholine. J Pharmacol Exp Ther 180:340–350, 1972.
19. Sperelakis N: Electrical properties of embryonic heart cells. In: De Mello WC (ed) Electrical phenomena in the heart. New York: Academic, 1972, pp 1–61.
20. Carmeliet EE, Horres CR, Lieberman M, Vereecke JS: Developmental aspects of potassium flux and permeability of the embryonic chick heart. J Physiol (Lond) 254:673–692, 1976.
21. Pappano AJ, Skowronek CA: Reactivity of chick embryo heart to cholinergic agonists during ontogenesis: decline in desensitization at the onset of cholinergic transmission. J Pharmacol Exp Ther 191:109–118, 1974.
22. Loffelholz K, Pappano AJ: Increased sensitivity of sinoatrial pacemaker to acetylcholine and to catecholamines at the onset of autonomic neuroeffector transmission in chick embryo heart. J Pharmacol Exp Ther 191:479–486, 1974.
23. Roeske WR, Wildenthal K: Responsiveness to drugs and hormones in the murine model of cardiac ontogenesis. Pharmacol Ther 14:55–66, 1981.

24. Biegon RL, Pappano AJ: Dual mechanism for inhibition of calcium-dependent action potentials by acetylcholine in avian ventricular muscle: relationship to cyclic AMP. Circ Res 46:353–362, 1980.
25. Reuter H: Effects of neurotransmitters on the slow inward current. In: Zipes DP, Bailey JC, Elharrar V (eds) The slow inward current and cardiac arrhythmias. Boston: Martinus Nijhoff, 1980, pp 205–219.
26. Inoue D, Hachisu M, Pappano AJ: Acetylcholine increases K^+ conductance in atrial but not in ventricular muscle during direct inhibition of Ca^{2+}-dependent action potentials in chick heart. Circ Res 53:158–167 1983.
27. Lane MA, Sastre A, Law M, Salpeter M: Cholinergic and adrenergic receptors on mouse cardiocytes in vitro. Dev Biol 57:254–269, 1977.
28. Pager J, Bernard C, Gargouïl Y: Evolution, au cours de la croissance foetale, des effets de l'acetylcholine au niveau de l'oreillette du Rat. C R Soc Biol (Poiters) 159:2470–2475, 1965.
29. Nukari-Siltovuori A: Postnatal development of adrenergic and cholinergic sensitivity in the isolated rat atria. Experientia 33:1611–1612, 1977.
30. Pappano AJ, Biegon RL: Mechanisms for muscarinic inhibition of calcium-dependent action potentials and contractions in developing ventricular muscle: the role of cyclic AMP. In: Paes de Carvalho AP, Hoffman BF, Lieberman M (eds) Normal and abnormal conduction of the heartbeat. Mt Kisco NY: Futura, 1983, pp. 327–344.
31. Josephson I, Sperelakis N: On the ionic mechanism underlying adrenergic–cholinergic antagonism in ventricular muscle. J Gen Physiol 79:69–86, 1982.
32. Reuter H: Über die Abhängigkeit der Acetylcholinwirkung von der äusseren Ca-Konzentration bei isolierten Meerschweinchenvorhofen. Experientia 22:39–40, 1966.
33. Hachisu M, Pappano AJ: A comparative study of the blockade of calcium-dependent action potentials by verapamil, nifedipine and nimodipine in ventricular muscle. J Pharmacol Ther 225:112–130, 1983.
34. Rodbell M: The role of hormone receptors and GTP-regulatory proteins in membrane transduction. Nature 284:17–22, 1980.
35. Watanabe AM, McConnaughey MM, Strawbridge RA, Fleming JW, Jones LR, Besch HR Jr: Muscarinic cholinergic receptor modulation of β-adrenergic receptor affinity for catecholamines. J Biol Chem 253:4833–4836, 1978.
36. Biegon RL, Epstein PM, Pappano AJ: Muscarinic antagonism of the effects of a phosphodiesterase inhibitor (methylisobutylxanthine) in embryonic chick ventricle. J Pharmacol Exp Ther 215:348–356, 1980.
37. Pappano AJ, Hartigan PM, Coutu MD: Acetylcholine inhibits the positive inotropic effect of cholera toxin in ventricular muscle. Am J Physiol 243:H434–H441, 1983.
38. Linden J, Vogel S, Sperelakis N.: Sensitivity of Ca-dependent slow action potentials to methacholine is induced by phosphodiesterase inhibitors in embryonic chick ventricles. J Pharmacol Exp Ther 222:383–388, 1982.
39. Ingbretsen CG: Interaction between alpha and beta adrenergic receptors and cholinergic receptors in isolated perfused rat heart: effects on cAMP-protein kinase and phosphorylase. J Cyclic Nucleotide Res 6:121–132, 1980.
40. Keely SL Jr, Lincoln TM, Corbin JD: Interaction of acetylcholine and epinephrine on heart cyclic AMP-dependent protein kinase. Am J Physiol 234:H432–H438, 1978.
41. Linden J, Brooker G: The questionable role of cyclic guanosine 3′:5′-monophosphate in heart. Biochem Pharmacol 28:3351–3360, 1979.
42. Lincoln TM, Keely SL: Effects of acetylcholine and nitroprusside on cGMP-dependent protein kinase in the perfused rat heart. J Cyclic Nucleotide Res 6:83–91, 1980.
43. Furchgott RF, Zawadzki JV: The obligatory role of endothelial cells in the relaxation of arterial smooth muscle by acetylcholine. Nature (Lond) 288:373–376, 1980.
44. Demey JG, Claeys M, Vanhoutte PM: Endothelium-dependent inhibitory effects of acetylcholine, adenosine triphosphate, thrombin and arachidonic acid in the canine femoral artery. J Pharmacol Exp Ther 222:166–173, 1982.
45. Chen F-CM, Yamamura HI, Roeske WR: Ontogeny of mammalian myocardial β-adrenergic receptors. Eur J Pharmacol 58:255–264, 1979.
46. Williams LT, Lefkowitz RJ: Receptor binding studies in adrenergic pharmacology, chap 9, New York: Raven, 1978.
47. Whitsett JA, Pollinger J, Matz S: β-Adrenergic receptors and catecholamine sensitive adenylate cyclase in developing rat ventricular myocardium: effect of thyroid status. Pediatr Res 16:463–469, 1982.
48. Alexander RW, Galper JB, Neer EJ, Smith TW: Non-co-ordinate development of β-adrenergic receptors and adenylate cyclase in chick heart. Biochem J 204:825–830, 1982.
49. Whitsett JA, Darovec-Beckerman C: Developmental aspects of beta adrenergic receptors and catecholamine-sensitive adenylate cyclase in rat myocardium. Pediatr Res 15:1363–1369, 1981.
50. Chen F-CM, Yamamura HI, Roeske WR: Adenylate cyclase and beta adrenergic receptor development in the mouse heart. J Pharmacol Exp Ther 222:7–13, 1982.
51. Ignarro LJ, Shideman FE: Appearance and concentrations of catecholamines and their biosynthesis in the embryonic and developing chick. J Pharmacol Exp Ther 159:38–48, 1968.
52. Higgins D, Pappano AJ: Development of transmitter secretory mechanisms by adrenergic neurons in the embryonic chick heart ventricle. Devel Biol 87:148–162, 1981.

53. Wacholtz MC, Sha'afi RI: Alprenol binding and cyclic AMP production in embryonic chick red cells during erythropoiesis. Membr Biochem 3:259–270, 1980.
54. Higgins D, Pappano AJ: Developmental changes in the sensitivity of the chick embryo ventricle to β-adrenergic agonist during adrenergic innervation. Circ Res 48:245–253, 1981.
55. Baker SP, Potter LT: Cardiac β-adrenoceptors during normal growth of male and female rats. Br J Pharmacol 68:65–70, 1980.
56. Bhalla RC, Sharma RV, Ramanathan S: Ontogenetic development of isoproterenol subsensitivity of myocardial adenylate cyclase and β-adrenergic receptors in spontaneously hypertensive rats. Biochim Biophys Acta 632:497–506, 1980.
57. Lau C, Slotkin TA: Maturation of sympathetic neurotransmission in the rat heart. II. Enhanced development of presynaptic and postsynaptic components of noradrenergic synapses as a result of neonatal hyperthyroidism. J Pharmacol Exp Ther 212:126–130, 1980.
58. Lau C, Slotkin TA: Maturation of sympathetic neurotransmission in the rat heart. VIII. Slowed development of noradrenergic synapses resulting from hypothyroidism. J Pharmacol Exp Ther 220:629–636, 1982.
59. Tsai JS, Chen A: Effect of L-triiodothyronine on $(-)^3$H-dihydroalprenolol binding and cyclic AMP response to (−) adrenaline in cultured heart cells. Nature 275:138–140, 1978.
60. Sperelakis N: Changes in membrane electrical properties during development of the heart. In: Zipes DP, Bailey JC, Elharrar V (eds) The slow inward current and cardiac arrhythmias. Boston: Martinus Nijhoff, 1980, pp 221–262.
61. Shigenobu K, Sperelakis N: Calcium current channels induced by catecholamines in chick embryonic hearts whose fast sodium channels are blocked by tetrodotoxin or elevated potassium. Circ Res 31:932–952, 1972.
62. Hagiwara S, Takahashi K: Surface density of calcium ions and calcium spikes in the barnacle muscle fiber membrane. J Gen Physiol 50:583–601, 1967.
63. Brown HF, McNaughton PA, Noble D, Noble SJ: Adrenergic control of cardiac pacemaker currents. Philos Trans R Soc Lond 270:527–537, 1975.
64. Tsien RW, Giles W, Greengard P: Cyclic AMP mediates the effects of adrenaline on cardiac Purkinje fibers. Nature 240:181–183, 1972.
65. Pappano AJ, Carmeliet EE: Epinephrine and the pacemaking mechanism at plateau potentials in sheep cardiac Purkinje fibers. Pflugers Arch 382:17–26, 1979.
66. Standen NB: The postnatal development of adrenoceptor responses to agonists and electrical stimulation in rat isolated atria. Br J Pharmacol 64:83–89, 1978.
67. Mackenzie E, Standen NB: The postnatal development of adrenoceptor responses in isolated papillary muscles from rat. Pflugers Arch 383:185–187, 1980.
68. Seidler FJ, Slotkin TA: Presynaptic and postsynaptic contributions to ontogeny of sympathetic control of heart rate in the pre-weanling rat. Br J Pharmacol 65:431–434, 1979.
69. Ishii K, Shigenobu K, Kasuya Y: Postjunctional supersensitivity in young rat heart produced by immunological and chemical sympathectomy. J Pharmacol Exp Ther 220:209–215, 1982.
70. Azuma J, Sawamura A, Harada H, Tanimoto T, Ishiyama T, Morita Y, Yamamura Y, Sperelakis N: Cyclic adenosine-monophosphate modulation of contractility via slow Ca^{2+} channels in chick heart. J Mol Cell Cardiol 13:577–587, 1981.
71. Polson JB, Goldberg ND, Shideman FE: Norepinephrine- and isoproterenol-induced changes in cardiac contractility and cyclic adenosine 3':5'-monophosphate levels during early development of the embryonic chick. J Pharmacol Exp Ther 200:630–637, 1977.
72. Renaud J-F, Sperelakis N, Le Douarin G: Increase of cyclic AMP levels induced by isoproterenol in cultured and non-cultured chick embryonic hearts. J Mol Cell Cardiol 10:281–286, 1978.
73. Marsh JD, Barry WH, Neer EJ, Alexander RW, Smith TW: Desensitization of chick embryo ventricle to the physiological and biochemical effects of isoproterenol. Circ Res 47:493–51, 1980.
74. Bobik A, Campbell JH, Carson V, Campbell GR: Mechanism of isoprenaline-induced refractoriness of the β-adrenoceptor-adenylate cyclase system in chick embryo cardiac cells. J Cardiovasc Pharmacol 3:541–553, 1981.
75. Hosey MM, Green RD: Effects of isoproterenol on cyclic AMP and cyclic AMP-dependent protein kinase in developing chick myocardium. Biochim Biophys Acta 500:152–161, 1977.
76. Haddox MK, Roeske WR, Russell DH: Independent expression of cardiac type I and II cyclic AMP-dependent protein kinase during murine embryogenesis and postnatal development. Biochim Biophys Acta 585:527–534, 1979.
77. Claycomb WC: Biochemical aspects of cardiac muscle differentiation: possible control of deoxyribonucleic acid synthesis and cell differentiation by adrenergic innervation and cyclic adenosine 3′:5′-monophosphate. J Biol Chem 251:6082–6089, 1976.
78. Au TLS, Collins GA, Walker MJA: Rate, force and cyclic adenosine 3′,5′-monophosphate responses to (−)-adrenaline in neonatal rat heart tissue. Br J Pharmacol 69:601–608, 1980.
79. Clark JB, Vinicor F, Carr L, Clark CM Jr: Adenylyl cyclase responsiveness to guanyl nucleotides in the developing rat heart. Pediatr Res 14:291–295, 1980.
80. Rockson SG, Homcy CJ, Quinn P, Manders WT,

Haber E, Vatner SF: Cellular mechanisms of impaired adrenergic responsiveness in neonatal dogs. J Clin Invest 67:319–327, 1981.
81. Hodach RJ, Hodach AE, Fallon JF, Folts JD, Bruyere HJ, Gilbert EF: The role of β-adrenergic activity in the production of cardiac and aortic arch anomalies in chick embryos. Teratology 12:33–46, 1975.
82. Oštádal B, Rychter Z, Rychterová V: The action of isoproterenol on the chick embryo heart. J Mol Cell Cardion 8:533–544, 1976.
83. Janatová T, Oštádal B, Dušek J: The effect of intraamnial administration of isoprenaline and dibutyryl cAMP on the chick embryonic heart. Physiol Bohemoslovaca 30:432, 1981.
84. Oštádal B, Krause E-G, Beyerdorfer I, Pelough V, Wollenberger A: Effect of intra-amnial administration of a cardiotoxic dose of isoproterenol on cyclic AMP levels in the chick embryo heart. J Mol Cell Cardiol 11:1183–1187, 1979.
85. Yamada S, Yamamura HI, Roeske WR: Ontogeny of α_1-adrenergic receptors in the mammalian myocardium. Eur J Pharmacol 68:217–221, 1980.
86. Yamada S, Yamamura HI, Roeske WR: The regulation of cardiac α_1-adrenergic receptors by guanine nucleotides and by muscarinic cholinergic agonists. Eur J Pharmacol 63:239–241, 1980.
87. Scholz H: Effects of beta- and alpha-adrenoreceptor activators and adrenergic transmitter releasing agents on the mechanical activity of the heart. Handbook Exp Pharmacol 54:651–733, 1980.
88. Benfey BG, Carolin T: Effect of phenylephrine on cardiac contractility and adenyl cyclase activity. Can J Physiol Pharmacol 49:508–512, 1971.
89. Higgins D: The development of the adrenergic innervation of the chick embryo ventricle. PhD thesis, University of Connecticut, Storrs, 1980.
90. Rosen MR, Hordof AJ, Ilvento JP, Danilo P Jr: Effects of adrenergic amines on electrophysiological properties and automaticity of neonatal and adult canine Purkinje fibers. Circ Res 40:390–400, 1977.
91. Hauswirth O, Wehner HD, Ziskoven R: α-Adrenergic receptors and pacemaker current in cardiac Purkinje fibers. Nature (Lond) 263:155–156, 1976.

17. MECHANISMS OF ADRENERGIC AND CHOLINERGIC REGULATION OF MYOCARDIAL CONTRACTILITY

August M. Watanabe
Jon P. Lindemann

Introduction

The autonomic nervous system is the major system extrinsic to the heart which regulates myocardial contractility. This system can be subdivided on the basis of anatomy, functional effects, and neurotransmitters released from postganglionic nerves into two major divisions: the sympathetic and parasympathetic nervous systems (fig. 17–1). In general, an increase in sympathetic nerve activity stimulates the heart (i.e., increases heart rate, conduction velocity through specialized conducting tissues, and myocardial contractility) whereas augmentation of parasympathetic activity inhibits the heart (i.e., reduces heart rate, conduction velocity through the atrioventricular node, and myocardial contractility). The heart is innervated by sympathetic nerves and the vagus, which is the parasympathetic innervation. The neurotransmitter released from preganglionic nerves in both the sympathetic and parasympathetic nervous systems is acetylcholine. Norepinephrine is the neurotransmitter that is released from postganglionic sympathetic nerves that innervates the heart. The transmitter released from postganglionic parasympathetic (vagal) nerve endings is acetylcholine (fig. 17–1). Both norepinephrine and acetylcholine produce their effects locally in the immediate area into which they are released, that is, they function as neurotransmitters. Epinephrine is a catecholamine which is released from the adrenal medulla and travels via the circulation to the heart and vasculature and thus functions as a hormone.

The sympathetic and parasympathetic nervous systems modify cardiac function by means of catecholamines and acetylcholine interacting with discrete proteins, referred to as receptors, which are located on the sarcolemma of cardiac cells (fig. 17–1). The receptors of the sympathetic nervous system have been broadly subdivided into alpha and beta, and both of these major types have been further subdivided into subclasses which have been designated alpha$_1$ and alpha$_2$ and beta$_1$ and beta$_2$. Norepinephrine stimulates alpha and beta$_1$ receptors and epinephrine stimulates alpha and both subclasses of beta receptors. Acetylcholine released from parasympathetic nerve endings interacts with muscarinic receptors.

In the intact animal or in conscious man, the cardiac effects of activation of the autonomic nervous system are very complex and dependent on multiple interrelating factors. Some of the most important of these factors are activation of reflexes, adrenergic–cholinergic interaction, and vascular effects. The nature and magnitude of interaction of these factors depend on how the autonomic nervous system is activated. For example, if the sympathetic nervous system is activated physiologically, such as by exercise,

The authors' work cited in this chapter was supported by the Herman C. Krannert Fund, by grants HL08795, HL06308, and HL07182 from the National Heart, Lung and Blood Institute, National Institutes of Health, Bethesda, Maryland, by the American Heart Association, Indiana Affiliate and the Veterans Administration. We gratefully acknowledge the secretarial assistance of Miss Terri Butcher.

N. Sperelakis (ed.), PHYSIOLOGY AND PATHOPHYSIOLOGY OF THE HEART.

Martinus Nijhoff Publishing, Boston/The Hague/ Dordrecht/Lancaster.

parasympathetic tone is likely to be reduced simultaneously and activation of reflexes and adrenergic–cholinergic interaction may not be pronounced. On the other hand, if the sympathetic system is activated by administration of a drug, interaction of these modulatory factors becomes very important in determining the ultimate cardiovascular effect of the administered agent. If norepinephrine is infused into an intact animal or human being, it will activate beta$_1$ receptors in the heart and also alpha-adrenergic receptors in the vasculature. The activation of alpha-adrenergic receptors will cause arteriolar vasoconstriction with resultant increases in peripheral vascular resistance and blood pressure. The norepinephrine-induced hypertension will cause activation of the baroreceptor reflex with consequent increases in efferent vagal nerve activity. The resultant augmentation of acetylcholine stimulation of muscarinic receptors on myocardial cells powerfully modulates the effects of the circulating norepinephrine, such that heart rate actually decreases rather than increases in response to beta$_1$-receptor stimulation and increases in myocardial contractility are blunted. The vasoconstriction produced by alpha-adrenergic stimulation also modulates cardiac function because of the increased resistance to ventricular ejection (i.e., increased afterload). If the animal or subject is pretreated with atropine prior to the administration of norepinephrine, a pure sympathetic effect, free of cellular responses to activation of reflexes and adrenergic–cholinergic interaction, will be seen. In this situation, heart rate will increase and myocardial contractility will be augmented to a greater extent in response to the norepinephrine administration.

Thus, activation of reflexes, hemodynamic effects, and adrenergic–cholinergic interaction are very important factors in determining the cardiac response to autonomic stimulation. The sympathetic and parasympathetic nervous systems interact dynamically in a coordinated manner to regulate cardiac function. The highest level of interaction occurs in vasomotor regulatory centers in the brain where afferent signals from the cardiovascular system are received and processed and efferent sympathetic and vagal nerve activities are regulated. In addition

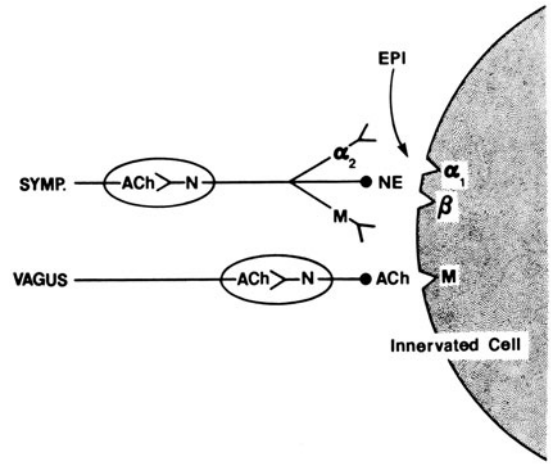

FIGURE 17–1. Schematic representation of relationship between sympathetic and vagal nerve terminals and the receptors with which their respective neurotransmitters interact. Acetylcholine (ACh) stimulates nicotinic (N) receptors in ganglia of both systems and muscarinic (M) receptors. Norepinephrine, released from sympathetic terminals and epinephrine (E), stimulate alpha$_1$ (α_1), alpha$_2$ (α_2), and beta (β) receptors. Symp, sympathetic.

to this CNS level of integration, important interactions occur between the two systems at the level of the nerve terminals (fig. 17–1). Histologic studies have shown that, in some regions of the heart, terminals of sympathetic and vagal nerves are in apposition one with the other. This physical relationship allows for interaction between the two systems at the nerve terminals. This interaction occurs both prejunctionally between nerves and postjunctionally at the level of membranes of innervated cells and within the cells. In the prejunctional level of interaction, acetylcholine released from parasympathetic nerve endings can stimulate muscarinic receptors on sympathetic terminals to inhibit the release of norepinephrine (fig. 17–1) (for review, see Levy and Martin [1]). Thus, vagal activity can modulate sympathetic effects by inhibiting norepinephrine release. In addition, stimulation of muscarinic receptors on the membranes of innervated cells can modulate the cellular response to beta-adrenergic-receptor stimulation (fig. 17–1). This postjunctional interaction allows vagal regulation of the cellular response to norepinephrine that is released

from sympathetic terminals and to circulating epinephrine.

This chapter discusses the cellular and subcellular mechanisms by which catecholamines and acetylcholine modify cardiac cell function and the cellular mechanisms of interaction between the sympathetic and parasympathetic nervous systems.

Mechanisms of Adrenergic Effects on the Heart

ADRENERGIC RECEPTORS

Catecholamines stimulate the heart by interacting with adrenergic receptors on myocytes. These receptors were originally defined and characterized functionally based on the response of intact tissues to a series of adrenergic agonists. These studies revealed two distinct rank orders of potency for agonists interacting with adrenergic receptors and therefore the receptors were subclassified into two classes, which were called alpha and beta. Subsequent studies with newer chemical entities suggested that further subclassification of the major classes was justified. With currently available adrenergic agonists and antagonists, the two major classes of adrenergic receptors have been further subclassified on the basis of functional response into $beta_1$ and $beta_2$ and $alpha_1$ and $alpha_2$ subtypes. The heart of mammals contains predominantly $beta_1$ receptors whereas vasculature appears to contain predominantly $beta_2$ receptors. Alpha-receptor subtypes also appear to be distributed according to organs. Vasculature contains predominantly $alpha_1$ receptors. In addition, based on both functional and radioligand binding studies, alpha-receptor subtypes appear to be differentially distributed among the pre- and postjunctional regions of sympathetic nerves (fig. 17–1). $Alpha_2$ receptors appear to be located on prejunctional sympathetic nerve terminals. It is believed that stimulation of these receptors inhibits norepinephrine release from the terminals. $Alpha_1$ receptors are the predominant type found on the innervated postjunctional sites of cardiovascular tissues.

While much important information about adrenergic receptors was gleaned from many functional studies with intact organs or tissues, it remained for the development of more direct radioligand binding assays of adrenergic receptors to reveal some of the biochemical and molecular properties of these receptors. Some of the most important discoveries relevant to the cardiovascular system from binding assays will be discussed in this section. For general reviews of new discoveries from radioligand binding assays, see references 2–7.

Beta-Adrenergic Receptors. Of the autonomic receptors (beta, alpha, and muscarinic), radioligand binding assays were first developed for beta-adrenergic receptors. This is perhaps the reason why, of these three major types of receptors, the most is known about the fundamental biochemistry of beta-adrenergic receptors. Probably because of the well-established importance of the sympathetic nervous system in regulating cardiac function, many of the studies of beta receptors have been done in heart. Thus, many of the new discoveries from binding assays regarding beta receptors are directly relevant to cardiovascular physiology and pharmacology.

Beta-adrenergic receptors are located on the sarcolemma of myocardial cells. It became possible to prove this after the development of preparations of highly purified sarcolemma and internal membrane systems (including sarcoplasmic reticulum) from heart [7–9]. By comparing the distribution of beta-adrenergic receptors with the distribution of marker enzymes known to be localized to sarcolemma, sarcoplasmic reticulum, and mitochondria, it was shown that beta receptors reside only on sarcolemma. Any beta-receptor binding activity found on internal membranes such as sarcoplasmic reticulum could be accounted for by contamination of the sarcolemma with sarcoplasmic reticulum [7–9]. The location of beta receptors on the outer surface of the sarcolemma makes them readily accessible to norepinephrine released from sympathetic nerve terminals or to circulating epinephrine.

Beta-adrenergic receptors in the heart are not static but rather dynamic entities whose properties can change in response to physiologic stresses, disease states, or administration of

drugs [3, 5–7]. The most readily detected and widely studied dynamic property of beta receptors is their density in plasma membranes. The number of beta receptors appears to vary according to the magnitude of their stimulation. As a broad generalization, the density of beta receptors increases when stimulation is low (called *up-regulation*) and decreases when stimulation is high (called *down-regulation*) [3–7]. These changes in receptor density are one of what are probably multiple alterations that may occur in an organ that renders it either desensitized or supersensitized to catecholamine stimulation. Alterations in receptor density may occur with physiologic variations in sympathetic activity. For example, when sodium intake by human subjects was increased from 10 to 400 mEq daily, a change that reduced sympathetic nervous system activity, the density of beta-adrenergic receptors on leukocyte membranes increased by approximately 50% [10]. That the changes in leukocyte-receptor density reflected receptor changes in the cardiovascular system was suggested by the observation that the subjects' sensitivity to the positive chronotropic effects of isoproterenol was also increased [10]. The density of beta-adrenergic receptors on leukocytes of these normal subjects was inversely correlated with circulating and 24-h urinary catecholamine levels [10]. The levels of catecholamines in the blood and urine presumably reflected sympathetic nerve activity. Thus, the higher the level of sympathetic nervous system activity (the greater the concentration of catecholamines in the receptor milieu), the more down-regulation had occurred. Changes in receptor density may also occur in response to drugs [3–6]. Drugs which diminish beta-receptor stimulation by destroying sympathetic nerves and/or depleting catecholamine stores (e.g., 6-hydroxydopamine and guanethidine) cause up-regulation. Beta-receptor blockers also cause increases in receptor density. On the other hand, chronic pharmacologic stimulation of beta receptors causes a reduction in receptor density.

Beta-receptor density also changes with certain disease states. The most extensively studied such association is that seen with abnormal thyroid states. Patients with hyperthyroidism exhibit signs suggestive of a hyperactive sympathetic nervous system whereas patients with hypothyroidism appear just the opposite. For example, hyperthyroid patients commonly have tachycardia, increased cardiac output, and tremulousness. Hypothyroid patients have bradycardia. Animal studies have shown that in hyperthyroidism the density of beta-adrenergic

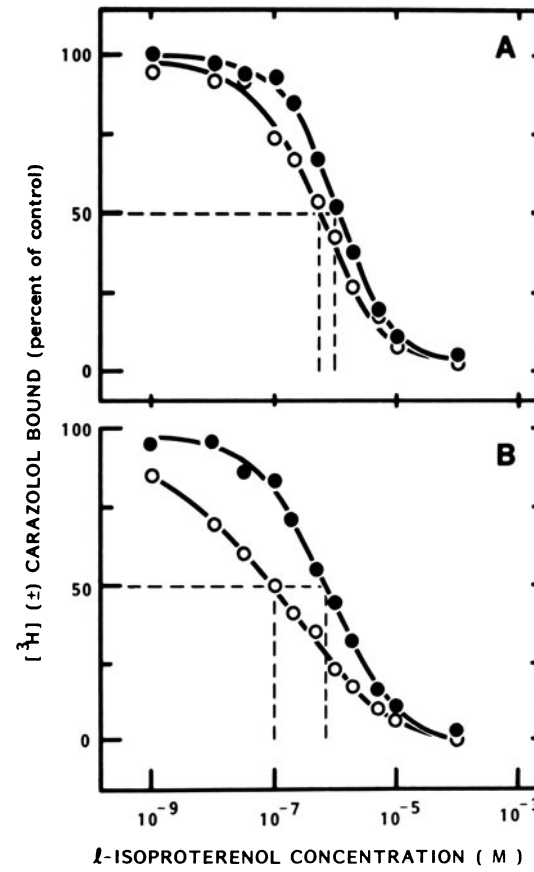

FIGURE 17–2. Curves describing competition of l-isoproterenol with [^{3}H](±)carazolol for binding to beta-adrenergic receptors in canine heart *(A)* and lung *(B)* membranes: ○——○ no added guanine nucleotide, ●——● 10^{-4} *M* added Gpp(NH)p. Note that in both heart and lung membranes, addition of Gpp(NH)p shifts the isoproterenol competition curve to a steeper slope (slope factor shift from 0.73 to 0.86 in heart and 0.42 to 0.74 in lung) and lower affinity (K_D change from 0.17 to 0.29 μ*M* in heart and from 0.026 to 0.23 μ*M* in lung). Because the curve in the absence of Gpp(NH)p was more shallow in lung than in heart, the guanine-nucleotide-induced shift is greater in the former than in the latter.

receptors is increased by 50%–100% whereas in hypothyroidism the density of beta-adrenergic receptors is reduced modestly [11, 12]. Clinical studies have shown that administration of triiodothyronine to normal subjects leads to an increase in density of beta-adrenergic receptors in leukocytes [13]. Although not yet proven, it has been speculated that these changes in leukocyte receptors reflect changes that also occur in the heart [13]. Thus, beta-receptor density in the heart is related to thyroid state and changes in the receptors may explain, at least partially, the cardiovascular changes that accompany altered thyroid status.

Studies with radiolabeled ligands have revealed differences in the molecular interactions of agonists and antagonists with beta-adrenergic receptors. The difference in the nature of agonist and antagonist binding is observed by analysis of the effects of guanine nucleotides on agonist competition curves. Addition of guanine nucleotides (GTP or Gpp[NH]p) to the assay medium decreases the affinity of beta receptors for agonists without changing the affinity for antagonists (fig. 17–2 and table 17–1) [2–7]. Partial agonists are affected in an intermediate manner proportional to their activity as agonists. This observation which was made originally in model systems has subsequently been extended to a variety of other tissues including heart (fig. 17–2 and table 17–1). In terms of their interaction with agonists, beta receptors can exist in two states [3–7]. Receptors in membrane preparations depleted of guanine nucleotides exist in both high- and low-affinity states [3–7]. This coexistence of two affinity states of the receptor is manifested in radioligand binding studies as shallow agonist competition curves, nonlinear Scatchard plots, and slope factors less than unity (fig. 17–2 and table 17–1). The addition of exogenous guanine nucleotides to such preparations is thought to convert a majority (or all) of the receptors into a single low-affinity state, thus transforming the agonist competition curve to a form with a steeper slope and shifting the dissociation constants to higher values (lower affinity) (fig. 17–2 and table 17–1) [3–7]. The data in figure 17–2 are from cardiac membranes (panel A), which generally demonstrate only a small guanine-nucleotide-induced shift in slope and affinity, and lung (panel B). Although in heart the change in receptor affinity for agonists is small compared to that seen in lung and in some other systems, these changes are consistent and reproducible. Antagonist competition curves are always steep and uniphasic, regardless of the presence or absence of guanine nucleotides, and these curves are not altered by the addition of guanine nucleotides (fig. 17–3 and table 17–1).

This agonist-specific two-state receptor conformation appears to be an in vitro manifestation of receptor changes induced by agents with intrinsic activity, these changes resulting under appropriate conditions in activation of adenylate cyclase [3–5]. It is postulated that beta-receptor agonists can induce a high-affinity state of receptor, resulting in a receptor–agonist complex which then interacts with a third component, a coupling protein. This ternary complex of hormone, receptor, and coupling protein then interacts with regulatory guanine nucleotides, which leads to a return of the receptor to a low-affinity state and dissociation of the hormone–receptor complex and at

TABLE 17–1. Effect of guanine nucleotide on interaction of beta-adrenergic receptors with the antagonist propranolol and with catecholamines

	Slope Factor		K_D	
Drug	$-G_{pp}(NH)_p$	$+G_{pp}(NH)_p$	$-G_{pp}(NH)_p$	$+G_{pp}(NH)_p$
l-Propranolol	0.91	0.91	5.8	5.6
l-Isoproterenol	0.73	0.86	0.17	0.29
l-Epinephrine	0.81	0.90	3.3	4.7
l-Norepinephrine	0.76	0.82	2.2	3.2

Values are means from 3–9 experiments. K_D for propranolol $\times 10^{-9}$ *M* and for catecholamines $\times 10^{-6}$ *M*.

the same time activation of adenylate cyclase [3, 5]. Antagonists (agents without intrinsic activity) cannot induce the high-affinity state and also do not activate adenylate cyclase. This concept is discussed in more detail in later sections of this chapter.

Alpha-Adrenergic Receptors. The existence and physiologic role of alpha-adrenergic receptors in vascular smooth muscle are well established, but their existence and role in cardiac muscle have been controversial [14]. Functional studies have shown that alpha agonists can increase myocardial contractility in certain species such as rat and rabbit [14]. The nature of the mechanical changes induced by alpha agonists is different from that of beta agonists, suggesting that different biochemical mechanisms mediate the contractile effects of stimulation of these two types of adrenergic receptors. For example, alpha agonists do not accelerate the rate of relaxation of cardiac muscle as do beta agonists [14]. Alpha agonists also produce electrophysiologic effects in isolated cardiac tissues studied in vitro, and these effects are different from those of beta agonists.

With the advent of radioligand binding assays, the presence of alpha receptors in the heart has been confirmed directly, but the role that these receptors play in mediating the inotropic effects of catecholamines is still not clear. Moreover, the biochemical mechanisms by which stimulation of alpha-adrenergic receptors might modify cardiac function are largely unknown [14].

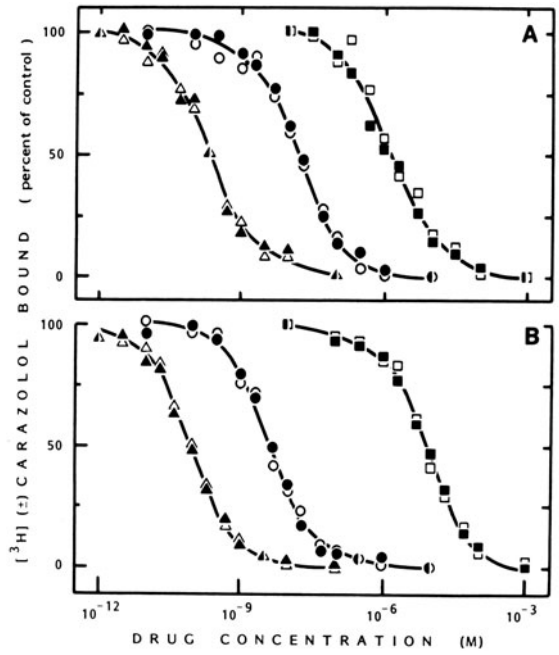

FIGURE 17–3. Competition of beta-adrenergic antagonists with [^{3}H](±)carazolol for binding to beta-adrenergic receptors present in membrane vesicles derived from canine ventricular myocardium *(A)* and canine lung *(B)*: S(−)carazolol (△▲); (−)propranolol (○●); (±)metoprolol (□■). Presence (filled symbols) or absence (unfilled symbols) of 10^{-4} *M* 5′-guanylylimidodiphosphate has no effect on the position or configuration of antagonist–radioligand competition curves. Reprinted with permission from Manalan et al. [79].

ADENYLATE CYCLASE

The proximate biochemical effector enzyme with which beta-adrenergic receptors interact to modify cardiac function is adenylate cyclase. Adenylate cyclase is located in sarcolemma, as are beta receptors, and not in internal membranes such as sarcoplasmic reticulum [15]. Hormone-regulated adenylate cyclase is comprised of at least three major units: receptors such as beta-adrenergic receptors, a catalytic unit which catalyzes the conversion of ATP into cyclic AMP (cAMP), and a coupling or regulatory unit which couples the receptor to the catalytic unit and translates the signal of hormone–receptor interaction to the catalytic unit whose activity is then altered (fig. 17–4). The details of the biochemistry and molecular biology of adenylate cyclase have been elucidated primarily in nonmammalian model systems (for a general review of adenylate cyclase, see Ross and Gilman [16]). However, most of the properties of the enzyme described in these systems appear to hold true also for myocardial adenylate cyclase.

It is now clearly established that adenylate cyclase can be regulated in both a stimulatory and an inhibitory manner, and that there are neurotransmitter and hormone receptors which can inhibit as well as those which can stimulate the enzyme [17–19]. Alpha$_2$ and muscarinic receptors interact with the enzyme in a manner which leads to inhibition of activity [18, 20].

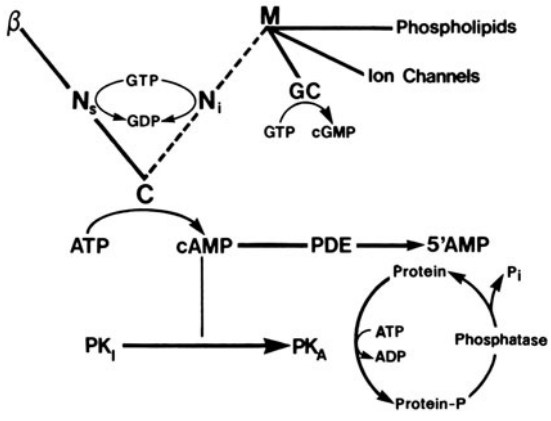

FIGURE 17–4. Schematic flow chart of interaction between autonomic receptors and intracellular effectors. Catecholamines interact with beta-adrenergic receptors (β) to stimulate, via a guanine-nucleotide-binding regulatory protein (N_s), the catalytic subunit (C) of adenylate cyclase. cAMP formed interacts with protein kinase (PK_I) to activate it (PK_A). The free catalytic subunit of protein kinase (PK_A) then catalyzes the phosphorylation of proteins. Proteins are dephosphorylated by phosphoprotein phosphatases. Muscarinic (M) receptors are also coupled to adenylate cyclase, possibly by an inhibitory guanine-nucleotide-binding protein (N_i). Muscarinic receptors are also coupled to guanylate cyclase (GC), ion channels and may regulate membrane phospholipid turnover.

The unit which couples receptors to the catalytic unit is called the G/F or N protein because it binds and is regulated by guanine nucleotides [16] (fig. 17–4). The N protein in turn is comprised of several subunits, one of which mediates the effects of stimulatory receptors, called N_s, and another which putatively mediates the effects of inhibitory receptors, called N_i [17–19]. Both N_s and N_i bind guanine nucleotides such as GTP. Both subunits also possess GTPase activity and are thereby able to hydrolyze GTP to GDP (fig. 17–4).

In most systems studied, including the heart, guanine nucleotides are necessary for regulation of adenylate cyclase activity. In cardiac membranes, guanine nucleotides themselves can stimulate enzyme activity (fig. 17–5). In addition, guanine nucleotides are required for hormonal regulation of enzyme activity. Catecholamines do not stimulate the enzyme unless guanine nucleotides (either GTP or nonhydrolyzable analogues) are present (fig. 17–5) [20]. In like manner, GTP must be present for expression of muscarinic inhibition of cardiac adenylate cyclase activity. Unlike beta-receptor stimulation of activity which can occur in the presence of GTP or nonhydrolyzable analogues, however, muscarinic inhibition of the enzyme occurs only when GTP is the guanine nucleotide present [20] (fig. 17–5). If nonhydrolyzable analogues are used, muscarinic inhibition of the enzyme does not occur (fig. 17–5) [20]. This observation has led to the speculation that muscarinic agonists might inhibit the enzyme by activating a GTPase and thereby reducing the availability of GTP for interaction with N_s. Data in cardiac membranes and in other systems coupled to nonmuscarinic inhibitory receptors are consistent with this conclusion. However, whether this is indeed a mechanism for muscarinic inhibition of adenylate cyclase and whether additional mechanisms are present remain to be established.

Thus, cardiac muscle sarcolemma contains both stimulatory (beta-adrenergic) and inhibitory (muscarinic) receptors which interact with N proteins. Included in the subunits comprising N proteins are a stimulatory component (N_s) and a putative inhibitory component (N_i), both of which bind GTP (fig. 17–4). When stimulatory or inhibitory receptors are activated by their respective agonists, the activity of the catalytic unit is either increased or reduced, this change in enzyme activity being mediated by the appropriate N protein (N_s or N_i). Intracellular cAMP levels then either increase or decrease.

Intracellular cAMP levels are controlled by the activity of two enzymes: adenylate cyclase and phosphodiesterase (fig. 17–4). The latter enzyme converts cAMP into 5′-AMP and thereby restores cellular levels of the cyclic nucleotide to prestimulation values. There is no evidence as yet that activation of autonomic receptors alters the activity of phosphodiesterase, but inhibition of this enzyme is a well-known important mechanism of action of certain drugs, most notably methyxanthines. Some of the newer nonglycoside, noncatecholamine-positive inotropic agents such as amrinone may also produce part of their contractile effects by

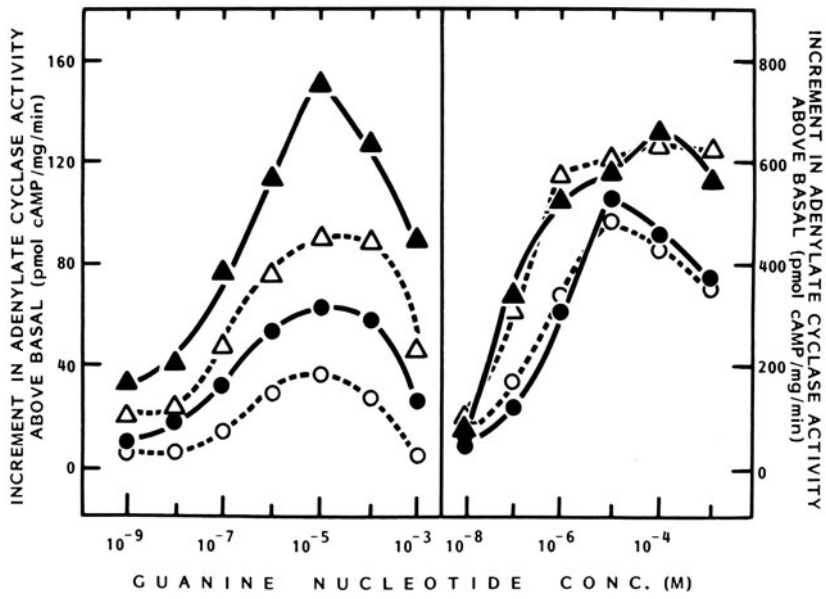

FIGURE 17–5. Guanine nucleotide stimulation of adenylate cyclase activity in canine cardiac membrane vesicles. Guanine nucleotide added was GTP in *left panel* and Gpp(NH)p in *right panel*. Circles are values with guanine nucleootides alone and triangles with guanine nucleotides plus 10^{-7} *M* isoproterenol. Unfilled symbols designate the presence of 10^{-5} *M* methacholine in addition to guanine nucleotide alone or with isoproterenol. Note that methacholine significantly inhibits GTP or GTP plus isoproterenol activation of adenylate cyclase *(left panel)*, but does not affect adenylate cyclase activity when the guanine nucleotide added is Gpp(NH)p *(right panel)*.

inhibiting phosphodiesterase, thereby increasing tissue levels of cAMP.

PHOSPHORYLATION OF PROTEINS: cAMP-DEPENDENT PROTEIN KINASE, PROTEIN PHOSPHATASES

When cAMP is increased within myocardial cells by the increased catalytic activity of adenylate cyclase, it then produces its effects on cellular function by interacting with another protein called cAMP-dependent protein kinase (for a review of protein kinases, see Krebs and Beavo [21]) (fig. 17–4). This enzyme exists in sarcolemma as well as in soluble form in the cytosol. cAMP-dependent protein kinase is an enzyme which is composed of two units, which are referred to as the regulatory and catalytic subunits [21]. When cAMP-dependent protein kinase exists as a holoenzyme, it is not catalytically active. The regulatory subunit is a receptor for cAMP, so that when cAMP is increased within the cell it binds to the regulatory subunit, and this interaction then causes the regulatory and catalytic subunits to dissociate [21]. When the catalytic subunit is released from the regulatory subunit, it becomes catalytically active and catalyzes the transfer of the terminal phosphate of ATP to various proteins within the myocardial cell (fig. 17–4). This phosphorylation changes the properties of the protein in such a manner that its interaction with ions, e.g., Ca^{2+}, is altered and thus the contractile properties of the heart are modified. Various cardiac muscle proteins have been shown in vitro to be substrates of cAMP-dependent protein kinase. Only a few of these proteins, however, have been shown to be phosphorylated, presumably by cAMP-dependent protein kinase, in intact functioning hearts. These include phosphorylase kinase, TN-I, myosin, and phospholamban [22].

Phosphorylation of phosphorylase kinase is involved in beta-agonist-induced activation of phosphorylase. While this effect of catecholamines is likely important in meeting the increased metabolic demands of cardiac muscle

functioning at an increased inotropic state, phosphorylation of this protein probably does not participate directly in increasing contractility.

Because TN-I, myosin, and phospholamban are intimately associated with components of the heart cell that either bind Ca^{2+} or regulate Ca^{2+} flux, it has been speculated that phosphorylation of one or more of these proteins might mediate the contractile effects of catecholamines [22]. TN-I is a component of troponin, one of the regulatory proteins of the myofibrillar contractile protein complex. It was first shown that TN-I could be phosphorylated by cAMP-dependent protein kinase in vitro [22]. Subsequently, it was shown that infusion of catecholamines to intact hearts caused phosphorylation of TN-I and that this correlated with increased contractile state [23]. The onset and development of increased contractile state correlated with phosphorylation of TN-I, but the reversal of these processes could be dissociated [23]. Upon removal of catecholamines, TN-I remained phosphorylated while contractile force returned to control values. Other agents (ouabain, increased Ca^{2+}, X537A) or maneuvers (reduced Na^{2+} in perfusion medium, Treppe) which produced positive inotropic effects but did not elevate cAMP levels did not cause phosphorylation of TN-I [23].

Studies of the effect of TN-I phosphorylation on the function of the troponin complex have been conflicting, so the significance and role of this phosphorylation remains uncertain. To the present, there are not consistent observations regarding the effect of TN-I phosphorylation on Ca^{2+} regulation of actomyosin-ATPase activity. If this phosphorylation were functionally important, it would be expected that phosphorylation of TN-I would either increase or decrease the sensitivity of this complex to Ca^{2+}. In fact, both types of alterations have been observed. It has been reported that phosphorylation of TN-I from guinea pig hearts reduced the Ca^{2+} requirement of actomyosin ATPase, i.e., increased the Ca^{2+} sensitivity [24]. Others have reported no difference in Ca^{2+} stimulation of actomyosin-ATPase activity of nonphosphorylated or phosphorylated myofibrils [25]. Finally, it has been reported that protein phosphorylation was associated with a decreased Ca^{2+} stimulation of actomyosin-ATPase activity [26]. If the latter observation were correct, it could be speculated reasonably that phosphorylation of TN-I, which results in reduced Ca^{2+} sensitivity of actomyosin ATPase to Ca^{2+}, partially accounts biochemically for the enhanced rate of relaxation of cardiac muscle exposed to catecholamines. However, the conflicting results regarding the effects of TN-I phosphorylation prevent any firm conclusions at the present regarding its physiologic significance [22]. The major remaining unresolved questions regarding the role of TN-I phosphorylation in response to cAMP elevation are: (a) What is the biochemical or ionic result of this phosphorylation? and (b) What is the role of this phosphorylation in mediating the mechanical effects of adrenergic stimulation?

The phosphorylation state of the 19,000-dalton light chain of myosin in intact cardiac muscle has been examined [22]. Similar to the situation for TN-I, the results have been contradictory. It has been reported that the 19,000-dalton light chain of cat papillary muscle was phosphorylated during exposure to norepinephrine [27]. On the other hand, others have reported that rabbit cardiac muscle light chain was fully phosphorylated in the resting state and addition of epinephrine resulted in a decrease in protein-bound phosphate [28]. More recently, it has been reported that a variety of inotropic maneuvers (both negative and positive inotropic interventions) did not alter myosin light-chain phosphorylation in rabbit and rat cardiac muscle [29]. Specifically, isoproterenol caused activation of phosphorylase (thus demonstrating a biochemical effect of cAMP elevation) in perfused rabbit hearts but did not affect phosphorylation of myosin light chain [29]. Thus, what effect, if any, catecholamines have on myosin phosphorylation in intact cardiac muscle remains to be established. Furthermore, what biochemical role phosphorylation of cardiac muscle light chain has in the overall function of myosin remains to be demonstrated [22].

In vitro studies on the role of phosphorylation in regulating sarcoplasmic reticulum func-

tion revealed that a major substrate for cAMP-dependent protein kinase was a 22,000-molecular-weight protein which appeared to be intrinsic to sarcoplasmic reticulum membranes [30, 31]. It was shown that addition of cAMP to sarcoplasmic reticulum membranes, with or without exogenous cAMP-dependent protein kinase, resulted in phosphorylation of this 22,000-dalton protein and associated with this increased Ca^{2+}-ATPase activity [30, 31]. Subsequent studies showed that this 22,000-dalton protein could be reduced in size to approximately 8,000–11,000 by appropriate treatment of membranes (e.g., boiling in detergent), suggesting that the protein is an oligomer composed of two or more subunits [32]. This protein has been named phospholamban (Greek for phosphate acceptor), and it has been suggested that this protein regulates Ca^{2+}-ATPase activity of sarcoplasmic reticulum [31].

Several laboratories have demonstrated that phospholamban can be phosphorylated in intact hearts [33–35]. This phosphorylation occurs rapidly (within 20 s of onset of catecholamine infusion) and occurs with low concentrations of drug, as low as $3 \times 10^{-9} M$ isoproterenol (fig. 17–6A) [35]. Ca^{2+}-ATPase activity of the same sarcoplasmic reticulum vesicles in which phospholamban is phosphorylated (i.e., sarcoplasmic reticulum isolated from intact ventricles) is increased in time and concentration dependence that parallels the time and concentration dependence of phospholamban phosphorylation (fig. 17–6B) [35]. Phospholamban phosphorylation and Ca^{2+}-ATPase activity closely parallel the onset and development of changes in relaxation parameters (i.e., rate of relaxation), but there may be a dissociation between the biochemical and mechanical parameters when reversal of the effects of isoproterenol is studied. Return of relaxation parameters to control values appeared to precede dephosphorylation of phospholamban and return of Ca^{2+}-ATPase to basal values [35]. There are several possible explanations for this latter observation, including: (a) that the discrepancy is more apparent than real, (b) that phosphorylation of phospholamban initiates the relaxant effects of catecholamines but other mechanisms (other than dephosphorylation of phospholam-

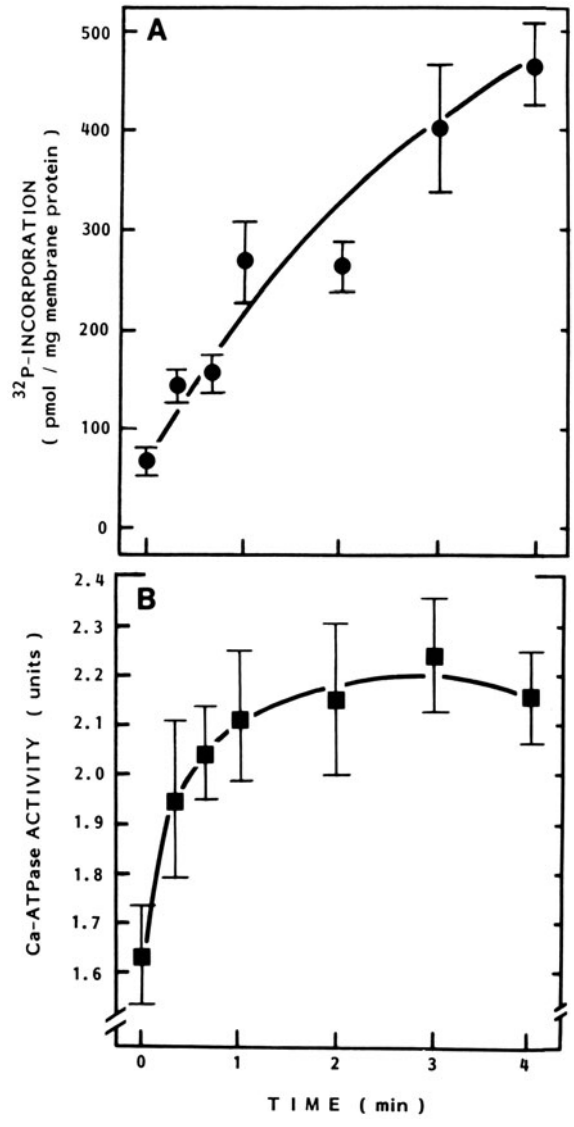

FIGURE 17–6. Time course of beta-adrenergic stimulation of phospholamban phosphorylation *(A)* and Ca^{2+}-ATPase activity *(B)* in guinea pig ventricles. Hearts were perfused with buffer containing 1.1–1.8 mCi $^{32}P_i$ for 30 min. Isoproterenol was then administered and hearts were frozen at the times indicated. Membrane vesicles were prepared and divided into aliquots for SDS–polyacrylamide-gel electrophoresis or assay of Ca^{2+}-ATPase activity. ^{32}P incorporation into phospholamban was quantified by counting the radioactivity in the bands from the dried gels (band identified by autoradiography) and dividing the value obtained by the specific activity of [γ-^{32}P]ATP, which was determined for each heart. Reprinted with permission from Lindemann et al. [35].

ban) terminate the mechanical effects, and (c) that phosphorylation of phospholamban has nothing whatsoever to do with the inotropic effects of catecholamines. Obviously, more studies will have to be done to resolve these questions.

Phosphorylation of all of the foregoing proteins discussed is reversed by the action of phosphoprotein phosphatases which remove the phosphate and thereby return the protein to its basal state (fig. 17–4). Thus far there is no evidence that neurotransmitters or hormones can regulate phosphoprotein phosphatase activities and thereby influence protein phosphorylation. However, such a mechanism of action is an attractive hypothesis for certain antiadrenergic agents, such as muscarinic agonists. This will be discussed in more detail in later sections.

Slow inward current (I_{si}) channels, putatively located in sarcolemma, presumably are also substrates for cAMP-dependent protein kinase [36]. Very little is known about this protein, however, and no convincing evidence has yet been provided regarding its phosphorylation in vitro or in vivo. Functional studies strongly suggest that one of the subcellular mechanisms by which catecholamines modify cardiac function is by causing phosphorylation of I_{si} channels.

Agents which elevate tissue cAMP levels increase I_{si}. This was first shown indirectly by studying so-called slow responses induced by various inotropic agents [37]. Intact cardiac tissue can be rendered inexcitable by inactivation of fast Na^+ channels, for example, by depolarization, administration of high concentrations of tetrodotoxin, or administration of buffer containing zero Na^+. Excitability can be restored to these cardiac tissues by administration of agents which elevate cAMP levels [37]. The inward depolarizing current in these excitability-restored hearts is carried by Ca^{2+} through I_{si} channels. This increase in I_{si} can be blocked by Ca^{2+} antagonists which do not alter catecholamine-induced elevation of cAMP levels [37]. cAMP levels in these same hearts were increased by the agents which induced slow responses (catecholamines, histamine, phosphodiesterase inhibitors, dibutyryl cAMP) [37]. Presumably agents which elevate cAMP levels increase I_{si} by causing phosphorylation of a protein component of I_{si} channels [38]. Positive inotropic agents or interventions which do not elevate cAMP, and therefore presumably do not activate cAMP-dependent protein kinase, do not increase I_{si} [37].

Subsequent more direct studies also suggest that catecholamines produce part of their effects by causing phosphorylation of I_{si} channels. Direct administration of cAMP or analogues to cardiac fibers caused increases in directly measured I_{si} (measured by voltage-clamp techniques) [39]. Recently, it has been shown that injection of the nonhydrolyzable analogue of GTP, Gpp(NH)p, and cholera toxin (which activates adenylate cyclase) directly into myocardial cells (by microiontophoresis) increased slow response and thus I_{si} [40]. Thus, substantial evidence suggests that I_{si} channels in sarcolemma are another subcellular site which is modified by catecholamines to effect functional changes, and that this modification involves protein phosphorylation [38, 39]. Further work will have to be done to document this directly with phosphorylation studies in intact myocardium.

To summarize this section, it seems likely that agents which increase cellular cAMP levels, such as catecholamines, alter myocardial cell function by causing phosphorylation of proteins. Several proteins which have been shown in intact hearts to be phosphorylated in response to catecholamine treatment have been considered. There are gaps or deficiencies in the evidence for a functional role of this phosphorylation for each of the proteins considered. The data regarding the biochemical effect of TN-I phosphorylation are contradictory and the reversal of phosphorylation appears to lag behind reversal of functional effects of catecholamines. Myosin light-chain phosphorylation does not seem to be modified by any inotropic intervention. The evidence for a role for phospholamban phosphorylation seems quite convincing, but the reversal of phosphorylation appears to lag behind reversal of the relaxant effects of catecholamines. Finally, although substantial evidence suggests that a component of I_{si} channels could be a substrate for cAMP-dependent protein kinase, no direct studies of phosphory-

lation of I_{si} channels either in vitro or in intact tissues have yet been accomplished. Thus, much remains to be studied to establish the functional role of phosphorylation of these proteins in mediating the positive inotropic effects of catecholamines. Other possible protein substrates which may be involved in regulating cardiac function should also be explored.

ROLE OF Ca^{2+} IN MEDIATING THE INOTROPIC EFFECTS OF CATECHOLAMINES

Ultimately, any change in contractile state of cardiac muscle is determined by the availability of Ca^{2+} to interact with the myofibrillar contractile protein complex. The effects of beta agonists must therefore ultimately involve changes in Ca^{2+} fluxes and availability to contractile proteins. As described above, these effects of catecholamines presumably include increased systolic inward Ca^{2+} flux via I_{si} channels, perhaps altered sensitivity of TN-C to Ca^{2+}, and increased Ca^{2+}-ATPase activity. Presumably, phosphorylation of proteins catalyzed by cAMP-dependent protein kinase is the biochemical change that mediates these effects.

Theoretically, Ca^{2+}-calmodulin-dependent protein kinase could also be activated by the increased intracellular Ca^{2+} resulting from catecholamine effects, and this kinase could also phosphorylate various proteins and thereby modify cardiac cell function. It has been shown in vitro that addition of calmodulin in the presence of Ca^{2+} to sarcoplasmic reticulum membranes leads to phosphorylation of phospholamban [41–43]. The amount of this phosphorylation is additive to that induced by cAMP-dependent protein kinase and therefore the two kinases are assumed to phosphorylate different sites [42]. Ca^{2+}-ATPase activity of sarcoplasmic reticulum is increased by calmodulin-kinase-induced phosphorylation just as it is by cAMP-dependent protein-kinase-induced phosphorylation [42, 43]. One study of functioning rat ventricles suggests that calmodulin-kinase-induced phosphorylation may also occur in vivo [33]. However, in extensive studies with guinea pig ventricles, a variety of inotropic interventions which do not elevate cAMP failed to cause phosphorylation of phospholamban (table 17–2) [35]. These interventions included perfusion with high Ca^{2+} buffer and the administration of ouabain and the Ca^{2+} ionophore A23187. Although the positive inotropic effects of these interventions were equivalent in magnitude to that induced by beta agonists, phospholamban phosphorylation was unaltered [35]. These positive inotropic agents which did not elevate cAMP levels did not accelerate the rate of relaxation of the guinea pig ventricles. Also, Ca^{2+}-ATPase activity of sarcoplasmic reticulum of these hearts was not altered (table 17–2). These results thus suggest that, in intact hearts, agents which increase intracellular Ca^{2+}, but do not elevate cAMP levels, do not cause phosphorylation of phospholamban, despite the fact that such phosphorylation can be shown in vitro and that sarcoplasmic reticulum membranes contain a Ca^{2+}-calmodulin-dependent protein kinase. The reason why phosphorylation by maneuvers

TABLE 17–2. Effects of various positive inotropic agents on phospholamban phosphorylation, Ca^{2+}-ATPase activity, and contractile parameters in intact myocardium

Treatment	^{32}P incorporation (pmol ^{32}P/mg protein)	Ca^{2+}-ATPase (μmol P_i/mg protein/h)	$+T_{max}$ (% control)	$\Delta t_{1/2}$ (ms)
H_2O, 60 s (control)	71 ± 11 (15)	1.63 ± 0.10 (15)		
Histamine, 1 μM, 60 s	191 ± 23 (6)*	2.10 ± 0.17 (6)*	190 ± 11 (6)	−22 ± 1* (6)
H_2O, 15 min (control)	59 ± 15 (8)	1.53 ± 0.11 (8)		
Bt_2cAMP, 3 mM, 15 min	118 ± 19 (9)*	1.98 ± 0.08 (9)*	115 ± 5 (9)	− 1 ± 1 (9)
Ouabain, 1 mM, 15 min	37 ± 7 (5)	1.47 ± 0.24 (5)	131 ± 4 (5)	
Propranolol, 6 μM + metiamide 10 μM, 5 min	37 ± 8 (3)	1.28 ± 0.05 (3)		
$+Ca^{2+}$, 5 mM 60 s	31 ± 4 (3)	1.25 ± 0.15 (3)		+ 2 ± 1 (3)

Results are mean ± SE of n hearts (in parentheses). $P < 0.05$ when compared to control.

which would be expected to activate calmodulin kinase cannot be demonstrated in vivo are unknown. Possibly, phosphate turnover at the calmodulin-kinase site is slow, and in vivo this site remains phosphorylated even in hearts not treated with positive inotropic agents.

Mechanisms of Cholinergic Effects on the Heart

One of the respects in which parasympathetic regulation of cardiac function differs from sympathetic regulation is that there is much more marked variability in response of different cardiac tissues to parasympathetic than to sympathetic stimulation [1]. All tissues of the heart generally respond similarly qualitatively and quantitatively to beta-adrenergic-receptor stimulation. By contrast, ventricular tissue is much less responsive to muscarinic agonists than is atrial tissue [1]. Choline esters potently decrease automaticity of spontaneously excitable atrial tissue and exert powerful negative inotropic effects on atrial muscle. By contrast, muscarinic agonists produce minimal negative inotropic effects on isolated ventricular tissues (in the absence of sympathetic stimulation) and minimal electrophysiologic effects on ventricular muscle. Muscarinic agonists may exert direct electrophysiologic effects on Purkinje fibers of some species. In both supraventricular and ventricular structures, muscarinic agonists antagonize the effects of beta agonists. Because of the relatively minimal effects of muscarinic agonists alone in ventricular tissues, the muscarinic antiadrenergic effect is pronounced compared to the effect seen with muscarinic agonists alone. This magnification of muscarinic effect during simultaneous sympathetic stimulation, which can be observed in isolated cardiac tissues as well as in intact animals with normal sympathetic and vagal innervation, has been termed *accentuated antagonism* [44]. These differences in responsiveness of supraventricular and ventricular structures to muscarinic stimulation suggest: (a) that multiple subcellular mechanisms mediate the cardiac effects of muscarinic stimulation, and (b) that only some of these subcellular mechanisms are shared by atrial and ventricular tissues. The various myocardial cell components that mediate muscarinic effects on the heart will be discussed in the following sections.

MUSCARINIC CHOLINERGIC RECEPTORS

Like adrenergic receptors, muscarinic receptors have also come to be studied directly with radioligand binding assays (for a general review of radioligand binding assays of muscarinic receptors, see Birdsall and Hulme [45] and Ehlert et al. [46]). These assays have demonstrated that muscarinic receptors exist in both atria and ventricles and that the density of receptors in ventricles is at least as great or greater than that in atria. Thus, the differences in atrial and ventricular responses to muscarinic agonists cannot be explained by muscarinic-receptor distribution. Binding studies indicate that muscarinic receptors are membrane associated and probably predominantly or exclusively located in the plasma membrane [9]. Muscarinic binding sites in purified sarcolemma and sarcoplasmic reticulum isolated from dog hearts copurified with the sarcolemmal marker Na^+, K^+-ATPase and away from the sarcoplasmic reticulum marker Ca^{2+}-ATPase [9]. Muscarinic binding activity also copurified with beta-adrenergic binding sites. Therefore, both beta-adrenergic and muscarinic receptors are localized to the sarcolemma in myocardium. Such a location would be optimal for accessibility of neurotransmitters to the receptors and for intracellular interaction between the two branches of the autonomic nervous system at the level of the receptors and their effectors (fig. 17–1).

Similar to beta-adrenergic receptors, muscarinic receptors are also regulated by a variety of influences [45, 46]. Binding assays have revealed that the interaction of agonists with muscarinic receptors is much more complex than that of antagonists, similar to the situation with beta-adrenergic receptors. Muscarinic receptors exist in multiple states in terms of their interaction with agonists [45, 46]. The same binding sites (i.e., muscarinic receptors) which interact with antagonists in a uniform manner interact with agonists heterogeneously. This is recognized by analysis of the curves relating the occupancy of muscarinic receptors to

the concentration of muscarinic agonists added to the receptors. The binding curves relating antagonist occupation of receptors to antagonist concentration are of the form predicted by the application of the law of mass action to the interaction of a ligand with a uniform set of binding sites (fig. 17–7). In contrast, the pattern of agonist binding curves deviates substantially from this simple mass-action relationship (fig. 17–7). These agonist curves are shallower than antagonist binding curves and have slope factors substantially less than 1.0. The most plausible explanation for this is that muscarinic receptors exist in multiple conformations in terms of their interaction with agonists [45, 46]. Three different classes of muscarinic binding sites, each with different affinities for agonists, have been described in rat brain membranes [45]. At least two binding sites (high and low affinity) for agonists have been described in several other organs, including heart [45, 46]. These different affinity binding sites are noninterconvertible in the binding assay, and therefore the slopes describing occupancy as a function of agonist concentration represent the sum of the interaction of ligand with multiple binding sites.

Muscarinic receptors, like beta-adrenergic receptors, are regulated by guanine nucleotides [46]. Analysis of agonist competition with antagonist radioligands for binding to muscarinic receptors in cardiac membrane preparations from which endogenous guanine nucleotides have been removed yields the shallow binding curves described above (fig. 17–7). If exogenous guanine nucleotides are added, however, the curves shift to a steeper form, a pattern compatible with the interaction of ligand with a single, homogeneous class of binding sites [46]. At the same time the affinity of the receptor for agonists is reduced substantially. These data have been interpreted as showing a guanine-nucleotide-induced conversion of receptors in a high-affinity state for agonists into a low-affinity state [46], analogous to the situation with guanine nucleotide regulation of beta-adrenergic receptors. Thus, with added guanine nucleotide binding curves are steeper (representing a single class of binding sites) and shifted to the right because most or all of the

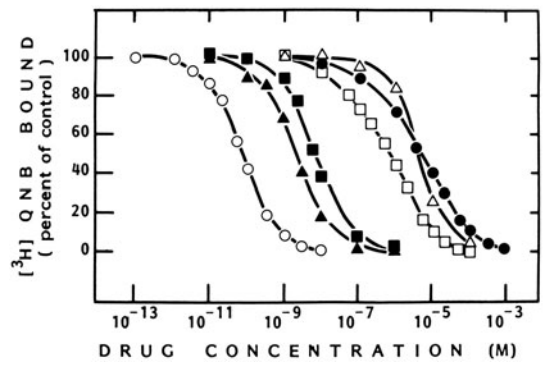

FIGURE 17–7. Competition curves for [^{3}H]QNB binding to muscarinic receptors in membrane vesicles derived from canine ventricular myocardium. Data from separate experiments performed in purified membrane preparations are presented, with binding expressed as a percent of control binding in the absence of competing drug. For all curves, [^{3}H]QNB concentration was approximately 80 p*M*. Note that oxotremorine (□) and methacholine (●) slopes are shallow compared to the antagonist slopes. Drugs are QNB (○), dexetimide (▲), atropine (■), oxotremorine (□), methacholine (●), and levetimide (△). Reprinted with permission from Mirro et al. [80].

receptors are in a low-affinity state. The interaction of guanine nucleotides, presumably via N proteins, with muscarinic receptors might be a mechanism for coupling of the receptor to intracellular effectors, analogous to the situation for beta-adrenergic receptors (fig. 17–4). However, as yet little is known about the detailed molecular interactions of muscarinic receptors with the other membrane components of the adenylate cyclase system.

Analogous to the situation with beta-adrenergic receptors, the density of cardiac muscarinic receptors varies depending on the ambient concentrations of muscarinic agonists. For example, cultured chick embryo heart cells exposed to carbamylcholine for various durations had a diminished negative chronotropic response to muscarinic agonists associated with a substantial reduction in receptor density [47]. Detailed analysis revealed a biphasic pattern to this agonist-induced receptor alteration, a rapid phase (occurring over 1 min) associated with a reduced affinity of receptors for agonists followed by a slower phase (occurring over several

hours) reflecting a true reduction in measurable receptor binding [47]. The agonist-induced reduction in cardiac muscarinic-receptor density has also been demonstrated in in vivo studies. Carbachol was administered to chicks in ovo. The negative chronotropic response to carbachol of hearts removed from these chicks was diminished compared to that of hearts from control chicks, and the density of muscarinic receptors in homogenates of these hearts was reduced markedly [48].

Like beta-adrenergic receptors, the density of cardiac muscarinic receptors can vary depending on thyroid status. Thyroidectomy increased the density whereas treatment with triiodothyronine resulted in a modest decrease in density of muscarinic receptors [49]. These effects of thyroid state on muscarinic receptors are exactly the opposite of the effects on beta-adrenergic receptors. Hyperthyroidism increases the density whereas hypothyroidism decreases the density of beta-adrenergic receptors in cardiac tissues [11, 12]. Thus, the tachycardia of hyperthyroid animals and the bradycardia of hypothyroid animals may reflect a reciprocal alteration in the density of receptors of both limbs of the autonomic nervous system.

INTRACELLULAR EFFECTORS COUPLED TO MUSCARINIC CHOLINERGIC RECEPTORS

Compared to the relatively detailed knowledge regarding the subcellular mechanisms by which beta agonists modify cardiac function, the intracellular mechanisms for producing muscarinic effects are sketchy. Several potential mechanisms will be discussed in this section.

Cation Channels. The electrophysiologic and inotropic effects of muscarinic activation of mammalian atria are associated with an increase in outward current carried by K^+ [50, 51]. This increase in K^+ outward current results in earlier repolarization of the membrane and thus shortening of action potential duration and decreases in contractility. The reduction in contractility is thought to be due to a secondary diminution in I_{si} [50]. Because action potential duration is shortened by increased outward currents, the plateau phase of the action potential during which time I_{si} occurs is abbreviated [50]. Whether this electrophysiologic mechanism can account entirely for the negative inotropic effects of muscarinic activation or whether additional mechanisms (to be discussed in later parts of this section) are operative remains to be established. Also, it is not known whether muscarinic receptors are coupled directly to K^+ channels or whether intermediary steps (e.g., altered phospholipid turnover, increased cyclic-GMP levels) must occur between activation of the receptors and increased K^+ current.

In mammalian atria, the effects of muscarinic activation on cation channels appears to depend on the concentration of muscarinic agonist used. With low concentrations of acetylcholine (sufficient to reduce twitch tension by 30%–40%), the previously described effects of muscarinic activation on K^+ currents occurred [50]. At this concentration of acetylcholine the changes in I_{si} were secondary or "indirect", i.e., these changes resulted from the shortening in plateau duration. With higher concentrations of acetylcholine (sufficient to reduce twitch tension by 70%–90%), a direct effect on I_{si} also was observed with voltage-clamp studies [50]. Thus, with high concentrations of muscarinic agonists, K^+ outward currents increased and I_{si} also decreased. These dual actions on ion flux would be expected to produce strong negative inotropic effects. As in the case of K^+ channels, the nature of the coupling between muscarinic receptors and I_{si} channels remains unknown.

Tissue differences also exist in muscarinic effects on I_{si}. In mammalian atria, high concentrations of acetylcholine directly reduced I_{si} [50]. However, in mammalian ventricular tissues, activation of muscarinic receptors even with high concentrations of acetylcholine did not appear to produce a direct effect on I_{si}.

Thus, one well-established effect of muscarinic activation is alterations in the properties of ion channels located in the sarcolemma of myocardial cells.

Cyclic GMP. It was first shown in cardiac tissue that cyclic-GMP (cGMP) levels could be elevated by activation of muscarinic cholinergic receptors. This original observation of musca-

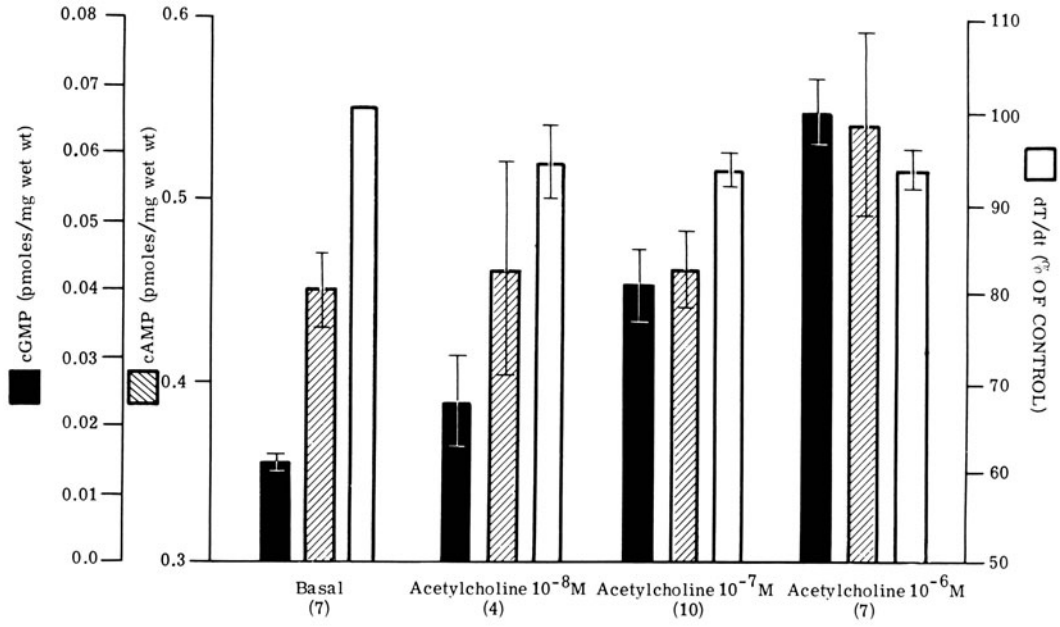

FIGURE 17–8. Effect of acetylcholine on cGMP and cAMP levels in guinea pig ventricles. Acetylcholine was perfused for 2 min prior to freezing hearts. Note the concentration-dependent increase in cGMP levels, without a change in cAMP levels except at 10^{-6} *M* acetylcholine. At this highest concentration of acetylcholine, catecholamines may have been released to account for the small elevation in cAMP level. Note also the lack of any significant negative inotropic effect of acetylcholine.

rinic-induced increases in cGMP levels in cardiac tissues was confirmed and extended by multiple subsequent studies done in hearts from a variety of different species (fig. 17–8) (for review, see Goldberg and Haddox [52]). Thus, there is no question that, under appropriate conditions, activation of muscarinic receptors can result in increases in myocardial tissue cGMP levels (fig. 17–8), but whether this muscarinic-induced elevation in cGMP levels has any physiologic role remains an issue of controversy [52, 53]. Moreover, the biochemical mechanisms by which changes in tissue cGMP might alter cardiac function are unknown [52].

The original studies which attempted to demonstrate a physiologic role for cGMP correlated a physiologic response (e.g., contractile state) with tissue cGMP levels. In these studies, acetylcholine was given to cardiac preparations in various concentrations for different durations, the mechanical or electrophysiologic responses of the hearts were observed, and cGMP levels determined in the same tissues. Although there appeared to be a fairly good correlation between tissue cGMP levels and the measured physiologic response, these studies could be criticized as being inconclusive because a sufficiently detailed concentration–response analysis was not performed [53].

The bulk of the additional evidence supporting a role for cGMP in mediating some of the physiologic effects of muscarinic activation comes from studies utilizing analogues of cGMP to attempt to increase directly the intracellular levels of the nucleotide. Analogues (e.g., dibutyryl cGMP or 8-bromo-cGMP) are used because they are less susceptible to degradation during superfusion or perfusion, and because they are thought to penetrate the sarcolemma more readily than does cGMP. It is reasoned that if intracellular cGMP levels can be increased directly with these agents, and if these agents mimic the action of acetylcholine, then this is evidence that cGMP mediates that action of acetylcholine. A similar rationale has

been applied to studies utilizing analogues of cAMP to establish the role of this nucleotide in mediating a given effect of a hormone or neurotransmitter. When using analogues of either cyclic nucleotide, the results must be interpreted cautiously, because the time course of action of these agents is slower than that of neurotransmitters and because relatively large concentrations are needed (in view of the low endogenous concentrations of these cyclic nucleotides) to produce the expected physiologic effects.

Analogues of cGMP have been shown to mimic certain of the electrophysiologic effects of acetylcholine. Dibutyryl cGMP slowed the spontaneous beating rate of isolated cultured rat heart cells [54]. Dibutyryl cAMP increased spontaneous beating rate [54]. cGMP injected directly into sinoatrial nodal cells by iontophoresis decreased the slope of spontaneous diastolic depolarization [55]. Acetylcholine administered by this same route was without effect, presumably because the choline ester must interact with muscarinic receptors on the outside of the sarcolemma to produce its effects [55]. Like acetylcholine, 8-bromo-cGMP inhibited atrial slow-response action potentials [56], an indirect assessment of I_{si}. Associated with this inhibition of the slow-response action potential was a negative inotropic effect [56]. 8-bromo-cGMP mimicked the effects of acetylcholine on action potential configuration and contractile state of rat atria [57]. In this same study, 8-bromo-cGMP decreased Ca^{2+} uptake by beating atrial preparations, but had no effect on K^+ content [57]. It was concluded that cGMP might mediate the effects of muscarinic activation on I_{si}, but not on K^+ channels [57].

Analogues of cGMP have also been used to assess the possible role of cGMP in the antiadrenergic effects of acetylcholine. Dibutyryl cGMP mimicked the effect of acetylcholine and antagonized the positive inotropic effects of catecholamines in isolated cardiac tissues [58]. These results have been confirmed by other laboratories. Like acetylcholine, dibutyryl cGMP also attenuated the positive inotropic effects of isoproterenol in hearts from hyperthyroid rats [59]. cGMP analogues also mimic acetylcholine in antagonizing certain of the electrophysiologic effects of catecholamines or cAMP. Isoproterenol antagonized the inhibition of 8-bromo-cGMP of slow responses to guinea pig atria [56]. This can be thought of as the reciprocal of cGMP antagonism of isoproterenol-induced augmentation of slow responses. cGMP analogues also mimicked the cholinergic antagonism of the cardiac metabolic effects of catecholamines [59]. Hearts from hyperthyroid rats were hyperresponsive to the metabolic effects of beta agonists compared to those from euthyroid animals [59]. Acetylcholine antagonized isoproterenol-induced activation of phosphorylase in such hearts [59]. Dibutyryl cGMP mimicked these effects of acetylcholine without lowering cAMP levels [59]. Thus, it has been shown that analogues of cGMP can mimic the effects of acetylcholine in antagonizing the electrophysiologic, inotropic, and metabolic actions of beta agonists.

If cGMP is involved in mediating some of the effects of muscarinic-receptor stimulation in the heart, the biochemical mechanism by which this occurs remains unknown. One hypothesis is that, analogous to the cAMP–protein-kinase system, cGMP interacts with a specific protein kinase which in turn phosphorylates certain substrates to alter protein function. A cGMP-dependent protein kinase has been identified in various tissues, including heart [60]. Recently, an assay has been developed for studying the activity of cGMP-dependent protein kinase in cardiac tissues [60]. With this assay, it has been shown for the first time that administration of acetylcholine to intact rat heart results in increases in cGMP-dependent protein kinase activity ratios associated with elevations in cGMP levels [60]. Both of these biochemical responses were associated with a negative inotropic effect in the same hearts. Na nitroprusside also increased cGMP levels, in fact to much greater levels than that caused by acetylcholine. However, Na nitroprusside did not increase cGMP-dependent protein kinase activity ratios nor did it change force of contraction [60]. These results suggest several conclusions: (a) they suggest a possible mechanism by which cGMP, the levels of which are altered in response to muscarinic stimulation, might modify protein function

and the physiologic properties of the heart; (b) they support the notion that cGMP and its intracellular effectors might be compartmentalized; and (c) they demonstrate the hazards of using agents other than muscarinic agonists to elevate cGMP levels and then drawing conclusions about the role of cGMP if these agents do not mimic the choline esters.

There is a body of evidence that has been interpreted to show that cGMP does not have any role in cardiac regulation [53]. One concentration–response study showed a dissociation between inotropic and cGMP-elevating effects of low concentrations of carbachol [61]. Low concentrations of carbachol (0.03–1.0 μM) decreased contractility whereas only high concentrations (2 or 10 μM) elevated cGMP levels [61]. Also, by using a low concentration of carbachol, a dissociation in time course of response was demonstrated. With 0.3 μM carbachol contractility fell whereas cGMP levels did not change [61]. These data were interpreted as showing that cGMP does not have a role in regulating the contractile state of atria. However, an alternative interpretation is that the contractile state of atria, as modified by muscarinic agonists, is determined by more than one factor, and cGMP regulates only one of those factors. It was shown by voltage-clamp studies that low concentrations of acetylcholine increased K^+ outward currents whereas high concentrations reduced I_{si} as well as increased outward currents in mammalian atria [50]. Even low concentrations (that only modified K^+ currents) produced negative inotropic effects, presumably because I_{si} was indirectly abbreviated owing to the shortened duration of the action potential [50]. High concentrations produced more marked negative inotropic effects presumably because I_{si} was directly inhibited as well as being abbreviated due to the shortened action potential duration. Thus, it is possible that with low concentrations of muscarinic agonists negative inotropic effects occur independently of cGMP and with high concentrations a second mechanism (e.g., inhibition of I_{si}) becomes operative and that this second mechanism involves cGMP. Such a conclusion would be compatible with studies that showed that cGMP modulates I_{si} or slow responses [57].

Another approach to test the cGMP hypothesis has been to elevate cGMP with drugs which do not interact with muscarinic receptors. Because of its potency in elevating tissue cGMP levels, Na nitroprusside has been widely used for such studies. It has been shown that Na nitroprusside did not mimic the inotropic, electrophysiologic, metabolic, or antiadrenergic effects of acetylcholine, even though it markedly increased cGMP levels (for a review, see Linden and Brooker [53]). However, because Na nitroprusside elevates cGMP levels in heart without producing physiologic effects, it does not necessarily follow that cGMP has no role in mediating the effects of acetylcholine. Immunohistochemical evidence in noncardiac [62] and cardiac [63] tissues has shown that cGMP can be compartmentalized within the cell and that muscarinic agonists and Na nitroprusside affect the concentrations of this nucleotide in different compartments. The recent observations that acetylcholine, but not Na nitroprusside, activates cGMP-dependent protein kinase in rat hearts provide further evidence for different compartments or pools of cGMP, each of which can be selectively regulated and which have different intracellular effectors [60]. Analogous evidence has been provided for compartmentation of cAMP and differential regulation of cAMP levels in different pools in myocardial cells.

The most convincing evidence against a role for cGMP in mediating certain physiologic effects are the observations that over a range of concentrations of muscarinic agonist certain physiologic effects can be induced without changing tissue cGMP levels. Acetylcholine decreased automaticity and shortened action potential duration of guinea pig atria and these changes appeared to occur without any relationship to tissue cGMP levels [64]. Muscarinic agonists antagonized the positive inotropic effects of agents that elevate cAMP levels (catecholamines, phosphodiesterase inhibitors, cholera toxin) without elevating cGMP levels [65]. These results could be interpreted as eliminating a role for cGMP in the electrophysiologic or antiadrenergic effects of muscarinic agonists. However, the following considerations should be kept in mind: (a) muscarinic receptors might be linked to multiple responses only one

or a few which are regulated by cGMP; each of these must be examined carefully before ruling out in a blanket fashion any physiologic role for cGMP; (b) cGMP might be compartmentalized and small undetectable (by available assays) changes in levels might have occurred in experiments that appeared to show no change in the levels of the nucleotide.

Thus, substantial evidence exists both in support of and against the concept that cGMP plays a role in mediating certain cardiac effects of muscarinic-receptor stimulation. It is clear that this is an unresolved issue. Further experiments must be done to establish or completely eliminate a role for this cyclic nucleotide in cardiac regulation.

cGMP levels are regulated by two enzymes: guanylate cyclase and cGMP phosphodiesterase [52]. Guanylate cyclase occurs as both a membrane-associated and soluble enzyme in cardiac tissues. The membrane-bound form of the enzyme is located in sarcolemma, the same location of muscarinic receptors [66]. The two forms of the enzyme in cardiac muscle are differentially regulated: nonionic detergents stimulated the particulate enzyme without modifying the activity of the soluble enzyme, whereas Na nitroprusside stimulated only the soluble enzyme [66]. These results showing both particulate and soluble forms of the enzyme and differential activation of the two forms of the enzyme provide further support for the notion of different intracellular pools of cGMP which can be modified selectively by certain agents. Acetylcholine presumably increases cGMP levels by stimulating guanylate cyclase. As noted, both muscarinic receptors and particulate guanylate cyclase are located in sarcolemma. Except for rare reports, however, investigators have failed to show any effect of muscarinic agonists on guanylate cyclase activity in broken cell preparations [52]. In intact tissues, Ca^{2+} is required for muscarinic-induced elevations in cGMP levels. The divalent cation ionophore A23187 increased cGMP levels in guinea pig ventricles presumably by elevating Ca^{2+} in certain critical areas of the myocardial cell [67]. Ca^{2+} has been shown to stimulate particulate guanylate cyclase activity [68]. Based on these types of results it has been suggested that Ca^{2+} might in some way function as an intermediary between the muscarinic receptor and guanylate cyclase. However, this conclusion remains to be established. Other studies have shown Ca^{2+} inhibition of guanylate cyclase [52]. In cardiac muscle, although Ca^{2+} is required for muscarinic-induced increases in cGMP levels, the physiologic response to muscarinic stimulation is either no change or a decrease in contractile state [58]. These mechanical effects suggest that muscarinic agonists do not produce a generalized increase in intracellular Ca^{2+} concentration. If activation of muscarinic receptors leads to mobilization of Ca^{2+}, this must occur in discrete intracellular pools (presumably in the region of guanylate cyclase) because contractile proteins and other intracellular enzymes (e.g., phosphorylase kinase) do not appear to be affected.

Cellular (Postjunctional)Mechanisms of Muscarinic Modulation of Adrenergic Effects on the Heart. In cardiac preparations from various mammalian species it has been shown clearly that choline esters antagonize the positive inotropic effects of beta-receptor agonists [58, 69] (fig. 17–9). In most of these studies with isolated tissues, the negative inotropic effects of muscarinic agonists given alone were prominent and easily detectable in atria [69], but were small or absent in ventricles [58]. Muscarinic antagonism of the positive inotropic effects of catecholamines was seen in both atria and ventricles. Thus, it appears that in atrial tissues muscarinic agonists produce negative inotropic effects both by a direct action and by antagonizing the effects of the beta-receptor agonists. By contrast, in ventricles the predominant muscarinic effect appears to be inhibition of the inotropic effects of beta agonists.

In isolated cardiac preparations, muscarinic agonists also antagonize the electrophysiologic effects of catecholamines. Choline esters attenuated the positive chronotropic effects of catecholamines on isolated atrial preparations, presumably by antagonizing the catecholamine-induced increase in spontaneous phase-4 depolarization. Muscarinic agonists antagonize the electrophysiologic effects of catecholamines on isolated Purkinje fibers or ventricular muscle. Acetylcholine inhibited isoproterenol-induced shortening of action potential duration in nor-

mally polarized paced cardiac Purkinje fibers. Acetylcholine also abolished isoproterenol-dependent slow responses in cardiac Purkinje fibers or guinea pig papillary muscles (fig. 17–10) [70].

Activation of muscarinic receptors also modulates the cardiac metabolic effects of beta-adrenergic-receptor stimulation. Acetylcholine completely antagonized the glycogenolytic effect of epinephrine in isolated perfused guinea pig hearts. Subsequent studies showed that this was due to a muscarinic antagonism of beta-adrenergic activation of glycogen phosphorylase [59, 71] (fig. 17–11).

Thus, in isolated cardiac preparations there is abundant evidence for intracellular interaction between activation of beta-adrenergic and muscarinic receptors. In isolated ventricular tissues, it appears that modulation of sympathetic effects is a major mechanism by which the parasympathetic nervous system exerts its effect. Choline esters alone produced little or no change in the inotropic, electrophysiologic, or metabolic properties of isolated ventricular tissues. Only when these physiologic or metabolic responses were stimulated by beta-adrenergic agonists did muscarinic cholinergic effects become readily apparent. In this situation, muscarinic agonists potently antagonized the beta-adrenergic alteration of these properties. The mechanisms for the intracellular interaction between the components of the sympathetic and parasympathetic systems are discussed in the next section.

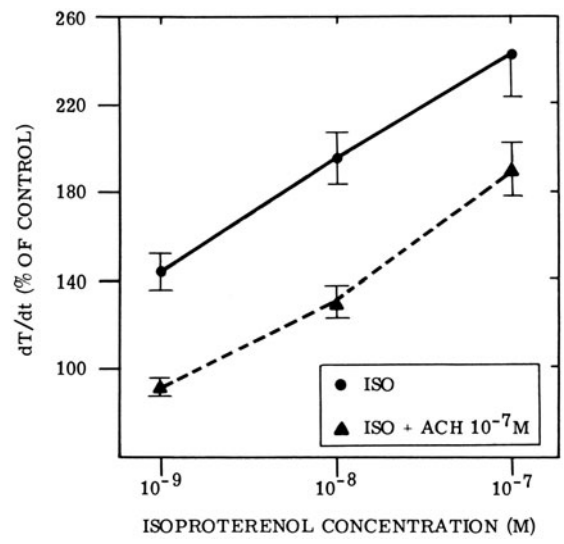

FIGURE 17–9. Effect of acetylcholine (ACh) (10^{-7} *M*) on the positive inotropic effect of isoproterenol (Iso) in isolated, perfused guinea pig ventricles. Measurements were taken after hearts had reached a stable level of contractions after 2 min of continuous drug infusion. Note that the inotropic response to isoproterenol is markedly attenuated by acetylcholine. Values are means ± SEM for 7–15 hearts. Reprinted with permission from Watanabe and Besch [58].

MUSCARINIC INHIBITION OF ADENYLATE CYCLASE. A number of investigators using different types of cardiac preparations from various species have shown that muscarinic agonists can attenuate beta-agonist-induced increases in steady-state tissue cGMP levels [59, 69, 71]. When physiologic or metabolic responses were measured, the muscarinic attenuation of cAMP generation paralleled the inhibition of the myocardial response to catecholamines. Muscarinic agonists inhibited catecholamine-induced increases in cAMP levels and concomitantly attenuated the positive inotropic effects [59, 69]. Muscarinic agonists also antagonized catecholamine-induced activation of phosphorylase while inhibiting cAMP generation [71]. These results are consistent with the conclusion that the muscarinic inhibition of cAMP generation is physiologically and metabolically important in cardiac cells, and that attenuation of cAMP generation might be a contributing mechanism for the antiadrenergic effects of muscarinic agonists.

The mechanism for muscarinic attenuation of catecholamine-induced cAMP generation involves inhibition of adenylate cyclase activity. It first was shown two decades ago, prior to any detailed knowledge regarding regulation of adenylate cyclase, that muscarinic agonists inhibited adenylate cyclase activity in crude preparations of dog myocardium [72]. Carbachol added to these preparations inhibited both basal and epinephrine-stimulated adenylate cyclase activity [72]. These results were confirmed in similar experiments which used a crude myocardial preparation from rabbit hearts [73]. As mentioned previously, adenylate cyclase activity in purified membranes from

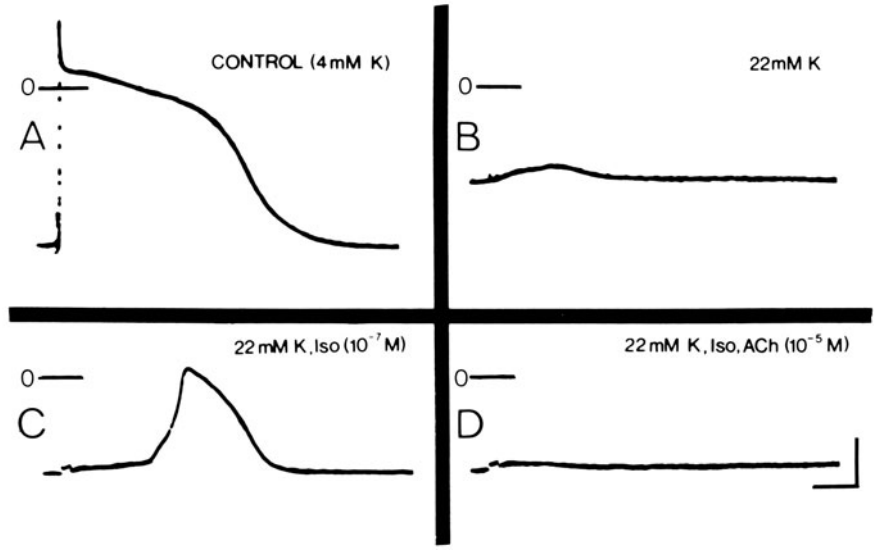

FIGURE 17–10. The effects of acetylcholine on an isoproterenol-dependent "slow response". *(A)* Control Purkinje fiber action potention in 4 m*M* potassium. *(B)* Generalized depolarization and loss of excitability produced by superfusion of Tyrode solution containing 22 m*M* potassium. *(C)* Restoration of excitability by the addition of 10^{-7} *M* isoproterenol. *(D)* The addition of acetylcholine (10^{-5} *M*) abolishes the "slow response" generated by the addition of isoproterenol. Zero potential indicated in each panel. Calibrations: horizontal bar = 50 ms; vertical bar = 25 mV. Reprinted with permission from Bailey et al. [70].

myocardial cells is not stimulated by hormones unless exogenous guanine nucleotides are added (fig. 17–5). Addition of exogenous guanine nucleotides stimulated the enzyme directly as well as facilitating hormone stimulation of the enzyme [20] (fig. 17–5). Thus, guanine nucleotides can activate cardiac adenylate cyclase directly and are required for hormone activation of the enzyme. In purified membrane preparations, muscarinic agonists had no effect on basal adenylate cyclase activity, i.e., that activity in the absence of added guanine nucleotides [20]. If GTP was added to the enzyme preparation, muscarinic agonists inhibited adenylate cyclase activity (fig. 17–5, left panel). This was true whether GTP was added alone or together with a catecholamine (fig. 17–5, left panel). In the earlier studies cited [72, 73], because the membrane preparations were crude it is likely that endogenous GTP was present. Thus, in these earlier studies it is likely that muscarinic effects on adenylate cyclase activity were also dependent on GTP. This dependency of the muscarinic inhibitory effect on GTP was specific for this guanine nucleotide. Cardiac adenylate cyclase activity was also increased by the nonhydrolyzable guanine nucleotide Gpp(NH)p (fig. 17–5, right panel). However, muscarinic agonists had no effect on enzyme activity in the presence of this nucleotide [20] (fig. 17–5, right panel). Similarly, muscarinic agonists did not modify NaF stimulation of adenylate cyclase activity [20]. The effects of muscarinic agonists were blocked by atropine [20]. It was concluded that the interaction of both muscarinic and beta-adrenergic receptors with adenylate cyclase was regulated by the naturally occurring guanine nucleotide GTP. These studies have been confirmed subsequently. Based on these findings and the data that show guanine nucleotide regulation of muscarinic-receptor affinity for agonists [45, 46], it is reasonable to hypothesize that an N protein, with which GTP interacts, is involved in "coupling" inhibitory muscarinic receptors to adenylate cyclase (fig. 17–4). Whether this is the same N_s protein that couples stimulatory receptors to the enzyme or whether muscarinic receptors are

coupled to the putative N_i protein is unknown (fig. 17–4). The detailed biochemical mechanism by which activation of muscarinic receptors leads to reduction of the efficacy of GTP is also unknown. The fact that this inhibition does not occur when the nonhydrolyzable analogue Gpp(NH)p is the guanine nucleotide present suggests the hypothesis that muscarinic agonists increase the activity of an adenylate-cyclase-associated GTPase. It has been shown in another system that muscarinic agonists can activate adenylate-cyclase-associated GTPase activity [74]. In studies indirectly assessing GTPase activity, this mechanism is suggested for cardiac membranes [75]. Other mechanisms are also possible instead of or in addition to that postulated. Thus, the specific details regarding the biochemical and molecular mechanisms by which activation of muscarinic receptors inhibits adenylate cyclase remain to be elucidated. Nevertheless, it seems clear that muscarinic agonists can diminish tissue cAMP levels by inhibiting catecholamine stimulation of adenylate cyclase.

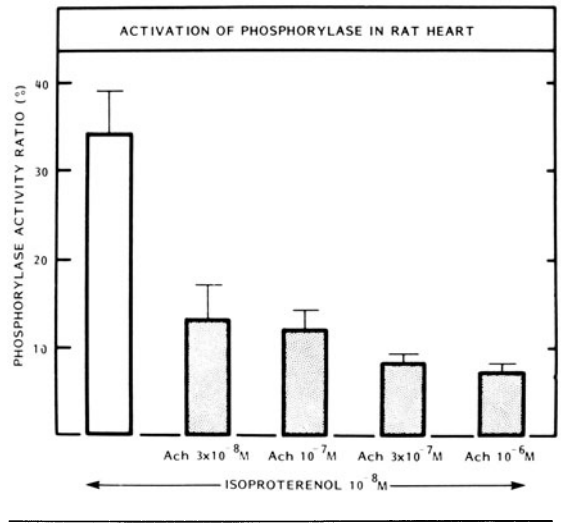

FIGURE 17–11. Muscarinic cholinergic antagonism of isoproterenol activation of glycogen phosphorylase in isolated perfused hearts taken from hyperthyroid rats. Basal phosphorylase activity ratio was 8%. Values were mean ± SEM of 6–8 hearts.

MUSCARINIC MODULATION OF cAMP EFFECTS INDEPENDENT OF CHANGES IN cAMP LEVELS. The muscarinic attenuation of catecholamine-induced cAMP generation cannot account entirely for the muscarinic antagonism of the cardiac effects of beta agonists. Under certain conditions, muscarinic agonists can potently inhibit the physiologic and metabolic effects of catecholamines without changing cAMP levels. Acetylcholine markedly antagonized the positive inotropic effects of isoproterenol in isolated perfused guinea pig ventricles [58] (fig. 17–9). cGMP levels in the acetylcholine-treated hearts were markedly elevated (fig. 17–12). However, cAMP levels in hearts receiving both acetylcholine and isoproterenol were not significantly different from those in hearts receiving isoproterenol alone [58] (fig. 17–12). These results have been confirmed subsequently by several other investigators. It has been shown either that muscarinic agonists attenuated a physiologic or metabolic response to catecholamines out of proportion to the magnitude of reduction in cAMP or that the inhibition of physiologic response occurred without any change in cAMP levels. Additional evidence for muscarinic antagonism of catecholamine effects by mechanisms not involving cAMP reduction comes from studies in which cAMP levels are increased independently of stimulation of beta receptors. It was observed many years ago that acetylcholine blocked the positive inotropic effects of both epinephrine and theophylline in isolated turtle hearts [76]. Although cAMP levels were not measured, it is reasonable to conclude that the positive inotropic effects of both epinephrine and theophylline were mediated at least partially by cAMP [76]. Subsequently, several investigators have utilized phosphodiesterase inhibitors to produce positive inotropic effects and elevate cAMP levels in cardiac preparations and then examine the effects of muscarinic agonists on these parameters. Methylisobutylxanthine (MIX) elevated cAMP levels and augmented Ca^{2+} -dependent action potentials and contraction in chick ventricles [77]. Acetylcholine (10^{-6} *M*) abolished the MIX-induced increase in tension without reducing tissue cAMP levels [77]. In isolated rat left atria, methacholine antagonized the positive inotropic effects of MIX without changing cAMP levels [69]. Myocardial cAMP levels also can be increased

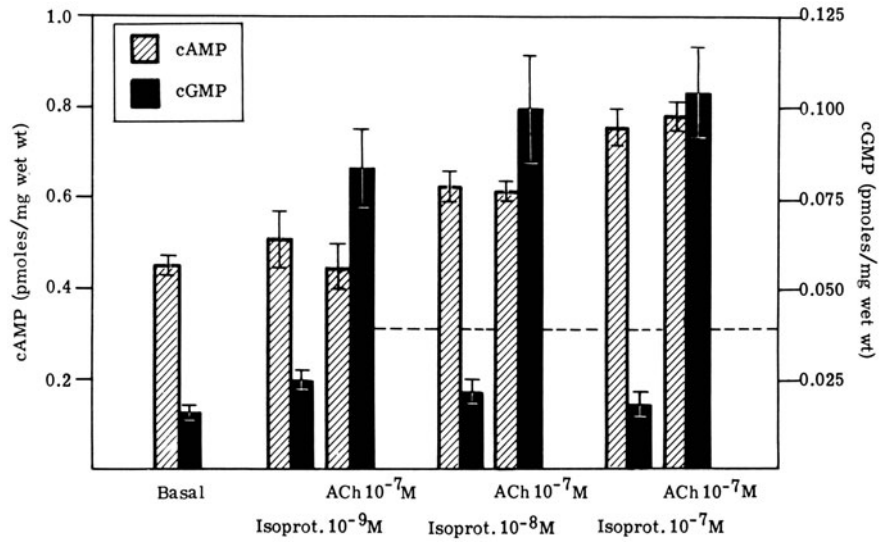

FIGURE 17–12. Cyclic nucleotide levels in hearts receiving isoproterenol (Isoprot.) alone or combined with acetylcholine (ACh) for 2 min of continuous infusion. Values are means ± SE for 7–16 hearts. The horizontal broken line is the mean value of cGMP found in hearts receiving 10^{-7} *M* acetylcholine alone for 2 min. Reprinted with permission from Watanabe and Besch [58].

by treating the intact tissue with cholera toxin [65]. The presumed mechanism is that cholera toxin inhibits the adenylate-cyclase-associated GTPase. Thus, the GTP concentration available to interact with the N protein is increased and adenylate cyclase thereby activated. Cholera toxin elevated cAMP levels [65] and increased contractions [65] of intact cardiac preparations. Muscarinic agonists inhibited the positive inotropic effect of cholera toxin without reducing cAMP levels [65]. These results thus provide additional evidence that muscarinic agonists can antagonize the effects of cAMP within the myocardial cell.

There are several potential sites beyond cAMP where muscarinic agonists could act to interfere with the intracellular effects of the nucleotide (fig. 17–4). One of these is cAMP activation of cAMP-dependent protein kinase. This has been examined in only a limited manner. However, the studies that have attempted to examine the relationship between cAMP levels and activation of cAMP-dependent protein kinase have failed to reveal any effect of acetylcholine on this relationship. That is, for a given level of cAMP, cAMP-dependent protein kinase was proportionately activated in the presence or absence of muscarinic agonists. Muscarinic agonists thus do not appear to interfere with cAMP activation of protein kinase.

Another potential site where muscarinic agonists might interfere with the intracellular effects of cAMP is at the level of phosphorylation of proteins which are thought to mediate the effects of hormones or drugs that elevate cAMP concentrations. Because TN-I and phospholamban have been shown to be phosphorylated in intact muscle in response to catecholamines, both proteins are good candidates for examining the effects of muscarinic agonists on protein phosphorylation. It has been shown in limited studies that acetylcholine reverses epinephrine-induced phosphorylation of TN-I [23]. Acetylcholine also potently attenuated isoproterenol-induced increases in ^{32}P incorporation into phospholamban while antagonizing the positive inotropic effects of the catecholamine [78] (fig. 17–13). Thus, muscarinic agonists can potently antagonize catecholamine-induced phosphorylation of myocardial cell proteins which may be involved in mediating the positive inotropic effects of catecholamines. It is not yet known whether this attenuation of

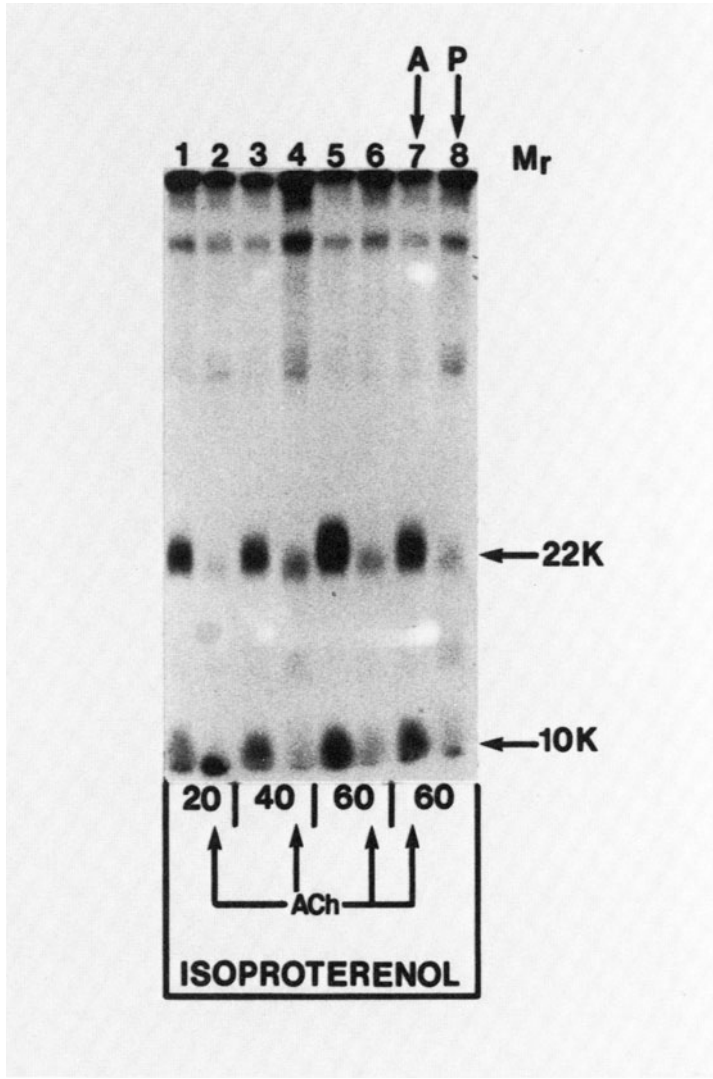

FIGURE 17–13. Autoradiogram of guinea pig ventricles perfused with $^{32}P_i$ and then treated with isoproterenol (10^{-8} *M*) alone or isoproterenol plus acetylcholine (10^{-7} *M*) for 20, 40, and 60 s. After perfusion with drugs for respective durations, ventricles were freeze-clamped and then membrane vesicles were prepared. Vesicles were subjected to gel electrophoresis and this autoradiogram was subsequently obtained. Acetylcholine was perfused simultaneously with and for the same duration as isoproterenol. Hearts in lanes 1, 3, and 5 received isoproterenol plus acetylcholine. Heart in lane 7 received atropine in addition to isoproterenol and acetylcholine, and heart in lane 8 received propranolol in addition to isoproterenol. Note that isoproterenol produces a time-dependent increase in ^{32}P incorporation into the 22,000- and 8,000- to 11,000-M_r proteins (lanes 1, 3, and 5). Propranolol antagonizes this effect of isoproterenol (lane 8). Acetylcholine clearly attenuates the isoproterenol-induced increase in ^{32}P incorporation (lanes 2, 4, and 6). Atropine reverses the effect of acetylcholine (lane 7). Reprinted with permission from Watanabe et al. [78].

protein phosphorylation can be accounted for entirely by muscarinic reduction in cAMP levels and thus in protein kinase activity. In view of the earlier studies mentioned, this seems unlikely. Rather, it seems more likely that cAMP may have been reduced somewhat and that this accounts partially for the reduced phosphorylation, but that some additional mechanism was also operative to produce the ultimate observed inhibition of ^{32}P incorporation. One reasonable hypothesis is that muscarinic agonists somehow activate a protein phosphatase (fig. 17–4).

There are, however, not yet any data available that address this question specifically.

Thus, muscarinic agonists appear to act at more than one level in modulating the cascade of reactions mediating the intracellular effects of beta-receptor stimulation. They can inhibit adenylate cyclase activity by somehow reducing the efficacy of GTP. In addition, they appear to be able to interfere with the intracellular effects of cAMP. The mechanism for this latter effect is yet unknown.

Summary

Catecholamines modify cardiac function by interacting with beta- and alpha-adrenergic receptors on myocyte cell surfaces. The intracellular effects of beta-adrenergic-receptor stimulation are mediated, at least partially, by the cAMP, cAMP-dependent protein kinase system. This ultimately involves cAMP-dependent protein-kinase-induced phosphorylation of proteins in myocardial cells to alter protein function and thereby change Ca^{2+} flux and binding to cellular components critical in regulating myocardial contractility. Several protein substrates of cAMP, which are involved in Ca^{2+} regulation of the myofibrillar contractile protein complex or in membrane control of Ca^{2+} movements, have been identified and shown to be phosphorylated in intact hearts treated with catecholamines. Although it seems likely that phosphorylation of one or more of these proteins is involved in mediating the cellular effects of cAMP, additional studies are needed to establish this and to elucidate the detailed biochemical mechanisms for these effects. Additional proteins, not yet identified, may also be involved in mediating these effects. It is possible that stimulation of beta-adrenergic receptors leads directly to altered cellular Ca^{2+} handling independent of changes in the cAMP, cAMP-dependent protein kinase system. However, no convincing evidence regarding such a mechanism is available.

Alpha agonists increase myocardial contractility in some species by activating myocardial alpha-adrenergic receptors. The intracellular mechanisms by which alpha agonists modify myocardial cell function are not known. Altered Ca^{2+} handling by myocytes must be involved, but how this occurs is unknown. It is known that the cAMP, cAMP-dependent protein kinase system does not mediate alpha-adrenergic effects on the heart.

The cellular mechanisms by which muscarinic agonists modify myocardial cell function are also less well elucidated than those for beta-adrenergic effects. Muscarinic activation in atria leads to increased K^+ flux. However, what "couples" muscarinic receptors to K^+ channels is unknown. cGMP levels can be elevated by muscarinic agonists, but the role of this nucleotide in modifying myocardial cell function remains questionable. One definite mechanism by which muscarinic agonists modify cardiac function is by modulating the cellular effects of beta agonists. This occurs by muscarinic inhibition of catecholamine stimulation of adenylate cyclase and muscarinic attenuation of phosphorylation of proteins. The detailed mechanisms of both of these muscarinic effects remain to be elucidated.

Thus, while there is substantial information about the cellular and subcellular mechanisms by which autonomic transmitters modify myocardial cell function, much remains to be established and to be elucidated in more detail. Future investigation in these areas should be fruitful and rewarding.

References

1. Levy MN, Martin PJ: Neural control of the heart. In: Handbook of physiology—the cardiovascular system I. Bethesda MD: American Physiological Society, 1979, pp 581–620.
2. Maguire ME, Ross EM, Gilman AG: Beta-adrenergic receptor: ligand binding properties and the interaction with adenylyl cyclase. Adv Cyclic Nucleotide Res 8:1–83, 1977.
3. Hoffman BB, Lefkowitz RJ: Radioligand binding studies of adrenergic receptors: new insights into molecular and physiological regulation. Annu Rev Pharmacol Toxicol 20:581–608, 1980.
4. Levitzki A: Catecholamine receptors. In: Cuatrecasas P, Greaves MF (eds) Receptors and recognition. London: Champ and Hall, 1976, pp 199–229.
5. Davies AO, Lefkowitz RJ: Regulation of adrenergic receptors. In: Lefkowitz RJ (ed) Receptor regulation. London: Chapman and Hall, 1981, pp 83–121.
6. Minneman KP: Adrenergic receptor molecules. In: Neurotransmitter receptors, part 2. London: Chapman and Hall, 1981, pp 185–268.
7. Watanabe AM, Jones LR, Manalan AS, Besch HR Jr: Cardiac autonomic receptors: recent concepts from

radiolabelled ligand binding studies. Circ Res 50:161–174, 1982.
8. Jones LR, Besch HR Jr, Fleming JW, McConnaughey MM, Watanabe AM: Separation of vesicles of cardiac sarcolemma from vesicles of cardiac sarcoplasmic reticulum. J Biol Chem 254:530–539, 1979.
9. Manalan AS, Jones LR: Characterization of the intrinsic cAMP-dependent protein kinase activity and endogenous substrates in highly purified cardiac sarcolemmal vesicles. J Biol Chem 257:10052–10062, 1982.
10. Fraser J, Nadeau J, Robertson D, Wood AJJ: Regulation of human leukocyte beta receptors by endogenous catecholamines: relationship of leukocyte beta receptor density to the cardiac sensitivity to isoproterenol. J Clin Invest 67:1777–1784, 1981.
11. McConnaughey MM, Jones LR, Watanabe AM, Besch HR Jr, Williams LT, Lefkowitz RJ: Thyroxine and propylthiouracil effects on alpha- and beta-adrenergic receptor number, ATPase activities, and sialic acid content of rat cardiac membrane vesicles. J Cardiovasc Pharmacol 1:609–623, 1979.
12. Williams LT, Lefkowitz RJ, Watanabe AM, Hathaway DR, Besch HR Jr: Thyroid hormone regulation of beta-adrenergic receptor number. J Biol Chem 252:2767–2769, 1977.
13. Ginsberg AM, Clutter WE, Shah SD, Cryer PE: Triiodothyronine-induced thyrotoxicosis increases mononuclear leukocyte beta-adrenergic receptor density in man. J Clin Invest 67:1785–1791, 1981.
14. Osnes J, Refsum H, Skomedal T, Oye I: Qualitative differences between beta-adrenergic and alpha-adrenergic effects on rat heart muscle. Acta Pharmacol Toxicol 42:235–247, 1978.
15. Besch HR Jr, Jones LR, Fleming JW, Watanabe AM: Parallel unmasking of latent Na^+,K^+ -ATPase and adenylate cyclase activities in cardiac sarcolemmal vesicles: a new use of the channel-forming ionophore alamethicin. J Biol Chem 252:7905–7908, 1977.
16. Ross EM, Gilman AF: Biochemical properties of hormone-sensitive adenylate cyclase. Annu Rev Biochem 49:533–564, 1980.
17. Seamon KB, Daly JW: Guanosine 5′- (β, γ -imido) triphosphate inhibition of forskolin-activated adenylate cyclase is mediated by the putative inhibitory guanine nucleotide regulatory protein. J Biol Chem 257:11591–11596, 1982.
18. Smith SK, Limbird LL: Evidence that human platelet alpha-adrenergic receptors coupled to inhibition of adenylate cyclase are not associated with the subunit of adenylate cyclase ADP-ribosylated by cholera toxin. J Biol Chem 257:10471–10478, 1982.
19. Hildebrandt JD, Hanoune J, Birnbaumer L: Guanine nucleotide inhibition of cyc^- S49 mouse lymphoma cell membrane adenylate cyclase. J Biol Chem 257:14723–14725, 1982.
20. Watanabe AM, McConnaughey MM, Strawbridge RA, Fleming JW, Jones LR, Besch HR Jr: Muscarinic cholinergic receptor modulation of beta-adrenergic receptor affinity for catecholamines. J Biol Chem 253:4833–4836, 1978.
21. Krebs EG, Beavo JA: Phosphorylation–dephosphorylation enzymes. Annu Rev Biochem 48:923–959, 1979.
22. Stull JT, Mayer SE: Biochemical mechanisms of adrenergic and cholinergic regulation of myocardial contractility. In: Handbook of physiology: the cardiovascular system. Bethesda, MD: American Physiological Society, 1979, pp. 741–774.
23. England PJ: Studies on the phosphorylation of the inhibitory subunit of troponin during modification of contraction in perfused rat heart. Biochem J 160:295–304, 1976.
24. Rubio R, Bailey C, Villar-Pilasi C: Effects of cyclic AMP dependent protein kinase on cardiac actomyosin: increase in Ca^{2+} sensitivity and possible phosphorylation of TN-I. J Cyclic Nucleotide Res 1:143–150, 1975.
25. Reddy YS, Wyborny LE: Phosphorylation of guinea pig cardiac natural actomyosin and its effect on ATPase activity. Biochem Biophys Res Commun 83:703–709, 1976.
26. Ray KP, England PJ: Phosphorylation of the inhibitory subunit of troponin and its effect on the calcium dependence of cardiac myofibril adenosine triphosphatase. FEBS Lett 70:11–16, 1976.
27. Lebowitz EA, Thibault LE, Adelstein RS: Phosphorylation of cat myocardial myosin and M-line protein enhancement by norepinephrine. Circulation 54:113, 1976.
28. Frearson N, Solaro RJ, Perry SV: Changes in phosphorylation of P light chain of myosin in perfused rabbit heart. Nature 264:801–802, 1976.
29. High CW, Stull JT: Phosphorylation of myosin in perfused rabbit and rat hearts. Am J Physiol 239:H756–H764, 1980.
30. Kirchberger MA, Tada M, Katz AM: Adenosine 3′:5′-monophosphate-dependent protein kinase-catalyzed phosphorylation reaction and its relationship to calcium transport in cardiac sarcoplasmic reticulum. J Biol Chem 249:6166–6173, 1974.
31. Tada M, Katz AM: Phosphorylation of the sarcoplasmic reticulum and sarcolemma. Annu Rev Physiol 44:401–423, 1982.
32. Lamers JMJ, Stinis JT: Phosphorylation of low molecular weight proteins in purified preparations of rat heart sarcolemma and sarcoplasmic reticulum. Biochim Biophys Acta 624:443–459, 1980.
33. LePeuch CJ, Guilleax JC, De Maille JC: Phospholamban phosphorylation in the perfused rat heart is not solely dependent on beta adrenergic stimulation. FEBS Lett 114:165–168, 1980.
34. Kranias EG, Solaro RJ: Phosphorylation of troponin I and phospholamban during catecholamine stimulation of rabbit heart. Nature 298:182–184, 1982.
35. Lindemann JP, Jones LR, Hathaway DR, Henry BG, Watanabe AM: Beta-adrenergic stimulation of

phospholamban phosphorylation and Ca^{2+} -ATPase activity in guinea pig ventricles. J Biol Chem 258:464–471, 1983.
36. Mirro MJ, Bailey JC, Watanabe AM: Role of cyclic AMP in regulation of the slow inward current. In: Role of the slow inward current in cardiac electrophysiology. The Hague: Martinus Nijhoff, 1980, pp 111–126.
37. Watanabe AM, Besch HR Jr: Cyclic adenosine monophosphate modulation of slow calcium influx channels in guinea pig hearts. Circ Res 35:316–324, 1974.
38. Sperelakis N, Schneider JA: A metabolic control mechanism for calcium ion influx that may protect the ventricular myocardial cell. Am J Cardiol 37:1079–1085, 1976.
39. Reuter H, Scholz H: The regulation of the Ca conductance of cardiac muscle by adrenaline. J Physiol (Lond) 264:49–62, 1977.
40. Li T, Sperelakis N: Stimulation of slow action potentials in guinea pig papillary muscle cells by intracellular injection of cyclic AMP, Gpp(NH)p and cholera toxin. Circ Res, 1983 (in press).
41. Jones LR, Maddock SW, Hathaway DR: Membrane localization of myocardial type II cAMP-dependent protein kinase activity. Biochim Biophys Acta 641:242–253, 1981.
42. Tada M, Inui M, Yamada M, Kadoma M, Kuzuya T, Abe H, Kakiuchi S: Effects of phospholamban phosphorylation catalysed by adenosine 3′:5′-monophosphate- and calmodulin-dependent protein kinases on calcium transport ATPase of cardiac sarcoplasmic reticulum. J Mol Cell Cardiol, 1983 (in press).
43. Kirchberger MA, Antonetz T: Calmodulin-mediated regulation of calcium transport and (Ca^{2+} + Mg^{2+})-activated ATPase activity in isolated cardiac sarcoplasmic reticulum. J Biol Chem 257:5685–5691, 1982
44. Levy MN: Sympathetic–parasympathetic interactions in the heart. Circ Res 29:437–445, 1971.
45. Birdsall NJM, Hulme EC: Biochemical studies on muscarinic acetylcholine receptors. J Neurochem 27:7–16, 1976.
46. Ehlert FJ, Roeske WR, Yamamura HI: The nature of muscarinic receptor binding. In: Iversen, Iversen, Snyder (eds) Handbook of physiology. New York: Plenum, 1982 (in press).
47. Galper JB, Smith TW: Properties of muscarinic acetylcholine receptors in heart cell cultures. Proc Natl Acad Sci USA 75:5831–5835, 1978.
48. Halvorsen SW, Nathanson NM: In vivo regulation of muscarinic acetylcholine receptor number and function in embryonic chick heart. J Biol Chem 256:7941–7948, 1981.
49. Sharma VK, Banerjee SP: Muscarinic cholinergic receptors in rat heart: effects of thyroidectomy. J Biol Chem 252:7444–7446, 1977.
50. Ten Eick R, Nawrath H, McDonald TF, Trautwein W: On the mechanism of the negative inotropic effect of acetylcholine. Pflugers Arch 361:207–213, 1976.
51. Trautwein W: Generation and conduction of impulses in the heart as affected by drugs. Pharmacol Rev 15:277–332, 1963.
52. Goldberg ND, Haddox MK: Cyclic GMP metabolism and involvement in biological regulation. Annu Rev Biochem 46:823–896, 1977.
53. Linden J, Brooker G: The questionable role of cyclic guanosine 3′:5′-monophosphate in heart. Biochem Pharmacol 28:3351–3360, 1979.
54. Krause EG, Halle W, Wollenberger A: Effect of dibutyryl cyclic GMP on cultured beating rat heart cells. In: Advances in cyclic nucleotide research, vol 1. New York: Raven, 1972, pp 301–305.
55. Tuganowski W, Kopec P, Kopyta M, Wezowska J: Iontophoretic application of autonomic mediators and cyclic nucleotides in sinus node cells. Naunyn Schmiedebergs Arch Pharmacol 299:65–67, 1977.
56. Kohlhardt M, Haap K: 8-bromo-guanosine-3′,5′-monophosphate mimics the effect of acetylcholine on slow response action potential and contractile force in mammalian atrial myocardium. J Mol Cell Cardiol 10:573–586, 1978.
57. Nawrath H: Does cyclic GMP mediate the negative inotropic effect of acetylcholine in the heart? Nature 267:72–74, 1977.
58. Watanabe AM, Besch HR Jr: Interaction between cyclic adenosine monophosphate and cyclic guanosine monophosphate in guinea pig ventricular myocardium. Circ Res 37:309–317, 1975.
59. Watanabe AM, Hathaway DR, Besch HR Jr: Mechanism of cholinergic antagonism of the effects of isoproterenol on hearts from hyperthyroid rats. In: Kobayashi T, Sano T, Dhalla N (eds) Recent advances in studies on cardiac structure and metabolism, vol 11. Baltimore: University Park Press, 1978, pp 423–429.
60. Lincoln TM, Keely SL: Regulation of the cardiac cyclic GMP-dependent protein kinase. Biochim Biophys Acta 676:230–244, 1981.
61. Brooker G: Dissociation of cyclic GMP from the negative inotropic action of carbachol in guinea pig atria. J Cyclic Nucleotide Res 3:407–413, 1977.
62. Ong SH, Steiner AL: Localization of cyclic GMP and cyclic AMP in cardiac and skeletal muscle: immunocytochemical demonstration. Science 195:183–185, 1977.
63. Mirro MJ, Harper JF, Steiner AL: Compartmentation of the cGMP in sinus node: subcellular localization by immunocytochemistry. Circulation 62:III-239, 1980.
64. Mirro MJ, Bailey JC, Watanabe AM: Dissociation between the electrophysiological properties and total tissue cyclic GMP content of guinea pig atria. Circ Res 45:225–233, 1979.
65. Pappano AJ, Hartigan PM, Coutu MD: Acetylcholine inhibits the positive inotropic effect of cholera toxin in ventricular muscle. Am J Physiol 243:H434–H441, 1982.

66. Revtyak G, Jones LR, Watanabe AM, Besch HR Jr: Canine myocardial guanylate cyclase: differential activation of sarcolemmal and cytoplasmic forms. Pharmacologist 20:147, 1978.
67. Lindemann JP, Besch HR Jr, Watanabe AM: Indirect and direct effects of the divalent cation ionophore A23187 on guinea pig and rat ventricular myocardium. Circ Res 44:472–482, 1979.
68. Wallach D, Pastan I: Stimulation of membranous guanylate cyclase by concentrations of calcium that are in the physiological range. Biochem Biophys Res Commun 72:859–865, 1976.
69. Brown BS, Polson JB, Krzanowski JJ, Wiggins JR: Influence of isoproterenol and methylisobutylxanthine on the contractile and cyclic nucleotide effects of methacholine in isolated rat atria. J Pharmacol Exp Ther 212:325–332, 1980.
70. Bailey JC, Watanabe AM, Besch HR Jr, Lathrop DR: Acetylcholine antagonism of the electrophysiological effects of isoproterenol on canine cardiac Purkinje fibers. Circ Res 44:378–383, 1979.
71. Gardner RM, Allen DO: The relationship between cyclic nucleotide levels and glycogen phosphorylase activity in isolated rat hearts perfused with epinephrine and acetylcholine. J Pharmacol Exp Ther 202:346–353, 1977.
72. Murad F, Chi YM, Rall TW, Sutherland EW: Adenyl cyclase. J Biol Chem 237:1233–1238, 1962.
73. La Raia PJ, Sonnenblick EH: Autonomic control of cardiac cAMP. Circ Res 28:377–384, 1971.
74. Koski G, Streaty RA, Klee WA: Modulation of sodium-sensitive GTPase by partial opiate agonists. J Biol Chem 257:14035–14040, 1982.
75. Strawbridge RA, O'Connor KW, Watanabe AM: Depression of canine cardiac adenylate cyclase activity by muscarinic cholinergic agonists: evidence that the effect is mediated by acceleration of the rate of decay of enzyme activity. Clin Res 29:244A, 1981.
76. Meester WD, Hardman HF: Blockade of the positive inotropic actions of epinephrine and theophylline by acetylcholine. J Pharmacol Exp Ther 158:241–247, 1967.
77. Biegon RL, Epstein PM, Pappano AJ: Muscarinic antagonism of the effects of a phosphodiesterase inhibitor (methylisobutylxanthine) in embryonic chick ventricle. J Pharmacol Exp Ther 215:348–356, 1980.
78. Watanabe AM, Lindemann JP, Jones LR, Besch HR Jr, Bailey JC: Biochemical mechanisms mediating neural control of the heart. In: Abboud FM, Fozzard HA, Gilmore JP, Reis DJ (eds) Disturbances in neurogenic control of the circulation. Baltimore: Waverly, 1981, pp 189–203.
79. Manalan AS, Besch HR Jr, Watanabe AM: Characterization of [^{3}H] (±) carazolol binding to beta adrenergic receptors: application to study of beta adrenergic receptor subtypes in canine ventricular myocardium and lung. Circ Res 49:326–336, 1981.
80. Mirro MJ, Manalan AS, Bailey JC, Watanabe AM: Anticholinergic effects of disopyramide and quinidine on guinea pig myocardium: mediation by direct muscarinic receptor blockade. Circ Res 47:855–865, 1980.

18. THE PHARMACOLOGY OF THE CARDIAC GLYCOSIDES

Theodore M. Brody
and Tai Akera

Background

The term digitalis encompasses a wide variety of steroids which have the property of increasing the force of contraction and eliciting characteristic electrophysiologic effects upon the heart. These substances are derived from a number of plant and animal sources. The medicinal actions of the squill, or sea onion, were recognized as early as 1600 B.C. Digitalis-like activity is present in the seeds of *strophanthus gratus,* which is the source of ouabain, used as an African arrow poison and in the skin of the toad, used by ancient Chinese herbalists. The glycosides most frequently used today are derived from the leaves of the foxglove, *Digitalis purpurea* and *D. lanata.* The classic study on the action of digitalis was published in 1785 by William Withering who described his long experience with digitalis in *An Account of the Foxglove, and Some of Its Medicinal Uses: With Practical Remarks on Dropsy, and other Diseases* [1]. Withering failed to recognize that its efficacy in reducing edema was secondary to its cardiac action. A second comprehensive monograph was published in 1799 by John Ferrier, who suggested that digitalis might have a cardiac effect distinct from its ability to promote a diuresis. Traube in 1850 also recognized the effect of digitalis in promoting the efficiency of cardiac muscle and further suggested that the bradycardia was the result of vagal stimulation.

N. Sperelakis (ed.), PHYSIOLOGY AND PATHOPHYSIOLOGY OF THE HEART.

Martinus Nijhoff Publishing, Boston/The Hague/ Dordrecht/Lancaster.

The usefulness of digitalis preparations in atrial fibrillation was first established in the early twentieth century. It was not many years ago, in 1938, that Cattell and Gold were able to show experimentally that the cardiac glycosides brought about their beneficial effects by increasing the force of contraction of the heart [2]. Following the purification of the digitalis glycosides and the establishment of methods for standardization of various preparations, digitalis became the mainstay of therapy for congestive heart failure.

Chemistry

The chemistry of the cardiotonic steroids and their structure–activity relationships have been the object of considerable research over the past 40 years [3]. Up until recently, those structural characteristics required for cardiotonic activity appeared to be well established, but more recent data suggest that the earlier hypotheses no longer hold. A recent review by Thomas et al. encompasses both the classic structure–activity relationship studies and some of the newer findings [4]. These workers have described a model for the interaction of a large number of the active chemicals with the putative digitalis receptor which is consistent with the effects of these agents to increase the force of contraction and to inhibit Na,K-ATPase activity. The cardiac glycosides are made up of a combination of an aglycone, or genin, combined with one or more sugar molecules. For example, digoxin, a cardiac glycoside exten-

sively used clinically, is made up of an aglycone, digoxigenin, with three molecules of digitoxose, attached at position 3 (see fig. 18–1). The aglycone and the glycoside both possess pharmacologic activity. The aglycones are generally shorter acting and less potent cardiotonic agents, but have the same therapeutic and toxic characteristics as the glycosides.

The classic structure–activity relationship studies of the digitalis-like compounds indicated that inotropic activity was to be found only with the 14β-hydroxysteroids substituted with a 17β-unsaturated lactone ring and additionally possessing the stereochemical features of the digitalis steroids; specifically, the cis/trans/cis configurations at the ring junctions [5]. These conclusions were difficult to reconcile with the observation that a number of compounds not possessing these features still exhibited significant digitalis-like activity. The model suggested by Thomas et al. does account for the wide spectrum of chemicals capable of producing an inotropic action, yet not conforming to the classic structural model. However, it does appear that the major functional group is the electrophilic center in the C-17 side chain which binds to the receptor and therefore is necessary for digitalis-like activity, although the lactone ring, per se, is not essential.

Among the various glycosides and aglycones there is a difference in the number and position of OH groups. Apparently the OH groups are important for determining lipid solubility, protein binding, metabolic biotransformation, and duration of action of the particular compound. While the aglycone portion of the molecule is responsible for the cardiac effects, the presence of sugar moieties influences potency and pharmacokinetics. The sugar in closest proximity to the genin has the greatest effect in the binding of the glycoside to its receptor. The second and third sugars have lesser influence. Not all digitalis-like compounds contain a five-membered unsaturated lactone ring at position 17 (see above), but those agents with the five-membered lactone ring are called cardenolides, the more common ones being digoxin, digitoxin, and ouabain.

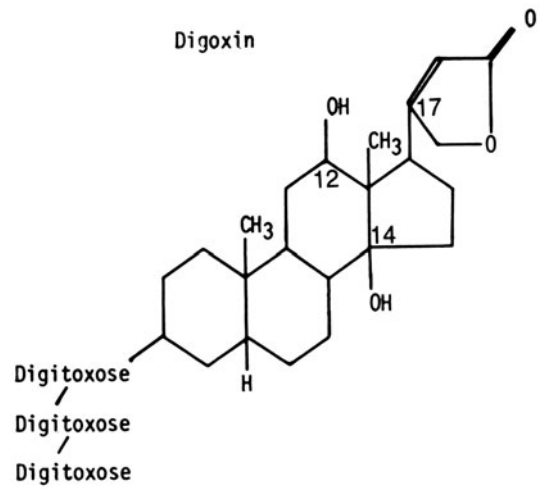

FIGURE 18–1. Chemical structure of the glycoside, digoxin. The aglycone, digoxigenin, lacks the sugars in the 3-position. Digitoxin differs from digoxin by the absence of an OH group at the C-12 position.

Pharmacokinetics

The two most widely used preparations are digoxin and digitoxin and these have been most extensively studied with respect to their pharmacokinetics in man.

In normal patients, the absorption of digoxin following oral administration varies from 65% to 85%, depending on the type of preparation used. Absorption of digoxin is more favorable from hydroalcoholic solutions and lower when tablets are the drug formulation. Variability is greatest with tablets and, although digoxin tablets must now meet a tablet dissolution test, physicians using a specific brand should probably maintain the patient on that preparation.

Following oral administration, a peak level of digoxin is achieved at 45–60 min which then falls to a plateau level 5–6 h after drug administration. This latter phase represents the predominant half-life ($t_{1/2}$) of approximately 35 h which results from the metabolism and excretion of the drug.

Because digitoxin is more lipid soluble than digoxin, its oral absorption is almost complete. The time required for one-half of the drug to

TABLE 18–1. Properties of some digitalis preparations

Preparation	Source	Dose	Peak effect	Half-Life	Absorption excretion, and metabolism
Digoxin (tablets, elixir, injection)	Glycoside from leaves of *D. lanata*	1.0–2.5 mg orally then 0.25–0.5 mg daily	4–6 h (oral)	35 h	Absorption 75%, eliminated by renal excretion
Digitoxin (tablets, injection)	Glycoside from *D. purpurea, D. lanata*, or other species	1.0–1.5 mg orally, then 0.1 mg daily	6–12 h (oral)	5 days	Absorption 90%–100%, hepatic biotransformation; renal elimination of metabolites
Lanatoside C (tablet)	Glycoside from *D. lanata*	1.0–1.5 mg orally, then 0.25–0.75 mg daily	4–6 h (oral)	33 h	Irregular absorption; 20% metabolized by liver
Deslanoside (injection)	Desacetyl derivative of lanatoside C	0.8–1.5 mg, then 0.2–0.5 mg daily	1–2 h	—	20% metabolized by liver; renal elimination
Powdered digitalis (pill, tablet, or capsule)	Leaves of *D. purpurea* or *D. lanata* mixture of various glycosides, primarily digitoxin	1.0 mg, then 100 mg daily	8–12 h	5–7 days	Irregular absorption; liver metabolism and renal excretion
Ouabain (injection)	Seeds of *Strophanthus gratus*	0.25–0.5 mg i.v., then 0.1 mg every h	0.5–2.0 h	—	Renal elimination

be eliminated from the body by metabolism and excretion is about 5–6 days in man.

The cardiac glycosides are widely distributed throughout the tissue and fluid compartments of the body. Plasma proteins are a significant site for glycoside binding; about 25% of digoxin and 90% of digitoxin are bound to plasma proteins. Both glycosides are distributed to all body tissues with highest concentrations found in kidney, skeletal muscle, heart, liver, and adrenal. Most tissues have concentrations up to 100 times greater than that of free drug found in plasma at equilibrium, indicating the avid binding of the glycosides to tissue protein.

Digoxin is essentially removed from the body by renal excretion, most of it being unchanged drug. The most important determinant of the fate of digoxin is renal function and the clearance of this glycoside is directly proportional to creatinine clearance. A small amount of digoxin is secreted by the kidney and some is reabsorbed from the tubular lumen.

Digitoxin, on the other hand, is largely metabolized and renal function does not significantly alter the half-life of this glycoside. In uremia the $t_{1/2}$ of digoxin and digitoxin are almost identical so that little is gained by using digitoxin in this regard. If dose adjustments are necessary during the course of therapy in uremic patients, however, digitoxin may be the preferred drug. Digitoxin is metabolized by the liver microsomal oxidative enzymes and those drugs or agents which stimulate or induce these enzymes facilitate the metabolic biotransformation of digitoxin. One of the products of digitoxin biotransformation is digoxin (table 18–1).

The cardiac glycosides are distributed relatively slowly throughout the body and have a large apparent volume of distribution. Their

onset of action is slow and is determined by the rate at which the drug is bound to Na,K-ATPase, the putative pharmacologic receptor. The binding of the drug to the tissue receptors is slow both in the intact animal and in isolated hearts and is largely dependent upon the concentrations of potassium and sodium ions in the extracellular environment [6]. For example, in a hypokalemic animal, or a patient with a low plasma potassium concentration as a result of vigorous diuretic therapy, the rate of binding of digitalis to its receptor is enhanced as is the rate of onset of its pharmacologic action. Hyperkalemia retards the onset of the digitalis effect [7]. The movement of sodium ion across the cardiac cell membrane also promotes the binding of the cardiac glycoside to its receptor so that the sodium concentration or the number of contractions or depolarizations per unit time will also influence the rate of onset of action [8]. It is possible therefore that digitalis might act more rapidly in a patient with a fast heart rate.

Among various animal species, the difference in sensitivity to the positive inotropic action of the cardiac glycosides is remarkable. A part of such species-dependent differences in glycoside sensitivity is apparently due to differences in the rate of metabolism and elimination of the glycosides. However, the primary cause of the difference is inherent within the heart muscle itself, as indicated by the differences in glycoside sensitivities which can be observed in isolated heart muscle preparations. Isolated myocardium from dog, cat, cow, or sheep is highly sensitive to the inotropic and toxic actions of the glycoside, whereas that from guinea pig or rabbit is approximately an order of magnitude less sensitive. The rat myocardium is more than two orders of magnitude less sensitive than the heart muscle obtained from guinea pigs or rabbits, requiring corresponding higher concentrations of the glycoside to produce positive inotropic effects. Human heart seems to have the highest glycoside sensitivity among the various animal species. These differences in the glycoside sensitivity are apparently due to the variation in affinity of the receptors for the glycosides [9], and a similar magnitude of inotropic effect can be obtained in each species when the myocardium is exposed to an appropriate concentration of the glycoside, i.e., the dose–response curves are parallel.

The doses (expressed as mg/kg of body weight) of the cardiac glycosides needed in neonates and young children are considerably larger than those in adults although there appears to be no significant difference in metabolic disposition or excretion. Thus, in younger individuals or animals, higher serum levels of drug are observed with no evidence of toxicity. Reasons for this tolerance to digitalis by the younger patient are presently unknown; apparently a difference in the interaction with the putative pharmacologic receptor, Na-ATPase does not appear to be the underlying event.

Pharmacodynamics

Digitalis has two useful clinical effects. These are to increase the force of myocardial contractions in patients with congestive failure and to slow the beating of the ventricle in atrial fibrillation or flutter. Although for many years it was thought that the beneficial effects in congestive heart failure might be the result of the slowing of the ventricular rate, it is now firmly established that the positive inotropic effect is the result of a direct action upon the heart subsequent to an interaction with the digitalis receptor (see below). Its effect on the electrophysiologic activity of the heart is also direct, but may be modified to some extent by input from the central nervous system. In addition to its effects upon the brain, which may also be responsible for some of its toxic manifestations, digitalis also has pronounced effects upon other tissues such as vascular smooth muscle, for example. The cardiac glycosides also have significant effects upon sympathetic and parasympathetic function in both therapeutic and toxic concentrations. Thus, the overall pharmacodynamics of this class of compounds is complex, influenced by indirect as well as by direct effects upon the target tissue.

INCREASE IN FORCE OF CONTRACTION

The cardiac glycosides increase the force of contraction of both atrial and ventricular heart

muscle. This *positive inotropic effect* can be demonstrated in various isolated cardiac muscle preparations from a variety of animals, including man. Increased contractility occurs in the normal as well as the failing heart, but is not generally seen in normal patients or animals because of reflex hemodynamic adjustments.

It can be readily shown in isolated heart muscle preparations that the cardiac glycosides increase peak developed tension and that this effect is dose or concentration dependent (fig. 18–2). With higher concentrations a negative inotropic effect may be observed associated with an increase in resting tension.

During congestive heart failure a number of pathophysiologic events occur which are ultimately modified by digitalis treatment. The basic defect is the inability of the heart to pump adequately to supply the tissues with blood. While the initial insult resulting in depression of myocardial contractility may vary, the pathologic sequelae are similar. When the heart fails to function, several mechanisms are triggered in an attempt to compensate for the deficit. There is an increase in end-diastolic volume, in which the heart is now operating at a new point on the Frank–Starling ventricular function curve; an increase in sympathetic tone; and, finally, a significant increase in ventricular size. The enhanced sympathetic tone is a consequence of reduced cardiac output and blood pressure influencing the baroreceptors. Thus, the result is a compensatory rise in blood pressure, heart rate, and peripheral resistance. However, ultimately this increase in sympathetic tone forces the heart to work harder to eject enough blood to perfuse the tissues, and cardiac efficiency is decreased.

During compensation, an increased preload is necessary to maintain the cardiac output. Myocardial oxygen consumption is increased and vascular and pulmonary congestion may result from the increase in preload. Any increase in metabolic demands upon the heart under these conditions can lead to dyspnea. Ventricular hypertrophy is also a consequence of the decrease in myocardial contractility. The rise in ventricular pressure promotes an increase in the number of myofibrils of the ventricle and in heart size. All these mechanisms act in concert in an attempt to maintain cardiac output and are reasonably successful except when increased demands are placed on the heart [10].

Intervention with digitalis is still the most effective treatment to maintain the patient with congestive failure. With the cardiac glycosides, the heart now operates on a new ventricular function curve, indicative of a higher level of cardiac contractility. Thus, at any designated ventricular filling pressure more stroke work is generated. Not only is peak tension development greater after digitalis, but also the time to reach a given tension at every load is reduced when the velocity of contraction is examined at various loads. The duration of systole is also reduced.

The effect of the glycosides to increase the force of contraction enhances stroke volume so that the sympathetic nervous system and catecholamines are no longer needed to maintain tissue perfusion. Since the kidney is now more effectively perfused, more salt and water is excreted and edema is reduced. Peripheral vasoconstriction is diminished, plasma volume is lowered, cardiac preload is decreased and the heart returns toward its normal size [10]. Oxygen consumption of the heart may be slightly increased by the cardiac glycosides, but efficiency is remarkably improved so that the net oxygen requirements may actually be less. The negative chronotropic effect of the cardiac glycosides may also tend to reduce oxygen consumption.

ELECTROPHYSIOLOGIC ACTIONS

The digitalis glycosides have both beneficial and toxic electrophysiologic effects upon the heart. In addition to their action to increase the force of cardiac contraction, the glycosides are used therapeutically to correct rhythm alterations of supraventricular origin. In high concentrations, the therapeutic actions of the glycosides are limited by the occurrence of life-threatening rhythm and conduction disturbances. Therefore, an understanding of the basic electrophysiology of the glycosides is important. Most of the pertinent experimental studies have been performed on either isolated preparations or in situ on species other than man although significant studies have also been

done on the human heart. Moreover, the glycosides have different actions on the specialized conducting tissues of the heart. Generally there has been good correspondence between observations in experimental animals and in man.

Direct Effects. The most extensively examined cardiac tissue from the viewpoint of the direct electrophysiologic actions of digitalis has been the mammalian Purkinje fiber [11]. The basis for the arrhythmogenic actions of the glycosides stems from studies on this tissue. Studies in which canine Purkinje fibers are exposed to the cardiac glycosides indicate that the glycosides promote spontaneous firing in this specialized conducting tissue which may become the origin of the electrical activity. Recent studies have demonstrated that a depolarization afterpotential, also referred to as a *transient depolarization* (TD) or delayed afterdepolarization (DAD), may be the causative underlying event. The TD is also capable of eliciting an aftercontraction. Generally, the transient depolarization is observed in Purkinje tissue following a train of several evoked action potentials in the presence of cardiac glycosides. This aberrant depolarization is frequency dependent and is observed more readily at high stimulation rates. When the transient depolarization reaches the threshold potential, a series of repetitive volleys are induced. These TDs have also been reported in atrial and ventricular muscle preparations using larger concentrations of cardiac glycosides. A transient inward current has been implicated in the genesis of the transient depolarizations.

Indirect Effects. It has been shown both experimentally and from clinical studies that efferent vagal activity is increased by the glycosides and that the slowing of heart rate observed can be blocked by atropine. Several sites appear to be implicated in this slowing of heart rate. Many studies have demonstrated that the slowing is dependent upon an intact automatic nervous system and both parasympathetic activation and sympathoinhibition play a role.

Sympathetic nervous activity may also be enhanced by digitalis and this action is observed with toxic doses of the glycosides. Whether the sympathetic stimulation originates within central nervous system or peripheral sites is still uncertain as is the importance of sympathetic stimulation in the genesis of the arrhythmias seen with the larger doses of digitalis. The role of the nervous system on the actions of digitalis has been reviewed by Gillis and Quest [12].

Effects on Various Cardiac Tissues. Atrial tissues are very sensitive to the indirect action of the cardiac glycosides because of its well-known responsiveness to acetylcholine. Acetylcholine markedly decreases the atrial refractory period (ERP), automaticity, and action potential duration (APD). The membrane potential (RMP) is increased and tissue becomes hyperpolarized, reducing conduction velocity. While the direct effects of the glycosides tend to *decrease* the resting membrane potential and to *increase* the action potential duration, the indirect effects predominate so that with therapeutic concentrations of digitalis the ERP and APD of atrial tissue are decreased. The atrioventricular (AV) nodal tissues are similarly influenced by acetylcholine so that digitalis has a significant effect on this tissue. Both the rate of rise and the amplitude of AV nodal tissue action potentials are decreased so that conduction is impaired and the ERP markedly increased. Thus, toxic doses of the glycosides can lead to AV block as a result of the conduction impairment. These effects are also of particular importance in the treatment of atrial fibrillation and atrial flutter. The Purkinje system and ventricular muscle are much less sensitive to acetylcholine and thus less influenced by the vagal effects of digitalis. As a result of the direct and indirect electrophysiologic actions of the cardiotoxic glycosides, the following may be observed on the ECG of patients with adequate digitalis to produce a positive inotropic effect. The heart rate is decreased due to the depressed sinoatrial (SA) nodal automaticity. The PR interval, the propagation through the AV node, is lengthened as a result of the decreased AV nodal conduction velocity. The QT interval, an estimate of the ERP, is shortened; a consequence of the increase in ventricular excitability. The ST segment may be depressed or inverted and the T wave inverted.

Treatment of Dysrhythmias. The cardiac glycosides are effective in the control of atrial fibrillation, atrial flutter, and supraventricular paroxysmal tachycardia.

In the treatment of atrial flutter, the aim is to reduce the ventricular rate. This is brought about by a direct action of digitalis on the AV node and also secondarily as a consequence of an increased blood pressure resulting from an enhanced cardiac output. This promotes vagal tone and reduces sympathetic drive. The direct effect on the AV node is to prolong the effective refractory period (ERP) so that a fewer number of impulses reach the ventricles; thus ventricular slowing is observed. The increased vagal tone shortens the atrial refractory period to further increase atrial rate. As a result, the AV node is bombarded at a greater frequency by impulses, but most of these are extinguished because the node is depressed and the refractory period is prolonged to a greater extent, further slowing the ventricular rate. Atrial flutter is also treated effectively with the cardiac glycosides. The increase in vagal activity shortens the ERP of the atria, as above, and the flutter is converted to atrial fibrillation which can be controlled more easily. Supraventricular paroxysmal tachycardias are generally relieved by maneuvers which enhance vagal activity; thus the use of digitalis is indicated. It is important to note that overdosage with digitalis can result in supraventricular paroxysmal tachycardia with AV block.

Digitalis Intoxication

All of the glycosides manifest similar toxic signs. In addition to cardiac rhythm disturbances, other untoward effects are frequently observed. These include such gastrointestinal effects as anorexia, nausea and vomiting, diarrhea, and abdominal pain. The genesis of the gastrointestinal side effects (particularly nausea and vomiting) is apparently the result of stimulation of the chemoreceptor trigger zone in the area postrema of the medulla. Headache, malaise, and drowsiness are prominent central nervous side effects which occur early in digitalis intoxication. Visual disturbances are seen in patients intoxicated with digitalis with blurring and color vision disturbances occurring most commonly.

The primary event which occurs most frequently in patients is arrythmogenesis. This includes rhythm abnormalities of both atria and ventricles and disturbances of AV conduction. Diagnosis rests on patient history and an estimation of the concentration of digitalis glycoside in the plasma. Since the therapeutic and toxic ranges of the glycosides in plasma overlap, clinical evaluation is clearly of primary importance.

TREATMENT

The treatment of digitalis toxicity, once the diagnosis is made, involves the use of one of several antiarrhythmic drugs. Lidocaine, procainamide, or propranolol are frequently used, effective agents. Phenytoin is also useful to treat atrial arrhythmias, although several instances of sudden death with this agent have been reported. Potassium administration is one of the most effective regimens when the plasma K^+ is either low or normal. If the plasma K^+ is high, further K^+ addition will enhance AV block and may induce cardiac arrest. Although the mechanism of the K^+-induced reversal of digitalis arrhythmogenesis has not been elucidated, several explanations have been proposed. Potassium is known to reduce the steady-state concentration of the glycoside-Na^+, K^+-ATPase complex, to have the ability to stimulate the sodium pump, and to alter cardiac cell membrane permeability. Data are presently not available to support any of these hypotheses, and an alternative mechanism is equally feasible.

DRUG INTERACTIONS

A recent interesting finding has been the observation of an interaction between the cardiac glycosides and quinidine. This is of particular clinical importance because of the use of quinidine in digitalized patients to convert atrial flutter to a sinus rhythm. It has been shown that certain of the cardiac glycosides, particularly digoxin, and quinidine occupy mutual binding sites in many tissues. Thus, the concomitant use of these two agents results in levels of the glycoside which are dangerously

high, and causes arrhythmias in a large number of patients [13]. When such a combined therapy is instituted it is necessary to reduce the maintenance dose of digoxin or increase the dosing interval. Quinidine reduces the clearance of the cardiac glycoside and also its volume of distribution in the body. Plasma digitoxin concentrations are less affected by quinidine administration, while ouabain's levels are apparently not influenced. The interaction between the digitalis glycosides and diuretics which promote the excretion of potassium is well known and has been discussed earlier. Hypokalemia results in an enhanced binding of the glycoside to its putative receptor in the heart and can lead to arrhythmias. Conversely, hyperkalemia will retard the binding of the glycoside to its receptor and slows the onset of the therapeutic action. Calcium ion potentiates the toxicity of the cardiac glycosides. Other drugs which must be used judiciously with the cardiac glycosides are the beta-adrenergic antagonists and the calcium channel blockers which may compromise the increased force of myocardial contraction induced by the glycosides.

Mechanisms of Therapeutic Action

Although the cardiac glycosides have a proven efficacy of increasing the force of myocardial contraction, especially in the failing heart, their clinical use has been compromised by their narrow margin of safety. For example, concentrations of digoxin in plasma observed in patients who are adequately treated with the glycosides are generally in the range of 1–2 ng/ml. These concentrations are approximately half those observed in patients showing signs of digitalis toxicity, representing an extremely narrow margin of safety for this group of compounds. Clinical studies have indicated that the therapeutic and toxic concentrations of digoxin or digitoxin in plasma overlap [14]. This narrow margin of safety of the cardiac glycosides has resulted in a high incidence of glycoside toxicity among patients on digitalis therapy. Because of this problem, many cardiologists recommend the use of alternative therapy such as diuretics or calcium antagonists to reduce preload and afterload in order to improve myocardial function, although only the cardiac glycosides reverse the cause of chronic heart failure, i.e., inadequate myocardial contractility. Another approach to this problem is to develop a drug which has a wider margin of safety. Therefore, it is necessary to understand the mechanisms responsible for both the therapeutic and toxic actions of the cardiac glycosides, since the strategy to develop safer compounds and also the rational treatment of patients are largely dependent on whether the receptors for the two actions of the glycoside are the same or different.

Cattel and Gold [15], pioneers of modern pharmacologic research into the mode of action of the cardiac glycosides, questioned in 1934 whether the therapeutic and toxic actions of the glycosides might not be separated by selecting a compound based on its chemical structure. Such a separation would be feasible only if the receptors for the two actions of the glycoside were different. Since that time, numerous compounds have been synthesized and tested for their therapeutic and toxic potencies. Occasionally, a partial improvement of the margin of safety has been reported; however, a complete separation of two actions of the glycoside derivatives has not yet been achieved. Since a large number of compounds with different structures have already been tested, the results should suggest that these two actions are probably not completely separable.

Na,K-ATPase AND THE SODIUM PUMP

Among numerous biochemical systems examined during the past four decades, the sodium pump of the cardiac plasma membrane or sarcolemma, or its enzymatic representation, Na,K-ATPase, has proven to be most sensitive to the cardiac glycosides. Various cardiac glycosides and their derivatives bind to Na,K-ATPase in a specific manner, and inhibit this enzyme activity [6, 8, 16]. The significant binding and the ensuing substantial enzyme inhibition observed in vitro occur in a range of glycoside concentrations which produce positive inotropic effects in isolated heart preparations or in intact animals. Moreover, when heart muscle is exposed to a therapeutic con-

centration of a cardiac glycoside, and Na,K-ATPase or sodium pump activity is assayed under conditions in which release of the glycoside bound to the enzyme is negligible; a 20%–40% inhibition of the enzyme or sodium pump activity can generally be observed. These findings suggested that the binding of cardiac glycosides to sarcolemmal Na,K-ATPase and the resulting sodium pump inhibition are involved in the mechanism of the positive inotropic action of these compounds.

CHARACTERISTICS OF THE POSITIVE INOTROPIC EFFECT

The positive inotropic effect of the cardiac glycoside has many salient characteristics. For example, the rate of onset of the inotropic effect is slow. This slow onset is apparently not due to a slow absorption of the glycoside, because the slow onset of the action can be observed even when the glycoside is injected intravenously, or in isolated heart preparations which are exposed to a uniform concentration of the glycoside. The rate of onset of the inotropic action can be accelerated by conditions which increase the rate of sodium influx into myocardial cells. These conditions include higher heart rate, driving of the heart with twin-pulse stimulation, or the presence of a sodium ionophore, monensin. The rate of onset is delayed by elevating the extracellular potassium concentration [16].

A slight change in the chemical structure of the active cardiac glycosides, e.g., saturation of the lactone ring, elimination of a hydroxyl group at the C-14 position, or a removal of the sugar moiety from glycosides, markedly reduces the potency of the compound [3, 4]. The loss of the positive inotropic effect of the cardiac glycosides in the intact animal is generally determined by the loss of the compound from the body, and therefore is dependent on the rate of metabolism and elimination. In isolated heart studies in which the glycoside concentration of extracellular fluid can be rapidly reduced to zero, the loss of the inotropic effect is dependent on the rate of release of the glycoside from the inotropic receptor. Under these conditions, the rate is dependent on the chemical structure of compounds and the animal species. Generally, the higher the potency of compound or the sensitivity of the myocardium, the slower the washout of the inotropic effect [16]. This slow rate is further delayed by elevating the extracellular potassium concentration.

These rather unique characteristics of the positive inotropic effect of the cardiac glycoside should be explained by any proposed mechanism of inotropic action of the glycosides.

BINDING OF CARDIAC GLYCOSIDES TO Na,K-ATPase

Na,K-ATPase is a membrane-bound enzyme which is responsible for the coupled, active transport of sodium and potassium ions across the cell membrane [6]. Apparently, the enzyme system spans the entire thickness of the cell membrane, binds sodium ions at the inner surface, and transports and releases sodium ions at the external surface. The enzyme system then binds potassium ions at the external surface and releases them at the inner surface. Each cycle of the above reaction is associated with a cycle of phosphorylation and dephosphorylation of, and also conformational changes in, the enzyme protein. The enzyme is phosphorylated from ATP which is hydrolyzed to ADP and inorganic phosphate during the reaction cycle, the free energy released from ATP being utilized for active cation transport.

Cardiac glycosides bind to Na,K-ATPase at the site accessible from extracellular side [16]. The binding normally occurs when the enzyme has just completed the transport of sodium ions, i.e., when the enzyme is in a sodium-induced conformation. If potassium ions induce a further conformational change in enzyme protein, the binding sites become less accessible to the glycoside. This means that the binding of the glycoside to Na,K-ATPase is promoted by conditions which either increase the intracellular sodium ions available to the sodium pump or reduce the extracellular potassium. Therefore, a higher heart rate, twin-pulse electrical stimulation, the presence of a sodium ionophore, such as monensin, or hypokalemia enhances the glycoside binding to Na,K-ATPase. Since glycoside binding occurs to the sodium-induced form of the enzyme, and the enzyme

spends only a comparatively short time in this form during its cycle of conformational changes, the binding of cardiac glycosides to Na,K-ATPase is relatively slow, resulting in a slow onset of glycoside action even when the drug is given intravenously.

Structure–activity relationship studies with various glycoside derivatives have shown that the ability of a compound to bind to and inhibit isolated Na,K-ATPase or the sodium pump is related well to its ability to increase the force of myocardial contraction in isolated heart muscle preparations [4]. Corresponding to the species-dependent differences in glycoside sensitivity, Na,K-ATPase preparations obtained from heart muscle of highly sensitive species have a high affinity for the glycoside, and those from relatively low sensitive species have a low affinity. These differences in the affinity of isolated Na,K-ATPase for various glycoside derivatives are primarily due to differences in the dissociation rate constants, or the rate at which the compounds are released from the binding sites on the enzyme [9]. Again, good correlation is observed between the rate of release of the compounds from isolated Na,K-ATPase and the rate of loss of the inotropic effect in isolated heart muscle preparations [17].

Finally, when Na,K-ATPase is isolated from cardiac muscle exposed to a positive inotropic concentration of the glycoside, one can generally observe that the enzyme is inhibited by 20%–40% [16], indicating that substantial glycoside binding to Na,K-ATPase must occur in the heart muscle at a time when the inotropic effect of the glycoside is apparent.

Because of these impressive relationships between the binding of cardiac glycosides to Na,K-ATPase and their inotropic effects, it is now generally believed that the binding of the glycoside to Na,K-ATPase is intimately related to the mechanisms of inotropic action of cardiac glycosides, i.e., Na,.K-ATPase is the receptor molecule for the pharmacologic action of the glycosides.

EVENTS WHICH CONNECT Na,K-ATPase INHIBITION TO INOTROPIC EFFECTS

Although the binding of cardiac glycosides to Na,K-ATPase seems to be essential for their positive inotropic effect, there are differences in opinion with regard to the mechanisms by which binding leads to an increase in the force of myocardial contraction. In cardiac muscle, membrane excitation is characterized by a rapid sodium influx, causing membrane depolarization, followed by a delayed potassium efflux which causes membrane repolarization. Unlike the action potential in the nerve cells, the time interval between membrane depolarization and repolarization in cardiac muscle, i.e., the plateau phase, is as long as 200–500 ms. During this time period, calcium ions enter the cell. These calcium ions combined with those released from intracellular sites, will cause a transient increase in the intracellular free calcium ion concentration shortly following each membrane excitation, resulting in muscle contraction. Cardiac glycosides have been shown to enhance this transient increase in calcium ion concentration, or calcium transient, thereby increasing the force of contraction [18]. Thus, it may be concluded that in some manner the glycosides increase the efficiency of events which connect membrane excitation to calcium transients.

The precise biochemical or electrophysiologic basis for the membrane-excitation–calcium-transient coupling mechanism, however, is presently unknown. Thus, it is somewhat difficult to understand how the glycoside modifies normal processes of the coupling mechanism to increase its efficiency. One obvious consequence of the glycoside binding to Na,K-ATPase is an inhibition of sodium pump activity. Therefore, several investigators have proposed that sodium pump inhibition causes an elevation of the intracellular sodium ion concentration, which in turn elevates intracellular calcium ion concentration by either stimulating a calcium-influx–sodium-efflux exchange reaction or inhibiting a sodium-influx–calcium-efflux exchange reaction [19]. The exchange reaction seems to work bidirectionally [20], i.e., during the systolic phase, calcium influx is coupled with sodium efflux, presumably due to the relatively high sodium concentration at the inner surface of the cell membrane, whereas during the diastolic phase, sodium influx is coupled with calcium efflux. Thus, it is more likely that sodium pump inhibition, with its

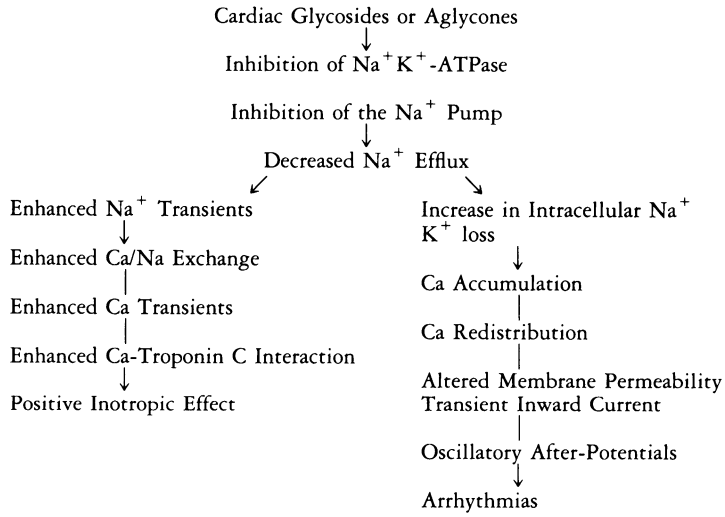

FIGURE 18–2. Proposed mechanisms of the positive inotropic and arrhythmogenic actions of the cardiac glycosides.

augmented increase in sodium ion concentration at the inner surface of the cell membrane during the systolic phase, enhances calcium influx. The problem with this explanation is that the increase in intracellular sodium ion concentration is minimal when as much as 40% inhibition of the sodium pump is caused by inotropic concentrations of the glycoside [21].

It is apparent that the sodium pump has a reserve capacity, since a substantial inhibition does not cause a corresponding increase in the intracellular sodium ion concentration. This must indicate that the remaining sodium pump, now turning over faster in response to a slightly higher intracellular sodium ion concentration, is adequate to pump out sodium ions entering the cell during a cycle of myocardial function. The presence of a reserve capacity of the sodium pump is also apparent when the rate of sodium influx is increased by increasing the heart rate or in the presence of agents which increase sodium influx. Under these conditions as well, the intracellular sodium ion concentration rises only minimally [22], indicating that the sodium pump is now turning over faster as a result of the slight increase in intracellular sodium ion concentration, and is adequate to handle the enhanced sodium influx rate. Thus, one has to question whether partial inhibition of a system which has a significant reserve capacity can have any physiologic significance.

Actually, a small increase in intracellular sodium may be sufficient to cause a substantial increase in intracellular calcium ion concentration, considering that the intracellular sodium ion concentration is approximately 5–10 m*M*, whereas the cytoplasmic calcium ion concentration is less than 0.01 m*M*. Alternatively, dynamic changes in the intracellular sodium concentration are such that one cannot experimentally determine, with the currently available methods, the changes in intracellular sodium ion concentration caused by a moderate sodium pump inhibition. During the early phase of membrane excitation, the rate of sodium influx suddenly increases. Such an increase may effectively elevate the sodium ion concentration at the inner surface of the cell membrane, thereby stimulating the sodium pump and also the calcium-influx–sodium-efflux exchange reaction [23]. During this period, individual sodium pump units may be turning over faster, in the absence of the glycoside, in response to an elevated intracellular sodium ion concentration and may now be operating at close to their maximum capacity to extrude sodium. Thus, an inhibition of the sodium pump by the glycosides may cause more

sodium ions to be extruded by the calcium–sodium exchange mechanism, resulting in an enhanced calcium influx, and augmented calcium transients. During the later phase of myocardial function, the rate of sodium influx declines, providing an opportunity for the inhibited sodium pump to "catch up" before the next membrane excitation.

This latter explanation is consistent with most observations, such as the finding that only a slight increase in intracellular sodium is observed in resting cardiac muscle exposed to inotropic concentrations of the glycoside, that sodium accumulation occurs more easily when the heart is stimulated at a higher frequency, that agents or conditions which enhance transmembrane sodium influx can increase the force of myocardial contraction, and that the augmentation of calcium transients by the cardiac glycosides has a relatively minor effect on the resting calcium concentration. In this regard, it should be noted that an enhancement of sodium influx, which would produce a similar net result as would sodium pump inhibition, also produces inotropic effects and toxicity quite similar to those caused by the cardiac glycosides. Nevertheless, this role for intracellular sodium has yet to be supported by the experimental demonstration of sodium transients. Additionally, that the magnitude of the sodium transients and calcium transients and the time course of the calcium–sodium exchange reaction are adequate to explain an augmentation of the calcium transient by this mechanism should be examined.

Alternative explanations for the enhancement of myocardial contraction resulting from the glycoside binding to Na,K-ATPase in the apparent presence of the sodium pump reserve capacity are also possible. For example, the glycoside binding to Na,K-ATPase might alter properties of membrane lipids associated with the enzyme so that the capacity and affinity of the calcium binding sites within the cell membrane are altered, favoring binding and release of calcium ions associated with membrane excitation [24, 25]. Such glycoside-enhanced calcium binding sites may be either inside or outside the membrane lipid bilayer.

Cardiac glycosides are capable of producing positive inotropic effects by their direct action on the heart, probably by binding to sarcolemmal Na,K-ATPase and inhibiting sodium pump activity. There is, however, no a priori reason to believe that this is the only mechanism by which the glycosides modify the force of myocardial contraction. For example, various cardiac glycosides alter the configuration of the action potential of cardiac muscle cells. The effect is both concentration and time dependent, i.e., in low concentrations and at an early time, the glycosides prolong the action potential duration, and at higher concentrations and after prolonged exposure, they shorten the action potential duration. These changes cannot be the primary mechanism for the positive inotropic action of the glycoside, as the inotropic effect can be observed at the time when the action potential duration is shortened, as well as prolonged. Nevertheless, these changes undoubtedly modify the force of contraction, which is anticipated to be enhanced when the action potential duration is prolonged. It is possible that the positive inotropic effect of the cardiac glycosides is mediated by two or more parallel pathways.

Mechanisms of Toxicity

While some of the toxic signs of cardiac glycosides, such as nausea, vomiting, fatigue, and yellow vision, are apparently due to their action on the central nervous system, the most important toxicity, cardiac dysrhythmia, probably involves both a direct action of the glycoside on the heart and indirect lesions, i.e., those on the nervous system. Since the arrhythmogenic actions of the glycoside can be demonstrated with isolated heart preparations, glycosides are apparently capable of producing arrhythmias by their direct action on the heart. Such a direct arrhythmogenic action of the glycoside is generally considered to result from inhibition of the sodium pump to a degree exceeding its reserve capacity [21]. In animal experiments with anesthetized dogs, cardiotoxicity of the glycoside is associated with a 60%–80% inhibition of the sodium pump. At this level of sodium pump inhibition, the remaining capacity of the sodium pump is insufficient

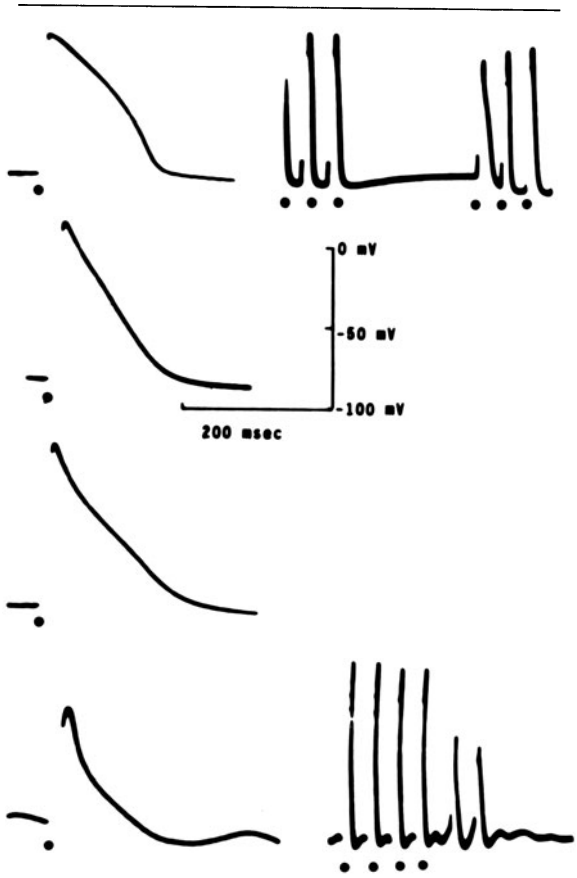

FIGURE 18–3. Membrane action potential of cat Purkinje fibers exposed to toxic concentrations of digoxin. Four driven action potentials, indicated by the solid points, are followed by two oscillatory afterpotentials in the presence of 2 μ*M* digoxin (lower trace). The upper trace is a control, prior to digoxin exposure.

to pump out sodium ions entering the cell associated with membrane excitation. This causes myocardial cells to accumulate sodium and lose potassium.

Sodium accumulation and potassium loss then cause partial depolarization, i.e., the transmembrane potentials become less negative, approaching the threshold potential for the activation of sodium channels. The concept that the reduced difference between the resting membrane potential and the threshold potential increases excitability of the myocardial cells, makes myocardial cells fire more easily without being driven by the normal pacemaker cells, and thereby causes arrhythmias, however, is not supported by studies which demonstrate that an elevation of the extracellular potassium concentration causes a further depolarization, yet reverses the glycoside-induced arrhythmias (fig. 18–3).

Electrophysiologic studies indicate that the ventricular tachycardia caused by toxic doses of the cardiac glycoside originates, at least initially, from Purkinje fibers [26]. When these fibers are exposed to toxic concentrations of the glycoside, oscillatory afterpotentials can be observed immediately following repolarization. The oscillatory afterpotentials are apparently caused by fluctuations in membrane permeability to various cations during the short time period which follows membrane repolarization. This increase in membrane permeability results in sodium, and perhaps calcium, ions to flow through the membrane into the cell, generating transient inward currents, which make the membrane potential less negative. Subthreshold oscillatory afterpotentials do not propagate; however, when the size of the afterpotential becomes large enough to reach the threshold potential, spontaneous firing occurs. This will propagate and cause arrhythmic contractions of the heart muscle. In glycoside-poisoned Purkinje fibers, such firing may become repetitive, resulting in ventricular tachycardia.

This transient increase in membrane permeability, which is responsible for oscillatory afterpotentials, seems to result from calcium overload at the inner surface of the cell membrane. Toxic doses of the cardiac glycosides inhibit the sodium pump beyond its reserve capacity, causes intracellular sodium accumulation, and subsequently results in a calcium overload via reduced calcium extrusion due to an inhibition of the coupled sodium-influx–calcium-efflux reaction. The calcium overload is speculated to cause oscillatory movements of calcium between intracellular stores and myoplasm with associated phasic changes in membrane conductance.

These phasic changes in membrane conductance and ensuing ventricular arrhythmias caused by oscillatory afterpotentials (triggered activity) should be distinguished from enhanced pacemaker (automatic) activity. Unlike

pacemaker activity, triggered activity is more difficult to overdrive, because triggered activity is enhanced by increasing stimulation frequency, whereas automatic activity is subject to postpacing depression. An elevation of the extracellular calcium concentration tends to depress automatic activity by reducing the slope of phase-4 depolarization, whereas it enhances the glycoside-induced oscillatory afterpotentials.

Cardiac glycosides may cause many different types of arrhythmias. Among them, ventricular tachycardia is perhaps most important as it poses the greatest danger to the patients. Clinically, however, the type of arrhythmia most frequently observed with the use of digitalis glycosides is that associated with the suppression of atrioventricular (AV) conduction. A slight increase in the PR interval, i.e., first-degree AV block, can be seen in most patients treated with "therapeutic" doses of digitalis. As the dose of the cardiac glycoside is increased, more advanced AV block can be observed. Stimulation of the parasympathetic nerve, presumably owing to the central action of the glycoside, is considered as the cause of the AV conduction block, since it is easily reversed by atropine or vagotomy in experimental animals, although there are also extra-vagal components. The blockade of the sympathetic nervous system by various means also increases the dose of the cardiac glycoside needed to cause arrhythmias. It is uncertain, however, whether the glycoside-induced increase in sympathetic nerve activity plays an important role in the arrhythmogenic action of the glycoside, or if the basal activity of the sympathetic nervous system is required to maintain the susceptibility of the heart to glycoside-induced toxicity. The latter view is favored by the observation that sympathetic discharge is not always increased in experimental animals exposed to toxic concentrations of the glycoside. As the baroreceptor is sensitized by the glycoside, sympathetic discharge becomes more phasic; a burst occurs during the diastolic phase, and the sympathetic activity almost ceases during the systolic phase [27]. Overall activity, however, may be somewhat decreased until the glycoside-induced arrhythmias cause a significant decrease in the mean arterial blood pressure.

Of particular interest is the hypothesis that the glycoside causes a nonuniform discharge within the cardiac sympathetic nerve, resulting in nonuniform electrophysiologic properties of cardiac muscle cells, predisposing the heart to arrhythmias [28]. If this were to occur, then sympathetic nerve activity contributes to the glycoside-induced arrhythmias, whether overall activity is decreased or increased.

Thus, the toxic effect of the cardiac glycoside may involve both a direct action of the glycoside on the myocardium and also indirect actions on the nervous system. The latter action of the glycoside may be due to alterations in sensitivity of the baroreceptor, central actions of the glycoside, and also an effect on nerve terminals. It is not surprising that the glycosides affect various systems, because Na,K-ATPase is ubiquitous and is likely to play important roles in various tissues. It is easy to understand these actions of the cardiac glycoside as stemming from sodium pump inhibition, since they can be explained from either reduced transmembrane potentials or via an enhancement of the coupled sodium efflux–calcium-influx exchange reaction.

References

1. Withering W: An account of the foxglove and some of its medicinal uses: with practical remarks on dropsy and other diseases. CGJ and J Robison, 1784. Reprinted in Med Class 2:305–443, 1937.
2. Cattell M, Gold H: The influence of digitalis glycosides on the force of contraction of mammalian cardiac muscle. J Pharmacol Exp Ther 62:116–125, 1938.
3. Chen KK, Henderson FG: Pharmacology of sixty-four cardiac glycosides and aglycones. J Pharmacol Exp Ther 111:365–383, 1954.
4. Thomas R, Brown L, Gelbart A: The digitalis receptor: inferences from structure activity relationships. Circ Res (Suppl 1)46:167–172, 1980.
5. Tamm C: The stereochemistry of the glycosides in relation to biological activity. In: Wellbrandt W, Lindgren P (eds) Proceedings of the First International Pharmacological Meeting. Vol 3: Newer aspects of cardiac glycosides. Oxford: Pergamon, 1963, pp 11–26.
6. Schwartz A, Lindenmayer GE, Allen JC: The sodium–potassium adenosine triphosphatase: pharma-

cological, physiological and biochemical aspects. Pharmacol Rev 27:3–134, 1975.
7. Goldman RH, Coltart DJ, Schweizer E, Snidow G, Harrison DC: Dose response in vivo to digoxin in normo- and hyperkalaemia-associated biochemical changes. Cardiovasc Res 9:515–523, 1975.
8. Akera T, Brody TM: The role of Na^+,K^+-ATPase in the inotropic action of digitialis. Pharmacol Rev 29:187–220, 1977.
9. Tobin T, Brody TM: Rates of dissociation of enzyme–ouabain complexes and $K_{0.5}$ values in $(Na^+ + K^+)$ adenosine-triphosphatase from different species. Biochem Pharmacol 21:1553–1560, 1972.
10. Mason DT: Regulation of cardiac performance in clinical heart disease: interactions between contractile state mechanical abnormalities and ventricular compensatory mechanisms. Am J Cardiol 32:437–448, 1973.
11. Tsien RW, Weingart R, Kass RS: Digitalis: inotropic and arrhythmogenic effects on membrane currents in cardiac Purkinje fibers. In: Morad M (ed) Biophysical aspects of cardiac muscle. New York: Academic, 1978, pp 345–368.
12. Gillis RA, Quest JA: The role of the nervous system in the cardiovascular effects of digitalis. Pharmacol Rev 31:19–97, 1979.
13. Doering W: Quinidine–digoxin interaction: pharmacokinetics, underlying mechanism and clinical implications. N Engl J Med 301:400–404, 1979.
14. Beller GA, Smith TW, Abelmann WH, Haber E, Hood WB: Digitalis intoxication: a prospective clinical study with serum level correlations. N Engl J Med 284:989–997, 1971.
15. Cattel M, Gold H: Studies on purified digitalis glucosides. III. The relationship between therapeutic and toxic potency. J Pharmacol Exp Ther 71:114–125, 1941.
16. Akera T: Effects of cardiac glycosides on Na^+,K^+-ATPase. In: Greeff K (ed) Handbook of experimental pharmacology. Vol. 56/I: Cardiac glycosides. Heidelberg: Springer-Verlag, 1981, pp 288–336.
17. Akera T, Baskin SI, Tobin T, Brody TM: Ouabain: temporal relationship between the inotropic effect and the in vitro binding to, and dissociation from, $(Na^+ + K^+)$-activated ATPase. Naunyn Schmiedebergs Arch Pharmacol 277:151–162, 1973.
18. Allen DG, Blinks JR: Calcium transients in aequorin-injected frog cardiac muscle. Nature 273: 509–513, 1978.
19. Langer GA: The intrinsic control of myocardial contraction—ionic factors. N Engl J Med 285:1065–1071, 1971.
20. Reuter H: Exchange of calcium ions in the mammalian myocardium. Circ Res 34:599–605, 1974.
21. Lee KS, Klaus W: The subcellular basis for the mechanism of inotropic action of cardiac glycosides. Pharmacol Rev 23:193–261, 1971.
22. Langer GA: Ion fluxes in cardiac excitation and contraction and their relation to myocardial contractility. Physiol Rev 48:708–757, 1968.
23. Akera T: Membrane adenosinetriphosphatase: a digitalis receptor? Science 198:569–574, 1977.
24. Gervais A, Lane LK, Anner BM, Lindenmayer GE, Schwartz A: A possible molecular mechanisms of the action of digitalis: ouabain action on calcium binding to sites associated with a purified sodium–potassium-activated adenosine triphosphatase from kidney. Circ Res 40:3–14, 1977.
25. Lullmann H, Peters T: Action of cardiac glycosides on the excitation–contraction coupling in heart muscle. Prog Pharmacol 2:1–57, 1979.
26. Ferrier GR, Saunders JH, Mendez C: A cellular mechanism for the generation of ventricular arrhythmias by acetylstrophanthidin. Circ Res 32:600–609, 1973.
27. Weaver LC, Akera T, Brody TM: Digoxin toxicity: primary sites of drug action on the sympathetic nervous system. J Pharmacol Exp Ther 197:1–9, 1976.
28. Lathers CM, Kelliher GJ, Roberts J, Beasley AB: Nonuniform cardiac sympathetic nerve discharge: mechanism for coronary occlusion and digitalis-induced arrhythmias. Circulation 57:1058–1065, 1978.

19. EFFECTS OF AND THE MECHANISM OF ACTION OF CALCIUM ANTAGONISTS AND OTHER ANTIANGINAL AGENTS

A. Fleckenstein
and G. Fleckenstein-Grün

General Considerations and History

It is one of the most important achievements in modern basic cardiology that many substances with a positive or negative inotropic effect on heart muscle act as promoters or inhibitors of the mediator function of Ca^{2+}-ions in excitation–contraction coupling. For instance, β-adrenergic stimulation with adrenaline, noradrenaline, or isoproterenol facilitates the transmembrane Ca^{2+} influx during excitation. Splitting of ATP by the Ca^{2+}-activated myofibrillar ATPase, and contractile tension development, are thereby augmented. Similarly, under the influence of cardiac glycosides, more Ca^{2+} is made available to the contractile myofibrils. Conversely, a number of negative inotropic substances can inhibit excitation–contraction coupling of heart muscle by a Ca^{2+}-antagonistic effect.

Nearly 20 years have passed since the first report from our laboratory on a new compound (later known under the different names of Isoptin, iproveratril, or verapamil) appeared which mimicked the cardiac effects of simple Ca^{2+} withdrawal [1]. This substance, like Ca^{2+} deficiency, diminished Ca^{2+}-dependent contractile force without a major change in action potential, reduced Ca^{2+}-dependent high-energy phosphate utilization of the beating heart, and lowered extra-oxygen consumption in parallel with contractile activity. However, these inhibitory effects of verapamil could be promptly neutralized with the help of additional calcium, β-adrenergic catecholamines, or cardiac glycosides, i.e., by measures able to restore the Ca^{2+} supply to the contractile system. Thus, verapamil represented the most interesting prototype in the series of further Ca^{2+}-antagonistic substances which were subsequently identified in our laboratory (see table 19–1). In fact, Ca^{2+} antagonism turned out to be a novel pharmacodynamic principle of cardiac inhibition clearly distinguishable from β-receptor blockade [2, 3]. Therefore in 1969, on the basis of our investigations with verapamil, methoxyverapamil (D-600), and prenylamine, we felt sufficiently entitled to introduce the term *calcium antagonist* for the sake of clarity [4].

As a result of comparative studies, however, it seemed feasible to subdivide the substances listed in table 19–1 into two groups: group A comprises the Ca^{2+} antagonists of outstanding efficacy and specificity such as verapamil, D-600, nifedipine, ryosidine, niludipine, nimodipine, and dilitiazem. The substances of group A are capable of inhibiting Ca^{2+}-dependent excitation–contraction coupling of the mammalian ventricular myocardium by 90% or more, before the fast Na^{+} influx, during the

N. Sperelakis (ed.), PHYSIOLOGY AND PATHOPHYSIOLOGY OF THE HEART.

Martinus Nijhoff Publishing, Boston/The Hague/Dordrecht/Lancaster.

TABLE 19–1

Group A: Calcium antagonists of outstanding specificity
Criteria: inhibition by 90%–100% of slow inward Ca current *without* concomitant influence on transmembrane Na conductivity

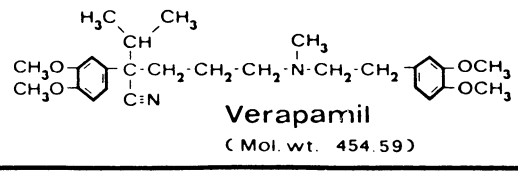

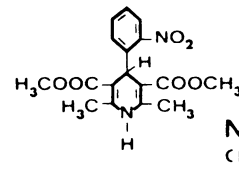

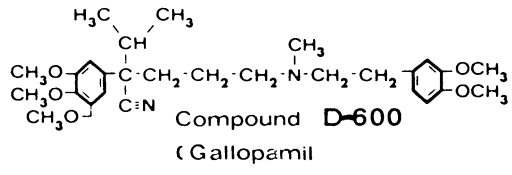

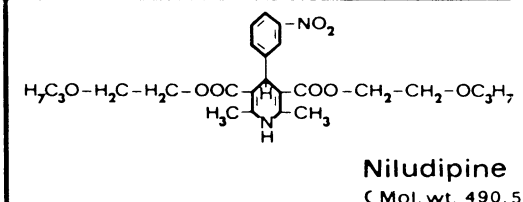

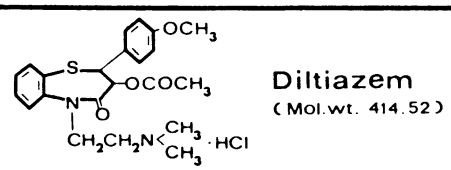

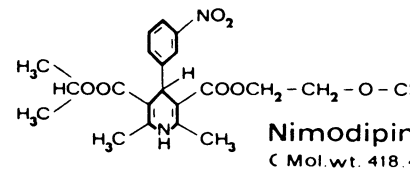

Group B: Calcium antagonists of satisfactory specificity
Criteria: inhibition by 50%–70% of slow inward Ca current *before* fast Na influx is also affected; additional blockade of Mg effects

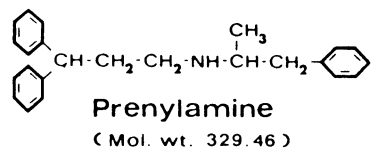

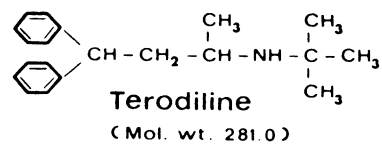

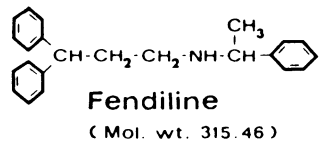

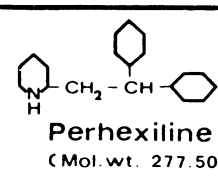

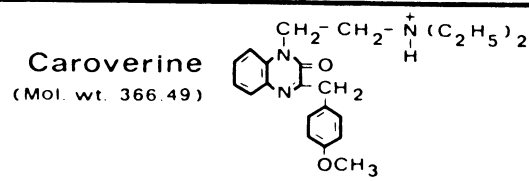

Evidence for the specific Ca^{2+}-antagonistic actions of the different compounds listed above was first presented in the following publications:
Verapamil: Fleckenstein [12], Fleckenstein et al. [3, 4].
D-600: Fleckenstein [12], Fleckenstein et al. [4].
Nifedipine: Fleckenstein [12], Fleckenstein et al. [8, 54, 55], Grün and Fleckenstein [11].
Niludipine: Fleckenstein et al. [56]. Nimodipine was simultaneously analyzed.
Diltiazem: The strong Ca^{2+}-antagonistic properties of diltiazem were first described by Japanese authors (Nakajima et al. [57]).
Prenylamine: Same papers as for verapamil.
Fendiline: Fleckenstein et al. [58].
Terodiline: Unpublished observations of Fleckenstein and Fleckenstein-Grün (1978).
Perhexiline: Fleckenstein-Grün et al. [59].

rising phase of action potential, which is also affected. Moreover, they do not interfere with electrogenic membrane effects of Mg^{2+} ions. Group B, on the other hand, includes prenylamine, fendiline, terodiline, caroverine, and perhexiline, which are somewhat less potent and specific. This means that, under their influence, a concomitant inhibition of the Na^{+}-dependent excitatory process can be seen when Ca^{2+}-dependent contractile tension development of isolated papillary muscles has been reduced by 50%–70%. Moreover, the substances of group B are also unable to discriminate clearly between Ca^{2+}- and Mg^{2+}-induced bioelectrical membrane effects. There are some indications that cinnarizine and flunarizine also belong to group B, but the poor water solubility of these drugs did not allow us a satisfactory electrophysiologic analysis on isolated myocardial tissue [5].

The scope of the Ca^{2+}-antagonistic drug responses is not merely confined to a dose-dependent limitation of cardiac contractile energy expenditure and oxygen requirement, since there are still a number of other therapeutically important actions:

1. On the *myocardium,* for instance, the Ca^{2+} antagonists also provide cardioprotection against deleterious intracellular Ca^{2+} overload, which is a major factor in the pathogenesis of myocardial necrosis.
2. On *cardiac pacemakers,* the principal action of Ca^{2+} antagonists consists of damping Ca^{2+}-dependent automaticity. This applies even more to ectopic foci. Moreover, reentry pathways may be blocked.
3. On *vascular smooth muscle,* Ca^{2+}-dependent tone is reduced and spastic contractions abolished. Accordingly, all Ca^{2+} antagonists are able, in very low concentrations, to relax the smooth musculature from coronary, cerebral, mesenteric, and renal arteries [5, 6–11].

However, these particular effects on myocardium, cardiac pacemakers, and vascular smooth muscle are accentuated differently, depending on the individual Ca^{2+} antagonist used. For instance, if verapamil or D-600 is systemically administered, their Ca^{2+}-antagonistic effects on myocardium, pacemakers, and vasculature appear almost equal in strength. On the other hand, nifedipine and its derivatives niludipine and nimodipine preferentially suppress vascular contractility whereas, at least in dogs and humans, their influence on cardiac pacemaker functions is modest. Due to these peculiarities, nifedipine and its derivatives are prominent vasodilators. Conversely, verapamil is particularly useful for direct cardioprotection, as in cardiomyopathies and for antidysrhythmic purposes. As for diltiazem, this substance too, although more related pharmacologically to verapamil than to nifedipine, interferes predominantly with vascular contractile activity.

Hence, certain characteristics indicate that the Ca^{2+} antagonists are not totally homogeneous. Nevertheless, there is ample evidence to show that all the Ca^{2+} antagonists listed in table 19–1 are members of a distinct pharmacologic family, having in common most of their therapeutic effects on the cardiovascular system. One is actually facing a Ca^{2+} antagonist boom, and thus the number of such compounds is rapidly growing. But among true Ca^{2+} antagonists there are also drugs which were launched under this designation without the necessary verification. For instance, lidoflazin has been claimed by its producers to represent a Ca^{2+} antagonist, but in our studies it turned out that this compound inhibits more

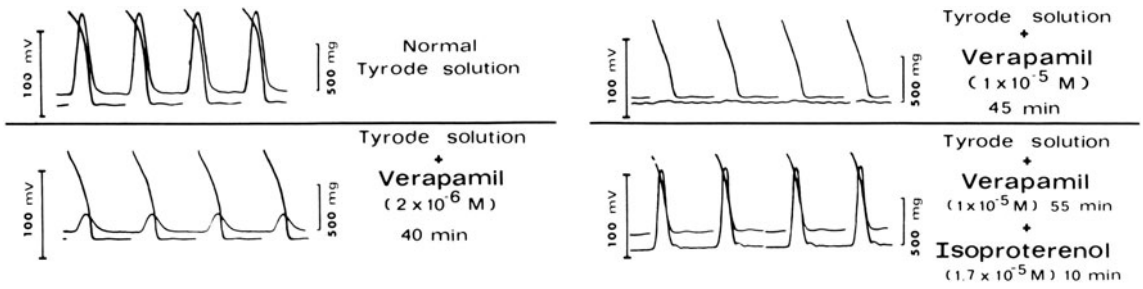

FIGURE 19–1

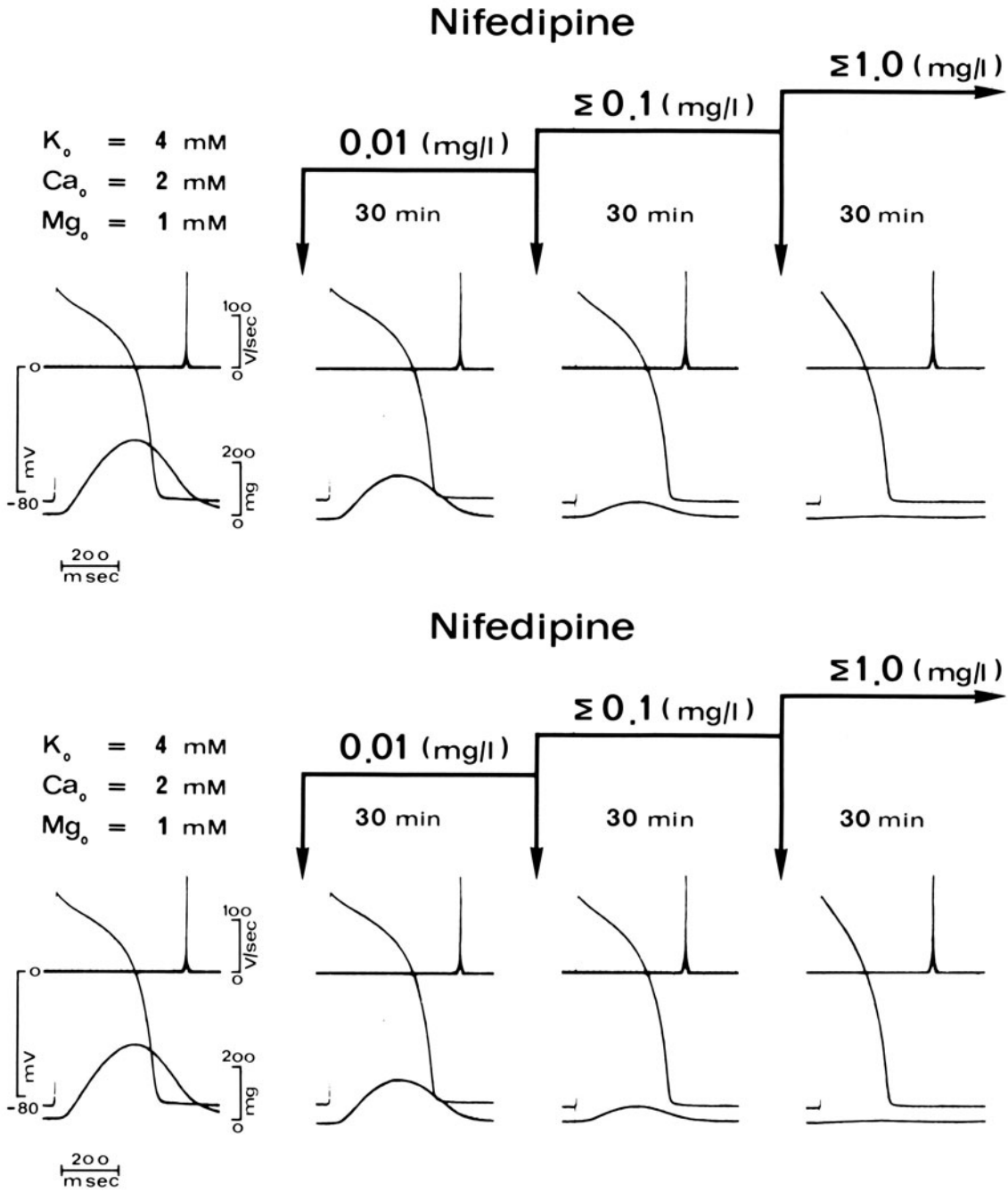

Guinea pig papillary muscle

Stimulation rate : 30 min^{-1}
Temperature : 30°C

FIGURE 19–3

the Na^+-dependent excitatory processes than the Ca^{2+}-dependent contractile parameters. Needless to say, the name of a Ca^{2+} antagonist should only be accredited to such drugs which exert Ca^{2+} antagonism so specifically that all other pharmacodynamic properties, at least in a reasonable dosage range, are more or less negligible (for more details, see review articles [6, 12, 13] and the recent monograph by Fleckenstein [5].

Opposite Effects of Calcium Antagonists and β-Adrenergic Catecholamines on Transsarcolemmal Calcium Influx and Contractile Tension Development

Crucial experiments illustrating the spectacular Ca^{2+}-antagonistic interference with the development of Ca^{2+}-dependent contractile tension in isolated guinea pig papillary muscles are shown in figures 19–1 to 19–3. Here the isometric contraction amplitude was totally suppressed by large doses of verapamil, nifedipine, or diltiazem. The high concentrations applied are sufficient to interrupt almost totally the "slow" inward current of Ca^{2+} ions across the excited myocardial sarcolemma membrane as established by direct measurements using a special voltage-clamp technique [14, 15]. In contrast, the "fast" influx of Na^+ ions which is responsible for the onset of action potential was unaffected. Therefore, in figures 19–2 and 19–3, upstroke velocity and height of overshoot of the action potential remained unchanged. Only the plateau of the action potentials appeared to be slightly abbreviated, because Ca^{2+} ions are no longer able to contribute to the maintenance of depolarization during the late phase of the plateau when the transmembrane Ca^{2+} conductivity has been blocked. As regards the control of the slow inward Ca^{2+} current, Ca^{2+} antagonists and sympathetic transmitter substances exert exactly opposite effects: Ca^{2+} antagonists restrict the transmembrane Ca^{2+} inflow, whereas β-receptor stimulation promotes the inward Ca^{2+} current, even in the presence of Ca^{2+} antagonists. When administered at excessively high concentrations, all specific Ca^{2+} antagonists of group A were able to selectively abolish cardiac contractile performance to the same extent of almost 100% and, in all these cases, suitable doses of β-adrenergic agents restored the mechanical responses [5].

There is no doubt that the sarcolemma membrane has to be considered the decisive site of action of Ca^{2+} antagonists. Thus it was shown in our laboratory that the possibility of controlling contractile force by Ca^{2+} antagonists is lost when the sarcolemmal membrane has previously been destroyed in "skinned" myocardial fibers by glycerin–water extraction or according to Winegrad's technique [16]. In such skinned fibers, Ca^{2+} antagonists caused no inhibition when contraction was directly induced by addition of ATP and Ca^{2+}. This indicated that the structural integrity of the cardiac sarcolemma membrane is an indispensable prerequisite for the Ca^{2+}-antagonistic drug action. Obviously, these agents lose their power if the Ca^{2+} ions have free access to the myofibrils where ATP is split. Hence, there is certainly no direct effect of Ca^{2+}-antagonistic compounds on the Ca^{2+}-dependent activation of myofibrillar ATPase and on energy transformation in the myofilaments. Similarly, in fractionated sarcoplasmatic reticulum, several attempts to demonstrate an inhibitory effect of negative inotropic doses of verapamil on binding, accumulation, or exchange of Ca^{2+} have failed [17–19]. Moreover, in isolated cardiac mitochondria, only an excessive concentration of verapamil, more than 1000 times greater than that required to produce contractile failure, suppressed Ca^{2+} uptake [20]. In other words, evidence for decisive action of negative inotropic concentrations of Ca^{2+} antagonists on intracellular sites is still lacking.

Many observations indicate that the sarcolemma membrane not only regulates the in-

FIGURES 19–1 to 19–3. Selective suppression of myocardial contractility by Ca^{2+} antagonists. No change in Na^+-dependent maximal rate of upstroke (dV/dt_{max}) and height of action potential (see upper record in figs. 19–2 and 19–3). Restitution of contractile force by isoproterenol (fig. 19–1) or by elevation of extracellular Ca^{2+} concentration (fig. 19–3). Isolated guinea pig papillary muscles in Tyrode solution with 2 m*M* Ca^{2+}. Figure 19–1 reproduced from Fleckenstein [60].

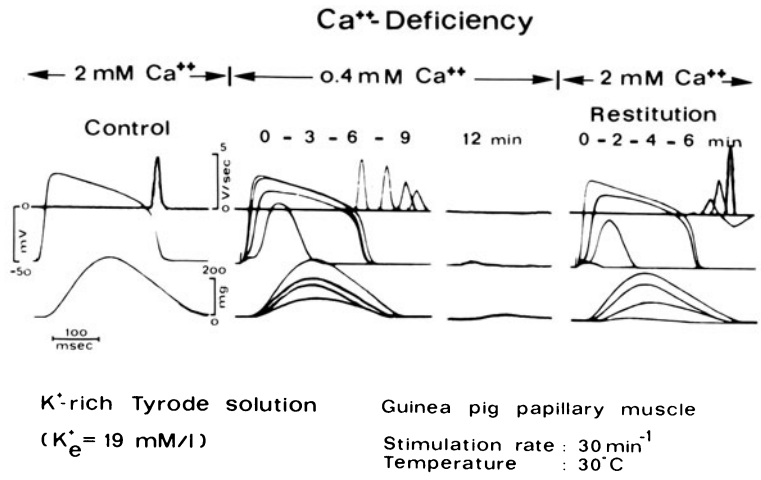

FIGURE 19–4. Parallel suppression of Ca^{2+}-dependent action potentials and contractile force of partially depolarized guinea pig papillary muscle in a K^+-rich (19 m*M*) Tyrode solution upon reduction of extracellular Ca^{2+} concentration from 2 to 0.4 m*M*. The records from top to bottom represent (a) dV/dt_{max}, (b) action potentials, (c) isometric mechanograms. Stimulation rate 30/min, temperature 30°C.

ward diffusion of Ca^{2+} into the myoplasm, but also plays an important role as *Ca^{2+}-accumulating system* which recruits Ca^{2+} actively from the environment. Presumably, the highest Ca^{2+} concentration is attained in those parts of the sarcolemma membrane which are invaginated in the form of the T tubules. From here the Ca^{2+} ions enter the interior of the myocardial fibers through the slow channels as soon as the excitation wave depolarizes these membrane structures. Although the basement membrane contains much negatively charged free or protein-bound mucopolysaccharide material with specific affinity for Ca^{2+} [21], the decisive reaction that leads to an accumulation of Ca^{2+} in the sarcolemmal membrane probably consists of the production of cyclic AMP [22, 23]. According to this concept, β-adrenergic catecholamines, through the formation of cyclic AMP, activate a membrane-bound protein kinase which, in turn, induces phosphorylation of membrane proteins in the vicinity of the slow channels or even within the slow channels. By this reaction, the number of fixed negative phosphate groups suitable for accumulation of Ca^{2+} ions is increased, whereas Mg^{2+} ions seem to be displaced [5]. In this way, β-adrenergic catecholamines probably fill the superficial Ca^{2+} pool with more loosely bound Ca^{2+} that is instantaneously available to the slow channels, as soon as depolarization has occurred. In other words, β-adrenergic catecholamines seem to increase the capacity of the superficial Ca^{2+} store so that the uptake of Ca^{2+} from the environment and the subsequent transsarcolemmal influx of Ca^{2+} are augmented, even in the case of considerable extracellular Ca^{2+} depletion or in the presence of Ca^{2+}-antagonistic drugs. Dibutyryl cyclic AMP increases the inward Ca^{2+} current more directly, i.e., without activation of adrenergic β-receptors.

The Ca^{2+} antagonists, on the other hand, exert exactly the opposite effects on superficial Ca^{2+} binding. They do not interfere with the formation of cyclic AMP [19], but they probably displace Ca^{2+} from the fiber surface apart from direct interference with the slow-channel-mediated inward Ca^{2+} current. Accordingly, isolated cardiac sarcolemma membranes could be depleted of bound Ca^{2+} by verapamil [18]. There are two different types of Ca^{2+} storage in cardiac sarcolemma membranes: one at low-affinity and another at high-affinity binding sites [24]. Verapamil specifically inhibited low-

affinity Ca^{2+} binding. The effective verapamil concentration that blocked low-affinity Ca^{2+} binding in isolated cardiac sarcolemma membranes proved to be as low as 1.4 μM [23]. Hence, verapamil and other Ca^{2+} antagonists seem to impair primarily the Ca^{2+}-binding capacity or the refilling of the superficial Ca^{2+} depots in the sarcolemma membrane, so that the availability of Ca^{2+} to the slow channels is critically diminished. Ca^{2+} antagonists of group A interfere with sarcolemmal Ca^{2+} binding and electrogenic Ca^{2+} influx selectively, whereas the Ca^{2+} antagonists of group B are less specific in that they also suppress Mg^{2+}-induced electrogenic membrane effects [5].

Linear Correlation between Inhibition by Calcium Antagonists of Transmembrane Calcium Supply and Contractile Performance

To study the quantitative correlation between the changes in Ca^{2+} influx and myocardial tension development, experiments have been carried out in our laboratory on isolated cat and guinea pig papillary muscles, in which the fast Na^+ transport system had previously been blocked [5, 25]. For instance, if the cardiac fiber membrane potential is reduced to -45 mV, the fast Na^+ inward current becomes inactivated, whereas the slow Ca^{2+} channels continue to respond to electrical stimulation. The simplest method of producing this critical degree of depolarization consists of placing additional KCl (19 mM) in the experimental Tyrode solution. Such predepolarized myocardial fibers are still capable of conducting propagated impulses. However, in this situation, not only contractile performance but also bioelectric activity depend on the slow inward Ca^{2+} current. Such Ca^{2+}-mediated action potentials of partially depolarized myocardial fibers are highly sensitive to changes in the extracellular Ca^{2+} concentration. Hence, upstroke velocity, height, and duration of the Ca^{2+}-carried action potentials decrease rapidly in a Ca^{2+}-deficient medium. In the experiment of figure 19–4, bioelectrical activity totally disappeared together with the contractile function within 12 min after the Ca^{2+} concentration had been reduced from 2 mM to 0.4 m M. However, the Ca^{2+}-dependent action potentials and contractile force recovered within 6 min following return to the original medium with 2 mM Ca^{2+}.

Figures 19–5 and 19–6 show how perfectly the Ca^{2+} antagonists mimic the effects of simple Ca^{2+} withdrawal on such partially depolarized guinea pig papillary muscles. As can be easily seen from the superimposed traces (registered with a storage oscilloscope), the papillary muscles (treated in fig. 19–5 with 0.2 mg nifedipine/l, 0.4 mg D 600/l, or 2 mg verapamil/l) behaved in the presence of a normal 2 mM Ca^{2+} concentration as if they were exposed to a Ca^{2+}-deficient medium. Obviously, in all these cases, the time course of inhibition of the Ca^{2+}-mediated action potentials coincides with the development of contractile incompetence. At the end of the experiment, the Ca^{2+} antagonists were neutralized by increasing the Ca^{2+} concentration up to 6 or 8 mM. Consequently, the bioelectrical membrane activity of the partially depolarized myocardium recovered again more or less in parallel with the mechanical performance. Figure 19–6 represents identical experiments with the use of the Ca^{2+} antagonists diltiazem, perhexiline maleate, and fendiline.

Partially depolarized ventricular myocardium offers unique possibilities of testing in this way the quantitative correlation between transmembrane Ca^{2+} influx, as indicated by the bioelectrical parameters of the Ca^{2+}-mediated action potentials, and by the mechanical responses. For instance, the upstroke velocity (dV/dt_{max}) of Ca^{2+}-mediated action potentials indicates the intensity of transsarcolemmal Ca^{2+} influx through the slow channel, whereas the duration of the Ca^{2+}-mediated action potentials reflects the length of time of Ca^{2+} entry. In fact, contractile tension changes in parallel with these bioelectrical parameters. As an example, the areas of the Ca^{2+}-dependent isometric mechanograms, representing tension time, as the most appropriate parameter of contractile performance, are plotted in figure 19–7 against the areas of the Ca^{2+}-mediated action potential curves. It is evident from this graph that there is a perfect linearity between the

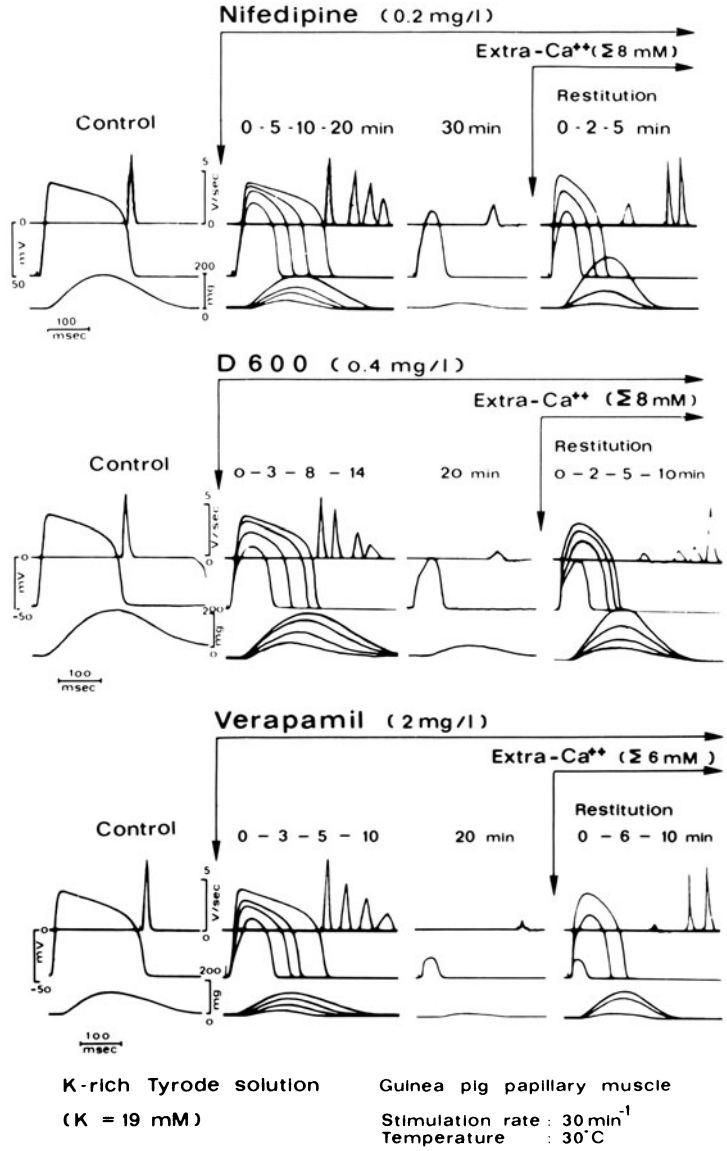

FIGURE 19–5

magnitude of the Ca^{2+}-dependent bioelectrical and mechanical responses. Hence the conclusion is justified that the various Ca^{2+} antagonists, tested in the present study on partially depolarized myocardium, act uniformly in that they inhibit contractile tension development always to the same extent as they are capable of restricting the slow transsarcolemmal inward Ca^{2+} current which is responsible, in this situation, for both the bioelectrical and the mechanical events.

Cardioprotective Actions of Calcium Antagonists: Decrease in Myocardial Oxygen Requirement—Prevention of Deleterious Intracellular Calcium Overload

The cardiac effects of β-adrenergic substances and Ca^{2+} antagonists counteract each other in almost every respect. Ca^{2+} binding in the superficial membrane pool, transmembrane Ca^{2+} influx through the slow channels, splitting of ATP by myofibrillar ATPase, contractile ten-

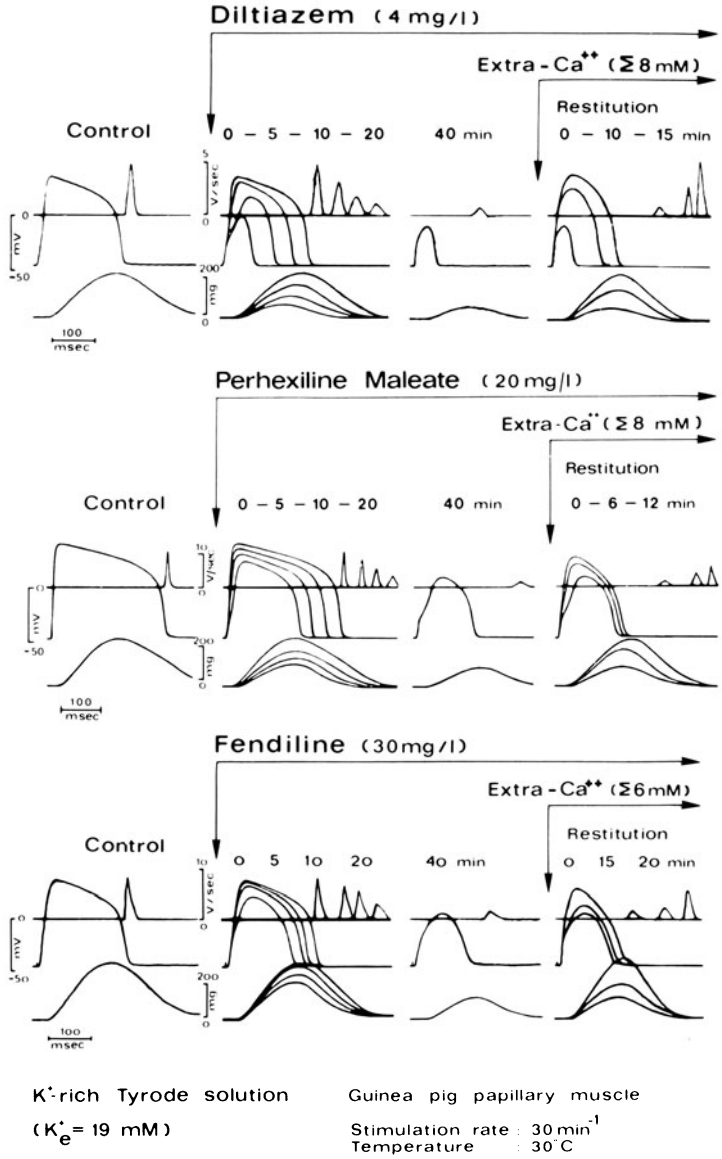

FIGURE 19–6

FIGURES 19–5 and 19–6. Parallel suppression of Ca^{2+}-dependent action potentials and contractile force of partially depolarized guinea pig papillary muscles in a K^+-rich (19 m*M*) Tyrode solution, containing 2 m*M* Ca^{2+}, by administration of various Ca^{2+} antagonists. Registration techniques and other experimental arrangements as in figure 19–4.

sion development, and oxygen requirement of the beating heart are increased by the β-adrenergic catecholamines. Conversely, the Ca^{2+} antagonists decrease all these Ca^{2+}-dependent parameters. It is commonly known that the intensity of oxidative cardiac metabolism depends on the rate of ATP consumption. Therefore the Ca^{2+} antagonists (like simple Ca^{2+} withdrawal) always lower the oxygen requirement to the same extent as they reduce the Ca^{2+}-dependent splitting of ATP and isometric tension development (fig. 19–8). Needless to say, the relatively small doses of Ca^{2+} antagonists administered in human therapy can produce only a modest reduction of heart work

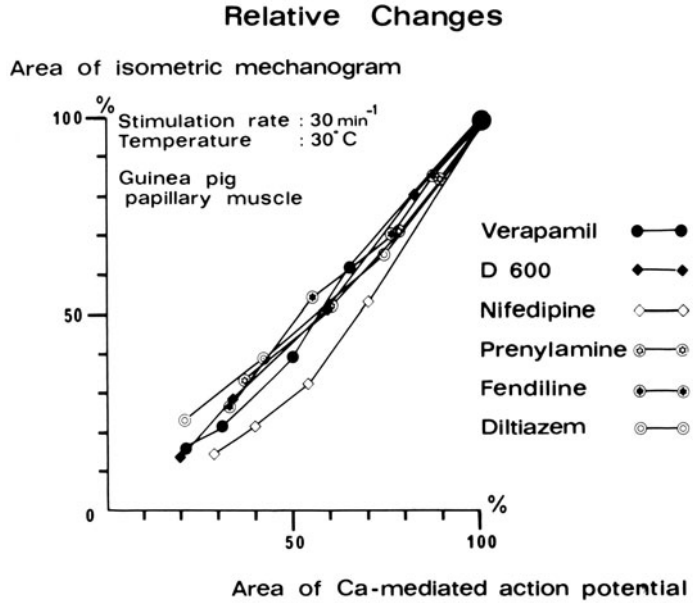

FIGURE 19–7. Linear relationship between decrease of area of isometric mechanograms and reduction of area of Ca^{2+}-mediated action potentials under the influence of various Ca^{2+} antagonists. The control data (= 100%) were obtained on partially depolarized guinea pig papillary muscles after 30-min incubation in K^+-rich (19 m*M*) Tyrode solution with 2 m*M* Ca^{2+}. Time of exposure to the Ca^{2+} antagonists was 20–40 min.

and oxygen demand. Nevertheless, adequate doses of Ca^{2+} antagonists can be successfully used for the treatment of patients with a hyperkinetic heart function or suffering from coronary heart disease. Here, a certain dose-dependent restriction of cardiac activity may be helpful in reestablishing a suitable balance between the reduced coronary oxygen supply and the actual cardiac oxygen requirement. In this respect, the Ca^{2+}-antagonistic compounds have a beneficial effect in patients with angina pectoris similar to that of the adrenergic β-receptor-blocking agents, although the mode of action is different: Ca^{2+}-antagonistic substances inhibit the transmembrane Ca^{2+} supply directly by acting on the slow channels; β-receptor-blocking agents, on the other hand, diminish transmembrane Ca^{2+} influx indirectly by neutralizing the promoter effects of β-adrenergic catecholamines. Nevertheless, both Ca^{2+} antagonists and β-blockers reduce the availability of Ca^{2+} to the contractile system so that, eventually, splitting of ATP, contractile energy expenditure, and cardiac oxygen requirement are lowered according to the same basic principle.

A rather unique property of Ca^{2+} antagonists is that they provide direct cardioprotection against Ca^{2+}-induced functional and structural damage. In fact, as we demonstrated in 1968, heart muscle fibers undergo severe alterations, finally resulting in necrosis, as soon as free Ca^{2+} ions penetrate excessively through the sarcolemma membrane into the myoplasm, so that the capacities of the Ca^{2+}-binding or extrusion processes become insufficient [5, 12, 13, 26–30]. The crucial event in the development of such lesions is high-energy phosphate deficiency which results (a) from excessive activation of Ca^{2+}-dependent intracellular ATPases, and (b) from Ca^{2+}-induced impairment of the mitochondria that mainfests itself as swelling vacuolization, cristolysis, loss of respiratory control, and phosphorylation capacity.

Table 19–2 shows the various pathogenic circumstances under which intracellular Ca overload proved to be the decisive etiologic fac-

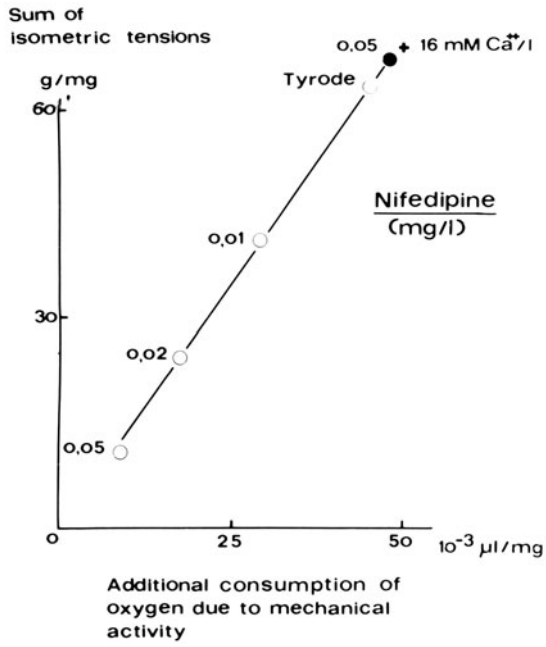

FIGURE 19–8. Nifedipine. Linear reduction of isometric tension and additional consumption of oxygen due to mechanical activity under the influence of increasing doses of the drug (0.01 mg, 0.02 mg, and 0.05 mg/l) in Tyrode solution containing 2.0 m*M* Ca^{2+}. With 0.05 mg/l, tension development and extra consumption of oxygen were greatly depressed. This drug effect could be completely neutralized by increasing the extracellular Ca^{2+} concentration up to 16 m*M* in the presence of 0.05 mg/l nifedipine. Experiment on a rabbit papillary muscle (wet weight, 0.8 mg). From Fleckenstein et al. [55].

tor in the production of myocardial fiber damage. Conversely in all these cases, Ca^{2+}-antagonistic compounds were capable of totally protecting structural and functional integrity. By restricting transmembrane Ca^{2+} influx, the Ca^{2+} antagonists minimized the ATP and creatine phosphate losses, and consequently prevented deleterious high-energy phosphate exhaustion. As an example, figures 19–9 and 19–10 show the tremendous increases in uptake of Ca and ^{45}Ca into rat hearts after subcutaneous injection of cardiotoxic doses of isoproterenol, and the strong inhibitory actions of Ca^{2+} antagonists. Verapamil and other Ca^{2+} antagonists prevented Ca^{2+} overload, high-energy phosphate breakdown, and structural damage. Chronic treatment of cardiomyopathic hamsters with Ca^{2+} antagonists also kept the myocardial Ca^{2+} content in the normal range and thereby provided complete cardioprotection [31]. In this context, it is to be remembered that the successful introduction of verapamil by Kaltenbach et al. [32] for the treatment of human hypertrophic obstructive cardiomyopathy was based on these experimental observations.

Ca^{2+} overload is also responsible to a significant extent for the impairment of the mitochondria in anoxic or ischemic cardiac tissue. Accordingly, Ca^{2+} antagonists such as verapamil [33], nifedipine [34] or diltiazem [35, 36] can even shield hypoxic and ischemic hearts from additional Ca^{2+}-induced myocardial fiber damage that would otherwise precipitate structural disintegration. Obviously, Ca^{2+} antagonists prolong the time of survival of ischemic hearts and mitigate the harmful influence of anoxia. Hence it is not surprising that, also in cardiac surgery, Ca^{2+} antagonists have recently been used as additives to cardioplegic solutions for better myocardial preservation [37].

Opposite Effects of Calcium Antagonists and Calcium Promoters on Calcium-dependent Nomotopic and Ectopic Pacemaker Activity

Ca^{2+} antagonists and β-adrenergic catecholamines also counteract each other on cardiac

TABLE 19–2. Key role of calcium overload in myocardial fiber necrotization

Myocardial destruction due to Ca^{2+} overload	① Overdoses of β-adrenergic catecholamines ② Overdoses of vitamin D_3 or dihydrotachysterol (AT 10) ③ Alimentary Mg or K deficiency ④ Genetic defects (hereditary cardiomyopathy of Syrian hamsters) ⑤ Anoxic or ischemic myocardial fiber membrane damage	Myocardial protection by calcium antagonists via prevention of Ca^{2+} overload

Ca Antagonists may be overpowered by higher degrees of sarcolemma membrane leakage that permit excessive influx of Ca ("calcium paradox"; "skinned fibers").

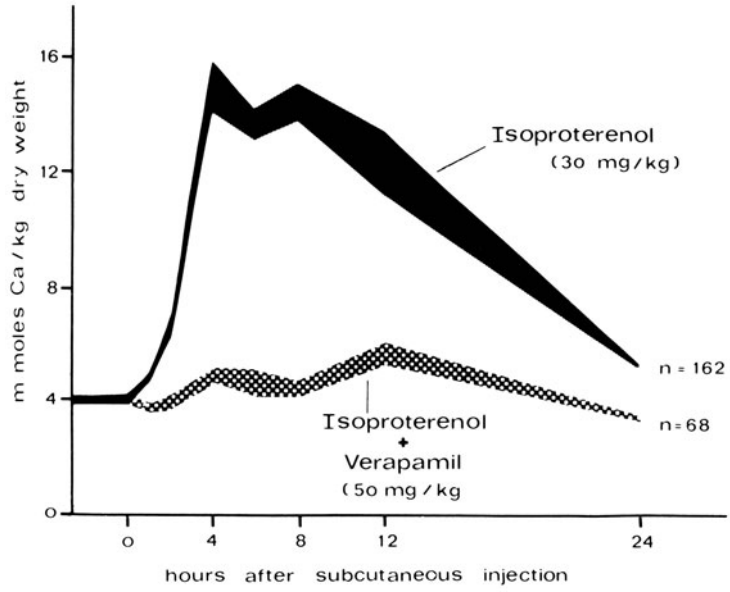

FIGURE 19–9. Protection by verapamil of the right ventricular myocardium of rats against isoproterenol-induced Ca^{2+} overload during an observation period of 24 h. Administration of 30 mg/kg isoproterenol with and without verapamil (50 mg/kg) at separate subcutaneous injection sites.

pacemakers, as schematically shown in figure 19–11. In fact, not only the initiation of myocardial contraction but also the fundamental process of sinus and atrioventricular node automaticity as well as atrioventricular conduction are necessarily linked with a transmembrane influx of Ca^{2+} ions. Moreover, the Ca^{2+} transport systems that operate in the nodal cell membranes closely resemble the "slow membrane channels" of ordinary myocardial fibers. Accordingly, in both nodal cells and ordinary myocardial fibers, these channels respond to virtually the same activators and inhibitors of the inward Ca^{2+} current [38–40]. Hence, β-adrenergic agents as well as dibutyryl cAMP, by promoting the transfer of Ca^{2+} through the slow channels, not only cause an increase in contractile force but also produce an analogous rise in heart rate and atrioventricular conduction velocity. Conversely, most Ca^{2+} antagonists exert negative inotropic, chronotropic, and dromotropic effects simultaneously [41, 42]. The Ca^{2+}-antagonistic divalent Co^{2+}, Ni^{2+}, and Mn^{2+} ions act similarly in that they also suppress, by inhibiting Ca^{2+} inflow across the slow membrane channels, contractility as well as pacemaker excitation. The same functional impairment results from simple Ca^{2+} withdrawal. On the other hand, tetrodotoxin (TTX), which is known to block the fast Na^{+} channels, does not inhibit sinus and atrioventricular node automaticity or atrioventricular conduction. Hence, there are two contrasting types of cardiac excitation that can be easily distinguished by their different sensitivities to drugs and by the typical shapes of their action potentials (fig. 19–12):

1. The fast, obviously Na^{+}-dependent, excitatory events in atrial myocardium, His bundle, Purkinje fibers, and ventricular myocardium (upstroke velocity = dV/dt_{max}: 170–400 V/s; propagation rate: 60–200 cm/s). This type of excitation is rather refractory to Ca^{2+} antagonists and Ca^{2+} promoters.
2. The slow, obviously Ca^{2+}-dependent, impulse generation and impulse conduction in the sinoatrial and atrioventricular nodes (upstroke velocity = dV/dt_{max}: 2–7 V/s;

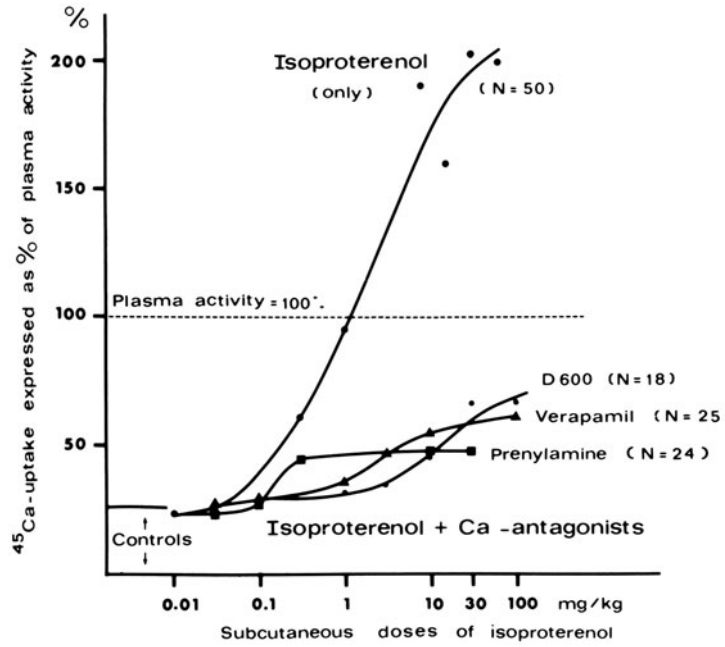

FIGURE 19–10. Prevention of excessive isoproterenol-induced uptake of labeled Ca^{2+} into the right ventricular myocardium of rats by Ca^{2+}-antagonistic compounds. Log dose–response curves of isoproterenol-induced radiocalcium incorporation obtained with or without simultaneous administration of D-600 (10 mg/kg), verapamil (17 mg/kg), or prenylamine (250 mg/kg). All measurements were made 6 h after subcutaneous injection of the drugs. Experiment by Janke and Fleckenstein (see Fleckenstein [12]).

propagation rate: 2–6 cm/s). This type of excitation readily responds to drugs that influence transmembrane Ca^{2+} conductivity.

However, the situation changes if ectopic automaticity develops in altered atrial or ventricular myocardium simultaneously with a drop in membrane potential. In this case, the excitatory process turns from the regular Na^{+}-dependent form into the slow-channel-mediated Ca^{2+}-dependent type which is characteristic of partially depolarized myocardium. Thus Ca^{2+} antagonists ("fourth class" of antidysrhythmic drugs according to Singh and Vaughan Williams [43]) will be able to extinguish the uncontrolled firing of such Ca^{2+}-dependent, atrial or ventricular ectopic foci, and also block Ca^{2+}-dependent slow-channel-mediated reentry pathways. Figure 19–13 illustrates the electrogenesis of ectopic automaticity in a low range of membrane potential (−30 to −50 mV). In this low range, automatic impulses appear in two typical forms: (a) as spontaneous local subthreshold oscillations of membrane potential, and (b) as propagated pacemaker action potentials if the depolarizing phase of these local oscillations reaches the threshold. The diagram further indicates that the influx of Ca^{2+} ions is the primary step responsible for spontaneous depolarization. This is true of both the depolarizing phase of the local oscillations and the Ca^{2+}-dependent upstroke of the propagated pacemaker action potentials. Then, in a second step, following the intrusion of Ca^{2+}, a delayed outward K^{+} current is elicited which drives the membrane potential back to the higher diastolic values. Needless to say, the Ca^{2+} antagonists, by inhibiting this Ca^{2+}-K^{+} exchange cycle, interrupt the fundamental process of ectopic automaticity, whereas β-adrenergic agents, by stimulating the inward Ca^{2+} current, promote spontaneous impulse discharge. With respect to these typical drug effects, nomotopic and ectopic pacemaker cells behave, at least in prin-

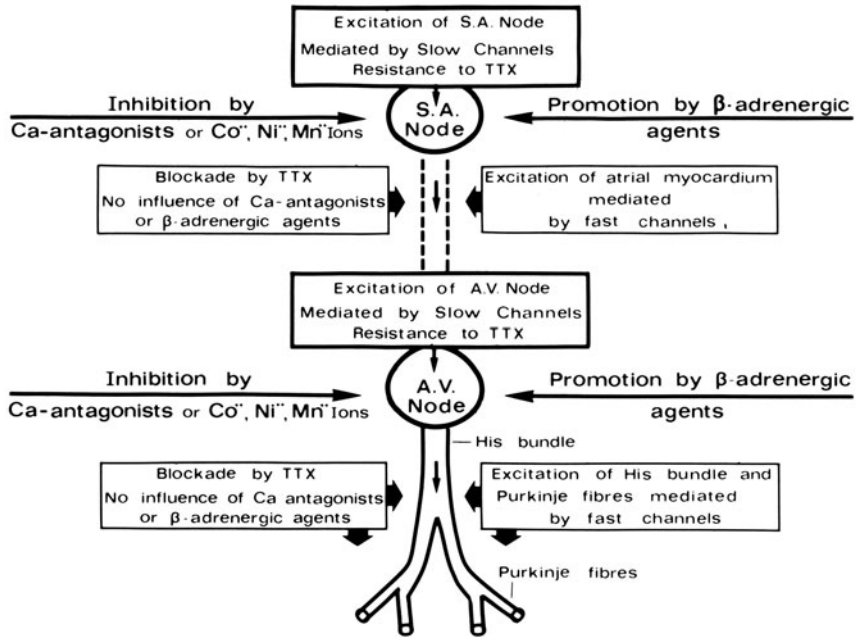

FIGURE 19–11. Opposite effects of Ca^{2+} antagonists and Ca^{2+} promoters (β-adrenergic agents) on slow-channel-mediated, TTX-insensitive SA node automaticity and AV node conductivity. Refractoriness to Ca^{2+} antagonists and β-adrenergic catecholamines of normal TTX-sensitive impulse propagation in atrial, His bundle, and Purkinje fibers.

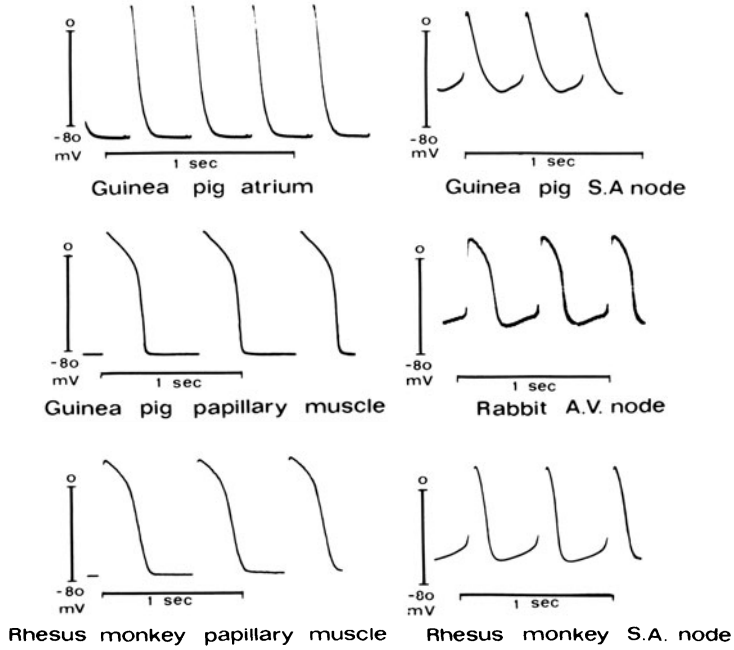

FIGURE 19–12. Comparison of transmembrane action potentials of electrically stimulated nonautomatic myocardial fibers from atrial or papillary muscles with those of spontaneously discharging sinoatrial (SA) or atrioventricular (AV) nodal cells. The characteristic feature of spontaneously active nodal cells is a slow diastolic depolarization that initiates a propagated pacemaker action potential as soon as the membrane potential is lowered to a critical level (threshold potential). The vertical calibrations of each record represent the zero potential and a membrane potential of −80 mV. The time calibrations indicate an interval of 1 s each.

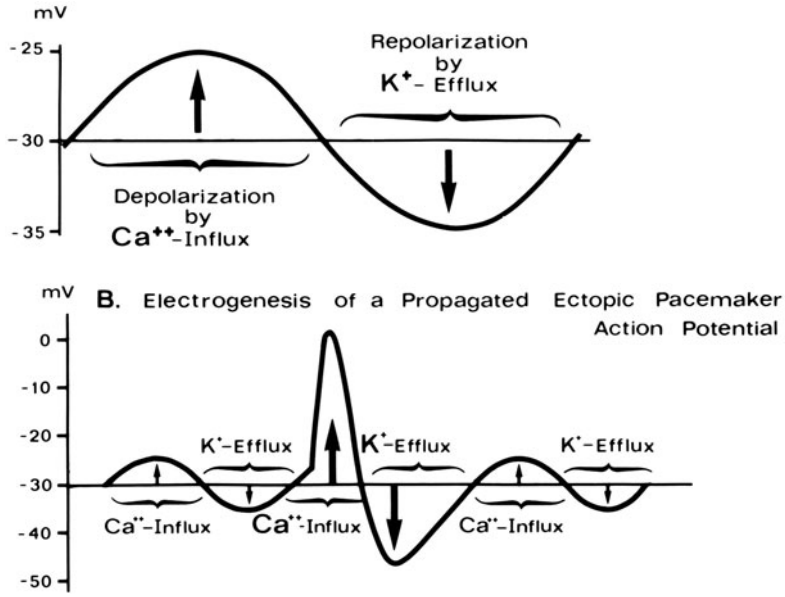

FIGURE 19–13. Scheme of coupled Ca^{2+}-K^+ exchange underlying electrogenesis of ectopic subthreshold oscillations *(A)* and propagated ectopic pacemaker action potentials *(B)* in a low range of membrane potentials (below −50 mV). In both cases, *A* and *B*, the depolarizing slow-channel-mediated inward current is carried by Ca^{2+} ions, while the subsequent repolarization is brought about by efflux of an equivalent amount of K^+ (I_K) which drives the membrane potential back to diastolic values. The greater influx of Ca^{2+}, in the case of a propagated ectopic pacemaker action potential, is apparently compensated for by an enhancement in that an overshooting repolarization is produced.

ciple, very much alike. For instance, figure 19–14 shows the inhibition of nomotopic sinoatrial and atrioventricular node automaticity by the Ca^{2+} antagonists verapamil and D-600. On the other hand, adrenaline resuscitates the spontaneous impulse discharge in previously paralyzed sinoatrial or atrioventricular nodes and restores atrioventricular conduction. Furthermore, as is generally known, adrenaline and other β-adrenergic agents also promote atrial and ventricular ectopic arrhythmias.

In parallel with such physiologic and pathophysiologic investigations, the efficacy of Ca^{2+} antagonists in the treatment of certain cardiac arrhythmias has also been established by many clinical studies. Thus, Bender found in 1966 that the damping effect of verapamil on the atrioventricular conduction can be practically used for the reduction of ventricular rate in cases of atrial fibrillation, and flutter [44]. Schamroth [45] and Krikler and his group [46–48] extended this work in demonstrating the outstanding potency of intravenously administered verapamil to interrupt reciprocating atrioventricular reentry tachycardias. Moreover ischemia-induced ventricular automaticity of vasospastic origin proved to be highly responsive to Ca^{2+} antagonists such as verapamil and even nifedipine. Also ventricular ectopic automaticity in connection with unstable angina or acute myocardial infarction is in numerous cases not refractory to this treatment.

Vascular Effects of Calcium Antagonists: Relaxation of Coronary Smooth Muscle, Reduction of Systemic Arteriolar Flow Resistance

Although the present chapter concentrates primarily on the cardiac effects of Ca^{2+} antagonists, the outstanding vasodilator potency of

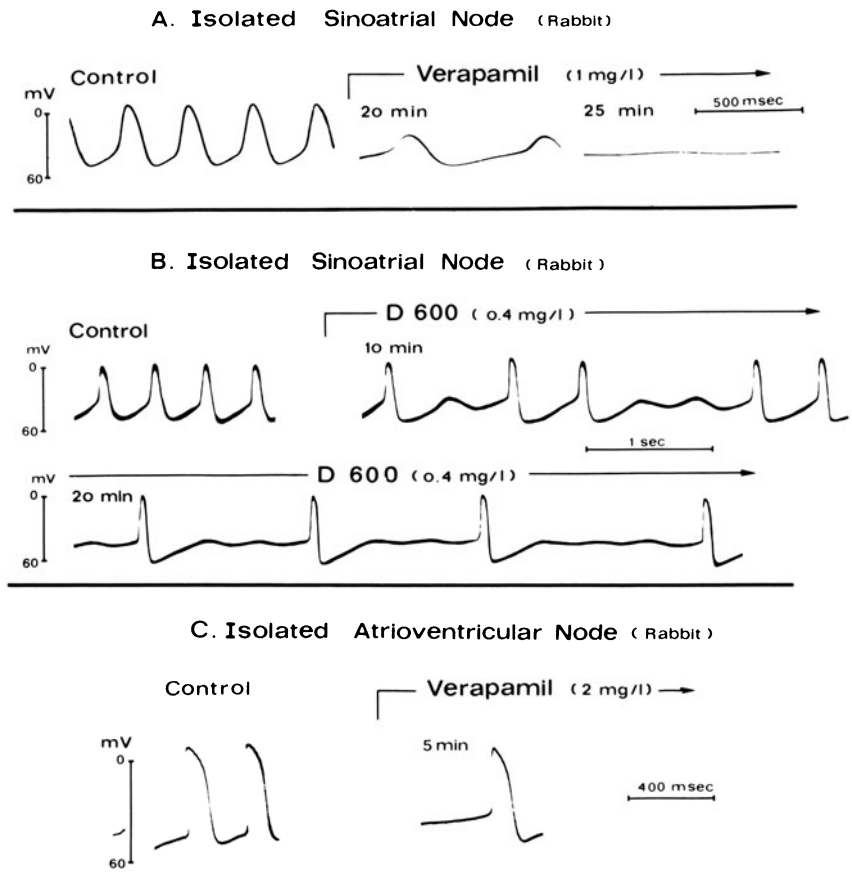

FIGURE 19–14. Inhibition by verapamil and D-600 of pacemaker function of isolated sinoatrial and atrioventricular nodes from rabbits. Verapamil and D 600 reduce both the steepness of slow diastolic depolarization, thereby producing a negative chronotropic effect, and the velocity of upstroke of propagated nodal action potentials. The height of the overshoot also decreases upon prolonged exposure to the drugs whereas there is a growing tendency to hyperpolarization during diastole. As shown in *B*, a nodal cell treated with the Ca^{2+} antagonist D 600, increasingly fails to elicit propagated pacemaker action potentials. This is due (a) to a reduction in the amplitude of intrinsic oscillatory potential changes, and (b) to a shift of threshold potential toward zero. Thus, an increasing number of spontaneous local depolarization waves remain unanswered. Each record in experiment *A*, *B*, and *C* was taken by steady impalement of a single cell. Record *A* reproduced from Kohlhardt et al. [41]. Record *B* from Tritthart et al. (unpublished data). Record *C* from Tritthart et al. [42].

these agents is another highly important factor on which their antianginal action is based. As schematically illustrated in figure 19–15, both tonic and phasic contraction of arterial smooth muscle depend on the availability of free Ca ions. They are either supplied from extracellular sources through potential-dependent or receptor-operated Ca^{2+} channels, sensitive to electric, mechanical, or pharmacologic stimuli, or alternatively released from cellular storage sites by nonelectrical mechanisms. The Ca^{2+} antagonists block directly, and most effectively, potential- or receptor-dependent transmembrane Ca^{2+} supply, but also impair transmembrane replenishment of the cellular stores, an effect that appears often with some delay. But lastly, under the influence of Ca^{2+} antagonists, every kind of contractile smooth muscle

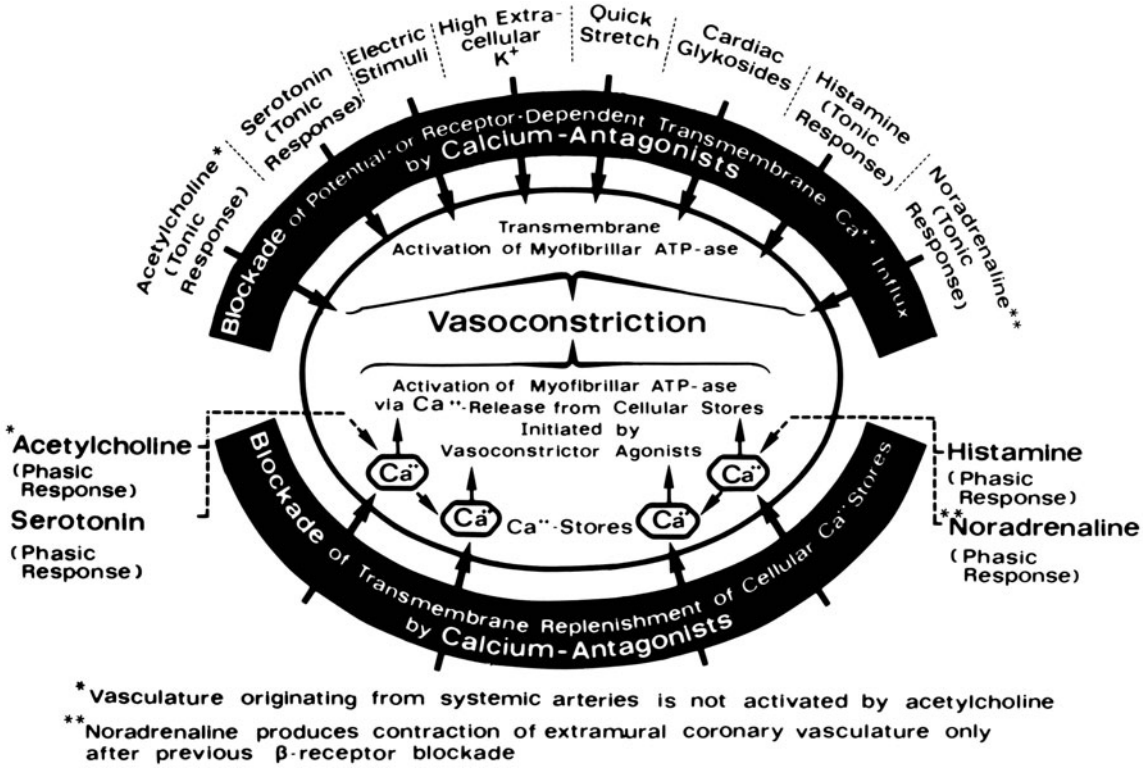

FIGURE 19–15. Scheme of the dual source of activator Ca^{2+} for tonic and phasic vascular smooth muscle contractions, i.e., (a) potential- or receptor-dependent transmembrane Ca^{2+} supply for tonic responses, and (b) release of Ca from cellular stores for phasic responses to vasoconstrictor agonists. Ca^{2+} antagonists inhibit directly and most effectively transmembrane Ca^{2+} influx, i.e., pathway (a). However, to a lesser extent, Ca antagonists also interfere with pathway (b), probably indirectly by impairing transmembrane replenishment of cellular Ca^{2+} stores. The exact anatomical location of these cellular Ca^{2+} stores is a pending problem (plasma membrane, inner surface of plasma membrane, SR structures ?).

activity can be damped on a dose-related manner [5, 7–10].

Interestingly enough, the vasodilator actions of Ca^{2+} antagonists manifest themselves most significantly on the coronary bed and the peripheral resistance vessels of the systemic circulation. Thus, under the influence of Ca^{2+} antagonists, any restriction of the mechanical energy expenditure of the myocardium—even of slight degree—is always accompanied by a powerful decrease of coronary vascular tone and by a concomitant reduction in systemic flow resistance leading to a diminution of cardiac afterload. For instance, coronary vasodilation by Ca^{2+} antagonists usually occurs in a dosage range which is only one-third to one-tenth of that required to produce negative inotropic effects on the heart in situ.

The decisive action of Ca^{2+} antagonists on coronary smooth muscle is excitation–contraction uncoupling, which can be easily demonstrated in vitro on the model of a potassium-induced spasm. In figure 19–16 are shown the results of a comparative study [5, 6] on pig coronary strips with different Ca^{2+} antagonists. The ordinate indicates the percentages of excitation–contraction uncoupling obtained. The abscissa shows on a logarithmic scale the molar concentrations of the Ca^{2+}-antagonistic compounds applied. Obviously, all Ca^{2+} antagonists tested in this series are more potent than papaverine. In comparison with papaverine, ni-

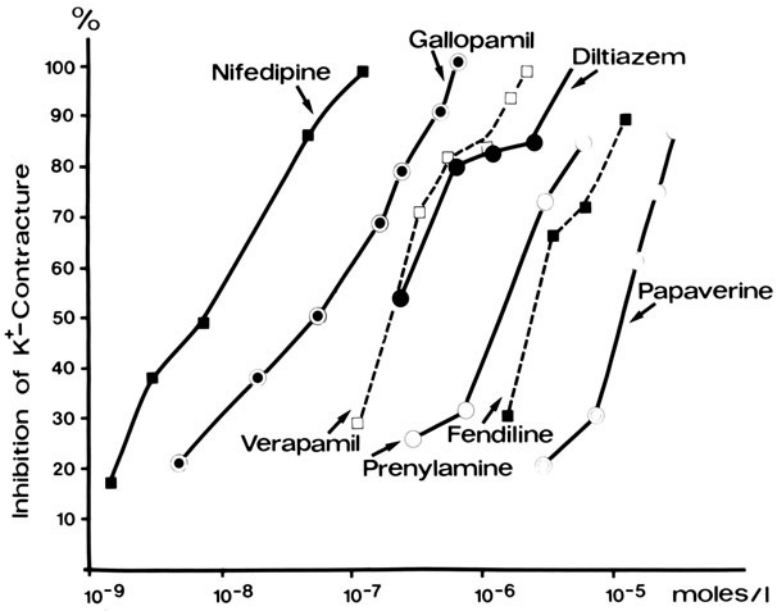

FIGURE 19–16. Relaxation (%) of K^+-depolarized pig coronary strips by various Ca^{2+} antagonists. Comparison of the relaxing potencies of these drugs administered to K^+-depolarized, fully contractured, pig coronary strips. In these experiments the time of exposure to the rich K^+-rich (43 m*M* KCl) Tyrode solution was kept constant (40 min). Then the Ca^{2+} antagonists were added and the maximum relaxation, reached within 1 h, measured. In comparison with the coronary relaxing potency of papaverine, nifedipine is approximately 3000 times, gallopamil 300 times, and verapamil and diltiazem 50–100 times stronger. Each point represents the average relaxation calculated from at least 15 individual experiments for each concentration, SE not exceeding ± 2%. Ca^{2+} content always 1 m*M*; temperature, 35°C; pH, 7.4; oxygenation with a gas mixture of 97% O_2 and 3% CO_2. Collection of experiments from Grün and Fleckenstein [11] and Fleckenstein [6].

fedipine is approximately 3000 times stronger, followed by D-600 (gallopamil), verapamil, and diltiazem. Thus the highly specific Ca^{2+} antagonists of group A proved to be the most effective coronary vasodilators as well. Furthermore, it is to be noted that they exert this coronary vasodilator action at the right place, that is to say, on the *great extramural coronary stem arteries* (including collaterals and anastomoses). In fact more than 95% of the stenosing atherosclerotic processes are located in this particular part of the coronary bed. Circulatory improvement is most evident in cases of Prinzmetal "variant" angina and other forms of coronary spasm that are frequently superimposed on eccentric atheromatous lesions or may even occur without angiographic evidence of structural obstacles.

However, the most important therapeutic prospects will possibly arise from the prophylactic efficacy of certain Ca^{2+} antagonists against arterial calcinosis. This effect has been studied extensively in our laboratory since 1971 on rats treated with high doses of vitamin D or dihydrotachysterol, or on diabetic animals after administration of alloxan. Interestingly enough, the destruction of the arterial media produced by these experimental procedures resembles the special form of calcific human arteriosclerosis described by Mönckeberg, or the spontaneous calcinosis of senescent arteries. Obviously, intracellular Ca^{2+} overload starts a pathogenic mechanism which is equally deleterious for both myocardial fibers and vascular smooth muscle cells. On the other hand, prophylactic treatment with Ca^{2+} antagonists such

as verapmil and diltiazem may protect myocardial *and* vascular integrity (for more details, see the research reports [5, 49–53]). It is now up to clinical studies to clarify what practical consequences will possibly ensue from these experimental observations with respect to an eventual long-term therapy with Ca^{2+} antagonists in coronary patients.

Summary

Ca^{2+} antagonists interfere with slow-channel-mediated transmembrane Ca^{2+} influx into excited atrial and ventricular fibers. Thereby Ca^{2+}-dependent splitting of ATP, mechanical tension development, and oxygen requirement of the beating heart are restricted. Apart from lowering contractile energy expenditure, Ca^{2+} antagonists also reduce the inward Ca^{2+} current into sinoatrial and atrioventricular nodal cells. This slows spontaneous impulse discharge from nomotopic pacemakers as well as atrioventricular conduction velocity. Ectopic focal activity arising from altered myocardial fibers is also damped by most of these drugs. Thus Ca^{2+} antagonists counteract the stimulatory cardiac effects of β-adrenergic catecholamines in almost every respect. Moreover, Ca^{2+} antagonists protect the heart against harmful intracellular Ca^{2+} overload, which has to be considered the decisive etiologic factor in cardiac necrosis due to (a) sympathetic over-stimulation, (b) high doses of vitamin D or dihydrotachysterol, (c) alimentary K^+ and Mg^{2+} deficiency, or (d) genetic defects as in cardiomyopathic Syrian hamsters. Even hypoxic and ischemic myocardial injury can be alleviated or retarded by Ca^{2+} antagonists since, also in this situation, early intracellular Ca^{2+} overload aggravates and precipitates structural decay.

Ca^{2+} antagonists also reduce Ca^{2+}-dependent tone and abolish spastic contractility in vascular smooth muscle. In coronary patients, they relax the vasculature of the great extramural coronary trunks. However, they also dilate the resistance vessels in systemic circulation, thereby relieving the heart indirectly. Moreover, experimental evidence exists indicating that certain Ca^{2+} antagonists can protect the arterial walls against Ca^{2+} overload, thus interfering with one of the most important etiologic factors of arteriosclerotic vascular destruction.

References

1. Fleckenstein A: Die Bedeutung der energiereichen Phosphate für Kontraktilität und Tonus des Myokards. Verh Dtsch Ges Inn Med 70:81–99, 1964.
2. Fleckenstein A, Döring HJ, Kammermeier H: Experimental heart failure due to inhibition of utilisation of high-energy phosphates. In: Proceedings of and International Symposium on the Coronary Circulation and Energetics of the Myocardium, Milan, 1966. Basle: Karger, 1967, pp 220–236.
3. Fleckenstein A, Kammermeier H, Döring HJ, Freund HJ: Zum Wirkungsmechanismus neuartiger Koronardilatatoren mit gleichzeitig Sauerstoff-einsparenden Myokard-Effekten, Prenylamin und Iproveratril. Z Kreisl Forsch 56:716–744 and 839–853, 1967.
4. Fleckenstein A, Tritthart H, Fleckenstein B, Herbst A, Grün G: A new group of competitive Ca-antagonists (Iproveratril, D 600, Prenylamine) with highly potent inhibitory effects on excitation–contraction coupling in mammalian myocardium. Pflugers Arch 307:R25, 1969.
5. Fleckenstein A: Calcium antagonism in heart and smooth muscle: experimental facts and therapeutic prospects. Monograph edited by John Wiley. New York: John Wiley, 1983.
6. Fleckenstein A: Specific pharmacology of calcium in myocardium, cardiac pacemakers, and vascular smooth muscle. Annu Rev Pharmacol Toxicol 17:149–166, 1977.
7. Fleckenstein-Grün G: Control of coronary spasms by calcium antagonists. In: Godfraind T, Albertini A, Paoletti R (eds) Calcium modulators. Amsterdam: Elsevier Biomedical, 1982, pp 141–154.
8. Fleckenstein-Grün G, Fleckenstein A: Ca-dependent changes in coronary smooth muscle tone and the action of Ca-antagonistic compounds with special reference to Adalat. In: Lochner W, Braasch W, Kroneberg G (eds) New therapy of ischemic heart disease. 2nd International Adalat Symposium, Amsterdam, 1974. Berlin: Springer-Verlag, 1975, pp 66–75.
9. Fleckenstein-Grün G, Fleckenstein A: Calcium-Antagonismus, ein Grundprinzip der Vasodilatation. In: Fleckenstein A, Roskamm H (eds) Calcium-Antagonismus. Proceedings of an international symposium on calcium antagonism, Frankfurt, December 1978. Berlin: Springer-Verlag, 1980, pp 191–207.
10. Fleckenstein-Grün G, Fleckenstein A: Calcium antagonism, a basic principle in vasodilation. In: Zan-

chetti A, Kirkler DM (eds) Calcium antagonism in cardiovascular therapy: experience with verapamil. Proceedings of an international symposium, Florence, 2–4 October 1980. Amsterdam: Excerpta Medica, 1981, pp 30–48.
11. Grün G, Fleckenstein A: Die elektromechanische Entkoppelung der glatten Gefässmuskulatur als Grundprinzip der Coronardilatation durch 4-(2′-Nitrophenyl)-2,6-dimethyl-1,4,dihydropyridin-3,5-dicarbonsäure-dimethylester (Bay a 1040, Nifedipin). Arzneimittelforsch 22:334–344, 1972.
12. Fleckenstein A: Specific inhibitors and promoters of calcium action in the excitation–contraction coupling of heart muscle and their role in the production or prevention of myocardial lesions. In: Harris P, Opie L (eds) Calcium and the heart. Proceedings of the meeting of the european section of the international study group for research in cardiac metabolism, London, 6 September 1970. London: Academic, 1971, pp 135–188.
13. Fleckenstein A, Döring HJ, Janke J, Byon YK: Basic actions of ions and drugs on myocardial high-energy phosphate metabolism and contractility. In: Schmier J, Eichler O (eds) Handbook of experimental pharmacology. New series vol 16/3. Berlin: Springer-Verlag, 1975, pp 345–405.
14. Kohlhardt M, Bauer B, Krause H, Fleckenstein A: Differentiation of the transmembrane Na and Ca channel in mammalian cardiac fibres by the use of specific inhibitors. Pflugers Arch 335:309–322, 1972.
15. Kohlhardt M, Fleckenstein A: Inhibition of the slow inward current by nifedipine in mammalian ventricular myocardium. Naunyn Schmiedebergs Arch Pharmacol 298:267–272, 1977.
16. Winegrad S: Studies of cardiac muscle with a high permeability to calcium produced by treatment with ethylenediamine-tetraacetic acid. J Gen Physiol 58:71–93, 1971.
17. Entmann ML, Allen JC, Bornet EP, Gillette PC, Wallick ET, Schwartz A: Mechanisms of calcium accumulation and transport in cardiac relaxing system (sarcoplasmic reticulum membranes): effects of verapamil, D 600, X 537 A and A 23187. J Mol Cell Cardiol 4:681–687, 1972.
18. Nayler WG, Szeto J: Effect of verapamil on contractility, oxygen utilization, and calcium exchangeability in mammalian heart muscle. Cardiovasc Res 6:120–128, 1972.
19. Watanabe AM, Besch HR Jr: Subcellular myocardial effects of verapamil and D 600: comparison with propranolol. J Pharmacol Exp Ther 191:241–251, 1974.
20. Frey M, Janke J: The effect of organic Ca-antagonists (verapamil, prenylamine) on the calcium transport system in isolated mitochondria of rat cardiac muscle. Pflugers Arch (Suppl) 359:R26, 1975.
21. Langer GA, Frank JS, Nudd LM, Seraydarian K: Sialic acid: effect of removal on calcium exchangeability of cultured heart cells. Science 193:1013–1015, 1976.
22. Watanabe AM, Besch HR Jr: The relationship between adenosine 3′,5′-monophosphate levels and systolic transmembrane calcium flux. In: Fleckenstein A, Dhalla NS (eds) Recent advances in studies on cardiac structure and metabolism. Vol 5: Basic functions of cations in myocardial activity. Baltimore: University Park Press, 1975, pp 95–102.
23. Wollenberger A: The role of cyclic AMP in the adrenergic control of the heart. In: Naylor WG (ed) Contraction and relaxation in the myocardium. London: Academic, 1975, pp 113–190.
24. Williamson JR, Woodrow ML, Scarpa A: Calcium binding to cardiac sarcolemma. In: Fleckenstein A, Dhalla NS (eds) Recent advances in studies on cardiac structure and metbolism. Vol 5: Basic functions of cations in myocardial activity. Baltimore: University Park Press, 1975, pp 61–71.
25. Späh F, Fleckenstein A: Nachweis einer strengen quantitativen Korrelation zwischen Hemmung des transmembranären Calcium-Influx und der mechanischen Spannungsentwicklung des Myokards unter dem Einfluss verschiedener Calcium-Antagonisten. In: Fleckenstein A, Rokamm H (eds) Calcium-Antagonismus. Berlin: Springer-Verlag, 1980, pp 29–41.
26. Fleckenstein A: Myocardstoffwechsel und Nekrose. In: Heilmeyer L, Holtmeier HJ (eds) In: VI Symposium "Herzinfarkt und Schock", dtsch Ges f Fortschritte auf dem Gebiet der Inneren Medizin, Freiburg, 8 November 1968. Stuttgart: Georg Thieme, 1968, pp 94–109.
27. Fleckenstein A, Döring HJ, Leder O: The significance of high-energy phosphate exhaustion in the etiology of isoproterenol-induced cardiac necrosis and its prevention by iproveratril, compound D 600, or prenylamine. In: Lamarche M, Royer R (eds) In: International symposium on drugs and metabolism of myocardium and striated muscle. Nancy: University of Nancy, 1969, pp 11–22.
28. Fleckenstein A, Janke J, Döring HJ, Leder O: Myocardial fibre necrosis due to intracellular Ca overload: a new principle in cardiac pathophysiology. In: Dhalla S (ed) Myocardial biology. Recent advances in studies on cardiac structure and metabolism, vol 4. Baltimore: University Park Press, 1974, pp 563–580.
29. Fleckenstein A, Janke J, Döring HJ, Leder O: Key role of Ca in the production of noncoronarogenic myocardial necroses. In: Fleckenstein A, Rona G (eds) Pathophysiology and morphology of myocardial cell alterations. Recent advances in studies on cardiac structure and metabolism, vol. 6. Baltimore: University Park Press, 1975, pp 21–32.
30. Fleckenstein A, Janke J, Döring HJ, Pachinger O: Ca overload as the determinant factor in the production of catecholamine-induced myocardial lesions. In: Bajusz E, Rona G (eds) Cardiomyopathies. Recent

advances in studies on cardiac structure and metabolism. vol 2. Baltimore: University Park Press, 1973, pp 455–466.
31. Lossnitzer K, Mohr W, Konrad A, Guggenmoos R: Hereditary cardiomyopathy in the Syrian golden hamster: influence of verapamil as calcium antagonist. In: Kaltenbach M, Loogen F, Olsen EGJ (eds) Cardiomyopathy and myocardial biopsy. Berlin: Springer-Verlag, 1978, pp 27–37.
32. Kaltenbach M, Hopf R, Keller M: Calciumantagonistische Therapie bei hypertroph-obstruktiver Kardiomyopathie. Dtsch Med Wochenschr 101:1284–1287, 1976.
33. Nayler WG, Grau A, Slade A: A protective effect of verapamil on hypoxic heart muscle. Cardiovasc Res 10:650–662, 1976.
34. Henry PD, Schuchleib R, Borda LJ, Roberts R, Williamson JR, Sobel BE: Effects of nifedipine on myocardial perfusion and ischemic injury in dogs. Circ Res 43:372–380, 1978.
35. Nagao T, Matlib MA, Franklin D, Millard RW, Schwartz A: Effects of diltiazem, a calcium antagonist, on regional myocardial function and mitochondria after brief coronary occlusion. J Mol Cell Cardiol 12:29–43, 1980.
36. Weishaar R, Ashikawa K, Bing RJ: Effect of diltiazem, a calcium antagonist, on myocardial ischemia. Am J Cardiol 43:1136–1143, 1979.
37. Clark RE, Christlieb IY, Ferguson TB, Weldon CS, Marbarger JP, Sobel BE, Roberts R, Henry PD, Ludbrook PA, Biello D, Clark BK: Laboratory and initial clinical studies of nifedipine, a calcium antagonist for improved myocardial preservation. Ann Surg 193:719–732, 1981.
38. Wit AL, Cranefield PF: Effect of verapamil on the sinoatrial and atrioventricular nodes of the rabbit and the mechanism by which it arrests reentrant atrioventricular nodal tachycardia. Circ Res 35:413–425, 1974.
39. Zipes DP, Fischer JC: Effects of agents which inhibit the slow channel on sinus node automaticity and atrioventricular conduction in the dog. Circ Res 34:184–192, 1974.
40. Zipes DP, Mendez C: Action of manganese ions and tetrodotoxin on atrioventricular nodal transmembrane potentials in isolated rabbit hearts. Circ Res 32:447–454, 1973.
41. Kohlhardt M, Figulla HR, Tripathi O: The slow membrane channel as the predominant mediator of the excitation process of the sinoatrial pacemaker cell. Basic Res Cardiol 71:17–26, 1976.
42. Tritthart H, Fleckenstein B, Fleckenstein A: Some fundamental actions of antiarrhythmic drugs on the excitability and contractility of single myocardial fibres. Naunyn Schmiedebergs Arch Pharmacol 269:212–219, 1971.
43. Singh BN, Vaughan Williams EM: A fourth class of antidysrhythmic action? Effect of verapamil on ouabain toxicity, on atrial and ventricular intracellular potentials and on other features of cardiac function. Cardiovasc Res 6:109–119, 1972.
44. Bender F: Die Behandlung der tachykarden Arrhythmien und der arteriellen Hypertonie mit Isoptin. Arzneimittelforsch 20:1310–1316, 1970.
45. Schamroth L, Krikler D, Garrett C: Immediate effects of intravenous verapamil in cardiac arrhythmias Br Med J 1:660–662, 1972.
46. Krikler D, Spurrell R: Verapamil in the treatment of paroxysmal supraventricular tachycardia. Postgrad Med J 50:447–453, 1974.
47. Spurrell R, Krikler D, Sowton E: Concealed bypasses of the atrioventricular node in patients with paroxysmal supraventricular tachycardia revealed by intracardiac electrical stimulation and verapamil. Am J Cardiol 33:590–595, 1974.
48. Spurrell R, Krikler D, Sowton E: Effects of verapamil on electrophysiological properties of anomalous atrioventricular connexion in Wolff–Parkinson–White syndrome. Br Heart J 36:256–264, 1974.
49. Fleckenstein A, Frey M, Leder O: Prevention by calcium antagonists of arterial calcinosis. In: Fleckenstein A, Hashimoto K, Herrmann M, Schwartz A, Seipel L (eds) New calcium antagonists: recent development and prospects. Proceedings of the diltiazem workshop, Freiburg, 10 May 1982. Stuttgart: G Fischer Verlag, 1983, pp 15–31.
50. Fleckenstein A, Frey M, v Witzleben H: Vascular calcium overload: a pathogenic factor in arteriosclerosis and its neutralization by calcium antagonists. In: Kaltenbach M, Neufeld HN (eds) 5th International Adalat Symposium: new therapy of ischaemic heart disease and hypertension. Proceedings, Berlin, 12–14 May 1982. Amsterdam: Excerpta Medica, 1983, pp 36–52.
51. Fleckenstein A, v Witzleben H, Frey M, Milner TG: Prevention of cataracts of alloxan-diabetic rats by long-term treatment with verapamil. Pflugers Arch (Suppl) 391:R12.
52. Frey M, Keidel J, Fleckenstein A: Verhütung experimenteller Gefäss-Verkalkungen (Mönckeberg's Typ der Arteriosklerose) durch Calcium-Antagonisten. In: Fleckenstein A, Roskamm H (eds) Calcium-Antagonismus. Proceedings of an international symposium on calcium antagonism, Frankfurt, December 1978. Berlin: Springer-Verlag, 1980, pp 258–264.
53. Janke J, Hein B, Pachinger O, Leder O, Fleckenstein A: Hemmung arteriosklerotischer Gefässprozesse durch prophylaktische Behandlung mit $MgCl_2$, KCl und organischen Ca^{++}-Antagonisten (quantitative Studien mit Ca^{45} bei Ratten). In: Betz E (ed) Vascular smooth muscle. Proceedings of a satellite symposium 25th Congress International Union Physiological Sciences, Tübingen, 20–24 July 1971. Berlin: Springer-Verlag, 1972, pp 71–72.
54. Fleckenstein A, Grün G, Byon YK, Döring HJ, Tritthart H: The basic Ca antagonistic actions of nifedipine on cardiac energy metabolism and vascular smooth muscle tone. In: Hashimoto K, Kimura E,

Kobayashi T (eds) New therapy of ischemic heart disease. First International Nifedipine (Adalat) Symposium, Tokyo, 1973. Tokyo: University of Tokyo, 1975, pp 31–44.

55. Fleckenstein A, Tritthart H, Döring HJ, Byon YK: Bay a 1040, ein hochaktiver Ca^{++}-antagonistischer Inhibitor der elektro-mechanischen Koppelungsprozesse im Warmblüter-Myokard. Arzneimittelforsch 22:22–33, 1972.
56. Fleckenstein A, Fleckenstein-Grün G, Byon YK, Haastert HP, Späh F: Vergleichende Untersuchungen über die Ca-antagonistischen Grundwirkungen von Niludipin (Bay a 7168) und Nifedipin (Bay a 1040) auf Myokard, Myometrium und glatte Gefässmuskulatur. Arzneimittelforsch 29:230–246, 1979.
57. Nakajima H, Hoshiyama M, Yamashita K, Kiyomoto A: Effect of diltiazem on electrical and mechanical activity of isolated cardiac ventricular muscle of guinea pig. Jpn J Pharmacol 25:383–392, 1975.
58. Fleckenstein A, Fleckenstein-Grün G, Byon YK: Fundamentale Herz- und Gefässwirkungen des Ca^{++}-antagonistischen Koronartherapeutikums Fendilin (Sensit^{R}). Arzneimittelforsch 27:562–571, 1977.
59. Fleckenstein-Grün G, Fleckenstein A, Byon YK, Kim KW: Mechanism of action of Ca^{2+}-antagonists in the treatment of coronary disease with special reference to perhexiline maleate. In: Proceedings of the symposium on perhexiline maleate, Strasbourg, 18 September 1976. Amsterdam: Excerpta Medica, 1978, pp 1–22.
60. Fleckenstein A: Experimentelle Pathologie der akuten und chronischen Herzinsuffizienz. Verh Dtsch Ges Kreisl-Forsch 34:15–34, 1968.
61. Fleckenstein, A: Fundamental actions of calcium antagonists on myocardial and cardiac pacemaker cell membranes. In: New Perspectives on Calcium Antagonists, GB Weiss ed., pp. 59–81, Am Physiol. Society, Clinical Physiological Series, 1981.
62. Fleckenstein, A: Pharmacology and electrophysiology of calcium antagonists. In: Calcium Antagonism in Cardiovascular Therapy: Experience with Verapamil; Proceed. of an Internat. Symp. on Calcium Antagonism in Cardiovascular Therapy, Florence, October 1980, A Zanchetti a. DM Krikler eds., pp. 10–29, Excerpta Medica, Amsterdam-Oxford-Princeton, 1981.

Acknowledgments

The figures 19–4, 19–5, 19–6 and 19–7 were reproduced from Fleckenstein [61] by courtesy of the American Physiological Society/Bethesda. The figures 19–11, 19–12, 19–13 and 19–14 originating from Fleckenstein [62] were released for reproduction by Excerpta Medica/Amsterdam-Oxford-Princeton.

20. CELLULAR ELECTROPHYSIOLOGY AND ISCHEMIA

Ralph Lazzara
and Benjamin J. Scherlag

Introduction

The conspicuous effects of ischemia on the electrocardiogram quickly caught the attention of clinicians who exploited them to diagnostic advantage. These electrocardiographic changes called for an explanation, which meant a description of the cellular electrophysiologic changes during ischemia that generated the electrocardiographic abnormalities. Although direct evidence bearing on the problem was scarce, constructs and schemas were plentiful. Textbooks of electrocardiography proudly displayed resting and action potentials from ischemic cells even before the technology for intracellular recording was well developed. The bases for these conceptions were the well-known depolarizing effect of injury on excitable cells and the idea that the duration of the action potential of ischemic cells was abbreviated. Explanations were built on the perception that the basic changes produced by ischemia were few and simple: partial depolarization, abbreviation of the action potential, or total loss of electrical activity because of cell death. Even after the development of intracellular recording, direct observations of cellular electrophysiologic changes during ischemia have been difficult and sparce. The true condition of ischemia occurs in the setting of the beating heart working under load and supplied with blood by the coronary circulation. Under these conditions intracellular recording is taxing, imprecise, and confined to the epicardial surface. Nonetheless, early recordings during acute ischemia confirmed the idea that ischemia caused a decrease in amplitude of the resting potential and abbreviation of the action potential [1, 2].

Recently the study of the cellular electrophysiologic effects of ischemia has been boosted by the growing interest in the arrhythmias that are caused by ischemia—an interest intensified by a full appreciation in the past decade of the awesome magnitude of the problem of sudden arrhythmic death in the western world. Frustrated by the unyielding difficulties in recording intracellular potentials in the beating heart, investigators have turned to oblique attacks on the problem. A common approach in recent years has been the isolation of tissues in vitro that had been ischemic in vivo. The obvious drawback of this approach is that the tissues are no longer ischemic at the time of study in vitro. Conclusions based on observations under these circumstances require the assumption that the cellular changes caused by ischemia in vivo persist for some time during superfusion in vitro even if the superfusate contains adequate oxygen and substrates.

Another favored approach has been to simulate ischemia in vitro by deprivation of oxygen and/or addition or alteration in concentrations of metabolites or ions to mimic changes thought to occur in ischemic regions in vitro. This approach suffers from the defects in knowledge of all the relevant changes occurring in ischemic regions in various stages and intensities of ischemia, and from the difficulty of

N. Sperelakis (ed.), PHYSIOLOGY AND PATHOPHYSIOLOGY OF THE HEART.

Martinus Nijhoff Publishing, Boston/The Hague/Dordrecht/Lancaster.

manipulating the intracellular environment to reproduce the changes occurring with ischemia. We do not have to dwell on the admonition that neither hypoxia nor metabolic inhibition is ischemia. Important effects of stagnant byproducts on cellular electrophysiology are receiving increasing scrutiny. This discussion will concentrate mainly on observations made from ischemic tissues in vivo and in vitro with selected references to studies of normal tissues superfused under simulated ischemic conditions, the most common of which has been simple hypoxia.

The Resting Potential

The earliest intracellular recordings of ischemic cells showed partial depolarization of subepicardial myocardial cells within a few minutes of coronary occlusion [1, 2]. Since these observations were made, the blood flow to subepicardial layers has been measured and appears to be about 25% of normal in the center of the ischemic region immediately after occlusion [3]. The partial depolarization of myocardial cells with ischemia was not startling, since it was known for a long time that hypoxia [4, 5] and metabolic inhibition [6] caused loss of resting potential. Also numerous studies have indicated that the extracellular concentration of potassium rises rapidly in ischemic regions because of leakage of potassium from the cell interior [7–10]. Recent evaluations with potassium-sensitive electrodes in vivo have quantified the changes in extracellular potassium in the myocardium following coronary occlusion [11]. The rise in extracellular potassium is greatest and most rapid in the subendocardial layers and least in the subepicardial layers, but concentrations in the neighborhood of 8 m*M*/l are reached in the subepicardial layers within a few minutes. These changes in extracellular potassium could account for the changes in resting potential in large part, if not entirely. The mechanism of the potassium loss from cells is not identified exactly. Studies of myocardial cells exposed to hypoxia in vitro indicate that a time-independent (background) potassium current is enhanced [12]. It was postulated that a rise in concentration of calcium in the cytosol may be the factor that augments the potassium current [13]. Also the rise in extracellular potassium would itself further enhance potassium permeability [14]. The time course of depression of the sodium–potassium pump during acute ischemia is uncertain [15]. The pump, if electrogenic in vivo, would contribute outward currents and augment the resting potential. Observations that potassium leak precedes depression of the sodium–potassium pump in hypoxia [16] suggest that depression of the pump is not a major factor in the depolarization that occurs very early in ischemia.

When the ischemia lasts hours or longer the living cells in the ischemic zone are variably depolarized. During these later stages it is unlikely that elevated extracellular potassium is the major determinant of the depolarization. Numerous studies show that the depolarization persists under conditions of superfusion with normal extracellular concentrations of potassium [17–29]. With prolonged ischemia it is probable that there is diminution of intracellular concentration (and activity) of potassium, with reduction of the ratio K_{in}–K_{out}, and attendant reduction of the potassium equilibrium potential. In addition, at later stages depression of the sodium–potassium pump [15] might reduce any contribution made by electrogenic pumping to the resting potential. Recently it was suggested that electrogenic pumping may contribute not only directly but also indirectly by providing hyperpolarizing current necessary to maintain the "normal" current–voltage relationship as opposed to another possible relationship that is downward (in the direction of inward current) shifted and has a stable resting potential at a more positive level [24]. The implication was that the membrane is capable of both relationships, but the "normal" predominates under the influence of hyperpolarizing current from the activity of the sodium–potassium pump, resulting in a normal resting potential.

The resting potentials of cells from chronically diseased human ventricle have been observed to be reduced (approximately 50 mV) and insensitive to changes in extracellular potassium concentration in the concentration range of 2–10 m*M* [24]. This finding sug-

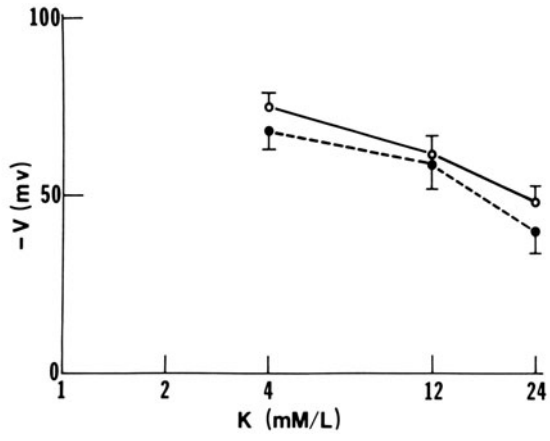

FIGURE 20–1. Relationship between transmembrane resting potential (V) and extracellular potassium (K) concentration for ischemic cells (solid circles) and bordering cells in the normal zone (circles) of epicardial preparations isolated from canine hearts 1–7 days after occlusion of the left anterior descending coronary artery. Means and standard deviations derived from ten separate studies of both ischemic and normal cells.

gested to the investigators that there might be a decrease in potassium conductance in these cells; that the membrane did not function primarily as a potassium electrode. Ischemic subepicardial cells isolated from canine hearts several days after coronary occlusion differ somewhat from normal subepicardial cells in the same hearts with respect to the relationship between extracellular potassium and membrane potential, but the differences are small. The relationship between extracellular potassium and membrane potential are depicted in figure 20–1. The downshift of the curve for the abnormal cells could be explained by decreased intracellular concentration of potassium.

The possibility that other specific ionic conductances contributed importantly to the resting potential of depolarized cells was investigated in human tissues by observing the effect of tetrodotoxin, a blocker of the fast channel, and methoxyverapamil, a blocker of the slow channel [24]. The failure of these agents to affect resting potential suggests that there was no significant resting inward current of sodium or calcium contributing a positive (depolarizing) component. However, observations of this type are sparse. There is a need for more information about the intracellular concentrations and comparative permeabilities of the various important ions after prolonged ischemia and about the effects of ischemia on steady-state current–voltage relationships of the membrane.

Cells of the specialized conducting system in ischemic regions are affected differently from adjacent myocardial cells. The Purkinje fibers in the region of supply of an occluded coronary artery are partially depolarized for several days after occlusion, but the superficial layers of Purkinje fibers survive and recover fully, unlike adjacent subendocardial myocardial cells which do not survive the first day of coronary occlusion in the dog [17–21]. Purkinje tissue is more resistant to oxygen deprivation in vitro than is working myocardium [5]. There is a possibility that the lesser requirements of Purkinje cells may be met in part by diffusion from the blood in the left ventricular chamber. One group of investigators has observed partial depolarization of Purkinje fibers in tissues isolated 20 min after coronary occlusion [29], a surprising finding in view of the comparative resistance of Purkinje fibers to hypoxia in vitro. There is uncertainty as to validity of these observations in tissues isolated during the unstable state of acute ischemia. It was speculated that a rise in extracellular potassium spilled from myocardial cells might be the operative factor in the depolarization.

The reasons for the depolarization of Purkinje fibers in later stages of ischemia (one day or more), as for that of myocardial cells, is unclear. The tendency of affected cells to recover toward normal amplitude of resting potential during several hours of superfusion, even with hypoxic solutions lacking foodstuffs, has suggested to some the action of a depressant agent(s) that is removed somewhat slowly (hours) during superfusion [19]. The recovery of Purkinje cells during superfusion is shown in figure 20–2. Of the various substances whose concentrations are elevated either intracellularly or extracellularly during ischemia, special notice recently has been taken of certain lipid breakdown products, the lysophosphoglycerides [30–32]. Cells exposed in vitro to

these substances in concentrations estimated to occur in ischemic regions developed electrophysiologic abnormalities resembling those of ischemic cells. There has been considerable interest in the concept that lipid breakdown products may lodge in the sarcolemma and alter its properties [33]. While this idea has some evidential support the role of this mechanism in electrophysiologic abnormalities in vivo remains to be defined precisely.

The survival for some time of myocardial and Purkinje cells with heterogeneously abnormal properties bears on the controversy concerning the size, configuration, and location of a "border zone" surrounding myocardial infarction [34]. It has been proposed that with ischemia cells are either normally oxygenated or lethally hypoxic; intermediate states constituting a substantial border zone do not exist [35]. In its simple form this hypothesis does not explain the prolonged survival of cells with abnormal function, a phenomenon definitively demonstrated in myocardium after ischemic injury. As a specific example, in the dog after coronary occlusion a canopy of myocardial cells just below the epicardium survives for some time and constitutes a border zone with abnormal cellular electrophysiologic properties, overlying the infarct. Since the method of recording of intracellular potentials is safe from the criticism that the sample is an admixture of normal and dead tissue, the hypothesis must be modified to include the possibilities that intermediate states of cellular oxygenation can persist for long times, or that normally oxygenated cells can be affected for a long time by the by-products of necrosis, or (the least plausible) that the cells can survive for a long time in a severely hypoxic state. Tissues exposed to uniform hypoxia in vitro are affected heterogeneously so the heterogeneity must be independent in part of blood flow [36].

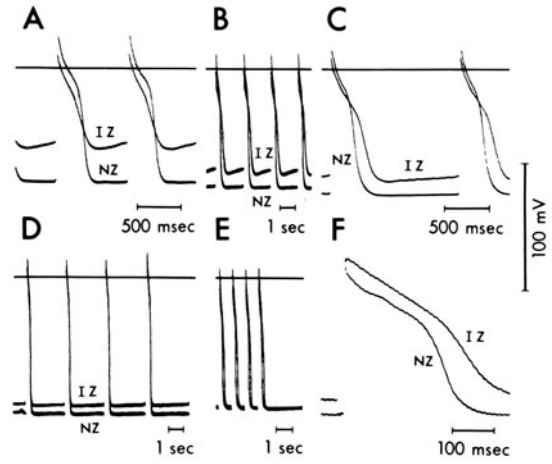

FIGURE 20–2. Recovery toward normal during superfusion of partially depolarized Purkinje fiber (IZ) isolated 24 h after coronary occlusion in the dog. Action potentials of the Purkinje fiber in the ischemic zone were recorded 10 min after isolation *(A)* along with a simultaneous recording from a Purkinje cell in the normal zone (NZ). The cell was partially depolarized, and showed enhanced diastolic depolarization and a prolonged action potential. After 1½ h of superfusion *(B)* the resting potential had increased significantly in amplitude. During continued superfusion for 12 h *(C-E)* both resting potential and the rate of diastolic depolarization were restored to normal. However, the prolonged action potential persisted *(F)*. The trace for the cell in the IZ was moved in *F;* the differences in resting potential are artifactual. Reproduced by permission of the American Heart Association from Lazzara et al. [19].

The Action Potential Upstroke: the Excitatory Current

Pronounced depression of the upstrokes of action potentials occurs early in ischemia [2, 37–40] and is a consistent feature of affected cells in later stages [17–28]. The depolarization of cells would entail depression of upstroke velocity and amplitude because of normal inactivation of the fast channel, but it is clear that there is more depression than can be accounted for on this basis. The relationship between membrane potential and $\dot{V}_{max}$ is downshifted in ischemic cells as illustrated in figures 20–3 and 20–4. The downshifted curves imply direct depression of the excitatory current. There is a great variability in the position of the abnormal curve compared with the normal. Often the curves are shifted severely downward and leftward, indicating that the excitatory current is not only severely depressed but is generated at levels of membrane potential where the normal fast channel is completely inactivated. This type of relationship (fig. 20–4) places suspicion

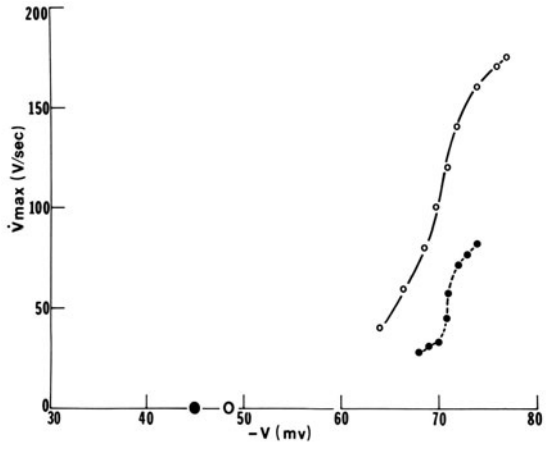

FIGURE 20–3. Relationship between maximal upstroke velocity (V_{max}) and transmembrane potential (V) at the time of excitation for a cell in the normal zone (circles) and a cell in the ischemic zone (solid circles) of an epicardial preparation isolated two days after coronary occlusion in the dog. The transmembrane potential was altered by changing concentration of K^+ in the superfusate. The symbols on the abscissa indicate resting potentials at K^+ concentration of 24 mM/l.

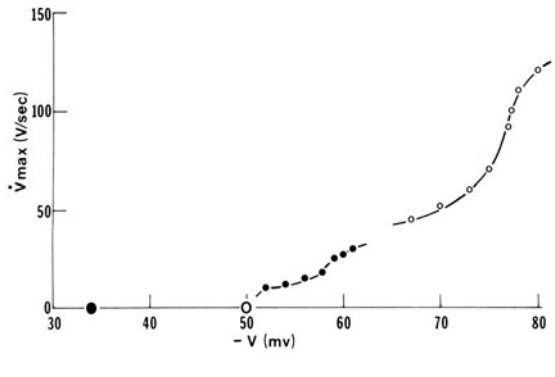

FIGURE 20–4. Relationship between maximal upstroke velocity (V_{max}) and transmembrane potential (V) at the time of excitation of a cell in the normal zone (circles) and the ischemic zone (filled circles) of an epicardial preparation isolated 24 h after coronary occlusion in the dog. The transmembrane potential was altered by changing the concentration of K^+ in the superfusate. The symbols on the abscissa indicate resting potentials at K^+ concentration of 24 mM/l.

on the slow channel. However, observations after blockade of the fast channel (tetrodotoxin) and the slow channel (methoxyverapamil) indicated that the fast channel can be altered with ischemia to generate depressed upstrokes at low levels of resting potential [27]. Apparently the voltage regulation of the "gates" is affected. The effect of tetrodotoxin on a greatly depressed upstroke from an ischemic subepicardial myocardial cell is shown in figure 20–5. In acutely ischemic porcine hearts where severe conduction depression and reentry occur in ischemic subepicardial layers, the excitatory current appears to be generated by depressed fast channels since lidocaine further depressed the responses [41]. Lidocaine also has pronounced effects on the tetrodoxtoxin-sensitive depressed responses of ischemic canine myocardium [42]. In human endocardial specimens taken from patients with ventricular aneurysms, however, depressed upstrokes sensitive to slow-channel blockers have been observed along with others sensitive to tetrodotoxin [24, 26]. The ineffectiveness of slow-channel blockers against ventricular tachycardia in ischemic heart disease and the effectiveness of agents that block the fast channel such as lidocaine and procainamide suggest that depressed rapid channels are most often involved in the generation of reentrant tachyarrhythmias in man. In the isolated whole heart, perfusion of the left anterior descending coronary artery with solutions having low P_{O_2}, no glucose, high K^+, and low pH depressed the upstrokes of action potentials as severely as acute coronary occlusion [43]. This finding was contrary to previous observations in vitro by this group of investigators, who had found that ischemic blood depressed action potentials in vitro more than superfusate with low P_{O_2}, no glucose, high K^+, and low pH [44]. The investigators suggested that the differences in the two studies might be due to the lack of contractile work and the higher oxygen tensions in vitro compared to the conditions in vivo. The available evidence indicates that the simple factors manipulated in those experiments could account in large part, if not entirely, for the depression of responsiveness with acute ischemia. In later stages it is likely that other factors are at work.

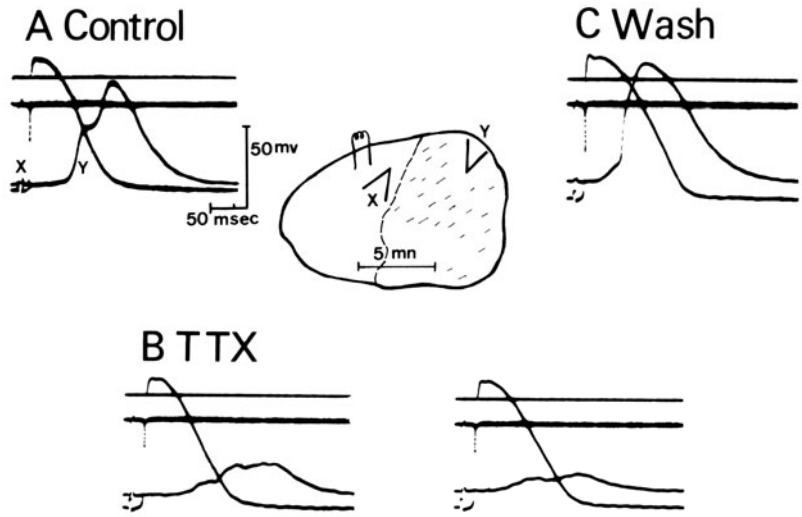

FIGURE 20–5. Influence of tetrodotoxin (TTX) on the severely depressed and irregular upstroke of an ischemic myocardial cell (Y) from an epicardial preparation isolated three days after coronary occlusion in the dog. Action potentials recorded from a cell bordering the ischemic zone (X) are also shown along with the upstroke velocity (middle trace) of the border cell. TTX added to the superfusate greatly depressed the response of the cell in the ischemic zone while depressing modestly (approximately 25%) $\dot{V}_{max}$ of the cell in the normal zone.

The upstrokes are not only depressed, but also frequently irregular. An illustration of this phenomenon is shown in figure 20–6, which displays action potentials generated by ischemic subepicardial cells. Such a phenomenon might derive from heterogeneity of fast channels on a microscale–groups of channels in the vicinity of the microelectrode with different voltage dependence and kinetics. Also there might be influence of irregular wavefronts of activation on the upstroke, that is, asynchrony of input into the impaled cell. A hint of this mechanism can be extracted from the recordings of figure 20–6. Differences between the action potentials in 6A and 6B were produced by alteration of the stimulus intensity (less in 6B). It is likely that the stimulus current affected the activation wavefront rather than the cell itself since the cell was activated 15–20 ms after the stimulus. The greater stimulus intensity (fig. 20–6A) was followed by an irregular upstroke, but the lesser intensity stimulus resulted in a long-step potential preceding a more irregular upstroke. It has been shown that the sequence of activation in ischemic regions may be very irregular especially at rapid rates when refractoriness is encountered [45–48]. The depressed and irregular upstrokes are reflected in part in the low-amplitude, polyphasic electrograms recorded from ischemic myocardium [48–53]. Although there is little direct evidence bearing on cell-to-cell coupling and internal resistance in ischemia, there is a suspicion that partial uncoupling of cells occurs, accompanied by a rise in internal resistance. It is known that elevation of free calcium and sodium and fall in pH in the cytosol, expected alterations in ischemia, causes cell uncoupling by increasing nexal resistance [54–56]. There is a rise in internal resistance in hypoxic myocardium associated with a rise in resting tension [57], findings that suggest cell uncoupling associated with increased concentration of cytosolic calcium. It is reasonable to presume that this uncoupling effect is heterogeneous and contributes to slowing and dishevelment of the sequence of activation and possibly to the irregularities of the upstroke. The consequences of this effect are not simple. Partial uncoupling could actually enhance the probability of excitation, and increase the ve-

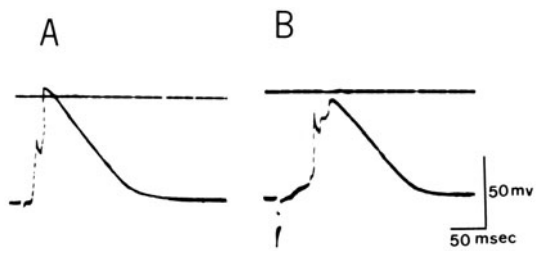

FIGURE 20–6. Irregular upstroke of a myocardial cell in the ischemic zone of an epicardial preparation isolated two days after coronary occlusion in the dog. Stimulus intensity in *A* was higher than that in *B* as shown by the differing amplitudes of the stimulus artifact. There was greater irregularity of the upstroke at the lower stimulus intensity *(B)*.

locity of the upstroke, given a depression of excitatory current [58]. With the reduced space constant, less of the debilitated current would be dissipated in flow along the sarcoplasm and more would be available to charge the membrane capacitor to the threshold potential.

Repolarization and Refractoriness

With acute ischemia there is consistently an abbreviation in the duration of the action potential, a hastening of repolarization mainly attributable to a shortened plateau [1, 2, 29, 38–40]. Hypoxia causes similar effects as acute ischemia except that it requires a longer time with hypoxia in vitro [44, 59] to produce changes that occur within minutes of ischemia in vivo [1, 2, 37–40]. The alteration in membrane properties that condition the change in configuration of the action potential have been examined in hypoxia [12]. It appears that with early and mild hypoxia there is enhancement of a time-independent potassium current. This finding is consonant with previous observations of increase in potassium efflux with hypoxia [16]. This increase in potassium conductance could be related to an increase in cytosolic calcium. Other observations indicate that, with more severe hypoxia, depression of the slow inward current contributes to the loss of the plateau [60]. The demonstration of the control of cyclic AMP and the dependence on energy of the slow inward current makes plausible the inference that the current is reduced in later stages of ischemia when ATP levels are low [61, 62]. It is not certain that similar mechanisms occur with ischemia, but the similarity in the changes in repolarization, the observed increases in potassium eflux, and the rapid decrease in contractile force with ischemia suggest that increase in potassium conductance and decrease in slow inward current may be operative factors. Whereas changes in repolarization may be the first change with hypoxia in vitro, with ischemia partial depolarization of the membrane appears at about the same time [1, 2, 37–40], probably because of the capture of leaked intracellular potassium in the extracellular space. The rise in extracellular potassium with ischemia in vivo would also be a factor in action potential shortening and increased potassium conductance.

In later stages of ischemia, the abnormalities of repolarization are varied. Repolarization has been observed to be abbreviated or prolonged [17–29]. In general the durations of repolarization of ischemic subepicardial myocardial cells studied 1–10 days after coronary occlusions are normal or slightly shortened, but greatly prolonged action potentials have been observed in deeper layers of ischemic myocardium [22] and in surviving subendocardial myocardial cells in the first few months after coronary occlusion in the cat [25]. Peripheral Purkinje cells isolated 1–5 days after coronary occlusion in the dog uniformly have prolonged action potentials [17–20]. The basis for the changes in later stages of ischemia are speculative at this time. Again, one may ruminate on the possible role of the products of ischemia. Prior elevation of lactate [63], CO_2 acidosis [64], and lysophosphoglycerides [30] among other things have been shown to delay repolarization of cardiac cells. The ionic mechanisms that condition delay in repolarization in ischemia are not known.

The relationship of repolarization to cycle length, i.e., the rate dependence, can be abnormal. Blunted or flat curves relating action potential duration to cycle length have been observed [22, 24]. The basis for the relative insensitivity of repolarization to changes in cy-

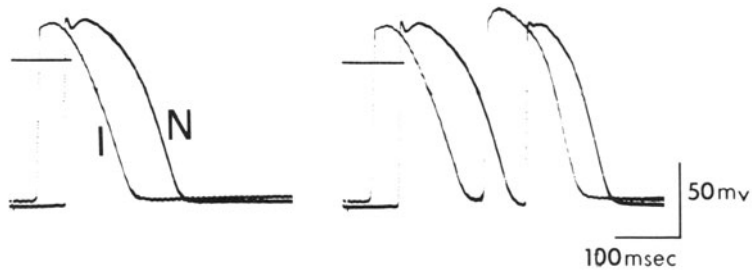

FIGURE 20–7. Anomalous response to premature stimulation of the action potential plateau of an ischemic myocardial cell. On the *left* are shown the action potentials recorded from a myocardial cell from the ischemic zone (I) and the normal zone (N) in an epicardial preparation isolated five days after coronary occlusion in the dog. On the *right* are shown the response of the two cells premature stimulation. The action potential of the cell in the ischemic zone has larger amplitude especially during the plateau phase, and the duration of the plateau is prolonged with the premature beat as compared with the driven beat. The cell from the normal zone has the normal response of shortening of plateau and action potential duration.

cle length in certain ischemic cells is speculative for lack of direct evidence. Depression of the slow inward current in later stages of ischemia might mitigate rate-dependent changes in free calcium in tthe cytosol and the consequent modulation of repolarizing potassium currents.

Ischemic subepicardial myocardial cells isolated in vitro frequently show an odd response to premature stimulation. There is often a range of coupling intervals for premature stimulation when there is anomalous prolongation of the plateau phase of the action potential. Along with the prolongation of the plateau there is an increase in amplitude of the action potential. This increase in the amplitude of the action potential is not accompanied by an increase in conduction velocity; rather the upstroke velocity is reduced. These changes could be explained by an increase in slow current, but the reason for the increase during this interval of the cardiac cycle is unclear. An example of this anomalous behavior is shown in figure 20–7.

Emphasis has been placed on the observation that the refractory periods of ischemic cells, especially more depressed ischemic cells, commonly exceed the durations of the action potentials, often substantially [21, 28]. The period of inexcitability (absolute refractory period) may occur throughout the action potential into diastole and a relatively long refractory period, marked by a greater requirement of excitatory current and a lesser response, may extend long into diastole. Moreover, it is commonplace for the relationship of postrepolarization refractoriness and rate to be anomalously direct; the greater the heart rate, the greater the refractory period. These features of postrepolarization refractoriness are shown in figure 20–8.

The anomalous refractoriness of ischemic cells, like the refractoriness of normal cells, has a rate dependence with a temporal evolution: the adjustment to a new rate is not complete within a single cycle. The time required for a new equilibrium and the magnitude of change over time may be greater with anomalous refractoriness than with normal refractoriness. Moreover there is a cycle-length dependence of the response that is superimposed on the refractory properties of a single cycle and that manifests also a temporal evolution to a new equilibrium state. In figure 20–8, at a cycle length of 3000 ms the refractory period of the ischemic cell approximated 400 ms. When the basic cycle length was reduced to 1000 ms, the refractory period of single cycle prolonged to approximately 650 ms, and the basic response, though outside the refractory period, was further depressed. The time dependence and cycle-length dependence of the response are illustrated in figures 20–9 and 20–10. When a

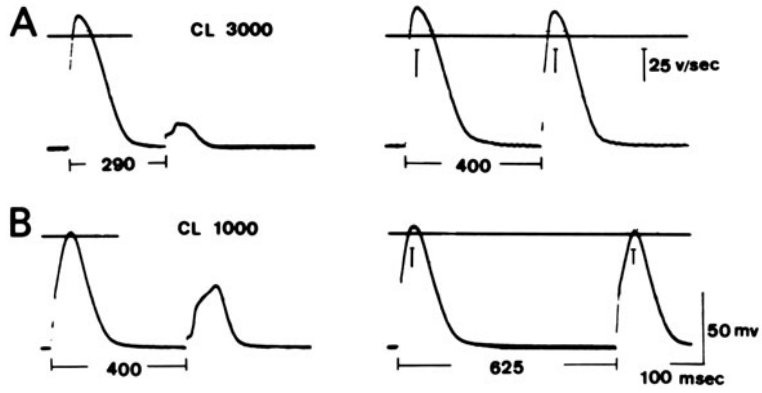

FIGURE 20–8. Anomalous refractory properties of ischemic myocardial cells. On the *left* are shown earliest responses of the ischemic cell at cycle length (CL) 3000 ms *(A)* and 1000 ms *(B)*. The absolute refractory period extends well into diastole and is longer at the shorter cycle length. Also shown are later responses that are nearly equivalent to the driven responses at the respective cycle lengths, marking the approximate ends of the relative refractory periods. The upstroke velocities of the driven and premature action potentials are represented by the vertical lines within the action potentials. The relative refractory periods of this are long in comparison with the relative refractory period associated with the terminal portion of repolarization in normal cells, and the durations of the relative refractory periods are longer at the shorter cycle length. Recordings were made from a cell in the ischemic zone of an epicardial preparation isolated three days after coronary occlusion in the dog.

more rapid rate is abruptly imposed there is a deterioration over time in the responses, sometimes culminating in quiescence. The introduction of a long cycle produces a response to the subsequent stimulus (fig. 20–10). This behavior has been referred to as "fatigue" [21]. This temporal evolution commonly is not dependent on changes in resting potential, but sometimes higher heart rates may be accompanied by progressive depolarization. This type of response is shown in figure 20–11. During short-term (minutes) changes in rate, loss of resting potential is not seen nearly as often as simple depression of response. Apparently there is an accumulation of a depressant factor or the depletion of an activator factor with time, these factors acting on the excitatory current. The greatly prolonged recovery times of excitatory current following an excitation apparently reflect delay in the recovery from inactivation of the depressed fast channel. The rate-related loss of resting potential could occur because of potassium accumulation in the extracellular space, but this seems unlikely in the superfused subepicardial preparation. Also rate-dependent depletion of ATP could depress an electrogenic pump.

It has been shown that the recovery from inactivation of the normal fast channel is delayed with partial depolarization [65] or with exposure to agents that depress the fast channel such as quinidine [66]. The recovery time observed with ischemic cells are too slow to be accounted for simply by partial depolarization. This observation implies a direct depressant effect of some ischemia-related factor on the fast channel. As with the atrioventricular node impingement of postrepolarization refractoriness at a certain range of rates causes a repetitive sequence in which successive responses deteriorate and conduct more slowly with each cycle, until a response is inadequate to propagate—the Wenckebach sequence, shown in figure 20–12.

The combination of heterogenous repolarization and variable postrepolarization recovery times of the excitatory current conspires to greatly disperse the refractory periods in ischemic regions. Moreover, a special feature of postrepolarization refractoriness is anomalously

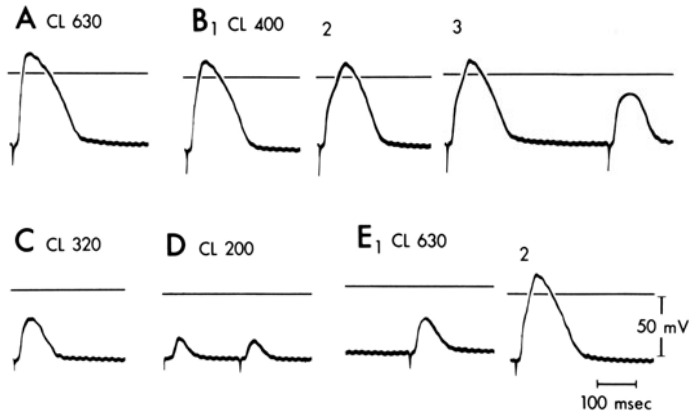

FIGURE 20–9. Rate-dependent and time-dependent (fatigue) depression of response in ischemic myocardial cells. Action potentials at various driven cycle lengths (CL) are shown in *A–D* with return to the original driving cycle in *E*. B-1 shows the response on immediate change form cycle length 630 ms to cycle length 400 ms whereas B-12 was recorded 20 s and B-3 40 s later. In B-3 there were alternating responses of greater and lesser magnitude. Immediately upon return to cycle length 630 ms in E-1 the response improved only slightly, but 15 s later (E-2) there was considerable improvement. The changes in responses occurred in the absence of appreciable changes in resting potential. Recordings were made from a cell in the ischemic zone of a epicardial preparation isolated five days after coronary occlusion in the dog.

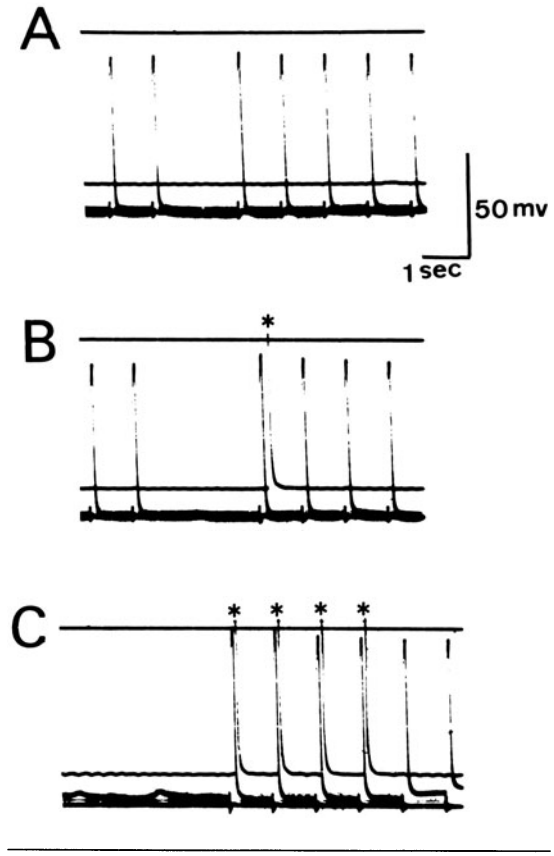

FIGURE 20–10. Restoration of excitation of a cell in the ischemic zone by the introduction of a pause. Action potentials were recorded from two cells in the ischemic zone of an epicardial preparation excised four days after coronary occlusion in the dog. Driving the preparation at a cycle length of 1 s resulted in quiescence of one cell after 10–15 s of drive. The introduction of a 2-s pause *(A)* was not followed by a response in the quiescent cell, but the introduction of a 3-s pause *(B)* was followed by a single response indicated by the asterisk. The introduction of a pause of 8 s *(C)* resulted in four consecutive responses, followed again by quiescence.

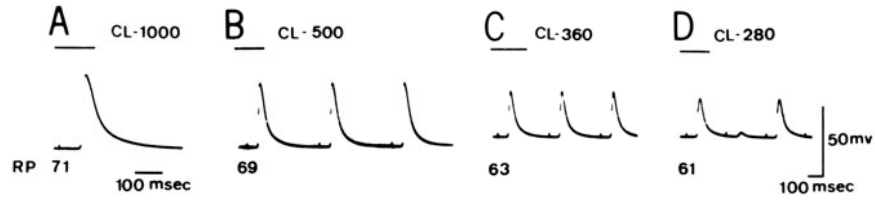

FIGURE 20–11. Rate-dependent loss of resting potential and depression of responsiveness in an ischemic myocardial cell of an epicardial preparation isolated one day after coronary occlusion in the dog. Resting potentials (RP) and action potentials at various cycle lengths are shown in *A* and *B*. There is increasing depolarization of the cell as the pacing cycle length (CL) was changed from 1000 ms to 280 msec. Along with the depolarization there was a depression of amplitude and upstroke velocity of the action potential.

long relative refractory periods, periods during which even more depressed responses are generated with greater disarray of the activation sequence. The likelihood of reentry in this environment is greatly enhanced. Detailed maps of the sequences of activation at the formation of reentrant excitation have documented the crucial role of the abnormal variability in refractory properties in producing the disordered activation sequence that culminates in reentry.

Automaticity

Diastolic depolarization of ischemic Purkinje fibers is more rapid and their automatic firing rate is increased [18, 19]. This disorder does not occur in the early phases of ischemia, but is prominent in the first day after occlusion and subsides gradually over several days. This behavior is illustrated in figure 20–2, which shows the devolution during superfusion of certain abnormalities, including enhanced automaticity, in an ischemic Purkinje fiber. During

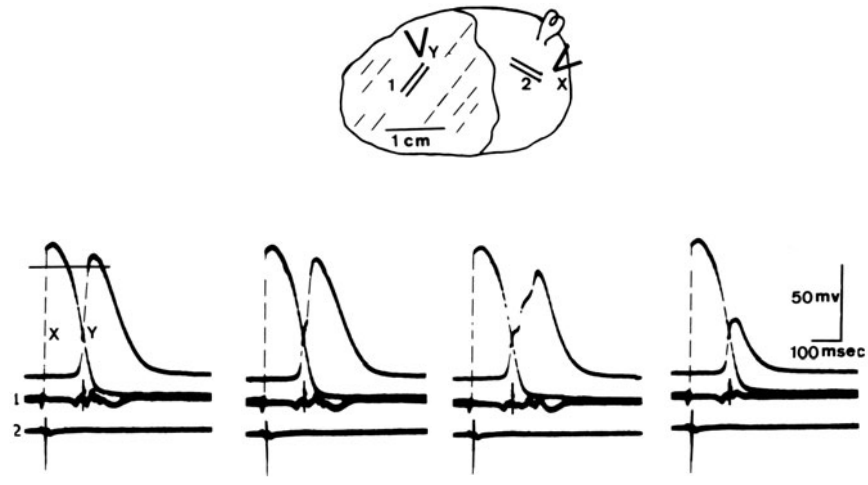

FIGURE 20–12. Progressive beat-by-beat depression of the upstroke of the action potential of an ischemic myocardial cell (Y) from an epicardial preparation isolated one day after coronary occlusion in the dog. Also shown are action potentials recorded from a cell in the normal zone (X) and electrograms recorded from the ischemic zone (1) and normal zone (2) in the vicinity of the respective action potential recordings.

superfusion, even with solutions low in oxygen and glucose, the rate of diastolic depolarization diminishes toward normal. The enhanced rate is sensitive to beta-adrenergic stimulation, but not dependent on it; restoration to normal is not achieved by beta blockade [19, 67]. It is less affected by lidocaine [68] than diastolic depolarization of normal Purkinje fibers and more affected by ethmozin [69]. These responses to the pharmacologic agents imply that the ionic currents that generate the diastolic depolarization may differ for ischemic fibers from those for normal fibers, but little else can be said at this time. Again, the action of a washable agent is suspect. A number of agents could be implicated. For example, lysophosphoglycerides enhance the rate of diastolic depolarization of Purkinje fibers.

Anomalous activity in the form of afterdepolarizations has been observed in Purkinje cells and deep myocardial cells within ischemic zones [22, 24, 70, 71]. Since afterdepolarizations have not been observed in subendocardial and subepicardial muscle cells, there is some question concerning the role of the dissection required to explore the deeper layers of myocardium in this phenomena. In view of the data supporting the conclusion that the phenomenon of delayed afterdepolarizations is dependent on oscillations of elevated concentrations of calcium in the cytosol [72], the occurrence of delayed afterdepolarizations would not be startling. The extent of the participation of this phenomenon in ectopic tachyarrhythmias in vivo remains to be ascertained. The ionic basis for early afterdepolarizations has received less attention, so comment in relation to ischemia is unwarranted.

Ectopy

Excitation of normal myocardium that originates in ischemic regions by whatever mechanism constitutes a form of ectopy. There is imposing evidence that reentrant excitation is the most common basis for ectopy. Reentry is a disorder of the sequence of activation that requires an ensemble of cells and a collusion of abnormal factors. The impulse must propagate continuously throughout the absolute refractory period of surrounding normal myocardium. Given the dimensions of the heart and the normal durations of refractoriness, this requirement entails abnormally slow conduction. It is characteristic of ischemic tissues that conduction is slowed to varying degrees. Slowed conduction is especially likely when excitation interrupts the anomalously long relative refractory periods. Therefore this abnormality has special relevance to ectopy. Since all the margins of the ischemic region are accessible to the original activation, for the impulse to avoid extinguishment by collision within the ischemic region, there must be a means of selectively directing the impulse, i.e., unidirectional block. Directionally selective propagation has been demonstrated abundantly in ischemic regions, most commonly on the basis of refractoriness. The impulse traveling along one direction encounters refractory tissues which recover in time for excitation by a delayed impulse arriving tardily from a route of slowed conduction. Finally, to complete a circuit there must be "holes"—regions between the outgoing and incoming limbs of the circuit which cannot be traversed so that the elements of the circuit retain their integrity, do not meld. This separatory region can be of abstract thickness, linear, as is proposed in the "leading circle" idea [73], wherein a line of refractoriness is supposed to separate the limbs of the circuit. In ischemic regions, the holes may be scars, or inexcitable but living myocardium. Inexcitability and prolonged quiescence of myocardium may be related to its refractory properties as we have seen (figs. 20–9 and 20–10). Thus, a complex temporal and spatial interaction of slowed conduction and heterogeneously abnormal refractory properties combines to form the elements of a reentry circuit.

The induction of repetitive firing, presumably reentrant, in a small, subepicardial preparation containing ischemic cells is shown in figure 20–13. The premature stimulation impinges on regions with differing refractory properties, producing quiescence in one region, greatly diminished responses in another and full responses in others. Because this reentry circuit was not mapped, it cannot be stated that the quiescent region provided any essential

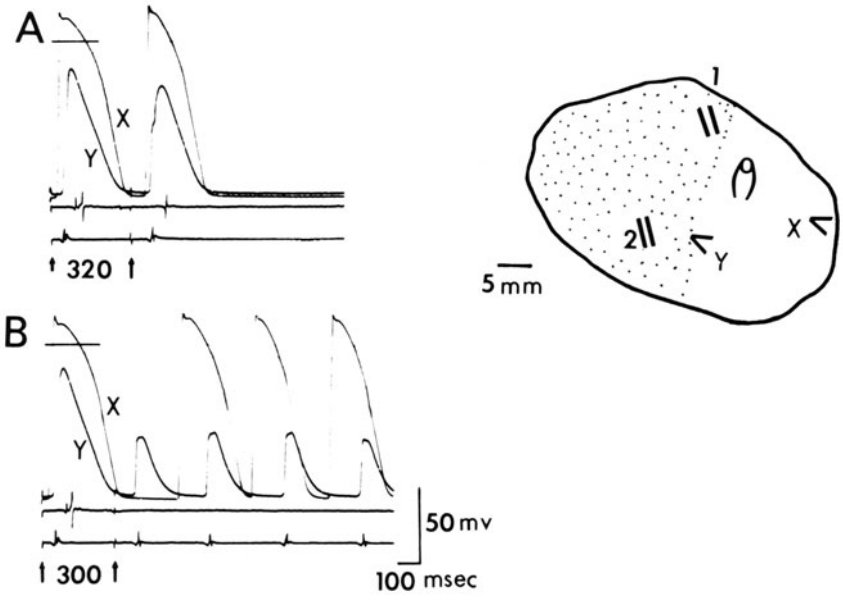

FIGURE 20–13. Induction of repetitive firing (tachyarrhythmia) in an epicardial preparation containing normal and ischemic (stippled) regions isolated four days after coronary occlusion in the dog. Action potentials are recorded from a cell at the border (Y) and in the normal zone and electrograms are recorded from the ischemic zone (1 and 2). At a premature coupling interval of 320 ms, all sites responded to the premature stimulation in a manner not much different from the driven responses. At a coupling interval of 300 ms, site 1 failed to respond and site Y responded with a diminutive action potential. Site X responded late with a full action potential which was followed by repetitive responses at sites 2, X and Y, the responses in Y all being diminutive. The tachycardia was accompanied by continuous block of propagation into site 1.

component of the reentry circuit. Nonetheless, it is clear that quiescent regions, holes, can be created from the abnormal refractory properties of the tissue. The premature stimulation that induced the tachycardia produced far greater variation in the timing and magnitude of responses of the various sites than the premature stimulation that did not lead to reentry.

Even the intrinsic generation of excitatory current, the automatic processes, can be influenced strongly by interaction among cells with different properties. For example, it has been shown that depolarizing current flow may induce or enhance diastolic depolarization in partially depolarized cells [74–76]. Current flow between cells at different levels of transmembrane potential could influence the automatic activity of a cell or cluster of cells. At sites of delayed conduction across an "excitatory gap", electrotonic interactions may occur between cells upstream that have repolarized and cells downstream that have been activated with delay—a phenomenon that has been called "reflection" [77]. This mechanism could enhance afterdepolarizations or produce electrotonic changes in transmembrane potentials that mimic intrinsic afterdepolarizations. Akin to this concept is the idea expressed in the phrase "focal reexcitation" [78], the excitation by flow of current between nearby cells at different levels of membrane potential because of differing rates of repolarization. There is little question that electronic currents during repolarization and diastole can be large around ischemic regions [45, 46]. They are the basis for the "injury currents" and "ST segment shifts" on the electrocardiogram, which are most prominent in acute ischemia. However, cell uncoupling would mitigate electrotonic current flow in later stages of ischemia. Excitation by electrotonic currents during repolarization and diastole is facilitated by conditions that produce

steep gradations or interruptions of properties, such as a sucrose gap in vitro. Where there is smooth, continuous gradation between cells the effect of electrotonic interaction is to minimize potential differences and current flow [79]. A case has been made for focal reexcitation or reflection in acute ischemia as a result of large "injury" currents and a narrow "inexcitable retion" between ischemic and normal tissues [80]. The extent to which heterogeneous properties result in electrotonic current flows which in turn lead to anomalous excitation is still uncertain. However, the prevailing role of heterogeneity in the production of reentrant excitation in ischemia regions is unquestionable.

Ischemia is exceedingly complex, comprising multiple factors of depletion and of production in varied temporal sequences, as well as interactions between heterogeneously abnormal and normal tissues, and indirect effects of ventricular dysfunction, mechanical stretch, altered autonomic activity, etc. The study of ischemia has proceeded haltingly because of the inability to record intracellular potentials in the ischemic condition in vivo. Nonetheless, understanding is growing and interest is thriving.

References

1. Kardesch M, Hogancamp CE, Bing RJ: Effect of complete ischemia on the intracellular electrical activity of the whole mammalian heart. Circ Res 6:715–725, 1958.
2. Samson WE, Scher AM: Mechanism of S-T segment alteration during acute myocardial injury. Circ Res 8:780–787, 1960.
3. Bishop SP, White FC, Bloor CM: Regional myocardial blood flow during acute myocardial infarction in the conscious dog. Circ Res 38:429–438, 1976.
4. Trautwein W, Gottstein U, Dudel J: Der Aktionsstrom der myokardfaser un sauerstoffmangel. Pflugers Arch 260:40–60, 1954.
5. Coraboeuf E, Gargouil YM, Laplaud J, Desplaces A: Action de l'anoxie sur les potentiels electriques des cellules cardiaques de mammiferes actives et enertes (tissu ventriculaire isole de cobaye). C R Acad Sci [D] (Paris) 246:3100–3103.
6. Webb JL, Hollander PB: Metabolic aspects of the relationship between the contractility and membrane potentials of the rat atrium. Circ Res 4:618–626, 1956.
7. Moore DJ: Potassium changes in the functioning heart under conditions of ischemia and congestion. Am J Physiol 123:443–447, 1938.
8. Harris AS, Bisteni A, Russel RA, Brigham JC, Firestone JE: Excitatory factors in ventricular tachycardia resulting from myocardial ischemia: potassium a major excitant. Science 119:200, 1954.
9. Regan TJ, Harman MA, Lehan PH, Burke WM, Odelwurtel HA: Ventricular arrhythmias and potassium transfer during myocardial ischemia and intervention with procainamide, insulin, or glucose solution. J Clin Invest 46:1657–1668, 1967.
10. Jennings RB, Crout JR, Smetters GW: Studies on distribution and localization of potassium in early myocardial ischemic injury. Arch Pathol 63:586–592, 1957.
11. Hill JL, Gettes LS: Effect of acute coronary artery occlusion on local myocardial extracellular K^+ activity in swine. Circulation 61:768–778, 1980.
12. Vleugels A, Vereecke J, Carmeliet E: Ionic currents during hypoxia in voltage-clamped cat ventricular muscle. Circ Res 47:501–508, 1980.
13. Bassingthwaighte JB, Fry CH, McGuigan JAS: Relationship between internal calcium and outward current in mammalian ventricular muscle: a mechanism for the control of the action potential duration? J Physiol (Lond) 262:15–37, 1976.
14. Carmeliet E: Chloride and potassium permeability in cardiac Purkinje fibers. Bruxelles: Arscia et Press Acad Europ, 1961.
15. Schwartz A, Wood JM, Allen JC, Bornet E, Entman ML, Goldstein MA, Sordahl LZ, Suzuki M, Lewis RM: Biochemical and morphologic correlates of cardiac ischemia. I. Membrane systems. Am J Cardiol 32:46–61, 1973.
16. Rau EE, Shine KI, Langer GA: Potassium exchange and mechanical performance in anoxic mammalian myocardium. Am J Physiol 232:H85, 1977.
17. Friedman PL, Stewart JR, Fenoglio JJ Jr, Wit AL: Survival of subendocardial Purkinje fibers after extensive myocardial infarction in dogs: in vitro and in vivo correlation. Circ Res 33:597–611, 1973.
18. Friedman PL, Stewart JR, Wit AL: Spontaneous and induced cardiac arrhythmias in subendocardial Purkinje fibers after extensive myocardial infarction in dogs. Circ Res 33:612–625, 1973.
19. Lazzara R, El-Sherif N, Scherlag BJ: Electrophysiological properties of Purkinje cells in one-day-old myocardial infarction. Circ Res 33:722–734, 1973.
20. Friedman PL, Fenoglio JJ, Wit AL: Time course for reversal of electrophysiological and ultrastructural abnormalities in subendocardial Purkinje fibers surviving extensive myocardial infarction. Circ Res 36:127–144, 1975.
21. Lazzara R, El-Sherif N, Scherlag BJ: Disorders of cellular electrophysiology produced by ischemia of the canine His bundle. Circ Res 36:444–453, 1975.
22. Ten Eick RE, Singer DH, Solberg LE: Coronary occlusion: effect on cellular electrical activity of the heart. Med Clin North Am 60:49–67, 1976.
23. Singer DH, Baumgarten CM, Ten Eick RE: Cellular electrophysiology of ventricular and other dysrhyth-

mias: studies on diseased and ischemic heart. Prog Cardiovasc Dis 24:97–156, 1981.
24. Ten Eick RE, Baumgarten CM, Singer DH: Ventricular dysrhythmia: membrane basis or of currents, channels, gates and cables. Prog Cardiovas Dis 24:157–188, 1981.
25. Myerburg RJ, Gelband H, Nilsson K, Sung RJ, Thurer RJ, Morales AR, Bassett AL: Long term electrophysiological abnormalities resulting from experimental myocardial infarction in cats. Circ Res 42:73–84, 1977.
26. Spear JF, Horowitz LN, Hodess AB: Cellular electrophysiology of human myocardial infarction. I. Abnormalities of cellular activation. Circulation 59:247–256, 1979.
27. Lazzara R, Scherlag BJ: The role of the slow current in the generation of arrhythmias in ischemic myocardium. In: Zipes DP, Bailey JC, Elharrar V (eds) The slow inward current and cardiac arrhythmias. The Hague: Martinus Nijhoff, 1980, pp 399–416.
28. Lazzara R, El-Sherif N, Hope RR, Scherlag BJ: Ventricular arrhythmias and electrophysiological consequences of myocardial ischemia and infarction. Circ Res 42:740–749, 1978.
29. Lazzara R, El-Sherif N, Scherlag BJ: Early and late effects of coronary artery occlusion on canine Purkinje fibers. Circ Res 33:597–611, 1973.
30. Corr PB, Cain ME, Witkowski FX, Price DA, Sobel BE: Potential arrhythmogenic electrophysiological derangements in canine Purkinje fibers induced by lysophosphoglycerides. Circ Res 44:822–832, 1979.
31. Sobel BE, Corr PB, Robinson AK, Goldstein RA, Witkowski FX, Klein MS: Accumulation of lysophosphoglycerides with arrhythmogenic properties in ischemic myocardium. J Clin Invest 62:546–553, 1978.
32. Arnsdorf MF, Sawicki GJ: The effects of lysophosphatidylcholine, a toxic metabolite of ischemia, on the components of cardiac excitability in sheep Purkinje fibers. Circ Res 49:16–30, 1981.
33. Katz AM, Messineo FC: Lipid–membrane interactions and the pathogenesis of ischemic damage in the myocardium. Circ Res 48:1–16, 1981.
34. Hearse DJ, Yellon DM: The "border zone" in evolving myocardial infarction: controversy or confusion? Am J Cardiol 47:1221–1334, 1981.
35. Simson MB, Harden W, Barlow C, Harken AH: Visualization of the distance between perfusion and anoxia along an ischemic border. Circulation 60:1151–1155, 1979.
36. Baumgarten CM, Cohen CJ, McDonald TF: Heterogeneity of intracellular potassium activity and membrane potential in hypoxic guinea pig ventricle. Circ Res 49:1181–1189, 1981.
37. Czarnecka M, Lewartowski B, Prokopczyk A: Intracellular recordings from the in situ working heart in physiological conditions and during acute ischemia and fibrillation. Acta Physiol Pol 24:331–337, 1973.
38. Downar E, Janse MJ, Durrer D: The effect of acute coronary artery occlusion on subendocardial transmembrane potentials in the intact porcine heart. Circulation 56:217–224, 1977.
39. Russell DC, Oliver MF, Wojtczak J: Combined electrophysiological technique for assessment of the cellular basis of the early ventricular arrhythmias. Lancet 1:686–688, 1977.
40. Kleber AG, Janse MJ, Van Capelle FJL, Durrer D: Mechanism and time course of S-T and T-Q segment changes during acute regional myocardial ischemia in the pig heart determined by extracellular recordings. Circ Res 42:603–613, 1978.
41. Cardinal R, Janse MJ, Van Eeden I, Werner G, d'Alnoncourt CN, Durrer D: The effects of lidocaine on intracellular and extracellular potentials, activation, and ventricular arrhythmias during acute regional ischemia in the isolated porcine heart. Circ Res 49:792–806, 1981.
42. Lazzara R, Hope RR, El-Sherif N, Scherlag BJ: Effects of lidocaine on hypoxic and ischemic cardiac cells. Am J Cardiol 41:872–879, 1978.
43. Morena H, Janse MJ, Fiolet JWT, Krieger WJG, Crijns H, Durrer D: Comparison of the effects of regional ischemia, hypoxia, hyperkalemia and acidosis on intracellular and extracellular potentials and metabolism in the isolated porcine heart. Circ Res 46:634–646, 1980.
44. Downar E, Janse MJ, Durrer D: The effect of "ischemic" blood on transmembrane potentials of normal porcine ventricular myocardium. Circulation 55: 455–462, 1977.
45. Janse MJ, Van Capelle FJL, Morsink H, Kleber AG, Wilms-Schopmen F, Cardinal R, d'Alnoncourt CN, Durrer D: Flow of "injury" current and pattern of excitation during early ventricular arrhythmias in acute regional myocardial ischemia in isolated porcine and canine hearts: evidence for two different arrhythmogenic mechanisms. Circ Res 47:151–165, 1980.
46. Janse MJ, Kleber AG: Electrophysiological changes and ventricular arrhythmias in the early phase of regional myocardial ischemia. Circ Res 49:1069–1081, 1981.
47. El-Sherif N, Smith RA, Evans K: Canine ventricular arrhythmias in the late myocardial infarction period. 8. Epicardial mapping of reentrant circuits. Circ Res 49:255–265, 1981.
48. Wit AL, Allessie MA, Bonke FIM, Lamemrs W, Smeets J, Fenoglio JJ Jr: Electrophysiologic mapping to determine the mechanism of experimental ventricular tachycardia initiated by premature impulses: experimental approach and initial results demonstrating reentrant excitation. Am J Cardiol 49:166–185, 1982.
49. Harris AS, Rojas AG: The initiation of ventricular fibrillation due to coronary occlusion. Exp Med Sug 1:105–122, 1943.
50. Waldo AL, Kaiser G: A study of ventricular arrhyth-

mias associated with acute myocardial infarction in the canine heart. Circulation 47:1222–1228, 1973.
51. Boineau JP, Cox JL: Slow ventricular activation in acute myocardial infarction: a source of reentrant premature ventricular contractions. Circulation 48:702–713, 1973.
52. Scherlag BJ, El-Sherif N, Hope RR, Lazzara R: Characterization and localization of ventricular arrhythmias resulting from myocardial ischemia and infarction. Circ Res 35:372–383, 1974.
53. El-Sherif N, Scherlag BJ, Lazzara R, Hope RR: Reentrant ventricular arrhythmias in the late myocardial infarction. I. Conduction characteristics in the infarction zone. Circulation 55:686–701, 1977.
54. De Mello WC: Effect of intracellular injection of calcium and strontium on cell communication in heart. J Physiol 250:231–245, 1975.
55. De Mello WC: Influence of the sodium pump on intracellular communication in heart fibers: effect of intracellular injection of sodium ion on electrical coupling. J Physiol 263:171–197.
56. De Mello WC: Intracellular injection of H^+ on the electrical coupling in cardiac Purkinje fibers. Cell Biol Int Rep 4:51–58, 1980.
57. Wojtczak J: Contractures and increase in internal longitudinal resistance of cow ventricular muscle induced by hypoxia. Circ Res 44:88–95, 1979.
58. Spach MS, Miller WT III, Geselowitz DB, Barr RC, Kootsey JM, Johnson EA: The discontinuous nature of propagation in normal canine cardiac muscle. Circ Res 48:39–54, 1981.
59. McDonald TF, MacLeod DP: Metabolism and the electrical activity of anoxic ventricular muscle. J Physiol (Lond) 229:559–582, 1973.
60. Payet MD, Schanne OF, Ruiz-Ceretti E, Demers JM: Slow inward and outward currents of rat ventricular fibers under anoxia. J Physiol (Paris) 74:31–35, 1978.
61. Watanabe AM, Besch HR Jr: Cyclic adenosine monophosphate modulation of slow calcium influx channels in guinea pig hearts. Circ Res 35:316–324, 1974.
62. Schneider JA, Sperelakis N: The demonstration of energy dependence of the isoproterenol-induced transcellular Ca^{2+} current in isolated perfused guinea pig hearts: an explanation for the mechanical failure of ischemic myocardium. J Surg Res 16:389–403, 1974.
63. Wissner SB: The effect of excess lactate upon the excitability of the sheep Purkinje fiber. J Electrocardiol 7:17–26, 1974.
64. Coraboeuf E, Deroubaix E, Hoerter J: Control of ionic permeabilities in normal and ischemia heart. Circ Res (Suppl 1) 38:92–97, 1976.
65. Gettes LS, Reuter H: Slow recovery from inactivation of inward currents in mammalian myocardial fibers. J Physiol 240:703–704, 1974.
66. Chen CM, Gettes LS: Combined effects of rate, membrane potential and drugs on maximum rate of rise (V max) of action potential upstroke of guinea pig papillary muscle. Circ Res 38:464–469, 1976.
67. Hope RR, Scherlag BJ, El-Sherif N, Lazzara R: Heirarchy of ventricular pacemakers. Circ Res 39:883–888, 1976.
68. Allen JD, Brennan JF, Wit AL: Actions of lidocaine on transmembrane potentials of subendocardial Purkinje fibers surviving in infarcted canine hearts. Circ Res 43:470, 1978.
69. Rosenshstraukh LV, Brachmann J, Scherlag BJ, Harrison L, Lazzara R: Mechanisms of ventricular automaticity in the normal and infarcted dog heart [abstr]. Clin Res 29:235A, 1981.
70. Dangman KH, Hoffman BF: Effects of nifedipine on electrical activity of cardiac cells. Am J Cardiol 46:1059–1067, 1980.
71. El-Sherif N, Zeiler R, Gough WB: Effects of catecholamines, verapamil, and tetrodotoxin on triggered automaticity in canine ischemic Purkinje fibers [abstr]. Circulation (Suppl 2) 62:281, 1980.
72. Kass RS, Lederer WJ, Tsien RW, Weingart R: Role of calcium ions in transient inward currents and aftercontractions induced by strophanthidin in cardiac Purkinje fibers. J Physiol (Lond) 281:187–208, 1978.
73. Allessie MA, Bonke FIM, Schopman FJG: Circus movement in rabbit atrial muscle as a mechanism of tachycardia. III. "The leading circle" involvement of an anatomical obstacle. Circ Res 41:9–18, 1977.
74. Katzung BG, Hondeghem LM, Grant AO: Cardiac ventricular automaticity induced by current of injury. Pflugers Arch 360:193–197, 1975.
75. Katzung BG, Morgenstern JA: Effects of extracellular potassium on ventricular automaticity and evidence for a pacemaker current in mammalian ventricular myocardium. Circ Res 40:105–111, 1977.
76. Jalife J, Moe GK: Effect of electrotonic potentials on pacemaker activity of canine Purkinje fibers in relation to parasystole. Circ Res 39:801–808, 1976.
77. Antzelevitch C, Jalife J, Moe GK: Characteristics of reflection as a mechanism of reentrant arrhythmias and its relationship to parasystole. Circulation 61:182–191, 1980.
78. Hoffman BF: The genesis of cardiac arrhythmias. Prog Cardiovasc Dis 8:319–329, 1966.
79. Moe GK, Mendez C: Physiological basis of premature beats and sustained tachycardia. N Engl J Med 288:250–254, 1973.
80. Janse MJ, Van Capelle FJL: Electrotonic interactions across an inexcitable region as a cause of ectopic activity in acute regional myocardial ischemia. Circ Res 50:527–537, 1982.

21. MECHANISM OF ACTION OF ANTIARRHYTHMIC DRUGS

Luc M. Hondeghem
and Bertram G. Katzung

Introduction

In this chapter we describe the *modulated receptor* hypothesis for the action of certain antiarrhythmic drugs. We briefly review the work that led to this hypothesis, present a detailed description of the mechanism, and apply it to a group of antiarrhythmic agents and the arrhythmias in which they are used.

A large number of drugs—e.g., antimalarials, local anesthetics, antiadrenergics, anticholinergics, antihistaminics, and antiepileptics—have antiarrhythmic effects. The search for a mechanism of action for such a diverse group of chemicals has led to several hypotheses. These hypotheses have had utility primarily as methods of classifying the drugs; few, if any, have come to grips with the basic question: how do useful antiarrhythmic drugs suppress abnormal electrical activity without similarly suppressing normal electrogenesis?

The application of electrophysiologic methods for studying the membrane actions of drugs has made it possible to identify some of the properties that appear to be associated with suppression of abnormal electrical activity.

This work was done during Dr. Hondeghem's tenure as an established investigator of the American Heart Association and with funds contributed in part by USPHS grants HL-21672 and HL-17452, and by a grant from Christiaens, N.V. Critical suggestions from Drs. C. Clarkson, C. Malecot, and J. Moyer were extremely valuable. The authors thank Dr. J. Moyer for his programming contributions, C. Cotner and J. Cowan for assistance with graphic illustrations, and D. Noack for secretarial assistance.

N. Sperelakis (ed.), PHYSIOLOGY AND PATHOPHYSIOLOGY OF THE HEART.

Martinus Nijhoff Publishing, Boston/The Hague, Dordrecht/Lancaster.

The first property to be clearly defined as an important correlate of antiarrhythmic action was *local anesthesia* [1]. This action, associated with blockade of sodium channels, is now recognized as the major action of the most commonly used antiarrhythmic agents, e.g., quinidine, lidocaine, and their congeners. In nerve, impulse propagation is blocked in healthy as well as injured fibers at the relatively high concentrations of local anesthetics used for infiltration anesthesia. In the heart, depressed conduction is suppressed but normal conduction is relatively less impaired—unless toxic doses are given. In other words, these drugs, at the concentrations used for the treatment of arrhythmias, *selectively* suppress impaired conduction in the heart. This selectivity is probably most important in abolishing reentry arrhythmias [2].

Two other effects of antiarrhythmic drugs can be at least partially ascribed to block of sodium channels. Blockade of sodium channels is important in the increase in *refractoriness* that is produced by some of these drugs. Block of sodium channels also plays a role in the suppression of *abnormal pacemaker activity* occurring at more negative diastolic potentials [3].

The calcium-channel-blocking agents were developed as vasodilators, but some members of this group also have antiarrhythmic effects [4]. These drugs relax normal vascular smooth muscle and cause moderate or little depression of the normal heart. Some of them, however, very markedly depress abnormal activity in myocardium, e.g., slow responses in ischemic and depolarized tissues [5]. There is some evidence indicating that the response of vascular

smooth muscle to the calcium-channel blockers is also modulated by the membrane potential [6]. Thus, some members of this class of drugs also seem to induce a *selective* blockade of the channels with which they interact.

Selective depression of membranes with impaired electrogenesis thus appears to be an effect common to at least two important subgroups of antiarrhythmic drugs. The mechanism for such selective depression is, at the present time, best explained by the *modulated receptor* hypothesis [7, 8]. This hypothesis postulates that the binding of a blocking drug to the receptor of a transmembrane channel is modulated by the state of the channel.

Because channel blockade, by definition, results in a decrease in ionic current through the channel, the voltage-clamp method is generally accepted as the most direct technique for defining the action of a channel-blocking drug. The voltage-clamp technique is relatively straightforward in some large cells (e.g., squid axon), but in cardiac muscle it has been limited by technical problems [9, 10]. These problems limit the speed with which large membrane currents can be controlled. This limitation applies especially to the sodium current, which is responsible for the rapid upstroke (phase O) of the normal action potential in atrial cells, His-Purkinje fibers, and ventricular myocardium. Therefore, most investigators have used the upstroke velocity (dV/dt or $\dot{V}$) of the action potential as an indirect measure of the sodium current. The maximum of $\dot{V}$($\dot{V}_{max}$ or dV/dt_{max}) has been validated as a reasonable measure of the peak sodium current by modeling [11, 12] as well as by direct measurement in small cardiac preparations where the sodium current can be successfully clamped [13–15]. (It should be stressed, however, that for $\dot{V}_{max}$ to give a valid estimate of sodium conductance, several criteria must be satisfied: [a] axial current flow must be zero [16], [b] membrane potential at which $\dot{V}_{max}$ occurs must remain constant between comparisons, [c] latency between stimulus and $\dot{V}_{max}$ must be kept constant [12], and [d] the nonsodium currents must contribute only negligibly at the time of $\dot{V}_{max}$ [11].)

Measurement of the calcium current I_{si} is not so difficult because it is both slower and smaller than the sodium current. For the same reason, estimates of I_{si} from the upstroke velocity of calcium-dependent action potentials are more hazardous; interference from sodium and potassium currents is much more likely. Therefore, most of the data relating to calcium-channel blockers described below are from voltage-clamp studies.

Background

The modulated receptor hypothesis explains the selective action of antiarrhythmic drugs on the basis of the differences between membrane electrogenesis in normal and in abnormal tissue. Such differences may include disparities in resting potential, in action potential shape and duration, and in recovery time between successive action potentials. Earlier work supporting these ideas is conveniently considered from the standpoint of the major variables involved: voltage and time.

ANTIARRHYTHMIC DRUG ACTION IS VOLTAGE DEPENDENT

In 1955 Weidman [1] showed that, in sheep Purkinje fibers, cocaine reduced $\dot{V}_{max}$ of the action potential without significantly changing the resting potential. In addition, he made the important observation that hyperpolarization, even in the continued presence of the drug, restored $\dot{V}_{max}$. He interpreted these observations as indicating that cocaine inactivates the system responsible for carrying sodium through the membrane. Jensen and Katzung [17] showed that therapeutic concentrations of phenytoin, which had little or no effect upon $\dot{V}_{max}$ in low-potassium solution, markedly reduced $\dot{V}_{max}$ when the membrane was depolarized by elevating the concentration of extracellular potassium. The same effect was observed for lidocaine [18] (also see fig. 21–1). Hondeghem et al. [2] and Hope et al. [19] proposed that a major mechanism of action of some antiarrhythmic drugs is to *selectively* block sodium channels that are depolarized by hypoxia or ischemia. This proposal has since been confirmed in several laboratories [20–24].

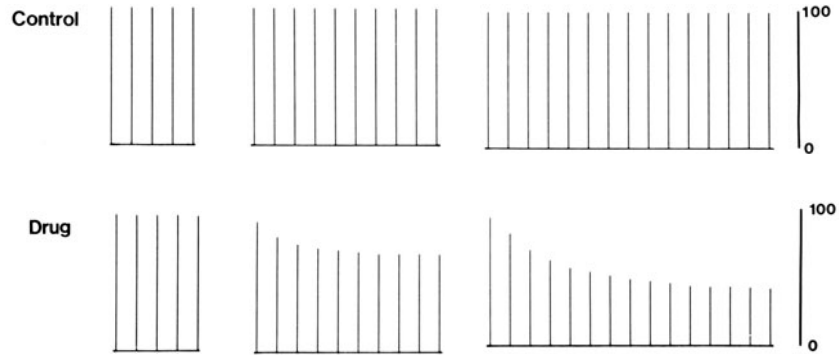

FIGURE 21–1. Voltage dependence of $\dot{V}_{max}$ reduction by procainamide (180 μ*M*). After a 20-s rest period, guinea pig papillary muscles were stimulated at 3.3 Hz. The resting membrane potential was altered by current injection. Note that the reduction of $\dot{V}_{max}$ is accentuated by depolarization (−70 mV) and that hyperpolarization (−100 mV) attenuates the procainamide effect.

ANTIARRHYTHMIC DRUG ACTION IS TIME DEPENDENT

Johnson and McKinnon [25] and Heistracher [26] showed that repetitive activation enhances sodium-channel block by quinidine (also see fig. 21–2). From studies of local anesthetic action in nerves, Strichartz [27] and Courtney [28] proposed that each time the channels were used (activated and inactivated) a fraction of them became blocked. In studies of quinidine and lidocaine, Chen et al. [29] showed that, during the interval between action potentials, sodium channels recover from block. In addition, they demonstrated that the rate of recovery is strongly voltage dependent; recovery is faster in well-polarized tissue than in partially depolarized tissue. We have found that upon clamping the membrane to −140 mV, recovery from block in the presence of therapeutic concentrations of lidocaine or quinidine is complete in less than 200 ms [30].

ANTIARRHYTHMIC DRUG ACTION IS STATE DEPENDENT

Hille [7] and Hondeghem and Katzung [8] proposed that the voltage- and time-dependent blockade of sodium channels caused by local anesthetic and antiarrhythmic drugs could be accounted for by a model based on the three channel states (fig. 21–3A) described by Hodgkin and Huxley [31]. At negative potentials the rested state is preferred; upon depolarization the channels rapidly pass through the activated state into the inactivated state, where they remain until the membrane is repolarized.

Data collected with protocols that measure the kinetics of block development as well as steady-state block suggest that a useful antiarrhythmic drug has a different set of association and dissociation rate constants for each of the three states (resting, activated, and inactivated), i.e., the drug interacts with a receptor that is modulated by the state of the channel (fig. 21–3B) [30, 32]. Channels that have drug bound to their receptors do not conduct ionic current; in addition, they behave as if the relationship between voltage and inactivation is shifted toward more negative potentials. The reasons for these assumptions are as follows:

Interaction of drug with the channel in the activated state is required to account for the fact that, for many drugs, the block becomes more marked as the frequency of channel opening is increased [27]. Since development of some block and recovery can occur at rest [28, 29, 32], the channels need not be open for some interactions to occur. However, since the rested-state receptor usually has a much lower affinity for the drug and much faster kinetics than the receptor in the inactivated state [8],

it is necessary that these states have different rate constants. The voltage shift of the inactivation relation is suggested because blocked channels behave as if they are at a potential less negative than the measured membrane potential [1, 28].

Quantitative aspects of the modulated receptor hypothesis have been formulated in a set of differential equations that describe the interactions of drugs with channels as a function of time and membrane voltage [8]. Several laboratories have tested the model and used it successfully to explain the effects of many antiarrhythmic drugs under various experimental conditions [30, 32–63].

In our laboratory we utilize a laboratory computer to solve the set of equations. The method provides an estimate of the proportion of channels in each of the Hodgkin–Huxley states: resting, activated, and inactivated, and the fraction of channels in each state that is complexed with drug. The total number of channels available is normalized to 1.0. All of the $\dot{V}_{max}$ estimates provided below are normalized in this way.

Mechanisms of State-Dependent Drug–Receptor Interactions

The modulated receptor model can provide a dynamic "moving picture" of the changes in state of membrane channels—changes brought about by the physiologic effect of time and membrane voltage, as well as the pharmacologic binding of drug molecules to channel receptors. To diagram these changes in static illustrations we have combined the basic Hodgkin-Huxley–drug-interaction diagram of figure 21–3B with a semiquantitative plot of the major fractions of the total pool of channels against time in figures 21–4 to 21–8. Each graph shows the results computed for one or more action potentials elicited after a rest of 20 s, plotted with the total number of channels normalized to 1.0 (ordinate), and the fraction of channels residing in each state designated by color. Throughout this series of figures rested channels are green, activated channels orange, and inactivated purple. The lightly colored

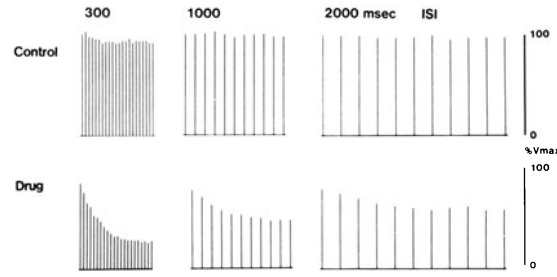

FIGURE 21–2. Time dependence of $\dot{V}_{max}$ reduction by aprindine (14 μ*M*). After a 20-s rest period, guinea pig papillary muscles were stimulated at 3.3, 1.0, or 0.5 Hz. Note that the depression of $\dot{V}_{max}$ is more marked at faster stimulus rates (less time at negative potentials; and more activations and more time at depolarized potentials).

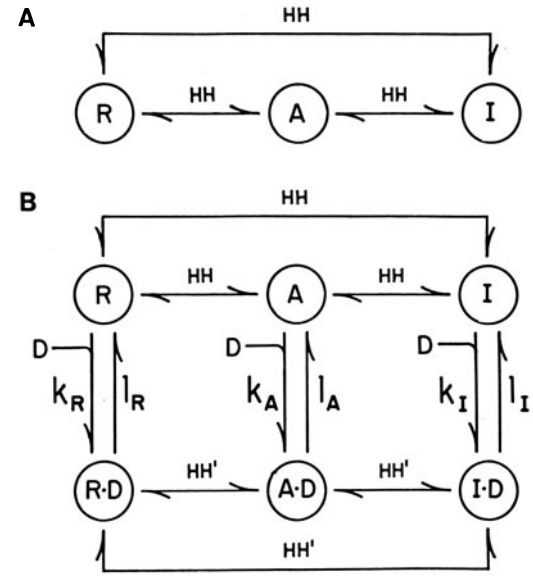

FIGURE 21–3. Schematic representation of the modulated receptor. *(A) Drug-free.* Sodium channels can exist in three states: rested (R; predominant at negative membrane potentials), activated (A; upon depolarization the channels open transiently) and inactivated (I; predominant at more positive potentials). The transitions between the three states have been described by Hodgkin and Huxley (HH) [31]. *(B) In the presence of drug.* Drug molecules (D) can associate (down arrow) or dissociate (up arrow) with the channels in all three states. Drug-associated channels (R·D, A·D, and I·D) behave as if they are at a less negative transmembrane potential, i.e., their Hodgkin–Huxley parameters are shifted to more positive potentials (HH′). Drug-associated channels are also blocked, i.e., they do not conduct ionic current.

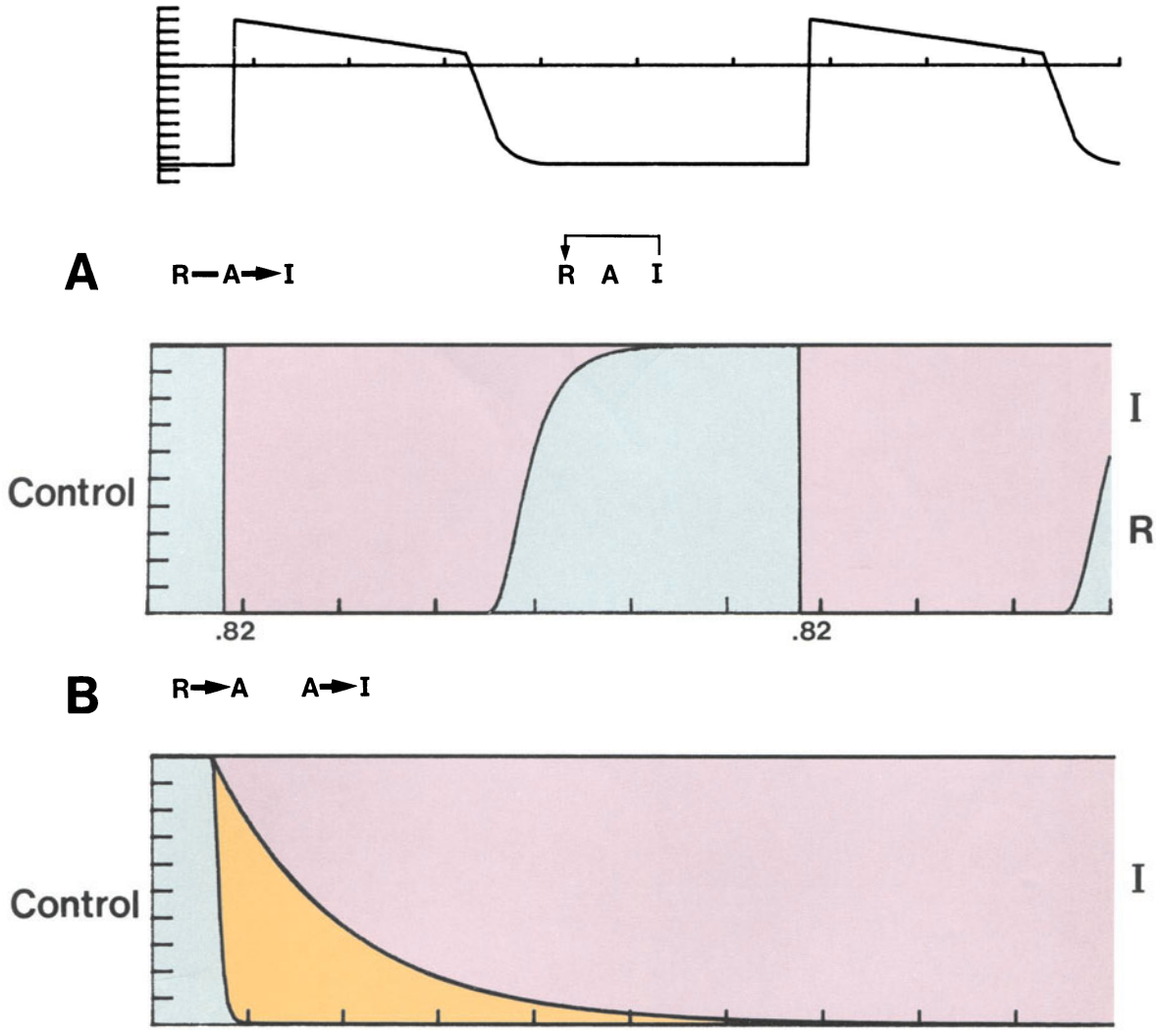

FIGURE 21–4. Computer simulations of channel states in the absence of drugs. The trace at the top shows two action potentials, at a frequency of 3.3 Hz, elicited after a 20-s rest period. The horizontal axis represents 500 ms. The distribution and shifts of channels from one state to another during these action potentials is shown in the panel below *(A)*. The pool diagram at the top of *A* (R — A → I) shows the rapid shift of channels from the rested, through the activated, to the inactivated state at the time of the first upstroke. The thickness of the arrow connecting R to I indicates the relative rate of conversion from one state to the other. The somewhat slower recovery of channels is indicated during repolarization of the first action potential (I → R).

The color graph diagrams these conversions quantitatively. In this figure and figures 21–5 to 21–8, light green represents channels in the rested, drug-free state, and light purple represents channels in the inactivated drug-free state. The sum of all the channel states is unity. As indicated in *A*, during the 500-ms duration of the sequence, the conversion of channels from the rested state to the inactivated state is so rapid that the activated state can be detected only by greatly expanding the time scale. In *B*, the horizontal axis represents 2.4 ms during the upstroke of the first action potential of *A*. Orange represents the fraction of channels in the open or activated state. The maximum normalized sodium conductance achieved during the upstroke of each of the two action potentials is 0.82, indicated below the upstroke in *A*. This value is less than unity, even in the absence of blocking drug, because a few channels inactivated before the rest of the channels open.

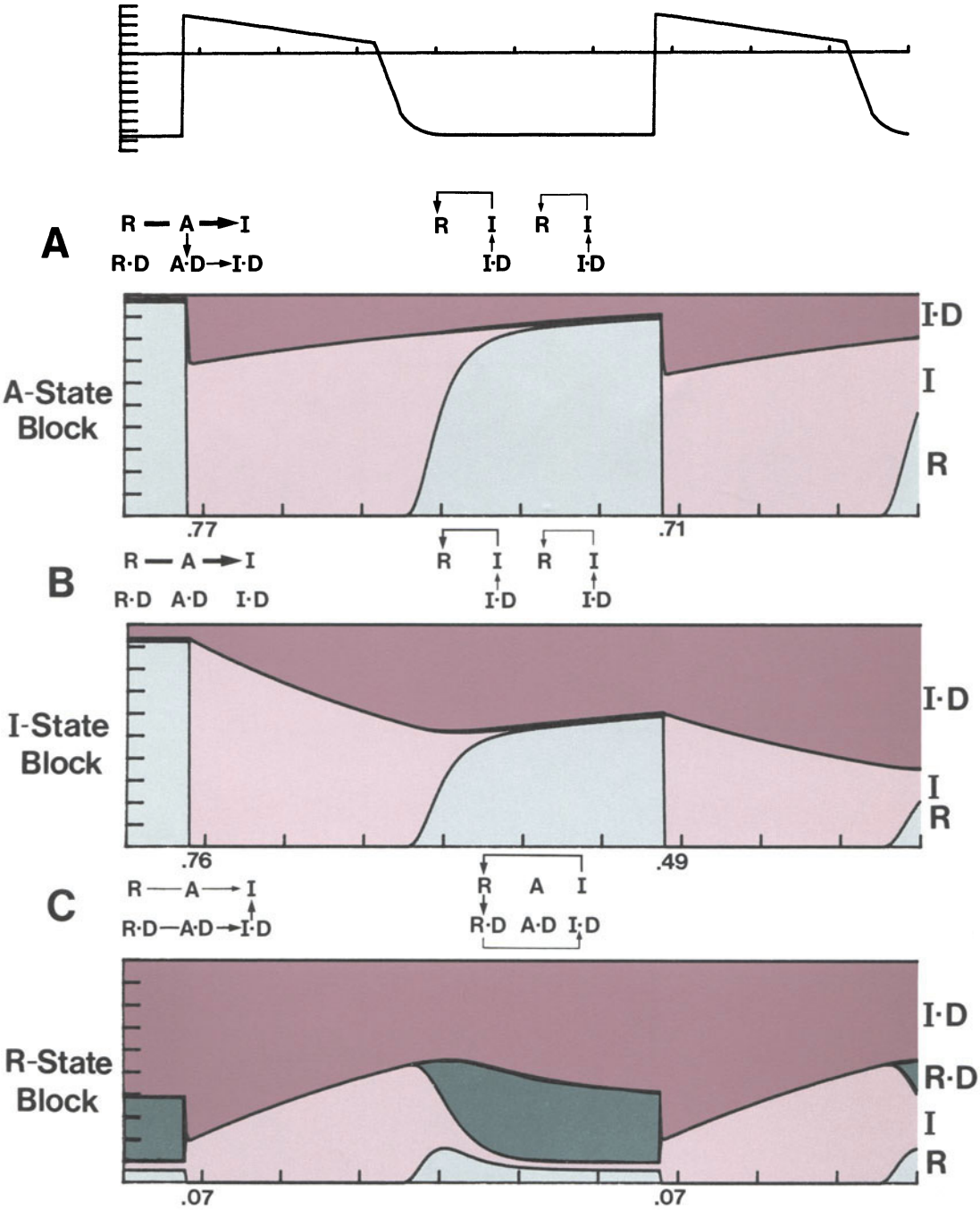

FIGURE 21–5. Channel states in the presence of an activated-state blocker *(A)*, inactivated-state blocker *(B)*, or rested-state blocker *(C)*. Simulated action potentials (top trace) and drug-free channels (light colors) are as defined in figure 21–4. Rested drug-associated channels (R·D) are represented in dark green. Dark purple represents the inactivated blocked channels (I·D). Activated blocked channels (A·D) are not resolved in the time resolution of the figure. Kinetic parameters for these hypothetical drugs were taken from table 21–1 (see text). In *A*, block develops exclusively during activation, i.e., at the time of the upstroke of the action potential (A → A·D). Throughout the plateau and diastolic phase the channels unblock (I·D → I). Depending upon the unblocking rate and the time that elapses before the next action potentials, some block may persist to attentuate the $\dot{V}_{max}$ of the next upstroke. In *B*, no block is associated with activation; instead it develops throughout the plateau of the action potential. Unblocking occurs only during diastole. The combination of more block development and less recovery time in *B* results in a substantial reduction of $\dot{V}_{max}$ from 0.76 to 0.49. In *C*, most of the rested channels are blocked (dark green), i.e., very few are available to become activated; hence the very low $\dot{V}_{max}$ (0.07). Channels only unblock during the plateau, i.e., when they are inactivated. Thus, the channels are either blocked or inactivated, and can never conduct the sodium current.

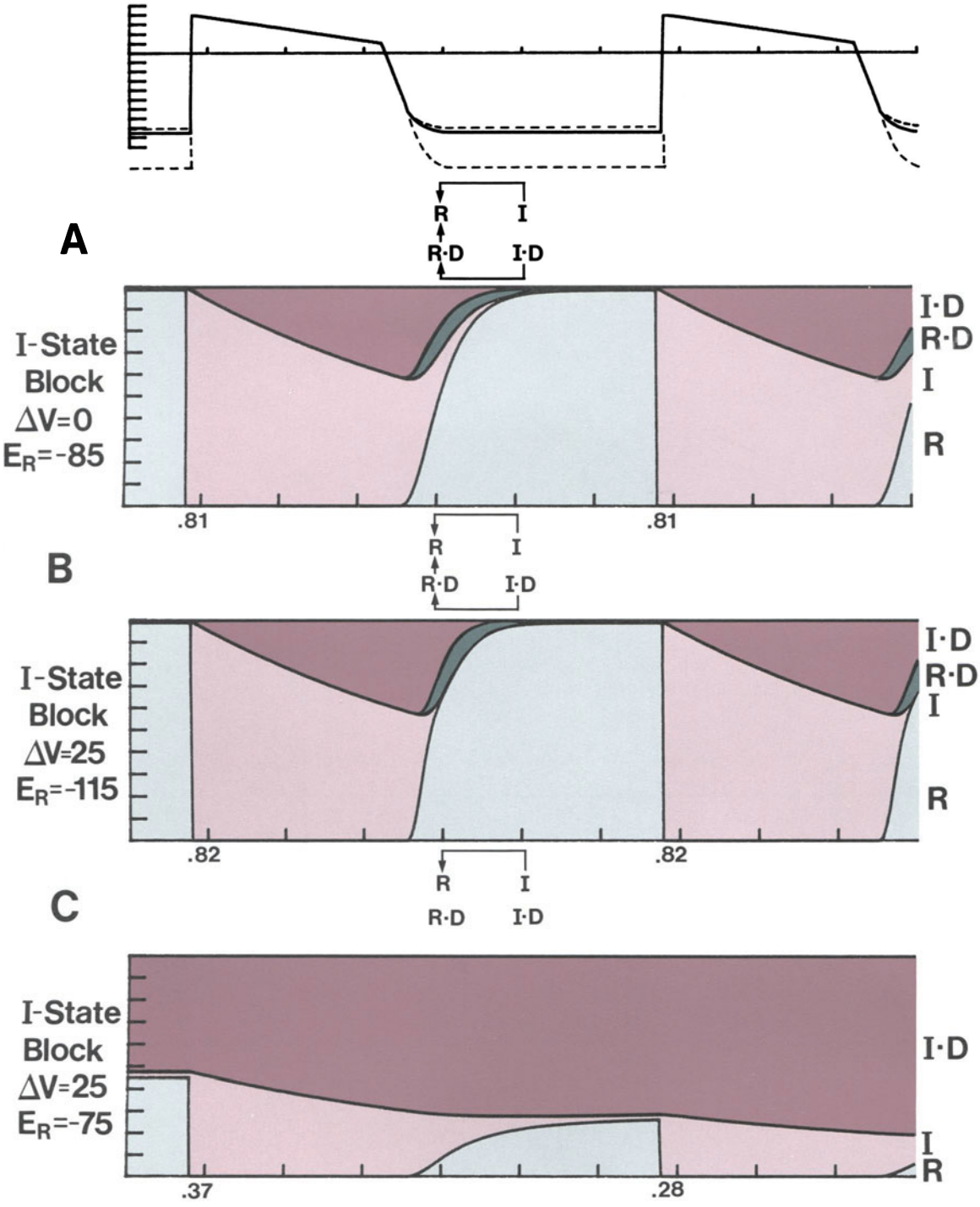

FIGURE 21–6. Effects of the omission of a voltage shift *(A)*, hyperpolarization *(B)*, and depolarization *(C)* upon the channel states. Except for the indicated changes in voltage parameters, the conditions are identical to those in figure 21–5B. In *A*, lack of voltage shift provides for recovery from the I·D block during repolarization through two routes: the slow I·D → I transition and the faster I·D → R·D transition. Since the latter is so much faster, most of the I·D channels quickly unblock to R via R·D, and the I·D to I path becomes relatively unimportant. In *B*, the same result is obtained in the presence of a voltage shift, by hyperpolarization of the cell membrane to −115 mV resting potential. In *C*, the cell membrane is slightly depolarized. Depolarization accentuates the effectiveness of the voltage shift, i.e., further closes the fast I·D → R·D route; and also promotes the I state, which in turn leads to block (cf., fig. 21–5B). Comparison of *B* and *C* clearly illustrates how an antiarrhythmic drug can *selectively* block depolarized tissue.

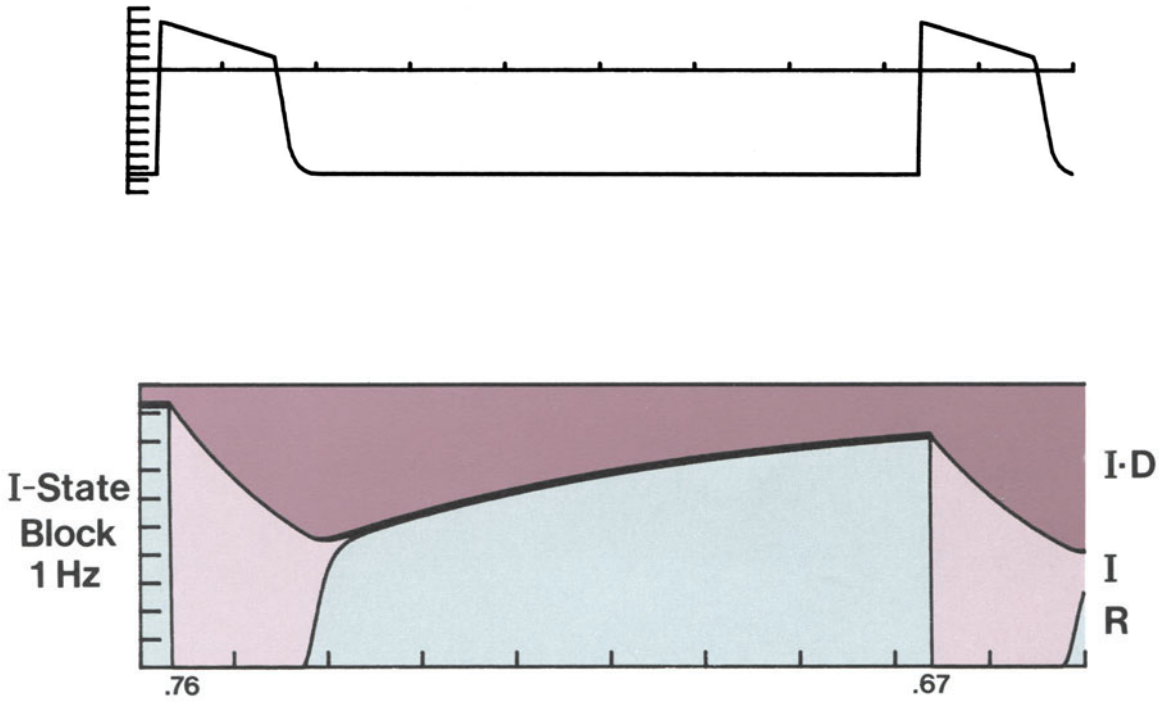

FIGURE 21–7. Effect of inactivated-state blocker at 1 Hz. All parameters in this figure are identical to those of figure 21–5B, except that heart rate was slowed from 3.3 Hz to 1 Hz and the horizontal axis represents 1.25 s. Thus, during the plateau of the first action potential the same amount of block develops as in figure 21–5B. Upon repolarization, unblocking occurs at exactly the same rate, but because of the slower heart rate, unblocking occurs for a longer time and hence recovery from block is more complete. As a result the upstroke of the second action potential is 0.67 as compared to 0.49 in figure 21–5B.

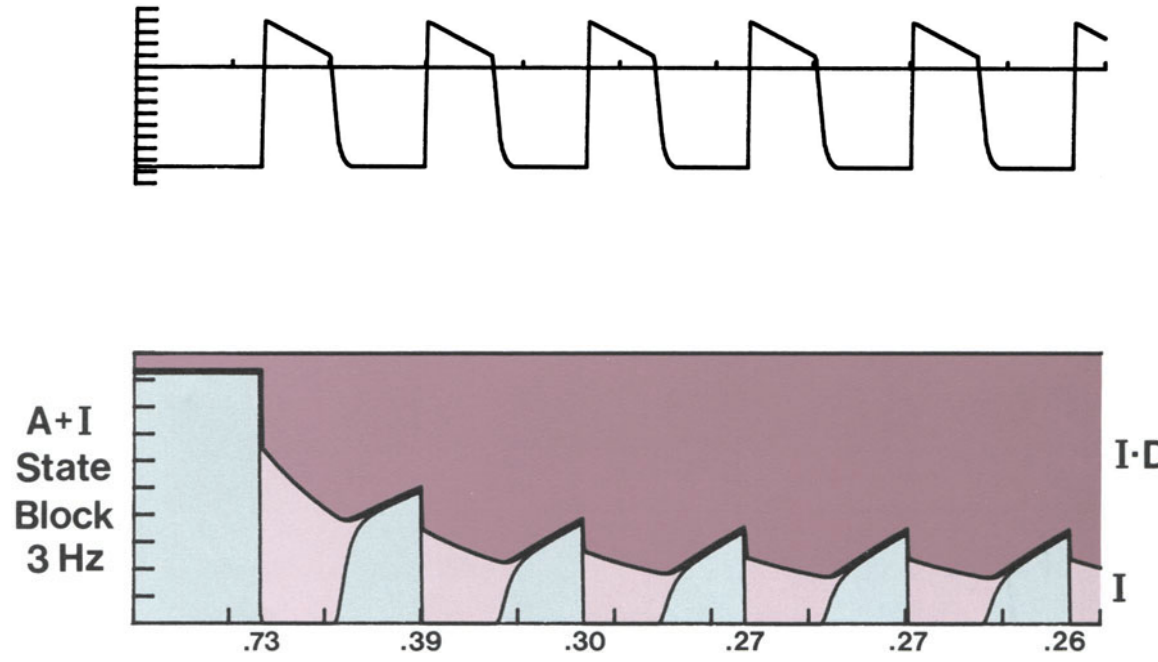

FIGURE 21–8. Cumulative block with a drug of high affinity for both the activated and inactivated states. Top trace shows a train of action potentials at 3.3 Hz (horizontal axis = 1.8 s). Note that block develops with each activation as well as during each inactivated (plateau) period. Since only the rested-state channel has a low affinity for the drug, recovery only proceeds when the membrane potential is negative, i.e., approaching or at the resting potential.

areas represent drug-free channels and the darker colors represent blocked channels.

Figure 21–4 illustrates the behavior of the model in the absence of drugs: Hodgkin–Huxley kinetics apply. When the cell membrane is maintained at a normal resting potential (e.g., −85 mV), all channels are in the rested state (light green in fig. 21–4). Upon depolarization the channels become activated but the activated state is so brief (less than 2 ms) that it cannot be resolved in figure 21–4A. This is indicated in the first subpicture above the graph by a heavy arrow from R (rested) via A (activated) to I (inactivated). Only when the time scale is greatly expanded can the transient activated state be visualized (orange in fig. 21–4B). Although the activated state is very brief, it is the time during which current flows. This current is proportional to the magnitude of the activated state; drugs that have a high affinity for the activated state can cause development of substantial block during this time. Activated channels quickly become inactivated (light purple in fig. 21–4A and B) for the duration of the plateau. Upon repolarization, the channels recover rather promptly (purple to green, I → A transition in fig. 21–4A).

CONSEQUENCES OF STATE-DEPENDENT AFFINITY

To illustrate the significance of varying affinities for the three channel states, we first consider a set of three hypothetical drugs, each with a high affinity (small dissociation constant, $K_d = 10^{-6}$ *M*) for one channel state, and low affinity (large $K_d = 10^{-3}$ *M*) for the other two states (table 21–1). The rate constants k and l were chosen to provide the K_d required for each state and a time constant in the range found for real drugs. To obtain a realistic degree of channel blockade, binding of the drugs is assumed to shift the inactivation curve 25 mV in the hyperpolarizing direction. This means that channels in which drug is bound to the receptor behave as though the membrane potential is 25 mV less negative than the measured potential. The effect of the voltage shift is discussed below.

Effects of a Hypothetical Drug with Highest Affinity for Channel Receptors in the Activated State. As shown in figure 21–5A, a long rest period permits accumulation of nearly all the channels in the unblocked rested state (light-green area) since neither the receptors in inactivated channels nor those in the rested channels have sufficient affinity for the drug. At the time of the action potential upstroke (channel activation) affinity increases 1000-fold and about 30% of the channel receptors bind drug. This shift from A to A·D (indicated in the first subpicture above fig. 21–5A) is not seen in the graph because it occurs too quickly, but the result—an abrupt increase in blocked-inactivated channels (I·D, dark purple in the graph) follows immediately. The predicted $\dot{V}_{max}$ for

TABLE 21–1. Kinetic parameters for the hypothetical drugs discussed in the text and displayed in Figs 4 - 8. Rate constants were selected to provide high (1 uM) or low (1 mM) affinities and realistic time constants for each drug. Time constants are calculated as: 1/(k•dose + l); dissociation constants (K_d) are calculated from K_d = l/k•dose (8).

	Rate constants				Time constant
	high affinity ($K_d = 10^{-6}$M)		low affinity ($K_d = 10^{-3}$M)		(ms)
State	k assoc. ($ms^{-1} M^{-1}$)	l dissoc. ms^{-1}	k assoc. ($ms^{-1} M^{-1}$)	l dissoc. (ms^{-1})	For drug concentrations 10^{-5} *M*
Rested	10^4	10^{-2}	10^2	10^{-1}	~ 10
Activated	1.5×10^5	0.15	1.5×10^3	1.5	~ 0.6
Inactivated	4×10^2	4×10^{-4}	4	4×10^{-3}	~ 230

Example: A hypothetical drug with highest affinity for the activated channel would be simulated using the high-affinity rate constants for the activated state (1.5×10^5 and 0.15) and the low-affinity constants for the rested and inactivated states (10^2, 10^{-1}; 4, 4×10^{-3}, respectively).

the first action potential (0.77) is slightly less than control (0.82, fig. 21–4) because a few channels enter the I·D pool during rest, and because some channels block during the first part of the upstroke before $\dot{V}_{max}$ has been achieved. During the ensuing plateau phase, channels equilibrate between the I and I·D pools (second subpicture above fig. 21–5A); since drug affinity for the inactivated channel is low, there is a slow exponential decrement of the I·D pool in favor of the I pool. At the end of the first plateau there is a rapid shift of drug-free inactivated channels (I pool, light purple) to the recovered state (R pool, light green) as the membrane potential returns to the resting level. However, the blocked channels (I·D pool, shown in dark purple) do not recover since the voltage shift associated with binding of drug makes them behave as though they were 25 mV more positive, i.e., −60 mV rather than −85 mV. At the time of the second action potential, 30% of the remaining unblocked channels become trapped in the I·D state. In a train of action potentials, this process would be repeated with each action potential until a steady-state level of blockade, in this case $\dot{V}_{max} = 0.70$, was reached.

Effects of a Hypothetical Drug with Highest Affinity for the Channel Receptor in the Inactivated State. As shown by the pool diagrams in the upper part of figure 21–5B, and by the slow increase in the I·D pool (dark purple) in the graph, most of the binding of this drug to receptor occurs during the plateau of the action potential, not during the upstroke. Repolarization at the end of the plateau reverses this process: the inactivated unblocked channels (light purple) are rapidly shifted to the rested state (light green). However, the inactivated blocked channels (dark purple) "see" a membrane potential of only −60 mV (because of the voltage shift) and therefore do not undergo removal of inactivation to the R·D state. Instead, they unblock slowly with the time-constant characteristic of I ↔ I·D kinetics. As a result, the $\dot{V}_{max}$ of the second action potential (0.49) is markedly reduced compared to the first action potential (0.76). The computed steady-state $\dot{V}_{max}$ for a long train of action potentials under these conditions is 0.33. Note that recovery from blockade by this drug occurs only during the diastolic interval. Therefore, the steady-state block caused by a drug with high affinity for the inactivated state will be dependent on the ratio of the action potential duration to the diastolic interval. In contrast, block caused by the drug with a high affinity only when the channel is activated (fig. 21–5A) decrements during both the plateau and the diastole; thus net steady-state block will be influenced by rate, but not by action potential duration.

Effects of a Drug with Highest Affinity for the Channel Receptor in the Rested State. As indicated in figure 21–5C, a drug with these characteristics would cause a large fraction of the channels to bind drug in the rested state (dark green). Because of the voltage shift, however, many of these move to the inactivated blocked (I·D) state—thus the preponderance of dark green and dark purple in the graph. Consequently, $\dot{V}_{max}$ of the first action potential is maximally reduced after a long rest period. In the example shown, $\dot{V}_{max}$ of the second action potential is unchanged. It is theoretically possible to reduce the degree of blockade by very rapid stimulation (to minimize the diastolic interval) with this type of drug. Thus a drug with a high affinity for channels in the rested state would be a cardiac poison, depressing normal, rested cells, rather than selectively depressing abnormal cells. Such drugs will be considered no further in this chapter.

VOLTAGE-DEPENDENCE OF CHANNEL BLOCKADE

The comparisons below are made using the inactivated-channel-blocking drug introduced in figure 21–5B. However, similar comparisons could be made for the activated-channel-blocking drug.

Significance of Drug-induced Shift of Inactivation. The hypothetical drugs described thus far (fig. 21–5) incorporate a voltage-shift effect. The importance of this shift can be appreciated by comparing figure 21–6A with figure 21–5B. The hypothetical drug modeled in figure

21–6A is identical to that of figure 21–5B except that it lacks a voltage shift. As a result, channels bind drug while they are inactivated and accumulate in the I·D pool as before. However, in contrast to the drug of figure 21–5B, the channels in figure 21–6A can leave the I·D pool during diastole by two routes: the relatively fast Hodgkin–Huxley recovery from inactivation (I·D → R·D) as well as the slower unbinding of drug (I·D → I). Since R·D → R also occurs relatively fast, recovery from block is completed rather quickly. Therefore, in the absence of a voltage shift, even a short diastolic interval is sufficient to allow all the channels to unblock and no accumulation of block occurs; the $\dot{V}_{max}$ of the second action potential is identical to that of the first.

Significance of Resting Membrane Potential. It can be easily shown that even for a drug that induces a significant inactivation voltage shift, e.g., the 25-mV shift of figure 21–5B, sufficient hyperpolarization, say from −85 to −115 mV (fig. 21–6B), will overcome the 25-mV voltage shift, causing the I·D channels to recover (I·D → R·D) and then quickly unblock (R·D → R). Conversely, a moderately depressed resting potential, e.g., −75 mV, markedly potentiates cumulative blockade by causing more trapping in the I·D state. This effect is shown in figure 21–6C for the same hypothetical inactivated-channel-blocking drug of figure 21–5B. Note that the $\dot{V}_{max}$ of the first action potential is much more inhibited in the depolarized preparation, and that repetitive activation leads to even more block. The predicted steady-state $\dot{V}_{max}$ for the depolarized cell of figure 21–6C is 0.13 compared to 0.33 for the cell of figure 21–5B.

TIME-DEPENDENT ASPECTS OF MODULATED RECEPTOR BLOCKADE

It has already been shown in figure 21–5A and B that the increment of blockade with successive action potentials is limited by the degree of recovery that occurs between periods of maximum drug-receptor affinity. Therefore, steady-state block at slow heart rates (other factors being constant) will be less than that achieved at fast heart rates. Figure 21–7 shows the first two action potentials of a train at 1 Hz using the same hypothetical inactivated-state-blocking drug displayed in figure 21–5B at 3.3 Hz. The steady-state $\dot{V}_{max}$ predicted at 1 Hz is 0.66 compared to the 0.33 $\dot{V}_{max}$ predicted for 3.3 Hz. The same analysis applied to the effects of drugs on early extrasystoles shows that such depolarizations manifest greater depression of $\dot{V}_{max}$ than the preceding regular action potential for both activated-state and inactivated-state-blocking drugs. The earlier the extrasystole, the less time for recovery and thus the more the inward current is reduced.

With continuous stimulation at a constant rate, $\dot{V}_{max}$ approaches a steady-state value slowly or rapidly, depending on the time constants of its interactions. This point has been discussed in some detail in a previous publication [30]. As shown in figure 21–8, a hypothetical drug with high affinity for the channel receptor in both the activated and inactivated states, and with the time constants indicated in table 21–1, will approach steady-state within 5–8 cycles.

EFFECTS OF ACTION POTENTIAL CONFIGURATION ON MODULATED RECEPTOR BLOCKADE

Some antiarrhythmic drugs depress $\dot{V}_{max}$ in atrial as well as Purkinje fibers and ventricular cells (e.g., quinidine) while others have much less effect on atrial cells (e.g., lidocaine) [64]. The modulated receptor hypothesis provides a mechanistic explanation for these observations based on the relatively short action potential plateau exhibited by atrial cells as compared to Purkinje and ventricular fibers.

Referring to figure 21–5A, it is apparent that a 50% change in action potential duration would have only a moderate effect on the depression of $\dot{V}_{max}$ of the second action potential of the train shown (as long as the rate is not changed) since recovery from block occurs at about the same rate during the plateau as during the diastolic interval. Therefore, a drug with high affinity only for the activated state will have the same effect regardless of action potential duration, i.e., the same effect on atrial as on Purkinje or ventricular cells.

In contrast, a drug with high affinity for the

TABLE 21–2. Relation of action potential duration to depression of steady-state $\dot{V}_{max}$ caused by pure activated channel and inactivated channel blocking drugs

	$\dot{V}_{max}$ for action potential duration of					
Drug[a]	20	50	100	150	200	300 ms[b]
Activated-channel Blocker	0.71	0.71	0.70	0.70	0.69	0.58
Inactivated-channel Blocker	0.64	0.56	0.45	0.35	0.26	0.08

[a]Kinetic parameters taken from table 21-1. Action potential frequency 3.3 Hz. Drug-free normalized $\dot{V}_{max}$ for all action potential durations was 0.82.
[b]Action potential duration measured at 100% repolarization.

inactivated channel (fig. 21–5B) would have much greater effect on a cell with a long plateau than on one with a short plateau since block continues to develop during the plateau period and diminishes only during diastole.

The predicted steady-state blockade caused by the two hypothetical agents (activated- and inactivated-channel blockers) as a function of action potential duration is given in table 21–2. Note that, for the range of durations given, the decrement in $\dot{V}_{max}$ produced by the activated-channel-blocking drug (from 0.71 to 0.58) is much less than the decrement produced by the blocker of inactivated channels (from 0.64 to 0.08). Since the plateau of atrial action potentials is typically 50 ms or less, while that of Purkinje fibers is 200 ms or more, it is apparent that a drug with high affinity only for inactivated channels would have a much greater effect in Purkinje tissue.

The Actions of Real Antiarrhythmic Drugs

To be clinically useful, an inward-channel-blocking drug must have significant affinity for the activated or for the inactivated channel (or for both), but not for the rested channel.

A meaningful classification of channel-blocking antiarrhythmic drugs should therefore be based on some measure of their affinities, e.g., dissociation constants, for each of the three channel states. To obtain such data requires experimental techniques that permit independent control of duration and membrane potential during each state. Obviously, the voltage-clamp technique is best for achieving such control. Because of the difficulty of voltage clamping cardiac tissue, only limited data for a few drugs are available: quinidine [30, 56, 57, 62], lidocaine [30, 32, 56, 57, 63, 65], procainamide [56, 65], amiodarone [66], and aprindine [65]. Similarly, the data for the calcium-channel blockers are still incomplete and limited to verapamil and its analogue D-600 [38, 67, 68], diltiazem [68, 69] and nifedipine [70, 71]. Consequently the description below is necessarily tentative.

MODULATED RECEPTOR MECHANISM OF ACTION OF SODIUM-CHANNEL-BLOCKING DRUGS

Of the sodium-channel-blocking drugs that we have studied, amiodarone appears to have the purest affinity for the inactivated state. This is shown by the following results: application of a fast pulse train of brief voltage clamps to the plateau level results in little or no block (fig. 21–9A). In contrast, a single long-plateau clamp pulse causes block to develop in an exponential fashion (fig. 21–9B). Application of clamps to different plateau voltages from −20 to +40 mV indicates no voltage dependence in this range for the development of block by amiodarone [66].

Similar studies have been carried out for lidocaine and a number of its analogues [65]. Bean et al. [32] studied lidocaine, utilizing the full voltage-clamp technique in rabbit Purkinje fibers. Both of these studies have obtained convincing evidence for predominantly inactivated-state blockade by lidocaine. Aprindine and a series of its analogues also show a marked affinity for the inactivated state [72]. However, both lidocaine and aprindine appear to have a higher affinity for the activated-channel receptor than does amiodarone. Quinidine also ap-

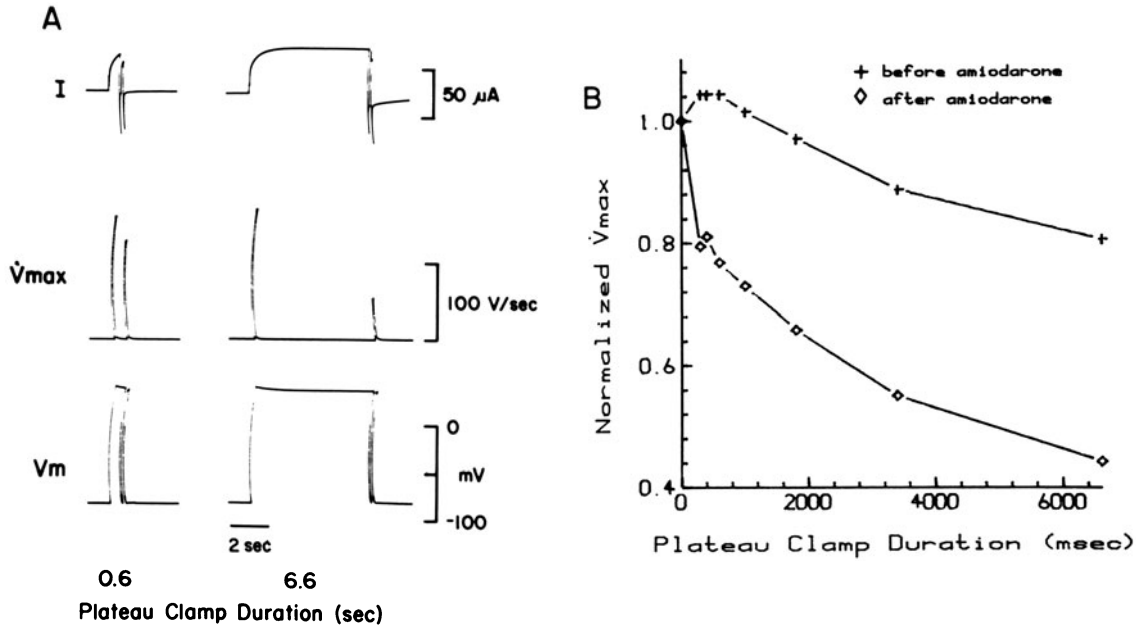

FIGURE 21–9. Time-dependent inactivated-channel block by amiodarone (8.8×10^{-5} *M*) is illustrated. *A*, recorded during superfusion with amiodarone, shows current (upper trace), $\dot{V}_{max}$ (middle trace), and intracellular potential (lower trace) during a 600-ms (left) and a 6600-ms (right) conditioning plateau clamp to +28 mV, followed by a test stimulus. The $\dot{V}_{max}$ of the test stimulus was mildly depressed after the short conditioning clamp, and severely depressed by the long clamp. A plot of $\dot{V}_{max}$ in this experiment, normalized to the control value, against duration of the plateau clamp before and after amiodarone administration is shown in *B*.

pears to have some affinity for the inactivated state, but not enough to account for all the block that develops during a pulse train [30, 62]. It is tempting to speculate that the "extra" block that develops with each action potential represents block of the activated state. Thus most of the currently used clinical agents have mixed effects on activated and inactivated channels. Figure 21–8 shows the effect of a drug with high affinity for both the activated and inactivated states.

MODULATED RECEPTOR MECHANISM OF ACTION OF ORGANIC CALCIUM-CHANNEL-BLOCKING DRUGS

Ehara and Kaufmann [67] showed that verapamil has a strongly use-dependent blocking effect on the slow inward (calcium) current and that recovery from block is potential dependent. McDonald et al. [38] showed that D-600 has a similar pattern of use-dependent onset of slow-channel blockade and voltage-dependent recovery from blockade. Results from this laboratory show that diltiazem also produces a use-dependent blockade (fig. 21–10); furthermore, the affinity for inactivated channels is much higher than for open (activated) channels [68].

Nifedipine, a very potent calcium-channel-blocking drug with little antiarrhythmic usefulness [73], appears to produce much less use-dependent blockade [71], suggesting that it may have significant affinity for the rested channel. These observations are further supported by comparison of the negative inotropic effects of verapamil and nifedipine. Verapamil has a markedly use-dependent negative inotropic action, manifested by reversal of the usual positive force–frequency relationship [74]. Furthermore, this effect is voltage dependent [75]. In contrast, nifedipine has a powerful negative inotropic effect that is relatively independent of stimulus frequency [76]. Unfortu-

nately, little voltage-clamp information is available regarding the kinetics of nifedipine action on the slow inward current.

Clinical Correlations

While it is not yet possible to predict exactly which drugs will be the most effective in a given patient's cardiac arrhythmia, it is now possible to predict whether new drugs will be useful in atrial arrhythmias, and to explain why some established agents are more useful for certain types of arrhythmias than for others.

ATRIAL TACHYCARDIA

The action potential of ordinary atrial muscle cells is characterized by a short plateau which shortens even more in tachycardia. Therefore, inactivated-channel blockers will cause relatively less sodium-channel block in atrial tissue. If the inactivated-channel blocker also has relatively fast recovery kinetics during diastole (e.g., lidocaine and phenytoin) the drug will have a low efficacy against atrial tachycardia. If, on the other hand, diastolic recovery is slowed by depolarization (e.g., digitalis toxicity) the blocked inactivated channels will accumulate and the drug may be expected to be more effective. This provides an explanation for the clinical observation that lidocaine is not very effective for atrial arrhythmias except those caused by digitalis toxicity [64]. It is important to note that amiodarone, which appears to act almost exclusively upon inactivated channels, is nevertheless more effective than lidocaine in atrial arrhythmias [77]. There are several possible explanations for this. Amiodarone has a slower diastolic recovery from block. Moreover, amiodarone lengthens the action potential duration, thus potentiating its inactivated-state block. Finally, amiodarone has additional effects, including calcium-entry blockade and antiadrenergic activity.

Quinidine is more effective as the number of action potentials per unit time is increased [30] while action potential duration is of relatively less importance in determining the fraction of channels blocked. Quinidine has a relatively slow time constant of recovery from block during diastole so block accumulates, especially at fast rates; hence the drug's effectiveness against atrial tachycardias.

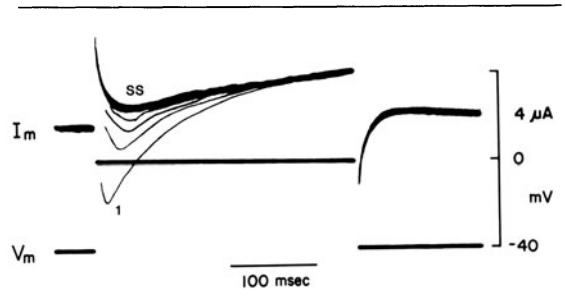

FIGURE 21–10. Effect of diltiazem, 4.4 μ*M* on slow inward current (Im) in voltage-clamped ferret papillary muscle. The drug had been present for 30 min. The numeral 1 indicates the first pulse of a train of clamps at 2 Hz after a rest period of several minutes, "SS" denotes the twentieth clamp. Traces for the first 20 clamp pulses are superimposed. Note that the current rapidly diminished toward a steady-state level with successive pulses.

AV NODAL ARRHYTHMIAS

Numerous conditions exist in which slow conduction through the atrioventricular (AV) node contributes to reentry arrhythmias. Since the major inward current in the AV node is a calcium current [78], it is not surprising that calcium-entry blockers can be quite effective against these arrhythmias. Like most of the sodium-channel blockers, these drugs have a high affinity for depolarized (i.e., inactivated) channels. Recovery from block proceeds slowly in depolarized cells and faster in cells with more negative resting potentials [38]. Therefore, in reciprocating rhythms involving an accessory pathway, these drugs will usually block the calcium-dependent pathway, especially if it is depolarized. Thus, the node is more likely to be blocked than the accessory bundle.

VENTRICULAR ARRHYTHMIAS

Ventricular and Purkinje fibers have long action potentials, hence inactivation block is much more important in these cells than in atrial tissue. Another important feature of healthy ventricular and nonpacemaker Purkinje cells is their fairly negative diastolic potential (-85 to -90 mV). Thus, although lidocaine

blocks a large fraction of the sodium channels during each plateau phase, the fast diastolic recovery (at −90 mV) ensures that most channels are unblocked by the time of the next normal action potential. There are, however, two exceptions: (a) $\dot{V}_{max}$ of early extrasystoles occurring *before* the drug–receptor complexes have dissociated are strongly suppressed, and (b) in tissues depolarized by disease, diastolic recovery from block proceeds much more slowly or not at all (compare figs. 21–5B and 21–6C). Hence, in depolarized tissue and especially for early extrasystoles, channels will be significantly blocked by a concentration of lidocaine that has no remarkable effect on conduction of the normal sinus impulse through healthy tissue.

Drugs that act on channels only when they are in the activated state are not assisted by the long plateau duration of Purkinje and ventricular cells. Only when a tachycardia develops will they succeed in blocking a substantial fraction of the sodium channels. It is then not surprising that lidocaine-like drugs appear more effective than quinidine [79] in suppressing premature depolarizations, while quinidine may be more effective in suppressing regular ventricular tachycardias [80].

OTHER CLINICAL APPLICATIONS

As indicated in an earlier publication [30], the combination of two antiarrhythmic drugs with different kinetic parameters may be considerably more effective than either drug alone, independent of dosage. In a clinical test of this prediction, Breithardt [81] showed that patients who were resistant to both disopyramide alone and mexiletine alone were successfully managed with a combination of these two dissimilar drugs.

Another predictable drug interaction results from the state-dependent model. If drug A lengthens the action potential duration and if drug B is an inactivated-state blocker, then at any given rate A will lengthen the effective time for inactivated-state block to develop and shorten the time for recovery from it. For example, amiodarone lengthens the action potential duration and therefore will enhance its own effect (see above), as well as that of any other inactivated-state blocker, e.g., lidocaine. Conversely, drugs that shorten action potential duration (e.g., acetylcholine in the atria) would be expected to reduce the effect of an inactivated-state blocker. Similarly, if a drug were found that safely and reliably reduced Purkinje or ventricular action potential duration, then such a drug might be useful in reversing conduction block induced by an overdose of an inactivated-state blocker.

At this stage in the development of the modulated receptor hypothesis, more extensive application to clinical drug selection would be premature. More information is needed on the cellular physiology of the cardiac tissue responsible for the abnormal rhythm. Especially valuable would be information on the resting potential in vivo. Unfortunately, this variable is most difficult to measure in patients.

Conclusion

We have discussed the modulated receptor hypothesis of sodium- and calcium-channel blockade and applied it to various types of drugs used in the treatment of arrhythmias. The model provides a mechanism by which useful antiarrhythmic drugs can selectively suppress abnormal electrical activity. A better understanding of the voltage- and time-dependent actions of antiarrhythmic drugs will allow a more rational selection of a drug for a particular arrhythmia, as well as the development of new drugs with optimized voltage–time characteristics. Our discussion has been limited to inward-current blockers. Other factors, like automaticity suppression, changes of action potential duration and refractoriness, and autonomic properties of antiarrhythmic drugs can also contribute in important ways to the control of certain arrhythmias.

References

1. Weidmann S: Effects of calcium ions and local anaesthetics on electrical properties of Purkinje fibres. J Physiol (Lond) 129:568–582,
2. Hondeghem L, Grant AO, Jensen RA: Antiarrhythmic drug action: selective depression of hypoxic cardiac cells. Am Heart J 87:602–605, 1974.
3. Grant AO, Katzung BG: The effects of quinidine

and verapamil on electrically-induced automaticity in the ventricular myocardium of guinea pig. J Pharmacol Exp Ther 196:407–419, 1976.
4. Fleckenstein A: Specific inhibitors and promotors of calcium action in the excitation–contraction coupling of heart muscle and their role in the prevention or production of myocardial lesions. In: Harris P, Opie LH (eds) Calcium and the heart. New York: Academic, 1971, pp 135–188.
5. Grant AO, Katzung BG: Ability of epinephrine, but not increased extracellular calcium, to reverse the effects of verapamil on ventricular automaticity in vitro. Proc West Pharmacol Soc 18:34–36, 1975.
6. Hondeghem LM, Ayad MJ: K Nifedipine blocks the voltage dependent potentiation of norepinephrine in vascular smooth muscle. Proc West Pharmacol Soc, 26:231–233, 1983.
7. Hille B: Local anesthetics: hydrophilic and hydrophobic pathways for the drug-receptor reaction. J Gen Physiol 69:497–515, 1977.
8. Hondeghem LM, Katzung BG: Time- and voltage-dependent interaction of antiarrhythmic drugs with cardiac sodium channels. Biochim Biophys Acta 472:373–398, 1977.
9. Attwell D, Cohen I: The voltage clamp of multicellular preparations. Prog Biophys Mol Biol 31:201–245, 1977.
10. Beeler GW, McGuigan JA: Voltage clamping of multicellular myocardial preparations: capabilities and limitations of existing methods. Prog Biophys Mol Biol 34:219–254, 1978.
11. Hondeghem LM: Validity of $\dot{V}_{max}$ as a measure of the sodium current in cardiac and nervous tissues. Biophys J 23:147–152, 1978.
12. Walton M, Fozzard HA: The relation of $\dot{V}_{max}$ to I_{Na}, G_{Nc} and h_x in a model of the cardiac Purkinje fiber. Biophys J 25:407–420, 1979.
13. Ebihara L, Shigeto N, Lieberman M, Johnson EA: The initial inward current in spherical clusters of chick embryonic heart cells. J Gen Physiol 75:437–456, 1980.
14. Colatsky TJ: Voltage clamp measurements of sodium channel properties in rabbit cardiac Purkinje fibres. J Physiol (Lond) 305:215–234, 1980.
15. Brown AM, Lee KS, Powell T: Sodium current in single rat heart muscle cells. J Physiol (Lond) 318:479–500, 1981.
16. Spach MS, Miller WT III, Geselowitz DB, Barr RC, Kootsey JM, Johnson EA: The discontinuous nature of propagation in normal canine cardiac muscle: evidence for recurrent discontinuities of intracellular resistance that affect the membrane currents. Circ Res 48:39–54, 1981.
17. Jensen RA, Katzung BG: Electrophysiological action of diphenylhydantoin on rabbit atria: dependence on stimulation frequency, potassium, and sodium. Circ Res 26:17–27, 1970.
18. Singh BN, Vaughan Williams EM: Effect of altering potassium concentration on the action of lidocaine and diphenylhydantoin on rabbit atrial and ventricular muscle. Circ Res 29:286–295, 1971.
19. Hope RR, Williams DO, El-Sherif N, Lazzara R, Scherlag BJ: The efficacy of antiarrhythmic agents during acute myocardial ischemia and the role of heart rate. Circulation 50:507–514, 1974.
20. Kupersmith J, Antman EM, Hoffman BF: In vivo electrophysiologic effects of lidocaine in canine acute myocardial infarction. Circ Res 36:84–91, 1975.
21. Michelson EL, Spear JF, Moore EN: Effects of procainmide on strength–interval relations in normal and chronically infarcted canine myocardium. Am J Cardiol 47:1223–1232, 1981.
22. Lamanna V, Antzelevitch C, Moe GK: Effects of lidocaine on conduction through depolarized canine false tendons and on a model of reflected reentry. J Pharmacol Exp Ther 221:353–361, 1982.
23. Wong SS, Myerburg RJ, Ezrin AM, Gelband H, Bassett AL: Electrophysiologic effects of encainide on acutely ischemic rabbit myocardial cells. Eur J Pharmacol 80:323–329, 1982.
24. Okumura K, Horio Y, Tokuomi H: Effects of lidocaine on conduction in normal and acutely ischemic ventricular myocardium of dogs. Arch Int Pharmacodyn 256:269–282, 1982.
25. Johnson EA, McKinnon MG: Differential effect of quinidine and pyridamine on the myocardial action potential at various rates of stimulation. J Pharmacol Exp Ther 120:460–465, 1957.
26. Heistracher P: Mechanism of action of antifibrillatory drugs. Naunyn Schmiedebergs Arch Pharmacol 269:199–212, 1971.
27. Strichartz G: The inhibition of sodium currents in myelinated nerve by quaternary derivatives of lidocaine. J Gen Physiol (Lond) 62:37–57, 1973.
28. Courtney KR: Mechanism of frequency-dependent inhibition of sodium currents in frog myelinated nerve by the lidocaine derivative GEA 968. J Pharmacol Exp Ther 195:225–236, 1975.
29. Chen C-M, Gettes LS, Katzung BG: Effect of lidocaine and quinidine on steady-state characteristics and recovery kinetics of $(dV/dt)_{max}$ in guinea pig ventricular myocardium Circ Res 37:20–29, 1975.
30. Hondeghem LM, Katzung BG: Effect of quinidine and lidocaine on myocardial conduction. Circulation 61:1217–1224, 1980.
31. Hodgkin AL, Huxley AF: The dual effect of membrane potential on sodium conductance in the giant axon of Loligo. J Physiol (Lond) 116:497–506, 1952.
32. Bean BP, Cohen CJ, Tsien RW: Lidocaine block of cardiac sodium channels. J Gen Physiol, 81:613–642, 1983.
33. Sada H: Effect of phentolamine, alprenolol, and prenylamine on maximum rate of rise of action potential in guinea-pig papillary muscles. Naunyn Schmiedebergs Arch Pharmacol 304:191–201, 1978.
34. Sada H, Kojima M, Ban T: Effect of procainamide on transmembrane action potentials in guinea-pig papillary muscles as affected by external potassium concentration. Naunyn Schmiedebergs Arch Pharmacol 309:179–190, 1979.
35. Courtney KR: Interval-dependent effects of small an-

tiarrhythmic drugs on excitability of guinea pig myocardium. J Mol Cell Cardiol 12:1273–1286, 1980.
36. Courtney KR: Antiarrhythmic drug design: frequency-dependent block in myocardium. In: Fink RB (ed) Molecular mechanisms of anesthesia. Progress in anesthesiology, vol 2. New York: Raven, 1980, pp 111–118.
37. Kohlhardt M, Seifert C: Inhibition of $\dot{V}_{max}$ of the action potential by propafenone and its voltage-, time-, and pH-dependence in mammalian ventricular myocardium. Naunyn Schmiedebergs Arch Pharmacol 315:55–62, 1980.
38. McDonald T, Pelzer D, Trautwein W: On the mechanisms of slow calcium channel block in heart. Pflugers Arch 385:175–179, 1980.
39. Oshita S, Sada H, Kojima M, Ban T: Effects of tocainide and lidocaine on the transmembrane action potentials as related to external potassium concentrations in guinea-pig papillary muscles. Naunyn Schmiedebergs Arch Pharmacol 314:67–82, 1980.
40. Sada H, Ban T: Effects of acebutolol and other structurally related *beta* adrenergic blockers on transmembrane action potential in guinea-pig papillary muscles. J Pharmacol Exp Ther 215:507–514, 1980.
41. Arlock P: Actions of lofepramine, a new tricyclic antidepressant, and desipramine on electrophysiological and mechanical parameters of guinea pig atrial and papillary muscles. Acta Pharmacol Toxicol 49:248–258, 1981.
42. Catterall WA: Inhibition of voltage-sensitive sodium channels in neuroblastoma cells by antiarrhythmic drugs. Mol Pharmacol 20:356–362, 1981.
43. Cardinal R, Janse MJ, Van Eeden I, Werner G, Naumann d'Alnoncourt C, Durrer D: The effects of lidocaine on intracellular and extracellular potentials, activation and ventricular arrhythmias during acute regional ischemia in the isolated procine heart. Circ Res 49:792–806, 1981.
44. Carson DL, Dresel PE: Effects of lidocaine on conduction of extrasystoles in the normal canine heart. J Cardiol Pharmacol 3:924–935, 1981.
45. Cordova MA, Bagwell EE, Lindenmayer GE: Studies on the interaction of propranolol and tetrodotoxin on dV/dt_{max} of canine Purkinje fiber action potentials. J Pharmacol Exp Ther 219:187–191, 1981.
46. Courtney KR: Comparative actions of mexiletine on sodium channels in nerve, skeletal and cardiac muscle. Eur J Pharmacol 74:9–18, 1981.
47. Courtney KR: Significance of bicarbonate for antiarrhythmic drug action. J Mol Cell Cardiol 13:1031–1034, 1981.
48. Gilmour RF, Ruffy R, Lovelace DE, Mueller TM, Zipes DP: Effect of ethanol on electrogram changes and regional myocardial blood flow during acute myocardial ischemia. Cardiovasc Res 15:47–58, 1981.
49. Gilmour RF, Chikharev VN, Jurevichus JA, Zacharow S, Zipes DP: Effect of aprindine on transmembrane currents and contractile force in frog atria. J Pharmacol Exp Ther 217:390–396, 1981.
50. Kolhardt M, Haap K: The blockade of V_{max} of the atrioventricular action potential produced by the slow channel inhibitors verapamil and nifedipine. Naunyn Schmiedebergs Arch Pharmacol 316:178–185, 1981.
51. Nattel S, Elharrar V, Zipes DP, Bailey JC: pH-dependent electrophysiological effects of quinidine and lidocaine on canine cardiac Purkinje fibers. Circ Res 48:55–61, 1981.
52. Rudiger HJ, Homburger H, Antoni H: Effects of a new antiarrhythmic compound [2-benzol-1-(2′ diisopropyl-amino-ethoxy-imino)-cycloheptome hydrogen fumarate] on the electrophysiological properties of mammalian cardiac cells. Naunyn Schmiedebergs Arch Pharmacol 317:238, 1981.
53. Sada H, Ban T: Time independent effects on cardiac action potential upstroke velocity (resting block) and lipid solubility of beta adrenergic blockers. Experientia 37:171–172, 1981.
54. Sada N, Ban T: Effects of various structurally related beta-adrenocepter blocking agents on maximum upstroke velocity of action potential in guinea-pig papillary muscles. Naunyn Schmiedebergs Arch Pharmacol 317:245–251, 1981.
55. Campbell TJ, Vaughan Williams EM: Electrophysiological and other effects on rabbit hearts of CCI22277, a new steroidal antiarrhythmic drug. Br J Pharmacol 76:337–345, 1982.
56. Carmeliet E, Saikawa T: Shortening of the action potential and reduction of pacemaker activity by lidocaine, quinidine, and procainamide in sheep cardiac Purkinje fibers: an effect on Na or K currents? Circ Res 50:257–272, 1982.
57. Colatsky TJ: Mechanisms of action of lidocaine and quinidine on action potential duration in rabbit cardiac Purkinje fibers. Circ Res 50:17–27, 1982.
58. Connors BW, Prince DA: Effects of local anesthetic OX314 on the membrane properties of hippocampal pyramidal neurons. J Pharmacol Exp Ther 220:476–481, 1982.
59. Grant AO, Trantham JL, Brown KK, Strauss HC: pH-dependent effects of quinidine on the kinetics of dV/dt_{max} in guinea pig ventricular myocardium. Circ Res 50:210–217, 1982.
60. Kojima M, Ban T, Sada H: Effects of disopyramide on the maximum rate of rise of the potential (V_{max}) in guinea-pig papillary muscles. Jpn J Pharmacol 32:91–102, 1982.
61. Hohnloser S, Weirich J, Antoni H: Effects of mexiletine on steady-state characteristics and recovery kinetics of V_{max} and conduction velocity in guinea pig myocardium. J Cardiovasc Pharmacol 4:232–239, 1982.
62. Weld FM, Coromilas J, Rothman JN, Bigger JT Jr: Mechanisms of quinidine-induced depression of maximum upstroke velocity in ovine cardiac Purkinje fibers. Circ Res 50:369–376, 1982.
63. Payet MD: Effect of lidocaine on fast and slow inactivation of sodium current in rat ventricular cells. J Pharmacol Exp Ther 223:235–240, 1982.
64. Rosen MR, Hoffman BF, Wit AL: Electrophysiology

and pharmacology of cardiac arrhythmias. V. Cardiac antiarrhythmic effects of lidocaine. Am Heart J 89:526–536, 1975.

65. Ehring GR, Moyer JW, Hondeghem LM: Implications from electrophysiological differences resulting from small structural changes in antiarrhythmic drugs. Proc West Pharmacol Soc 25:65–67, 1982.
66. Mason JW, Hondeghem LM, Katzung BG: Amiodarone blocks inactivated cardiac sodium channels. Pflugers Arch 396:79–81, 1983.
67. Ehara T, Kaufmann R: The voltage- and time-dependent effects of (−)-verapamil on the slow inward current in isolated cat ventricular myocardium. J Pharmacol Exp Ther 207:49–55, 1978.
68. Kanaya S, Arlock P, Katzung BG, Hondeghem LM: Diltiazem and verapamil preferentially block inactivated calcium channels. J Mol Cell Cardiol 15:145–148, 1983.
69. Morad M, Tung L, Greenspan AM: Effect of diltiazem on calcium transport and development of tension in heart muscle. Am J Cardiol 49:595–601, 1982.
70. Kolhardt M, Fleckenstein A: Inhibition of the slow inward current by nifedipine in mammalian ventricular myocardium. Naunyn Schmiedebergs Arch Pharmacol 298:267–272, 1977.
71. Bayer R, Ehara T: Comparative studies with calcium antagonists. In: Van Zwieten PA, Schonbaum E (eds) The action of drugs on calcium metabolism. Stuttgart: Fischer Verlag, 1978, pp 31–37.
72. Moyer J, Hondeghem LM: Characterization of activation and inactivation block in a series of aprindine derivatives using voltage clamp technique. Fed Proc 42:634, 1983.
73. Kawai C, Konishi T, Matsuyama E, Okazaki H: Comparative effects of three calcium antagonists, diltiazem, verapamil, and nifedipine, on the sinoatrial and atrioventricular nodes: experimental and clinical studies. Circulation 63:1035–1042, 1981.
74. Bayer R, Hennekes R, Kaufmann R, Mannhold R: Inotropic and electrophysiological actions of verapamil and D600 in mammalian myocardium. I. Patterns of inotropic effects of racemic compounds. Naunyn Schmiedebergs Arch Pharmacol 290:49–68, 1975.
75. Linden J, Brooker G: The influence of resting membrane potential on the effect of verapamil on atria. J Mol Cell Cardiol 12:325–331, 1980.
76. Bayer R, Rodenkirchen R, Kaufmann R, Tec JH, Hennekes R: The effect of nifedipine on contraction and monophasic action potential of isolated cat myocardium. Naunyn Schmiedebergs Arch Pharmacol 301:29–37, 1977.
77. Rowland E, Krikler DM: Electrophysiological assessment of amiodarone in treatment of resistant supraventricular arrhythmias. Br Heart J 44:82–90, 1980.
78. Kokubun S, Nishimura M, Noma A, Irasawa H: Membrane currents in the rabbit atrioventricular node cell. Pflugers Arch 393:15–22, 1982.
79. Sami M, Harrison DC, Kraemer H, Houston N, Shimasaki C, De Busk RF: Antiarrhythmic efficacy of encainide and quinidine: validation of a model of drug assessment. Am J Cardiol 48:147–156, 1981.
80. Mason JW, Winkle RA: Electrode-catheter arrhythmia induction in the selection and assessment of antiarrhythmic drug therapy for recurrent ventricular tachycardia. Circulation 58:971–985, 1978.
81. Breithardt G, Seipel L, Abendroth RR: Comparison of antiarrhythmic efficacy of disopyramide and mexiletine against stimulus-induced ventricular tachycardia. J Cardiovasc Pharmacol 3:1026–1037, 1981.
82. Singh BN, Vaughan Williams EM: The effect of amiodarone, a new anti-anginal drug, on cardiac muscle. Br J Pharmacol 39:657–667, 1970.

22. CALCIUM AND THE INJURED CARDIAC MYOCYTE

Winifred G. Nayler
and M.J. Daly

Introduction

Injured cardiac myocytes accumulate Ca^{2+}. It does not seem to matter whether the injury is due to reperfusion after prolonged periods of normothermic ischemia [1, 2], sustained hypoxia [3], a naturally occurring cardiomyopathy, or the reintroduction of Ca^{2+} after only a few minutes of Ca^{2+}-free perfusion [4–6], the end result is the same—that is, the cells become overloaded with Ca^{2+}. The primary aim of this chapter is to establish why the injured myocytes accumulate Ca^{2+}, and then to define the route by which this Ca^{2+} enters. Finally we will consider the consequences of the resultant Ca^{2+} overloading.

Calcium Gain during Postischemic Reperfusion

THE AMOUNT OF Ca^{2+} INVOLVED

Shen and Jennings [1] were the first to describe a gain in tissue Ca^{2+} associated with postischemic reperfusion. Before considering how or why this happens, it is possibly worth spending a few moments considering how much Ca^{2+} is involved and why it is so important. The data summarized in figure 22–1 go some way toward accomplishing this, because they show the magnitude of the gain in Ca^{2+} that is involved and the linear relationship which exists between it and the recovery of active tension-generating capacity upon reperfusion. These particular data were obtained during a series of experiments [7] in which isolated, retrogradely perfused rabbit hearts were being made totally ischemic for 60 min at temperatures ranging between 25° and 37° and then reperfused at 37°C. After 15 min of reperfusion the hearts were dissolved in concentrated nitric acid and assayed for Ca^{2+} by atomic absorption spectrophotometry [8]. All the time the hearts were being perfused, and while they were globally ischemic or being reperfused, tension development was monitored [3]. Now, as this figure 22–1 shows, when the percentage recovery of developed tension that occurred upon reperfusion was plotted as a function of the gain in tissue Ca^{2+} a straight line was obtained, with those hearts which had accumulated the least Ca^{2+} exhibiting the best recovery. Some idea of the relevance of a gain in Ca^{2+} of between 2 and 10 μmol/g dry weight (fig. 22–1) can be obtained by recalling that the cytosol of cardiac myocytes usually contains only submicromolar concentrations of ionized calcium. Even the total amount of Ca^{2+} which is present in normal heart muscle, including that which is stored in the various intracellular compartments (the mitochondria and the sarcoplasmic reticulum), is only about 2.0–2.5 μmol/g dry weight. Hence, as Shen and Jennings [1] pointed out over a decade ago, reperfusion after a relatively short period of ischemia can result in as much as fivefold increase in the calcium content of the tissue.

These investigations were supported by a grant from the National Health and Medical Research Council of Australia.

N. Sperelakis (ed.), PHYSIOLOGY AND PATHOPHYSIOLOGY OF THE HEART.

Martinus Nijhoff Publishing, Boston/The Hague/ Dordrecht/Lancaster.

Confirmation of the fact that there is a straight-line relationship between the percentage recovery of active tension-generating capacity during post ischemic reperfusion and the accompanying gain in tissue Ca^{2+} has come from some recently published data relating to the effects of ischemia and postischemic reperfusion on the Ca^{2+} content of rabbit interventricular septum preparations [9]. Likewise, on searching through the literature it is not difficult to find evidence to support the conclusion that, upon reperfusion, mammalian hearts which have been allowed to become ischemic accumulate Ca^{2+}. Thus, for example, Peng et al. [10] reported a fourfold increase in the Ca^{2+} content of pig hearts which had been made ischemic (by occluding the left anterior descending coronary artery) for 2 h and then reperfused. Other data are summarized in table 22–1.

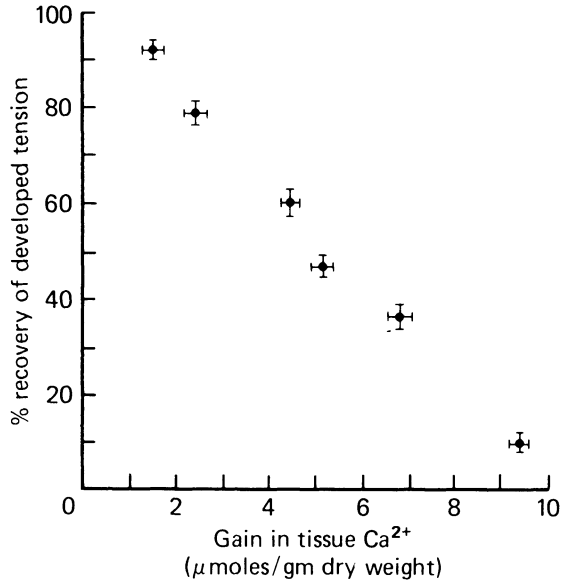

FIGURE 22–1. Relationship between the gain in tissue Ca^{2+} during postischemic reperfusion and the recovery of active tension-generating capacity. Hearts were made ischemic for 60 min before being reperfused for 15 min at 15°C. Percentage recovery of developed tension refers to the percentage recovery relative to the tension developed immediately before the hearts were made globally ischaemic. Each result is the mean ± SE of at least six estimations.

THE RELEVANCE OF THE DURATION AND INTENSITY OF THE ISCHEMIC INSULT

The data listed in table 22–1 relate only to the effect of reperfusion after a fairly prolonged period of total ischemia. In their earlier experiments Shen and Jennings [1, 11] noted that reperfusion after a relatively short episode of ischemia is not necessarily accompanied by a gain in Ca^{2+}. What happens, then, if there is only a partial reduction in coronary flow—as may happen, for example, during coronary artery spasm or following the formation and subsequent removal of a thrombus? Table 22–2 helps to answer this question, because it shows that in rabbit hearts, for example, restoring full flow after 60 or more minutes of reperfusion at one-fifth of the normal flow rate does not necessarily result in a complete recovery of the active tension-generating capacity of the hearts. Moreover this table also shows that such a restoration of flow may still be accompanied by a raised tissue Ca^{2+}. Apart from confirming that ischemic heart muscle gains Ca^{2+} upon reperfusion, and that there is a positive correlation between a failure to regenerate the active tension-generating capacity of the myocardium and the gain in tissue Ca^{2+}, table 22–2 contains at least one other point of interest—the magnitude of the gain in Ca^{2+} and loss of con-

TABLE 22–1. Reperfusion-induced gain in myocardial Ca^{2+} content

Preparation	Minutes of ischemia	Minutes of reperfusion	Gain in Ca^{2+} (μmol/g)	Ref
Dog posterior papillary muscle	40	20	3.8	1
Rabbit interventricular septum	60	30	6.7 ± 0.7	9
Rabbit left ventricle	60	15	6.3 ± 0.2	8

Gain in Ca^{2+} is expressed as μmol/g dry weight tissue.

TABLE 22–2. Recovery of developed tension and gain in tissue Ca^{2+} during reperfusion after 30, 60, or 90 min of graded ischemia at 37°C

Duration of ischemia (min)	30	60	90
Moderate low flow (3 ml/min)			
% Recovery	100	72	55
Gain in Ca^{2+}	0.6 ± 0.2	0.9 ± 0.3	1.1 ± 0.2
Severe low flow (1 ml/min)			
% Recovery	80	39	22
Gain in Ca^{2+}	2.6 ± 0.3	5.4 ± 0.9	9.8 ± 0.6
Global ischemia (zero flow)			
% Recovery	36	18	0
Gain in Ca^{2+}	4.6 ± 0.4	8.2 ± 0.3	9.6 ± 2.1

The percentage recovery developed tension refers to tension recovered after 30 min of reperfusion expressed as a percentage of the tension developed immediately before reducing the coronary flow rate from the control level of 15 ml/min to 3, 1, or 0 ml/min as indicated. Ca^{2+} is measured as μmol/g dry weight. The experiments were performed at 37°C, using adult New Zealand White male rabbits.

tractility is roughly proportional to (a) the *duration* of the ischemic episode, and (b) the *severity* of the reduction in coronary flow.

KINETIC CONSIDERATIONS

Some idea of the rapidity with which the ischemic myocardium accumulates Ca^{2+} upon reperfusion was provided by Shen and Jennings [11]. Using an ischemic period of 40 min they followed the rate of $^{45}Ca^{2+}$ uptake when coronary flow was reintroduced, and found that asymptote had been reached within about 10 min. These earlier findings have subsequently been confirmed by others [9]. We can safely conclude, therefore, that the uptake of Ca^{2+} is a rapid process. Nevertheless it does not appear to be instantaneous–or could it be that some cells have been more damaged than others by the ischemic episode, and that upon reperfusion the most damaged cells accumulate Ca^{2+} instantaneously, while the less damaged cells accumulate the Ca^{2+} more slowly, or perhaps at a later time?

TABLE 22–3. Effect of the duration of the ischemic episode on the reperfusion-induced gain in Ca^{2+}

Perfusion	Gain in Ca^{2+} after 30-min reperfusion (μmol/g dry wt)
30-min ischemia	4.0 ± 0.2
60-min ischemia	6.7 ± 0.7

These data relate to studies on rabbit interventricular septa [9]. The preparations were made ischemic at 28°C for the indicated times and then reperfused for 30 min.

SPECIFICITY OF THE REPERFUSION-INDUCED GAIN IN Ca^{2+}

As discussed by Shine et al. [12], theoretically there is no reason why the net accumulation of cellular Ca^{2+} that occurs during postischemic reperfusion need depend solely on a defect in Ca^{2+} influx. Maybe it could involve a decrease in Ca^{2+} efflux from the cell. This does not seem to be the case, however, because Ca^{2+} efflux remains relatively undisturbed at a time when Ca^{2+} influx is progressing rapidly, as if out of control [2]. The amount of Ca^{2+} that is accumulated depends, to some extent, upon the duration of the preceding ischemic episode. Thus table 22–3 shows, for example, that rabbit interventricular septa that are reperfused after 30 min of ischemia at 28°C gain 4.0 ± 0.2 μmol Ca^{2+}/g dry wt, whereas similar preparations that have been reperfused after 60 min of ischemia gain 6.7 ± 0.7 μmol/g dry weight [9]. There appears to be no specificity for Ca^{2+} in this uptake process. Thus studies in which either ^{133}Ba or ^{85}Sr have been added to the perfusion buffer instead of ^{45}Ca [1] or ^{47}Ca [9] have shown [12] that both of these isotopes are accumulated during postischemic reperfusion. In the case of ^{133}Ba, reperfusion after only 15 min of ischemia at 37°C does not cause an enhanced uptake of ^{133}Ba; reperfusion after 30 min of ischemia causes the rate of ^{133}Ba uptake

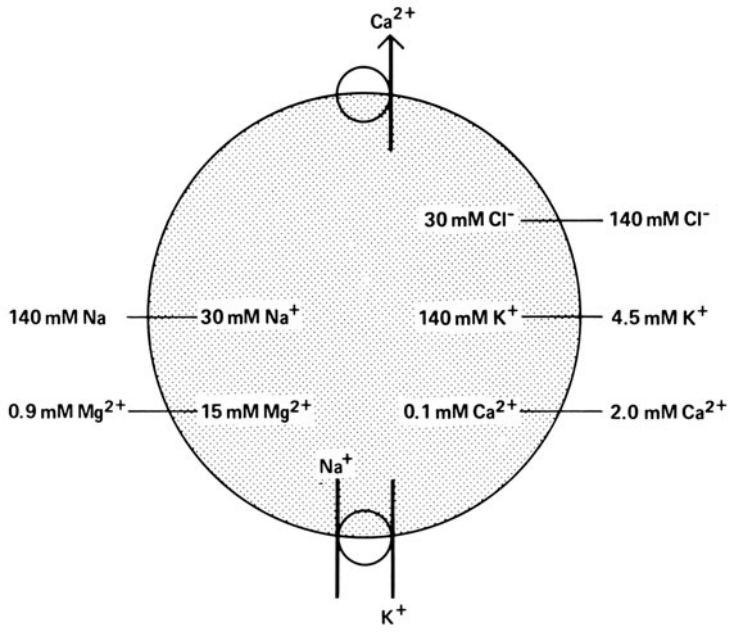

FIGURE 22–2. Schematic representation of the differential distribution of ions across the plasmalemma of cardiac myocytes.

to increase by 33% [12], while after 60 min of ischemia the rate of ^{133}Ba uptake is more than doubled. If ^{85}Sr is used as the marker a less dramatic effect is obtained [12], with no increase in uptake after up to 45 min of ischemia, but an enhanced rate of uptake when the duration of the ischemia episode is extended to 60–70 min. This lack of specificity extends beyond the divalent cations. Thus marked changes occur in the tissue content of other electrolytes. Tissue Na^+ rises, and K^+ falls; there is also a gain in tissue H_2O, and loss of Mg^{2+} [1]. Looking at the distribution of these ions in normal mammalian heart muscle (fig. 22–2) it could be imagined that reperfusion after a prolonged period of ischemia has simply allowed the various ions to flow down their electrochemical gradient. Could this be why we do not see an enhanced rate of Ca^{2+} efflux? Is it simply because there is an inward driving force for Ca^{2+} across what may now be a nonselectively permeable membrane? Before considering this possibility in greater detail we need to establish what happens to the Ca^{2+} that accumulates under these conditions.

LOCALIZATION OF THE ACCUMULATED Ca^{2+}

The Ca^{2+} that is accumulated upon reperfusion is located intracellularily—and in particular within the mitochondria where it accumulates to form dense, rosette-shaped bodies [8, 11]. The significance of these intramitochondrial Ca^{2+} deposits should not be overlooked or underestimated. Thus, as figure 22–3 shows, if the percentage increase in the Ca^{2+} content of mitochondria harvested from ischemic-reperfused hearts is plotted against the percentage recovery of the active tension-generating capacity of the hearts from which the mitochondria were harvested we again find a linear relationship. Clearly the hearts which recover best are those in which the mitochondria have accumulated the least Ca^{2+}. Perhaps this is not altogether surprising, because, as table 22–4 shows, mitochondria that are exposed to excessive amounts of Ca^{2+} show an impaired ATP-producing activity, even when the mitochondria are incubated in a well-oxygenated, substrate and precursor-enriched environment.

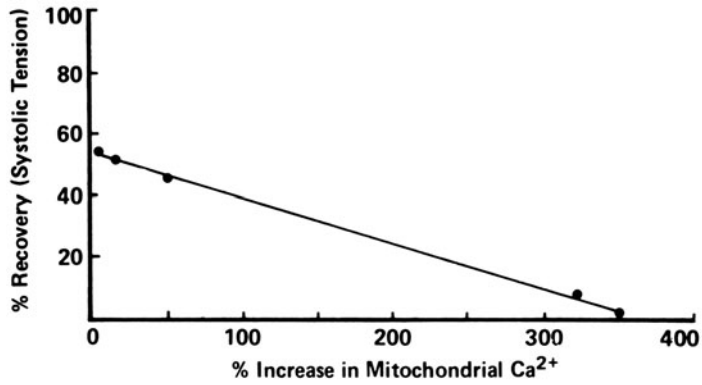

FIGURE 22–3. Relationship between the Ca^{2+} content of mitochondria harvested from hearts that had been made globally ischemic at 37°C and then reperfused, and the recovery of active tension generation. Each point refers to a single experiment.

One way of slowing down the rate at which cardiac mitochondria accumulate Ca^{2+} is to reduce the temperature. Thus (fig. 22–4), depending upon the concentration of Ca^{2+} in the incubation medium, cooling the temperature of the reaction mixture from 37°C to 25°C may actually halve the rate at which the mitochondria accumulate Ca^{2+}. We will return to this point later in this chapter, when we are discussing ways of protecting the myocardium against reperfusion-induced damage.

ISCHEMIC-INDUCED CHANGES IN CYTOSOLIC Ca^{2+} WITHOUT A NET GAIN IN Ca^{2+}

So far we have concentrated our attention on the gain in Ca^{2+} that occurs during post-ischemic reperfusion. Obviously there can be no net gain during periods of total ischemia apart from any Ca^{2+} which is taken upon from the extracellular space. If we assume that the extracellular fluid contains about 2.5 μmol/l Ca^{2+} this would only account for an uptake of about 0.35 μmol Ca^{2+}/g wet tissue weight. There may, however, be a redistribution of the tissue Ca^{2+}, so that cytosolic Ca^{2+} may rise in the absence of a net gain. There are several reasons for believing that this may occur. First, as the tissue stores of adenosine triphosphate (ATP) and creatine phosphate (CP) fall, the ionic pumps which normally operate to maintain intracellular ionic homeostasis will fail, due to substrate depletion. Some of these pumps are shown schematically in figure 22–5. They include:

TABLE 22–4. Effect of Ca^{2+} on the ATP-producing activity of cardiac mitochondria

μ*M* Ca^{2+}	% Reduction in ATP production
5	0
12.5	58 ± 4
30	68 ± 6
50	72 ± 10

Each result is the mean ± SE of six separate experiments, using mitochondria harvested from the freshly exercised hearts of six rabbits. The Ca^{2+} concentration is the free-ionized level of Ca^{2+}, obtained by buffering with EGTA. The mitochondria were incubated at 25°C in the presence of the indicated amounts of Ca^{2+} for 10 min before being assayed [8] for their ATP-producing activity.

1. The plasmalemmal-located, Ca^{2+}-activated ATPase which functions to pump Ca^{2+} out of the cell, against the prevailing concentration gradient [13]. If this pump fails we can expect any Ca^{2+} which has entered the cell, irrespective of its route of entry, to be trapped there unless it can leave in exchange for Na^{+} [14, 15].
2. The Ca^{2+}-activated ATPase of the sarcoplasmic reticulum. Since the function of this pump is to drive Ca^{2+} into the sarcoplasmic reticulum [16], its failure, whether it be due to energy depletion or some other cause, must result in a raised cytosolic Ca^{2+}

3. The plasmalemmal-located Na^+,K^+-activated ouabain-sensitive ATPase. Since this pumps Na^+ out of and K^+ into the cells against their respective concentration gradients, its failure must result in a loss of tissue K^+ and a gain in Na^+. Such ionic movements are known to occur when the myocardium is made ischemic [1]. At first sight the raised tissue Na^+ might be thought to be insignificant, but when it is recalled that a raised cytosolic Na^+ may *indirectly* trigger a raised cytosolic Ca^{2+} because: (a) Na^+ displaces Ca^{2+} from mitochondria [17], and (b) Ca^{2+} from the extracellular space may enter in exchange for Na^+ via the Na^+-Ca^{2+} exchange reaction [14, 15], its probable importance begins to emerge.

Ca^{2+} GAIN AND ATP DEPLETION

Within seconds of the onset of severe ischemia the myocardial reserves of energy-rich phosphates (adenosine triphosphate and creatine phosphate) begin to fall. After about 1 min the creatine phosphate reserves may have fallen by as much as 80% [18]; within 15 min about 65% of the tissue ATP and about 55% of the total adenine nucleotides have disappeared [19]. After about 40 min of ischemia the high-energy phosphate reserves have been virtually depleted [18] and the tissue has become irreversibly injured to such an extent that it fails to recover upon reperfusion [19, 20]. According to Reimer et al. [21], so long as the tissue levels of ATP remain above 5 μmol/g dry weight, the subsequent readmission of 0_2 does not prompt the development of cellular abnormalities. Conversely, if the tissue levels of ATP have fallen to around 2 μmol/g dry weight, reoxygenation or reperfusion precipitates overt membrane damage. Probably the depletion of the energy-rich stores and the overloading of the system with Ca^{2+} are linked, but the depletion of the energy-rich phosphate reserves *precedes* any net gain in Ca^{2+}. Thus, as Jennings and his colleagues [1, 20, 21] have shown, reperfusion after relatively short periods of ischemia is not associated with a net gain in tissue Ca^{2+}, despite the depletion ATP and CP reserves. After longer periods of ischemia (>40

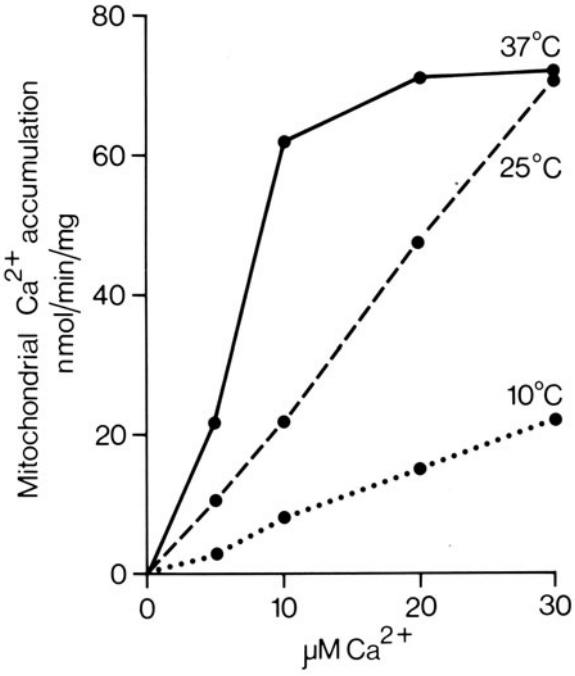

FIGURE 22–4. Effect of temperature on the rate of Ca^{2+} accumulation by isolated mammalian cardiac mitochondria.

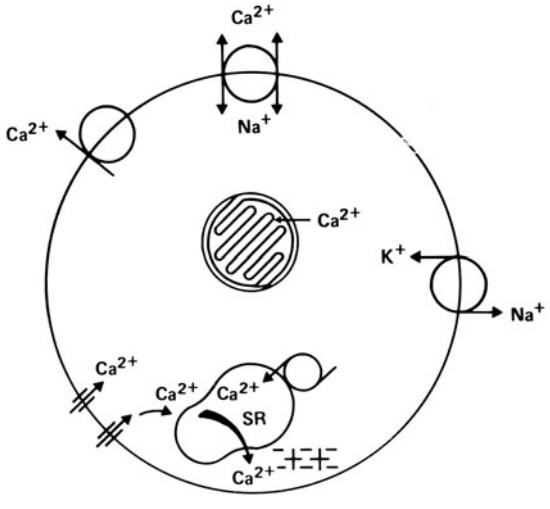

FIGURE 22–5. Schematic representation of the various Ca^{2+}-sensitive pumps in a cardiac myocyte: S.R., sarcoplasmic reticulum.

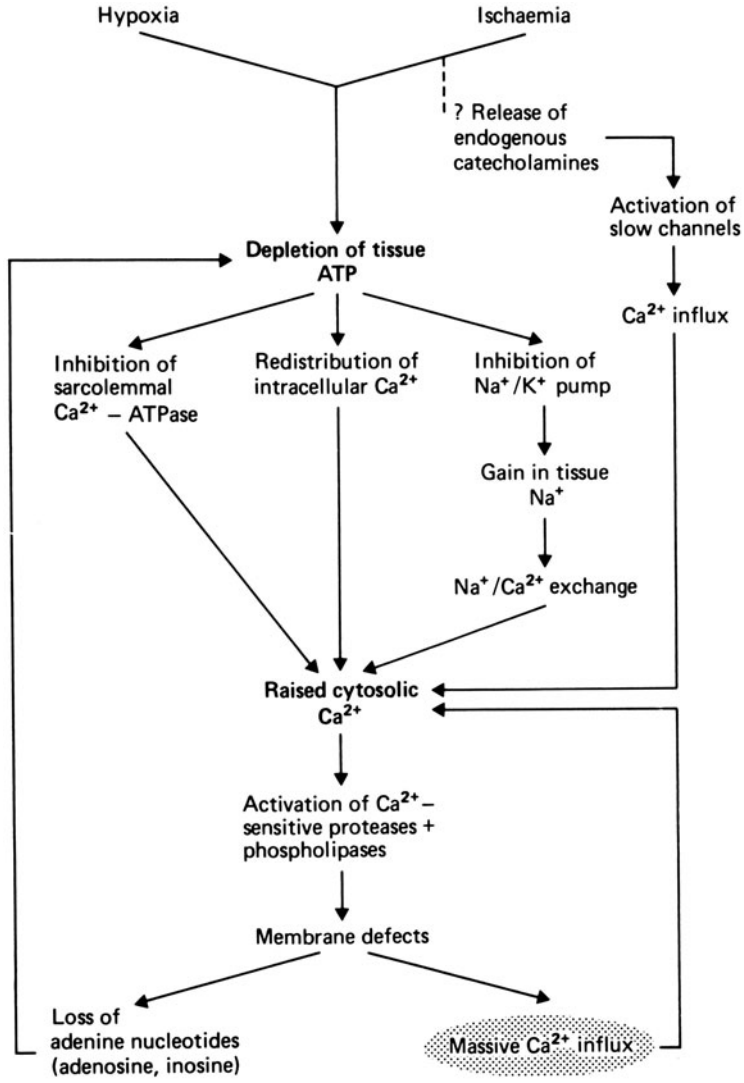

FIGURE 22–6. Possible sequence of events triggered by a prolonged period of hypoxia or ischemia.

min), however, reperfusion is most definitely accompanied by a gain in tissue Ca^{2+}, unless certain protective procedures have been invoked. In the absence of those protective procedures we can imagine there being a sequence of events that occur, similar to those described in figure 22–6. Thus, early during the hypoxic or ischemic episode, and at a time when the tissue reserves of ATP and CP are already drastically reduced, cytosolic Ca^{2+} may rise without any, or only a minor, rise in total tissue Ca^{2+}. This raised cytosolic Ca^{2+} may involve an ATP-depletion-induced inhibition of the Ca^{2+} ATPase in the sarcoplasmic reticulum, inhibition of the sarcolemmal Ca^{2+} ATPase, and inhibition of the Na^+-K^+ pump. Inhibition of this later pump must be responsible for the early rise in tissue Na^+ that occurs under these conditions [1] and this in turn may facilitate an entry of Ca^{2+} in exchange for some of the Na^+. The raised Na^+ may also promote a release of Ca^{2+} from the mitochondria [17]. All of these events will trigger a raised cyto-

solic Ca^{2+}, and once this happens a secondary phase of the response may be switched on. The second phase probably involves the activation of Ca^{2+}-sensitive proteases and phospholipases [22, 23], leading possibly to irreversible changes in the structure and integrity of the sarcolemmal complex. Once this stage has been reached we can expect there to be a massive and rapid influx of Ca^{2+}, similar to that described originally by Shen and Jennings [1], and a loss of intracellular constituents—including the adenine bases that are the precursors for ATP production [24].

In summary, therefore, the overloading of the ischemic myocardium with Ca^{2+} is a complex phenomenon triggered by an early depletion of the energy-rich phosphate reserves. *Initially* cytosolic Ca^{2+} may rise without any accompanying rise in total tissue Ca^{2+}. Some of the Ca^{2+} which appears in the cytosol may have entered in exchange for Na^+, some may have been displaced from the mitochondria, and some may have been released from the sarcoplasmic reticulum in response to the rapidly accumulating H^+ [25]. This Ca^{2+} will tend to remain in the cytosol, because of the substrate-depletion-induced failure of the various ATPases which are responsible for maintaining a low cytosolic Ca^{2+}. Once the cytosolic Ca^{2+} reaches a critical level we can expect to see an almost explosive disruption of the sarcolemma and other lipid-protein membranes, due to the activation of the endogenous Ca^{2+}-sensitive phospholipases and proteases. When this stage has been reached there is nothing to stop the extracellular Ca^{2+} from entering the cell. Hence upon reperfusion with Ca^{2+}-containing solutions we can anticipate that there will be an exacerbation of the ischemic-induced damage.

POSTISCHEMIC REPERFUSION AND THE FUNCTIONING OF THE SUBCELLULAR SYSTEMS

The Sarcolemma. Comparatively little is known about the direct effects of ischemia and postischemic reperfusion on the biochemical functioning of the sarcolemma. Its passive permeability to Ca^{2+} remains unchanged for periods of up to 1 h of ischaemia [26]. After 3 h or more, however, its passive permeability toward Ca^{2+} is increased [26]–at least in some species.

In marked contrast to the prolonged period of ischemia that is needed to alter the passive permeability of the membrane toward Ca^{2+} is a relatively early decline, within 10–20 min, in the activity of the Na^+,K^+-ATPase enzyme [26]. This decline in the activity of the Na^+,K^+-ATPase is not accompanied by, and therefore presumably is not dependent upon, a change in the phospholipid composition of the plasmalemma. Presumably, therefore, it is dependent either upon some as yet unrecognized defect in the sarcolemma or alternatively the appearance of an inhibitory substance which survives the techniques used for isolating sarcolemmal vesicles. No matter what it is due to, this early decline in the functioning of the Na^+,K^+-ATPase, when coupled to the decline in activity that may be due to substrate depletion, fits in well with the observation that early during the ischemic episode tissue Na^+ rises and K^+ falls.

The Na^+,K^+-ATPase is not the only plasmalemmal-located enzyme that is affected by an ischemic episode. Thus recently Bersohn et al. [26] described an early decline in adenylate cyclase activity. At about the same time the Na^+-Ca^{2+} exchange mechanism slows [26]. Hence there are at least three systems: Na^+-Ca^{2+} exchange, the adenylate cyclase enzyme, and the Na^+, K^+-ATPase enzyme whose functions are slowed early during an ischemic episode, at a time when the passive permeability of the sarcolemma to Ca^{2+} is unchanged.

The Myofibrils. These appear to be remarkably resistant to the effects of ischemia [27], but it is possible that as yet unrecognized changes do occur.

The Sarcoplasmic Reticulum. Quite apart from a possible inhibitory effect of ATP depletion on the Ca^{2+}-accumulating activity of the sarcoplasmic reticulum, ischemia and postischemic reperfusion *directly* affect its functioning, slowing its rate of Ca^{2+} retrieval [28]. Once again, however, this effect appears only after prolonged periods of ischemia.

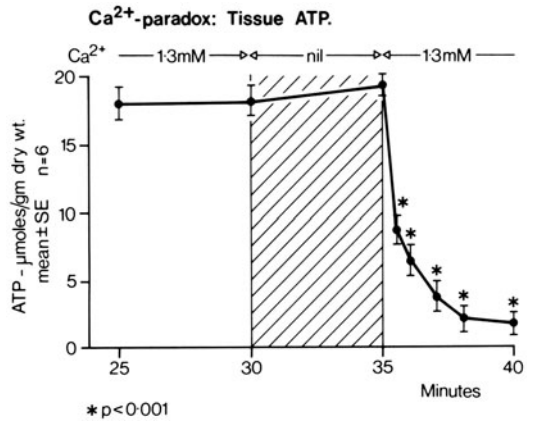

FIGURE 22–7. Tissue levels of ATP in rabbit heart muscle to which Ca^{2+} was added back after 5 min of Ca^{2+}-free perfusion at 37°C. Note that the decline in the tissue stores of ATP occurs at the time of Ca^{2+} repletion. Reproduced with permission from *Am J Pathol.*

The Mitochondria. There are numerous studies now which show that the ATP-generating activity of cardiac mitochondria declines in response to an ischemic episode [3, 10], and that the decline is exaggerated during reperfusion. This decline is paralleled by a rapid rise in their Ca^{2+} content [2, 8, 10]. These two events are probably interdependent because maintenance of normal homeostasis with respect to Ca^{2+} is dependent upon a supply of ATP, but mitochondria that are exposed to Ca^{2+}-enriched environment rephosphorylate ADP (adenosine diphosphate) slowly [8].

At the moment we are not sure why the various organelles display these changes in response to ischemia and postischemic reperfusion, but it is tempting to assume that they all reflect a basic and fundamental change in the organization of phospholipid- and proteolipid-containing membranes that occurs because of an early loss of ionic homeostasis and an accompanying rise in cytosolic Ca^{2+}.

Before describing the possible routes of Ca^{2+} entry into injured cardiac myocytes we should consider the gain in Ca^{2+} which occurs under other conditions—including that of the Ca^{2+} paradox and during posthypoxic reoxygenation.

Calcium Entry during the Calcium Paradox

DEFINITION

When isolated mammalian hearts are perfused with Ca^{2+}-free buffers, mechanical [6], but not electrical [29], activity ceases abruptly. In adult, but not in neonatal [30], hearts the readmission of Ca^{2+} a few minutes later triggers a sequence of events which has become known as *the calcium paradox* [6]. This is characterized by a rapid and massive influx of Ca^{2+} [4, 5], depletion of the energy-rich phosphate reserves [31], impaired functioning of the sarcoplasmic reticulum [32], and the extrusion of intracellular components, including creatine kinase and myoglobin, into the extracellular space. Although the occurrence of the Ca^{2+} paradox is well documented, its pathophysiology remains obscure. A major and as yet unresolved problem relates to the route of Ca^{2+} entry that is involved [33]. Some investigators have proposed that the slow channels provide the major route of Ca^{2+} entry [33]; others maintain that Ca^{2+} transport through the slow channels need not be involved [5].

FACTORS AFFECTING THE MAGNITUDE OF THE GAIN IN Ca^{2+} DURING THE PARADOX

To reiterate for a moment, a Ca^{2+} paradox is an irreversible phenomenon that is induced by reintroducing Ca^{2+} after a relatively brief period of Ca^{2+}-free perfusion. At the outset it must be realized that the conditions which have already been described, and which are associated with the massive influx of Ca^{2+} that occurs upon postischemic reperfusion, are quite different from those of the paradox. In the case of the reperfused ischemic heart a decline in the energy-rich phosphate reserves of the myocardium *precedes* the gain in Ca^{2+}, whereas during the paradox the tissue stores of ATP and CP are well maintained, or even elevated, until Ca^{2+} repletion begins [2]. Hence in the paradox the high-energy phosphate reserves are depleted *after,* and as a result of, the gain in tissue Ca^{2+} (fig. 22–7) whereas in the reperfused ischemic heart depletion of the energy-rich phosphate reserves *precedes* and may indirectly trigger the enhanced influx of Ca^{2+}.

TABLE 22–5. Myocardial Ca^{2+} and Na^+ during the Ca^{2+} paradox

Duration of Ca^{2+}-free perfusion (min)	Tissue Ca^{2+} and Na^+ (μmol/g dry wt)	
	Ca^{2+}	Na^+
0 (control hearts)	3.7 ± 0.13	44.5 ± 2.21
1	4.0 ± 0.22	45.7 ± 4.37
5	17.6 ± 0.94	132.9 ± 7.22
10	19.3 ± 0.55	129.9 ± 5.22

These results are from experiments in which isolated rat hearts were used [4]. Except during the period of Ca^{2+}-free perfusion, the perfusion buffer contained 1.25 m*M* Ca^{2+}. The experiments were performed at 37°C.

Some idea of the magnitude of the paradox-induced gain in tissue Ca^{2+} is shown by the data summarized in table 22–5. Clearly it exceeds that encountered when ischemic hearts are reperfused (compare tables 22–3 and 22–5).

The gain in Ca^{2+} that occurs during the Ca^{2+}-repletion phase of the Ca^{2+} paradox is accompanied (table 22–5) by a massive gain in Na^+ (table 22–5) and a loss of K^+ [4]. Hence it must not be assumed that the Ca^{2+} paradox is associated with a highly specific change in the selective ionic permeability of the membranes that surround the muscle cells. Instead the various ions may simply flow along their respective ionic gradients. It is pertinent to ask, however, whether measurements of cationic contents that are made after 5 or 10 min of Ca^{2+} repletion provide data which are pertinent to the changes which occur during the first few seconds of Ca^{2+} repletion? We will return to this question shortly.

The factors that affect the amount of Ca^{2+} that is gained under these conditions include the duration of the Ca^{2+}-free perfusion (table 22–5), the temperature at which the Ca^{2+}-free perfusion buffer is maintained [34], the Na^+ content of the perfusion buffer [4], and the presence of other divalent cations, including Co^{2+} and Mn^{2+} [35]. Neither Mg^{2+} [4] nor the presence of verapamil [5] appears to affect the amount of Ca^{2+} overloading that occurs under these conditions. However (table 22–6), the Ca^{2+} content of the Ca^{2+}-repletion buffer has a profound effect on the gain in Ca^{2+} that occurs upon Ca^{2+} repletion, with a larger and an earlier gain in Ca^{2+} occurring when Ca^{2+}-enriched Ca^{2+}-repletion buffers are used.

There is widespread agreement that the presence of >0.05/mmol Ca^{2+}/l in the Ca^{2+}-free perfusion buffer is sufficient to protect against the occurrence of the paradox. Perfusion with buffers containing less than this amount of Ca^{2+} ensures that it will occur, unless protective measures have been introduced. Before considering how and why this massive overloading with Ca^{2+} occurs it may be useful to summarize the factors which have been shown to attenuate the paradox. Unfortunately, in many experiments, protein or enzyme release has been used as a marker for the occurrence of the paradox, and since the gain in tissue Ca^{2+} does not necessarily parallel enzyme (or protein) release we cannot be certain that the attenuation of the paradox which has been described has always been associated with an attenuation of the gain in Ca^{2+}. Factors which appear to attenuate the paradox include less than 1 min of Ca^{2+}-free perfusion [4], replacing some of the Na^+ in the Ca^{2+}-repletion perfusion buffer with Li^+ [4], acidosis [36], hypothermia [34], and adding Co^{2+} and Mn^{2+}—provided that

TABLE 22–6. Effect of Ca^{2+} content of the Ca^{2+}-repletion buffer on tissue Ca^{2+} gain during the Ca^{2+} paradox (μmol/g dry weight)

Duration of Ca^{2+}-free perfusion (min)			
0	2	5	10
	0.1 m*M* Ca^{2+}-repletion buffer		
2.7 ± 0.27	5.1 ± 0.55	7.0 ± 0.63	7.3 ± 1.23
	2.5 m*M* Ca^{2+}-repletion buffer		
2.5 ± 0.11	17.2 ± 1.18	22.7 ± 0.34	23.2 ± 1.09

These data were obtained from experiments with isolated rat hearts [4] perfused at 37°C. Data from the 0 min of Ca^{2+}-free perfusion provide the control data.

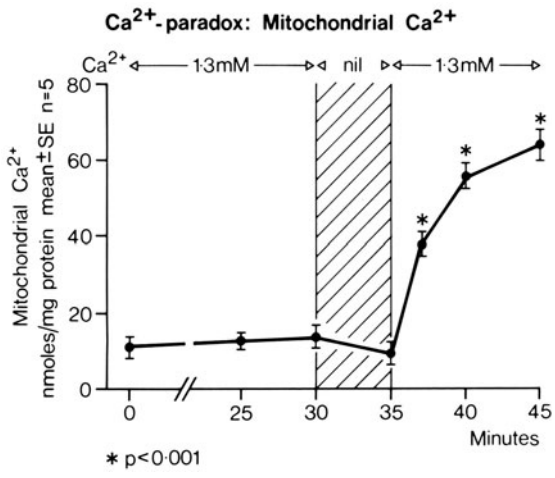

FIGURE 22–8. Ca^{2+} content of mitochondria isolated from hearts which had been perfused with Ca^{2+}-free solutions for 5 min and then reperfused with Ca^{2+}-containing solutions. The mitochondria were isolated in an EDTA-free medium [8] to ensure that they retained their endogenous Ca^{2+}. *$P<0.001$; each point is mean ± SEM of six experiments. Reproduced with permission from the *Am J Pathol.*

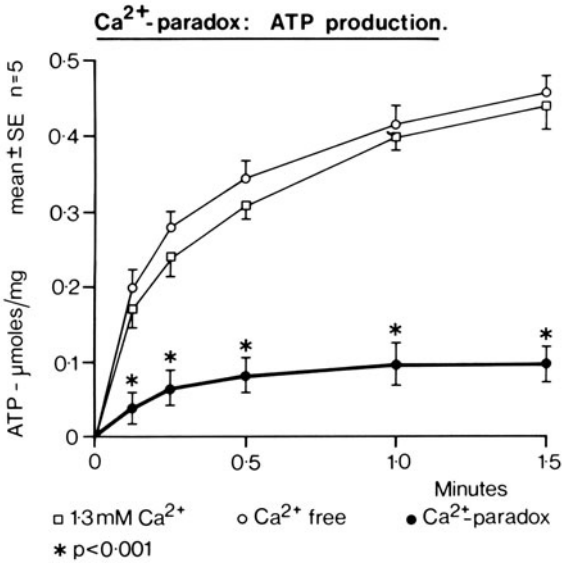

FIGURE 22–9. As for figure 22–8 except that the mitochondria was assayed for their ATP-producing activity. * $P<0.001$; each point is the mean ± SEM of six experiments. Reproduced with permission from the *Am J Pathol.*

they are added prior to the period of Ca^{2+}-free perfusion [35]. Factors which cause an exacerbation of the paradox include increasing the duration of the period of Ca^{2+}-free perfusion and raising the Ca^{2+} content of the Ca^{2+}-repletion buffer.

LOCALIZATION OF THE ACCUMULATED Ca^{2+}

Having established that the Ca^{2+} paradox results in cardiac myocytes becoming overloaded with Ca^{2+} it is again pertinent to ask where this Ca^{2+} accumulates within the cell. So far as we can ascertain the Ca^{2+} is again avidly accumulated by the mitochondria, so that (fig. 22–8) they become overloaded with Ca^{2+}—just as we have described for the reperfused ischemic heart. As mitochondrial Ca^{2+} rises, their capacity to produce ATP declines (fig. 22–9). We are left, therefore, with a metabolic situation which closely resembles that described for the reperfused ischemic heart. The difference between these two conditions lies in the fact that (a) in the paradox, but not during postischemic reperfusion, the decline in the tissue reserves of ATP is directly attributable to the massive influx of Ca^{2+}; (b) in the paradox, but not during postischemic reperfusion, the massive influx of Ca^{2+} occurs despite the presence of a normal tissue concentration of ATP and CP; and (c) in the paradox, but not necessarily during postischemic reperfusion, the ultrastructure of the cell surface is distorted before the massive influx in Ca^{2+} occurs.

ALTERATIONS IN THE MORPHOLOGY OF THE CELL SURFACE CAUSED BY Ca^{2+} REPLETION AFTER BRIEF PERIODS OF Ca^{2+}-FREE PERFUSION

The surface of cardiac muscle cells has a complex ultrastructure. Beyond the enzymatically active plasmalemma there is an electron-dense, carbohydrate-rich layer known as the glycocalyx, or basement coat [37]. This glycocalyx (or basement coat) can be divided into an inner surface coat and an outer external lamina [38]. The plasmalemma, the surface coat, and the external lamina are normally continuous and together they provide the outer boundary to the cell. However, upon perfusion with Ca^{2+}-

deficient solutions the components of the glycocalyx separate. The surface coat remains attached to the plasmalemma whereas fluid-filled spaces appear inbetween the surface coat and the external lamina [38]. When this happens the reintroduction of Ca^{2+}-containing solutions causes irreversible damage, accompanied by a massive influx of Ca^{2+} [4, 6]. Some investigators believe that this disorganization of the cell surface renders the underlying plasmalemma freely permeable to Ca^{2+} [38]. Others believe that the route of Ca^{2+} entry may be far more complex [39]. Nor should it be forgotten that a derangement of the glycocalyx is not the only change that occurs in the morphology of the cell surface. For instance, the intercalated discs, which are normally closely adherent, become widely separated [40]. The question naturally arises, therefore, as to whether some of the Ca^{2+} that enters upon Ca^{2+} repletion enters via these altered and distorted intercalated discs?

THE CONSEQUENCES OF Ca^{2+} OVERLOADING ASSOCIATED WITH THE PARADOX

Having established that Ca^{2+} overloading does occur under these conditions it may be useful to consider the consequences of it. These include disruption of mitochondrial function (fig. 22–9); activation of the Ca^{2+}-sensitive proteases, phospholipases, and ATPases; inhibition of the Na^+,K^+-ATPase enzyme (which is inhibited by concentrations of Ca^{2+} of about 0.1 mmol/1); and activation of the myofibrillar apparatus, causing the development of sustained contracture and excessive ATP utilization. Possibly the rapid development of this sustained contracture may be responsible, in part at least, for further disruption of the cell membrane and intercalated disc ultrastructure, leading in turn to an exacerbation of the Ca^{2+}-overload phenomenon. The end result is an ATP-depleted, supercontracted tissue, which has become damaged to such an extent that it expels substantial amounts of its intracellular constituents into the extracellular space. As might have been expected, even the Ca^{2+}-accumulating activity of the sarcoplasmic reticulum [32] is depressed under these conditions.

Calcium Gain during Posthypoxic Reoxygenation

TIME COURSE OF THE GAIN IN Ca^{2+}

Earlier in this chapter we described the gain in tissue Ca^{2+} that occurs during the reperfusion of ischemic heart muscle. It may be logical to ask whether a similar gain in Ca^{2+} occurs when heart muscle becomes hypoxic and is reoxygenated.

Recent studies have shown that heart muscle does accumulate Ca^{2+} after prolonged periods of substrate-free hypoxia [41]. This gain in Ca^{2+} is small, however, when compared with the gain that occurs when hypoxic heart muscle is reoxygenated. It occurs without a concomitant change in the rate of Ca^{2+} efflux [41]. It occurs immediately at the time of reoxygenation and therefore may even precede the onset of contracture. The amount of Ca^{2+} that enters during this process is about 6–8 μmol Ca^{2+}/g dry weight and therefore is approximately the same as that encountered during postischemic reperfusion.

CONSEQUENCES OF THE GAIN IN Ca^{2+}

These closely resemble those already described for the reperfused ischemic heart. They include loss of membrane integrity, the development of sustained contracture, mitochondrial Ca^{2+} overload, and cell death.

Why should the enhanced influx occur only upon reoxygenation? There is no easy answer to this question, but one possibility is that it is associated with the resumption of ATP production by the mitochondria. Once ATP becomes available, the myofibrils will shorten, and in so doing they may mechanically disrupt a membrane already damaged or made fragile by the preceding period of hypoxia (fig. 22–6).

The Route of Ca^{2+} Entry

We are faced now with the problem of deciding how Ca^{2+} enters the damaged myocytes. In normal myocytes, and under normal conditions, there are at least four different routes available for the entry of Ca^{2+}. These are: (a) in exchange for Na^+ [14], (b) by passive dif-

fusion, (c) in exchange for K^+, and (d) through the voltage-activated slow channels [42].

The question naturally arises, therefore, as to whether the excessive entry of Ca^{2+} that occurs during the Ca^{2+} paradox, during postischemic reperfusion, and during reoxygenation involves one or more of these routes, or whether some abnormal route of entry is involved. At first sight it may seem puzzling that the answer to such a fundamental question is not readily available. There may be two reasons for this: first, many of the substances which have been introduced to block one of these routes of entry — for example, inhibitors of the slow channels [33]—have many other actions [43], apart from their well-documented effects on slow-channel transport. For example, these substances also exert an energy-sparing effect [8] so that it is impossible to determine whether an efficacious effect which they may exert in limiting the entry of Ca^{2+} under any of these conditions is due to a direct inhibitory effect on the slow channels, whether it is due to a better-maintained supply of energy, as adenosine triphosphate, for the maintenance of intracellular homeostasis with respect to Ca^{2+}, or to some other and possibly as yet unrecognized action. The same difficulty applies when hypothermia [34] or acidosis [36] has been used, because both of these interventions alter several parameters of cell function, including that of slow-channel activity, Na^+-Ca^{2+} exchange, and energy production.

DURING POSTISCHEMIC REPERFUSION

The gain in tissue Ca^{2+} that occurs during postischemic reperfusion probably represents the end-result of a chain of events triggered initially by the failure of the cell to produce sufficient ATP to maintain a low cytosolic Ca^{2+}. The sequence of events may resemble that shown in figure 22–6, with some Ca^{2+} entering early in exchange for Na^+; some may enter through slow channels activated by the released catecholamines and some may enter by passive diffusion. Later, however (fig. 22–6), we can expect a massive increase in Ca^{2+}, due to the entry of Ca^{2+} through a plasmalemma that has been damaged. Under these conditions Ca^{2+} entry need not depend upon an enhanced entry through the slow channels — a conclusion which is supported by the observation [9] that the late addition of slow-channel-blocking substances does not prevent Ca^{2+} gain during postischemic reperfusion. Conversely the prophylactic use of these substances reduces or prevents the gain in Ca^{2+}, presumably because their energy-sparing effect [8] ensures that sufficient ATP remains available to maintain intracellular homeostasis. Once an excessive entry of Ca^{2+} has been triggered we can expect a further change to occur, due to the mechanical disruption of the plasmalemma associated with the rapid onset of contracture. In conclusion, therefore, during postischemic reperfusion there may be at least three stages of Ca^{2+} overloading: (a) an early rise in cytosolic Ca^{2+} due to an altered distribution of tissue Ca^{2+} and an uptake of Ca^{2+} in exchange for Na^+; (b) a second stage which probably involves the entry of Ca^{2+} through a membrane which has become leaky, or developed holes [18]; and (c) finally, as contracture develops, there may be mechanical disruption of the cell surface, including the intercalated discs.

Ca^{2+} GAIN DURING THE PARADOX

Here the situation may be even more complex. Perfusion of the myocardium with Ca^{2+}-deficient solutions is known to cause the components of the glycocalyx — which provides the outermost surface of the cell membrane complex — to separate. This glycocalyx can be separated into an inner and outer layer, and upon perfusion with a Ca^{2+}-free buffer these two layers separate. Thus the inner coat (or surface coat) remains attached to the plasmalemma and separated from the outer coat (the external lamina) by fluid-filled spaces. Some investigators [38] believe that this disorganization of the cell surface renders the underlying plasmalemma freely permeable to Ca^{2+}

A derangement of the glycocalyx is not the only change that occurs in the morphology of the cell surface. The intercalated discs, instead of being closely adherent, become widely separated [40]. Whatever causes this disruption of the intercalated discs may, at the same time, render them freely permeable to Ca^{2+}.

In the case of the paradox there is an addi-

tional problem, which is that the gain in Ca^{2+} may not be the primary event. Thus recent experiments have shown that perfusion with Ca^{2+}-free buffers that contain a chelating agent alters the functioning of the slow channels, rendering them permeable to Na^{+} [44]. This could facilitate a small increase in cytosolic Na^{+} which may in turn be of sufficient magnitude to trigger the Ca^{2+}-Na^{+} exchange mechanism, producing a gain in tissue Ca^{2+}. There is, therefore, no need to assume that an excessive entry of Ca^{2+} through the slow channels provides a major [39] or only route of Ca^{2+} entry during the paradox. Nor is there any reason to conclude that this gain in Ca^{2+} depends upon an earlier depletion of the energy-rich phosphate reserves. Clearly the etiology of the gain in Ca^{2+} which occurs under these conditions is complex.

Ca^{2+} ENTRY DURING POSTHYPOXIC REOXYGENATION

To explain the massive increase in Ca^{2+} uptake that occurs during posthypoxic reoxygenation it is difficult to escape the conclusion that some entry involves diffusion across a membrane which has been mechanically disrupted [45]. Others argue, however, that the enhanced entry reflects the development of a specific change in the selective permeability of the sarcolemma [41]. Irrespective of whether this is true, the fact that when added at the time of reoxygenation the Ca^{2+} antagonists do not prevent the gain in Ca^{2+}, whereas they do so when added early and prior to the period of hypoxia [46], argues against the entry of Ca^{2+} depending solely upon an enhanced slow-channel transport.

Consequences of Ca^{2+} Overloading and Protective Procedures

From the foregoing discussion it has become clear that there may be multiple routes for the entry of Ca^{2+} into injured cardiac myocytes. In addition we could be faced with the existence of a raised cytosolic Ca^{2+} without a net gain — due to an internal redistribution of Ca^{2+} Whatever its cause, the consequences of a massive influx of Ca^{2+} are the same: (a) ATP wastage due to the excessive activation of Ca^{2+}-sensitive ATPases; (b) tissue destruction due to excessive phospholipase and protease activation, and possibly due to the stresses imposed by the sudden development of contracture; (c) loss of mitochondrial function due to the avidity with which cardiac mitochondria accumulate Ca^{2+} and the attendant loss of oxidative phosphorylating activity [8]; and (d) depletion of the adenine nucleotide bases, due to their displacement from the tissue into the extracellular spaces.

When combined, these factors are sufficient to precipitate cell death and tissue necrosis. How, then, do the various protective procedures work? The most likely explanation as far as the myocytes are concerned is that their early addition and, in the case of hypothermia, implementation ensure that sufficient ATP remains available to ensure the maintenance of intracellular homeostasis with respect, not only to Ca^{2+}, but also to Na^{+}.

References

1. Shen AC, Jennings RB: Myocardial calcium and magnesium in acute ischemic injury. Am J Pathol 67:417–440, 1972.
2. Nayler WG: The role of calcium in the ischemic myocardium. Am J Pathol 102:126–134, 1981.
3. Nayler WG, Ferrari R, Poole-Wilson PA, Yepez CE: A protective effect of a mild acidosis on hypoxic heart muscle. J Mol Cell Cardiol 11:1053–1071, 1979.
4. Alto LE, Dhalla NS: Myocardial cation contents during induction of calcium paradox. Am J Physiol 237:H713–H719, 1979.
5. Nayler WG, Grinwald PM: Dissociation of Ca^{2+} accumulation from protein release in calcium paradox: effect of barium. Am J Physiol 242:H203–H210, 1982.
6. Zimmerman ANE, Daems W, Hulsmann WC, Snijder J, Wisse E, Durrer D: Morphological changes of heart muscle caused by successive perfusion with calcium-free and calcium containing solutions (calcium paradox). Cardiovasc Res 1:201–209, 1967.
7. Nayler WG: Protection of the myocardium against post ischemic reperfusion damage: the combined effect of hypothermia and nifedipine. J Thorac Cardiovasc Surg, 1982 (in press).
8. Nayler WG, Ferrari R, Williams A: Protective effect of pretreatment with verapamil, nifedipine and propranolol on mitochondrial function in the ischemic

and reperfused myocardium. Am J Cardiol 46:242–248, 1980.
9. Bourdillon PD, Poole-Wilson PA: The effects of verapamil, quiescence, and cardioplegia on calcium exchange and mechanical function in ischemic rabbit myocardium. Circ Res 50:360–368, 1982.
10. Peng CF, Kane JJ, Murphy ML, Straub KD: Abnormal mitochondrial oxidative phosphorylation of ischemic myocardium reversed by Ca^{2+}-chelating agents. J Mol Cell Cardiol 9:897–908, 1977.
11. Shen AC, Jennings RB: Kinetics of calcium accumulation in acute myocardial ischemic injury. Am J Pathol 67:441–452, 1972.
12. Shine KI, Douglas AM, Ricchiuti NV: Calcium, strontium, and barium movements during ischemia and reperfusion in rabbit ventricle: implications for myocardial preservation. Circ Res 43:712–720, 1978.
13. Caroni P, Carafoli E: The Ca^{2+}-pumping ATPase of heart sarcolemma: characterization, calmodulin dependence, and partial purification. J Biol Chem 256:3263–3270, 1981.
14. Reuter H: Exchange of calcium ions in the mammalian myocardium: mechanisms and physiological significance. Circ Res 34:599–605, 1974.
15. Langer GA: Sodium–calcium exchange in the heart. Annu Rev Physiol 44:435–449, 1982.
16. Tada M, Yamamoto T, Tonomura Y: Molecular mechanism of active calcium transport by sarcoplasmic reticulum. Physiol Rev 58:1–79, 1978.
17. Carafoli E, Tiozzo R, Lugli G, Crovetti F, Kratzing C: The release of calcium from heart mitochondria by sodium. J Mol Cell Cardiol 6:361–371, 1974.
18. Jennings RB, Hawkins HK, Lowe JE, Hill ML, Klotman S, Reimer KA: Relation between high energy phosphate and lethal injury in myocardial ischemia in the dog. Am J Pathol 92:187–214, 1978.
19. Jennings RB, Reimer KA, Hill ML, Mayer SE: Total ischemia in dog hearts, in vivo. 1. Comparison of high energy phosphate production, utilization, and depletion, and of adenine nucleotide catabolism in total ischemia in vivo vs. severe ischemia in vivo. Circ Res 49:892–900, 1981.
20. Jennings RB, Reimer KA: Lethal myocardial ischemic injury. Am J Pathol 102:241–255, 1981.
21. Reimer KA, Jennings RB, Hill ML: Total ischemia in dog hearts, in vitro. 2. High energy phosphate depletion and associated defects in energy metabolism, cell volume regulation, and sarcolemmal integrity. Circ Res 49:901–911, 1981.
22. Beckman JK, Owens K, Knauer TE, Weglicki WB: Hydrolysis of sarcolemma by lysosomal lipases and inhibition by chlorpromazine. Am J Physiol 242:H652–H656, 1982.
23. Chien KR, Reeves JP, Buja LM, Bonte F, Parkey RW, Willerson JT: Phospholipid alterations in canine ischemic myocardium: temporal and topographical correlations with Tc-99m-PPi accumulation and an in vitro sarcolemmal Ca^{2+} permeability defect. Circ Res 48:711–719, 1981.
24. La Noue KF, Watts JA, Koch CD: Adenine nucleotide transport during cardiac ischemia. Am J Physiol 241:H663–H671, 1981.
25. Dunnett J, Nayler WG: Effect of pH on calcium accumulation and release of isolated fragments of cardiac and skeletal muscle sarcoplasmic reticulum. Biochim Biophys Acta 198:434–438, 1979.
26. Bersohn MM, Philipson KD, Fukushima JY: Sodium–calcium exchange and sarcolemmal enzymes in ischemic rabbit hearts. Am J Physiol 242:C288–C295, 1982.
27. Katz AM, Tada M: The "stone heart": a challenge to the biochemist. Am J Cardiol 29:578–580, 1972.
28. Feher JJ, Briggs FN, Hess ML: Characterization of cardiac sarcoplasmic reticulum from ischemic myocardium: comparison of isolated sarcoplasmic reticulum with unfractionated homogenates. J Mol Cell Cardiol 12:427–432, 1980.
29. Locke FS, Rosenheim O: Contributions to the physiology of the isolated heart: the consumption of dextrose by mammalian cardiac muscle. J Physiol (Lond) 36:205–220, 1907.
30. Chizzonite RA, Zak R: Calcium-induced cell death: susceptibility of cardiac myocytes is age-dependent. Science 213:1508–1510, 1981.
31. Boink ABTJ, Ruigrok TJ, Zimmerman ANE: Changes in high energy phosphate compounds of isolated rat hearts during Ca^{2+}-free perfusion and reperfusion with calcium. J Mol Cell Cardiol 8:973–979, 1976.
32. Alto LE, Dhalla NS: Role of changes in microsomal calcium uptake in the effects of reperfusion of Ca^{2+}-deprived rat hearts. Circ Res 48:17–24, 1981.
33. Hearse DJ, Baker JE, Humphrey SM: Verapamil and the calcium paradox. J Mol Cell Cardiol 12:733–740, 1980.
34. Holland CE Jr, Olson RE: Prevention by hypothermia of paradoxical calcium necrosis in cardiac muscle. J Mol Cell Cardiol 7:917–928, 1975.
35. Nayler WG: Cobalt, manganese and the calcium paradox. J Mol Cell Cardiol (Suppl 2) 14:11, 1982.
36. Bielecki K: The influence of changes in pH of the perfusion fluid on the occurrence of the calcium paradox in the isolated rat heart. Cardiovasc Res 3:268–271, 1969.
37. Muir AR: A calcium-induced contracture of cardiac muscle cells. J Anat 102:148–149, 1968.
38. Crevey BJ, Langer GA, Frank JS: Role of Ca^{2+} in the maintenance of rabbit myocardial cell membrane structural and functional integrity. J Mol Cell Cardiol 10:1081–1100, 1981.
39. Grinwald PM, Nayler WG: Calcium entry in the calcium paradox. J Mol Cell Cardiol 3:867–880, 1981.
40. Winegrad S, Robinson TF: Force generation among cells in the relaxing heart. Eur J Cardiol (Suppl) 7:63–70, 1978.
41. Harding DP, Poole-Wilson PA: Calcium exchange in rabbit myocardium during and after hypoxia: ef-

fect of temperature and substrate. Cardiovasc Res 14:435–445, 1980.
42. New W, Trautwein W: The ionic nature of slow inward current and its relation to a contraction. Pflugers Arch 334:24–38, 1972.
43. Nayler WG, Thompson JE, Jarrott B: The interaction of calcium antagonists (slow channel inhibitors) with myocardial alpha adrenoceptors. J Mol Cell Cardiol 14:13–20, 1982.
44. Krishtal OA, Pidoplichko VI, Shaknovalov Yu A: Conductance of the calcium channel in the membrane of snail neurones. J Physiol 310:410–434, 1981.
45. Ganote CE, Kaltenbach JP: Oxygen-induced enzyme release: early events and a proposed mechanism. J Mol Cell Cardiol 11:389–406, 1979.
46. Nayler WG, Fassold E, Yepez C: Pharmacological protection of mitochondrial function in hypoxic heart muscle: effect of verapamil, propranolol and methylpridesolone. Cardiovasc Res 12:152–161, 1978.

23. CELL COUPLING AND HEALING-OVER IN CARDIAC MUSCLE

Walmor C. De Mello

Introduction

As in many other tissues the internal milieu of cardiac fibers is separated from the extracellular fluid by an insulating surface layer characterized by a high electrical resistance.

When the surface cell membrane is injured an electrical potential difference appears between damaged and nondamaged cells *(injury potential)*. In 1877, Engelmann demonstrated that when the cardiac muscle is injured the injury potential soon vanishes (see fig. 23–1). An explanation for this interesting phenomenon *(healing-over)* is that the cells located near damage are depolarized and consequently the flow of injury current is interrupted. This is not the case, however, because the injury potential can be reestablished by damaging the cells located near the previous lesion [1].

In many types of cells the injury of the surface cell membrane is immediately followed by an extrusion of protoplasm through the damaged area. This "healing process", which avoids the loss of intracellular material, is based on the formation of a new membrane at the injured area and has been described in protozoa, marine eggs, and skeletal muscle [2].

If a skeletal muscle fiber is immersed in a Ca-free Ringer solution and ulteriorly lesioned film formation does not occur and disintegration inevitably follows, the formation of a new membrane at the site of damage is dependent on Ca [2]. The establishment of this membrane has been ascribed to a chemical reaction (surface precipitation reaction) involving a substance, "ovothrombin", formed from some precursor in the cell in the presence of Ca^{2+} [2].

Is myocardial healing-over due to the establishment of a new membrane at the site of damage? To answer this question we must enquire if the *surface precipitation reaction* provides a good electrical sealing. It is known that healing-over as described in cardiac muscle does not exist in skeletal muscle where the injury currents spread along the muscle fiber, rendering it wholly depolarized [3]. In isolated sartorius muscle fibers, small lesions produced by punching the cell membrane with a microelectrode depolarize the fiber irreversibly (see fig. 23–2) [4].

So, under normal conditions the establishment of a plug at the area of cell damage is not enough to provide an electrical sealing. Of some interest in this context is that in skeletal muscle fibers immersed in isotonic Ca solution, the depolarization of the muscle fibers elicited by small lesions is completely reversed in a few seconds [4]. Some observations suggest that membrane lipids are involved in this process. So, calcium is known to induce coalescence of phospholipid films [5] and phospholipase C impairs the sealing process in high-Ca solution [4].

As the formation of a new membrane at the damage area does not represent an effective ionic barrier under normal conditions, it seems reasonable to conclude that the healing-over of cardiac muscle is not explained by a surface precipitation reaction. The other plausible alternative is that a high-resistance barrier is established between damaged and nondamaged cells.

N. Sperelakis (ed.), PHYSIOLOGY AND PATHOPHYSIOLOGY OF THE HEART.

Martinus Nijhoff Publishing, Boston/The Hague/ Dordrecht/Lancaster.

In frog ventricular muscle the depolarization caused by lesion is quickly reversed regardless of the size of the preparation. This finding led Rothschuh [3] to postulate the hypothesis that cardiac muscle is composed of small functional units—Mikroelementen separated by polarized ionic barriers.

Ulterior studies by Weidmann [6] demonstrated that in cardiac Purkinje fibers the core resistivity is quite low (105 Ωcm) and the space constant high (1.9 mm) compared with the length of a single cell (about 125 μm). This certainly rules out the possibility that cardiac cells are separated by preestablished ionic barriers.

Evidence is, indeed, available that cardiac cells are electrically coupled [6–9]. When one-half of a bundle of ventricular fibers is exposed to radioactive K and the other half is continuously washed with nonradioactive Tyrode, a steady state with respect to tissue ^{42}K is reached in about 6 h [10]. At the end of this time an appreciable amount of ^{42}K is found in the half of the bundle not exposed to radioactive potassium. The exponential decay of radioactivity along the muscle has a length constant of 1.55 mm, which clearly indicates that the longitudinal movement of ^{42}K is not hindered by the intercellular junctions [10]. The quantitative analysis of these results led to the conclusion that the permeability of the intercellular junctions is about 5000 times greater than that of the nonjunctional membrane.

The intercellular channels are also permeable to different molecules. Cell-to-cell diffusion of Procion Yellow (mol wt 697) [11], tetraethylammonium (mol wt 130) [12], $^{14}cAMP$ (mol wt 328) [13], and fluorescein (mol wt 330) [14, 15] has been reported in cardiac tissues.

Recently, a new compound, Lucifer Yellow (mol wt 473) was introduced by Stewart [16] as a fluorescent probe and proved extremely valuable in studies of cell-to-cell communication. Lucifer Yellow is sui generis— it does not diffuse through the nonjunctional membrane, but crosses the gap junctions in several tissues [16, 17]. Studies carried out in our laboratory showed that the dye diffuses longitudinally along dog trabeculae after its introduction into the cell with cut-end method [11]. As is shown

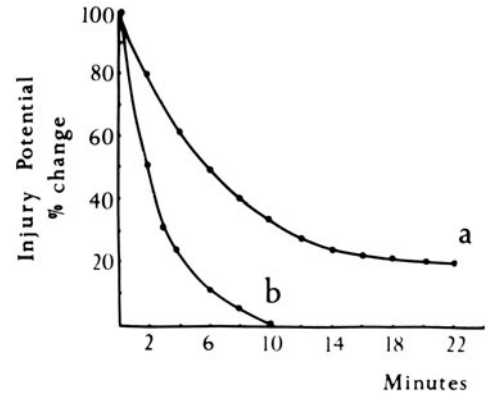

FIGURE 23–1. Healing-over of toad ventricular muscle immersed in normal Ringer solution *(b)*. Curve *(a)* shows the influence of Ca-free solution on the healing-over process. From De Mello et al. [18].

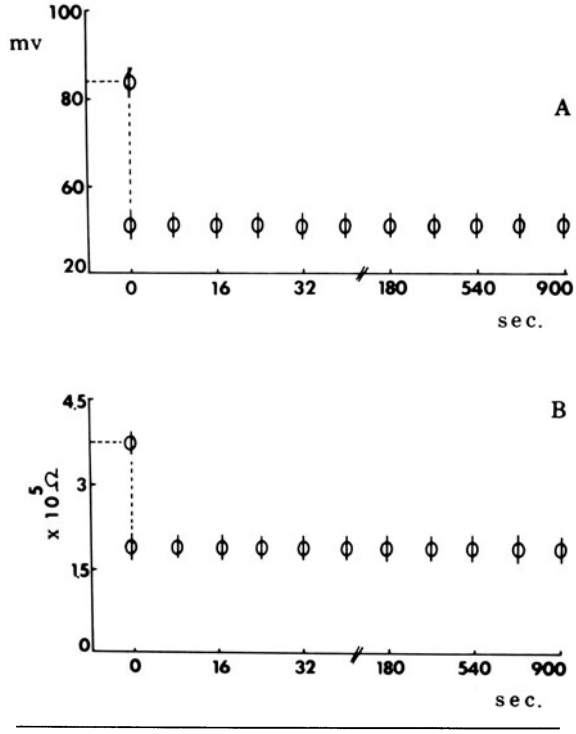

FIGURE 23–2. Lack of sealing in frog skeletal muscle fibers immersed in normal Ringer solution. Irreversible drop of resting potential *(A)* and input resistance *(B)* produced by puncture of the cell membrane with a micropipette (about 4 μm in diameter). Each curve is the average from 25 fibers. Vertical dotted line indicates moment of lesion. Vertical line at each point indicates SE of the mean. From De Mello [4].

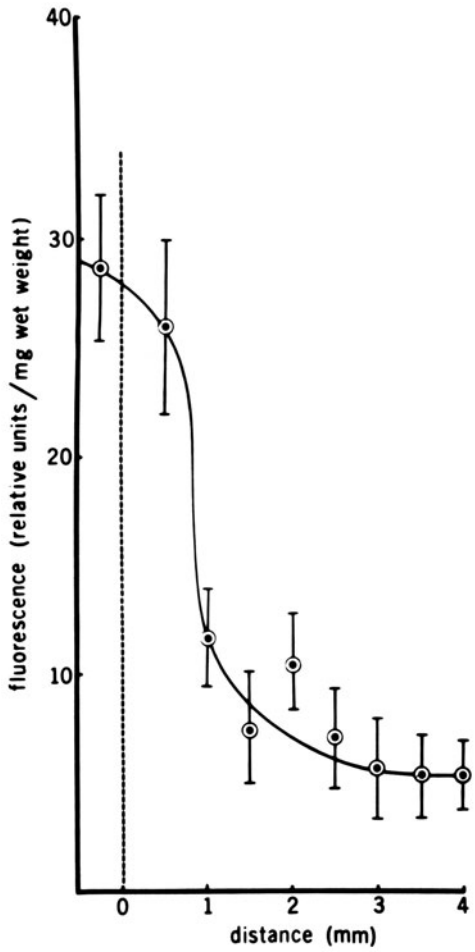

FIGURE 23–3. Longitudinal diffusion of Lucifer Yellow along dog trabeculae immersed in normal Tyrode solution. Diffusion period, 90 min. The vertical dotted line separates the loaded (left) from the unloaded area (right). Average from 20 muscles. Vertical line at each point, SD of the mean. From De Mello and Castillo, unpublished.

in figure 23–3, the dye can be detected by spectrofluorometric methods 4 mm away from the rubber partition 1½ h after its introduction into the cell.

The question of whether the longitudinal movement of the dye is due to intracellular diffusion can be answered by performing washout studies. Figure 23–4 shows that the washout curve for Lucifer Yellow consists of a first rapid component ($t_{1/2} = 1\frac{48}{}$ min) which represents the loss of Lucifer Yellow from the extracellular space and a second slow component which correlates to the outward movement of the dye through the surface cell membrane. The second component has an extremely long half-life ($t_{1/2} = 2 \times 10^3$ min), supporting the view that the permeability of the surface cell membrane to Lucifer Yellow is, indeed, negligible. The meaning of these results is that the dye diffuses longitudinally along cardiac fibers through the intercellular channels.

Since cardiac cells are connected through low-resistance channels it might be reasonable to think that following damage the junctional conductance can be markedly reduced suppressing the flow of injury currents from damaged to nondamaged cells [18]. On the other hand, it is known that Ca ions are essential for the healing-over process [18–20]. These findings led to the hypothesis that the junctional conductance in heart might be modulated by variations in free $[Ca^{2+}]_i$ [20]. In order to check this idea, I injected Ca iontophoretically inside a cardiac cell and searched for possible changes in cell-to-cell coupling. The results show that the electrical coupling of the heart cells is gradually reduced and cell decoupling is finally achieved in about 600 s [9, 20] (see fig. 23–5). Concurrently with fall in intercellular communication the input resistance (V_0/I_0) of the injected cell increases appreciably (see fig. 23–5). Both effects of Ca are completely reversible. Rose and Loewenstein [21], using aequorine, demonstrated that the injection of Ca ions into salivary gland cells of *Chironomus* produces a quick decline of the electrical coupling when the light emission is seen to spread all the way to the intercellular junctions.

These findings are indicative that healing-over can be ascribed to a marked increase in electrical resistance of the intercellular junctions located between normal and damaged cells and due to a rise in free Ca.

The mechanism by which Ca ions change the junctional conductance is not known. Two hypotheses seem worth consideration: (a) Ca ions bind to negative polar groups of gap junction phospholipids and abolish the permeability of the hydrophilic channels. Phospholipids and proteins are normal constituents of gap junc-

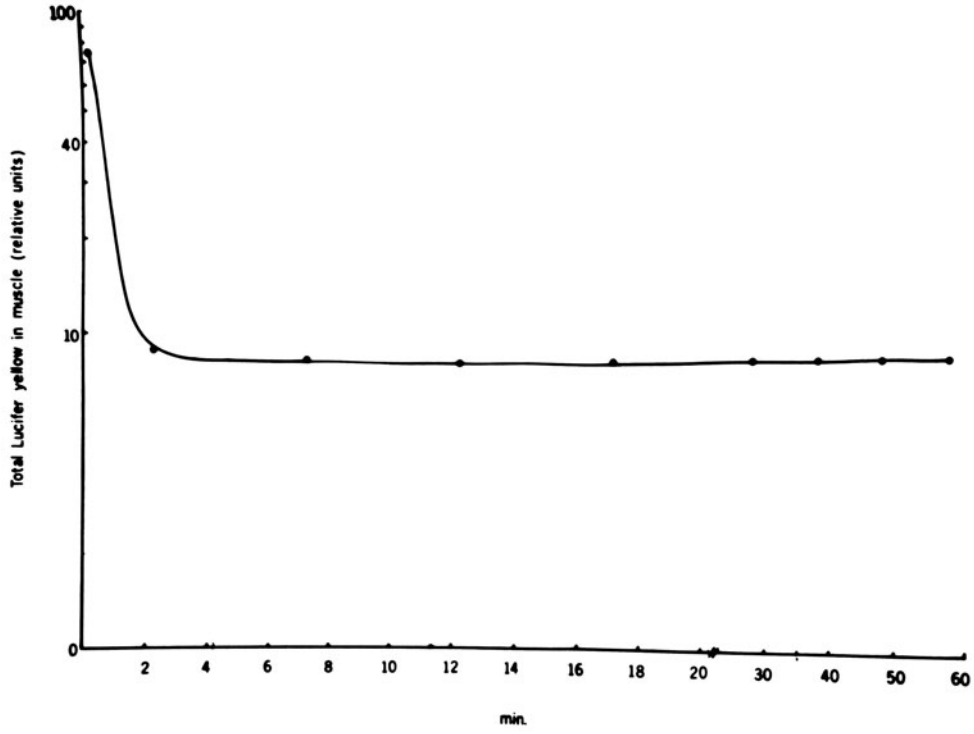

FIGURE 23–4. Loss of Lucifer Yellow from a dog trabecula. The washout curve shows a first rapid component ($t_{1/2}$, 1^{48} min) and an extremely slow second component ($t_{1/2}$, 2×10^3 min). Temperature, 37°C. From De Mello and Castillo, unpublished.

tions [22]. (b) Ca activates enzyme reactions which lead to closure of the intercellular channels through a conformational change in gap junction proteins. As the intracellular injection of La^{3+} causes a quick suppression of cell-to-cell coupling [23] it seems reasonable to think that the binding of the cation to negative sites at the gap junctions might, indeed, alter the channel permeability.

Influence of Na-Ca Exchange on Cell-to-Cell Coupling

In cardiac muscle, like in nerve fibers, the extrusion of Ca ions is dependent upon the energy provided by the Na concentration gradient across the nonjunctional membrane [24, 25]. The Na-K pump produces a sodium electrochemical gradient across the nonjunctional membrane which is used to energize the Ca extrusion from the cell. The Na-Ca exchange can be reversed if the intracellular Na concentration is increased with consequent increase in Ca influx [26].

As a rise in $[Na^+]_i$ reverses the Na-Ca exchange the obvious question is—can the injection of Na ions into the cell impair the cell-to-cell coupling? The answer is yes. When Na is injected iontophoretically into a cardiac cell the intracellular longitudinal resistance is increased and cell decoupling is produced [27, 28] (see fig. 23–6). The suppression of the electrical coupling elicited by high $[Na^+]_i$ is dependent on the extracellular Ca concentration. So, when $[Ca^{2+}]_0$ is low, the effect of Na injection on cell-to-cell communication is negligible [28], supporting the view that the abolishment of the electrical coupling is accomplished by the activation of the Na-Ca exchange and ulterior rise in free $[Ca^{2+}]_i$.

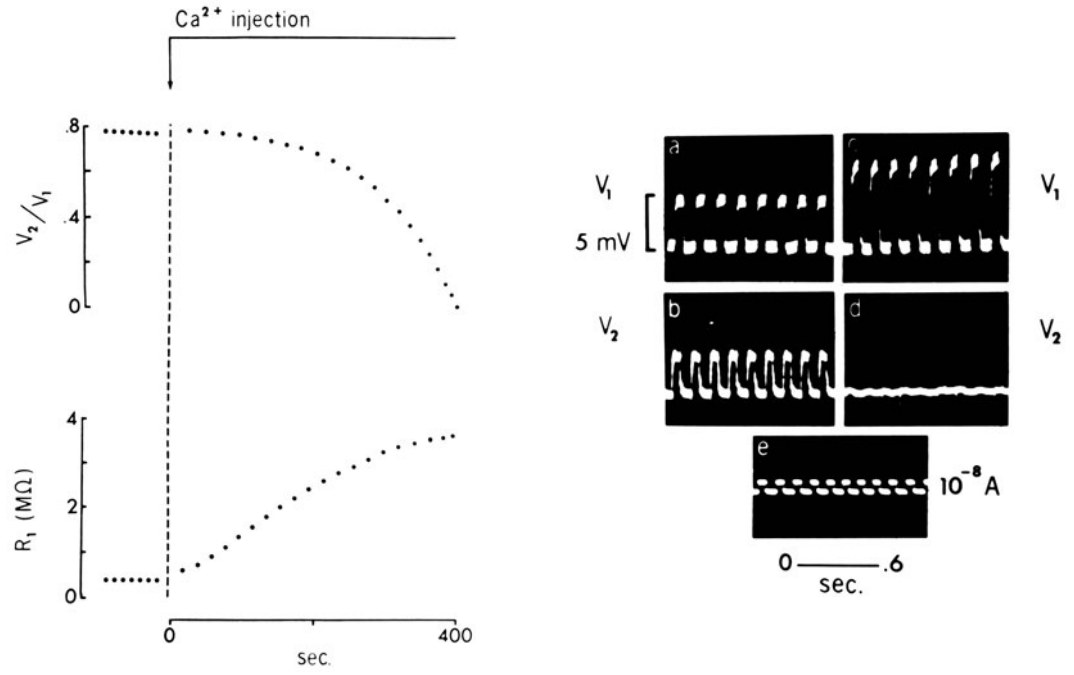

FIGURE 23–5. Effect of intracellular Ca injection on the electrical coupling of cardiac Purkinje cells. *(Left)* Typical effect of Ca injection on coupling coefficient (V_2/V_1) and input resistance (R_1) (average from six experiments). *(Right)* (a) and (b) show V_1 and V_2 controls; (c) and (d) recorded after 410 s of Ca injection showing cell decoupling. From De Mello, unpublished.

The Cost of Cell-to-Cell Communication

Since the enhancement of $[Na^+]_i$ impairs or even abolishes the electrical coupling of cardiac cells, it seems logical that the inhibition of the Na-K pump can also change intercellular communication. Indeed, when cardiac fibers are exposed to certain concentrations of ouabain, the intracellular longitudinal resistance increases appreciably and finally cell decoupling is produced [28, 29]. The effect of the glycoside on cell-to-cell coupling is greatly due to the increase in free $[Ca^{2+}]_i$. So, in fibers exposed to ouabain, the time required for cell decoupling was dependent upon the extracellular Ca concentration [29].

In cardiac Purkinje partially depolarized by recent dissection the activation of the Na-K pump with norepinephrine increases the resting potential and the electrical coupling of the heart cells [30].

The conclusion drawn from these observations is that the Na extrusion exerts a remarkable influence on the transference of electrical and chemical signals between cells. The changes in junctional permeability brought about by alterations of $[Na^+]_i$ are due to the rise or fall in free $[Ca^{2+}]_i$ which are related to the rate of Na-Ca exchange.

Rapidity of sodium transport across the nonjunctional membrane is also essential for the maintenance of conduction velocity.

It is known that the conduction velocity (θ) is proportional to: $\theta \propto 1/\sqrt{ar_i}$, where a is the fiber diameter and r_i the intracellular longitudinal resistance. Contrary to previous ideas, the intracellular longitudinal resistance is now considered a variable parameter which depends among other things on the free $[Ca^{2+}]_i$ [9, 31]. Therefore, an increase in r_i reduces the conduction velocity in cardiac fibers.

The maintenance of a high junctional permeability, however, is not free. The cell must spend energy on the extrusion of Na ions and

in deeping the free $[Ca^{2+}]_i$ low. ATP is supplied from metabolism solely by oxidative phosphorylation in mitochondria and by glycolisis. Metabolic inhibition decreases the rates of active ion transports by reducing the rate of ATP production. 2-4 Dinitrophenol, for instance, an uncoupler of oxidative phosphorylation, increases the intracellular longitudinal resistance in cardiac fibers, and abolishes the electrical coupling and the cell-to-cell diffusion of fluorescein [15]. These effects of dinitrophenol are related to the elevation of free $[Ca^{2+}]_i$ [15]. Indeed, when EDTA is injected into the heart cells exposed to dinitrophenol, the electrical coupling is partly recovered. Although the evidence available from these studies is that the modulation of junctional permeability is a smooth process it is not clear whether the number of active channels varies with the changes in free $[Ca^{2+}]_i$ or whether all the channels are simultaneously involved.

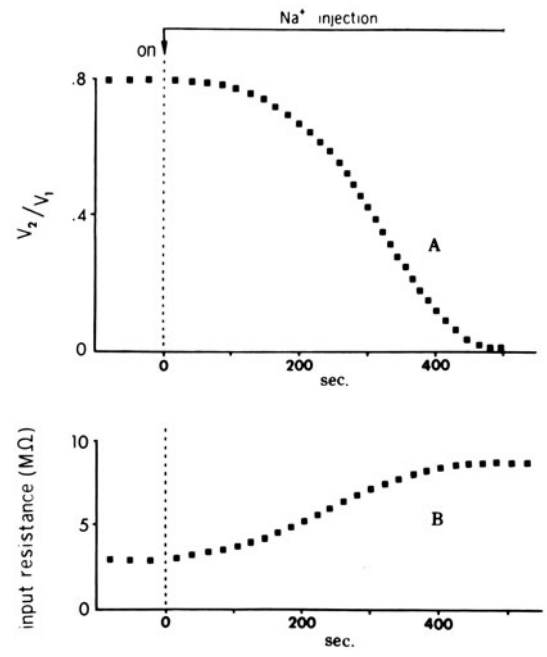

FIGURE 23–6. Typical effect of intracellular Na injection on the electrical coupling (V_2/V_1) *(A)* and input resistance *(B)* of a canine Purkinje fiber. Modified from De Mello [28].

Is the Junctional Permeability Influenced by Intracellular pH?

In 1977, Turin and Warner [32] demonstrated that the exposure of embryonic cells of Xenopus to 100% CO_2 not only reduces the pH_i but also depolarizes the cells and abolishes the cell-to-cell coupling.

More recently it has been shown that the intracellular injection of H^+ ions into cardiac cells increases the intracellular longitudinal resistance and causes cell decoupling [33, 34]. In sheep Purkinje fibers exposed to 100% CO_2 a similar increase in r_i has been reported [35].

The question remains as to whether the effect of low pH_i on the electrical coupling is due to a rise in free $[Ca^{2+}]_i$. In *Chironomus* salivary gland cells [36] or in barnacle muscle [37] the changes in pH_i caused by high P_{CO_2} are seen concurrently with an increase in free $[Ca^{2+}]_i$. The exposure of sheep Purkinje fibers to high P_{CO_2} reduces pH_i but the free $[Ca^{2+}]_i$ also falls [38]. Myocardial healing-over, a phenomenon related to a drastic increase in junctional resistance [20], can be accomplished in the absence of Ca if the pH_o is reduced to 5 (De Mello, unpublished).

The evidence reviewed above suggests that H ions have a direct effect on junctional resistance in cardiac fibers. In embryonic cells of *Fundulus,* acidification of the cytosol causes cell decoupling — an effect due to a direct interaction of protons with gap-junction molecules [39].

As the buffer capacity of heart cells is quite high [40] it is not clear whether pH_i plays a role in the control of junctional resistance under physiologic conditions. During myocardial ischemia, however, when the pH_i and pH_o are reduced it is easy to visualize that H ions contribute to the healing-over process, avoiding the spread of injury currents and the flow of metabolites between injured and normal cells [31].

Cyclic AMP and Cell-to-Cell Coupling

Ca and cyclic nucleotides are intimately related in the process of modulation of cell function

induced by hormones [41]. Evidence is available that in some systems Ca plays the important role of second messenger. The intracellular free $[Ca^{2+}]_i$ seems to regulate the concentration of cyclic AMP. So, Ca, an activator of guanylate cyclase [41], reduces the intracellular concentration of cyclic AMP in part due to the inactivation of adenylate cyclase [42].

These findings lead to an important question — are cyclic nucleotides involved in the regulation of junctional permeability? In salivary glands of *Drosophila,* cyclic AMP enhances the coupling between cells [43].

Recently, studies have been performed on rat ventricular fibers exposed to theophylline (0.4 m*M*), an inhibitor of phosphodiesterase. The results show an increase in the spread of electrotonic activity and in conduction velocity [44]. As the time constant of the cell membrane is not altered by the drug it seems possible to conclude that the increase in space constant (59%) is not related to change in resistance of the nonjunctional membrane. Calculations of the intracellular longitudinal resistance (r_i) on the basis of conduction velocity (θ) and the time constant of the foot of the action potential $\left(\tau \text{ foot} = \frac{1}{\theta^2 r_i Cm}\right)$ indicated that r_i is reduced [44].

Assuming that theophylline is not changing myoplasmic resistivity the results presented above indicate that the drug enhances cell-to-cell coupling by reducing the junctional resistance.

The effect of theophylline on the electrical coupling is probably related to the increase in concentration of cyclic AMP. Indeed, when the cardiac fibers are exposed to dB-cyclic AMP (5×10^{-5} *M*) the conduction velocity is enhanced and r_i is decreased (Estapé and De Mello, unpublished). It is known that cyclic AMP activates a protein kinase which in the presence of ATP leads to the phosphorylation of different proteins [45]. Therefore, the phosphorylation of gap junction proteins might cause conformational changes which increase the diameter of the intercellular channels.

The possible interactions between Ca and cyclic nucleotides in the regulation of junctional permeability seems to represent a novel aspect in the study of cell-to-cell communication.

Namm et al. [46] found, for instance, that augmented supplies of Ca ions to perfused rat hearts produced a decrease in their content of cAMP. Conversely, increased concentrations of this nucleotide have been reported in papillary muscles exposed to Ca-free solution [47].

As a substantial rise in concentration of cyclic AMP lead to an increase in permeability of the nonjunctional membrane to Ca [48, 49] it seems reasonable to assume that the effect of cyclic AMP on cell-to-cell coupling depends on the concentration of the nucleotide. Small increments in concentration of cyclic AMP might decrease r_i through a phosphorylation of gap junction proteins while a marked increase in concentration of the nucleotide might impair cell communication because the free $[Ca^{2+}]_i$ is increased. Supporting this view is the finding that theophylline at low concentration (0.4 m*M*) enhances cell-to-cell coupling [44] while at high concentration (4 m*M*) impairs the electrical coupling of heart cells [50].

Physiologic and Pathologic Implications of Cell-to-Cell Communication

The organization of cardiac muscle is based on isolated functional units connected through low-resistance intercellular channels. This morphologic arrangement enables the electrical impulse to travel without delay throughout the cardiac fibers, allowing the heart cells to beat synchronously. Contrary to skeletal muscle in which the intracellular longitudinal resistance is provided by the myoplasm only, in heart the junctional resistance represents an important regulatory factor of the spread of the electrical impulse. When the junctional conductance is increased, as for example when the concentration of cyclic AMP is enhanced, the spread of electrical activity is greatly augmented. On the other hand, when the free $[Ca^{2+}]_i$ is elevated or the intracellular pH is reduced the conductance of the intercellular channels declines, impairing the impulse conduction. Consequently, slow conduction is produced which facilitates the generation of cardiac arrhythmias. The

finding that the junctional resistance is highly dependent on metabolic energy, which is necessary to pump Na out of the cell and maintain a low free $[Ca^{2+}]_i$, indicates that parameters such as conduction velocity are also dependent upon cell metabolism and ATP synthesis. Changes in cardiac rhythm elicited by digitalis toxicity or myocardial ischemia are in part due to the rise in free $[Ca^{2+}]_i$ or the fall in pH_i. In both situations the electrical coupling is greatly impaired or abolished in part due to membrane depolarization, but also because the intracellular resistance is markedly enhanced [3].

In the atrioventricular node the size and number of gap junctions is smaller than in the atrium or ventricle [51, 52] and the intracellular longitudinal resistance is normally high [53]. This explains, in part, the delay of impulse conduction typical of this cardiac area. Here, more than in atrial or ventricular muscle the impulse conduction is extremely vulnerable to further enhancement of intracellular resistance. The so-called "fatigue" phenomenon of the atrioventricular node is known to be frequency dependent. A reasonable explanation for this phenomenon is the increase in intracellular resistance produced by stimulation at high rate and probably related to the increment in free $[Ca^{2+}]_i$. As the number of hydrophilic channels connecting the node cells is small and the generation of action potentials is dependent upon a slow current carried by Ca and Na [54], it is expected that in the atrioventricular node the impulse propagation is highly dependent on frequency of stimulation.

Evidence has been provided, indeed, that in myocardial fibers the intracellular longitudinal resistance is increased by stimulation at high rate [55].

Thanks to the compartmentalized structure of cardiac muscle "death of a cell does not necessarily mean the death of adjacent cells". The lesion of the surface cell membrane enhances the free $[Ca^{2+}]_i$, markedly suppressing cell communication and the flow of injury current which would depolarize large masses of normal cardiac cells. The healing-over process represents, indeed, an important mechanism of preservation of heart function during injury.

References

1. Engelmann TW: Vergleichende Untersuchungen zur Lehre von der Muskel- und Nervenelektricität. Pflugers Arch 15:116–148, 1877.
2. Heilbrunn LV: Dynamics of living protoplasm. Heilbrunn LV (ed). New York: Academic, 1956.
3. Rothschuh KE: Ueber den funktionellen Aufbau des Herzens aus elektrophysiologischen Elementen and ueber den Mechanisms der Erregungsleitung in Herzen. Pflugers Arch 253:238–251, 1951.
4. De Mello WC: Membrane sealing in frog skeletal muscle fibres. Proc Natl Acad Sci USA 70:982–984, 1973.
5. Blioch ZL, Glagoleva JM, Lieberman EA, Nenashev VA: A study of the mechanism of quantal transmitter release at a chemical synapse. J Physiol (Lond) 199:11–35, 1968.
6. Weidmann S: The electrical constants of Purkinje fibres. J Physiol (Lond) 118:348–360, 1952.
7. Woodbury JW, Crill WE: On the problem of impulse conduction in the atrium. In: Florey E (ed) Nervous inhibition. Oxford: Pergamon, 1961, pp 124–125.
8. Barr L, Dewey MM, Berger W: Propagation of action potentials and the nexus in cardiac muscle. J Gen Physiol 48:797–823, 1965.
9. De Mello WC: Effect of intracellular injection of calcium and strontium on cell communication in heart. J Physiol 250:231–245, 1975.
10. Weidmann S: The diffusion of radiopotassium across intercalated discs of mammalian cardiac muscle. J Physiol (Lond) 187:323–342, 1966.
11. Imanaga I: Cell-to-cell diffusion of Procion Yellow in sheep and calf Purkinje fibres. J Membr Biol 16:381–388, 1974.
12. Weingart R: The permeability to tetraethylammonium ions of the surface membrane and the intercalated disks of the sheep and calf myocardium. J Physiol (Lond) 240:741–762, 1974
13. Tsien R, Weingart R: Inotropic effect of cyclic AMP in calf ventricular muscle studied by a cut end method. J Physiol (Lond) 260:117–141, 1976.
14. Pollack GH: Intercellular coupling in the atrioventricular node and other tissues of the heart. J Physiol (Lond) 255:275–298, 1976.
15. De Mello WC: Effect of 2-4 dinitrophenol on intercellular communication in mammalian cardiac fibres. Pflugers Arch 380:267–276, 1979.
16. Stewart WC: Functional connections between cells as revealed by dye-coupling with a high fluorescent naphthalimide tracer. Cell 14:741–759, 1978.
17. Bennett MVL, Spira ME, Spray DC: Permeability of gap junctions between embryonic cells of *Fundulus:* a reevaluation. Dev Biol 65:114–125, 1978.
18. De Mello WC, Motta G, Chapeau M: A study on the healing-over of myocardial cells of toads. Circ Res 24:475–487, 1969.
19. Déleze J: Calcium ions and the healing-over of heart fibres. In: Taccardi B, Marchetti G (eds) Electro-

physiology of the heart. London: Pergamon, 1965, pp 147–148.
20. De Mello WC: The healing-over process in cardiac and other muscle fibers. In: De Mello WC (ed) Electrical phenomena in the heart. New York: Academic, 1972, pp 323–351.
21. Rose B, Loewenstein WR: Calcium ion distribution in cytoplasm visualized by aequorin: diffusion in cytosol restricted by energized sequestering. Science 190:1204–1206, 1975.
22. Griepp EB, Revel JP: Gap junctions in development. In: De Mello WC (ed) Intercellular communication. New York: Plenum, 1977, pp. 1–32.
23. De Mello WC: Effect of intracellular injection of La^{3+} and Mn^{2+} on electrical coupling of heart cells. Cell Biol Int Rep 3:113–119, 1979.
24. Reuter H, Seitz N: The dependence of calcium efflux from cardiac muscle on temperature and external ion composition. J Physiol (Lond) 195:451–470, 1968.
25. Baker PF, Blaustein MP, Hodgkin AL, Steinhardt RA: The influence of calcium on sodium efflux in squid axons. J Physiol (Lond) 200:431–458, 1969.
26. Blaustein MP, Hodgkin AL: The effect of cyanide on the efflux of calcium from squid axons. J Physiol (Lond) 200:497–527, 1969.
27. De Mello WC: Electrical uncoupling in heart fibres produced by intracellular injection of Na or Ca. Fed Proc 17:3, 1974.
28. De Mello WC: Influence of the sodium pump on intracellular communication in heart fibres: effect of intracellular injection of sodium ion on electrical coupling. J Physiol (Lond) 263:171–197, 1976.
29. Weingart R: The action of ouabain on intercellular coupling and conduction velocity in mammalian ventricular muscle. J Physiol (Lond) 264:341–365, 1977.
30. De Mello WC: Factors involved on the control of junctional conductance in heart. Proc Int Union Physiol Sci 12:319, 1977.
31. De Mello WC: Intercellular communication in cardiac muscle. Cir Res 50:2–35, 1982.
32. Turin L, Warner AE: Carbon dioxide reversibly abolishes ionic communication between cells of early amphybian embryon. Nature (Lond) 270:56–57, 1977.
33. De Mello WC: On the decoupling action of ouabain in cardiac fibers. Fed Proc 22:4, 1979.
34. De Mello WC: Influence of intracellular injection of H^+ on the electrical coupling in cardiac Purkinje fibres. Cell Biol Int Rep 4:51–57, 1980.
35. Weingart R, Reber W: Influence of internal pH on r_i of Purkinje fibres from mammalian heart. Experientia 35:929, 1979.
36. Rose B, Rick R: Intracellular pH, intracellular free Ca, and junctional cell–cell coupling. J Membr Biol 44:377–415, 1978.
37. Lea TJ, Ashley CC: Increase in free Ca^{2+} in muscle after exposure to CO_2. Nature (Lond) 275:236–238, 1978.
38. Hess P, Weingart W: Intracellular free calcium modified by pH_i in sheep Purkinje fibres. J Physiol (Lond) 307:60, 1980.
39. Spray DC, Harris AL, Bennett MVL: Gap junctional conductance is a simple and sensitive function of intracellular pH. Science 211:712–715, 1981.
40. Ellis D, Thomas RC: Direct measurements of the intracellular pH of mammalian cardiac muscle. J Physiol (Lond) 262:755–771, 1976.
41. Goldberg N: Cyclic nucleotides and cell function. In: Weismann G, Claiborne R (eds) Cell membranes: biochemistry, cell biology and pathology. New York: HP Publishing, 1975, 185 pp.
42. Rasmussen H: Ions as "second messengers". In: Weismann G, Claiborne R (eds) Cell membranes: biochemistry, cell biology and pathology. New York: HP Publishing, 1975, 203 pp.
43. Hax Werner MA, Van Venrooij Ger EPM, Vossenberg Joost BJ: Cell communication: a cyclic-AMP mediated phenomenon. J Membr Biol 19:253–266, 1974.
44. Estapé E, De Mello WC: Effect of theophylline on the spread of electrotonic activity in heart. Fed Proc 41:1505, 1982.
45. Greengard P: Possible role for cyclic nucleotides and phosphorylated membrane proteins in postsynaptic actions of neurotransmitters. Nature 260:101–108, 1976.
46. Namm DH, Mayer SE, Maltbie M: The role of potassium and calcium ions in the effect of epinephrine on cardiac cyclic adenosine 3′-5′ monophosphate, phosphorylase kinase and phosphorylase. Mol Pharmacol 4:522–530, 1968.
47. Endoh M, Brodde OE, Reinhardt D, Schumman HJ: Frequency dependence of cyclic AMP in mammalian myocardium. Nature 261:716–717, 1976.
48. Reuter H: Properties of two inward membrane currents in the heart. Annu Rev Physiol 41:413–424, 1979.
49. Sperelakis N: Changes in membrane electrical properties during development of the heart. In: Zipes DP, Bailey JC, Elharrar V (eds) The slow inward current and cardiac arrhythmias. The Hague: Martinus Nijhoff, 1980, 221 pp.
50. De Mello WC: Cell-to-cell diffusion of fluorescein in heart fibers. Fed Proc 37:3, 1978.
51. James TN, Scherf L: Ultrastructure of the atrioventricular node. Circulation 37:1049–1070, 1968.
52. Masson-Pevet M: The fine structure of cardiac pacemaker cells in the sinus node and in tissue culture. Thesis. Amsterdam: Rodopi.
53. De Mello WC: Passive electrical properties of the atrioventricular node. Pflugers Arch 371:135–139, 1977.
54. Mendez C, Moe GK: Atrioventricular transmission. In: De Mello WC (ed) Electrical phenomena in the heart. New York: Academic, 1972, pp. 263–291.
55. Bredikis J, Bukauskas F, Veteikis R: Decreased intercellular coupling after prolonged rapid stimulation in rabbit atrial muscle. Circ Res 49:815–820, 1981.

24. EFFECTS OF CARDIOTOXINS ON MEMBRANE IONIC CHANNELS

M. Lazdunski
and J.F. Renaud

Introduction

Various ionic currents and conductance changes underlie the normal electrogenesis and automacity of the heart. A number of drugs and therapeutic agents act on the membranes of myocardial cells in a more or less specific manner on sodium, calcium, and potassium channels.

One of the most remarkable developments in neurobiology in the last decade has been the increasing interest in the large number of neurotoxins synthesized by microorganisms, plants, snakes, scorpions, spiders, and marine organisms. Each toxin is valuable because of its extreme specificity of action and high affinity for its receptor, allowing it to be used for the fine pharmacologic analysis of important physiologic functions. Many neurotoxins are also cardiotoxins.

In this chapter, we review natural substances that are toxic to cardiac cells through their interaction with the plasma membrane [1]. Toxins that specifically act on nerve terminals to alter the storage and release of neurotransmitters, like α-latrotoxin, botulinium toxin, tetanus toxin, β-bungarotoxin, and crototoxin, are excluded from this discussion [2].

It turns out that most of the interesting cardiotoxins are specifically active on the fast sodium channel of cardiac cells.

N. Sperelakis (ed.), PHYSIOLOGY AND PATHOPHYSIOLOGY OF THE HEART.

Martinus Nijhoff Publishing, Boston/The Hague/Dordrecht/Lancaster.

Toxins that Are Specific for the Fast Sodium Channel

TETRODOTOXIN AND SAXITOXIN

Tetrodotoxin (TTX) (fig. 24–1) is a heterocyclic guanidine found in the puffer fish and in some species of newt, octopus, frog, and goby. TTX provokes a reversible inhibition of the fast Na^+ current in myelinated nerve, skeletal muscle, and a number of other excitable cells [3]. The concentration dependence of TTX inhibition is hyperbolic with a half-maximum effect between 1 and 5 n*M* in different nerve preparations [4, 5].

Saxitoxin (STX) like TTX is a heterocyclic guanidine with two guanidine groups per molecule instead of one for TTX (fig. 24–1). It is produced by *Gonyaulax* dinoflagellates and is found to be concentrated in shellfish that feed on these organisms. The mechanism of action of TTX and STX on the Na^+ channel is the same and both are specific for this channel [3, 6]. The inhibitory effect of saxitoxin on the fast Na^+ current is also reversible; the dose–response curve is hyperbolic with a half-maximum inhibition at 1–5 n*M* [6].

Quantitative biochemical studies of the binding of TTX and STX to their common receptor site were made possible by the availability of tritiated TTX, labeled by the Wilzbach method, and of tritiated STX [6] and more recently of new and highly radioactive derivatives which have been synthesized by chemical modification of TTX [7]. Photoactivated TTX derivatives which can irreversibly block the Na^+

channel upon irradiation have also synthesized [8]. It has been proposed that TTX and STX bind to the selectivity filter of the Na^+ channel [6, 9]. This model of interaction assumes that guanidinium moieties of TTX and STX enter the sodium channel like the free guanidinium cation itself, and that the bulky part of the toxins occludes the mouth of the channel, like a cork, blocking the passage of Na^+ ions. Hydroxyl groups on the toxin molecule would be involved in the formation of hydrogen bonds with the Na^+-channel protein in order to stabilize the toxin–channel interaction. However, recent chemical modification of the Na^+ channel does not seem to fully support this mechanism of association. TTX binding is irreversibly blocked by treatment of nerve membranes with carboxyl-modifying reagents [10–12], suggesting the presence of an essential carboxylate at the toxin receptor site. If TTX binds to the selectivity filter which normally recognizes Na^+, such a chemical modification should also abolish the Na^+ channel conductance. Instead, Na^+ channels that have been made TTX insensitive by chemical modifications are still active in the generation of action potentials with the same kinetics of activation and inactivation, with the same ionic selectivity and with only a slightly reduced unit conductance [13, 14]. The TTX receptor has been solubilized and partially purified from the electric organ of *Electrophorus electricus,* from the brain and muscle of rat [15–17]. The best data [15] indicate that the binding site is situated on a 250,000- to 270,000-dalton polypeptide, in agreement with independent results obtained from irradiation inactivation experiments [18, 19].

The most characteristic aspect of TTX action on the mammalian heart is the marked insensitivity of cardiac muscle to TTX. A substantial reduction in the rate of rise of action potentials in ventricular trabeculae and Purkinje fibers does not occur until a TTX concentration of about 1 μM is reached [20, 21]. In a preliminary series of experiments designed to determine whether the reported difference in sensitivity to TTX reflects basic differences in the TTX receptor of cardiac muscle, as compared to nerve and skeletal muscle, voltage dependence of TTX block of the Na^+ channel in rat papillary muscle was found [22]. In these experiments, the TTX sensitivity of the Na^+ channel was markedly increased when the membrane potential was more positive. Such an action of TTX would indeed be characteristic for the cardiac membrane since it has never been seen for Na^+ channels in nerve cells. These conclusions have been criticized, however, on the basis that they relate to upstroke velocity measurements that are not a good measure of the true variations of the Na^+ conductance. In a more recent series of experiments several groups have found no voltage dependence for steady-state TTX block of excitatory and background Na^+ channels when measuring I_{Na} under voltage clamp [21, 23, 24]. TTX block of Na^+ channels in voltage-clamped dog and rabbit Purkinje fibers is well described by a 1:1 binding reaction with a voltage-independent dissociation constant of 1 μM [21, 23, 24]. This dissociation constant is about 3 or-

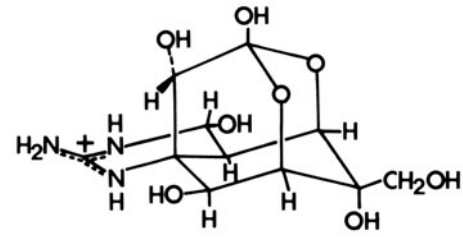

TETRODOTOXIN (TTX)

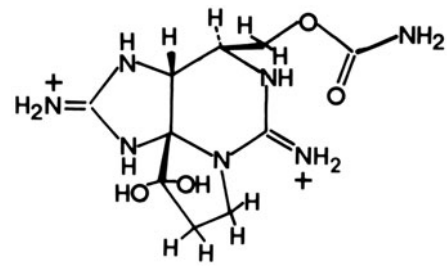

SAXITOXIN (STX)

FIGURE 24–1. The structure of tetrodotoxin and saxitoxin.

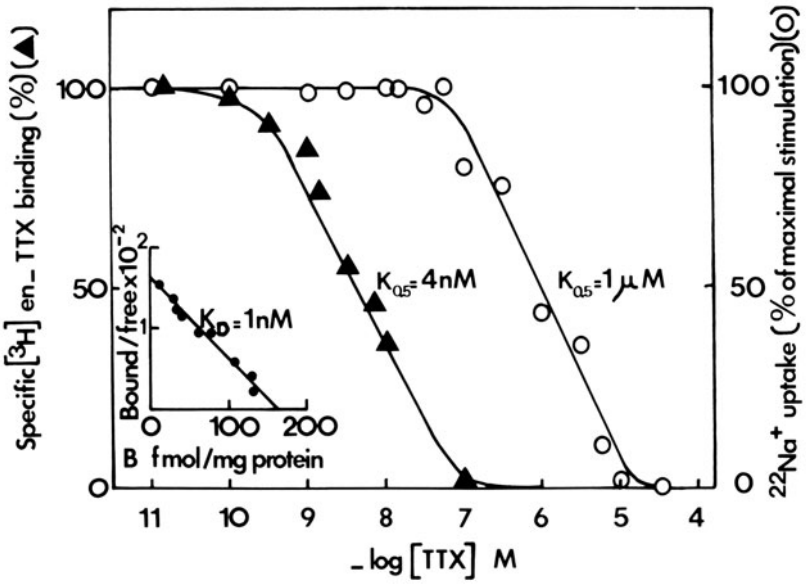

FIGURE 24–2. Interaction of TTX with the Na^+ channel of rat heart ventricle. Scarchard plot of the specific [^{3}H]en-TTX binding (●) and displacement of specific [^{3}H]en-TTX binding in rat heart homogenates by TTX (▲) give a dissociation constant of the [^{3}H]en-TTX receptor complex (K_D) and half-displacement of TTX ($K_{0.5}$) of 1 n*M* and 4 n*M*, respectively. The inhibition by TTX of the rate of ^{22}Na uptake (○) gives a half-maximum effect of TTX action ($K_{0.5}$) of 1 μ*M*.

ders of magnitude higher than normally found for TTX–receptor interactions in nerve membranes [6].

In fact, the affinity of TTX for its cardiac receptor seems to be very dependent on the animal species. The dissociation constant of the TTX–receptor complex measured with voltage-clamped frog atrial fibers is 3.4 n*M* and is not voltage dependent [25]. This value is close to those found in nerve and skeletal muscle. Different families of TTX receptors corresponding to different classes of Na^+ channels have also been postulated for Purkinje fibers in the dog heart [26].

The problem of the low sensitivity to TTX has now been studied using rat cardiac cells in culture and two biochemical approaches, one involving utilization of a tritiated TTX derivative in which tritiated ethylenediamine is grafted to TTX ([^{3}H]en-TTX) [27], the other involving $^{22}Na^+$ flux experiments which will be explained in more detail later in this chapter. Direct-binding experiments with [^{3}H]en-TTX measure all kinds of Na^+ channels, i.e., both functional and nonfunctional species. $^{22}Na^+$ flux studies measure only functional Na^+ channels [28, 29]. [^{3}H]en-TTX-binding experiments reveal a family of high-affinity binding sites with a dissociation constant (K_D) near 1 n*M*, whereas $^{22}Na^+$ flux studies reveal a family of low-affinity binding sites with a K_D near 1 μ*M*, i.e., about threefold higher than the K_D for the high-affinity binding site (fig. 24–2).

The electrophysiology of these rat cardiac cells in culture also indicates the presence of a Na^+ channel with a low sensitivity for TTX [30], confirming the results of $^{22}Na^+$ flux studies.

The conclusion from these studies is that high-affinity and low-affinity binding sites coexist in mammalian cardiac cells although only Na^+ channels with a low affinity for TTX seem to be electrically expressed. The same situation has been encountered with rat skeletal muscle in culture where the two families of TTX-binding sites coexist with the same affinities as those found for rat cardiac cells [31]. Here

again only the low-affinity binding site (K_D = 1 μM) is expressed electrically. In the case of the mammalian muscle, the physiologic expression of one or other of the classes is dependent upon innervation. Na^+ channels with a high affinity for TTX are physiologically expressed when the muscle is innervated; the preparation is then TTX sensitive, whereas Na^+ channels with low-affinity binding sites for TTX become electrically expressed after denervation, the preparation then becoming resistant to TTX [32].

Saturable high-affinity binding of [^{3}H]en-TTX was identified in rat, rabbit, guinea pig, and embryonic chick heart membranes, i.e., in preparations displaying either sensitivity (chick heart cells) or resistance (rat, rabbit, guinea pig) to TTX [27]. The saturation isotherm showed a single population of TTX receptors with a K_D of 0.5–1.0 nM, independent of the regional distribution of the receptors. TTX and STX specifically displaced [^{3}H]en-TTX binding with K_D values of 4.0 nM and 3.4 nM, respectively (fig. 24–2). [^{3}H]en-TTX binding is inhibited at acidic pH and half-inhibition is observed at pH 6.2. This pH value was ascribed to the pK of an essential ionizable group on the cardiac Na^+ channel and is close to values that have been found for nerve membranes [33]. This essential ionizable group is probably the carboxylate which can be modified by carbodiimides or trialkyloxonium salts in other preparations that are sensitive to TTX [10, 12, 13]. Monovalent cations selectively displaced [^{3}H]en-TTX binding, indicating that the toxin binds to a specific ion coordination site. The displacement of [^{3}H]en-TTX binding by monovalent cations occurs in the sequence of efficacy: guanidinium > Tl^+ > NH_4^+ > Li^+ > Na^+ > K^+ > Rb^+ > Cs^+. The interesting feature of inorganic monovalent cation binding to the Na^+ channel is a positive cooperativeness that suggests that there are multiple and coupled monovalent ion binding sites at the mouth of the Na^+ channel. Divalent cations also displaced [^{3}H]en-TTX binding in the sequence Mg^{2+} (K_D; = 1.3 mM) > Ca^{2+} (K_D = 3.2 mM). Since cations like Na^+, K^+, or Ca^{2+} prevent TTX association to the TTX receptor, K_D values measured in a Ringer solution are six times higher than in a choline medium [27].

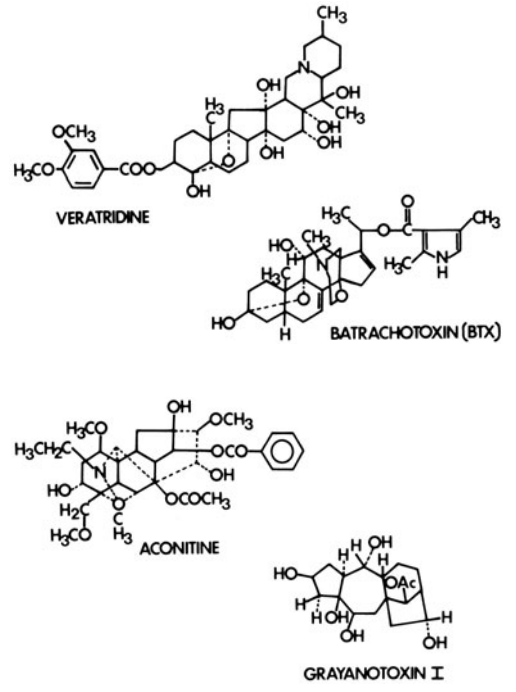

FIGURE 24–3. Structure of lipid-soluble molecules of veratridine, batrachotoxin, aconitine, and grayanotoxin I.

These biochemical studies indicate that the interaction of TTX with high-affinity binding sites in cardiac cells has properties similar to those found for nerve and muscle membranes [6].

CEVERATRUM ALKALOIDS, BATRACHOTOXIN, ACONITINE, AND GRAYANOTOXINS

These compounds (fig. 24–3) represent a series of lipid-soluble molecules which have dramatic effects on cardiac and other excitable cells [1].

Veratridine and other veratrum alkaloids are steroid alkaloids that occur in liliaceous plants belonging to the genera *Veratrum, Zygadenus, Stenanthium,* and *Schoenocaulon* [34].

Batrachotoxin (BTX) is a steroidal alkaloid extracted from the skin of a Colombian frog *Phyllobates aurataenia*. It is one of the most toxic substances known and its lethal effect on mammals appears to be mainly due to its car-

diac arryhthmogenic action. Work on this toxin has also been reviewed in detail [35].

Aconitine is the main alkaloid of the plant *Aconitum napellus*. Its structure is not closely related to that of veratridine and BTX.

Grayanotoxins (GTXs) are toxic diterpenoids found in various species of *Rhododendron, Kalmia,* and *Leucothoe* (Eriacaceae).

Veratridine, BTX, and aconitine depolarize the nerve or muscle membrane by causing the voltage-sensitive Na^+ channels to become persistently active at the resting membrane potential [36–38]. The hyperexcitability and depolarization of excitable cells induced by these toxins is caused by two effects: (a) a shift of the voltage dependence of activation of sodium channels toward more negative potentials, and (b) a block of the inactivation process of these channels. In addition, these three toxic compounds not only alter the gating mechanism of the voltage-sensitive Na^+ channel, they also change its ion selectivity and increase its permeability for larger cations [39, 40].

These three types of toxins may bind preferentially to an open state of the Na^+ channel since repetitive stimulation to activate Na^+ channels facilitates their action [36, 38, 41]. Depolarization of excitable cells by veratridine, BTX, and aconitine is blocked by TTX [3, 42, 43].

GTXs, although they are very different in structure from the veratrum alkaloids [44, 45], aconitine and BTX, seem to have essentially the same type of mechanism of action (and maybe of receptor) on Na^+ channels [3, 33].

Two different types of techniques have been used to analyze the fine mechanism of action of these neurotoxic compounds. The first is the voltage-clamp technique which provides information on the kinetics and the voltage dependency of the activation and inactivation steps as well as on the ion-transport properties of the open form of the channel. The second approach uses fluxes of radioactive monovalent cations [46]. Veratridine, BTX, and GTXs all increase the initial rate of $^{22}Na^+$ entry into neuroblastoma or skeletal muscle cells [31]. This stimulation is due to the chemical activation of Na^+ channels by these toxins and is inhibited by TTX. BTX is by far the most powerful of this class of toxins.

Considerable literature has been devoted to the cardiac action of cerveratrum alkaloids, BTX, aconitine, and GTXs. A very critical analysis of all the available results has recently been published [42].

Voltage-clamp experiments with veratrine using frog atrial fibers and with aconitine using sheep Purkinje fibers [47–49] have shown that these lipid-soluble molecules have an action on cardiac fast Na^+ channels similar to that found in nerve or skeletal muscle cells. Both toxic preparations blocked the inactivation mechanism of the Na^+ channel. (Veratrine is a mixture of toxic alkaloids containing the pure compound veratridine. It is always preferable to use veratridine.)

Ceveratrum alkaloids, aconitine, and BTX at low concentrations prolong the repolarization phase of the action potential in different cardiac preparations; their effect is both dose dependent and frequency dependent and inhibited by TTX [42]. This effect is seen at concentrations in the nanomolar range for BTX [50–52] or in the micromolar range for other compounds [42, 49, 53]. At higher concentrations, all these lipid-soluble toxins depolarize the cardiac cell membrane. Again toxin-induced depolarization is blocked by TTX.

Moreover, $^{22}Na^+$ flux experiments using chick embryonic cardiac cells in culture [54] have shown that veratridine maximally increases the initial rate of $^{22}Na^+$ influx in these cells by a factor of about 5 at a concentration of 0.1 m*M* (fig. 24–4). Dose–response curves indicate a half-maximum effect at 22 μM. Veratridine stimulation of the rate of Na^+ influx is inhibited by TTX ($K_{0.5[TTX]}$ = 6.6 n*M* at 22 μM veratridine).

GTXs also activate Na^+ channels in cardiac preparations [55, 56] in the same way that they activate the Na^+ channel in nerve cells. The effect of GTX I has even been observed on the sinoatrial node although this cell type is characterized by a TTX-resistant electrical activity [57]. This is one example where the presence of Na^+ channels can be demonstrated by using toxins which specifically affect the gating mechanism of the channel.

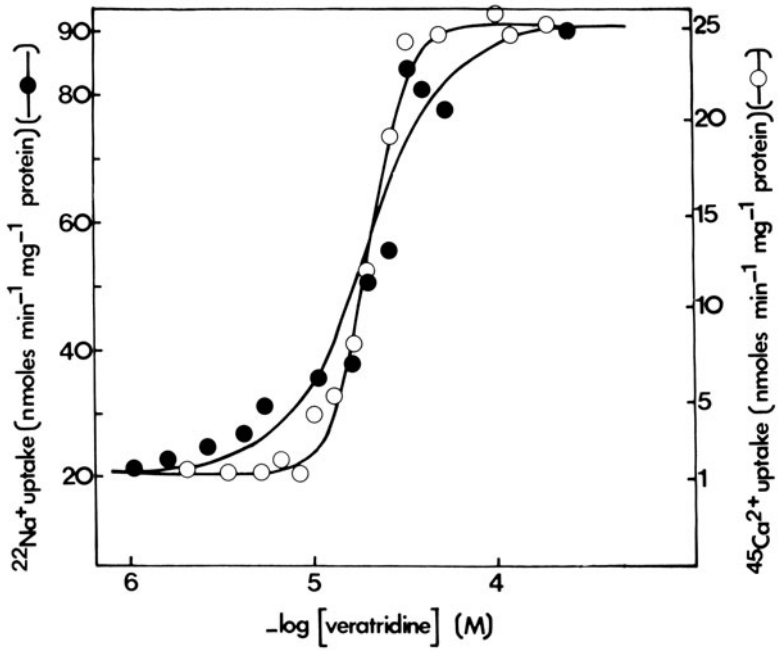

FIGURE 24–4. Activation by veratridine of the initial rate of $^{22}Na^+$ (—●—) and $^{45}Ca^{2+}$ uptake (—○—) by embryonic cardiac cells in culture [54].

Veratridine and other ceveratrum alkaloids, BTX, and GTXs all produce a concentration-dependent and reversible positive inotropic effect [42]. Aconitine is the only compound for which no inotropic effect has been reported. Detailed comparisons of the concentration–effect relationships have been made for a large number of ceveratrum ester alkaloids [42] and for a series of structurally related GTXs [58]. It has been shown that the maximum increase in force of contraction is nearly the same for the different ceveratrum alkaloids [42], but there are large differences in the concentration range at which the different compounds are active on cardiac contraction with half-maximum effects between 10 n*M* and 100 μ*M*. Ceveratrum alkaloids like germitetrine, protoveratrines, or germitrine produce a positive inotropic effect at concentrations more than 1 order of magnitude lower than those necessary to obtain the same action with veratridine. These differences between the ceveratrum alkaloids are not yet explained since $^{22}Na^+$ flux studies, with neuroblastoma cells, do not demonstrate important differences in affinity for the Na^+ channel among all these compounds [59].

At least two calcium-entry systems are involved in the coupling between excitation and contraction in the heart: the slow Ca^{2+} channel and the Na^+-Ca^{2+} exchange system [60, 61]. The positive inotropic effect of veratridine (and related compounds), BTX, and GTXs is the indirect result of their action on the Na^+ channel. By triggering a persistent activation of the Na^+ channel, these toxins increase the intracellular Na^+ concentration, which provokes an influx of Ca^{2+} through the Na^+-Ca^{2+} exchange system. The inotropic effect due to the lipid-soluble toxins is of course blocked by TTX [42]. The implication of the Na^+-Ca^{2+} exchange system in the mechanism of the inotropic effect produced by the lipid-soluble toxins has been demonstrated directly both by voltage-clamp studies on frog atrial trabeculae [48] and by $^{22}Na^+$ and $^{45}Ca^{2+}$ flux studies with embryonic ventricular cardiac cells in culture [54]. When veratridine stimulates $^{22}Na^+$ influx by a factor of 5, it increases the initial rate of $^{45}Ca^{2+}$ entry by a factor of 25 (fig. 24–

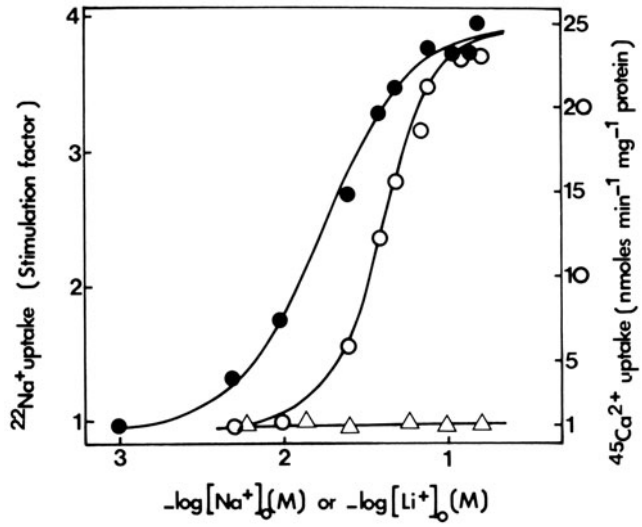

FIGURE 24–5. The effect of extracellular Na^+ concentration upon $^{22}Na^+$ (●—●) and $^{45}Ca^{2+}$ (○—○) uptake stimulated by veratridine on cultured chick embryonic heart cells. Na^+ replacement by Li^+ fails to stimulate Ca^{2+} uptake (△—△) [54].

4). As expected for an indirect effect of veratridine on the Na^+-Ca^{2+} exchange system, veratridine-stimulated Ca^{2+} influx is inhibited by TTX, is Na dependent, and Na^+ cannot be replaced by Li^+ (fig. 24–5).

Unlike TTX, STX, or the polypeptide toxins which will now be described, veratridine and BTX do not appear to be specific for the fast Na^+ channel. It has been recently shown that these lipid-soluble toxins block slow Ca^{2+} channels in neuroblastoma cells in exactly the same concentration range in which they activate Na^+ channel [62]. It would be of interest to analyze their effect on the slow Ca^{2+} channel of cardiac cells.

SCORPION AND SEA ANEMONE TOXINS

Toxins from both North American and North African scorpions have been purified and sequenced [63] (fig. 24–6). These toxic molecules are all single-chain polypeptides extensively cross-linked by disulfide bonds; they are miniproteins with a molecular weight of about 7000. Scorpion venom contains a mixture of multiple toxins, some being more specific to mammals, others to insects or to crustaceans. A lysine residue (ϵ-amino side-chain) has been identified as one of the essential aminoacids at the active site of these toxins [64]. Voltage-clamp experiments on various nerve preparations with the pure toxins from *Androctonus australis, Leiurus quinquestriatus,* and *Buthus Eupus* [65–67] have shown that their main effect is to slow down considerably the inactivation of the Na^+ channel. These toxins have no effect on the activation of the channel. Whole venoms seem to have essentially the same properties as the pure toxins [3].

Anemone toxins (ATXs) active on different animal species have been isolated from a variety of sea anemone species [68], some which have been sequenced [69–72] (fig. 24–6). They are single-chain basic polypeptides of 2500 to about 5000 molecular weight, cross-linked with disulfide bridges. An arginine residue (guanidine group) has been identified as the essential amino acid at the active site of these toxins [73]. ATX and scorpion toxins (ScTXs) have no obvious sequence homology (fig. 24–6). Similarly to ScTXs, ATXs specifically slow down the inactivation of Na^+ channels in nerve membranes without altering the activation step [74, 75]. This effect is inhibited by TTX. Both ScTXs and ATXs enhance the action of veratridine or BTX, aconitine, and GTXs on

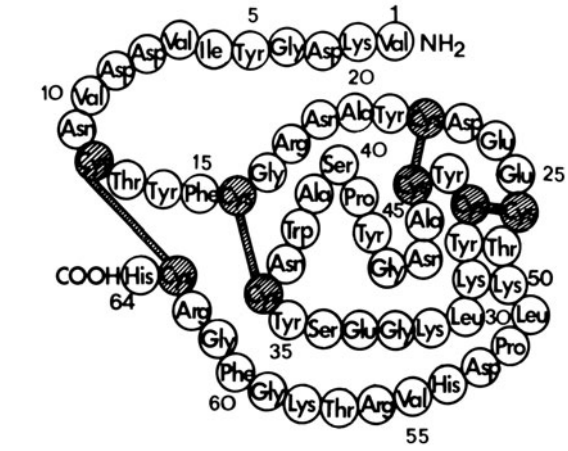

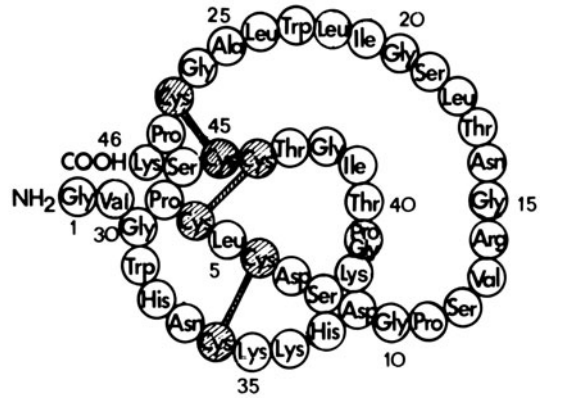

FIGURE 24–6. The structure of toxin II from scorpion venom *Androctonus australis Hector* and toxin V (ATX) from the sea anemone *Anemonia sulcata*.

the Na^+ permeability of neuroblastoma cells [33, 59, 76]. However, the scorpion toxins do not have the same mechanism of action, i.e., the venom of the American scorpion *Centruroides sculpturatus* has no effect on the inactivation of the Na^+ channel, but it shifts the voltage dependence of activation to more negative membrane potentials [77].

ScTXs and ATXs can be radiolabeled and their receptor subunit of the Na^+ channel of nerve preparations has been biochemically identified [63, 78, 79]. They both provide a tool to analyze the biochemical properties of the inactivation gate. The main properties of binding studies with ^{125}I-labeled toxins are the following: (a) Both toxins bind to sites at the external face of the Na^+ channel that are different but interdependent; the stoichiometry of binding is higher for ^{125}I-labeled ATXs [79]. (b) The binding of ScTXs to their specific sites is voltage dependent and does not occur on a depolarized membrane [63, 66, 78, 80] whereas the binding of ATXs can be found on both polar-

ized and depolarized synaptosomes [79]. (c) There are about two ATX-binding sites per TTX binding site.

Chemical modification of the carboxylates in ATX hardly alters the binding activity of the toxin, but completely suppresses both its toxicity and of course its effects on the Na^+ channel. In other words the chemically modified toxin is an antagonist of the native toxin [73].

Scorpion toxin II from *Androctonus australis Hector* dramatically prolongs the repolarization phase of the cardiac action potential. This prolongation is inhibited by TTX and is not seen in low-Na^+ solutions [81]. Pure anemone toxins from *Anemonia sulcata* and from *Anthopleura xanthogrammica* display the same type of effect on a variety of cardiac preparations [82–84]. The most probable conclusion from these results is that these two classes of polypeptide toxins slow down the inactivation of the cardiac Na^+ channel and may even induce an incomplete inactivation. In other words, their action on the cardiac cells is the same as their action on nerve Na^+ channels. This has been confirmed (a) by voltage-clamp studies of the effect of ATX on chick embryonic cardiac aggregates [43], and (b) by binding experiments of ^{125}I-labeled toxin II from the *Androctonus* scorpion to chick heart cells [85].

Both types of polypeptide toxins produce a positive inotropic effect on a variety of cardiac preparations and at very low toxin concentrations [82, 84, 86, 87].

Among a large number of polypeptide toxins extracted either from different scorpion venoms or from different sea anemones, the most potent for their positive inotropic effect are toxin V from *Anemonia sulcata* (fig. 24–6) and toxin II from *Anthopleura xanthogrammica* at concentrations between 1 and 5 n*M* [87]. Their half-maximal activity for the Na^+ channel of mammalian cardiac cells is observed at concentrations of the order of 1 n*M*. It is interesting to remark that mammalian cardiac cells that are TTX resistant are highly sensitive to ATXs, whereas nerve cells or chick cardiac cells that are TTX sensitive are more resistant to ATXs. The difference between the affinities of ATXs for Na^+ channels in sensitive or resistant cells is about 100-fold. An important part of the work devoted to the analysis of the mechanism of action of ATXs on the heart has been carried out with chick embryonic cardiac cells in culture using (a) electrophysiologic measurements with the simultaneous recording of contraction, and (b) measurements of $^{22}Na^+$ and $^{45}Ca^{2+}$ flux. Results obtained with ATXs [83] indicate: (a) The toxin induces action potentials of long duration, a slowing of the beating rate, and a simultaneous increase in amplitude and duration of cardiac contractions. (b) The toxin maximally increases the rate of $^{22}Na^+$ and of $^{45}Ca^{2+}$ entry in ventricular cells by a factor of about 1.5 and of 12, respectively. This effect is blocked by TTX, is dependent upon the external Na^+ concentration, and is not seen when Li^+ replaces Na^+; (c) ATX and veratridine work in synergy to stimulate both $^{22}Na^+$ and $^{45}Ca^{2+}$ influx. (d) ATX still induces contractions when the slow Ca^{2+} channel is blocked by verapamil, D-600 or Mn^{2+} (fig. 24–7A–C), but toxin-induced contractions are blocked in external Li^+ (fig. 24–7C). All these results taken together indicate that the increase in amplitude and duration of cardiac contractions caused by the toxin is most likely due (as for lipid-soluble toxins) to an indirect activation of the Na^+-Ca^{2+} exchange system. *Androctonus australis Hector* scorpion toxins have probably the same mechanism of action since they also stimulate the rates of both $^{22}Na^+$ and $^{45}Ca^{2+}$ influx into cardiac cells and since this stimulation is also inhibited by TTX [88] and synergically increased by veratridine [85].

A polypeptide toxin isolated from the coral *Goniopora* spp. provokes inotropic effects that are suppressed by TTX [89]. The mechanism of the cardiostimulant action of this peptide is probably the same as for ScTXs and ATXs.

A new category of polypeptide scorpion toxins has just been discovered [90]. They are extracted from the venoms of scorpions from Central or South America such as *Centruroides suffusus suffusus* or *Tityus serrulatus* [91]. These toxins block the activity of Na^+ channels in muscle cells. Although their physiologic effect is, at first sight, similar to that of TTX or STX, their binding site is different. These toxins can be radiolabeled with iodine and their properties of associations with the Na^+ channel

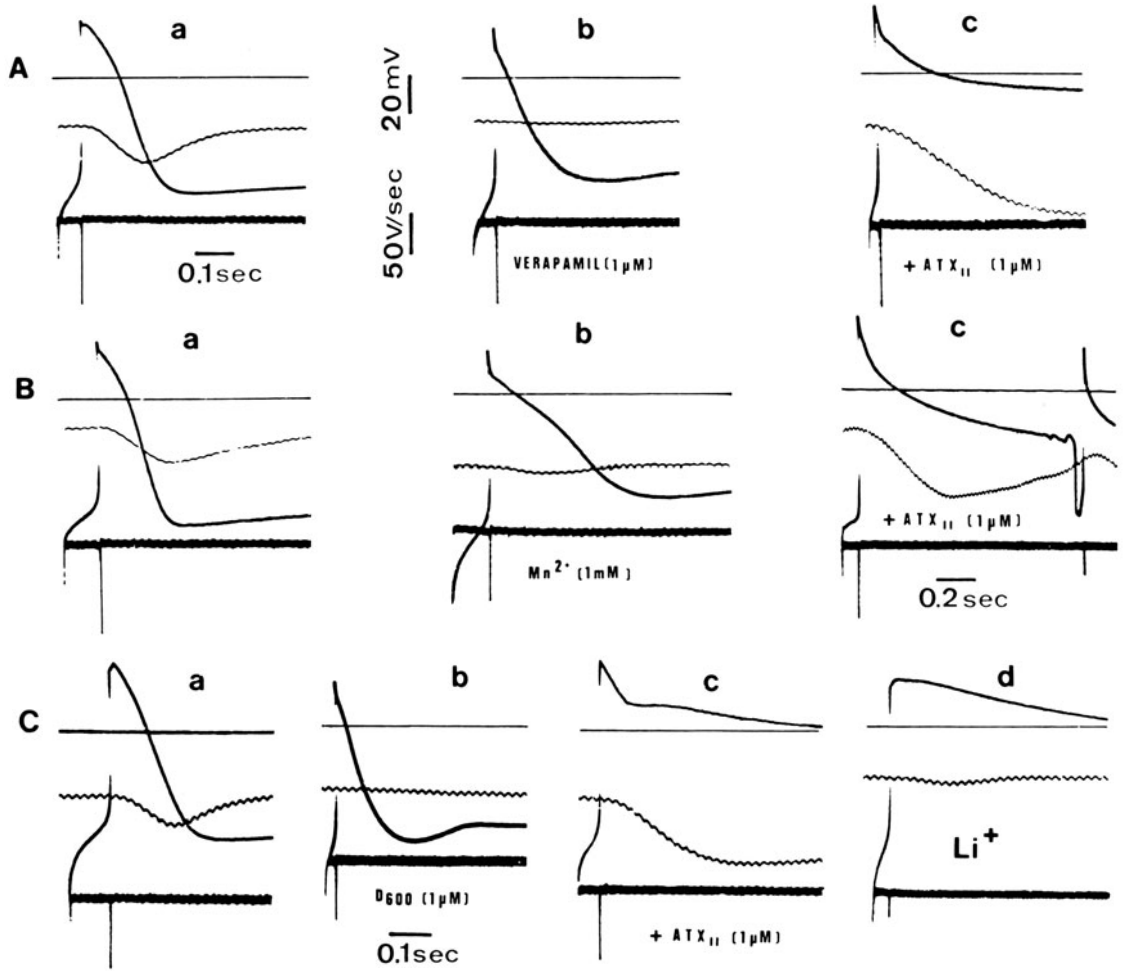

FIGURE 24–7. Effects of ATX-II on cultured chick embryonic heart cells in the presence of verapamil, Mn^{2+} ions, and D-600. (A) Verapamil. (B) Mn^{2+}. In each series of records, (a) control; (b) steady-state effect of blockers of the slow Ca^{2+} channel (note the suppression of contractibility); (c) after addition of ATX-II to the medium containing blockers of the Ca^{2+} channel (note the presence of contraction). *(C)* Suppression of the contraction induced by ATX-II in the presence of D-600 after external Na^+ replacement by Li^+: (a) control; (b) steady-state effect of 1 μ*M* D-600 in Na^+ medium (note the absence of contraction); (c) after addition of 1 μ*M* ATX-II in the Na^+ medium containing 1 μ*M* D-600 (the contraction reappears); (d) after complete replacement of external Na^+ by Li^+ in the presence of 1 μ*M* D-600 and 1 μ*M* ATX-II (note the suppression of contractibility). Records in this figure display the usual traces for the zero voltage line for dV/d*t* (lower trace), for the action potential, and for the contraction (middle trace) represented by a downward deflexion.

have been studied in detail. The dissociation constant of *Tityus* γ toxin with the Na^+ channel in nerve cells or in the electric organ of *Electrophorus electricus* is as low as 10^{-12} *M* [91]. There is a 1:1 stoichiometry between receptors of *Tityus* or *Centruroides* toxins and TTX. Moreover these polypeptide toxins discriminate between surface and T-tubular Na^+ channels in the muscle cell [90]. A study of these toxins on cardiac cells would be of a great interest. We have already demonstrated that there are binding sites for these toxins on chick embryonic cardiac cells in culture. Interactions are strong since dissociation constants for the *Ti-*

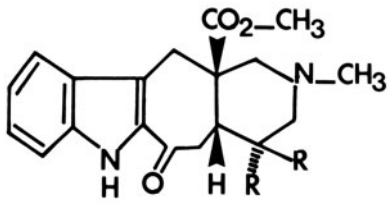

ERVATAMINE : R=H ; $R'=C_2H_5$

EPIERVATAMINE : $R=C_2H_5$; R'=H

FIGURE 24–8. The structure of ervatamine and of epiervatamine.

tyus γ toxin–cardiac membrane interaction are near 15 p*M*, about 2 orders of magnitude lower than dissociation constants found for the TTX–Na^+-channel complex ($K_D \simeq 1$ n*M*).

TOXINS AS TOOLS TO STUDY THE DIFFERENTIATION OF CARDIAC Na^+ CHANNELS

Most groups working on embryonic heart ontogenesis have observed that the maximum upstroke velocity of the cardiac action potential and the susceptibility of both action potential and contraction to blockade by TTX increase during the embryonic development of the chick and rat heart [92, 93]. In early stages of development (both in vivo and in vitro), the inward current responsible for the rising phase of the action potential is a slow Na^+ current that is sensitive to D-600 but not to TTX. The TTX-sensitive fast Na^+ channel appears at later stages of development. Electrophysiologic and biochemical studies using specific neurotoxins have shown [43] (a) that veratridine, BTX, ATX, and TTX receptors are present at the early stage when action potentials are insensitive to TTX; (b) that the fast Na^+ channel at this stage is in a nonfunctional (or silent) form which cannot be electrically activated, but which can be activated by the gating system toxins (veratridine, BTX, and ATX); and (c) that the transition from the early to the late stage of development corresponds both to the transformation of silent into functional channels and to an increase of the density of channels by a factor of 4–5.

Silent Na^+ channels that are present but not physiologically expressed at the very early stage of embryonic heart ontogenesis are similar to those which have been found in fibroblasts [94].

OTHER TOXINS

Ervatamine. Ervatamine is a toxic alkaloid (fig. 24–8) isolated from an Australian tree, *Ervatamina orientalis* [95]. Analyses of the mechanism of action of ervatamine and epiervatamine (a structural analogue 4–8 times more potent than ervatamine) on nervous preparations [96, 97] have shown (a) that ervatamine and epiervatamin provoke a frequency-dependent block of the fast Na^+ channels; (b) that the two molecules inhibit the effects of veratridine, BTX, ScTXs, and ATXs on the Na^+ channel similarly to TTX; (c) that ervatamine and epiervatamine do not bind to receptors specific for TTX, ScTXs, or ATXs; and (d) that the toxin alkaloids associate with the gating system of the Na^+ channel and are competitive inhibitors of BTX action, suggesting that the two classes of molecules have a common receptor site; epiervatamine and BTX have similar affinities for the Na^+ channel.

Ervatamine blocks the action potential of cardiac cells without altering the resting potential [98]. It inhibits the fast Na^+ current by binding to a single class of receptors ($K_D = 20$ μ*M*). The inhibition is frequency dependent and ervatamine prolongs the rate of reactivation of the Na^+ channel. Ervatamine also inhibits the slow Na^+ channel which is seen in Ca^{2+}-free solutions containing TTX as well as the slow Ca^{2+} channel [98].

Cardiotoxins. Although these toxins do not really belong to the family of natural compounds that are specific for ionic channels, it is useful to discuss them here mainly because of their name. Cardiotoxins form a family of single-chain toxic polypeptides of about 60 amino acids that are abundant in venoms belonging to snakes of the *Elapidae* family. Cardiotoxins

TABLE 24–1. A summary of the different classes of toxins acting on the Na^+ channel

Toxin	Physiologic effect	References
Tetrodotoxin (TTX) Saxitoxin (STX)	Blocks Na^+ currents	3, 21
Lipid-soluble molecules Veratridine Batrachotoxin (BTX) Aconitine Grayanotoxins (GTXs)	Causes persistent activation of Na^+ channels	34, 35, 37, 38, 42, 44, 49
North American or North African scorpion toxins (ScTXs) *Androctonus australis* Hector (toxin II) *Leiurus quinquestriatus* *Buthus Eupus*	Specifically slows Na^+ current inactivation	63, 65–67
Polypeptide toxins from sea anemone (ATXs) *Anemonia sulcata* (toxins II and V) *Anthopheura xanthogrammica* (toxins I and II)		68, 73–75, 86
Central or South American scorpion toxins *Centruroides suffusus suffusus* (Css-II) *Tityus serrulatus* (*Tityus* γ)	Blocks the early Na^+ current	77, 90, 91
Pyrethroids	Modifies the closing of fast Na^+ channels	105, 106

have extensive sequence homologies with snake neurotoxins that block nicotinic receptors [99].

This class of miniproteins is called cardiotoxins because they provoke systolic arrest in isolated heart preparations and death by ventricular fibrillation when administered to animals. Cardiotoxins bind to a lipid type of receptor structure [100, 101], provoking spectacular morphologic changes in membranes [102]. They affect various kinds of cells, both excitable and nonexcitable, causing irreversible depolarization and consequently impairing both the structure and function of the cells. The structural rearrangement that follows binding to essentially negatively charge lipids leads, among other things, to irreversible destruction of the Na^+,K^+-ATPase [101], but also of ionic channels (Romey, personal communication). Most cardiotoxin preparations contain traces of phospholipases [102] and the membrane effects that are seen are often due to the synergistic action of these two classes of proteins [102].

Palytoxin. Palytoxin has been isolated from zoanthids of the genus *Palythoa* [103]. This molecule is the most potent marine toxin yet isolated. It inhibits phasic tension production and initiates tonic contracture in isolated paced ventricle strips at concentrations of about 0.1 n*M*. Palytoxin-induced contracture is associated with $^{45}Ca^{2+}$ uptake [104]. The mechanism of action of this toxin is still unknown.

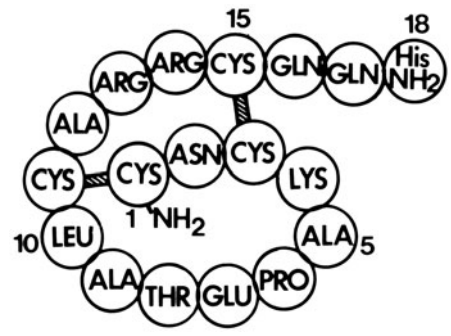

FIGURE 24–9. The structure of apamin from bee venom.

Summary and Conclusions

Most of the known natural cardiotoxins are also active on nerve and skeletal muscle and are specific for the fast Na^+ channel of the heart cell. Their mechanism of action and the available information concerning their receptor sites put them in three main different classes: (a) TTX and STX; (b) veratrum alkaloids, aconitine, BTX and GTXs; and (c) polypeptide toxins from some scorpion venoms and from sea anemone and coral venoms. Through their action on the fast Na^+ channel these toxins can either block contraction, produce positive inotropic effect and spontaneous contractions, or induce arrhythmia and cell fibrillation. Pyrethroids (a new generation of insecticides) are another class of molecules acting on the fast Na^+ channel [105, 106] which deserve study as possible cardiotoxins. A summary of the different types of toxins active on the Na^+ channel is presented in table 24–1.

Other natural cardiotoxins include ervatamine, which essentially acts as a local anaesthetic; snake cardiotoxins, which are in fact cytotoxins; and palytoxin, which has not yet been studied in sufficient detail to ascribe a function.

There is no natural toxic compound available that is specific for other ionic channels, like the classic K^+ channel or the slow Ca^{2+} channel, that are important for the cardiac action potential and the excitation–contraction coupling. The present pharmacology of these channels has been defined using compounds like TEA, aminopyridines, D-600 verapamil, nitrendipine, and analogues [107–109] which are not natural substances, which in many cases are not absolutely specific for a given channel, and which in general do not act at very low concentrations with the exception of the nitrendipine analogues. Only nitrendipine and its analogues look promising for the analysis of the properties of the Ca^{2+} channel at the molecular level [108, 109]. The discovery of natural toxins specific for the slow Ca^{2+} channel, for the Na^+-Ca^{2+} exchange system, or for other channels involved in the pacemaker mechanisms would be of a considerable interest.

One polypeptide toxin extracted from bee venom has been shown recently to be active on the Ca^{2+}-dependent K^+ channel of nerve, skeletal muscle, and smooth muscle cells [110]. This toxin, called apamin (fig. 24–9), forms very tight interactions with the Ca^{2+}-dependent K^+ channel (K_D = 15–20 p*M*). Because of the importance of the Ca^{2+}-dependent K^+ channel in the generation of a repetitive electrical activity in many excitable cells [111, 112] and because of the importance of the channel in linking cellular Ca^{2+} metabolism to membrane polarization, apamin will certainly become a tool as widely used as TTX itself. There is therefore an urgent need to test this toxin on a variety of cardiac preparations.

References

1. Lazdunski M, Renaud JF: The action of cardiotoxins on cardiac plasma membranes. Annu Rev Physiol 44:463–473, 1982.
2. Howard BD, Gunderson CB Jr: Effects and mechanisms of polypeptide neurotoxins that act presynaptically. Annu Rev Pharmacol 20:307–336, 1980.
3. Narahashi T: Chemicals as tools in the study of excitable membranes. Physiol Rev 54:813–889, 1974.
4. Schwartz JR, Ulbricht W, Wagner HH: The rate of action of tetrodotoxin on myelinated nerve fibers of *Xenopus Laevis* and *Rana esculenta*. J Physiol (Lond) 233:167–194, 1973.
5. Cuervo LA, Adelman WJ: Equilibrium and kinetic properties of interaction between tetrodotoxin and the excitable membrane of the squid giant axon. J Gen Physiol 55:309–355, 1970.
6. Ritchie JM, Rogart RB: The binding of saxitoxin and tetrodotoxin to excitable tissue. Rev Physiol Biochem Pharmacol 79: 1–50, 1977.
7. Chicheportiche R, Balerna M, Lombet A, Romey G, Lazdunski M: Synthesis of new, highly radioactive tetrodotoxin derivatives and their binding properties to the sodium channel. Eur J Biochem 104:617–625, 1980.
8. Chicheportiche R, Balerna M, Lombet A, Romey G, Lazdunski M: Synthesis and mode of action on axonal membranes of photoactivable derivatives of tetrodotoxin. J Biol Chem 254:1552–1557, 1979.
9. Ritchie JM: The sodium channel as a drug receptor. In: Straub RW, Bolis L (eds) Cell membrane receptors for drugs and hormones: a multidisciplinary approach. New York: Raven, 1978, pp 227–242.
10. Baker PF, Rubinson KA: Chemical modification of crab nerves can make them insensitive to the local anaesthetics tetrodotoxin and saxitoxin. Nature 257:412–414, 1975.
11. Reed JK, Raftery MA: Properties of the tetrodotoxin binding component in plasma membranes iso-

lated from *Electrophorus electricus*. Biochemistry 15:944–953, 1976.
12. Shrager P, Profera C: Inhibition of the receptor for tetrodotoxin in nerve membranes by reagents modifying carboxyl groups. Biochim Biophys Acta 318:141–146, 1973.
13. Sigworth FJ, Spalding BC: Chemical modification reduces the conductance of sodium channels in nerve. Nature 283:293–295, 1980.
14. Spalding BC: Properties of toxin-resistant sodium channels produced by chemical modification in frog skeletal muscle. J Physiol (Lond) 305:485–500, 1980.
15. Moore HPH, Fritz LC, Raftery MA, Brockes JP: Isolation and characterization of a monoclonal antibody against the saxitoxin-binding component from the electric organ of the eel *Electrophorus electricus*. Proc Natl Acad Sci USA 79: 1673–1677, 1982.
16. Hartshorne RP, Catterall WA: Purification of the saxitoxin receptor of the sodium channel from rat brain. Proc Natl Acad Sci USA 78:4620–4624, 1981.
17. Barchi RL, Murphy LE: Size characteristics of the solubilized sodium channel saxitoxin binding site from mammalian sarcolemma. Biochim Biophys Acta 597:391–398, 1980.
18. Levinson SR, Ellory JC: Molecular size of the tetrodotoxin binding site estimated by irradiation inactivation. Nature [New Biol] 245:122–123, 1973.
19. Barhanin J, Schmid A, Lombet A, Wheeler KP, Lazdunski M, Ellory J: Molecular size of different neurotoxin receptors on the voltage-sensitive Na^+ channel. J Biol Chem 258:700–702, 1983.
20. Dudel J, Peper K, Rüdel R, Trautwein W: The effect of tetrodotoxin on the membrane current in cardiac muscle (Purkinje fibers). Plugers Arch 295:213–226, 1967.
21. Cohen CJ, Bean BP, Colatsky TJ, Tsien RW: Tetrodotoxin block of sodium channels in rabbit purkinje fibers. J Gen Physiol 78:383–411, 1981.
22. Baer M, Best PM, Reuter H: Voltage-dependent action of tetrodotoxin in mammalian cardiac muscle. Nature 263:344–345, 1976.
23. Colatsky TJ, Gadsby DC: Is tetrodotoxin block of background sodium channels in canine cardiac Purkinje fibres voltage-dependent? J Physiol (Lond) 306:20P, 1980.
24. Gadsby DC, Colatsky TJ: Kinetics and voltage-independence of tetrodotoxin (TTX) block of background sodium channels in dog cardiac Purkinje fibers. Fed Proc 39:2076, 1980.
25. Sauviat MP: Le canal sodium des fibres atriales de grenouille. Mode d'action de la tétrodotoxine et de l'ervatamine. Thesis, University of Orsay, 1980.
26. Coraboeuf E, Deroubaix E, Coulombe A: Effect of tetrodotoxin on action potential of the conducting system in the dog heart. Am J Physiol 236:561–567, 1979.
27. Lombet A, Renaud JF, Chicheportiche R, Lazdunski M: A cardiac tetrodotoxin binding component: biochemical identification, characterization, and properties. Biochemistry 20:1279–1285, 1981.
28. Catterall WA, Coppersmith J: Pharmacological properties of sodium channels in cultured rat heart cells. Mol Pharmacol 20:533–542, 1981.
29. Renaud JF, Kazazoglou T, Lombet A, Chicheportiche R, Jaimovich E, Romey G, Lazdunski: The Na^+ channel in mammalian cardiac cells. Two kinds of tetrodotoxin receptors in rat heart membranes. J Biol Chem 258:8799–8805, 1983.
30. Jourdon P, Sperelakis N: Electrical properties of cultured heart cell reaggregates from newborn rat ventricles: comparison with intact non-cultured ventricles. J Mol Cell Cardiol 12:1441–1458, 1980.
31. Lombet A, Frelin C, Renaud JF, Lazdunski M: Na^+ channels with binding sites of high and low affinity for tetrodotoxin in different excitable and non-excitable cells. Eur J Biochem 124:199–203, 1982.
32. Harris JB, Thesleff S: Studies on tetrodotoxin-resistant action potentials in denervated skeletal muscle. Acta Physiol Scand 83:382–388, 1971.
33. Catterall WA: Neurotoxins that act on voltage-sensitive sodium channels in excitable membranes. Annu Rev Pharmacol Toxicol 20:15–43, 1980.
34. Kupchan SM, By AW: Steroid alkaloids; the veratrum group. In: Manske RHF (ed) Alkaloids, vol 10. New York: Academic, 1968, pp193–285.
35. Albuquerque EX, Daly JW: Batrachotoxin, a selective probe for channels modulating sodium conductances in electrogenic membranes. In: Chapman and Hall (eds) The specificity and action of animal, bacterial and plant toxins. 1976.
36. Khodorov BI, Revenko SV: Further analysis of the mechanisms of action of batrachotoxin on the membrane of myelinated nerve. Neuroscience 4:1315–1330, 1979.
37. Schmidt H, Schmitt O: Effect of aconitine on the sodium permeability of node of Ranvier. Pflugers Arch 349:133–148, 1974.
38. Ulbricht W: The effect of veratridine on excitable membranes of nerve and muscle. Erg Physiol 61:18–71, 1969.
39. Lazdunski M, Balerna M, Barhanin J, Chicheportiche R, Fosset M, Frelin C, Jacques Y, Lombet A, Pouysségur J, Renaud JF, Romey G, Schweitz H, Vincent JP: Molecular aspects of the structure and mechanism of the voltage-dependent sodium channel. Ann N Y Acad Sci 358:169–182, 1980.
40. Mozhayeva GN, Naumov AP, Negulyaev YA, Nosyreva ED: The permeability of aconitine-modified sodium channels to univalent cations in myelinated nerve. Biochim Biophys Acta 466:461–473, 1977.
41. Jacques Y, Fosset M, Lazdunski M: Molecular properties of the action potential Na^+ ionophore in neuroblastoma cells. J Biol Chem 253:7383–7392, 1978.

42. Honerjäger P: Cardioactive substances that prolong the open state of sodium channel. Rev Physiol Biochem Pharmacol 92:1–74, 1981.
43. Renaud JF, Romey G, Lombet A, Lazdunski M: Differentiation of the fast sodium channel in embryonic heart cells followed by its interaction with neurotoxins. Proc Natl Acad Sci USA 78:5348–5352, 1981.
44. Kakisawa H, Kozima T, Yanai M, Nakanishi K: Stereochemistry of grayanotoxins. Tetrahedron Lett 21:3091–3104, 1965.
45. Kumazawa Z, Iriye R: Stereochemistry of grayanotoxin II. Tetrahedron Lett 12:927–930, 1970.
46. Catterall WA: Activation of the action potential Na ionophore of cultured neuroblastoma cells by veratridine and batrachotoxin. J Biol Chem 250:4053–4059, 1975.
47. Horackova M, Vassort G: Ionic mechanism of inotropic effect of veratrine on frog heart. Pflugers Arch 341:281–284, 1973.
48. Horackova M, Vassort G: Excitation–contraction coupling in frog heart: effect of veratrine. Pflugers Arch 352:291–302, 1974.
49. Peper K, Trautwein W: The effect of aconitine on the membrane current in cardiac muscle. Pflugers Arch 296:328–336, 1967.
50. Hogan PM, Albuquerque EX: The pharmacology of batrachotoxin III. Effect on the heart Purkinje fibers. J Pharmacol Exp Ther 176:529–537, 1971.
51. Honerjäger P, Reiter M: The cardiotoxic effect of batrachotoxin. Naunyn Schmiedebergs Arch Pharmacol 299:239–252, 1977.
52. Shotzberger GS, Albuquerque EX, Daly JW: The effects of batrachotoxin on cat papillary muscle. J Pharmacol Exp Ther 196:433–444, 1976.
53. Sperelakis N, Pappano AJ: Increase in P_{Na} and P_K of cultured heart cells produced by veratridine. J Gen Physiol 53:97–114, 1969.
54. Fosset M, De Barry J, Lenoir MC, Lazdunski M: Analysis of molecular aspects of Na^+ and Ca^{2+} uptakes by embryonic cardiac cells in culture. J Biol Chem 252:6112–6117, 1977.
55. Akera T, Ku DD, Frank M, Brody TM, Iwasa J: Effects of grayanotoxin I on cardiac Na^+ K^+ adenosine triphosphatase activity, transmembrane potential and myocardiac contractile force. J Pharmacol Exp Ther 247:199–254, 1976.
56. Ku DD, Akera T, Frank M, Brody TM, Iwasa J: The effects of grayanotoxin I and α-dihydrograyanotoxin II on guinea-pig myocardium. J Pharmacol Exp Ther 200:363–372, 1977.
57. Seyama I: Effect of grayanotoxin I on sa node and right atrial myocardia of the rabbit. Am J Physiol 235:C136–C142, 1978.
58. Hotta Y, Takeya K, Kobayashi S, Harada N, Sakakibara J, Shirai N: Relationship between structure, positive inotropic potency and lethal dose of grayanotoxins in guinea pig. Arch Toxicol 44:259–267, 1980.
59. Honerjäger P, Frelin C, Lazdunski M: Actions, interactions and apparent affinities of various cevera-trum alkaloids at sodium channels of cultured neuroblastoma and cardiac cells. Naunyn Schmiedebergs Arch Pharmacol 321:123–129, 1982.
60. Reuter H: Divalent cations as charge carriers in excitable membranes. Prog Biophys Mol Biol 26:1–43, 1973.
61. Reuter H: Exchange of calcium ions in the mammalian myocardium: mechanisms and physiological significance. Circ Res 34:599–605, 1974.
62. Romey G, Lazdunski M: Lipid-soluble toxins thought to be specific for Na^+ channels block Ca^{2+} channels in neuronal cells. Nature 297:79–80, 1982.
63. Rochat H, Bernard P, Couraud F: Scorpion toxins: chemistry and mode of action. Adv Cytopharmacol 3:325–334, 1979.
64. Sampieri F, Habersetzer-Rochat C: Structure–function relationships in scorpion neurotoxins: identification of the superreactive lysine residue in toxin I of *Androctonus australis Hector.* Biochim Biophys Acta 535:100–109, 1978.
65. Romey G, Chicheportiche R, Lazdunski M, Rochat H, Miranda F, Lissitzky S: Scorpion neurotoxin a presynaptic toxin which affects both Na^+ and K^+ channel in axons. Biochem Biophys Res Commun 64:115–121, 1975.
66. Mozhayeva GN, Naumov AP, Nosyreva ED, Grishin EV: Potential-dependent interaction of toxin from venom of the scorpion *Buthus Eupus* with sodium channels in myelinated fibre. Biochim Biophys Acta 597:587–602, 1980.
67. Gillespie JI, Meves H: The effect of scorpion venoms on the sodium currents of the squid giant axon. J Physiol 308:479–499, 1980.
68. Schweitz H, Vincent JP, Barhanin J, Frelin C, Linden G, Hugues M, Lazdunski M: Purification and pharmacological properties of eight sea anemone toxins from *Anemonia sulcata, Anthopleura xanthogrammica, Stoichactis giganteus* and *Actinodendron plumosum.* Biochemistry 20:5245–5252, 1981.
69. Martinez G, Kopeyan C, Schweitz H, Lazdunski M: Toxin III from *Anemonia sulcata:* primary structure. FEBS Lett 84:247–252, 1977.
70. Tanaka M, Haniu M, Yasunobu KT, Norton TR: Amino acid sequence of the *Anthopleura xanthogrammica* heart stimulant, Anthopleurin A. Biochemistry 16:204–208, 1977.
71. Wunderer G, Fritz H, Wachter E, Machleidt W: Amino-acid sequence of a coelenterate toxin: toxin II from *Anemonia sulcata.* Eur J Biochem 68:193–198, 1976.
72. Wunderer G, Eulitz M: Amino acid sequence of toxin I from *Anemonia sulcata.* Eur J Biochem 89:11–17, 1978.
73. Barhanin J, Hugues M, Schweitz H, Vincent JP, Lazdunski M: Structure–function relationship of sea

anemone toxin II from *Anemonia sulcata*. J Biol Chem 256:5764–5769, 1980.
74. Bergman C, Dubois JM, Rojas E, Rathmayer W: Decreased rate of sodium conductance inactivation in the node of Ranvier induced by a polypeptide toxin from sea anemone. Biochim Biophys Acta 455:175–184, 1976.
75. Romey G, Abita JP, Schweitz H, Wunderer G, Lazdunski M: Sea anemone toxin: a tool to study molecular mechanisms of nerve conduction and excitation–secretion coupling. Proc Natl Acad Sci USA 73:4055–4059, 1976.
76. Jacques Y, Fosset M, Lazdunski M: Molecular properties of the action potential Na^+ ionophore in neuroblastoma cells: interactions with neurotoxins. J Biol Chem 253:7383–7392, 1978.
77. Cahalan MD: Modification of sodium channel gating in frog myelinated nerve fibers by *Centruroides sculpturatus* scorpion venom. J Physiol (Lond) 244:511–534, 1975.
78. Ray R, Morrow CS, Catterall W: Binding of scorpion toxin to receptor sites associated with voltage-sensitive sodium channels in synaptic nerve ending particles. J Biol Chem 253:7307–7317, 1978.
79. Vincent JP, Balerna M, Barhanin J, Fosset M, Lazdunski M: Binding of sea-anemone toxin to receptor sites associated with the gating system of the sodium channel in synaptic nerve endings in vitro. Proc Natl Acad Sci USA 77:1646–1650, 1980.
80. Catterall WA: Membrane potential-dependent binding of scorpion toxin to the action potential sodium ionophore: studies with a toxin derivative prepared by lactoperoxidase catalyzed iodination. J Biol Chem 252:8660–8668, 1977.
81. Coraboeuf E, Deroubaix E, Tazieff-Depierre F: Effect of toxin II isolated from scorpion venom on action potential and contraction of mammalian heart. J Mol Cell Cardiol 7:643–653, 1975.
82. Ravens U: Electromechanical studies of an *Anemonia sulcata* toxin in mammalian cardiac muscle. Naunyn Schmiedebergs Arch Pharmacol 296:73–78, 1976.
83. Romey G, Renaud JF, Fosset M, Lazdunski M: Pharmacological properties of the interaction of a sea anemone polypeptide toxin with cardiac cells in culture. J Pharmacol Exp Ther 213:607–615, 1980.
84. Shibata S, Izumi T, Seriguchi DG, Norton TR: Further studies on the positive inotropic effect of the polypeptide anthopleurin A from a sea anemone. J Pharmacol Exp Ther 205:683–692, 1978.
85. Couraud F, Rochat H, Lissitzky S: Binding of scorpion neurotoxins to chick embryonic heart cells in culture and relationship to calcium uptake and membrane potential. Biochemistry 19:457–462, 1980.
86. Alsen C, Beress L, Fischer K, Proppe D, Reinberg T, Sattler RW: The action of a toxin from the sea anemone *Anemonia sulcata* upon mammalian heart muscles. Naunyn Schmiedebergs Arch Pharmacol 295:55–62, 1976.
87. Shibata S, Norton TR, Izumi T, Matsuo T, Katsuki S: A polypeptide (AP.A) from sea anemone *(Anthopleura xanthogrammica)* with potent positive inotropic action. J Pharmacol Exp Ther 199:298–309, 1976.
88. Couraud F, Rochat H, Lissitzky S: Stimulation of sodium and calcium uptakes by scorpion toxin in chick embryo heart cells. Biochim Biophys Acta 433:90–100, 1976.
89. Fujiwara M, Muramatsu I, Hidaka H, Ikushima S, Ashida K: Effects of goniopora toxin, a polypeptide isolated from coral, on electromechanical properties of rabbit myocardium. J Pharmacol Exp Ther 210: 153–157, 1979.
90. Jaimovich E, Ildefonse M, Barhanin J, Rougier O, Lazdunski M: *Centruroides* toxin, a selective blocker of surface Na^+ channels in skeletal muscle: voltage-clamp analysis and biochemical characterization of the receptor. Proc Natl Acad Sci USA 79:3896–3900, 1982.
91. Barhanin J, Giglio JR, Leopold P, Schmid A, Sampaio SV, Lazdunski M: *Tityus serrulatus* venom contains two classes of toxins: *Tityus* γ toxin is a new tool with a very high affinity for studying the Na^+ channel. J Biol Chem 257:12553–12558, 1982.
92. Sperelakis N, Shigenobu K, McLean MJ: Membrane cation channels: changes in developing hearts, in cell culture and in organ culture. In: Lieberman M, Sano T (eds) Developmental and physiological correlates of cardiac muscle. New York: Raven, 1975, pp 209–234.
93. Bernard C: Establishment of ionic permeabilities of the myocardial membrane during embryonic development of the rat. In: Lieberman M, Sano T (eds) Developmental and physiological correlates of cardiac muscle. New York: Raven, 1975, pp 169–184.
94. Frelin C, Lombet A, Vigne P, Romey G, Lazdunski M: Properties of Na^+ channels in fibroblasts. Biochem Biophys Res Commun 107:202–208, 1982.
95. Knox JR, Slobbe J: Three novel alkaloids from *Ervatamina orientalis*. Tetrahedron Lett A:2149–2151, 1971.
96. Frelin C, Vigne P, Ponzio G, Romey G, Tourneur Y, Husson HP, Lazdunski M: The interaction of ervatamine and epiervatamine with the action potential Na^+ ionophore. Mol Pharmacol 20:107–112, 1981.
97. Pichon Y, Sauviat MP: Effect of ervatamine on the sodium current in squid giant axons. J Physiol (Lond) 280:29–30P, 1978.
98. Sauviat MP: Effects of ervatamine chlorhydrate on cardiac membrane currents in frog atrial fibres. Br J Pharmacol 71:41–49, 1980.
99. Lee CY: Recent advances in chemistry and pharmacology of snake toxins. In: Ceccarelli B, Clementi F (eds) Advances in cytopharmacology, vol 3. New York: Raven, 1979, pp 1–16.
100. Vincent JP, Schweitz H, Chicheportiche R, Fosset

M, Balerna M, Lenoir MC, Lazdunski M: Molecular mechanism of cardiotoxin action on axonal membranes. Biochemistry 15:3171–3175, 1976.

101. Vincent JP, Balerna M, Lazdunski M: Properties of association of cardiotoxin with lipid vesicles and natural membranes: a fluorescence study. FEBS Lett 85:103–108, 1978.
102. Gulik-Krzywichi T, Balerna M, Vincent JP, Lazdunski M: Freeze-fracture study of cardiotoxin action on axonal membrane and axonal membrane lipid vesicles. Biochim Biophys Acta 643:101–114, 1981.
103. Moore RE, Scheuer PJ: Palytoxin: a new marine toxin from Coelentarate. Science 172:495–498, 1971.
104. Rayner MD, Sanders BJ, Harris SM, Lin YC, Morton BE: Palytoxin: effects on contractility and $^{45}Ca^{2+}$ uptake in isolated ventricle strips. Res Commun Chem Pathol Pharmacol 11:55–65, 1975.
105. Narahashi T: Effects of insecticides on nervous conduction and synaptic transmission. In: Wilkinson CF (ed) Insecticide biochemistry and physiology. New York: Plenum, 1976, pp327–352.
106. Jacques Y, Romey G, Cavey MT, Kartalovski B, Lazdunski M: Interaction of pyrethroids with the Na^+ channel in mammalian neuronal cells in culture. Biochim Biophys Acta 600:882–897, 1980.
107. Sperelakis N: Effects of cardiotoxic agents on the electrical properties of myocardial cells. In: Balazs T (ed) Cardiac toxicology, vol 1. Boca Raton FL: CRC, 1981, pp 39–108.
108. Ehlert FJ, Itoja E, Roeske WR, Yamamura HI: The interaction of [^{3}H]nitredipine with receptors for calcium antagonists in the cerbral cortex and heart of rats. Biochem Biophys Res Commun 104:937–943, 1982.
109. Bolger GT, Gengo PJ, Luchowski EM, Siegel H, Triggle DJ, Janis RA: High affinity binding of a calcium channel antagonist to smooth and cardiac muscle. Biochem Biophys Res Commun 104:1604—1609, 1982.
110. Hugues M, Romey G, Duval D, Vincent JP, Lazdunski M: Apamin as a selective blocker of the calcium-dependent potassium channel in neuroblastoma cells: voltage-clamp and biochemical characterization of the toxin receptor. Proc Natl Acad Sci USA 79:1308–1312, 1982.
111. Meech RW: Calcium-dependent potassium activation in nervous tissue. Annu Rev Biophys Bioeng 7:1–18, 1978.
112. Barrett JN, Barrett EF, Dribin LB: Calcium-dependent slow potassium conductance in rat skeletal myotubes. Dev Biol 82:258–266, 1981.

25. CARDIAC HYPERTROPHY AND ALTERED CELLULAR ELECTRICAL ACTIVITY OF THE MYOCARDIUM

Possible Electrophysiologic Basis for Myocardial Contractility Changes

Robert E. Ten Eick
and Arthur L. Bassett

Introduction

The myocardial cell hypertrophies in response to a sustained increase in workload. Increased workload can result from factors including: pressure overload due to ventricular or systemic hypertension; volume overload because of an AV fistula, other defects in the heart pump, or hypervolemia; sustained increase in heart rate. It can be subsequent to regional damage brought about by acute or chronic ischemia and infarction, by nutritional and hormonal disturbances, and by dynamic [1] and isometric exercise [2]. There are numerous physiologic changes concomitant with and perhaps associated with hypertrophy of the myocardial cell. These include mechanical, biochemical, structural and ultrastructural, and most recently described, electrophysiologic alterations. The notion has developed that hypertrophy is compensatory, allowing the heart to meet the increased workload, and that cardiac failure ensues if hypertrophy is insufficient [3, 4]. The literature on hypertrophy and failure is extensive. This review will be limited to an examination of changes occurring in a common (and the most studied) form of hypertrophy, i.e., that provoked by pressure overload. We described the electrophysiologic changes associated with this form of hypertrophy and consider pertinent mechanical, structural, and biochemical data which are concomitant and may be related to the electrical changes. We will refer to other models or to naturally occurring disease-induced hypertrophy when they reflect areas of special significance or pertinence. The interested reader is directed to several recent reviews of biochemical changes in the myocardium during hypertrophy, including those of Rabinowitz and Zak [5], Wikman-Coffelt et al. [4], and Zak and Rabinowitz [6].

Original data reported in this review supported in part by grants HL 26027 to RET and HL 19044 to ALB from the USPHS, National Institutes of Health, Heart, Lung and Blood Division.

N. Sperelakis (ed.). PHYSIOLOGY AND PATHOPHYSIOLOGY OF THE HEART.

Martinus Nijhoff Publishing. Boston/The Hague/ Dordrecht/Lancaster.

Structural Changes in Hypertrophy

A number of studies have focused on the ultrastructural and structural changes occurring in dilated and hypertrophic heart to determine whether such changes can provide at least a partial explanation for altered contractile properties. Clearly, there are changes in sarcomere length and sarcomere banding patterns, including slippage of fibrils and an increase in mass, i.e., enlargement of the cross-sectional area of muscle cells, in myocardial hypertrophy [7]

This enlargement reflects changes in a number of subcellular structures and compartments including those involved in excitation and excitation–contraction coupling such as: the sarcolemma and T tubules, the interstitial "extracellular space", the sarcoplasmic reticulum, and the mitochondria, the "energy source" for establishing and maintaining the ionic concentration gradients required for excitability [8].

The myocardial cell can double in size during hypertrophy. The increase in sarcoplasmic volume is associated with a high degree of vesiculation of the sarcolemmal membranes [7]. These sarcolemmal vesiculations have been described as "cardiac villi" or arcade-like diverticulae. Multiple pinocytotic vesicles are seen in close approximation to either surface of the sarcolemmal membranes and may reflect the need of the hypertrophied cell for an increased membrane surface area. Mitochondria tend to congregate near the sarcolemma, suggesting that there are energy-dependent transport processes occurring at or near the surface membranes during hypertrophy [9].

Less is known about hypertrophy-induced changes in the intercalated discs which contain the structures permitting the cardiac impulse to conduct from cell to cell through low-resistance pathways. Apparently in response to prolonged exercise, which is known to increase heart size and myocardial cell mean diameter, there is an alteration in intercalated disc structure [7]. There are focal increases of up to five times normal in the width of the intercellular gap junction of the intercalated disc, and vesicles exhibiting a moderately dense matrix appear in the gap region. The vesiculation serves to increase both the volume and surface area in the intercellular gap region believed to be involved in intercellular transfer of ions and cell-to-cell communication. Whether these focal increases in the width of the gap junction affect either impulse conduction or contraction has not been clarified. Data are available which suggest that some dissociation of intercalated discs in human hearts occurs with mitral stenosis, congenital heart disease, myocardial fibrosis [10], and idiopathic cardiomyopathy [11]. The qualitative and quantitative correlation of dissociation of the intercalated discs in hypertrophy to electrophysiologic disturbances in such hearts remains to be fully elucidated [12].

Numerous studies have demonstrated that hypertrophy is characterized by an increase in the number of mitochondria in the myocardial cell. There is some controversy with respect to the ratio of the myofibrils to mitochondria. It has been suggested that hypertrophy evokes an increase in the relative amount of contractile material to be supplied with energy by the mitochondria such that an imbalance of energy relationships may develop [13]. This matter is not entirely clear because some studies fail to show a change in the ratio of these two structures [7]. The mitochondria of hypertrophied hearts are said to be slightly larger than those of nonhypertrophied hearts, and there are indications that there are differences in their internal ultrastructure. Mitochondrial degeneration is evident in end-stage hypertrophy and idiopathic cardiomyopathy [11]. While there are indications that mitochondrial function is altered in hypertrophy, the relation of changes in energy "status" to concomitant electrical and contractile changes is unclear.

Dilatation of the transverse tubule (T tubule) system has been noted in a number of studies on hypertrophied hearts. A similar dilatation has been noted in anoxic, hypoxic, and ischemic hearts [7]. Several studies have shown that during hypertrophy the T-system develops markedly, dilating [14] as well as enlarging longitudinally. In clinical cases of idiopathic cardiac hypertrophy with or without muscular aortic stenosis, the T tubules are particularly enlarged and expanded; enlargement is longitudinal and often proceeds to the intermediate sarcolemma [11, 14]. The appearance of a fine granular material within the T tubules has also been noted [7]. The significance of these changes in ultrastructural morphology with respect to changes in function associated with hypertrophy remains to be elucidated. To this end, several models have received attention.

The rat heart has been used for numerous studies of myocardial mechanical and, more recently, electrical alterations in hypertrophy (see below). Therefore, the concomitant changes in cellular anatomy and ultrastructure are of inter-

est. A particularly detailed examination of pressure-overload-induced changes in the proportions and absolute amounts of the various structures that make up rat ventricular cells has been carried out by Page and McCallister [13] using a quantitative morphometric approach. Pressure-overload-induced hypertrophy was produced by partial constriction of the ascending aorta with a silver band. As a result, there is left ventricular systolic hypertension and the progressive increase in the size of the myocardial cells. It is clear that, ten or more days after constriction of the aorta, the fraction of cell volume made up of myofibrils is uniformly increased while the fraction of cell volume made up of mitochondria shows a significant decrease. This suggested that the energy-producing organelles may be diminished relative to the contractile apparatus, and this may somehow be related to the ultimate development of heart failure. Microchemical assays of pressure-overloaded left ventricles of rats confirmed the results obtained by the quantitative morphometric analyses using electromicrographs. As noted previously, similar observations have been made in other animal models.

Changes in the external sarcolemma and T systems have also been documented. The cross-sectional diameter and area, and thus volume of hypertrophied cells, increase. By virtue of their larger diameter and volume, the hypertrophied myocardial cells have a smaller surface-area–volume ratio, i.e., the ratio of external sarcolemmal membrane area per unit of cell volume, falls as cell size increases. It has been suggested that the ratio change may affect the hypertrophic cell's ability to maintain homeostasis because of the increased demand on the plasma membrane portion of the external sarcolemmal envelope to perform vital functions including uptake of metabolic nutrients from the blood and interstitial spaces, outward transport of waste products and metabolic intermediates into the interstitial spaces and blood, and, finally, movements of ions associated with electrical excitation. However, Page and McCallister have suggested that the pressure-overloaded hypertrophied rat ventricular cell compensates for the decrease in surface–volume ratio by increasing the area of the plasma membrane lining the T-system. As the cell expands in diameter, additional T-system membrane is generated so that the ratio of sarcolemmal membrane that encloses both the external and internal cell volume remains constant. As a result the cell becomes honeycombed with T-system channels containing a fluid presumed to have the composition of extracellular fluid.

Wendt-Gallitelli and Jacob [15] used electron-microscopic investigations to evaluate the morphologic changes in heart tissue of Goldblatt rats during the compensatory stage of gradually provoked pressure-induced cardiac hypertrophy. They observed a marked increase in myocardial cell size within the first four weeks after renal artery coarctation; particularly evident was an enlargement of the T-tubule system. The observation that the transverse tubular system and the sarcoplasmic reticulum increase in parallel with the enlarging cell volume and myofibrillar mass agrees with the report by Page and McCallister [13]. Also using aortic constriction, Goldstein et al. [16] described ultrastructural changes in the left ventricle resulting when aortic constriction in the rabbit was gradually imposed. Distortions of the intercalated discs and widening of the Z bands were noted. The significance of these changes with respect to the changes in electrical activity noted by Aronson [17] in the Goldblatt rat model is considered below.

The nature of the stimulus provoking enlargement of the T-tubular space is unclear. Acute exercise, anoxic cardiac arrest, and ischemia produce T-tubule enlargement [18]. Transmitter-induced efflux of Cl^- produces T-tubule dilation in crayfish skeletal muscle, and it is known that intracellular Cl^- activity (a_i^{Cl}) decreases significantly in skeletal muscle during exhaustive work (see Tomanek and Banister [18] for a review). A number of papers (e.g., Horwood and Beznak [19]) document myocardial fluid and electrolyte shifts after imposition of aortic coarctation, but whether an efflux of cellular Cl^- occurs in the chronically pressure-overloaded hypertrophied ventricle is not known.

Anversa et al. [20] and Weiner et al. [21] have, in interesting and significant studies, ad-

dressed the morphometry of cardiac hypertrophy induced by experimental renal hypertension by evaluating endocardial and epicardial myocytes in the left ventricle of normal and hypertensive rats. In the normal ventricle, endocardial regions contain 30% more myocytes, 27% less interstitial space, 48% less capillary volume, and 17% less capillary surface than epicardium, while the same capillary length per unit of tissue volume occurs in both regions. In terms of the relative and absolute volumes and surface areas of their organelles, the cytoplasmic composition of normal endocardial and epicardial myocytes are nearly identical. In contrast, after 1–4 weeks of hypertension induced by renal arterial constriction, endocardial myocytes enlarged 26%, whereas epicardial myocytes enlarged 37%, although the number of myocytes and total length of capillaries remained constant in both areas. In the epicardial region of the interstitial volumes increased proportionately while in the endocardium there was a disproportionate 55% increase in interstitial components. Expansion of capillary lumens accounted for much of the interstitial enlargement throughout the myocardium [22]. Hypertrophy of myocytes in the epicardial region was accompanied by a reduced mitochondrial–myofibril ratio and proportionately large increases (two- to threefold) in both smooth endoplasmic reticulum and T-system volume and surface area. Thus, on a cellular basis, the morphometric characteristics of myocytes from hypertensive rats are significantly different from normal, and significant differences occur between the inner and outer layers of the myocardium. In this vein, it is interesting that fibrosis induced clinically or experimentally by aortic stenosis or coarctation is greatest in the subendocardial region where presumably blood supply is less (relative to subepicardium) [23]. Gulch [24] believes cell location (endocardial vs epicardial) during pressure overload to be a factor in determining the degree of action potential changes associated with hypertrophy (see below).

In summary, it appears from detailed ultrastructural studies primarily done in the rat heart that the surface area of the cardiac cell increases during hypertrophy. This is accompanied by an increase in the apparent surface area and volume of the T-tubule system. The total area including the area contiguous with the cell surface and the area in abutment with the sarcoplasmic reticulum are increased. This suggests that the modification of the T-tubule system may reflect, in part, an adaptation intended to maintain normal excitation–contraction coupling mechanisms in the cells. In other words, it has been suggested that the marked development of the T-tubule system during hypertrophy serves a useful purpose because, through these canals which penetrate the cell interior, the action potential can "reach" efficiently into the depths of the enlarged cell, and also the luminal membranes of the T-tubule canals may serve as carriers of cations, especially Ca^{2+}

Numerous studies have documented biochemical changes in the hypertrophied heart. These include alterations in protein synthesis [25–27] including myosin [28]; decrease in myosin-ATPase activity [29] which may relate to alterations in myosin isoenzymes [30] and myosin cross-bridge cycling [31] which in turn affects maximum velocity of isotonic shortening; heat production [32]; energy pathways [33]; collagen content [34]; and its distribution [35]; and DNA synthesis [36].

Stimulus to Hypertrophy

The biochemical nature of the stimulus to hypertrophy as well as the phenomenon of hypertrophy and its reversibility have been considered by various researchers. It has been suggested that these events may be incited by cyclic-AMP changes mediated by norepinephrine or pressure per se, perhaps by fiber stretch. The stimulus may act directly on the myocardial nucleus, or may act indirectly by the following sequence of events: Ca^{2+} from the sarcoplasmic reticulum may increase cyclic AMP and protein phosphorylation. This immediate elevation of cyclic AMP and its effect on protein phosphorylation would increase protein synthesis, whereas decreased cyclic AMP would cause decreased protein synthesis. Thus, nu-

clear cyclic AMP, which has been shown to control the synthesis of selective proteins in several types of tissues, may be an important regulating factor in the hypertrophy process, but this hypothesis has not been proven.

Meerson [3] has described three states of ventricular hypertrophy in the mammalian ventricle after chronic partial aortic or pulmonary artery occlusion. Stage 1 is a period of developing hypertrophy often with contractile dysfunction. Stage 2 is a stable phase of hypertrophy with "normal or even enhanced contractility". During stage 3, the hypertrophied heart demonstrates gradual contractile impairment and eventually "failure". Hatt et al. [37] have reviewed the structural characteristics of hypertrophy in terms of Meerson's scheme and have found that degenerative changes are more frequent when the load is more severe [38].

The biochemical and structural factors related to the development of physiologic (stage 1) vs pathologic hypertrophy (stage 2) have been reviewed recently by Wikman-Coffelt et al. [4]. They note that there are a number of major determinants; which include the degree of ventricular wall stress, the duration of such stress, and the nature of the inciting stimulus, the specific ventricle affected as well as the species, age, and health of the animal. Most inducers of hypertrophy appear to initiate the process by a common mechanical–biochemical coupling mechanism. The work overload causes an increased wall tension and pressure on the myocardial cells, and stretches the muscle fibers. Perhaps mediated or modulated by norepinephrine release, the stretch and associated increased strain in the fibers augments RNA transcription and protein synthesis, perhaps via the cyclic-AMP mechanism previously discussed. Then, depending on the severity of the workload, secondary factors such as increased tissue P_{CO_2} may determine whether the heart can adjust to an elevation in workload by developing the characteristics of either physiologic or pathologic hypertrophy, i.e., does the force developed during contraction remain the same or even increase, or does a major deficit in ventricular function and contractility ensue?

Electrical and Mechanical Alterations in Hypertrophy

During the past two decades, a number of investigators have quantified myocardial contractility using isolated ventricular muscles from normal hearts of mammals. The effects of drugs and changes in the extracellular ionic environment on both the electrical and mechanical properties of normal myocardial muscles have been delineated. In addition, the temporal stages of contractile function during pressure overload (ventricular systolic hypertension) have been studied and found to vary both with the degree and duration of pressure overload, and the species of animal used.

Several groups have established that chronic pressure overload of the right ventricle without cardiac failure (via sudden imposition of partial pulmonary artery occlusion) results in a depression in the force–velocity relationship of isolated feline right ventricular muscles studied in vitro [39, 40]. The active force and the maximum rate of development of force are reported to be reduced in such hypertrophied muscles [41], and there are significant differences in the force–interval relation as demonstrated by changes in the responses to altered rhythms including postextrasystolic potentiation [42, 43]. Time-dependent factors involved in contractile function during right ventricular systolic hypertension were recently emphasized by Williams and Potter [43]. They demonstrated that the active length–force relation, maximum rate of force development during the twitch, and force–velocity relations of right ventricular muscles are significantly depressed six weeks after pulmonary artery occlusion; however, these variables reverted toward normal within 24 weeks after occlusion. Only the time to peak force remained slightly elevated. Cooper et al. [44] have produced right ventricular hypertrophy by a nonacute progressive overload, and documented depressed velocity of shortening and active force while time to peak force is prolonged. Recent studies have indicated an increase in passive stiffness of hypertrophied right ventricular papillary muscles from cats with pulmonary artery constriction [45, 46].

An important advance toward understanding

the pathophysiology of hypertrophic heart was development of pressure-overload-induced chronic cardiac failure in a cat model. Spann et al. [39] clearly demonstrated that active force and the force–velocity relation were markedly decreased in right ventricular muscles isolated from cats with overt chronic right heart failure (Meerson, stage 3 of depressed contractility). The contractility of the intact right ventricle of cat was also found to be depressed [47]. Depression of active force has been confirmed by other workers [48].

Most of the early studies of the electrophysiologic effects of pressure-overload-induced hypertrophy also have involved the cat model of right ventricular hypertrophy induced by partial occlusion of the pulmonary artery; these studies have been the source of a variety of data showing changes in the cellular action potential. Although Kaufmann et al. [40] reported no differences in the electrophysiologic properties of normal vs hypertrophied papillary muscles despite decreased velocity of shortening, a later study by the same group revealed prolonged action potentials, decreased resting potential, and reduced upstroke velocity after three weeeks of exposure to pressure overload [49]; however, no contractile data were reported in this latter study.

An acutely (1–3 h) imposed elevation to two times normal systolic pressure in the right ventricle of cats during partial pulmonary artery occlusion had no effect on action potential configuration (Bassett et al., unpublished observations). However, cats in a slightly less early stage of hypertrophy (three days after partial banding of the pulmonary artery and without congestive heart failure) can exhibit action potentials with a rather depressed voltage during the plateau phase [50]; the plateau voltage depression was associated with a decrease in active force and rate of force development *and* increased time to peak force. Although indices of contractility remained depressed, the action potential appeared to normalize after 21 days with no marked difference discernible between action potentials from sham controls and those from banded hearts after 90 or more days except for a slight increase in the time for 70% repolarization [51]. In contrast, Ten Eick et al. [52] reported that in specimens of right ventricle, hypertrophied by the identical banding procedure performed in Bassett's laboratory 5–7 months prior to study, plateau voltage was depressed and action potential duration was significantly prolonged. These latter results suggested that the action potential changes do not return to normal in time, but rather they can persist for at least 5–7 months following the initiation of pressure overload. Ten Eick and Bassett then considered possible reasons for the apparently conflicting results. Bassett and Gelband's [50, 51] data for 110-day banding were obtained from right ventricles that were only mildly to moderately hypertrophic, whereas Ten Eick et al.'s data [52] were obtained on severely hypertrophied right ventricular free walls. The two studies also employed slightly different experimental protocols. Gelband and Bassett [48] examined the action potentials at a single stimulus rate of 30/min while Ten Eick et al. [52] used several stimulus rates ranging from 12 to 240 beats/min. In collaboration, Ten Eick and Bassett [53] therefore examined the possibilities that the magnitude of the changes in the action potential were determined by either the severity of the hypertrophy or by the stimulus rate. What they found was that the more hypertrophied the right ventricle, the greater was the depression of the plateau and the more prolonged was the action potential duration. When a stimulus rate of 30/min was used in mildly hypertrophied papillary muscle, however, the action potentials were indistinguishable from normal except for a very slight decrease in the repolarization rate during phase 3. This finding supports Bassett and Gelband's [51] earlier data. Interestingly, even in mildly hypertrophic preparations, when stimulated at rates of 60 beats/min or greater it was possible to detect some prolongation of the duration associated with a slowing of the repolarization rate during phase 3. In the mildly hypertrophied case, under these conditions of more rapid stimulation, plateau voltage may have been slightly depressed; but at slower stimulus rates, the plateau voltage was either unchanged or even slightly more positive than normal. In moderately and severely hypertrophic specimens, at

all stimulus rates plateau voltage was depressed, repolarization rate during phase 3 was slowed and duration was increased, particularly during the latter portion of phase 3. The plateau depression was about 5–8 mV, ranging from 4 to as much as 15 mV. The implications of such a change in plateau voltage with regard to depression of cardiac contractility will be discussed later. The recent results reported by Ten Eick and Bassett [53, 54] therefore, confirm the earlier results reported by these workers and indicate (a) the changes in the action potentials of cat heart subjected to pressure overload do not normalize with time, but rather persist; (b) the changes become more intensified as the severity of the right heart hypertrophy becomes more severe; and (c) the extent of the changes are more evident at heart rates of 60/min or more than at slower rates.

Regional variations in the transient depression of the plateau voltage in cat right ventricular pressure overloaded for three days also have been documented [55, 56]. The regional variations in the action potential changes also persist as they can be found in cat heart after pressure overload for 5–7 months [54]. Regional variation is not restricted to the cat model. Aronson [57] has indicated that action potentials recorded from endocardial and epicardial sites in the Goldblatt rat model of hypertrophy also have a much wider variation in action potential configuration than in normal rat heart.

In another study using cats with cardiac failure 1–3 days after pulmonary artery banding, Gelband and Bassett [48] noted decreased resting potential, overshoot, and upstroke velocity with impaired conduction and lengthened action potential duration.

Right ventricular hypertrophy induced by partial pulmonary artery constriction in the rabbit [58, 59] is associated with decreased velocity of shortening, decreased rate of force development but without change in active force, and an increase in the time to peak force. In an electrophysiologic study of long-term (21–39 weeks) pressure overload induced by pulmonary artery or aortic constriction, also in rabbits, Konishi [60] reported no change in ventricular resting potential and action potential duration and amplitude; contractile properties were not measured. However, inspection of his data reveals a depression in action potential plateau voltage similar to that noted by Ten Eick et al. [52–54]. We are unaware of any other studies defining the electrophysiologic effects of left ventricular systolic hypertension and hypertrophy induced by aortic constriction. However, using a rabbit volume-overload model of ventricular hypertrophy produced by experimentally induced hyperthyroidism, Sharp [61] has recently reported depression of the plateau voltage and slowing of repolarization during phase 3.

Recently, Cameron et al. (submitted for publication) have characterized several cellular morphologic and electrical abnormalities occurring in cats with partial supracoronary aortic constriction that may underlie the associated incidence of lethal cardiac arrhythmias [62]. In situ, during or after vagally induced slowing of sinus rate, premature ventricular depolarizations occurred in eight (26%) of the 31 experimental animals and three of the 31 developed ventricular fibrillation. In contrast, arrhythmias during vagally induced sinus slowing were not observed in 31 normal or seven sham-operated cats. Left ventricular endocardial fibrosis and connective tissue infiltration were found in most aortic-banded cats. During stimulation of isolated left ventricular specimens at cycle lengths of 630–1000 ms in tissue bath, subendocardial muscle cells within fibrotic regions elicited heterogenous electrical abnormalities. Included were action potentials with shorter-than-normal duration, low-amplitude action potentials generated by cells with low resting potentials, stepped or fragmented upstrokes, as well as electrically silent areas. The electrical abnormalities were concentrated near the interfaces between fibrotic and morphologically normally appearing tissues. Cells exhibiting abnormal action potentials were interspersed with other having normal activity. The durations of randomly sampled action potentials recorded from left ventricular myocardium outside of patchy fibrotic areas were prolonged. Overall, the findings in the nonfibrotic tissues were quite similar to those of Ten Eick et al. [53, 54] obtained from hypertrophic right ventricular myocardium of cat.

The electrophysiologic changes brought about by pressure overload of the rat left ventricle have been studied by several groups, notably Aronson [17], Gulch et al. [63], and Gulch [24, 64]. Capasso et al. [65] have recently reviewed the electrical and mechanical physiologic alterations in the hypertrophied rat heart. When left ventricular hypertrophy is gradually induced by renal hypertension, developed tension increases [65–68] or remains unchanged [65], time to peak tension increases [24, 65–68], maximum velocity of shortening decreases [65–67], and action potential duration [17, 24, 63] invariably seems to increase without significant changes in resting potential, amplitude of action potential overshoot, or maximum rate of rise of the action potential upstroke. Moreover, Gulch et al. [63] observed that the prolongation of action potential duration became more marked as the degree of hypertrophy became more severe. Again, the changes in cellular electrical activity in the hypertrophic rat heart are qualitatively rather similar to those seen in the hypertrophic cat right ventricle [53, 54].

Studies of the mechanical properties of rat left ventricle during hypertrophy induced by aortic constriction have reported a decrease in developed force [42] or no change [69–72], an increase [65, 70] or no change [42, 72] in time to peak force, an increase in time to peak shortening [70], and a decrease in the velocity of shortening [42, 69, 71]. Gradual pulmonary artery constriction in young rats also can produce significant hypertrophy with no impairment of force-generating properties or shortening velocity [73]. None of these latter studies included data on electrical properties.

Lengthening of action potential duration in rat and cat is not restricted only to hypertrophy induced by pressure overload. Tibbits et al. [74] noted that left ventricular papillary muscles from female rats run on a treadmill had altered electrical and mechanical properties when they were studied in tissue bath. Muscles from the trained rats generated greater peak isometric twitch tension per unit cross-sectional area than the control group. At the same time, while the action potentials were unchanged with respect to resting potential, action potential amplitude or overshoot, and APD_{90}, there was a significant prolongation of the action potential measured as time to repolarize to -50 mV. These investigators suggested that the treadmill exercise might cause an adaptation in the sarcolemma which increases Ca^{2+} "availability" to the contractile proteins. The differences between the changes in the mechanical properties induced by exercise and those induced by pathology make it difficult to assess these findings.

In the rat, renovascular hypertension produced by unilateral renal artery occlusion is a stable model of progressive ventricular pressure overload which takes two weeks to develop and is associated with a 50% increase in heart weight, no loss in body weight, and no signs of congestive heart failure. Using this model, Capasso et al. [65] report resting muscle compliance is unaltered by hypertrophy. Others have reported a decreased distensibility 24 weeks after renal occlusion in the same model [67, 75] which may be related to an increase in cardiac collagen content [76]. However, the renal hypertensive rat model of gradually induced myocardial hypertrophy does not appear to develop a phase of severe cellular damage and loss of myocardial contractility. Thus, the *phase 1* stage of hypertrophy (depressed contractility with suddenly imposed overload) described by Meerson [3] may not be applicable to all models.

Hayashi and Shibata [77] examined ventricular muscle action potentials in spontaneously hypertensive rats. Again, the transmembrane action potential was significantly longer in such hearts, but there were no significant differences in resting potential, action potential, amplitude overshoot, conduction velocity, and repolarization rate. These data have been confirmed by Heller [78] and Heller et al. [79]. Additionally, Heller [78] has demonstrated prolongation of ventricular action potentials in rats made hypertensive with deoxycorticosterone acetate when compared to those in control rats, and evaluated contractions and aftercontractions in papillary muscles from rats with spontaneous hypertension and cardiac hypertrophy [72, 78]. Although electrical studies were not done in the latter experiments, it was noted

that in the rats with myocardial hypertrophy the after contractions were larger than in their respective controls. Additionally, the mechanical refractory periods increased as the duration of hypertension increased.

Aronson [57] has examined, using the renal hypertensive rat model, oscillations in membrane potential which have been termed *afterdepolarizations* [80, 81] or *afterpotentials*. He reported that afterpotentials can be induced in hypertrophied rat myocardium selectively. Three kinds of afterpotentials were observed: early afterdepolarizations, delayed afterdepolarizations, and early afterhyperpolarizations. The first two types could give rise to triggered spontaneous activity while the third does not. Delayed afterdepolarizations were induced in hypertrophied muscles exposed to high Ca^{2+}, while early afterdepolarizations occurred in hypertrophied fibers exposed to tetraethylammonium (TEA). Neither of these treatments produced afterpotentials in normal myocardium. The delayed afterdepolarizations became larger when the stimulation frequency, number of preceding beats, or external Ca^{2+} concentration was increased. The interval coupling the upstroke of the last driven action potential to the positive-going peak of the delayed afterdepolarization decreased when the stimulation frequency or number of preceding beats was increased. This suggests that the afterpotentials and the associated triggered activity seen in the pressure-overloaded myocardium may be important factors underlying arrhythmia in these hearts. Spontaneously occurring afterpotentials and aftercontractions [72, 78] may be related, but this is not clear.

Keung and Aronson [82] showed that the ventricular hypertrophy induced by renal hypertension in rats which is associated with a generalized lengthening of the action potential duration also causes a reproducible decrease in T-wave magnitude. The change in T-wave configuration of the ECG may result from a difference in the duration of endocardial and epicardial action potentials. This notion is supported by a good correlation between cellular epicardial-to-endocardial repolarization gradients (as measured by action potential duration in isolated muscle preparations) and the change in T-wave morphology associated with cardiac hypertrophy [83].

There are few data defining the electrophysiologic properties of cardiac tissue from humans with cardiomyopathies, but action potentials recorded from ventricular tissue taken from the heart of a 42-year-old female with hypertrophic cardiomyopathy have been reported to have longer durations than action potentials recorded from "normal" papillary muscles taken from patients undergoing mitral valve replacement [84]. While this finding has been generally confirmed by Singer and Ten Eick and their co-workers, the changes in cellular electrical activity in hypertrophic diseased human heart are much more extensive and intensive than that described by Coltart and Meldrum [84]. The electrophysiologic changes observed in diseased human ventricle were recently reviewed by Singer et al. [85] and Ten Eick et al. [86]. The interested reader is referred to these two articles.

Of interest is the fact that, as in the case of the exercised rats [74], the right atrial monophasic action potential obtained during cardiac catheterization increases in amplitude and duration after physical training in healthy human volunteers [87]. Although not reported even though chest x-rays were taken, it is interesting to speculate that their exercise and training regimen led to hypertrophy of the right atrium.

Relationship between the Electrical and Mechanical Changes and Hypertrophy

In the cat model of cardiac hypertrophy produced by long-term right ventricular pressure overload, generally the extent of the electrophysiologic changes is increased as the severity of the hypertrophy is increased [53]. At the same time, however, the pressure overload may also be associated with production of morphologic evidence of damage to the ventricular myocardium which has been forced to work harder and against an elevated wall tension [88]. This raises the question of whether it is *damage* per se, *hypertrophy* per se, or both which underlie the electrophysiologic and mechanical changes which have been reported.

In this vein, studies by Cutilletta et al. [89] on the spontaneously hypertensive rat may provide some clues. This group noted that in the spontaneously hypertensive rat, cardiac hypertrophy developed even though hypertension was prevented by treatment beginning at birth with nerve-growth-factor antiserum. They suggested that myocardial hypertrophy in these rats is a primary manifestation of an underlying myocardial abnormality, and that it is the hypertrophic heart that produces the hypertension rather than the hypertension causing hypertrophy.

There is a significant decrease in capillary density, variably increased folding of the intercalated discs, and a significant cardiac hypertrophy in the myocardium of spontaneously hypertensive rats [90]. Additionally, the ECG of these rats changes markedly during progressive development of left ventricular hypertrophy [91]. Findings that QRS and P-wave durations progressively increased led to the suggestion that the specialized conducting system does not increase in parallel to the cardiac muscle mass as the hypertrophy progresses. It was further suggested that it was the resulting disparity that slowed the spread of the impulse. An alternate explanation would be that either hypertrophy, damage, or mechanical stress of the conducting system causes changes in the membrane and/or cable properties of the conducting system.

A recent clinical study suggests that hypertrophy-induced increased QRS duration may be more closely associated with development of intercellular fibrosis than with increased muscle mass [92]. Whether similar fibrotic changes occur in the spontaneously hypertensive rat heart and could underlie change in either the cellular membrane or cable properties [82] is unclear at this time. Of particular importance in this regard would be results indicating whether or not the hypertrophic hearts of spontaneously hypertensive rats, in which hypertension was prevented by treatment with nerve-growth-factor antiserum, developed a wider-than-normal QRS or other evidence of conduction disturbances. However, the broad significance of such findings will be limited by the fact that the available data characterizing the electrical and mechanical changes associated with experimentally induced or spontaneously occurring cardiac hypertrophy in animal models or clinically in man vary widely between species and are strongly influenced by the duration and nature of the stimulus employed to provoke the hypertrophic response.

Meaning and Basis for the Electromechanical Changes

Certain generalizations about hypertrophy emerge from the currently available data. Most studies on isolated cardiac muscle mechanics in rats and rabbits with cardiac hypertrophy produced by ventricular pressure overload report normal or increased developed tension, decreased velocity of shortening, increased time to peak tension, and increased time to peak shortening; in the rat model of left ventricular hypertrophy induced by renal hypertension or spontaneous hypertension, action potential duration is prolonged. In cats with right ventricular hypertrophy, developed tension is reduced, the velocity of shortening and maximal rate of tension development are decreased, and these mechanical changes are generally associated with depression of plateau voltage, reduced rate of repolarization, and prolonged action potential duration. These data suggest that despite decreased shortening velocity and rate of tension development, normal levels of developed tension apparently can be maintained in rats and rabbits with left ventricular hypertrophy because the duration of contraction is increased, possibly mediated by the prolongation of the plateau phase of the action potentials [17, 63]. There are several studies which demonstrate that the characteristics of the isometric contraction can be influenced by the voltage-time course of the membrane depolarization [93–96]. The nature of the relationship between contraction and membrane depolarization is complex and varies with species and experimental conditions, but it is not unreasonable to speculate that the longer action potentials in hypertrophied rat ventricular muscle may prolong the duration of the contraction event so as to maintain normal levels of developed force despite the diminished velocity of

shortening or rate of force development. Aronson [17] has shown for rat ventricular muscle that the correlation between contraction and the duration of depolarization was best for APD_{50} when muscles exhibited relatively short action potentials (sham and pressure-overload relieved muscles), yet the correlation virtually disappeared in hypertrophied muscles which had very long action potentials. Since maximum force development in rat ventricular muscle is affected very little by depolarizations lasting more than 100 ms [97], it may be that once the duration of the action potential reaches a certain length, active force is no longer influenced by this parameter [17].

Alternatively, the long action potentials noted for hypertrophied ventricle may be either secondary to or caused by altered contraction. There are recent data [98] which clearly demonstrate that the mechanical deformation can affect cardiac cellular electrical activity in frog heart. Previously, Kaufmann et al. [40] proposed that the duration of the myocardial action potential is influenced by the mode of contraction. They had noted that isotonic shortening of cat papillary muscle prolongs action potential duration while isometric force development tends to shorten it. Although extrapolation of these findings in isolated muscle to the behavior of muscle fibers in situ in the hypertrophying heart is uncertain, especially in view of pressure-overload-induced or dilatation-induced changes in the connective tissue of the cardiac skeleton [99], they clearly have implications for physiologic function. The length of various fiber bundles may vary within the walls of a particular chamber, not only during phasic ventricular contraction but also during pressure overload [100] (reviewed by Wikman-Coffelt et al. [4]). Wall stress and therefore location of fibers also apparently determine the degree of their hypertrophy [20] and, in turn, the degree of prolongation of the action potential duration.

Gulch [24, 64] extended his electrophysiologic study on muscle preparations from hypertrophied hearts of Goldblatt rats to nonhypertrophied cat hearts. He noted that *right ventricular* action potentials in the Goldblatt rat are prolonged in comparison to the corresponding controls, and suggested this relates to the slight degree of hypertrophy demonstrated by the right ventricles. This phenomenon is not specific for the rat since in cat heart action potentials elicited by papillary muscles from the left ventricle are also prolonged compared to those of the right ventricle; qualitatively similar responses were obtained in guinea pig hearts. Gulch [64] suggested that the differences between left and right ventricular action potentials may be attributed to the differing mechanical loading to which the corresponding myocardial cells are subjected in situ. If this is the case, one must likewise propose that differences in the durations of action potentials of subendocardial cells will be prolonged relative to subepicardial cells because of the higher wall stress to which cells in wall layers located in the endocardial region are subjected. Indeed, Gulch [64] has noted that prolonged action potentials are found in subendocardial as compared to subepicardial cells as well as in cells of left ventricular versus cells in right ventricular papillary muscle. Thus, degree of pressure overload (and indirectly the cell location) particularly with respect to the ventricular chamber in which it is located, is a highly significant factor defining the duration of the action potential. It is curious that in five-month-old dogs there is a relative paucity of T tubules in myocardium of the low-working-pressure right ventricle when compared to the higher-pressure left ventricle [101]. One wonders what effect the additional excitable membrane area represented by the T tubules might have on action potential duration.

Changes in collagen synthesis and content accompany ventricular pressure overload in cat [102] and rat [103]. One might speculate as to whether this could alter cellular electrical coupling and inhibit propagation of the repolarization wave. Keung and Aronson [82] attempted to assess whether an alteration in cellular electrical coupling contributes to the electrophysiologic changes associated with hypertrophy. They analyzed the spatial steady-state electrotonic voltage profile produced by intracellularly applied constant current pulses, and found the effective input resistance was unaffected by hypertrophy in rat ventricular cells.

They also demonstrated that the action potential prolongation accompanying hypertrophy was not uniform throughout the heart. While the entire time course of repolarization was prolonged in endocardial and papillary muscle fibers, only the latter half of repolarization was prolonged in epicardial fibers. They concluded that altered electrotonic coupling between cells was not an important factor contributing to the prolonged action potential durations seen in hypertrophied myocardium. Therefore, logically one should expect a change in membrane function to underlie the changes in the action potential configuration. Biochemical alterations associated with hypertrophy may affect the intracellular concentration of Ca^{2+} and thus may modulate membrane properties and ionic gradients or both, and even dissociate the time course of the action potential from contractile performance.

An almost universal finding in muscle fibers from mammalian hearts exposed to ventricular pressure overload and hypertrophy is increased action potential duration. The ionic basis for this has not been clarified, yet it has been the subject of several recent studies. Aronson [17] has evaluated the responses of hypertrophied rat myocardium (Goldblatt procedure) to changes in extracellular fluid composition and during exposure to ionic channel blockers. They found that in pressure-overloaded and sham-operated control ventricles the action potential changes brought about by the various testing treatments differed quantitatively. Exposure of the hypertrophic isolated myocardium to high Ca^{2+}-containing or low-Na^{+}–Tyrode solution produced greater decreases in action potential duration than in normal myocardium. Exposure to D-600, an inhibitor of slow inward current, also produced a greater shortening, but its effect was limited to APD_{50} in pressure-overloaded muscles. In contrast, exposure to Sr^{2+} Tyrode and TEA Tyrode produced an increase in APD_{50} and ADP_{75}, but the effect was similar in both pressure-overloaded and sham-operated muscle action potentials. Treatment with Ca^{2+}-free–Tyrode solution had little effect on action potential duration in either group. None of the treatments had a significantly different effect on resting membrane potential or action potential amplitude in either group. Aronson [17] felt the most likely basis for the prolongation of the duration of the action potential in hypertrophied rat myocardium was that the inactivation of a Ca^{2+}-inactivated inward current was slowed. This notion remains to be proven using a voltage-clamp approach. Gulch has also manipulated the extracellular environment in hypertrophied (Goldblatt procedure) rat myocardium [63]. After depression of the fast Na^{+} inward current by either tetrodotoxin, depolarization produced by augmentation of extracellular K^{+} concentration, or by reduction of the extracellular Na^{+} concentration, action potentials prolonged by hypertrophy remain prolonged. They concluded that Na current did not contribute importantly to the prolongation of APD. They also manipulated the extracellular Ca^{2+} concentration after inhibiting fast Na^{+} channel conductance, and suggested that the membrane slow inward current was primarily carried by Ca^{2+} ions in the hypertrophied cells. From this report [63], it appears that prolongation of APD results from either an augmentation of either phasic or steady-state net slow inward current or a decrease in net outward repolarizing current, either time dependent or time independent. Changes in either or both the maximal conductance or the kinetics of channel function could be involved. However, it is more difficult to explain decreased contractile force if slow current is in fact increased. The more likely explanation should involve the potassium channels.

Recently the power of the voltage-clamp approach was brought to bear on this question. Ten Eick et al. [54], using the single sucrose gap technique, examined the voltage-clamping membrane currents recorded from fine papillary muscles which had been isolated from the right ventricles of cats both with normal hearts and with hearts subjected to right ventricular pressure overload for 5–7 months. Their analysis indicated that, while the overall time course of the membrane current was qualitatively unchanged by hypertrophy, several parameters quantifying the total current and its component parts were altered. The amplitude of the slow inward current was reduced at all levels of

membrane potential, but neither its voltage dependence nor its time course of decay (inactivation rate) were affected. The finding that ventricular hypertrophy reduces myocardial slow inward current [54] has recently been confirmed by Hemwall and Houser [104] using a more indirect approach. They found that the amplitude and duration of the slow-response, calcium- and catecholamine-dependent action potentials were smaller and shorter in hypertrophic cat ventricular myocardium than that in normal heart. The time course for the development of the time-dependent outward-rectifying potassium current was prolonged and its amplitude was reduced at all voltages; its voltage dependence was also shifted positively by about 10 mV [54]. The shift in the current–voltage relation did not account for the entire reduction in this component of membrane current. The shape of the current–voltage curve for the instantaneous background current was strikingly altered, having developed a region of negative slope between about -30 and 0 mV. It should be mentioned that while inward rectification is seen in the instantaneous background current of normal cat papillary muscle, a negative slope region has never been reported [54, 105]. Ten Eick et al. [54] have suggested that these changes in the slow-inward- and outward-directed components of the membrane current flowing at voltage levels associated with the action potential plateau and late repolarization phase can qualitatively explain the depression of the plateau voltage, the slowing of the repolarization rate during phase 3, and the prolongation of the action potential duration that have been observed in severely hypertrophic cat right ventricular myocardium. Verification of this notion awaits the results of computer-generated action potential modeling using the voltage-clamp data. While it is uncertain to what extent results obtained from hypertrophic cat heart can be applied to hypertrophic rat heart, these results of [54] do not support the notion that action potential prolongation is due to an hypertrophy-associated slowing of the inactivation of a Ca-inactivated inward current [17]. In fact, the inactivation kinetics of the slow inward current were found to be unaffected by hypertrophy. The data from cats, however, support the hypothesis that a Ca-dependent conductance, a Ca-dependent potassium conductance for instance, may be inhibited and its kinetics slowed.

The mechanisms underlying the shift in the voltage dependence of the time-dependent potassium current and the negative slope region in the instantaneous background current are not even poorly understood at this time. Some speculations in this regard will be expressed later in this chapter. One point does seem clear, however: the shift in the time-dependent potassium current–voltage curve cannot be explained by an alteration in surface charge either on the inner or outer surfaces of the sarcolemma because, it this were the case, the voltage dependence of the slow inward current would be expected to shift also. Because the slowing of the repolarization rate during phase 3 became more pronounced as the severity of hypertrophy increased, at least in the cat heart, it is reasonable to suggest that the changes in the outward-directed repolarizing currents observed during voltage clamp are similarly graded as function of the severity of hypertrophy.

In order to extrapolate from the effects of hypertrophy on any of the components of the membrane current to effects on the membrane conductances for each of the currents, one assumes that the transmembrane concentration gradient for the involved ion species is unaltered by either the experimental intervention or the voltage-clamping pulse. The field is well aware that the latter is certainly not true and there are compelling reasons to believe that hypertrophy and failure also affect the ionic concentration gradients. These conclusions relative to K^+ are supported by the recent work of Martin et al. [106].

Fluid and electrolyte shifts occur in pressure-overloaded rat and dog ventricle [107, 108]. Martin et al. [106] studied electrogenic Na^+ pumping in failing cat papillary muscle. They noted that papillary muscles from the failing hearts had slightly lower resting potentials than those from normal animals and, when the muscles were cooled, resting potentials in both groups fell to low levels. However, after 2 h of hypothermia, upon rewarming to 37°C in 10

m*M* K^+, the muscles from normal cat hearts abruptly hyperpolarized upon rewarming to -82 mV and then slowly leveled off to -66 mV. In contrast, muscles from animals in heart failure hyperpolarized, but to a lesser extent, during rewarming. The steady-state potential also leveled off at -66 mV. They suggested that the Na^+ pump for electrogenicity is depressed in hearts from cats with pulmonary-artery-constriction-induced heart failure. These data can also support other hypotheses. For instance, simple Na-K exchange could have been depressed or electrogenic Na-Ca exchange could have been enhanced. In short, these results are rather difficult to interpret.

Martin et al. [106] studied drive-related changes in extracellular K^+ activity (a_0^k) in muscles from hypertrophied hearts. Ion selective microelectrodes and morphometric techniques were used. Upon the imposition of a higher driving rate, the a_0^k in the extracellular space reached a maximum and then returned toward a lower steady-state level. This pattern of extracellular K^+ accumulation took significantly longer to unfold in failing muscles than it did in normal muscles, and the steady-state concentration of the K accumulated in the interstitial spaces of failing tissue was significantly higher. However, the maximum a_i^k obtained in failing muscles was found to be slightly lower than that in normal muscles. These changes are consistent with previously reported differences in the patterns of drive-related changes in resting potentials measured in normal and failing muscles and are explained by an increase in the volume of the interstitial space of hypertrophic heart and an increase in the ionic load on the Na^+-K^+ exchange pump. Such an hypothesis also can explain the apparent slowing of the development of the outward-directed repolarizing currents during voltage clamp to voltages in the plateau range that has been reported by Ten Eick et al. [54]. If this is the case, one should expect the component of the time-dependent outward current attributable to accumulation of potassium in the interstitium to be larger and more slowly developing in hypertrophic heart. Preliminary data (Ten Eick, unpublished observations) suggest the results are as predicted.

Relaxation is also affected in myocardial hypertrophy. For example, Capasso et al. [65] noted time to one-half relaxation is increased; the relation of this change to action potential lengthening is unclear. Relaxation in normal mammalian heart muscle is sensitive to the loading conditions [109]. Recently, Le Carpentier et al. [110] have demonstrated a decrease in the maximum velocity of relaxation of hypertrophied rat ventricular muscle which parallels the decrease in maximum velocity and extent of shortening. However, there were no changes in the load sensitivity of relaxation even in the terminal stages of congestive heart failure. They indicated the maintenance of an efficient intracellular Ca^{2+}-sequestering system so as to preserve the homeostasis of the sensitivity of relaxation to loading conditions even in the presence of pressure overload.

Reversibility of Hypertrophy-induced Changes

The question of whether the changes induced by hypertrophy are reversible has been addressed by numerous studies. They indicate that the changes regress rapidly when excessive pressure or volume load on the heart are relieved. Regression can occur after relief of systemic hypertension, repair of ventricular septal defect, and operative correction of aortic regurgitation. Whether regression will be complete or partial seems to depend on the degree of hypertrophy as well as on the age and health of the animal. Although ventricular hypertrophy regresses after correction of experimental or clinical hemodynamic overload, contractility usually remains depressed. Failure of contractility to return to normal may be related to the fact that the connective tissue changes do not appear to regress as readily as do the changes in myocardial mass; possibly irreversible biochemical and structural changes are involved.

Investigations using the cat model have delineated the temporal aspects of regression in right ventricular hypertrophy *after* release of chronic pulmonary artery occlusion [111]. Coulson et al. [112] noted that relief of pressure overload allows reversal of the depression of velocity of shortening and ability to develop

force, although catecholamine depletion is still present. A study of intermittent pressure loading on the development of right ventricular hypertrophy in the cat demonstrates that the regression of hypertrophy is a slower process than its progression [113].

Few data exist with which reversibility of the electrophysiologic changes can be assessed. This question bears importantly on the hypothesis that electrophysiologic changes partially underlie the contractility changes. Capasso et al. [65, 114] have evaluated the electrical and mechanical changes brought about by reversal of pressure overload induced by renal hypertension in rats. Removal of the stimulus for hypertension consists of surgical excision of the left kidney of rats which had undergone previously clipping of the left renal artery. Capasso et al. [114] simultaneously recorded mechanical and electrical activity in sham and the hypertrophied papillary muscles. The mechanical and electrical abnormalities described in their earlier studies were reversed in muscles from rats which were made normotensive for ten weeks subsequent to ten weeks of hypertension. The story, however, is far from clear. In one study on a rat model, anomalous contractile properties were reported to persist even after regression of hypertrophy induced by banding the aorta for 5–15 days [70]; in addition, certain biochemical abnormalities also are not completely reversed [115].

The Electrophysiologic Basis for Decreased Contractility

Hypertrophy of the myocardium is associated with and appears to set into motion events at the molecular level which can culminate in depression of contractility and altered sarcolemmal electrophysiologic function. The alterations in electrophysiologic function are manifested as changes in the membrane action potential and transmembrane current. Voltage-clamp study of the excitation–contraction process in normal sheep [116, 117], beef [96], and cat [118] hearts indicates that at least one change in the action potential and one in the membrane current of hypertrophic heart should predictably reduce the force of contraction. Force of contraction is strongly influenced both by plateau voltage and by the maximal slow-inward-current amplitude. The relationships between contractile force and these two parameters are intimately intertwined. The membrane potential during the plateau of the action potential also influences the magnitude of the slow inward current; the plateau voltage is influenced by the strength of the slow inward current; both are required to initiate excitation–contraction coupling and both influence the force of the twitch.

The relationship between membrane potential and the force of contraction during the myocardial twitch is an S-shaped function with a threshold near -60 mV which reaches a maximum at approximately $+10$ to $+20$ mV when defined by 250- to 800-ms-long step voltage clamps. Inspection of the voltage–tension relationship reveals that any significant loss of membrane potential during the action potential plateau will exert a negative inotropic effect on twitch force. If the average level of potential during the plateau is reduced from 0 mV to about -10 mV, which we have indicated is not untypical for severely hypertrophic myocardium, the force of contraction would be expected to be reduced by about 15% from normal just by virtue of the depolarization and the function defining the relationship between twitch force and membrane potential. The reduction of twitch force by 15%, however, is predicted making the assumption that hypertrophy does not affect the voltage–tension relationship. This assumption may not be valid. Recently, Ten Eick et al. [54] have defined the voltage–tension relationships of papillary muscles from both normal and hypertrophic right ventricles of cat (see fig. 25–1). They found that in the voltage range of the plateau the position of the voltage–tension curve for hypertrophic heart is about 10 mV positive to that of the curve for normal heart. The voltage threshold for tension development is not much changed by hypertrophy, but the maximal tension in hypertrophic myocardium occurs when membrane potential is about $+30$ mV. This shift of 10 mV in the voltage–tension relationship means that, even if the plateau voltage were unchanged by hypertrophy, twitch force

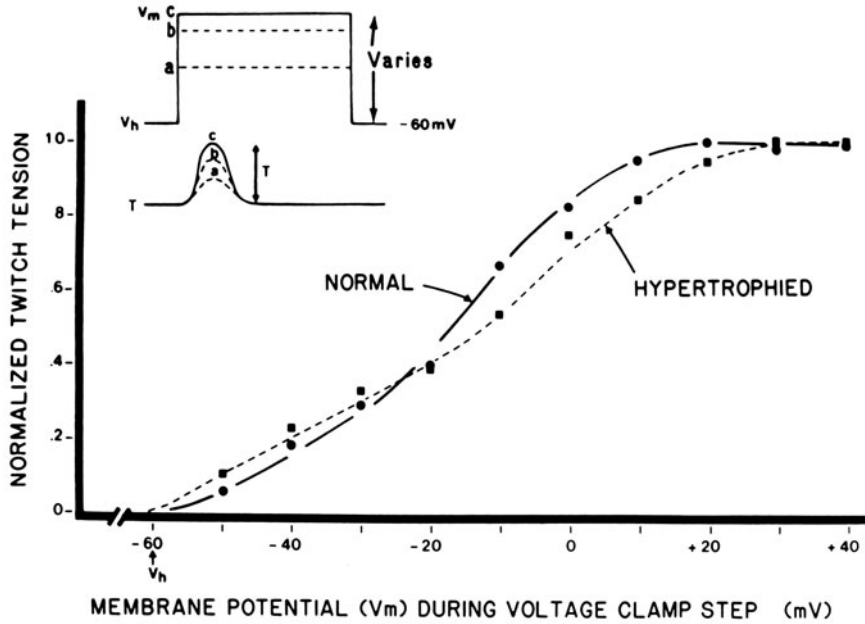

FIGURE 25–1. Normalized functions defining the voltage dependence of the peak tension developed during the twitch (ordinate, normalized to the maximally obtained tension) evoked during voltage clamp to selected levels of membrane potential (V_m) (abscissa, in mV). The inset depicts the family of voltage clamps to the selected levels of V_m and the grading of the twitches evoked by the voltage clamps. Notice the shift toward more positive potentials in the maximum of the RVH curve without apparent change in the voltage threshold for tension development. Modified from Ten Eick et al. [54].

would be reduced by about 15%. Add to the 15% reduction in twitch force due to the shift in the voltage–tension relationship the 15% reduction due to the loss of plateau voltage, and the loss of twitch force due to hypertrophy-induced electrophysiologic changes now accounts for a sizable, functionally significant decrease in myocardial contractility.

Consideration of the relationship between twitch force and the duration of the action potential plateau suggests that the prolongation of the action potential duration and the reduction in the repolarization rate attending the reduction in outward repolarizing current found in hypertrophic myocardium are compensations which ensure that the action potential plateau will activate the excitation–contraction process as completely as is possible for the level of potential achieved by the hypertrophy-inhibited plateau. Given the reduction in the slow inward current, it is fortunate that the repolarizing outward current is also reduced because, if it were not, the plateau in hypertrophied myocardium would be rather abbreviated and even greater loss of twitch force would occur.

The mechanism underlying the 10-mV positive shift in the voltage–tension curve is not understood. However, it does not seem to result from any shift in the voltage dependence of the slow inward current because the normalized show-inward-current–voltage curve obtained for hypertrophic muscle was found to be coincident with that for normal muscle [54]. Curiously, the direction and extent of the shifts in the voltage dependence of the time-dependent delayed rectifier potassium current and in the voltage–tension relationship seem to be nearly identical [54]. This suggests that the shifts could have a common underlying basis.

Let us suppose that the primary effect of hypertrophy is to reduce the density of the slow inward current. This could be the result of (a) a reduction in the number of conducting slow channels per cell or per unit area of sarcolem-

mal membrane (i.e., the same number of channels has to serve a larger membrane area in hypertrophied cells), or (b) hypertrophic-induced change in the probability that slow channels will conduct under a particular set of conditions, or both. The reduction in slow-inward-current density would be expected to cause the amount of activator Ca^{2+} released from the sarcoplasmic reticulum (SR) to be less than normal. There are two reasons for believing this. First, the transsarcolemmal slow-inward-current density is less and, second, because of the cellular hypertrophy and the attendant proliferation of T-tubular membrane, the slow-current density and related ohmic voltage drop available to trigger release of activator Ca^{2+} from the SR are expected to be reduced. It would be the second expectation that would underlie the reduction in Ca^{2+}-dependent components of the delayed outward-rectifying current and of the potassium-carried component of the inward-rectifying instantaneous background current. The shift in the voltage dependence of the time-dependent potassium current and in the voltage–tension relationship would, therefore, occur because a greater voltage drop across the surface membrane of the hypertrophic cell would be required to provoke a maximal Ca^{2+} release by the more remote SR. The upshot would be that the voltage or current signal supplied by the excitatory process (i.e., the action potential) in hypertrophic muscle, even if it were normal in amplitude, would be "perceived" by the SR as being less than normal and a smaller-than-normal fraction of the readily releasable pool of SR Ca^{2+} would be released to affect activation of the contractile proteins.

Conclusion

Ten Eick et al. [54] have argued that slow inward current is reduced and the voltage–tension relationship is shifted, but what might this mean to cardiac function? Do these changes affect the operation of the in vivo heart in situ with its sympathetic innervation intact? It is well known that contractility of the normal heart can be modulated by the level of sympathetic nervous activity playing on the myocardium. It is also well known that the slow inward current can be enhanced by norepinephrine and other β-receptor agonists. Therefore one might wonder whether it matters that hypertrophy inhibits the slow current when it can be greatly enhanced by catecholamines in the intact in situ heart. The answer is not clear and may be parodoxical. It is well known that in Meerson's stage 3 of hypertrophy the in situ myocardium can be moderately to severely depleted of its intrinsic catecholamines. In addition, hypertrophic myocardium has been found to have, relative to normal heart, a reduced number of β receptors [119–121]. This situation is quite different from that found in hearts depleted of catecholamines by chronic sympathectomy. Denervated hearts have an increased number of β receptors and are supersensitive to the effects of catecholamines on both electrical and mechanical activity. Hypertrophied cat heart, on the other hand, may be subsensitive to catecholamines as judged by their effects on the twitch and on slow inward current [104] (Ten Eick, unpublished observations). Subsensitivity probably reflects the decrease in the number of β receptors since receptor ligand binding affinity is either unchanged [120] or increased [121]. From this discussion it appears that the effectiveness of the extrinsic neurally mediated compensatory mechanisms to modulate cardiac function may be blunted in the hypertrophic heart. However, because the effects of the catecholamines on the slow inward current seem intimately related to their effects on the cellular level of cyclic AMP, this question will not be resolved until more complete information is available on the effect of hypertrophy on the coupling mechanisms between β-receptor activation and cyclic-AMP generation and metabolism, between cyclic-AMP level and slow current enhancement, and between slow current and the release of activator calcium. The possible effects on impulse conduction of the hypertrophy-induced reduction in slow current must also be considered because a well-coordinated electrical beat is required if the heart is to deliver a well-coordinated contraction. A fully developed discussion of this facet of cardiac function during hypertrophy is outside the

scope of this chapter. Nevertheless the reader should keep this point in mind as it too has important bearing on hemodynamic function of the hypertrophied and failing heart.

Whatever the mechanism or mechanisms underlying the changes in contractility and in the electrophysiologic function of hypertrophic heart muscle, and irrespective of whether the mechanism or mechanisms are common to both types of changes, it is clear that any attempt to account for the loss of contractility associated with cardiac hypertrophy must include contributions from the effects of the loss of plateau voltage and the shift in the voltage–tension relationship on contractile force. That is to say, the effect of altered cellular electrophysiologic function on contractility must be considered in any accounting which attempts to explain the reduced contractility associated with hypertrophy, at least in the cat model with a long-term pressure-overloaded right ventricle. This concept remains to be established in humans.

References

1. Scheuer J, Tipton CM: Cardiovascular adaptation to physical training. Annu Rev Physiol 39:221–251, 1977.
2. Muntz KH, Gonyea WJ, Mitchell JH: Cardiac hypertrophy in response to an isometric training program in the cat. Circ Res 49:1092–1101, 1981.
3. Meerson FZ: The myocardium in hyperfunction, hypertrophy and heart failure. Circ Res (Suppl 2) 25:1–163, 1969.
4. Wikman-Coffelt J, Parmley WW, Mason DJ: The cardiac hypertrophy process: analyses of factors determining pathological vs physiological development. Circ Res 45:697–707, 1979.
5. Rabinowitz M, Zak R: Mitochondria and cardiac hypertrophy. Circ Res 36:367–376, 1976.
6. Zak R, Rabinowitz M: Molecular aspects of cardiac hypertrophy. Annu Rev Physiol 41:539–552, 1969.
7. Leyton RA, Sonnenblick EH: Ultrastructure of the failing heart. Am J Med Sci 258:304–327, 1969.
8. Bishop SP, Cole CR: Ultrastructural changes in the canine myocardium with right ventricular hypertrophy and congestive heart failure. Lab Invest 20:219–229, 1969.
9. Lin HL, Katele KV, Grimm AF: Functional morphology of the pressure- and the volume-hypertrophied rat heart. Circ Res 41:830–836, 1977.
10. Kawamura K, Konishi T: Symposium on function and structure of cardiac muscle. 1. Ultrastructure of the cell junction of heart muscle with special reference to its functional significance in excitation, conduction and to the concept of "disease of intercalated disc". Jpn Circ J 31:1533–1543, 1967.
11. Sekiguchi M: Electron microscopical observation of the myocardium in patients with idiopathic cardiomyopathy using endomyocardial biopsy. J Mol Cell Cardiol 6:111–122, 1974.
12. Kawamura K, James TN: Comparative ultrastructure of cellular junctions in working myocardium and the conduction system under normal and pathologic conditions. J Mol Cell Cardiol 3:31–60, 1971.
13. Page E, McCallister LP: Quantitative electron microscopic description of heart muscle cells. Am J Cardiol 31:172–181, 1973.
14. Meessen H: Ultrastructure of the myocardium: its significance in myocardial disease. Am J Cardiol 22:319–327, 1968.
15. Wendt-Gallitelli MF, Jacob R: Time course of electron microscopic alterations in the hypertrophied myocardium of Goldblatt rats. Basic Res Cardiol 72:209–213, 1977.
16. Goldstein MA, Sordahl LA, Schwartz A: Ultrastructural analysis of left ventricular hypertrophy in rabbits. J Mol Cell Cardiol 6:265–273, 1974.
17. Aronson RS: Characteristics of action potentials of hypertrophied myocardium from rats with renal hypertension. Circ Res 47:443–454, 1980.
18. Tomanek RJ, Banister EW: Myocardial ultrastructure after acute exercise stress with special reference to transverse tubules and intercalated discs. Cardiovasc Res 6:671–679, 1972.
19. Horwood DM, Beznak M: Fluid and electrolyte shifts relating cardiac hypertrophy with normal growth. Can J Physiol Pharmacol 49:951–958, 1971.
20. Anversa P, Loud AV, Giacomelli F, Wiener J: Absolute morphometric study of myocardial hypertrophy in experimental tension. II. Ultrastructure of myocytes and interstitium. Lab Invest 38:597–609, 1978.
21. Weiner J, Giacomelli F, Loud AV, Anversa P: Morphometry of cardiac hypertrophy induced by experimental renal hypertension. Am J Cardiol 44:919–929, 1979.
22. Breisch EA, Houser SR, Carey RA, Spann JF, Bove AA: Myocardial blood flow and capillary density in chronic pressure overload of the feline left ventricle. Cardiovasc Res 14:469–475, 1980.
23. Cheitlin MD, Rabinowitz M, McAllister H, Hoffman JIE, Bharati S, Lev M: The distribution of fibrosis in the left ventricle in congenital aortic stenosis and coarctation of the aorta. Circulation 62:823–830, 1980.
24. Gulch RW: The effect of chronic loading on the action potential of mammalian myocardium. J Mol Cell Cardiol 12:415–420, 1980.
25. Rabinowitz M: Protein synthesis and turnover in normal and hypertrophied heart. Am J Cardiol 31:202–210, 1973.

26. Schreiber SS, Rothschild MA, Oratz M: Investigation into the causes of increased protein synthesis in acute hemodynamic overload. In: Rona G, Ito Y (eds) Recent advances in studies on cardiac structure and metabolism, vol 12. Baltimore: University Park Press, 1978, pp 49–60.
27. Sims JM, Patzer B, Kumudavalli-Reddy M, Martin AF, Rabinowitz M, Zak R: The pathways of protein synthesis and degradation in normal heart and during development and regression of cardiac hypertrophy. In: Rona G, Ito Y (eds) Recent advances in studies on cardiac structure and metabolism, vol 12. Baltimore: University Park Press, 1978, pp 19–28.
28. Ueda S, Nagai R, Yayahi Y: Synthesis and enzymatic properties of myosin from hypertrophied and failing hearts: difference in behavior of right and left ventricular free walls and interventricular septum. In: Advances in: Tajuddin M, Das PK, Tarig M, Dhalla NS (eds) Advances in myocardiology, vol 1. Baltimore: University Park Press, 1980, pp 523–533.
29. Scheuer J, Bahn AK: Adenosine triphosphatase activity and physiological function. Circ Res 45:1–12, 1979.
30. Mercadier JJ, Lompre AM, Wisnewski C, Samuel JL, Bercovici J, Swynghedauw B, Schwartz K: Myosin isoenzymatic changes in several models of rat cardiac hypertrophy. Circ Res 49:525–532, 1981.
31. Maughan D, Low E, Litten R III, Brayden J, Alpert N: Calcium activated muscle from hypertrophied rabbit hearts. Circ Res 44:279–287, 1979.
32. Alpert NR, Mulieri LA: Increased myothermal economy of isometric force generation in compensated cardiac hypertrophy induced by pulmonary artery constriction in the rabbit: a characterization of heat liberation in normal and hypertrophied right ventricular papillary muscles. Circ Res 50:491–500, 1982.
33. Zimmer HG, Ibel H, Steinkopff G: Studies on the hexose monophosphate shunt in the myocardium during development of hypertrophy. In: Tajuddin M, Das PK, Tarig M, Dhalla NS (eds) Advances in myocardiology vol 1. Baltimore: University Park Press, 1980, pp 487–492.
34. Bonnin CM, Sparrow MP, Taylor RR: Collagen synthesis and content in right ventricular hypertrophy in the dog. Am J Physiol 241:h708–h713, 1981.
35. Frederiksen DW, Hoffnung JM, Frederiksen RT, Williams RB: The structural proteins of normal and diseased human myocardium. Circ Res 42:459–466, 1978.
36. Yabe Y, Abe H: Change in DNA synthesis in significantly hypertrophied human cardiac muscle. Tajddin M, Das PK, Tarig M, Dhalla MS (eds) Advances in myocardiology, vol 1. Baltimore: University Park Press, 1980, pp 553–564.
37. Hatt PY, Berjal G, Moraver J, Swynghedauw B: Heart failure: an electron microscopic study of the left ventrical papillary muscle in aortic insufficiency in the rabbit. J Mol Cell Cardiol 1:235–247, 1970.
38. Hatt PY: Cellular changes and damage in mechanically overloaded hearts. In: Fleckenstein A, Rona G (eds) Recent advances in studies on cardiac structure and metabolism, vol 6. Baltimore: University Park Press, 1975, pp 325–334.
39. Spann JF, Buccino RA, Sonnenblick EH, Braunwald E: Contractile state of cardiac muscle obtained from cats with experimentally produced ventricular hypertrophy and heart failure. Circ Res 21:341–354, 1962.
40. Kaufman RL, Homburger H, Wirth H: Disorder in excitation–contraction coupling of cardiac muscle from cats with experimentally produced right ventricular hypertrophy. Circ Res 28:346–357, 1971.
41. Cooper G IV, Satavan M Jr, Harrison CE, Coleman HN III: Mechanisms for the abnormal energetics of the pressure induced hypertrophy of the cat myocardium. Circ Res 33:213–223, 1973.
42. Meerson FZ, Kapelko VI: The contractile function of the myocardium in two types of cardiac adaptation to a chronic load. Cardiology 57:183–199, 1972.
43. Williams JF Jr, Potter RD: Normal contractile state hypertrophied myocardium after pulmonary constriction in the cat. J Clin Invest 54:1266–1272, 1974.
44. Cooper G IV, Tomanek RJ, Ehrhardt JC, Marcus ML: Chronic progressive pressure overload of the cat right ventricle. Circ Res 48:488–497, 1981.
45. Natarajan G, Bove AA, Coulson RL, Carey RA, Spann JF: Increased passive stiffness of short term pressure overload hypertrophied myocardium in cat. Am J Physiol 237:H676–H680, 1979.
46. Williams JF Jr, Potter RD: Passive stiffness of pressure induced hypertrophied cat myocardium. Circ Res 49:211–215, 1981.
47. Spann JF, Covell JW, Eckberg DL, Sonnenblick EH, Ross J, Braunwald E: Contractile performance of the hypertrophied and chronically failing cat ventricle. Am J Physiol 223:1150–1157, 1972.
48. Gelband H, Bassett AL: Depressed transmembrane potentials during experimentally induced ventricular failure in cats. Circ Res 32:625–634, 1973.
49. Tritthart H, Leudcke H, Bayer R, Sterle H, Kauffmann R: Right ventricular hypertrophy in the cat: an electrophysiological and anatomical study. J Mol Cell Cardiol 7:163–174, 1975.
50. Bassett AL, Gelband H: Chronic partial occlusion of the pulmonary artery in cats: change in ventricular action potential configuration during early hypertrophy. Circ Res 32:15–26, 1973.
51. Bassett AL, Gelband H: Electrical and mechanical properties of cardiac muscle during chronic right ventricular pressure overload. In: Dhalla NS (ed) Myocardial biology. Recent advances in studies on cardiac structure and metabolism, vol 4. Baltimore: University Park Press, 1973, pp 3–20.

52. Ten Eick RE, Gelband H, Kahn J, Bassett AL: Changes in outward currents of papillary muscles of cats with right ventricle hypertrophy. Circulation 56:III-46, 1977.
53. Ten Eick RE, Bassett AL, Robertson LL: Severity of hypertrophy grades the changes induced in the myocardial action potential. Fed Proc, 1983 (1983).
54. Ten Eick RE, Bassett AL, Robertson LL: Possible electrophysiological basis for decreased contractility associated with myocardial hypertrophy in cat: a voltage clamp approach. In: Alpert N (ed) Perspectives in cardiovascular research, vol. 7: Myocardial hypertrophy and failure, New York, Raven Press, 1983, pp. 245–259.
55. Ten Eick RE, Gleband H, Goode M, Bassett AL: Increased inward rectifying potassium current in cat ventricle subjected to chronic pressure overload. Circulation 56:II-77, 1978.
56. Bassett AL, Gelband H, Nilsson K, Myerburg RJ: Localized transmembrane action potential abnormalities in right ventricles subjected to pressure overload. Circulation 47:II-47, 1977.
57. Aronson RS: Afterpotentials and triggered activity in hypertrophied myocardium from rats with renal hypertension. Circ Res 48:720–727, 1981.
58. Alpert NR, Hamrell BB, Halpern W: Mechanical or biochemical correlates of cardiac hypertrophy. Circ Res (Suppl 2) 34/35:71–82, 1974.
59. Hamrell BB, Alpert NR: The mechanical characteristics of hypertrophied rabbit cardiac muscle in the absence of congestive heart failure: the contractile and series elastic elements. Circ Res 40:20–25, 1977.
60. Konishi T: Electrophysiological study on the hypertrophied cardiac muscle experimentally produced in the rabbit. Jpn Circ J 29:491–503, 1965.
61. Sharp NA: Alterations in ventricular action potentials in pressure overload and thyrotoxic hypertrophy. In: Alpert N (ed) Perspectives in cardiovascular research, vol. 7: Myocardial hypertrophy and failure, New York, Raven Press, 1983, pp. 245–259.
62. Bassett AL, Myerburg RJ, Nilsson K, Sung RJ, Morales AR, Gelband H: Electrophysiologic consequences of experimental chronic left ventricular systolic hypertension. Circulation 4:II-7, 1978.
63. Gulch RW, Baumann R, Jacob R: Analysis of myocardial action potential in left ventricular hypertrophy of the Goldblatt rats. Basic Res Cardiol 74:69–82, 1979.
64. Gulch RW: Alterations in excitation of mammalian myocardium as a function of chronic loading and their implications in the mechanical events. Basic Res Cardiol 75:73–80, 1980.
65. Capasso JM, Strobeck JE, Sonnenblick EH: Myocardial mechanical alterations during gradual onset long term hypertension in rats. Am J Physiol 10:H435–H441, 1981.
66. Jacob R, Ebrecht G, Kammereit A, Medugorac L, Wendt-Gallitelli MF: Myocardial function in different models of cardiac hypertrophy: an attempt at correlating mechanical, biochemical and morphological parameters. Basic Res Cardiol 72:160–167, 1977.
67. Kammereit A, Jacob R: Alterations in rat myocardial mechanics under Goldblatt hypertension and experimental aortic stenosis. Basic Res Cardiol 74:389–405, 1979.
68. Wendt-Gallitelli MF, Ebrecht G, Jacob R: Morphological alterations and their functional interpretation in the hypertrophied myocardium of Goldblatt hypertensive rats. J Mole Cell Cardiol 11:275–287, 1979.
69. Bing OHL, Matsushita S, Fanburg BL, Levine HJ: Mechanical properties of rat cardiac muscle during experimental hypertrophy. Circ Res 28:234–245, 1971.
70. Jouannot P, Hatt PY: Rat myocardial mechanics during pressure induced hypertrophy development and reversal. Am J Physiol 299:355–364, 1975.
71. Bing OHL, Fanburg BL, Brooks WW, Matsushita S: The effect of the lathyrogen β-aminoproprionitrile (BAPN) on the mechanical properties of experimentally hypertrophied rat cardiac muscle. Circ Res 43:632–637, 1978.
72. Heller LJ: Augmented aftercontractions in papillary muscles from rats with cardiac hypertrophy. Am J Physiol 237:H649–H654, 1979.
73. Julian FJ, Morgan DL, Moss RL, Gonzalez M, Dwivedi P: Myocyte growth without physiological impairment in gradually induced rat cardiac hypertrophy. Circ Res 49:1300–1310, 1981.
74. Tibbits GF, Barnard RJ, Baldwin DM, Cugalj N, Roberts NK: Influence of exercise on excitation contraction coupling in rat myocardium. Am J Physiol 240:H472–H480, 1981.
75. Jacob R, Brenner B, Ebrecht G, Holubarsch C, Medugorac I: Elastic contractile properties of the myocardium in experimental cardiac hypertrophy of the rat: methodological and pathophysiological considerations. Basic Res Cardiol 75:253–261, 1980.
76. Holubarsch CH: Contractive type and fibrosis type of decreased myocardial distensibility: different changes in elasticity of myocardium in hypertension and hypertrophy. Basic Res Cardiol 75:244–252, 1980.
77. Hayashi H, Shibata S: Electrical properties of cardiac cell membrane of spontaneously hypertensive rat. Eur J Pharmacol 27:355–359, 1974.
78. Heller LJ: Cardiac muscle mechanics from doca- and aging spontaneously hypertensive rats. Am J Physiol 235:H82–H86, 1978.
79. Heller LJ, Stauffer EK: Altered electrical and contractile properties of hypertrophied cardiac muscles. Fed Proc 38:975, 1979.
80. Ferrier GR, Moe GK: Effect of calcium on acetylstrophanthidin-induced transient depolarizations in

canine Purkinje tissue. Circ Res 33:508–515, 1973.
81. Ferrier GR, Saunders JH, Mendez C: A cellular mechanism for the generation of ventricular arrhythmias by acetylstrophanthidin. Circ Res 32: 600–609, 1973.
82. Keung ECH, Aronson RS: Non-uniform electrophysiological properties and electrotonic interaction in hypertrophied rat myocardium. Circ Res 49: 150–158, 1981.
83. Keung ECH, Aronson RS: Transmembrane action potentials and the electrocardiogram in rats with renal hypertension. Cardiovasc Res 15:611–614, 1981.
84. Coltart DJ, Meldrum SJ: Hypertrophic cardiomyopathy: an electrophysiological study. Br Med J 4:217–218, 1970.
85. Singer DH, Baumgarten CM, Ten Eick RE: Cellular electrophysiology of ventricular and other dysrhythmias: studies on diseased and ischemic heart. Prog Cardiovasc Dis 24:97–156, 1981.
86. Ten Eick RE, Baumgarten CM, Singer DH: Ventricular dysrhythmias: membrane basis, or, of currents, channels, gates and cables. Prog Cardiovasc Dis 24:157–188, 1981.
87. Brorson L, Conradson TB, Olsson B, Varnauskas E: Right atrial monophasic action potential and effective refractory periods in relation to physical training and maximum heart rate. Cardiovasc Res 10:160–168, 1976.
88. Bishop SP, Melsen LR: Myocardial necrosis, fibrosis and DNA synthesis in experimental cardiac hypertrophy induced by sudden pressure overload. Circ Res 39:238–245, 1976.
89. Cutilletta AF, Benjamin M, Culpepper WS, Oparil S: Myocardial hypertrophy and ventricular performance in the absence of hypertension in spontaneously hypertensive rats. J Mol Cell Cardiol 10:689–703, 1978.
90. Tomanek RJ, Davis JW, Anderson SC: The effects of alpha-methyldopa on cardiac hypertrophy in spontaneously hypertensive rats: ultrastructural, stereological and morphometric analysis. Cardiovasc Res 13:173–182, 1979.
91. Dunn FG, Pfeffer MA, Frohlich ED: ECG alterations with progressive left ventricular hypertrophy in spontaneous hypertension. Clin Exp Hypertens 1:67–86, 1978.
92. Mazzoleni A, Curtin ME, Wolfe R, Reiner L: On the relationship between heart weights, fibrosis, and QRS duration. J Electrocardiol 8:233–236, 1975.
93. Kavaler F: Membrane depolarization as a cause of tension development in mammalian ventricular muscle. Am J Physiol 196:968–970, 1959.
94. Morad M, Trautwein W: The effect of the duration of the action potential on contraction in the mammalian heart muscle. Pflugers Archiv 299:66–82, 1968.
95. Wood EH, Hoppner RL, Weidmann S: Inotropic effects of electrical currents. I. Positive and negative of constant electrical currents or current pulses applied during cardiac action potentials. II. Hypotheses: calcium movements, excitation contraction coupling and inotropic effects. Cir Res 24:409–445, 1969.
96. Beeler GW Jr, Reuter H: Relation between membrane potential, membrane current and activation of contraction in ventricular myocardial fibers. J Physiol 207:211–229, 1970.
97. Leoty C: Membrane currents and activation of contraction in rat ventricular fibers. J Physiol 239:237–249, 1974.
98. Lab MJ: Mechanically dependent changes in action potentials recorded from the intact frog ventricle. Circ Res 42:519–528, 1978.
99. Spotnitz HM, Sonnenblick EH: Structural conditions in the hypertrophied and failing heart. Am J Cardiol 32:398–406, 1973.
100. Morady F, Laks MM, Parmley WW: Comparison of sarcomere lengths from normal and hypertrophied inner and middle canine right ventricle. Am J Physiol 225:1257–1259, 1973.
101. Legato MJ: Cellular mechanisms of normal growth in the mammalian heart. II. A quantitative and qualitative comparison between the right and left ventricular myocytes in the dog from birth to five months of age. Circ Res 44:263–279, 1979.
102. Bonnin CM, Sparrow MP, Taylor RR: Collagen synthesis and content in right ventricular hypertrophy in the dog. Am J Physiol 241:H708–H713, 1981.
103. Medugorac I: Characteristics of the hypertrophied left ventricular myocardium in Goldblatt rats. Basic Res Cardiol 72:261–267, 1977.
104. Hemwall EL, Houser SR: Alterations of slow response action potentials in right ventricular hypertrophy. Circulation 66:II-77, 1982.
105. McDonald TF, Trautwein W: Membrane currents in cat myocardium: separation of inward and outward components. J Physiol 274:193–216, 1978.
106. Martin FG, Houser SR, Marino TA, Freeman AR: Comparison of normal and failing cardiac muscles: the drive related changes in extracellular potassium activity. Biophys J 37:24, 1982.
107. Moulder PV, Eichelberger L, Daily PO: Segmental water and electrolyte distribution in canine hearts with right ventricular hypertrophy. Fed Proc 26:382, 1967.
108. Nachev P: The effect of aortic coarctation on the concentration of water and electrolytes in cardiac muscle. Proc Soc Exp Biol Med 147:137–139, 1974.
109. Brutsaert DL, De Clerk NM, Gothals MA, Housmans PR: Relaxation of ventricular cardiac muscle. J Physiol 203:469–480, 1978.
110. Le Carpentier Y, Martin JL, Gastineau P, Hatt PY: Load dependence of mammalian heart relaxation

during cardiac hypertrophy and heart failure. Am J Physiol 242:H855–H861, 1982.
111. Cooper G IV, Satava RM, Harrison CE, Coleman HN III: Normal myocardial function and energetics after reversing pressure overload hypertrophy. Am J Physiol 226:1158–1165, 1974.
112. Coulson RL, Yazdanfar S, Rubio E, Bove AA, Lemole GM, Spann JF: Recuperative potential of cardiac muscle following relief of pressure overload hypertrophy and right ventricular failure in the cat. Circ Res 40:41–49, 1977.
113. Marcus ML, Eckberg DL, Braxmeier JL, Abboud FM: Effects of intermittent pressure loading on the development on ventricular hypertrophy in the cat. Circ Res 40:484–488, 1977.
114. Capasso JM, Strobeck JE, Malhotra A, Scheuer J, Sonnenblick EH: Contractile behavior of rat myocardium after reversal of hypertensive hypertrophy. Am J Physiol 242:H882–H889, 1982.
115. Cutilletta AF, Dowell RT, Rudnik M, Arcilla RA, Zak R: Regression of myocardial hypertrophy. I. Experimental model, changes in heart weight, nucleic acids and collagens. J Mol Cell Cardiol 7:767–781, 1975.
116. Gibbons WR, Fozard HA: Voltage dependence and time dependence of contraction in sheep cardiac Purkinje fibers. Circ Res 28:446–460, 1971.
117. Gibbons WR, Fozzard HA: Relationships between voltage and tension in sheep cardiac Purkinje fibers. J Gen Physiol 63:345–366, 1975.
118. Trautwein W, McDonald TF, Tripathi O: Calcium conductance and tension in mammalian ventricular muscle. Pflugers Archiv 354:55–74, 1976.
119. Limas C, Limas CJ: Reduced number of β-adrenergic receptors in the myocardium of spontaneously hypertensive rats. Biochem Biophys Res Commun 83:710–714, 1978.
120. Woodcock EA, Funder JW, Johnston CI: Decreased cardiac β-adrenergic receptors in deoxycorticosterone-salt and renal hypertensive rats. Circ Res 45:560–565, 1979.
121. Cervoni P, Herzlinger H, Lai FM, Tanikella T: A comparison of cardiac reactivity and β-adrenoceptor number and affinity between aorta-coarcted hypertensive and normotensive rats. Br J Pharmacol 74:517–523, 1981.

26. DEVELOPMENTAL CHANGES IN MEMBRANE ELECTRICAL PROPERTIES OF THE HEART

Nicholas Sperelakis

Introduction

Important physiologic, electrophysiologic, pharmacologic, biochemical, and ultrastructural changes occur during the embryonic development of avian and mammalian hearts. For example, striking changes occur in the electrical properties of ventricular myocardial cells during embryonic development of chick heart. In many mammalian hearts, some of the changes extend into the early postnatal period. These changes affect and determine the functional behavior and properties of the heart at each stage of development and differentiation. Therefore, it is the purpose of this chapter to review and summarize many of these changes in properties. The attention of the reader will be called to a number of recent review articles that summarize these properties, as well as go into greater detail.

Studies of the electrophysiologic properties of embryonic heart cells are useful, not only to elucidate the changes during differentiation, but also to obtain clues for understanding the complex electrophysiology of adult hearts. Most of the data presented are for the chick, although some data are presented for developing mammalian hearts. Some findings on organ-cultured hearts and cultured heart cells will be presented for comparison. Since the electrical properties may be affected by morphologic and biochemical properties, relevant changes in these properties are also discussed.

The work of the author summarized and reviewed in this chapter was supported by grants from the National Institutes of Health (HL-18711). The author wishes to acknowledge the collaborative efforts with his colleagues, particularly Drs. K. Shigenobu, M.J. McLean, J.-F. Renaud, and I. Josephson.

N. Sperelakis (ed.), PHYSIOLOGY AND PATHOPHYSIOLOGY OF THE HEART.

Martinus Nijhoff Publishing, Boston/The Hague/ Dordrecht/Lancaster.

Intact Hearts Developing In Situ

PRECARDIAC AREAS OF THE BLASTODERM

The early embryo (up to 1 somite) possesses cells which are destined to form the heart. These cells migrate through the early embryo and congregate bilaterally into the so-called precardiac areas (mesoderm) of the anterior half of the flattened 16- to 17-h (head process) blastoderm [1].

Explants of the blastodermal and precardiac areas, after several days in culture, develop spontaneous action potentials (APs) of about 50-mV amplitude [2]. In culture, a tubular heart develops within a vesicle and it beats spontaneously for several days, but further differentiation does not proceed in vitro. The precardiac area can be treated with trypsin to facilitate mechanical separation of the three germ layers, and culture of the precardiac mesoderm gives rise to a solid mass of cells which fire spontaneous APs and contract [3]. If the postnodal piece (posterior third of blastoderm) is dissected from the 19-h chick blastoderm and placed into culture, it does not normally give rise to heart tissue. If, however, the postnodal piece is cultured in the presence of an RNA-enriched fraction obtained from adult chicken

hearts, a typical spontaneously-beating tubular heart forms within a vesicle, as in the case of the precardiac areas described above [4]. The beating cells in the induced hearts were shown to possess some myofilaments. In addition, the induced tubular hearts exhibit spontaneous APs [5]. Thus, it appears that either RNA or some other material within the extract obtained from the adult heart can induce cells in the postnodal piece, normally not destined to form the heart, to take on many of the properties of cardiac myoblasts.

Subsequently in development in situ, twin tubular primordia form bilaterally from the precardiac mesoderm, and they fuse to form a single tubular heart. This fusion begins from the head end and proceeds posteriorly by a zipper-like process, such that the first region fused (ventricle) begins contracting first; the atria are added posteriorly later. The tubular heart begins contracting spontaneously at 30–40 h (9–19 somite state). Cutting the two-day heart into bulbus, ventricle and sinoatrium regions shows that each region has a characteristic automaticity, the sinoatrium region being the fastest.

The tubular heart begins to propel blood shortly after it starts to beat. The blood pressure is very low (1–2 mmHg) at this stage, and it increases progressively during embryonic development (approximately 30 mmHg by day 18) and during postembryonic life [6, 7]. The velocity of propagation of the peristaltic contraction wave in three-day hearts is approximately 1 cm/s [7].

The heart rate of the chick embryo increases from about 50 beats/min at day 1.5 to the maximal value of about 220 beats/min by day 8; it has been suggested that the increase in beating rate may result from the concomitant rise in blood pressure [7]. The influence of temperature on heart rate decreases markedly during development [7]. The Q_{10} decreases from about 3.6 on day 3 to about 2.0 on day 18 for the same temperature range [8]. Breaks in the Arrhenius plots (of spontaneous heart rate vs temperature) also occur at different temperatures in young hearts compared to old hearts.

RESTING MEMBRANE AND K^+ PERMEABILITY

Resting Potentials. The resting potential (E_m), measured by intracellular microelectrodes, of the ventricular portion of the chick and rat hearts increases during embryonic development [9–15]. In embryonic chick heart (table 26–1), the greatest changes occur between days 2 and 7, and thereafter the increase is smaller. For example, in a two-day-old heart, the mean resting E_m is about -40 mV, and this increases to about -51 mV on day 3. The resting potential is close to -80 mV by day 12, nearly the final adult value. As discussed below, the large increase in resting E_m during the first few days may be due mainly to an increase in K^+ permeability (P_K) and not in K^+ equilibrium potential (E_K) (or $[K]_i$). However, some investigators [2] have reported larger values of resting E_m for young hearts, i.e., less of a change during development, and attributed low recorded potentials in young hearts to current leakage around the electrode tip due to improper sealing of the microelectrode (this effect would be most prominent in cells having a high input resistance).

Resting Potential vs log $[K]_0$ Curves. The relationship between resting E_m and external K^+ concentration ($[K]_0$) was determined for embryonic hearts of different ages [14, 16]. Data for three-day, five-day, and 15-day-old embryonic chick hearts are shown in figure 26–1. $[K]_i$ was estimated by extrapolation of the curves to zero potential, and the values varied between 125 m*M* (for two-day hearts) and 155 m*M* (for 14- to 20-day hearts) (table 26–1). Also plotted in figure 26–1 are the theoretical curves (calculated from the Goldman constant-field equation given in the inset) for five different ratios of P_{Na}/P_K: 0.001, 0.01, 0.05, 0.1, and 0.2. As indicated in the figure, it was assumed that $[Na]_i$ was 30 m*M* and $[K]_i$ was 150 m*M* for these calculations. The data points for the three-day hearts most closely fit the theoretical curve for a P_{Na}/P_K ratio of 0.2; those for the five-day hearts fit the curve for a P_{Na}/P_K of 0.1, and those for the 15-day hearts most closely fit between the 0.05 and 0.01 curves. These data

TABLE 26–1. Summary of data obtained from E_m vs log $[K]_0$ curves and from input resistance (r_{in}) measurements for chick embryonic hearts (ventricular cells) at various stages of development

Embryonic age (days)	E_m (mV)	Slope (mV/decade)	Extrapolated $[K]_i$ (m*M*)	E_K (mV)	P_{Na}/P_K ratio	r_{in} (mΩ)
2	−40	30	125	−100	0.21	13.0
3	−51	40	130	−101	0.17	8.5
4	−57	46	140	−103	0.08	6.5
5–6	−58	50	130	−101	0.08	5.5
7–9	−71	51	145	−104	0.07	5.5
11–13	−80	53	145	−104	0.07	4.7
14–20	−78	52	155	−106	0.05	4.5

The resting potential (E_m) values are given for a $[K]_0$ of 2.7 m*M*. The slope is the average at $[K]_0$ levels between 10 and 100 m*M*. $[K]_i$ was estimated from the extrapolation of fitted curves to zero potential. The P_{Na}/P_K ratios were calculated from the Goldman constant-field equation at every $[K]_0$ level for which E_m was measured, and an average value was calculated for each heart; some individual values for hearts in the 14- to 20-day age group were as low as 0.02. Data were taken from Sperelakis and Shigenobu [13], and Sperelakis et al. [49]. Similar values for slope and $[K]_i$ were obtained by Pappano [17] for embryonic chick atrium at four days, six days, and 12 days; the 18-day values were −59 mV/decade and 125 m*M* $[K]_i$, respectively.

suggest that the P_{Na}/P_K ratio is very high in young hearts, and that this accounts for the low measured resting E_m. That is, the low resting E_m is not due to a greatly lower $[K]_i$ and E_K. As shown in table 26–1, only a very small increase in the calculated E_K occurs during development: from about −100 mV on day 2 to −106 mV on days 14–20. Thus, in the young hearts, the resting E_m is far from E_K due to the high P_{Na}/P_K ratio. In this respect, the myocardial cells in young embryonic hearts resemble sinoatrial (SA) nodal cells in adult hearts.

In old embryonic chick or adult hearts, the E_m vs log $[K]_0$ curve is nearly linear above 10 m*M* K^+, with a slope approaching the theoretical 61 mV/decade (from the Nernst equation). If the slope were exactly 61 mV/decade, then E_m would be equal to E_K, and the membrane would be completely K^+ selective in high $[K]_0$. The data in figure 26–1 and table 26–1 show that the slope for hearts 7–20 days old is 51–53 mV/decade, whereas the average slopes (curves continually bend) for four-day, three-day, and two-day hearts are 46, 40, and 30 mV/decade, respectively. Similar values for $[K]_i$ and slope were found for embryonic chick atrial cells at various stages of development [17].

Membrane Resistance. In order to ascertain whether the P_{Na}/P_K ratio is high in young embryonic chick hearts because of high Na^+ permeability or because of a low K^+ permeability, input resistance (r_{in}) was determined from steady-state voltage–current curves. The r_{in} of the ventricular cells is high (13 MΩ) in young two-day-old hearts, and rapidly declines over the next few days, reaching the final adult value of about 4.5 MΩ by day 14 (table 26–1). If the average cell size and the degree of electrical coupling between the cells remains unchanged during this period, the high r_{in} of the young hearts would suggest that membrane resistivity (R_m) is very high. The latter would be consistent with a low K^+ conductance and K^+ permeability in the young hearts. These results suggest that the P_{Na}/P_K ratio is high in young hearts because P_K is low, and not because P_{Na} is high.

Consistent with the interpretation that P_K is low in hearts is the finding that the chronaxie of young hearts (two-day-old) is about fourfold higher than that of nine- to 16-day hearts [9]. This indicates that the membrane time constant is about fourfold higher in young hearts and, if membrane capacitance remains constant, membrane resistivity must be fourfold higher.

Carmeliet et al. [18] have reported, on the basis of ^{42}K flux measurements, that P_K is about two- to threefold lower in six- to eight-day hearts than in 18- to 20-day hearts, consistent with the conclusions from the electrical studies described above. (Although they re-

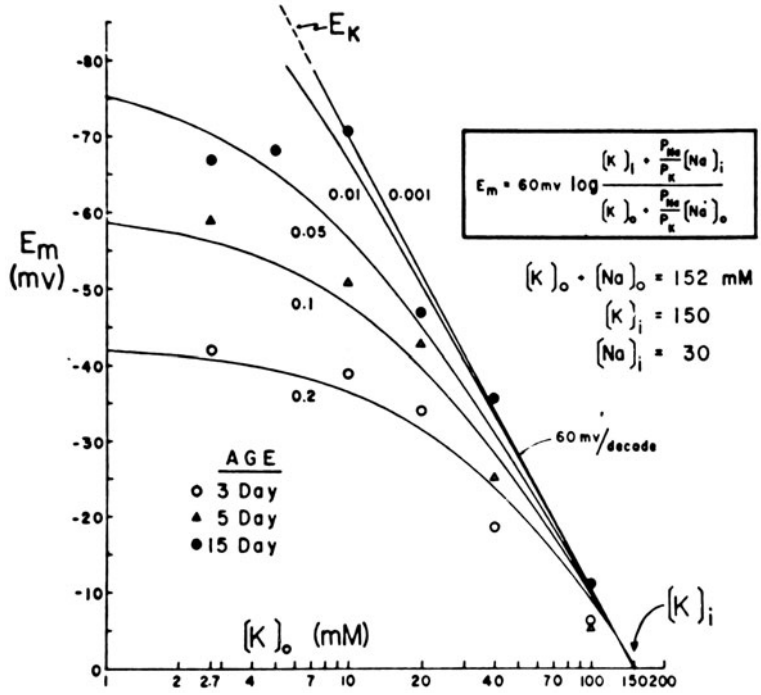

FIGURE 26–1. Resting potential (E_m) plotted as a function of $[K]_o$ on a logarithmic scale for representative hearts of three different ages. $[K]_o$ was elevated by substitution of K^+ for equimolar amounts of Na^+. Continuous lines give theoretical calculations from the constant-field equation (inset) for P_{Na}/P_K ratios of 0.001, 0.01, 0.05, 0.1, and 0.2. Calculations were made assuming $[K]_i$ and $[Na]_i$ values shown. For a P_{Na}/P_K ratio of 0.001, the curve is linear over the entire range with a slope of 60 mV/decade, i.e., it closely follows E_K. Symbols give representative data obtained from embryonic chick hearts at days 3 (0), 5 (▲), and 19 (●). The data for the three-day heart follow the curve for a P_{Na}/P_K ratio of 0.2, those for the five-day heart follow the curve for 0.1, and those for the 15-day heart fall between the curves for 0.01 and 0.05. The estimated intracellular K^+ activities ($[K]_i$) obtained by extrapolation to zero potential are nearly the same for all ages. Taken from Sperelakis and Shigenobu [13].

ported that the calculated P_K for three- to five-day hearts was nearly as high as that for the 18- to 20-day hearts, which disagrees with the electrical measurements, they did not control for spontaneous beating and APs (hence increased K^+ efflux) which occurs in the three- to five-day hearts; this might cause them to calculate an erroneously high P_K.) The values for the P_K coefficients were 13.2×10^{-8} cm/s for seven-day hearts and about 27.5×10^{-8} cm/s for 19-day hearts (at a $[K]_0$ of 2.5–5.0 m*M*). P_K was greatly reduced in 0 m*M* $[K]_0$. The P_{Na}/P_K ratios calculated from the constant-field equation were 0.018 for the 19-day hearts and 0.037 for the seven-day hearts. The P_{Na} coefficient, as calculated from P_K and P_{Na}/P_K ratio, did not change during development (constant at about 0.50×10^{-8} cm/s).

Sensitivity to Elevated $[K]_0$. Since flattening of the resting potential vs log $[K]_0$ curve at lower $[K]_0$ levels is much more prominent for young hearts, i.e., they are depolarized less by a given increment in $[K]_0$ (see fig. 26–1), young hearts should be less affected by elevation of $[K]_0$. Young hearts are indeed less affected by elevation of $[K]_0$ than are older hearts [13, 19]. This is true for both inhibition of automaticity of the whole heart as well as for loss of excitability of the ventricle to electrical stimulation [13]. Automaticity and excitability of two- to three-day hearts fail at about 25 m*M* K^+,

whereas failure occurs at about 15 m*M* (automaticity) and 20 m*M* (excitability) for the 14- to 20-day hearts. Depression of automaticity was evident by 12 m*M* in hearts of all ages.

Lack of Effect of Acetylcholine on P_K. The young ventricular cells are not hyperpolarized by acetylcholine (ACh), even though a large hyperpolarization is theoretically possible because the resting E_m is much below E_K [13]. Therefore, it is likely that ACh does not significantly increase P_K in ventricular cells. In ventricular muscle of old embryonic chick, ACh has little or no effect on shortening the AP also, whereas the atrial AP is markedly shortened. The atrial cells of young hearts are slightly depolarized by ACh in normal medium, and slightly hyperpolarized in Na^+-free medium, suggesting that ACh increases both Na^+ conductance and K^+ conductance in young hearts [17, 20, 21]. Pappano [17] interpreted the small hyperpolarization produced by ACh in Na^+-free solution to be consistent with a low P_K, namely, that few K^+ channels are available to be opened by ACh.

(Na,K)-ATPase ACTIVITY

The specific activity of the (Na,K)-ATPase is low in young embryonic chick hearts and rises during development [22]. The average value on day 4 is about 35% of that on day 16 (7.4 ± 0.7 mol P_i/h/mg protein), that on day 6 is about 42%, that on day 9 is about 57%, and that on day 13 is about 77%. This enzyme activity is highest on day 20 (about 144% of that on day 16). The adult level is about equal to that on embryonic day 16.

Thus, while P_K is increasing during development, and hence the outward passive leak of K^+ and inward leak of Na^+ (due to the increased electrochemical driving force), the capability of the Na^+-K^+ pump is increasing correspondingly. That is, the increased cation pump capability tends to compensate for the increased demand on the pump due to increased cation leak. However, the pumping capacity of the very young hearts must be sufficient to maintain the relatively high $[K]_i$ and low $[Na]_i$ already present in the young cells.

When the ventricular myocardial cells from 16-day hearts are placed into monolayer cell culture, the specific activity of the (Na,K)-ATPase decreases by more than threefold [23]. The lower Na^+-K^+ pumping capability of the cultured cells is consistent with the lower K^+ permeability and somewhat lower $[K]_i$ generally observed in these cells [22].

ION CONTENT

Sodium. Tissue electrolyte analyses in chick embryonic hearts (ventricles) show that the total tissue content of Na^+ in young hearts is very high, and that it decreases gradually until about day 13, after which the level remains constant [10, 24]. Sodium ion exchangeability is low in young hearts and rises gradually during development to about 70% near hatching. Thus, there may be a great amount of bound Na^+ in young hearts, including in the nucleus [25] and in the extracellular (subendocardial) mucopolysaccharide cardiac jelly (which serves a valve-like function) [26]. The data from electrophysiologic studies [10, 13] indicated that the thermodynamically active free intracellular Na^+ concentration must not be extremely high because the Na^+-dependent APs already overshoot to +11 mV in day-2 hearts; the overshoot increases rapidly, reaching +28 mV by day 8; the latter value is the same as the adult value. McDonald and De Haan [14] reported that the Na^+ content of the chick heart did not change during development. Carmeliet et al. [18] measured $[Na]_i$ values of 16 m*M* and 15 m*M* for seven-day and 19-day embryonic chick hearts, respectively. Harsch and Green [27] reported that the $[Na]_i$ levels remained relatively constant (23–38 m*M*) between days 8 and 18. Thus, there seems little doubt that the free $[Na]_i$ is relatively low in young hearts.

Extracellular Space; Chloride. There is a decrease in extracellular space during development of embryonic chick heart. The inulin space was reported to decrease from 39% at day 8 to 19% at day 18 [27]. The extracellular space determined by radioactive chromium–EDTA decreased from 34% on days 6–8 to 27% on days 18–20 [18].

The estimates of intracellular Cl^- for days

8–18 were 36–45 m*M* [27]. These values are too high to be consistent with the measured resting potentials (of −70 to −80 mV) if Cl^- were passively distributed. There is hardly any compelling evidence for a Cl^- pump in myocardial cells (see Sperelakis [28]).

Potassium. The K^+ content of chick hearts was reported to gradually increase during development, from about 68 mmol/kg on days 2–3 to a plateau level of about 86 mmol/kg on day 13 [24]. However, it was reported that the calculated $[K]_i$ levels may actually decrease during development: from 145 m*M* on day 8 to 91 m*M* on day 18 [27]. Similarly, McDonald and De Haan [14] reported that $[K]_i$ changed from 167 m*M* on day 2 to 118 m*M* on days 14–18, and Carmeliet et al. [18] calculated $[K]_i$ values of 151 m*M* and 122 m*M* for chick hearts on days 6–8 and days 18–20, respectively. The electrophysiologic data from resting E_m vs log $[K]_0$ curves [13] indicate that $[K]_i$ is about 125 m*M* on day 2, and that it increases gradually to about 155 m*M* on days 14–20 (table 26–1). The calculated E_K increases from about −100 mV at day 2 to −106 mV at days 14–20 (table 26–1). Pappano [17] also reported high values of $[K]_i$ (145 m*M*) on day 4 for chick atrial cells. Thus, $[K]_i$ is already high in young hearts, and so the cardiac cells must actively transport cations before day 2.

ELECTROGENIC PUMP POTENTIAL

The energy-dependent pump located in the cell membrane, which maintains the ionic gradients for Na^+ and K^+ ions across the cell membrane, becomes electrogenic when the ratio of Na^+ ions pumped out to K^+ ions pumped in is greater than 1; that is, the pump directly produces a potential (V_{ep}) which contributes to the measured resting potential, usually by between 2 and 15 mV, depending on the type of cell and the physiologic conditions (see reviews by Thomas [29] and Sperelakis [28]). An electrogenic Na^+ pump potential has been demonstrated in various tissues of the heart [30–35].

Using flux studies, Lieberman et al. [36] found evidence for an electrogenic pump in cultured embryonic chick (11-day-old) myocardial cells. Pelleg et al. [37] observed an electrogenic pump potential of a few millivolts in cultured embryonic heart cell reaggregates derived from early (three-day-old) and late (16-day-old) stages of development that were subjected to overdrive stimulation. These studies indicate that electrogenic transport is present in early stages of ontogenesis, and that this ability is retained in vitro. If $[Na]_i$ is somewhat higher in young hearts and if the pump coupling ratio (Na/K) is a function of $[Na]_i$, V_{ep} might be expected to be higher in young hearts, especially in view of the higher membrane resistance, but there is no evidence for this. This lack of a larger V_{ep} might be partly explained on the basis of a lower density of pump sites in the young hearts.

POSTDRIVE HYPERPOLARIZATION AND OVERDRIVE SUPPRESSION OF AUTOMATICITY

When automatic heart cells are driven at a faster rate than their intrinsic rate, upon termination of the drive there is a transient pause followed by a gradual recovery to the predrive firing rate [32, 37]. This phenomenon of overdrive suppression of automaticity is caused by a small transient hyperpolarization of a few millivolts; this transient hyperpolarization is the cause of the suppression of the automaticity. Vassalle [32] presented evidence that the hyperpolarization was due to stimulation of an electrogenic Na^+ pump potential, presumably resulting from an increase in $[Na]_i$ and in $[K]_0$ during the drive. The high frequency of APs during the overdrive, with the accompanying increased Na^+ influx and K^+ efflux, initially overwhelm the Na-K pump capability, leading to elevation of $[Na]_i$ and $[K]_0$. This, in turn, stimulates the Na-K pump, and perhaps increases the Na/K coupling ratio of the pump, thus increasing V_{ep} and hyperpolarizing.

Overdrive suppression was observed in intact young three-day-old hearts (prior to innervation of the heart), and was attributed to the release of an ACh-like substance from within the heart cells [38]. However, it was recently demonstrated by Pelleg et al. [37] that cultured heart cells (ventricular and atrial), isolated from both young and old embryonic

chick hearts, which are automatic in vitro, exhibit the phenomena of postdrive hyperpolarization and overdrive suppression of automaticity that are blocked by ouabain but not by atropine. These findings support the view that stimulation of an electrogenic pump is the cause of this behavior. These results also indicate that young embryonic heart cells are capable of exhibiting electrogenic Na-K pumping.

AUTOMATICITY

Requirements for automaticity include: (a) a low Cl^- conductance (g_{Cl}), as is generally true for myocardial cells, and (b) a low K^+ conductance (g_K). A low g_K enhances membrane inductance in series with one type of K^+ channel (the inward-rectifying anomalous rectification channel having a negative slope conductance region), and tends to cause oscillations in E_m. The low g_K also is responsible for the low resting potential (moves the resting E_m farther from E_K) and places E_m in the region that can support pacemaker oscillations.

Pronounced changes in automaticity of the ventricular cells also occur during development, as could be predicted from the changes in P_K. The incidence of hyperpolarizing afterpotentials and pacemaker potentials is very high (80–100) in the young hearts, and this incidence decreases to 0% in the old embryonic hearts (table 26–2) [13]. If a portion of the ventricle is cut and isolated to remove drive from the nodal cells, the incidence of pacemaker potentials is 100% for embryos up through day 10, whereas the incidence is 0% in embryos day 12 or older (table 26–2 and fig. 26–2). These results indicate that the ventricular myocardial cells possess automaticity capability when they are young, but that this capability diminishes as the cells age.

TABLE 26–2. Incidence (%) of pacemaker potentials and hyperpolarizing afterpotentials found in ventricular myocardial cells during embryonic development of chick hearts

Embryonic age (days)	Hyperpolarizing afterpotentials	Pacemaker potentials	
	Intact hearts	Intact hearts	Cut ventricles
2–3	81	80–100	100
4	63	60–100	100
7	38	20–40	100
10	0	0	100
12	0	0	0
17	0	0	0
20	0	0	0
27	0	0	0

Cells which exhibit pacemaker potentials usually also possess hyperpolarizing afterpotentials, but the converse is not always true. Data taken from Sperelakis and Shigenobu [13], Sperelakis et al. [49], Sperelakis and McLean [131], and Sperelakis and McLean [132].

However, old ventricular cells again become automatic when trypsin dispersed and placed into monolayer cell culture. For example, ventricular myocardial cells dispersed from 16-day-old chick embryos and cultured as monolayers usually revert back toward the young embryonic state with respect to their electrical properties, including gain of automaticity [13]. When the cells are allowed to reaggregate into small spheres, however, they often retain their highly differentiated electrical properties, including lack of automaticity [39, 40]. Some reaggregates exhibit automaticity, even though the APs are relatively fast rising and tetrodotoxin (TTX) sensitive. The gain in automaticity of cultured cells appears to reflect a decrease in P_K [41–43]. In some cases, isolated single ventricular cells in culture have such a low P_K that they are depolarized too far and do not normally exhibit automaticity or excitability [44]. However, if these cells are hyperpolarized by intracellular application of current pulses, spontaneous APs and contractions occur [44].

It has been suggested that mechanical stretch of the wall of the tubular heart of the young chick embryo, by the gradual buildup of the blood volume and blood pressure, may play a role in the initiation of the heartbeat and in the gradual increase in the heart rate during development [45]. However, it is difficult to reconcile this view with other facts, such as (a) the demonstration that the precardiac tissue of the chick blastoderm can develop in vitro into spontaneously contracting heart-like tubes, vesicles, or cell clusters [2, 4, 5, 46, 47] with no evidence of an intraluminal buildup of pressure, and (b) the retention of automaticity of cultured isolated single heart cells or monolayers.

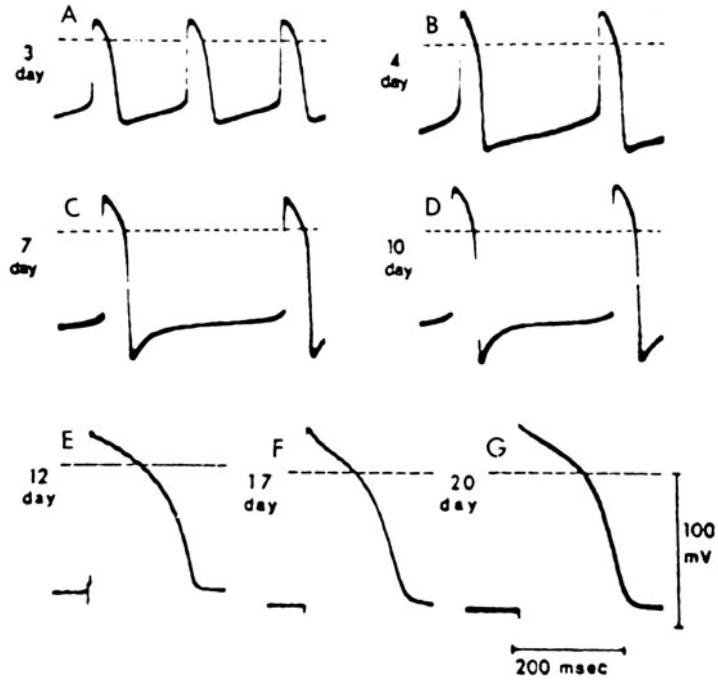

FIGURE 26–2. Electrophysiologic recordings from ventricular fragments cut from chick embryonic hearts of various ages. *(A–D)* Pacemaker potentials preceded the APs in impaled cells within fragments from hearts aged three, four, seven, and ten days. Maximal rate of rise and maximal diastolic potentials in the fragments were the same as in the intact heart. The fragments contracted spontaneously. *(E–G)* Cut ventricular fragments from hearts 12 days old and older did not exhibit automaticity. Action potentials with fast rates of rise (equal to those recorded from cells in the intact hearts of the respective ages) were elicited by field stimulation (shock artifacts visible) from fragments of 12-, 17-, and 20-day ventricles. Time calibration in *D* applied to *A–D* and that in *G* to *E–G*. Modified from Sperelakis et al. [49].

ACTION POTENTIAL CHANGES

Rate of Rise and Overshoot. The action potentials (APs) of the cells of intact chick hearts undergo sequential changes during development in situ [13, 48, 49], as shown in figure 26–3. There is a progressive increase in maximal rate of rise ($+\dot{V}_{max}$) (figs. 26–3 and 26–4) and overshoot of the AP (fig. 26–3), as well as an increase in resting potential. The overshoot averaged +11 mV on day 2, and increased progressively over the next few days, reaching the maximal value of about +28 mV by day 8. The duration (at 50% repolarization) was hardly changed during development, the average value being 110 ms. The time course of the increase in $+\dot{V}_{max}$ was not parallel to the increase in resting E_m, the increase in resting E_m preceding the increase in $+\dot{V}_{max}$ by several days; that is, in young hearts, it was not unusual to find a cell with a large resting potential but with a low $+\dot{V}_{max}$.

Young (2–3 days in ovo) myocardial cells possess slowly rising (10–40 V/s) (fig. 26–4) APs preceded by pacemaker potentials (fig. 26–3A). Hyperpolarization does not greatly increase the rate of rise (fig. 26–5), thus indicating that the low $+\dot{V}_{max}$ is not due to inactivation of fast Na^+ channels at the low resting potential, but rather to a low density of fast Na^+ channels. Excitability is not lost until the membrane is depolarized to less than −20 mV (fig. 26–5), thus indicating the preponderance of slow channels. The AP upstroke in young

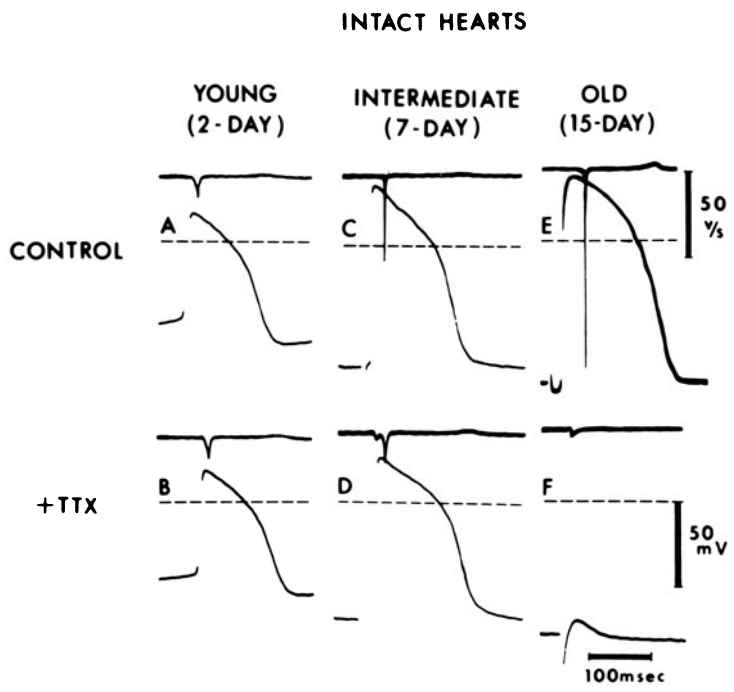

FIGURE 26–3. Characteristics of the action potentials in intact embryonic chick hearts at different stages of development. *(A–B)* Intracellular recordings from a two-day-old heart before *(A)* and 20 min after *(B)* the addition of tetrodotoxin (TTX) (20 μg/ml). *(C–D)* Recordings from a seven-day-old heart before *(C)* and 2 min after *(D)* the addition of TTX (2 μg/ml). Note depression of the rate of rise in *D*. *(E–F)* Records from a 15-day-old heart prior to *(E)* and 2 min after *(F)* the addition of TTX (1 μg/ml). The APs were abolished and excitability was not restored by strong field stimulation in *F*. Thus, the hearts became progressively more responsive to TTX during development, i.e., the effect of TTX increased with increasing embryonic age. The upper traces give dV/dt; this trace has been shifted relative to the V-*t* trace to prevent obscuring dV/dt. The horizontal broken line in each panel represents zero potential. dV/dt calibration (in *E*) and voltage and time calibrations (in *F*) pertain to all panels. Modified from Sperelakis and Shigenobu [13].

hearts is generated by Na^+ influx through (TTX-insensitive) slow Na^+ channels, as indicated by the dependence of the AP overshoot (fig. 26–6A) and rate of rise (fig. 26–6B) on the external Na^+ concentration. The slope of overshoot as a function of $[Na]_0$ approaches the theoretical 61 mV/decade from the Nernst equation at the lower $[Na]_0$ concentrations (fig. 26–6A).

Kinetically fast Na^+ channels are substantial in number by day 5. This is about the time that circulation is established to the chorioallanoic membrane for gas exchange. At this time, $+\dot{V}_{max}$ is about 50–70 V/s (fig 26–4 and table 26–3). During this intermediate stage of development (from about day 5 to 7), a large number of slow channels still coexist with the fast Na^+ channels in the membrane.

By day 8, depolarization to less than −50 mV abolishes excitability (fig. 26–5). This indicates that the AP-generating Na^+ channels now consist predominantly of fast Na^+ channels. The dependence of the inward current on $[Na]_0$ during the AP in old embryonic hearts is also shown in figure 26–6A and B. The density of fast Na^+ channels continues to increase until about day 18, when the adult maximal rate of rise of about 150 v/s is achieved (fig. 26–4). This conclusion has been strengthened by confirmatory observations reported by Iijima and Pappano [50] and Marcus and Fozzard [51]. A large fraction of the slow Na^+ channels

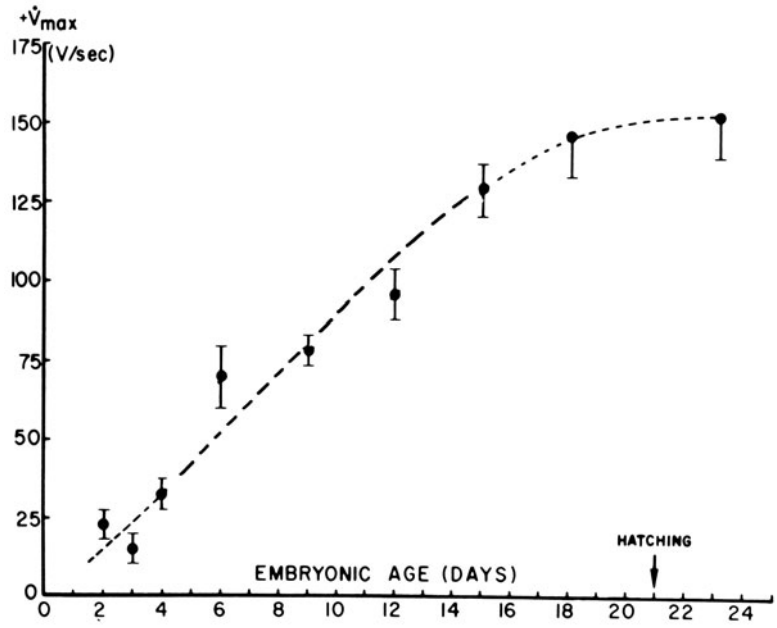

FIGURE 26–4. Changes in the maximum rate of rise of the cardiac action potential ($+\dot{V}_{max}$) during embryonic development of chicks. There is a progressive increase in $+\dot{V}_{max}$ during development, with a plateau level being reached by about day 18. Vertical bars give ± SE. Data taken from Sperelakis and Shigenobu [13], and Jourdon et al. (unpublished observations).

appear to have been lost functionally, and insufficient numbers remain to support regenerative excitation. (However, the simultaneous increase in resting potential during development might render propagation more difficult for any given density of slow channels, because of the greater critical depolarization required to reach threshold and because of the increased K^+ conductance.) Addition of some positive inotropic agents rapidly increases the number of slow Ca^{2+}-Na^+ channels available in the membrane, and leads to the regaining of excitability in cells whose fast Na^+ channels have been voltage inactivated or blocked [52–54].

Sensitivity to TTX and to Calcium Antagonistic Drugs. Tetrodotoxin (TTX), a specific blocker of fast Na^+ channels, has no effect or only little effect on the AP rate of rise or overshoot of the young (two- to three-day-old) hearts (fig. 26–3B and table 26–3). During the intermediate stage (days 5–7), TTX causes a reduction in $+\dot{V}_{max}$ to about 10–20 V/s, but the APs and accompanying contractions persist (fig. 26–3C and D, and table 26–3). After day 8, the APs are completely abolished by TTX despite increased stimulation intensity (fig. 26–3E and F, and table 26–3).

The Ca^{2+}-antagonist drugs, verapamil and D-600, block the APs of the young embryonic hearts [55, 56]. This indicates that these agents block slow Na^+ channels as well as slow Ca^{2+} and slow Ca^{2+}-Na^+ channels, and so are not specific for blockade of Ca^{2+} current. In contrast, Mn^{2+} at 1 m*M* does not depress the APs of young hearts, although it does block the contractions, indicating a greater specificity for slow Ca^{2+} channels and not for the slow Na^+ channels [13].

In recent experiments (Kojima and Sperelakis, unpublished observations) on three-day-old chick embryonic hearts, it was confirmed that verapamil and D-600 depress and block the AP. Elevation of $[Ca]_0$ did not antagonize

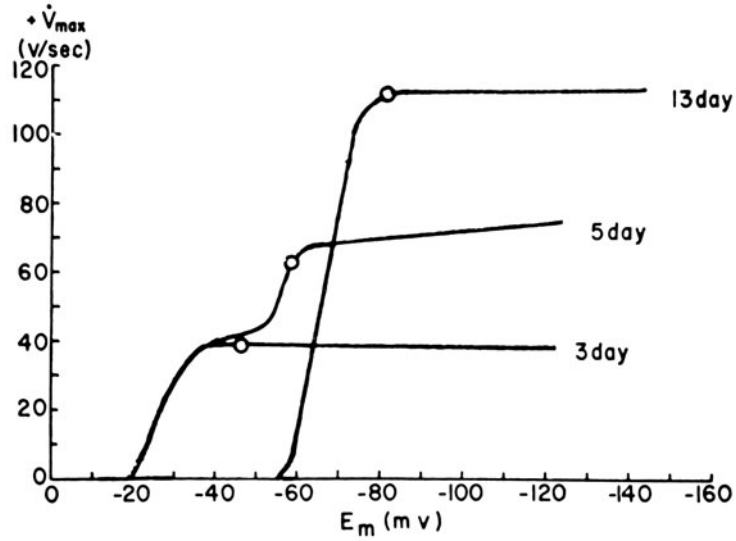

FIGURE 26–5. Evidence for two types of Na^+ channels. Data illustrating changes in the maximal rate of rise of the AP ($+\dot{V}_{max}$) as a function of membrane potential (E_m) for representative hearts of three different embryonic ages (three, five, and 13 days). The membrane potential was changed by applying rectangular polarizing current pulses of long duration (several seconds). The circles give the mean resting potential (polarizing pulses not applied). Note that complete inactivation for the 13-day heart occurs at about −55 mV, whereas complete inactivation does not occur until about −25 mV for the three-day and five-day hearts. For the three-day and 13-day hearts, there appears to be only one type of channel: slow and fast, respectively. The data for the five-day heart (transition period) suggest that there are two sets of channels, one set inactivating at about −55 mV and the other set at −25 mV. Modified from Sperelakis and Shigenobu [13].

this blocking effect of the drugs, whereas elevation of $[Na]_0$ (starting from 50% of normal $[Na]_0$) did antagonize, consistent with the channel being a slow Na^+ rather than a slow Ca^{2+} channel. In addition, it was found that nifedipine also blocked, whereas diltiazem, bepridil, and mesudipine did not.

Galper and Catterall [57] reported that the early embryonic chick heart was insensitive to TTX (with no regard to contractions), but was sensitive to D-600. During subsequent development, the sensitivity to TTX increased and the sensitivity to D-600 decreased in a reciprocal manner. Kasuya et al. [58] also reported that the slowly rising APs of three-day-old embryonic chick hearts involved cation channels that were pharmacologically different from those of old embryonic hearts. Nathan and DeHaan [59] found that TTX-sensitive fast Na^+ conductance channels were absent or nonfunctional in cultured cell reaggregates derived from three-day-old embryonic chick hearts. Ishima [60] reported that the contractions of three- to five-day-old embryonic chick hearts were not affected by TTX.

Consistent with the findings reported from several laboratories, from electrophysiologic experiments, that there is a large increase in number of fast Na^+ channels during development, it was demonstrated by Renaud et al. [61] that the number of specific TTX-binding sites (using ^{3}H-ethylenediamine–TTX) is very low in three-day-old embryonic chick hearts, and increases four- to fivefold during embryonic development. They also confirmed that the APs in the two- to three-day hearts were insensitive to TTX. Iijima and Pappano [50] and Marcus and Fozzard [51] reported that there are some fast Na^+ channels detectable on day 3, and that the sensitivity of the fast Na^+

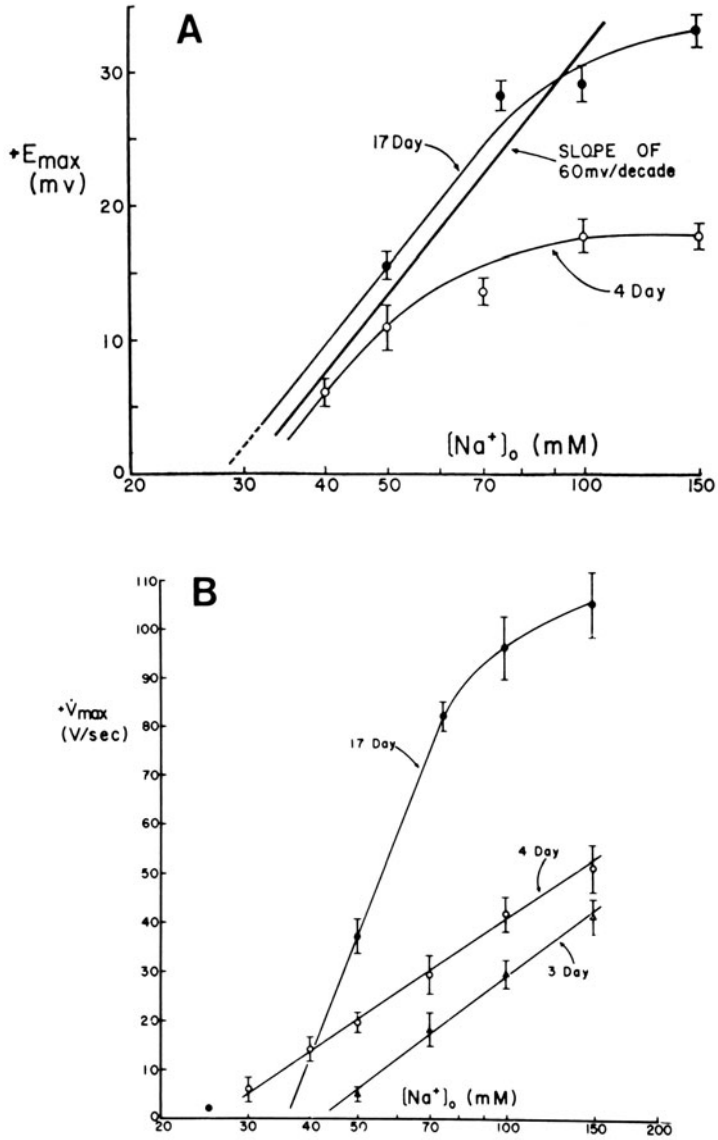

FIGURE 26–6. Evidence that Na^+ is the predominant carrier of inward current in both young and old embryonic chick hearts. *(A)* The mean overshoot values ($+E_{max}$) for one representative four-day-old heart and one representative 17-day-old heart plotted as a function of external Na^+ concentration on a logarithmic scale. A line having a slope of 60 mV/decade has been arbitrarily superimposed. The curves are nearly linear with a slope approaching 60 mV/decade at lower $[Na]_o$, but flatten at high $[Na]_o$ levels. *(B)* The effect of variation of $[Na]_o$ on maximum rate of rise of the action potential ($+\dot{V}_{max}$). $[Na]_o$ was lowered by replacing the NaCl with equimolar amounts of choline–Cl. Plotted are the mean $+\dot{V}_{max}$ ($\pm$ SE) values for three-day, four-day, and 17-day-old hearts. The curve for the old heart is linear at lower $[Na]_o$ levels, and flatten at higher levels; for the young hearts, the curves are linear over the entire range. Taken from Sperelakis and Shigenobu [13].

TABLE 26–3. Effect of tetrodotoxin (TTX) on the action potential maximal rate of rise ($+\dot{V}_{max}$) of chick embryonic hearts (ventricular muscle) as a function of developmental age

Embryonic age (days)	$+\dot{V}_{max}$ (V/s)		TTX sensitivity
	Control	+TTX	
2–3	15–35	10–30	Little or none
5–6	50–70	10–30	Partial
8–10	75–90	0	Complete
12–16	90–140	0	Complete
17–21	140–170	0	Complete

Data taken from Sperelakis and Shigenobu [13].

channels to blockade by TTX does not change during development. Renaud et al. [61] found that there was degradation of the TTX receptors, with a half-time of 9 h in monolayer cultures that were reverted, and that the TTX receptors were stable 24 h after inhibition of protein synthesis in reaggregate cultures containing highly differentiated cells.

Summary. In summary, young (two- to three-day-old) embryonic chick hearts have APs with relatively low rates of rise and which are only little depressed by TTX [13, 48, 62–65]. Since hyperpolarization does not greatly increase the rate of rise, the density of functional fast Na^+ channels is low. In contrast, the density of slow Na^+ channels is high in the young hearts, and verapamil-type agents block the slow Na^+ channels, whereas Mn^{2+} does not [13, 55]. During development, the number of functional fast Na^+ channels increases progressively, reaching the final adult level by about day 18. In contrast, the number of available slow channels, in the absence of positive inotropic agents, decreases during development, reaching the adult level by about day 8. At this time, TTX completely blocks the APs, indicating that the number of available slow channels is not enough to support regenerative excitability. However, addition of a positive inotropic agent, such as beta-adrenergic agonists, histamine, or methylxanthines, rapidly increases the number of available slow channels, and thus allows regenerative slow APs to be generated in the presence of TTX blockade or voltage inactivation (in 25 m*M* $[K]_0$) of the fast Na^+ channels. During an intermediate stage of development, days 5–7, a sizable number of functional fast Na^+ channels coexist with the originally high density of functional slow channels, so that blockade of the fast Na^+ channels by TTX unmasks slow APs, resembling those present in young (two- to three-day-old) hearts.

BIOCHEMICAL CHANGES

Cyclic-AMP Levels. Pronounced changes in cyclic-AMP (cAMP) content occur during embryonic development of the chick heart [49, 66, 67]. The cAMP level is highest in young hearts and it decreases during development. McLean et al. [66] found a cAMP level of 116 pmol/mg protein on day 4, and this decreased sharply by day 5 to about 41; there was a gradual further decline to 9.4 pmol/mg protein, which is about the adult level, by day 16. Renaud et al. [67] found a cAMP level of 33.6 pmol/mg protein on day 4 and 11.7 on day 16.

The relationship between changes in membrane properties and changes in cAMP levels during development of heart remains to be clarified. In cultured skeletal muscle, however, the cAMP level decreases sharply as the myoblasts fuse into myotubes, i.e., when the cells further differentiate. In addition, increase in cAMP level is associated with increase in the number of available slow channels. Therefore, it is tempting to speculate that the decrease in number of available slow channels during development of chick heart, as described above, results from the concomitant drop in cAMP level. This would allow positive inotropic agents that increase the cAMP level to increase the number of available slow channels transiently back toward the density present in young embryonic hearts. In other words, the developmental change in steady-state level of cAMP allows the fraction of slow channels that are available for activation to be modulated by inotropic agents.

It appears that the cAMP level in cultured hearts cells is either about the same (e.g., 16 pmol/mg protein in cells derived from 16-day hearts) [66] or reduced (e.g., 4.5 pmol/mg protein) [67]. A reduction in cAMP was ob-

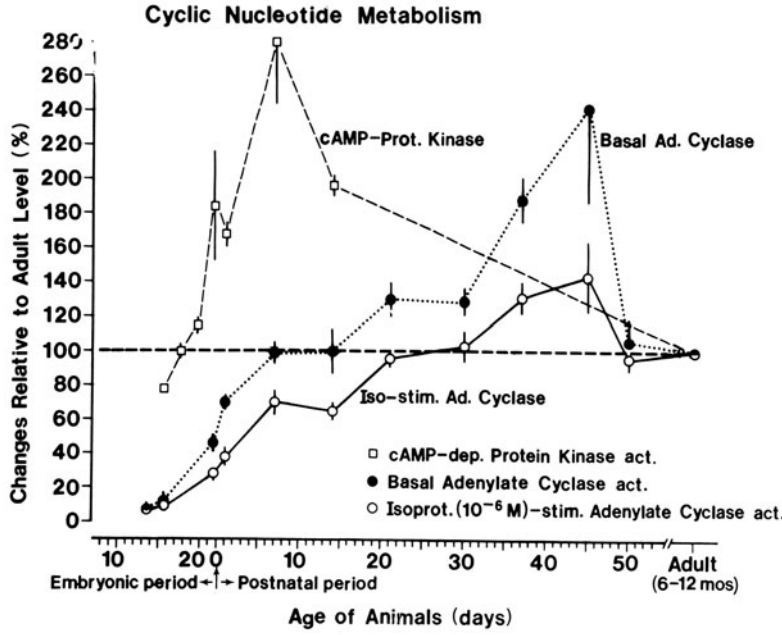

FIGURE 26–7. Developmental changes in cAMP-dependent protein kinase and adenylate cyclase activity in mouse hearts. The ordinate shows percent changes (expressed as percent of adult level (6–12 months old)) in total cAMP-dependent protein kinase activity (type I and type II [□]) and basal (●) and isoproterenol (10^{-6} *M*)-stimulated adenylate cyclase activities (○). Values for cAMP-dependent protein kinase were recalculated from the values given in the papers by Haddox et al. [71], and those for the basal and ISO-stimulated adenylate cyclase activity from Chen et al. [72]. The author thanks Dr. Michio Kojima for preparation of this figure by recalculation of data in the original articles.

served in cell cultures prepared from four-day-old chick hearts. The cAMP level of young (four-day) hearts placed into organ culture for two weeks declines (to 5.6 pmol/mg protein), even though the cells do not further differentiate electrically or ultrastructurally [67]. A similar decline in cAMP level (to 5.3 pmol/mg protein) was observed in organ-cultured 16-day-old chick hearts.

Isoproterenol was capable of markedly elevating the cAMP level in all cases—young or old, cultured or noncultured—thus demonstrating the presence of functional beta-adrenergic receptors. For example, 10^{-6} *M* isoproterenol raised the cAMP level of seven- to eight-day hearts from a control level of 35 pmol/mg to 80 pmol/mg protein at 3 min (time of peak effect) [66]. Isoproterenol elevated the cAMP level of four-day-old hearts from 34 pmol/mg to 119 pmol/mg protein, thus clearly showing that young hearts prior to innervation have functional beta-adrenergic receptors. The organ cultures and cell cultures of four-day-old and 16-day-old hearts also responded markedly to isoproterenol.

In rat heart, the cAMP level was reported to increase during the period from just before birth to postnatal day 10 [68]. The changes in cAMP in rat skeletal muscle were similar to those for the heart. Likewise, in embryonic chick skeletal muscle, there was an increase in cAMP level between days 7 and 15 [69, 70].

In mouse hearts, Haddox et al. [71] found that there was an increase in activity of the cAMP-dependent protein kinase from prenatal day 16 to postnatal day 10, following which activity gradually declined to the adult level (fig. 26–7, squares). Chen et al. [72] found that the basal adenylate cyclase activity was very low at prenatal day 14 and progressively increased through postnatal day 45 (fig. 26–7,

filled circles). The isoproterenol (10^{-6} *M*)-stimulated adenylate cyclase activity increased in parallel to the basal activity (fig. 26–7, unfilled circles).

Glucose Uptake, Amino Acid Uptake, and Membrane Fluidity. Changes in other membrane properties also occur during development. For example, glucose uptake is very high in young hearts and decreases during development. A carrier-mediated saturable glucose transport system appears on about day 7, and an enhancement of glucose uptake by insulin can be first demonstrated shortly thereafter [73]. Thus, insulin had no effect on glucose uptake of five-day-old embryonic chick hearts, but did on seven-day-old hearts. Glucose uptake by hearts five days old and younger seems to be by simple diffusion across the membrane [74, 75]. Ouabain stimulates glucose uptake in ten-day-old hearts, but not in five-day hearts [76]. As development proceeds, the heart myocytes also become progressively less permeable to sorbitol.

Amino acids are actively transported against concentration gradients in five-day-old embryonic chick hearts, and insulin enhances the rate of amino acid transport [77]. The amino acid uptake decreases with development.

There are also changes in membrane fluidity (microviscosity) during development of chick hearts [75]. There is a trend toward increase in fluidity as development proceeds. The cholesterol–phospholipid ratio of the sarcolemma increases during development, concomitant with an increase in the number of unsaturated fatty acid residues. In general, the changes seem to be too complex to correlate with changes in the electrical properties, as, for example, with changes in K^+ permeability. The membrane fluidity of cultured chick skeletal myoblasts increases concomitant with fusion and myotube formation [78].

Metabolic Changes. Young (two- to three-day-old) embryonic chick hearts have large pools of glycogen, and their metabolism is mainly by anaerobic glycolysis. The circulation to the chorioallantoic membrane under the eggshell for gas exchange is not established until day 5. Following this event, there is a shift toward aerobic metabolism, accompanied by changes in various enzymes. For example, there is an increase in pyruvate kinase activity [79, 80]. Many of the biochemical changes that occur in hearts during development have been summarized in a review by Harary [81].

Hearts of young chick embryos utilize the phosphogluconate pathway to a greater extent, relative to the tricarboxylic acid cycle pathway, than do hearts of older embryos or adults [82]. Proliferating cells in general are characterized by high activity of pentose cycle enzymes [83]. Enzymes of the pentose shunt pathway, such as glucose-6-P dehydrogenase and 6-P-gluconic dehydrogenase, decrease from day 4 to day 20, whereas enzymes of the Krebs cycle, such as isocitric dehydrogenase and α-ketoglutaric dehydrogenase, increase during development [84]. In addition, hexokinase activity increases severalfold. The capacity to metabolize long-chain fatty acids appears late in development (after day 12) [85].

In rat hearts, lactic dehydrogenase (LDH) shifts from the embryonic M-form isoenzyme (which catalyzes the reduction of pyruvate to lactate) to the adult-like H form (which facilitates pyruvate oxidation to CO_2 and H_2O) [86]. Similar changes were shown to occur in embryonic chick skeletal muscle [87]. When old embryonic chick myocardial cells are cultured in monolayers, they begin to synthesize the early embryonic M-LDH [88]. Isoenzyme transformation also occurs during rat heart development with respect to creatine phosphokinase [89].

Consistent with the fact that young embryonic hearts have a low rate of aerobic metabolism, being mainly dependent on glycolysis, the young hearts are relatively resistant to metabolic interventions. For example, hypoxia does not block the slow APs of young embryonic chick hearts [90]. Similarly, ventricular cells of seven-day-old chick embryonic hearts are much less sensitive than those of 15-day-old hearts to a variety of metabolic poisons [91]. In mammalian atrial muscle, which has a high glycogen content, the isoproterenol-induced slow APs are only slightly depressed by hypoxia [92].

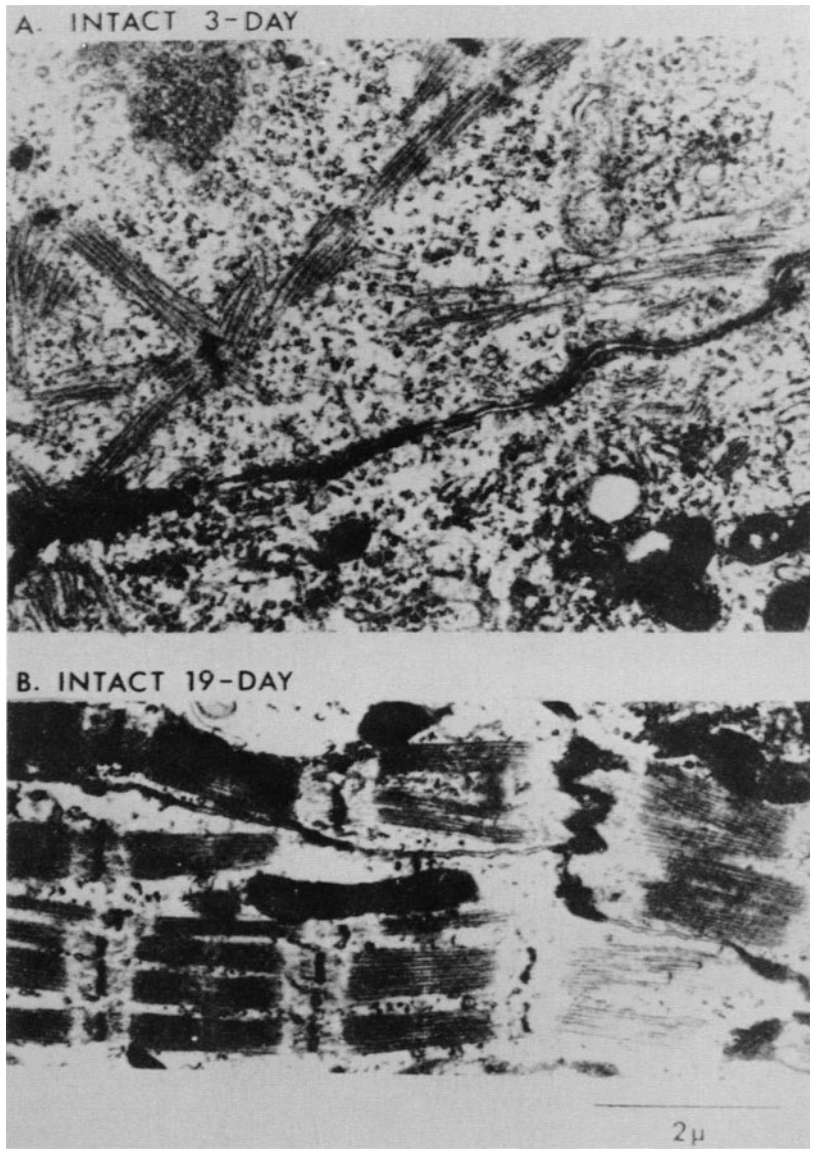

FIGURE 26–8. Cell ultrastructure of young (three days in ovo) and old (19 days in ovo) embryonic chick hearts in situ. *(A)* Three-day ventricular cell demonstrating paucity and nonalignment of myofibrils. Ribosomes are abundant in the cytoplasm. The contiguous cells are held in close apposition by desmosomes. *(B)* 19-day ventricular cells with abundant and aligned myofibrils. A convoluted intercalated disc appears between contiguous cells. Taken from Sperelakis et al. [49], Sperelakis and McLean [131], and Sperelakis and McLean [132].

ULTRASTRUCTURAL CHANGES

Thin myofilaments are clearly present at 30 h, and they begin to collect into groups at about 36 h [93]. Thin filaments are found without thick filaments, but thick filaments usually occur in association with thin filaments. The myofibrils in the two- to three-day hearts are relatively sparse and in various stages of formation (fig. 26–8A). The myofibrils are not aligned, and they run in all directions, including perpendicular to one another. Bundles of myofilaments attached to one Z line often radiate in several directions (fig. 26–8A). The sarcomeres are usually incomplete early in their

formation, and the myofibrils are short. H zones first become obvious at day 8, and M lines do not appear until about day 18. Free cytoplasmic polyribosomes are abundant and rough ER tubules lined with ribosomes are prominent in young hearts; ribosomes are frequently in close association with the developing myofibrils. Large pools of glycogen are observed in the young (two- to three-day-old) hearts.

Organ-Cultured Embryonic Hearts

YOUNG EMBRYONIC HEARTS

Cultivation of embryonic hearts in vitro aids in the analysis of the changes that occur during normal development in situ. When young (three-day-old) embryonic chick hearts, which have not yet become innervated by either cholinergic or adrenergic fibers, are placed into organ culture, they fail to gain TTX-sensitive fast Na^+ channels [94, 95]. Instead, the APs continue to be generated by TTX-insensitive slow Na^+ channels, the rates of rise remain slow, and pacemaker potentials precede the APs (fig. 26–9). These APs resemble those recorded from three-day-old hearts in situ. Similar findings were obtained when young hearts were grafted on to the chorioallantoic membrane of host chicks for blood perfusion [96]. Thus, organ-cultured young hearts do not differentiate further in vitro, but appear to be arrested in the young embryonic state.

When young hearts which have been arrested in the early developmental state are treated with RNA-enriched fractions obtained from adult chicken hearts, they gain fast Na^+ channels and become completely sensitive to TTX [97–99]; that is, young hearts in vitro can be induced to undergo further membrane differentiation. Cultured young hearts thus provide a useful model for studying the regulation of membrane differentiation.

INTERMEDIATE AND OLD EMBRYONIC HEARTS

Organ-cultured intermediate (five- to seven-day-old) hearts have both fast and slow Na^+ channels, just as in situ [94–96]. The APs have moderate rates of rise (40–70 V/s), and TTX reduces the maximal rate of rise of the AP to about 10 V/s. Cultured 17-day hearts tend to retain their fast-rising APs and complete sensitivity to TTX, but survival is limited to a few days. Thus, in organ culture, the embryonic hearts tend to retain the state of differentiation achieved at the time of placement into culture.

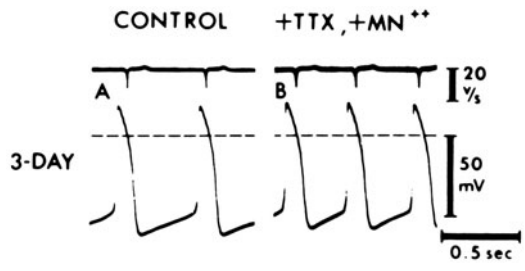

FIGURE 26–9. Failure of appearance of fast Na^+ channels in a three-day-old heart organ-cultured for six days. The APs recorded from one cell prior to *(A)* and another cell after *(B)*, the addition of tetrodotoxin (TTX) are almost identical; dV/D*t* values (upper traces) are similar for the two cells. Subsequent addition of Mn^{2+} (1 m*M*; panel *B*) in the presence of TTX had no effect on the maximal rate of rise of the AP, thus indicating that the inward current during the APs is not predominantly carried by Ca^{2+} ion. Modified from Sperelakis and Shigenobu [13].

Cultured Heart Cells

Various stages of cardiac electrical differentiation can be simulated in vitro using cell cultures, and their study may facilitate elucidation of the mechanisms operating during normal cardiogenesis. The electrophyisologic properties observed depend to a large extent on the age of the hearts from which the cells are isolated and on the method of cell culture.

OLD EMBRYONIC HEARTS

Monolayer Cultures. When cells are dispersed from old embryonic hearts using trypsin and standard monolayer cultures are prepared, the cells are found to possess slowly rising TTX-insensitive APs with pacemaker potentials (fig. 26–10C and D); that is, the APs are similar to

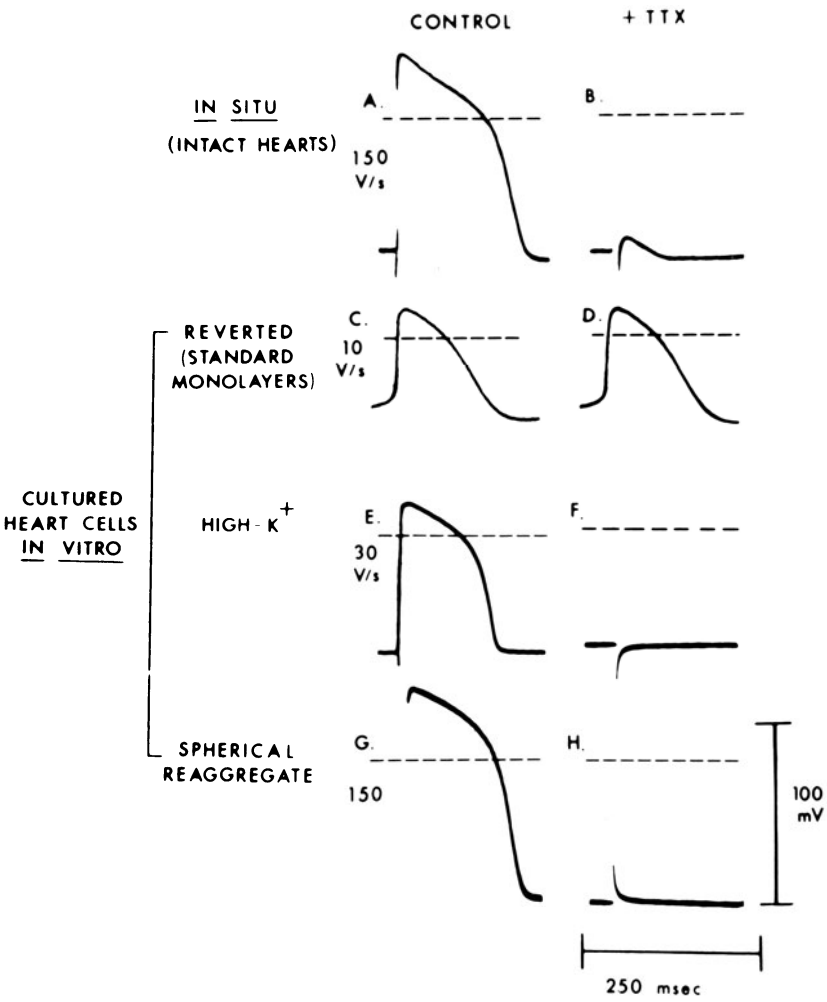

FIGURE 26–10. Comparison of the electrophysiologic properties of the intact old (16-day) embryonic chick heart in situ *(A* and *B)* with those of trypsin-dispersed old ventricular myocardial cells in cultures prepared by three different methods *(C–H). (A* and *B)* Intact heart; control AP *(A)* was rapidly rising (150 V/s), had a high stable resting potential (about −80 mV), and was completely abolished by tetrodotoxin (TTX; 0.1 g/ml) *(B). (C* and *D)* Standard reverted monolayers; control AP was slowly rising (10 V/s) and was preceded by a pacemaker potential; the resting potential was low (about −50 mV) *(C),* and TTX did not alter the AP *(D). (E* and *F)* Partially reverted cells cultured as monolayers in media containing elevated K^+ concentration (25 m*M*); control AP had a rate of rise of 30 V/s *(E),* lacked a pacemaker potential, had a moderately high resting potential (−60 mV), and was completely abolished by TTX *(F). (G* and *H)* Highly differentiated cells in spherical reaggregate culture; control APs were rapidly rising (150 V/s), the resting potentials were high (−80 mV) *(G),* and TTX abolished the APs *(H).* Taken from Sperelakis et al. [49], Sperelakis and McLean [131], and Sperelakis and McLean [132].

those recorded in young (two- to three-day-old) hearts, rather than in old hearts from which the cells were taken (fig. 26–10A and B). It thus appears that cell separation results in a rapid reversion toward the young embryonic state [3, 55, 62, 100, 101].

This reversion can be partially prevented (or reversed) by separating the cells in trypsinizing solutions containing elevated K^+ concentrations (12–60 m*M*; by isomolar substitutions of K^+ for Na^+) and 5 m*M* ATP [39]. Action potentials recorded from cells prepared in this

manner are initiated from moderately high stable resting potentials of about −60 mV, and they are completely sensitive to TTX; however, the maximal rate of rise of the AP is still rather slow, averaging about 30 V/s (fig. 26–10E and F). The mechanism whereby elevated K^+ and ATP helps to minimize reversion of the cultured cells is not known, although $[K]_i$ is reduced in the reverted cells to about 90–100 m*M* and this does not occur in highly differentiated cultured cells.

Jones et al. [102] reported that multilayer-cultured ventricular cells can be made to exhibit highly differentiated morphology (e.g., densely packed and aligned myofibrils with mitochondria between the fibrils), as well as advanced electrical properties, if the fetal calf serum concentration is lowered from 10% to 0.1% after the first few days, presumably to remove growth-promoting factors, and the cells are subsequently allowed to age in vitro for several weeks.

Renaud et al. [103] recently demonstrated that monolayer heart cells maintained in a lipoprotein-deficient serum differentiate electrically compared to cells cultured in normal media. The cells in lipoprotein-deficient media had greater resting potentials, faster-rising APs that were greatly decreased by TTX, and muscarinic agonists now blocked automaticity. The authors found that the cholesterol content of the cell membranes was decreased in monolayer culture, and that the lipoprotein-deficient medium returned it to normal levels. It was also reported that the TTX receptor and muscarinic receptor remained stable for over 25 h after protein synthesis was blocked in the highly differentiated cells, whereas in the reverted cells these receptors were rapidly degraded (with half-times of 9–14 h).

Spherical Reaggregate Cultures. Cells with highly differentiated electrophysiologic properties can be obtained following trypsinization (in solutions containing elevated K^+ and 5 m*M* ATP) and subsequent reaggregation to form small spheres (0.1–0.5 mm in diameter) in vitro [39]. (It must be emphasized that not all reaggregates contain cells that are highly differentiated, i.e., many are reverted.) Reaggregation is achieved either by gyrotation for 24–48 h or by plating the cells on cellophane to which the cells adhere poorly. Action potentials recorded from cells in such reaggregates possess rapid rates of rise (up to 200 V/s) and are initiated from high stable resting potentials (about −80 mV), and TTX completely abolishes all excitability (fig. 26–10G and H). The intracellular records are indistinguishable from those made from the intact 16-day ventricle (fig. 26–10A and B). As in the case of the intact old embryonic hearts, positive inotropic agents induce slowly rising APs in the highly differentiated cultured cells following blockade of the fast Na^+ channels with TTX [39, 104, 105]. Acetylcholine was without noticeable effect on the APs of cultured ventricular cells, both reverted [106] and highly differentiated [39].

YOUNG EMBRYONIC HEARTS

When young (two- to three-day-old) embryonic hearts are trypsin dispersed and the cells are allowed to reaggregate in vitro, the cells retain electrical activity characteristic of the intact young heart; that is, the cells have low resting potentials, and they fire spontaneous slowly rising APs that are unaffected by TTX. As observed in the case of young organ-cultured intact hearts, however, the addition of RNA-enriched extracts from adult chicken hearts to the reaggregated young myocardial cells induces the appearance of rapidly rising (e.g., 100 V/s) APs, which fire from high stable resting potentials (−70 to −80 mV), and which are completely sensitive to TTX [96, 97]. This further differentiation results in the achievement of adult-like electrophysiologic properties, as normally occurs in situ. The mechanism of action of the active principle in the extract remains to be elucidated. Nathan and De Haan [59] reported that they can achieve further differentiation of young cells in reaggregate culture without the addition of special extracts.

Meaning of Veratridine Depolarization

It was first shown by Sperelakis and Pappano [107] that veratridine depolarizes the reverted

cultured (monolayer) heart cells and that TTX prevents this depolarization, even though TTX had no obvious effect on the APs. They interpreted these findings to suggest that veratridine opens up a resting type (i.e., time independent) of Na^+ channel (i.e., resting P_{Na} is increased by veratridine), and that TTX blocks this action. (Since veratridine actually hyperpolarized the cells in the presence of TTX, they concluded that veratridine also increases the resting K^+ permeability, P_K.) Other investigators subsequently saw similar effects of veratridine and related toxins (such as batrachotoxin and grayanotoxin) on neurons and myocardial cells (see the review by Sperelakis [108]). Because veratridine depolarized and increased Na^+ influx in monolayer culture heart cells that were reverted (i.e., exhibited slowly rising TTX-insensitive APs), it was suggested that there must be "silent" (i.e., inoperable) fast Na^+ channels present in the reverted cells that could be opened by veratridine [61, 109]. But this conclusion is based on the premise that veratridine can only act on fast Na^+ channels, which seems to be an assumption that is equivocal. In support of their conclusion, Renaud et al. [61] reported that there was some specific TTX binding in the young hearts (the number of such binding sites increased about sixfold during embryonic development), i.e., that there were some "silent" fast Na^+ channels in young hearts.

However, Pang and Sperelakis [110] showed that the veratridine-stimulated ^{45}Ca influx into the heart cells, which should reflect a parallel Na^+ influx because of the Ca-Na exchange system, was independent of embryonic age of the developing chick, i.e., the curve was flat. These investigators therefore concluded that veratridine must act on a second channel (in addition to the fast Na^+ channel) to increase Na^+ influx and Ca^{2+} influx and depolarize, since the number of TTX-binding sites increases during embryonic development [61], as does the rate of rise of the APs [8, 13, 62], reflecting the number of fast Na^+ channels; that is, more and more fast Na^+ channels were available to be opened as a function of embryonic age, and yet the veratridine effect on Ca^{2+} influx was independent of embryonic age. The second channel opened by veratridine could be the resting P_{Na} channel and/or the voltage-dependent slow Na^+ channel.

Relevant to the evidence presented above that veratridine is not a specific opener of fast Na^+ channels in myocardial cells, Romey and Lazdunski [111] have now shown that veratridine, aconitine, batrachotoxin, and grayanotoxin are not specific for the fast Na^+ channels of neuroblastoma cells either, but also act to block the voltage-dependent slow Ca^{2+} channels, at the same or even lower concentrations.

Induction and Properties of Myocardial Slow Channels

ACTION OF POSITIVE INOTROPIC AGENTS

A number of positive inotropic agents exert an effect on the myocardial cell membrane to increase the number of available slow channels, and this action may at least partly explain their effect on increasing cardiac contractility. It is through the slow channels that Ca^{2+} influx occurs during the cardiac AP, and the amount of Ca^{2+} ion entering the myocardial cell controls the force of contraction. The Ca^{2+} entering directly helps to elevate $[Ca]_i$ involved in activating the myofilaments, and indirectly does so by bringing about the further release of Ca^{2+} from the intracellular stores in the SR [112]. Blockade of the slow channels, and hence Ca^{2+} influx, by Ca^{2+}-antagonistic agents, such as verapamil, D-600, nifedipine, Mn^{2+}, Co^{2+}, and La^{3+}, depresses or abolishes the contractions without greatly affecting the normal fast AP, i.e., contraction is uncoupled from excitation.

The positive inotropic agents which have been shown to affect the number of available slow channels include: catecholamines (beta-adrenergic receptor agonists), histamine (H_2 receptor), methylxanthines, angiotensin II, and fluoride ion. The action of most of these agents is very rapid, the peak effect often occurring within 1–3 min.

One method of detecting the effect of positive inotropic agents on the myocardial slow channels is to first block the fast Na^+ channels and excitability by TTX or to voltage inactivate the fast Na^+ channels by partially depo-

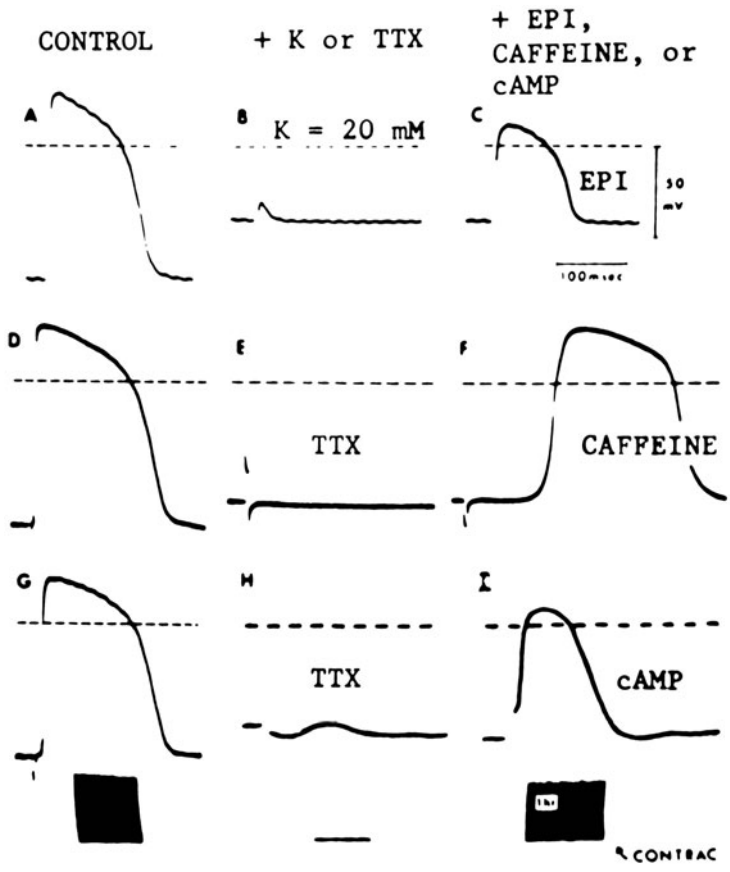

FIGURE 26–11. Induction of slow action potentials by positive inotropic agents in chick embryonic (16-day-old) hearts whose fast Na^+ channels have been inactivated by elevated $[K]_o$ *(A–C)* or tetrodotoxin (TTX) *(D* and *F, G–I). (A–C)* K^+ inactivation of the fast Na^+ channels, and induction by catecholamine. *(A)* Control fast AP. *(B)* Abolition of excitability by elevation of $[K]_o$ to 20 m*M*, despite a tenfold increase in stimulus intensity. *(C)* Slowly rising electrical response produced rapidly (1 min) after addition of epinephrine (Epi, 1×10^{-5} *M*); contractions (not shown) accompanied the electrical responses. Addition of Mn^{2+} or La^{3+} (1 m*M*) blocked the slow APs within 5 min (not shown). *(D* and *F)* TTX inactivation of the fast Na^+ channels. *(D)* Control fast AP. *(E)* Abolition of APs 2 min after exposure to TTX (4 μg/ml). *(F)* Restoration of electrical (and contractile) activity by addition of caffeine (1 m*M*). *(G–I)* Induction of the slow channels by cAMP. *(G)* Control fast AP. *(H)* Abolition of excitability in TTX. *(I)* Restoration of slowly rising electrical responses 20–60 min after addition of cAMP (3 m*M*). The insets in *G–I* give the contraction recorded on a penwriter at slow speed. Note that the contractile force in *I* is about equal to that in *G*. Modified from Sperelakis and Shigenobu [13].

larizing the cells (e.g., to −40 mV) in elevated $[K]_o$ (e.g., 25 m*M*) [52]. Then, addition of agents, such as catecholamines, which rapidly increase the number of slow channels available for activation upon stimulation, causes the appearance of slowly rising overshooting APS (the "slow responses") which resemble the plateau component of the normal fast AP (fig. 26–11C and F). The slow APs are accompanied by contractions, and it has been shown that both Ca^{2+} and Na^+ inward currents participate in the slow AP [53, 113]. The slow APs are blocked by agents which block inward slow Ca^{2+} current, including Mn^{2+}, La^{3+}, verapamil, and D-600 [56, 113, 114].

RELATIONSHIP TO CYCLIC AMP

Histamine and beta-adrenergic agonists, subsequent to binding to their specific receptors, are known to lead to rapid stimulation of aden-

ylate cyclase with resultant elevation of cAMP levels [114, 115]. The methylxanthines enter into the myocardial cells and inhibit phosphodiesterase, thus causing an elevation of cAMP [114]. These positive inotropic agents also rapidly induce the slow APs by making more slow channels available in the membrane. Hence, cAMP is somehow involved in the functioning of the slow channels [53, 113, 114, 116, 117].

Consistent with this, cAMP itself and its dibutyryl derivative also induce the slow APs, but only after a much longer lag period (peak effect in 15–30 min), as would be expected from slow penetration through the membrane [53, 113]. Another test of the cAMP hypothesis was done by using a GTP analogue (5′-guanylimidodiphosphate [GPP(NH)P]), an agent known to directly activate adenylate cyclase in a variety of broken cell preparations. The addition of GPP(NH)P (10^{-5}–10^{-3} *M*) induced the slow APs in cultured reaggregates of chick heart cells within 5–30 min [118]. These results support the hypothesis that the intracellular level of cAMP controls the availability of the slow channels in the myocardial sarcolemma.

In another test of the cAMP hypothesis, cAMP was microinjected intracellularly into dog Purkinje fibers and guinea pig ventricular muscle [119]. It was found that cAMP injections induced the slow APs in the injected cell for a transient period of 1–2 min; the amplitude and duration of the induced slow AP was a function of the amount of cAMP injected. When a slow AP was induced by theophylline, cAMP injections increased their rate of rise and amplitude also for a transient period.

METABOLIC DEPENDENCE

The induced slow APs are blocked by hypoxia, ischemia, and metabolic poisons (including cyanide, dinitrophenol, and valinomycin), accompanied by a lowering of the cellular ATP level [54]. This suggests that interference with metabolism somehow leads to blockade of the slow channels. This effect is relatively rapid; for example, the blockade occurs within 5–15 min. In contrast, the fast APs are unaffected, thus indicating that the fast Na^+ channels are essentially unaffected. Thus, there is a dependence of the functioning of the slow channels on metabolic energy. The contractions accompanying the fast APs are depressed or abolished, indicating that contraction is uncoupled from excitation, as expected if the slow channels were blocked.

In addition to the effect of metabolism on the slow channels, with prolonged metabolic intervention, e.g., 60–120 min of hypoxia, there is a gradual shortening of the duration of the normal fast AP, until a relatively brief spike-like component only remains, but which is still rapidly rising [54, 91]. Thus, metabolic interference exerts a second, but much slower effect on the membrane, namely, to increase the kinetics of g_K turnon, thereby shortening the AP. This effect could be mediated by a gradual rise in $[Ca]_i$, since a steady-state elevation in $[Ca]_i$ can cause an increase in g_K, by turning on the Ca^{2+}-activated g_K [120].

The myocardial slow channels are selectively blocked by acidosis [121]. For example, the slow APs induced by isoproterenol (in 25 m*M* $[K]_0$) are depressed in rate of rise, amplitude and duration as the pH of the perfusing solution is lowered below 7.0 [122]. Complete block occurs at about pH 6.1, and 50% inhibition occurs at about pH 6.6. The contractions are depressed in parallel with the slow APs. Acidosis has little or no effect on the fast APs, but the accompanying contractions become depressed and abolished as a function of the degree of acidosis [123]; that is, excitation–contraction uncoupling occurs, as expected from a selective blockade of the slow channels. Since the myocardium becomes acidotic during ischemia and hypoxia, it is likely that the effects of these metabolic interventions on the slow channels are partly mediated by the accompanying acidosis [123].

PHOSPHORYLATION HYPOTHESIS

Because of the relationship between cAMP and the number of available slow channels, and because of the dependence of the functioning of the slow channels on metabolic energy, it has been postulated that a membrane protein must be phosphorylated in order for the slow channel to become available for voltage activation [53, 54, 116, 124–127] (fig. 26–12). The only

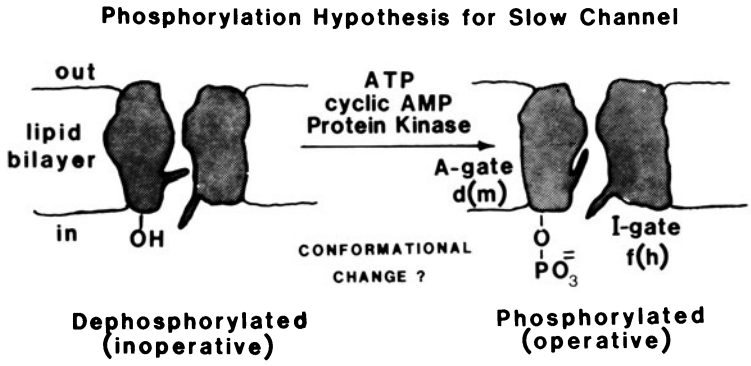

FIGURE 26–12. Cartoon model for a slow channel in myocardial cell membrane. Two hypothetical forms of the channel are depicted: dephosphorylated form *(left diagram)* and phosphorylated form *(right diagram)*. It is postulated that a protein constituent of the slow channel must be phosphorylated in order for the channel to be in a functional state available for voltage activation. There are two gates associated with each channel: an activation (A) gate, and an inactivation (I) gate. The gates are presumably charged positively so that they can sense the membrane potential. The I gate moves more slowly than the A gate. The slow-channel gates are kinetically much slower than those of the fast Na^+ channel. In the resting state, the A gate is closed and the I gate is open. In the active state, both gates are open. Depolarization causes the A gate to open relatively quickly, so that the channel becomes conducting (the active state). However, the I gate slowly closes during depolarization and inactivates the channel (the inactive state). During recovery upon repolarization, the A gate closes and the I gate opens (returns to the resting state). Verapamil and Mn^{3+} block the slow channel. Tetrodotoxin (TTX) blocks fast Na^+ channels from the outside, presumably by binding in the channel mouth. Modified from Sperelakis [8].

well-documented effect of cAMP is the activation of a cAMP-dependent protein kinase (dimer split into two active monomers), and the latter enzyme, in the presence of ATP, phosphorylates a variety of proteins. Several membrane proteins are phosphorylated under appropriate conditions [128], and similar results have been shown for cardiac membrane preparations [129, 130].

The protein that is phosphorylated might be a constituent of the slow channel itself. Phosphorylation could make the slow channel available for activation by causing a conformational change that either allowed the activation gate to be opened upon depolarization or effectively increased the diameter of the water-filled pore so that Ca^{2+} and Na^+ could pass through. Regardless of mechanism, the phosphorylated form of the slow channel would be the active (operational) form, and the dephosphorylated form would be the inactive (inoperative) form; that is, only the phosphorylated form would be available to become activated upon depolarization to threshold. The dephosphorylated channels would be electrically silent. Thus, agents that act to elevate the cAMP level, either by stimulating the adenylate cyclase or by inhibiting the phosphodiesterase, would increase the fraction of the slow channels that are in the phosphorylated form, and hence available for voltage activation. Some positive inotropic agents that do not elevate cAMP, but yet induce the slow channels, may act by inhibiting the phosphatase which dephosphorylates the slow-channel protein, thereby resulting in a larger fraction of phosphorylated channels [105].

The developmental changes in the autonomic receptors of mouse hearts are summarized in figure 26–13. Changes in the adrenergic receptors (β-adrenergic and α_1-adrenergic) are given in panel A, and changes in the cholinergic muscarinic receptors are given in panel B. The details of the developmental changes in the autonomic receptors in chick and mouse hearts are summarized in chapter 16.

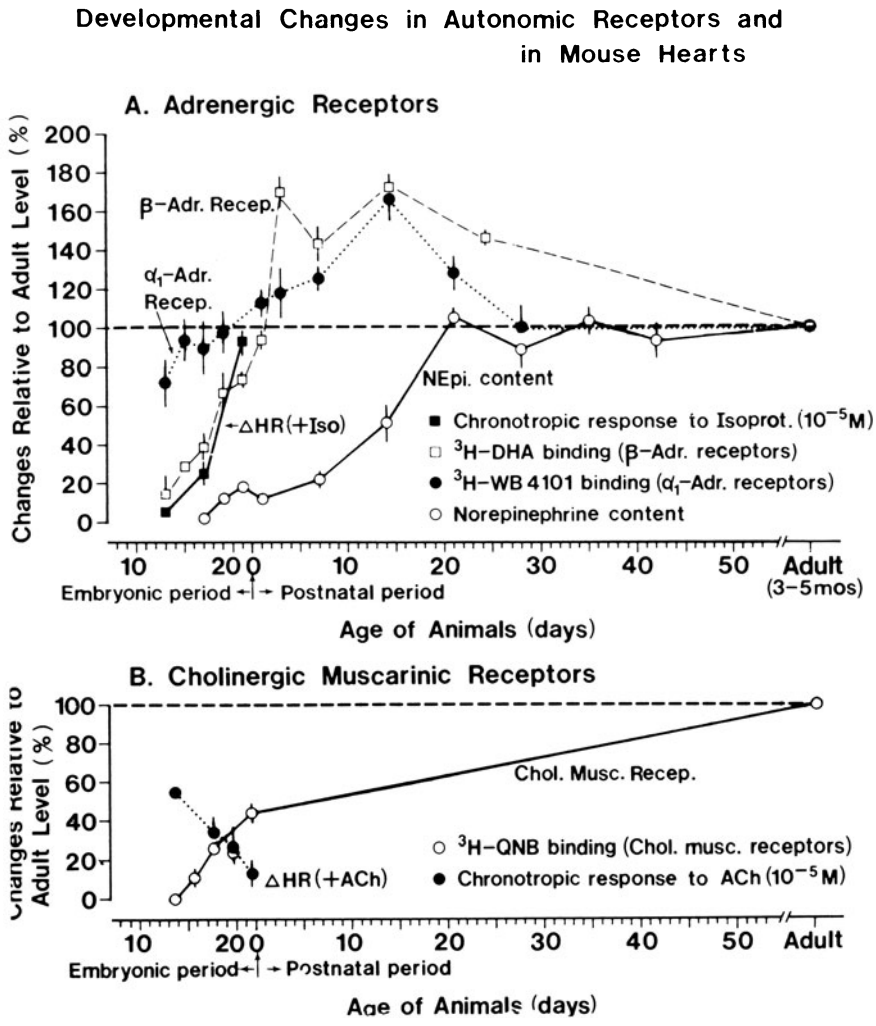

FIGURE 26–13. Summary of developmental changes in autonomic receptors in mouse hearts relative to the adult level. *(A)* Changes in cardiac adrenergic receptors, norepinephrine content, and chronotropic response to isoproterenol. Changes in number of α_1-adrenergic receptors (●), β-adrenergic receptors (□), norepinephrine content (○), and heart rate responses (as percent of the control level) to isoproterenol (10^{-5} *M*) (■) are plotted. The abscissa gives developmental age in days prenatal (10–22 days) and postnatal (0–55 days and adult). α_1-Adrenergic receptors were determined by ^{3}H-WB4101 (^{3}H-2-N [2,6-dimethoxyphenoxyethyl] amino ethyl-1,4 benzodioxane) binding, and the β-adrenergic receptors by ^{3}H-DHA (^{3}H-dehydroalprenolol) binding. Values plotted are mean ± SE. (The SE was not shown when it was smaller than the size of a symbol.) There was no change in binding affinity for the antagonists, ^{3}H-WB4101 and ^{3}H-DHA, during this period (not shown). Values for α_1-adrenergic binding studies and norepinephrine content were recalculated from the data given in Yamada et al. [133] and those for the β-adrenergic binding studies and for the chronotropic response to ISO from Chen et al. [134]. *(B)* Changes in cholinergic muscarinic receptors and chronotropic response to acetylcholine (ACh). Changes in muscarinic receptor density (○) and heart rate response to ACh (10^{-5} *M*) (●), expressed as percent of the adult level and control level, respectively. The cholinergic muscarinic receptors were assayed by ^{3}H-QNB (^{3}H-quiniclidinyl benzilate) binding. Values plotted are mean ± SE. There was no change in binding affinity for the antagonist ^{3}H-QNB during development (not shown). The values were recalculated from the data given in Roeske and Yamamura [135]. The author wishes to thank Dr. Michio Kojima for preparation of this figure by recalculation of data in the original articles.

Summary and Conclusions

Striking changes occur in the electrical properties of the myocardial cell membrane during embryonic development of chick hearts. The young tubular hearts (2–3 days old) have a low resting potential of about −40–50 mV, even though $[K]_i$ is nearly as high as the adult value. The low resting potential is caused by a low K^+ permeability (P_K). The low P_K can also account for the high degree of automaticity observed in the ventricular cells of young embryonic hearts. P_K increases rapidly during development, attaining nearly the final adult value by day 12; the resting potential increases to about −80 mV, and automaticity of the ventricular cells is suppressed. The young heart has a low (Na,K)-ATPase activity, and this enzyme activity increases during development along with P_K.

The young (two- to three-day-old) hearts have action potentials (APs) with slow maximal rates of rise ($+\dot{V}_{max}$) of 10–30 V/s. The slowly rising APs are not affected by tetrodotoxin (TTX), and hyperpolarization does not greatly increase the rate of rise. The APs are dependent mainly on $[Na]_0$. Thus, it appears that fast Na^+ channels are absent or relatively few in number in young hearts, the inward current during the AP being carried predominantly through TTX-insensitive slow Na^+ channels. The slow Na^+ channels are blocked by verapamil, but not by 1 m*M* Mn^{2+}. Mn^{2+} does block the contractions, presumably by blockade of the Ca^{2+} influx during the AP. This Ca^{2+} influx presumably occurs through some slow Ca^{2+} channels that are likely to be present. In many respects, the young tubular hearts resemble pulsating blood vessels, and their electrical properties are somewhat similar to those of vascular smooth muscle.

There is a progressive increase in $+\dot{V}_{max}$ of the AP during development. By day 5, $+\dot{V}_{max}$ is about 50–80 V/s, and TTX now reduces $+\dot{V}_{max}$ to 10–30 V/s, i.e., to the value observed in two- to three-day-old hearts. Thus, the TTX-sensitive fast Na^+ channels progressively increase in number until they attain the final adult level by day 18. Between days 5 and 7, fast Na^+ channels and a high density of slow Na^+ channels coexist. After day 8, TTX completely abolishes excitability, suggesting that the number of functional slow channels has decreased sufficiently so as not to support regenerative excitation.

The cAMP level is very high in young hearts and decreases during development. The high cAMP level in young hearts may keep most or all of the slow channels in a phosphorylated state, and hence available for voltage activation. Decrease in the cAMP level during development allows control to be exercised over the number of available slow channels. The fact that isoproterenol can elevate the cAMP level in even young (four-day-old) hearts (that already have high levels of cAMP) indicates that functional beta-adrenergic receptors are present prior to innervation.

The slow channels in young hearts are predominantly of the slow Na^+ type, whereas those slow channels induced by some positive inotropic agents, e.g., isoproterenol, in older hearts are of the slow Ca-Na type.

Young embryonic rat hearts also have slowly rising TTX-insensitive APs. The major difference from the embryonic chick is that the slow channels that pass the inward current for the AP appear to be predominantly of the slow Ca^{2+} type rather than of the slow Na^+ type.

Young embryonic chick hearts (three days old), removed prior to innervation and placed into organ culture for two weeks or grafted on the chorioallantoic membrane of a host chick for blood perfusion, do not gain fast Na^+ channels or otherwise differentiate. This suggests that something in the in situ condition, such as neurotrophic or other factors, is required for triggering further differentiation. If, however, these young organ-cultured hearts are exposed for several days to an RNA-enriched fraction obtained from adult chicken hearts, they do gain TTX-sensitive fast Na^+ channels. This induction is blocked by inhibitors of protein synthesis, such as cyclohexamide. Thus, the synthesis of specific membrane proteins controls the appearance of fast Na^+ channels. Hence, cardiac myoblasts whose development, with respect to some membrane electrical properties, has been arrested in vitro can be induced to differentiate further. Trypsin-dispersed myocardial cells obtained from young embryonic chick

hearts and placed in cell culture for several weeks also do not proceed with differentiation in vitro, unless exposed to the RNA extract from adult heart.

Monolayer cultures of heart cells prepared from old embryonic heart (ventricles) rapidly revert back to the young embryonic state; that is, they lose most or all of their fast Na^+ channels, gain slow Na^+ channels, and gain automaticity because of a low P_K; they also lose many of their myofibrils. If however, the cells are allowed to reaggregate into small spheres and incubate for a period of 1–3 weeks, they often will regain highly differentiated electrical properties. These cells also retain their membrane receptors for catecholamines, histamine, and angiotensin. The cultured ventricular (and atrial) cells possess receptors for acetylcholine. Thus, highly differentiated myocardial cells can be maintained in cell culture under appropriate conditions. Exposure of monolayer cultures possessing reverted electrical properties to media containing lipoprotein-deficient serum caused the cells to gain highly differentiated electrical characteristics concomitant with increase in cholesterol content of the cell membrane.

Based on veratridine-induced depolarization of and stimulation of Na^+ influx and Ca^{2+} influx into monolayer cultured heart cells that possess reverted electrical properties, and TTX block of the veratridine effect, it has been postulated that there are some silent (nonfunctional) fast Na^+ channels in the reverted cells which can be opened by veratridine. Consistent with this view, there are some binding sites for a ^{3}H-TTX analogue (for assessing specific binding sites presumably on fast Na^+ channels) in the young (three-day-old) embryonic chick hearts. But the number of ^{3}H-TTX binding sites increases about sixfold during embryonic development in ovo in parallel with the increase in $+\dot{V}_{max}$ of the AP, thus confirming by a different approach the fact that the number of fast Na^+ channels increases during development. The fact that the degree of veratridine stimulation of ^{45}Ca uptake is independent of embryonic age argues against the concept of silent fast Na^+ channels in the young hearts, and for the likelihood that veratridine exerts effects on other types of channels, e.g., on slow channels or resting P_{Na} channels, as well as on fast Na^+ channels.

Positive inotropic agents, such as norepinephrine, histamine, and methylxanthine, rapidly induce slow Ca-Na channels in old embryonic myocardial cells. Following blockade of the fast Na^+ channels with TTX, these agents rapidly allow the production of slowly rising APs by increasing the number of slow channels available for voltage activation. Since norepinephrine, histamine, and methylxanthines rapidly elevate intracellular cAMP levels, these results suggest that cAMP controls the number of operational slow channels. Exogenous cAMP produces the same effect but much more slowly, whereas intracellular injection of cAMP increases the number of available slow channels within seconds.

The myocardial slow channels induced by the positive inotropic agents are very sensitive to blockade by metabolic poisons, hypoxia, and ischemia. In contrast, the fast Na^+ channels are essentially unaffected; however, the contractions accompanying the fast APs are depressed or abolished, i.e., contraction is uncoupled from excitation, as expected from the slow-channel blockade. Therefore, the slow channels are metabolically dependent, whereas the fast Na^+ channels are not. The slow channels are also selectively sensitive to blockade by acid pH.

Because of the dependence of the myocardial slow channels on cAMP level and on metabolism, phosphorylation of a membrane protein constituent of the slow channel, by a cAMP-dependent protein kinase and ATP, may be required to make it available for voltage activation. By virtue of these special properties of the slow channels, the Ca^{2+} influx of the myocardial cell can be controlled by extrinsic factors, such as by autonomic nerve stimulation or circulating hormones, or by intrinsic factors, such as intracellular pH or ATP level.

References

1. Rosenquist G, De Haan RL: Migration of precardiac cells in the chick embryo: a radioautographic study. Contrib Embryol Carnegie Inst Wash 263:113–121, 1966.

2. LeDouarin G, Obrecht G, Coraboeuf E: Déterminations reégionales dans l'air cardiaque presomptive mises en évidence chez l'embryon de poulet par la méthode microelectrophysiologique. J Embryol Exp Morphal 15:153–167, 1966.
3. Renaud D: Etude electrophysiologique de la différentiation cardiaque chez l'embryon de poulet. Thesis, University of Nantes, 1973.
4. Niu MC, Deshpande AK: The development of tubular heart in RNA-treated post-nodal pieces of chick blastoderm. J Embryol Exp Morphol 29:485–501, 1973.
5. McLean MJ, Renaud JF, Sperelakis N: Cardiac-like action potentials recorded from spontaneously-contracting structures induced in post-nodal pieces of chick blastoderm exposed to an RNA-enriched fraction from adult heart. Differentiation 11:13–17, 1978.
6. Girard H: Arterial pressure in the chick embryo. Am J Physiol 224:454–460, 1974.
7. Romanoff A: In: The avian embryo: structure and functional development. New York: Macmillan, 1960.
8. Sperelakis N: Changes in membrane electrical properties during development of the heart. In: Zipes DP, Bailey JC, Elharrar V (eds) The slow inward current and cardiac arrhythmias. Boston: Martinus Nijhoff, 1980, pp 221–262.
9. Shimizu Y, Tasaki K: Electrical excitability of developing cardiac muscle in chick embryos. Tohoku J Exp Med 88:49–56, 1966.
10. Yeh BK, Hoffman BF: The ionic basis of electrical activity in embryonic cardiac muscle. J Gen Physiol 52:666–681, 1967.
11. Couch JR, West TC, Hoff HE: Development of the action potential of the prenatal rat heart. Circ Res 24:19–31, 1969.
12. Boethius J, Knutsson E: Resting membrane potential in chick muscle cells during ontogeny. J Exp Zool 174:281–286, 1970.
13. Sperelakis N, Shigenobu K: Changes in membrane properties of chick embryonic hearts during development. J Gen Physiol 60:430–453, 1972.
14. McDonald TF, De Haan RL: Ion levels and membrane potential in chick heart tissue and cultured cells. J Gen Physiol 61:89–109, 1973.
15. Bernard C: Establishment of ionic permeabilities of the myocardial membrane during embryonic development of the rat. In: Lieberman M, Sano T (eds) Developmental and physiological correlates of cardiac muscle. New York: Raven, 1976, pp 169–184.
16. Sperelakis N: Pacemaker mechanisms in myocardial cells during development of embryonic chick hearts. In: Developments in cardiovascular medicine. Vol 17: Bouman LN, Jongsma HJ (eds) Cardiac rate and rhythm: physiological, morphological, and developmental aspects. The Hague: Martinus Nijhoff, 1982, pp 129–165.
17. Pappano AJ: Sodium-dependent depolarization of non-innervated embryonic chick heart by acetylcholine. J Pharmacol Exp Ther 180:340–350, 1972.
18. Carmeliet EE, Horres CR, Lieberman M, Vereecke JS: Developmental aspects of potassium flux and permeability of the embryonic chick heart. J Physiol (Lond) 254:673–692, 1976.
19. De Haan RL: The potassium-sensitivity of isolated embryonic heart cells increases with development. Dev Biol 23:226–240, 1970.
20. Löffelholz K, Pappano AJ: Increased sensitivity of sinoatrial pacemaker to acetylcholine and to catecholamines at the onset of autonomic neuroeffector transmission in chick embryo heart. J Pharmacol Exp Ther 191:479–486, 1974.
21. Pappano AJ: Action potentials in chick atria: ontogenic changes in the dependence of tetrodotoxin-resistant action potentials on calcium, strontium, and barium. Circ Res 39:99–105, 1976.
22. Sperelakis N: (Na^+-K^+)-ATPase activity of embryonic chick heart and skeletal muscles as a function of age. Biochim Biophys Acta 266:230–237, 1972.
23. Sperelakis N, Lee EC: Characterization of (Na^+-K^+)-ATPase isolated from embryonic chick hearts and cultured chick heart cells. Biochim Biophys Acta 233:562–579, 1971.
24. Klein RL: Ontogenesis of K and Na fluxes in embryonic chick heart. Am J Physiol 199:613–618, 1970.
25. Klein RL, Horton CR, Thureson-Klein A: Studies on nuclear amino acid transport and cation content in embryonic myocardium of the chick. Am J Cardiol 25:300–310, 1970.
26. Thureson-Klein A, Klein RL: Cation distribution and cardiac jelly in early embryonic hearts: a histochemical and electron microscopic study. J Mol Cell Cardiol 2:31–40, 1971.
27. Harsch M, Green JW: Electrolyte analyses of chick embryonic fluids and heart tissue. J Cell Comp Physiol 62:319–326, 1963.
28. Sperelakis N: Origin of the cardiac resting potential. In: Berne RM, Sperelakis N (eds) Handbook of physiology: the cardiovascular system. Vol 1: The heart. Bethesda MD: American Physiological Society, 1979, pp 187–267.
29. Thomas RC: Electrogenic sodium pump in nerve and muscle cells. Physiol Rev 52:563–594, 1972.
30. Deleze J: Possible reasons to drop of resting potential of mammalian heart preparations during hypothermia. Circ Res 8:553–557, 1960.
31. Page E, Storm SR: Cat heart muscle in vitro. VIII. Active transport of sodium in papillary muscles. J Gen Physiol 48:957–972, 1965.
32. Vassalle M: Electrogenic suppression of automaticity in sheep and dog Purkinje fibers. Circ Res 27:361–377, 1970.
33. Glitsch HG: An effect of the electrogenic sodium pump on the membrane potential in beating guinea-pig atria. Pflugers Arch 344:169–180, 1973.
34. Isenberg G, Trautwein W: The effect of dihydro-

ouabain and lithium ions on the outward current in cardiac Purkinje fibers: evidence for electrogenicity of active transport. Pflugers Arch 350:41–54, 1974.
35. Noma A, Irisawa H: Contribution of an electrogenic sodium pump to the membrane potential in rabbit sinoatrial node cells. Pflugers Arch 358:289–301, 1975.
36. Lieberman M, Horres CR, Aiton JF, Johnson EA: Active transport and electrogenicity of cardiac muscle in tissue culture. In: 27th Proceedings of the International Congress of Physiological Sciences, Paris, vol 13, 1977, p 446.
37. Pelleg A, Vogel S, Belardinelli L, Sperelakis N: Overdrive suppression of automaticity in cultured chick myocardial cells. Am J Physiol 238:H24–H30, 1980.
38. Coraboeuf E, Le Douarin G, Obrecht-Coutris G: Release of acetylcholine by chick embryo heart before innervation. J Physiol (Lond) 206:383–395, 1970.
39. McLean MJ, Sperelakis N: Retention of fully differentiated electrophysiological properties of chick embryonic heart cells in culture. Dev Biol 50:134–141, 1976.
40. Jongsma HJ, Masson-Pevet M, De Bruyne J: Synchronization of the beating frequency of cultured rat heart cells. In: Lieberman M, Sano T (eds) Developmental and physiological correlates of cardiac muscle. New York: Raven, 1976, pp 185–196.
41. Sperelakis N, Lehmkuhl D: Effect of current on transmembrane potentials in cultured chick heart cells. J Gen Physiol 47:895–927, 1964.
42. Sperelakis N, Lehmkuhl D: Ionic interconversion of pacemaker and non-pacemaker cultured chick heart cells. J Gen Physiol 49:867–895, 1966.
43. Sperelakis N: Electrophysiology of cultured chick heart cells. In: Sano T, Mizuhira V, Matsuda K (eds) Electrophysiology and ultrastructure of the heart. Tokyo: Bunkodo, 1967, pp 81–108.
44. Pappano AJ, Sperelakis N: Low K^+ conductance and low resting potentials of isolated single cultured heart cells. Am J Physiol 217:1076–1082, 1969.
45. Rajala GM, Pinter MJ, Kaplan S: Response of the quiescent heart tube to mechanical stretch in the intact chick embryo. Dev Biol 61:330–337, 1977.
46. Rosenquist GC: Localization and movement of cardiogenic cells in the chick embryo: heart-forming portion of the primitive streak. Dev Biol 22:461–475, 1970.
47. Deshpande AK, Siddiqui MAQ: A reexamination of heart muscle differentiation in the postnodal piece of chick blastoderm mediated by exogenous RNA. Dev Biol 58:230–247, 1977.
48. Shigenobu K, Sperelakis N: Development of sensitivity to tetrodotoxin of chick embryonic hearts with age. J Mol Cell Cardiol 3:271–286, 1971.
49. Sperelakis N, Shigenobu K, McLean MJ: Membrane cation channels: changes in developing hearts, in cell culture, and in organ culture. In: Lieberman M, Sano T (eds) Developmental and physiological correlates of cardiac cells. New York: Raven, 1976, pp 209–234.
50. Iijima T, Pappano AJ: Ontogenetic increase of the maximal rate of rise of the chick embryonic heart action potential: relationship to voltage, time and tetrodotoxin. Circ Res 44:358–367, 1979.
51. Marcus NS, Fozzard H: Tetrodotoxin sensitivity in the developing and adult chick heart. J Mol Cell Cardiol 13:335–340, 1981.
52. Pappano AJ: Calcium-dependent action potentials produced by catecholamines in guinea pig atrial muscle fibers depolarized by potassium. Circ Res 27:379–390, 1970.
53. Shigenobu K, Sperelakis N: Ca^{++} current channels induced by catecholamines in chick embryonic hearts whose fast Na^+ channels are blocked by tetrodotoxin or elevated K^+. Circ Res 31:932–952, 1972.
54. Schneider JA, Sperelakis N: The demonstration of energy dependence of the isoproterenol-induced transcellular Ca^{++} current in isolated perfused guinea pig hearts: an explanation for mechanical failure of ischemic myocardium. J Surg Res 16:389–403, 1974.
55. McLean MJ, Shigenobu K, Sperelakis N: Two pharmacological types of slow Na^+ channels as distinguished by verapamil blockade. Eur J Pharmacol 26:379–382, 1974.
56. Shigenobu K, Schneider JA, Sperelakis N: Blockade of slow Na^+ and Ca^{++} currents in myocardial cells by verapamil. J Pharmacol Exp Ther 190:280–288, 1974.
57. Galper JB, Catterall WA: Developmental changes in the sensitivity of embryonic heart cells to tetrodotoxin and D 600. Dev Biol 65:216–227, 1978.
58. Kasuya Y, Matsuki N, Shigenobu K: Changes in sensitivity to anoxia of the cardiac action potential plateau during chick embronic development. Dev Biol 58:124–133, 1977.
59. Nathan RD, De Haan RL: In vitro differentiation of a fast Na^+ conductance in embryonic heart cell aggregates. Proc Natl Acad Sci USA 75:2776–2780, 1978.
60. Ishima Y: The effect of tetrodotoxin and sodium substitution on the action potential in the course of development of the embryonic chicken heart. Proc Jpn Acad 44:170–175, 1978
61. Renaud JF, Romey G, Lombet A, Lazdunski M: Differentiation of the fast Na^+ channel in embryonic heart cells: interaction of the channel with neurotoxins. Proc Natl Acad Sci USA 78:5248–5352, 1981.
62. Sperelakis N: Electrical properties of embryonic heart cells. In: De Mello WC (ed) Electrical phenomena in the heart. New York: Academic, 1972, pp 1–61.
63. McDonald TF, Sachs HG, De Haan RL: Development of sensitivity to tetrodotoxin in beating chick

embryo hearts, single cells, and aggregates. Science 176:1248–1250, 1972.
64. McDonald TF, Sachs HG: Electrical activity in embryonic heart cell aggregates. Pflugers Arch 354:151–164, 1975.
65. De Haan RL, McDonald TF, Sachs HG: Development of tetrodotoxin sensitivity of embryonic chick heart cells in vitro. In: Lieberman T, Sano T (eds) Developmental and physiological correlates of cardiac muscle. New York: Raven, 1976, pp 155–168.
66. McLean MJ, Lapsley RA, Shigenobu K, Murad R, Sperelakis N: High cyclic AMP levels in young embryonic chick hearts. Dev Biol 42:196–201, 1975.
67. Renaud J-F, Sperelakis N, Le Douarin G: Increase of cyclic AMP levels induced by isoproterenol in cultured and non-cultured chick embryonic hearts. J Mol Cell Cardiol 10:281–286, 1978.
68. Novak E, Drummond GI, Skala J, Hahn P: Development changes in cyclic AMP, protein kinase, phosphorylase kinase, phosphorylase in liver, heart and skeletal muscle of the rat. Arch Biochem Biophys 150:511–518, 1972.
69. Zalin RJ, Montague W: Changes in cyclic AMP, adrenylate cyclase and protein kinase levels during the development of embryonic chick skeletal muscle. Exp Cell Res 93:55–62, 1975.
70. Sperelakis N, Pappano AJ: Physiology and pharmacology of developing heart cells. In: Papp JG (ed) International encyclopedia of pharmacology and therapeutics. Oxford: Pergamon, 1983 (in press).
71. Haddox MK, Roeske WR, Russell DH: Independent expression of cardiac type I and II cyclic AMP-dependent protein kinase during murine embryogenesis and postnatal development. Biochim Biophys Acta 585:527–534, 1979.
72. Chen F-CM, Yamamura HI, Roeske WR: Adenylate cyclase and *beta* adrenergic receptor development in the mouse heart. J Pharmacol Exp Ther 222:7–13, 1982.
73. Guidotti G, Kanemeishi D, Foa PP: Chick embryo heart as a tool for studying cell permeability and insulin action. Am J Physiol 201:863–868, 1961.
74. Guidotti G, Loreti L, Gaja G, Foa PP: Glucose uptake in the developing chick embryo heart. Am J Physiol 211:981–987, 1966.
75. Kutchai H, King SL, Martin M, Daves ED: Glucose uptake by chicken embryo hearts at various stages of development. Dev Biol 55:92–102, 1977.
76. Guidotti G, Foa PP: Development of an insulin-sensitive glucose transport system in chick embryo hearts. Am J Physiol 201:869–872, 1961.
77. Elsas LJ, Wheeler FB, Dannes DJ, De Haan RL: Amino acid transport by aggregates of cultured chicken hearts: effect of insulin. J Biol Chem 250:9381–9390, 1975.
78. Herman BA, Fernandez BS: Developmental changes in membrane fluidity of cultured myogenic cells [abstr]. Physiologist 19:223, 1976.
79. Harris W, Days R, Johnson C, Flinkelstein I, Stallworth J, Hubert C: Studies on avian heart pyruvate kinase during development. Biochem Biophys Res Commun 75:1117–1121, 1977.
80. Cardenas JM, Bandman E, Strohman RC: Hybrid isozymes of pyruvate kinase appear during avian cardiac development. Biochem Biophys Res Commun 80:593–599, 1978.
81. Harary I: Biochemistry of cardiac development: In vivo and in vitro studies. In: Berne RM, Sperelakis N (eds) Handbook of physiology: the cardiovascular system. Vol 1: The Heart. Bethesda MD: American Physiological Society, 1979, pp 43–60.
82. Coffey R, Chendelin V, Newburgh R: Glucose utilization by chick embryo heart homogenates. J Gen Physiol 48:105–112, 1964.
83. Paul J: In: Wilmer ED (ed) Cells and tissues in culture. Vol 1. New York: Academic, 1965, pp 239–276.
84. Seltzer JL, McDougal DB: Enzyme levels in chick embryo heart and brain from 1–21 days of development. Dev Biol 42:95–105, 1975.
85. Warshaw JB: Cellular energy metabolism during fetal development. IV. Fatty acid activation, acyl transfer and fatty acid oxidation during development of the chick and rat. Dev Biol 28:537–544, 1972.
86. Fine IH, Kaplan NV, Kuftinec D: Developmental changes of mammalian lactic dehydrogenase. Biochemistry 4:116–124, 1963.
87. Cahn RD, Kaplan NO, Levine L, Zwilling E: Nature and development of lactic dehydrogenase. Science 136:962–969, 1962.
88. Cahn RD: Developmental changes in embryonic enzyme patterns: the effect of oxidative substrates on lactic dehydrogenase in beating chick embryonic heart cell cultures. Dev Biol 9:327–346, 1964.
89. Ziter FA: Creatine kinase in developing skeletal and cardiac muscle of the rat. Exp Neurol 43:539–546, 1974.
90. Sperelakis N, Lehmkuhl D: Effects of temperature and metabolic poisons on membrane potentials of cultured heart cells. Am J Physiol 213:719–724, 1967.
91. Vleugels A, Carmeliet E, Bosteels S, Zaman M: Differential effects of hypoxia with age on the chick embryonic hearts: changes in membrane potential, intracellular K and Na, K efflux and glycogen. Pflugers Arch 365:159–166, 1976.
92. Thyrum PT: Reduced transmembrane calcium flow as a mechanism for the hypoxic depression of cardiac contractility. J Int Res Commun 1:1b, 1973.
93. Hibbs RG: Electron microscopy of developing cardiac muscle in chick embryos. Am J Anat 99:17–52, 1956.
94. Sperelakis N, Shigenobu K: Organ-cultured chick embryonic hearts of various ages. I: Electrophysiology. J Mol Cell Cardiol 6:449–471, 1974.
95. Shigenobu K, Sperelakis N: Failure of development of fast Na^+ channels during organ culture of young

embryonic chick hearts. Dev Biol 39:326–330, 1974.
96. Renaud JF, Sperelakis N: Electrophysiological properties of chick embryonic heart grafted and organ cultured in vitro. J Mol Cell Cardiol 8:889–900, 1976.
97. McLean MJ, Renaud JF, Sperelakis N, Niu MC: mRNA induction of fast Na^+ channels in cultured cardiac myoblasts. Science 191:297–299, 1976.
98. Sperelakis N, McLean MJ, Renaud JF, Niu MC: Membrane differentiation of cardiac myoblasts induced in vitro by an RNA-enriched fraction from adult heart. In: Niu MC, Chuang HH (eds) The role of RNA in development and reproduction (Second International Symposium, Peking, China, 23–30 April 1980). New York: Science Press, Beijing and Van Nostrant Reinhold, 1981, pp 730–771.
99. McLean MJ, Renaud JF, Niu MC, Sperelakis N: Membrane differentiation of cardiac myoblasts induced in vitro by an RNA-enriched fraction from adult heart. Exp Cell Res 110:1–14, 1977.
100. Sperelakis N, Lehmkuhl D: Effect of current on transmembrane potentials in cultured chick heart cells. J Gen Physiol 47:895–927, 1964.
101. Sperelakis N: Cultured heart reaggregate model for studying cardiac toxicology. Proceedings of the conference on cardiovascular toxicology, Washington, D.C. Environ Health Perspect 26:243–267, 1978.
102. Jones JK, Paull K, Proskauer CC, Jones R, Lepeschkin E, Rush S: Ultrastructural changes produced in cultured myocardial cells by electric shock [abstr]. *Fed Proc* 34:972, 1975.
103. Renaud JF, Scana AM, Kazazoglou T, Lombet A, Romez G, Lazdunski M: Normal serum and lipoprotein-deficient serum give different expressions of excitability, corresponding to different stages of differentiation, in chick cardiac cells in culture. Proc Natl Acad Sci USA, 1983. (in press).
104. Josephson I, Renaud JF, Vogel S, McLean M, Sperelakis N: Mechanisms of the histamine-induced positive inotropic action in cardiac muscle. Eur J Pharmacol 35:393–398, 1976.
105. Vogel S, Sperelakis N, Josephson I, Brooker G: Fluoride stimulation of slow Ca^{++} current in cardiac muscle. J Mol Cell Cardiol 9:461–475, 1977.
106. Sperelakis N, Lehmkuhl D: Insensitivity of cultured chick heart cells to autonomic agents and tetrodotoxin. Am J Physiol 209: 693–698, 1965.
107. Sperelakis N, Pappano AJ: Increase in P_{Na} and P_K of cultured heart cells produced by veratridine. J Gen Physiol 53:97–114, 1969.
108. Sperelakis N: Effects of cardiotoxic agents on the electrical properties of myocardial cells. In: Balazs T (ed) Cardiac toxicology, vol 1. Boca Raton FL: CRC, 1981, pp 39–108.
109. Catterall WA: Activation of the action potential Na^+ ionophore of cultured neuroblastoma cells by veratridine and batrachotoxin. J Biol Chem 250:4053–4059, 1975.
110. Pang DC, Sperelakis N: Veratridine stimulation of calcium uptake by chick embryonic heart cells in culture. J Mol Cell Cardiol 14:703–709, 1982.
111. Romey G, Lazdunski M: Lipid-soluble toxins thought to be specific for Na^+ channels block Ca^{2+} channels in neuronal cells. Nature 297:79–80, 1982.
112. Fabiato A, Fabiato F: Calcium and cardiac excitation–contraction coupling. Am Rev Physiol 41:473–484, 1979.
113. Schneider JA, Sperelakis N: Slow Ca^{++} and Na^+ current channels induced by isoproterenol and methylxanthines in isolated perfused guinea pig hearts whose fast Na^+ channels are inactivated in elevated K^+. J Mol Cell Cardiol 7:249–273, 1975.
114. Watanabe AM, Besch HR Jr: Cyclic adenosine monophosphate modulation of slow calcium influx channels in guinea pig hearts. Circ Res 35:316–324, 1974.
115. Pappano AJ, Biegon RL: Mechanisms for muscarinic inhibition of calcium-dependent action potentials and contractions in developing ventricular muscle: the role of cyclic AMP. In: Hoffman BF, Lieberman M, Paes de Carvalho AP (eds) Normal and abnormal conduction of the heartbeat. Mt Kisco NY: Futura, in press (1983).
116. Sperelakis N, Schneider JA: A metabolic control mechanism for calcium ion influx that may protect the ventricular myocardial cell. Am J Cardiol 37:1079–1085, 1976.
117. Reuter H: Localization of beta adrenergic receptors, and effects of noradrenaline and cyclic nucleotides on action potentials, ionic currents and tension in mammalian cardiac muscle. J Physiol (Lond) 242:429–451, 1974.
118. Josephson I, Sperelakis N: 5′-Guanylimidodiphosphate stimulation of slow Ca^{++} current in myocardial cells. J Mol Cell Cardiol 19:1157–1166, 1978.
119. Vogel S, Sperelakis N: Induction of slow action potentials by microiontophoresis of cyclic AMP into heart cells. J Mol Cell Cardiol 13:51–64, 1981.
120. Isenberg G: Is potassium conductance of cardiac Purkinje fibers controlled by $[Ca^{++}]_i$? Nature 243:273–274, 1975.
121. Chesnais JM, Coraboeuf E, Sauviat MP, Vassas JM: Sensitivity to H, Li and Mn ions of the slow inward sodium current in frog atrial fibres. J Mol Cell Cardiol 7:627–642, 1975.
122. Vogel S, Sperelakis N: Blockade of myocardial slow inward current at low pH. Am J Physiol 233:C99–C103, 1977.
123. Belardinelli L, Vogel SM, Sperelakis N, Rubio R, Berne RM: Restoration of inward slow current in hypoxic heart muscle by alkaline pH. J Mol Cell Cardiol 11:877–892, 1979.
124. Tsien RW, Giles W, Greengard P: Cyclic AMP mediates the effects of adrenaline on cardiac Purkinje fibers. Nature [New Biol] 240:181–183, 1972.

125. Li T, Sperelakis N: Stimulation of slow action potentials in guinea pig papillary muscle cells by intracellular injection of cyclic AMP, Gpp(NH)p, and cholera toxin. Circ Res 52:111–117, 1983.
126. Reuter H, Scholz H: The regulation of the calcium conductance of cardiac muscle by adrenaline. J Physiol (Lond) 264:49–62, 1977.
127. Sperelakis N, Belardinelli L, Vogel SM: Electrophysiological aspects during myocardial ischemia. In: Proceedings of the 8th world congress of cardiology (Tokyo 1978). Amsterdam: Excerpta Medica, 1979, pp 229–236.
128. Greengard P: Cyclic nucleotides, phosphorylated proteins, and neuronal function. New York: Raven, 1978.
129. Carty D, Sperelakis N, Villar-Palasi C: Ca^{++}-antagonistic drugs reverse cyclic AMP-dependent phosphorylation of heart sarcolemmal proteins. Biochem Pharmacol (submitted for publication).
130. Rinaldi ML, Capony JP, Demaille JC: The cyclic AMP-dependent modulation of cardiac sarcolemmal slow calcium channels. J Mol Cell Cardiol 14:279–289, 1982.
131. Sperelakis N, McLean MJ: The electrical properties of embryonic chick cardiac cells. In: Longo LD, Reneau DD (eds) Fetal and newborn cardiovascular physiology. Vol 1: Developmental aspects. New York: Garland, 1978, pp 191–236.
132. Sperelakis N, McLean MJ: Electrical properties of cultured chick heart cells. In: Dhalla NS, Sano T (eds) Recent advances in studies on cardiac structure and metabolism, vol 12. Baltimore: University Park Press, 1978, pp 645–666.
133. Yamada S, Yamamura HI, Roeske WR: Ontogeny of c_1-adrenergic receptors in the mammalian myocardium. Eur J Pharmacol 68:217–221, 1980.
134. Chen F-CM, Yamamura HI, Roeske WR: Ontogeny of mammalian myocardial β-adrenergic receptors. Eur J Pharmacol 58:255–264, 1979.
135. Roeske WR, Yamamura HI: Maturation of mammalian myocardial muscarinic cholinergic receptors. Life Sci 23:127–132, 1978.

27. AGING OF THE ADULT HEART

Edward G. Lakatta

Introduction

Both quantitative and qualitative assessment of normal cardiovascular function differ with age of the organism studied [1–4]. Thus, functional studies of the normal heart at a single age are incomplete and represent only a point on a continuum. A full understanding of heart function in stressful or pathologic states must consider that age-related changes modify the substrate upon which the stress or disease process is superimposed and that the expression of a given pathologic state is not solely due to the disease per se, but represents an age–disease interaction. Striking examples of this interaction can be observed in cardiac overload states [5] or in the effect of adaptation of the myocardium to chronic physical conditioning [6].

The present chapter summarizes the results of studies which have investigated the effect of aging on some aspects of cardiac function discussed elsewhere in this volume. This approach appears optimal for integration of the aging variable into our current understanding of the function of the heart in normal and pathlogic states. Primary emphasis is given to studies of cardiac function over the adult range, i.e., from adulthood to senescence; in addition, since the majority of these studies have been implemented in the rat aging model, this species is the focus of discussion.

Cardiac Mass and Ultrastructure

An increase in cardiac mass has been noted to occur with advancing age in many species, including man [2, 7]. In man, the gradual increase in systolic blood pressure likely due to progressive stiffening of the central arteries is an apparent cause of the cardiac hypertrophy [2]. In some rodent strains, while hypertension is present in advanced age and may be causally related to the cardiac hypertrophy, in others hypertrophy occurs even in the absence of an elevated blood pressure at rest [7, 8]. In the Wistar strain, in which several aspects of cardiac biochemistry and physiology have been studied with respect to advanced age, the extent of left ventricular hypertrophy occurring between adulthood (six months) and senescence (24 months) is 20%–40% depending on whether heart mass is referenced to body size, i.e., tibial length, or to body weight (fig. 27–1). Since body weight decreases during senescence, the 40% hypertrophy assessed by the left ventricular/body weight is probably an overestimate [9]. Absolute left ventricular weight increases 20%. There is no change in water content and, while hydroxyproline concentration nearly doubles [10], the absolute amount can account for only 1%–2% increase in mass. The average cell volume increases approximately 20% between adulthood and senescence and thus nearly all of the increase in heart mass is due to an increase in cell mass [9]. The density of subcellular organelles has not been precisely quantitated over this age range. Coronary atherosclerosis is not present in this rat strain and under light microscopy the age of the hearts cannot be determined on the basis of coronary artery appearance [10]. Quantitative studies of capillary density and fiber densities have demonstrated a decrease in the former and a reduction in their ratio [11, 12]. As in most other tissues, lipofuscin granules within the cell increase with advancing age

N. Sperelakis (ed.), PHYSIOLOGY AND PATHOPHYSIOLOGY OF THE HEART.

Martinus Nijhoff Publishing, Boston/The Hague/
Dordrecht/Lancaster.

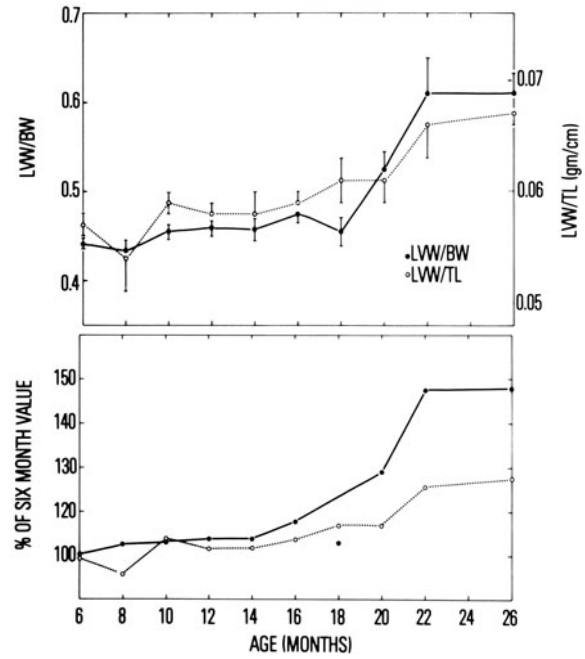

FIGURE 27–1. The effect of age on the ratios of left ventricle to body weight (LVW/BW) and to tibial length (LVW/TL) in the Wistar rat. In the lower panel these ratios have been normalized to the 6 month value. From Yin et al. [9].

[13], but these have no apparent functional significance.

Many functional aspects of the senescent heart resemble those in hearts which have hypertrophied in response to an experimentally increased work load. These include changes in myocardial catecholamine content, action potential configuration, contraction duration, viscoelastic properties, velocity of sarcoplasmic reticulum Ca^{2+} accumulation, myofibrillar ATPase activity, and protein synthesis [1, 4]. As we proceed to discuss age-related changes in the heart it is important to determine whether these apparent age-related changes in the heart can be attributed to hypertrophy per se.

Excitation–Contraction

ACTION POTENTIAL

The effect of adult age on cardiac action potential characteristics has been studied in rat atria and ventricles, guinea pig ventricles, and canine Purkinje fibers. Resting membrane potential does not vary with age [14–19]. In unstretched rat atria [14, 15], a substantial increase in action potential duration occurs during maturation from the neonatal period (two months) to adulthood (6–12 months) with no further change through senescence (28 months). Similarly, in unloaded rat ventricular endocardium, no changes were observed in action potential duration or refractory period between adult and senescent hearts [16], and a similar effect of age on the duration of unstretched canine Purkinje fiber action potential has been observed [17].

The characteristics of the cardiac action potential are not fixed, but vary with many experimental factors. One such factor is the feedback interaction between excitation and contraction, i.e., either mechanical factors or Ca^{2+} loading of the cell modulate the action potential duration [20]. To examine the relation between the action potential and contraction, the two must be studied simultaneously. In isolated guinea pig right ventricular papillary muscles [18], si-

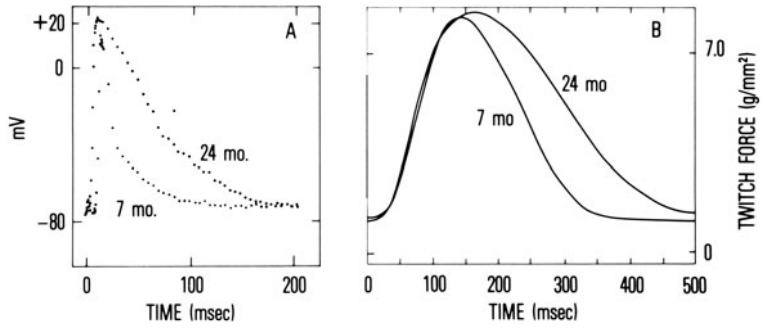

FIGURE 27–2. *(A)* Typical transmembrane action potentials measured in right ventricular papillary muscles isolated from adult (seven-month) and senescent (24-month) rat hearts. Muscles were stimulated to contract regularly at 24 min^{-1} at 29°C in Krebs–Ringer solution containing $[Ca^{2+}]$ of 2.5 m*M*. The length of the muscles was that at which optimal force development in response to excitation occurred (L_{max}). *(B)* Typical isometric contractions in right ventricular papillary muscles isolated from adult and senescent rat hearts and measured under conditions as in *A*. Redrawn from Wei et al. [19].

multaneous measurements of the isometric twitch and transmembrane action potential made over a wide range of stimulation frequencies (30–400/min) indicate that both the plateau phase of the action potential and the contraction duration were prolonged in muscles from three- to four-month versus 26- to 40-month animals. With respect to the consideration of *adult* aging it cannot be determined whether the age changes observed in this study occur over the adult to senescent period or, like the studies in unloaded rat cardiac tissues [14], occur mainly over the maturational period in this species. In right ventricular papillary muscles contracting isometrically at the peak of their length–tension curve, prolongation of both action potential and contraction duration were observed in muscles from senescent (24-months) versus adult (6–8 months) animals [19]. Typical action potentials from a senescent and adult muscle are illustrated in figure 27–2A, and typical isometric contractions in figure 27–2B. Greater overshoot and substantially greater area above 0 mV and repolarization times were observed in the senescent versus adult [19] muscles, and these differences persisted across a wide range of perfusate $[Ca^{2+}]$. The particular alterations in ionic currents during the "slow" and repolarization phases of the action potential that change with age in each of the studies cited remain to be established. Plausible hypotheses include that with advancing age: (a) slow inward current is enhanced, or (b) electrogenic Na^+-Ca^{2+} exchange or outwardly directed K^+ current is retarded, possibly due to a delay or other differences in the excitation-induced increase myoplasmic Ca^{2+} transient.

Prolongation of the isometric twitch with advancing age (fig. 27–2B) has been observed in a variety of preparations from a variety of species [16, 21, 22]. The precise relationship between the prolongation of the action potential and contraction duration in the senescent heart also remains to be established. Plausible explanations include that with advancing age: (a) prolonged depolarization retards the restitution of myoplasmic Ca^{2+} to is preexcitation level, and this retards relaxation; (b) a delayed cellular Ca^{2+} transient causes a delay in outwardly directed currents; or (c) prolongation of the electrical and mechanical parameters are unrelated and independently reflect prolonged restitution of preexcitation ionic gradients at the cell membrane and within the myoplasmic space. The prolonged excitation–contraction cycle observed in the senescent rat myocardium is of particular functional significance when the interval between the two successive stimuli becomes progressively shortened (fig. 27–3). Note that when the interstimulus interval is reduced to 160 ms, a contraction can be elicited

in only 20% of senescent muscles while at 120 ms all senescent muscles studied fail to contract. This could be due primarily to electrical refractoriness, e.g., delayed restitution of those aspects of excitation required to trigger the release of Ca^{2+} within the cell and/or to delay restitution of Ca^{2+} cycling within the cell from the previous contraction, possibly representing electromechanical dissociation which can be elicited in this species [23].

SARCOPLASMIC RETICULUM

In isolated cardiac cells or mechanically skinned cell fragments, a small increase in myoplasmic Ca^{2+} effects the release of Ca^{2+} from the sarcoplasmic reticulum [24, 25] and this has been referred to as *Ca^{2+} induced-Ca^{2+} release*. Once initiated, the cycle of Ca^{2+} release and reuptake can perpetuate itself without requiring additional Ca^{2+} input into the cell, i.e., under some Ca^{2+}-loading conditions, spontaneous Ca^{2+}-Ca^{2+} release occurs [24, 25]. Recent evidence that sarcoplasmic-reticulum-generated Ca^{2+} induced-Ca^{2+} release occurs in intact preparations of a wide variety of species has been recently obtained using laser-spectroscopic methods [26, 27]. The rat, in particular, demonstrates spontaneous sarcoplasmic-reticulum-generated Ca^{2+} oscillation under experimental conditions similar to those in figures 27–2 and 27–3, i.e., those usually employed in studies of excitation-contraction mechanisms in cardiac muscle in vitro.

Age differences in Ca^{2+} uptake or release by sarcoplasmic reticulum could in part explain the failure to generate a contraction in response to a premature stimulus (fig. 27–3). Indeed, under some conditions, cell fragments from the senescent rat heart require a greater trigger concentration of $[Ca^{2+}]$ to release Ca^{2+} from the sarcoplasmic reticulum [28]. In addition, the rate of Ca^{2+} accumulation in isolated sarcoplasmic reticulum over that range of pCa expected to occur within the cell subsequent to excitation is substantially reduced in vesicles isolated from senescent versus adult hearts (fig. 27–4). A similar result was obtained comparing isolated sarcoplasmic reticulum from maturational (3–4 months) hearts to that from senescent (24–25 months) hearts [29]. In addition, since no age difference was observed in the (Mg^{2+},Ca^{2+})-ATPase activities in that study, it has been suggested that the diminution in Ca^{2+} transport resulted from an age effect on the efficiency of coupling of ATP hydrolysis to Ca^{2+} transport [29]. However, since sarcoplasmic reticulum from adult, i.e., six- to 12-month rat hearts was not examined

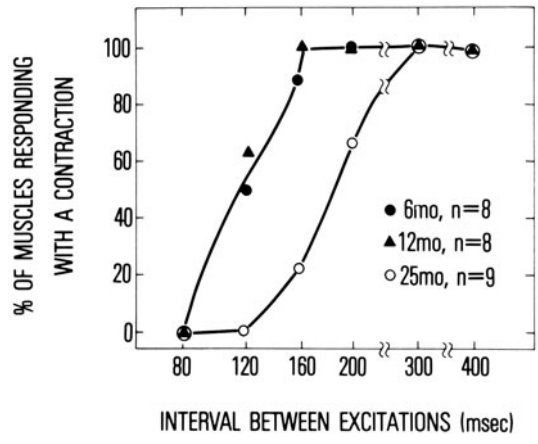

FIGURE 27–3. The effect of adult age on the mechanical response to a reduction in the interval between successive stimuli. Redrawn from Lakatta et al. [16].

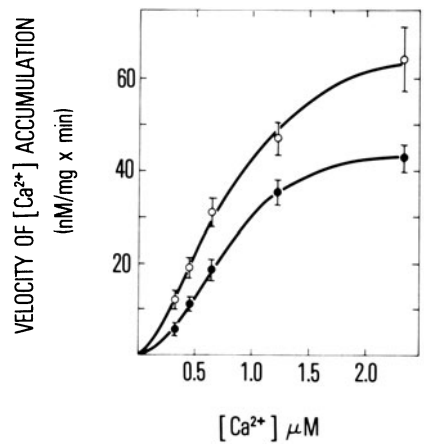

FIGURE 27–4. The velocity of Ca^{2+} accumulation in sarcoplasmic reticulum isolated from six- to eight-month (○) and 24- to 25-month (●) rat hearts. The curves are different at the $P < 0.001$ by analysis of variance. From Froehlich et al. [30].

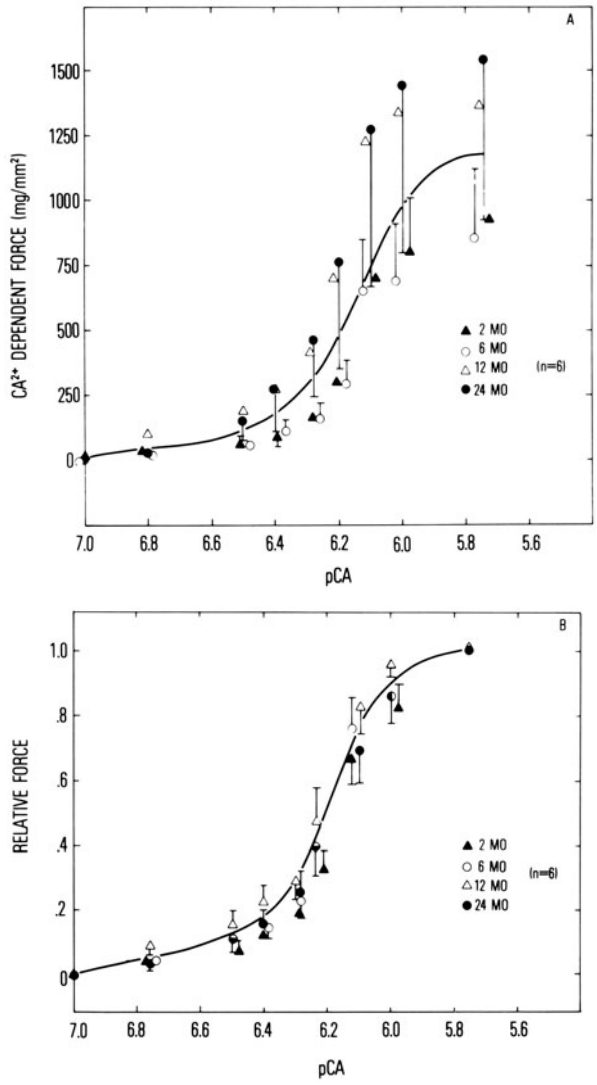

FIGURE 27–5. *(A)* The effect of age from the neonatal to senescent period on steady levels of force across a range of pCa. *(B)* The data in each preparation have been normalized to their maximal level. From Bhatnagar et al. [32].

in this study, it cannot be determined whether this conclusion pertains to adult aging of the heart or reflects a maturational process.

A reduced rate of sarcoplasmic reticulum Ca^{2+} sequestration could result in delayed relaxation not only in a given contraction (fig. 27–2B), but also in response to a subsequent premature stimulus (fig. 27–3), since the extent of Ca^{2+} reloading within the sarcoplasmic reticulum might not be sufficient to respond to a trigger for its release [28]. Thus, both prolonged contraction duration and delayed restitution of the excitation–contraction cycle in the senescent heart could be explained by age differences in the rate of sarcoplasmic Ca^{2+} transport or in requirements for its release. Although the fundamental mechanisms for the age differences evident in figures 27–2 to 27–4 require further elucidation, these differences are so striking that the rat-aging model would appear to be an important tool for studies of excitation-contraction coupling in the heart [30].

Force Production, Stiffness, and Shortening

In Ca^{2+}-activated muscle, force and stiffness are determined by the interaction between the myofilaments (i.e., number of cross-bridges) and their geometric linkage to nonactivation-dependent structures, e.g., collagen and membranes. The force and stiffness properties of the latter, i.e., passive properties, can be separated from activation-dependent force and stiffness under conditions in which Ca^{2+} activation of the myofilaments is assumed to be absent. In classic mechanics this assumption has been made during the interval between stimuli (i.e., diastolic period) or in the unstimulated state. Some recent studies, however, suggest that this assumption may not be valid in cardiac muscle, especially that from the rat, where intermittent random asychronous Ca^{2+} activation of the myofilaments in the unstimulated state results from spontaneous Ca^{2+} oscillations and accounts for a small portion of resting force [26, 31].

Under conditions when the purely passive properties of muscle might be measured, precise characterization of myofilament activation from force and stiffness measurements requires modeling of the geometric arrangement or linkage of myofilaments and passive viscoelastic structures. Measurement of force or stiffness over a range of Ca^{2+} activation rather than at a single level can circumvent this problem to a certain extent and may provide information regarding myofilament interaction.

In muscle preparations chemically skinned with detergent, steady-state force production across the range of pCa that is likely to occur subsequent to excitation is not altered by age (fig. 27–5A). That the shape of the relative force–pCa curve is not age-related (fig. 27–5B) also suggests that sensitivity of troponin C to Ca^{2+} also may not be age-related.

In muscles with intact membranes, because of the sarcolemmal barrier and sequestration of Ca^{2+} within the cell, force production in response to an excitation varies over a higher range of perfusate $[Ca^{2+}]$, $[Ca^{2+}]_e$. In intact adult rat cardiac muscle, force development varies over a rather relatively narrow range of $[Ca^{2+}]_e$ compared to most other species (fig. 27–6). This marked shift of the $[Ca^{2+}]_e$-developed force relationship in the rat to lower $[Ca^{2+}]_e$ cannot result from a difference in the force–pCa relationship as in figure 27–5, because this is fairly constant among species [28]. Rather it is most likely attributable to a species difference in cellular Ca^{2+} loading. Since the frequency and amplitude of Ca^{2+} oscillations referred to earlier vary with the extent of cellular Ca^{2+} loading, changes in the intensity fluctuations in scattered light which result from these oscillations can monitor changes in cellular Ca^{2+} loading even in the absence of stimulation [26, 33]. As illustrated in figure 27–6A, a marked shift in Ca^{2+} loading as monitored by this technique is observed in the rat and likely determines the shift in the force–$[Ca^{2+}]_e$ relationship observed in this species (fig. 27–6B). It is also important to note that in isolated cardiac muscle, when $[Ca^{2+}]_e$ exceeds a maximum, force production falls (see rat in fig. 27–6B) and, thus, studies of the effect of $[Ca^{2+}]_e$ or other inotropic perturbations that enhance $[Ca^{2+}]_e$ loading should be performed over the optimal range of $[Ca^{2+}]_e$, i.e., less than 3m*M* in the rat muscle stimulated at low frequencies at moderately low temperatures; when $[Ca^{2+}]_e$ is kept low, the response in rat cardiac muscle to inotropic perturbation is qualitatively similar to that of other species [21, 31, 34]. Over the adult range, aging does not affect the $[Ca^{2+}]_e$-developed force relationship over the optimal range of $[Ca^{2+}]_e$ (fig. 27–7A). In addition, at optimal $[Ca^{2+}]_e$, the effect of resting muscle length, which also modulates the extent of myofilament activation at a given $[Ca^{2+}]_e$ [35, 36]. on developed force production is not altered by age (fig. 27–7B).

While peak twitch force is not altered with advancing age, other characteristics of the twitch do exhibit age-related changes. The prolong twitch time (fig. 27–2B) is accompanied by prolonged stiffness (fig. 27–8A). Both the time to peak stiffness and force as well as the time for their relaxation times are prolonged. These findings have consistently been observed in several studies [6, 7, 37] and suggest that the time course of activation is prolonged with adult aging of the myocardium [4]. In addition, the slope stiffness coefficient, α, as deter-

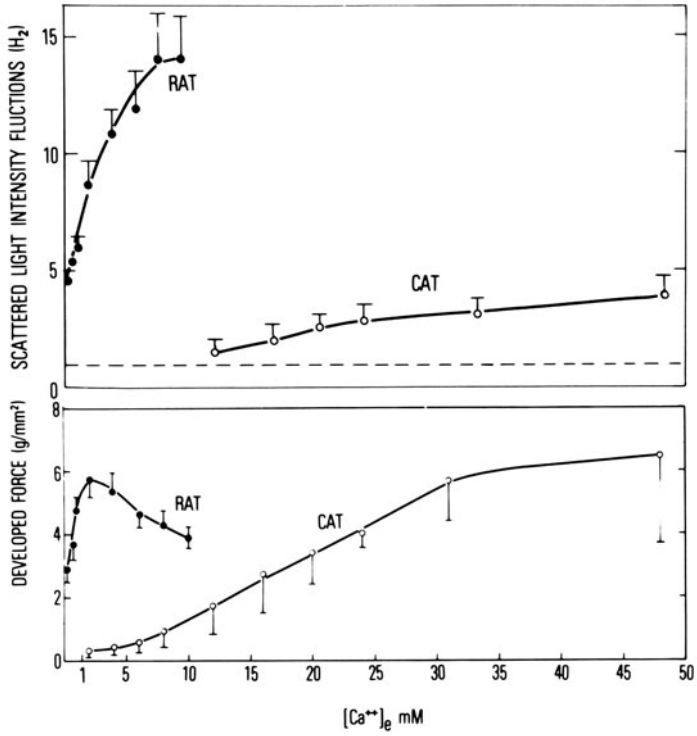

FIGURE 27–6. The effect of $[Ca^{2+}]_e$ on scattered light intensity fluctuations caused by spontaneous diastolic cellular Ca^{2+} oscillations *(A)* measured prior to an excitation and force developed in response to that excitation *(B)* is isolated rat ($n = 3$) and cat ($n = 3$) cardiac muscles. Stimulus frequency was 2 min^{-1} and temperature was 29°C. It is important to note that the curves in the figure are not unique, but vary with stimulation frequency, particularly in the cat. Also, the frequency of scattered light fluctuations is greater than the frequency of the underlying cellular Ca^{2+} oscillations because the amplitude of cellular motion caused by the Ca^{2+} oscillations is up to severalfold greater than the wavelength of the laser beam (0.5 nm) used to detect the microscopic motion.

mined from the relationship of stiffness to force during the twitch is increased with advancing age (fig. 27–8B). This apparently does not result from an age difference in passive (i.e., nonmyofilament activation related) viscoelastic properties, since prior to excitation in "resting" muscle, the slope stiffness coefficient is not age-related [7, 37].

The prolonged time-course twitch of force and stiffness and the enhanced slope stiffness coefficient during twitch observed in cardiac muscles from senescent versus adult rats are not fixed, but can be modified by chronic physical conditioning [6]. Figure 27–9 illustrates the effect of mild daily exercise (treadmill running) for five months (approximately 20% of the rat's lifespan) on contraction duration as a function of length (figure 27–9A) and $[Ca^{2+}]_e$ (fig. 27–9B). Note that this mild exercise protocol had no effect on twitch characteristics or contraction duration in muscles from adult animals. In muscles from senescent animals, however, contraction duration was reduced to those levels observed in their younger adult counterpart. Similarly, the time course of stiffness and the slope stiffness coefficient, α, were reduced by exercise in the senescent, but not in the adult muscles [6]. In addition to demonstrating that certain properties commonly observed in the myocardium from aged rats can be modified by exercise, these results also provide a striking example on the influence of age on the effects of physical conditioning in cardiac muscle. Since physical conditioning does not alter the

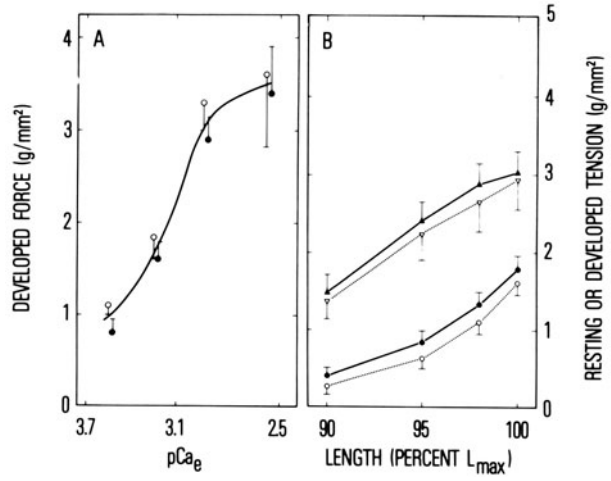

FIGURE 27–7. *(A)* The effect of $[Ca^{2+}]_e$ on twitch force in left ventricular trabeculae carneae isolated from adult (6–8 months), ●, and senescent (25 months), ○, Wistar rats. Muscles were stimulated to contract isometrically at 24 min^{-1} at 29°C. From Lakatta and Yin [4]. *(B)* The effect of resting muscle length on resting force (circles) and twitch force (triangles) in left ventricular trabeculae carneae from adult (closed symbols) and senescent (open symbols) rat hearts. Stimulation rate was 24 min^{-1} and $[Ca^{2+}]_e$ was 2.5 m*M*. L_{max} is that length at which twitch force was optimal. Redrawn from Yin et al. [7].

collagen content in the heart [38, 39], reversal of prolonged contraction duration and altered stiffness properties in the senescent heart suggests that these properties of the senescent heart are not attributable to enhanced collagen content [10]. In addition, it is important to note this level of physical conditioning did not alter heart weight or heart weight/body weight either group of animals, but did obliterate the prolonged time-course twitch force and stiffness in the senescent heart. This indicates that these properties of senescent myocardium cannot be attributed to the cardiac hypertrophy per se of the senescent heart. This point is also clearly illustrated by the results of another study, which created the same extent of hypertrophy present in the senescent heart in middle-aged adult rats by banding the aorta [7]. Although muscles from the hypertrophied left ventricles of the banded animals exhibited a prolonged twitch and increased α compared to controls, the magnitudes of these were not as great as those observed in the senescent heart.

While one major function of cardiac muscle is to stiffen to produce force, the other major and ultimate function is to shorten in order to eject blood. The speed of shortening, according to the cross-bridge, sliding-filament, theories of muscle contraction, is ultimately determined by the kinetics of cross-bridge cycling. The velocity of shortening is inversely related to the load which the filaments bear. At very light loads (or zero load if this experiment were feasible) the maximum velocity of shortening will occur and will reflect the maximum cross-bridge cycling rate. The maximum velocity of shortening also depends on the level of myofilament Ca^{2+} activation, which is not constant but varies with time during the twitch. Studies of the effect of age on velocity of shortening have documented a decline over the maturational period [22, 40, 41] and have suggested that a further decline may occur with adult aging [40]. It is important to note that these measurements of the effect of age on shortening velocity have not taken into consideration that the time course of Ca^{2+} activation may be altered with age. Thus, differences in shortening velocity observed in muscles from different aged rats following a release (i.e., permitted to shorten) at a given time following stimulation

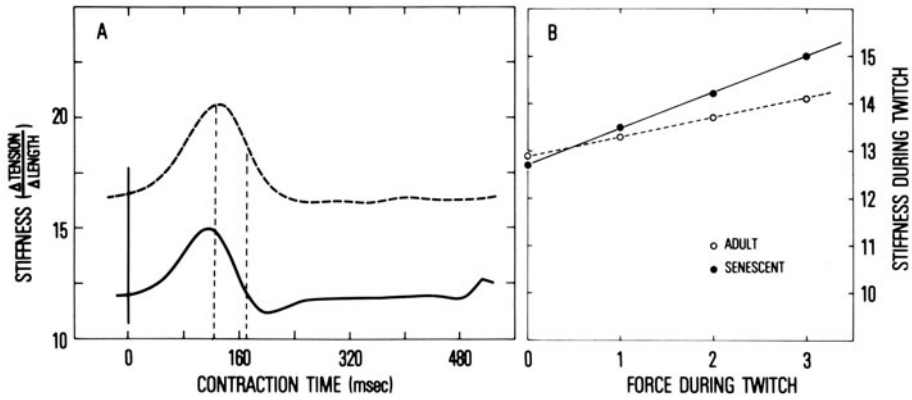

FIGURE 27–8. *(A)* The average time course of stiffness in left ventricular trabeculae carneae isolated from senescent (n = 17, dotted) and adult (n = 8, solid) rats. To permit the measurement of stiffness during an isometric twitch, a servomotor system capable of producing fine gradations in length superimposed on the basic isometric preparation was designed. By means of this system a length perturbation with any forcing function desired up to a peak amplitude of 0.24 mm at frequencies from DC to 100 Hz could be superimposed on the study length. These particular studies employed a sinusodial length function with maximum amplitude limited to 0.025 mm. Control circuits limited the application of perturbation to 20 successive cycles at the probing frequency (25 Hz in this case) and generated a synchronization pulse field stimulation of the muscle via platinum electrodes (5 ms, supramaximal voltage) by a Grass SD5 stimulator after precisely 1.5 perturbations. The sequence was repeated at 5-s intervals. An additional reference contraction (devoid of perturbations) was evoked midway between each of the perturbed cycles. By subtracting unperturbed twitches, an approximation of force development due only to the length of perturbation throughout the time course of the muscle contraction was derived. Combining the force and length data, a resulting dynamic stiffness, defined at dT/dL is obtained. *(B)* Slope stiffness coefficient derived from the relationship of stiffness to force during the twitch in muscles in *A*. Active contraction stiffness is a linear function of force (stiffness = α F + B) and is given for both age groups. The age difference is in α or the slope (0.41 ± 0.14 in the adult muscles, n = 8, versus 0.76 ± 0.05 in the senescent muscles, n = 17, $P < 0.03$) while the intercept, B, is not age-related (12.9 ± 0.14 in the adult versus 12.7 ± 1.3 in the senescent muscles). Redrawn from Spurgeon et al. [37].

may in part be due to age-related differences in Ca^{2+} activation at that time rather than indicative of specific age-related differences of intrinsic cross-bridge kinetics.

Parameters of the isometric twitch in some instances can provide indirect assessment of cross-bridge cycling rate. The maximum rate of force production, dF/dt, is determined in part by the velocity of cross-bridge cycling. However, other factors, i.e., both active and passive stiffness, and the synchrony of activation among cells comprising the muscle, also determine maximum dF/dt and, since these may vary with age, the observation that maximum dF/dt maximum is unaffected by age (fig. 27–10A) over a broad age range does not necessarily indicate that the cross-bridge cycling rate at a particular level of Ca^{2+} activation is unaltered by aging. Time to peak force and contraction duration, which have been observed to vary inversely with shortening velocity [42, 43], increase with age over a broad range (fig. 27–10A), but these are also determined by the time courses of the myoplasmic Ca^{2+} transient and myofilament activation, which are apparently prolonged with age. The fact that shortening velocity is dependent on the level of Ca^{2+} activation precludes the interpretation that prolonged time to peak tension or contraction duration necessarily indicate a diminished cross-bridge cycling rate in senescent versus adult cardiac muscle.

The maximum myofilament ATPase activity correlates directly with shortening velocity and inversely with contraction times [42, 43]. Actomyosin, myosin, and myofibrillar ATPase

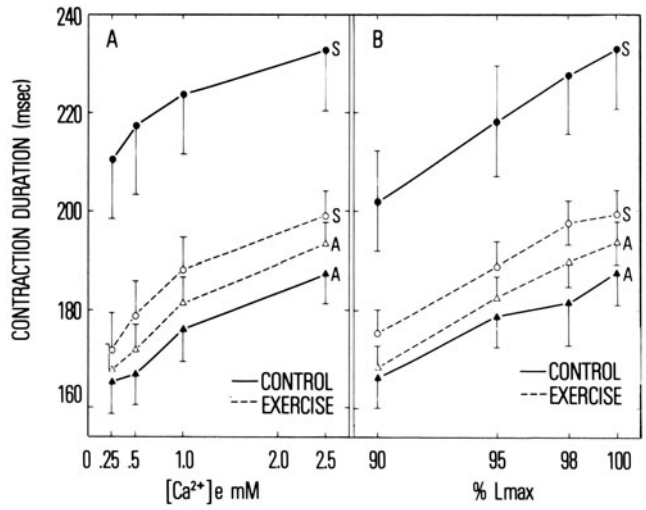

FIGURE 27–9. The effect of chronic daily wheel exercise on contraction duration (time from stimulus artifact to half-relaxation of force) in left ventricular trabeculae carneae from adult and senescent rats as a function of resting muscle length *(A)*, and $[Ca^{2+}]_e$ *(B)*: S, senescent (24 months); A, adult (6–8 months); C, control; E, exercised. Muscles were stimulated at 24 min^{-1} at 29°C, $[Ca^{2+}]_e$ = 2.5 m*M* in *A* and muscle length is L_{max} in *B*. The exercise protocol did not significantly change developed force or maximal rate of force development in either age group. Reprinted from Spurgeon et al. [6].

(fig. 27–10A) do decline with age, but the major portion of this decline occurs during the maturational period, with very little additional change from midlife to senescence. The Ca^{2+} dependence of myofibrillar ATPase activity over that range of pCa expected to occur during a twitch does not vary with age (fig. 27–10B). It is noteworthy that while expressed as *ATPase activity* of a given preparation, ATP hydrolysis per se is not the rate-limiting step of the cross-bridge cycle, and that the methods employed measure the overall sequence of intermediate reactions that occur in the enzyme hydrolytic cycle from Ca^{2+} binding to product release [44]. In this regard, the off rate of Ca^{2+} from troponin may be a determinant both of cross-bridge kinetics of the duration of activation. The effect of age on Ca^{2+} dissociation from the myofilaments remains to be determined.

Adrenergic Modulation

A substantial literature in man and intact animals suggests that adrenergic responsiveness of the cardiovascular system diminishes with advancing age [45]. Studies in isolated tissue demonstrate a diminished postsynaptic component of the beta responsiveness with age [46–48]. Two main aspects of beta-adrenergic modulation of the cardiac cell are to increase contractility and to reduce contraction duration (the relaxant response). Figure 27–11 illustrates that in the myocardium the contractile response to isoproterenol decreases with adult age, while relaxant response is unaltered with aging. Similar results were observed in response to norepinephrine [46]. In isolated sarcoplasmic reticulum, in the presence of exogenous protein kinase, the increase in Ca^{2+} velocity in response to a wide range of cAMP (cyclic AMP) concentrations is not age-related [49, 50]. Since stimulation of the Ca^{2+} accumulation rate in sarcoplasmic reticulum is a potential mechanism to explain the relaxant effect of beta-adrenergic stimulation in cardiac muscle, these results in isolated sarcoplasmic reticulum are in accord with the results obtained in figure 27–11A. That the contractile and relaxant effects of beta-adrenergic stimulation can be separated in the senescent heart

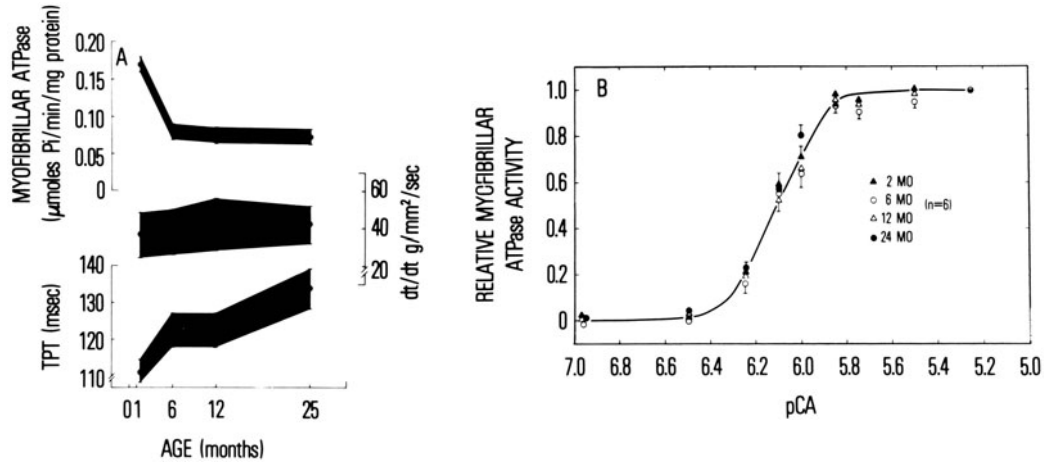

FIGURE 27–10. *(A)* The effect of age on the maximum rate of myofibrillar ATPase activity, time to peak twitch force, and maximum rate of twitch force development. Myofibrillar ATPase activity was measured in detergent-purified myofibrils at pCa of 5.8 (see *B*). Mechanical parameters were measured at L_{max} at $[Ca^{2+}]_e$ = 2.5 m*M* in right ventricular papillary muscles stimulated to contract regularly at 24 min^{-1} at 29°C. Reprinted from Bhatnagar et al. [32].

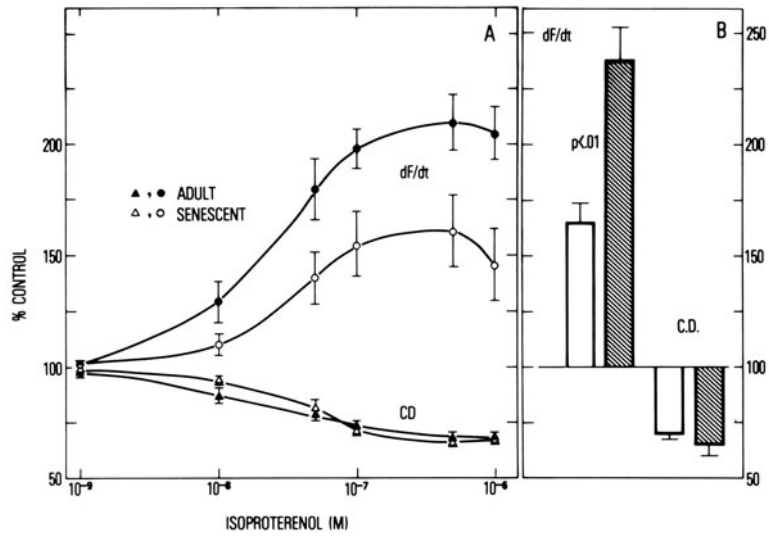

FIGURE 27–11. *(A)* The contractile (dF/d*t*) and relaxant (CD) effects of isoproterenol in vascularly perfused interventricular septa from adult (●) and senescent (○) rats. Prior to isoproterenol, dF/d*t* was not age-related, but CD was significantly greater in the septa from senescent hearts. *(B)* The effect of dibutyryl cAMP on the maximum rate of force production (dF/d*t*) and contraction duration (CD). Redrawn from Lakatta et al. [46].

suggests that this model may be useful for studies designed to elucidate further the mechanism of catecholamines at the subcellular level. The mechanism for the diminished effect of beta-adrenergic agonists on contractility cannot be explained solely by diminished myofilament or energetic responses to enhanced myoplasmic Ca^{2+} resulting from beta stimulation, because when Ca^{2+} is enhanced without stimulation of the beta-adrenergic pathway, the contractile response does not differ with age (fig. 27–7). Age differences in the extent of myofilament phosphorylation which would alter Ca^{2+} binding and ATPase activity at a *given* pCa may be a potential mechanism to explain the age difference. Conversely, age differences in phosphorylation or the change in Ca^{2+} transport resulting from cAMP-dependent phosphorylation of the sarcolemma are also viable hypotheses to explain the results in figure 27–11. In either case, the mechanism of the age difference in contractile response is apparently distal to cAMP-dependent activation of protein kinase, since isoproterenol increases cAMP and activates protein kinase to the same extent in adult and senescent hearts [47]. This suggests that age differences at the beta receptor do not occur or are not implicated in the diminished response. That the age deficit in contractile response is still observed when dibutyryl cAMP rather than Isoproterenol is employed as the agonist (fig. 27–11B) provides additional support for this hypothesis.

Measurements of beta-receptor numbers and affinity by agonist and antagonist binding indicate that these are not altered with adult aging [47, 51]. However, a difference in beta-receptor affinity for catecholamine agonist was observed when senescent rats (24 months) were compared to rats in the maturational stage of development [52]. Furthermore, a diminution in adenylate cyclase activity in response to guanine nucleotides, NaF, and isoproterenol has been observed to occur with maturation [52, 53]. This age difference in adenylate cyclase stimulation occurs apparently somewhere between maturation and adulthood, i.e., between three and 12 months of age, because no difference was observed between preparations from 12- and 24-month animals [53]. It is of

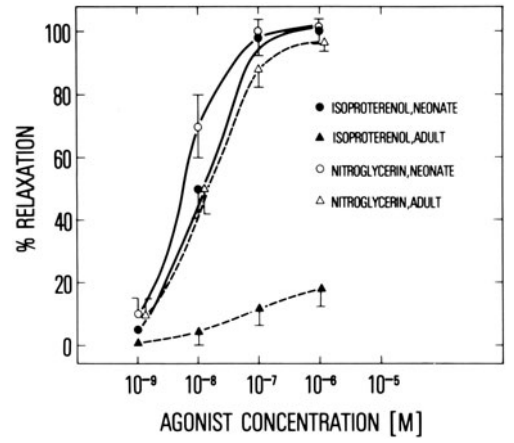

FIGURE 27–12. The effect of isoproterenol and nitroglycerin on relaxation of thoracic aorta isolated from neonatal (46–59 days) and adult (279–294 days) rats. Note that, while the response to isoproterenol is markedly reduced in the older rats, the response to nitroglycerin remains intact. Redrawn from Fleisch and Hooker [56].

interest to note also that the hyperthyroid state stimulates an increase in beta-receptor density in the rat at all ages, including senescence [54, 55].

Several studies have indicated that a loss of beta-adrenergic-induced relaxation of systemic vasculature occurs with aging [48, 56]. The extent of this decline is marked, occurs over the maturational period (fig. 27–12), and persists into advanced age [57, 58]. Treatment of animals with large quantities of thyroxine for three months restored a significant portion of the relaxant response to beta-adrenergic stimulation in those elderly (22 months) rats [58].

Not many studies have focused on the age-related changes in cholinergic modulation of the heart at the cellular level. Vagotomy failed to increase heart rate in senescent versus adult anesthetized rats [59]. It has been observed that concentrations of acetylcholine in rat atria become markedly depressed with adult aging [60]. In addition, threshold responsiveness to vagal nerve stimulation declines [61] and response to high-frequency stimulation is diminished in senescence [59]. Direct application of methacholine in vagotomized rats resulted in a diminished slowing of heart rate in senescent

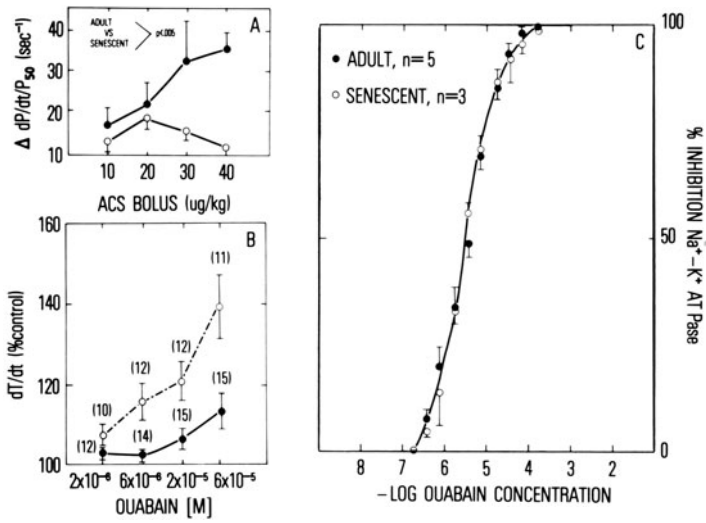

FIGURE 27–13. *(A)* The inotropic (dP/dT/P) response to acute bolus infusion of acetylstrophanthidin (ACS) in awake unanesthetized adult (13 years and senescent ● (11–13 years) ○ beagles. *(B)* The contractile (dT/d*t*) response to ouabain in left ventricular trabeculae carneae from adult (○) and senescent (●) rat hearts. Muscles were stimulated at 24 min^{-1} at 29°C at L_{max} in $[Ca^{2+}]_e$ of 0.25 m*M*. dT/d*t* prior to ouabain was not age-related. Redrawn from Gerstenblith et al. [34]. *(C)* The effect of ouabain inhibition of (Na, K)-ATPase in membrane preparation from adult and senescent beagles studies in *A*. No age difference was present in the absolute activity of ouabain-sensitive (Na, K)-ATPase. Redrawn from Guarnieri et al. [66].

versus adult and neonatal anesthetized rats [59]. While acetylcholine in low concentrations affected a greater change in guanosine monophosphate in tissue slices from senescent versus adult rat hearts, at higher acetylcholine concentrations, no age difference was observed [62].

Cardiac Glycosides

The sensitivity to cardiac glycosides changes dramatically with age in the rat model such that at moderate temperatures and low rates of stimulation the response virtually disappears after approximately the first 21 days of life [63]. Adult rat muscles under these conditions will respond to glycosides when Ca^{2+} loading is lowered by a prior reduction in $[Ca^{2+}]_e$. However, the range of concentrations of glycosides required to elicit an inotropic response is high compared to adult cardiac muscle from other species, in part, to decreased ability of the glycosides to bind to rat cardiac sarcolemma [64, 65]. Studies of the effect of adult age on the inotropic response to glycosides demonstrate a marked reduction in muscles from senescent adult rats (fig. 27–13A), while the inotropic response in these same senescent muscles to continual paired pacing is greater than that to ouabain and equal to that in the adult muscles [34]. The effect of adult age on neither the total density of (Na^+,K^+)-ATPase sites nor ouabain binding to these sites has been determined. It is noteworthy that, in purified sarcolemmal preparations isolated from senescent rats, the density of Na^+-K^+ receptor sites is not substantially changed from that in preparations from maturational animals [29]. The relative ouabain inhibition of (Na^+,K^+)-ATPase in rat membrane preparations is not altered with adult age [34]. A similar picture emerges from studies of the inotropic response to acetylstrophanthidin in adult (1–3 years) and senescent (11–13 years) beagles [66], i.e., a substantial reduction in the inotropic response was observed in the elderly dogs (fig. 27–13B), while relative inhibition of ATPase was not age-related (fig. 27–13C). Additional studies

to delineate the mechanism(s) of the reduced response to glycosides in senescent myocardium might provide a useful tool to probe the long-standing enigma of precisely how glycosides alter the Ca^{2+} loading of the cardiac cell.

Metabolism

ENERGY METABOLISM

In order for cyclic actomyosin interaction to occur, energy is required in diastole for intracellular pumps to maintain $[Na^+]_i$ and $[Ca^{2+}]_i$ at levels far from their thermodynamic equilibria, and during systole for contractile protein displacement. In order to precisely relate energy metabolism to function, the two must be studied simultaneously; this has been accomplished in a single study examining the effect of adult age on oxidative metabolism in isolated perfused working rat hearts [67]. In that study following 30 min of the most strenuous conditions employed, moderate (i.e., approximately 20%) decrements in oxygen consumption, palmitate oxidation, ATP, creatine phosphate, and ATP/ADP were observed in hearts isolated from 24- to 28-month Fischer rats versus those from five- to 12-month animals. An increase in the glycolytic flux of about the same magnitude (though not statistically significant) also occurred in the hearts of animals of advanced age. Measurements of total work, i.e., wall stress during the cardiac cycle, were not made and it is impossible to determine whether the reduction in aerobic metabolism was actually appropriate for decreased external component of work in the senescent hearts as estimated from heart rate $\times$ systolic pressure [67]. An alternate hypothesis is that the reduction in maximum coronary flow per gram heart weight of approximately 20% observed in this and another study [68] compromises maximum oxygen supply, which limits oxidative metabolism and an increased glycolysis under strenuous work loads. A more marked increase in glycoloytic rate accompanied by a diminution in aerobic metabolism has also been observed in homogenates from senescent versus adult rat hearts and it has been hypothesized that with advanced age a "shift" from aerobic to glycolytic energy production occurs [69]. In that study, however, the functional status of the hearts was not monitored. Oxidation of palmitate is diminished in mitochondria isolated from senescent versus adult hearts [70] and this represents an additional plausible mechanism for the diminution in respiration observed in the intact heart when palmitate is employed as a substrate. Respiration of other substrates, i.e., glutamate–pyruvate, or glutamate–malate, is also reduced, but other substrates, i.e., succinate and ascorbate, are oxidized equally well in mitochondria from senescent and adult hearts. The effect of age on mitochondrial energetics has been recently extensively reviewed elsewhere [71].

With a reduction of perfusate P_{O_2}, a shift to more glycolytic energy production occurs. Senescent cardiac muscle is able to withstand extended periods of hypoxia as well as adult muscles (fig. 27–14). During recovery from hypoxia developed force recovery is equal in both age groups. Contraction duration exhibits a marked overshoot in both groups, but this is much more pronounced in the senescent muscles [20]. With reoxygenation, myoplasmic $[Ca^{2+}]$ increases transiently and the exaggerated contraction duration in the senescent myocardium may be attributable to the altered Ca^{2+} sequestration characteristics observed in isolated sarcoplasmic reticulum from senescent rat hearts (fig. 27–4).

PROTEIN METABOLISM

The effect of age on myocardial protein turnover has been studied in mouse and rat strains, in intact animals, isolated hearts, and cell-free systems. All studies in either species have demonstrated that a decrease in protein synthesis occurs from the maturational or growth phase to the adult period [72–77]. In hearts from three-month versus 24-month animals, the older group had a diminution in myocardial RNA concentration of 20%, a 50% reduction in the rate of RNA synthesis, and a 35% reduction in protein synthesis [76]. The results suggested that, with aging, the number of ribosomes decreased, and since RNA degradation in the aged hearts was also decreased to 40% of that observed in the maturational animals,

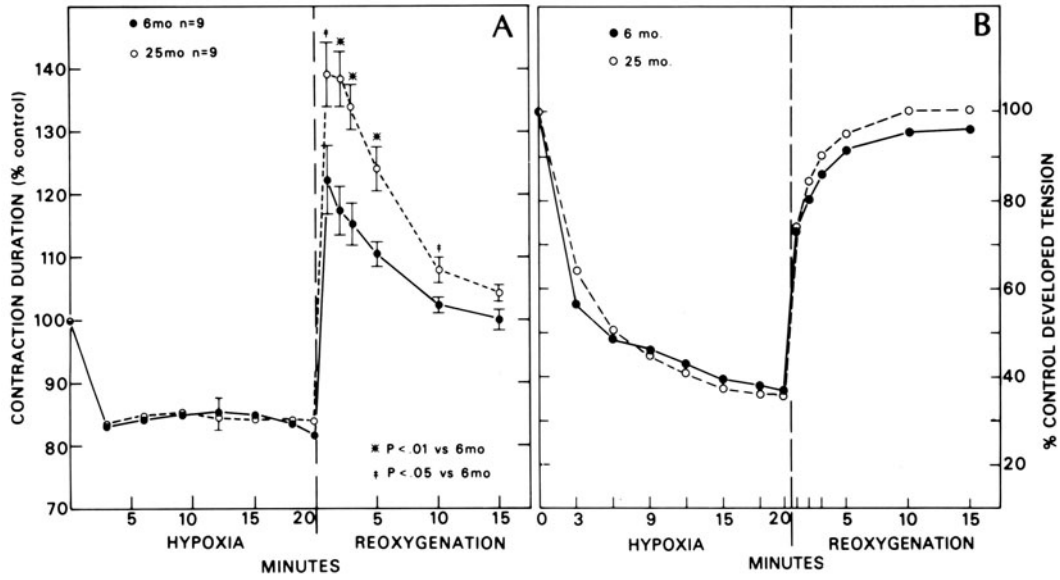

FIGURE 27–14. The effect of advanced adult age on twitch force *(B)* and contraction *(A)* duration during hypoxia and recovery from hypoxia. Muscles were stimulated to contract at 24 min^{-1} at L_{max} at 29°C in $[Ca^{2+}]_e$ of 2.2 m*M*. Prior to hypoxia, twitch force was not age-related, but contraction duration was increased in muscles from 24-month animals. Redrawn from Lakatta et al. [16].

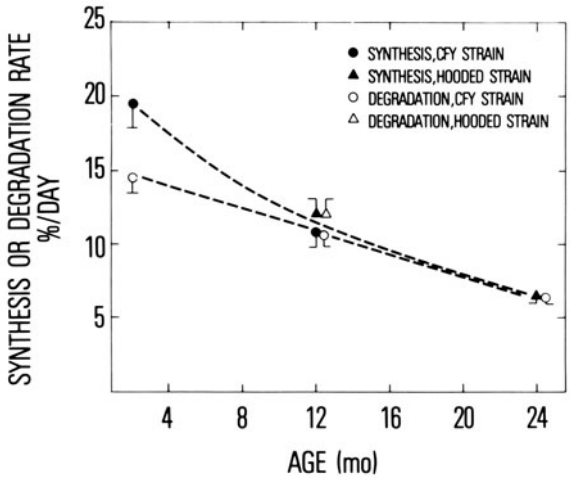

FIGURE 27–15. The effect of age on in vivo protein synthesis in two strains of rats. Redrawn from Crie et al. [77].

that the rate of transcription is also reduced. Since exogenous transfer RNA was without effect at three months but increased the rate of protein synthesis in cell sap preparations from the senescent hearts by 40%–50%, a slowing down at the translational step was also suggested. In toto, these studies clearly demonstrate that the rate of protein synthesis decreases after the growth phase and suggest that this is attributable to decreases in the rate of both transcription and translation. The question of whether protein synthesis or degradation is altered with *adult* aging in rats has been addressed more recently in a study which compared the rate of protein synthesis and degradation at three points across a broad age range [77]. Note that between 12 and 24 months an approximate 45% decrease was observed in the rates of both protein synthesis and degradation (fig. 27–15). In the mouse model a 26% decrease in the rate of protein synthesis was also observed between seven and 26 months; thyroid injections enhanced the rate of synthesis in the older animals to levels near those in younger animals [73]. Thus, even after the growth phase ends, a further reduction in the rate of protein turnover occurs between adulthood and senescence in both mice and rats. The diminu-

tion in protein turnover rates suggests that the "lifespan" of cardiac proteins is increased in the senescent heart, but no effects of the rates of protein synthesis and degradation on function are currently known. It is noteworthy that, in cardiac hypertrophy in younger animals caused by left ventricular pressure overload, the rate of protein synthesis and degradation were, as in the aging heart, also diminished, and this has led to the hypothesis that this form of hypertrophy represents *accelerated aging* [75, 76, 78]. However, additional studies are required to substantiate this hypothesis [4].

References

1. Gerstenblith G, Lakatta EG, Weisfeldt ML: Age changes in myocardial function and exercise response. Prog Cardiovasc Dis 19:1–21, 1976.
2. Lakatta EG: Alterations in the cardiovascular system that occur in advanced age. Fed Proc 38:163–167, 1979.
3. Lakatta EG: Heart. In: Masoro EJ (ed) CRC handbook of physiology of aging. Boca Ranton FL: CRC, 1981, pp 269–282.
4. Lakatta EG, Yin FCP: Myocardial aging: functional alterations and related cellular mechanisms. Am J Physiol 242:H927–941, 1982.
5. Walford GD, Spurgeon HA, Lakatta EG: Volume overload hypertrophy in mid-late adult life diminishes contractile performance and prolongs contraction duration. Circulation 62:III-13, 1980.
6. Spurgeon HA, Steinbach MF, Lakatta EG: Chronic exercise prevents characteristic age-related changes in rat cardiac contraction. Am J Physiol (Heart Circ Physiol 13): H513–H518, 1983.
7. Yin FCCP, Spurgeon HA, Weisfeldt ML, Lakatta EG: Mechanical properties of myocardium from hypertrophied rat hearts: a comparison between hypertrophy induced by senescence and by aortic banding. Circ Res 46:292–300, 1980.
8. Rothbaum DA, Shaw DJ, Angell CS, Shock NW: Cardiac performance in the unanesthetized senescent male rat. J Gerontol 28:287–292, 1973.
9. Yin FCP, Spurgeon HA, Rakusan K, Weisfeldt ML, Lakatta EG: Use of tibial length to quantify cardiac hypertrophy: application in the aging rat. Am J Physiol 243 (Heart Circ Physiol 12): H941–H947, 1982.
10. Weisfeldt ML, Loeven, Shock NW: Resting and active mechanical properties of trabeculae carneae from aged male rats. Am J Physiol 220:1921–1927, 1971.
11. Rakusan K, Poupa O: Capillaries and muscle fibres in the heart of old rats. Gerontologia 9:107–112, 1964.
12. Tomanek RJ: Effects of age and exercise on the extent of the myocardial capillary bed. Anat Rec 167:55–62, 1970.
13. Travis DF, Travis A: Ultrastructural changes in the left ventricular rat myocardial cells with age. J Ultrastruct Res 39:124–148, 1972.
14. Cavoto FV, Kelliher GJ, Robert J: Electrophysiological changes in the rat atrium with age. Am J Physiol 226:1293–1297, 1974.
15. Roberts J, Goldberg PB: Changes in cardiac membranes as a function of age with particular emphasis on reactivity to drugs. In: Cristofalo VJ, Roberts J, Adelman RC (eds) Advances in experimental medicine and biology. Vol 61: Explorations in aging. New York: Plenum, 1975, pp 119–148.
16. Lakatta EG, Gerstenblith G, Angell CS: Prolonged contraction duration in aged myocardium. J Clin Invest 55:61–68, 1975.
17. Rosen MR, Reder RF, Hordof AJ, Davies M, Danilo P Jr: Age-related changes in Purkinje fiber action potentials of adult dogs. Circ Res 43:931–938, 1978.
18. Rumberger E, Timmermann J: Age-changes of the force–frequency-relationship and the duration of action potential isolated papillary muscles of guinea pig. Eur J Appl Physiol 34:277–284, 1976.
19. Wei JY, Spurgeon HA, Lakatta EG: Excitation-contraction in rat myocardium: alteration with adult aging. Am J Physiol (in press).
20. Gülch RW: The effect of elevated chronic loading on the action potential of mammalian myocardium. J Mol Cell Cardiol 12:415–420, 1980.
21. Lakatta EG: Excitation–contraction. In: Weisfeldt ML (ed) Aging. Vol 12: The aging heart: its function and response to stress. New York: Raven, 1980, pp 77–100.
22. Urthaler F, Walker AA, James TN: The effect of aging on ventricular contractile performance. Am Heart J 96:481–485, 1978.
23. Lee SE Mainwood GW, Korecky B: The electrical and mechanical response of rat papillary muscle to paired pulse stimulation. Can J Physiol Pharmacol 48:216–225, 1970.
24. Fabiato A, Fabiato F: Contraction induced by a calcium-triggered release of calcium from the sarcoplasmic reticulum of single skinned cardiac cells. J Physiol 249:469–495, 1975.
25. Dani AM, Cittadini A, Inesi G: Calcium transport and contractile activity in dissociated mammalian heart cells. Am J Physiol 237:C147–C155, 1979.
26. Stern MD, Kort AA, Bhatnagar GM, Lakatta EG: Scattered-light intensity fluctuations in diastolic rat cardiac muscle caused by spontaneous Ca^{++}-dependent cellular mechanical oscillations. J Gen Physiol 82:119–153, 1983.
27. Kort AA, Lakatta EG: Ca^{2+}-dependent mechanical oscillations occur spontaneously in unstimulated mammalian cardiac tissue. Circ Res, 1984 (in press).
28. Fabiato A: Calcium release in skinned cardiac cells: variations with species, tissues, and development. Fed Proc 41:2238–2244, 1982.

29. Narayanan N: Differential alterations in ATP-supported calcium transport activities of sarcoplasmic reticulum and sarcolemma of aging myocardium. Biochim Biophys Acta 678:442–459, 1981.
30. Froelich JP, Lakatta EG, Beard E, Spurgeon HA, Weisfeldt ML, Gerstenblith G: Studies of sarcoplasmic reticulum function and contraction duration in young adult and aged rat myocardium. J Mol Cell Cardiol 10:427–438, 1978.
31. Lakatta EG, Lappe DL: Diastolic scattered light fluctuation, resting force and twitch force in mammalian cardiac muscle. J Physiol (Lond) 315:369–394, 1981.
32. Bhatnagar GM, Walford DG, Beard ES, Humphries SH, Lakatta EG: ATPase activity and force production in myofibrils and twitch characteristics in intact muscle from neonatal, adult, and senescent rat myocardium. J Mol Cell Cardiol 1984 (in press).
33. Lappe DL, Lakatta EG: Intensity fluctuation spectroscopy monitors contractile activation in "resting" cardiac muscle. Science 207:1369–1371, 1980.
34. Gerstenblith G, Spurgeon HA, Froelich JP, Weisfeldt ML, Lakatta EG: Diminished inotropic responsiveness to ouabain in aged rat myocardium. Circ Res 44:517–523, 1979.
35. Jewell RB: A reexamination of the influence of muscle length on myocardial performance. Circ Res 40:221–230, 1977.
36. Lakatta EG, Spurgeon HA: Force staircase kinetics in mammalian cardiac muscle: modulation by muscle length. J Physiol (Lond) 299:337–352, 1980.
37. Spurgeon HA, Thorne PR, Yin FCP, Shock NW, Weisfeldt ML: Increased dynamic stiffness of trabeculae carneae from senescent rats. Am J Physiol 232:H373–380, 1977.
38. Holloszy JO, Booth FW: Biochemical adaptations to endurance exercise in muscle. Annu Rev Physiol 38:273–291, 1976.
39. Tomanek RJ, Taunton CA, Liskop KS: Relationship between age, chronic exercise, and connective tissue of the heart. J Gerontol 27:33–38, 1972.
40. Alpert NR, Gale HH, Taylor N: The effect of age on contractile protein ATPase activity and the velocity of shortening. In: Tanz RD, Kavaler F, Robert J (eds) Factors influencing myocardial contractility. New York: Academic, 1976, pp 127–133.
41. Heller LJ, Whitehorn WV: Age-associated alterations in myocardial contractile properties. Am J Physiol 222:1613–1619, 1972.
42. Close R: The relation between intrinsic speed of shortening and duration of the active state of muscle. J Physiol (Lond) 180:542–559, 1965.
43. Barany M: ATPase activity of myosin correlated with speed of muscle shortening. J Gen Physiol (Suppl) 50:197–216, 1967.
44. Marston SB, Taylor EW: Comparison of the myosin and actomyosin ATPase mechanisms of the four types of vertebrate muscles. J Mol Biol 139:573–600, 1980.
45. Lakatta EG: Age-related alterations in the cardiovascular response to adrenergic mediated stress. Fed Proc 39:3173–3177, 1980.
46. Lakatta EG, Gerstenblith G, Angell CS, Shock NW, Weisfeldt ML: Diminished inotropic response of aged myocardium to catecholamine. Circ Res 36:262–269, 1975.
47. Guarnieri T, Filburn CR, Zitnik G, Roth GS, Lakatta EG: Contractile and biochemical correlates of β-adrenergic stimulation of the aged heart. Am J Physiol 239:H501–H508, 1980.
48. Fleisch JH: Age-related decrease in beta adrenoceptor activity of the cardiovascular system. Trends Pharmacol Sci 2:337–339, 1981.
49. Beard ES, Lakatta: 1984 (in preparation).
50. Kadoma M, Froehlich J: Regulation of Ca^{2+} transport activity in sarcoplasmic reticulum from young and old hearts: effects of cAMP and protein kinase. 1984 (in preparation).
51. Abrass IB, Davis JL, Scarpace PJ: Isoproterenol responsiveness and myocardial β-adrenergic receptors in young and old rats. J Gerontol 37:156–160, 1982.
52. Narayanan N, Derby J-A: Alterations in the properties of β-adrenergic receptors of myocardial membranes in aging: impairments in agonist–receptor interactions and guanine nucleotide regulation accompany diminished catecholamine-responsiveness of adenylate cyclase. Mech Ageing Dev 19:127–139, 1982.
53. O'Connar SW, Scarpace PJ, Abrass IB: Age-associated decrease of adenylate cyclase activity in rat myocardium. Mech Ageing Dev 16:91–95, 1981.
54. Scarpace PJ, Abrass IB: Thyroid hormone regulation of β-adrenergic receptor number in aging rats. Endocrinology 108:1276–1278, 1981.
55. Zitnik G, Roth GS: Effects of thyroid hormones on cardiac hypertrophy and β-adrenergic receptors during aging. Mech Ageing Dev 15:19–28, 1981.
56. Fleisch JH, Hooker CS: The relationship between age and relaxation of vascular smooth muscle in the rabbit and rat. Circ Res 38:243–249, 1976.
57. Godfraind T: Alternative mechanisms for the potentiation of the relaxation evoked by isoprenaline in aortae from young and aged rats. Eur J Pharmacol 53:273–279, 1979.
58. Parker RJ, Berkowitz BA, Lee C-H, Denckla WD: Vascular relaxation, aging and thyroid hormones. Mech Ageing Dev 8:397–405, 1978.
59. Kelliher GJ, Conahan ST: Changes in vagal activity and response to muscarinic receptor agonists with age. J Gerontol 35:842–849, 1980.
60. Verkhratsky NS: Acetylcholine metabolism peculiarities in aging. Exp Gerontol 5:49–56, 1970.
61. Frolkis VV, Berzrukov VV, Schevchuk VG: Hemodynamic response and its regulation in old age. Exp Gerontol 10:251–271, 1975.
62. Kul'chitskii OK: Effect of acetylcholine on the cyclic GMP level in the rat heart at different ages. Bull Exp Biol Med 90:1237–1239, 1980.

63. Langer GA, Brady AJ, Tan ST, Serena SD: Correlation of the glycoside response, the force staircase and the action potential configuration in the neonatal rat heart. Circ Res 36:744–752, 1975.
64. Erdmann E, Philipp G, Scholz H: Cardiac glycoside receptor, (Na^+ + K^+)-ATPase activity and force of contraction in rat heart. Biochem Pharmacol 29:3219–3229, 1980.
65. Ku DD, Akera T. Robin T, Brody TM: Comparative species studies on the effect of monovalent cations and ouabain on cardiac Na^+, K^+-adenosine triphosphatase and contractile force. J Pharmacol Exp Ther 197:458–469, 1976.
66. Guarnieri T, Spurgeon H, Froehlich JP, Weisfeldt ML, Lakatta EG: Diminished inotropic response but unaltered toxicity to acetylstrophanthidin in the senescent beagle. Circulation 60:1548–1554, 1979.
67. Abu-Erreish GM, Neely JR, Whitmer JT, Whitman V, Sanadi DR: Fatty acid oxidation by isolated perfused working hearts of aged rats. Am J Physiol 232:E258–262, 1977.
68. Weisfeldt ML, Wright JR, Shreiner DP, Lakatta E, Shock NW: Coronary flow and oxygen extraction in the perfused heart of senescent male rats. J Appl Physiol 30:44–49, 1971.
69. Frolkis VV, Bogatskaya LN: The energy metabolism of myocardium and its regulation in animals of various age. Exp Gerontol 3:199–210, 1968.
70. Hansford RG: Lipid oxidation by heart mitochrondria from young adult and senescent rats. Biochem J 170:285–295, 1978.
71. Hansford RG: Metabolism and energy production. In: Weisfeldt ML (ed) Aging. vol 12: The aging heart: its function and response to stress. New York: Raven, 1980, pp 25–76.
72. DU JT, Beyer TA, Lang CA: Protein biosynthesis in aging mouse tissues. Exp Gerontol 12:181–191, 1977.
73. Florini JR, Saito Y, Manowitz EJ: Effect of age on thyroxine-induced cardiac hypertrophy in mice. J Gerontol 28:293–297, 1973.
74. Geary S, Florini JR: Effect of age on rate of protein synthesis in isolated perfused mouse hearts. J Gerontol 27:325–332, 1972.
75. Meerson FZ: The myocardium in hyperfunction, hypertrophy and heart failure. Circ Res (Suppl 2)25:1–163, 1969.
76. Meerson, FZ, Javich MP, Lerman MI: Decrease in the rate of RNA and protein synthesis and degradation in the myocardium under long-term compensatory hyperfunction and on aging. J Mol Cell Cardiol 10:145–159, 1978.
77. Crie JS, Millward DJ, Bates PC, Griffin EE, Wildenthal K: Age-related alterations in cardiac protein turnover. J Mol Cell Cardiol 13:589–598, 1981.
78. Grimm AF, Kubota R, Whitehorn WV: Ventricular nucleic acid and protein levels with myocardial growth and hypertrophy. Circ Res 19:552–558, 1966.

28. HORMONAL EFFECTS ON CARDIAC PERFORMANCE

Eugene Morkin

Introduction

Alterations in cardiac function have been described in a number of experimental and clinical disorders of the endocrine system. For the most part, however, the mechanisms of these effects has been obscure. New insight into the problem has been provided by recognition that thyroid hormone regulates ventricular myosin isoenzyme composition [1, 2]. Now the increase in cardiac mechanical performance and myosin ATPase in the presence of excess thyroid hormone can be explained, at least in part, by increased synthesis of a myosin isoenzyme with high ATPase activity, which normally represents only a minor component of the total ventricular myosin. A similar change in myosin isoenzyme composition has been found in thyroid-deficient rats treated with triiodothyronine (T_3) [3, 4]. In addition, the existence of ventricular myosin isoenzymes and the control of their expression by thyroid hormone and other factors may provide explanations for some otherwise perplexing reports of changes in myosin ATPase activity in various animal models of endocrine disorders.

Thyroid Hormone and Myosin Isoenzymes

MYOSIN STRUCTURE AND FUNCTION

The thick filaments are constructed from parallel myosin molecules and the actin filaments from repeating units of globular actin that are arranged like a double strand of pearls twisted on their long axis. Cardiac myosin is a hexamer composed of two heavy polypeptide chains of 210,000 daltons each. The heavy chains coil round each other to form an α-helical tail region, which imparts rigidity and length to the molecule, and divide to form two globular head regions. Each globular head region has a site for ATP binding and hydrolysis and a separate but closely related site for actin binding. In addition to its two heavy chains, myosin contains two light chains; the precise location of the light chains is uncertain, but appears to be near the ATP- and actin-binding sites on the heavy chains. Three troponin components and tropomyosin, proteins involved in the regulation of contraction, lie along a longitudinal groove between the actin monomers.

It is now almost universally accepted that, in both cardiac and skeletal muscle, contraction involves the sliding of the thick (myosin) filament of the sarcomere past the thin (actin) filament, utilizing energy supplied by hydrolysis of ATP. This process is controlled by variations in the cystolic concentration of Ca^{2+}, which binds to the troponin complex in the thin filament. As a result, tropomyosin undergoes a conformational change which facilitates the interaction of myosin heads with the actin filament. The sliding between the filaments is thought to be caused by a cyclic interaction between cross-bridges, which are comprised of the globular head region of myosin molecules, and specific sites on the actin filament.

Initially, experiments with hydrid myosins, in which light chains derived from fast skeletal muscle are combined with heavy chains from

This work was supported by grants from the Gustavus and Louis Pfeiffer Research Foundation and the National Institutes of Health (HL-20984).

N. Sperelakis (ed.), PHYSIOLOGY AND PATHOPHYSIOLOGY OF THE HEART.

Martinus Nijhoff Publishing, Boston/The Hague/ Dordrecht/Lancaster.

slow skeletal muscle, and vice versa, appeared to show that both myosin ATPase activity, and hence muscle-shortening velocity, might be determined by the type of myosin light chains. Later hybridization experiments have failed to confirm the effect of myosin light chains on the rate of Ca^{2+}-ATPase activity or actin-stimulated Mg^{2+}-ATPase activity. Furthermore, full ATPase activity of skeletal myosin has been found to be retained in the bare heavy subunits.

To relate the chemistry of actin–myosin interaction to mechanical events during muscle contraction, Lymn and Taylor [5] proposed a four-step reaction mechanism: (a) binding of ATP and rapid dissociation of actomysin, (b) hydrolysis of ATP on the free myosin head, (c) recombination of actin with the myosin products complex, and (d) release of myosin products. This mechanism was attractive because it could be related easily to the cycling of myosin cross-bridges during contraction: (a) dissociation of the myosin head or cross-bridge from the filament, (b) movement of the myosin cross-bridge, (c) recombination of the myosin cross-bridge with actin, and (d) the drive stroke of the cycle.

Subsequent studies [6, 7] indicated that this schema had to be made more complex to be realistic. Some of these newer concepts are presented in figure 28–1. Rather than a single hydrolysis step, as proposed in the original Lymn and Taylor model, several additional intermediate states in hydrolysis of ATP by the free myosin head have been identified from changes in myosin fluorescence. Other evidence suggests that the reaction products of ATP hydrolysis, adenosine diphosphate (ADP) and inorganic orthophosphate (P_i), are released sequentially from the active site. Furthermore, kinetic studies have revealed that association–dissociation between actin and the myosin-products complex occurs with great rapidity; this reaction is estimated to occur 1000 times more rapidly than hydrolysis of ATP. In terms of the sliding-filament model of contraction, this would imply that cross-bridges (myosin heads) cycle on and off the thin filament many times during a single turn of the ATP cleavage cycle. Presumably, only after myosin heads have undergone the conformational changes associated with ATP hydrolysis would the complexes formed with actin contribute to force development. With a mechanochemical mechanism of this type, several myosin isoenzymes could coexist in a single contractile unit (sarcomere) and work together, without the differences in ATPase activity limiting the speed of contraction.

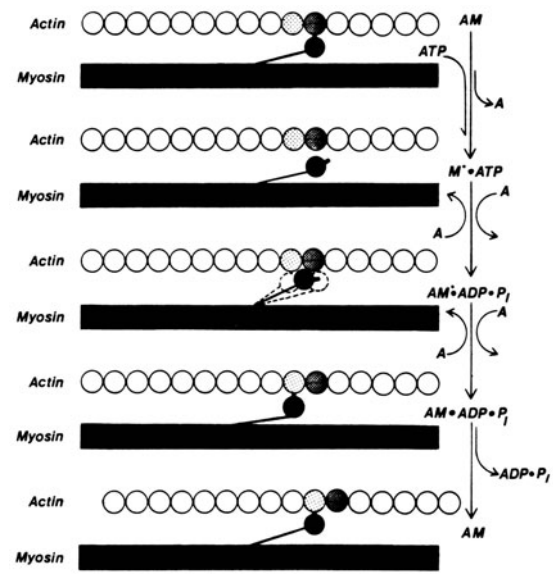

FIGURE 28–1. A current model of the relationship between muscle contraction and ATP hydrolysis by actomyosin. Upon binding of ATP to myosin, actin and myosin dissociate, and conformational changes take place in the myosin heads (M*) during which there is rapid attachment and detachment of the myosin heads to actin monomers. The myosin heads or cross-bridges contribute to force development only after undergoing conformational changes associated with ATP cleavage.

CARDIAC MYOSIN ISOENZYMES

Ventricular muscle consists of a dominant fiber type with properties similar to red skeletal myosin. Despite their uniform histologic appearance, ventricular muscle cells in most species contain varying amounts of three myosin forms which are designated V_1, V_2, V_3, in order of decreasing electrophoretic mobility and ATPase activity. These three myosin forms are structurally distinct from one another because

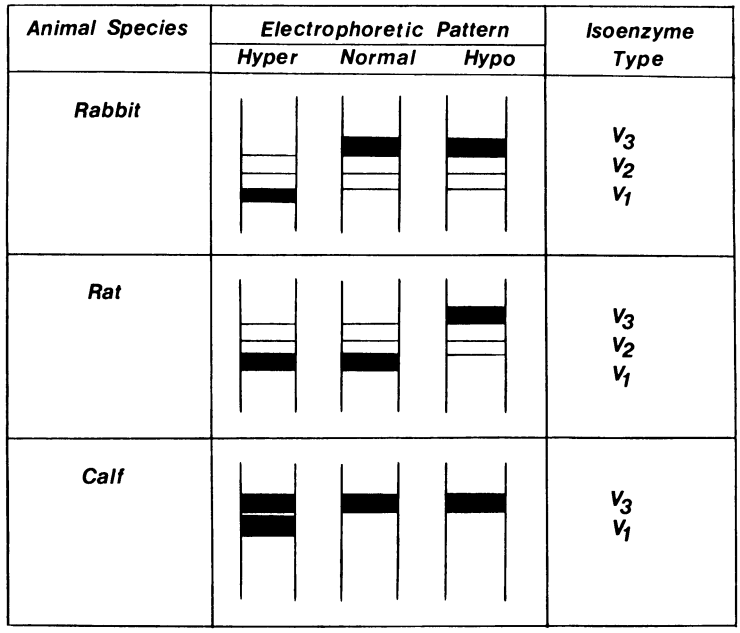

FIGURE 28–2. Effects of thyroid status on the distribution of ventricular myosin isoenzymes. In the calf, the faster-migrating band in the hyperthyroid state also may contain the V_2 form.

they are formed from several combinations of two heavy chains (HC) types, referred to as α- and β-heavy chains. The light chains appear to be the same in all three myosin forms. Thus, each molecule of the V_1 isoenzyme consists of two HC-α, whereas V_3 isoenzyme has two HC-β. V_2 is a heterodimer of HC-α and HC-β. Since myosin plays a major role in the cross-bridge cycle, any alterations in the proportion of myosin isoenzymes would be expected to alter the mechanical performance of the ventricle.

EFFECTS OF THYROID STATUS ON MYOSIN ISOENZYME PATTERN

The influence of the thyroid status of the animal on the composition of ventricular myosin isoenzymes is illustrated schematically in figure 28–2. In normal adult rats, thyroid deficiency induced by hypophysectomy or thyroidectomy stimulates synthesis of the V_3 myosin form and depresses synthesis of the V_1 form. By contrast, in adult euthyroid rabbits, thyroid hormone administration stimulates synthesis of the V_1 form and depresses synthesis of the V_3 form. Since, in both these animal species, myosins differ only by virtue of their heavy-chain structure, these results were interpreted to indicate that thyroid hormone must stimulate synthesis of α chains and depress synthesis of β chains. This conclusion has been confirmed by the demonstration that thyroid hormone administration stimulates synthesis of mRNA specific for α chains and depresses synthesis of the mRNA for β chains [8].

The extent of species differences in ventricular myosin isoenzyme composition when quantified are quite striking. In rats, about 80%–85% is in the V_1, 5%–10% V_2, and 10%–15% V_3. After thyroidectomy followed by treatment with ^{131}I to ablate residual thyroid tissue, V_3 represents essentially all of the myosin present. In euthyroid adult rabbits, about 85% of myosin is in the V_3 form and administration of thyroid hormone causes a complete reversal with 85% becoming the V_1 form.

The extent of myosin isoenzyme changes due to thyroid hormone may prove to be less dra-

matic in other species. For example, in the calf, ventricular myosin migrates in pyrophosphate-containing gels as a single band, thought to represent V_3. After thyroxine is administered for two weeks, a faster-migrating band appears (V_1) representing about 50%–60% of the total myosin. Thyroid deficiency induced by treatment with propylthiouracil for two weeks has no discernible effect on the normal predominance of the V_3 form.

Human ventricular tissue obtained at postmortem shows a pattern closely similar to that in rabbit. All three myosin forms are seen, but there is a strong predominance of the low-activity V_3 isoenzyme. To date, the effects of thyroid status on ventricular myosin isoenzyme composition have not been documented. There may be further isoenzyme forms to be discovered. If not, this distribution may restrict the potential for change or for redirection of human myosin genes. Since the V_3 content is near an upper limit, it cannot increase much further. However, the amount of V_1 might increase if properly stimulated.

CORRELATION BETWEEN CHANGES IN MYOSIN ISOENZYMES AND MECHANICAL PERFORMANCE

Cardiac output, heart rate, and systemic blood pressure are generally elevated in thyrotoxicosis [9]. These alterations have been attributed, in part, to changes in the peripheral circulation mediated by the metabolic effects of thyroid hormone. However, there also are now known to be direct chronotropic and inotropic effects on the heart.

A positive chronotropic effect of thyroid hormone was established nearly 50 years ago by experiments demonstrating that isolated hearts or excised atria from animals administered thyroid hormone beat at a faster rate than similar control preparations. Direct inotropic effects of thyroid hormone have been shown by measurements of the mechanical performance of isolated papillary muscles from thyrotoxic cat hearts [10]. In isotonic experiments, muscles from thyrotoxic cats showed a significant increase in the velocity of shortening compared to euthyroid muscles. In isometric experiments, the rate of tension development was increased without much change in maximum active tension. These findings occurred in the presence and absence of intact norepinephrine stores and over a wide range of temperature and contraction frequency. An increase in the rate of isometric tension development also has been found in both intact and glycerinated muscles from thyrotoxic rabbits, which is consistent with a direct effect of thyroid hormone on the contractile proteins.

Although the results of these experiments on isolated cardiac muscle seem consistent with a positive inotropic response to excess thyroid hormone, extrapolation to the intact circulation has been uncertain because of the increases which occur in heart rate and ventricular dimensions. To gain a clearer description of the effects of the hormone on the intact heart, LV mechanical performance has been assessed recently in calves with implanted sonomicrometer crystals and pressure transducers [11]. As would be expected, heart rate, LV systolic pressure and dP/dt are increased significantly after treatment. LV internal diameter is increased in both systole and diastole, but fractional shortening is unchanged. The increases in LV end-diastolic diameter and systolic blood pressure combine to increase peak wall stress by about 30%. Despite the increase in afterload, mean velocity of circumferential fiber shortening (V_{cf}) remains normal. Thus, in the intact heart at rest, the direct inotropic effect of thyroid hormone does not produce a greater speed of shortening; speed of shortening remains normal despite a greater afterload.

The cardiovascular effects of hypothyroidism are often viewed as the opposite of thyrotoxicosis, yet, according to the hypotheses developed here, thyroid deficiency would not be expected to alter myosin isoenzymes or cardiac performance in species such as man, calf, and rabbit, which have a marked predominance of the V_3 isoenzyme. Nevertheless, reductions in cardiac output, stroke volume, and heart rate have been reported in hypothyroid subjects and thyroid-deficient animals [9]. Changes in these parameters could reflect alterations in peripheral oxygen demands, rather than direct negative inotropic effects on the myocardium. However, experimental studies of hypothyroid-

ism in open-chested dog preparations [12] or isolated papillary muscles [10] also have found depressed myocardial mechanical performance. It is perhaps noteworthy that in these studies the differences between hypothyroid and control hearts generally were smaller than between euthyroid and hyperthyroid hearts and not always statistically significant. Particularly in isotonically contracting papillary muscles the velocity of contraction may have been underestimated because of the slower activation process in hypothyroid muscles. Under these circumstances contraction would begin later in the cycle than usual, which would tend to reduce the speed of shortening. More accurate assessments of contraction velocity probably could be obtained in quick-release experiments.

These explanations may not be adequate to encompass all the evidence of reduced contractile performance in hypothyroid hearts, particularly in human subjects. Pericardial effusion is clinically quite common in hypothyroidism, and can be easily recognized by echocardiography. In addition, several other explanations should be considered, including a defect in excitation–contraction coupling, impairment in myocardial performance related to myxedematous infiltration, hypertrophy secondary to hypertension, and severe coronary atherosclerosis.

CARDIAC MYOSIN ISOENZYMES IN OTHER CONDITIONS

Recently, alterations in ventricular myosin isoenzyme composition have been noted in a number of conditions not clearly associated with an alteration in thyroid status. In some cases, there seem to be subtle changes in plasma thyroid hormone concentration. For example, a switch from the V_3 to the V_1 form has been described in the rat ventricle during the first two weeks after birth [13]. At about the same period of development, rabbit ventricular myosin changes from a predominance of the V_3 to the V_1 form [14]. In both instances, the changes in myosin isoenzyme composition coincide with a postnatal elevation of plasma T_4 concentration. It seems well established that expression of certain other enzymes during the neonatal period is related to changes in plasma thyroid hormone concentration [15].

As another example, streptozotocin-induced diabetes in the rat causes depression of myocardial performance in association with reduction in myosin ATPase activity and a switch in myosin isoenzymes from the V_1 and the V_3 form [16, 17]. Plasma thyroid hormone concentrations are reduced in this model and administration of the hormone returns myosin ATPase activity toward normal.

Changes in myosin isoenzyme composition from the V_1 to the V_3 form also have been reported in the rat in association with aging [18] and hypertrophy secondary to pressure-volume overload [19, 20]. With aging in the rat, decreases in mechanical performance and myosin ATPase activity have been described. There also is a decrease in plasma T_4 concentration [21], but plasma-free T_4 concentration remains normal. No information is available with regard to the effects of hemodynamic overload on plasma thyroid hormone concentration. However, administration of T_4 has been shown to prevent the decrease in myosin ATPase activity that occurs after aortic coarctation in the rat [22].

These examples suggest that plasma thyroid hormone concentration may play some role in mediating the changes in cardiac myosin isoenzymes that have been described in various animal models. In some cases, however, the hormone may exert only a permissive action, with other factors playing a more direct role in the isoenzyme changes. It should be emphasized that these actions of thyroid hormone, as well as most other effects of the hormone, are highly species specific. Many of the changes in myosin isoenzymes that have been reported in experimental models, particularly the rat, may have no direct counterpart in man.

REGULATION OF MYOSIN ISOENZYMES BY THYROID ANALOGUES AND OTHER FACTORS

The effects of thyroid hormone analogues, nonthyroidal hormones, and dietary carbohydrate on expression of ventricular myosin analogues recently have been studied by Sheer and Morkin [23]. First, they determined the relative ability of thyroid analogues to stimulate the V_1 myosin form in thyroid-deficient rats relative to their ability to stimulate oxidative metabolism.

For this purpose, ventricular myosin isoenzyme patterns, myocardial $^{14}CO_2$ production from ^{14}C-labeled glucose or palmitate, and hepatic α-glycerolphosphate dehydrogenase (GPDH) activity were studied in thyroidectomized and hypophysectomized rats using L-3,5,3′-triiodothyronine (T_3), D-3,5,3′-triiodothyronine (dT_3), L-3,3′,5′-triiodothyronine (rT_3), L-3,5,3′-triiodothyroacetic acid (Triac), and 3,5-diiodothyronine (T_2). The results showed no clear separation of the effects of these analogues on myosin isoenzyme expression relative to their stimulation of CO_2 production and GPDH activity. However, since the maximum effect of the analogues was much less than T_3, that is, they act as partial agonists, it might be possible to induce small increases in V_1 without much risk of undesirably large stimulation of CO_2 production.

Also, cardiac myosin composition was found to be subject to modification by several other factors. High carbohydrate feeding (74% total calories as fructose or glucose) in hypophysectomized rats, which is known to induce a number of respiratory enzymes, increased V_1 from 12% to 36%; myocardial CO_2 production and hepatic GPDH activity also were stimulated to a similar extent. An even more impressive myosin isoenzyme switch occurred in thyroidectomized animals fed a high fructose diet. In this model the V_1 myosin form increased from undetectable levels to 28% of total myosin. Partial replacement with T_3 and fructose feeding in these animals had synergistic actions on myosin isozyme expression, GPDH activity, and CO_2 production. With respect to nonthyroidal hormones, isoproterenol, a β-adrenergic agonist, and propranolol, a β-adrenergic antagonist, had no effect on T_3 dose–response curves. Adrenalectomy in normal rats caused a 33% decrease in V_1 and a corresponding increase in V_3.

These results were interpreted to indicate that the relative rates of ventricular myosin α- and β-chain synthesis are regulated by two distinct mechanisms: (a) thyroid hormone acting through nuclear receptors to stimulate α-chain synthesis and depress β-chain synthesis, and (b) an independent mechanism involving dietary carbohydrate, glucocorticoids, and perhaps other factors which have been implicated in modulating myosin isoenzyme expression.

In the case of malic enzyme, which also is induced by thyroid hormone and high-carbohydrate diet, it has been proposed that T_3 acts to amplify a primary glucose-induced signal [24]. Whether or not the latter possibility is correct, it seems likely that the signal created by the T_3-receptor complex probably interacts with the signal created by high-carbohydrate diet, glucocorticoids, etc., at a pretranslational level.

Other Mechanisms of Thyroid Hormone Action

CATECHOLAMINES

Before 1960, several investigators found support for the hypothesis that excess thyroid hormone enhances or potentiates the cardiovascular actions of catecholamines [9]. Subsequently, a large amount of evidence has accumulated to refute this contention. For example, the positive inotropic and chronotropic responses to epinephrine, norepinephrine, and cardiac sympathetic nerve stimulation were comparable in T_4-treated and normal dogs [25, 26]. Similar results were obtained with catecholamine infusions in thyrotoxic human subjects [27]. The enhanced contractile performance of isolated papillary muscles from thyroxine-treated cats was not influenced by depletion of catecholamine stores with reserpine [10]. No increase was found in myocardial concentration of norepinephrine or epinephrine or in urinary excretion of catecholamines and their metabolites. Furthermore, low levels of plasma catecholamines and dopamine β-hydroxylase activity has been reported in thyrotoxic subjects.

This evidence indicates that thyrotoxicosis is not associated with increased β-adrenergic activity or supersensitivity to β-adrenergic stimulation. However, there have been suggestions of a more subtle interplay between thyroid hormone and catecholamines. For example, thyroid hormone has been found to increase the number of cardiac β-adrenergic receptors in rat heart. As with many of the other actions of thyroid hormone, this increase in β-adrenergic

receptors seems to be species specific and is not found in rabbit or calf. In addition, amplification by thyroid hormone of the intracellular system for expression of β-adrenergic stimulation was suggested by experiments showing an increase in myocardial phosphorylase-*a* activation by catecholamines in rats pretreated with T_4. Despite extensive further study, the mechanism responsible for this interesting observation has not come to light.

Experiments making use of β-adrenergic antagonists also have failed to reveal a clear role for catecholamines in mediating the cardiovascular effects of thyroid hormone. Recently, the effects of β-adrenergic blockade have been examined in conscious animals [28], thereby avoiding some of the problems associated with anesthesia or the use of isolated heart preparations. Intravenous treatment with full β-adrenergic-blocking doses of propranolol had no effect on hemodynamic parameters or LV mechanical performance. However, the average dose of propranolol required to achieve β-adrenergic blockade was twice that needed in the euthyroid state.

MEMBRANE ACTIONS

A second possible site of thyroid action is on the membrane properties of the heart. Thus, there are effects on heart rate, rhythm, and electrical excitability. The most striking electrophysiologic abnormality in experimental hyperthyroidism is a decrease in the duration of the action potential recorded from individual atrial muscle cells. In contrast, the duration of the action potential is prolonged in hypothyroidism. A reduction in action potential duration increases the electrical excitability of the atrium, as shown by a reduction in stimulation threshold for a given coupling interval. This may explain the tendency of thyrotoxic patients to develop atrial fibrillation.

Several possible mechanisms have been offered by way of explanation for these effects of thyroid hormone on myocardial membrane properties. Since both diastolic depolarization and repolarization of the action potential are thought to be related in part to changes in transmembrane K^+ conductance, it has been proposed that thyroid hormone may selectively influence these changes. A decrease in Na^+ conductance relative to the increase in K^+ conductance also could explain the changes in diastolic depolarization. In addition, thyroid hormone administration appears to increase sarcolemmal (Na^+,K^+)-ATPase activity. The numbers of (Na^+,K^+)-ATPase molecules in the membrane are reported to increase without changing the specific activity of the enzyme. Consistent with increased Na^+-K^+ pump activity, there is evidence of a decrease in intracellular Na^+ concentration. Also, thyroid hormone has been reported to stimulate Ca^+ uptake by isolated sarcoplasmic reticulum, possibly by a cAMP-mediated increase in the extent of phosphorylation of a 22,000-molecular-weight regulatory protein (phospholamban).

Nonthyroidal Hormones and Cardiac Performance

Secretions from several endocrine organs, including the anterior pituitary and adrenal cortex, may modulate myocardial performance. It is difficult in some cases, however, to distinguish the effects of these hormones on the heart from their influences on the peripheral circulation. Also, some of their actions may be mediated through interactions with catecholamines or thyroid hormone. Cardiac performance is sometimes impaired with diabetes mellitus, a complex group of disorders characterized by an absolute or relative lack of insulin. Whether this represents a distinct cardiomyopathy is controversial, but recent experimental evidence lends some support to the view. A number of hormones, including parathyroid hormone (parathormone), aldosterone, angiotension II, and vasopressin have important peripheral effects, but there is little evidence that they have major actions on the heart. With these caveats in mind, the actions of several nonthyroidal hormones on cardiac performance are reviewed briefly below.

ANTERIOR PITUITARY HORMONES

The anterior pituitary gland secretes at least seven polypeptide hormones. Four (ACTH, FSH, LH, and TSH) primarily produce their biologic effect indirectly by altering hormonal

secretions from specific target organs (adrenal cortex, gonad, and thyroid). Thus, their effects on the cardiovascular systems will be the same as those of the hormones secreted by the target gland. There are no known clinical cardiovascular manifestations of altered secretion of prolactin or isolated growth hormone deficiency. However, excessive secretion of growth hormone produces a syndrome known as acromegaly, which may be associated with signs and symptoms of cardiac dysfunction. An increase in cardiac mass usually is present, occasionally to an extreme degree [29]. Also, there appears to be an increased incidence of hypertension, coronary arteriosclerosis, and cardiac dysrhythmias. Since 10%–20% of these patients exhibit overt congestive heart failure in the absence of other explanations, the suggestion has been made that a specific acromegalic cardiomyopathy exists. At postmortem, subendocardial fibrosis and septal hypertrophy have been found in addition to biventricular dilation and hypertrophy [30].

The incidence of acromegalics with subclinical evidence of cardiac dysfunction is controversial. Jonas et al. [31] reported shortening of LV ejection time (LVET), prolongation of the preejection period (PEP), and elevation of PEP/LVET ratio in seven out of ten patients studied. On the other hand, Mather et al. [32] found a normal ejection fraction by echocardiography in all but one of 23 patients, and in those with increased LV mass there was no detectable impairment of LV performance by noninvasive techniques. They also pointed out that the abnormal PEP/LVET ratios reported by Jonas et al. [31] were largely the result of a shortened LVET with a relatively normal preejection period, which would not be a typical pattern of subclinical cardiac dysfunction. Possibly, some of the variability noted in these and other studies may be related to the duration of the disease before institution of definitive treatment.

The effects of growth hormone on cardiac growth, ventricular performance, and blood pressure have been studied experimentally in the rat [33]. It was found that hypophysectomy prevents development of cardiac hypertrophy in response to aortic banding. In the absence of banding, cardiac atrophy and low blood pressure were observed. The decrease in cardiac weight relative to body weight in hypophysectomized rats was not corrected by growth hormone, but the weight of the heart increased after aortic constriction to about one-half of the expected weight. Growth hormone treatment did not influence cardiac output and work of hypophysectomized rats, but after aortic constriction these values were higher in hypophysectomized rats treated with growth hormone than in untreated controls. Treatment of hypophysectomized rats with thyroxine restored the weight and rate of the heart, the blood pressure, cardiac output, and work to near normal levels. After aortic constriction, on the other hand, no significant further increase in the weight of the heart took place. These results indicate that, in the rat, growth hormone is essential to cardiac growth and maintainence of normal cardiac mass, but thyroid hormone is principally responsible for the reduction in cardiac performance after hypophysectomy.

A significant reduction in the activity of cardiac myofibrils from hypohysectomized or thyroidectomized rats also has been found [34]. It was possible to completely restore myofibrillar ATPase activity by treatment with T_4, although it did not stimulate general body growth or return the heart-weight–body-weight ratio to normal. This conclusion with regard to the effect of hypophysectomy on myofibrillar ATPase was later confirmed using purified myosin [35].

ADRENAL CORTICAL HORMONES

The most common cardiovascular manifestation of adrenal cortical insufficiency (Addison disease) is arterial hypotension. Orthostatic hypotension and syncope are common. These are thought to be secondary to marked hypovolemia and electrolyte abnormalities. In severe cases, the heart size may be small, perhaps reflecting a reduction in work load. In experimental adrenal insufficiency in the rat, similar changes in blood pressure and heart weight are found. In addition, as pointed out above, a decrease in the high ATPase activity V_1 myosin form occurs which can be reversed by glucocorticoid replacement [23].

Hypertension is present in 80%–90% of patients with glucocorticoid excess (Cushing syndrome). Hemodynamic, electrocardiographic, and x-ray examinations of patients with this condition have revealed no specific cardiac abnormalities except those that are usually associated with either hypertension or electrolyte disturbances.

Hypersecretion of aldosterone (Cohn syndrome) is associated with arterial hypertension and hypokalemia. Both in the clinical disorder and a related experimental model, hypertension induced by desoxycorticosterone acetate and salt in the rat, there is no evidence that mineralocorticoids directly affect cardiac function.

DIABETES MELLITUS

The incidence of congestive heart failure is increased in diabetics even when such factors as age, blood pressure, plasma cholesterol, weight, and coronary artery disease are taken into account [36]. These data, together with postmortem reports [37, 38] of cardiomegaly, interstitial fibrosis, and subendocardial thickening of the small coronary arteries in diabetics with clinical evidence of congestive failure, have led to proposals that diabetes is associated with a discrete form of cardiomyopathy.

Further work has been done to establish the pathologic basis for a diabetic cardiomyopathy. Regan et al. [39] have reported variable degrees of interstitial and perivascular fibrosis; significant accumulations of acid-Schiff-positive material was found in the interstitium. The walls of intramural blood vessels were thickened in some cases, usually to a mild extent. There was no evidence that either large or small blood vessel occlusive disease contributed to the pathologic alterations in the myocardium.

The study by Regan et al. [39] also included hemodynamic assessment of a small group of diabetic patients without hypertension or angiographically significant coronary artery disease. A consistent reduction in stroke volume index and elevation of LV diastolic pressure was found. Increments in afterload caused a significant increase in filling pressure compared to normals without a stroke volume response. These changes, which are indicative of reduced ventricular compliance, were interpreted as signifying a preclinical cardiomyopathy. Noninvasive studies [40, 41] also have suggested myocardial dysfunction in diabetics; however, the type of abnormalities reported have been somewhat variable.

Further support for the concept of a diabetic cardiomyopathy has come from experimental studies of drug-induced diabetes. Studies by Regan et al. [42] in chronically diabetic dogs have indicated that the stiffness of the LV is increased, possibly because of increased collagen content. Regulation of postprandial hyperglycemia with insulin did not reverse these changes [43]. In the early period after induction of diabetes in the rat with large doses of alloxan, cardiac function and high-energy phosphate stores were reduced due to impaired glucose utilization [44]. Acute correction of substrate deficiency in the perfused hearts with insulin or high concentrations of glucose restored ATP levels and returned ventricular function toward normal. Work on chronically diabetic rats, employing both isolated LV papillary muscles and perfused hearts, has shown slowing of relaxation and depression of contractility in diabetic hearts [45, 46]. Efforts have been made to correlate these mechanical changes to alterations in calcium uptake by the sarcoplasmic reticulum [47] and to a change in myosin isoenzymes toward a predominance of the low-activity V_3 form [17]. These latter experimental changes were reversible with insulin [48], but as pointed out above, thyroid hormone levels also are depressed in this model and could be responsible for some of the abnormalities.

References

1. Flink IL, Morkin E: Evidence for a new cardiac myosin species in thyrotoxic rabbit. FEBS Lett 81:391–394, 1977.
2. Flink IL, Rader JH, Morkin E: Thyroid hormone stimulates synthesis of a cardiac myosin isozyme: comparison of the two-dimensional electrophoretic patterns of the cyanogen bromide peptides of cardiac myosin heavy chains from euthyroid and thyrotoxic rabbits. J Biol Chem 254:3105–3110, 1979.
3. Hoh JFY, McGrath PA, Hale PT: Electrophoretic analysis of multiple forms of rat cardiac myosin: ef-

fects of hypophysectomy and thyroid replacement. J Mol Cell Cardiol 10:1053–1076, 1978.
4. Hoh JFY, Egerton LJ: Action of triiodothyronine on the synthesis of rat ventricular myosin isozymes. FEBS Lett 101:143–148, 1979.
5. Lymn RW, Taylor EW: Mechanism of adenosine triphosphate hydrolysis by actomyosin. Biochemistry 10:4617–4624, 1971.
6. Taylor EW: Mechanism of actomyosin ATPase and the problem of muscle contraction. CRC Crit Rev Biochem 6:103–165, 1979.
7. Stern LA, Chock PB, Eisenberg E: Mechanism of the actomyosin ATPase: effect of actin on the ATP hydrolysis step. Proc Natl Acad Sci USA 78:1346–1350, 1981.
8. Sinha AM, Umeda PK, Kavinsky CJ, Rajamanickam C, Hsu H-J, Jakovcic S, Rabinowitz M: Molecular cloning of mRNA sequences for α- and β-form myosin heavy chains: expression in ventricles of normal, hypothyroid, and thyrotoxic rabbits. Proc Natl Acad Sci USA 79:5847–5851, 1982.
9. Morkin E, Flink IL, Goldman S: Physiological and biochemical effects of thyroid hormone on cardiac performance. Prog Cardiovasc Dis 25:435–464, 1983.
10. Buccino RA, Spann JF, Pool PE, Sonnenblick EH, Braunwald E: Influence of the thyroid state on the intrinsic contractile properties and energy stores of the myocardium. J Clin Invest 46:1669–1682, 1967.
11. Goldman S, Olajos M, Friedman H, Roeske WR, Morkin E: Left ventricular performance in conscious thyrotoxic calves. Am J Physiol 242:H113–H121, 1981.
12. Stauer BE, Schulze W: Experimental hypothyroidism: depression of myocardial contractile function and hemodynamics and their reversibility by substitution with thyroid hormone. Basic Res Cardiol 71:624–644, 1976.
13. Zak R, Chizzonite RA, Everett AW, Clark WA: Study of ventricular isomyosins during normal and thyroid hormone induced cardiac growth. J Mol Cell Cardiol (Suppl 3) 14:111–117, 1982.
14. Dussault JH, Labie F: Development of the hypothalamic–pitituary–thyroid axis in the neonatal rat. Endocrinology 97:1321–1324, 1975.
15. Greengard O, Jaindar SC: The prematurely promoted formations of liver enzymes in suckling rats. Biophys Biochem Acta 237:476–483, 1971.
16. Dillman WH: Diabetes mellitus induced changes in cardiac myosin of the rat. Diabetes 29:579–582, 1980.
17. Malhotra A, Penpargkul S, Fein F, Sonnenblick EH, Scheuer J: The effects of streptozotocin induced diabetes in rats on cardiac contractile proteins. Circ Res 49:1243–1250, 1981.
18. Lompre AM, Mercadier JJ, Wisnewsky C, Bouveret P, Pantaloni C, d'Albis A, Schwartz K: Species and age-dependent changes in the relative amounts of cardiac myosin isoenzymes in mammals. Dev Biol 84:286–290, 1981.
19. Rupp H: The adaptive changes in the isoenzyme pattern of myosin from hypertrophied rat myocardium as a result of pressure overload and physical training. Basic Res Cardiol 76:79–88, 1981.
20. Mercadier JJ, Lompre AM, Wisenewsky C, Samuel JL, Bercovici J, Swynghedauw B, Schwartz K: Myosin isozyme changes in several models of rat cardiac hypertrophy. Circ Res 49:525–532, 1981.
21. Frolkis VV, Valueva GV: Metabolism of thyroid hormones during aging. Gerentology 24:81–94, 1978.
22. Litten RA III, Martin BJ, Low RB, Alpert NR: Altered myosin isozyme patterns from pressure overload and thyrotoxic hypertrophied rabbit hearts. Circ Res 50:856–864, 1982.
23. Sheer D, Morkin E: Effects of thyroid hormone analogs, non-thyroidal hormones, and high carbohydrate diet on cardiac myosin isozyme expression the rat. Fed Proc 42:2212, 1983.
24. Mariash CN, McSwigan CR, Towle HC, Schwartz HL, Oppenheimer JH: Glucose and triiodothyronine both induce malic enzyme in the rat hepatocyte culture. J Clin Invest 65:1126–1134, 1981.
25. Margolius HS, Gaffney T: Effect of injected norepinephrine and sympathetic nerve stimulation in hypothyroid and hyperthyroid dogs. J Pharmacol Exp Ther 149:329–335, 1965.
26. Van der Shoot JB, Moran NC: An experimental evaluation of the reputed influence of thyroxine on the cardiovascular effects of catecholamines. J Pharmacol Exp Ther 149:336–345, 1965.
27. Aoki VS, Wilson WR, Theilen EO: Studies of the reputed augmentation of the cardiovascular effects of catecholamines in patients with spontaneous hyperthyroidism. J Pharmacol Exp Ther 181:362–368, 1972.
28. Goldman S, Olajos M, Pieniaszek H, Perrier D, Mayersohn M, Morkin E: Beta-adrenergic blockade with propranolol in conscious euthyroid and thyrotoxic calves: dosage requirements and effects on heart rate and left ventricular performance. J Pharmacol Exper Ther 219:394–399, 1981.
29. Heljtmancik MR, Bradfield JY, Herman GR: Acromegaly and the heart: a clinical and pathologic study. Ann Intern Med 34:1445–1456, 1951.
30. Rossi L, Theine G, Caregaro L, Giordano R, Lauro S: Dysrhythmias and sudden death in acromegalic heart disease: a clinicopathological study. Chest 72:496–498, 1977.
31. Jonas EA, Aloia JF, Lane JF: Evidence of subclinical heart muscle dysfunction in acromegaly. Chest 67:190–194, 1975.
32. Mather HM, Boyd MJ: Jenkins JS: Heart size and function in acromegaly. Br Med J 41:697–701, 1979.
33. Beznak M: Effect of growth hormone and thyroxin on cardiovascular system of hypophysectomized rats. Am J Physiol 204:279–283, 1963.

34. Lifschitz MD, Kayne HL: Cardiac myofibrillar ATPase activity in hypophysectomized or thyroidectomized rats. Biochem Pharmacol 15:405–407, 1966.
35. Rovetto MJ, Hjalmarson AC, Morgan HE, Barrett MJ, Goldstein RA: Hormonal control of cardiac myosin adenosine triphosphatase in the rat. Circ Res 31:397–409, 1972.
36. Kannel WB, Hjortland M, Castelli WP: Role of diabetes in congestive heart failure: the Framingham study. Am J Cardiol 34:29–34, 1974.
37. Rubler S, Diugash J, Yuceoglu YZ, Kumral T, Branwood AW, Grishman A: New type of cardiomegaly associated with diabetic glomerulosclerosis. Am J Cardiol 30:595–602, 1972.
38. Hamby RI, Zoneraich S, Sherman L: Diabetic cardiomyopathy. JAMA 229:1749–1754, 1974.
39. Regan TJ, Lyons MM, Ahmed SS, Levinson GE, Oldewurtel HA, Ahmad MR, Haider B: Evidence for cardiomyopathy in familial diabetes mellitus. J Clin Invest 60:885–899, 1977.
40. Amed SS, Jafferi GA, Narang RM, Regan TJ: Preclinical abnormalities of left ventricular function in diabetes mellitus. Am Heart J 89:153–158, 1975.
41. Rubler S, Sajadi RM, Araoye MA, Holford FD: Noninvasive estimate of performance in patients with diabetes. Diabetes 27:127–134, 1978.
42. Regan TJ, Ettinger PO, Khan MI, Jesranc MV, Lyons MM, Oldewurtel HA, Weber M: Altered myocardial function in chronic diabetes without ischemia in dogs. Circ Res 35:222–237, 1974.
43. Regan TJ, Wu CF, Yeh CK, Oldewurtel HA, Haider B: Myocardial composition and function in diabetes: chronic insulin use. Circ Res 49:1268–1277, 1981.
44. Miller TB Jr: Cardiac performance in isolated perfused hearts from alloxan diabetic rats. Am J Physiol 236:H808–H812, 1979.
45. Fein FS, Kornstein LB, Strobeck JE, Capasso JM, Sonnenblick EH: Altered myocardial mechanics in diabetic rats. Circ Res 47:922–933, 1980.
46. Penpargkul S, Schaible T, Yiptinsoi T, Scheuer J: The effect of diabetes on performance and metabolism of rat heart. Circ Res 47:911–921, 1980.
47. Penpargkul S, Fein F, Sonnenblick EH, Scheuer J: Depressed cardiac sarcoplasmic reticular function from diabetic rats. J Mol Cell Cardiol 13:303–309, 1981.
48. Fein FS, Strobeck JE, Malhotra A, Scheuer J, Sonnenblick EH: Reversibility of diabetic cardiomyopathy with insulin in rats. Circ Res 49:1251–1261, 1981.

29. CARDIOPLEGIA

Principles and Problems

Hans Jürgen Bretschneider
Martha Maria Gebhard
and Claus Jürgen Preusse

The Globally Ischemic Heart

Interruption of the coronary circulation with ensuing depletion of cardiac oxygen reserves and shift from aerobic to anaerobic energy gain leads to disturbances of contractile function, to acidosis and changes in electrolyte and water distribution between intracellular and extracellular compartments, and thereby to disturbances of basic electrophysiologic processes, to structural alterations, and, finally, to organ death. Irreversible damage to the left ventricular myocardial muscle occurs much more rapidly than in the right ventricle, the atria, and the central and peripheral conductive system. In considering partial or complete reversibility of an ischemic stress by reperfusion and reoxygenation, three phases of global ischemia can be defined using the terminology originally applied to functional changes in the brain under global ischemia [1]:

The first phase of undisturbed function or *latency period* is identical with the duration of myocardial aerobic energy supply from the oxygen reserves available at the time of coronary circulatory arrest, oxyhemoglobin, oxymyoglobin, and physically dissolved oxygen, which total about 1–2 ml/100g left ventricular myocardium. Depending on the level of myocardial performance and O_2 demand prior to ischemia, these reserves last for no more than 1–20 s under normothermic conditions.

When the level of O_2 reserves becomes critical, at partial pressures of O_2 of less than 5 mmHg, myocardial energy is derived from anaerobic glycolysis and high-energy phosphate bonds. The initial drop of creatine phosphate (CP)—to approximately 3 μmol/g left ventricular muscle in the canine heart—is accompanied by functional disturbances to complete cardiac arrest as well as by first minute ultrastructural changes in the myocardial muscle of left ventricle. Reperfusion and reoxygenation in this phase, however, immediately result in resumption of full preischemic function. For this reason, we call this phase *"survival period"* or, after its biochemical criteria, CP time (t_{CP}). It lasts for about 5 min in the hypothermic ischemic dog heart following coronary circulatory arrest at 25°C (fig. 29–1).

If one exceeds the survival period, myocardial adenosine triphosphate (ATP) is utilized in addition to anaerobic energy sources. Ultrastructural alterations now increase significantly. Reperfusion and reoxygenation lead to recovery of preischemic function only after a latency period which exponentially increases with increasing duration of global ischemia and becomes infinite in the canine heart at an ATP level of approximately 2 μmol/g left ventricular myocardium. The phase from the beginning of

This work was supported by the Deutsche Forschungsgemeinschaft SFB 89—Kardiologie Göttingen.

ischemia to the limit of reversibility of ischemic damage is called *revival time*. We distinguish from it the so-called practical period of revival which correlates with a recovery latency of about 20 min and in the dog heart with an ATP content of 4 μmol/g left ventricular myocardium. We therefore call it ATP time (t_{ATP}). Depending on preischemic cardiac O_2 demands, t_{ATP} is approximately 40 min in the hypothermic dog heart at 25°C (fig. 29–1).

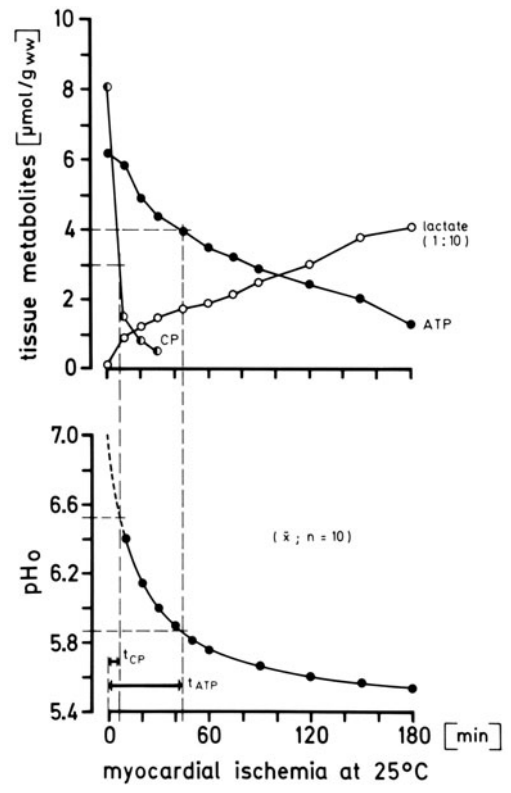

FIGURE 29–1. Metabolites and extracellular pH in the left ventricular myocardium of dog hearts during ischemic cardiac arrest.

Cardioplegia: Principles and Results

Generally, any method which prolongs cardiac tolerance to global ischemia is called *cardioplegia*. Theoretically, this can be reached in each of the three phases by improving the energy-supply–energy-demand ratio in the heart, which following coronary circulatory arrest drops below 1, indicating an increasing and finally irreversible energy deficit under a given limitation of O_2 supply [1, 2]. The ratio may be improved by: (a) decreasing cardiac energy demands which prior to ischemia can be equated with oxygen consumption ($M\dot{V}O_2$) but during ischemia must be assumed to equal or exceed the anaerobic energy turnover $\dot{E} = (1.5 \times \triangle\text{lactate} + \triangle\sim P):\triangle t$; (b) increasing myocardial energy reserves in the form of oxygen, of glycogen, or of high-energy phosphate bonds; or (c) improving the metabolic yield of energy by improving the ATP gain per molecule of oxygen (ATP/O quotient) under aerobic conditions or the energy-gain–energy-turnover ratio $\eta = (1.5 \times \triangle\text{lactate}):(1.5 \times \triangle\text{lactate} + \triangle\sim P)$ under anaerobic conditions.

The *energy demands* of any organ are the sum of its basal energy requirement and those during work. In the heart the latter is essentially determined by the level of performance of the contractile system. It varies by a factor of approximately 15 when comparing $M\dot{V}O_2$ at maximum work with that of the empty beating or fibrillating heart [2, 3], and by a factor of 100 in comparison to that of the heart arrested in diastole (fig. 29–2). The membranous ion pumping systems, however, contribute relatively little to this [3]. The basal energy requirement of the heart results from the needs for structural preservation and for metabolic and electrophysiologic readiness for function. The differing functional reversibility of global ischemia during the aerobic latency, during t_{CP}, or after t_{CP} indicates that energy-consuming systems determining work output can be temporarily "switched off" without ill effects. However, a fall of the basal energy turnover below the minumum requirement is always accompanied by at least reversible damage of the organ.

Suspension of the work output of the heart can be achieved by any electrophysiologic or pharmacologic intervention which inactivates the electrophysiologic mechanisms and the contractile system and leads to diastolic cardiac arrest. Of the numerous known methods, we mention only those currently in clinical use (for review, see Hearse et al. [4]):

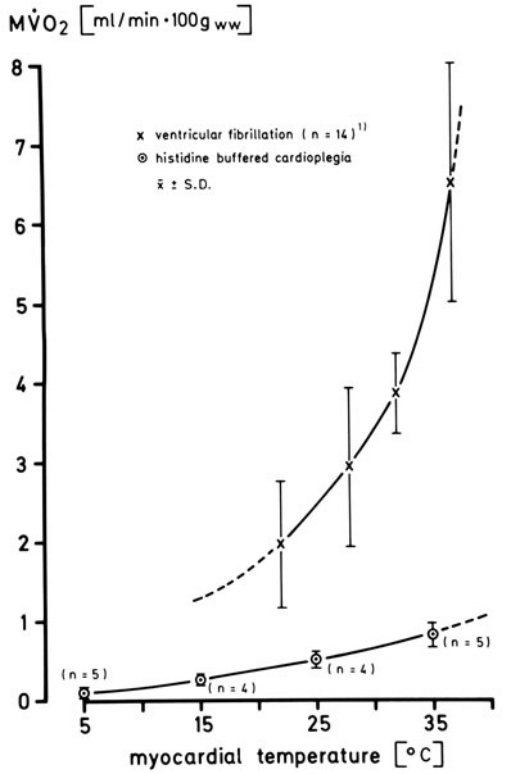

FIGURE 29–2. Temperature dependence of $M\dot{V}O_2$ of canine hearts during ventricular fibrillation (1) data from Buckberg et al. [6] and during cardioplegic coronary perfusion with the sodium-poor, calcium-free, histidine-buffered solution [17].

1. The elevation of extracellular potassium concentration $[K]_0$ which—depending on its degree—leads to inactivation of the rapid as well as the slow Na and Ca-Na channels and thereby to electrical and mechanical cardiac arrest [5].
2. The elevation of extracellular magnesium concentration $[Mg]_0$ primarily causing displacement of calcium from its loci in the outer membrane and particularly in the contractile system and thus leading to mechanical arrest and relaxation of the heart [5].
3. The reduction of extracellular sodium concentration $[Na]_0$ to a cytoplasmic level with simultaneous minimizing of free extracellular calcium concentration $[Ca]_0$ in order to effect not only electrical but also complete mechanical inactivation of cardiac muscle cells according to the well-known efficacy of $[Ca]_0$ in the contractile system inversely correlating with the square of $[Na]_0$ [5].
4. Pharmacologic cardiac arrest by administration of beta blockers, local anesthetics, or calcium antagonists alone or in combination with the above-mentioned electrophysiologically acting principles.

We have stopped using method 4 because of an unusually firm binding of these substances in the myocardium during anaerobic ischemia, leading the prolongation of their effects into the postischemic phase and delaying functional recovery of the heart. Method 1 or a combination of 1 and 2, or method 2 or a combination of 2 and 3 has generally to be preferred. The efficacy of these latter in comparison to purely ischemic cardiac arrest as well as their equivalence in minimizing cardiac energy demand for work is shown by the comparison of $M\dot{V}O_2$ during ventricular fibrillation with that during cardioplegic coronary perfusion with our low-Na, Ca-free, histidine-buffered solution (fig. 29–2) or with data from the literature on $M\dot{V}O_2$, e.g., during hyperkalemia coupled with beta blockade [6].

The basal metabolism of the heart like that of other organs can be increased by catecholamines, thyroid hormone, or similarly acting pharmacologic agents. But if these special metabolic situations are excluded, $M\dot{V}O_2$ is identical with the minimal value necessary for preservation of structural integrity and readiness for function, i.e., the $M\dot{V}O_2$ under the conditions of complete electrical as well as mechanical inactivation of the heart during coronary perfusion with cardioplegic solution (fig. 29–2). This minimum $M\dot{V}O_2$ is only temperature dependent in regard to its absolute value (Q_{10} around 2.0). The much higher temperature dependence of $M\dot{V}O_2$ of the fibrillating heart—with Q_{10} values of more than 2.5—shows that under such conditions a decrease in temperature also means decrease in work output, e.g., a decrease in frequency of fibrillation (fig. 29–2).

During the anaerobic phase of global isch-

emia, the energy turnover E of cardioplegically arrested hearts is lower than that of hearts arrested by pure ischemia (fig. 29–3). With Q_{10} values around 2.0, the temperature dependence is comparable to that of $M\dot{V}O_2$ during the aerobic phase of cardioplegic coronary perfusion and likewise clearly lower than the temperature dependence of $\dot{E}$ of hearts arrested in pure ischemia (figs. 29–2 and 29–3). This again is due to the much higher degree of activation of contractile systems even during anaerobiosis of pure ischemia which is clinically apparent by the increased myocardial tone of those hearts. The high standard deviation of these results, moreover, indicates that the individually variable preischemic level of turnover can be extensively equalized by complete cardioplegia, but remains effective into anaerobiosis under conditions of pure ischemic cardiac arrest.

For principal reasons there are only limited possibilities of prolonging the revival time of the heart under global ischemia by direct or indirect *increase of myocardial energy reserves.* When maximizing myocardial O_2 reserves in the effort to achieve an increase in aerobic latency after coronary circulatory arrest, the following has to be considered:

1. Only the intravascular space is available for adding O_2 carriers in the form of oxyhemoglobin or oxyfluorocarbons. But only 40%–50% of it—the capillaries, venules, and small veins—is effective for supplying O_2 to the myocardium by diffusion. In the canine heart this usable vascular space totals maximally 10 ml/100 g left ventricular myocardium.
2. Even a manifold increase of O_2 reserves can achieve significant prolongation of aerobic latency only when combined with an $M\dot{V}O_2$ which is decreased to a minimum level by optimal cardioplegia (table 29–1).
3. Hyperbaric partial pressures of oxygen, partially in the presence of minimum MVO_2 values, have toxic effects by inducing free radical and peroxide formation [7] and by this or other yet unknown mechanisms increase the basal energy requirement of the heart (unpublished results).

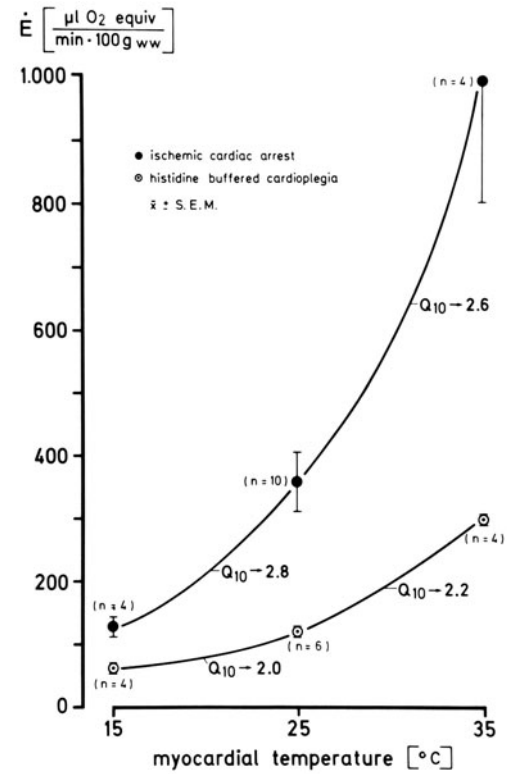

FIGURE 29–3. Temperature dependence of anaerobic energy turnover during t_{ATP} in dog hearts ischemically arrested or cardioplegically perfused prior to ischemia.

4. In myocardial preservation under deep hypothermia with hyperbaric P_{O_2}, moreover, quantitative considerations of the penetration depth of O_2 by diffusion from the external and internal myocardial surfaces are demanded. According to Warburg's diffusion equation, only approximately two-thirds to three-fourths of an unhypertrophied left ventricular wall can be reached even under the most favorable conditions (temperature of the heart 5°C, $M\dot{V}O_2$ 0.1 ml/min/100 g, P_{O_2} 5 atm). In an overall analysis of the myocardial ATP content we thus may obtain extremely prolonged t_{ATP} and good structural preservation of the subepicardial as well as of the subendocardial regions with simultaneous irreversible damage of the core.

TABLE 29–1. Calculation of under different experimental conditions maximally reachable aerobic latency

Experimental conditions	Myocardial temperature (°C)	Myocardial O_2 pressure (mm Hg)	$\dot{M}VO_2$ $\left(\frac{ml}{min \times 100\ g}\right)$	Myocardial O_2 reserves (ml/min/100 g) (= Hb-O_2 + Mb-O_2 + solved O_2)	Aerobic latency (min)
Pure ischemia		40	5.0	1.5 + 0.5 + 0.1	0.4
Cardioplegia	35	150	0.8	— 0.5 + 0.4	1.1
Cardioplegia		700	0.8	— 0.5 + 1.8	2.9
Pure ischemia		40	2.4	1.5 + 0.5 + 0.1	0.9
Cardioplegia	25	150	0.4	— 0.5 + 0.5	2.5
Cardioplegia		700	0.4	— 0.5 + 2.1	6.5
Pure ischemia		40	1.2	1.5 + 0.5 + 0.1	1.8
Cardioplegia	15	150	0.2	— 0.5 + 0.5	5.0
Cardioplegia		700	0.2	— 0.5 + 2.5	15
Pure ischemia		40	0.5	1.5 + 0.5 + 0.2	4.4
Cardioplegia	5	150	0.1	— 0.5 + 0.7	12
Cardioplegia		700	0.1	— 0.5 + 3.2	37

The high-energy phosphate bonds in the myocardium are not energy reserves in the strict sense of the word, because they are necessary for preservation of structure and function. There appears to be no constant tissue level of CP and adenine nucleotides. Rather, depending on energy demands, there is a changing equilibrium between CP and the pool of linked adenine nucleotides. From this it also follows that at the onset of global ischemia in hearts arrested by pure ischemia the initial contents of CP and ATP are clearly less than after cardioplegic coronary perfusion (figs. 29–1 and 29–7).

The reserves of glycogen, which in regard to the yield of ATP under anaerobic conditions is the most favorable substrate for glycolysis, are never the factor limiting t_{ATP} in all presently used methods of cardiac arrest and cardioplegia (fig. 29–7). In contrast, methods which raise myocardial glycogen content prior to ischemia increase $\dot{E}$ and/or reduce membrane permeability to protons produced intracellularly during anaerobiosis and thereby diminish the effectiveness of cardioplegic methods which are combined with an increase of buffer capacity of the heart (unpublished results).

The possibility of *improving the efficacy of metabolic energy gain* under aerobic conditions is indicated by the quotient ATP/O during oxidation of various substrates. The oxidation of glucose residues from glycogen yields an ATP/O ratio of 3.2 and that of palmitate of 2.8 [8]. Such a theoretical and in vitro attainable increase in ATP gain of 15% per molecule oxygen, however, cannot be reached in vivo because of the necessarily mixed substrates. Therefore it can be neglected for prolongation of aerobic latency during global ischemia. However, it may be important in the balance of energy of underperfused margins of regional myocardial ischemia [8].

Under anaerobic conditions, glycolysis is the essential metabolic pathway for ATP gain. The efficacy of anaerobic energy gain η in pure ischemia as in all cardioplegic methods mentioned above is on the average 0.65 or 65% (fig. 29–4) [9, 10]. The adaptation of glycolytic energy production to anaerobic energy turnover always leaves a deficit of 35% under these conditions, which fundamentally limits t_{ATP}. Up to now the only possibility of favorably influencing η in order to prolong t_{ATP} lies in the increase of buffer capacity of the myocardium. Mean values of η obtained during t_{ATP} under these conditions are around 80% (fig. 29–4). This increase of η by about 25% over that in pure ischemia effects a prolongation of t_{ATP} by a factor of approximately 2 (fig. 29–4).

The artificial increase of myocardial buffer

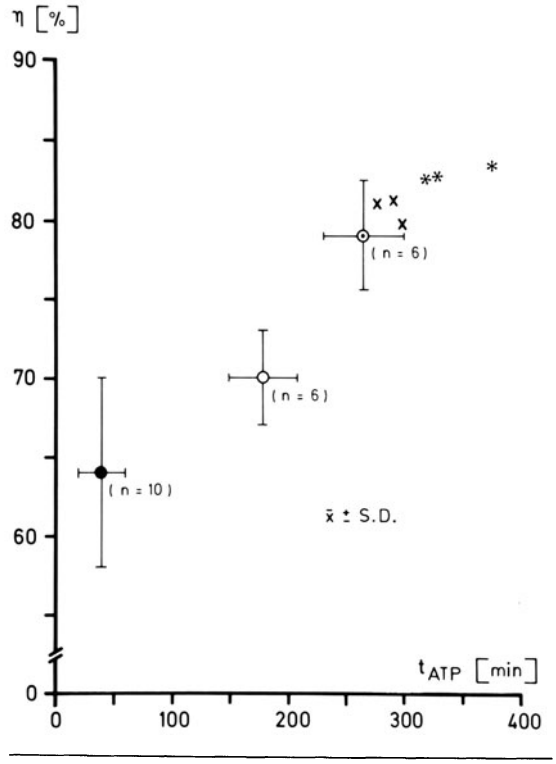

FIGURE 29–4. Mean efficacy of anaerobic energy gain during t_{ATP} in the left ventricular myocardium of dog hearts at 25°C, depending on preischemic treatment. For symbols, see figure 29–6.

capacity β under conditions of global ischemia calls for (a) the identification of the critical pH range in need of buffering for the ischemic myocardium, and (b) an evaluation of the quantitative limits for an increase of β.

From the physiologic cytoplasmic pH of around 7.0 [11], the specific sensitivity of the myocardium to alkaline pH and, at the same time, marked limitation of the activity of certain key enzymes of glycolysis near pH 6.0 [9, 10], one can conclude that the critical pH range lies between 7.0 and 6.0. Thus, buffer substances with a pk near 6.5 are suitable.

From osmotic considerations additional introduction of a buffer is limited to the extracellular compartment of the myocardium. Buffer substances which significantly diffuse into myocardial cell simultaneously cause cellular edema by the accompanying water shifts. In limitation to the extracellular space, however, even with best use of this compartment by optimal equilibration with the buffer solution [12], the increase of β/kg myocardial muscle can only attain one-fourth to maximally one-third of β/kg buffer solution used.

The nonbicarbonate buffer capacity of the left ventricular myocardium within the physiologic pH range amounts 20–30 mmol/kg/pH [11]. In order to double β of the left ventricular myocardium between pH 7.0 and 6.0, one therefore needs an approximately 100-m*M* solution of a buffer with pk of 6.5 or a solution well in excess of 200 m*M* of a buffer with pk 5.5. Thus, an effective artificial increase of myocardial buffer capacity can be achieved at the present only in combination with the cardioplegic concept of low $[Na]_0$ and minimum

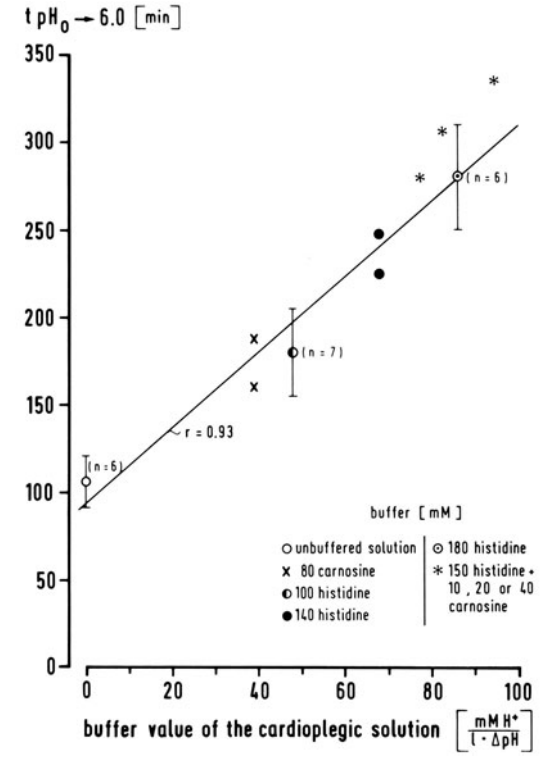

FIGURE 29–5. Delay of extracellular acidification in the left ventricular myocardium of dog hearts during global ischemia at 25°C, depending on buffer capacity between pH 7.0 and 6.0 of the sodium-poor, calcium-free, cardioplegic solution used prior to ischemia. x̄ ± S.D.

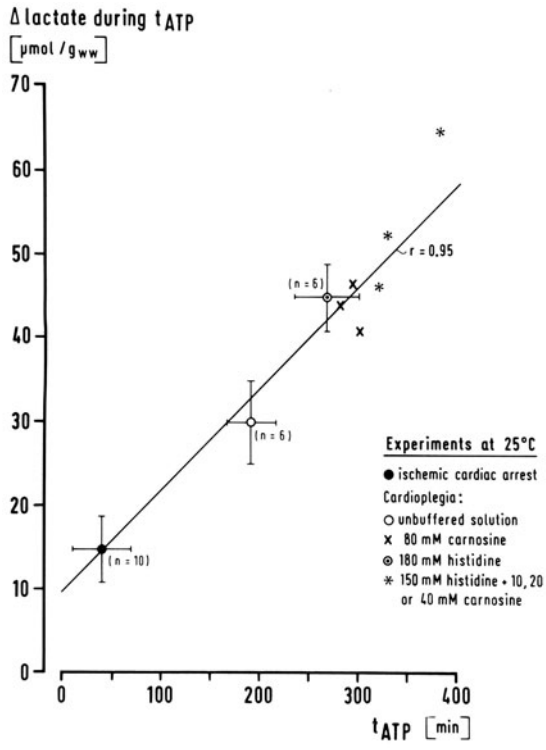

FIGURE 29–6. Lactate accumulation during t_{ATP} in the left ventricular myocardium of dog hearts, depending on buffer substance and buffer capacity between pH 7.0 and 6.0 (see fig. 29–5) of the sodium-poor, calcium-free, cardioplegic solution used prior to ischemia. $\bar{x} \pm$ S.D.

$[Ca]_0$, since such a cardioplegic solution alone offers the necessary osmotic margin. The accuracy of these quantitative considerations is shown in dog hearts in which an excellent correlation was found between the time interval from the onset of global ischemia until pH_0 6.0 and β of the cardioplegic solution used prior to ischemia (fig. 29–5). The prolongation of t_{ATP} thus attained is coupled with a prolonged glycolysis of slightly increased intensity (figs. 29–1, 29–6, and 29–7). It seems therefore plausible to consider phosphofructokinase, the glycolytic enzyme with specific pH dependence which is almost inactivated at pH 6.0, as playing an essential role in effective protection [10, 13].

The low-sodium, calcium-free, histidine-buffered cardioplegic solution, developed from the considerations detailed above [2, 17], prolongs t_{ATP} between normothermia and 15°C always by a factor of 6–7 as compared to pure ischemia, while the same solution without buffer, just as all other unbuffered cardioplegic solutions, increases it by a factor of 3–4 (fig. 29–8) [2]. The particularly large increase of t_{ATP} by the histidine-buffered solution at temperatures decreasing from normothermia to 25°C ($Q_{10} \rightarrow 2.7$) is due to the largely temperature-dependent pk_2 of histidine (approximately 5.9 at 35°C, 6.1 at 25°C, and 6.3 at 15°C). Therefore, the buffering capacity of the solution between pH 7.0 and 6.0 and hence the additional t_{ATP} gained by increasing the role of glycolysis during anaerobic energy turnover at 35°C are less than at 25° or even 15°C.

With the considerable increase in t_{ATP}, ex-

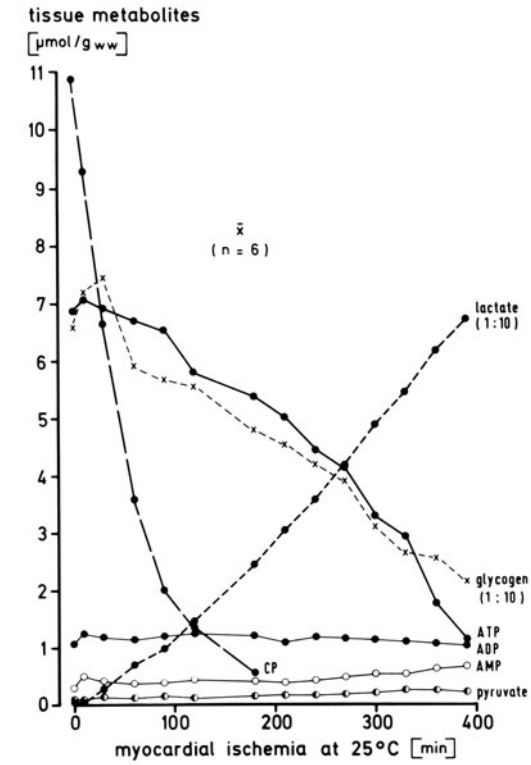

FIGURE 29–7. Metabolites in the left ventricular myocardium of dog hearts during global ischemia after protection with the sodium-poor, calcium-free, histidine-buffered cardioplegic solution [17].

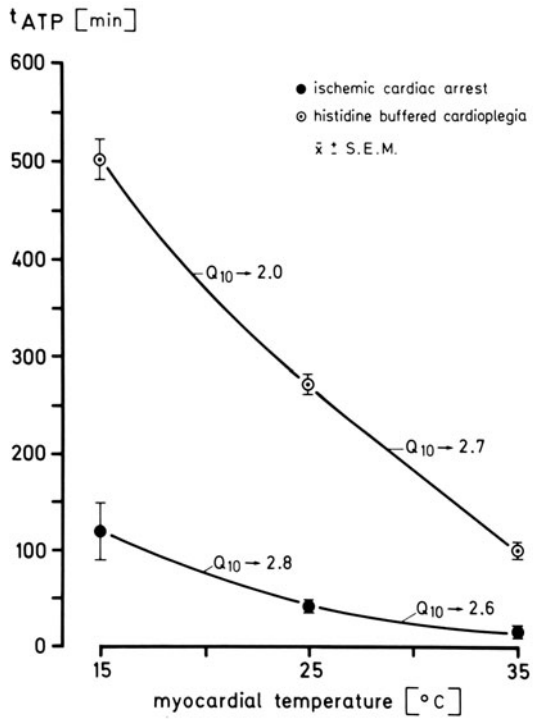

FIGURE 29–8. Temperature dependence of t_{ATP} of ischemically and cardioplegically arrested hearts.

perimental ischemia of 300 min at a mean myocardial temperature of 23°C and a recovery latency of 20 min is reversible in dog hearts without significant structural or functional damage (figs. 29–9 to 29–11) [14]. When applying the revival time achieved under optimal myocardial protection and global ischemia in dog hearts to the hearts of patients undergoing cardiac surgery, one has to take into consideration the various kinds and extent of preexisting damage. If one corrects the experimental results by a factor of 2 for such possibly limiting factors, an ischemic period of 150 min at approximately 23°C of mean myocardial temperature is available to the surgeon [2]. This has now been proven by clinical results [15].

Problems of Cardioplegia

In pure ischemia as well as in ischemia under cardioplegic conditions, there is a close correlation between the state of energy of the heart, the degree of structural alteration, and the functional reversibility. Nevertheless, this correlation is by no means absolute. Preliminary results of the analysis of the passive electrical properties of the myocardium in comparison with its state of energy during ischemia indicate that there are variations in protection of myocardial energy state and structure, depending on treatment of the heart before ischemia (fig. 29–12) [16]. Moreover, under special experimental conditions, an ischemic stress can become irreversible because of rather specific alterations of functional integrity of cellular and subcellular membranes and despite optimal protection of at least the energy state of the heart. For example:

1. If one reduces the amount of calcium bound to the surface coat of myocardial cell membranes below a certain minimum level, abrupt reintroduction of calcium results in irreversible damage to the heart even at physiologic levels of CP and ATP in the tissue, i.e., the so-called calcium paradox [17].
2. If one substitutes carnosine with its more favorable pk of approximately 6.7 at 25°C for histidine as buffer substance in a low-sodium, calcium-free, cardioplegic solution [18], t_{ATP} remains the same (fig. 29–6). Nevertheless, the same ischemic stress of 300 min at a mean myocardial temperature of 23°C is not reversible (fig. 29–10). Severe intracellular edema immediately follows postischemic reperfusion (figs. 29–11 and 29–13), while the myocardial ATP content decreases from approximately 4.7 μmol/g left ventricular myocardium at the end of ischemia to a level of 3.0 μmol/g during 20 min of postischemic reperfusion (fig. 29–10).

Preliminary experimental as well as clinical results indicate that even specific "protection of structures" can be afforded, e.g., by the addition of quinine to our histidine-buffered cardioplegic solution [19]. Its effect becomes apparent by accelerating of the metabolic recovery of

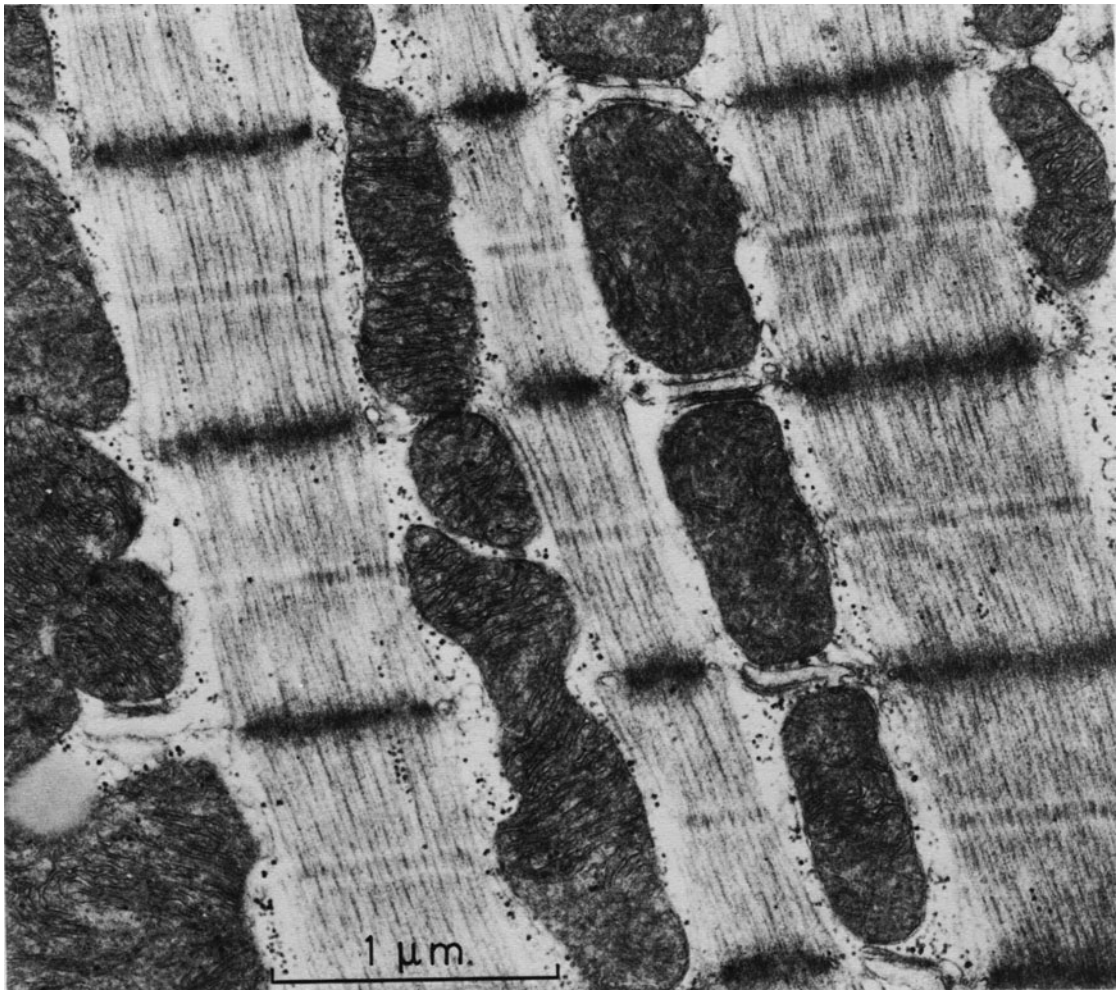

FIGURE 29–9. Electron micrograph of left ventricular subendocardium of a dog heart after protection with the sodium-poor, calcium-free, histidine-buffered cardioplegic solution, 300 min of global ischemia at 23°C, and 21 min of reperfusion with a modified Tyrode solution: almost normal mitochondria, sufficient glycogen granules between the sarcomeres, minute cellular edema. Original magnification ×20,000.

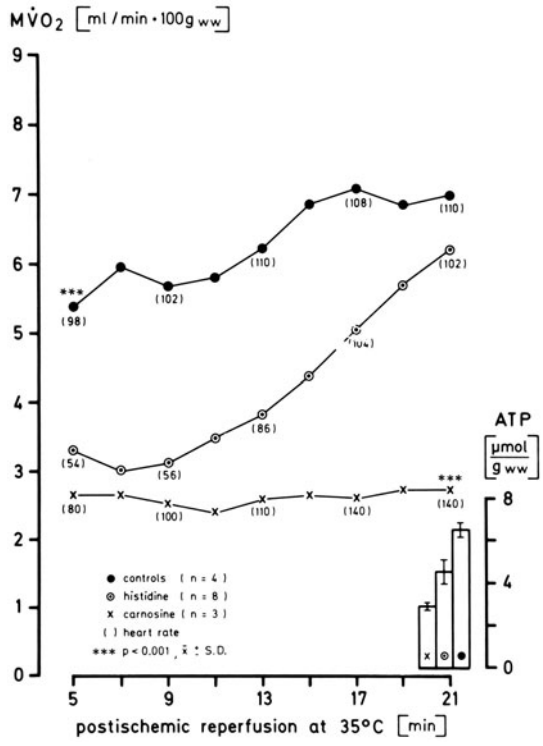

FIGURE 29–10. O_2 consumption of empty beating canine hearts during perfusion with a modified Tyrode solution (controls), and under the same conditions after protection with histidine-buffered [17] or carnosine-buffered [18] sodium-poor, calcium-free cardioplegic solution and consecutive 300 min of ischemia at 23°C. Left ventricular ATP content at the end of 21 min of Tyrode perfusion.

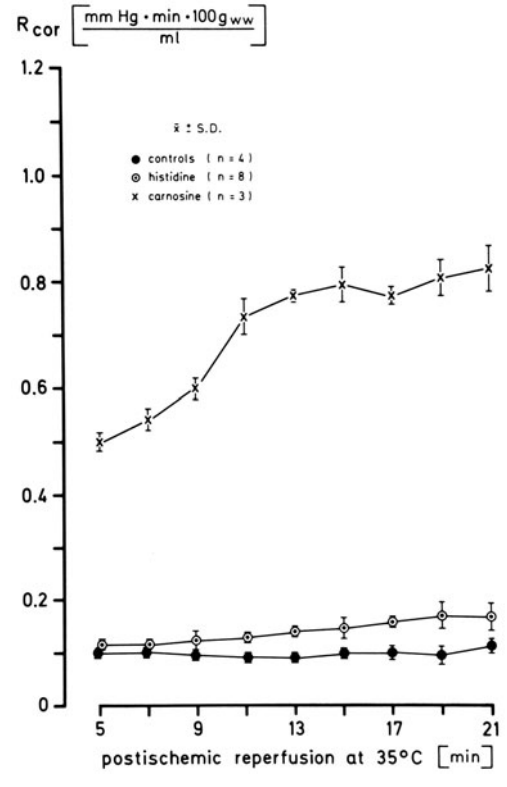

FIGURE 29–11. Coronary resistance during perfusion with modified Tyrode solution in the experimental groups shown in figure 29–10.

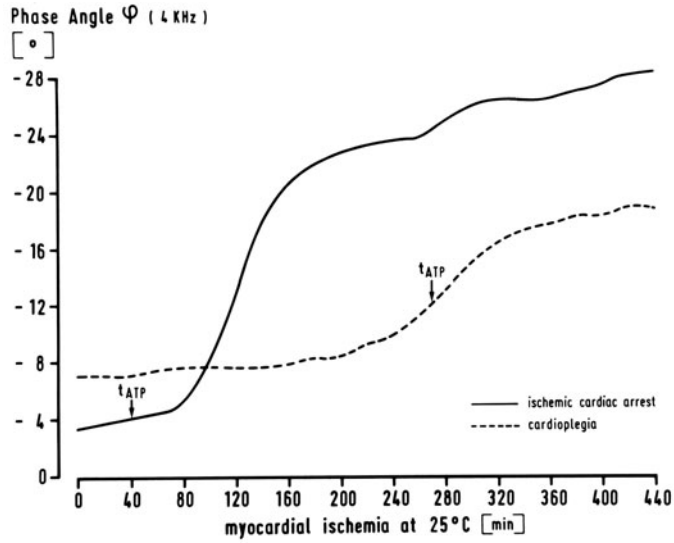

FIGURE 29–12. Phase angle of the alternating current resistance of left ventricular myocardium of dog hearts at 4 kHz of a.c. frequency, during global ischemia and during ischemia after cardioplegic perfusion with out histidine-buffered solution. Note the shift of t_{ATP} in relation to the time course of the phase angle in protected in comparison to unprotected hearts. For details, see Bretschneider et al. [16].

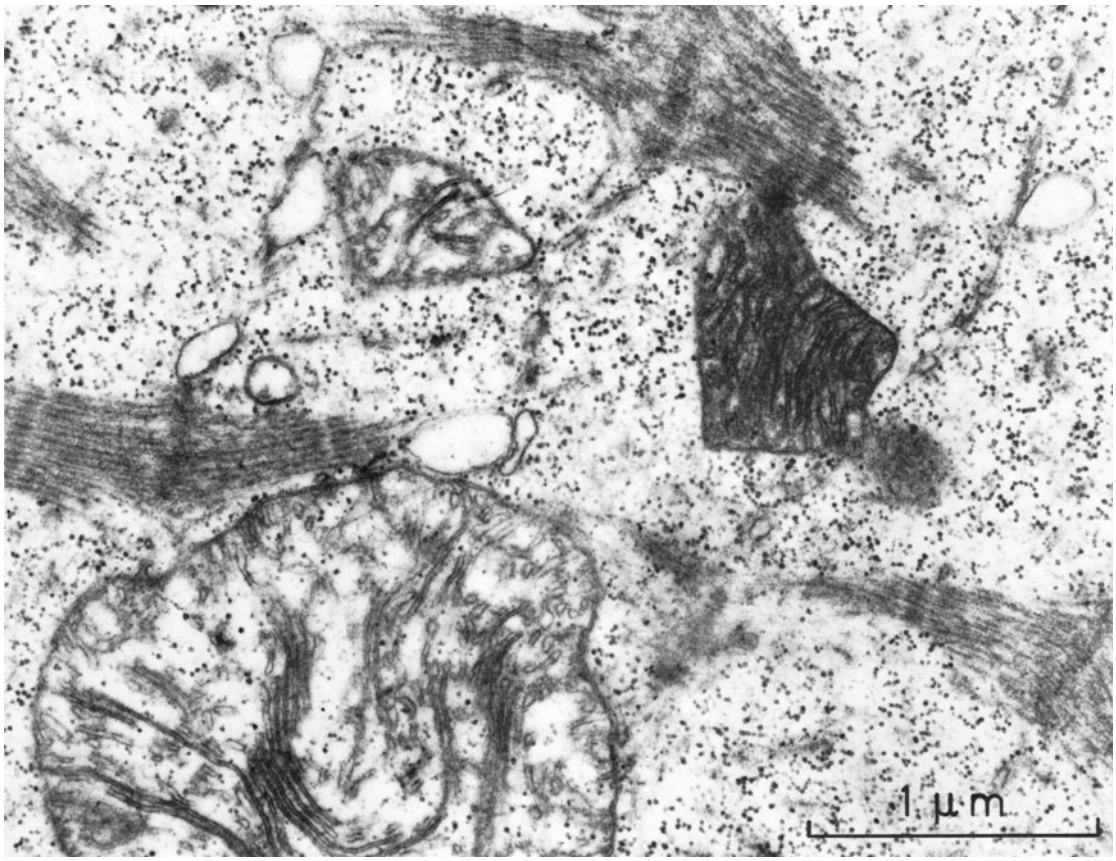

FIGURE 29–13. Electron micrograph of left ventricular subendocardium of a canine heart after protection with sodium-poor, calcium-free, carnosine-buffered cardioplegic solution [18], 300 min of ischemia at 23°C, and 21 min of reperfusion with a modified Tyrode solution: severe intracellular edema and laceration of myofibrills; in the major part of mitochondria edema, fragmentation of cristae, and loss of matrix structure, in some tendency of recovery. Original magnification ×20,000.

the heart, by lowering the incidence of arrhythmias, and by optimizing minimal coronary resistance during postischemic reperfusion. The possibility of such a specific intervention represents a decisive improvement in protection of the heart during global ischemia, because it reduces untoward postischemic phenomena which otherwise—in the manner of a vicious cycle—aggravate the metabolic, structural, and functional restitution of the organ.

Acknowledgments

The above detailed concept of cardioplegia and protection of the heart under global ischemia has been developed in close scientific cooperation with W. Kübler, MD, Professor of Cardiology, Heidelberg (FRG); P.G. Spieckermann, MD, Professor of Physiology, Göttingen; E. Gersing, PhD, and Ph.A. Schnabel, MD, Physiology, Göttingen; and with the help of always excellent technical assistants.

References

1. Bretschneider HJ: Überlebenszeit und Wiederbelebungszeit des Herzens bei Normo- und Hypothermie. Verh Dtsch Ges Kreislaufforsch 30:11–34, 1964.
2. Bretschneider HJ, Gebhard MM, Preusse CJ: Reviewing the pros and cons of myocardial preservation within cardiac surgery. In: Longmore DB (ed) Towards safer cardiac surgery. Lancaster: MTP, 1981, pp 21–53.
3. Bretschneider HJ, Hellige G: Pathophysiologie der Ventrikelkontraktion—Kontraktilität, Inotropie, Suffizienzgrad und Arbeitsökonomie des Herzens. Verh Dtsch Ges Kreislaufforsch 42:14–30, 1976.
4. Hearse DJ, Braimbridge MV, Jynge P: Protection of the ischemic myocardium: cardioplegia. New York: Raven, 1981.
5. Noble D: The initiation of the heart beat. Oxford: Clarendon, 1979.
6. Buckberg GD, Brazie JR, Nelson RL, Goldstein SM, McConnell DH, Cooper N: Studies on the effects of hypothermia on regional myocardial blood flow and metabolism during cardiopulmonary bypass. I. The adequately perfused beating, fibrillating, and arrested heart. J Thorac Cardiovasc Surg 73:87–94, 1977.
7. Chance B, Sies H, Boveries A: Hydroperoxide metabolism in mammalian organs. Physiol Rev 59:527–605, 1979.
8. Hütter JF, Schweickhardt C, Piper HM, Spieckerman PG: Inhibition of fatty acid oxidation and decrease of oxygen consumption of working rat heart by 4-bromocrotonic acid. J Mol Cell Cardiol 16:105–108, 1984.
9. Neely JR, Morgan HE: Relationship between carbohydrate and lipid metabolism and the energy balance of the heart muscle. Annu Rev Physiol 36:413–459, 1974.
10. Kübler W, Spieckermann PG: Regulation of glycolysis in the ischemic and the anoxic myocardium. J Mol Cell Cardiol 1:351–377, 1970.
11. Roos A, Boron WF: Intracellular pH. Physiol Rev 61:296–434, 1981.
12. Preusse CJ, Gebhard MM, Bretschneider HJ: Myocardial "equilibration processes" and myocardial energy turnover during initiation of artificial cardiac arrest with cardioplegic solution. Thorac Cardiovasc Surg 29:71–76, 1981.
13. Kallerhoff M, Hölscher M, Kläss G, Helmchen U, Bretschneider HJ: Influence of different kidney-protective solutions on metabolism and energetics of ischemic kidneys. Pflügers Arch 382:R15, 1982.
14. Schnabel PhA, Gebhard MM, Preusse CJ, Richter J, Schwartz P, Spieckermann B, Bretschneider HJ: Protektion der Ultrastruktur im ischämischen Myokard durch die kardioplegische Lösung HTK nach Bretschneider bei 25°C. Verh Anat Ges 77:605–608, 1983.
15. Schulte HD, Preusse CJ, Groschopp C, Bircks W, Bretschneider HJ: Crystalloid cardioplegia: experience with the Bretschneider solution. In: Engelman RM, Levitsky S (eds) A textbook of clinical cardioplegia. Mt Kisco NY: Futura, 1982.
16. Bretschneider HJ, Gebhard MM, Gersing W, Preusse CJ: Problems of myocardial protection under view of the heterogeneity of the affected tissues and the different vulnerability of subcellular structures. In: Caldarera CM, Harris P (eds) Advances in studies on heart metabolism. Bologna: CLUEB, 1982.
17. Gebhard MM, Bretschneider HJ, Gersing E, Preusse CJ, Schnabel PhA, Ulbricht LJ: Calcium-free cardioplegia—pro. Europ Heart J 4 (Suppl. H):151–160, 1983.
18. Gercken G, Bischoff H, Trotz M: Myokardprotektion durch eine Carnosin-gepufferte kardioplegische Lösung. Drug Res 30:2140–2143, 1980.
19. Bretschneider HJ, Gebhard MM, Gersing E, Preusse CJ, Schnabel PhA: Recent advances for myocardial protection. In: Kaplitt MJ, Borman JB (eds) Concepts and controversies in cardiovascular surgery. Norwalk, Connecticut: Appleton-Century-Crofts, 1983.

30. THE EFFECTS OF THE VOLATILE ANESTHETIC AGENTS ON THE HEART

Margaret G. Pratila
and Vasilios Pratilas

Introduction

It took only just over a year after William Morton showed the feasibility of surgical anesthesia to demonstrate the marked effects of volatile anesthetic agents on the heart. On 28 January 1848, Hannah Greener, aged 15, was the first patient to die during chloroform anesthesia (presumably of ventricular fibrillation).

Increasing amounts of research at the cellular level and in intact animals in addition to clinical studies have emphasized this effect. The many hundreds of papers that have been written on the cardiac effects of the anesthetic agents and the many millions of dollars spent on monitoring the heart in the perioperative period attest to the importance of the effects of anesthetic agents on the heart.

One of the exciting advances in understanding the effects of anesthetic agents on the heart has been the application of microelectrode techniques of electrophysiology which allow us to study the effects of anesthetic agents on the cell uninfluenced by uncontrolled autonomic nervous system activity. It is to these studies that we shall mainly direct our attention. Anesthetic effects influencing the coronary circulation have also become increasingly important with the advent of coronary bypass surgery.

The Sinoatrial Node

Hauswirth and Schaer [1] in 1967 described the effects of halothane on action potentials from single rabbit sinoatrial (SA) nodal fibers. They showed a decrease of the maximal diastolic potential (MDP) and a decreased rate of diastolic depolarization. These effects were confirmed by Reynolds and his colleagues [2]. At 1% concentration, halothane had a moderate negative chronotropic action on the SA nodal fibers. This was the result of a reduced rate of diastolic depolarization and an increase in threshold potential. At 2% halothane the rate of diastolic depolarization was further reduced and maximal diastolic potential, overshoot, and amplitude of the action potential were also decreased. At 4% halothane a progressive reduction in maximal diastolic potential, overshoot, and amplitude occurred. Arrest of the fiber followed. The arrest did not follow progressive slowing of rate, but was associated with marked loss of maximal diastolic potential, increase in the threshold potential, and ultimate loss of excitability. These fibers were unresponsive to electrical stimulation. The arrest was completely reversed when halothane was washed out. The effects are summarized in figure 30–1.

Maylie et al. [3] have recently indicated that generation of the pacemaker potential in the SA node is related to the activation of an inward current with high equilibrium potential rather than decreasing potassium ion conductance. Kampine and his colleagues [4] have further examined the SA nodal suppression caused by halothane in the light of the findings of Maylie et al. Halothane has been shown to inhibit inward Ca^{2+} current through the slow ionic channel in myocardium, demonstrated by depression of the maximum rate of rise

N. Sperelakis (ed.), PHYSIOLOGY AND PATHOPHYSIOLOGY OF THE HEART.

Martinus Nijhoff Publishing, Boston/The Hague/
Dordrecht/Lancaster.

($+\dot{V}_{max}$) of the slow action potential [5]. The negative chronotropic action of halothane and the dose-dependent depression of $+\dot{V}_{max}$ in phase 4 and phase 0 demonstrated by Kampine et al. are consistent with inhibition of slow calcium channels in the SA node. Introduction of calcium (2× concentration) produced a parallel shift in the dose–responsive curve in an upward direction and blunted the overall depression of phases 4 and 0. Introduction of a calcium-channel blocker (verapamil) produced a parallel depression of the dose–response curve and potentiated depression of the heart rate and $+\dot{V}_{max}$ of phase 0. It would appear that halothane interacts with calcium competitively.

Halothane 0.5% and initial exposure to 1% halothane resulted in hyperpolarization of the transmembrane potential in guinea pig and cat SA nodal fibers [6]. Initial exposure to 1.12% and 2.25% enflurane did not produce the same effect. Enflurane 2.25% and 4.50% produced a significant negative chronotropic action, an increase in duration of phase 4, and a decreased rate of rise in phase 4. The rate of rise of phase 0 was decreased and the duration of the action potential prolonged at 4.5% enflurane (fig. 30–2). The effects of enflurane are obviously less marked than those of halothane.

The clinical use of methoxyflurane has decreased markedly due to its adverse renal effects and its slow uptake and elimination. However, it is the prototype of the halogenated ethers. Reynolds and his co-workers [2] demonstrated a biphasic effect on the SA node. There is a decrease in rate which is preceded by a brief initial acceleration. This acceleration is due chiefly to a slight loss in maximal diastolic potential. It is not reversed by propranolol. The decrease in rate is associated with a further decrease in maximal diastolic potential and an increase in threshold potential. Overshoot is reduced. An arrest of activity invariably occurred at 1% methoxyflurane and frequently occurred at 0.5%. Arrest followed a loss of MDP, increase in threshold potential, and finally a loss of excitability. As with the other volatile agents this effect was reversible. When the rate was increased by epinephrine, exposure to methoxyflurane had little effect.

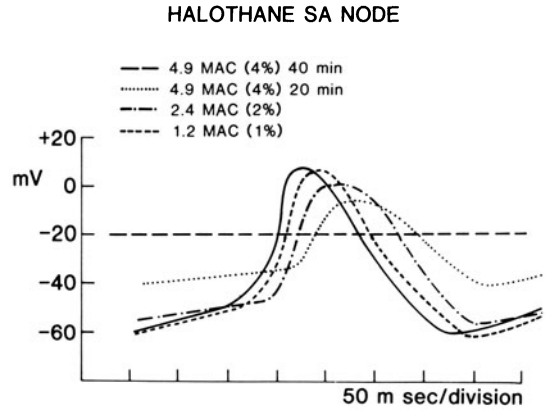

FIGURE 30–1. A schematic presentation of the effects of halothane on the SA nodal action potential [1, 2]. The effects of concentration and time are shown. MAC values allow comparison between agents.

THE ATRIA

Hauswirth [7] has shown that single rabbit atrial fibers are not very sensitive to even 2% halothane. Although the overshoot was significantly decreased and repolarization slightly prolonged, there was no marked change in resting potential or amplitude of the action potential as is seen in the SA node. Similar effects are seen with 1% methoxyflurane [8]. Enflurane [9] also produced a decreased overshoot and prolonged repolarization, but 6% enflurane

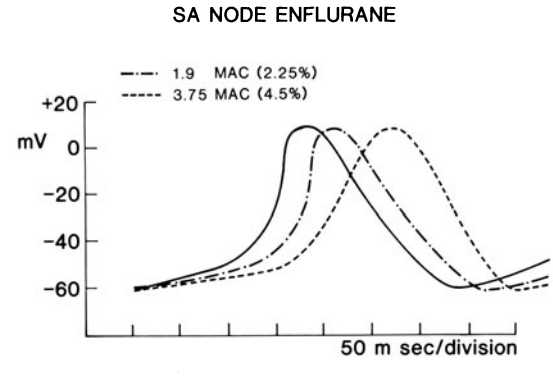

FIGURE 30–2. A schematic presentation of the effects of enflurane on the SA nodal action potential [6].

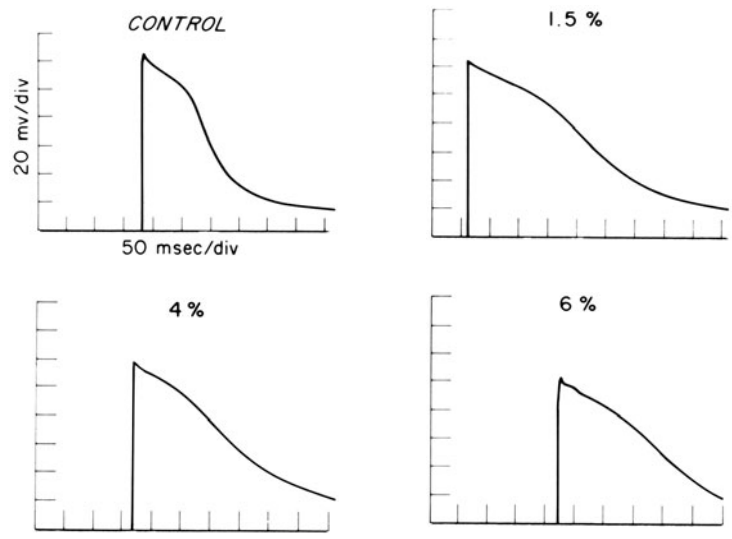

FIGURE 30–3. The effects of enflurane on rabbit atrium at 1.5% (1.25 MAC), 4% (3.3 MAC), and 6% (5 MAC).

(a dose far in excess of clinical values) was necessary before reduction in amplitude occurred. Resting potential was virtually unchanged (fig. 30–3).

THE ATRIOVENTRICULAR NODE

There is no doubt clinically that the presently used volatile anesthetic agents have a marked effect on the atrioventicular (AV) node. It is not uncommon to see P waves unrelated to QRS complexes on the monitoring ECG during anesthesia. With the termination of anesthesia there is termination of the dysrhythmia.

Scherlag et al. [10] and Damato et al. [11] described a method of studying AV nodal conduction in intact dogs by His bundle stimulation and recording. This His bundle electrogram allows subdivision of the PR interval into two components [12, 13]. Conduction time between the atrial depolarization potential and the His bundle deflection (AH interval) primarily represents impulse propagation in the region of the AV node. Conduction to the distal bundle of His and Purkinje network (HV interval) is measured from the His deflection to the beginning of the QRS complex.

The effects of the anesthetic agents on AV nodal conduction have mainly been studied by His stimulation and recording. Atlee and Rusy [14] in their initial studies utilizing catheter electrocardiography found a concentration-dependent depression of AV conduction by halothane. This depression was most marked proximal to the bundle of His (intraatrial and AV node, AH recording). Since atropine did not significantly alter the effect of halothane, vagal stimulation was not felt to be a factor. Beta-blockade with propranolol further slowed conduction, indicating sympathetic enhancement of AV conduction was present even at 2% halothane. Rapid atrial pacing also slowed conduction. The arrival of an impulse during the absolute refractory period with no transmission or during the relative refractory period when decremental conduction occurs was felt to be the probable cause. Prolongation of the refractory period was considered the most likely mechanism of halothane-produced depression of AV conduction.

In a later study [15], Atlee and Alexander showed that an increased concentration of halothane prolonged AV nodal and His–Purkinje conduction time in spontaneously beating hearts in which heart rate was constant and rate did not influence conduction time. The functional refractory period was prolonged at slow heart rates (120 beats/min), but unaffected at rapid rates (200 beats/min).

Atlee et al. [16] also studied the effects of the antidysrhythmics lidocaine and diphenylhydantoin in the presence of halothane. There was further prolongation of AV conduction to that produced by halothane. AV conduction was more sensitive to drug affect than His–Purkinje or total intraventricular conduction. They believed this might represent potentiation of the normal slowing of conduction through the AV node in response to increases in heart rate (fatigue response). They concluded that the antidysrhythmics failed to reverse the depressant effects of halothane on AV conduction. This may explain their ineffectiveness in the treatment of certain dysrhythmias during halothane anesthesia.

The problem with these early studies is that light anesthesia with halothane was used as a control. In a more recent study, chronically instrumented dogs were used and the true awake-to-anesthetized state obtained [17]. The results of these studies with halothane seem to indicate that halothane-induced prolongation of AV nodal conduction is more apparent at light levels of anesthesia (1%–1.5% halothane) and is more a function of changes in autonomic tone than of increasing concentration. Hantler and his colleagues [18] also studied halothane related to an "unanesthetized" control by using total spinal anesthesia. Sympathetic nervous system activity was thereby eliminated. AH interval was prolonged at fast rates following exposure to halothane, but not at slow rates.

In intact unpremedicated dogs, methoxyflurane produced a dose-dependent increase in the effective refractory period of the AV conduction system [19]. This was not influenced by vagotomy, which suggests the effect is independent of parasympathetic control.

Methoxyflurane is one of the few agents on which microelectrode studies are available. Reynolds et al. [8] showed that the activity of the AV node remained normal even after complete arrest of the SA nodal fiber. This finding correlates well with the frequent development of nodal rhythm during methoxyflurane anesthesia [20].

His bundle studies in the presence of 1–2 MAC (minimal alveolar concentration) enflurane slowed a prolongation of AV nodal, but not His–Purkinje or ventricular, conduction times [21]. (Minimum alveolar concentration is that concentration (vol/vol) of an inhalational anesthetic which prevents 50% of subjects from moving in response to a painful stimulus.) AV nodal conduction time increased as heart rate was increased. This rate dependency was enhanced by enflurane. His–Purkinje and ventricular conduction were not affected by rate or enflurane. The atrial effective refractory period, functional refractory period of the AV node, and AV nodal conductivity were depressed by enflurane. Halothane does not prolong the atrial effective refractory period [22]. This may be important in explaining the decreased incidence of supraventricular dysrhythmias during enflurane anesthesia compared to halothane. The effects of enflurane on the His–Purkinje and ventricular conduction system contrast with those the authors report for halothane. Since conduction changes are necessary for ventricular dysrhythmias caused by reentry of excitation, they felt their findings might partially explain the clinical impression of a decreased incidence of ventricular dysrhythmias with enflurane compared to halothane.

Zaidan et al. [23] have shown that ¾ MAC enflurane did not influence ventricular pacing employed as treatment of third-degree heart block produced by cardioplegic solutions during cardiopulmonary bypass. This is support from a clinical source for the findings at Atlee et al.

Blitt et al. [24] studied the effects of 1.25, 2, and 2.5 MAC isoflurane on AV conduction by His bundle electrocardiography during atrial pacing in dogs. There were no changes in AH interval. Atrial pacing to 200 beats/min did not influence the AH interval, unlike the effects of halothane. The stability of cardiac rhythm observed clinically with isoflurane may be related to this lack of effect on the AV node.

Purkinje Fibers

Reynolds et al. [2] reported that, when quiescent canine Purkinje fibers were exposed in vitro to 1% halothane, the resting membrane potential (RMP) was unchanged and the rate of phase-4 depolarization virtually unaffected.

Hauswirth [7], however, found in sheep Purkinje fibers RMP was increased and overshoot and duration of the action potential was decreased at 1% halothane. This disparity could be due to species differences. At 2% halothane or above, rate slowed in spontaneously beating fibers as a result of increase in threshold potential and a decreased rate of rise in phase-4 depolarization. A steep increase in the slope of phase 2 caused almost a complete loss of plateau. Action potential (AP) duration was shortened. In driven fibers the same effect on the plateau was seen. In many fibers, AP duration was not shortened due to a decrease in phase-3 repolarization. Pruett and his co-workers [25] have also shown similar results at equivalent concentrations—a shortened AP duration, decreased overshoot, depressed rate of phase-4 depolarization, and reduced maximum diastolic potential. $+\dot{V}_{max}$, however, increased and membrane responsiveness was enhanced. Amplitude and $+\dot{V}_{max}$ were decreased in the slow-response APs of fibers partially depolarized by 20 m*M* KCl.

Quiescent Purkinje fibers exposed to 1% methoxyflurane had a slightly less negative resting potential, but did not develop automatically. In spontaneously beating fibers, 0.5% and 1% methoxyflurane caused marked increases in rate mainly due to an increase in the slope of phase-4 depolarization. While a sharp increase in phase-2 repolarization occurred, the duration of action potential remained about the same due to a decrease in the terminal part of phase-3 repolarization. $+\dot{V}_{max}$ in phase 0 was also slightly decreased.

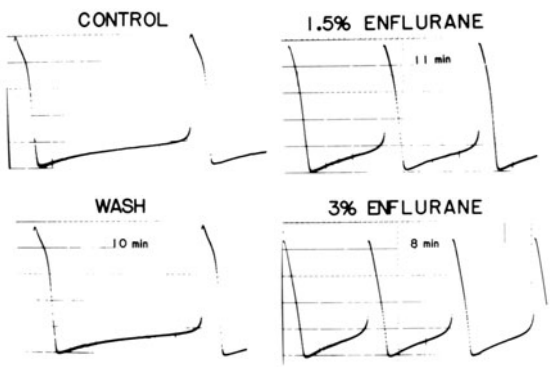

FIGURE 30–4. The effects of enflurane on spontaneously firing canine Purkinje fibers at 1.5% (0.73 MAC) and 3% (1.5 MAC).

The actions of enflurane are similar to those observed with halothane. In spontaneously active Purkinje fibers, however, enflurane enhances the rate of phase-4 depolarization and significantly reduces MDP (fig. 30–4). Threshold potential also appears to be at a less negative voltage. These findings have also been reported by Pruett and his colleagues [25]. These authors showed enhancement of membrane responsiveness in Purkinje fibers by both halothane and enflurane. Since membrane responsiveness reflects the fast inward current carried by sodium ions, they suggest normalization of membrane responsiveness after exposure to halothane and enflurane might be due to alteration in voltage- and/or time-dependent changes in sodium conductance similar to that reported by Chen et al. [26] for lidocaine.

Ventricular Muscle

Halothane depresses intraventricular conduction, but to a lesser extent than conduction through the AV node [16]. Ventricular automaticity is somewhat depressed by halothane as shown by studies in isolated cell preparations [2, 27] and in intact animals [27, 28]. At 2% halothane, Hauswirth [7] found in sheep ventricular cells an unchanged resting membrane potential, a decreased overshoot, a reduced duration of the action potential and a shortened effective refractory period. The $+\dot{V}_{max}$ of phase-0 depolarization was also decreased. Recent work has confirmed Hauswirth's findings [5]. Up to 2% halothane had little effect on normal APs. At 2% and above, a slight decrease in amplitude and duration occurred so that the plateau was shortened. $+\dot{V}_{max}$ of the normal fast AP was not depressed at any concentration of halothane.

Enflurane also has little effect on the resting membrane potential of normal guinea pig APs [29]. Amplitude and $+\dot{V}_{max}$ were virtually unaffected by even 6% enflurane. However, loss

of plateau and AP duration occurred at higher concentrations (fig. 30–5).

Since the slow inward current is in part responsible for maintaining the plateau of the action potential [30], the decrease in duration may be attributed to the depression of the slow inward currents by the volatile anesthetic agents which we shall discuss later. We cannot, however, exclude the possibility that potassium conductance is increased by these agents. This also would shorten the duration of the action potential.

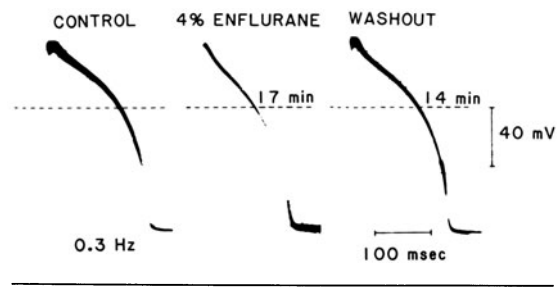

FIGURE 30–5. The effect of enflurane 4% (2.35 MAC) on normal guinea pig ventricular muscle action potential showing some loss of plateau and AP duration.

Ventricular Contraction

All volatile anesthetic agents are known to depress myocardial contractility. Even nitrous oxide, for so many years thought to be innocuous, is now known to be a cardiac depressant [31]. This depressant effect of the anesthetic agents has been shown both in clinical situations [32–36] and in the laboratory [37–42].

The mechanism of myocardial depression by the volatile anesthetic agents has been and continues to be the basis for a great number of investigations. It is unlikely that a single factor will provide an adequate explanation.

The volatile agents could influence the cardiac excitation–contraction process in a number of ways:

1. An effect on myocardial contractile proteins.
2. An effect on calcium ion release by the sarcoplasma reticulum.
3. An effect on myocardial slow channels.

It has been suggested that the volatile anesthetic agents interact directly with the myocardial contractile protein by changing its shape, blocking ionic channels, or preventing structural change in the protein. Evidence for this direct action is provided by the work of Seeman [43], Halsey [44, 45] Woodbury [46], Metcalfe [47], and Cheng [48] and their co-workers. Trudell has suggested a change in the fluidity of the phospholipid bilayer at anesthetic concentrations thus affecting the membrane lipoproteins involved in slow channel gating [49]. It has been postulated that alterations in fluidity would affect fast and slow channel gating equally, and fast sodium channel gating is unaffected by both halothane [5] and enflurane [29]. However, the work of Rosenberg et al. [50] and of Pang et al. [51] showed that variation in structure of phospholipid molecules, phospholipid–cholesterol ratio, and anesthetic concentration caused an increase or a decrease in the internal fluidity of the bilayer. These findings may partially explain the differing anesthetic actions on fast and slow channel gating.

The sarcoplasmic reticulum (SR) is a membranous system in the cardiac muscle that controls the amount and duration of calcium ion availability for contraction. Lipophilic volatile anesthetics have been shown to accumulate in the SR [52]. It has been suggested that the SR might be an important site at which anesthetic agents act to inhibit contractility [53]. Lain et al. [54] showed decreased uptake of calcium in homogenized and differentially centrifuged muscle. Although they showed a decreased calcium uptake, their halothane concentration was much greater than that which is clinically relevant. The work of Lee and colleagues [55], which also shows decreased Ca^{2+} uptake, suffers also from an uncertain concentration of halothane. Su and Kerrick have shown inhibition of Ca^{2+} uptake by the cardiac SR in the presence of clinically relevant concentrations of both halothane and enflurane [56–58]. They used mechanically skinned myocardial fibers, which allows free movement of the perfusing medium through the outer cell membrane.

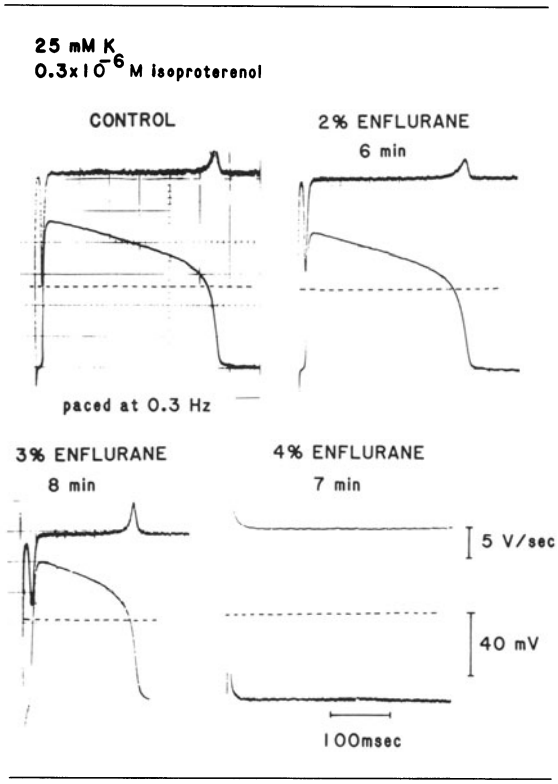

FIGURE 30–6. Effect of enflurane on slow cardiac action potentials from guinea pig ventricular muscle at 2% (1.2 MAC), 3% (1.8 MAC), and 4% (2.35 MAC). Note marked effects on slow AP at 4% compared to figure 30–5, the fast AP.

Price and Ohnishi have expressed contrary views [59]. Measurements of La^{3+} displaceable calcium ions in dog trabecular muscle indicate that halothane reduces the amount of superficially bound calcium ions [60]. Blanck [61–63] and co-workers have also studied the effects of halothane, enflurane, and isoflurane. All stimulate Ca^{2+} uptake by the SR in vitro. This occurs at low ATP concentrations and clinical ranges of the anesthetic agents. Their data suggest that all three agents increase the affinity of (Ca^{2+},Mg^{2+})-ATPase for ATP. Since rate of uptake is not stimulated beyond maximum velocity of the enzyme, the authors suggest that ATP availability is improved rather than enzyme alteration. At higher concentrations of ATP (>5 m*M*) and higher clinical concentrations of the anesthetic agents, inhibition of Ca^{2+} uptake occurs. However, at normal ATP levels and clinical concentration, all three agents seem to have little effect on Ca^{2+} uptake. Clinical significance, if any, lies in the fact that, if ATP declines as in ischemic heart disease or during ischemic arrest during cardiopulmonary bypass, Ca^{2+} uptake might be depressed.

Recently Komai and Rusy have concluded from their work on the effects of halothane in rested-state and potential-state contractions in rabbit papillary muscle that transsarcoleminal calcium influx and stored calcium are equally influenced, resulting in a negative inotropic action. Halothane reduces the amount of stored calcium by inhibiting uptake and accelerating the loss of the cation during rest [64].

During phase 2 or plateau of the action potential, an inward movement of calcium ions occurs through the kinetically slow ion transport system [65]. If this system is blocked by verapamil, a marked negative inotropism occurs in the presence of virtually normal action potentials [66]. The calcium entering the cell through these channels contributes to the contractile process [67]. Early workers [7, 68] showed halothane produced this negative inotropism with little effect on cardiac action potentials. Electromechanical dissociation is not uncommon clinically, and is manifested as severe hypotension with a virtually normal electrocardiogram.

The effects of halothane [5], enflurane [29] (fig. 30–6), and methoxyflurane [69] (fig. 30–7) on the slow channels have been studied by simultaneous measurements of action potentials and contractions in guinea pig papillary muscles. All three agents produce a depression of the inward calcium current that enters the myocardial cells through the voltage-dependent slow channels. Slow-channel action potentials were obtained by depolarization to −40 mV with 26 m*M* K^+ thus inactivating fast sodium channels [70]. Cells at this level of depolarization are inexcitable due to lack of inward current [71]. Slow-channel current can be increased by elevating the intracellular cyclic adenosine monophosphate (cAMP) level [72–74]. The $+\dot{V}_{max}$ of the slow action potential reflects the rate of depolarizing current flow [75]. The depressant effects of halothane on

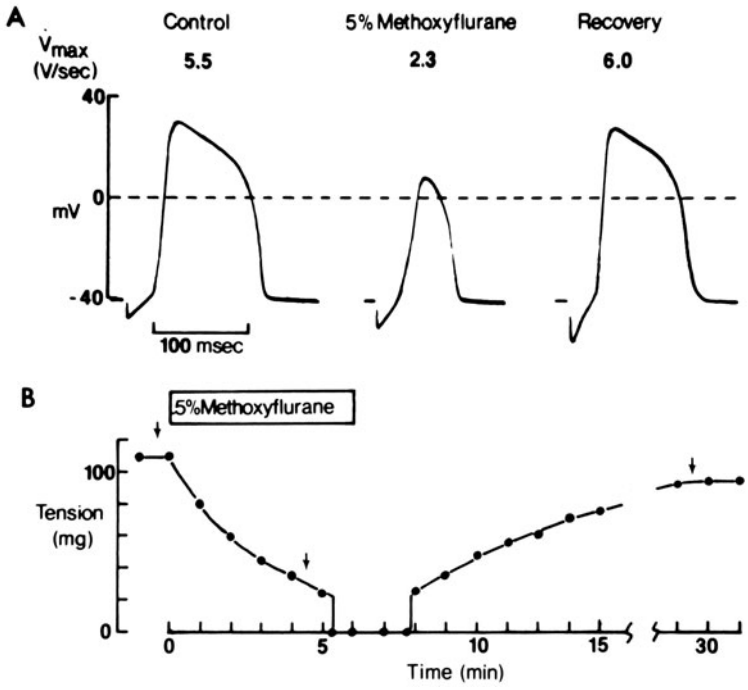

FIGURE 30–7. Effect of methoxyflurane 5% on *(A)* the slow action potentials of guinea pig papillary muscle and *(B)* tension developed.

$+\dot{V}_{max}$ are more marked than those of enflurane. Halothane is slightly more depressant than enflurane also on tension produced by the muscle during the slow AP. These findings appear to support investigators who have found halothane to be more depressant [34, 35, 39] rather than those who have suggested that enflurane [36, 40–42] was more or equally depressant.

At lower concentrations, halothane 0.5% (0.65 MAC) [5] and enflurane 1% (0.6 MAC) [29] both produced a negative inotropic effect without an effect on the slow AP. Obviously a mechanism other than slow-channel depression is involved in this early cardiac depression.

Clinical Implications

Halothane like many antidysrhythmic drugs produces depression of phase-4 depolarization. It has been shown to moderate the cardiotoxic effects of digitalis [76, 77] and even have therapeutic value in ouabain-induced ventricular tachycardia [78]. Ectopic pacemaker cells in digitalis-induced ventricular tachycardia are situated either in the left bundle branch or more distal Purkinje fibers with retrograde activation of the bundle of His [79]. Logic and Morrow [80] have shown that halothane can suppress glycocide enhancement of these ectopic pacemakers. Digitalis inhibits the ATP-dependent Na^+-K^+ pump [81]. The resultant increase in intracellular sodium ionic concentration stimulates the sodium–calcium transport system [82]. Intracellular calcium concentration increases and myocardial contractility improves. Cardiotoxicity of digitalis is a result of a greater inhibition of the pump. Halothane antagonizes the increased rate of phase-4 depolarization and may therefore prevent the increased automaticity in ectopic pacemaker cells. The enhanced membrane responsiveness reported by Pruett and Gramling [83] may also contribute to the prevention of reentrant dysrhythmias not only of digitalis toxicity but

those produced by ischemia. Finally, the competitive action of halothane with calcium on the slow channel may also be a factor [4].

Diethyl ether, methoxyflurane, enflurane, and isoflurane also increase tolerance to digitalis toxicity when administered prior to ouabain infusion and restore sinus rhythm when administered acutely during ouabain-induced ventricular tachycardia [84]. Methoxyflurane and enflurane both increase the rate of phase-4 depolarization in lower centers while decreasing the rate of phase-4 depolarization in the SA node. This would tend to produce nodal rhythm, which is frequently seen during anesthesia with these agents. Enflurane has also been shown to increase membrane responsiveness [25] so this may in part explain their action in moderating digitalis-induced dysrhythmias. While their effect on the AV node remains somewhat unclear, they certainly do not antagonize the AV nodal depression of digitalis. Like digitalis, effective refractory periods of the ventricles are also shortened. The sympathetic nervous system is thought to be involved in the genesis of digitalis-induced ventricular dysrhythmias [85]. Halothane [86], enflurane [87], and isoflurane [88] are thought to decrease sympathetic nervous activity and thus confer increased tolerance to digitalis.

While we have discussed the antidysrhythmic effects of the volatile anesthetic agents, in clinical situations dysrhythmias are not infrequent. This is particularly true in the presence of catecholamines. Initially there was discussion as to whether the underlying mechanism was that of increased automaticity or reentry [89–91]. All evidence now points to reentry. In Zink's work there were critical levels for both blood pressure and atrial rate. A rise in intraventricular systolic pressure causes stretch of Purkinje fibers. This in turn slows conduction velocity and increases the rate of diastolic depolarization, both of which favor reentry [92]. The bigeminal beat is thought to be a fusion beat of a reentrant impulse that has its origins in the upper interventricular septum with the next normal beat conducted through the AV node [93]. The findings of Reynolds and Chiz support this work [93]. Epinephrine, in concentrations without effect on velocity of impulse conduction in Purkinje fibers, markedly potentiated a modest slowing of conduction produced by halothane. This effect was antagonized by alpha blockade, but not by beta blockade.

Clinically we term these findings "sensitization of the myocardium by halothane", i.e., the dose of intravenous exogenous epinephrine needed to produce ventricular premature contractions (VPCs) is lower in the presence of halothane anesthesia than in the awake state. In comparing the presently used volatile agents, Joas and Stevens [94] have shown, in dogs, that in the presence of isoflurane four times the dose of epinephrine necessary during halothane anesthesia is required to produce VPCs. Human studies confirm these findings [96]. During epinephrine injection the stability of heart rhythm is greatest with isoflurane, then enflurane, and least with halothane. Both Johnston et al. [95] for halothane and Horrigan et al. [96] for enflurane have shown it requires larger doses of epinephrine when the vehicle of injection is lidocaine. This contradicts the often quoted adage that lidocaine should not be given during halothane-induced dysrhythmias because it depresses an already depressed (by halothane) AV conduction.

Verapamil, a slow-calcium-channel inhibitor, has only recently been introduced into clinical practice in the United States. We have briefly alluded to its actions while discussing some of the electrophysiologic findings. It is known to inhibit myocardial contractility, depress the SA and AV nodes, and decrease vascular smooth muscle tone [97]. Dysrhythmias occurring during anesthesia have been successfully treated with verapamil [98]. Verapamil also produces blockade of the fast sodium channels [99], which contributes to its depression of cardiac output [100].

The effects of verapamil during halothane [101], enflurane [102], and isoflurane [103, 104] anesthesia have been studied. Verapamil produced a rise in the epinephrine dysrhythmogenic threshold and epinephrine-induced ventricular dysrhythmia in the intact dog during 1 MAC halothane anesthesia [101]. There

was a further depression in mean arterial pressure and cardiac function compared to halothane alone. Cardiac output, however, varied. After a uniform initial rise, cardiac output remained high in some dogs or fell in others. This may represent an additive effect of halothane on the balance of the two cardiovascular effects of verapamil, i.e., beneficial afterload reduction vs deleterious direct myocardial depression [105].

Verapamil in the presence of enflurane anesthesia decreased mean arterial pressure, cardiac output, and heart rate, and left ventricular dP/dt decreased. Enflurane caused hemodynamic depression below control at 25% of the verapamil dosage [102]. Animals receiving 1 MAC isoflurane compared to those receiving 1 MAC enflurane had a greater sympathetic tone and tolerated higher plasma levels of verapamil. There was also less reflex increase in epinephrine [103]. These findings may indicate isoflurane as the inhalational agent of choice in patients taking verapamil. Kates et al. [104] confirm the additive myocardial depressant effects of isoflurane and verapamil. They also showed only partial reversal by calcium, which might indicate depression of the slow channels is not the sole mechanism in the cardiac depression.

Coronary Circulation

Ischemic heart disease has become increasingly important to the anesthesiologist for several reasons. These include aging population, the increased incidence of coronary bypass surgery, and the acceptance of patients for noncardiac surgery who previously would have been considered too great a risk. The following is a highly simplified outline of myocardial oxygenation so that we may discuss the effects of the volatile anesthetic agents.

Myocardial oxygen supply is mainly dependent upon blood flow through the coronary arteries and the oxygen-carrying capacity of the blood. Coronary blood flow is greatest in early diastole. The pressure gradient across the coronary vessels is influenced by the aortic diastolic pressure and the left ventricular end-diastolic pressure (LVEDP). Heart rate also influences coronary blood flow because of its effects on length of diastole. If diastolic pressure or LVEDP are changed, coronary flow changes unless coronary vascular resistance also changes. In ischemic heart, atheromatous changes preclude this decrease in coronary vascular resistance and coronary flow depends upon pressure and diastolic time.

Anemia, acid–base balance, and adequate ventilation are more important than the anesthetic agents per se on the oxygen-carrying capacity of the blood.

Factors influencing myocardial oxygen consumption have been well reviewed [105, 106]. The most important are heart rate, the myocardial contractile state, and myocardial wall tension. Increased heart rate means increased myocardial work. N. Ty Smith [107] has listed 58 indicators in assessing the myocardial contractile state. This itself indicates a lack of agreement on both method of evaluation and definition of contractility. LV^{dP}/dt has been considered a reasonable index [108–111]. Increases are associated with increased myocardial oxygen consumption while decreases have the opposite effect. The rate–pressure product (heart rate × systolic blood pressure) also has an adequate correlation with myocardial oxygen consumption under clinical conditions [112, 113]. A rate–pressure product of +11,000 occurred in patients who developed ischemic changes during surgery [114]. Myocardial wall tension is determined by ventricular pressure, intraventricular volume, and myocardial mass. Increases in intraventricular pressure or volume increase wall tension and thus myocardial work.

The effects of the inhalational agents on myocardial contractility have been discussed in the previous section on ventricular contraction and also reviewed by Smith [107] and Sonntag [115]. Suffice it to say that halothane, enflurane, and isoflurane all caused myocardial depression and, therefore, decreased myocardial work.

The restriction of coronary blood flow during systole is greatest at the endocardium and least at the epicardium [116]. The endocardium is therefore more vulnerable to ischemic changes [117]. Another important facet of the coronary

circulation is the division into the larger conductance vessels on the epicardial surface and the smaller precapillary resistance vessels within the myocardium [118]. The larger vessels do not play a part in overall coronary resistance until neurogenic stimulation occurs [119]. This factor may be of importance in view of the effects of volatile anesthetic agents on autonomic control of the circulation [120].

Early work performed in anesthetized animals with open chests showed only slight effects on stimulation of adrenergic nerves [121, 122]. More recent investigations in chronically instrumented animals have shown adrenergic stimulation or blockade has profound effects on coronary blood flow [123, 124]. Alpha and beta receptors have been demonstrated in the coronary vascular bed [125]. The rather complicated and as yet incompletely understood effects of sympathetic influences on the coronary circulation have been succinctly reviewed by Klocke and his colleagues [126].

The effects of the volatile anesthetics on coronary circulation have been investigated in animal studies and in man.

Animal Studies

Eberlein [127], Saito et al. [128], and Weaver [129], utilizing flowmeters, have shown that halothane and methoxyflurane decreased coronary artery flow while diethyl ether increased flow in dogs. Other experiments using washout of ^{85}Kr from the coronary vein as an estimate of myocardial blood flow have shown decreases in ventricular function and oxygen consumption accompanied by equivalent decreases in myocardial blood flow [130]. Since the heart of *Sus scrofa* more nearly resembles that of man [131], Merin et al. studied the effect of halothane in pigs [132]. Dose-related depression in left ventricular function by halothane was again accompanied by equivalent decreases in coronary blood flow and oxygen consumption.

Decrease in coronary blood flow with halothane and increase with diethyl ether are most likely due to alterations in cardiac oxygen requirements [133]. However, Domenech et al. studied the circumflex diastolic coronary vascular resistance in the working heart and total mean coronary resistance in the isolated nonworking heart of the dog during 100% oxygen and 2%–3% halothane in oxygen. They concluded that the decreased resistance they observed was due to a direct action of halothane on coronary vessels. This action was not modified by beta-adrenergic block [134]. Sawyer et al. [136] were able to contrast local and systemic effects of halothane on the vascular bed supplied by the right coronary artery by using an extracorporeal circuit containing an isolated donor lung. Local administration of halothane caused marked coronary vasodilation without effect on RV^{dP}/dt or systemic pressure. Systemic halothane caused marked reduction of systemic pressure and RV^{dP}/dt and was without effect on coronary resistance. They concluded that, while the direct local effect is to produce dilation, reflex baroreceptor stimulation and decreased cardiac metabolism during systemic halothane antagonize local effects. This was supported by the finding that systemic halothane during alpha blockade produced a significant decrease in coronary resistance. They also compared the effects of halothane and enflurane on the right coronary circulation in the pig. Halothane and enflurane both cause coronary vasodilation as a direct effect. Systemically halothane and enflurane cause decreases in systemic pressure without change in coronary resistance, local effects being effectively antagonized by indirect effects [136].

Verrier and his colleagues [137] measured myocardial blood flow as an indicator of oxygen supply during autoregulation and maximal vasodilation at various coronary arterial perfusion pressures at stable oxygen demand. The relationship between pressure and blood flow provided an index of coronary vascular reserve. Pressure–flow relations in the left circumflex coronary artery were compared during halothane (approx. 1 MAC) and nitrous oxide anesthesia. Myocardial oxygen demand and blood flow decreased during halothane anesthesia. The interesting point was that the pressure–flow relationship during maximal vasodilation shifted to the left. This reflects the lower coronary arterial perfusion pressure at which flow became zero. The authors aptly explain this by the vascular waterfall theory. This shift also re-

flects the lower coronary arterial perfusion at which subendocardial ischemia occurs during autoregulation of blood flow. Greater coronary vascular reserve is present during halothane anesthesia than with nitrous oxide.

The use of lightly anesthetized animals as controls may produce erroneous results [120, 138]. Vatner and Smith, using chronically instrumented dogs, showed that halothane produced a dose-related decrease in ventricular function at 1% and 2% [139], but coronary flow did not decrease with increased concentration. Merin et al. [37] found a dose-related decrease in myocardial blood flow. The latter group felt that the presence of tachycardia with its effect on oxygen demand was a factor in the conflicting findings. These authors also studied the effects of enflurane [41]. Dose-dependent depression of ventricular function was accompanied by depression of myocardial blood flow and oxygenation. Comparison with halothane in the same dog showed dose-dependent negative inotropic effects accompanied by equivalent decreases in cardiac oxygen demand.

Human Studies

Sonntag et al. [140] investigated the effects of 0.7% and 1.54% halothane in healthy patients. Myocardial function decreased in a dose-related manner without change in heart rate. Myocardial blood flow and oxygen consumption also showed a dose-related decrease. Myocardial oxygenation was adequate as evidenced by decreased oxygen extraction and unchanged lactate levels. The rate–pressure product correlated poorly with myocardial oxygen consumption although there was a dose-related decrease during halothane anesthesia. Changes in arterial blood pressure and contractile function of the heart were more closely related to myocardial oxygen consumption, but still not ideal. They felt an ideal clinical correlate of myocardial oxygen demand during anesthesia is still unavailable.

Ischemic Heart Disease

Ischemic heart disease is a situation where there is an imbalance between myocardial oxygen supply and myocardial oxygen consumption. Experimentally produced ischemia by ligation of coronary arteries has been studied in dog under halothane [141, 142] and epidural anesthesia [143] with improvement in myocardial perfusion and oxygenation. However, as Merin [144] has pointed out, the control state was hyperdynamic with rapid heart rates. Anesthesia reduced heart rate and blood pressure. These together with depression of cardiac contractility might depress myocardial oxygen demand more than a decreased coronary perfusion pressure decreased myocardial oxygen supply. The work of Prys-Roberts et al. in chronically instrumented animals also does not show a beneficial effect of halothane on the ischemic heart [145]. Nor did halothane at ½ or 1 MAC protect ventricular function following global myocardial ischemia [146]. Gerson et al. [147] used elevation of the ST segment on epicardial electrocardiogram in response to temporary occlusion of the left descending coronary artery as an index of ischemia. They compared 1% halothane to nitroprusside–propranolol and found reduction of the ST segment to be significantly greater with halothane.

More recently, investigations have utilized narrowed rather than completely occluded vessels in an attempt to provide conditions nearer to those present in clinical situations. Lowenstein and his co-workers [148] studied the effects of halothane between 0.5% and 2% upon left ventricular myocardium supplied by a critically narrowed coronary artery (left anterior descending) and a normal coronary artery (left circumflex). An inspired halothane concentration well tolerated by myocardium supplied by the normal coronary artery produced dysfunction and paradox (i.e., ischemia) in the myocardium supplied by the narrowed coronary artery despite normal global left ventricular function. They hypothesized that clinically unsuspected intraanesthetic compromise of such an area may be an important cause of perioperative myocardial infarction despite the absence of an ischemic episode or hemodynamic instability. They felt a local decrease in perfusion pressure was the cause of the dysfunction. This is supported by the work of Behrenbeck et al. [149], which showed no difference in re-

gional myocardial function in ischemic or nonischemic areas with increasing concentrations of halothane as long as perfusion was maintained. The former group also produced critical constriction of the left circumflex coronary artery [150]. Critical constriction of a coronary artery supplying a large area of the myocardium may cause a severe loss of regional myocardial perfusion that is accompanied by an equally severe loss of global perfusion. The effects of enflurane in the presence of critical constriction of the left anterior descending coronary artery were to produce marked reduction in segmental wall function with matching global dysfunction [151]. Critical constriction produced slightly greater depression of left anterior descending segmental function compared with the left circumflex segment and significantly more depression of global function. Hickey et al. [152] saw virtually no effect on hemodynamics, metabolism, or ECG findings at 40% decrease in left anterior descending coronary flow as a result of stenosis at 1.2 MAC halothane anesthesia. Low arterial pressure and 2.1 MAC produced evidence of ischemia. Merin et al. [153] caused a 60% reduction in flow to the left anterior descending coronary artery in swine, which resulted in ischemia of the cardiac muscle supplied by that vessel. Their object was to compare the effects of halothane with fentanyl-supplemented nitrous oxide anesthesia. Neither protected against the ischemia and the degree of ischemia and depression of ventricular function was not different. They concluded decrease in oxygen supply due to coronary stenosis was no more deleterious to metabolic function when oxygen supply/demand was high as with fentanyl or when it was low as with halothane. Lowenstein et al. [154], however, using values from Merin et al. [153], Waters et al. [155], and Verrier et al. [137], calculated that, with the degree of narrowing reported by Merin et al. and the hemodynamic state, a low-demand–low-pressure anesthetic (halothane) will be better tolerated than a high-demand–high-pressure anesthetic (fentanyl).

There are inherent problems in these studies. The first is that coronary stenosis is imposed upon a preexisting stable anesthetic state unlike the clinical situation where anesthesia is imposed upon severe narrowing of one or more coronary arteries [154]. Secondly, such localized constrictions are unlikely clinically. More widespread coronary artery involvement might produce more obvious evidence of global ischemia with hemodynamic correlates. A recent article by Hoffman et al. [156] showed cardiovascular and regional hemodynamic differences in young compared to aged rats. Whether these are applicable to man or not is questionable, but does point to the fact that further studies are needed.

Clinical Investigations

Lieberman et al. [157] studied the effect of halothane in patients undergoing coronary artery bypass grafting by monitoring a V_5 surface ECG. Of their patients, 73% had evidence of left ventricular dysfunction prior to surgery. No evidence of new ischemic changes occurred prior to coronary artery bypass. Slogoff et al. [158] showed a 26% incidence of ischemia in patients given a morphine-based anesthetic with a markedly higher incidence when beta blockade was withheld. Kistner et al. [159] also compared halothane and morphine in patients undergoing coronary artery bypass and found in a well-monitored situation that halothane was superior in avoidance of ischemic and adverse hemodynamic changes. Delaney and his colleagues [32] have compared halothane and enflurane (¾ MAC) in patients with coronary artery disease. Their findings indicate that halothane decreases the contractile state, heart rate, and afterload, and therefore presumably myocardial consumption, while slightly increasing preload. Enflurane reduced afterload only. Similar findings have been described for isoflurane [160], which reduces systemic vascular resistance to a greater extent than enflurane, while stroke volume and cardiac output are less impaired [161]. Isoflurane causes significantly less impairment of myocardial contractile performance compared to halothane and enflurane despite the fact that its effects on contractile proteins and their enzyme systems are similar [162]. Prys-Roberts et al. have also noted the limited effect of halothane on systemic vascular resistance [163].

In conclusion, we have summarized the effects of the volatile anesthetics in clinical use today on the electrophysiology of the heart and their effects on the heart and coronary circulation with particular reference to ischemic heart disease, the major coincidental pathologic process faced by an anesthesiologist today. For the sake of completeness, we should mention the enthusiasm for high-dose opiate (fentanyl) anesthesia for coronary artery surgery which is presently in vogue. We briefly mentioned this subject above. Interested readers are directed to articles by Lowenstein and Philbin [164], Waller et al. [165], Stanley et al. [166], Lunn et al. [167], Zurick et al. [168], Merin et al. [153], and Sonntag et al. [169]. It will be seen that there is no *single* anesthetic agent which provides ideal conditions for surgery in patients with coronary artery disease. Judicious combination of various pharmacologic agents and careful monitoring is the "best" anesthesia.

References

1. Hauswirth O, Schaer H: Effects of halothane on the sinoatrial node. J. Pharmacol Exp Therap 158:36–39, 1967.
2. Reynolds AK, Chiz JF, Pasquet AF: Halothane and methoxyflurane: a comparison of their effects on cardiac pacemaker fibers. Anesthesiology 33:602–610, 1970.
3. Maylie J, Morad M, Weiss J: A study of pacemaker potential in rabbit sino-atrial node: measurement of potassium activity under voltage-clamp conditions. J Physiol 311:161–178, 1981.
4. Kampine JP, Bosnjak ZJ, Turner LA: Effects of halothane on SA node: role of calcium. Anesthesiology 55:A58, 1981.
5. Lynch C, Vogel S, Sperelakis N: Halothane depression of myocardial slow action potentials. Anesthesiology 55:360–368, 1981.
6. Merlos JR, Bosnjak ZJ, Purlock RV, Turner LA, Kampine JR: Halothane and enflurane effects on SA node cells. Anesthesiology 53:S143, 1980.
7. Hauswirth O: Effects of halothane on single atrial, ventricular, and Purkinje fibers. Circ Res 24:745–750, 1969.
8. Reynolds AK, Chiz JF, Pasquet AF: Pacemaker migration and sinus node arrest with methoxyflurane and halothane. Can Anaesth Soc J 18:137–144, 1971.
9. Pratila MG, Vogel S, Sperelakis N: Effects of enflurane on rabbit atrium. Unpublished data.
10. Scherlag BJ, Helfant RH, Damato AN: A catheterization technique for His-bundle stimulation and recording in intact dog. J Appl Physiol 25:425–428, 1968.
11. Damato AN, Lau SH, Bobb GA, Wit AL: Recording of AV nodal activity in the intact dog heart. Am Heart J 80:353–366, 1970.
12. Narula OS, Scherlag BJ, Samet P, Javier RP: Atrioventricular block: localization and classification by His-bundle recordings. Am J Med 50:146–165, 1971.
13. Kastor JA: Atrioventricular block. N Engl J Med 292:462–465, 572–574, 1975.
14. Atlee JL, Rusy BF: Halothane depression of A-V conduction studied by electrograms of the bundle of His in dogs. Anesthesiology 36:112–118, 1972.
15. Atlee JL, Alexander SC: Halothane effects on conductivity of the AV node and His Purkinje system in the dog. Anesth Analg (Cleve) 56:378–386, 1977.
16. Atlee JL, Homer LD, Tober RE: Diphenylhydantoin and lidocaine modification of AV conduction in halothane anesthetized dogs. Anesthesiology 43:49–60, 1975.
17. Atlee JL III, Houge JC, Malkinson CE: Halothane and AV conduction: awake vs anesthesia. Anesthesiology 55:A53, 1981.
18. Hantler CB, Kroll DA, Tait AR, Knight PR: Cardiac effects of halothane with spinal anesthesia. Anesthesiology 55:A4, 1981.
19. Morrow DH, Haley JV, Logic JR: Anesthesia and digitalis. VII. The effect of pentobarbital halothane and methoxyflurane on the AV conduction and inotropic responses to ouabain. Anesth Analg (Cleve) 51:430–438, 1972.
20. Jacques A, Hudon F: Effect of epinephrine on the human heart during methoxyflurane anesthesia. Can Anaesth Soc J 10:53, 1963.
21. Atlee JR III, Rusy BF: Atrioventricular conduction times and atrioventricular nodal conductivity during enflurane anesthesia in dogs. Anesthesiology 47:498–503, 1977.
22. Atlee JL, Rusy BF, Kreul JF: Supraventricular excitability in dogs during anesthesia with halothane and enflurane. Anesthesiology 49:407–413, 1978.
23. Zaidon JR, Curling PE, Kaplan JA: Effect of enflurane on pacing threshold. Anesthesiology 55: A59, 1981.
24. Blitt CD, Raessler KL, Wightman MA, Groves BM, Wall CL, Geha DG: Atrioventricular conduction in dogs during anesthesia with isoflurane. Anesthesiology 50:210–212, 1979.
25. Pruett JK, Mote PS, Grover TE, Augeri JM: Enflurane and halothane effects on cardiac Purkinje fibers. Anesthesiology 55:A65, 1981.
26. Chen C, Gettes LS, Katzung BG: Effect of lidocaine and quinidine on steady-state characteristics and recovery kinetics of $(dV/dt)_{max}$ in guinea pig ventricular myocardium. Circ Res 37:20–29, 1975.
27. Hashimoto K, Endoh M, Kimura T: Effects of halothane on automaticity and contractile force of iso-

lated blood-perfused canine ventricular tissue. Anesthesiology 42:15–25, 1975.
28. Logic JR, Morrow DH: The effect of halothane on ventricular automaticity. Anesthesiology 36:107–118, 1972.
29. Lynch C, Vogel S, Pratila MG, Sperelakis N: Enflurane depression of myocardial slow action potentials. J Pharmacol Exp Ther 222:405–409, 1982.
30. Vassalle M: Electrogenesis of the plateau and pacemaker potential. Am Rev Physiol 41:425–440, 1979.
31. Lappas DC, Buckley MJ, Laver MB, Daggett WM, Lowenstein E: Left ventricular performance and pulmonary circulation following addition of nitrous oxide to morphine during coronary-artery surgery. Anesthesiology 43:61–69, 1975.
32. Delaney TJ, Kistner JR, Lake CL, Miller ED Jr: Myocardial function during halothane and enflurane anesthesia in patients with coronary artery disease. Anesth Analg (Cleve) 59:240–244, 1980.
33. Stevens WC, Cromwell TH, Halsey MJ, Eger EI II, Shakespeare TF, Bahlman SH: The cardiovascular effects of a new inhalational anesthetic, Forane, in human volunteers at constant arterial carbon dioxide tension. Anesthesiology 35:8–16, 1971.
34. Rathod R, Jacobs HK, Kramer NE, Rao TLK, Salem MR, Towne WD: Echocardiographic assessment of ventricular performance following induction with two anesthetics. Anesthesiology 49:86–90, 1978.
35. Kaplan JA, Miller ED, Bailey DR: A comparative study of enflurane and halothane using systolic time intervals. Anesth Analg (Cleve) 55:263–268, 1976.
36. Smith NT, Calverley RK, Prys-Roberts C, Eger EI II, Jones CW: Impact nitrous oxide on the circulation during enflurane anesthesia in man. Anesthesiology 48:345–349, 1978.
37. Merin RG, Kumazawa T, Luka NL: Myocardial function and metabolism in the conscious dog and during halothane anesthesia. Anesthesiology 44:402–415, 1976.
38. Kemmotsu O, Hashimoto Y, Shimosato S: Inotropic effects of isoflurane on mechanics of contraction in isolated cat papillary muscles from normal and failing hearts. Anesthesiology 39:470–477, 1973.
39. Kemmotsu O, Hashimoto Y, Shimosato S: The effects of fluroxene and enflurane on contractile performance of isolated papillary muscles from failing hearts. Anesthesiology 40:252–260, 1974.
40. Ritzman RJ, Erickson HH, Miller ED: Cardiovascular effects of enflurane and halothane in the rhesus monkey. Anesth Analg (Cleve) 55:85–91, 1976.
41. Merin RG, Kumazawa T, Luka NL: Enflurane depresses myocardial function perfusion and metabolism in the dog. Anesthesiology 45:501–507, 1976.
42. Brown BR, Crout JR: A comparative study of the effects of five general anesthetics on myocardial contractility. Anesthesiology 34:236–245, 1971.
43. Seeman P: The membrane expansion theory of anesthesia. In: Fink BR (ed) molecular mechanisms of anesthesia. Progress in anesthesiology, vol 1. New York: Raven, 1975, pp 243–252.
44. Halsey MJ: Structure–activity relationships of inhalational anesthetics. In: Halsey MJ, Millar RA, Sutton JA (eds) Molecular mechanisms in general anesthesia. Edinburgh: Churchill Livingstone, 1974, pp 3–16.
45. Halsey MJ, Brown FF, Richards RE: Perturbations of model protein systems as a basis for the central and peripheral mechanisms of general anaesthesia. Molecular interactions and activity in proteins, Ciba Foundation Symposium 60. Amsterdam: Excerpta Medica, 1978.
46. Woodbury JW, d'Arrigo JS, Eyring H: Molecular mechanism of general anesthesia lipoprotein conformation change theory. In: Fink BR (ed) Molecular mechanisms of anesthesia. Progress in anesthesiology, vol 1. New York: Raven, 1975, pp 253–276.
47. Metcalfe JC, Hoult JRS, Colley CM: The molecular implications of a unitary hypothesis of anesthetic action. In: Halsey MJ, Millar RA, Sutton JA (eds) Molecular mechanisms in General Anaesthesia. Edinburgh: Churchill Livingstone, 1974, pp 145–163.
48. Cheng SC, Brunner EA: Is anesthesia caused by excess GABA? In: Fink BR (ed) Molecular mechanisms of anesthesia. Progress in anesthesiology, vol 2, New York: Raven, 1980, pp 137–144.
49. Trudell JR: A unitary theory of anesthesia based on lateral phase separations in nerve membranes. Anesthesiology 46:5–10, 1977.
50. Rosenberg PH, Eibl H, Stier A. Biphasic effects of halothane on phospholipid and synaptic plasma membranes: a spin label study. Mol Pharmacol 11:879–882, 1975.
51. Pang KY, Chang TL, Miller KW: On the coupling between anesthetic induced membrane fluidization and cation permeability in lipid vesicles. Mol Pharmacol 15:729–738, 1979.
52. Mastrangelo CJ, Trudell JR, Edmunds HN, Cohen EN: Effect of clinical concentrations of halothane on phospholipid membrane fluidity. Mol Pharmacol 14:463–467, 1978.
53. Menn RG: Inhalational anesthetics and myocardial metabolism: possible mechanism of functional effects. Anesthesiology 34:236–245, 1971.
54. Lain RF, Hess ML, Gertz EW, Briggs FN: Calcium uptake activity of canine myocardial sarcoplasmic reticulum in the presence of anesthetic agents. Circ Res 23:597–604, 1968.
55. Lee SL, Alto LE, Dhalla NS: Subcellular effects of some anesthetic agents on rat myocardium. Can J Physiol Pharmacol 57:65–70, 1974.
56. Su JY, Kerrick WGL: Effects of halothane on Ca^{++}-activated tension development in mechanically disrupted rabbit myocardial fibers. Pflugers Archiv 375:111–117, 1978.
57. Su JY, Kerrick WGL: Effects of halothane on caf-

feine-induced tension transients in functionally skinned myocardial fibers. Pflugers Archiv 380:29–34, 1979.
58. Su JY, Kerrick WGL: Effects of enflurane on functionally skinned myocardial fibers from rabbits. Anesthesiology 52:385–389, 1980.
59. Price HL, Ohnishi ST: Effects of anesthetics on the heart. Fed Proc 39:1575–1579, 1980.
60. Ohnishi ST, Di Camillo Ca, Singer M, Price HL: Correlation between halothane-induced myocardial depression and decreases in La^{3+}–displaceable Ca^{2+} in cardiac muscle cells. J Cardiovasc Pharmacol 2:67–75, 1980.
61. Blanck TJJ, Thompson M: Calcium transport by cardiac sarcoplasmic reticulum: modulation of halothane action by substrate concentration and pH. Anesth Analg (Cleve) 60:390–394, 1981.
62. Conahan TJ, Blanck TJJ: Sarcoplasmic reticulum: enflurane effect on Ca^{++} dynamics. Anesthesiology 51:S146, 1979.
63. Blanck TJJ, Thompson M: Enflurane and isoflurane stimulate calcium transport by cardiac sarcoplasmic reticulum. Anesth Analg (Cleve) 61:142–145, 1982.
64. Komai H, Rusy BF: Effect of halothane on rested-state and potentiated-state contractions in rabbit papillary muscle: relationship to negative inotropic actions. Anesth Analg (Cleve) 61:403–409, 1982.
65. Weidmann S: Heart: electrophysiology. Annu Rev Physiol 36:155–169, 1974.
66. Shigenobu K, Schneider JA, Sperelakis N: Blockade of slow Na^+ and Ca^{++} currents in myocardial cells by verapamil. J Pharmacol Exp Ther 190:280–288, 1974.
67. Fabiato A, Fabiato F: Calcium and cardiac excitation–contraction coupling. Annu Rev Physiol 41:473–484, 1979.
68. Awalt CH, Frederickson EL: The contractile and cell membrane effects of halothane. Anesthesiology 25:90, 1964.
69. Lynch C, Vogel S, Pratila MG, Sperelakis N: Methoxyflurane depression of myocardial slow action potentials. Unpublished findings.
70. Shigenobu K, Sperelakis N: Calcium current channels enduced by catecholamines in chick embryonic hearts whose fast Na^+ channels are blocked by TTX or elevated K^+. Circ Res 31:932–952, 1972.
71. Reuter H, Scholz H: A study of the ion selectivity and kinetic properties of the calcium-dependent slow inward current in cardiac muscle. J Physiol (Lond) 264:17–47, 1977.
72. Watanabe AM, Besch HR Jr: Cyclic adenosine monophosphate modulation of slow Ca^{++} influx channels in guinea pig hearts. Circ Res 35:316–324, 1974.
73. Sperelakis N, Schneider JA: A metabolic control mechanism for calcium ion influx that may protect the ventricular myocardial cell. Am J Cardiol 37:1079–1085, 1976.
74. Reuter H, Scholz H: The regulation of the calcium conductance of cardiac muscle by adrenalin. J Physiol (Lond) 264:49–62, 1977.
75. Kass RS, Siegelbaum SA, Tsien RW: Three-microelectrode voltage clamp experiments in calf Purkinje fibers: is slow inward current adequately measured? J Physiol (Lond) 290:201–225, 1979.
76. Morrow DH, Townley NT: Anesthesia and digitalis toxicity: an experimental study. Anesth Analg (Cleve) 43:510–519, 1964.
77. Reynolds AK, Horne ML: Studies on the cardiotoxicity of ouabain. Can J Physiol Pharmacol 47:165–170, 1969.
78. Morrow DH, Knapp DE, Logic JR: Anesthesia and digitalis toxicity. V. Effect of the vagus on ouabain-induced ventricular automaticity during halothane. Anesth Analg (Cleve) 49:23–27, 1970.
79. Damato AN, Lau SH, Bobb GA: Digitalis-induced bundle-branch ventricular tachycardia studied by electrode catheter recordings of the specialized conducting tissues of the dog. Circ Res 28:16–22, 1971.
80. Logic JR, Morrow DH: The effect of halothane on ventricular automaticity. Anesthesiology 36:107–118, 1972.
81. Matsui H, Schwartz A: Mechanism of cardiac glycoside inhibition of the (Na^+-K^+)-dependent ATPase from cardiac tissue. Biochim Biophys Acta 151:655–663, 1968.
82. Baker PF, Blaustein MP, Hodgkin AL, Steinhardt RA: The influence of calcium on sodium efflux in squid axons. J Physiol (Lond) 200:431–458, 1969.
83. Pruett JK, Gramling ZW: Halothane enhanced membrane responsiveness in canine Purkinje fibers. Fed Proc 38:589, 1979.
84. Ivankovich AD, Miletich DJ, Grossman RK, Albrecht RF, El-Etr AA, Cairoli VJ: The effect of enflurane, isoflurane, fluroxene, methoxyflurane and diethyl ether anesthesia on ouabain tolerance in the dog. Anesth Analg (Cleve) 55:360–365, 1976.
85. Pearle DL, Gillis RA: Effect of digitalis on response of the ventricular pacemaker to sympathetic neural stimulation and to isoproterenol. Am J Cardiol 34:704–710, 1974.
86. Skovsted P, Price ML, Price HL: The effects of carbon dioxide on preganglionic sympathetic activity during halothane, methoxyflurane and cyclopropane anesthesia. Anesthesiology 37:70–75, 1972.
87. Brown FF III, Owens WD, Felts JA, Spitznagel EL Jr, Cryer PE: Plasma epinephrine and norepinephrine levels during anesthesia: enflurane-N20-02 compound with fentanyl-N20-02. Anesth Analg (Cleve) 61:366–370, 1982.
88. Skovsted P, Sapthavichaikul S: The effects of isoflurane on arterial pressure, pulse rate, autonomic nervous activity and barostatic reflexes. Can Anaesth Soc J 24:304–314, 1977.
89. Hashimoto K, Hashimoto K: The mechanism of sensitization of the ventricle to epinephrine by halothane. Am Heart J 83:652–658, 1972.
90. Hashimoto K, Endoh M, Kimura T: Effects of hal-

othane on automaticity and contractile force of isolated blood-perfused canine ventricular tissue. Anesthesiology 42:15–25, 1975.
91. Zink J, Sasyniuk BI, Dresel PE: Halothane–epinephrine induced cardiac arrhythmias and the role of heart rate. Anesthesiology 43:548–555, 1975.
92. Singer DH, Lazzara R, Hoffman BF: Electrophysiological effects of canine peripheral A-V conducting system. Circ Res 26:361–378, 1970.
93. Reynolds AK, Chiz JF: Epinephrine-potentiated slowing of conduction in Purkinje fibers. Res Commun Chem Pathol Pharmacol 9:633–642, 1974.
94. Joas TA, Stevens WC: Comparison of the arrhythmic doses of epinephrine during Forane, halothane and fluroxene anesthesia in dogs. Anesthesiology 35:48–53, 1971.
95. Johnston RR, Eger EI II, Wilson C: A comparative interaction of epinephrine with enflurane, isoflurane and halothane in man. Anesth Analg (Cleve) 55:709–712, 1976.
96. Horrigan RW, Eger EI II, Wilson C: Epinephrine-induced arrhythmias during enflurane anesthesia in man: a non-linear dose–response relationship and dose-dependent protection from lidocaine. Anesth Analg (Cleve) 57:547–550, 1970.
97. Singh BN, Ellrodt G, Peter GT: Verapamil: a review of its pharmacological properties and therapeutic use. Drugs 15:169–197, 1978.
98. Brichard G, Zimmerman PE: Verapamil in cardiac dysrhythmias during anesthesia. Br J Anaesth 42:1005–1012, 1970.
99. Bayer R, Kalusche D, Kaufmann R, Mannhold R: Inotropic and electrophysiological actions of verapamil and D600 in myocardium. III. Effects of the optical isomers on transmembrane action potentials. Naunyn Schmiedebergs Arch Pharmacol 290:81–97, 1975.
100. Merin RG: Slow channel inhibitors, anesthetics and cardiovascular function. Anesthesiology 55:198–200, 1981.
101. Kapur PA, Flacke WE: Epinephrine-induced arrhythmias and cardiovascular function after verapamil during halothane anesthesia in the dog. Anesthesiology 55:218–225, 1981.
102. Kapur PA, Flacke WE, Olewine SK, Van Etten PA: Cardiovascular and catecholamine responses to verapamil during enflurane anesthesia. Anesthesiology 55:A14, 1981.
103. Kapur PA, Flacke WE, Olewine SK: Comparison of effects of isoflurane versus enflurane on cardiovascular and catecholamine responses to verapamil in dogs. Anesth Analg (Cleve) 61:193–194, 1982.
104. Kates RA, Kaplan JA, Hug CC, Guyton R, Dorsey LM: Hemodynamic interactions of verapamil and isoflurane in dogs. Anesth Analg (Cleve) 61:194–195, 1982.
105. Ellrodt G, Chew CYC, Singh BN: Therapeutic implications of slow-channel blockade in cardio-circulatory disorders. Circulation 62:669–679, 1980.
106. Braunwald E: Control of myocardial oxygen consumption. Am J Cardiol 27:416–432, 1971.
107. Smith NT: Myocardial function and anaesthesia. In: Prys-Roberts (ed) The circulation in anaesthesia. Oxford: Blackwell Scientific, 1980, pp 59–60.
108. Shimosato S: Isovolumic intraventricular pressure change: an index of myocardial contractility during anesthesia. Anesthesiology 31:327–333, 1969.
109. Pollack GH: Isovolumic intraventricular pressure. Anesthesiology 32:381–383, 1970.
110. Mason DT, Braunwald E, Covell JW, Sonnenblick EH, Ross J Jr: Assessment of cardiac contractility: the relation between the rate of pressure rise and ventricular pressure during isovolumic systole. Circulation 44:47–58, 1971.
111. Prys-Roberts C, Gersh BJ, Baker AB, Reuben SR: The effects of halothane on the interactions between myocardial contractility, aortic impedance and left ventricular performance. I. Theoretical considerations and results. Br J Anaesth 44:634–639, 1972.
112. Nelson RR, Gobel FL, Jorgensen CR, Wang K, Wang Y, Taylor HL: Hemodynamic predictors of myocardial oxygen consumption during static and dynamic exercise. Circulation 50:1179–1189, 1974.
113. Gobel FL, Nordstrom LA, Nelson RR, Jorgensen CR, Wang Y: Rate–pressure product as an index of myocardial oxygen consumption during exercise in patients with angina pectoris. Circulation 57:549–556, 1978.
114. Roy WL, Edelist G, Gilbert B: Myocardial ischemia during non-cardiac surgical procedures in patients with coronary-artery disease. Anesthesiology 51:393–397, 1979.
115. Sonntag H: Actions of anesthetics on the coronary circulation in normal subjects and patients with ischemic heart disease. Int Anesthesiol Clin 18:111–135, 1980.
116. Brandi G, McGregor M: Intramural pressure in the left ventricle of the dog. Cardiovasc Res 3:472–475, 1969.
117. Hoffman JIE: Determinants and prediction of transmural myocardial perfusion. Circulation 58:381–391, 1978.
118. Cohen MV, Kirk ES: Differential response of large and small coronary arteries to nitroglycerin and angiotensin: autoregulation and tachyphylaxis. Circ Res 33:445–453, 1973.
119. Braunwald E, Ross J Jr, Sonnenblick EH: Regulation of coronary blood flow: mechanisms of contraction of the normal and failing heart, 2nd edn. Boston: Little Brown, 1976, pp 200–231.
120. Vatner SF, Franklin D, Braunwald E: Effects of anesthesia and sleep on circulatory response to carotid sinus nerve stimulation. Am J Physiol 220:1249–1255, 1971.
121. Berne RM: Effect of epinephrine and nor-epinephrine on coronary circulation. Circ Res 6:644–655, 1958.
122. Hardin RA, Scott JB, Haddy FJ: Effect of epineph-

rine and norepinephrine on coronary vascular resistance in dogs. Am J Physiol 201:276–280, 1961.
123. Hackett JG, Abboud FM, Mark AL, Schmid PG, Heistad DD: Coronary vascular responses to stimulation of chemoreceptors and baroreceptors: evidence for reflex activation of vagal cholinergic innervation. Circ Res 31:8–17, 1972.
124. Vatner SF, Higgins CB, Braunwald E: Effects of norepinephrine on coronary circulation and left ventricular dynamics in the conscious dog. Circ Res 34:812–823, 1974.
125. Pitt B, Elliot EC, Gregg DE: Adrenergic receptor activity in the coronary arteries of the unanesthetized dog. Circ Res 21:75–84, 1967.
126. Klocke FJ, Ellis AK, Orlick AE: Sympathetic influences on coronary perfusion and evolving concepts of driving pressure, resistance and transmural flow regulation. Anesthesiology 52:1–5, 1980.
127. Eberlein HJ: Der Einfluss von Anästhetika auf das Koronargefässsystem. Wien Z Inn Med 46:400–403, 1965.
128. Saito T, Wakisaka K, Yudate T: Coronary and systemic circulation during (inhalation) anesthesia in dogs. Far East J Anesth 5:105–111, 1966.
129. Weaver PC: Study of the cardiovascular effects of halothane. Ann R Coll Surg Engl 49:114–136, 1971.
130. Kumazawa T, Merin RG: Effects of inhalation anesthetics on cardiac function and metabolism in the intact dog. Recent Adv Cardiac Struct Metab 10:71–79, 1975.
131. Douglas WR: Of pigs and men and research: a review of applications and analogies of the pig *Sus scrofa,* in human medical research. Space Life Sci 3:226–234, 1972.
132. Merin RG, Verdouw PD, De Jong JW: Dose-dependent depression of cardiac function and metabolism by halothane in swine *(Sus scrofa).* Anesthesiology 46:417–423, 1977.
133. Wolff G, Claudi B, Rist M, Wardak MR, Niederer W, Graedel E: Regulation of coronary blood flow during ether and halothane anaesthesia. Br J Anaesth 44:1139–1149, 1972.
134. Domenech RJ, Macho P, Valdes J, Penna M: Coronary vascular resistance during halothane anesthesia. Anesthesiology 46:236–240, 1977.
135. Sawyer DC, Ely SW, Korthuis RJ, Scott JB: Effects of halothane in right coronary circulation in the dog. Anesth Analg (Cleve) 59:559, 1980.
136. Sawyer DC, Ely SW, Scott JB: Halothane and ethrane effects on the coronary circulation. Anesthesiology 53:S129, 1980.
137. Verrier ED, Edelist G, Consigny PM, Robinson S, Hoffman JIE: Greater coronary vascular reserve in dogs anesthetized with halothane. Anesthesiology 53:445–459, 1980.
138. Muggenburg BA, Mauderly JL: Cardiopulmonary function of awake, sedated and anesthetized beagle dogs. J Appl Physiol 37:152–157, 1974.
139. Vatner SP, Smith NT: Effects of halothane on left ventricular function and distribution of regional blood flow in dogs and primates. Circ Res 34:155–167, 1974.
140. Sonntag H, Merin RG, Donath U, Radke J, Schenk HD: Myocardial metabolism and oxygenation in man awake and during halothane anesthesia. Anesthesiology 51:204–210, 1979.
141. Bland JHL, Lowenstein EL: Halothane-induced decrease in experimental myocardial ischemia in the non-failing canine heart. Anesthesiology 45:287–293, 1976.
142. Smith G, Rogers K, Thorburn J: Halothane improves the balance of oxygen supply to demand in acute experimental myocardial ischemia. Br J Anaesth 52:577–583, 1980.
143. Klassen GA, Bramwell RS, Bromage PR: Effect of acute sympathectomy by epidural anesthesia on the canine coronary circulation. Anesthesiology 52:8–15, 1980.
144. Merin RC: Is anesthesia beneficial for the ischemic heart? Anesthesiology 53:439–440, 1980.
145. Prys-Roberts C, Roberts JG, Foex P, Clarke TNS, Bennett MJ, Ryder WA: Interaction of anesthesia, betareceptor blockade and blood loss in dogs with induced myocardial infarction. Anesthesiology 45:326–339, 1976.
146. Nugent M, Walls JT, Tinker JH, Harrison CE: Post-ischemic myocardial function: no anesthetic protection. Anesthesiology 53:S108, 1980.
147. Gerson JL, Hickey RF, Bainton CR: Treatment of myocardial ischemia with halothane or nitroprusside–propranolol. Anesth Analg (Cleve) 62:10–14, 1982.
148. Lowenstein E, Foex P, Francis CM, Davies WL, Yusuf S, Ryder WA: Regional ischemic ventricular dysfunction in myocardium supplied by a narrowed coronary artery with increasing halothane concentration in the dog. Anesthesiology 55:349–359, 1981.
149. Behrenbeck T, Nugent M, Quasha A, Hoffman E, Ritman E, Tinker J: Halothane and ischemic regional myocardial wall dynamics. Anesthesiology 53:S140, 1980.
150. Francis CM, Glazebrook C, Lowenstein E, Davies WL, Foex P, Ryder WA: Effect of halothane on the performance of the heart in the case of critical constriction of the L circumflex coronary artery. Br J Anaesth 52:631P, 1980.
151. Cutfield GR, Francis CM, Foex P, Lowenstein E, Davies WL, Ryder WA: Myocardial function and critical constriction of the L anterior descending coronary artery: effects of enflurane. Br J Anaesth 52:953P, 1980.
152. Hickey RF, Verrier ED, Baer RW, Vlahakes GJ, Hoffman JIE: Does deliberate hypotension produce myocardial ischemia when the coronary artery is stenotic? Anesthesiology 53:S89, 1980.
153. Merin RG, Verdouw PD, De Jong JW: Myocardial functional and metabolic responses to ischemia in swine during halothane and fentanyl anesthesia. Anesthesiology 56:84–92, 1982.

154. Lowenstein E, Hill RD, Rajogopalan B, Schneider RC: Winnie the Pooh revisited, or, the more recent adventures of Piglet. Anesthesiology 56:81–83, 1982.
155. Waters DD, Daluz P, Wyatt HL, Swan JHC, Forrester JS: Early changes in regional and global left ventricular function induced by graded reductions in regional coronary perfusion. Am J Cardiol 39:537–543, 1977.
156. Hoffman WE, Miletich DJ, Albrecht RF: Cardiovascular and regional blood flow changes during halothane anesthesia in the aged rat. Anesthesiology 56:444–448, 1982.
157. Lieberman RW, Jobes DR, Schwartz AJ, Andrews RW: Incidence of ischemia during CABG using halothane. Anesthesiology 51:S90, 1979.
158. Slogoff S, Keats AS, OH E: Preoperative propranolol therapy and aorta-coronary bypass operation. JAMA 240:1487–1490, 1978.
159. Kistner JR, Miller ED, Lake CL, Ross WT Jr: Indices of myocardial oxygenation during coronary-artery revascularization in man with morphine versus halothane anesthesia. Anesthesiology 50:324–330, 1979.
160. Calverly RK, Smith NT, Jones CW, Prys-Roberts C, Eger EI II: Ventilatory and cardiovascular effects of enflurane anesthesia during spontaneous ventilation in man. Anesth Analg (Cleve) 57:610–618, 1978.
161. Tarnow J, Eberlein HJ, Oser G, Patschke D, Schneider E, Schweichel E, Wilde J: Influence of modern inhalational anesthetics on haemodynamics, myocardial contractility, LV volumes and myocardial oxygen supply. Anaesthetist 26:220–230, 1977.
162. Pask HT, England PJ, Prys-Roberts C: Effects of volatile inhalational anesthetic agents on isolated bovine cardiac myofibrillar ATPase. J Mol Cell Cardiol 13:293–301, 1981.
163. Prys-Roberts C, Lloyd JW, Fisher A, Kerr JH, Patterson TJS: Deliberate profound hypotension induced with halothane: studies of haemodynamics and pulmonary gas exchange. Br J Anaesth 46:105–116, 1974.
164. Lowenstein E, Philbin DM: Narcotic "anesthesia" in the eighties. Anesthesiology 55:195–197, 1981.
165. Waller JL, Hug CC, Nagle DM, Craver JM: Hemodynamic changes during fentanyl-oxygen anesthesia for aortocoronary bypass operation. Anesthesiology 55:212–217, 1981.
166. Stanley TH, Philbin DM, Coggins CH: Fentanyl-oxygen anesthesia for coronary artery surgery: cardiovascular and antidiuretic hormone responses. Can Anaesth Soc J 26:168–172, 1979.
167. Lunn JK, Stanley TH, Eisele J, et al.: High-dose fentanyl anesthesia for coronary artery surgery: plasma fentanyl concentrations and influence of nitrous oxide on cardiovascular responses. Anesth Analg (Cleve) 58:390–395, 1979.
168. Zurick Am, Urzua J, Yared J-P, Estafanous FG: Comparison of hemodynamic and hormonal effects of large single dose fentanyl anesthesia and halothane/N20 anesthesia for coronary artery surgery. Anesth Analg (Cleve) 61:521–526, 1982.
169. Sonntag H, Larsen R, Hilfiker O, Kettler D, Brockschnieder B: Myocardial blood flow and oxygen consumption during high-dose fentanyl anesthesia in patients with coronary disease. Anesthesiology 56:417–422, 1982.

II. CORONARY CIRCULATION

31. EFFECTS OF TOXIC SUBSTANCES ON THE HEART

Victor J. Ferrans

Introduction

The reactions of the heart to toxic injury can be classified according to whether they represent: (a) a direct toxic effect of the agent, (b) the result of an exaggeration of the pharmacologic effects of the agent either on the myocardium itself or on the coronary or systemic circulation, or (c) an allergic or hypersensitivity phenomenon. These etiologic distinctions are not always clear on anatomic study of the heart lesions resulting from toxic injury, as a wide spectrum of complex cardiac morphologic changes has been associated with the effects of toxic drugs and chemicals on humans and on experimental animals.

Most cardiotoxic drugs produce the features of either an acute toxic or an acute allergic reaction, and these develop either shortly after administration of a single dose of a particular drug or during (and even after) a course of treatment requiring administration of multiple doses. These lesions demonstrate an unequivocal cause-and-effect relationship, whether they result from an overdose, a side effect, or a hypersensitivity reaction. The clinical features of these reactions usually are those of acute toxic phenomena, with electrocardiographic ischemic changes, arrhythmias, acute cardiac failure, and sudden death. From the morphologic standpoint, drug-induced myocardial lesions usually consist of multifocal areas of myocardial degeneration, necrosis, inflammation, or fibrosis; however, large, confluent areas of necrosis and fibrosis resembling myocardial infarcts develop in certain toxic reactions. Total absence of anatomic changes may be found in the case of certain agents such as digitalis and quinidine, which can cause rapidly fatal changes in cardiovascular function (particularly arrhythmias) without accompanying morphologic alterations. Cardiomegaly in these circumstances is attributable to preexisting heart disease. Less frequently, certain drugs or chemicals may produce long-term cardiac alterations with clinical and morphologic manifestations of a chronic cardiomyopathy.

In this review, the morphologic reactions of the heart to toxic injury are described under the following categories: (1) cardiac hypertrophy; (2) cardiomyopathies; (3) cardiac necrosis, including infarct-like myocardial necroses, hypersensitivity (allergic) myocarditis, and toxic myocarditis; (4) pericarditis; and (5) vascular changes, including hypersensitivity vasculitis, toxic vasculitis, fibromuscular hyperplasia, and thromboembolism. Cardiovascular developmental abnormalities also may be produced by drugs or chemicals. Considerations of these effects is outside the scope of this chapter.

Cardiac Hypertrophy

Cardiac hypertrophy is defined as an increase in the mass of the heart muscle beyond the limits of normal for age, sex, and body weight. This increase in mass usually develops as a compensatory response to an increase in the work load of the heart. Such an increase may result from congenital lesions, acquired valvular dysfunction, pulmonary disease (cor pulmonale), systemic hypertension, variously mediated drug

N. Sperelakis (ed.), PHYSIOLOGY AND PATHOPHYSIOLOGY OF THE HEART.

Martinus Nijhoff Publishing, Boston/The Hague/ Dordrecht/Lancaster.

effects (thyroid hormone, growth hormone, catecholamines), or from unknown causes, as in the case of the cardiomyopathies. Up to a certain limit, known as the critical heart weight (500 g), hypertrophy of human hearts is thought to be mediated by an increase in the size of the individual cardiac muscle cells. It has been suggested that an increase in cardiac mass beyond this critical heart weight is associated with the formation of additional cardiac muscle cells; however, the mechanism of formation of new cardiac muscle cells under these circumstances is not known, and this concept remains controversial [1].

The rate of mitosis of cardiac muscle cells falls to negligible levels within a short period of time after birth, and evidence of new cell division in greatly hypertrophied hearts has not been observed. However, it has been demonstrated that under certain circumstances atrial muscle cells in adult hearts can be induced to undergo DNA synthesis and mitosis [2]. It is also known that pathologic increases in cardiac mass during early neonatal life may be associated with hyperplasia of the muscle cells [1].

Cardiac hypertrophy can be classified as being concentric (pressure overload, characterized by thick chamber walls and normal or smaller-than-normal chamber volumes) or eccentric (volume overload, characterized by large chamber volumes and by walls of variable thickness). Hypertrophy also can be classified as being symmetric or asymmetric. In most types of heart disease, the degree of hypertrophy is similar in the various regions of a given cardiac chamber (symmetric hypertrophy). The exception to this is hypertrophic cardiomyopathy, in which the ventricular septum becomes thickened to a much greater extent than do the free walls of both ventricles.

Cardiac hypertrophy can exist in three stages : (a) the stage of developing hypertrophy, which is characterized by rapid synthesis of new cellular components; (b) the stage of stable hyperfunction or compensated hypertrophy; and (c) the stage of cellular exhaustion, in which cardiac function deteriorates and various degenerative changes become prominent in the muscle cells. Most of the increment in muscle mass that occurs in hypertrophy is mediated through increases in mitochondrial and myofibrillar components. However, the quantitative relations between these two components vary considerably according to the cause and stage of the hypertrophy.

Very considerable degrees of cardiac hypertrophy can be induced in experimental animals by the administration of growth hormone [3], thyroid hormone [4], triiodothyroacetic acid (TRIAC) [5, 6], norepinephrine [7], and isoproterenol [8]. The last two agents induce hypertrophy at dose levels which are lower than those necessary to produce cardiac necroses. In fact slow, long-term infusion of norepinephrine produces cardiac hypertrophy at doses which do not result in elevation of the systemic arterial pressure [7]. The hypertrophy produced in newborn animals by administration of TRIAC to their mothers during pregnancy is of special interest in that it resembles in some respects the hypertrophy which occurs in hypertrophic cardiomyopathy [5, 6]. The types of hypertrophy produced by growth hormone and thyroid hormone in experimental animals have duplicated most of the features found in the hypertrophy occurring in human patients with acromegaly and hyperthyroidism.

Cardiomyopathies

The cardiomyopathies (heart muscle diseases) can be classified into: (a) hypertrophic, (b) congestive or ventricular-dilated, and (c) restrictive [9].

HYPERTROPHIC CARDIOMYOPATHY

In hypertrophic cardiomyopathy, the ventricular cavities are abnormally small, the ventricular walls are abnormally thick, and the ventricular septum becomes thickened to a greater extent than does the posterolateral free wall of the left ventricle at the level of the inferior border of the posterior leaflet of the mitral valve. In addition, the ventricular septal muscle in hypertrophic cardiomyopathy shows considerable cellular and myofibrillar disarray (as do the ventricular free walls). In most patients, this disorder is familial; however, in a few instances, it is associated with other diseases such as Friedreich ataxia, hyperthyroidism, and len-

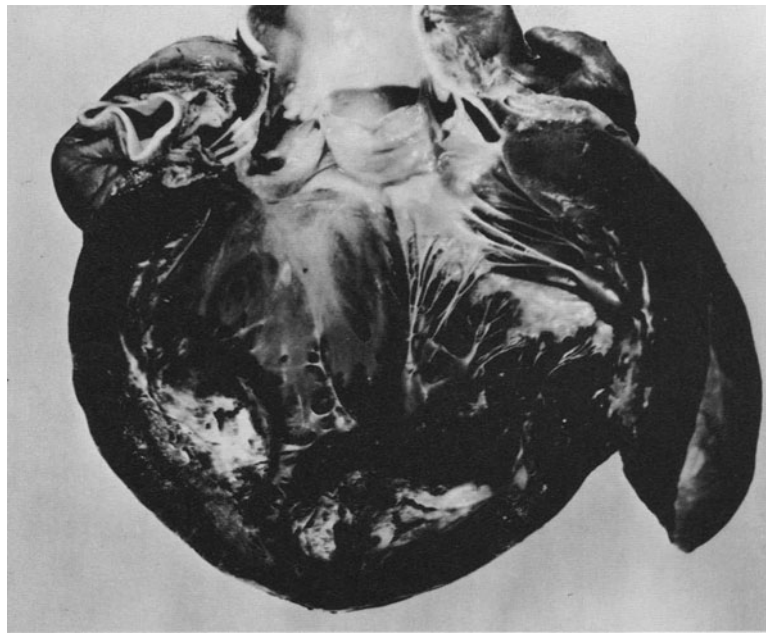

FIGURE 31–1. Gross photograph of dilated heart of patient with cardiomyopathy and history of chronic alcoholism. Mural thrombi fill the apical region of the left ventricle.

tiginosis [10]. It also occurs in cats, pigs, and dogs, but a suitable model strain of these animals has not been developed yet [11, 12]. The nature of the basic defect is unknown, but the disease is of great pharmacologic interest because of the many complex ways in which its clinical manifestations can be drastically altered by β-adrenergic blockers, various inotropic agents, and substances that modify calcium transport (verapamil). Nevertheless, at the present time, there is no drug-induced model of hypertrophic cardiomyopathy.

DILATED CARDIOMYOPATHIES

The term congestive or ventricular-dilated cardiomyopathy describes a heterogeneous group of muscle diseases (in which congenital, hypertensive, valvular, and pulmonary heart disease are excluded as etiologic factors) which have congestive heart failure (systolic pump failure) and dilatation of both ventricular chambers as common features (fig. 31–1). Mural thrombi and focal endocardial thickening are common, as are small foci of myocytolysis and myocardial fibrosis [9].

The eccentric hypertrophy and cardiac dilatation that occur in dilated cardiomyopathy are mediated mainly through gradual rearrangement of the layers of muscle cells forming the ventricular walls. The arrangement of these layers becomes more and more tangential to the wall as dilatation develops. Overstretching of sarcomeres does not account for the chronic dilatation, although it certainly does occur in acute dilatation. The possible contribution of longitudinal cell growth (leading to elongation of the cells) to eccentric hypertrophy remains to be fully assessed. The etiology of the changes described above remains unknown in many patients with dilated cardiomyopathy (idiopathic dilated cardiomyopathy); in other patients, the cardiomyopathy is associated with chronic alcoholism (alcoholic cardiomyopathy), with sequelae of viral infection, or with the administration of toxic agents. Ethyl alcohol, antineoplastic agents of the anthracycline family, cobalt, and furazolidone have been identified as toxic agents capable of inducing syndromes of chronic cardiomyopathy.

Alcoholic Cardiomyopathy. Ethyl alcohol has

several detrimental effects on myocardial metabolism, including: depression of mitochondrial functions, decrease in the uptake of calcium by sarcoplasmic reticulum, accumulation of lipid, and indirect effects mediated by acetaldehyde (which can inhibit protein synthesis and promote release of catecholamines), by acetate. and by thiamine. Nevertheless, the pathogenetic mechanisms of alcoholic cardiomyopathy remain uncertain [13–15]. Cardiomyopathy develops only in a small percentage of alcoholic patients, although a much higher percentage of these patients shows less obvious cardiac anatomic and functional abnormalities. Furthermore, the complete clinical picture of alcoholic cardiomyopathy seen in humans has not been reproduced in experimental animals by ethanol feeding, even though various morphologic and functional changes have been observed in such animals. It appears likely that the toxic effect of ethanol on myocardium is modified by other factors and that the "alcoholic" cardiomyopathy observed clinically in human patients is a multifactorial disease [13].

Histologic and ultrastructural studies have been useful in the recognition of some of the diseases leading to the nonspecific picture of progressive cardiac dilatation and failure seen in dilated cardiomyopathy [16]. Nevertheless, the anatomic findings in patients with congestive cardiomyopathy do not differ significantly in patients with and without a history of chronic alcoholism. Myocardial biopsies in these patients have revealed a wide variety of nonspecific degenerative changes, which tend to reflect the duration and severity of the heart disease. Alcoholic patients often show accumulations of large numbers of lipid droplets in cardiac muscle cells; however, this is a nonspecific change. Alcoholic cardiomyopathy in some patients is complicated by concomitant deficiency of thiamine or other nutrients. It also may be complicated by other toxic materials ingested along with the ethanol. The most striking example of this was illustrated by the epidemics of severe, acute cardiomyopathy, often associated with pericardial effusion and lactic acidosis, which developed in chronically malnourished alcoholic patients who had ingested large amounts of beer to which cobalt salts had been added during the manufacturing process to improve the quality of the foam. Structural findings in these patients included prominent vacuolization, myofibrillar lysis, glycogen accumulation, and edema of the muscle cells. Experiments in animals showed that protein malnutrition was an important factor modulating the absorption of cobalt from the gastrointestinal tract [13].

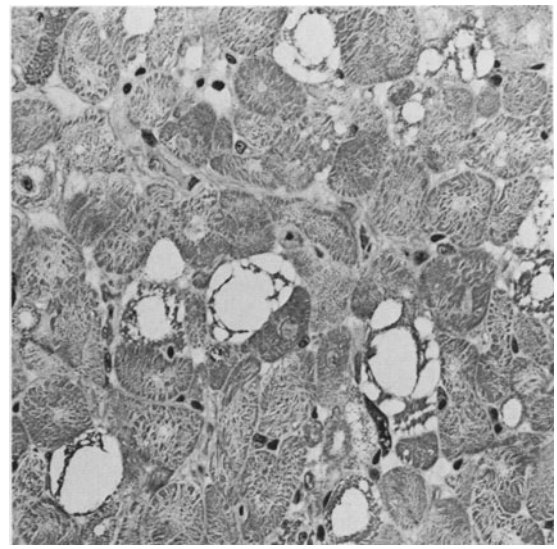

FIGURE 31–2. Severe cytoplasmic vacuolization of cardiac myocytes is the characteristic finding in anthracycline cardiotoxicity. Plastic-embedded tissue, alkaline toluidine blue stain, ×400.

Anthracycline Cardiomyopathy. Although anthracycline antibiotics also can produce acute (ventricular arrhythmias and depression of contractility) and subacute (pericarditis and myocarditis) cardiac toxicity, these agents are well known for the distinctive type of chronic congestive cardiomyopathy that they produce in humans and experimental animals. The pathogenesis of this complication, which generally is dose dependent (usually at least >400 mg/m^2 total cumulative dose), remains uncertain, but a number of possible mechanisms have been proposed, including drug binding by intercalation into the DNA in cardiac muscle cells, inhibition of several enzyme systems, and promotion of peroxidative damage, mediated by free radicals, to cell membranes, mitochon-

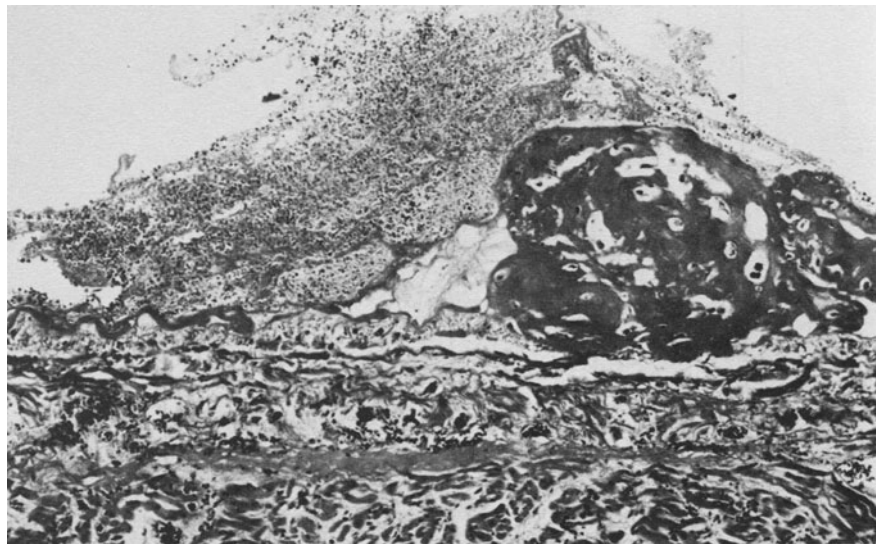

FIGURE 31–3. Fibrinous pericarditis and epicardial hemorrhage in heart of patient with acute cardiomyopathy due to administration of large amounts of cyclophosphamide in preparation for bone marrow transplantation, H & E stain, ×40.

drial membranes, DNA, enzymes, and membranes of sarcoplasmic reticulum [17–19]. Regardless of the causes, the drug toxicity leads to two major cardiac morphologic lesions, which are ventricular dilatation and myocardial cellular degeneration. The degeneration is manifested microscopically by myofibrillar loss and cytoplasmic vacuolization (fig. 31–2). The latter is a prominent but focal finding that involves individual cells rather than large, confluent areas of myocardium, and is caused by massive dilatation of tubules of sarcoplasmic reticulum. These changes also can involve the conduction system of the heart. The severity of the cardiac morphologic changes induced by anthracyclines has been evaluated by myocardial biopsies, which have been considered useful in determining whether or not patients at risk of developing anthracycline cardiomyopathy can receive additional amounts of the drug [20]. Previous radiation to the heart is known to be a significant risk factor in the development of anthracycline cardiomyopathy. This cardiomyopathy constitutes a new model system for the study of idiopathic chronic congestive cardiomyopathy; however, other side effects of anthracyclines, including bone marrow toxicity, gastrointestinal toxicity, and cutaneous lesions, may limit the practical usefulness of this model.

The anthracycline antibiotics, particularly doxorubicin and daunorubicin, are among the most effective antineoplastic agents available at the present time. For this reason, considerable efforts have been made to diminish their cardiotoxicity without compromising their therapeutic effectiveness. The most successful results in this regard have been obtained with ICRF-187, a compound which appears to act by chelating iron (which is needed to mediate the peroxidative reactions promoted by anthracyclines). When given concomitantly with doxorubucin, ICRF-187 reduces markedly the severity of the cardiomyopathy which develops in rabbits, rats, dogs, and pigs [21–24]. Compounds which act as free-radical scavengers (vitamin E, N-acetylcysteine) have been considerably less successful in blocking the cardiotoxic effects of doxorubicin [24–28]. Intensive efforts are under way to synthesize less cardiotoxic antibiotics of the anthracycline family.

It is important to note that antineoplastic agents other than the anthracyclines also are capable, but only rarely, of producing cardiac damage. Among these are: cyclophosphamide, busulfan, mitomycin C, cisplatinum, 5-fluorouracil, vincristine, VP-16, and m-AMSA

FIGURE 31–4. Same heart as in figure 31–3, showing microthrombi (arrowheads) in left ventricular capillaries. Periodic acid-Schiff stain, ×400.

[29–31]. Cyclophosphamide is cardiotoxic only when administered in massive doses [29, 30]. This is the case in patients being prepared for bone marrow transplantation, in whom cyclophosphamide has been reported to precipitate an acute cardiomyopathy characterized by hemorrhagic myocardial necrosis and pericardial effusion (figs. 31–3 and 31–4). Busulfan has caused endocardial fibrosis; mitomycin C, myocardial fibrosis. Myocardial infarctions have followed the administration of vincristine, 5-fluorouracil, and VP-16. ECG changes have been reported after cisplatinum therapy, and severe arrhythmias have followed treatment with m-AMSA (however, the solvent used in preparation of the latter is suspected of being the toxic agent) [31].

Furazolidone Cardiomyopathy. Furazolidone, an antibiotic of the nitrofuran group, produces congestive cardiomyopathy in ducks, chickens, and turkeys [32–37]. When administered to the young of these avian species it causes, in a dose-dependent manner, congestive cardiomyopathy and severe ventricular dilatation without microscopic evidence of hypertrophy, necrosis, or fibrosis. Ultrastructural study has shown that the principal alteration in cardiac muscle cells is diffuse myofibrillar lysis [36]. The sarcoplasm of affected myocytes contains scattered masses of free thick and thin myofilaments, clumps of Z-band material, and accumulations of cytoskeletal filaments. Supplements of selenium, vitamin E, and taurine do not protect against furazolidone-induced cardiomyopathy [37], but propranolol has been reported to be protective [38]. The biochemical mechanisms mediating this cardiomyopathy remain unknown. Ducklings with furazolidone-induced cardiomyopathy offer an attractive model for studies of the biochemical and structural alterations of myofibrillar lysis and drug-induced cardiac failure.

Other Agents which Induce Toxic Cardiomyopathies. In addition to the agents mentioned above, which cause well-defined syndromes of congestive cardiomyopathy, other drugs can induce depression of myocardial contractility, with or without associated brady- or tachyarrhythmias, and with or without the morphologic changes of toxic myocarditis (see below). Important among these are: tricyclic antidepressants, phenothiazines, lithium carbonate, emetine, chloroquine, quinidine, calcium

blockers, and radiographic contrast agents [15, 39–41].

Amytriptyline has been responsible for most of the cardiovascular reactions attributed to tricyclic antidepressants. The cardiotoxic actions of these agents usually occur only with preexisting ischemic heart disease or after drug overdosage and are manifested by arrhythmias and direct depression of myocardial function. Phenothiazines also are prone to producing hypotension, by virtue of their α-adrenergic-blockading effects and inhibition of central pressor reflexes; in addition, patients on phenothiazines show a tendency toward prolongation of the QT interval, which facilitates the development of arrhythmias. It has been suggested that myocardial changes induced by tricyclic antidepressants and phenothiazines persist after withdrawal of these drugs; however, no controlled studies have been made of these problems. Emetine, an alkaloid used in the treatment of amebiasis and schistosomiasis, frequently produces electrocardiographic changes; these may persist for several months after termination of treatment. Rarely, emetine causes depression of cardiovascular function and death from cardiac failure or arrhythmias [39–41].

Electrocardiographic alterations are frequent in patients receiving lithium carbonate. T-wave changes are common; tachyarrhythmias, atrioventricular conduction disturbances, and left bundle branch block occur at toxic serum lithium concentrations. These effects are reversible in the majority of patients, but a few patients receiving lithium carbonate develop congestive cardiomyopathy which does not improve after the drug is discontinued [39–41].

Chloroquine occasionally produces electrocardiographic changes, usually bundle branch block; impairment of cardiac function also may occur.

Radiographic contrast agents often produce electrocardiographic changes and depression of myocardial function, particularly when used for ventriculography or coronary arteriography. This effect seems to be mediated by a calcium-chelating action rather than by osmolarity changes. Significant depression of myocardial function also can result from the use of other agents which interfere with the movement of calcium ions, i.e., verapamil and quinidine [39–41].

OBLITERATIVE AND RESTRICTIVE CARDIOMYOPATHIES

Obliterative cardiomyopathies are a group of disorders characterized by endocardial fibrous thickening and endocardial mural thrombosis, changes which lead to partial obliteration of the ventricular cavities. Löffler syndrome and endomyocardial fibrosis are the most important entities in this group. Restrictive cardiomyopathies are those in which infiltrative processes (for example, amyloidosis) of diffuse accumulation of fibrous tissue in the ventricular walls reduce myocardial compliance and interfere with ventricular filling.

Löffler syndrome (fibroplastic parietal endocarditis) is a disorder of unknown etiology in which hypereosinophilia in blood and heart (and often also in other tissues) is accompanied by marked endocardial fibrous thickening and mural thrombosis [42]. These processes also can involve the cardiac valves. The eosinophilia can be transient, and it is thought that Löffler syndrome and endomyocardial fibrosis (in which eosinophilia is lacking at the time when heart disease becomes clinically evident) represent two parts of the spectrum of endomyocardial disease associated with eosinophilia. Evidence has been presented to suggest that eosinophilic leukocytes can release products capable of inducing endocardial damage by mechanisms that remain unclear.

Endocardial mural thickening of mild degree can occur in association with toxic or ischemic lesions that cause myocardial necrosis [16]; however, marked fibrous thickening of mural and valvular endocardium also can be produced by methysergide and ergotamine tartrate [43–46]. The cardiac valves most frequently involved are the mitral and aortic, which become thickened and distorted by a layer of dense fibrous tissue. This tissue is devoid of elastic fibers and resembles that found in the lesions of carcinoid heart disease [47]. In the atrioventricular valves, the fibrosis may lead to thickening and fusion of the chordae tendineae. These lesions can lead to valvular stenosis and

regurgitation. Mural endocardial thickening also occurs in the late stages of allylamine cardiotoxicity and in radiation-induced myocardial fibrosis.

Cardiac Necrosis and Myocarditis

CARDIAC NECROSIS

Although much of the research on the mechanisms of cardiac muscle cell necrosis has centered on ischemic injury and its modification by pharmacologic agents, many of the principles derived from these studies are applicable to toxic myocardial injury. Two basic forms of cardiac muscle cell necrosis are recognizable: coagulation necrosis and necrosis with contraction bands (myofibrillar damage leading to myocytolysis) [16].

Coagulation Necrosis. Ischemia of less than 20 min duration produces reversible damage characterized by glycogen depletion, mitochondrial swelling, mild intracellular edema, and relaxation of sarcomeres (reflecting loss of contractility). Irreversible injury with the features of coagulation necrosis develops when the period of ischemia exceeds 20 min. The percentage of irreversibly damaged cells increases as the period of ischemia is prolonged up to 60 min, at which time most of the cells in the ischemic areas become irreversibly injured. In addition to the changes mentioned above, coagulation necrosis is characterized by: (a) intramitochondrial flocculent precipitates, which are thought to be derived from mitochondrial lipids; (b) margination of nuclear chromatin, which is regarded as evidence of irreversible nuclear damage; (c) small holes or defects in the plasma membrane, signifying loss of its permeability barrier function; and (d) various degrees of dissociation of the intercellular junctions, leading to electrical uncoupling of the cells. These changes progress to fully developed coagulation necrosis, in which the muscle cells have relaxed myofibrils with indistinct myofilaments. For these reasons, coagulation necrosis is characteristically limited to central areas of myocardial infarcts, in which reflow does not occur after ischemic damage develops.

Necrosis with Contraction Bands. In contrast to coagulation necrosis, peripheral areas of infarcts show a different type of necrosis, known as necrosis with contraction bands, which is characterized by: (a) hypercontraction of myofibrils; (b) intramitochondrial, electron-dense calcific deposits; and (c) progression to myocytolysis. The distinctive features of this type of necrosis are related to the entry of large amounts of calcium ions, which originate from partial perfusion of peripheral areas of ischemic lesions, into cells which are damaged by ischemia. The passage of calcium through damaged, abnormally permeable plasma membranes is responsible for the hypercontraction; this passage occurs either when severely but temporarily ischemic tissue is reperfused with arterial blood or when necrosis develops because of other factors not related to a reduction in coronary blood flow. For these reasons, necrosis with contraction bands is seen in many forms of cardiac toxic injury, including the lesions caused by catecholamines and vasodilating antihypertensive agents [16]. Progression of necrosis with contraction bands to myocytolysis is mediated through lysis of the myofilaments, a change that results in an empty appearance of the cells. The time course of this progression is highly variable. Of interest is the fact that the lysis of contractile elements in infarcted myocytes is retarded by therapy with corticosteroids, under which circumstances the cells appear "mummified" [48].

As explained above, the morphologic appearance of irreversibly injured, ischemic cardiac myocytes differs according to whether or not cell death occurs with or without the ischemic tissue having been reperfused. It should be noted, however, that flow through the ischemic area often cannot be reestablished when attempts are made to reperfuse tissue that has been ischemic for a long time (in excess of 90 min). Under these circumstances, the microcirculation in the ischemic area may have suffered irreversible damage, giving rise to the "no reflow" phenomenon [16].

INFLAMMATION

Inflammation basically is a protective response by which injured tissue is restored to its normal state or damage produced by injury is re-

paired. However, inflammation also can be the cause of additional tissue damage, and modification of myocardial inflammatory responses constitutes an important aspect of cardiac pharmacology.

Acute Inflammation. Acute inflammation is manifested by vascular dilatation, tissue edema, and infiltration by leukocytes. These manifestations result from the release of vasopermeability factors (kinins, vasoactive amines, leukokines, anaphylatoxins from complement, and prostaglandins) and leukotactic factors (these vary in their ability to attract different types of inflammatory cells in areas of cellular injury or necrosis). The diagnosis of acute myocarditis (due to infection, drug reaction, or many other causes) is dependent on the finding of acute inflammatory cells, which have the capacity to neutralize offending chemical and infective agents and to destroy remnants of injured cells and extracellular components of connective tissue [16].

Polymorphonuclear neutrophilic leukocytes, which are strongly phagocytic cells, constitute the most prominent features of acute inflammation in the heart, where they first become marginated (i.e., adherent to the luminal surfaces of capillaries) before passing into the extravascular compartment through gaps in the junctions connecting endothelial cells. Mononuclear cells, i.e., monocytes and lymphocytes, invade tissues at somewhat later stages of acute inflammation. As they leave the vascular compartment, blood monocytes undergo a gradual transformation into macrophages, thereby also participating in phagocytic processes. Lymphocytes have the capacity of mediating responses involving specific humoral (B lymphocytes) or cell-mediated (T lymphocytes) immune responses.

Mast cells, which are abundant in myocardium, also participate in acute inflammatory and hypersensitivity reactions by serving as mediator cells capable of releasing histamine, together with other components of mast cell granules, either on direct contact of the cell with a chemical or through the interaction of antigens with IgE bound to the mast cell surface. Many of the properties of mast cells in tissues are shared by basophilic leukocytes in blood.

Eosinophilic leukocytes, which also are phagocytic, can participate in acute inflammation as well as in chronic inflammation, and are well known to be associated with allergic and parasitic disorders; however, their specific role in these processes is not well understood. They represent an important component in the inflammatory reaction associated with allergic myocarditis, but they also occur in other, unrelated cardiac disorders such as Löffler syndrome of hypereosinophilia and endomyocardial fibrosis.

Subacute Inflammation. Subacute inflammation is a delayed phase of acute inflammation, and is characterized by the accumulation of monocytes and lymphocytes and by the formation of granulation tissue. The latter is composed of rapidly proliferating fibroblasts, pericytes, and capillary endothelial cells in a matrix of developing connective tissue. The synthesis of connective tissue proteins by these cells mediates the fibrous tissue deposition by which healing occurs.

Chronic Inflammation. Chronic inflammation is characterized by the continuing presence of lymphocytes, monocytes (or monocyte-derived cells such as macrophages and epithelioid cells), and plasma cells in the tissues. It usually results from the persistence of material that elicits an immunologic reaction, and it causes continuing tissue damage either because of immunologic injury or because of excessive deposition of collagen. Chronic inflammation can be granulomatous, in which the inflammatory cells are associated with multinucleated giant cells (of either histiocytic or myogenic origin) and form nodular masses.

CARDIAC CELLULAR DAMAGE PRODUCED BY TOXIC AGENTS

It is obvious that many highly specific biochemical and pharmacologic mechanisms can mediate the cardiac cellular damage produced by toxic drugs and chemical agents. It is difficult to establish structural–functional correlations with respect to such lesions; even highly

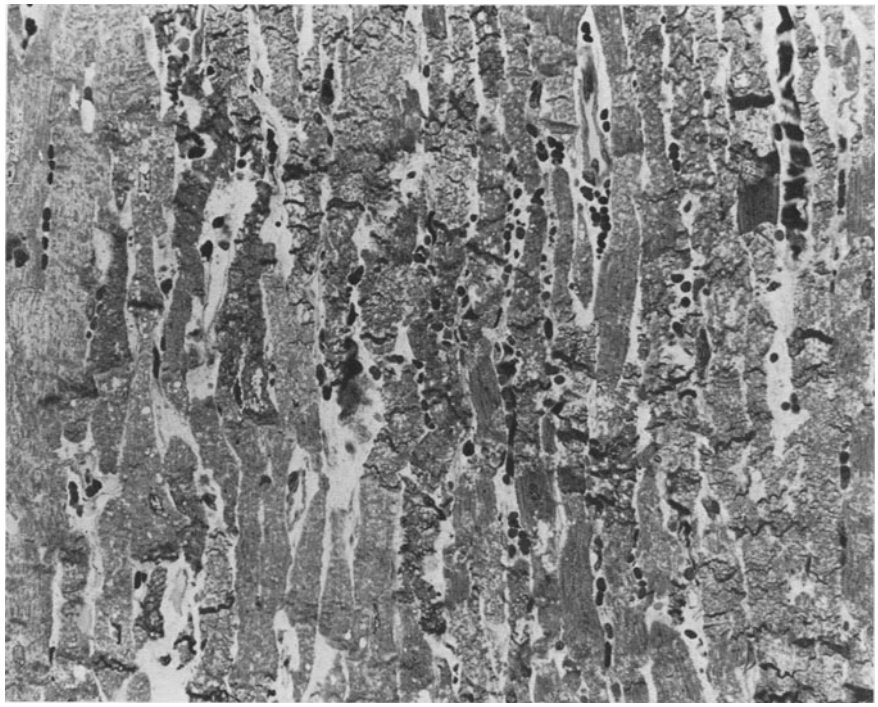

FIGURE 31–5. Necrosis with contraction bands in left ventricular papillary muscle of dog given overdose of minoxidil. Plastic-embedded tissue, alkaline toluidine blue stain, ×250.

specific, localized disturbances of the delicate equilibrium of cell functions can lead rapidly to a picture of generalized cell damage or cell necrosis. Examples of toxic agents producing specific damage to various subcellular organelles of cardiac muscle cells include (a) compounds which interfere with mitochondrial enzymes (cyanide [49], thyroid hormone [4]), uncouple oxidative phosphorylation (dinitrophenol [50]), or bind to mitochondrial DNA (acriflavine [51]) and produce a number of alterations in mitochondrial morphology; (b) compounds which induce intracellular calcification, usually localized within mitochondria (dehydrotachysterol [52], sodium phosphate [53]); (c) compounds which primarily cause myofibrillar lesions (sympathomimetic amines [54–57], plasmocid [58], diuretics, or other conditions leading to potassium deficiency [59]); (d) compounds which cause accumulations of electron-dense lamellae (chloroquine [60]); (e) compounds which produce massive dilation of sarcoplasmic reticulum (anthracyclines [17–20]) (figs. 31–5 to 31–7).

Although the changes just cited seldom are specific, they can provide valuable clues as to the mode of action of a given agent. Many of the changes in the contractile apparatus, nucleus, or membrane systems (plasma membrane/T tubules and sarcoplasmic reticulum) are associated with complex alterations in the overall concentrations of Ca, Mg, Na, and K, as well as with changes in the intracellular compartmentalization of these ions [61]. Furthermore, these ionic alterations, and changes in intracellular pH, can be associated with activation and release of lysosomal hydrolytic enzymes, including cathepsin D and other proteases and phospholipases [62, 63]. These variously interrelated changes, together with alterations in the permeability of plasma membranes, act as determinants of whether or not cellular injury progresses to the point of irreversibility, i.e., cellular necrosis [16].

On the basis of the pathogenesis and morphology of the resulting lesions, acute toxic cardiac damage can be classified into the following categories: (a) myocardial infarcts and

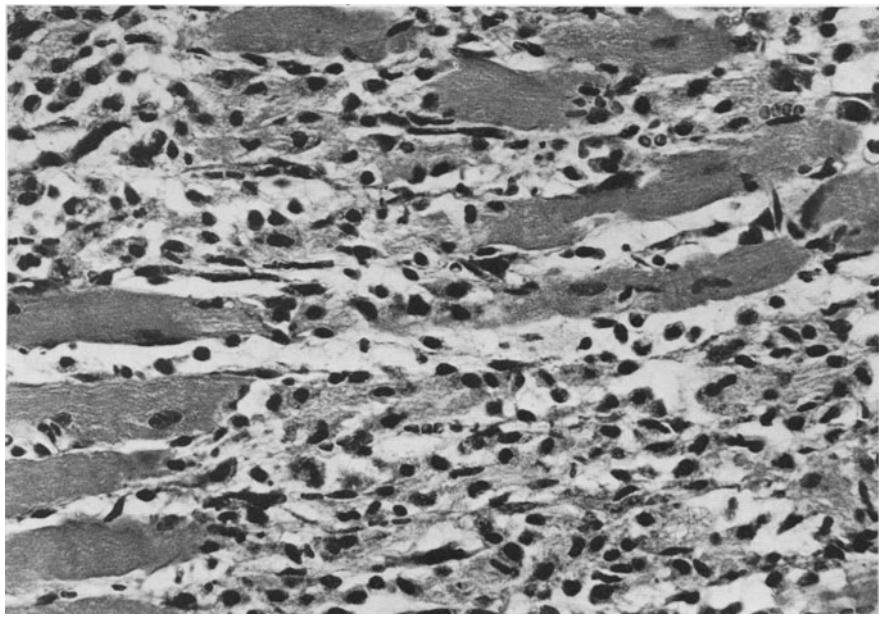

FIGURE 31–6. Left ventricular myocardium of rat with hydralazine-induced necrosis. Necrotic myocytes are being invaded by inflammatory cells. H & E stain, ×400.

infarct-like lesions, (b) hypersensitivity myocarditis, and (c) toxic myocarditis.

MYOCARDIAL INFARCTION ASSOCIATED WITH TOXIC REACTIONS

Grossly evident myocardial infarction may occur when the coronary arteries are involved by drug-induced arteritis (as from amphetamines), fibromuscular intimal proliferation (oral contraceptives), embolization from infective endocarditis (associated with intravenous drug abuse), or, in patients with normal coronary arteries, following exposure to toxic levels of carbon monoxide, nitrates, thyroid preparations, methysergide or ergot derivatives, and certain antineoplastic agents [40]. Large, infarct-like areas of necrosis, not related to obstruction of large, extramural coronary arteries, have been produced in experimental animals by the administration of large, toxic doses of isoproterenol [54, 57]. It was originally thought that this necrosis resulted from isoproterenol-induced increases in cardiac rate, contractility, and oxidative metabolism to an extent beyond the limits of the oxygen supply system. More recently, however, it has become evident that isoproterenol also produces other highly complex effects, including a marked increase in calcium uptake, stimulation of the adenyl-cyclase system, aggregation of platelets, and induction of the formation of free radicals capable of causing peroxidative damage [15, 64]. Other symphathomimetic amines are capable of inducing myocardial necroses (norepinephrine, epinephrine), which are small, patchy, and multifocal, and usually localized in left ventricular subendocardium [54–57].

Other effects of catecholamines are of practical importance. Catecholamine-induced cardiac lesions in experimental animals have several human counterparts, as is the case in patients with pheochromocytomas, tetanus, subarachnoid hemorrhage, and other CNS lesions [15]. In these conditions, release of large amounts of catecholamines can lead to focal cardiac damage. Ischemic cardiac damage can be aggravated by high circulating levels of catecholamines in patients with acute myocardial infarction [15]. The ingestion of certain foods containing tyramine can produce severe hypertensive crises in patients undergoing therapy with monoamine oxidase inhibitors [65]. Therapy with β-adrenergic blockers and exposure to chloroform and other halogenated hy-

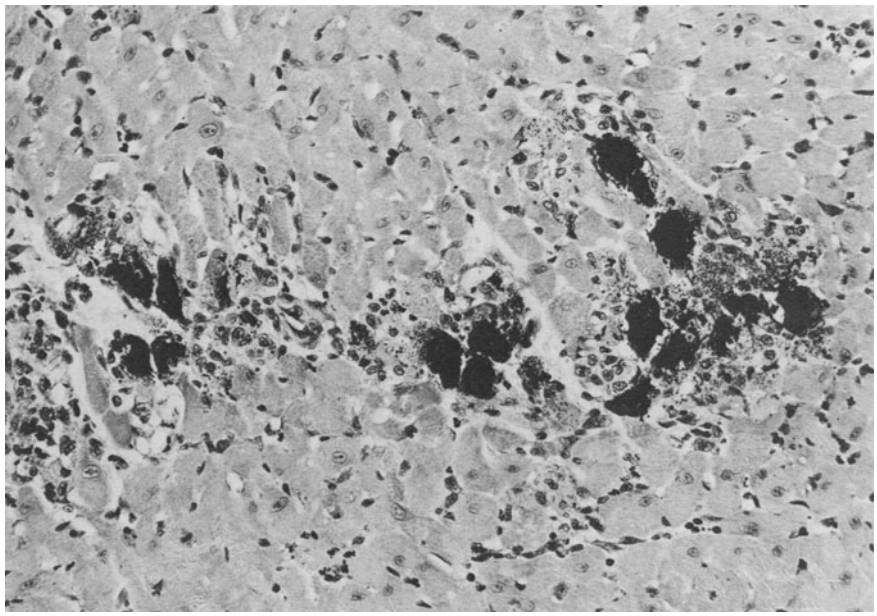

FIGURE 31–7. Heavily calcified, necrotic myocytes are surrounded by moderate inflammatory infiltrate in heart of rat given large dose of dehydrotachysterol. Von Kossa stain, ×250.

drocarbons (including a number of fluorinated compounds and halogen-containing anesthetic and refrigerating agents) can sensitize the myocardium to the effects of sympathomimetic amines [39].

HYPERSENSITIVITY MYOCARDITIS

Hypersensitivity myocarditis associated with drug therapy is characterized by infiltration of the heart muscle with numerous eosinophils admixed with mononuclear cells, predominantly lymphocytes and plasma cells [40, 41]. The cellular infiltrate may be focal or diffuse and is associated with foci of myocytolysis. Fibrotic changes are absent and all lesions are similar in age and appearance. True granulomatous lesions are not present, although giant cells of myogenic origin may be found. Vascular involvement is frequent and consists of a bland-appearing vasculitis affecting small arteries, arterioles, and venules. The inflammatory reaction also may involve the pericardium, but characteristically spares the cardiac valves. The absence of extensive myocardial necrosis or fibrosis distinguishes drug-related hypersensitivity myocarditis from other forms of myocarditis in which eosinophils are prominent. Endocardial fibrosis is not a feature of hypersensitivity myocarditis. Hypersensitivity myocarditis represents the most common form of drug-induced heart disease. The clinical criteria for the diagnosis of this disorder are: (a) previous use of the drug without incident; (b) the hypersensitivity reaction bears no relationship to the magnitude of the dose of the drug; (c) the reaction is characterized by classic allergic symptoms, symptoms of serum sickness or syndromes suggesting infectious disease; (d) immunologic confirmation; and (e) persistence of symptoms until the drug is discontinued. The following drugs have been associated with hypersensitivity myocarditis: methyldopa, hydrochlorothiazide, sulfadiazine, sulfisoxazole, sulfonylureas, chloramphenicol, *p*-aminosalicylic acid (PAS), amitriptyline, carbamazepine, indomethacin, penicillin, phenindione, phenylbutazone, oxyphenbutazone, tetracycline, diphenylhydantoin, acetazolamide, ampicillin, chlorthalidone, spironolactone, and streptomycin. Many of these drugs also have been associated with hypersensitivity vasculitis. The pathogenesis of drug-induced hypersensitivity myocarditis remains unclear, but appears to be immunologically mediated, perhaps as a delayed hypersen-

sitivity reaction in which the drug or one of its metabolites act as haptens and combine with an endogenous macromolecule; it is this combination that is antigenic. Hypersensitivity myocarditis also has developed after injection of horse serum, tetanus toxoid, and smallpox vaccine.

TOXIC MYOCARDITIS

Drugs can cause myocardial injury not only by producing allergic (hypersensitivity) myocarditis, but also by direct toxic effects which result in cell damage and cell death. This type of drug toxicity is dose-related; depending upon its rate of progression, it can cause either acute toxic myocarditis or a more chronic picture of drug-induced cardiomyopathy. In acute toxic myocarditis there is interstitial edema, multifocal areas of cardiac muscle cell necrosis with contraction bands, and an inflammatory cell infiltrate consisting of lymphocytes, plasma cells, and polymorphonuclear leukocytes. The areas of necrosis show different stages of progression. Eosinophils may be present, but seldom are prominent. There is endothelial cell damage, but not a true vasculitis. Microthrombi have been reported in toxicity due to ADP, cyclophosphamide (fig. 31–4), catecholamines, and thromboxane A. The paucity of eosinophils and the presence of various stages of cell death and healing by fibrosis serve to differentiate toxic myocarditis from hypersensitivity myocarditis. Among the drugs and chemicals known to cause toxic myocarditis are: daunorubicin, doxorubicin, 5-fluorouracil, emetine, antimony compounds, amphetamines, cyclophosphamide, catecholamines, lithium carbonate, phenothiazines, plasmocid, paraquat, and mitomycin C [40, 41]. It should be remembered that a cellular inflammatory reaction may be poorly developed or totally absent in toxic myocarditis due to antineoplastic or immunosuppressive agents.

Other agents capable of inducing focal myocardial fibrosis and necrosis are: monensin, a polyether antibiotic that acts as a Na-selective carboxylic ionophore [66]; rapeseed oil, the most important ingredient of which is erucic acid [67]; arsenicals, which also can cause peripheral vascular disease (black leg) [40, 41]; and allylamine, a highly toxic aliphatic amine used in industry [68]. Corticosteroids produce degenerative lesions in the hearts of animals and to a lesser extent in those of humans [40, 69]. Cobalt, copper, tellurium, cadmium, and zinc, when given in toxic doses, can precipitate systemic lesions, often with cardiac and skeletal muscle involvement, which resemble those resulting from deficiency of selenium and vitamin E and which can be at least partially prevented by dietary supplements of selenium and vitamin E [70, 71]. Finally, oral hypoglycemic agents have been associated with adverse cardiovascular effects that have not been completely elucidated [15].

A peculiar type of chronic inflammatory myocarditis associated with marked, grossly evident reddening of the tissue and with hemorrhage and fibrosis (fig. 31–8) has been observed in atrial myocardium of dogs and pigs treated with minoxidil, a vasodilating antihypertensive agent that also can produce foci of left ventricular papillary muscle necrosis [72, 73]. For reasons that are not clear, the atrial lesions in dogs are localized mainly in the right atrium; those in pigs, in the left atrium. The papillary muscle necroses (fig. 31–5) are thought to be consequences of the tachycardia, hypotension, and hypoperfusion which occur when large doses of minoxidil are given. The pathogenesis of the atrial lesions is unknown. It is of interest that similar right atrial lesions are produced in dogs by the administration of large doses of theobromine [74].

Pericarditis

Pericarditis with or without effusion has been reported to occur in patients with drug-induced systemic lupus erythematosus. In the majority of these patients, the pericarditis is only one of the many manifestations of the lupus-like syndrome. A relatively large number of drugs has been implicated in the induction of lupus-like syndromes. Among these agents are: hydralazine, procainamide, isoniazid, *p*-aminosalicylic acid, diphenylhydantoin, methylphenylethylhydantoin, mephenytoin, primidone, trimethadione, ethosuximide, methsuximide, trimethadone, penicillin, penicillamine,

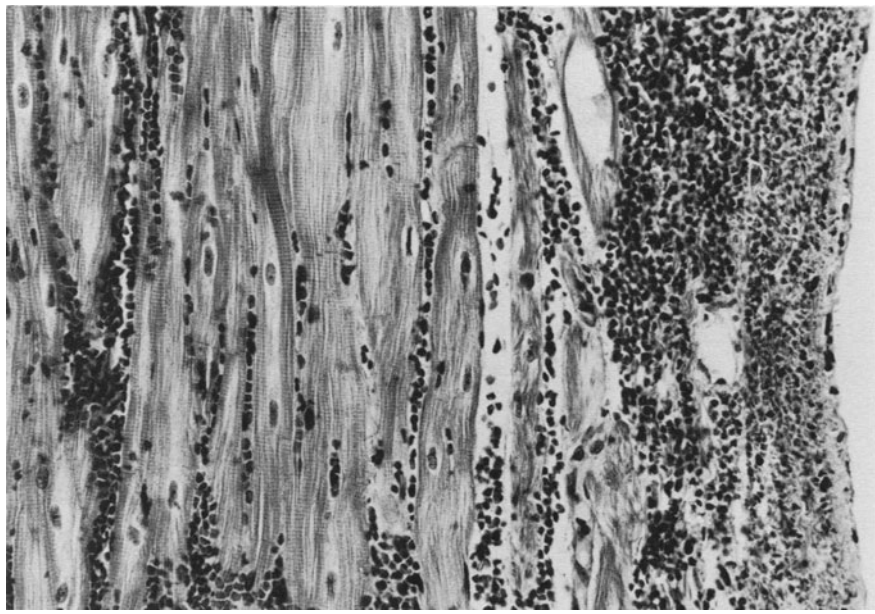

FIGURE 31–8. Extensive subendocardial hemorrhage in left ventricle of dog given toxic dose of minoxidil. H & E stain, × 100.

sulfonamides, tetracycline, propylthiouracil, methyldopa, barbiturates, griseofulvin, streptomycin, quinidine, phenylbutazone, chlorpromazine, methotrimeprazine, perphenazine, promazine, and reserpine. It is to be noted that, in many of the reports of the agents just mentioned, the evidence linking drug usage to the lupus-like syndrome is highly circumstantial, and, in some instances, the symptoms suggestive of lupus have antedated the use of the drug in question. The syndromes have been most clearly documented in the case of hydralazine and procainamide [40].

Drugs that cause toxic myocarditis, hypersensitivity myocarditis, or large areas of myocardial necrosis often also cause pericarditis by extension of the inflammation to the pericardium, particularly the visceral pericardium. Pericardial hemorrhage (fig. 31–3) can occur as a result of cyclophosphamide toxicity [29, 30] and therapy with anticoagulants. The latter problem is encountered in some patients with uremia who are given heparin during the course of hemodialysis [40].

Vascular Changes

Morphologic changes of considerable practical importance are induced by drugs or chemicals that modify the lesions of atherosclerosis, either through changes in plasma lipids and lipoproteins or through more direct effects on vascular walls. Other toxic chemicals exert their effects on blood vessels by inducing connective tissue changes leading to the formation of nonatherosclerotic aneurysms in the aorta and other large arteries. These effects usually are mediated through biochemical inhibition of specific steps in the synthesis of connective tissue proteins, as in the cause of penicillamine and β-aminopropionitrile [75].

HYPERSENSITIVITY VASCULITIS

The anatomic features of hypersensitivity vasculitis may be summarized as follows: (a) only small vessels, primarily arterioles, capillaries, and venules, are involved, (b) muscular and elastic arteries and large veins are spared, (c) aneurysms are not found, (d) all lesions appear to be of about the same age, (e) fibrinoid necrosis is not present, and (f) eosinophils and mononuclear cells are the predominant components of the inflammatory reaction and are present in all three layers of the involved vessel

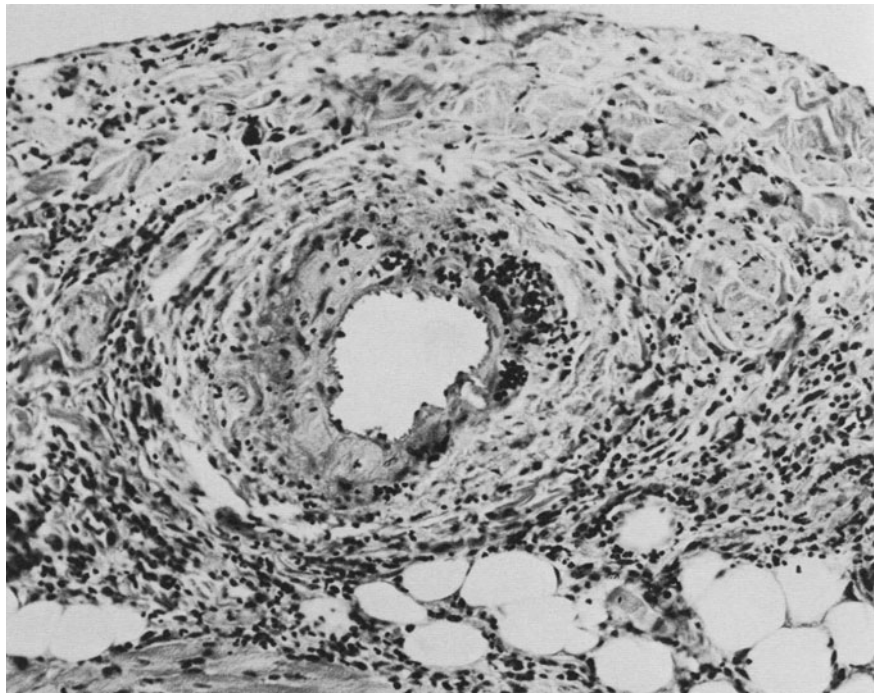

FIGURE 31–9. Inflammatory reaction surrounds area of fibrinoid necrosis and intramural hemorrhage in small artery in right atrial epicardium of dog receiving toxic dose of minoxidil. H & E stain, ×80.

and in adjacent areas of interstitial connective tissue [40, 76, 77]. Drugs reported to induce hypersensitivity vasculitis include: allopurinol, ampicillin, bromide, carbamazepine, chloramphenicol, chlortetracycline, chlorpropamide, chlorthalidone, chromolyn sodium, colchicine, dextran, diazepam, diphenylhydantoin, diphenhydramine, griseofulvin, indocin, isoniazide, levamisole, methylthiouracil, oxyphenbutazone, phenylbutazone, potassium iodide, procainamide, propylthiouracil, quinidine, spironolactone, sulfonamides, tetracycline, and trimethadione [40, 76, 77].

In contrast to drug-induced vasculitis, the lesions of periarteritis nodosa, a collagen-vascular disease of unknown origin, are characterized by: (a) involvement of muscular arteries, (b) fibrinoid necrosis of the vascular walls, (c) frequent occlusion of the vascular lumina by thrombus or granulation tissue, and (d) weakening of the media, with formation of aneurysms. Vascular lesions in other collagen-vascular diseases have nonspecific features, and occasionally may resemble those in periarteritis nodosa. The exception is Wegener granulomatosis, in which the lesions affect small arteries, arterioles, and venules (pulmonary vessels often are involved), forming granulomas with acute and chronic inflammatory cells and multinucleated giant cells. Nevertheless, granulomatous lesions are not diagnostic of Wegener granulomatosis, and fibrinoid necrosis is not diagnostic of collagen-vascular diseases, as these lesions occur in other diseases [40].

TOXIC VASCULITIS

Toxic vasculitis is usually necrotizing, with morphologic features similar to those of periarteritis nodosa. Medium-sized and small arteries are most often affected; however, smaller vessels also may be involved. The lesions tend to be segmental and to be heavily infiltrated by polymorphonuclear leukocytes. Fibrinoid necrosis, superimposed thrombi, and aneurysm formation are usually found in various stages of evolution. These lesions are most frequently associated with the use of penicillin or sulfonamides; less frequently, with organic arsenicals, gold

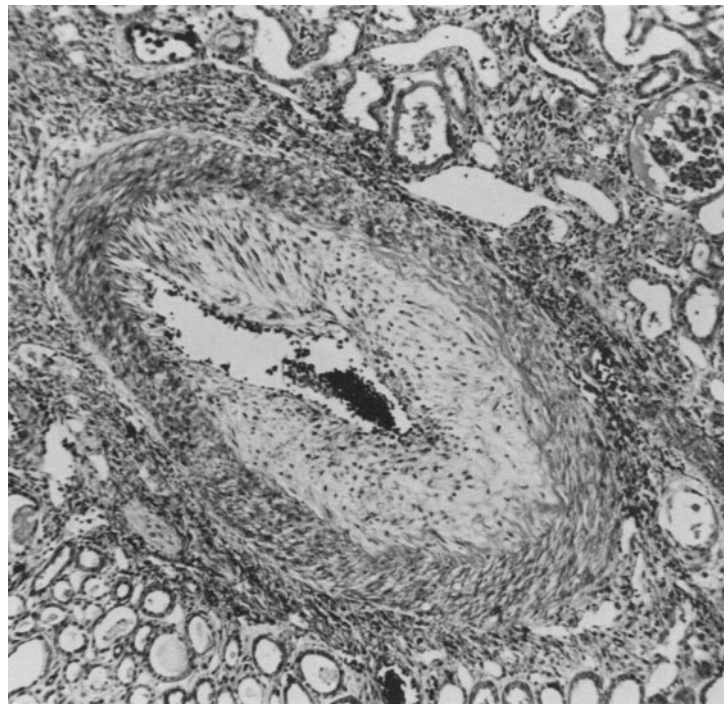

FIGURE 31–10. Fibromuscular intimal proliferation, presumed to be due to oral contraceptives, has caused considerable luminal narrowing in small renal artery. Movat pentachrome stain, ×80.

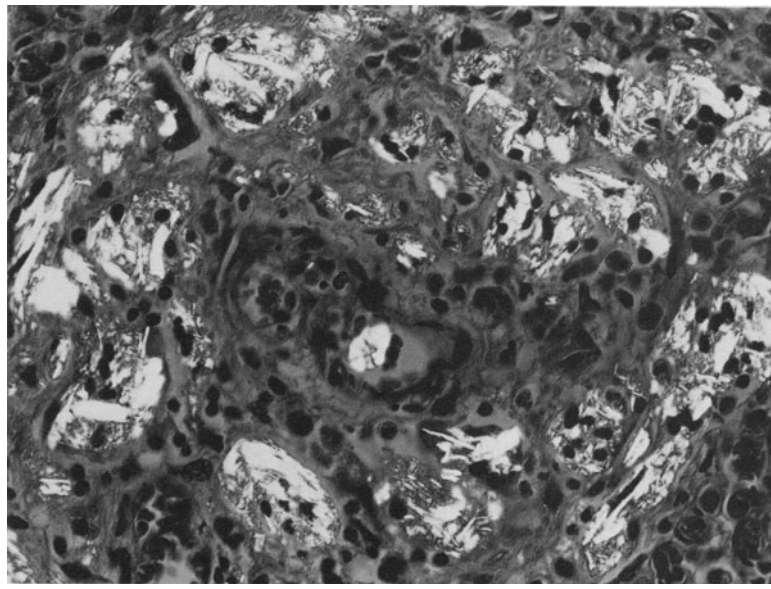

FIGURE 31–11. Micrograph taken with partially polarized light to demonstrate numerous talc deposits around small pulmonary blood vessel of patient who had history of intravenous drug abuse. H & E stain, ×100.

salts, minoxidil (fig. 31–9), mercurials, bismuth, amphetamine, metamphetamine, DDT, heterologous serum, and sulfonamides. The pathogenesis of drug-induced toxic vasculitis remains incompletely understood [40, 41].

VASCULAR LESIONS ASSOCIATED WITH ORAL CONTRACEPTIVES

Vascular proliferative lesions, not related to atherosclerosis, have been found in women taking oral contraceptives (fig. 31–10), in pregnant women and immediately postpartal women, and in a few men with severe liver disease (the implication in the latter patients being that of inadequate inactivation of certain steroids). These lesions may be associated with thrombosis, and may occur in the systemic, portal, or pulmonary circulation. The lesions consist of fibromuscular intimal thickenings containing smooth muscle cells, collagen, and proteoglycans; inflammatory cells and vascular necrosis usually are not present. The exact pathogenesis of these lesions is uncertain [76].

OTHER DRUG-INDUCED VASCULAR LESIONS

Other drug-induced arterial lesions include those induced by: (a) ergotamine (intimal proliferation, medial hypertrophy, and hyalinization, with or without superimposed thrombosis and gangrene); (b) methysergide maleate (intimal proliferation often leading to vascular occlusion), a compound which, as mentioned previously, also can aggravate coronary artery disease symptoms and produce retroperitoneal, endocardial, and mediastinal fibrosis; and (c) vitamin D (calcification of arterial elastic lamina [40, 41]). In addition, disseminated arterial lesions similar to those in periarteritis nodosa are found in patients using amphetamines intravenously; pulmonary arteriolar granulomatous lesions (fig. 31–11) occur in patients who inject themselves intravenously with suspensions of drug tablets containing talc or other silicates [77], and drug-related infective vasculitis can develop in patients receiving intravenously administered drugs. In the latter patients, the infection may be only a localized phlebitis or may progress to infective arteritis or endocarditis. Drug-induced thrombophlebitis not related to infection also is a common complication of intravenous therapy.

References

1. Ferrans VJ: Morphology of the heart in hypertrophy. Hosp Pract 18:67–78, 1983.
2. Oberpriller JO, Ferrans VJ, Carroll RJ: Changes in DNA content, number of nuclei and cellular dimensions of young rat atrial myocytes in response to left coronary ligation. J Mol Cel Cardiol 15:31–42, 1983.
3. Powis L: Growth hormone in cardiac hypertrophy induced by nephrogenous hypertension. Recent Adv Stud Cardiac Struct Metab 8:413–425, 1975.
4. Gerdes AM, Kriseman J, Bishop SP: Changes in myocardial cell size and number during development and reversal of hyperthyroidism in neonatal rats. Lab Invest 48:598–602, 1983.
5. Symons C, Olsen EGJ, Hawkey CM: The production of cardiac hypertrophy by triiodothyroacetic acid. J Endocrinol 65:341–346, 1975.
6. Hawkey CM, Olsen EGJ, Symons C: Production of cardiac muscle abnormalities in offspring of rats receiving triiodothyroacetic acid (triac) and the effect of beta adrenergic blockade. Cardiovasc Res 15:196–205, 1981.
7. Laks MM, Morady F: Norepinephrine—the myocardial hypertrophy hormone? Am Heart J 91:674–675, 1976.
8. Bartolome JV, Trepanier PA, Chait EA, Slotkin TA: Role of polyamines in isoproterenol-induced cardiac hypertrophy: effects of α-difluoromethylornithine, an irreversible inhibitor of ornithine decarboxylase. J Mol Cell Cardiol 14:461–466, 1982.
9. Roberts WC, Ferrans VJ: Pathologic anatomy of the cardiomyopathies (idiopathic dilated and hypertrophic types, infiltrative types and endomyocardial disease with and without eosinophilia). Hum Pathol 6:287–342, 1975.
10. Perloff JK: Pathogenesis of hypertrophic cardiomyopathy: hypotheses and speculations. Am Heart J 101:219–226, 1981.
11. Liu SK: Cardiac disease in the dog and cat. In: Roberts HR, Dodds WJ (eds) Pig model for biomedical research. Taipei: Pig Research Institute, 1982, pp 110–133.
12. Hsu FS, Du S-J: Cardiac diseases in swine. In: Roberts HR, Dodds WJ (eds) Pig model for biomedical research. Taipei: Pig Research Institute, 1982, pp 134–142.
13. Ferrans VJ, Buja LM, Roberts WC: Cardiac morphologic changes produced by ethanol. In Rothschild MA, Oratz M, Schreiber S (eds) Alcohol and abnormal protein biosynthesis. New York: Pergamon, 1974, pp 139–185.
14. Regan TJ, Khan MI, Ettinger PO, Heider B, Lyons MM, Oldewurtel HA: Myocardial function and lipid

metabolism in the chronic alcoholic animal. J Clin Invest 54:740–752, 1974.
15. Opie LH: Metabolic and drug-induced injury to the myocardium. In: Bristow MR (ed) Drug-induced heart disease. Amsterdam: Elsevier/North Holland Biomedical, 1980, pp 81–102.
16. Ferrans VJ, Butany JW: Ultrastructural pathology of the heart. In: Trump BF, Jones RT (eds) Diagnostic electron microscopy, vol 4. New York: John Wiley and Sons, 1983, pp 319–473.
17. Ferrans VJ: Overview of cardiac pathology in relation to anthracycline cardiotoxicity. Cancer Treat Rep 62:955–961, 1978.
18. Ferrans VJ: Morphologic assessment of cardiac lesions caused by anthracyclines. In: Muggia FM, Young CW, Carter SK (eds) Anthracycline antibiotics in cancer therapy. The Hague: Martinus Nijhoff, 1982, pp 331–347.
19. Ferrans VJ: Anthracycline cardiotoxicity. In Spitzer JJ (ed) Myocardial injury. New York: Plenum, 1982, pp 519–532.
20. Billingham ME, Mason JW, Bristow MR, Daniels JR: Anthracycline cardiomyopathy monitored by morphologic changes. Cancer Treat Rep 62:865–872, 1978.
21. Herman EH, Ferrans VJ, Jordon W, Ardalan B: Reduction of chronic daunorubicin cardiotoxicity by ICRF-187 in rabbits. Res Commun Chem Pathol Pharmacol 31:85–97, 1981.
22. Herman EH, Ferrans VJ: Reduction of chronic doxorubicin cardiotoxicity in dogs by pretreatment with (±)-1,2-bis(3,5-dioxopiperazinyl-1-yl) propane (ICRF-187). Cancer Res 41:3436–3440, 1981.
23. Herman EH, El-Hage AN, Ferrans VJ, Witiak DT: Reduction by ICRF-187 of acute daunorubicin toxicity in Syrian golden hamsters. Res Commun Chem Pathol Pharmacol 40:217–231, 1983.
24. Herman EH, Ferrans VJ: Influence of vitamin E and ICRF-187 on chronic doxorubicin cardiotoxicity in miniature swine Lab Invest 49:69–77, 1983
25. Van Vleet JF, Ferrans VJ, Weirich WE: Cardiac disease induced by chronic adriamycin administration in dogs and an evaluation of vitamin E and selenium as cardioprotectants. Am J Pathol 99:13–32, 1980.
26. Van Vleet JF, Ferrans VJ: Cutaneous lesions and hematologic alterations in chronic adriamycin intoxication in dogs with and without vitamin E and selenium supplementation. Am J Vet Res 41:691–699, 1980.
27. Van Vleet JF, Ferrans VJ: Evaluation of vitamin E and selenium protection against chronic adriamycin toxicity in rabbits. Cancer Treat Rep 64:315–317, 1980.
28. Unverferth DV, Mehegan JP, Nelson RW, Scott CC, Leier CV, Hamlin RL: The efficacy of N-acetylcysteine in preventing doxorubicin-induced cardiomyopathy in dogs. Semin Oncol (Suppl 1) 10:2–6, 1983.
29. Applebaum FR, Strauchen JA, McGraw RG, Jr, Savage DD, Kent KM, Ferrans VJ, Herzig GP: Acute lethal carditis caused by high-dose combination chemotherapy: a unique clinical and pathological entity. Lancet 1:58–62, 1976.
30. Gottdiener JS, Applebaum FR, Ferrans VJ, Deisseroth A, Ziegler J: Cardiotoxicity associated with high-dose cyclophosphamide therapy. Arch Intern Med 141:758–763, 1981.
31. Von Hoff DD, Rozencweig M, Piccart M: The cardiotoxicity of anticancer agents. Semin Oncol 9:23–33, 1982.
32. Jankus EF, Noren GR, Staley NA: Furazolidone-induced cardiac dilatation in turkeys. Avian Dis 16:958–961, 1972.
33. Czarnecki CM: Furazolidone-induced cardiomyopathy: biomedical model for the study of cardiac hypertrophy and congestive heart failure. Avian Dis 24:120–138, 1980.
34. Van Vleet JF, Ferrans VJ: Congestive cardiomyopathy induced in ducklings fed graded amounts of furazolidone. Am J Vet Res 44:76–85, 1983.
35. Van Vleet JR, Ferrans VJ: Furazolidone-induced congestive cardiomyopathy in ducklings: regression of cardiac lesions after cessation of furazolidone ingestion. Am J Vet Res 44:1007–1013, 1983.
36. Van Vleet JF, Ferrans VJ: Furazolidone-induced congestive cardiomyopathy in ducklings: myocardial ultrastructural alterations. Am J Vet Res 44:1014–1023, 1983.
37. Van Vleet JF, Ferrans VJ: Furazolidone-induced congestive cardiomyopathy in ducklings: lack of protection from selenium, vitamin E, and taurine supplements. Am J Vet Res 44:1143–1148, 1983.
38. Gwathmey J, Hamlin RL: Protection of turkeys against furazolidone-induced cardiomyopathy. Am J Cardiol 52:626–631, 1983.
39. Horowitz JD: Drugs that induce heart problems. Which agents? What effects? J Cardiovasc Med 8:308–315, 1983.
40. McAllister HA Jr, Mullick FG: The cardiovascular system. In: Riddell R (ed) Pathology of drug-induced and toxic diseases. New York: Churchill-Livingstone, 1982, pp 201–228.
41. Fenoglio JJ Jr: The effects of drugs on the cardiovascular system. In: Silver MD (ed) Cardiovascular pathology. New York: Churchill-Livingstone, 1982, pp 1085–1107.
42. Fauci AS, Harley JB, Roberts WC, Ferrans VJ, Gralnick HR, Bjornson BH: The idiopathic hypereosinophilic syndrome: clinical, pathophysiologic and therapeutic considerations. Ann Intern Med 97:78–92, 1982.
43. Graham JR: Cardiac and pulmonary fibrosis during methysergide therapy for headache. Am J Med Sci 254:1–12, 1967.
44. Kunkel RS: Fibrotic syndromes with chronic use of methysergide. Headache 11:1–5, 1971.
45. Bana DS, McNeal PS, Le Compte PM, Shah Y, Graham JR: Cardiac murmurs and endocardial fibrosis associated with methysergide therapy. Am Heart J 88:640–655, 1975.

46. Mason JW, Billingham ME, Friedman JP: Methysergide-induced heart disease: a case of multivalvular and myocardial fibrosis. Circulation 56:889–890, 1977.
47. Ferrans VJ, Roberts WC: The carcinoid endocardial plaque: an ultrastructural study. Hum Pathol 7:387–409, 1976.
48. Kloner RA, Fishbein MC, Lew H, Maroko PR, Braunwald E: Mummification of the infarcted myocardium by high dose corticosteroids. Circulation 57:56–63, 1978.
49. Suzuki T: Ultrastructural changes of heart muscle in cyanide poisoning. Tohoku J Exp Med 95:271–287, 1968.
50. Poche R: Über den Einfluss von Dinitrophenol und Thyroxin auf die Ultrastruktur des Herzmuskels bei der Ratte. Virchows Arch [Pathol Anat] 335:282–297, 1962.
51. Laguens R, Meckert PC, Segal A: Effects of acriflavin on the fine structure of the heart muscle cell mitochondria of normal and exercised rats. J Mol Cell Cardiol 4:185–193, 1972.
52. Raute-Kreinsen U, Berlet H, Bühler F, Rixner P: Elektronen-mikroskopische Befunde am Herzmuskel der Ratte bei experimentell induzierten Elektrolyt-veränderungen. Virchows Arch [Pathol Anat] 375:331–344, 1977.
53. Neinhaus H, Poche R, Reimold E: Elektrolytverschiebungen, histologische Veränderungen der Organe and Ultrastruktur des Herzmuskels nach Belastung mit Cortisol, Aldosteron und primären Natriumphosphat bei der Ratte. Virchows Arch [Pathol Anat] 337:245–269, 1963.
54. Ferrans VJ, Hibbs RG, Weily HS, Weilbaecher DG, Walsh JJ, Burch GE: A histochemical and electron microscopic study of epinephrine-induced myocardial necrosis. J Mol Cell Cardiol 1:11–22, 1970.
55. Kawanami O, Ferrans VJ, Fulmer JD, Crystal RG: Ultrastructure of pulmonary mast cells in patients with fibrotic lung disorders. Lab Invest 40:717–734, 1979.
56. Ferrans VJ, Hibbs RG, Cipriano PR, Buja LM: Histochemical and electron microscopic studies of norepinephrine-induced myocardial necrosis in rats. Recent Adv Stud Card Struct Metab 1:495–525, 1972.
57. Rona G, Hüttner I, Boutet M: Microcirculatory changes in myocardium with particular reference to catecholamine-induced cardiac muscle cell injury. In: Meesen H (ed) Handbuch der allgemeinen Pathologie, vol 3, part 7, Mikrozirkulation/Microcirculation. Berlin: Springer-Verlag, 1977, pp 791–888.
58. Berger JM, Bencosme SA: Divergence in patterns of atrial and ventricular cardiocyte degeneration: studies with plasmocid. J Mol Cell Cardiol 2:41–49, 1971.
59. Sarkar K, Levine DZ: Repair of the myocardial lesion during potassium repletion of kaliopenic rats: an ultrastructural study. J Mol Cell Cardiol 11:1165–1172, 1979.
60. Ridout RM, Decker RS, Wildenthal K: Chloroquine-induced lysosomal abnormalities in cultured foetal mouse hearts. J Mol Cell Cardiol 10:175–183, 1978.
61. Trump BF, Berezesky IK, Laiho KU, Osornio AR, Mergner WJ, Smith MW: The role of calcium in cell injury: a review. Scan Electron Microsc II, SEM Inc, AMF O'Hare, Ill, 1980, pp 437–462.
62. Decker RS, Wildenthal K: Lysosomal abnormalities in hypoxic and reoxygenated hearts. I. Ultrastructural and cytochemical changes. Am J Pathol 98:425–444, 1980.
63. Decker RS, Poole AR, Crie JS, Dingle JT, Wildenthal K: Lysosomal alterations in hypoxic and reoxygenated hearts. II. Immunohistochemical and biochemical changes in cathepsin D. Am J Pathol 98:445–455, 1980.
64. Singal PK, Beamish RE, Dhalla NS: Potential oxidative pathways of catecholamines in the formation of lipid peroxides and genesis of heart disease. In: Spitzer JJ (ed) Myocardial injury. New York: Plenum, 1982, pp 391–401.
65. Blackwell B, Marley E, Price J, Taylor D: Hypertensive interactions between monoamine oxidase inhibitors and foodstuffs. Br J Psychiatry 113:349–365, 1967.
66. Van Vleet JF, Amstutz HE, Weirich WE, Rebar AH, Ferrans VJ: Clinical, clinicopathologic, and pathologic alterations in monensin toxicosis in cattle. Am J Vet Res 44:1629–1636, 1983.
67. Bhatnagar MK, Yamashiro S: Ultrastructural alterations of the myocardium of rats fed rapeseed oils. Res Vet Sci 26:183–188, 1979.
68. Boor PJ, Ferrans VJ: Ultrastructural alterations in allylamine-induced cardiomyopathy: early lesions. Lab Invest 47:76–86, 1982.
69. Clark AF, Tandler B, Vignos PJ: Glucocorticoid-induced alterations in the rabbit heart. Lab Invest 47:603–610, 1982.
70. Van Vleet JF, Boon GD, Ferrans VJ: Induction of lesions of selenium–vitamin E deficiency in weanling swine fed silver, cobalt, tellurium, zinc, cadmium, and vanadium. Am J Vet Res 42:789–799, 1981.
71. Van Vleet JF, Boon GD, Ferrans VJ: Induction of lesions of selenium–vitamin E deficiency in ducklings fed silver, cobalt, cadmium, copper, tellurium or zinc and protection by selenium or vitamin E supplements. Am J Vet Res 42:1206–1217, 1981.
72. Herman EH, Balazs T, Ferrans VJ, Young RSK: Divergent effects of propranolol and furosemide pretreatment on acute cardiomyopathy induced by minoxidil in beagle dogs. Toxicology 20:155–164, 1981.
73. Herman EH, Ferrans VJ, Balazs T: Minoxidil and cardiac lesions. Circulation 64:1299–1300, 1981.
74. Gans JH, Korson R, Cater MR, Ackerly CC: Effects of short-term and long-term theobromine administration to male dogs. Toxicol Appl Pharmacol 53:481–496, 1980.
75. Pinnell SR: Disorders of collagen. In: Stanbury JB, Wyngaarden JB, Fredrickson DS (eds) The metabolic

basis of inherited disease. New York: McGraw-Hill, 1978, pp 1366–1394.
76. Irey NS, Norris HJ: Intimal lesions associated with female reproductive steroids. Arch Pathol 96:227–234, 1973.
77. Arnett EN, Battle WE, Russo JV, Roberts WC: Intravenous injection of talc-containing drugs intended for oral use: a cause of pulmonary granulomatosis and pulmonary hypertension. Am J Med 60:711–718, 1976.

32. VASCULAR SMOOTH MUSCLE CELLS AND OTHER PERIENDOTHELIAL CELLS OF MAMMALIAN HEART

Michael S. Forbes

Introduction

The mammalian heart is characterized by a vascular supply which is truly prodigious. It is curious that, of the many studies addressed to the heart, few have been directly concerned with ultrastructure of the *medial* or *periendothelial* cells of myocardial blood vessels. The term *vascular smooth muscle cells* comes most readily to mind when one is describing such cells, but it has become apparent that less highly developed cells occupy the walls of the heart's microvessels. Such cells, which include entities known as *primitive smooth muscle cells* and *pericytes,* are the positional and—perhaps—the functional equivalents of the definitive smooth muscle cells of the larger myocardial blood vessels. This chapter describes the structure of true vascular smooth muscle cells (VSMC), and considers, in addition, the spectrum of periendothelial cells within the vasculature of the heart.

"Definitive" Vascular Smooth Muscle Cells

GENERAL FEATURES

The packing and orientation of smooth muscle cells of the major arteries and veins of the heart may vary considerably according to the species under examination, the particular vessel being investigated, and perhaps even the individual selected for study. Though the conventional picture of arteries is one in which the muscle cells wind in circles or spirals about the endothelial cylinder (figs. 32–1, 32–3, and 32–4), it is not unusual to find longitudinally running bundles of cells at the outermost level of the tunica media, for example, in the anterior descending [1] and right coronary arteries [2] of the dog, and the right coronary artery of shrew [2]. It is intriguing, furthermore, to consider the orientation of smooth muscle cells in the right coronary artery of the vervet *(Cercopithecus aethiops);* in some planes of section an inner longitudinal, a central circular, and an outer longitudinal muscle layer can be detected (fig. 32–6). Further observation along lengths of this artery indicate that only the central layer intrinsically forms a complete covering of the vessel. The inner and outer "layers" appear to be spiral bundles of cells whose longitudinal axes are aligned at an extremely steep pitch with respect to the vessel axis. The cells of the central layer themselves are slightly canted, forming an angle of ca. 30° with respect to true circular orientation (fig. 32–4).

It should be recalled that the physiologic state of the blood vessel at the time of fixation will be a major factor in the orientation of smooth muscle cells which is observed with the microscope [e.g., 3]. Thus the morphologic study of the blood vessel wall requires thorough appreciation of the conditions under which a vessel has been preserved, and benefits from the use of techniques which effectively reconstruct the three-dimensional architecture (or allow its visualization in toto, as with scanning electron microscopy of enzymatically digested vessels [e.g., 2, 4–6]).

N. Sperelakis (ed.), PHYSIOLOGY AND PATHOPHYSIOLOGY OF THE HEART.

Martinus Nijhoff Publishing, Boston/The Hague/ Dordrecht/Lancaster.

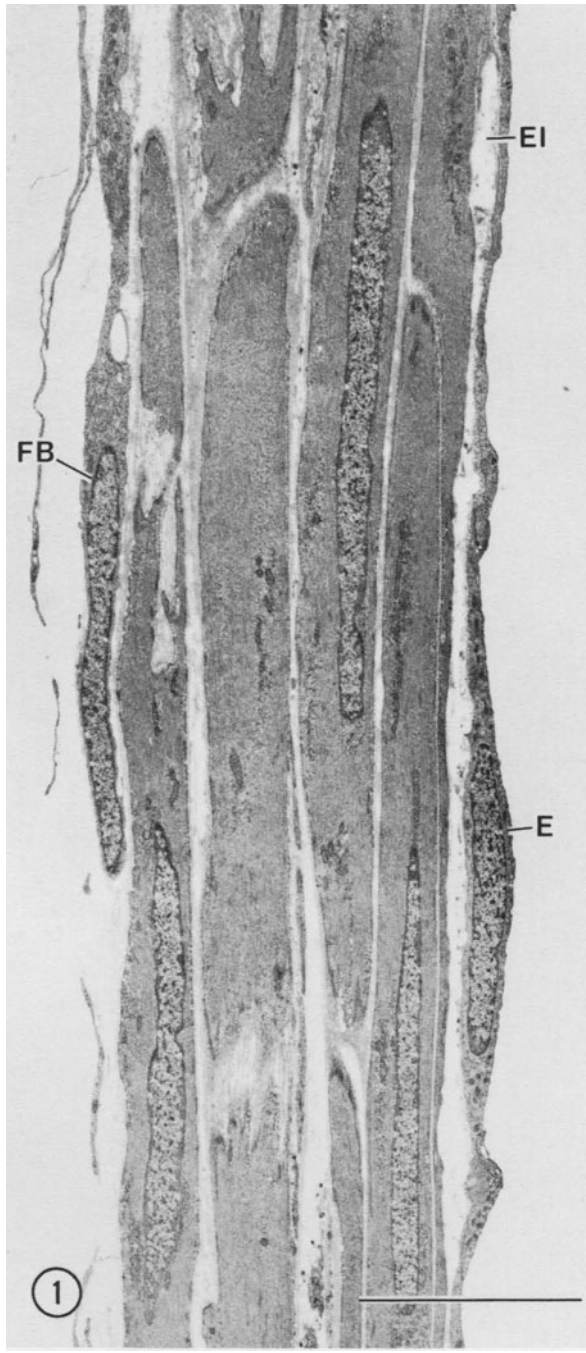

FIGURE 32–1. Myocardial blood vessels of squirrel monkey *(Saimiri sciureus)*. Survey micrograph of wall of anterior descending coronary artery, the vessel viewed here in transverse thin section. Approximately four layers of vascular smooth muscle cells form the tunica media of the artery along its largest segments. The medial layer is bordered on its adluminal side by the tunica intima, the complex of a layer of endothelial cells (E) and the elastica interna (EI), and on its abluminal surface by connective tissue elements including collagen and fibroblasts (FB), which together with occasional examples of nerve tissues comprise the tunica adventitia. Scale bar represents 5 μm.

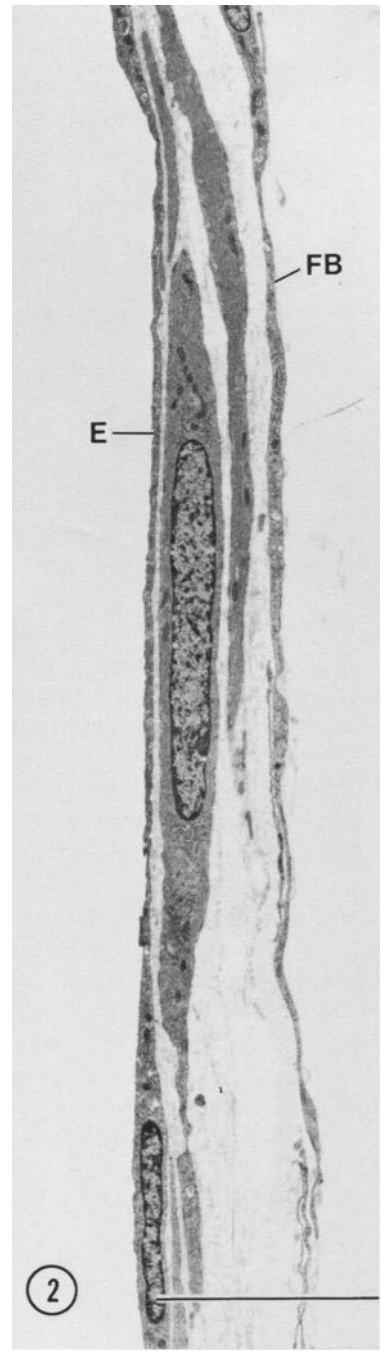

FIGURE 32–2. Myocardial blood vessels of squirrel monkey *(Saimiri sciureus)*. The accompanying vein of the artery shown in figure 32–1. Micrograph equivalent in magnification and orientation, which serves to demonstrate the profound contrast in wall structure which exists between the two divisions of the myocardial circulatory system. The three tunicae are extant, the t. adventitia perhaps constituting the greatest portion of the vessel wall. Labels as in figure 32–1. Scale bar represents 5 μm.

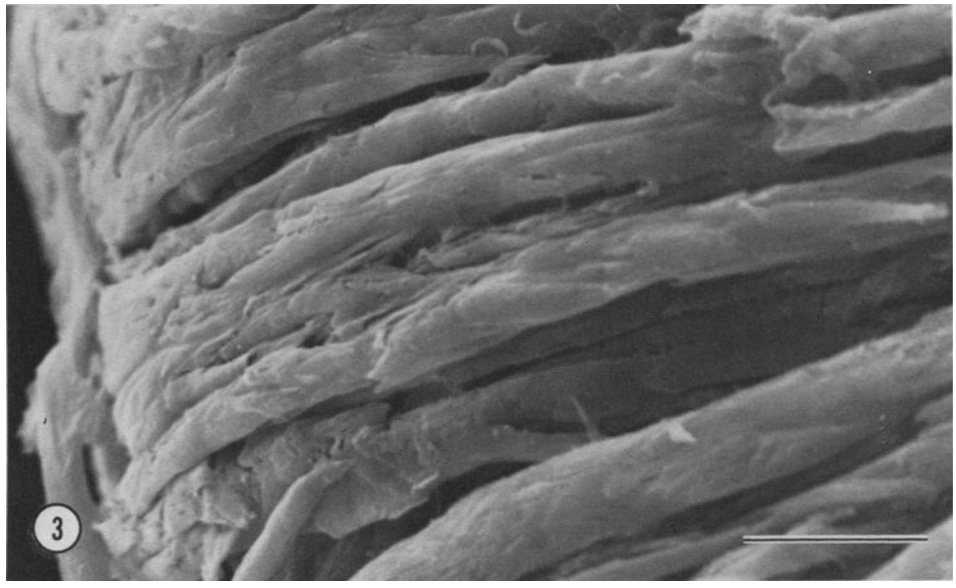

FIGURE 32–3. Scanning electron micrograph of smooth muscle cells of a dog right coronary artery from which the adventitial material has been removed by sequential exposure to hydrochloric acid and collagenase, coupled with mechanical dissection. At this point on the vessel's circumference, all the smooth muscle cells wind about the vessel axis in circumferential orientation (cf. fig. 32–5, however, for a more complete appreciation of the medial architecture of this vessel). The overall fusiform shape of the cells is evident, but their topography is noticeably irregular, marked by various excrescences and indentations. Scale bar represents 10 μm.

FIGURE 32–4. Low-power transmission electron micrograph of right coronary artery of vervet monkey (*Cercopithecus aethiops*). At the upper regions of the field there appear bundles of spirally oriented smooth muscle cells (cf. fig. 32–6). The major component of the wall is invested in cells which are sectioned en face, but are obliquely oriented with respect to the vessel axis (large arrow). Note fusiform nuclei and minor cytoplasmic projections (small arrows). Scale bar represents 10 μm.

The tunica media of coronary arteries and their branches is usually an unbroken covering composed primarily of vascular smooth muscle cells (VSMC). The other broad categories of myocardial blood vessels (veins, venules, arterioles, and capillaries) frequently are characterized by large gaps in the tunica media. The muscular arteries of the heart do not contain distinct strata of VSMC, delimited by sheets of elastin, as is the case in larger "elastic" arteries. Thus to speak of the relative numbers of "layers" in myocardial blood vessels is inexact at best. Still the general conclusion can be drawn that, as the size of the mammal (and its heart) increases, so do the overall diameters and wall thicknesses of comparably located arterial segments. For example, the coronary arteries of a mouse seldom achieve medial thicknesses of more than 6–7 μm, and contain a maximum of only 3–4 layers of VSMC; in comparison, the medial layer of dog right coronary artery is massive, possessing 12–15 layers of muscle cells (fig. 32–5).

In overall form, arterial VSMC are flattened, tapered, strap-like cells (figs. 32–1, 32–3, and 32–4). In many instances, the cells from arteries of larger mammalian hearts do not taper to rounded ends, but instead exhibit distinct indentations which may originate from nearly any point on the sarcolemma (figs. 32–1, 32–3, 32–4, and 32–8). In such cases, the tips of the cells are particularly elaborate (fig. 32–8). The VSMC of smaller vessels (and this is true as well for most of the vessels from smaller mammals) tend to be less complex in their surface contours (e.g., fig. 32–7). Such cells are more tightly fitted together within the medial layer, perhaps in part because of the lower incidence there of elements of connective tissue.

Arterial VSMC are individually noteworthy by dint of the extreme degree of polarity observed by their cytoplasmic components, including nuclei (see *The Nucleus*. . . .), cytoskeletal and contractile fibrils (See *Fibrillar elements*. . .), and various other organelles (see *"Miscellaneous" organelles*). The bipolar form is not necessarily retained in the smallest myocardial vessels, however, and secondary ("circumferential") projections are prominent features of pericytes on venules and capillaries (see *Cytoskeletal elements* and figs. 32–28 to 32–33), and venous VSMC as well may be branched [3] (see *Comparison of arterial/arteriolar*. . .).

ORGANELLES AND CELL SYSTEMS

As pointed out above, a striking characteristic of the muscle cells in coronary arteries is their marked bipolar conformation. Not only is this embodied in the overall shape of these cells (figs. 32–1, 32–3, and 32–4), but it is also evident in their internal construction, which—in each cell—is developed around the nucleus and the associated cytoplasm which extends from each of its poles. These and other constituents are described below in greater detail.

The Nucleus, Associated Organelles, and the Central Sarcoplasmic Core. Most VSMC in the cardiac circulatory system appear to be mononucleate. The nucleus in each muscle cell is distinctly fusiform, its tips aimed directly at the cell ends (figs. 32–1 and 32–4). Though infoldings of the nuclear membrane can be found (fig. 32–4), these are rather infrequent, and the profile that the nucleus presents in thin section usually is unremarkable, save for its occasional great length (up to ca. 25 μm).

Golgi saccules and centrioles are generally located near the nucleus (fig. 32–9). The Golgi apparatus seldom displays a memorable morphology, though in other vessels this organellar system has been shown to react noticeably to the administration of ionophoric agents [7]. As many as four centrioles may be encountered; given the rarity of multiple nuclear profiles in VSMC, the significance of this observation is unclear.

There is a distinct association between each smooth muscle nucleus and the sharply delimited cylinders or cones of cytoplasm which extend from its apices out toward the cell ends (fig. 32–9). There results a compartmentation of the cell contents, such that certain organelles (Golgi saccules, centrioles, microtubules, intermediate filaments, mitochondria, and lysosomes) are lodged primarily within the *central sarcoplasmic core* (figs. 32–9 to 32–11), whereas the remaining voluminous cortical region of the cell is virtually completely filled with myofilaments (see below). The central sarcoplasmic

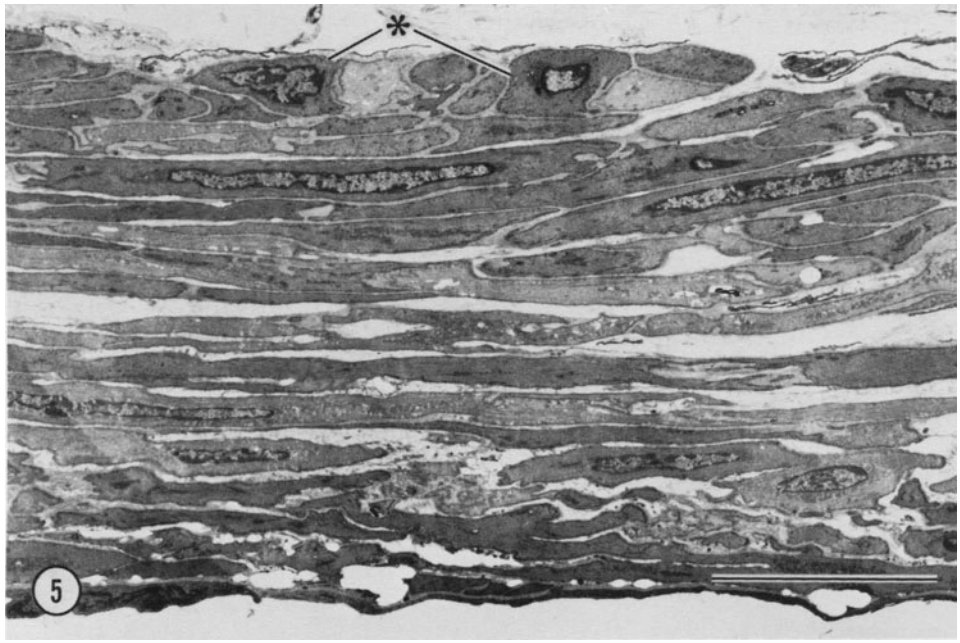

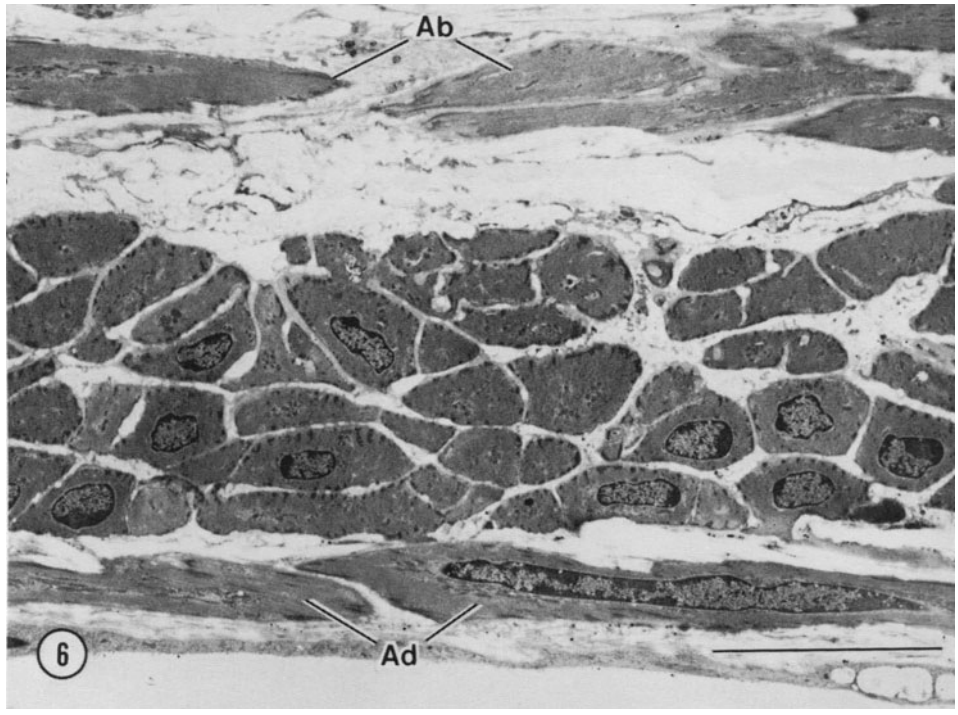

FIGURE 32–5. Right coronary artery of dog; vessel viewed in transverse section. The bulk of the medial layer is composed of smooth muscle cells which are arranged circularly about the vessel and therefore are caught in longitudinal section (cf. figs. 32–1 and 32–3). The farthest abluminal layers of smooth muscle, however, are seen in cross section (*), which indicates that they are longitudinally oriented along the outer surface of the vessel wall. Scale bar represents 10 μm.

FIGURE 32–6. Right coronary artery of vervet monkey; longitudinal section. Three distinct strata of smooth muscle cells constitute the tunica media of this vessel. The immediately adluminal cells (Ad) run parallel to vessel axis, while a central stratum of approximately circularly oriented cells forms the major portion of the medial layer. It is the latter cells which are equivalent to the cells seen en face in figure 32–4, the spirally oriented cells in figure 32–4 may correspond to either the adluminal band or the abluminal (Ab) layer which is separated from the medial wall by a large gap. Scale bar represents 10 μm.

FIGURE 32–7. Longitudinal section of mouse anterior descending coronary artery; the circularly applied smooth muscle cells thus appear in transverse section, and in this orientation display profiles closely fitted to one another. Accordingly there is a minimum of intervening connective tissue. Scale bar represents 2 μm.

FIGURE 32–8. Squirrel monkey right coronary artery, viewed at the same magnification and similar orientation to that of the mouse artery shown in figure 32–7. In contrast to that vessel, the VSMC here are strikingly pleiomorphic in profile, and are characterized by involved sarcolemmal indentations and cavities (*). The cells are separated by large spaces, which are occupied by the thick surface coats of the cells and by connective tissue elements. Scale bar represents 5 μm.

core can be envisioned as an entity which forms a medullary zone within the muscle cell and surrounds the nucleus; its major portion is fusiform, but a retinue of thin digit-like ramifications also extends into the peripheral regions of the cell (fig. 32–10). This internal compartment provides both enclosure and transcellular distribution of the cytoskeleton (see below) and the mitochondrial complement (see *"Miscellaneous" organelles*) of the smooth muscle cell.

Fibrillar Elements (Cytoskeletal and Contractile). The cytoskeleton and contractile apparatus of coronary arterial VSMC are largely isolated from one another, as discussed in the preceding section. The cytoskeleton is composed of longitudinally oriented microtubules and intermediate filaments (figs. 32–10 to 32–12). In many sections which pass through the central sarcoplasmic core, intermediate filaments ("10-nm" filaments, "skeleton" filaments [8]) appear as the predominant fibril (figs. 32–10 and 32–11), but their overall incidence may vary considerably between adjacent cells in the blood vessel wall. Microtubules accompany—or are accompanied by—intermediate filaments in the various recesses of the sarcoplasmic core system (figs. 32–10 to 32–12); they observe the same longitudinal disposition, and frequently appear surrounded by a "halo," 10 nm or so in width, which emphasizes their presence (figs. 32–10 and 32–12). The orientation of microtubules may in fact be a dictating force for the similar alignment observed for intermediate filaments [9, 10]. In visceral smooth muscle cells, intermediate filaments have been implicated [11] as forming segmental frameworks which interact via their anchorage in intracellular dense bodies (see the following section). This sort of system seems absent from cardiac vessels [2]. Rather there exists a system of cytoskeletal supports, consisting solely of filaments and tubules which are distributed—albeit thinly at some points in the cytoplasm— throughout the smooth muscle cell, without the intercalation of stationary points of attachment.

The collection of myofilaments which characterizes the peripheral myoplasm appears to consist largely of 5- to 8-nm-diameter actin filaments (figs. 32–10 and 32–12). The occurrence of myosin filaments is often sporadic in specimens of myocardial vessels. When these 15- to 19-nm-"thick" filaments are preserved, they usually appear in the majority of VSMC in the particular vessel, and yet may be absent from certain cells; no particular distribution of "haves" and "have-nots" is evident within the vessel wall, however.

The consensus among investigators concerned with the mechanics of smooth muscle is that arterial and venous VSMC are dependent for their contractile activity upon the presence of filamentous myosin (for reviews, see Murphy [12] and Somlyo [13]). It therefore seems likely that a total lack of thick filaments bespeaks inadequate fixation of the specimen under examination. Still, a failproof fixation regimen—that which consistently produces thick filaments—has not yet been offered, nor has the mosaic occurrence of thick filaments among adjacent VSMC been investigated.

The propensity of myofilaments to be grouped into bundles is most evident in longitudinal sections of myocardial VSMC (fig. 32–11). Many such bundles terminate in the opaque subsarcolemmal substance of the *dense bodies* (fig. 32–11; see below). Stereoscopic images have served to demonstrate this association, in VSMC, of myofilaments with dense bodies [2, 13], and profiles of actin filaments frequently can be discerned in thin transverse sections of dense bodies (fig. 32–12).

Surface Coat, Sarcolemma, Dense Bodies, and Caveolae. The outermost covering of VSMC is composed of lightly opaque, amorphous material. This material is likely constituted in the main by glycoproteinaceous moieties; the most general (and least chemically committal) term for the material seen by electron microscopy is the *surface coat.* Surface coats can display a wide array of appearances in different mammals and in vessels of different sizes. Specifically, where VSMC are closely packed (fig. 32–7) the surface coat is a consistently thin layer, the most opaque portion of which is at most 50 nm thick and often separated from the sarcolemma proper by a relatively lucent space, 30–50 nm in width [2]. In contrast, where the VSMC are

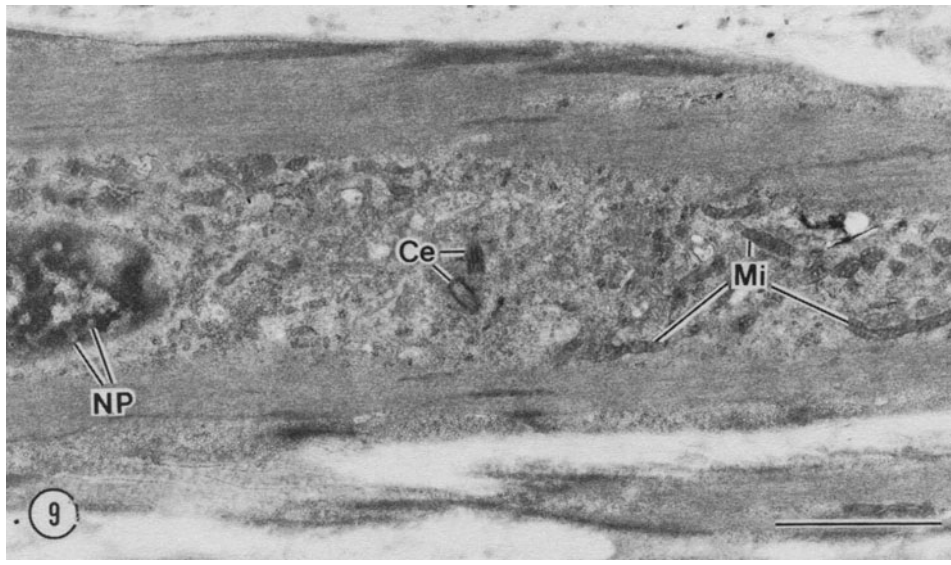

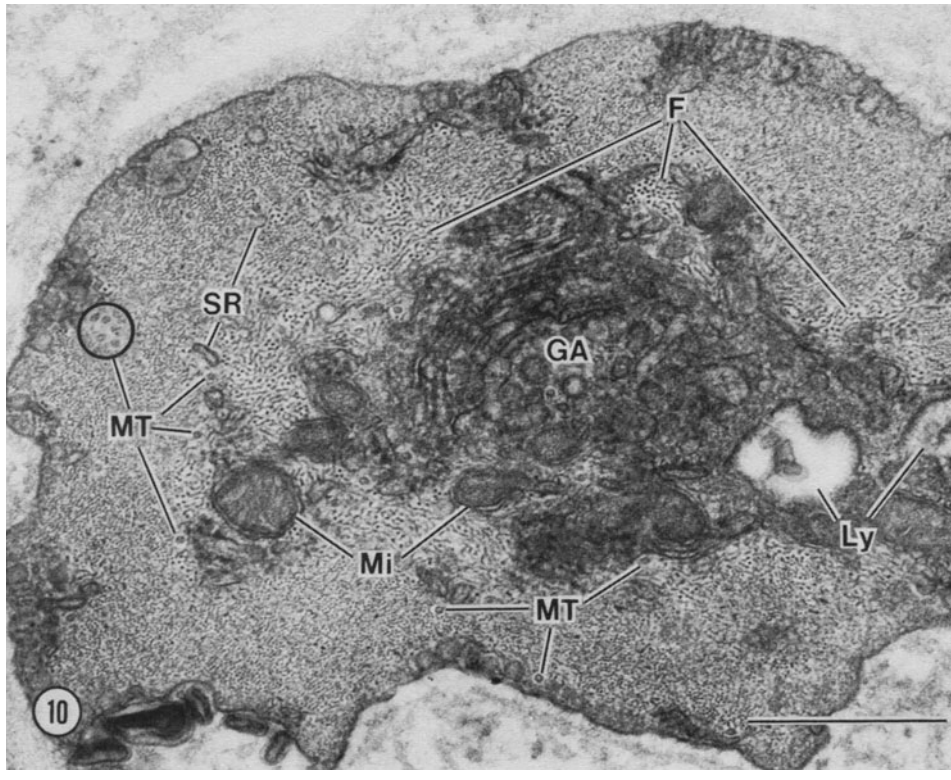

FIGURE 32–9. Longitudinal thin section through the center of a VSMC from vervet right coronary artery; the relationship between the nucleus (NP, nuclear pores) and the central sarcoplasmic core is demonstrated. A pair of centrioles (Ce) are located in the core, as is the nucleus; other organelles indigenous to the core include mitochondria (Mi) and ribosomes. The peripheral regions of the cells are filled for the most part with myofilaments. Scale bar represents 2 μm.

FIGURE 32–10. Squirrel monkey right coronary artery. Transverse section through VSMC at point distal to the nucleus. The central sarcoplasmic core here is dominated by saccules and tubules of the Golgi apparatus, and is characterized as well by numerous intermediate filaments (F) and microtubules (MT), all cut as well in transverse section. Profiles of mitochondria (Mi) and sarcoplasmic reticulum (SR) also occupy the core, as do lysosomes (Ly), here represented by multivesicular bodies. Thin, peripheral extensions of the core are represented by microtubule profiles, typically surrounded by electron-lucent halos. Scale bar represents 0.5 μm.

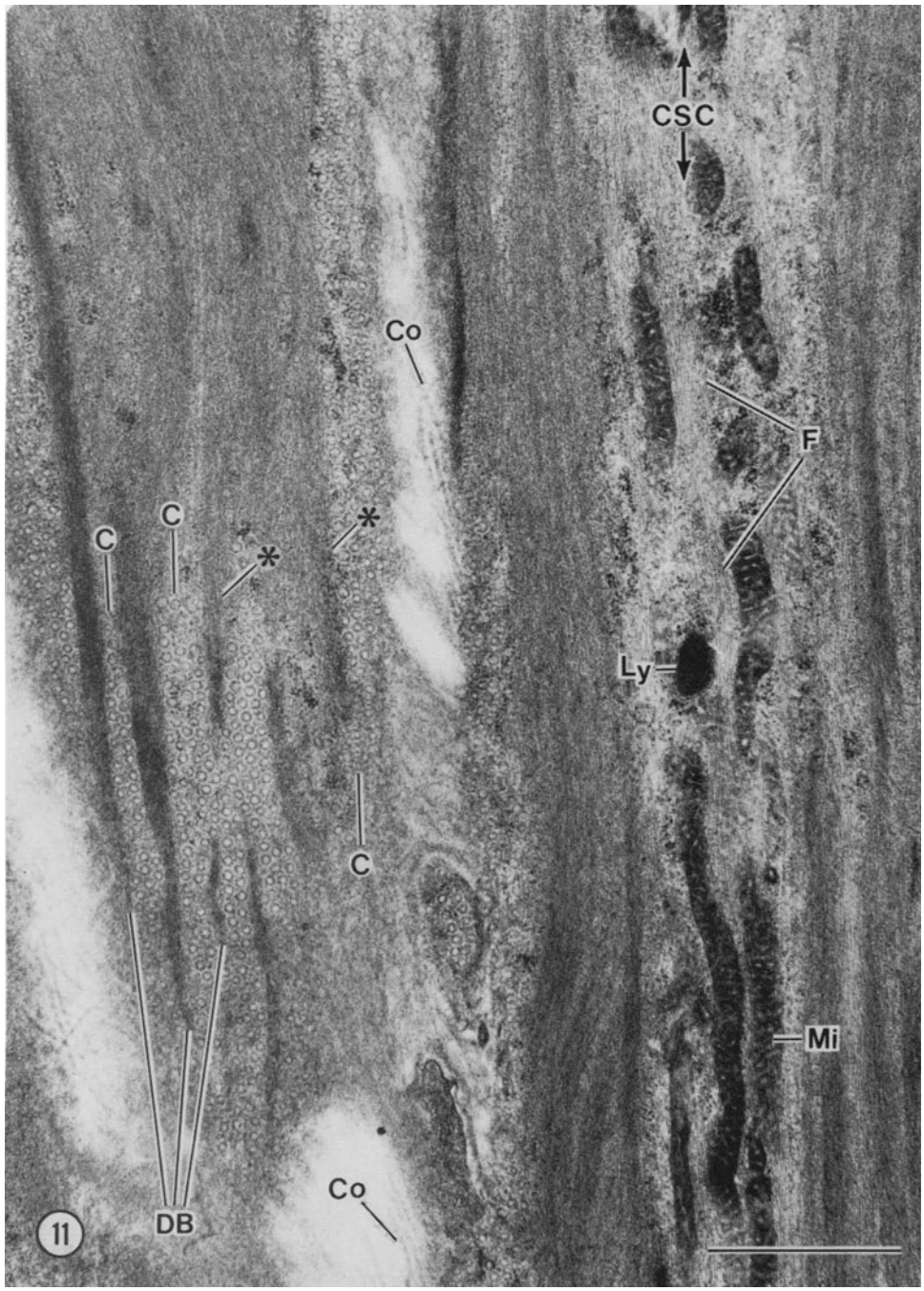

FIGURE 32–11. Vervet right coronary artery. In this section, the smooth muscle cells are cut longitudinally. The surface of one cell (at the left) is exposed en face, and in the cell at the right the central sarcoplasmic core (CSC) is evident as a relatively clear zone which contains longitudinally oriented mitochondria (Mi), numerous intermediate filaments (F), and a lysosome (Ly). Microtubules also observe preferential location in this region (cf. fig. 32–10), but their lower numbers render them less obvious in longitudinal sections. The myofilaments of these smooth muscle cells tend to group in large bundles which lead, at their extremities, into dense subsarcolemmal adhesion plaques (dense bodies: DB); transitions between myofilament bundles and dense bodies are indicated by asterisks. Alternating with the subsarcolemmal stripes formed by dense bodies are rows of sarcolemma decorated with numerous surface—connected caveolae (C). Collagen fibrils (Co) are closely associated with the surfaces of the muscle cells. Scale bar represents 1 μm.

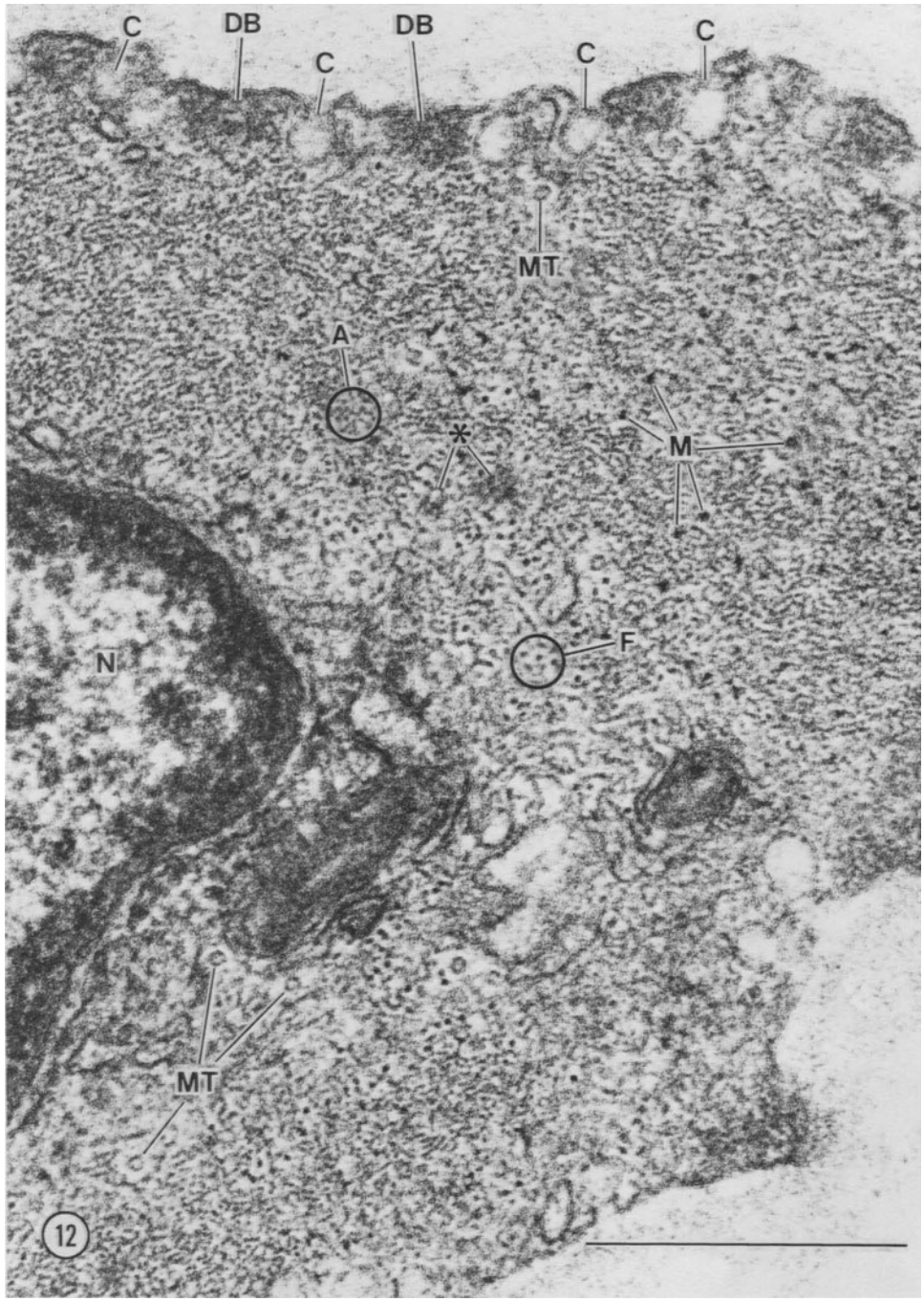

FIGURE 32–12. Transverse section of VSMC from right coronary artery of squirrel monkey. All the categories of fibrils are visible in this field, including actin (A) and myosin (M) filaments, which are the basis of the cell's contractile apparatus and occupy the cortical portion of the myoplasm. The alternation of caveolae (C) with subsarcolemmal dense bodies (DB) is evident (cf. fig. 32–11). Small internal dense bodies (*) appear in limited numbers. Punctate actin profiles can be discerned within the subsarcolemmal dense bodies, indicating their probable termination there. The cytoskeletal fibrils—microtubules (MT) and intermediate filaments (F)—are far less numerous at this level of the cell, though they specifically populate the central sarcoplasmic core (figs. 32–10 and 32–11) and its ramifications. N, nucleus. Scale bar represents 0.5 μm.

widely separated (e.g., in monkey coronary arteries) the surface coats (fig. 32–8 and 32–13) are thick and thrown into irregular profiles, and form elaborate whorls and filigrees, particularly within the recesses that characterize the muscle cell tips in such vessels [2] (figs. 32–8 and 32–16).

Much of the sarcolemma of arterial VSMC is segmented into a series of lengthwise divisions by the alternation of stripe-like dense bodies and bands of caveolae (fig. 32–11). Relatively few isolated, intracellular dense bodies (fig. 32–12) are found in coronary artery VSMC, in contrast to VSMC of larger vessels such as carotid artery (unpublished observations) and PAMV [13], for which the terminologic distinction has been made between the intracellular, "free-floating" densities and the longitudinal, subsarcolemmal striations; the former have been denoted as dense bodies and the latter as *surface patches* [13]. There has also been drawn an analogy between the Z discs of striated muscle and dense bodies of VSMC, both of which serve as regions in which actin filaments anchor [13]. Similarly, the subsarcolemmal dense bodies of VSMC are analogous to the fasciae adherentes of heart, those portions of the intercalated discs in which the thin filaments belonging to the myofibrils terminate [14, 15]. A partial substitute for internal dense bodies in coronary VSMC may reside in smearings of the opaque material which extend away from subsarcolemmal locations to points deep in the myoplasm.

Sarcolemmal inpocketings (*caveolae,* lit. "small caves") are a substantial component of muscle cells. Such flask-shaped invaginations add considerable surface area to certain myocardial cells [16–18]. Caveolae appear to be permanently connected to the sarcolemma, with their lumina open to the extracellular fluid space. This stands in contrast to the mobile "micropinocytotic" vesicles of vascular endothelial cells. The caveolae of smooth muscle are not limited to single invaginations, but may participate in extensive structures, so-called *beaded tubules* (figs. 32–14 and 32–17) of varying lengths [2, 19]. These complexes bear close resemblance to the forming elements of the system of transverse tubules of skeletal and cardiac muscle [2, 15, 20], and for this reason smooth muscle caveolae collectively may be considered to represent the equivalent of T tubules—in both the analogous and homologous senses [2, 19].

Most surfaces of arterial VSMC—abluminal, adluminal, and lateral—are decorated with caveolae (e.g., figs. 32–10 to 32–12). Farther down the vascular tree, the VSMC of arterioles become thinner and presumably less voluminous, and frequently lack caveolae on their adluminal surfaces, as do pericytes on the smallest vessels (figs. 32–30 and 32–31; see *Cytoskeletal elements*).

Sarcoplasmic Reticulum. A variety of smooth-surfaced tubules and saccules are present in smooth muscle cells. Some are concentrated in the Golgi apparatus (see *The nucleus. . .* and fig. 32–10), but the majority of these profiles—primarily located in the central sarcoplasmic core and its ramifications, or close beneath the sarcolemma—are known collectively as *sarcoplasmic reticulum* (SR). This collection of intracellular membranous structures is considered functionally equivalent to the more structured SR networks in striated and cardiac muscle [21–24]. In large vessels, the division of SR into *peripheral, deep,* and *central* categories has been made [25]. The relatively small volumes of coronary artery VSMC usually allow a more limited distinction, that between the peripheral and central SR (figs. 32–10 and 32–13). The alternation of dense bodies and caveolae creates a subtle subsarcolemmal compartmentation which exists in addition to the more noticeable overall cortical and medullary arrangement of cell components (see *The nucleus. . .* and *Fibrillar elements. . .*). Thus much of the sarcoplasmic reticulum is specifically located beneath the ribbons of sarcolemma which bear caveolae.

The more notable component of the peripheral SR division is *junctional SR* (J-SR), those segments which are juxtaposed to the inner surface of the sarcolemma (figs. 32–13 to 32–15). The J-SR winds as multibranched tubules among the sarcolemmal invaginations formed by caveolae (figs. 32–13 to 32–15), and appears to make connection with both surface sarcolemma and caveolae through the interposition of so-called *junctional processes.* One form

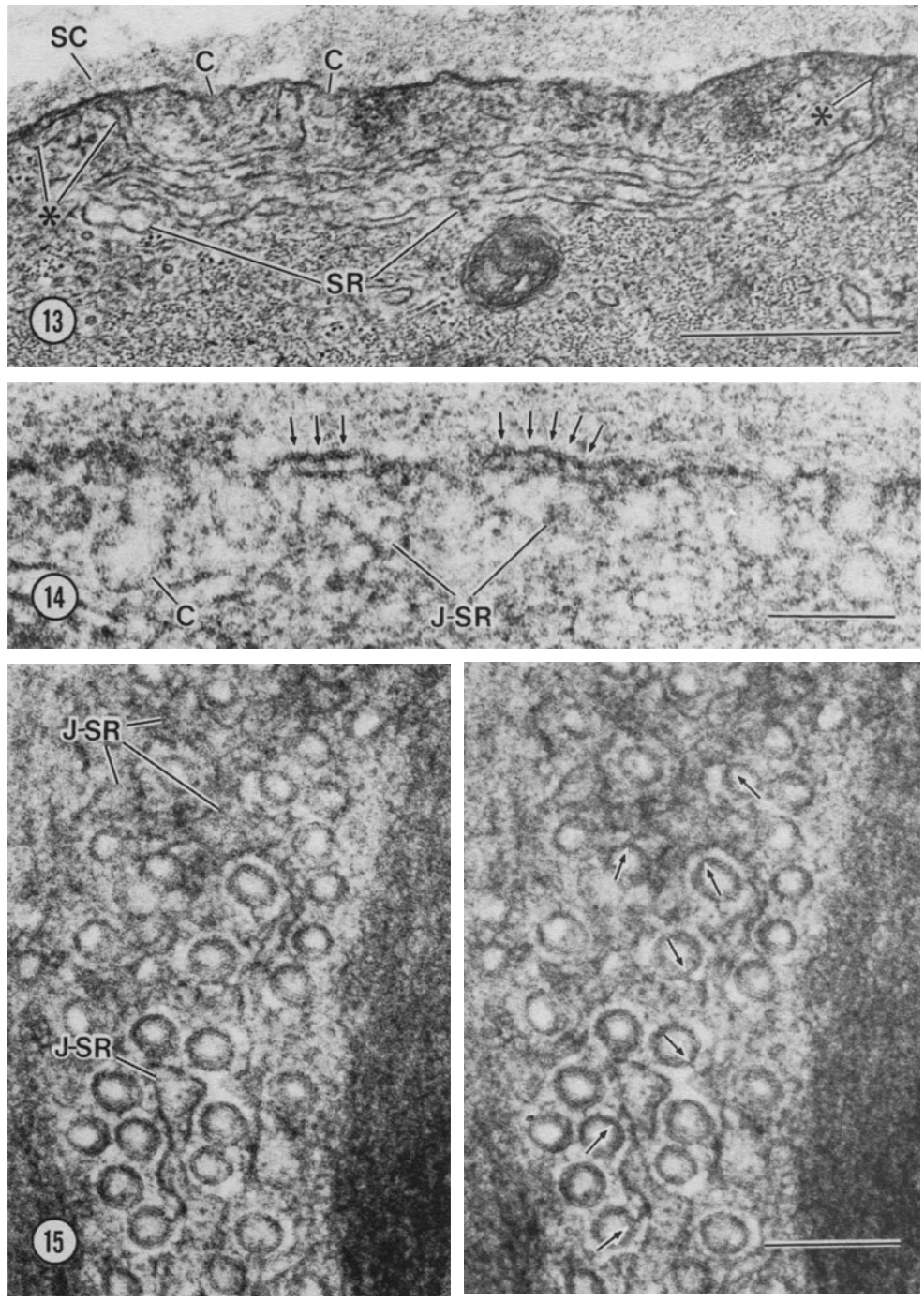

FIGURE 32–13. Squirrel monkey anterior descending coronary artery; smooth muscle cell in transverse section. Layered profiles of sarcoplasmic reticulum (SR) are present, tubular extensions of which are closely apposed (*) to the sarcolemma. C, caveolae. Note the varying thickness of the muscle cell's surface coat (SC). Scale bar represents 0.5 μm.

FIGURE 32–14. Same vessel as in figure 32–13. Subsarcolemmal couplings formed between the sarcolemma and saccules of junctional sarcoplasmic reticulum (J-SR). Distinct linear structures (pillars: arrows) connect the apposed membranes. The J-SR profiles are interspersed with caveolae, two of which (at C) are fused to form a short "beaded tubule." Scale bar represents 0.1 μm.

FIGURE 32–15. Squirrel monkey anterior descending artery. Stereo micrograph pair (10° separation) showing the marked interdigitation of junctional SR (J-SR) and surface-connected caveolae, and demonstrating the pillar-like structures (arrows) that connect the two. Scale bar represents 0.2 μm.

taken by the processes is that of thin profiles ("pillars" [26]), which resemble unit membranes and whose opaque limiting substance frequently can be seen to fuse with the apposed membrane leaflets of the J-SR and sarcolemma/caveola (figs. 32–13 to 32–15) [2, 27]. As has been discussed [2, 19], the T tubules of smooth muscle are likely represented by caveolae; the complexes constituted by appositions of caveolae with J-SR are therefore the equivalent of the "internal couplings" typical of other muscle types [e.g., 15, 20], while the J-SR–sarcolemma complexes clearly are the homologues of peripheral couplings [2, 19].

Junctions (Homo- and Heterocellular). A multitude of intermembranous connections are demonstrable in the walls of myocardial blood vessels [2]. *Homocellular* junctions form both between individual medial cells and also within them (i.e., they are *intracellular,* developing at points of juxtaposition of sarcolemmal regions belonging to the same cell). *Heterocellular* junctions are those which join the adluminal VSMC with the underlying endothelium [2].

A wide variety of VSMC homocellular junctions has already been described in coronary arteries [2]. These include *simple appositions,* in which sarcolemmal surfaces are poised in parallel array with one another, separated by a space of ca. 17–20 nm (fig. 32–16) which usually does not admit the electron-opaque substance of the cell coat. *Intermediate* junctions (fig. 32–17) display a spectrum of morphologies—which range from a short pair of intracellular densities which face one another across an empty-appearing, 17- to 20-nm gap to *quasi*-desmosomal complexes which are characterized by structured extracellular material. *Desmosomes* themselves appear between VSMC of cat coronary arteries [2]. Short *gap junctions* are present in coronary arterial VSMC of mouse, guinea pig, dog, and squirrel monkey [2] (fig. 32–18), and these may be located either *inter*cellularly or *intra*cellularly.

The heterocellular junctions of myocardial arteries are less varied in morphology than the homocellular connections. Most often seen between smooth muscle and endothelium are simple appositions, which usually incorporate an endothelial extrusion which extends abluminally to approach the overlying smooth muscle cell. No discernible intracellular structures are present in either of the cells which participate in a simple myoendothelial junction. On the other hand, there is encountered, on occasion, a heterocellular junction of the intermediate category (fig. 32–19), which is marked by intracellular accumulations of opaque substance similar to those of homocellular counterparts.

A third category of heterocellular junctions —myoendothelial gap junctions—has been clearly identified in arteries and arterioles of the mouse heart [2] (fig. 32–20), but examples have not yet been found in equivalent vessels of other species. Myoendothelial gap junctions are frequently characterized by an abluminal endothelial protrusion or an adluminal VSMC protrusion. The frequent presence of such junctions in these thin-walled vessels of mouse heart may be indicative of a function of adhesion and structural stabilization, rather than necessarily one of electrical continuity [2].

Heterocellular junctions (including gap-like junctions: fig. 32–21) are frequently encountered in veins, venules, and capillaries. In veins in particular, unusual junctional profiles are found (fig. 32–22) which do not clearly correspond in form to the junctional categories already described.

"Miscellaneous" Organelles. In a review of this kind, there inevitably accumulate categories of cell structures which are lumped together and accounted for, both for the purposes of completeness and—primarily—because relatively little research has been devoted to them. Such is the case, to greater or lesser degrees, with the mitochondria, rough endoplasmic reticulum, ribosomes, glycogen particles, and lysosomes of vascular smooth muscle cells, all of which are considered below. The Golgi apparatus and centrioles have already been dealt with in this chapter.

As noted earlier, mitochondria of myocardial VSMC are in large part restricted in their occurrence to the central sarcoplasmic core and its extensions, these last including subsarcolemmal cavities in which mitochondria may

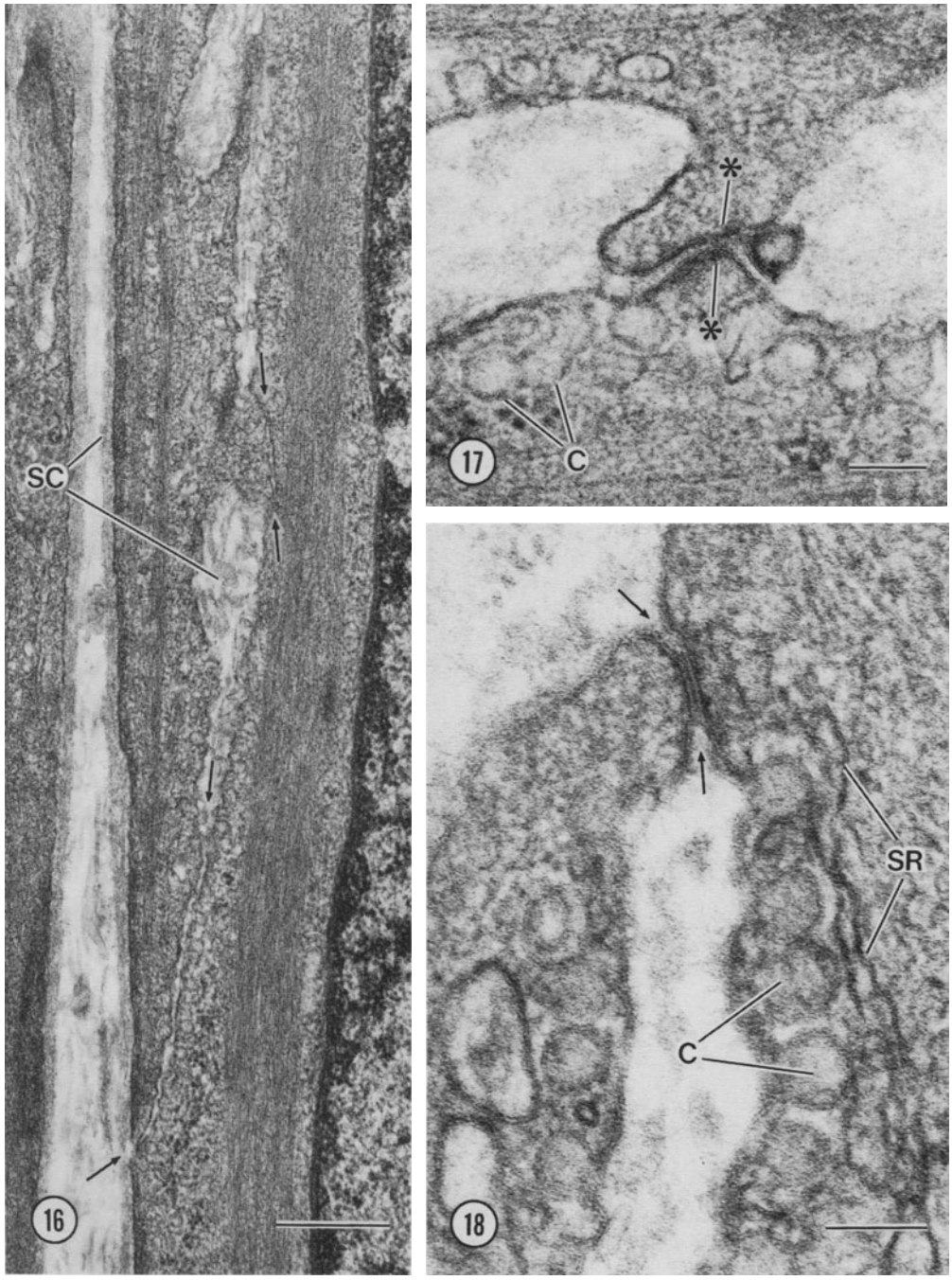

FIGURE 32–16. Anterior descending artery of squirrel monkey. Two VSMC form two junctional regions known as simple appositions (between arrows). Although the apposed sarcolemmata run parallel for rather great distances, no intra- or extracellular densities can be discerned, nor does the structured surface coat (SC) appear to enter the intercellular gaps at these points. Scale bar represents 0.5 μm.

FIGURE 32–17. Right coronary artery of dog heart. The upper muscle cell has formed a small digital protrusion which approaches the lower cell, forming an "intermediate" contact, characterized primarily by accumulations of electron-opaque material (*) immediately beneath the apposed sarcolemmal regions. Numerous caveolae appear in the adjacent sarcolemmata, some of which (C) are fused to form a beaded caveolar chain. Scale bar represents 0.1 μm.

FIGURE 32–18. Squirrel monkey right coronary artery. Gap junction (between arrows), ca. 59 nm in length, formed between a slender process of one smooth muscle cell with the main cell body of another. Homocellular gap junctions are frequently found in coronary arteries, but most are of a limited size such as the one shown here. Note the close association of caveolae (C) with tubules of sarcoplasmic reticulum (SR). Scale bar represents 0.1 μm.

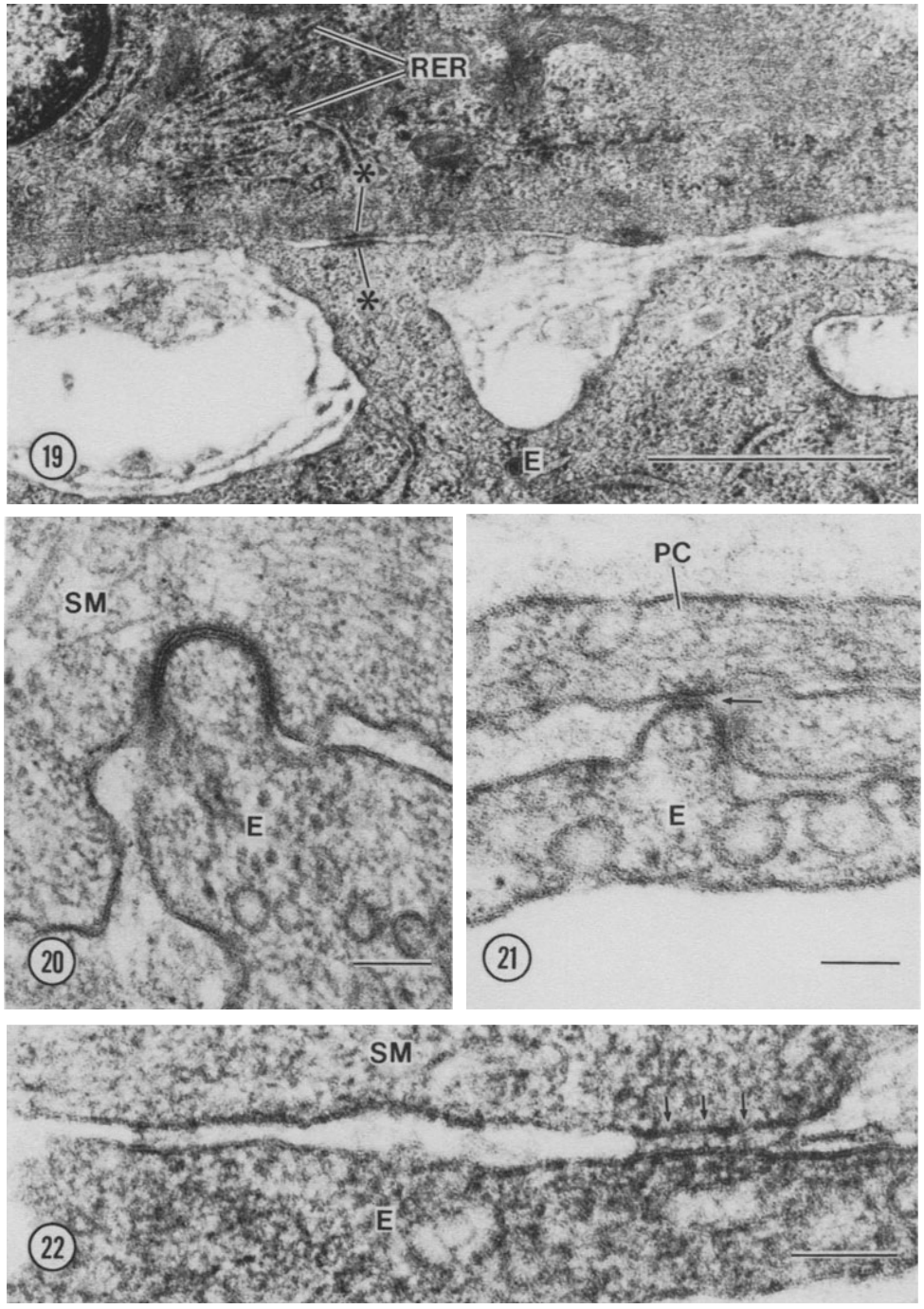

FIGURE 32–19. Myointimal region of a large artery in rhesus monkey right papillary. Two hummocks of an endothelial cell (E) approach the adluminal surface of the subjacent smooth muscle cell. The left-hand endothelial protrusion comes into close contact with the smooth muscle sarcolemma, and part of the apposition is composed of a heterocellular intermediate contact, identifiable by its thin opaque plaques (*) (cf. fig. 32–17). RER, rough endoplasmic reticulum. Scale bar represents 1 μm.

FIGURE 32–20. Myoendothelial gap junction in mouse right coronary artery. This example is formed by a dome-like endothelial process (E) which fits into a closely correspondent invagination of the overlying smooth muscle cell (SM). Scale bar represents 0.1 μm.

FIGURE 32–21. Wall of a venule from rhesus monkey right papillary muscle. The endothelium (E) juts up to abut the process of a pericyte (PC), there forming a short, close apposition (arrow) which resembles the myoendothelial gap junction seen in figure 32–20. Scale bar represents 0.1 μm.

FIGURE 32–22. Transverse section through anterior coronary vein of squirrel monkey. The limiting membranes of the smooth muscle (SM) and endothelial cell (E) run in approximately parallel array, and along this length two regions appear which are notable because of the presence in the intercellular gap of strands of material, some of which is collected into linear bodies (arrows) which extend to contact both apposed membranes. Scale bar represents 0.1 μm.

contact the SR and caveolae [19]. Such complexing may be related to the intracellular transfer of Ca^{2+} ion within the smooth muscle cell [13]. Mitochondria of coronary artery VSMC are small and elongate, and usually are aligned with the longitudinal axis of the cell (e.g., fig. 32–11).

Ribosome-decorated tubules—"rough" endoplasmic reticulum—and α-rosettes of glycogen are much in evidence in VSMC of the neonatal animal, but disappear for the most part from mature cells, though occasional examples of rough ER may persist in the central sarcoplasmic core (fig. 32–19), along with free ribosomes and scattered glycogen particles.

Lysosomes of myocardial VSMC assume a number of forms [2], including uniformly opaque membrane-bounded spheroids (fig. 32–11), variegate bodies with light and dark components (probably secondary lysosomes), and multivesicular structures (fig. 32–10). The occurrence, in the extracellular spaces of the rat coronary artery media, of collections of multisized vesicles, has suggested the hypothesis that VSMC waste products are liberated from the cell via exocytosis of lysosomes [28].

Comparison of Arterial/Arteriolar vs Venous/Venular Smooth Muscle Cells

The two major blood vessel categories of the heart can be readily distinguished from one another at light-microscopic levels on the basis of the thick muscular walls of arteries, and the thin walls and large lumina of veins (fig. 32–1). Arterioles (fig. 32–26) and venules usually exhibit characteristics similar to those of the respective "parent" vessels. Some vessel segments, however, offer highly equivocal profiles whose periendothelial components are, to more or less degrees, intermediate in structure between smooth muscle cells and pericytes (fig. 32–27); these transitional forms are considered further in the following section.

A good deal more information is available on the structure of the arterial side of the heart's circulatory system than is the case for its venous complement. Veins in general are frequently described as bearing longitudinally oriented smooth muscle cells, but in fact the shape and orientation of these cells can vary tremendously with the vein type, the particular segment, the point on the vessel circumference, etc. [3, 29]. In fact it may be difficult to discern clearly delineated tunics in veins, since VSMC may appear within levels of the vessel wall which—in arteries—would rightly belong to the tunica intima or tunica adventitia [3] (fig. 32–24). The great variation in incidence and orientation of VSMC in a collection of human veins studied by Kügelgen (data summarized by Rhodin [3]) is tacit promotion for evaluation, on an individual basis, of any particular segment of any particular vein, of any particular species. Therefore the descriptions of myocardial veins given here may be anecdotal, in view of the relatively few observations thus far made on such vessels. At its widest points, the anterior vein of rhesus monkey (which accompanies the right coronary artery) displays 4–5 "layers" of VSMC bodies and processes at some points around its circumference (fig. 32–23), and at others none at all. Fibroblasts and bands of collagen may abut the endothelium while VSMC are located farther abluminally; in certain regions, connective tissue is the major vessel wall component. Additional variations are found in the VSMC orientation (as judged by the alignment of myofilaments); abluminal longitudinal VSMC profiles are intermingled with more adluminal, concentric elements, and vice versa (fig. 32–23). "Stellate" VSMC have been reported as well [3]. This suggests that some venous VSMC possess both longitudinal and circumferential processes—thus resembling the pericytes of venules and capillaries [30]—and this would account in part for the multiplicity of VSMC orientation in veins.

There is probably only a single generality that can be made concerning the structure of the VSMC of myocardial veins: they present notably thinner profiles than those of VSMC in corresponding arteries (figs. 32–1 and 32–23 to 32–25). Examples of the organelles and cell systems described in the preceding sections can be found in venous VSMC (fig. 32–25), though some specific complexes such as homocellular gap junctions have not yet been encountered. It is interesting to note that in the same vein thick (myosin) filaments may appear in some

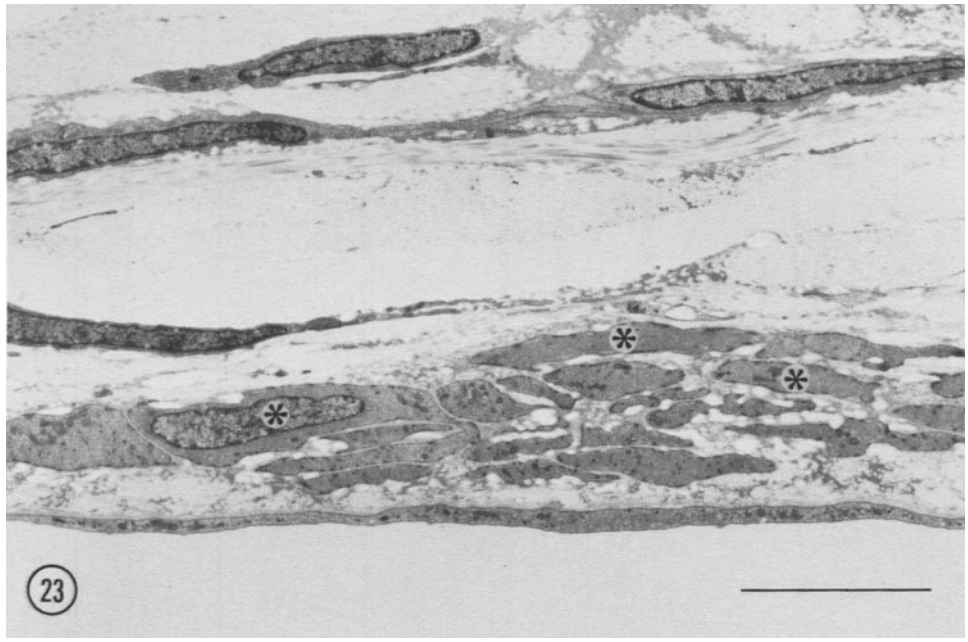

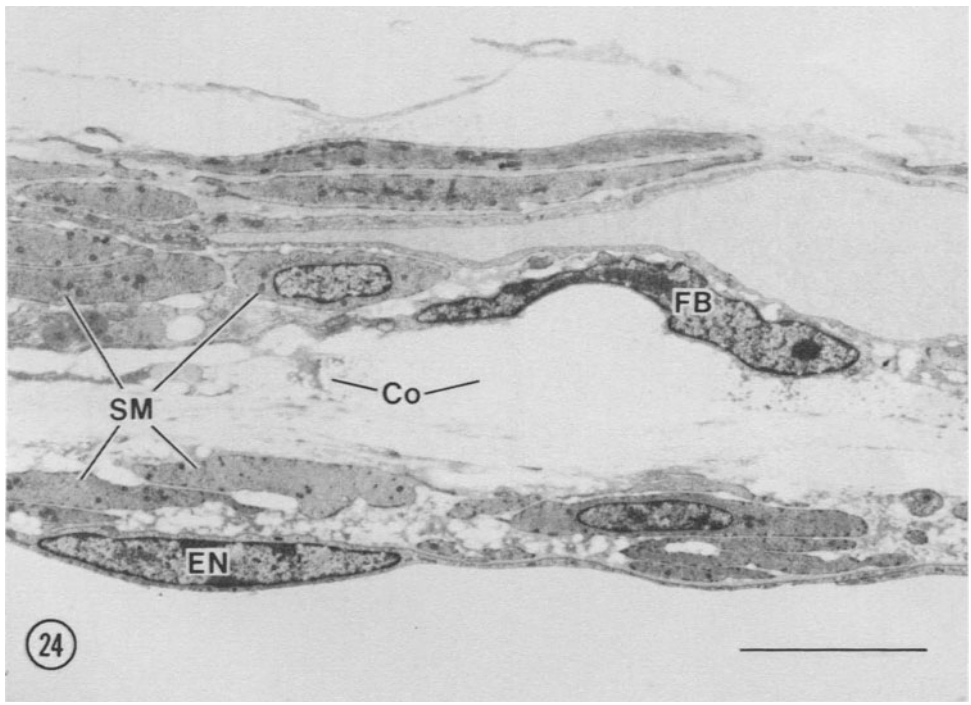

FIGURE 32–23. Anterior vein of rhesus monkey; vessel cut in transverse section. At this point on the circumference of the vein, the smooth muscle cells occupy positions equivalent to the tunica media of arteries. The orientations of these cells are varied, however, there being an admixture of circumferentially (*) and longitudinally aligned cells. Scale bar represents 5 μm.

FIGURE 32–24. Same vein as in figure 32–23, at another point on its circumference. Smooth muscle cells (SM) are located both in subendothelial positions (EN, endothelial cell nucleus) and in "adventitial" regions (note the fibroblast [FB] and bands of collagen [Co] which are interposed between the two groups of VSMC). Scale bar represents 5 μm.

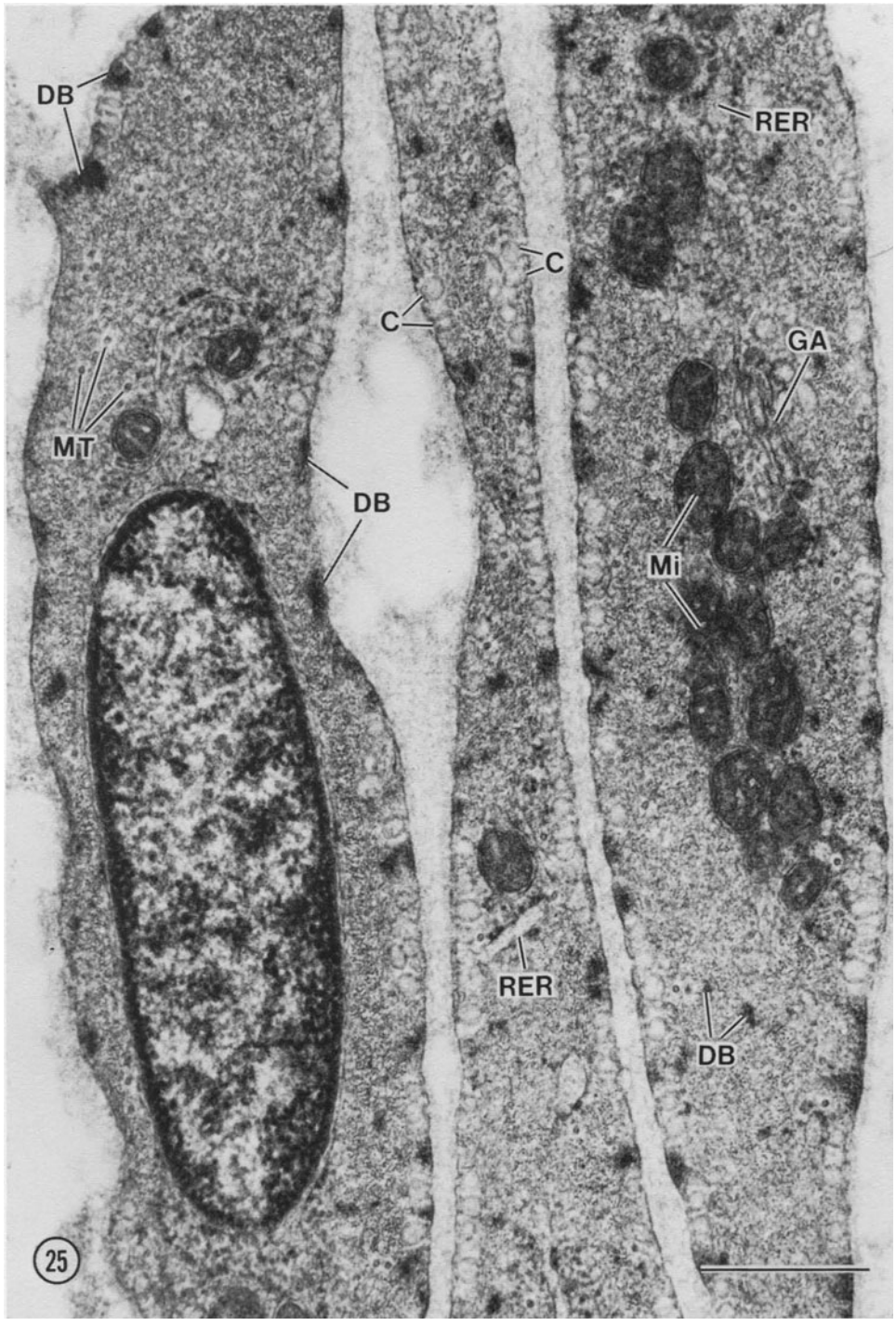

FIGURE 32–25. VSMC in transversely sectioned anterior vein of rhesus monkey heart. Such cells are characterized by thin, flattened profiles. Present in this field are a number of organelles and structures which are found in arterial VSMC as well. These include mitochondria (Mi), Golgi saccules (GA), and cisternae of rough endoplasmic reticulum (RER); in venous VSMC, these last appear more prominent than in arterial VSMC. In these transversely sectioned profiles, fibrillar elements such as microtubules (MT) and myofilaments also are caught in transverse section (thus indicating that the cell bodies and processes are aligned along the length of the vessel). Dense bodies (DB) are present free in the myoplasm, as well as apposed to the sarcolemma, where they are interspersed with groups of caveolae (C). Scale bar represents 0.5 μm.

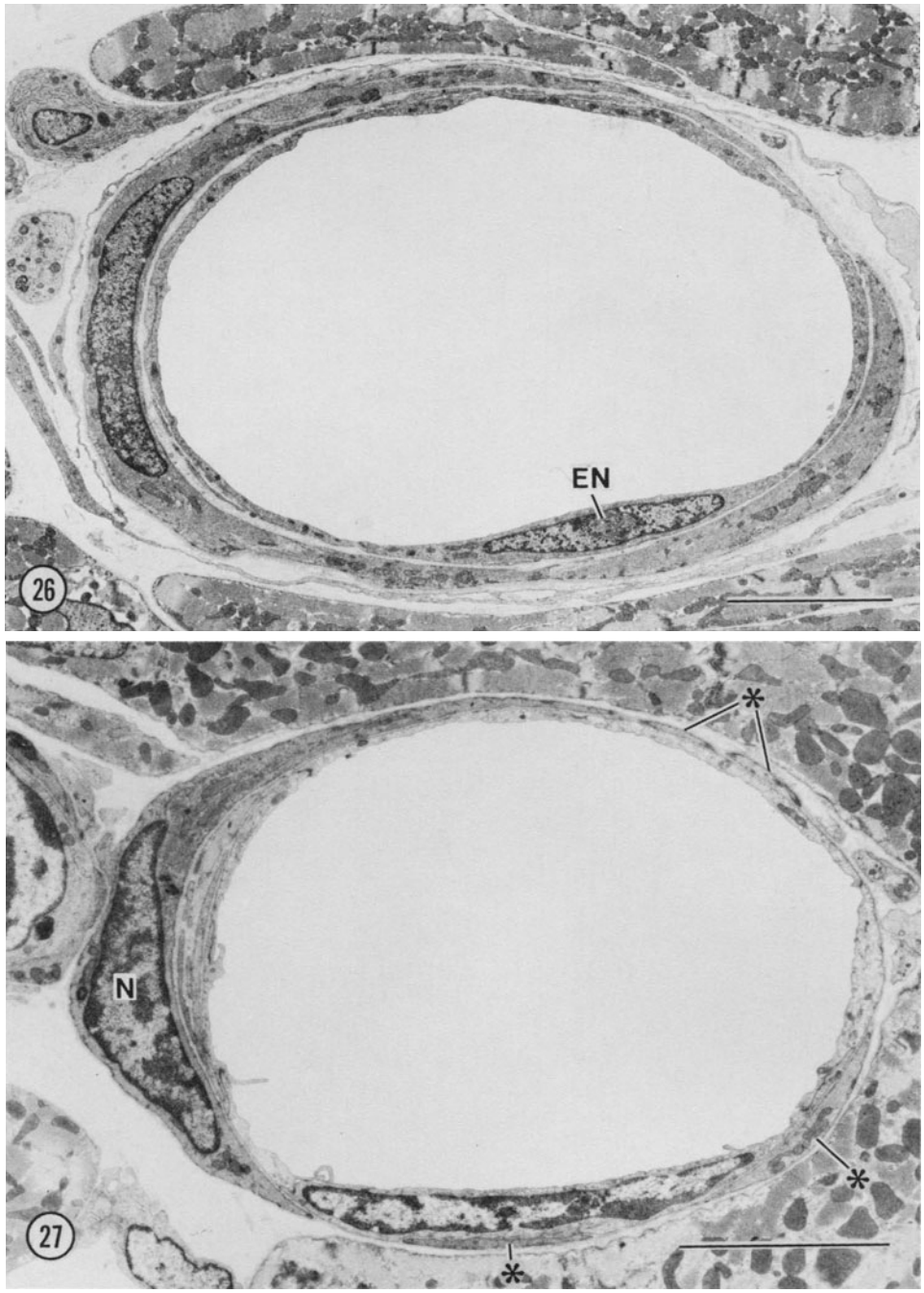

FIGURE 32–26. Transverse section through "typical" arteriole in right ventricular wall of squirrel monkey *(Saimiri sciureus)*. At most points of the circumference of this vessel, a single layer of smooth muscle is present, almost completely enveloping the endothelial cylinder. The VSMC component is in its essence identical to that of coronary arteries in its organellar content, though the individual cells appear less voluminous. EN, endothelial cell nucleus. Scale bar represents 5 μm.

FIGURE 32–27. Blood vessel in mouse left ventricular wall. Although this vessel is of a diameter (ca. 14 μ, lesser axis) characteristic of arterioles or venules (cf. fig. 32–26), its medial layer consists of a "primitive smooth muscle cell" which displays features intermediate between those of pericytes and smooth muscle cells; these features include a protruding nuclear profile (N) and extensive cytoplasmic processes (*) which appear as isolated profiles in this micrograph, but were found—in succeeding sections—to be confluent with the nucleated portion of the cell. In such cells, surface caveolae appear at both abluminal and adluminal surfaces, in contrast to pericytes which form the periendothelial layer of small vessels (cf. figs. 32–30 and 32–31). Scale bar represents 5 μm.

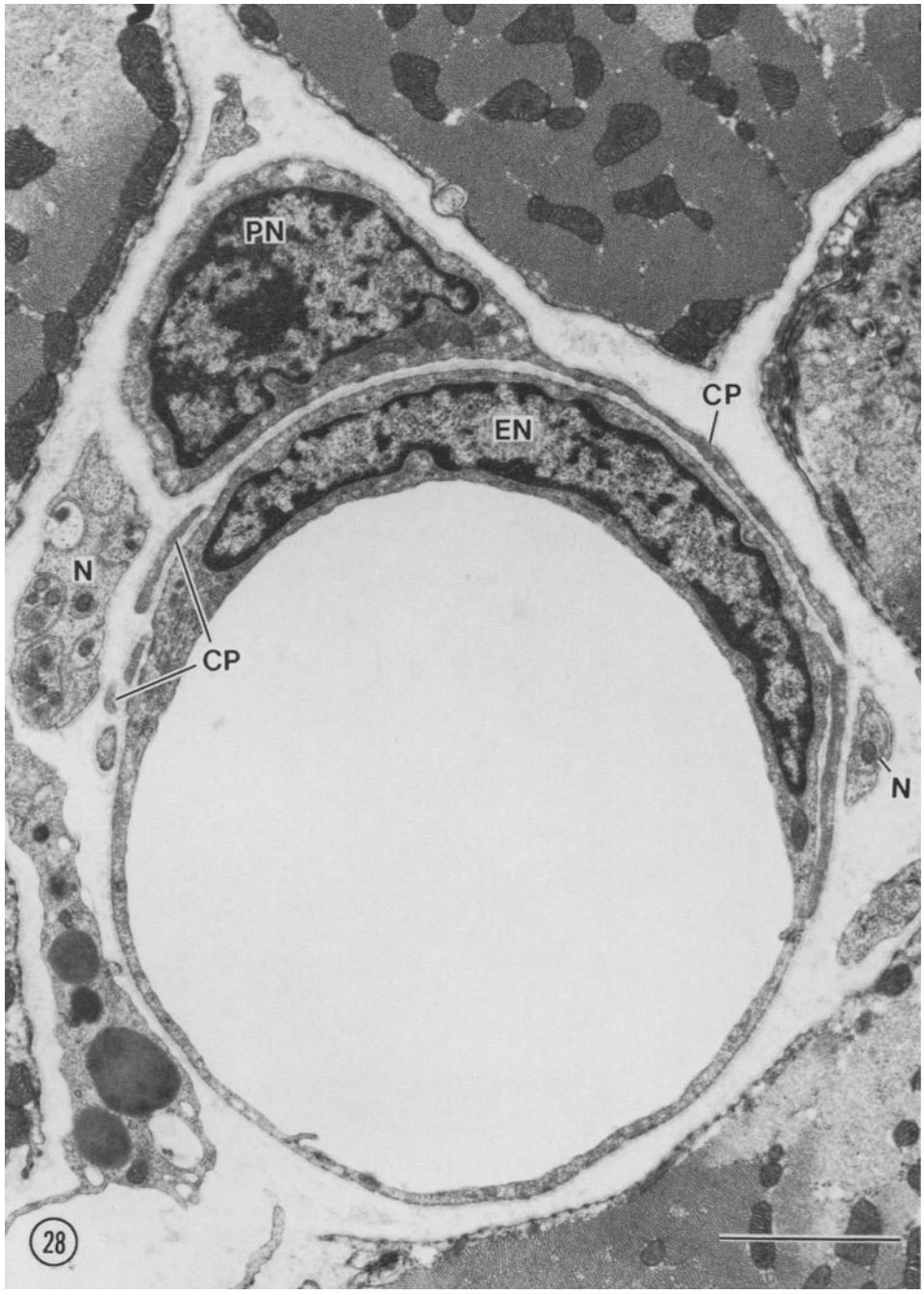

FIGURE 32–28. Transverse section of small vessel (luminal diameter ca. 7.9 μm: probably a venous capillary) of rhesus monkey papillary muscle. The cell body of the pericyte is characterized by a protrusive nucleus (PN); profiles of its circumferential process (CP) appear at various points about the endothelial cylinder (EN, nucleus of endothelial cell). The vessel is hemmed in by cardiac muscle cells, and elements of nervous tissue (N) are closely associated with the vessel's abluminal surface. Scale bar represents 2 μm.

VSMC, but not in others, as is the case in arteries (see *Fibrillar elements . . .*). Certainly the possibility of branching complicates the concept of the *central sarcoplasmic core* (see *The nucleus . . .*) in venous VSMC, as does their relative thinness. A great deal of study—specifically addressed to cardiac vein ultrastructure—will be required before further generalities can be established.

Comparative Structural Aspects of Vascular Smooth Muscle Cells and Other Periendothelial Cells

Pericytes are classically recognized as those cells of periendothelial location which partially envelop the endothelial profiles of microvessels—such as capillaries and postcapillary venules—and, in addition, bear surface coat material (*basal lamina*) which is continuous with that intrinsic to the endothelial cells (figs. 32–28 and 32–30). The *Rouget cells,* periendothelial cells of amphibian microcirculation, have clearly visible contractile abilities [31]. On the other hand, belief in the contractile abilities of their phylogenetic counterparts, the pericytes, has truly waxed and waned since the time of Rouget's observations. During the 1920s, Zimmerman [32], Vimtrup [33], and Krogh [34] supported the contractile role, whereas later—perhaps coincidental with the advent of transmission electron microscopy—the function of pericytes was deemed less clear, and their contractile ability in some cases came to be denied outright (see Majno [35] and Zweifach [36]). The concept did not die out, however, and supporting evidence has resurfaced in force recently [6, 30, 37–41].

In microvascular networks, there is seen a gradual transition between capillaries and venules (and sometimes between arterioles and capillaries) with respect to luminal diameter and types and numbers of periendothelial cells [32, 35, 42]. The ultrastructure of periendothelial cells also changes gradually from that which is characteristic of pericytes to that exemplified by features typical of smooth muscle cells. Thus in many vessels there can be found intermediate forms (*primitive smooth muscle cells:* fig. 32–27). In several studies of mouse myocardium, it has been documented that many basic ultrastructural features are mutually comparable for smooth muscle cells, primitive smooth muscle cells, and pericytes [19, 30, 37]. These features fall into five categories:

1. Cytoskeletal elements.
2. Excitation–contraction coupling system (SR and "T system").
3. Contractile (force-generating) apparatus.
4. Force-transmitting devices (heterocellular junctions).
5. Effector system (efferent innervation).

CYTOSKELETAL ELEMENTS

Microtubules and intermediate filaments form an organized skeletal network within periendothelial cells such as pericytes. A structural study of mouse heart microcirculation [30] showed that these fibrils are likely responsible for the configuration and maintenance of the pericyte's numerous cytoplasmic processes, and this seems likely to be the case in primate heart as well (figs. 32–30 and 32–31). Microtubules are especially prominent within the longitudinal stems of pericytes (figs. 32–30 and 32–31), and intermingle in both longitudinal stems and circumferential processes with varying numbers of intermediate filaments (fig. 32–33; also see Forbes et al. [30]).

The cytoskeletal fibrils of pericytes are notable in that they are restricted to the abluminal cytoplasmic region, whereas microfilaments are massed next to the adluminal surfaces (figs. 32–30 and 32–33). A bilayered internal segmentation is therefore typical of pericytes; this sort of cytoplasmic compartmentation compares favorably with the arrangement characteristic of the definitive VSMC of the myocardial vascular supply—a myofilament-filled cortex about a central core which is free of contractile elements.

EXCITATION–CONTRACTION COUPLING SYSTEM

Smooth-surfaced saccules and tubules, the structural analogues of sarcoplasmic reticulum in VSMC (see *Sarcoplasmic reticulum*), in pericytes are primarily present as subplasmalemmal

profiles (figs. 32–30 and 32–31). The subsarcolemmal endoplasmic reticulum of pericytes frequently generates bridging structures which contact the inner plasmalemmal leaflet and strongly resemble the junctional processes of VSMC couplings (see *Sarcoplasmic reticulum*).

Caveolae, which are abundant on all surfaces of the thicker VSMC, generally occupy only abluminal plasmalemmal positions in pericytes; limited numbers of adluminal caveolae are found in the primitive smooth muscle cells of larger microvessels and the VSMC of arterioles. Examples of caveolar tubules, consisting of 2–3 vesicular elements fused end to end, can be found both in pericytes and in the transitional forms of periendothelial cells; these are not so extensive as the "beaded tubules" of mouse coronary arterial VSMC [19], yet demonstrate the propensity of the limiting membrane to form significant invaginations in periendothelial cells of all vessel categories.

CONTRACTILE APPARATUS

A major identifying feature of most myocardial pericytes is the collection of 7- to 8-nm-diameter *microfilaments* which populate the adluminal layer of the cell, that portion which is closest to the underlying endothelium (figs. 32–30 and 32–33). In the microvascular beds of brain [43] and retina [41], these microfilaments have been shown, by means of decoration with heavy meromyosin, to be chemically equivalent to the F-actin of muscle cells. In myocardial pericytes, the microfilaments are aligned along the longitudinal axes of the various processes; this, together with their juxtaendothelial location, places them in ideal position to exert contractile influence, particularly in the numerous circumferential processes, which may in some instances nearly surround the endothelial cylinder [30]. A major failing in the promotion of the concept of pericyte contractility is the general absence of thick, myosin-like filaments; under certain conditions, however, tactoidal bodies reminiscent of myosin aggregates have been detected in the cytoplasm of brain pericytes [43]. Mechanisms have been proposed for smooth muscle contraction which do not require the palpable presence of thick filaments [44]; I have already noted the capricious occurrence of myosin filaments in VSMC of myocardial vessels (see *Fibrillar elements . . .*) [2]. Added to these circumstances is the relative difficulty which attends the capture of transverse sections of pericyte processes—in which authoritative identification of myosin filaments, if present, could best be made.

FORCE-TRANSMITTING DEVICES

The arteries and veins of mammalian heart incorporate numerous appositions between the medial and intimal tunics (see *Junctions . . .*). A variety of heterocellular junctions are present in microvessels as well, including simple appositions (fig. 32–30), intermediate contacts [30], and gap junctions (fig. 32–21). Pericytes vary in their encompassment of individual myocardial vessels, and may in fact be inferior in this parameter in comparison to their counterparts in the skeletal muscle microcirculation [39, 40]. Still, the presence of numerous traction points between myocardial pericytes and the accompanying endothelium may provide sites for transfer of contractile force to the vessel lining, thereby providing graded amounts of deformation to the luminal contour of capillaries and venules.

EFFECTOR SYSTEM

Both efferent and afferent axon terminals are known to accompany myocardial vessels at all levels of the circulatory bed [37]. The chemical nature of the efferent nerves associated with pericytes on capillaries and postcapillary venules varies between species. In the mouse, the majority of terminals appear to be cholinergic (as judged in animals treated by administration of 5- or 6-hydroxydopamine, which labels adrenergic terminals [37]). On the other hand, cat myocardium, which is profusely supplied with adrenergic nerves [45], contains a system of blood vessels which at all its levels is similarly supplied with terminals filled with numerous small dense-cored vesicles (unpublished observations).

The gap between axon terminal and abluminal vessel surface is smallest in microvessels (in mouse averaging ca. 170 nm, with a minimum distance of 46 nm [37]); this is perhaps related in some instances to the progressive

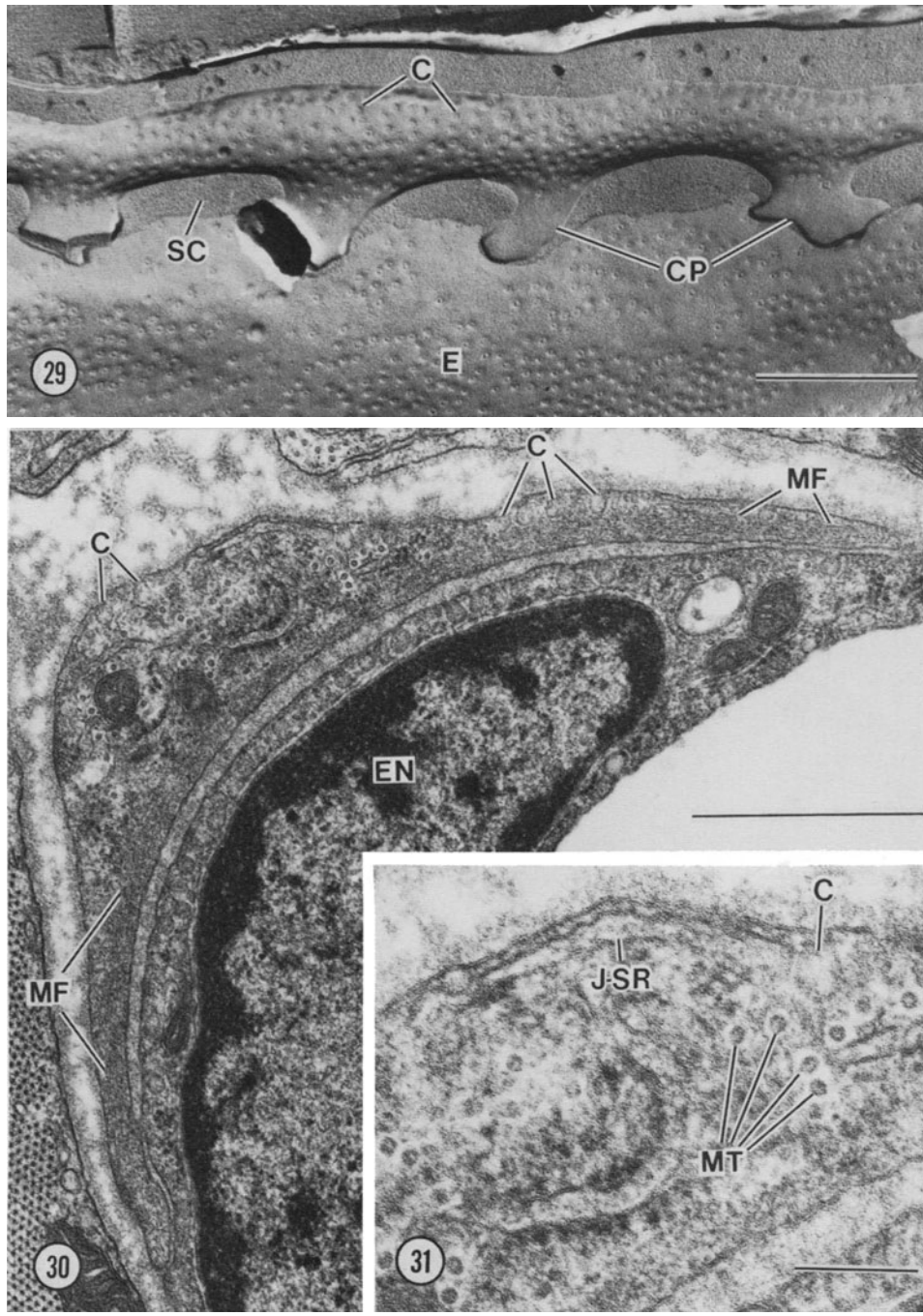

FIGURE 32–29. Freeze-fracture replica of a small blood vessel (fractured longitudinally) from right papillary of rhesus monkey. Reproduced in the field are the contours of a pericyte which overlies the vessel's endothelial wall (E). The circumferential processes of the pericyte (CP) lack caveolar openings (C) at their thinnest portions; this image corresponds favorably to the appearance of these processes in thin sections (fig. 32–30). SC, replica of surface coat material between pericyte and endothelium. Scale bar represents 1 μm.

FIGURE 32–30. Transverse section through capillary (5.4 μm luminal diameter) from rhesus right papillary muscle. A profile of pericyte cytoplasm is closely applied to the endothelium (EN, endothelial nucleus). Caveolae (C) are restricted in occurrence to the upper (abluminal) plasmalemma of the pericyte and there appear only within the thicker portions. The attenuated tips of the processes are completely filled with microfilaments (MF), which elsewhere are massed subjacent to the adluminal plasmalemma. Microtubules are located only in the abluminal cytoplasm, and thus are segregated from the more basal microfilaments. Both tips of the pericyte come into close apposition with the endothelium. Scale bar represents 1 μm.

FIGURE 32–31. Detail of figure 32–30, showing subplasmalemmal saccule (J-SR) equivalent to junctional SR of vascular smooth muscle. Orientation of microtubules (MT) is predominantly along the longitudinal stem of the pericyte. C, caveola. Scale bar represents 0.2 μm.

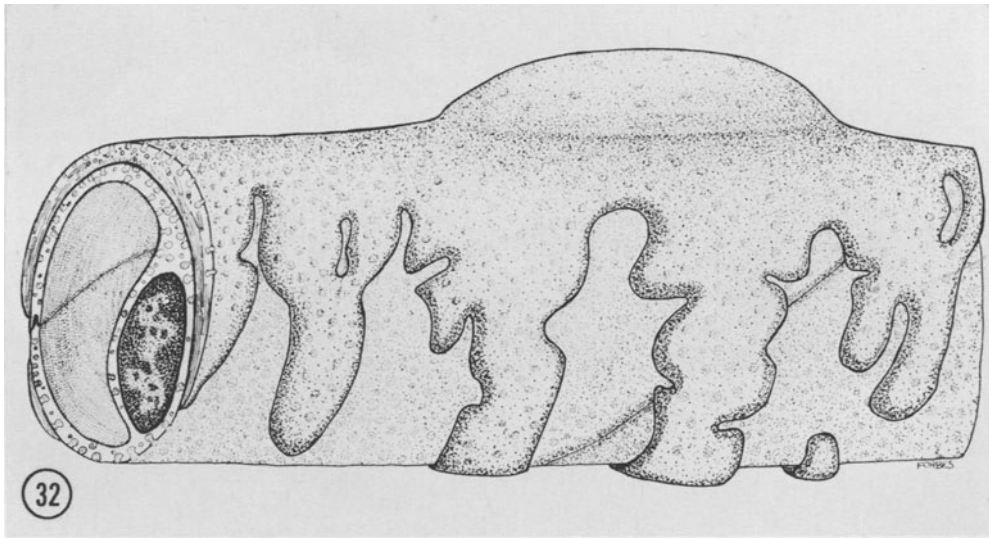

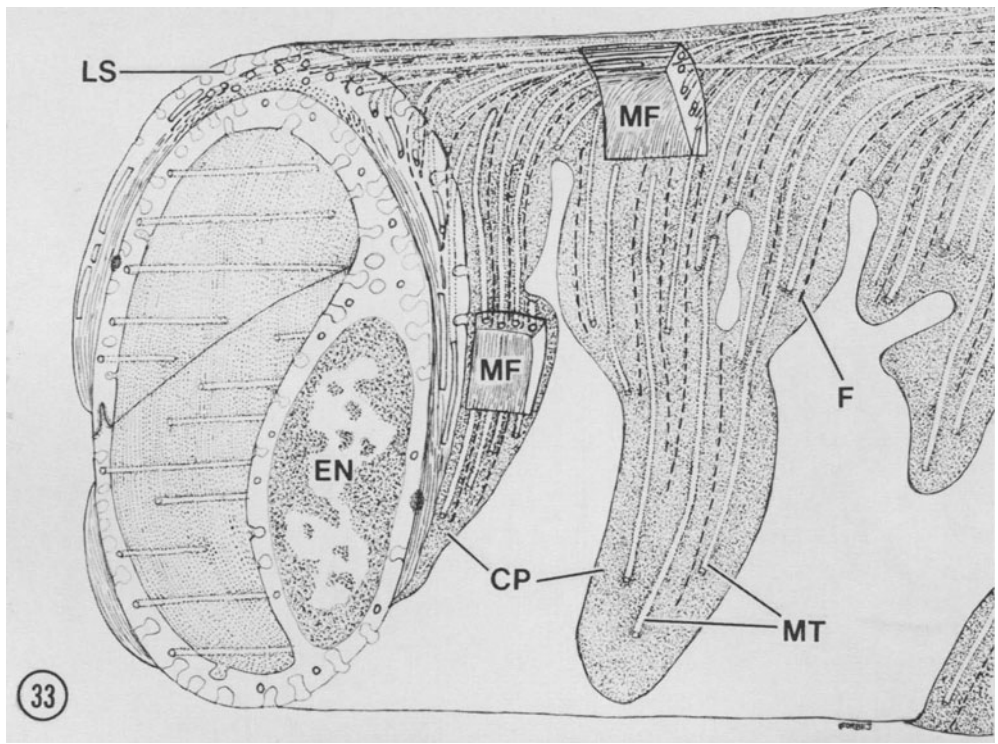

FIGURE 32–32. Diagram of the three-dimensional relationship borne by a pericyte to its accompanying cylinder of capillary endothelium (drawn on the basis of observations made on mouse heart). The pericyte's nucleus typically is protrusive (cf. fig. 32–28), and its cytoplasm forms two major longitudinal stems and numerous, less-extensive circumferential processes, the latter of which may branch from either the main cell body or the longitudinal stems (see fig. 32–33). The outer (abluminal) surfaces of the pericyte are characterized by caveolar indentations. From Forbes et al. [30], courtesy of Alan R. Liss, Inc.

FIGURE 32–33. Drawing based on the diagram shown in figure 32–32, demonstrating by surface projection and cutaway views the intracytoplasmic organization of pericyte fibrils. Microfilaments (MF), presumably composed of actin, are restricted to the adluminal cytoplasm, whereas the cytoskeletal fibrils, microtubules (MT) and intermediate filaments (F), occupy the more abluminal cytoplasmic regions. Note that numbers of all three categories of fibrils are diverted from the longitudinal stem (LS) into the circumferential processes (CP), so that the same stratification of fibrils is maintained in all branches of the pericyte. EN, endothelial nucleus. From Forbes et al. [30], courtesy of Alan R. Liss, Inc.

narrowing of the perivascular space which accompanies the diminution of vessel bore. The fact remains that a substantial structural relationship exists between terminal axons and pericytes in mammalian heart, such that the pericyte surfaces are within reasonable diffusion distances of neurotransmitter substances. It has been demonstrated [40] that skeletal pericytes contract in response to intravascularly administered norepinephrine, angiotensin, or vasopressin, and that myocardial pericytes are unaffected by such treatment. The pericytes of skeletal muscle differ from myocardial pericytes in that they generally are not associated with efferent axon terminals [39]. It remains to be seen what effects would result in heart either from extravascular application of vasoactive agents or induced release of neurotransmitter from the terminal axons themselves.

Conclusion and Summary

The walls of myocardial blood vessels in mammals are occupied by a spectrum of muscle and muscle-like cells, various forms of which are collectively known by numerous appellations: smooth muscle cells, primitive smooth muscle cells, transitional cells, medial cells, mural cells, perivascular cells, pericapillary cells, Rouget cells, etc. A reasonable unifying term which at once encompasses this spectrum of vascular components is, simply, *periendothelial cells,* for this term aptly describes their positioning, yet does not relegate them to strict residence within a medial tunic (consider, for example, the far-flung VSMC which appear in veins: see *Comparison of arterial/arteriolar . . .* and fig. 32–24). The use of "periendothelial cells" furthermore sidesteps the debate as to whether three distinct tunics can be identified in microvessels such as capillaries. (Incidentally, for capillaries of mammalian myocardium, the answer is clear to this reviewer: the *tunica intima* is of course represented by the endothelial cylinder, the *t. media* by pericyte bodies and processes, and the *t. adventitia* by the fibroblasts and the numerous elements of neural tissue [including Schwann cells] which appear in the perivascular space.)

The spectrum of fine structure attributes possessed by periendothelial cells is not restricted solely to the stretches of "microvessels" which connect arteries and veins in the individual heart, but can also exist interspecifically, such as is demonstrated in the numerous instances when anatomically equivalent vessels display strikingly different profiles and distributions of VSMC (e.g., figs. 32–7 and 32–8). With the application of more effective regimens of preservation it has become apparent that VSMC are far more complex than was indicated by early electron micrographs. This has been shown to be the case as well with "minor" periendothelial cells such as myocardial pericytes, which in well-fixed tissue displays obvious complements of microfilaments which may prove to be the basis of a contractile apparatus. Thus there must remain the possibility, which would be of great physiologic significance, that modulation of vessel bore occurs, to one or another degree, at all levels of the circulatory system of the heart.

Acknowledgments

The research which contributed to this work as reported was carried out at the University of Maryland (PHS grants NS-06779 and NS-08261) and at the University of Virginia (grants-in-aid from the American Heart Association [78-753] and its Virginia affiliate [A81-737], as well as PHS grant HL-28329, all the Virginia-based support to M.S. Forbes) and PHS grant HL-19242. Dr. Forbes is recipient of Research Career Development Award 5-K04 HL00550 from the National Institutes of Health.

The contributions made during the course of this research by Drs. Erland R. Nelson, Marshall L. Rennels, and S. David Gertz, and especially by Miss Barbara A. Plantholt, are acknowledged, as is the able technical assistance of Messrs. Rafa Rubio and Lawrence A. Hawkey. Primate heart material was generously contributed by Drs. S.K. Jirge and K.R. Brizzee of the Tulane University Delta Regional Primate Research Center (Covington, Louisiana: Dr. Peter Gerone, Director). Some of the electron-microscopic instrumentation with which this study was carried out is located in the Central Electron Microscope Facility of the University of Virginia School of Medicine.

References

1. Boucek RJ, Takashita R, Fojaco R: Relation between microanatomy and functional properties of the coronary arteries (dog). Anat Rec 147:199–207, 1963.
2. Forbes MS: Ultrastructure of vascular smooth-muscle cells in mammalian heart. In: Kalsner S (ed) The coronary artery. London: Croom-Helm, 1982, pp 3–58.
3. Rhodin JAG: Architecture of the vessel wall. In: Bohr DF, Somlyo AP, Sparks HV Jr (eds) Handbook of physiology. Sect 2: The cardiovascular system. Vol 2: Vascular smooth Muscle. Bethesda MD: American Physiological Society, 1980, pp 1–32.
4. Uehara Y, Suyama K: Visualization of the adventitial aspect of the vascular smooth muscle cells under the scanning electron microscope. J Electron Microscopy 27:157–159, 1978.
5. Murakami M, Sugita A, Shimada T, Nakamura K: Surface view of pericytes on the retinal capillary in rabbits revealed by scanning electron microscopy. Arch Histol Jpn 42:287–303, 1979.
6. Mazanet R, Franzini-Armstrong C: Scanning electron microscopy of pericytes in rat red muscle. Microvasc Res 23:361–369, 1982.
7. Somlyo AP, Garfield RE, Chacko S, Somlyo AV: Golgi organelle response to the antibiotic X537A. J Cell Biol 66:425–443, 1975.
8. Eriksson A, Thornell L-E: Intermediate (skeletin) filaments in heart Purkinje fibers: a correlative morphological and biochemical identification with evidence of a cytoskeleton function. J Cell Biol 80:231–247, 1979.
9. Goldman RD: The role of three cytoplasmic fibers in BHK-21 cell motility. I. Microtubules and the effects of colchicine. J Cell Biol 51:752–762, 1971.
10. Forbes MS, Dent JN: Filaments and microtubules in the gonadotrophic cell of the lizard, *Anolis carolinensis*. J Morphol 143:409–434, 1974.
11. Cooke P: A filamentous cytoskeleton in vertebrate smooth muscle fibers. J Cell Biol 68:539–556, 1976.
12. Murphy RA: Mechanics of vascular smooth muscle. In: Bohr DF, Somlyo AP, Sparks HV Jr (eds) Handbook of physiology. Sect 2: The cardiovascular system. Vol 2: Vascular smooth muscle. Bethesda MD: American Physiological Society, 1980, pp 325–352.
13. Somlyo AV: Ultrastructure of vascular smooth muscle. In: Bohr DF, Somlyo AP, Sparks HV Jr (eds) Handbook of physiology. Sect 2: The cardiovascular system. Vol 2: Vascular smooth muscle. Bethesda MD: American Physiological Society, 1980, pp 33–68.
14. Forbes MS, Sperelakis N: Structures located at the level of the Z bands in mouse ventricular myocardial cells. Tissue Cell 12:467–489, 1980.
15. Forbes MS, Sperelakis N: Ultrastructure of mammalian cardiac muscle. In: Sperelakis N (ed) Physiology and pathophysiology of the heart. Boston: Martinus Nijhoff, 1984, pp. 3–42.
16. Gabella G: Inpocketings of the cell membrane (caveolae) in the rat myocardium. J Ultrastruct Res 65:135–147, 1978.
17. Masson-Pévet M, Gros D, Besselsen E: The caveolae in rabbit sinus node and atrium. Cell Tissue Res 208:183–196, 1980.
18. Levin KR, Page E: Quantitative studies on plasmalemmal folds and caveolae of rabbit ventricular myocardial cells. Circ Res 46:244–255, 1980.
19. Forbes MS, Rennels ML, Nelson E: Caveolar systems and sarcoplasmic reticulum in coronary smooth muscle cells of the mouse. J Ultrastruct Res 67:325–339, 1979.
20. Forbes MS, Sperelakis N: The membrane systems and cytoskeletal elements of mammalian myocardial cells. In: Shay JW, Dowben RM (eds) Cell and muscle motility, vol 3. New York: Plenum, 1983, pp 89–155.
21. Somlyo AP, Devine CE, Somlyo AV, North SR: Sarcoplasmic reticulum and the temperature-dependent contraction of smooth muscle in calcium-free solutions. J Cell Biol 51:722–741, 1971.
22. Somlyo AV, Somlyo AP: Strontium accumulation by sarcoplasmic reticulum and mitochondria in vascular smooth muscle. Science 174:955–958, 1971.
23. Somlyo AP, Devine CE, Somlyo AV: Sarcoplasmic reticulum, mitochondria and filament organization in vascular smooth muscle. In: Betz E (ed) Vascular smooth muscle. Berlin, Springer, 1979, pp 119–121.
24. Devine CE, Somlyo AV, Somlyo AP: Sarcoplasmic reticulum and mitochondria as cation accumulation sites in smooth muscle. Philos Trans R Soc Lond [B] 265:17–23, 1973.
25. Popescu LM, Diculescu I: Calcium in smooth muscle sarcoplasmic reticulum in situ: conventional and X-ray analytical electron microscopy. J Cell Biol 32:911–919, 1975.
26. Forbes MS, Sperelakis N: Bridging junctional processes in couplings of skeletal, cardiac, and smooth muscle. Muscle Nerve 5:674–681, 1982.
27. Somlyo AV: Bridging structures spanning the junctional gap at the triad of skeletal muscle. J Cell Biol 80:743–750, 1979.
28. Joris I, Majno G: Cellular breakdown within the arterial wall: an ultrastructural study of the coronary artery in young and aging rats. Virchows Arch [Pathol Anat] 364:111–127, 1974.
29. Franklin KJ: The physiology and pharmacology of veins. Physiol Rev 8:346–364, 1928.
30. Forbes MS, Rennels ML, Nelson E: Ultrastructure of pericytes in mouse heart. Am J Anat 149:71–92, 1977.
31. Rouget C: Mémoire sur le dévelopment, la structure et les propriétés physiologiques des capillaires sanguins et lymphatiques. Arch Physiol Norm Pathol 5:603–663, 1873.
32. Zimmerman KW: Der feinere Bau der Blutcapillaren. Z Anat Entwicklungsgesch 68:3–109.
33. Vimtrup BJ: Beiträge zur Anatomie der Kapillaren. I. Ueber kontraktile Elemente in der Gafässwand der Blutkapillaren. Z Gesamte Anat 65:150–182, 1922.
34. Krogh A: The anatomy and physiology of capillaries. New Haven: Yale University, 1929.

35. Majno G: The ultrastructure of the vascular membrane. In: Hamilton WF, Dow P (eds) Handbook of physiology. Circulation. Washington DC: American Physiological Society, 1965, pp 2293–2375.
36. Zweifach BW: Microcirculation. Annu Rev Physiol 35:117–150, 1973.
37. Forbes MS, Rennels ML, Nelson E: Innervation of myocardial microcirculation: terminal autonomic axons associated with capillaries and postcapillary venules in mouse heart. Am J Anat 149:71–92, 1977.
38. Rennels ML, Nelson E: Capillary innervation in the mammalian central nervous system: an electron microscopic demonstration. Am J Anat 144:233–241, 1975.
39. Tilton RG, Kilo C, Williamson JR: Pericyte–endothelial relationships in cardiac and skeletal muscle capillaries. Microvasc Res 18:325–335, 1979.
40. Tilton RG, Kilo C, Williamson JR, Murch DW: Differences in pericyte contractile function in rat cardiac and skeletal muscle microvasculatures. Microvasc Res 18:336–352, 1979.
41. Wallow IH, Burnside B: Actin filaments in retinal pericytes and endothelial cells. Invest Ophthalmol Vis Sci 19:1433–1441, 1980.
42. Rhodin JAG: Ultrastructure of mammalian venous capillaries, venules, and small collecting veins. J Ultrastruct Res 25:452–500, 1968.
43. Le Beux YJ, Willemot J: Actin- and myosin-like filaments in rat brain pericytes. Anat Rec 190:811–826, 1978.
44. Panner BJ, Honig CR: Filament ultrastructure and organization in vertebrate smooth muscle. J Cell Biol 35:303–321, 1967.
45. Yamauchi A: Ultrastructure of the innervation of the mammalian heart. In: Challice CE, Virágh S (eds) New York: Academic 1973, pp 127–178.

33. THE PATHOGENESIS OF CORONARY ATHEROSCLEROSIS

S. David Gertz
and Adi Kurgan

Introduction

In the United States between 1974 and 1977, 52% of all causes of death were attributed to cardiovascular diseases [1]. Ischemic heart diseases accounted for 65% of all cardiovascular diseases and were responsible for every third death (34%) in the USA during this period. The purported increase in incidence of ischemic heart disease in civilized communities during the first two-thirds of this century has been attributed variously to the decline and/or extinction of infectious diseases, to a "less than optimal adaptation to changing patterns of life style", and to advances in diagnostic techniques. Although the mortality rate for ischemic heart disease in the USA declined significantly (21%) during the period 1968–1976 [2, 3], its incidence has not, and this entity remains the cause of more deaths in the USA than any other disease.

Ischemic heart disease is a general term which includes all myocardial disorders resulting from insufficient blood flow relative to requirement. Arteriosclerotic stenosis (primarily atherosclerosis) of the coronary arteries has been considered to be the underlying causative factor for this insufficiency in as many as 99% of the cases with thrombosis of the coronary arteries alone; emboli; arterites such as syphilitic, rheumatic, temporal or polyarteritis; congenital anomalies of the coronary vessels; or spasm with "normal coronary arteries" all accounting for a very small percentage of pathogenetic factors in ischemic heart disease. Progress in our understanding of the pathogenesis of atherosclerosis has been inhibited in part because of its insidious onset and its usually protracted period of asymptomatic development. Unfortunately, "asymptomatic" coronary atherosclerosis is still, in the majority of cases, detected only when death occurs from other causes or when coronary vessels are visualized by angiography. Indeed, it was not until studies of American males who died in the Korean war that the higher prevalence of this disease within the second decade of life was documented. Since then, considerable effort has been directed toward increasing our understanding of the pathogenesis of atherosclerosis—a task whose successful completion is essential in order to prolong man's active life span.

In this chapter it is our intention to review current concepts concerning the major theories of the pathogenesis of atherosclerosis and recent advances based on these theories. In advance of this discussion, a brief review of the major pathologic changes in the coronary vessels in atherosclerosis is presented.

This work was supported in part by the Irving E. Meller Research Fund.

N. Sperelakis (ed.), PHYSIOLOGY AND PATHOPHYSIOLOGY OF THE HEART.

Martinus Nijhoff Publishing, Boston/The Hague/ Dordrecht/Lancaster.

Normal Coronary Arterial Wall

The coronary artery wall, like that of all muscular arteries, consists of three distinct layers or tunicae: intima, media, and adventitia.

INTIMA

This, the innermost layer, is bounded on its luminal side by a usually single, continuous, interdigitated layer of endothelial cells which are attached to one another by a series of junctional complexes of varying types depending on location and vessel caliber. These cells are arranged to permit marginal overlap which provides for a degree of cellular reserve, and hence maintenance of continuity, when the vessel is subjected to excessive dilatation or other mechanical stresses associated with normal pulsatile flow. The endothelial junctions inhibit the intercellular passage of macromolecules as evidenced by the nonpenetration of horseradish peroxidase. Small macromolecules of the size of the low-density lipoproteins may be transported across the endothelium in vesicular chains [4]; disruption of this transport system is considered by some to contribute to the accumulation of these lipids within the arterial wall.

The intima is limited on its external side by the internal elastic lamina—a perforated, circular sheet of elastic tissue. The internal elastic membrane in the fetus is essentially a continuous tube of elastic tissue with localized splitting occurring only a few days after birth prior to the more-advanced development of the media [5]. The 2- to 7-micra fenestrations in the internal elastic lamina appear to restrict the migration of cells from the media to the subendothelial space to only limited passage. This is supported by numerous studies which have confirmed the morphologic association between the intimal fibromuscular hyperplasia characteristic of atherosclerosis and disruption of the internal elastic lamina.

Between the endothelium and internal elastic lamina are found a variety of loose connective tissue components including an often ill-defined connective tissue meshwork, the basal lamina. The endothelium is tenuously attached to this lamina by half-desmosomes. In the fetus and newborn, the endothelium is closely apposed to the internal elastic lamina; however, shortly after birth, the subendothelial space becomes widened by the influx of cells and connective tissue such that, in the main coronary arteries of the adult, the intima represents approximately one-sixth of the total wall thickness. In general, only an occasional smooth muscle cell can be found between the two limiting layers of the intima. With increasing age, however, and at sites of intimal cushions (usually found at branch points), the number of intimal smooth muscle cells increases.

The intima, particularly the endothelium, is unique in the wide variety of functions it performs which are designed to maintain the integrity of the vascular system and hence the tissues supplied. The role of the endothelium as a nonthrombogenic surface has been considered by some to be related to the secretion of the thin layer of complex carbohydrate which is found on the luminal surface of the endothelial lining. This glycocalyx has a particular affinity for ruthenium red staining, and has been shown to be thinner in areas of the arterial tree prone to atherosclerosis [6]. In recent years it has been accepted that the nonthrombogenicity of the endothelial surface is due, at least in part, to the secretion by the endothelium of prostacyclin (PGI_2), a potent inhibitor of platelet aggregation, and by secretion of antifactor VIII for interference with instrinsic coagulation. Other functions of the endothelium include: the mediation of thrombolysis, its regenerative and proliferative role in response to vascular injury, controlled exchange of fluids and metabolic substances of various molecular sizes between blood and surrounding tissues including the metabolism of lipoproteins and chylomicrons through the action of lipoprotein lipase, and the formation of a relative barrier to blood cells and particulate matter [7, 8].

MEDIA

The media consists primarily of smooth muscle cells arranged in multiple concentric spiral lamellar units.[1] The collagen and elastic fibers (as well as glycosaminoglycans) which surround the smooth muscle cells are presumably elaborated by the smooth muscle cells themselves [9–11]. The smooth muscle cell is considered to be a multipotential cell whose capabilitites of migration, proliferation, and synthesis are manifest in the intimal thickening of atherosclerosis (see the section on *Pathologic changes*. . .). On the external, abluminal as-

pect of the media is the less continuous, and not always present, external elastic lamina. The presence of elastic tissue is essential for the mechanical adaptation of the arterial wall in response to increased wall tension which occurs with systole and for elastic recoil in diastole to permit proper distal propulsion of blood and gradual dampening of the pulsatile aspects of flow toward the smaller vessels.

ADVENTITIA

This, the outermost layer of the coronary vessels, consists of loose connective tissue composed of bundles of collagen and elastic fibers with a mixture of loosely arranged smooth muscle cells and fibroblasts. The latter represents the predominant cell type in this layer. Vaso vasora are found in this layer extending, according to Wolinsky and Glagov, as far luminally as the approximately 29th lamellar unit of the media [12]. The area of supply of these vessels extends further inward such that only the innermost layers of the media are supplied exclusively from the lumen. The presence and significance of perivascular nerves and their terminals, often found in the outer media and adventitia of coronary vessels, and even abutting on pericytes at the capillary level, are discussed in chapter 32.

Pathologic Changes in the Arterial Wall in Atherosclerosis

Atherosclerosis is the form of arteriosclerosis which involves generally the larger arteries and which also forms the pathogenetic basis underlying most circumstances of ischemic coronary artery disease. From the standpoint of pathologic anatomy, atherosclerosis is primarily a disease of the arterial intima, although secondary changes can also be found at times in the media. Atherosclerotic lesions generally are classified into three types: fatty streaks, fibrous plaques, and complicated lesions. (For reviews, see references 5, 6, and 13–19).

FATTY STREAKS

The fatty streak is considered to be the earliest of these three lesion types and can generally be found in all persons by age ten. Fatty streaks increase in frequency up to the third decade and in absolute surface area involved during all decades [17]. This is a nonobstructive lesion characterized by focal accumulation within the intima of relatively small numbers of smooth muscle cells, macrophages, and foam cells.

The degree of luminal protrusion of fatty streaks ranges from slightly raised to not at all. The yellow color seen upon gross inspection of these lesions is associated with the lipid deposition found within these intimal cells as well as extracellularly. Fatty streaks are distributed throughout the aterial tree, but display a predilection for arterial curvatures and branch orifices [20].

Of interest, macrophages found here have been shown to have the ability, among a variety of other functions, to secrete collagenase and elastase [21], which is of particular significance in view of the fact that rupture of the internal elastic lamina is considered to represent one of the first steps in atherogenesis [22].

It remains a matter of controversy as to whether the foam cells, which increase in number with increased lipid deposition, have their origin from smooth muscle cells or from macrophages. This question has arisen because of the fact that foam cells exhibit phagocytic properties and often show ultrastructural features resembling leukocytes, particularly monocytes, and have the ability to produce acid hydrolases and catalases. On the other hand, it has been shown that smooth muscle in tissue culture can be transformed into foam cells following lipid imbibition. A recent study by Fowler et al. has shown that, in all likelihood, these cells have their origin both from monocytes and from smooth muscle cells with a greater proportion being derived from the latter [23].

FIBROUS PLAQUES

Fibrous plaques are generally considered to be the characteristic lesion of well-developed atherosclerosis. Lesions in the coronary vessels occur generally later than in the aorta and occur earlier, and are more pronounced, in male coronaries as a rule than in those of women. Macroscopically, fibrous plaques are white in appearance and routinely protrude to varying de-

grees into the vascular lumen accounting for their often being referred to as "raised lesions". The principal component of the fibrous plaque is the substantial accumulation of intimal smooth muscle cells with a highly variable degree of intra- as well as extracellular lipid (see *Lipids and atherogenesis*). The smooth muscle cells are also intertwined with variable amounts of collagen, elastic fibers, and glycosaminoglycans such that the contribution of the smooth muscle cell to intimal thickening is not only by virtue of its multiplication and migration, but also because of the products it synthesizes. It has been suggested that the glycosaminoglycans, possibly in combination with these other connective tissue components, participate in the accumulation of extracellular lipids within the plaque and within the media [24].

The accumulated smooth muscle cells, macrophages, foam cells, and intercellular substances within the intima take the form of a dome-shaped fibrous cap covering a deeper central core of necrotic cellular debris mixed with extracellular lipid deposition. The distribution of fibrous plaques, as a rule, is not as ubiquitous as the fatty streak, being localized, to a much greater extent, to areas of the arterial tree considered to be subjected to increased wall shear such as ostia and curvatures. Thus, although in many cases, the fatty streak and the fibrous plaque occupy the same anatomic position in the coronary arteries, with the former occurring generally earlier, this is not always the case, and the suggestion that the fatty streak represents the unequivocal precursor to the fibrous plaque remains unconfirmed. It has been shown that fibrous plaques occur with greatest frequency in the main coronary vessels just distal to the coronary sinuses [25]. In the latter study it was also shown that 39 of 41 patients (up to the age of 40, who died of noncardiovascular-related causes) had evidence of fatty streaks or fibrous plaques with involvement of 5%–10% of the surface area of the coronary intima. The great majority of these lesions was found to be localized to the cardiac half of the vessel circumference rather than the epicardial half. Atherosclerotic lesions may be found throughout the extramural portions of the coronary vessels, but the intramural portions of these vessels are usually spared [26].

COMPLICATED LESIONS

Complicated lesions are fibrous plaques which have been altered by increased cellular necrosis, calcification, desquamation of the overlying edothelial surface and thrombus formation, or hemorrhage.

The origin of intimal calcium deposition, in addition to the possibility of its being attracted to the injured intima from the lumen, is also considered to be derived from precipitation of this ion during injury and necrosis of intimal smooth muscle cells. Another possible source is from deterioration of attached platelets which have internal calcium-transport systems very similar to those of smooth muscle cells [22].

The complicated lesion can result in a compromise of coronary perfusion as a result of partial or total arterial occlusion due to the marked luminal protrusion of the lesion itself or because of the superimposed thrombus formation which may also result in occlusion of smaller coronary vessels distally following platelet shower or embolization. Progression of central necrosis within the plaque and accumulation of its "gruel" is often associated with weakening of the arterial wall which may result in dissection within the wall, aneurysm, hemorrhage, or embolization of fragments of the plaque or adjacent areas of the arterial wall.

Endothelium and Atherogenesis

ENDOTHELIAL REGENERATION

The life span of "normal" endothelial cells, as determined from studies of DNA synthesis, has been shown to vary between 100 and 180 days in most areas of the vascular tree with the cellular turnover at vascular curvatures or branch orifices ranging between 60 and 120 days [27]. By contrast, Spaet and Gaynor reported that endothelial cells are replaced only a few times during life [28]. However, these authors are in agreement that the rate of endothelial turnover is greatest at branch orifices.

The regenerative capacity of vascular endothelium has been the subject of extensive investigation. Early studies of endothelial injury by Poole et al. (1958) suggested that repair by regeneration was dependent upon endothelial ingrowth from the periphery of the lesion [29].

It has also been proposed that blood leukocytes might be the source of regenerating endothelium [30]. A third suggestion, based on studies of regeneration following balloon-catheter injury, considered the formation of new endothelium to be from intimal migration and redifferentiation of underlying smooth muscle cells [31]. In a later correlative light, scanning, and transmission electron-microscopic study by Fishman et al. [32], in which endothelial denudation was induced by brief drying with a gentle stream of air to avoid simultaneous damage to the media, endothelial regeneration was shown from the periphery of the denuded region. However, a simultaneous origin of new endothelium from blood monocytes could not be excluded. Moreover, their finding of marked intimal thickening, particularly in that area not yet completely covered by regenerating endothelium and without lipid deposition, and in the rat carotid artery which is generally not considered to be prone to spontaneous atherosclerosis, indicates that an origin from underlying smooth muscle cells remains a third possibility.

ENDOTHELIAL INJURY

It is now widely accepted that atherosclerosis develops at the site of prior damage to the endothelial lining. Such damage may expose subendothelial tissues to formed and fluid elements of the blood and thus facilitate the initiation of atherogenesis. A variety of factors have been implicated as being capable of directly causing, or contributing to, endothelial cell injury. These include severe changes in pH, temperature and osmolality [16]; ischemia [33, 34]; hypoxia [35]; ligation [36]; experimental hypertension [37]; carbon monoxide poisoning [38]; injections of bradykinin, serotonin, epinephrine, angiotensin I and II, acetoacetic acid (a diabetes metabolite), and nicotine [39]; as well as a variety of mechanical manipulations including occlusion with microsurgical clips [40]; balloon catheterization and even brushing with a soft camel brush [16]. Other mediators of endothelial injury include homocystinemia [41], endotoxin [42], antigen–antibody complexes [43], hyperlipidemia [44], formed elements of the blood including leukocytes [45] and platelets [46], endothelial compression associated with arterial spasm [47], and hemodynamic forces associated with partial constriction [48].

In general, endothelium responds in a limited number of ways to this wide variety of injurious stimuli. This response, as determined from a variety of light, scanning,[2] and transmission electron-microscopic studies, has been shown to range, depending on the intensity and duration of the noxious stimulus, from disruption of the plasma membrane, focal necrosis, cellular fragmentation, and desquamation to the "nondenuding" structural alterations in individual or contiguous endothelial cells. These alterations include intracytoplasmic vacuoles of various types, membrane-bound pseudopodia from adjacent endothelial cells or underlying smooth muscle cells, endothelial blebs of variable size which protrude into the vascular lumen, and disruption of interendothelial junctions [16, 34, 36, 47].

Participation of the endothelium in the atherogenic process includes its influence on the thickness of the intimal lesion, its control of lipid transport to the site of plaque formation, and the degree to which its absence permits platelet attachment and release. Intimal thickening has been shown to be greatest in areas which have not been reendothelialized; whereas endothelial regrowth seems to enhance regression [49]. By virtue of the vesicular transport system (molecules up to 100 n*M* in width) which accounts for the majority of the transmural lipid transport, the lipid concentration in the arterial wall has been shown, e.g., in the thoracic aorta, to be down to as little as one-thirtieth of that found in the blood [50]. Alteration of this transport system by endothelial injury, or disruption of the endothelial lining, may subject the subendothelial tissues to a much higher concentration of lipid which may be stimulatory to smooth muscle proliferation. Of interest, Stemerman [16] has shown lipid accumulation to be limited almost exclusively to the area beneath regenerating endothelium. Thus, this complex interrelationship between endothelium and lipid accumulation is far from completely understood. Regardless of the method of injury, damage to the endothelial lining, in addition to the above, results in the attachment of platelets to exposed subendothe-

lial tissues. These platelets are considered to be capable of stimulating smooth muscle proliferation by release of mitogenic factor(s) during the platelet release reaction [13, 14]. (For further details, see *Response to injury theory.*)

Theories of Atherogenesis: Introduction

Scarpa (1804) and Lobstein (1833) [51] are credited with providing the first pathologic descriptions of arteriosclerosis and its association to ischemic heart disease. Since that time, numerous theories of the etiology and pathogenesis of atherosclerosis have been presented. Each of these theories attempts to identify the mechanism(s) responsible for one or all of the pathologic alterations which characterize atherosclerosis, namely, smooth muscle cell proliferation, connective tissue formation, and variable degrees of lipid deposition. It is the purpose of this section to present the major theories which have been entertained and which have not been excluded by scientific investigation. It should be emphasized that the question of which of the presented mechanisms represents the most likely remains unanswered. Moreover, the available evidence indicates that atherogenesis may be initiated by a wide variety of pathogenetic factors singly or in combination.

Since current concepts concerning the pathogenesis of atherosclerosis continue to be influenced by the two major theories advanced in the middle of the last century—the thrombogenic theory and the insudation theory—a brief review of these theories will be presented first.

THROMBOGENIC OR ENCRUSTATION THEORY

This, the oldest theory, was first initiated by Von Rokitansky [52] and later revised by Duguid [53, 54]. This theory suggests that atherogenesis is preceded by deposition of thrombi (platelets, fibrin, and leukocytes) on the intimal surface which are later incorporated into the arterial wall by overgrowth of endothelium. The lipid content of the atherosclerotic plaque was considered to be derived from breakdown products of the platelets and leukocytes which form these thrombi. At this early stage, the importance of intimal smooth muscle cell proliferation had not been recognized.

INSUDATION-INFLAMMATION THEORY

This theory, advanced by Virchow [55, 56], holds that atherosclerosis is initiated by local (mechanical) intimal injury which is followed by the increased passage (imbibition or insudation) and accumulation of blood constituents (fluid and cellular) from the arterial lumen into the intima. Virchow suggested that this insudation results in an inflammatory process with edema, "fatty degeneration" of the intimal cells, and connective tissue proliferation in reaction to the degenerative "mucoid pool". It was not intended by Virchow to imply that the inflammation was initiated by lipid insudation—as many investigators often misinterpreted—rather that the intimal injury occurred first thus predisposing the arterial wall to increased permeability followed by a secondary inflammatory process.

At this stage, the insudation theory did not define the precise form in which lipid is transported to the atheroma. Anitschkow [57, 58] showed that the addition of cholesterol to the diet of rabbits resulted in hypercholesterolemia followed by "lipid-filled lesions" in the aorta. He thus modified the theory of Virchow by suggesting that hypercholesterolemia is the inciting cause of atherosclerosis on the basis of his finding cholesterol and its esters as components of the atherosclerotic plaque. This modification thus holds that the increased blood lipoproteins have the tendency to settle in the intima and initiate the resulting changes typical of atherosclerosis. Other factors such as mechanical or pharmacologic were considered to be of secondary importance. Because of these observations, it was the general consensus for years that conquering the problem of atherosclerosis was dependent solely upon clarifying and reversing the biochemical alterations of plasma lipids.

Lipids and Atherosclerosis

The source, nature, and fate of the lipids which accumulate in atherosclerotic lesions have been the subject of considerable investigation. It has been suggested variously that the extracellular lipids are themselves capable of contributing to the initiation of the atherogenic process, or, al-

ternatively, that these lipids represent by-products of this process. It has generally been accepted that most lipids which are found in the vascular wall arrive there by crossing the endothelial "barrier" in the form of lipoproteins, although there is some evidence for a smooth muscle cell origin for some of the arterial lipids.

The lipoproteins have the general structure of a "pseudomicelle" being composed of an outer surface coat of peptides (apoproteins) and polar lipids (unesterified cholesterol, phospholipids, etc) and an inner core of non-polar lipids (cholesterol ester, triglycerides) [59]. Five major types of plasma lipoproteins have been identified which are classified based on ultracentrifugation fractions or electrophoretic mobility: 1. chylomicrons 2. very low density lipoproteins (VLDL) (pre-B-lipoproteins) 3. intermediate density lipoproteins (IDL). 4. low density lipoproteins (LDL) (B-lipoproteins). 5. high density lipoproteins (HDL) (a-lipoproteins). These lipoproteins are heterogeneous with regard to their lipid content such that each of the major plasma lipids, cholesterol, tryglycerides, and phospholipids, is present in the different lipoprotein groups, but their proportions vary such that in chylomicrons and VLDL, the major lipid is triglyceride with the concentration of triglycerides in VLDL being lower. In LDL, cholesterol is the lipid of highest concentration while in HDL, the protein fraction predominates with phospholipids being the next in concentration in this group. The principle functions of plasma lipoproteins are to transport synthesized and absorbed cholesterol and triglycerides to sites of utilization and a storage [59–62].

It is generally accepted that the major component of the lipids in atheromatous lesions is derived from circulating cholesterol in the form of LDL. Triglycerides and phospholipids, which also enter the arterial wall as components of LDL or VLDL, and which are also actively synthesized and metabolized by the arterial wall, represent a relatively minor component of the lipid composition of most atheromatous lesions [63]. Nonetheless, a number of studies have shown a significant correlation between hypertriglyceridemia and coronary heart disease [64], and indeed apoprotein characteristics of very low density lipoproteins (VLDL) have been found in human atherosclerotic lesions [65, 66].

Since the observation of the presence of cholesterol (free and esterified) in arterial lesions [57, 58, 64], hypercholesterolemia has been known to be an important risk factor for the development of atherosclerosis. It is known that in persons with familial hypercholesterolemia, cholesterol accumulates more rapidly in the arterial wall, and clinical manifestations of cardiovascular pathology appear earlier in life [67, 68]. A variety of epidemiologic studies have provided evidence for a high degree of correlation between dietary-induced hypercholesterolemia and increased prevalence of coronary disease [69]. Moreover, experimental studies involving high-cholesterol diets have repeatedly shown accumulation of cholesterol in large arteries associated with the other pathologic characteristics of more-advanced atherosclerosis [70]. Evidence for the accumulation of LDL, the principal carrier of endogenous cholesterol, in arterial lesions is provided by the finding of its apoprotein (Apo-B) in these lesions [71, 72].

In order to understand current hypotheses concerning the role of lipids (particularly LDL) in the genesis of the atherosclerotic plaque, a brief review of recent concepts of LDL–cell interaction is in order [73]: (a) Cells bind LDL to specialized, high-affinity, membrane-bound receptors. (b) LDL is internalized, probably by endocytosis, and fuses with primary lysosomes. (c) LDL is broken down into protein and cholesterol ester. (d) Protein is broken down into free amino acids which leave the cell. (e) Cholesterol ester is hydrolyzed into free cholesterol which is released from the lysosome into the cell. (e) The cholesterol then suppresses endogenous cholesterol synthesis, stimulates esterification as "stored" cholesterol, and suppresses synthesis of new LDL receptors reducing LDL–cell interaction.

As indicated by Steinberg [73] it has been suggested that patients with familial hypercholesterolemia (phenotype II-a) have a deficiency in LDL receptors, which presumably accounts for the markedly elevated LDL levels in these patients. The relationship between such a receptor deficiency and the accelerated atherogenesis which occurs in these patients is unclear. Interestingly, Ross and Harker [44] suggested that chronic hyperlipidemia may initiate atherogenesis by itself inducing endothelial cell damage.

The possibility that chylomicrons (containing exogenous cholesterol and triglycerides) might be atherogenic has been discussed by Zilversmit, who hypothesized that the interaction of triglyceride-rich lipoprotein with arterial lipoprotein lipase constitutes an atherogenic process [72]. According to this hypothesis, chylomicrons may bind to subendothelial tissues exposed following endothelial cell loss. Triglycerides would then be hydrolyzed by lipoprotein lipase followed by internalization of cholesterol-rich chylomicron remnants by arterial smooth muscle cells.

A negative correlation has been reported between plasma high-density lipoproteins (HDL) and coronary heart disease. It has been suggested that HDL may exert an antiatherogenic effect by way of reverse cholesterol transport out of cells and toward the liver for catabolism and excretion [74], and that interference with HDL molecules may be a common cause of premature atherosclerosis [59, 74].

In summary, the most widely entertained theories concerning factors responsible for lipid accumulation in large vessel walls include: (a) Defect in membrane LDL receptor function (b) Altered transcellular (endocytotic) transport of lipoproteins. (c) Impaired lysosomal degradation of lipoproteins (d) Altered endothelial permeability [62]. Although accumulation of lipid is an undisputed, major component of the atherosclerotic plaque, and indeed the lipid-insudation hypothesis has virtually dominated atherosclerotic research for most of this century, a number of serious questions have arisen. These include inconsistencies in ability to demonstrate the known complications of human atherosclerosis including plaque ulceration and thrombosis in dietary-induced lesions; wide variations in histopathologic characteristics between dietary and "spontaneous" lesions found in man; and the fact that lipid accumulation may be detected in a variety of species including man even without elevated levels of serum lipids [75]. In addition, although there have been suggestions of a causative relationship between lipid insudation and smooth muscle cell proliferation, this theory has not adequately explained this cellular proliferation which forms a major, if not the principal, component of the atherosclerotic plaque.

Degeneration and Clonal Senescence Theories

The *degeneration theory* is considered to have been advanced initially by Thoma in 1833 [76], who suggested that the components of the atherosclerotic plaque have their origin as products of fatty and hyaline degeneration of connective tissue components of the arterial wall. Evidence of degenerative processes in the arterial wall exists particularly in the late stages of plaque development [77, 78], and, indeed, aging is an undisputed risk factor. On the other hand, it is known that atherosclerotic lesions occur in the young and in the absence of other signs of tissue degeneration.

A related hypothesis is that often referred to as the *clonal senescence theory*. Martin and Sprague [79] suggested that atherogenesis is a function of declining stem cell activity. According to this theory, the intimal smooth muscle cell proliferation is normally controlled by reciprocal feedback by way of "chalones" which are considered to be endocrine substances which inhibit mitosis and which possibly are secreted by smooth muscle cells themselves [78]. With age, these smooth muscle cells are not adequately replaced, which results in a failure of this inhibitory control system, thus permitting "uncontrolled" smooth muscle cell proliferation.

Monoclonal Theory

Benditt and Benditt [80] suggested that individual atherosclerotic lesions are clones from single smooth muscle cells which serve as progenitors for all subsequent cells. This was based on their observations that most individual atherosclerotic lesions from subjects with glucose-6-phosphate dehydrogenase defficiency (G-6-PD) contained either one or the other of the two isoenzymes of G-6-PD, whereas most tissues from control subjects contained both isoenzymes. According to this theory, each atherosclerotic lesion represents a benign neoplasm derived from a cell that has been subjected to mutation by noxious agents such as chemical or viral [81].

Although support for this theory is not widespread, it has yet to be disproven. Arguments against this theory of smooth muscle cell

proliferation include the observation that the finding of a single enzyme phenotype consistently throughout a lesion does not necessarily imply a clonal origin since a single lesion could arise from more than one cell that contained the same isoenzyme [82].

Immune Mechanisms in the Initiation of Atherogenesis

The implication of immune mechanisms in atherogenesis is based primarily on their ability to induce arterial damage—particularly to the endothelium [43]. Endothelium is known to possess a number of antigens including ABO antigens, factor-VIII antigen, α-2-macroglobulin antigen, and thromboplastin antigen [16]. This wide variety of antigens on the endothelial surface has been suggested to account at least in part for the susceptibility of the endothelium to such injury [16]. Evidence of arterial damage associated with immune mechanisms is derived from studies of graft rejection such as human kidney transplant and chronic failure of heart transplants [43, 83] where intimal cellular proliferation and lipid deposition may be found in arteries of almost any size. Regarding circulating autoantibodies, some evidence for the existence of antigens specific to the arterial intima does exist. Indeed, in rheumatic fever, in addition to the widely recognized histopathologic changes associated with calcification of the aortic and atrioventricular valve leaflets, changes common to arteriosclerosis are also seen with the rheumatic arteritis of the coronary vessels themselves. The delayed hypersensitivity reaction has also been implicated in the initiation of arterial wall damage because of evidence of infiltration of small lymphocytes as well as fibrinoid necrosis and because of its association with induction of hypertension and its subsequent sequelae [84]. Circulating antigen–antibody complexes have also been implicated in atherogenesis because of their known effect in induction of tissue injury. In immune complex diseases, arteritis is an established component [85], and, in serum sickness, lesions resembling atherosclerosis have been found in coronary arteries and at aortic branch points [86]. It is suggested that the similarity of the distribution of immune-complex-induced disease to the "spontaneous" lesions is related to the fact that similar hemodynamic and permeability mechanisms are responsible for deposition of immune complexes as are lipoproteins [43]. The arterial damage by immune complexes may also be due to activation of complement and attraction of polymorphs which result in fibrinoid necrosis of the arterial wall. Although this marked infiltration of polymorphs is generally considered to be atypical of atheroma, studies by Minick et al. [87] and Howard et al. [88] have shown that atherosclerotic lesions, induced by synergy of immune complex diseases and lipid feeding, display both the proliferative and the lipid deposition aspects of histologically demonstrable human lesions. It has also been suggested that immune complexes may further contribute to atherogenesis by way of the thrombogenic mechanism—by combination with, and activation of, platelets and initiation of the platelet release reaction [89].

Although the role of immune complexes in the initiation of atherogenesis is well established in experimental animals, their role in human disease requires additional testing. Interestingly, however, it has been shown, on the basis of studies of patients with monoclonal gammaglobulinopathy, that hyperlipidemia can be induced by an autoimmune response—for example, by way of antiheparin autoantibodies capable of inhibition of lipoprotein lipase resulting in marked hyperlipidemia [90]. To what extent autoimmune hyperlipidemia exists as a significant contribution to human atherogenesis is not certain. However, this emphasizes our serious lack of information concerning the role of immune systems in the pathogenesis of atherosclerosis.

Role of Platelets in Atherogenesis and the Response-to-Injury Theory

This theory, as advocated most recently by Ross and colleagues [13–15], represents a synthesis of ideas from a number of other theories and is predicated upon the presupposition that atherogenesis is preceded by damage to the endothelial lining. Indeed, prior damage to the arterial intima is a presupposition for both the

lipid imbibition theory of Virchow and the *thrombosis encrustation theory* of Rokitansky.

According to this theory, injury to the endothelial lining, whether continual or repetitive, might be so subtle as to result in alteration of the permeability characteristics of the endothelial lining without obvious morphologic changes or severe enough to result in extensive endothelial damage in the form of cellular fragmentation or desquamation. This results in exposure of the arterial wall to increased concentrations of plasma constituents, including various lipoprotein fractions, and results in the adherence of platelets to exposed subendothelial connective tissue. The discharge of products of the platelet release reaction is associated with further platelet aggregation and thrombus formation. According to Ross et al., one component ot the platelet aggregation release reaction is the release of a mitogenic factor (shown to be a low-molecular-weight [10,000–30,000] cationic protein) which stimulates smooth muscle cell proliferation. In spite of some contradictory evidence suggesting the lack of requirement for platelets for this proliferative process [91], there is evidence that, in the absence of this platelet-derived growth factor, plasma will not support smooth muscle proliferation. Thus, this interaction between plasma components and/or platelet constituents and arterial smooth muscle results in proliferation and focal migration from the media into the intima through normal or pathologic fenestrations in the internal elastic lamina as well as further proliferation of smooth muscle cells already present in the intima. This proliferation, accompanied by increased formation of connective matrix by smooth muscle cells as well, constitutes intimal fibromuscular hyperplasia pathognomonic of arteriosclerosis.

Support for the proliferative role of discharge products of the platelet release reaction with respect to smooth muscle cells is also derived from studies by Moore et al. [92] in which rabbits were made thrombocytopenic with antiplatelet antibodies. Following endothelial damage, such animals showed a virtual absence of smooth muscle cell proliferation with consequent inhibition of atherosclerotic lesions and fibrous plaques. Studies of swine which were homozygous for Von Willebrand disease, in which platelet adhesion to the subendothelium is impaired, have shown the absence of atherosclerotic lesions in spite of dietary-induced hypercholesterolemia [93]. The hypercholesterolemic, non-Von-Willebrand swine showed extreme atherosclerosis. On the other hand, a more recent study on the susceptibility to atherosclerosis of coronary arteries of swine with Von Willebrand disease following balloon catheter injury and administration of an atherogenic diet did not appear to show any appreciable differences between affected and nonaffected animals [94]. It has been suggested, on the basis of studies using endothelial cell-conditioned medium, that the endothelium itself might exert a proliferative influence with respect to the smooth muscle cells [95, 96]. It has also been suggested that the macrophage might be a source of mitogen for fibroblast proliferation in wound healing [97], which raises the question of whether these cells could have a similar effect on smooth muscle.

Recent evidence indicates that platelets also release thromboxane A_2, one of the many prostaglandin derivatives of arachidonic acid. Thromboxane A_2 is a potent vasoconstrictor and stimulant of platelet aggregation. It should be mentioned, however, that the precursor of thromboxane A_2 can also be converted, in the endothelial cells, to another derivative, prostacyclin (PGI_2), which favors vasodilation and inhibits platelet aggregation presumably by increasing platelet cyclic AMP [73, 98, 99]. This further emphasizes the importance of intact endothelium for the structural and functional integrity of the vascular wall. In spite of considerable evidence in support of a proliferative role of discharge products of platelet release reaction in atherogenesis, evidence to date for a protective effect in experimental atherogenesis of antiplatelet-aggregating agents in general, and agents which prevent primary adhesion in particular, is only somewhat encouraging with considerable conflicting evidence [100, 101].

In accordance with the reaction-to-injury hypothesis, another possible explanation for the more severe and widespread atherogenesis in animals fed a hyperlipidemic diet may be found

in the reported effect of hypercholesterolemia on platelet aggregation. Carvalho et al. [102] reported a 25-fold increase in platelet aggregation to epinephrine in patients with type-II hyperlipoproteinemia. In another study, a significant increase in ADP-induced platelet aggregation following oral administration of cholesterol was reported [103]. Moreover, a significant decrease in collagen- and thrombin-induced platelet aggregation was found in human subjects fed a low-fat, low-cholesterol diet [104]. Accumulation of lipid at sites of endothelial injury in animals fed a high-cholesterol diet is well known. On the other hand, Moore and colleagues [92, 105] found a variety of atherosclerotic lesions following repeated catheter injury in normolipemic animals. These lesions included fatty streaks, edematous plaques, fibrous (lipid-free) plaques, and raised lesions with intra- as well as extracellular lipid deposition covered partially or totally with thrombus formation. Cholesterol clefts were also seen in such lesions as early as two weeks. Thus, evidence exists that lipid accumulation in atherosclerotic lesions is not dependent upon hypercholesterolemia; it may occur in animals fed normal diets provided that this be associated with repeated insult to the endothelial lining [92]. An added interrelationship is that a number of studies have provided evidence that the hyperlipoproteinemia itself may damage endothelial cells [44, 73, 92, 102].

It has been shown that smooth muscle cell proliferation in rats occurs only in those areas which require more than seven days for endothelial regeneration [47]. Thus, the possibility of the existence of a "critical lesion size" has been suggested in which a critical amount of endothelium must be desquamated before smooth muscle proliferation can be initiated. This is supported by studies suggesting that small areas of denudation up to approximately 20 cells in width do not result in smooth muscle cell proliferation [106, 107]. This raises another question of whether the mitogenecity of the platelet release reaction is immediate or whether an accumulation of mitogenic substance(s) may be required over a longer time period [47].

Considerable additional support for the reaction-to-injury hypothesis is obtained from information which has accumulated regarding the effects of hemodynamic forces on the arterial wall as discussed in the following section.

Hemodynamic Factors in Atherogenesis

That hemodynamic factors might contribute to the initiation of atherosclerosis has been suggested by the well-known predilection of this process for arterial curvatures and branch orifices. These areas have been shown to display increased intimal permeability as evidenced by increased accumulation of Evans blue dye in the intima and adjacent medial layers [108]. This altered permeability has been shown to correspond to the pattern of intimal lipid deposition as shown by increased sudanophilia seen in coronary arteries of animals subjected to an atherogenic diet [20]. Such areas represent frequent sites of atherosclerotic plaque formation [108]. Endothelial cell turnover is reported to be greater at branch orfices [27, 109] and the sensitivity of these cells to changing flow patterns is manifested by distinct variability in their axis of orientation at these sites [110]. At branch orifices, damage to endothelial cells in nontreated control animals has been detected with the aid of scanning electron microscopy. This damage has been found to range from crater- and balloon-like vesicular defects to focal areas of cellular desquamation [34, 108, 111, 112]. These sites have also been shown to be favored sites for the accumulation of platelet aggregates [113] and deposition of leukocytes—particularly monocytes [114].

Hemodynamic forces are considered to act on the arterial wall by two principal mechanisms: (a) Shear stress: acts parallel to the axis of the blood vessel and represents the drag force which the adjacent blood exerts on the endothelial lining. (b) Lateral pressure force: acts perpendicular to the axis of flow. This force is thought to facilitate the interaction of fluid and cellular elements of the blood with the vascular wall.

SHEAR FORCES

This force represents the drag or friction force of the blood on the luminal surface which is

independent of turbulence. It is proportional to the viscosity and rate of flow and inversely proportional to the luminal radius. That such forces might damage the vascular wall is suggested by several reports of functional and structural changes in the endothelial lining associated with areas such as arterial curvatures and branch orifices [20, 27, 108, 111]. This is supported by the classic studies of Fry in which an intravascular grooved plug was used to acutely narrow the arterial lumen [115]. He reported that when the shear force of the blood approached 379 ± 85 dyn/cm^2, the "acute yield stress of the endothelial surface", rapid cellular deterioration occurred, resulting in focal or widespread endothelial desquamation. That shear forces of this magnitude (at or exceeding the yield stress of the endothelial lining) might exist in vivo has been suggested previously [48, 108]. This is particularly true in highly pulsatile arterial systems such as the coronary arteries which are notorious for their numerous anatomic curvatures and rapid tapering, and which are frequently subjected to abrupt, rapid, and wide fluctuations in velocity and demand for flow [26]. Shear stress is also expected to be high in areas of arterial constriction such as coarctation, atherosclerotic stenosis, or arterial spasm. In a recent scanning electron-microscopic study combined with blood flow analyses, endothelial damage was found at the site of partial (50%) coronary artery constriction [48]. This damage ranged from vesicular defects (craters and balloons) to endothelial desquamation and was found to be more extensive on the proximal slope of the constriction where shear forces are expected to be greatest. Extensive platelet deposition and thrombus formation was found on exposed subendothelium at sites of focal constriction even though, and probably particularly because, the reduction in transluminal diameter was insufficient to alter the rate of distal arterial flow.

LATERAL PRESSURE FORCES

Increased lateral intravascular pressure which occurs in association with hypertension is thought to contribute to vascular injury in two major ways: First, it is known that endothelial cells contribute to the transport of plasma lipoproteins mediated in part by lipoprotein lipase thought to be located on the endothelial surface. Increased lateral pressure, particularly in circumstances such as hypertension, might alter lipid transport directly by pressure damage to the endothelial barrier or indirectly through some form of minimal cellular damage which may interfere with normal metabolic processes. Studies of experimental hypertension have shown that elevated arterial pressure increases the permeability of the vessel wall to lipids particularly in animals with experimental atherosclerosis [116–118] and that lesion formation in these animals, both in large vessels and in small vessels, is greater than in control, nonhypertensive animals [118].

A variety of studies have been concerned with pathologic changes in blood vessels associated with animal (spontaneous and experimental) and human hypertension. In studies of spontaneously hypertensive rats, increased intimal thickening with hyalinization and fibrosis have been reported, with medial hyperplasia and hypertrophy, resulting in overall thickening of vascular wall associated, in some instances, with total luminal obstruction [119]. Haudenschild et al. [120], in a combined scanning and transmission electron-microscopic study of deoxycorticosterone–salt-treated rats and spontaneously hypertensive rats, showed intimal changes in both models as evidenced by distortion of endothelial shape, subintimal thickening due to accumulation of extracellular material including precipitated plasma proteins, reticulated basement membrane and collagen fibers, and fragments of elastin which appeared to show a blood as well as a vessel wall origin. Of interest, withdrawal of the hypertensive stimulus (DOC–salt) and normalization of blood pressure, even when combined with a prolonged period of low-salt diet, did not result in a discernible regression of these intimal changes, suggesting that vascular injury, once induced, may not completely reverse, and that areas of prior damage might serve as foci for subsequent more-advanced damage to the vascular wall. It has also been shown that permeability is increased in elastic and muscular arteries in hypertension as evidenced by enhancement of vesicular transport and by increased

protein passage through endothelial junctions and through discontinuities in the endothelial lining [121–123].

In conclusion, increased arterial pressure can alter intimal permeability by: (a) increasing filtration pressure, (b) stretching the endothelial surface and increasing its permeability, and (c) direct mechanical damage to the endothelial surface resulting in exposure of subendothelial layers. Microscopic studies have provided evidence for most if not all of the known histopathologic alterations in vascular intima and media associated with hypertension which are common to atherogenesis. Moreover, it has repeatedly been confirmed that the risk of hypertension for atherosclerosis—particularly in ischemic heart disease and cerebrovascular disease—increases progressively with increasing blood pressure; and, conversely, the risk for atherosclerosis appears diminished by therapeutic reduction of blood pressure.

Vasoconstriction, Vasospasm, and Atherogenesis

The observations of the effect of hemodynamic forces on the integrity of the vascular wall have provided greater insight into the relationship between episodes of arterial constriction, such as atherosclerotic stenosis and coronary vasospasm, and the pathogenesis of ischemic heart disease. Considerable evidence has accumulated implicating coronary vasospasm as a major, if not the principal, causative factor in Prinzmetal variant angina [124–126] and as a contributory factor to classic angina pectoris and acute myocardial infarction [127–129]. It has been assumed that the threat posed by such episodes for the initiation of myocardial ischemia depends on the degree to which the reduction in luminal diameter results in the interference with distal coronary blood flow. However, the results of several studies suggest a modification to this assumption [48, 108, 130]. Coronary vasospasm may result in myocardial ischemia and/or infarction not only as a result of a "critical" vascular constriction, when coronary flow would be dangerously reduced, but also as a result of marked endothelial damage that may occur even, and perhaps particularly, when the reduction in luminal diameter is not sufficient to alter the rate of distal coronary flow. Such endothelial damage may result in thrombus formation at the site of spasm or constriction, followed by partial or total arterial occlusion at that site (especially if superimposed upon preexisting arteriosclerosis), or occlusion of smaller coronary vessels distally after platelet shower or embolization.

Of particular significance, Turitto and Baumgartner [131] determined that the rate and extent of formation of platelet microthrombi on exposed subendothelium actually increase with increasing shear rate up to the highest shear rate tested of 10,000 s^{-1}. It is not certain whether shear rates in excess of this would continue to favor an increased rate and extent of thrombus formation or at what point such increased shear forces might favor embolization. Nonetheless, the latter report further supports the suggestion that a focal partial arterial constriction such as spasm is a much-favored site for marked endothelial damage, platelet deposition, and thrombus formation even, and possibly particularly, when the reduction in luminal diameter is insufficient to alter the rate of flow. Finally, it is also necessary to confirm whether this sequence of increased shear forces, marked endothelial damage, and thrombus formation might also occur at sites of arteriosclerotic stenosis, suggesting another cause for a sudden compromise of coronary perfusion.

The possibility that coronary arterial spasm might itself contribute to the initiation of atherogenesis is suggested on the basis of observations of endothelial damage and platelet attachment at these sites in experimental systems [48]. As per the response-to-injury hypothesis, the endothelial damage at sites of spasm (whether from mechanical effects of shear forces or endothelial compression associated with the vascular constriction) would be followed by platelet attachment to exposed subendothelial tissues, infiltration of lipoprotein molecules and lipid-laden macrophages, and proliferation and intimal migration of arterial smooth muscle cells. Support for this hypothesis is also obtained from the work of Gutstein et al. [132], who showed that rats, whose aortae were sub-

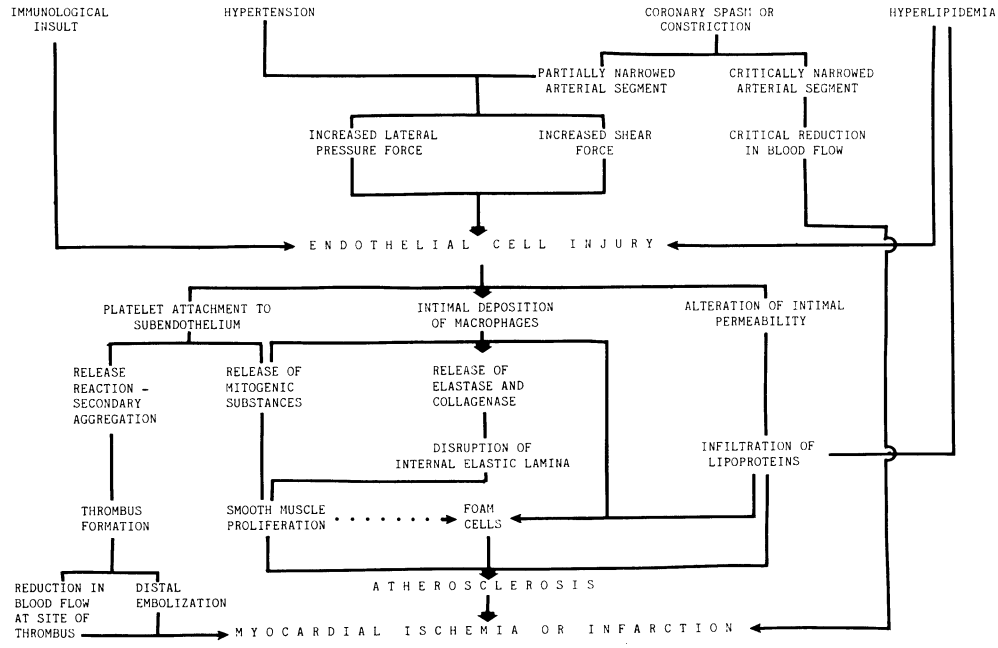

FIGURE 33–1. Diagram depicting the role of four of the many risk factors in the pathogenesis of atherosclerosis and ischemic heart disease as per the reaction-to-injury hypothesis.

jected to repetitive vasoconstriction, manifest fibrocalcific lesions as well as many of the intermittent stages associated with atherogenesis, and by the report of Betz and Scholte [133], who showed arteriosclerotic lesions following vasoconstriction induced by electrical stimulation.

As of the writing of this chapter, very little direct clinical evidence exists for this pathogenetic relationship [134] with the exception of the report by Marzilli et al. [135], who described the case of one patient who showed spontaneously occurring coronary spasm which, after eight months, presented with a fixed stenosis at the same site. On the other hand, as emphasized by Gutstein [136], experimental evidence for a relationship between coronary vasospasm and atherosclerosis does exist, and this relationship should be subjected to confirmation. Although the prevalence of coronary spasm in the total spectrum of ischemic heart diseases has classically been considered to be minimal, recent clinical studies have emphasized that this entity may be far more prevalent than previously thought [127, 129, 137]. Thus, confirmation of this pathogenetic relationship between vasospasm and coronary atherosclerosis should expand considerably the role of spasm in the pathogenesis of classic angina pectoris and acute myocardial infarction.

Conclusion

A variety of theories have been advanced concerning mechanisms of atherogenesis, but, as current thinking still holds, nearly all are predicated upon alterations in the structural or functional integrity of the endothelial lining (Fig. 33–1). A number of recent studies have been concerned with the nature of the endothelial damage which may precede the development of more advanced vascular lesions. However, the identification of endothelial damage associated with or preceeding the more advance vascular lesions associated with ischemic heart disease in man has not yet been achieved, and our information remains exclusively within the realm of experimental model systems. Conse-

quently, even though prior endothelial damage is presumed, its nature in man in vivo remains uncertain and thus its treatment or prevention cannot be reliably tested.

Possibilities for prevention of atherosclerosis at the clinical level are hampered by a number of factors. First, we still lack an effective, reliable, noninvasive method for the assessment of atherosclerotic lesions in vivo. Techniques of ultrasound and arteriography associated with scanning following injection of various markers have not yet proved to be totally reliable for this purpose, and not at all for the assessment of endothelial lesions. This has prevented us from following the progression of lesions in individual patients, and has therefore precluded the effective assessment of potentially antiatherosclerotic agents. Consequently, efforts thus far toward the control of coronary atherosclerosis have been concentrated primarily on dietary or pharmacological intervention directed toward the elimination or reduction of the effect of one or more of the 246 known risk factors for coronary heart disease [138]. Efforts should also be directed toward the possibility of intervention at the local arterial level including prevention or reversal of initial endothelial cell damage, inhibition or retardation of the massive smooth muscle cell proliferation, and modification of mural lipoprotein transport. Success at the local arterial level is essential in order to mitigate or eliminate the need for drastic abstentions, deprivations and interventions which seriously affect the quality of our lives.

Notes

1. One lamellar unit consists of two smooth muscle cell layers divided by one layer of elastic membrane containing variable amounts of collagen, elastin, and glycosaminoglycans.

2. The contribution of the scanning electron microscope (SEM) to the study of atherogenesis is based upon its ability to detect endothelial damage over a large area of the luminal surface, permitting three-dimensional observation of surface alterations. Although the nondenuding, fine structural changes in the endothelium, such as the nonprotuding intracytoplasmic vacuoles or membranous whorls, may escape detection by the SEM, these alterations are usually associated with changes such as endothelial blebs and other protruding vacuoles which are detectable with scanning electron microscopy as craters and balloons [34]. Recent improvements in techniques of tissue preparation for SEM have greatly increased the reliability of this instrument for the identification of damage at the endothelial surface particularly when used with correlative light and transmission electron microscopy.

References

1. World Health Statistics Annual. Vol 1: Vital statistics and causes of death. Geneva: World Health Organization, 1977, pp 272–279; 1978, pp. 218–225; 1979, pp 134–141; 1980, pp 108–115.
2. Cooper R, Stamler L, Dyer A, Garside D: The decline in mortality from coronary heart disease, USA, 1968–1975. J Chronic Dis 31:709–720, 1978.
3. Stern MP: The recent decline in ischemic heart disease mortality. Ann Intern Med 91:630–640, 1979.
4. Stein O, Stein Y, Eisenberg S: Radioautographic study of the transport of ^{125}iodine-labeled serum lipoproteins in rat aorta. Z Zellforsch Mikrosk Anat 138:223–237, 1973.
5. Vlodaver Z, Edwards JE: Pathology of coronary atherosclerosis. Prog Cardiovasc Dis 14:256–274, 1971.
6. Wissler RW: Principles of the pathogenesis of atherosclerosis. In: Braunwald E (ed) Heart disease: a text book of cardiovascular medicine. Philadelphia: WB Saunders, 1980, pp 1221–1245.
7. Wall RT, Harker LA: The endothelium and thrombosis. Annu Rev Med 31:361–371, 1980.
8. Hoak JC, Czervionke RL, Fry GL, Haycraft DL, Brotherton AA: Role of the vascular endothelium. Philos Trans R Soc Lond [B] 294:331–338, 1981.
9. Ross R, Klebanoff SJ: The smooth muscle cell. I. In vivo synthesis of connective tissue proteins. J Cell Biol 50:159, 1971.
10. Wight TN, Ross R: Proteoglycans in primate arteries. II. Synthesis and secretion of glycosaminoglycans by arterial smooth muscle cells in culture. J Cell Biol 67:675–686, 1975.
11. Narayanan S, Sanberg LB, Ross R, Layman D: The smooth muscle cell. III. Elastin synthesis in arterial smooth muscle cell culture. J Cell Biol 68:411–419, 1976.
12. Wolinsky H, Glagov S: Comparison of abdominal and thoracic aortic medial structure in mammals: deviation of man from the usual pattern Circ Res 25:677–686, 1969.
13. Ross R, Glomset JA: The pathogenesis of atherosclerosis I. N Engl J Med 295:369–377, 1976.
14. Ross R, Glomset JA: The pathogenesis of atherosclerosis II. N Engl J Med 295:420–425, 1976.
15. Ross R: The arterial wall and atherosclerosis. Annu Rev Med 30:1–15, 1979.
16. Stemerman MB: Hemostasis, thrombosis and atherogenesis. Atheroscl Rev 6:105–146, 1979.
17. Oeser J, Fehr R, Brinkmann B: Aortic and coronary

atherosclerosis in a Hamburg autopsy series. Virch Arch [Pathol Anat] 384:131–148, 1979.
18. Bierman EL: Atherosclerosis and other forms of arteriosclerosis. In: Isselbacher KJ, Adams RD, Baunwald E, Petersdorf RG, Wilson D (eds) Harrison's principles of internal medicine, 9th edn. London: McGraw-Hill, 1980, pp 1156–1166.
19. Velican C, Velican D: Coronary intimal necrosis occurring as an early stage of atherosclerotic involvement. Atherosclerosis 39:479–496, 1981.
20. Flaherty JT, Ferrans VJ, Pierce JE, Carew TE, Fry DL: Localizing factors in experimental atherosclerosis. In: Likoff W, Segal BL, Insull W, Mayer JH (eds) Atherosclerosis and coronary heart disease. New York: Grune and Stratton, 1972, pp 40–84.
21. Werb Z, Gordon S: Elastase secretion by stimulated macrophages. J Exp Med 142:361–377, 1975.
22. Mendlowitz M: Arterial calcium metabolism, hypertension and arteriosclerosis. Cardiology 67:81–89, 1981.
23. Fowler S, Shiu H, Haley NJ: Characterization of lipid-laden aortic cells from cholesterol-fed rabbits. Lab Invest 41:372–378, 1979.
24. Smith EB, Smith RH: Early changes in the aortic intima. Atheroscl Rev 3:119–136, 1976.
25. Fox B, James K, Morgan B, Seed A: Distribution of fatty and fibrous plaques in young human coronary arteries. Atherosclerosis 41:337–347, 1982.
26. Texon M: Hemodynamic basis of atherosclerosis. New York: McGraw-Hill, 1970.
27. Wright HP: Endothelial turnover. Thromb Diath Haemorrh (Suppl) 40:79–85, 1970.
28. Spaet TH, Gaynor E: Vascular endothelial damage and thrombosis. Adv Cardiol 4:47–66, 1970.
29. Poole JCP, Sanders AG, Florey HW: The regeneration of aortic endothelium. J Pathol Bacteriol 175:133–143, 1958.
30. Baumgartner HR, Spaet TH: Endothelial replacement in rabbit arteries. Fed Proc 29:710, 1970.
31. Spaet TH, Stemerman MB, Lejnecks I: The role of smooth muscle cells in repopulation of rabbit aortic endothelium following balloon catheter injury. Fed Proc 32:219, 1973.
32. Fishman JA, Ryan GB, Karnovsky MJ: Endothelial regeneration in the rat carotid artery and the significance of endothelial denudation in the pathogenesis of myointimal thickening. Lab Invest 32:339–351, 1975.
33. Chiang J, Kowada M, Ames A III, Wright RL, Majno G: Cerebral ischemia. III. Vascular changes. Am J pathol 52:455–76, 1968.
34. Gertz SD, Forbes MS, Sunaga T, Kawamura J, Rennels ML, Shimamoto T, Nelson E: Ischemic carotid endothelium: transmission electron microscopic studies. Arch Pathol Lab Med 100:522–526, 1976.
35. Yu MC, Bakay L, Lee JC: Ultrastructure of the central nervous system after prolonged hypoxia. II. Neuroglia and blood vessels. Acta Neuropathol (Berl) 22:235–244, 1972.
36. Hoff HF: Vascular injury: a review. In: Koller F, Brinkhous KM, Biggs R, Rodman NF, Hinnom S (eds) Vascular factors and thrombosis. Stuttgart: FK Schattauer Verlag, 1970, pp 121–136.
37. Gardner DL, Mathews MA: Ultrastructure of the wall of small arteries in early experimental rat hypertension. J Pathol 97:51–62, 1969.
38. Kjeldson K, Astrup P, Wanstrup J: Ultrastructural intimal changes in the rabbit aorta after a moderate carbon monoxide exposure. Atherosclerosis 16:67–87, 1972.
39. Constantinides P: The important role of endothelial changes in atherogenesis. In: Shimamoto T, Numano F (eds) Atherogenesis II. Amsterdam: Excerpta Medica 1973, pp 51–65.
40. Gertz SD, Kurgan A, Wajnberg RS, Nelson E: Endothelial cell damage and thrombus formation following temporary arterial occlusion: effects of pretreatment with aspirin or heparin. J Neurosurg 50:578–586, 1979.
41. Harker L, Ross R, Slichter S: Homocystine-induced arteriosclerosis: the role of endothelial injury and platelet response in its genesis. J Clin Invest 58:731–741, 1976.
42. Gaynor E, Bouvier CA, Spaet TH: Vascular lesions: possible pathogenetic bases of the generalized Schwartzman reaction. Science 170:986–988, 1970.
43. Poston RN: Immunological aspects of atheroma: a review. R Soc Med 72:674–681, 1979.
44. Ross R, Harker L: Hyperlipidemia and atherosclerosis. Science 193:1094–1100, 1976.
45. Stewart GJ, Ritchie WGM, Lynch PR: Venous endothelial damage produced by massive sticking and emigration of leukocytes. Am J Pathol 74:507–522, 1974.
46. Marchesi VT: Some electron microscopic observations on interactions between leukocytes, platelets and endothelial cells in acute inflammation. Ann NY Acad Sci 116:174–488, 1964.
47. Joris I, Majno G: Endothelial changes induced by arterial spasm. Am J Pathol 102:346–358, 1981.
48. Gertz SD, Uretzky G, Wajnberg RS, Navot N, Gotsman MS: Endothelial cell damage and thrombus formation after partial arterial constriction: relevance to the role of coronary artery spasm in the pathogenesis of myocardial infarction. Circulation 63:476–486, 1981.
49. Karnovsky MJ: Endothelial–vascular smooth muscle cell interactions. Am J Pathol 105:200–206, 1981.
50. Bratzler RL, Chisolm GM, Colton CK, Smith KA, Lees RS: The distribution of labeled-low-density lipoprotein across the rabbit thoracic aortic in vivo. Atherosclerosis 25:289–307, 1977.
51. Leibowitz JO: The history of coronary heart disease. Berkeley: University of California, 1970.
52. Von Rokitansky C: A manual of pathological anatomy (trans GE Day). London: New Sydenham Society, 1852.
53. Duguid JB: Thrombosis as a factor in the pathogenesis of aortic atherosclerosis. J Pathol Bacteriol 60:57–61, 1948.

54. Duguid JB: Mural thrombosis in arteries. Br Med Bull 2:36–38, 1955.
55. Virchow R: Phlogose und Thrombose im Gefässsystem. In: Gesammelte Abhandlungen zur wissenschaftlichen Medizin. Frankfurt-am-Main: Meidinger, 1856.
56. Virchow R: Gesammelte Abhandlungen zur wissenschaftlichen Medizin: Phlogose und Thrombose im Gefasssystem. Berlin: Max Hirsch, 1862.
57. Anitschkow NN: Über Veranderungen der Kaninchenaorta bei experimentelle Cholesterinsteatose. Beitr Pathol Anat 56:379–404, 1913.
58. Anitschkow NN: A history of experimentation on arterial atherosclerosis in animals. In: Blumenthal HT (ed) Cowdry's arteriosclerosis. 2nd edn. Springfield IL: CC Thomas, 1967, pp 21–44.
59. Miller NE: Plasma lipoproteins, lipid transport, and atherosclerosis: recent developments. J Clin Pathol 32:639–650, 1979.
60. Asmal AC, Leary WP: Classification of hyperlipidaemias: a time for review? South Afr Med J 50:915–918, 1975.
61. Brown MS, Goldstein JL: The hyperlipoproteinemias and other disorders of lipid metablism. In: Isselbacher KJ, Adams RD, Braunwald E, Petersdorf RG, Wilson JD (eds) Harrison's principles of internal medicine. London: McGraw-Hill, 1980, pp 507–518.
62. Wolinsky H: A proposal linking clearance of circulating lipoproteins to tissue metabolic activity as a basis for understanding atherogenesis. Circ Res 47:301–311, 1980.
63. Haimovici H: Atherogenesis: recent biological concepts and clinical implications. Am J Surg 134:174–178, 1977.
64. Dolder MA, Oliver MF: Myocardial infarction in young men: study of risk factors in nine countries. Br Heart J 37:493–503, 1975.
65. Hoff HF, Heideman CL, Jackson RL, Bayardo RJ, Kim H, Gotto AM Jr: Localization patterns of plasma apolipoproteins in human atherosclerotic lesions. Circ Res 37:72–79, 1975.
66. Onitini AC, Lewis B, Bentall H, Jamieson C, Wisheart J, Faris I: Lipoprotein concentrations in serum and in biopsy samples of arterial intima: a quantitative comparison. Atherosclerosis 23:513–519, 1976.
67. Castelli, WP, Doyle JT, Gordon T, Hames CG, Hjortland MC, Hulley SB, Kagan A, Zukel WJ: HDL, cholesterol and other lipids in coronary heart disease: the co-operative lipoprotein phenotyping study. Circulation 55:767–72, 1977.
68. Fredrickson DS, Goldstein JL, Brown MS: The familial hyperlipoproteinemias. In: Stanbury JB, Wyngaarden JB, Fredrickson DS (eds) The metabolic basis of inherited disease, 4th edn. New York: McGraw-Hill, 1978, pp 604–655.
69. Stamler J: Life styles, major risk factors, proof and public policy. Circulation 58:3–19, 1978.
70. Scott RF, Daoud AS, Florentin RA: Animal models in atherosclerosis. In: Wissler RW, Geer JC (eds) The pathogenesis of atherosclerosis. Baltimore: Williams and Wilkins, 1972, pp 120–146.
71. Hoff HF, Heideman CL, Gaubatz JW, Titus JC, Gotto AM Jr: Quantitation of apo-B in human aortic fatty streaks: a comparison with grossly normal intima and fibrous plaques. Atherosclerosis 30:263–272, 1978.
72. Zilversmit DB: Atherogenesis: a postprandial phenomenon. Circulation 60:473–485, 1979.
73. Steinberg D: Underlying mechanisms in atherosclerosis. J Pathol 133:75–87, 1981.
74. Miller GJ: High density lipoproteins and atherosclerosis. Annu Rev Med 31:97–108, 1980.
75. Stehbens WE: The role of lipid in the pathogenesis of atherosclerosis. Lancet 1:724–726, 1975.
76. Thoma R: Uber die Abhangigkeit der Hindegewebsneubildung in der Arterienintima von den mechanischen Bendingungen des Blutumlaufes. Virchows Arch [Pathol Anat] 93:443–505, 1883.
77. Blumenthal HT, Lansing AL, Wheeler PA: Calcification of the media of the human aorta and its relation to intimal arteriosclerosis, aging and disease. Am J Pathol 20:665–679, 1944.
78. Walton KW: Pathogenetic mechanisms in atherosclerosis. Am J Cardiol 35:542–558, 1975.
79. Martin GM, Sprague CA: Symposium on in vitro studies related to atherogenesis: life histories of hyperplastoid cell lines from aorta and skin. Exp Mol Pathol 18:125–141, 1973.
80. Benditt EP, Benditt JM: Evidence for a monoclonal origin of human atherosclerotic plaques. Proc Natl Acad Sci USA 70:1753–1756, 1973.
81. Benditt EP: The monoclonal theory of atherogenesis. Atheroscl Rev 3:77–85, 1978.
82. Fialkow PJ: The origin and development of human tumors studied with cell markers. N Engl J Med 291:26–35, 1974.
83. Kosek JC, Bieber C, Lower RR: Heart graft arteriosclerosis. Transplant Proc 3:512–514, 1971.
84. Svendsen UG: The importance of thymus in the pathogenesis of the chronic phase of hypertension in mice following partial infarction of the kidney. Acta Pathol Microbiol Scand [A] 85:539–547, 1977.
85. Cochrane CG, Koffler D: Immune complex disease in experimental animals and man. Adv Immunol 16:185–264, 1973.
86. Kniker WT, Cochrane CG: Pathogenetic factors in vascular lesions of experimental serum sickness. J Exp Med 122:83–97, 1965.
87. Minick CR, Murphy GE, Campbell WG: Experimental induction of atheroarteriosclerosis by the synergy of allergic damage to arteries and a lipid rich diet. J Exp Med 124:635–652, 1966.
88. Howard AN, Patelski J, Bowyer DE, Gresham GA: Atherosclerosis induced in hypercholesterolaemic baboons by immunological injury and the effects of intravenous polyunsaturated phosphatidyl choline. Atherosclerosis 14:17–29, 1971.
89. Pfueller SL, Lüscher EF: The effects of aggregated immunoglobulins on human blood platelets in re-

lation to their complement fixing abilities. J Immunol 109:517–533, 1972.
90. Beaumont JL, Beaumont V: Autoimmune hyperlipidemia. Atherosclerosis 26:405–418, 1977.
91. Guyton JR, Karnovsky MJ: Smooth muscle cell proliferation in the occluded rat carotid artery: lack of requirement for luminal platelets. Am J Pathol 94:585–596, 1979.
92. Moore S, Friedman RJ, Singal DP, Gauldie J, Blajchman MA, Roberts RS: Inhibition of injury induced thromboatherosclerotic lesions by antiplatelet serum in rabbits. Thromb Haemost 35:70–81, 1976.
93. Fuster V, Bowie EJW, Lewis JC, Fass DN, Owen Ca Jr, Brown AL: Resistance to arteriosclerosis in pigs with von Willebrand's disease. J Clin Invest 61:722–730, 1978.
94. Griggs TR, Reddick RL, Sultzer D, Brinkhous KM: Susceptibility to atherosclerosis in aortas and coronary arteries of swine with von Willebrand's disease. Am J Pathol 102:137–145, 1981.
95. Fass DN, Dawning MR, Meyers P, Bowie EJ, Witte LD: Cell growth stimulation by normal and von Willebrand's porcine platelets and endothelial cells [abstr]. Blood (Suppl 1) 52:181, 1978.
96. Gajdusek C, Schwartz S, Di Corleto Ross R: Endothelial cell derived mitogenic activity. Fed Proc 38:1075, 1979.
97. Leibovich S, Ross R: A macrophage-dependent factor that stimulates the proliferation of fibroblasts in vitro. Am J Pathol 84:501–514, 1976.
98. Moncada S, Gryglewski R, Bunting SL, Vane JR: An enzyme isolated from arteries transforms prostaglandin endoperoxides to an unstable substance that inhibits platelet aggregation. Nature 163:663–665, 1976.
99. Mustard JF, Kinlough-Rathbone RL, Packham MA: Prostaglandins and platelets. Annu Rev Med 31:89–96, 1980.
100. Weis HJ: Antiplatelet therapy. N Engl J Med 298:1344–1347, 1978.
101. Weiss HJ: Antiplatelet therapy. N Engl J Med 298:1403–1406, 1978.
102. Carvalho ACA, Colman RW, Lees RS: Platelet function in hyperlipoproteinemia. N Engl J Med 290:434–438, 1974.
103. Yamazaki H, Sano T, Kobayashi I, Takahashi T, Shimamoto T: Enhancement of ADP-induced platelet aggregation by adrenaline and cholesterol in vivo and its prevention. In: Shimamoto T, Numano F (eds) Atherogenesis II. Amsterdam: Excerpta Medica, 1973, pp 177–194.
104. Iacono JM, Binder RA, Marshall MW, Shoene NW, Jencks JA, Mackin JF: Decreased susceptibility to thrombin and collagen platelet aggregation in man fed low fat diet. Haemostasis 3:306–318, 1975.
105. Moore S: Endothelial injury and atherosclerosis. Exp Mol Pathol 31:182–190, 1979.
106. Hirsch EZ, Robertson AL: Selective acute arterial endothelial injury and repair. I. Methodology and surface characteristics. Atherosclerosis 28:271–287, 1977.
107. Reidy MA, Schwartz SM: Endothelial regenerating. III. Time course of intimal changes after small defined injury to rat aortic endothelium. Lab Invest 44:301–308, 1981.
108. Fry DL: Hemodynamic forces in atherogenesis. In: Scheinberg P (ed) Cerebrovascular diseases. New York: Raven, 1976, pp 77–95.
109. Caplan BA, Schwartz CJ: Increased endothelial cell turn-over in areas of in vivo Evans blue uptake in the pig aorta. Atherosclerosis 17:401–417, 1973.
110. Langille BL, Adamson SL: Relationship between blood flow direction and endothelial cell orientation at arterial branch sites in rabbits and mice. Circ Res 48:481–488, 1981.
111. Nelson E, Gertz SD, Forbes MS, Rennels ML, Heald FD, Khan MA, Farber TM, Miller E, Husain MM, Earl FL: Endothelial lesions in the aorta of egg yolk-fed miniature swine: a study by scanning and transmission electron microscopy. Exp Mol pathol 25:208–220, 1976.
112. Lewis JC, Kottke BA: Endothelial damage and thrombocyte adhesion in pigeon atherosclerosis. Science 196:1007–1009, 1977.
113. Geissinger HD, Mustard JF, Rowsell HC: The occurrence of microthrombi on the aortic endothelium of swine. Can Med Assoc J 87:405–408, 1962.
114. Gerrity RG, Naito HK, Richardson M, Schwartz CJ: Dietary induced atherogenesis in swine: morphology of the intima in prelesion stage. Am J Pathol 95:775–786, 1979.
115. Fry DL: Acute vascular endothelial changes associated with increased blood velocity gradients. Circ Res 22:165–197, 1968.
116. Veress B, Balint A, Kocze A, Nasy Z, Jellinek H: Increasing aortic permeability by atherogenic diet. Atherosclerosis 11:369–371, 1970.
117. Bretherton KN, Day AJ, Skinner SL: Effect of hypertension on the entry of ^{125}I-labeled low density lipoprotein into the aortic intimal in normal-fed rabbits. Atherosclerosis 24:99–106, 1976.
118. Schwartz SM: Hypertension, endothelial injury and atherosclerosis. Cardiovasc Med 2:991–1002, 1977.
119. Wexler BC, Iams SG, Judd JT: Arterial lesions in repeatedly bred spontaneously hypertensive rats. Circ Res 38:494–501, 1976.
120. Haudenschild CC, Prescott MF, Chobanian AV: Effects of hypertension and its reversal on aortic intima lesions of the rat. Hypertension 2:33–44, 1980.
121. Giacomelli F, Weiner J, Spiro D: The cellular pathology of experimental hypertension. V. Increased permeability of cerebral arterial vessels. Am J Pathol 59:133–160, 1970.
122. Huttner I, Boutet M, More RH: Studies on protein passage through arterial endothelium. III. Effect of blood pressure levels on the passage of fine struc-

tural protein tracers through rat arterial endothelium. Lab Invest 29:536–546, 1973.
123. Bevan RD: An autoradiographic and pathological study of cellular proliferation in rabbit arteries correlated with an increase in arterial pressure. Blood Vessels 13:100–128, 1976.
124. Dhurandhar RW, Watt DL, Silver MD, Trimble AS, Adelman AG: Prinzmetal's variant form of angina with arteriographic evidence of coronary spasm. Am J Cardiol 30:902–905, 1972.
125. Chahine RA, Luchi RJ: Coronary arterial spasm: culprit on bystander? Am J Cardiol 37:936–937, 1976.
126. Meller J, Pichard A, Dack S: Coronary arterial spasm in prinzmetal's variant angina: a proved hypothesis. Am J Cardiol 37:938–940, 1976.
127. Maseri A, l'Abbate A, Baroldi G, Chierchia S, Marzilli M, Ballestra AM, Severi S, Parodi O, Biagini A, Distante A, Pesola A: Coronary vasospasm as a possible cause of myocardial infarction. N Engl J Med 299:1271–1277, 1978.
128. Braunwald E: Coronary artery spasm as a cause of myocardial ischemia. J Lab Clin Med 97:299–312, 1981.
129. Hellstrom HR: The injury-spasm and vascular autoregulatory hypothesis of ischemic disease. Am J Cardiol 49:802–810, 1982.
130. Folts JD, Crowell EB, Rowe GG: Platelet aggregation in partially obstructed vessels and its elimination with aspirin. Circulation 54:365–370, 1976.
131. Turitto VT, Baumgartner HR: Platelet interaction with subendothelium in flowing rabbit blood: effect of blood shear rate. Microvasc Res 17:38–54, 1979.
132. Gutstein WH, Lataillade JN, Lewis L: Role of vasoconstriction in experimental arteriosclerosis. Circ Res 10:925–932, 1962.
133. Betz E, Schlote W: Responses of vessel walls to chronically applied electrical stimuli. Basic Res Cardiol 74:10–20, 1979.
134. Lown B, De Silva RA: Is coronary arterial spasm a risk factor for coronary atherosclerosis. Am J Cardiol 45:901–903, 1980.
135. Marzilli M, Goldstein S, Trivella MG, Palumbo C, Maseri A: Some clinical considerations regarding the relation of coronary vasospasm to coronary atherosclerosis: a hypothetical pathogenesis. Am J Cardiol 45:882–886, 1980.
136. Gutstein WH: Coronary spasm and coronary atherosclerosis. Am J Cardiol 48:389–390, 1981.
137. Luchi RJ, Chahine RA: Coronary artery spasm, coronary artery thrombosis, and myocardiol infarction. Ann Intern Med 95:502–505, 1981.
138. Hopkins PN, Williams RR: A survey of 246 suggested coronary risk factors. Atherosclerosis 40:1–52, 1981.

34. ELECTROPHYSIOLOGY OF VASCULAR SMOOTH MUSCLE

Nicholas Sperelakis

Introduction

This chapter provides an overview of the electrophysiology of vascular smooth muscle, and of how the actions of some vasoactive substances are mediated by changes in electrical properties of the cell membrane. Emphasis is given to the role of Ca^{2+} ion and to the action of inhibitor drugs.

Compared to skeletal muscle or cardiac muscle, less is known about the electrical properties of vascular smooth muscle (VSM), because of the difficulty of making satisfactory microelectrode impalements in the very small smooth muscle cells and because of the tough connective tissue that is often present. However, considerable progress has been made during the past few years. For the sake of convenience, I will draw heavily upon the work done in my own laboratory, even though many of the facts and principles concerning VSM resulted from the efforts of numerous other investigators. To attempt to give proper credit to all these published studies would make this chapter unwieldy.

Vascular smooth muscle consists of an assembly of short (e.g., 200 μm in length) and thin (e.g., 5 μm in diameter) cells. Contiguous cells often come into close contact, forming various types of specialized junctions. The degree of low-resistance electrical coupling between the VSM cells is uncertain and controversial. Some investigators who conclude that low-resistance connections exist in one vessel conclude that they may not exist in another vessel [1]. Motor nerves of the autonomic nervous system innervate the muscle cells and exercise some control over their state of contraction. The neurons release neurotransmitters, such as norepinephrine and acetylcholine, at periodic neuron varicosities distributed along the length of the blood vessels. The nerve fibers are generally confined to the border between the outer adventitia layer and the media (muscle) layer. Thus, many VSM cells become influenced by neurotransmitter secreted at a relatively distant point, i.e., there usually are no close neuromuscular junctions as found in skeletal muscle.

The neurotransmitters, some vasoactive hormones and autacoids, and some vasoactive drugs appear to exert their primary effect on the electrical properties of the cell membrane of the VSM cells. Changes in the level of the "resting" membrane potential control the level of contraction of the VSM cells, depolarization increasing the state of contraction and hyperpolarization diminishing the state of contraction (i.e., producing relaxation). Changes in the conductance of the cell membrane for certain ions, e.g., Ca^{2+}, have profound effects on the degree of contraction.

The Ca^{2+} necessary for raising the myoplasmic Ca^{2+} to activate the contractile myofilaments (e.g., elevating free $[Ca]_i$ $<10^{-7}$ *M* to $>10^{-5}$ *M*) may come from two sources: (a) Ca^{2+} influx across the surface membrane, and (b) Ca^{2+} release from some internal store, such as the sarcoplasmic reticulum (SR), brought about by the Ca^{2+} influx and/or a change in potential across the SR membrane. Some vasoactive substances may exert a primary or secondary effect to facilitate or depress Ca^{2+} re-

N. Sperelakis (ed.), PHYSIOLOGY AND PATHOPHYSIOLOGY OF THE HEART.

Martinus Nijhoff Publishing, Boston/The Hague/ Dordrecht/Lancaster.

lease from the SR. Some vasoactive agents produce contraction without an associated change in membrane potential, termed pharmacomechanical coupling, but often changes in membrane conductance can be detected [2, 3].

It is often mentioned that there are two general categories of VSM: those that generate action potentials in vitro (*spiking* VSM) and those that normally do not fire action potentials in vitro (*nonspiking* VSM) [4–6]. The spikes, when they occur, bring about contraction or increase the state of contraction. An example of spiking VSM is the rat portal vein, while examples of nonspiking muscle are some of the large arteries in rabbit [4, 7]. However, some of the nonspiking VSM in vitro (and electrically inexcitable) may actually fire spikes in situ in response to summated excitatory junction potentials (EJPs) [8]. In addition, the nonspiking VSM can be made to spike in vitro by simply lowering the K^+ conductance with Ba^{2+} or tetraethylammonium (TEA^+) [3, 9]. This means that the membrane possesses a full complement of voltage-dependent slow channels for inward current and is capable of regenerative excitation.

VSM cells have relatively low resting potentials (of about -55 mV), due to a low K^+ permeability (P_K), although in some vessels the resting potentials are often greater than -70 mV. The VSM cells are capable of exhibiting automaticity, at least under certain experimental conditions. An inward slow current (I_{si}), carried almost exclusively by Ca^{2+} ion in many types of VSM cells, is responsible for the depolarizing phase of the spikes. There appear to be no functional fast Na^+ channels and inward fast Na^+ current. Therefore, agents like tetrodotoxin (TTX) that block fast Na^+ channels have no effect on the VSM spikes, whereas agents like verapamil that block slow channels depress and block the VSM spikes.

For a detailed description of the electrical properties of VSM and electromechanical and pharmacomechanical coupling, the reader is referred to a number of reviews, including those by Kumamoto [10], Horn [11], Johansson [7], Bolton [12], and Johansson and Somlyo [13].

Electrical Properties of Vascular Smooth Muscles

RESTING MEMBRANE POTENTIALS

In general, the basic electrical properties of VSM cells, such as resting potentials and action

TABLE 34–1. Summary of some electrical properties of the resting membrane in arterial smooth muscle

	Condition	Resting E_m (mV)	Input resistance r_{in} (MΩ)	P_{Na}/P_K Ratio
A.	Guinea pig superior mesenteric artery			
	Control ringer	-54 ± 0.6	8.5 ± 0.3	—
	Ouabain (10^{-5} *M*)†	-46 ± 1.0*	—	0.17
	Cl^--free solution	-55 ± 0.6	8.5 ± 0.4	—
	Ba^{2+} (1.0 m*M*)	-24 ± 0.8*	24.0 ± 1.8*	0.42
	Low Na^+ solution	-66 ± 1.3*	—	—
B.	Dog coronary arteries			
	Large diameter	-56 ± 2	9.0 ± 0.4	—
	Small diameter	-53 ± 2	10.0 ± 1.0	—
	Small diameter	-55 ± 1.0; -54 ± 1.3	—	—

Values given are the mean ± 1 SE.

*Significantly different from control value at $P < 0.05$.

The small coronary arteries were intramural and less than 0.5 mm in diameter; the large coronary arteries were extramural and more than 1.0 mm in diameter. Measurements of E_m were made after only 1–5 min exposure to ouabain, so that depolarization due to ion shifts (i.e., rundown of the ionic gradients) did not occur. Value listed is for a $[K]_0$ of 4.0 m*M*. Data taken from Harder and Sperelakis [14], Harder et al. [15], and Belardinelli et al. [16].

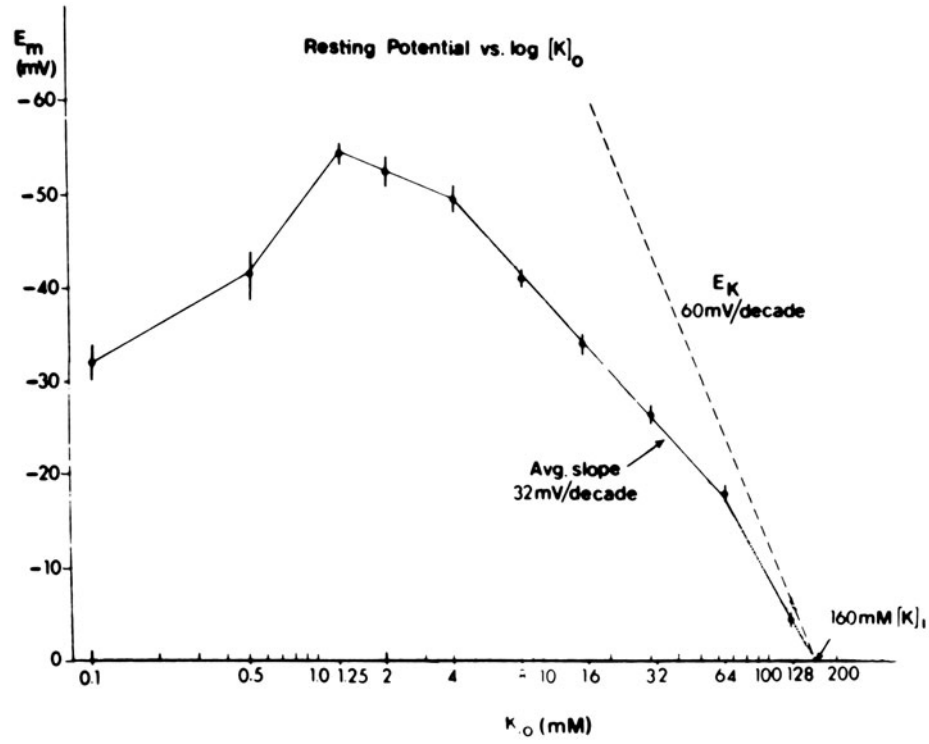

FIGURE 34–1. Resting potential (E_m) as a function of external K^+ concentration, $[K]_o$ (log scale) for vascular smooth muscle of guinea pig superior mesenteric artery. The vertical bars represent the mean ± 1 SEM for 10–23 impalements in 4–6 muscles. The curve extrapolated to zero potential gives an estimated internal K^+ concentration, $[K]_i$, of 160 m*M*. The broken line gives the K^+ equilibrium potential (E_K) as calculated from the Nernst equation and has a slope of 60 mV/tenfold change in $[K]_o$. From Harder and Sperelakis [14].

potential (AP) characteristics, are similar to those in other types of smooth muscle, for example, circular intestinal muscle.

The resting membrane potential of vascular smooth muscles (VSM) is usually about −55 mV. For example, Harder and Sperelakis [14] found a mean resting potential (E_m) in guinea pig superior mesenteric artery of −54 ± 0.6 mV (table 34–1A). The mean resting potential for the small coronary arteries of the dog was −54 ± 1.0 mV and that for the large coronary arteries was −56 ± 2 mV (table 34–1B) [15, 16].

There is a small contribution of the electrogenic pump potential to the resting E_m in VSM cells. For example, Harder and Sperelakis [14] found a contribution of about 8 mV in guinea pig superior mesenteric artery; that is, the resting E_m rapidly decreased from a control value of −54 mV to −46 mV when ouabain (10^{-5} *M*) was added to inhibit the (Na,K)-ATPase and thus stop the Na-K pump (table 34–1A). Thus −46 mV represents the net diffusion potential (E_{diff}) that reflects the ionic distributions and the relative ionic conductances (for a discussion of this, see Sperelakis [17]). The electrogenic pump potential (V_{ep}) is in parallel with E_{diff}, so that removal of V_{ep} (i.e., −54 mV) permits the measurement of E_{diff} (namely, −46 mV) (see fig. 34–18).

The P_{Na}/P_K ratio can be calculated from E_{diff} using the Goldman constant-field equation, adopting values for $[Na]_i$ and $[K]_i$ and assuming that Cl^- is passively distributed. The value of $[K]_i$ can be estimated by running a complete curve of E_m vs log $[K]_o$ and extrapolating to zero potential (fig. 34–1). By this method, a

value of 160 m*M* was obtained for $[K]_i$ in guinea pig superior mesenteric artery, and a P_{Na}/P_K ratio of 0.17 was calculated (in 4 m*M* $[K]_o$) [14]. This ratio is considerably higher than that found for skeletal muscle or cardiac muscle. The ratio is high because of a low P_K and not because of a high P_{Na}.

In guinea pig superior mesenteric artery, Cl^- ions appear to be passively distributed, i.e., Cl^- distributes itself in accordance with the average membrane potential [14]. This means that, for a membrane at rest for a long period, the Cl^- equilibrium potential (E_{Cl}), calculated from the Nernst equation, equals the resting E_m. The evidence for passive Cl^- distribution is based on the fact that the resting E_m upon equilibration in Cl^--free Ringer solution was nearly exactly equal to that in Ringer solution in the presence of Cl^- (table 34–1A); that is, following a transient depolarization that is expected to occur during Cl^- washout from the cells, the potential returns to the original value within 10 min. If $[Cl]_i$ was higher than that predicted from the resting E_m (due to an inwardly directed Cl^- pump), then hyperpolarization should have been observed after equilibration in Cl^--free solution. The fact that the input resistance (r_{in}) in Cl^--free solution was about the same as that in the presence of Cl^- (table 34–1A) suggests that the Cl^- conductance (g_{Cl}) is relatively low in this muscle. This conclusion is also supported by the fact that Ba^{2+} ion (1 m*M*), a relatively specific depressant of K^+ conductance (g_K), rapidly produced a large depolarization in normal Cl^--containing Ringer solution (table 34–1A). When g_{Cl} is high, Ba^{2+} has relatively little effect [18]. Hence, there is no evidence for a Cl^- pump in this tissue.

In low-Na^+ solution, the membrane should become hyperpolarized, as expected because of the removal of much of the depolarizing Na^+ influx. Under such conditions, guinea-pig superior mesenteric artery cells became hyperpolarized by about 12 mV, from the control of -54 mV to a value of -66 mV in low-Na^+ solution (table 34–1A).

The input resistance (r_{in}), that is, the resistance that the impaled microelectrode "looks into," may be calculated from the slope of the steady-state voltage–current curve through the origin (i.e., at infinitesimally small applied current). Depolarizing and hyperpolarizing current pulses are applied through the voltage-recording microelectrode by means of a balanced bridge circuit [19] or by a second independent voltage-recording microelectrode impaled very close to the current-injecting microelectrode in the same cell. r_{in} generally ranges between 5 and 15 MΩ for VSM. For example, the average value was 8.5 MΩ in guinea pig superior mesenteric artery (table 34–1A), and 9 and 10 MΩ, respectively, in large and small coronary arteries of the dog (table 34–1B). Assuming a cell length (L) of 200 μm and a radius (*a*) of 2.5 μm, and assuming no low-resistance coupling between cells, an r_{in} of 9 MΩ gives a membrane resistivity (R_m) of 283 Ω cm^2 ($R_m = r_{in} \times \pi 2aL$). This value would be underestimated if the cells are connected by low-resistance pathways. Addition of Ba^{2+} ion (0.5 or 1.0 m*M*), a blocker of K^+ conductance, greatly increases r_{in}.

The degree of low-resistance coupling between VSM cells is not really known and the interpretations are controversial. Since much of the basic data obtained in electrical coupling studies in smooth muscle are similar to those in cardiac muscle, the reader is referred to a review article by Sperelakis [20] that summarized many of the facts and arguments for cardiac muscle. Mekata [1] recently reported that r_{in} (measured from polarizing current pulses of 0.5 nA or less injected through the voltage-recording microelectrode by means of a bridge circuit) of the circumflex coronary artery of the dog varied over a wide range of 10–400 MΩ (mean of 181 MΩ). Since he could not measure any electrotonic potential beyond 0.4 mm, when external polarizing current pulses were applied by a partitioned-chamber method of Tomita [21], Mekata concluded that low-resistance coupling between VSM cells must be poor in this vessel. In contrast, Mekata concluded that the cells in the anterior descending coronary artery were well coupled (length constant of 2.44 mm).

It was reported by Harder [22] that the slope of the curve of E_m vs log $[K]_o$ was much higher (58 mV/decade) in the middle cerebral

artery of the cat than that in the cat mesenteric artery (36 mV/decade) or guinea pig superior mesenteric artery (32 mV/decade) (fig. 34–1); that is, the VSM cell membrane in the cerebral artery was more K^+ selective (lower P_{Na}/P_K ratio). This property would make the membrane potential more sensitive to changes in $[K]_0$.

Depolarization produced in low $[K]_0$ (<1.25 m*M*) (fig. 34–1) may be due to two factors: (a) inhibition of the electrogenic Na-K pump, and (b) a reduction in g_K (and P_K). After a period in low $[K]_0$ (or K^+-free solution), elevation of $[K]_0$ back to the normal level (e.g., 4m*M*) causes a pronounced hyperpolarization that "overshoots" the normal resting E_m; this is thought to be due to great stimulation of the electrogenic pump due to the preceding Na^+ loading (i.e., increase in $[Na]_i$) [23, 24]. This K^+-induced hyperpolarization is associated with relaxation of the VSM. Webb and Bohr [25, 26] reported that the K^+-induced relaxation was greater in VSM from spontaneously hypertensive rats (SHR) than in normotensive rats. This finding was consistent with the results of Bonaccorsi et al. [23], who found that the contribution of the electrogenic pump potential to the resting E_m was greater in the SHR animals.

Development of tension in VSM is closely associated with changes in E_m; for example, this is well known for K^+ contractures. In addition, the amplitude of the norepinephrine-induced contraction is altered by changes in the resting E_m level, e.g., depolarization by a few millivolts greatly increases tension development [27, 28]. Hyperpolarization has the opposite effect, decreasing the contractile response to norepinephrine [28]; nitroprusside-induced hyperpolarization reduces the tension developed by K^+ and by norepinephrine [29].

In some experiments, the norepinephrine-induced contractions occurred without depolarization at low doses (10^{-9}–10^{-7} *M*) and with depolarization at high doses (10^{-6}–10^{-5} *M*) [3, 27, 30, 31], but, in other cases, 10^{-8} *M* norepinephrine (10^{-9} *M* in SHR animals) produced significant depolarization with the contraction in rat pulmonary artery. However, norepinephrine brings about additional tension in arteries that are already maximally depolarized by K^+ [2, 4, 28] perhaps by releasing Ca^{2+} sequestered in the SR.

EXCITED MEMBRANE PROPERTIES

Inexcitability of Some VSM Preparations In Vitro. The VSM cells in some isolated arterial strip preparations are often inexcitable by electrical stimulation for unknown reasons. There are some exceptions to this, including cultured rat aortic VSM cells (see below). Venous VSM cells are usually excitable in isolated preparations, and may even be spontaneously active. Mesenteric arteries of guinea pig also can exhibit spontaneous electrical activity under appropriate conditions of temperature and pressure [32]. The arterial VSM cells that are electrically inexcitable in vitro probably fire action potentials in situ, in response to summated EJPs following neurotransmitter release.

Induction of Excitability by TEA or Ba^{2+} Ion. Exposure of the isolated arterial VSM to agents that depress K^+ conductance (g_K) at rest and during excitation, such as Ba^{2+} ion (fig. 34–2A and B) and tetraethylammonium ion (TEA^+) (fig. 34–2C and D), induce electrical excitability. These agents allow large overshooting APs to be elicited by electrical stimulation (fig. 34–2D) and sometimes spontaneous discharge also occurs (fig. 34–2B). Inhibition of g_K suppresses the outward K^+ current, which should permit a greater net inward current and thus facilitate regenerative excitation; that is, for a given amount of inward current (through voltage-dependent slow channels), a decrease in the simultaneous K^+ outward current gives a greater net inward current. A minimum net inward current is required before a regenerative AP can occur. Ba^{2+} and TEA^+ not only depress the resting g_K but also slow the kinetics of g_K turn-on during depolarization, thus allowing the inward slow current (I_{si}) to predominate. The lack of electrical excitability in vitro in normal Ringer solution may be due to one or more factors, such as: (a) too early a turn-on of g_K, (b) lack of anomalous rectification (i.e., instantaneous decrease in g_K with depolarization), (c) inactivation of some of the slow channels causing in-

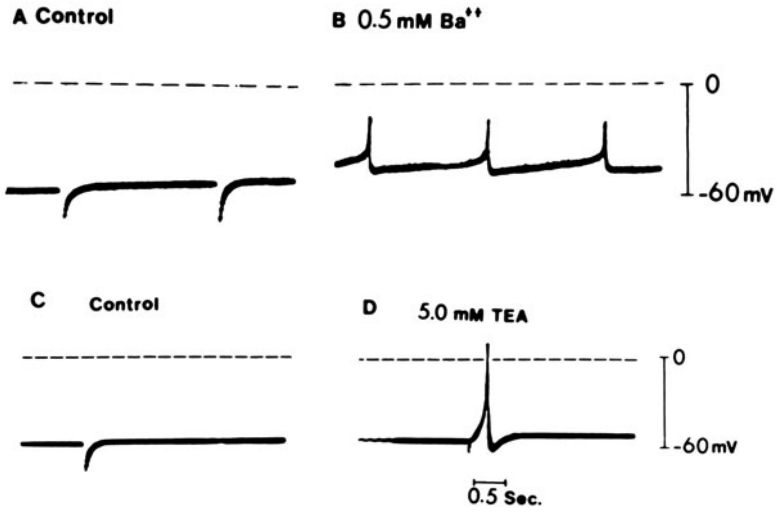

FIGURE 34–2. Induction of excitability by Ba^{2+} *(A* and *B)* and by tetraethylammonium ion (TEA^+) in guinea pig superior mesenteric artery muscle. *(A)* Control showing a large resting potential of about −55 mV and lack of spontaneous action potentials (APs) or responses to external electrical stimulation (two shock artifacts shown). *(B)* Record taken from same cell 5 min after the addition of 0.5 m*M* Ba^{2+}, illustrating the partial depolarization and production of spontaneous APs. *(C)* Control showing a large resting potential of about −58 mV and lack of spontaneous APs or responses to intense external electrical stimulation (one shock artifact depicted). *(D)* Record taken from the same cell 5 min after the addition of 5 m*M* TEA^+, illustrating a large overshooting AP produced in response to electrical stimulation. Modified from Harder and Sperelakis [9].

sufficient I_{si}, or (d) an increase in g_{Cl} (which tends to clamp or hold the E_m at E_{Cl}.

TEA has been shown to induce spikes in common carotid artery of the rabbit [33], the rabbit saphenous artery [34], and low doses of TEA allow norepinephrine to induce spike activity [35]. Droogmans et al. [3] showed that the spontaneous APs induced by TEA in rabbit ear artery were Ca^{2+} dependent. Hence, the TEA-induced APs in arterial smooth muscle should provide a useful assay system for the effect of various vasoactive substances on the inward Ca^{2+} current (Ca^{2+} influx) of VSM cells.

When APs are induced by agents like TEA^+, their maximal rate of rise ($+\dot{V}_{max}$) varies from 2 to 12 V/s. For example, in guinea pig superior mesenteric artery [9], the average $+\dot{V}_{max}$ (in 1.8 m*M* Ca^{2+}) was 6 ± 0.7 V/s (table 34–2). The AP duration (measured at 50% repolarization) was 50–75 ms. The average amplitude of these spikes was 59 mV, i.e., there usually was a small overshoot of about 5 mV (table 34–2). However, in some conditions, the APs undershoot to various degrees, i.e., their peak does not reach the zero potential level. This may be due to a premature increase in g_K.

The $+\dot{V}_{max}$ increases only slightly with hyperpolarization (produced by injected hyperpolarizing current pulses), whereas $+\dot{V}_{max}$ decreases greatly with depolarization [9]. Decrease of $+\dot{V}_{max}$ to 50% of its maximal value (half-inactivation of the slow channels) occurs by −47 mV, and complete inactivation ($+\dot{V}_{max} = 0$) occurs at −22 mV. This behavior is consistent with the behavior of slow channels in visceral smooth muscle and cardiac muscle (although inactivation does not begin until about −50 mV in myocardial cells). The curve of $+\dot{V}_{max}$ vs E_m is more or less typical of slow-channel APs.

The specific blocker of fast Na^+ channels, TTX, has no effect on the rate of rise or overshoot of the APs of VSM cells (or of visceral smooth muscle). This was shown, for example, in guinea pig superior mesenteric artery [9].

TABLE 34–2. Summary of the properties of the TEA-induced action potentials in arterial smooth muscles

Parameter	Dog coronary arteries		Guinea pig superior mesenteric artery[a]
	Small diameter (<0.5 mm)	Large diameter (>1.0 mm)	
Resting E_m (mv)	−53 ± 2	−56 ± 2	−54 ± 1.3
Amplitude of TEA-induced action potential (mV)	54 ± 1	56 ± 1	59 ± 1
$+\dot{V}_{max}$ (V/s)	6 ± 1	5 ± 1	6 ± 0.7
Ca^{2+} dependency (mV/decade)	31	30	29

The data are given as the mean ± SE.
[a]The duration (at 50% repolarization) of the spikes in the guinea pig was 50–75 ms. From Harder et al. [15] and Harder and Sperelakis [9].

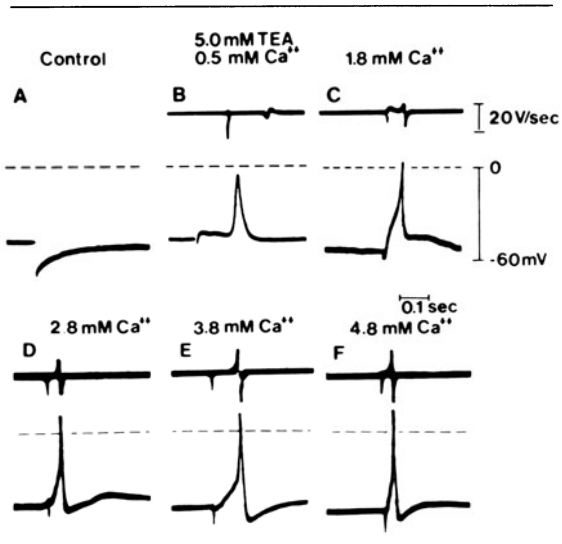

FIGURE 34–3. Ca^{2+} dependency of stimulated action potentials in presence of TEA^+ in normally inexcitable vascular smooth muscle from guinea pig superior mesenteric artery. All records were taken from one impalement. *(A)* Control record showing a large resting potential of −58 mV and lack of spontaneous action potentials or responses to intense external electrical stimulation (one shock artifact depicted). *(B–F)* Production of APs (in response to electrical stimulation) after addition of 5 m*M* TEA, illustrating increase in amplitude and maximal rate of rise ($+\dot{V}_{max}$) of APs as $[Ca]_o$ is increased from 0.5 m*M* *(B)* to 1.8 m*M* *(C)*, 2.8 m*M* *(D)*, 3.8 m*M* *(E)*, and 4.8 m*M* *(F)*. The upper trace in *B–F* gives dV/dt, the maximal deflection of which is proportional to $+\dot{V}_{max}$. The horizontal broken line gives the zero potential level. From Harder and Sperelakis [9].

This indicates that an inward fast Na^+ current does not contribute to the depolarizing phase of the AP, and that fast Na^+ channels are either absent or nonfunctional ("silent"). This conclusion is supported by the fact that hyperpolarization does not greatly increase $+\dot{V}_{max}$ (see above).

The $+\dot{V}_{max}$ and overshoot of the APs of most types of VSM are increased greatly by elevation of $[Ca]_o$ and decreased by lowering of $[Ca]_o$. This was shown, for example, in guinea pig superior mesenteric artery [9] (fig. 34–3) and in dog coronary arteries [15]. In both arteries, a plot of AP amplitude (proportional to overshoot) against log $[Ca]_o$ gave a straight line with a slope of about 30 mV/decade (table 34–2). Since this is about the same as the theoretical slope of 30.5 mV/decade calculated from the Nernst equation for a divalent cation, the results indicate that the inward current during the APs in these two types of arteries is carried almost exclusively by Ca^{2+} ion; that is, Na^+ ion carries little or no inward current. This conclusion is further supported by the results of experiments in which $[Na]_o$ was varied (and $[Ca]_o$ held constant). Variation in $[Na]_o$ over a wide range (0–150 m*M*) had little or no effect on the amplitude or $+\dot{V}_{max}$ of the APs [9]. In addition, a plot of $+\dot{V}_{max}$ vs log $[Ca]_o$ (between 1.0 and 5.0 m*M*) gave a straight line.

The results with Ca^{2+}-antagonistic agents, such as verapamil and bepridil, are consistent with the conclusion that the inward current during the APs is carried entirely by slow channels, i.e., fast Na^+ channels do not participate. Verapamil and bepridil, at concentrations that markedly depress the slow channels,

were shown to cause only slight depression of the fast Na^+ channels; that is, these agents are relatively specific for slow channels. In guinea pig superior mesenteric artery [9] (fig. 34–4A and B), in dog coronary arteries [15, 16], and in cultured rat aortic cells [39], it was demonstrated that verapamil depresses and blocks the Ca^{2+}-dependent APs. The same was true for bepridil on dog coronary artery [40] and cultured rat aortic cells [41]. If a significant participation of fast Na^+ channels occurred in VSM, then one could expect that verapamil and bepridil would not completely block the APs. Mn^{2+}, another Ca^{2+} antagonist, also blocked the APs [9] (fig. 34–4C and D). Verapamil and bepridil also depress the K^+ contracture and norepinephrine contracture of isolated rabbit aortic rings [42]. A number of other calcium antagonists, including mesudipine, nifedipine, and diltiazem, were also shown to block the K^+ contracture of both arterial and venous smooth muscles [43].

Because of the complete Ca^{2+} dependence of the APs, the TEA-induced APs should make a good assay system for determining the effects of vasoactive substances on the Ca^{2+} influx and on other membrane properties of the VSM cells, as will be shown below. The rate of rise of the AP is proportional to the inward current (for a constant membrane capacitance, C_m), and the inward current (assuming the electrochemical driving force is unchanged) is proportional to the number of activated slow channels. Thus, if a drug depresses the $+\dot{V}_{max}$ by 50%, this corresponds to a block of half of the slow channels (assuming the conductance per channel is unaffected). This analysis also assumes that the drug did not affect other membrane properties such as g_K. As we have seen above, changes in g_K can have profound effects on the $+\dot{V}_{max}$ of the AP, because the rate of rise is proportional to the *net* inward current and not the absolute inward slow current.

Relatively little is known about propagation in VSM, including velocity of propagation. In intestinal smooth muscle, propagation velocity is about 5 cm/s, and occurs from muscle cell to muscle cell, independent of the nerves (although the nerves influence activity). In VSM, there is not much evidence for muscle-cell-to-muscle-cell propagation over long distances. Relatively little is known about the degree of low-resistance coupling between contiguous cells. In arterial VSM particularly, the muscle cells seem to be under greater control by the innervation. Excitatory (EJPs) and inhibitory (IJPs) junction potentials [1] are produced in the VSM cells by action of neurotransmitters. Depolarizing JPs increase the state of contraction, as well as trigger spike activity, which further increases the state of contraction. Hyperpolarizing JPs have the opposite effect.

The spikes may lead to relatively rapid phasic contractions superimposed on the basal tonus (tonic contraction) that is a function of the resting E_m. A high frequency of spikes

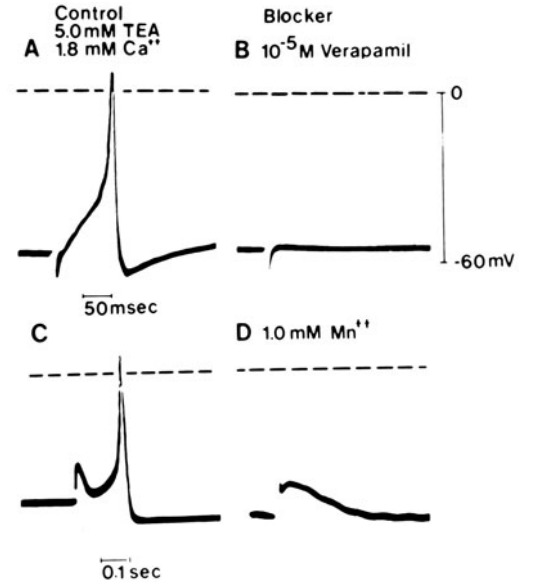

FIGURE 34–4. Blockade of TEA-induced action potential by slow channel blockers in isolated vascular smooth muscle from guinea pig mesenteric arteries. *(A)* Control record illustrating large overshooting AP induced by 5 m*M* TEA upon electrical stimulation. *(B)* Record taken from the same cell, illustrating complete blockade of AP within 5 min after the addition of 10^{-5} *M* verapamil (shock artifact only visible). *(C)* Another control record depicting the large overshooting AP induced by 5 m*M* TEA upon electrical stimulation. *(D)* Record taken from same cell showing complete blockade of action potential within 30 s after addition of 1.0 m*M* Mn^{2+} (shock artifact only visible). From Sperelakis [64].

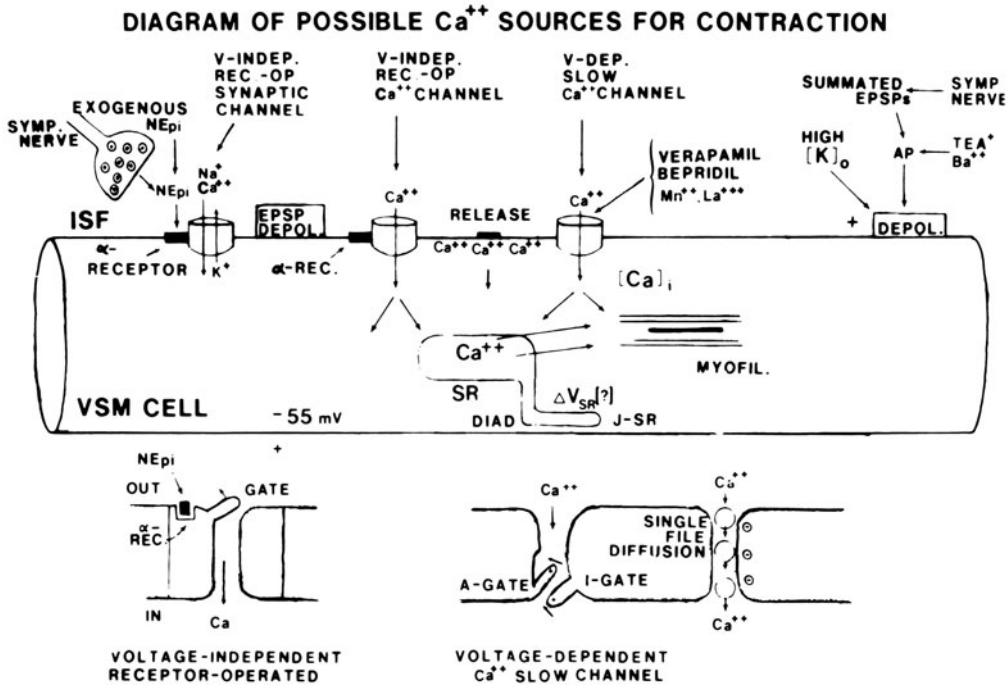

FIGURE 34–5. Diagrammatic representation of the various possible sources of Ca^{2+} ions for contraction of vascular smooth muscle. Three major extracellular sources are depicted: (1) A voltage-independent receptor-operated postsynaptic channel that is nonspecific, allowing Na^+, Ca^{2+}, and K^+ to pass through; this channel is responsible for the excitatory postsynaptic potentials (EPSPs or EJPs). (2) A voltage-independent, receptor-operated Ca^{2+} channel that is specific for Ca^{2+} ions; (2a) A variant of this mechanism is a receptor-operated release of Ca^{2+} ions bound to fixed negative charges at the inner surface of the cell membrane. (3) A voltage-dependent, time-dependent, gated Ca^{2+} slow channel that is specific for Ca^{2+}; this is the channel responsible for the rising phase of the action potential, and is the site of action of several Ca-antagonistic drugs (slow-channel blockers) or multivalent ions. The receptors involved in mechanisms 1, 2, and 2a are depicted as alpha-adrenergic receptors and norepinephrine (NEpi) as the neurotransmitter. The major intracellular sources of Ca^{2+} ions are the SR, and perhaps Ca^{2+} bound to the inner surface of the cell membrane; Ca^{2+} release from the SR may be brought about by a rise in $[Ca]_i$ and by a potential change across the SR membrane. High $[K]_o$ depolarizes and thereby leads to activation of the voltage-dependent Ca^{2+} slow channels (mechanism 3), causing a contracture. Exogenous NEpi activates the alpha receptors, which in turn (a) depolarize by activating the synaptic channels (mechanism 1) and thereby activating the Ca^{2+} slow channels (mechanism 3), and (b) cause a direct rise in $[Ca]_i$ either by mechanism 2 or 2a. Not depicted is the possibility that NEpi penetrates into the cell to act directly on the SR to release Ca^{2+}. Some Ca^{2+} may enter through activated postsynaptic channels. The lower two diagrams depict the functioning of a receptor-operated channel and a voltage-operated channel. From Sperelakis [64].

would bring about a smooth tetanic contraction of greater amplitude.

SOURCES OF Ca^{2+} FOR CONTRACTION

The Ca^{2+} ions for activation of the contractile proteins come from two major sources: (a) Ca^{2+} influx from the interstitial fluid bathing the cells, and (b) release of Ca^{2+} from the sarcoplasmic reticulum (SR) stores. In addition, it has been postulated that there may be a contribution from Ca^{2+} released from binding sites on the inner surface of the cell membrane, e.g., triggered by the action of some drugs. These various possible sources of Ca^{2+} for contraction are diagrammatically depicted in figure 34–5.

The Ca^{2+} influx across the sarcolemma is down an electrochemical gradient and through the voltage-dependent and time-dependent Ca^{2+} slow channels, one major focus of this

chapter. This Ca^{2+} inward slow current is responsible for the rising phase of the AP in most VSM cells. It is these slow channels that are blocked by agents like verapamil, bepridil, Mn^{2+}, and La^{3+}, as indicated in figure 34–5.

The Ca^{2+} influx acts to directly elevate $[Ca]_i$ and, in addition, it might cause the release of more Ca^{2+} from the SR, by the Ca-triggered–Ca-release mechanism of Fabiato and Fabiato [44]. It is also possible that Ca^{2+} release from the SR may be controlled by depolarization of the sarcolemma, which could lead to depolarization of the SR by somehow being reflected across the diadic junctions formed between sarcolemma and SR[1] (junctional SR is continuous with the network SR surrounding bundles of myofilaments). The level of $[Ca]_i$ in a noncontracting cell is about 1×10^{-7} M, and the $[Ca]_i$ necessary for peak contraction is 10^{-5}–10^{-4} M; half-maximal contraction occurs at about 2×10^{-6} M.[2]

Contractions initiated by action potentials or by elevated $[K]_0$ presumably occur by means of activation of the voltage-dependent slow channels to allow Ca^{2+} influx down its electrochemical gradient. Ca^{2+} release from the SR may also contribute. High $[K]_0$ depolarizes by reducing E_K, as calculated from the Nernst equation ($E_K = -61$ mV log $[K]_i/[K]_0$). Since verapamil blocks Ca^{2+} influx through the voltage-dependent slow channels, this agent would also prevent the Ca^{2+} release from the SR triggered by Ca^{2+} influx, and hence should nearly completely block the contractions; in addition, because the AP spike depends on an inward Ca^{2+} current, verapamil should also block the APs.

Contractions initiated by norepinephrine (NEpi) may be brought about by somewhat different mechanism(s):

(a) NEpi binding to alpha-adrenergic receptors on the VSM cell (postsynaptic) membrane increases conductance for Na^+ (and perhaps Ca^{2+}), thereby producing the equivalent of a large excitatory postsynaptic potential (EPSP) (or excitatory junctional potential [EJP]). This EPSP depolarization should activate the voltage-dependent Ca^{2+} slow channels and cause a large Ca^{2+} influx. A cartoon model of how the receptor-operated gate mechanism could work is depicted in the lower left side of figure 34–5, for comparison with the model for a voltage-dependent Ca^{2+} slow channel depicted in the lower right. (Also depicted is the likely possibility that Ca^{2+} ions pass through the slow channel by single-file diffusion with several binding sites (to negative charges) along the way, and that the ions pass from energy well to energy well successively by bumps from neighboring ions.)

(b) If there is some similarity to the ion channels in postsynaptic membrane at the vertebrate skeletal neuromuscular junction activated by acetylcholine (ACh) (nicotinic receptor), this receptor-operated channel being nonspecific so that a number of cations, including Na^+, Ca^{2+}, and K^+, can pass through, then some Ca^{2+} influx may occur through these voltage-independent synaptic channels. Casteels et al. [27] have shown that NEpi increases the permeability for Na^+, Ca^{2+}, K^+, and Cl^- ions. There is no evidence that verapamil blocks Ca^{2+} influx through the postsynaptic channels (similar to the lack of effect of tetrodotoxin [TTX] on Na^+ influx through the ACh-operated postsynaptic channels).

(c) It has been postulated (see reviews by Bolton [12], Johansson and Somlyo [13], Casteels [46], and Van Breeman et al. [47]) that there is a separate set of alpha-receptor-operated, voltage-independent channels that allows only Ca^{2+} ions to pass through. Major evidence for this view comes from the fact that addition of exogenous norepinephrine, to VSM completely depolarized by elevated $[K]_0$ and in contracture, produces a considerably greater force of contraction. However, it is difficult to distinguish between mechanisms (b) and (c). Even if Na^+ influx is increased upon addition of NEpi to K^+-depolarized VSM cells, this would not rule out the possibility of this type of receptor-operated Ca^{2+} channel. The most compelling argument for this type of channel is Casteels' finding that low concentrations of NEpi bring about some contraction without an accompanying depolarization (higher doses produced depolarization and greater contraction).

(d) A variation of the third mechanism is that, instead of a protein channel imbedded in the lipid bilayer membrane and coupled to the alpha receptor, activation of the alpha receptor

could instead somehow cause the release of Ca^{2+} bound to negative charges at the inner surface of the cell membrane (see fig. 34–5). It may be presumed that verapamil does not greatly affect Ca^{2+} influx through this receptor-operated mechanism, because the NEpi-induced contractures are depressed only about 50% by 10^{-5} *M* verapamil [42].

In summary, it is likely that, since the (maximal) NEpi-induced contracture is often greater than the (maximal) K^+-induced contracture, and since agents such as verapamil depress the K^+ contracture more than the NEpi-contracture [42], NEpi produces contraction via two Ca^{2+} sources: (a) the V-dependent Ca^{2+} slow channels (activated by EPSP depolarization), and (b) the receptor-operated channels (of the nonspecific postsynaptic type or the postulated specific Ca^{2+} type). Presumably, agents such as verapamil block the V-dependent Ca^{2+} slow channels, but have relatively little or no effect on the receptor-operated channels. Since the NEpi-induced contracture is less depressed by low $[Ca]_0$ than is the K^+-induced contracture, this suggests that NEpi also causes some release of Ca^{2+} internally. The latter could occur by release of Ca^{2+} bound to the internal surface of the cell membrane. Alternatively, it is possible that NEpi crosses the cell membrane and acts directly on the SR membrane to bring about Ca^{2+} release (if so, then the alpha-receptor antagonists would also have to gain access to the same sites.)

It has been reported by Motalsky et al. [48] that some calcium-antagonistic drugs, such as verapamil and methoxy-verapamil (D-600) (but not nifedipine and diltiazem), also act as antagonists for α_1- and α_2-adrenergic receptors, and that this might partially explain some of their vasodilatory action and inhibition of NEpi-induced contractures in VSM.

Effects of Some Vasoactive Substances

INTRODUCTION

Experiments were done on large (>1.0 mm o.d.) and small (<0.5 mm) coronary arteries of the dog to investigate the mechanism of action of certain vasoactive substances, namely, the vasodilators adenosine, nitroglycerin, and verapamil, and the vasoconstrictor ouabain. Patients under treatment with cardiac glycosides sometimes develop coronary constriction, and Fleckenstein et al. [49] suggested that this effect is mediated by an increase in Ca^{2+} influx. Schnaar and Sparks [50] found that the contractile responses of small coronary arteries were relaxed by adenosine but not by nitroglycerin, whereas the large vessels were relaxed by nitroglycerin but not by adenosine. They suggested that these effects were mediated by inhibition of Ca^{2+} influx.

Verapamil was first shown by Kohlhardt et al. [51] (reviewed by Fleckenstein [52]) to produce a decrease in contraction of cardiac muscle by inhibition of the Ca^{2+} influx from the extracellular fluid. The methoxy derivative of verapamil, D-600, had the same effect, but was somewhat more potent. Another Ca^{2+}-antagonistic agent, nifedipine, was also shown to block the inward slow current in cardiac muscle [36]. Verapamil is not specific for Ca^{2+} influx, but also depressed Na^+ influx through myocardial slow channels, i.e., verapamil is a nonspecific blocker of slow channels [37, 53]. Bepridil, a newer antianginal agent and coronary vasodilator, also blocks the slow APs and slow channels of myocardial cells [38]. Similar findings were made by Labrid et al. [54]. In smooth muscle, verapamil inhibits Ca^{2+} influx in VSM cells [55–58] and in visceral smooth muscle [59]. The Ca-antagonistic drugs have vasodilatory effects, including on the coronary arteries. Bepridil also was shown to have coronary vasodilatory effects [60, 61] and an antianginal effect [62]. Since VSM cells possess slow channels, fast Na^+ channels being either absent or nonfunctional, it might be predicted that agents like verapamil and bepridil would block the APs in VSM cells

GENERAL CHARACTERISTICS OF THE ACTION POTENTIALS

The VSM cells in both small and large arteries are quiescent and have stable resting potentials [15, 16]. Action potentials (APs) usually are not initiated when intracellular or extracellular current pulses are applied (fig. 34–6A). However, addition of 10 m*M* TEA allows over-

shooting (by about 5–10mV) APs to be elicited on application of extracellular current pulses (rectangular pulses, 20–30 ms in duration) in both large and small arteries (fig. 34–6B). Intracellularly applied polarizing current pulses also produce APs. The TEA caused only a small depolarization of about 4 mV. The mean amplitude of the TEA-induced AP was 54 ± 1 (SE) mV in the small arteries and 56 ± 1 mV in the large arteries (table 34–2). The $+\dot{V}_{max}$ of the APs was 6 ± 1 V/s (small arteries) and 5 ± 1 V/s (large arteries).

Ca^{2+} DEPENDENCY OF THE ACTION POTENTIALS

The amplitude and $+\dot{V}_{max}$ of the TEA-induced APs increased as a function of $[Ca]_0$ (fig. 34–3) [9, 15]. As can be seen in figure 34–3, the APs were undershooting when $[Ca]_0$ was only 0.5 m*M*, and the amplitude of the response increased as $[Ca]_0$ was increased. In high $[Ca]_0$, a spontaneous second AP sometimes followed the first stimulated one. The relationship between the amplitude and log $[Ca]_0$ was linear and had an average slope of 30 mV/decade —between 0.5 and 5.0 m*M* $[Ca]_0$ in the large arteries and 31 mV/decade in the small arteries (fig. 34–7 and table 34–2). These values agree with the theoretically predicted value from the Nernst equation of 30.5 mV/decade for a membrane selective for a divalent cation (at 37° C). These data indicate that the inward current during the AP is carried primarily by Ca^{2+} ions.

BLOCKADE BY Ca^{2+} -ANTAGONISTIC AGENTS

Verapamil and Bepridil Blockade. Verapamil–HCl (10^{-5} *M*), a known blocker of slow channels [36, 37, 51, 53, 63], rapidly depressed and abolished (fig. 34–6) the TEA-induced APs in both small and large coronary arteries (table 34–3). The verapamil blockade is consistent with the Ca^{2+} dependency of the AP. As expected, the inhibitory effect of verapamil could be reversed by elevation of $[Ca]_0$.

The antianginal agent and coronary vasodilator, bepridil, was shown to depress and block the inward slow current in myocardial cells [38, 54]. In the dog coronary artery (0.5–1.0 mm o.d.), bepridil also rapidly depressed (10^{-6} *M*) and abolished (10^{-5} *M*) the TEA-induced APs (table 34–3) [40]. Thus, these results can explain the antianginal action of bepridil, namely, inhibiting Ca^{2+} influx into the VSM cells of the coronary arteries, and thereby exerting a relaxing effect on the VSM cells.

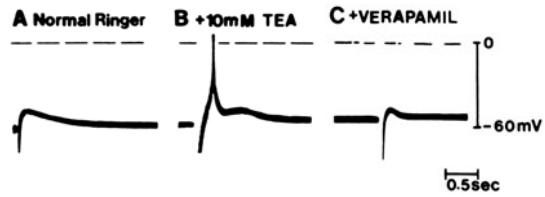

FIGURE 34–6. Induction of action potentials by TEA in the vascular smooth muscle of dog coronary artery, and their blockade by calcium-antagonistic drugs. *(A)* Control record in normal Ringer solution showing a lack of spontaneous action potentials or responses to external electrical stimulation (one shock artifact visible); resting potential was −55 mV. *(B)* Record taken from the same cell 10 min after addition of 10 m*M* TEA, illustrating a large overshooting AP in response to electrical stimulation. *(C)* Addition of verapamil (5×10^{-6} *M*) abolished the APs within 5 min. The horizontal broken line gives the zero potential. From Harder and Sperelakis [9].

Verapamil and bepridil also depress the K^+-induced contractures of isolated rabbit aortic rings in a dose-dependent manner (fig. 34–8) [42]. These drugs also depress the norepinephrine-induced contractures, but to a lesser extent (than for the K^+ contractures) [42].

TABLE 34–3. Summary of the effects of some vasoactive substances on the TEA-induced action potentials of small and large coronary arteries of the dog heart

Substance	Small diameter (<0.5 mm)	Large diameter (>1.0 mm)
Verapamil (1.5×10^{-6} *M*)	Blocked	Blocked
Bepridil (1×10^{-5} *M*)	Blocked[a]	—
Mn^{2+} (10^{-3} *M*)	Blocked	Blocked
Adenosine (10^{-5} *M*)	Blocked	No effect
Nitroglycerin (10^{-5} *M*)	No effect	Blocked
Cardiac glycosides (10^{-8}–10^{-6} *M*)	Potentiated	—

[a]Tested on intermediate-sized arteries (0.5- to 1.0-mm diameter).
Data taken from Harder and Sperelakis [9], Harder and Sperelakis [14], Harder et al. [15], Belardinelli et al. [16], and Sperelakis [64].

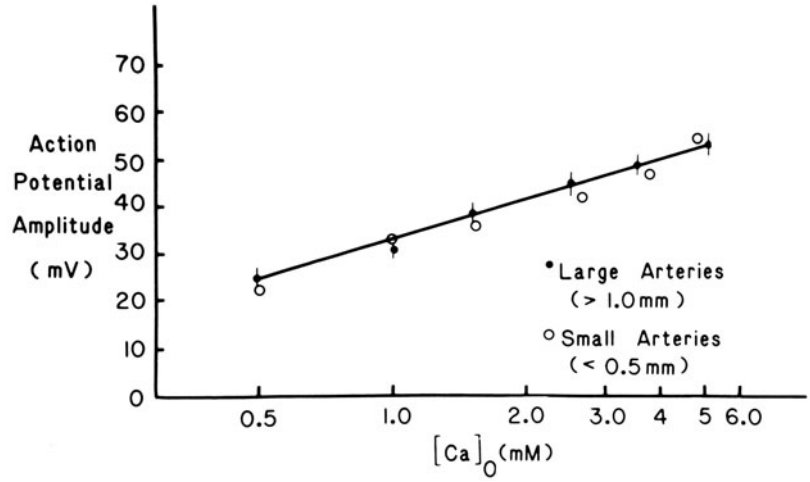

FIGURE 34–7. Effect of increasing external Ca^{2+} concentration ($[Ca]_o$) on the amplitude of the TEA-induced action potentials in large (filled circles) and small (unfilled circles) coronary arteries of the dog heart. Each point plotted is the mean value (± SE) of 10–21 values. The curve through the filled circles was fitted by linear regression analysis. The average slope of this line is 30 mV/decade. Modified from Harder et al. [15].

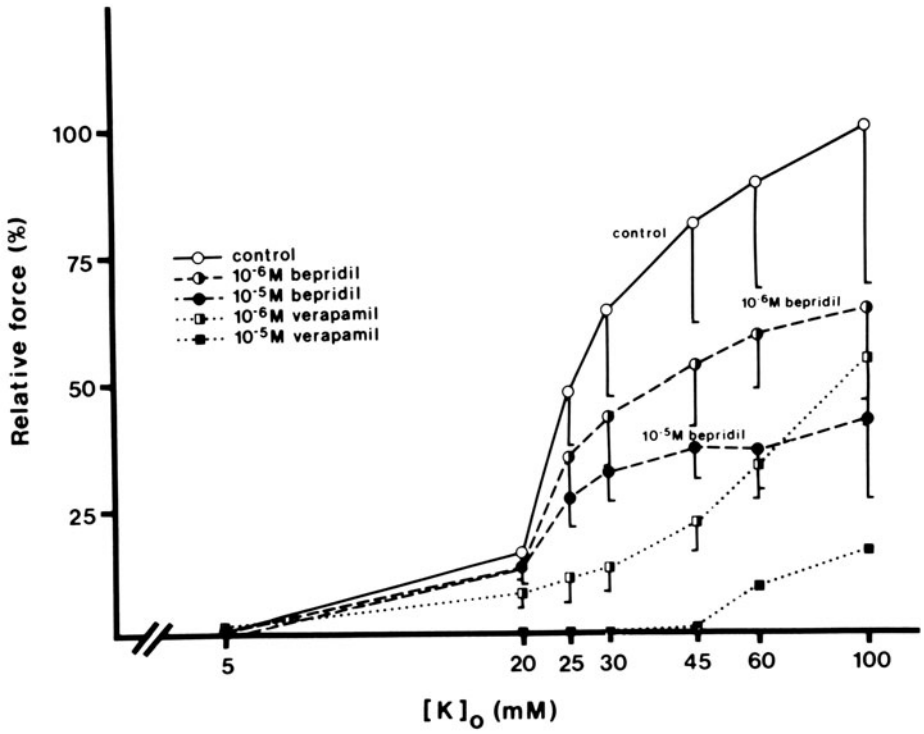

FIGURE 34–8. Effect of verapamil and bepridil on the contractions of rabbit aortic rings induced by elevated K^+. Cumulative K^+ dose–response curves were obtained in the presence and absence of verapamil (10^{-5} and 10^{-6} *M*) and bepridil (10^{-5} and 10^{-6} *M*). Tissues were equilibrated with the blocking agents for 20 min before assaying. Contractile responses are plotted relative to the maximum response of the control tissue. From Mras and Sperelakis [42].

Mn^{2+}-Ion Blockade. $MnCl_2$ (1 m*M*) exerted effects similar to those of verapamil and bepridil, namely, depression and block of the TEA-induced APs in both small and large coronary arteries [64] (table 34–3 and fig. 34–4C and D). Since Mn^{2+} at 1 m*M* is a relatively specific blocker of slow channels that allow Ca^{2+} ion to pass through, but does not block slow Na^+ channels or fast Na^+ channels [37], these results also are consistent with the conclusion that the inward current during the TEA-induced AP is carried almost exclusively by Ca^{2+} ion.

Propafenone Blockade. Propafenone, another coronary vasodilator, was also found to depress (at 10^{-6} *M*) and abolish (at 10^{-5} *M*) the TEA-induced spikes in dog coronary artery [35].

EFFECTS OF ADENOSINE AND NITROGLYCERIN

Adenosine Blockade in Small Coronary Arteries. Adenosine (10^{-5} *M*) abolished the TEA-induced Ca^{2+}-dependent action potentials in small coronary arteries within 1 min (table 34–3) [15]. When the VSM cells blocked by adenosine were superfused with adenosine deaminase to destroy the adenosine, there was nearly complete recovery of the APs within 2 min. Figure 34–9 (unhatched bars) summarizes the dose dependency of the effect of adenosine on $+\dot{V}_{max}$ (fig. 34–9A) and amplitude (fig. 34–9B) of the APs. As shown, depression of the APs began at 1×10^{-7} *M* and was complete at 1×10^{-5} *M*. The depression of the $+\dot{V}_{max}$ by adenosine reflects an inhibition of the inward Ca^{2+} current. Adenosine had no significant effect on the resting potential (E_m) or input resistant (r_{in}).

Adenosine Insensitivity of Large Coronary Arteries. Adenosine (10^{-5} *M*) had no effect on the amplitude or $+\dot{V}_{max}$ of the TEA-induced Ca^{2+}-dependent APs in the large coronary arteries (table 34–3) [15]. Adenosine also had no significant effect on the resting E_m or r_{in}.

Nitroglyerin Blockade in Large Coronary Arteries. Nitroglycerin (10^{-5} *M*) completely abolished the TEA-induced Ca^{2+}-dependent APs in the large coronary arteries within 5 min (table 34–3) [15]. Figure 34–9 (hatched bars) summarizes the dose dependency of the effect of nitroglycerin on $+\dot{V}_{max}$ (fig. 34–9A) and amplitude (fig. 34–9B) of the APs. As shown, 50% depression of both parameters was produced by about 5×10^{-6} *M* nitroglycerin, and 10^{-7} *M* had a slight effect. The depression of $+\dot{V}_{max}$ by nitroglycerin corresponds to a depression of the inward Ca^{2+} current. Elevation of $[Ca]_0$ by 3 m*M* restored the APs depressed by nitroglycerin, indicating that the inhibitory effects of the drug are antagonized by Ca^{2+} ion. Nitroglycerin had no significant effect on the resting E_m or r_{in}.

Nitroglycerin Insensitivity of Small Coronary Arteries. Nitroglycerin (10^{-5} *M*) had no effect on either the amplitude of $+\dot{V}_{max}$ of the Ca^{2+}-dependent APs in the small coronary arteries (table 34–3) [15]. Nitroglycerin also did not affect the resting E_m or r_{in}.

CARDIAC GLYCOSIDE POTENTIATION OF THE Ca^{2+} INWARD CURRENT

The effects of the cardiac glycosides, ouabain and digoxin, known to produce coronary vasoconstriction, were studied on the electrical activity of isolated small (0.5 mm o.d.) coronary arteries of the dog [16]. The cardiac glycosides (4×10^{-9} to 1×10^{-7} *M*) increased the amplitude and maximal rate of rise ($+\dot{V}_{max}$) of the TEA-induced Ca^{2+}-dependent APs in a dose-dependent manner (fig. 34–10 and table 34–3). In most experiments, a submaximal dose of TEA (usually 5 m*M*) was used so that the potentiating effects of the cardiac glycosides could be readily discerned. Figure 34–11 summarizes the dose dependency of the effect of digoxin on $+\dot{V}_{max}$ (fig. 34–11A) and amplitude (fig. 34–11B) of the APs. As can be seen, significant increase in both parameters occurred at 4×10^{-9} *M*, and maximal potentiation occurred at 1×10^{-7} *M*. Increase in digoxin concentration to 10^{-6} *M* produced a smaller potentiation than did 10^{-7} *M*, consistent with a blocking effect of high concentrations of cardiac glycosides on the slow channels [63–65] and with some depolarization.

The cardiac glycosides also rapidly (e.g., 3–

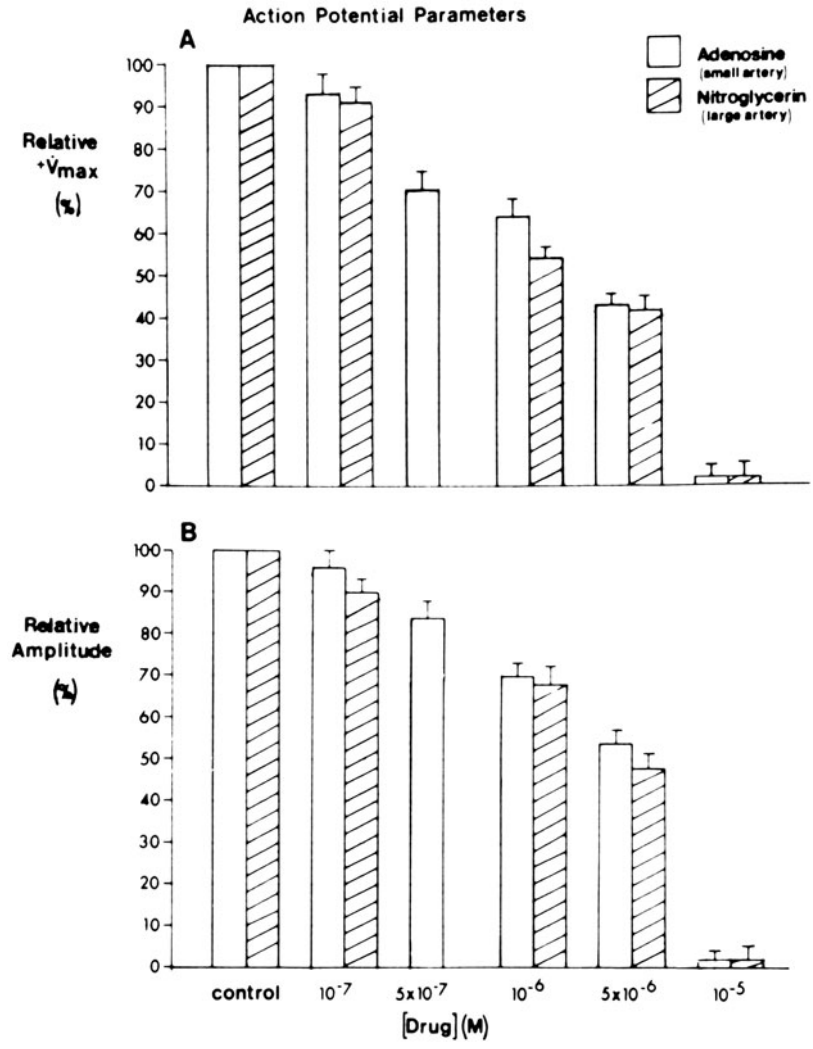

FIGURE 34–9. Dose dependency of adenosine (unfilled bars) and nitroglycerin (cross-hatched bars) on the maximal rate of rise ($+\dot{V}_{max}$) *(A)* and amplitude *(B)* of the TEA-induced action potentials of dog coronary artery. The ordinates give the AP parameters as a percentage of the control value in the absence of the drug. Each bar gives the mean ± SE for 6–8 cells sampled from 3–4 coronary arteries. The adenosine data were obtained from small arteries, and the nitroglycerin data from large arteries. With both adenosine and nitroglycerin, complete blockade occurred at 10^{-5} *M*. From Harder et al. [15].

10 min) produced spontaneous APs in the presence of subthreshold doses of TEA (e.g., 5 m*M*), and increased the frequency of the spontaneous APs produced by 10 or 15 m*M* TEA (fig. 34–12) [16]. A small elevation in $[Ca]_0$ (e.g., by 1 m*M*) caused a marked increase in frequency, amplitude, and rate of rise of the APs, i.e., the effects of the glycosides were greatly enhanced in elevated $[Ca]_0$, consistent with the effect of the glycosides being mediated by increase in Ca^{2+} conductance, hence Ca^{2+} influx. Verapamil (5×10^{-6} *M*) abolished all APs produced by the glycosides.

Phentolamine (5×10^{-6} *M*), an alpha-adrenergic antagonist, did not prevent the effects of the glycosides, and phenylephrine (5×10^{-6} *M*), an alpha-adrenergic agonist, did not mimic the effects of the glycosides and had no

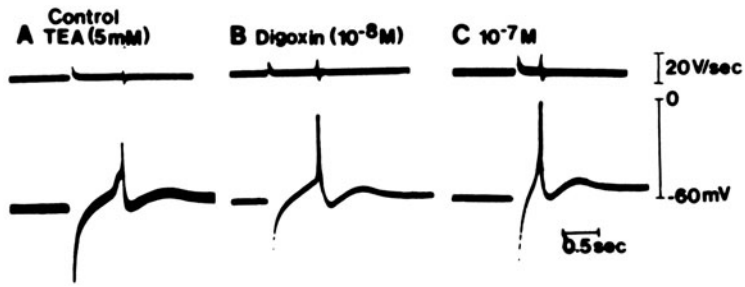

FIGURE 34–10. Illustration of the potentiating effect of digoxin on the amplitude and maximal rate of rise of the AP. *(A)* Elicitation of an undershooting AP by electrical stimulation in the presence of a low dose of TEA (5 m*M*). *(B)* and *(C)* Records taken from same cell within 2 min after addition of 10^{-8} *M (B)* and 10^{-7} *M (C)* digoxin, showing a marked increase in the amplitude and maximal rate of rise of the APs. Upper trace gives dV/d*t*. From Belardinelli et al. [16].

significant effect on the resting potential or action potentials [16]. These results suggest that the effects of the glycosides were not mediated by release of catecholamines from sympathetic nerve terminals or by activation of the alpha-adrenergic receptors.

The effects of the cardiac glycosides occurred before any significant depolarization was evident [16]. Significant depolarization was observed only after relatively long periods (e.g., 15 min) in high doses of glycoside, 10^{-6} *M* for digoxin and 10^{-7} *M* for ouabain. At 10^{-6} *M*, ouabain depolarized by 12 mV (from the control value of -54 mV to -42 mV) within 15 min.

In summary, the data indicate that the low concentrations of cardiac glycosides ($<10^{-7}$ *M*) increase inward Ca^{2+} slow current in VSM by a mechanism that is independent of membrane depolarization, i.e., independent of the well-known action of the glycosides to inhibit the (Na,K)-ATPase, and hence the Na-K cation pump. This Ca^{2+}-influx potentiating action of cardiac glycosides can account for their coronary vasoconstrictor effect and may be important in digitalis toxicity.

HISTAMINE POTENTIATION OF CA^{2+} INFLUX

Harder [22] demonstrated that histamine (10^{-7}–10^{-5} *M*) increased the amplitude and the $+\dot{V}_{max}$ of the TEA-induced APs in dog coronary arteries (<0.5 mm o.d.), and that this effect was blocked by the H_1-receptor antagonist, pyrilamine maleate. In quiescent preparations in the absence of TEA, histamine (10^{-6} *M*) hyperpolarized by 9 mV (from -55 to -64 mV) and reduced r_{in} to about half of the control value, consistent with an increase in g_K. Because the histamine-induced hyperpolarization was prevented by 1 m*M* Mn^{2+}, it was suggested that this increase in g_K was mediated by an increased Ca^{2+} influx and elevated $[Ca]_i$ due to the Meech-Gardos effect (Ca^{2+}-induced increase in g_K).

Casteels and Suzuki [66] had reported, on rabbit ear artery, that histamine activates both H_1 receptors (blocked by mepyramine) and H_2 receptors (blocked by cimetidine), H_1 activation tending to depolarize and increase force development, and H_2 activation tending to hyperpolarize and decrease force development. Since K^+-free medium prevented the hyperpolarizing effect of H_2 activation, it appears that stimulation of the electrogenic pump is responsible for the hyperpolarization. Because they found that the effects of histamine on force were independent of changes in E_m, they concluded that H_1 activation induces release of Ca^{2+} from intracellular stores and that H_2 activation inhibits this release.

NERVE–MUSCLE INTERACTIONS

In dog coronary arteries, Mekata [1] also reported that the VSM cells were electrically quiescent and that APs could not be evoked by electrical stimulation. However, electrical-field stimulation (brief pulses as short as 0.5 ms) of

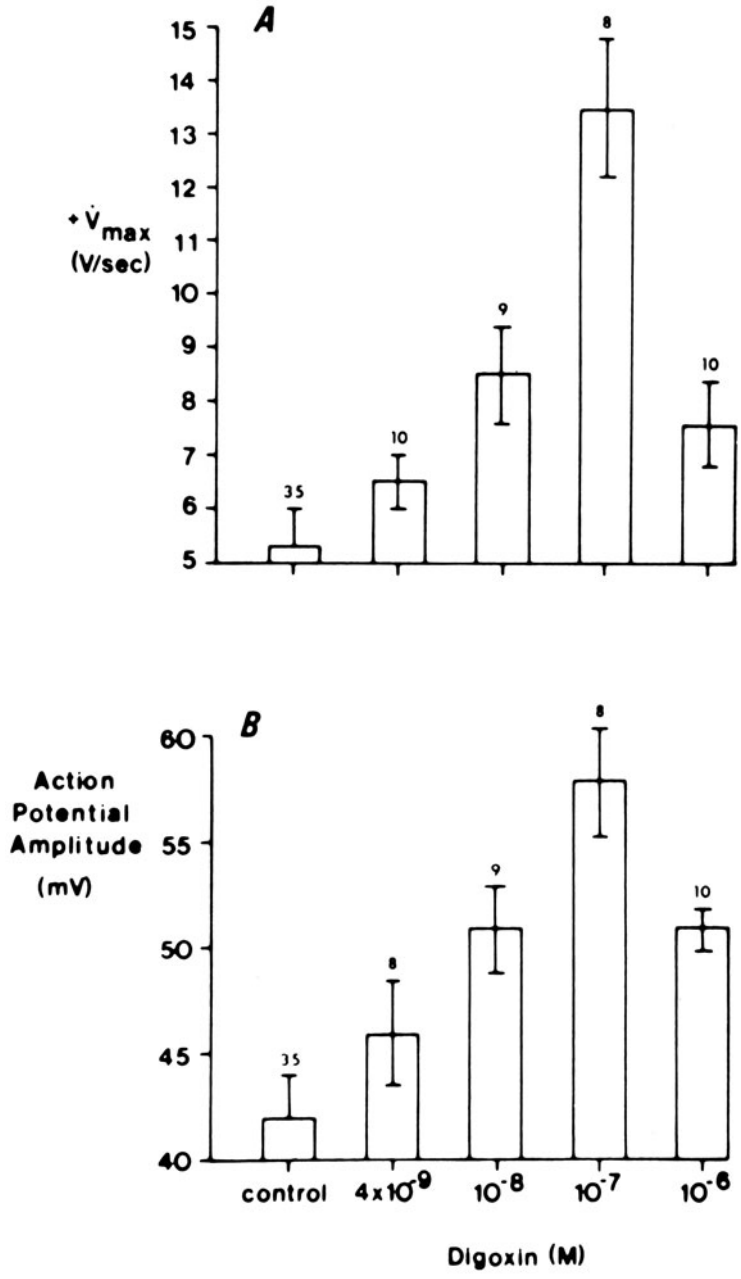

FIGURE 34–11. Summary of data demonstrating the dose dependency of digoxin on the maximal rate of rise *(A)* and amplitude *(B)* of the action potentials in dog coronary arteries (small size). The tissue was bathed in 5 m*M* TEA to permit the elicitation of APs. Each bar gives the mean ± SE of 24–60 values. Significant increases in both $\dot{V}_{max}$ and amplitude occurred at 10^{-8} *M*, and the peak effect occurred at 10^{-7} *M*. At higher doses of digoxin (10^{-6} *M*), the effect was less. From Belardinelli et al. [16].

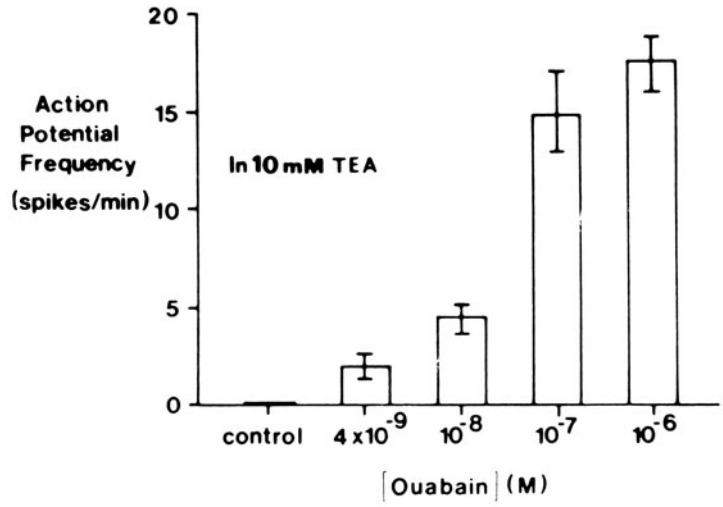

FIGURE 34–12. Summary of data demonstrating the dose dependency of ouabain on the frequency of spontaneous action potentials of the dog coronary artery in presence of TEA (10 m*M*). Each bar gives the mean ± SE for 4–12 impalements in 2–7 coronary arteries. From Belardinelli et al. [16].

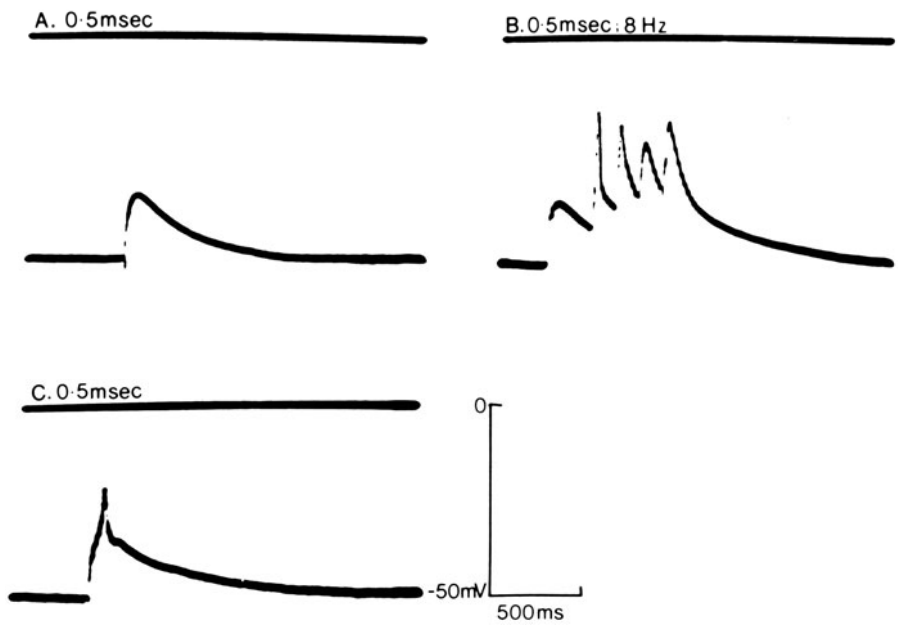

FIGURE 34–13. Effects of nerve stimulation in small mesenteric arteries of guinea pig. All records are from one cell. *(A)* A single EJP recorded intracellularly following a single field stimulus (0.5-ms duration). *(B)* Stimulation with repetitive pulses (8 Hz, 0.5-ms duration) evokes spikes and contraction. *(C)* On some occasions, a single stimulating pulse evoked a single EJP which reached threshold for a spike. Modified from Zelcer and Sperelakis [8].

the intramural nerves produced either contraction, associated with depolarization of the VSM, or relaxation, associated with hyperpolarization. Depolarization occurred when the resting potential was more negative than −60 mV, and hyperpolarization occurred when resting E_m was less negative than −50 mV. These responses were blocked by TTX, suggesting that the potential changes in the VSM cells were excitatory and inhibitory junction potentials due to neurotransmitter release with nerve excitation. Mekata concluded that, even in such relatively large arteries (about 2.5 mm diameter), most of the VSM cells, including the innermost cells (closest to the vessel lumen), can be controlled by the nerves (generally confined to the adventitiomedial border).

The characteristics of the excitatory junction potentials have been examined in a number of vessels, including guinea pig mesenteric arteries and arterioles and saphenous and ear arteries [8, 34, 67–74]. Illustration of several EJPs is given in figure 34–13.

Electrical Properties of Cultured VSM Cells

ADVANTAGES OF CULTURED CELLS

Over the past decade, many investigators have exploited the cell culture systems for VSM cells. These preparations have been used extensively to study lipid metabolism and other biochemical reactions [75], but very few electrophysiologic studies have been done. Most of the biochemical studies have been done on explant cultures. In this preparation, a minced fragment of blood vessel media layer is maintained for several weeks to allow cells to "grow" out of the explant; the cell outgrowth is subcultured for several passages (for a detailed description, see Sperelakis [76]). However, such cultured cells generally lose their contractile ability after a few days, i.e., they dedifferentiate to an undetermined extent (e.g., see Chamley and Campbell [77]). The electrical studies have been done on primary cell cultures, in which the smooth muscle is dissociated into its individual component cells by enzymatic means, and the dissociated cells are plated out and cultured for a few days before experimentation [39, 41, 78–81]. However, spontaneously contracting monolayer cultures of VSM cells from rat aorta, which were passed several times and maintained for up to three months, have also been produced and characterized [82].

Study of cultured VSM cells offers several advantages, including the following: (a) They are easier to impale for long periods with microelectrodes because of the absence of tough connective tissue and because of weaker contractions. Cultured cells allowed to reaggregate into small (e.g., 50–300 μm in diameter) spheres (by gyration for 24 h) are especially useful for microelectrode impalements (summarized by Sperelakis [76]). (b) A relatively pure population of myocytes can be prepared, thus enabling chemical determinations to be made on the muscle cells and not on the other cell types found in intact blood vessels. (c) The cultured VSM cells are denervated; hence the effect of various vasoactive substances can be ascertained in the absence of neural effects. (d) Studies on changes in VSM muscle function under various conditions can be made free of systemic influences, e.g., circulating substances. (e) The effects of long-term exposure of the VSM cells to various drugs or altered environment can be determined. (f) Ion-flux studies can be done in monolayer cultures where there is no interstitial compartment, thus simplifying the analysis and interpretation.

CULTURED EMBRYONIC CHICK VSM CELLS

McLean and Sperelakis [79] produced cultured reaggregates of VSM cells which contracted spontaneously. Single cells were trypsin-dispersed from arteries and veins (great vessels near the heart and mesenteric vessels) isolated from ten- to 20-day-old chick embryos, and allowed to reaggregate into small spheres (100–300 μm in diameter) by gyrotation. Many of these spherical reaggregates contracted spontaneously or in response to electrical stimulation during culture periods of up to six weeks. When the reaggregates were allowed to adhere to a glass substrate, cells emigrated from the spheres to form aprons of monolayered cells which continued to contract. Thick and thin myofilaments and "dense bodies" characteristic

of smooth muscle cells were observed in a large fraction of the cells examined by electron microscopy.

The vascular smooth muscle cells in these primary cultures had resting potentials of −40 to −60 mV and overshooting APs with maximal rates of rise usually of about 4–10 V/s. In addition, the APs were insensitive to tetrodotoxin (TTX), a blocker of fast Na^+ channels. Such electrophysiologic properties are characteristic of smooth muscle cells. The APs were preceded by pacemaker potentials, which are responsible for the spontaneous firing.

Therefore, these results indicate that identifiable vascular smooth muscle cells can be successfully maintained in primary culture as reaggregates for several weeks, and that these cells retain electrical and contractile properties similar to those of smooth muscle cells in intact adult blood vessels. Thus, this preparation provides a convenient system for electrophysiologic and pharmacologic studies of VSM cells.

Spontaneously contracting cultures of VSM cells from embryonic chick omphalomesenteric vessels have been reported [78]. Electrophysiologic studies on cultured reaggregates of smooth muscle cells from guinea pig vas deferens have also been made [83].

CULTURED RAT AORTIC CELLS

Recent success has been made in producing and impaling cultured reaggregates of VSM cells from adult rat aorta [39, 41, 81, 84]. The cells were dispersed by collagenase/elastase, and allowed to reaggregate into small spheres (50–200 μm in diameter) by plating on to cellophane or by gyrotation, and these primary cultures were incubated for 5–14 days.

In the first study [39], the mean resting potential was −55 mV, and the mean input resistance was 9.0 MΩ (table 34–4). The cells were quiescent, electrically and mechanically, and electrical stimulation often did not elicit responses. However, some cells did respond to electrical stimulation, and in these cases the AP response consisted of an initial spike component and a second long-lasting plateau component of about 5 s in duration. In cells that were unresponsive to electrical stimulation, addition of Ba^{2+} (1 m*M*) or tetraethylammonium

TABLE 34–4. Summary of some electrical properties of cultured vascular smooth muscle cells enzyme dispersed from adult rat aorta

Condition	E_m (mV)	r_{in} (MΩ)
Control	−55 ± 1.0	9.0 ± 0.6
Ba^{2+} (1.0 m*M*)	−36 ± 1.5	17.0 ± 1.0*
TEA^+: 5.0m*M*	−52 ± 1.6	10.5 ± 1.0
15.0 m*M*	−35 ± 0.5*	16.3 ± 0.6*
Epinephrine: 10^{-7} *M*	−46 ± 1.2*	—
10^{-6} *M*	−35 ± 1.2*	—

Data given are the mean ± 1 SE.
*Statistically significant difference from the control value at $P < 0.05$.
From Harder and Sperelakis [39] and Mras and Sperelakis [41].

ion (TEA; 5–15 m*M*) induced excitability (with accompanying contraction), either as spontaneous APs or by allowing responses to electrical stimulation (fig. 34–14). The cells became partially depolarized (e.g., to −36 mV) by Ba^{2+}, and the input resistance increased (table 34–4). The frequency of spontaneous firing of the Ba^{2+} -induced spikes was affected by polarizing current pulses, as expected for pacemaker behavior (fig. 34–14B–D). Elevation of Ca^{2+} in the bathing solution increased the amplitude (overshoot) of the APs, and prolonged the plateau component (fig. 34–15). The APs were blocked by verapamil (10^{-5} *M*). The reaggregates consisted of a tight packing of elongated small-diameter cells, some of which exhibited thick and thin myofilaments, "dense bodies", and surface membrane caveolae. The results of this study demonstrated that reaggregates of arterial smooth muscle in primary culture can maintain functional and morphologic characteristics of intact arterial smooth muscle, and therefore provide a useful preparation for the study of vascular smooth muscle function and control.[3]

In subsequent studies [41, 81, 84] it was confirmed that the APs that were evoked by electrical stimulation (in the absence of any added agent, such as Ba^{2+} or TEA) were of long duration (3–5 s) and consisted of spike and plateau components and that verapamil and Mn^{2+} blocked both components. Sometimes the plateau component occurred without a spike component. The initial spike compo-

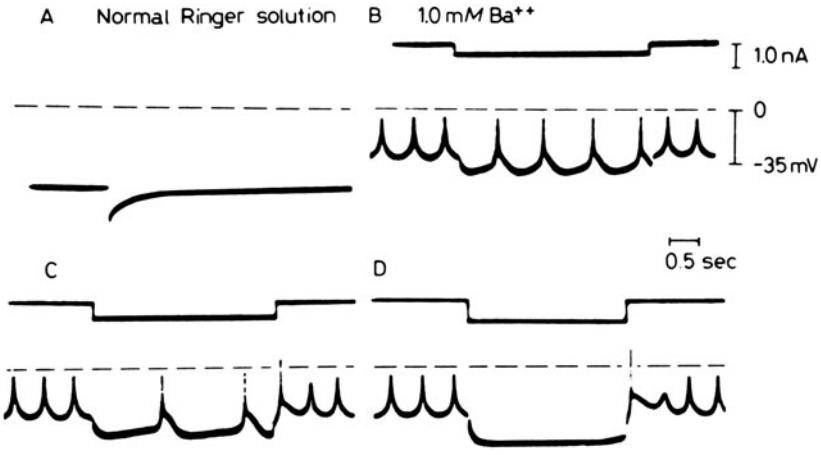

FIGURE 34–14. Spontaneous action potential generation in primary cultures of rat aortic smooth muscle cells exposed to Ba^{2+} ion. *(A)* Record illustrating absence of spontaneous APs and lack of response to extracellular electrical stimulation (one shock artifact depicted). *(B* and *C)* Records illustrating the partial depolarization and the induction of spontaneous APs by 1.0 m*M* Ba^{2+}. There was an increase in amplitude and reduction in frequency of the spontaneous APs during intracellular application of 0.5-nA *(B)* and 0.9-nA *(C)* hyperpolarizing current pulses. *(D)* Record illustrating abolition of spontaneous spike activity during a 1.2-nA hyperpolarizing current pulse. Note the stimulation of an AP at the cessation of the hyperpolarizing current pulse in *(C)* and *(D)*. All records were taken from the same cell. From Harder and Sperelakis [39].

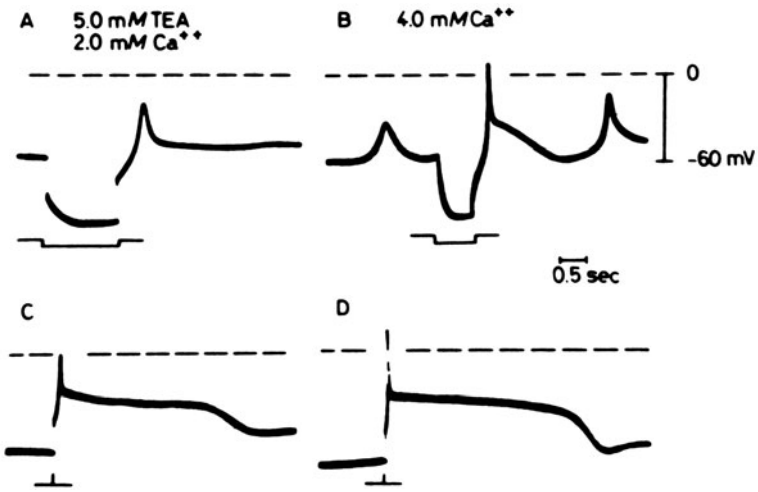

FIGURE 34–15. Electrical activity of cultured vascular smooth muscle cells enzyme-dispersed from aorta of adult rat. *(A)* Record illustrating a small spike response to anodal-break stimulation in normal Ca^{2+} solution containing 5 m*M TEA*. *(B)* Record from the same cell illustrating the large overshooting AP having a prominent depolarizing afterpotential in response to anodal-break stimulation when Ca^{2+} was elevated to 4.0 m*M*. Spontaneous activity also occurred. *(C* and *D)* Records from a cell in another reaggregate illustrating the response to brief (3 ms) depolarizing current pulses in 2 m*M* Ca^{2+} *(C)* and in 4 m*M* Ca^{2+} *(D)*. Note the marked increase in amplitude of the spike component in duration of the "plateau" component produced by elevation of Ca^{2+}. The times of application of the hyperpolarizing *(A* and *B)* and depolarizing *(C* and *D)* current pulses are indicated by the lower trace in each panel. From Harder and Sperelakis [39].

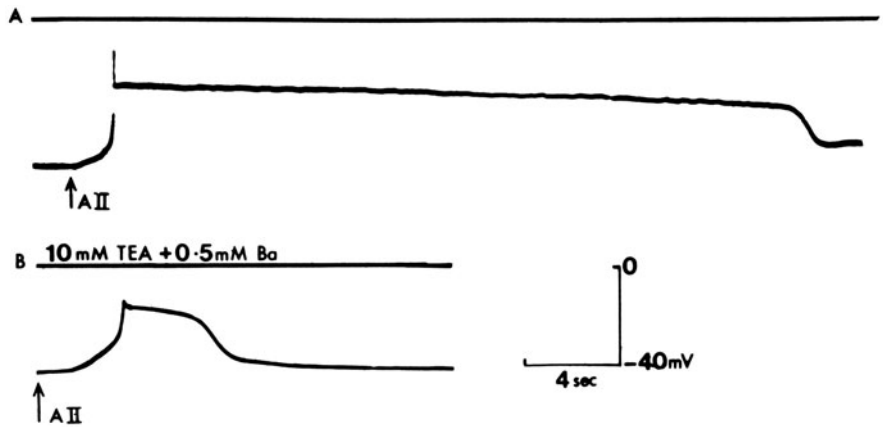

FIGURE 34–16. The effects of angiotensin (AII) on cultured reaggregates of rat aortic smooth muscle cells. *(A)* AII (20 μL of 10^{-6} *M* in a 1.0-ml bath) rapidly depolarizes and initiates an AP containing a spike and plateau. *(B)* In the presence of 10 m*M* TEA^+ and 0.5 m*M* Ba^{2+}, AII (same concentration as in *A*) also depolarizes and induces an AP. From Zelcer and Sperelakis [81].

nent had a maximum rate of rise ($+\dot{V}_{max}$) of 1–3 V/s and an amplitude of 30–40 mV (sometimes nearly reaching the zero potential level). When the plateau component occurred alone, it was much slower rising (0.1–0.3 V/s). It was also shown that the APs have a sharp threshold, and that the APs fatigue when the frequency of stimulation is too high. Addition of bepridil, a Ca^{2+} -antagonist agent like verapamil, also depressed and blocked the APs in a dose-dependent manner (10^{-7}–10^{-5} *M*). These results agree with external recordings showing that APs with long duration plateaus are recorded from isolated strips of rat aorta [85].

Angiotensin II (AII) (10^{-6} *M*), given as a bolus, rapidly depolarized the cultured cells by about 10–30 mV [81]. Sometimes the AII-induced depolarization triggered APs (with spike and plateau components) (fig. 34–16). The AII-induced depolarization disappeared in Na^+-free solution, suggesting that the depolarization may be due to an increase in Na^+ conductance. These experiments demonstrate that AII has a direct effect on VSM cells to depolarize them and that this may be one important mechanism whereby angiotensin increases the degree of contraction of VSM cells. The results also demonstrate that functional angiotensin receptors are present in the cultured cells.

Cultured reaggregates of rat aortic VSM cells prepared from spontaneously hypertensive rats (SHR) gave similar responses to AII [81]. There were no significant differences between the resting potentials of the SHR cells (-45.6 ± 0.5 mV) compared to the nonhypertensive Wistar-Kyoto (WKY) cells (-44.7 ± 0.5 mV), or between the APs.

In further studies on angiotensin by Johns and Sperelakis [84], continuous exposure of the cultured rat aortic VSM cells to angiotensin II (rather than bolus injection) also produced an angiotensin-induced peak depolarization of about 20 mV, which triggered an action potential consisting of a spike plus plateau (ca. 20-s duration). Membrane resistance was also lowered significantly, consistent with an angiotensin-induced increase in conductance for an inward-depolarizing current. This could explain the potent vasoconstricting action of angiotensin.

Conclusions

The resting potential of VSM cells in small and large coronary arteries of the dog, superior mesenteric artery of the guinea pig, and cultured rat aortic cells is about -54 mV. There is a contribution by the electrogenic pump potential to the resting potential of about 8 mV in guinea pig superior mesenteric artery, i.e.,

the net diffusion potential (E_{diff}) is about -46 mV. The p_{Na}/P_K ratio calculated from the Goldman constant-field equation for this E_{diff} value, for a $[K]_i$ of 160 m*M* and an assumed $[Na]_i$ of 15 m*M* is 0.18 (at $[K]_o$ of 4 m*M*). The value of $[K]_i$ was 160 m*M* for the guinea pig superior mesenteric artery, as extrapolated from the curve of E_m against log $[K]_o$. In guinea pig superior mesenteric artery, Cl^- ion appears to be passively distributed, i.e., Cl^- distributes itself in accordance with the average membrane potential ($E_{Cl} = E_m$) and there is no electrical evidence for a Cl^- pump. The average input resistance was about 9 MΩ, which, assuming a cell length of 200 μm and radius of 2.5 μm, gives a membrane resistivity (R_m)

ELECTRICAL EQUIVALENT CIRCUIT FOR CELL MEMBRANE OF VASCULAR SMOOTH MUSCLE OF DOG CORONARY ARTERY

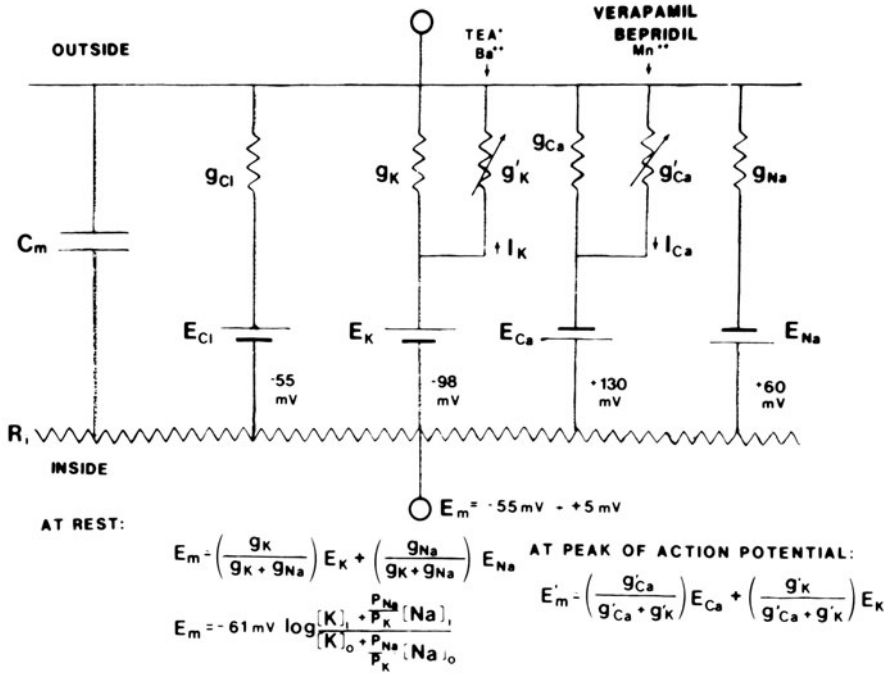

FIGURE 34–17. Electrical equivalent circuit for the cell membrane of arterial vascular smooth muscle cells. The conductance pathways (channels) are shown both for the resting membrane (g_K, g_{Na}, g_{Ca}, and g_{Cl}) and for the excited membrane (g'_{Ca} and g'_K). The arrow through the resistances (for the excited membrane) represent the fact that the resistance (conductance) varies with the membrane potential and time, i.e., these are voltage-dependent conductances. The equilibrium potentials for the four major ions of concern (E_K, E_{Na}, E_{Ca}, and E_{Cl}), as calculated from the Nernst equation for the known ion distributions, are depicted as batteries of differing polarities and magnitudes as indicated. The resistance channels are presumably due to protein molecules floating in the phospholipid bilayer matrix of the membrane, and the parallel capacitance (C_m) component is due to the lipid bilayer. Verapamil, bepridil, and Mn^{2+} block the Ca^{2+} slow channels, whereas TEA^+ and Ba^{2+} block the resting K^+ channels (depress g_K) and depress the kinetics of activation of g'_K. There may be only one type of voltage-dependent K^+ channel, one that allows K^+ to pass more readily outward (outwardly directed rectification or delayed rectification). The AP rising velocity and overshoot is determined by the inward slow Ca^{2+} current carried through the slow channels. The repolarization of the AP is brought about by a sharp increase in g'_K which is activated by the depolarization. Inexcitability may be produced when ($g_K + g'_K$) is too high. From Sperelakis [64].

TABLE 34–5. Calculation of contribution of electrogenic Na^+ pump potential to resting potential for different values of membrane resistivity from the circuit depicted in figure 34–18

R_m (Ω-cm^2)	E_{diff} (mv)	V_{ep} (mV)	E_m (mV)	ΔV ($E_m - E_{diff}$) (mV)
1,000	−46	−60	−55.3	− 9.3
5,000	−46	−60	−58.7	−12.7
1,000	−46	−70	−62.0	−16.0
1,000	−46	−46	−46.0	0
1,000	−46	0	−46.0	0
1,000	−77	−91	−86.3	− 9.3
5,000	−77	−91	−89.7	−12.7
1,000	−77	−85	−82.3	− 5.3
5,000	−77	−85	−84.3	− 7.3

$$E_m = \left(\frac{R_m}{R_m + R_p}\right) V_{ep} + \left(\frac{R_p}{R_m + R_p}\right) E_{diff}$$

R_p, the pump resistance, assumed to be constant (independent of R_m) at 500 Ω-cm^2 when the pump is operating, and infinite resistance when the pump is stopped. E_{diff} is the net diffusion potential based on the ion distributions (equilibrium potentials) and relative conductances. V_{ep} is the electrogenic Na^+ pump potential produced by a net outward positive current (e.g., three Na^+ ions extruded to two K^+ ions pumped in). E_m is the resting potential calculated from the equation given above. ΔV is the difference between E_m and E_{diff}, i.e., it gives the contribution of V_{ep} to the resting potential. Note that the resting potential (E_m) increases, due to a large contribution from V_{ep}, when R_m is increased; this is consistent with experimental observations. Also note that the contribution from V_{ep} to E_m is the same in cells that have a greater E_{diff}, when the difference between V_{ep} and E_{diff} (14 mV) is the same.

of 283 Ω-cm^2. (If low-resistance connections between cells exist, R_m would be underestimated.)

The arterial VSM cells in isolated strip preparations are generally electrically inexcitable in vitro (with the exception of some cultured rat aortic VSM cells), although these cells probably fire APs in situ in response to summated EJPs from neurotransmitter release. Addition of agents, such as Ba^{2+} and TEA^+, that depress K^+ conductance at rest and during excitation, and hence the outward K^+ current, allow large overshooting spike APs to be elicited by electrical stimulation. Suppression of the outward current should allow a greater net inward current, and thus facilitate regenerative excitation.

The maximal rate of rise ($+\dot{V}_{max}$) of the TEA-induced APs averages about 5 V/s. Depolarization reduces $+\dot{V}_{max}$, as expected, and complete inactivation of the slow channels ($+\dot{V}_{max} = 0$) occurs at a resting E_m of about −22 mV. The APs overshoot often to about +10 mV; in some cases, however, the APs undershoot, i.e., fail to reach the zero potential level. The degree of overshoot is a function of $[Ca]_0$, higher $[Ca]_0$ levels giving greater overshoots. The amplitude (and $+\dot{V}_{max}$) of the APs give straight lines when plotted against log $[Ca]_0$ (between 0.5 and 5.0 m*M*), with a slope of about 30 mV/decade. Since this slope is nearly exactly the theoretical value calculated from the Nernst equation for a divalent ion, and since variation in $[Na]_0$ has little or no effect on the amplitude or $+\dot{V}_{max}$ of the APs, the inward current during the TEA-induced APs is carried almost exclusively by Ca^{2+} ion.

Verapamil blocks the Ca^{2+}-dependent APs, as expected, whereas TTX has no effect on their amplitude or $+\dot{V}_{max}$. These results indicate that an inward fast Na^+ current does not contribute to the inward current of the AP, but that the inward current is entirely a slow current carried through slow channels. Thus, fast Na^+ channels are either absent or nonfunctional. In this respect, the VSM cells of adult animals are like the myocardial cells in very young embryonic hearts which possess many slow channels but little or no functional fast Na^+ channels (young tubular hearts may be considered as pulsating blood vessels) [85].

The TEA-induced Ca^{2+}-dependent APs make a good assay system for determining the effect of vasoactive substances on the VSM cells. For example, verapamil and bepridil,

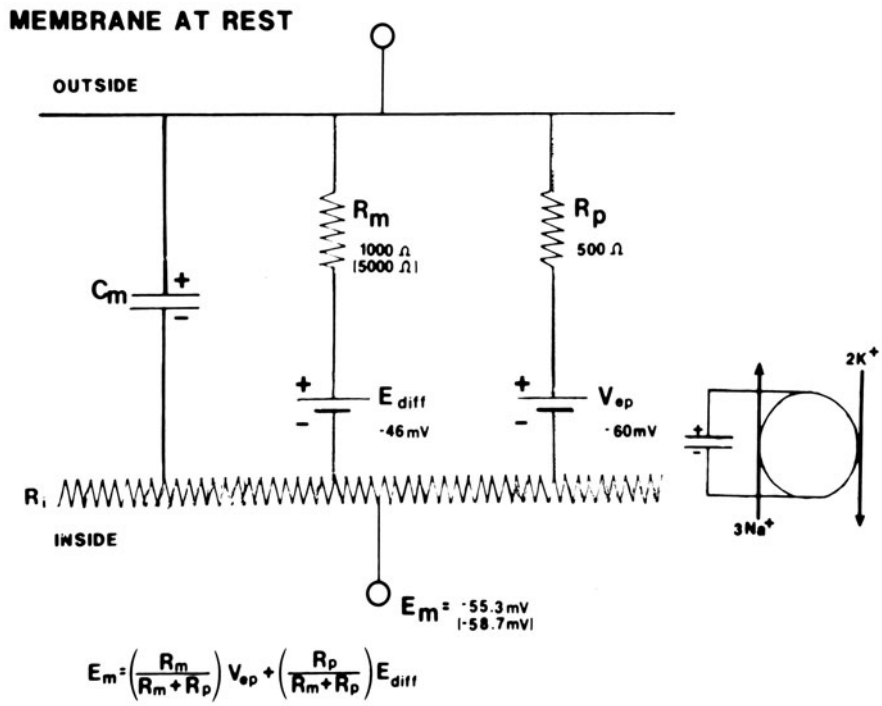

FIGURE 34–18. Hypothetical electrical equivalent circuit for an electrogenic sodium pump in vascular smooth muscle cells. Model consists of a pump pathway (R_p) in parallel with the membrane resistance (R_m) pathway and the membrane capacitance (C_m). The pump protein (Na,K)-ATPase and the ion-channel conductance proteins are floating in the lipid bilayer membrane as parallel elements. The net diffusion potential (E_{diff}) (determined by the ion equilibrium potentials and relative ion conductances) is depicted in series with R_m. The electrogenic Na^+ pump potential (V_{ep}) (determined by the rate of the pump turnover and the Na^+-K^+ coupling ratio) is depicted in series with the pump resistance (R_p). R_p is assumed to have a constant value close to R_m, but to be independent of changes in R_m, when the pump is operating at a constant rate; R_p is assumed to become infinite when the pump is stopped. (Alternatively, the internal resistance of V_{ep} can be considered as becoming infinite when the pump is stopped.) The inset provides another representation for the battery V_{ep}, namely, a capacitance in parallel with (and being charged by) the Na^+-K^+ exchange pump which is electrogenic (i.e., the Na^+/K^+ coupling ratio is greater than 1.00) and generating a constant outward current. From Sperelakis [64].

known coronary vasodilators, depress and block the APs, and hence the Ca^{2+} influx into the VSM cells during excitation. This action most likely accounts for the vasodilatory effect of these Ca^{2+}-antagonistic drugs. Another Ca^{2+}-antagonistic agent, Mn^{2+} ion, also abolishes the TEA-induced APs. Similarly, adenosine, a known vasodilator that may play a role in the local regulation of blood flow [86], was shown to depress and block the Ca^{2+}-dependent APs in small coronary arteries of the dog, but had no effect in the larger vessels. In contrast, nitroglycerin, another vasodilator, depressed and blocked the APs in large coronary arteries, but had no effect in the smaller vessels. Cardiac glycosides, known coronary vasoconstrictors, potentiate the inward Ca^{2+} current in small coronary arteries of the dog. This action of the cardiac glycosides can account for their vasoconstrictor action and may be important in digitalis toxicity.

Cultured VSM cells, prepared from arteries, retain many of the same electrical properties that the cells in the intact arteries possessed.

It is concluded that the electrical equivalent circuit of the cell membrane of arterial VSM cells is as depicted in figure 34–17. As shown in figure 34–17, there are voltage-dependent

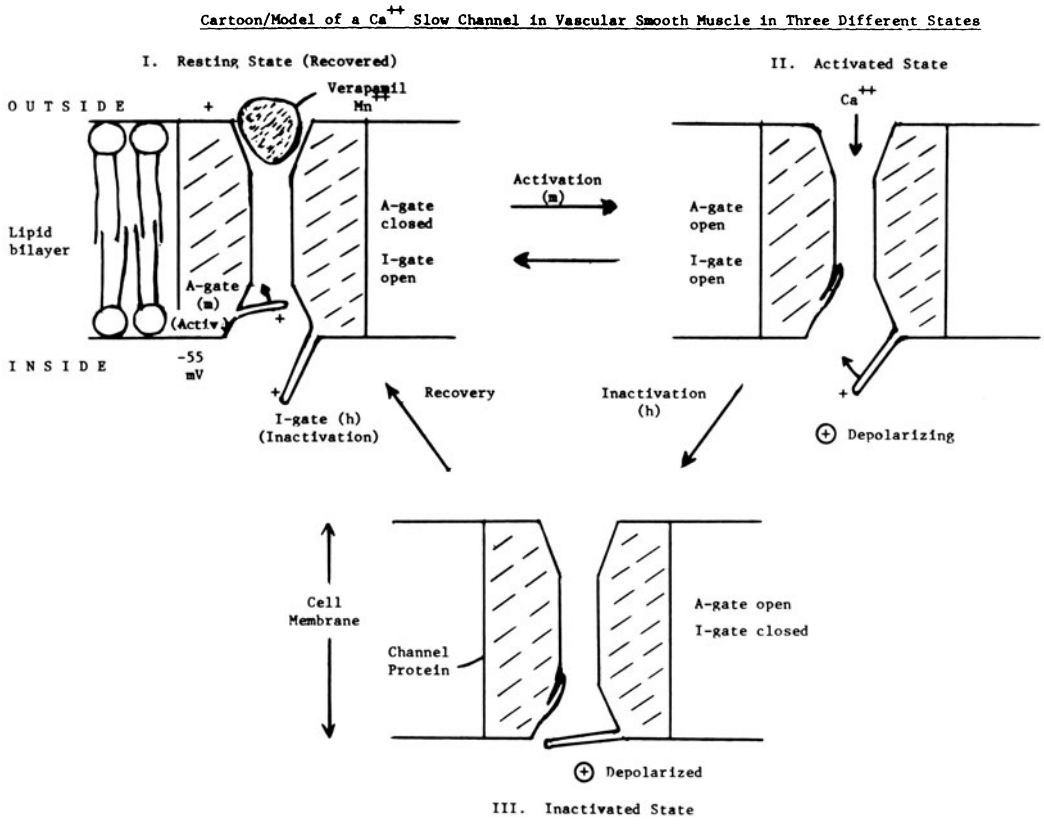

FIGURE 34–19. Cartoon/model of a Ca^{2+} slow channel in vascular smooth muscle. The channel protein spans the thickness of the cell membrane, and floats in the phospholipid bilayer matrix. Three different states of the channel gates are depicted. In the resting state, the activation (A) gate is closed and the (I) gate is open; thus, the channel is nonconducting. The voltage dependency of the channel is presumably due to the gates carrying a net positive charge. With depolarization to threshold, the channel changes into the activated (conducting) state, because the A gate opens quickly (by electrostatic repulsion) while the I gate is still open; that is, the kinetics of the A-gate movements are faster than those for the I gate. With continued depolarization, however, the I gate closes while the A gate is still open, and the channel passes into the inactivated state, which is also nonconducting. Upon repolarization, the two gates can move back into their original resting positions (recovery process). The main differences between slow channels in comparison with fast Na^+ channels are (a) that the kinetics of the gate movements appear to be much slower; (b) that the voltage range at which the gates open and close are at less negative voltages; and (c) that the drugs that block the channels are different, agents like verapamil and Mn^{2+} blocking slow channels, whereas agents like TTX block the fast Na^+ channels. The gates are depicted simply as physical barriers, but they might actually reflect conformational changes in the channel protein. The I gate is presumably located at the inner orifice of the channel, because proteolytic enzymes functionally remove the I gates without affecting the A gates (in perfused squid axons). From Sperelakis [64].

slow channels that are specific for Ca^{2+} ion, and are blocked by the slow-channel blockers verapamil, bepridil, and Mn^{2+}. There is probably only one type of voltage-dependent K^+ channel, the outward-going delayed-rectifier channel, which is responsible for repolarization of the AP. Agents like Ba^{2+} and TEA^+ affect both types of K^+ channels, namely, the resting g_K and the delayed-rectifier channel. The resting potential, more correctly E_{diff}, is determined by the resting values for the K^+ and Na^+ conductances (g_{Na}/g_K ratios) and the magnitude of E_K and E_{Na}. The electrogenic pump potential (V_{ep}) contribution to the resting po-

tential is illustrated in figure 34–18. Calculations based on the equivalent circuit depicted here are presented in table 34–5 to illustrate how the magnitude of the contribution of V_{ep} to the resting E_m is affected by membrane resistance (R_m).

The three states of the Ca^{2+} slow channel, modeled after the Hodgkin–Huxley hypothesis for the fast Na^+ channel. are schematized in figure 34–19. Some Ca^{2+}-antagonistic drugs may act to plug the channel physically by binding to its outer mouth or inner surface. In addition, because of the frequency dependency of the action of such agents, it seems likely that these drugs also depress and slow the recovery process of the channel, namely, the conversion from the inactive state back to the resting state. Binding of drug to the slow channel may occur primarily in the activated or inactivated states of the channel.

Since some Ca^{2+}-antagonistic drugs readily enter the muscle cells, it is possible that they may have a primary or secondary site of action intracellularly. For example, methoxy-verapamil has been shown to block the slow channels by acting on the inner surface of the cell membrane [87, 88]. Consistent with this, it was demonstrated that ^{3}H-bepridil and ^{3}H-verapamil readily enter vascular smooth muscle cells (rabbit aorta) [89, 90], thus consistent with the view that bepridil may also act to depress Ca^{2+} release from the SR [38]. In smooth muscle and cardiac muscle, the order of uptakes observed was: bepridil > verapamil >> nifedipine > diltiazem [90]. This order of uptakes was in the same order as their lipid solubilities [91]. In addition, verapamil and bepridil inhibit Ca^{2+} binding to isolated sarcolemma from guinea pig heart in a dose-dependent manner, verapamil being the more potent of the two agents; in contrast, nifedipine and diltiazem did not exert such an effect [92, 93].

Acknowledgments

The work of the author and his associates summarized in this chapter was supported by NIH grant HL-19242 and by grants from Wallace Laboratories and from Smith, Kline and French Laboratories. The author would like to acknowledge his associates who were involved in these studies: M.J. McLean, MD, PhD; D. Harder, PhD; E. Zelcer, PhD; S. Mras, PhD; P.-A. Molyvdas, MD; D. Johns, MD; and D. Pang, PhD.

Notes

1. Forbes and Sperelakis [94] have shown that there are junctional processes and pillars that connect the sarcolemma and surface caveolae with the membrane of the junctional SR, which may be involved in the transfer of excitation from the sarcolemma to the SR.

2. It has been demonstrated by Ridgeway et al. [45] that, in barnacle muscle, there is hysteresis in the force–$[Ca]_i$ relationship, such that the curve is shifted to the left as $[Ca]_i$ is decreased. Thus, a particular $[Ca]_i$ can maintain a higher force level than it can create, and contraction modulates Ca^{2+} sensitivity.

3. Thakkar et al. [95] demonstrated that the cultured rat aortic cells possess a potent phospholipase A_2 activity.

References

1. Mekata F: Electrophysiological properties of the smooth muscle cell membrane of the dog coronary artery. J Physiol (Lond) 298:205–212, 1980.
2. Somlyo AP, Somlyo AV: Vascular smooth muscle. I. Normal structure, pathology, biochemistry and biophysics. Pharmacol Rev 20:197–272, 1968.
3. Droogmans G, Raeymaekers L, Casteels R: Electro- and pharmacomechanical coupling in the smooth muscle cells of the rabbit ear artery. J Gen Physiol 70:129–148, 1977.
4. Somlyo AV, Somlyo AP: Electromechanical and pharmacomechanical coupling in vascular smooth muscle. J Pharmacol Exp Ther 159:129–145, 1968.
5. Somlyo AV, Vinall P, Somlyo AP: Excitation–contraction coupling and electrical events in two types of vascular smooth muscle. Microvasc Res 1:354–373, 1969.
6. Johansson B: Electromechanical and mechanoelectrical coupling in vascular smooth muscle. Angiologia 8:129–143, 1971.
7. Johansson B: Processes involved in vascular smooth muscle contraction and relaxation. Circ Res 43:14–20, 1978.
8. Zelcer E, Sperelakis N: Ionic dependence of electrical activity in small mesenteric arteries of guinea pig. Pflugers Arch 392:72–78, 1981.
9. Harder DR, Sperelakis N: Action potentials induced in guinea pig arterial smooth muscle by tetraethylammonium. Am J Physiol 237:C75–86, 1979.
10. Kumamoto M: Electrophysiological basis for drug action on vascular smooth muscle. In: Carnier O, Shibata S (eds) Factors influencing vascular resistivity. Tokyo: Igaku-Shoin, 1977, pp 106–131.

11. Horn L: Electrophysiology of vascular smooth muscle. In: Kaley G, Altura B (eds) Microcirculation, vol 2. Baltimore: University Park Press, 1978 pp 119–157.
12. Bolton TB: Mechanisms of action of transmitters and other substances on smooth muscle. Physiol Rev 59:606–718, 1979.
13. Johansson B, Somlyo AP: Electrophysiology and excitation–contraction coupling. In: Bohr DF, Somlyo AP, Sparks HV (eds) Handbook of physiology, Sect 2: The cardiovascular system. Vol 2: Vascular smooth muscle. Bethesda MD: American Physiological Society, 1980, pp 301–323.
14. Harder D, Sperelakis N: Membrane electrical properties of vascular smooth muscle from guinea pig superior mesenteric artery. Pflugers Arch 378:111–119, 1978.
15. Harder D, Belardinelli L, Sperelakis N, Rubio R, Berne RM: Differential effects of adenosine and nitroglycerin on the action potentials of large and small coronary arteries. Circ Res 44:176–182, 1979.
16. Belardinelli L, Harder D, Sperelakis N, Rubio R, Berne RM: Cardiac glycoside stimulation of inward Ca^{++} current in vascular smooth muscle of canine coronary artery. J Pharmacol Exp Ther 209:62–66, 1979.
17. Sperelakis N: Origin of the cardiac resting potential. In Berne RM, Sperelakis N (eds) Handbook of physiology Sect 2: The cardiovascular system. Vol 1: The heart. Bethesda MD: American Physiological Society, 1979, pp 187–267.
18. Sperelakis N, Schneider MF, Harris EJ: Decreased K^+ conductance produced by Ba^{++} in frog sartorius fibers. J Gen Physiol 50:1565–1583, 1967.
19. Sperelakis N, Lehmkuhl D: Effect of current on transmembrane potential in cultured chick heart cells. J Gen Physiol 47:895–927, 1964.
20. Sperelakis N: Propagation mechanisms in heart. Annu Rev Physiol 41:441–457, 1979.
21. Tomita T: Electrical responses of smooth muscle to external stimulation in hypertonic solution. J Physiol (Lond) 183:450–468, 1966.
22. Harder DR: Membrane electrical effects of histamine on vascular smooth muscle of canine coronary artery. Circ Res 46:372–377, 1980.
23. Bonaccorsi A, Hermsmeyer K, Aprigliano O, Smith CP, Bohr DF: Mechanism of potassium relaxation of arterial muscle. Blood Vessels 14:261–276, 1977.
24. Haddy FJ: The mechanism of potassium vasodilation. In: Vanhoutte PM, Leusen I (eds) Mechanisms of vasodilation. Basel: Karger, 1978, pp 200–205.
25. Webb RC, Bohr DF: Potassium-induced relaxation as an indicator of Na^+-K^+ ATPase activity in vascular smooth muscle. Blood Vessels 15:198–207, 1978.
26. Webb RC, Bohr DF: Potassium relaxation of vascular smooth muscle from spontaneously hypertensive rats. Blood Vessels 16:71–79, 1979.
27. Casteels R, Kitamura K, Kuriyama H, Suzuki H: The membrane properties of the smooth muscle cells of rabbit pulmonary artery. J Physiol 271:41–61, 1977.
28. Haeusler G: Relationship between noradrenaline-induced depolarization and contraction in vascular smooth muscle. Blood Vessels 15:46–54, 1978.
29. Ito Y, Suzuki H, Kuriyama H: Effects of sodium nitroprusside on smooth muscle cells of rabbit pulmonary artery and portal vein. J Pharmacol Exp Ther 207:1022–1031, 1978.
30. Mekata F, Niu H: Biophysical effects of adrenaline on the smooth muscle of the rabbit common carotid artery. J Gen Physiol 59:92–102, 1972.
31. Kuriyama H, Suzuki H: Electrical property and chemical sensitivity of vascular smooth muscles in normotensive and spontaneously hypertensive rats. J Physiol (Lond) 285:409–424, 1978.
32. Zelcer E, Sperelakis N: Spontaneous electrical activity in pressurized small mesenteric arteries. Blood Vessels 19:301–310, 1982.
33. Mekata F: Electrophysiological studies of the smooth muscle cell membrane of rabbit common cartotid artery. J Gen Physiol 57:738–751, 1971.
34. Holman ME, Surprenant AM: Some properties of the excitatory junction potentials recorded from saphenous arteries of rabbits. J Physiol 287:337–351, 1979.
35. Harder DR: Membrane electrical activation of arterial smooth muscle. In Crass C, Barnes CD (eds) Research topics in physiology: vascular smooth muscle. New York: Academic, 1981, pp 71–97.
36. Kohlhardt M, Fleckenstein A: Inhibition of the slow inward current by nifedipine in mammalian ventricular myocardium. Naunyn Schmiedebergs Arch Pharmacol 298:267–272, 1977.
37. Shigenobu K, Schneider JA, Sperelakis N: Verapamil blockade of slow NA^+ and Ca^{++} responses in myocardial cells. J Pharmacol Exp Ther 190:280–288, 1974.
38. Vogel S, Crampton R, Sperelakis N: Blockade of myocardial slow channels by bepridil (CERM-1978). J Pharmacol Exp Ther 210:378–385, 1979.
39. Harder DR, Sperelakis N: Action potential generation in reaggregates of rat aortic smooth muscle cells in primary culture. Blood Vessels 16:186–201, 1979.
40. Harder DR, Sperelakis N: Bepridil blockade of Ca^{++}-dependent action potentials in vascular smooth muscle of dog coronary artery. J Cardiovasc Pharmacol 3:906–914, 1981.
41. Mras S, Sperelakis N: Bepridil (CERM-1978) blockade of action potentials in cultured rat aortic smooth cells. Eur J Pharmacol 71:13–19, 1981.
42. Mras S, Sperelakis N: Bepridil (CERM-1978) and verapamil depression of contractions of rabbit aortic rings. Blood Vessels 18:196–205, 1981.
43. Sperelakis N, Mras S: Depression of contractions of rabbit aorta and guinea pig vena cava by mesudipine and slow channel blockers. Blood Vessels, 1983 (in press).
44. Fabiato A, Fabiato F: Calcium and cardiac excita-

tion–contraction coupling. Annu Rev Physiol 41:473–484, 1979.
45. Ridgway EB, Gordon AM, Martyn DA: Hysteresis in the force–calcium relation in muscle. Science 219:1075–1077, 1983.
46. Casteels R: Electro- and pharmacomechanical coupling in vascular smooth muscle. Chest (Suppl) 78:150–156, 1980.
47. Van Breeman C, Aaronson T, Loutzenhifer R: Sodium–calcium interactions in mammalian smooth muscle. Pharmacol Rev 30:167–208, 1979.
48. Motulsky HJ, Snavely MD, Hughes RJ, Insel PA: Interaction of verapamil and other calcium channel blockers with α_1- and α_2-adrenergic receptors. Circ Res 52:226–231, 1983.
49. Fleckenstein A, Nakayama K, Fleckenstein-Grün G, Byon YK: Interactions of vasoactive ions and drugs with Ca-dependent excitation–contraction coupling of vascular smooth muscle. In Carafoli E (ed) Calcium transport in contraction and secretion. Amsterdam: North Holland, 1975, pp 555–564.
50. Schnaar RC, Sparks HV: Response of large and small coronary arteries in nitroglycerin, $NaNO_2$ and adenosine. Am J Physiol 223:223–228, 1972.
51. Kohlhardt M, Bauer B, Krause H, Fleckenstein A: Differentiation of the transmembrane Na and Ca channels in mammalian cardiac fibers by the use of specific inhibitors. Pflugers Arch 335:309–322, 1972.
52. Fleckenstein A: Specific pharmacology of calcium in myocardium, cardiac pacemaker and vascular smooth muscle. Annu Rev Pharmacol Toxicol 17:149–166, 1977.
53. McLean MJ, Shigenobu K, Sperelakis N: Two pharmacological types of cardiac slow Na^+ channels as distinguished by verapamil. Eur J Pharmacol 26:379–382, 1974.
54. Labrid C, Grosset A, Dureng G, Mironneau J, Duchene-Marullaz P: Some membrane interactions with bepridil, a new antianginal agent. J Pharmacol Exp Ther 211:546–554, 1979.
55. Peiper U, Griebel L, Wende W: Activation of vascular smooth muscle of rat aorta by noradrenaline and depolarization: two different mechanisms. Pflugers Arch 330:74–89, 1971.
56. Haeusler G: Differential effect of verapamil on excitation–contraction coupling in smooth muscle and on excitation–secretion coupling in adrenergic nerve terminals. J Pharmacol Exp Ther 180:672–682, 1972.
57. Massingham R: A study of compounds which inhibit vascular smooth muscle contraction. Eur J Pharmacol 22:75–82, 1973.
58. Bilek I, Laven R, Peiper R, Regnat K: The effect of verapamil on the response to noradrenaline or to potassium-depolarization in isolated vascular strips. Microvasc Res 7:181–189, 1974.
59. Golenhofen K: Theory of P and T systems for calcium activation in smooth muscle. In: Bulbring F, Shuba MF (eds) Physiology of smooth muscle. New York: Raven, 1976, pp 197–202.
60. Cosnier D, Duchene-Marullaz P, Rispat G, Streichenberger G: Cardiovascular pharmacology of bepridil (1-[3-Isobutoxy-2-(benzyl-phenyl) amino] propyl pyrrolidine hydrochloride): a new potential anti-anginal compound. Arch Int Pharacodyn Ther 225:131–151, 1977.
61. Michelin FT, Cheucle M, Duchene-Marullaz P: Comparative influence of bepridil, dipyridimole and propranolol on cardiac activity and coronary venous blood flow in the anesthetized dog. Therapie 32:485–490, 1977.
62. Romano JP, Jouve A: Utilization clinique d'un nouvel anti-angineaux, le 1978 CERM (Bepridil, RL). Vie Med 1:1789–1791, 1978.
63. Schneider JA, Sperelakis N: Slow Ca^{++} and Na^+ responses induced by isoproterenol and methylxanthines in isolated perfused guinea pig hearts exposed to elevated K^+. J Mol Cell Cardiol 7:249–273, 1975.
64. Sperelakis N: Electrophysiology of vascular smooth muscle of coronary artery. In: Kalsner S (ed) The coronary artery. London: Croom Helm, 1982, pp 118–167.
65. Josephson I, Sperelakis N: Ouabain blockade of inward slow current in cardiac muscle. J Mol Cell Cardiol 9:409–418, 1977.
66. Casteels R, Suzuki H. The effect of histamine on the smooth muscle cells of the ear artery of the rabbit. Pflugers Arch 387:17–25, 1980.
67. Hirst GDS: Neuromuscular transmission in arterioles of guinea-pig submucosa. J Physiol 273:263–275, 1977.
68. Hirst GDS, Neild TO: An analysis of excitatory junctional potentials recorded from arterioles. J Physiol 280:87–104, 1978.
69. Hirst GDS, Neild TO: Some properties of spontaneous excitatory junction potentials recorded from arterioles of guinea-pigs. J Physiol 303:43–60, 1980.
70. Hirst GDS, Neild TO: Evidence for two populations of excitatory receptors for noradrenaline on arteriolar smooth muscle. Nature 283:767–768, 1980.
71. Hirst GDS, Neild TO: Localization of specialized noradrenaline receptors at neuromuscular junctions on arterioles of the guinea-pig. J Physiol 313:343–350, 1981.
72. Holman ME, Surprenant AM: Effects of tetraethylammonium chloride on sympathetic neuromuscular transmission in saphenous artery of young rabbits. J Physiol 305:451–465, 1980.
73. Holman ME, Surprenant AM: An electrophysiological analysis of the effects of noradrenaline and α-receptor antagonists on neuromuscular transmission in mammalian muscular arteries. Br J Pharmacol 71:651–661, 1980.
74. Surprenant A: A comparative study of neuromuscular transmission in several mammalian muscular arteries. Pflugers Arch 386:85–91, 1980.
75. Ross R, Glomset J, Kariya B, Harker L: A platelet-dependent serum factor that stimulates the prolifer-

ation of arterial smooth muscle cells in vitro. Proc Natl Acad Sci USA 71:1207–1210, 1974.
76. Sperelakis N: Cultured heart cell reaggregate model for studying problems in cardiac toxicology. In: Van Stee EW (ed) Cardiovascular toxicology. New York: Raven, 1982, pp 57–108.
77. Chamley J II, Campbell GR: Mitosis of contractile smooth muscle cells in tissue culture. Exp Cell Res 84:105–110, 1974.
78. Hermsmeyer K, De Cino P, White R: Spontaneous contractions of dispersed vascular smooth muscle in cell culture in vitro 12:628–634, 1976.
79. McLean MJ, Sperelakis N: Electrophysiological recordings from spontaneously contracting reaggregates of cultured vascular smooth muscle cells from chick embryos. Exp Cell Res 104:309–318, 1977.
80. Hermsmeyer K: High shortening velocity of isolated single arterial muscle cells. Experientia 35:1599–1602, 1979.
81. Zelcer E, Sperelakis N: Angiotensin induction of active responses in cultured reaggregates of rat aortic smooth muscle cells. Blood Vessels 18:263–279, 1981.
82. Kimes BW, Brandt BL: Characterization of two putative smooth muscle cell lines from rat thoracic aorta. Exp Cell Res 98:349–366, 1976.
83. McLean MJ, Pelleg A, Sperelakis N: Electrophysiological recordings from spontaneously contracting reaggregates of cultured vascular smooth muscle cells from guinea pig vas deferens. J Cell Biol 890:439–452, 1979.
84. Johns DW, Sperelakis N: Angiotensin-II depolarization of cultured vascular smooth muscle cells [abstr 815]. Circulation (Suppl 2) 66:II--204, 1982.
85. Biamino E, Kruckenberg P: Synchronization and conduction of excitation in the rat aorta. Am J Physiol 217:276–282, 1969.
86. Sperelakis N: Changes in membrane electrical properties during development of the heart. In: Zipes DP, Bailey JC, Elharrar V (eds) The slow inward current and cardiac arrhythmias. The Hague: Martinus Nijhoff, 1980, pp 221–262.
87. Berne RM: Cardiac nucleotides in hypoxia: possible role in regulation of coronary blood flow. Annu J Physiol 204:317–322, 1963.
88. Hescheler J, Pelzer D, Trube G, Trautwein W: Does the organic calcium channel blocker D600 act from inside or outside on the cardiac cell membrane? Pflugers Arch 393:287–291, 1982.
89. Mras S, Sperelakis N: Comparison of ^{3}H-bepridil and ^{3}H-verapamil uptake into rabbit aortic rings. J Cardiovasc Pharmacol 4:777–783, 1982.
90. Pang DC, Sperelakis N: Nifedipine, diltiazem, bepridil and verapamil uptakes into cardiac and smooth muscles. Eur J Pharmacol 87:199–207, 1983.
91. Pang DC, Sperelakis N: Uptakes of calcium antagonists into muscles as related to their lipid solubilities. Biochem Pharmacol 1983 (in press).
92. Pang DC, Sperelakis N: Inhibitory action of bepridil (CERM-1978) on calcium binding to cardiac sarcolemma of guinea pig. Biochem Pharmacol 30:2356–2358, 1981.
93. Pang DC, Sperelakis N: Differential actions of calcium antagonists on calcium binding to cardiac sarcolemma. Eur J Pharmacol 81:403–409, 1982.
94. Forbes MS, Sperelakis N: Bridging junctional processes in couplings of skeletal, cardiac, and smooth muscle. Muscle Nerve 5:674–681, 1982.
95. Thakkar JK, Sperelakis N, Pang D, Franson RC: Characterization of phospholipase A_2 activity in rat aorta smooth muscle cells. Biochim Biophys Acta 750:134–140, 1983.

35. ELECTROMECHANICAL AND PHARMACOMECHANICAL COUPLING IN VASCULAR SMOOTH MUSCLE

G. Droogmans
and R. Casteels

Introduction

The contractile response of smooth muscle cells is triggered by an increase of the free cytoplasmic concentration of calcium ions. In skinned smooth muscle fibers, i.e., tissues from which the cell membrane has been chemically removed by detergent treatment, the threshold Ca concentration for initiating contraction amounts to approximately 10^{-7} *M*, and full activation of the contractile proteins occurs at about 10^{-5} *M* calcium [1–3].

This change in Ca concentration can be brought about by an increased net influx of calcium ions from the extracellular medium, or by a mobilization of calcium ions from intracellular stores. When smooth muscle preparations are exposed to Ca-free solutions, or to solutions containing La^{3+} or Mn^{2+}, which block the entry of calcium ions, K depolarization does not evoke a contraction, whereas constrictor agents only induce a transient contraction. A second stimulation with these agonists does not evoke a second response [4, 5]. These findings indicate that a continuous supply of calcium ions from the extracellular medium is required to maintain a tonic force development in smooth muscle cells. They also illustrate that a recycling of Ca ions between sarcoplasmic reticulum and cytoplasm, as it occurs in striated muscle [6, 7], does not exist in smooth muscle.

N. Sperelakis (ed.), PHYSIOLOGY AND PATHOPHYSIOLOGY OF THE HEART.

Martinus Nijhoff Publishing, Boston/The Hague/ Dordrecht/Lancaster.

The early observations that K-depolarized smooth muscle cells, in which no electrical responses occur, can still be contracted by agonists [8, 9] suggested that these substances can affect the contractile state through other mechanisms than a change in membrane potential. It was further shown that the differences in the maximal contractile effects of different agonists are maintained in K-depolarized smooth muscle cells. These observations led to the introduction of the term pharmacomechanical coupling, as opposed to electromechanical coupling, to define the processes which lead to activation of contraction without a necessary change in resting potential [10].

This subdivision of activation of contraction into electro- and pharmacomechanical coupling ultimately led to the postulation of two types of Ca channels in smooth muscle cell membranes, i.e., voltage-sensitive Ca channels which are opened upon depolarization of the cell membrane, and receptor-operated Ca channels, which are opened by the interaction of agonists with their receptor [11].

Electromechanical Coupling and Voltage-sensitive Calcium Channels

RESTING POTENTIAL

In normal physiologic conditions, the resting membrane potential of vascular smooth muscle cells measured with intracellular microelectrodes ranges from −50mV to −70mV. This transmembrane potential difference is largely

due to passive diffusion. Active processes build up concentration gradients across the cell membrane, and the diffusion of ions down their electrochemical gradient induces a diffusion potential. Its magnitude is determined by the intra- and extracellular concentrations of the different permeating ionic species and by their relative permeabilities [12, 13]. The observation that changes in extracellular ion concentrations affect the resting potential is in agreement with such a mechanism. Because the membrane potential does not change by 62 mV for a tenfold change in $[K^+]_0$, it can be concluded that the membrane is not selective permeable for K ions, and that the permeability for other ions and/or other processes also contributes to the resting potential. From the experimental values of intra- and extracellular ionic concentrations and their relative permeabilites, a value of -31 mV for the diffusion potential has been calculated in rabbit main pulmonary artery [14], whereas the measured value of the resting potential amounts to -57 mV. The discrepancy between both values could be partly explained if some of the active transmembrane transport processes are electrogenic, i.e., the transfer of net electrical charges across the cell membrane by these pumps creates an additional potential difference. Evidence for the existence of an electrogenic Na-K pump has been presented for both visceral and vascular smooth muscle [15–17]. The nonpassive Cl distribution [18, 19] might also be caused by an active electrogenic Cl influx, which contributes to the membrane potential, as has been observed in guinea pig taenia coli [20]. This brief description of the mechanisms contributing to the membrane potential indicates that changes in this parameter can be induced by changes of the ion gradients or the ionic permeabilities, or by affecting the active ion transport. The latter action can modify the ionic gradients and/or the electrogenic component of the resting potential. These changes in membrane potential might directly affect vascular smooth muscle tone, or they might modulate the contractions induced by agonists.

ACTION POTENTIALS

Spontaneous action potentials of different configurations have been recorded in a number of vascular smooth muscle preparations, whereas in other preparations action potentials could be induced by K depolarization, electrical stimulation, or by application of excitatory agents [21–25]. In the larger vessels, however, the appearance of action potentials seemed to be exceptional, and could be induced only under rather unphysiologic conditions, e.g., in the presence of K-channel-blocking agents tetraethylammonium (TEA) and procaine [5, 26–39]. More recent experiments showed that exogenously applied noradrenaline and endogenous noradrenaline released from the nerve endings upon stimulation have different effects on the membrane potential [30, 31]. The release of neurotransmitter from the perivascular nerves induces excitatory junction potentials which can summate and reach threshold for eliciting an action potential when the stimulus frequency is sufficiently high. On the other hand, stimulation with exogenous noradrenaline does not affect the resting potential in these tissues. This discrepant action of exogenous and endogenous noradrenaline has been explained by assuming the existence of two different populations of α adrenoceptors, [32,33]: the classic extrajunctional α receptors, which are activated by exogenous noradrenaline, and the intrajunctional γ receptors, which are activated by endogenous noradrenaline released from the nerve terminals and which cannot be accessed by exogenous noradrenaline in a sufficiently high concentration to activate them. However, in guinea pig ear artery [34] and mesenteric vein [35] there was no discrepancy between the effects of endogenous and exogenous noradrenaline on the resting potential.

VOLTAGE-SENSITIVE CALCIUM CHANNELS

As discussed in chapter 34, the inward current responsible for the upstroke of the action potential in spike discharging tissues is probably carried by both Ca^{2+} and Na^+ ions. The contribution of each cation depends mainly on the ion selectivity of the channel and might vary between different vascular smooth muscles.

The amount of Ca^{2+} ions entering during a single action potential has been estimated from the amount of charge required to discharge the membrane capacity from the resting potential to the peak of the action potential, and by as-

suming that this charge is entirely carried by Ca^{2+} ions. This estimated value is an order of magnitude below the amount necessary to activate a maximal contraction. A possible explanation for this discrepancy might be that the net transmembrane current is an underestimated value of the inward Ca current because of the existence of an appreciable outward K current (net inward current << inward Ca current). Experimental evidence for such an important overlap between inward and outward membrane currents is lacking, because the technical limitations of the voltage-clamp technique applied to multicellular smooth muscle preparations do not allow a quantitative analysis of the ionic currents underlying the action potential. However, such an overlap might explain why some vascular smooth muscles generate action potentials in normal physiologic solutions, and others only do when the outward K current is blocked by TEA. An alternative explanation for the discrepancy between the amount of calcium estimated from the amplitude of the action potential and that required to activate a maximal contraction might be that the depolarization of the cell membrane, or the small amount of Ca^{2+} ions entering the cell during the action potential, triggers the release of calcium ions from an intracellular compartment, analogous to the excitation–contraction coupling in striated muscle. Convincing evidence in favor of the latter hypothesis is also lacking.

A graded depolarization of the cell membrane, e.g., by increasing $[K^+]_0$, stimulates ^{45}Ca influx and induces a contraction. Any experimental conditions which block spontaneous or induced action potentials and the concomitant contractile responses, such as exposure to Ca-free solutions, or application of Ca antagonists such as D-600, Mn^{2+}, or La^{3+}, also inhibit to a large extent the stimulation of the ^{45}Ca influx and the contraction induced by K depolarization [5]. This observation therefore favors the hypothesis that both activation mechanisms, action potentials and graded depolarizations, depend on the opening of the same type of Ca channels. K depolarization does not evoke a contractile response in Ca-free medium, and this suggests that a depolarization of the cell membrane does not trigger a release of intracellular Ca. Therefore it is also unlikely that the depolarizing phase of the action potential does induce such a release, but a Ca-induced Ca release during the action potential or during a graded depolarization cannot be excluded.

Pharmacomechanical Coupling and Receptor-operated Channels

RECEPTOR-OPERATED CHANNELS

In a number of vascular smooth muscle cells a change of the membrane potential is not the primary trigger for the contraction induced by agonists, because it occurs without a concomitant change of the resting potential [5, 31, 36, 37]. Similar observations have been obtained for the stimulation of pig coronary artery with acetylcholine [38]. In guinea pig coronary artery [39] and in rabbit mesenteric artery [40], acetylcholine elicits a contraction while hyperpolarizing the cell membrane. The constrictor effect of histamine in canine coronary artery is also accompanied by a hyperpolarization of the cells [41]. In basilar artery a close relationship was observed between membrane depolarization and contraction at low noradrenaline concentrations, but the amplitude of the contraction increases without a further depolarization at higher concentrations of the agonist [42]. In other preparations, such as rabbit pulmonary artery [14] and guinea pig aorta [43], noradrenaline induces a contraction at concentrations which do not affect the resting potential. This nonelectrical or pharmacomechanical activation depends both on an influx of Ca from the extracellular medium through receptor-operated channels (ROC) and on a release of Ca from intracellular stores [5, 44–47]. The latter is responsible for the initial phasic component of the contractile response, whereas the former causes the later tonic component of the contraction [48, 49].

These receptor-operated channels are not affected by organic Ca antagonists at concentrations which block the voltage-dependent Ca channels [50–52]. In guinea pig portal vein it was shown that part of the noradrenaline contraction was insensitive to 10^{-5} *M* verapamil, whereas at this drug concentration the sponta-

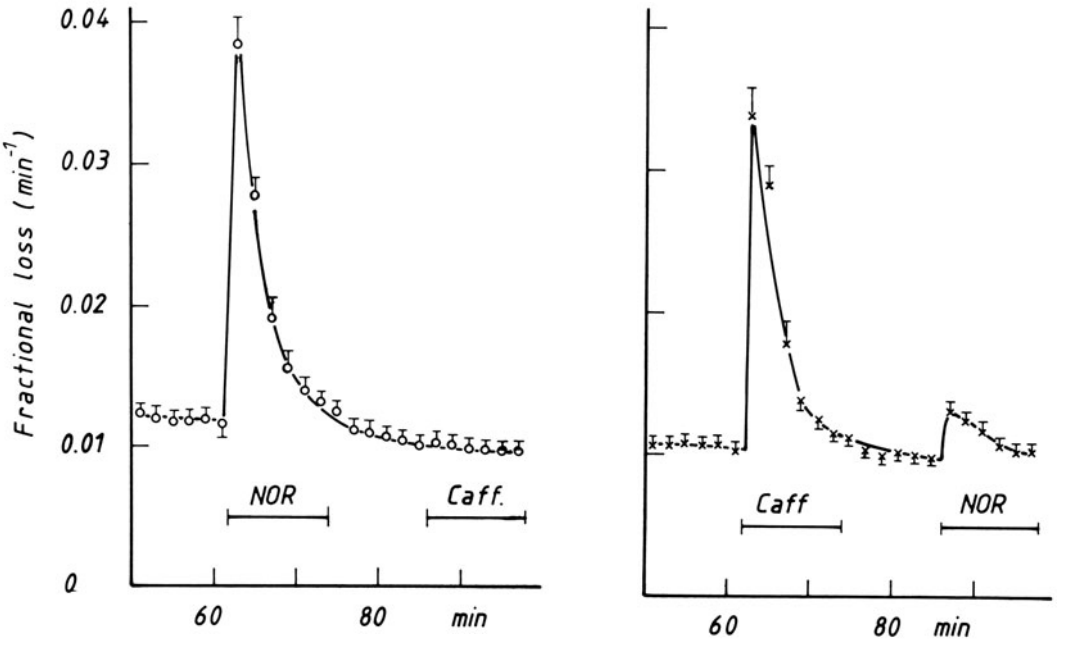

FIGURE 35–1. Effect of successive stimulations with 10^{-5} *M* noradrenaline (NOR) and 10 m*M* caffeine (caff) on the ^{45}Ca-efflux rate from rabbit ear artery. The efflux has been performed at 20°C in a Ca-free solution, and the initial 50 min of washout are not shown. Each curve represents the mean of four tissues.

neous electrical and mechanical activity, as well as the K-induced contraction, were completely blocked [53]. These observations strongly suggest that the ROC constitute a population of Ca channels which is different from the voltage-dependent channels. Also the observation that agonist-induced contractions and contractions induced by K depolarization have a different temperature sensitivity [54–57] is consistent with this hypothesis. The finding that different agonists produce unequal maximal contractile responses is not inconsistent with the existence of a single type of ROC, but might arise from a different degree of coupling of the various receptor types to these channels.

AGONIST-SENSITIVE CALCIUM STORES

The observation that excitatory agents, but not membrane depolarization, can evoke a transient contraction in smooth muscle preparations exposed to Ca-free solutions suggests that agonists may release calcium from intracellular Ca stores. Different agonists might act on the same intracellular Ca store, but release different amounts of stored calcium and induce contractions of different magnitudes in Ca-free solution [46, 58, 59]. This is illustrated in figure 35–1. Both caffeine (10 m*M*) and noradrenaline (10^{-5} *M*) induce a release of ^{45}Ca in rabbit ear artery. However, caffeine is no longer able to release Ca after a stimulation with noradrenaline, whereas, after a stimulation with caffeine, noradrenaline induces an additional Ca release. These findings suggest that both substances act on the same Ca compartment, but that noradrenaline is more effective than caffeine in depleting this store. Such a release mechanism has been described for most smooth muscle tissues, but there exists a large tissue variability concerning the capacity of this store or/and the rate at which calcium is lost from this compartment during exposure to Ca-free medium. In guinea pig taenia coli after about 3 min of exposure to Ca-free solution at 35°C the tissues no longer respond to stimulation with carbachol, suggesting that the intracellular carbachol-sensitive Ca store is depleted of

Ca [60]. On the other hand, vascular smooth muscle preparations, such as rabbit main pulmonary artery [61], rabbit ear artery [62], and rabbit aorta [47], respond to a stimulation with noradrenaline even after an exposure of 60 min to Ca-free solution. In dog coronary artery [63] and in rabbit basilar artery [64] the contractile response induced by noradrenaline in Ca-free solution declines very rapidly. Lowering the temperature reduces significantly the rate of Ca loss from this store [57, 65].

The transient nature of the contractile response in Ca-free medium is not due to a reuptake of the released calcium ions, but it is rather due an extrusion of these ions across the cell membrane. This explains why α-adrenergic activation is accompanied by a transient stimulation of the ^{45}Ca-efflux rate, and also why a second stimulation of these tissues in Ca-free medium does not induce a second phasic contractile response nor a stimulation of the ^{45}Ca efflux [5, 46, 58].

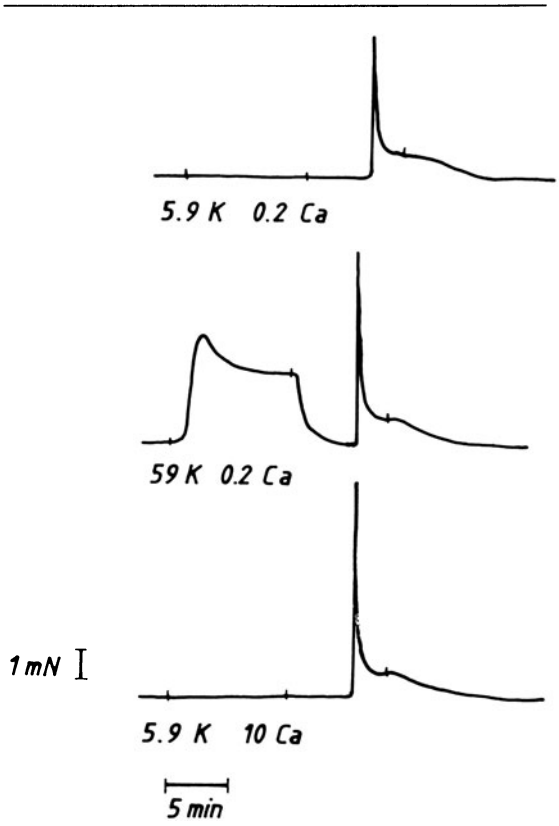

FIGURE 35–2. Effect of different loading procedures on the transient contractions induced by noradrenaline in Ca-free solutions. Ca-depleted tissues have been exposed during 10 min to solutions containing 5.9 m*M* K, 0.2 m*M* Ca (top); 59 m*M* K, 0.2 m*M* Ca (middle); or 5.9 m*M* K, 10 m*M* Ca (bottom). This loading procedure is followed by an exposure of 5 min to Ca-free solution and a subsequent stimulation with 10^{-5} *M* noradrenaline.

The absence of a recycling mechanism, such as it occurs in skeletal muscle between cytoplasm and sarcoplasmic reticulum, therefore raises the question of how the agonist-sensitive Ca store is refilled after it has been depleted by stimulation with an agonist in Ca-free solution. This refilling by reexposing these Ca-depleted tissues to Ca-containing solutions has been investigated in rabbit aorta [66] and in rabbit ear artery [62]. In the latter tissue it was found that the refilling of the noradrenaline-sensitive Ca store is much faster than its depletion during exposure to Ca-free solution. In addition, the filling rate and the final amount of Ca taken up in the agonist-sensitive Ca store strongly depend on the extracellular calcium concentration, suggesting that $[Ca^{2+}]_0$ is the main determinant of the amount of stored calcium and that the filling of the store might occur by a more direct pathway between extracellular and intracellular space. The secondary role of $[Ca^{2+}]_i$ in the filling of the store is demonstrated by the following experimental observation (fig. 35–2). Ca-depleted tissues which have been exposed to a solution containing 5.9 m*M* K and 10 m*M* Ca take up more calcium in the noradrenaline-sensitive Ca store (measured by the amplitude of the transient contraction induced by noradenaline in Ca-free solution) than tissues which have been exposed to a solution containing 59 m*M* K and 0.2 m*M* Ca, and this in spite of the fact that the tissues were contracted during the exposure to the latter solution ($[Ca^{2+}]_i$ high), whereas they remained relaxed ($[Ca^{2+}]_i$ low) during the exposure to the 5.9 m*M* K, 10 m*M* Ca-containing solution. At the same calcium concentration, however, a greater amount of calcium is taken up in the store during exposure to 59 m*M* K than during exposure to 5.9 m*M* K, indicating that also $[Ca^{2+}]_i$ might play some role in the refilling of that store.

Such a direct pathway between the extracellular space and the noradrenaline-sensitive Ca store might be formed by the anatomic couplings between the junctional sarcoplasmic reticulum and the surface membrane [67]. These are specialized regions where the SR membrane is separated from the cell membrane by a 10- to 12-nm gap traversed by periodic, electron-opaque processes.

The different rate of filling and of depletion of the noradrenaline-sensitive Ca store can be explained by assuming that the permeability of these junctions for calcium ions depends either on the direction of the electrochemical Ca gradient across this barrier or on the amount of calcium in the store. The dependency of the degree of filling on the extracellular Ca concentration is consistent with the first hypothesis, although convincing evidence in favor of any of these two mechanisms is lacking. An attractive extrapolation of this hypothesis is that receptor-operated channels and agonist-sensitive calcium stores can be integrated into a single mechanism. Receptor activation releases calcium from its storage sites, and thereby evokes the phasic component of contraction. The depletion of this calcium compartment causes an increase in the Ca permeability of its connection with the extracellular space. The concomitant influx of calcium through that pathway induces the tonic component of the contractile response in Ca-containing media.

Although the ability of different smooth muscles to contract in Ca-free solutions correlates with their SR volume [67], it has not been proven beyond any doubt that the agonist-sensitive Ca store corresponds to the SR. Freeze-fracture studies revealed the existence of particles on the SR membranes of smooth muscle which are implicated in Ca transport, although they are fewer in number than in skeletal and cardiac muscle [68]. By means of the electron microprobe it could be shown that this structure contains calcium [69]. Also an ATP-dependent Ca accumulation in the sarcoplasmic reticulum of skinned vascular smooth muscle fibers could be demonstrated [70]. The noradrenaline-sensitive Ca store in rabbit ear artery has been estimated at about 60 μmol/kg tissue weight [5]. By assuming that the calcium concentration in this store is the same as in the extracellular medium, it can be calculated that this structure occupies about 8% of the cell volume, and this value is close to the value for the SR volume determined morphometrically (2%–7.5%). These considerations suggest that the agonist-sensitive Ca store and the SR might be the same structure, although a release of calcium from the sarcoplasmic reticulum in situ or from isolated SR vesicles has not been demonstrated as yet.

Calcium Extrusion and Calcium Sinks

The dependency of the tonic force development on extracellular Ca^{2+} ions and the limited capacity of the intracellular organelles as Ca sinks suggest that vascular smooth muscle cells require an efficient transmembrane Ca-extrusion mechanism in order to maintain a constant Ca content and in order to induce relaxation.

CALCIUM-EXTRUSION MECHANISMS

Two different Ca-extrusion mechanisms have been proposed. In the first one the energy required to extrude calcium ions against their electrochemical gradient is derived from the electrochemical gradient of Na ions (Na-Ca exchange), which is created by the Na-K pump. An attractive feature of this hypothesis is that it not only explains the extrusion of calcium ions and relaxation, but it also predicts that a reduction of the electrochemical gradient of Na ions drives calcium ions into the cell and induces contraction [71]. The observations that Na-free solutions, and Na-K pump inhibition by cardiac glycosides or by exposure to K-free solutions which leads to a dissipation of the electrochemical Na gradient, induce vasoconstriction, and that the reestablishment of this gradient induces relaxation, are consistent with this hypothesis.

A detailed analysis of experimental data, obtained in rabbit ear artery [72], shows some inconsistencies with the Na-Ca exchange hypothesis. The effects of Na-free solutions on contraction and on ^{45}Ca efflux are similar to the effects of K depolarization, and therefore suggest a common mode of action, i.e., the opening of voltage-sensitive Ca channels. Both Na-

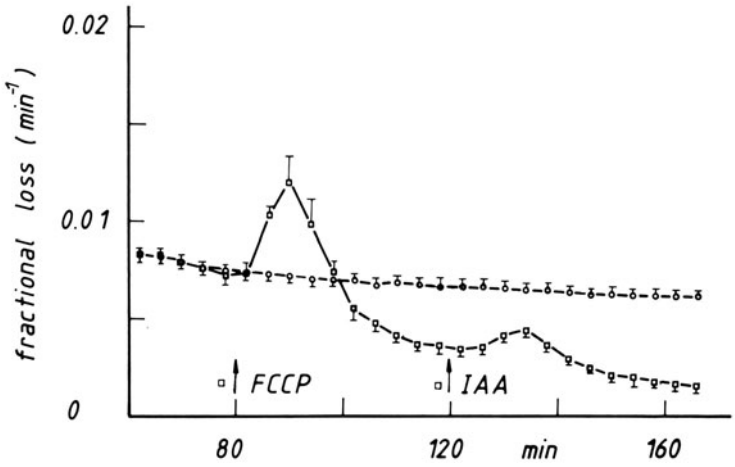

FIGURE 35–3. Effect of metabolic inhibition on the ^{45}Ca efflux from rabbit ear artery. The efflux has been performed at 20°C in a solution containing 0.5 m*M* Ca and 2 m*M* EGTA (pCa = 7), and the first 60 min of efflux are not shown. The open circles represent the control efflux. In the efflux curve represented by the open squares 10^{-5} *M* FCCP has been added after 80 min of efflux, and 10^{-3} *M* IAA has been added additionally after 120 min of efflux. Each curve represents the mean of four tissues.

free solutions and high K solutions induce a transient increase of the ^{45}Ca efflux when calcium is present in the external medium. This transient stimulation of the efflux, as well as the concomitant contractile response, are blocked by La^{3+} ions, which block the voltage-sensitive Ca channels. Na-free solutions induce a depolarization with a magnitude of 10–20 mV depending on the Na substitute. The amplitude of the concomitant contraction can be correlated with this depolarization, but it is greater than the contraction evoked by an equivalent depolarization induced by increasing $[K^+]_0$. These findings therefore suggest that Na-free solutions induce contraction by causing depolarization and the opening of voltage-sensitive channels. The absence of Na ions removes the competition between Na and Ca ions for these channels, which might be responsible for the greater contractile response observed in Na-free medium compared to that in a Na-containing solution at the same membrane potential.

The Na-Ca exchange hypothesis also predicts that Na-free solutions should affect the extrusion of Ca ions which are released from intracellular stores by stimulation with agonists, or which are released from mitochondria by the application of uncoupling agents, such as DNP or FCCP. However, this extrusion as measured by the transient stimulation of the ^{45}Ca-efflux rate is not significantly affected when the electrochemical Na gradient is reduced by lowering $[Na]_0$ or by a prolonged exposure of the tissues to K-free solutions [72]. Also the effect of Na-free solutions on the transient contraction induced by noradrenaline in Ca-free solutions is not consistent with the Na-Ca exchange hypothesis.

The alternative mechanism, an ATP-dependent Ca-extrusion pump, has been described in human erythrocytes [73]. A direct demonstration of such a pump in intact vascular smooth muscle preparations is difficult, because there are no known specific inhibitors for it. The interpretation of the effects of metabolic inhibition on the ^{45}Ca efflux is complicated by the fact that any interference with the energy supply of smooth muscle cells causes a release of calcium from intracellular structures [58, 72, 74]. Figure 35–3 shows the effect of metabolic inhibition on the ^{45}Ca-efflux rate from rabbit ear artery into a medium containing 10^{-7} *M* calcium. The extracellular calcium concentration has been decreased because a prolonged ex-

posure to metabolic inhibitors in Ca-containing media induces membrane leakiness [75], which is probably due to the increase in cellular calcium. It is obvious that the successive application of the inhibitors FCCP and IAA induces, after a transient stimulation, a significant reduction of the ^{45}Ca efflux below its control value. These observations and also the pronounced temperature effect on the ^{45}Ca-efflux rate [57] are consistent with an ATP-dependent Ca-extrusion mechanism, but, because of the redistribution of the cellular Ca under these conditions, they are not a foolproof demonstration of such a Ca pump.

More recent studies have focused on the demonstration of an ATP-dependent Ca accumulation in microsomal fractions prepared from smooth muscle tissues [76–78]. In all microsomal preparations it was possible to demonstrate a very efficient ATP-dependent Ca accumulation, but there is some controversy about the nature and the purity of these membrane fractions. In some preparations [79] a small component of Ca uptake dependent on the electrochemical Na gradient has been observed, but it has a low affinity for Ca ions and also a low capacity compared to the ATP-dependent extrusion pump.

INTRACELLULAR CALCIUM SINKS AND RELAXATION

Transmembrane Ca extrusion probably represents the ultimate step in the relaxation of vascular smooth muscle, because of the limited capacity of the intracellular Ca stores and because of the absence of a recycling mechanism for stored calcium in these tissues. However, this does not necessarily imply that there is a direct contribution of transmembrane Ca extrusion to the relaxation process, because intracellular organelles might function as an intermediate storage site preceding the extrusion of activator calcium. There is only scarce experimental evidence for the direct contribution of each of these processes to relaxation.

In rabbit ear artery, reducing the temperature from 35°C to 20°C does not affect the amount of ^{45}Ca released by noradrenaline in Ca-free solution. However, the amplitude of the concomitant contraction is much smaller at 35°C, because the transmembrane Ca extrusion is much faster at this temperature and the released Ca will therefore induce a smaller increase in $[Ca^{2+}]_i$ [57]. This observation suggests that transmembrane Ca extrusion might play a direct role in the relaxation process.

Experimental evidence for an ATP-dependent Ca uptake in the sarcoplasmic reticulum of skinned vascular smooth muscle cells has been presented [70]. Also the observation that the noradrenaline-sensitive Ca store takes up more calcium when the intracellular calcium concentration is increased, such as during K depolarization, is consistent with an intermediate storage function of the SR. A stimulation of Ca uptake in the agonist-sensitive Ca store by β-agonists also fits this hypothesis [43, 60]. In guinea pig mesenteric artery, isoprenaline induces a relaxation which is accompanied by an increase in cyclic AMP. On the other hand, it was found that application of cyclic AMP and protein kinase to a skinned preparation of this tissue increases the uptake of calcium ions into an intracellular store [80].

Isolated mitochondria show a great capacity for Ca uptake [81, 82]. In intact preparations the uncouplers of oxidative phosphorylation DNP and FCCP induce a release of ^{45}Ca from the mitochondria. Based on these observations it could be argued that mitochondria might also function as an additional Ca storage site. However, electron-probe analysis revealed the presence of Ca granules in mitochondria of smooth muscle fibers which had been damaged, but not in normal smooth muscle cells [69]. Therefore it is rather unlikely that mitochondria play an important role in excitation–contraction coupling.

It has also been suggested that the inner edge of the cell membrane serves as a Ca store, which can be released upon stimulation and which can be filled directly from the outside [47]. These calcium ions might directly activate the contractile proteins or they might serve as trigger calcium for the release of calcium from other intracellular stores (calcium-induced Ca release). Histochemical studies showed electron-opaque precipitates of calcium salts close to the cell membrane and its translocation during stimulation [83–87]. Because

of the limited resolution of these techniques, these precipitates might correspond to calcium bound to the cell membrane or to calcium in junctional SR vesicles. Because these findings could not be confirmed by electron-probe analysis, and because a membrane-bound Ca fraction is not present in more accessible cell types, it is rather unlikely it plays an important role in excitation–contraction coupling.

References

1. Endo M, Kitazawa T, Yagi S, Iino M, Kakuta Y: Some properties of chemically skinned smooth muscle fibers. In: Casteels R, Godfraind T, Ruegg JC (eds) Excitation–contraction coupling in smooth muscle. Amsterdam: North Holland, 1977, pp 199–209.
2. Gordon AR: Contraction of detergent-treated smooth muscle. Proc Natl Acad Sci USA 75:3527–3530, 1978.
3. Saida K, Nonomura Y: Characteristics of Ca^{2+} and Mg^{2+}-induced tension development in chemically skinned smooth muscle cells. J Gen Physiol 72:1–14, 1978.
4. Van Breemen C, Farinas BR, Gerba P, McNaughton ED: Excitation–contraction coupling in rabbit aorta studied by the lanthanum method for measuring calcium influx. Circ Res 30:33–54, 1972.
5. Droogmans G, Raeymaekers L, Casteels R: Electro- and pharmacomechanical coupling in the smooth muscle cells of the rabbit ear artery. J Gen Physiol 70:129–148, 1977.
6. Ebashi S: Regulation of muscle contraction. Proc R Soc Lond [B] 207:259–286, 1980.
7. Caputo C: Excitation and contraction processes in muscle. Annu Rev Biophys Bioeng 7:63–83, 1978.
8. Evans DHL, Schild HO, Thesleff S: Effects of drugs on depolarized plain muscle. J Physiol (Lond) 143:474–485, 1958.
9. Waugh WH: Adrenergic stimulation of depolarized arterial muscle. Circ Res 11:264–276, 1962.
10. Somlyo AV, Somlyo AP: Electromechanical and pharmacomechanical coupling in vascular smooth muscle. J Pharmacol Exp Ther 159:129–145, 1968.
11. Bolton TB: Mechanism of action of transmitters and other substances on smooth muscle. Physiol Rev 59:606–718, 1979.
12. Goldmann DE: Potential, impedance and rectification in membranes. J Gen Physiol 27:37–60, 1943.
13. Hodgkin AL, Katz B: The effect of sodium ions on the electrical activity of the giant axon of the squid. J Physiol (Lond) 108:37–77, 1949.
14. Casteels R, Kitamura R, Kuriyama H, Suzuki H: The membrane properties of the smooth muscle cells of the rabbit pulmonary artery. J Physiol (Lond) 271:41–61, 1977.
15. Casteels R, Droogmans G, Hendrickx H: Electrogenic sodium pump in smooth muscle cells of the guinea-pig's taenia coli. J Physiol (Lond) 217:297–313, 1971.
16. Hendrickx H, Casteels R: Electrogenic sodium pump in arterial smooth muscle cells. Pflugers Arch 346:299–306, 1974.
17. Bonaccorsi A, Hermsmeyer K, Aprigliano O, Smith CB, Bohr DF: Mechanism of potassium relaxation of arterial muscle. Blood Vessels 14:261–276, 1977.
18. Casteels R: The distribution of chloride ions in the smooth muscle cells of the guinea-pig's taenia coli. J Physiol (Lond) 214:225–243, 1971.
19. Aickin CC, Brading AF: Measurement of intracellular chloride in guinea-pig vas deferens by ion analysis, ^{36}chloride efflux and micro-electrodes. J Physiol (Lond) 326:139–154, 1982.
20. Droogmans G, Casteels R: Membrane potential and ion transport in smooth muscle cells. In: Buelbring E, Shuba MF (eds) Physiology of smooth muscle. New York: Raven, 1976, pp 11–18.
21. Funaki S: Spontaneous spike-discharges of vascular smooth muscle. Nature 191:1102–1103, 1961.
22. Steedman WM: Micro-electrode studies on mammalian vascular muscle. J Physiol (Lond) 186:382–400, 1966.
23. Somlyo AV, Vinall P, Somlyo AP: Excitation–contraction coupling and electrical events in two types of vascular smooth muscle. Microvasc Res 1:354–373, 1969.
24. Golenhofen K, Von Loh D: Intracellulare Potentialmessungen zur normalen Spontanaktivitat des isolierten Portalvene des Meerschweinchens. Pflugers Arch 319:82–100, 1970.
25. Harder DR: Comparison of electrical properties of middle cerebral and mesenteric artery in cat. Am J Physiol 239:C23–C26, 1980.
26. Harder DR, Sperelakis N: Membrane electrical properties of vascular smooth muscle from guinea-pig superior mesenteric artery. Pflugers Arch 378:111–119, 1978.
27. Harder DR, Sperelakis N: Action potentials induced in guinea-pig arterial smooth muscle by tetraethylammonium. Am J Physiol 237:C75–C80, 1979.
28. Itoh T, Kuriyama H, Suzuki H: Excitation–contraction coupling in smooth muscle cells of the guinea-pig mesenteric artery. J Physiol (Lond) 321:513–535, 1981.
29. Harder DR, Belardinelli L, Sperelakis N, Rubio R, Berne RM: Differential effects of adenosine and nitroglycerin on the action potentials of large and small coronary arteries. Circ Res 44:176–182, 1979.
30. Hirst GDS: Neuromuscular transmission in arterioles of guinea-pig submucosa. J Physiol (Lond) 273:263–275.
31. Holman ME, Surprenant A: Some properties of the excitatory junction potentials recorded from saphenous arteries of rabbits. J Physiol (Lond) 287:337–351, 1979.
32. Hirst GDS, Neild TD: Evidence for two populations

of excitatory receptors for noradrenaline in arteriolar smooth muscle. Nature 283:767–768, 1980.
33. Hirst GDS, Neild TD: Localization of specialized noradrenaline receptors at neuromuscular junctions on arterioles of the guinea-pig. J Physiol (Lond) 313:343–350, 1981.
34. Kajiwara M, Kitamura K, Kuriyama H: Neuromuscular transmission and smooth muscle membrane properties in the guinea-pig ear artery. J Physiol (Lond) 315:283–302, 1981.
35. Suzuki H: Effects of endogenous and exogenous noradrenaline on the smooth muscle of guinea-pig mesenteric vein. J Physiol (Lond) 321:495–512, 1981.
36. Su C, Bevan JA, Ursillo RC: Electrical quiescence of pulmonary artery smooth muscle during sympathomimetic stimulation. Circ Res 15:20–27, 1964.
37. Vonderlage M: Spread of contraction in rabbit ear artery preparations in response to stimulation by norepinephrine. Circ Res 49:600–608, 1981.
38. Ito Y, Kitamura K, Kuriyama H: Effects of acetylcholine and catecholamines on the smooth muscle cells of the porcine coronary artery. J Physiol (Lond) 294:595–611, 1979.
39. Kitamura K, Kuriyama H: Effects of acetylcholine on the smooth muscle cell of isolated main coronary artery of the guinea-pig. J Physiol (Lond) 293:119–133, 1979.
40. Kuriyama H, Suzuki H: The effects of acetylcholine on the membrane and contractile properties of smooth muscle cells of the rabbit superior mesenteric artery. Br J Pharmacol 64:493–501, 1978.
41. Harder DR: Membrane electrical effects of histamine on vascular smooth muscle of canine coronary artery. Circ Res 46:372–377, 1980.
42. Harder DR, Abel PW, Hermsmeyer K: Membrane electrical mechanism of basilar artery constriction and pial artery dilation by norepinephrine. Circ Res 49:1237–1242, 1981.
43. Kajiwara M: General features of electrical and mechanical properties of smooth muscle cells in the guinea-pig abdominal aorta. Pflugers Arch 393:109–117, 1982.
44. Godfraind T, Kaba A: The role of calcium in the action of drugs on vascular smooth muscle. Arch Int Pharmacodyn 196:35–49, 1972.
45 Bohr DF: Vascular smooth muscle updated. Circ Res 32:665–671, 1973.
46. Deth R, Van Breemen C: Relative contributions of Ca^{++} influx and cellular Ca^{++} release during drug-induced activation of the rabbit aorta. Pflugers Arch 348:13–22, 1974.
47. Deth R, Van Breemen C: Agonist induced release of intracellular Ca^{++} in the rabbit aorta. J Membr Biol 30:363–380, 1977.
48. Bevan JA, Waterson JG: Biphasic constrictor response of the rabbit ear artery. Circ Res 28:655–661, 1971.
49. Steinsland OS, Furchgott RF, Kirpekar SM: Biphasic constriction of the rabbit ear artery. Circ Res 32:49–58, 1973.
50. Peiper U, Griebel L, Wende W: Activation of vascular smooth muscle cells of rat aorta by noradrenaline and depolarization: two different mechanisms. Pflugers Arch 330:74–89, 1971.
51. Bilek I, Laven R, Peiper U, Regnat K: The effect of verapamil on the response to noradrenaline or to potassium-depolarization in isolated vascular strips. Microvasc Res 7:181–189, 1974.
52. Golenhofen K, Hermstein N: Differentiation of calcium activation mechanisms in vascular smooth muscle by selective suppression with verapamil and D600. Blood Vessels 12:21–37, 1975.
53. Golenhofen K, Hermstein N, Lammel E: Membrane potential and contraction of vascular smooth muscle (portal vein) during application of noradrenaline and high potassium, and selective inhibitory effects of iproveratril (verapamil). Microvasc Res 5:73–80, 1973.
54. Vanhoutte PM, Shepherd JT: Effect of temperature on reactivity of isolated cutaneous veins of the dog. Am J Physiol 218:1746–1750, 1970.
55. Vanhoutte PM, Lorenz RR: Effect of temperature on reactivity of saphenous, mesenteric and femoral veins of the dog. Am J Physiol 218:317–329, 1970.
56. Peiper U, Griebel L, Wende W: Unterschiedliche Temperaturabhangigkeit der Gefassmuskelkontraktion nach Aktivierung durch Kalium-Depolarization bzw. Noradrenalin. Pflugers Arch 324:67–78, 1971.
57. Droogmans G, Casteels R: Temperature-dependence of ^{45}Ca fluxes and contraction in vascular smooth muscle cells of rabbit ear artery. Pflugers Arch 391:183–189, 1981.
58. Deth R, Casteels R: A study of releasable Ca^{2+} fractions in smooth muscle cells of the rabbit aorta. J Gen Physiol 69:401–416, 1977.
59. Deth R, Lynch CJ: Mobilization of a common source of smooth muscle Ca^{2+} by norepinephrine and methylxanthines. Am J Physiol 240:C239–C247, 1981.
60. Casteels R, Raeymaekers L: The action of acetylcholine and catecholamines on an intracellular calcium store in the smooth muscle cells of the guinea-pig taenia coli. J Physiol (Lond) 294:51–68, 1979.
61. Casteels R, Kitamura K, Kuriyama H, Suzuki H: Excitation–contraction coupling in the smooth muscle cells of the rabbit main pulmonary artery. J Physiol (Lond) 271:63–79, 1977.
62. Casteels R, Droogmans G: Exchange characteristics of the noradrenaline sensitive calcium store in vascular smooth muscle cells of rabbit ear artery. J Physiol (Lond) 317:263–279, 1981.
63. Van Breemen C, Siegel B: The mechanism of α-adrenergic activation of the dog coronary artery. Circ Res 46:426–429, 1980.
64. McCalden TA, Bevan JA: Sources of activator calcium in rabbit basilar artery. Am J Physiol 241:H129–H131, 1981.
65. Somlyo AP, Devine CE, Somlyo AV, North SR: Sarcoplasmic reticulum and the temperature-dependent contraction of smooth muscle in calcium free solution. J Cell Biol 51:722–741, 1971.

66. Karaki H, Kubota H, Urakawa N: Mobilization of stored calcium for phasic contraction induced by norepinephrine in rabbit aorta. Eur J Pharmacol 56:237–245, 1979.
67. Devine CE, Somlyo AV, Somlyo AP: Sarcoplasmic reticulum and excitation–contraction coupling in mammalian smooth muscle. J Cell Biol 52:690–718, 1972.
68. Devine CE, Rayns DG: Freeze fracture studies of membrane systems in vertebrate muscle. II. Smooth muscle. J Ultrastruct Res 51:293–306, 1975.
69. Somlyo AP, Somlyo AV, Shuman H: Electron probe analysis of vascular smooth muscle: composition of mitochondria, nuclei and cytoplasm. J Cell Biol 67:911–918, 1979.
70. Raeymaekers L, Casteels R: Measurement of Ca uptake in the endoplasmic reticulum of the smooth muscle cells of the rabbit ear artery. Arch Int Physiol Biochim 75:33–34, 1981.
71. Blaustein MP: Sodium ions, calcium ions, blood pressure regulation and hypertension: a reassessment and an hypothesis. Am J Physiol 232:C165–C173, 1977.
72. Droogmans G, Casteels R: Sodium and calcium interactions in vascular smooth muscle cells of rabbit ear artery. J Gen Physiol 74:57–70, 1979.
73. Schatzmann HJ, Vincenzi FF: Calcium movements across the membrane of human red cells. J Physiol (Lond) 201:369–395, 1969.
74. Van Breemen C, Wuytack F, Casteels R: Stimulation of ^{45}Ca efflux from smooth muscle cells by metabolic inhibition and high K depolarization. Pflugers Arch 359:183–196, 1975.
75. Casteels R, Van Breemen C, Wuytack F: Effect of metabolic depletion on the membrane permeability of smooth muscle cells and its modification by La^{3+} Nature 239:249–251, 1972.
76. Fitzpatrick DF, Landon EJ, Debbas G, Hurwitz L: A calcium pump in vascular smooth muscle. Science 176:305–306, 1972.
77. Wei J-W, Janis RA, Daniel EE: Isolation and characterization of plasma membrane from rat mesenteric arteries. Blood Vessels 13:279–292, 1976.
78. Wuytack F, Landon E, Fleischer S, Hardman JG: The calcium accumulation in a microsomal fraction from porcine coronary artery smooth muscle: a study of the heterogeneity of the fraction. Biochim Biophys Acta 540:253–269, 1978.
79. Grover AK, Kwan CY, Daniel EE: Na-Ca exchange in rat myometrium membrane vesicles highly enriched in plasma membranes. Am J Physiol 240:C175–C182, 1981.
80. Itoh T, Izumi H, Kuriyama H: Mechanisms of relaxation induced by activation of β-adrenoceptors in smooth muscle cells of the guinea-pig mesenteric artery. J Physiol (Lond) 326:475–493, 1982.
81. Batra S: The role of mitochondrial calcium uptake in contraction and relaxation of human myometrium. Biochim Biophys Acta 305:428–432, 1972.
82. Raeymaekers L, Wuytack F, Batra S, Casteels R: A comparative study of the calcium accumulation by mitochondria and microsomes isolated from the smooth muscle of the guinea-pig taenia coli. Pflugers Arch 368:217–223, 1977.
83. Popescu LM, Diculescu I, Zelck U, Ionescu N: Ultrastructural distribution of calcium in smooth muscle cells of guinea-pig taenia coli. Cell Tissue Res 154:357–378, 1974.
84. Debbas G, Hoffman L, Landon EJ, Hurwitz L: Electron microscopic localization of calcium in vascular smooth muscle. Anat Rec 182:447–472, 1975.
85. Atsumi S, Sugi H: Localization of calcium-accumulating structures in the anterior byssal retractor muscle of *Mytilus Edulis* and their role in the regulation of active and catch contractions. J Physiol (Lond) 257:549–560, 1976.
86. Sugi H, Daimon T: Translocation of intracellularly stored calcium during the contraction–relaxation cycle in guinea-pig taenia coli. Nature 269:436–438, 1977.
87. McGuffee LJ, Hurwitz L, Little SA, Skipper BE: A ^{45}Ca autoradiographic and stereological study of freeze-dried smooth muscle of the guinea-pig vas deferens. J Cell Biol 90:201–210, 1981.

36. VASCULAR MUSCLE MEMBRANE PROPERTIES IN HYPERTENSION

Kent Hermsmeyer

Introduction

Although it would be ideal to present a discussion of how the coronary circulation is altered at the cell level in hypertension, there exist virtually no data comparing membrane properties of coronary vascular muscle cells from hypertensive and normotensive animals. However, the elevated peripheral resistance in hypertension is believed to be a predisposing influence to cardiac pathology. In this light, the present chapter is included to identify the changes in vascular muscle that result in increased peripheral resistance and so increase the workload of the heart. It might be hoped that the properties of the coronary circulation will be sufficiently different from the peripheral vasculature that new antihypertensive agents (e.g., perhaps selective Ca^{2+} antagonists such as nitrendipine) might cause relaxation of specifically the peripheral vasculature without diminishing the regulatory mechanisms operating in the coronary circulation. In any event, the specific comparative study of the coronary vascular muscle cells of normotensive and hypertensive animals is needed.

Several animal models have contributed to our understanding of mechanisms involved in hypertension. One of the most studied animal forms of genetic hypertension is the Okamoto-Aoki strain of spontaneously hypertensive rat (SHR) and the precisely genetically matched strain of normotensive rats (all derived from the same parents), designated Wistar-Kyoto normotensive rats (WKY). Although cardiac contractility is not different in SHR and WKY during the developmental stages of hypertension, cardiac function in SHR is dependent on an exaggerated β-adrenergic drive, which is, however, apparently not essential to the development of hypertension because pharmacologic blockade of the increased β-adrenergic drive does not hinder development of the hypertensive state in SHR [1]. However, older SHR develop ventricular hypertrophy and cardiac performance deteriorates [2]. The cardiac hypertrophy is associated with a decrease in the mitochondria per unit cell volume [3,4]. Even when cardiac hypertrophy is reversed by removing the pressure overload, the normalization of cardiac mass does not necessarily follow. For example, hydralazine lowers blood pressure without decreasing left ventricular mass [5]. Furthermore, α-methyldopa normalized the mitochondria to myofibril ratio even when administered in dosages that did not lower blood pressure, but only in animals treated beginning at one month of age [6]. There thus appears to be a selective effect of α-methyldopa on myocardial cell changes independent of blood pressure.

It is clear that hypertension is the most common cause of left ventricular hypertrophy and the most common precursor of congestive heart failure [7]. Even in borderline hypertensive children, there is significant cardiac hypertrophy and perhaps the early stages of cardiac problems [8]. Studies to determine whether reduction in systolic blood pressure and thus the work load of the heart would improve coronary flow or further aggravate coronary blood flow

This research was supported by grants HL 14388 and HL 16328 from the National Institutes of Health.

N. Sperelakis (ed.), PHYSIOLOGY AND PATHOPHYSIOLOGY OF THE HEART.

Martinus Nijhoff Publishing, Boston/The Hague/ Dordrecht/Lancaster.

(by causing coronary insufficiency) have suggested that, in all cases, the reduction of the pressure load and excessive myocardial oxygen requirements improves cardiac function, provided that the extent of vasodilator therapy did not excessively lower blood pressure [7]. Thus, humans with hypertension suffer a loss of cardiac function, possibly beginning in early stages of elevated blood pressure, if blood pressure is not normalized.

Evidence for Altered Vascular Muscle Function

The extensive evidence for the broad range of altered vascular muscle function in hypertension has been presented in several excellent reviews [e.g., 9, 10], so only main features with mechanisms suggested by data will be pointed out here. A central feature of genetic hypertension is the increased vascular reactivity to NE [11], serotonin [12], and the extracellular Ca^{2+} requirement for contraction [13, 14]. A further feature is the impaired ability to relax under the influence of powerful vasodilators, such as papaverine [9]. One important contributor to the increased peripheral resistance has been established by Folkow et al. [15] as vessel wall hypertrophy and thickening. Medial hypertrophy of hypertensive subjects and experimental animals has been documented and is agreed on [9]. However, the structural component cannot account for more than part of the increased resistance because antihypertensive drugs can lower blood pressure to normal levels by direct relaxation. Furthermore, in young animals there is the development of increased reactivity preceding the development of either increased blood pressure or medial thickening [16]. Undoubtedly, one of the most important clues for determining cause and effect in hypertension is which alterations precede development of increased blood pressure, as opposed to those which might occur as a consequence of it.

One change that has been identified as part of the sequence of development is the active transport of Na^+ and K^+ ions. Jones et al. [17] have shown in the DOCA–salt form of hypertension, in which the development of increased blood pressure and the transport of Na^+ and K^+ in strips of aorta can be conveniently correlated at each stage in the development of hypertension, that altered ion fluxes precede rather than follow the development of hypertension. Furthermore, there is substantial additional evidence for altered ion transport associated with vascular muscle cells in hypertension, at least some of which are associated with a humoral agent that might be similar to digitalis (as an endogenous circulating substance), possibly also present in humans [18].

The consequence of altered ion transport for the membrane function of vascular muscle cells appears to be greater stimulation by norepinephrine (NE), at least in the SHR form of hypertension. As a result of altered ion flux regulation in SHR there is a lower intracellular K^+ concentration and a higher intracellular Na^+ concentration, which then causes increased activity of the electrogenic Na^+ pump (possibly a change to a 3:1 ratio of Na^+/K^+) that contributes importantly to E_m in vascular muscle [11]. The review presented in the latter reference argues, by subdivision of the possibilities leading to altered sensitivity due to change in membrane properties, for the cause being ion transport. A summary of the cellular mechanisms contributing to membrane potential is shown in figure 36–1. The schematic diagram shows membrane potential (E_m) of WKY and SHR cells in either the resting state or stimulated by NE. In the resting state, the principal alterations are that the SHR have an inappropriately low intracellular K^+ concentration of 150 m*M*, a Na^+ of 20 m*M*, and a E_m contributed by electrogenic ion transport (E_t) of -12 mV. Although the total E_m is -54 mV in both cases, the component ion movements leading to the potential (electrogenesis) are different. Those differences are exacerbated by NE stimulation, where the greater ion transport in the SHR is effectively short-circuited by the increased passive ion permeability due to NE. During stimulation, increased Ca^{2+}, Na^+, K^+, and Cl^- fluxes, determined according to electrochemical gradients (passively), dominate E_m even though the Na^+-K^+ pump is still active. With increased membrane permeabilities, the ion gradients become the dominant factor

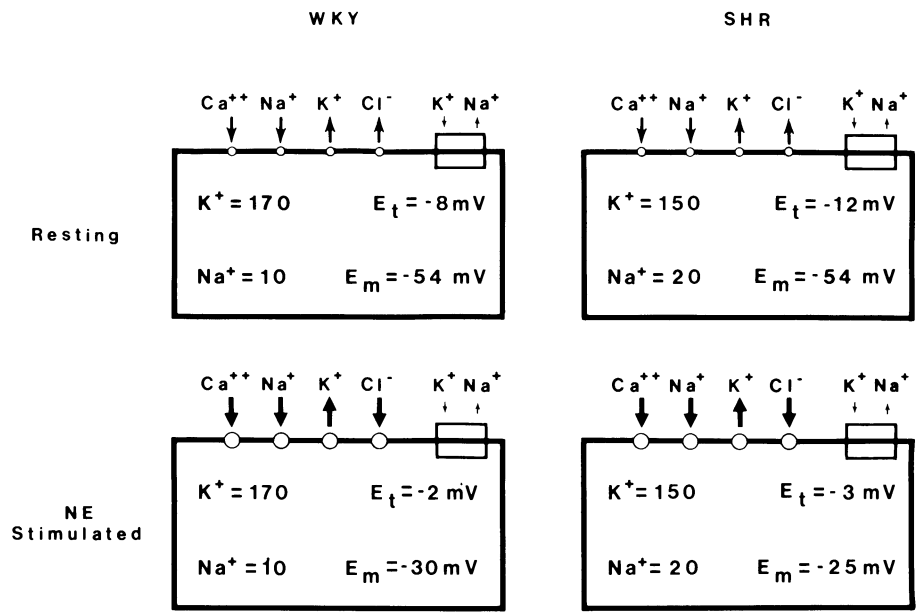

FIGURE 36–1. Ion gradient and electrogenic ion transport (E_t) differences that lead to higher norepinephrine (NE) sensitivity in caudal artery of SHR are summarized in a comparison diagram based partly on measurements and partly on estimates. Intracellular free K^+ and Na^+ concentrations (and thus membrane gradients) are different in SHR and WKY as shown. The greater Na^+ in SHR cells may enhance the electrogenicity of the pump by conversion from 3 Na^+:2 K^+ to 3 Na^+:K^+, increasing the voltage contributed by E_t while transporting less K^+.

At rest, the smaller K^+ gradient of SHR is compensated for by larger E_t (rectangles at right end of each cell), giving membrane potential (E_m) that is the same in SHR and WKY. During NE stimulation, ion conductances for Ca^{2+}, Na^+, K^+, and Cl^- are increased (larger circles and heavy flux arrows), depolarizing the cell by ion movements much in excess of ion transport and revealing the ion gradient difference between SHR and WKY [19].

During NE stimulation, E_m would be determined primarily by the balance of increased conductances for the four ions shown, with K^+ gradient particularly important because K^+ is the only outward gradient which could cause hyperpolarization (more intracellular K^+ means greater electronegativity). Ca^{2+} and Na^+ are always depolarizing forces (inward gradients) and Cl^- is assumed to change from depolarizing at rest to hyperpolarizing during NE stimulation (but Cl^- substitution experiments have ruled Cl^- relatively unimportant). Because of NE-increased membrane conductance, E_t does not contribute much more than 3 or 2 mV (SHR/WKY) because a given ion flow produces less voltage through a lower resistance (Ohm's law).

Na^+ concentrations are based on the assumption that about 33% of the total Na represents free concentration and the values measured by electron-probe microanalysis in our laboratory (unpublished observations). The higher intracellular Na^+ concentration probably leads to the greater voltage contributed by ion transport in SHR, with E_t by chance being just enough to make E_m equal to WKY in the resting state.

The most important feature for explaining why SHR are more reactive to NE is the lower intracellular K^+ concentration because during the NE-stimulated increase in ion conductances (larger flux arrows and conductance circles), E_m is determined primarily by ion gradients. Intracellular K^+ concentration and E_t values are from Hermsmeyer [19]. Intracellular Na^+ concentrations are based on electron-probe measurements and the constraints of isotonicity [25].

in E_m and the lower K^+ gradient in SHR leads to a less negative E_m. Thus, under the influence of a moderate NE concentration, SHR depolarize more and, because E_m is the principal determinant of contraction in vascular muscle, there is greater contraction.

This mechanism of increased NE sensitivity was established by measurements of E_m in caudal arteries of SHR and WKY in normal physiologic solutions or with the electrogenic Na^+ pump inhibited [19]. Such a change in E_m electrogenesis between SHR and WKY is not

found in cardiac muscle or in venous cells [20]. Mesenteric veins of anesthetized SHR in situ had different E_m from those of WKY only when sympathetic nerves were functioning; after blockade by TTX, there was no difference in E_m, indicating that venous muscle cells were the same in SHR and WKY [21]. The normal electrogenesis of cardiac and hepatic portal venous E_m of SHR would seem to indicate an alteration specific to the arterial muscle membrane and might explain the elevated peripheral resistance found in hypertension.

Because the concept of pharmacomechanical coupling has recently been argued as being more important than E_m [22], a comment on the control of tension by voltage in vascular muscle is in order here. Although it is entirely possible that Ca^{2+} permeability of a muscle cell could be increased, triggering contraction, with the simultaneous and perfectly compensating increase in conductance for K^+ or Cl^-, the specific instance providing the data for that argument has been countered [23]. Reviews summarizing arguments for the dominance of voltage-controlled tension in vascular muscle have recently been presented [24, 25]. Although it is still possible that there are changes in tension produced without accompanying E_m alterations, and, in fact, the important vessel remaining to be explored is the coronary artery under the influence of acetylcholine [26, 27], there is not sufficient evidence at this point to suggest that the peripheral vasculature is normally regulated independently of E_m.

The alteration in E_m electrogenesis found in SHR does not appear to be common to other forms of hypertension studied to date. In both the DOCA–salt and the Dahl genetic forms of hypertension, there was no alteration of the K^+ or Na^+ activity or the electrogenic Na^+ pump activity [28]. It is more likely that ion transport in isolated peripheral arteries in DOCA–salt hypertension may only secondarily be altered in response to primary changes in humoral factors and neural control mechanisms. In the case of Dahl hypertension, it would appear that altered neural mechanisms may sufficiently explain the altered reactivity.

A direct corollary of the hypothesis that SHR peripheral arteries have a decreased K^+ activity and increased Na^+ activity, and therefore an increased activity level of the electrogenic Na^+ pump, is the prediction that transient stimulation of the electrogenic pump might produce a larger effect in hypertensive than in normotensive animals. In fact, that prediction is borne out in what can be called the K^+ return relaxation. In the K^+ return relaxation, a segment of artery which has been freed of adrenergic nerve endings is exposed to O K^+ solution and to an agent such as NE, which will induce tension, for a period of at least several minutes and then is returned to solution containing K^+ (still in the presence of the NE). This was the basic protocol used to directly demonstrate increased electrogenic ion transport in the original observation [19, 24, 25]. The contractile correlate of the increased electrogenic ion transport causing increased hyperpolarization is an increased relaxation in SHR, which is exactly what is found [19, 29]. The direct correlation (same time course) of E_m and tension has been demonstrated [23–25], also supporting the hypothesis that E_m is the controlling factor during NE contractions and K^+ return relaxations. These experiments thus suggest the importance of the Na^+-K^+ pump in the increased reactivity seen in hypertension and suggest how increased intracellular Na^+ activity is translated into higher NE sensitivity.

Membrane Mechanisms of Increased Peripheral Resistance

Having identified alterations in vascular muscle in hypertension, it is next important to determine what mechanisms caused the altered vascular muscle properties. The first step taken by my laboratory to investigate this question is an experiment designed to determine whether the altered vascular muscle function is inherent in SHR arterial muscle or is the result of a neural or humoral influence. We carried out cross-transplantation experiments using the caudal artery of SHR rats, which is our most often studied artery, in the anterior eye chamber of rats, which is an immunologically privileged site supplied with the circulation and innervation of the iris. In the anterior eye chamber, a

dense adrenergic innervation grows into the artery transplant over a period of several weeks, reestablishing a pattern very much like that found in the caudal artery in situ [30]. As the result of the four possible combinations of host and donor (within the strain or cross-transplantation between SHR and WKY), the arterial muscle always took on the characteristics of the host animal; that is, caudal arteries from SHR were converted to the E_m-electrogenesis and NE-sensitivity characteristics of a WKY host, whereas WKY caudal arteries were converted conversely, and noncrosses were not converted [30].

However, the conversion of membrane properties occurred only when the donor tissue was from animals two weeks old, not from donor animals 12 weeks old. Since adrenergic innervation of the caudal artery normally occurs at age 3–4 weeks, it appears that the sympathetic nervous system releases a trophic substance which triggers the subsequent characteristics of development of the artery [30].

With evidence for a neural or humoral factor as triggering the abnormal membrane property development in SHR, the next step was to define whether it was the sympathetic nervous system, as hypothesized from the extensive evidence for altered function of the sympathetic nervous system in hypertension [10], or some humoral factor, for which there is also extensive evidence [31]. The experimental design was similar to the cross-transplantation experiments just explained, with the exception that in half of the animals, the sympathetic innervation to the iris was interrupted by superior cervical ganglionectomy before the transplantation. The result of the experiment, now with eight categories of arteries, is shown in figure 36–2. E_m electrogenesis and NE sensitivity followed the host animal only when sympathetic innervation was allowed to occur, as is shown in figure 36–2. These experiments strongly suggest the importance of the sympathetic nervous system, which we hypothesize is in the form of a trophic substance released from the sympathetic nervous system, to cause the development of higher intracellular Na^+ activity and lower intracellular K^+ activity, the subsequent increased activity of the electrogenic Na^+ pump, and consequently increased NE sensitivity that causes elevated peripheral resistance. The sequence of events is thus begun with an abnormal trophic substance released by the sympathetic nervous system of SHR, which leads to altered E_m electrogenesis and NE sensitivity.

At this point, one cannot rule out a relative excess or deficiency of the trophic substance normally produced by WKY as possibly leading to the same result. It is only possible to conclude that an abnormal trophic influence of SHR sympathetic nervous system is present, which can even convert otherwise inherently normal arterial muscle cells from WKY into the abnormal behavior seen in SHR. Further experiments will be necessary to establish the exact timing of the sympathetic trophic trigger event in both SHR and WKY and to define what may alter the process, and perhaps identify the chemical nature of the substance. From such an understanding, it may be possible to therapeutically manage or even prevent the development of hypertension from this cause.

Of course, the altered E_m electrogenesis in vascular muscle of arteries is by no means the only mechanism leading to hypertension. Substantial evidence is presented in other reviews on this subject for factors acting directly and immediately on the peripheral vasculature (see Abboud [10] and Brody [31]). Certainly the central nervous system has a role in the production of hypertension. In fact, Brody and coworkers have identified an area in the anterior-ventral portion of the third cerebral ventricle (AV3V) that is critical for the maintenance of normal fluid homeostasis and cardiovascular responses to central stimuli affecting water balance and blood pressure [32]. The degree to which altered vascular muscle behavior is caused by circulating substances (e.g., vasopressin, endogenous digitalis-like substance, converting enzyme) would provide other classes of mechanisms for the development of high blood pressure. Similarly, cardiovascular reflexes which are normally such a powerful regulator of blood pressure (see Abboud [10]) must play a role in the maintenance of long-term elevated blood pressure. However, the evidence cited in this chapter is almost entirely

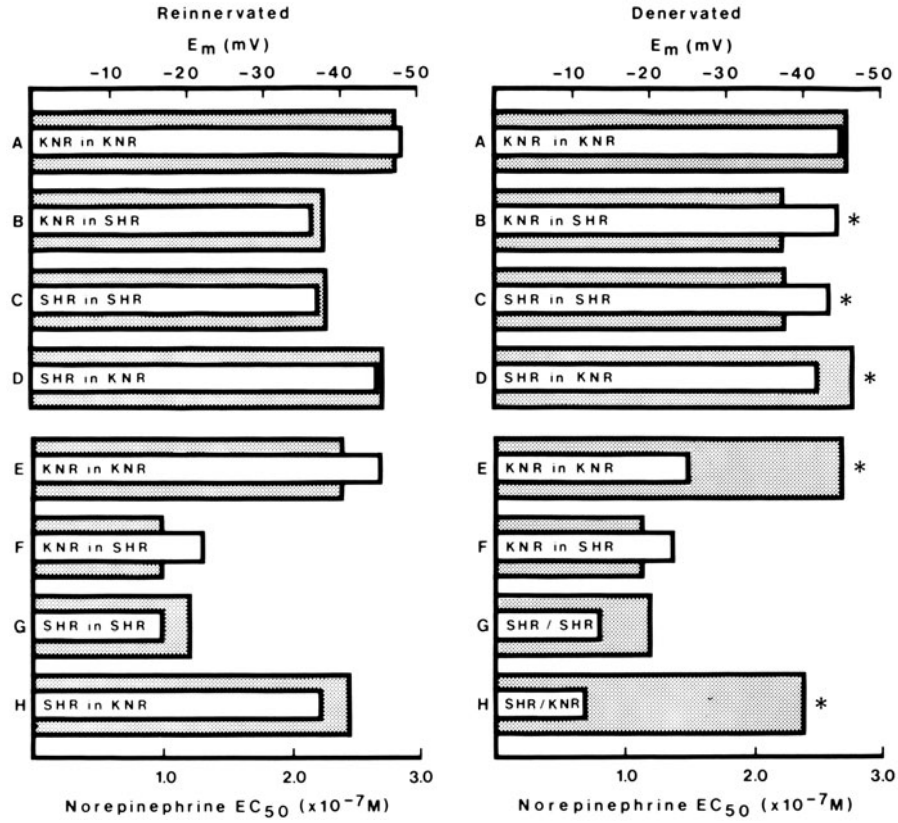

FIGURE 36–2. Interconversion of membrane properties in reinnervated caudal artery transplants (left side) and nonconversion (right), when reinnervation was prevented by superior cervical ganglionectomy, demonstrate the importance of a trophic influence of the sympathetic nervous system (from Abel and Hermsmeyer [33]). Both the E_m determined at 16°C (upper) and the NE sensitivity (lower) show conversion by the reinnervation process.

from experiments in which the blood vessels have been isolated from the animal, freed of adrenergic nerve endings by 6-hydroxydopamine (a substance which rapidly destroys adrenergic nerve endings) or similar procedures, and washed free of any circulating blood-borne substance. The demonstration of abnormally increased NE sensitivity under these conditions is a strong argument that the arterial muscle cells are involved in elevated peripheral resistance.

Conclusions

This chapter has reviewed a specific mechanism, suggesting that altered membrane properties of arterial muscle in hypertension appear to be the result of an abnormal sympathetic trophic influence rather than inherent in the muscle cells. That there are also important humoral and neural contributions to elevated peripheral resistance has also been acknowledged. Many of the data for hypertension studies, like those cited here for cellular mechanisms, are derived principally from hypertension induced in rats, either by genetic selection or by surgical and pharmacologic manipulation of the animal. The question has been raised about the applicability of data from rat experiments to the human condition of hypertension. It is important to recognize that no animal model is exactly the same as human hypertension, and that one should not expect any single model to provide the answers necessary for understand-

ing and controlling human hypertension. That group of diseases with unknown etiology which we call human essential hypertension has characteristics that can and should be explored in different animal models.

What is important is to identify and thoroughly understand the mechanisms that produce hypertension in experimental animals. It is highly likely that some of the same altered physiologic control mechanisms found in experimental animals will in some way be guidelines to mechanisms of human essential hypertension. Therefore, the correct question is not which experimental model is closest to human essential hypertension, but rather what altered blood pressure regulatory mechanisms identified in experimental animals might exist in humans.

Then the answer to the question of which model is important is that all animal models of hypertension are important because they may lead us to an understanding that will allow increasing control and even prevention of human hypertension. By its nature, the disease hypertension is one requiring the skills of several disciplines for rapid improvement in understanding. The extent to which each specialist approaches the problem with the realization that he is contributing one aspect of a large multidisciplinary effort will determine the success and the rate of progress in further understanding this important disease.

References

1. Pfeffer MA, Frohlich ED, Pfeffer BA, Weiss AK: Pathophysiological implications of the increased cardiac output of young hypertensive rats. Circ Res (Suppl 1) 34 and 35:I-235–I-242, 1974.
2. Pfeffer MA, Frohlich ED: Hemodynamic and myocardial function in young and old normotensive and spontaneously hypertensive rats. Circ Res (Suppl 1) 32 and 33:I-28–I-38, 1973.
3. Page E, Polimeni PI, Zak R, Earley J, Johnson M: Myofibrillar mass in rat and rabbit heart muscle: correlation of microchemical and stereological measurements in normal and hypertrophic hearts. Circ Res 30:430, 1972.
4. Lund DD, Tomanek RJ: Myocardial morphology of spontaneously hypertensive and aortic-constricted rats. Am J Anat 152:141, 1978.
5. Sen S, Tarazi RC, Bumpus FM: Cardiac hypertrophy and antihypertensive therapy. Cardiovasc Res 11:427, 1977.
6. Tomanek RJ: Selective effects of α-methyldopa on myocardial cell components independent of cell size in normotensive and genetically hypertensive rats. Hypertension 4:499–506, 1982.
7. Tarazi RC, Levy MN: Cardiac responses to increased afterload. Hypertension (Suppl 2) 4:II-8–II-18, 1982.
8. Schieken RM, Clarke WR, Lauer RM: Left ventricular hypertrophy in children with blood pressures in the upper quintile of the distribution: the Muscatine Study. Hypertension 3:669, 1981.
9. Brody MJ, Zimmerman BG: Peripheral circulation in arterial hypertension. Prog Cardiovasc Dis 18:323–340, 1976.
10. Abboud FM: The sympathetic system in hypertension. Hypertension (Suppl 2) 4:II-208–II-225, 1982.
11. Hermsmeyer K: Membrane potential mechanisms in experimental hypertension. In: Worcel M, et al. (eds) New trends in arterial hypertension. Inserm symposium 17. Amsterdam: Elsevier/North Holland Biomedical, 1981, pp 175–187.
12. Haeusler G, Finch L: Vascular reactivity to 5-hydroxytryptamine and hypertension in the rat. Naunyn Schmiedebergs Arch Pharmacol 272:101, 1972.
13. Jones AW: Altered ion transport in large and small arteries from spontaneously hypertensive rats and the influence of calcium. Circ Res (Suppl 1) 34 and 35:I-117–I-122, 1974.
14. Daniel EE, Kwan CY: Control of contraction of vascular muscle: relation to hypertension. Trends Pharmacol Sci 2:220–222, 1981.
15. Folkow B, Hallback M, Lundgren Y, Weiss L: Structurally based increase of flow resistance in spontaneously hypertensive rats. Acta Physiol Scand 79:373–378, 1970.
16. Lais LT, Brody MJ: Vasoconstrictor hyperresponsiveness: an early pathogenic mechanism in the spontaneously hypertensive rat. Eur J Pharmacol 47:177–189, 1978.
17. Jones AW, Heidlage JF, Meyer R, Day B, Freeland A: Non-specific supersensitivity of aortic ^{42}K effluxes during DOCA hypertension in the rat, and the effects of anti-hypertensive therapy. In: Worcel M, et al. (eds) New trends in arterial hypertension. Inserm symposium 17. Amsterdam: Elsevier/North-Holland Biomedical, 1981, pp 163–173.
18. Haddy FJ, Pamnani MB, Clough DL: Humoral factors and the sodium–potassium pump in volume expanded hypertension. In: Worcel M, et al. (eds) New trends in arterial hypertension. Inserm symposium 17. Amsterdam: Elsevier/North-Holland Biomedical, 1981, pp 189–199.
19. Hermsmeyer K: Electrogenesis of increased norepinephrine sensitivity of arterial vascular muscle in hypertension. Circ Res 38:362–367, 1976.
20. Hermsmeyer K, Walton S: Specificity of altered electrogenesis of membrane potential in hypertension. Circ Res (Suppl 1) 40:I-153–I-156, 1977.

21. Harder DR, Contney SJ, Willems WJ, Stekiel WJ: Norepinephrine effect on in situ venous membrane potential in spontaneously hypertensive rats. Am J Physiol 240:H837–H842, 1981.
22. Droogmans G, Raeymaekers L, Casteels R: Electro- and pharmacomechanical coupling in the smooth muscle cells of the rabbit ear artery. J Gen Physiol 70:129–148, 1977.
23. Trapani A, Matsuki N, Abel PW, Hermsmeyer K: Norepinephrine produces tension through electromechanical coupling in rabbit ear artery. Eur J Pharmacol 72:87–91, 1981.
24. Hermsmeyer K, Trapani A, Abel PW: Membrane potential-dependent tension in vascular muscle. In: Vanhoutte PM, Leusen I (eds) Vasodilatation. New York: Raven, 1981, pp 273–284.
25. Hermsmeyer K: Sodium pump hyperpolarization–relaxation in rat caudal artery. Fed Proc 41, 1982 (in press).
26. Kitamura K, Kuriyama H: Effects of acetylcholine on the smooth muscle cell of isolated main coronary artery of the guinea-pig. J Physiol 293:119–133, 1979.
27. Ito Y, Kitamura K, Kuriyama H: Effects of acetylcholine and catecholamines on the smooth muscle cell of the porcine coronary artery. J Physiol 294:595–611, 1979.
28. Hermsmeyer K, Abel PW, Trapani AJ: Norepinephrine sensitivity and membrane potentials of caudal arterial muscle in DOCA–salt, Dahl, and SHR hypertension in the rat. Hypertension (Suppl 2) 4:II-49–II-51, 1982.
29. Webb RC, Bohr DF: Potassium relaxation of vascular smooth muscle from spontaneously hypertensive rats. Blood Vessels 16:71–79, 1979.
30. Campbell GR, Chamley-Campbell J, Short N, Robinson RB, Hermsmeyer K: Effect of cross-transplantation on normotensive and spontaneously hypertensive rat arterial muscle membrane. Hypertension 3:534–543, 1981.
31. Brody MJ: New developments in our knowledge of blood pressure regulation. Fed Proc 40:2257–2261, 1981.
32. Brody MJ, Johnson AK: Role of the anteroventral third ventricle region in fluid and electrolyte balance, arterial pressure regulation, and hypertension. In: Martini L, Ganong WF (eds) Frontiers in neuroendocrinology, vol 6. New York: Raven, 1980, pp 249–292.
33. Abel PW, Hermsmeyer K: Sympathetic cross-innervation of SHR and genetic controls suggests a trophic influence on vascular muscle membranes. Circ Res 49:1311–1318, 1981.

37. MECHANICAL PROPERTIES, CONTRACTILE PROTEINS, AND REGULATION OF CONTRACTION OF VASCULAR SMOOTH MUSCLE

Steven P. Driska

Introduction and Scope

An understanding of vascular smooth muscle contraction is important to cardiologists and cardiac researchers because ultimately vascular smooth muscle determines both the amount of work the heart must do (by altering total peripheral resistance) and the amount of oxygen and substrates available to do it (by regulating coronary perfusion). With this relationship in mind this chapter presents a description of our present knowledge of the contractile process in vascular smooth muscle based on biochemical, biophysical, physiologic, and mechanical studies. Since other chapters in this book cover the ultrastructure, electrophysiology, and metabolism and energetics, these subjects will not be covered in any detail, and will serve to delimit the boundaries of this chapter.

Mechanical responses of vascular smooth muscle and the regulatory processes involved have been studied in a variety of preparations, ranging from intact cylindrical arteries to helical or circular strips of the arterial media. At the subcellular level, various protein preparations from smooth muscle have been studied, but the ability to develop force or shorten is lost and usually MgATPase activity or superprecipitation (defined later) is taken as the manifestation of the actin–myosin interaction responsible for muscular contraction. Midway between these two approaches is that of "skinned" preparations. In these preparations, the plasma membrane has been damaged or destroyed by mechanical methods, detergents, bacterial toxins, or freezing, yet the array of myofilaments presumably remains intact because the preparations can develop measurable active force when they are bathed in appropriate solutions. These "skinned" preparations have advantages and disadvantages like isolated proteins and intact tissues do, but their major contribution has been in bridging the large gap between the biochemistry of isolated proteins and the physiology of intact muscle. They have done this by demonstrating the applicability of biochemical findings to more organized systems capable of transducing chemical energy into mechanical work. While the primary focus of this chapter is vascular smooth muscle, much of our knowledge, particularly in biochemistry, comes from the study of nonvascular smooth muscle, especially chicken gizzard. With the implicit understanding that there might be species and tissue differences, these findings from nonvascular smooth muscles will be assumed to apply to vascular smooth muscle as well.

The preparation of this manuscript was supported by NIH grants HL 24881 and HL 25383.

N. Sperelakis (ed.), PHYSIOLOGY AND PATHOPHYSIOLOGY OF THE HEART.

Martinus Nijhoff Publishing, Boston/The Hague/ Dordrecht/Lancaster.

Mechanical Properties

This section of the chapter describes the most widely used preparations for studying mechan-

ical properties of vascular smooth muscle (VSM), the underlying assumptions for each, which properties are measured and which are calculated, and the general utility of each for studying different aspects of vascular function. Then a brief summary of findings obtained from such preparations will be presented. The order of coverage is from the most physiologic to the least physiologic.

ISOLATED ARTERIES IN VITRO

Studies on excised arteries in vitro have been important in building an understanding of how smooth muscle functions when forming part of the wall of a pressurized tube. In these studies an artery is dissected from its location, cannulated at both ends, stretched to its in vivo length, and immersed in a suitable bathing solution. The longitudinal (axial) length is set and the axial force can be measured. The blood vessel is pressurized with either a gas or with a saline solution, which may be flowing through it or static. The pressure within the vessel is measured with the outside of the blood vessel being at atmospheric pressure. (Actually the difference, or transmural pressure, is measured.) The pressure can be set at any level by the apparatus, and pressure becomes the independent variable. The diameter of the vessel is a dependent variable, and is measured by caliper devices or optical methods (for the external diameter) or radiologic methods (for the internal diameter). Knowledge of the wall thickness at a known length and diameter allows the wall thickness to be computed at any tissue length and diameter, because the arterial wall itself has been shown to be essentially incompressible [1]. This then allows the computation of internal diameter from external diameter measurements and vice versa. It is important to point out that the diameter cannot be set at a specified value like the length of a muscle can be in a one-dimensional experiment. To achieve a given diameter the pressure and/or level of activation have to be varied and, if a constant diameter is to be maintained, a feedback system has to be used to vary the pressure. The orientation of the smooth muscle cells is usually assumed to be circumferential in these preparations; this means that the diameter, radius, and circumference are all approximately proportional to the average smooth muscle cell length. Complications arising from the fact that the wall has a finite thickness, and the influence of this on cell-length homogeneity, have been discussed [2].

By application of the law of Laplace for cylinders, $T = Pr$, the circumferential tension per unit length of artery can be computed. Here T is tension, P is transmural pressure, and r is the internal radius. This characteristic (T) is independent of wall thickness and has units of force/length, typically given in either dyn/cm or Newtons/m. Frequently it is desirable to estimate the stress arising from the distending pressure, which tends to stretch circumferentially oriented smooth muscle cells. This is the circumferential or tangential stress, which has units of force/wall cross-sectional area (typically dyn/cm^2 or $Newtons/m^2$). This can be compared to the stress developed by strips of smooth muscle. The average circumferential stress can be estimated by assuming that the wall is made of a uniform material, and is isotropic and thin in relation to the radius of the cylinder. In this case, the circumferential stress is given by $S = Pr/h$, where S is stress and h is wall thickness. Since these assumptions are generally not good ones, particularly that of a thin wall, a more refined approach can be taken which allows the calculation of circumferential stress throughout the thickness of the wall as a function of the radius [3]. Here stress is calculated by the formula $S = P(1+r_o^2/r^2)/[(r_o/r_i)^2 - 1]$, with r_i and r_o being the inner and outer radii, respectively. This formula has been used to compute circumferential stress as a function of radius within the wall and compare it to the average stress in figure 37—1. This is useful in illustrating the profile of stress within the arterial wall (fig. 37–1), but it still assumes the wall to be uniform, isotropic, and linearly elastic. Doyle and Dobrin [4] derived a similar result from finite deformation theory. They suggested that the higher circumferential stresses calculated for the inner layers of the arterial wall were responsible for the greater occurrence of elastic lamellae they observed in the inner layers of the carotid artery. The arterial wall is made of different structures (primarily

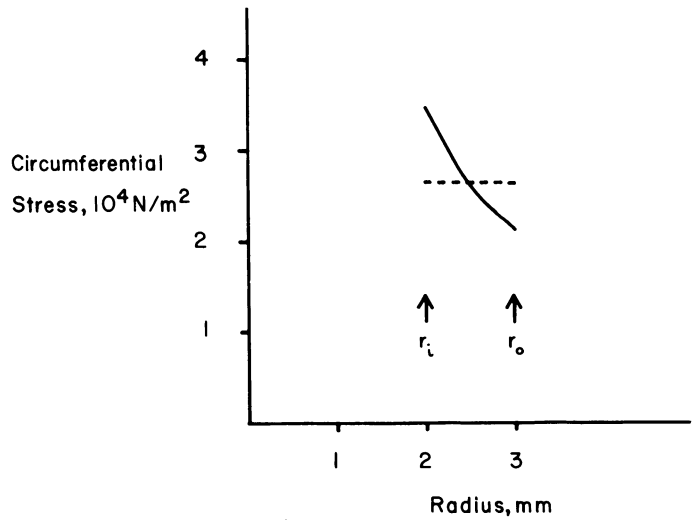

FIGURE 37–1. Circumferential stress as a function of radial position in the wall of a pressurized artery. Stress was computed by the equation $S = P\,(1 + r_o^2/r^2)/[(r_o/r_i)^2 - 1]$ for a relatively thick walled vessel with an inner radius of 2 mm and a wall thickness of 1 mm. The transmural pressure used for calculation was 1.33×10^4 N/m^2 (100 mmHg). The dashed line indicates the average circumferential stress, given by $S = Pr_i/h$, where h is wall thickness. The stress is highest near the lumen and decreases toward the outside. In thin-walled vessels the dependence of stress on radial location is not as steep.

endothelial cells, smooth muscle cells, elastin, and collagen) which differ in stiffness and radial location and have nonrandom orientations, so the analytic treatment in figure 37–1 is an oversimplification. Clearly a more complete mathematical model of an artery needs to consider the nonlinear stiffness of given elements, their orientation, and the radius at which they are located.

In studies with intact excised arteries, it is common to measure the diameter over a wide range of transmural pressures, and to repeat this process under varying degrees of smooth muscle activation. Changes in diameter and length are usually expressed as strains, strain being the length change divided by a reference length. From a number of such measurements it is possible to compute values of circumferential and longitudinal elastic moduli. (The elastic modulus is the change in stress divided by the change in strain.) The circumferential incremental Young's modulus is given by

$$E = \frac{\Delta P_i 2 d_e d_i^2 (1 - \sigma^2)}{\Delta d_e (d_e^2 - d_i^2)}$$

where d_e and d_i refer to the exterior and internal diameters, respectively, ΔP_i is the change in pressure, and Δd_e is the change in external diameter. Sigma (σ) is the Poisson ratio which is 0.5 for an incompressible isotropic material undergoing small deformations. The Poisson ratio describes the ratio of strains in perpendicular directions when three-dimensional solids are deformed. This equation was popularized by Bergel [5] and applies when a blood vessel is held at constant length. In studies such as these, the value of E usually increases with pressure, meaning the vessel wall is becoming stiffer, i.e., less extensible with inflation. This is generally understood to be a result of more stress being borne by collagen, which is the stiffest element of the wall. One of the most interesting findings to come from these studies was that contraction of vascular smooth muscle was found to *decrease* the elastic modulus, when the elastic moduli of stimulated and control arteries were compared at the same pressures. This is because, in the constricted arteries, less of the load was borne by the stiff collagen.

However, when they were compared at the same diameter (and hence the same strain), the arteries with stimulated VSM were stiffer [6].

Dobrin and Rovick [6] calculated circumferential stress as a function of arterial diameter for both passive and norepinephrine-stimulated arteries. The difference between the two stresses at a given diameter was taken as the active circumferential stress. They obtained a maximum value of 0.88×10^5 N/m^2 for the whole wall, or 2.73×10^5 N/m^2 for the estimated smooth muscle component. This is in reasonable agreement, considering the low muscle content of the canine carotid artery [7], with the active stress development found in many VSM strip preparations (summarized by Murphy [2]). This finding gives an idea of the loads applied to vascular smooth muscle in arteries compared to loads imposed in one-dimensional studies of VSM strips. The maximum active stress was found to be developed at a diameter that corresponded to that found with relaxed smooth muscle at a pressure of 150 mmHg [8]. Maximum shortening is usually found when arteries are stimulated at pressures ranging from 50 to 175 mmHg (summarized by Dobrin [9]). Excitation of vascular smooth muscle in very distended arteries leads to decreased active stress development [8], presumably analogous to the results of overstretching smooth muscle. When arteries are removed from their in vivo location, they retract approximately 30% [9], indicating that they had been under longitudinal (axial) stress. Interaction of this axial stress with circumferential stress leads to complicated analytic relationships between stresses and strains in different directions. The arterial wall is not isotropic, meaning that its properties, such as stiffness, are different in different directions, and this makes the interactions between stresses in different axes more important. Dobrin and Doyle [10] analyzed the error arising from the assumption of isotropic mechanical properties and concluded from their data on canine carotid arteries that the error in the calculated circumferential elastic modulus was small between 75 and 135 mmHg pressure and larger at both higher and lower pressures. The dynamic elastic properties have been studied with sinusoidal volume changes and, in general, the dynamic elastic moduli are 1.5- to twofold greater than the static values for the same artery (summarized by Dobrin [9]).

The study of three-dimensional mechanical properties of arteries and changes with aging or hypertension has provided valuable insights into these conditions. Cox [11] found that the value of the passive incremental elastic modulus was greater in carotid arteries of older rats when the vessels were compared at the same value of strain. Larger values of maximum active stress development and also of maximum active constriction were found with carotid arteries from DOCA [12], Goldblatt [12], and spontaneously hypertensive [13] rats compared to the appropriate controls.

Studies on excised arteries have made important contributions to our understanding of vascular function but, like studies using other techniques, they have limitations. Their major strength is that they provide information about the internal diameter as the final dependent variable, under the effect of physiologic forces (i.e., distending pressure). So in this sense, it is the best preparation to study to learn how arteries work. There are some limitations, however. It is always assumed that the outside pressure is zero or atmospheric. Clearly this is not always the case in many situations, particularly for arteries within the ventricular wall. Secondly, it is sometimes just assumed that the VSM is circularly oriented, and that circumferential stress can be equated with VSM cell stress. In most cases the arterial wall has been considered to be isotropic, meaning that it has the same elastic modulus in all directions, which is not true. Recent progress has been made in theoretical treatments of anisotropy, allowing better calculations of circumferential moduli [14]. Even when anisotropy is considered, the wall is viewed as being uniform in the radial direction (yet it has long been known to be a layered structure). Often calculations require the use of the Poisson ratio, which is 0.5 for isotropic materials undergoing small deformations. But in many experiments the deformations are much larger and the Poisson ratio would be less than 0.5 even for an isotropic material. Most of these problems are due to the application of classic physical methods to soft

biologic tissues which undergo much larger deformations than the steel wires or tubes on which classic theories were based. There has been some use of finite deformation analysis, and this is encouraging because it is more appropriate when strains are as large as those that occur with blood vessels [15]. The final limitation is that most studies use static pressures. The arterial wall has viscoelastic properties, so a pressure–diameter tracing depends on the rate of change of pressure and the direction of change.

Investigators usually inflate and deflate the arteries until reproducible responses are obtained, but the dynamic relationship of arterial diameter to the pulse pressure is required for complete physiologic relevance. In spite of these limitations, the study of excised arteries has made major contributions to the knowledge of vascular function. Recent technological advances have made it possible to extend these studies from large arteries to resistance vessels and terminal arterioles [16, 103]. The mechanical properties of arteries have recently been the subject of a thorough review [9].

RING AND STRIP PREPARATIONS

The most commonly studied vascular smooth muscle preparation is the smooth muscle strip. These are either circularly oriented or (especially in the case of smaller vessels) helically oriented. Great care must be taken with helical strips because arterial diameter, strip width, and helix angle are all interrelated. Herlihy [17] has pointed out that the different helix angle could compromise comparisons between arteries of different diameters even if strip width is the same, because stress development is a function of the helix angle. These preparations may or may not have the adventitial and intimal layers removed. The presence or absence of endothelial cells of the intimal layer is a major determinant of pharmacologic responsiveness [18]. With these preparations, length changes and forces are measured in just one direction, which is hoped to be the axis of the smooth muscle cells. Ring preparations have more in common with strip preparations than with intact arteries because, as with strips, force and length changes are imposed and measured in only one dimension. Rings are often everted so that the adventitia forms the inside and agonists, nutrients, and O_2 can reach the smooth muscle cells more easily.

In contrast to studies on intact arteries where diameter (and hence smooth muscle length) is dependent on transmural pressure and muscle activation, muscle length is the independent variable with muscle strips and rings. By analogy with striated muscle research, the length–isometric-force and force–velocity relationships are most commonly studied. This approach has been quite fruitful for understanding how vascular smooth muscle functions, but it tells less about how arteries function. For cardiovascular relevance it would be most important to know the final length of the muscle after shortening against a nonconstant load. This would be analogous to knowing the inside diameter of an artery after stimulation at some pressure. Some studies of nonvascular smooth muscle have addressed this question, namely, whether the length–isometric-tension curve is the same as the length–tension curve obtained by measuring the final length obtained after contraction against constant loads. The length–tension curves were found to be essentially the same regardless of the method used up to a length of 0.8 L_o. At greater lengths, a shortening defect was found, meaning that the muscle did not shorten as much as expected from the isometric length–tension curve [19].

The Length–Tension Curve. The elegant correlation of mechanical and morphologic data that forms the basis for the sliding-filament model of striated muscle contraction [20] is lacking in smooth muscle. However, the sliding-filament model is generally accepted even though the precise dimensions of a smooth muscle sarcomere are not known. The thick filaments are slightly longer in smooth muscle, being 2.2 microns in smooth vs 1.5 microns in striated muscle [21]. The thin filament length in smooth muscle is not known because of numerous technical difficulties. Filament counts from electron micrographs of transverse sections of smooth muscles show a much higher ratio of thin to thick filaments, ranging from 12:1 to 18:1, than occurs in striated muscle. These fil-

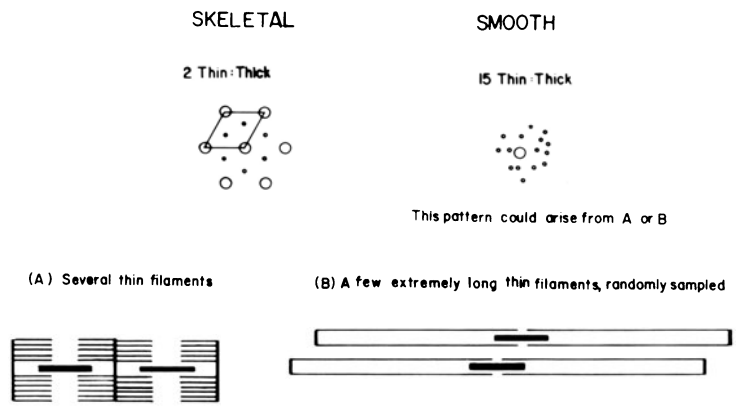

FIGURE 37–2. Possible explanations of filament counts in electron micrographs of cross sections of smooth muscle. In the overlap region of vertebrate skeletal muscle (left) the area encompassed by the parallelogram contains a total of one thick filament and two thin filaments. The smooth muscle does not show as much order (right) and there are generally 12–18 thin filament profiles per thick filament profile. Because thick filaments in smooth muscle are not in good lateral registration, the plane of section might pass through the thick filament of one sarcomere, but only intersect thin filaments in adjacent sarcomeres. This makes sectioning a random sampling process, and the high number of thin filament profiles could arise from large numbers of thin filaments (*A*, lower left) or a smaller number of extremely long thin filaments (*B*, lower right). Both models represent extreme cases that are consistent with the 15 : 1 filament count and contain equal amounts of myosin and actin. In *B* the thin filaments are 8.25 microns long, giving rise to a 16.5-micron sarcomere; in *A* the sarcomere length is 2.9 microns. Both models use a 2.2-micron-thick filament.

ament counts are in good agreement with the amounts and ratios of myosin and actin in smooth muscles [22], but because thick filaments are not in good lateral registration this has to be regarded as a random sampling process. Therefore, these data are consistent with a spectrum of sarcomere models ranging from one where the thin to thick filament length ratio is the same as in skeletal muscle, but there are more thin filaments interacting with each thick filament, to the opposite extreme where only two thin filaments interact with each end of the thick filament, but the thin filaments are much longer. These extremes are shown in figure 37–2. The idea that long thin filaments could explain the high force generation and economy of smooth muscle has been proposed [21, 23]. Calculations of how long the thin filaments would have to be (for a 15 : 1 filament count) show that the hypothetical thin filament length would be 8.25 microns (from tip to Z-line equivalent) making a 16.5-micron sarcomere. If the proteins of *skeletal* muscle were arranged in this type of sarcomere, only 18% as much myosin would be needed. The muscle would develop 47% more force and it would shorten only 12% as fast. While the true situation can be anywhere on this spectrum, the long sarcomere model has many attractive features in explaining mechanical data, and it maximizes the fraction of the limited number of thick filaments present that can develop force in parallel. At present all these models must be considered as possibilities when interpreting mechanical properties.

The previous paragraph has explained the inability to describe a "sarcomere length" in smooth muscle, but it is still possible to compare the length–tension curves of skeletal and smooth muscle, if the muscle length is expressed in relation to the optimum length for force development, L_o. (In skeletal muscle, L_o would correspond to sarcomere lengths of 2.0–2.2 microns.) All muscles develop a certain amount of passive tension (arising from elastic and connective tissue) when stretched. This passive tension is particularly prominent in vascular smooth muscle, and it must be subtracted

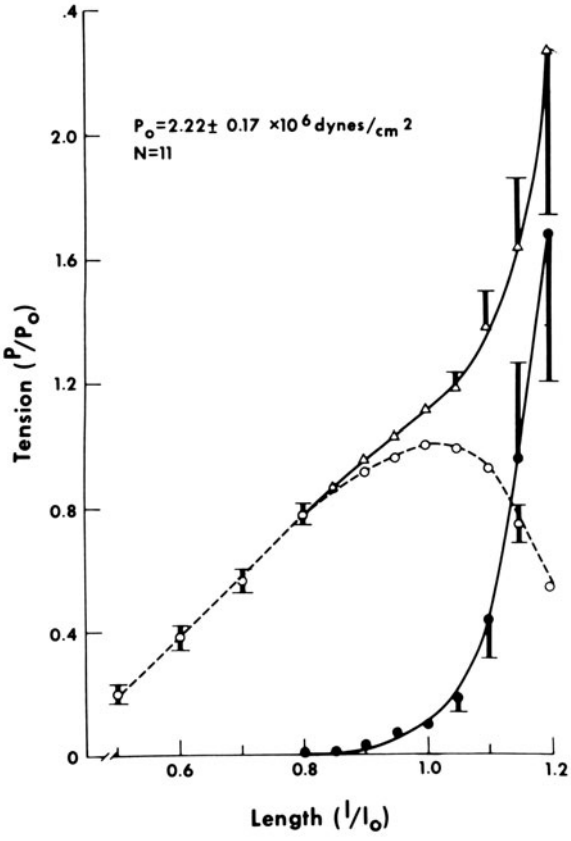

FIGURE 37–3. Length–tension curve of hog carotid artery smooth muscle strips. Muscle length is expressed as a fraction of L_o, the optimum length for active force generation; tension is expressed as a fraction of P_o, the maximum active force. Closed circles: passive force estimated by quick release of the muscle from a longer length; triangles: isometric force during stimulation with K^+; open circles: active tension (the total tension in the stimulated muscle minus the passive tension at that length). Error bars represent ± 1 SE. From Herlihy and Murphy [104] with permission of the American Heart Association.

from the total tension of the stimulated muscle to obtain the active tension. The active tension is attributed to force generation by myosin cross-bridges, and the accuracy of its measurement depends on the ability to measure and subtract passive tension accurately. The length–passive-tension curve is usually estimated by relaxing the tissue with drugs or calcium chelators, or it may be determined by imposing rapid shortening steps (quick releases) that discharge any force developed by the cross-bridges before they can recover, revealing the passive tension due to elastic structures at the new length.

The active tension curve typical of vascular smooth muscle (fig. 37–3) shows an optimum length with decreasing forces developed at both longer and shorter lengths. Usually a smooth curve is obtained; sharp corners (like those found with single skeletal fibers) are not obtained, but this is not surprising in view of the complexity of most preparations relative to the single fiber studied with the spot follower servo system [20]. There has been one report of a plateau on the length–tension curve of smooth muscle [24], but this was found with an invertebrate smooth muscle, the anterior byssus retractor of *Mytilus edulis*. Little data are available on force development in highly stretched VSM because tissues often are damaged by extreme stretching, and the high passive tensions subject the active tension measurements to large error. However, the decline of active force is steeper at lengths greater than L_o than it is at muscle lengths less than L_o. At short muscle lengths, smooth muscle retains its ability to develop force better than skeletal muscle. The common assertion that smooth muscle can shorten much more than striated muscle is probably an exaggeration; Murphy [25] has pointed out (fig. 37–4) that published length–tension curves of skinned skeletal fibers are similar to those of smooth muscle tissues, implying that the limited capacity of skeletal muscle is a more consequence of length-dependent activation, rather than myofibrillar geometry.

If one compares the values of F_0 (the maximum active force developed per unit cross-sectional area) obtained for skeletal and vascular smooth muscle, it is found that the smooth muscle can develop as much or more force. This is particularly surprising because the smooth muscle contains only about one-fourth as much myosin [22]. The ability of vascular smooth muscle tissues to develop this much force has been shown to be a cellular property, and not the result of a complicated tissue architecture that confers a mechanical advantage to cells [26–28]. Thus, the length–tension curve and the high force development of vas-

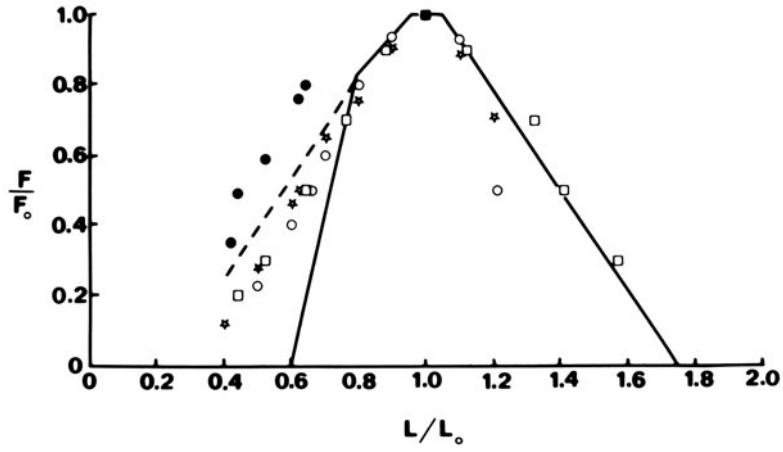

FIGURE 37–4. Comparison of the active tension–length curves of smooth and skeletal muscle. Forces are normalized to peak forces generated by each preparation, and lengths are normalized to the optimum length for each preparation, which represents a 2.1-μm sarcomere length in skeletal muscle. Solid line: single skeletal fiber, data from Gordon et al. [20]; dashed line and filled circles: skinned skeletal fibers activated directly by Ca^{2+}; open circles: hog carotid artery strips, data from Herlihy and Murphy [104]; open squares: cat duodenal circular muscle; stars: dog tracheal smooth muscle. Note that the smooth muscle preparations develop force at shorter lengths than the intact skeletal fibers, but that skinned skeletal fibers are able to develop force relatively better than intact smooth muscle at short lengths. From Murphy [2] with the permission of the American Physiological Society and S. Karger.

cular smooth muscle are a property of the individual cells. This finding is corroborated by direct evidence from studies on the very large smooth muscle cells of amphibian stomach. Force development by single cells from this tissue, when expressed relative to cross-sectional area, shows the same high value seen in smooth muscle strips [29].

Application of the length–tension curve obtained from smooth muscle strips to intact arteries leads to some complications. As a first approximation, the mean circumference (average of inner and outer) can be equated to the muscle length. As the muscle contracts, however, there has to be a greater extent of contraction by the inner layer, since the wall thickening displaces mass toward the lumen. For example, in the case of an artery with a r_i/r_o ratio of 0.7, constriction leading to a decrease of r_o to 80% of its initial value causes r_i to decrease to 52% of its initial value. Circumferences are of course proportional to radii. This implies that there could be slippage between layers. The point to be made here is that the shortening capacity of vascular smooth muscle is adequate to cause pronounced constriction, but it is not possible to define equivalent muscle cell length or "strip length" at a given radius precisely. Even if all muscle cells in the artery had exactly the same length at some radius, cell-length inhomogeneity would appear at other radii [2].

The Force–Velocity Curve. The force–velocity relationship in vascular smooth muscle is qualitatively similar to that seen in skeletal muscle, in that both are fit reasonably well by the hyperbolic equation of A.V. Hill: $(F+a)(V+b) = (F_o+a)b$. Values of $\dot{V}_{max}$, the maximum shortening velocity, can be extrapolated from a linearization of the equation and expressed in muscle lengths/s. At 37°C these values are much lower in vascular smooth muscle (0.02–0.7 L_o/s) than in skeletal muscle (typically 1–10 L_o/s). Recent evidence, however, has pointed out some difficulties involved in measuring $\dot{V}_{max}$ in smooth muscle. Foremost among these is the finding that shortening ve-

locities obtained with a given load are time dependent, i.e., the velocity depends on how long the muscle has been stimulated isometrically before it is allowed to shorten isotonically [30–34]. In these experiments, muscles are usually stimulated isometrically as tension develops and then rapidly released to shorten against selected constant loads. Surprisingly, the highest values of $\dot{V}_{max}$ (the unloaded shortening velocity) are measured before isometric tension is fully developed. This phenomenon will be discussed at length in a subsequent section, but its importance here is that it suggests that values of $\dot{V}_{max}$ in the literature may be underestimates. Another complication with $\dot{V}_{max}$ measurements made by the method of isotonic quick releases is the transiently high shortening velocity observed following quick releases. It is not clear whether this is a manifestation of cross-bridge kinetics [34] or a damped series elastic component [35]. In either case, these initial rates are about six times greater than steady-state shortening velocities and could lead to overestimates of the true $\dot{V}_{max}$. In afterloaded isotonic contractions, load (force) is an independent variable, and velocity is the dependent variable. The opposite approach is sometimes taken, with velocity being the independent variable by imposing constant velocity shortenings on the muscle and measuring the force the muscle can exert under these conditions.

The maximum shortening velocity can also be estimated by a procedure known as the "slack test" method. In this method, a stimulated muscle is rapidly shortened to a new length beyond the point where force drops to zero, and the portion of the length change when force was zero is divided by the time that force remains at zero to compute an unloaded shortening velocity.

The Series Elastic Component. The contractile component (CC) of muscle behaves like it is transmitting force to an external load through a spring, the series elastic component (SEC). In the early analogue models of muscle, the anatomic feature responsible for the SEC was not known, and it was treated as something independent of the myofilaments which constitute the contractile component. Later studies on skeletal muscle led to the more modern view that much of the SEC is in the myosin cross-bridge itself. One way of measuring the SEC is to rapidly shorten a muscle during the peak of an isometric tetanus, so that all force is discharged. With a very stiff SEC, very little shortening is required. A plot of length and force during this procedure defines the characteristics of the SEC. For skeletal muscles, rapid shortening by 3% totally discharges tension [36] and using faster length changes with single fibers a shortening of less than 1% is needed [37, 38]. The force–length relationship is not linear at low values of force so the linear region is often extrapolated to zero force. This intercept represents about 0.5% shortening with single fibers [37, 38], and about 1.5% with whole muscle [36]. When similar experiments were performed with vascular smooth muscle strips, shortening of 2%–3% was adequate to totally discharge force and the linear extrapolation had an intercept of 1.5% shortening [39]. Unfortunately the estimates of the series elasticity depend on the quality of the instrumentation and the speed with which the releases can be performed; series elasticities of 5%–10% of muscle length have been reported in the past. In summary it appears that isometrically contracting vascular smooth muscle is almost as stiff as skeletal muscle. The series elastic component has an important influence on measurement of isotonic shortening velocities because it has been reported to be responsible for transiently high shortening velocities after a release [35]. This undesirable influence of the SEC on shortening velocities could be avoided by using afterloaded isotonic contractions, but with this method shortening under different isotonic loads starts at different times after stimulation, a real disadvantage because of the dependence of shortening velocities on the duration of stimulation [32, 33].

Estimation of Cellular Mechanical Properties in Multicellular Preparations. The small size of vascular smooth muscle cells has prohibited the use of single cells for mechanical studies, although this has been achieved with the much larger cells from amphibian stomach [29]. This

means that vascular smooth muscle cellular properties have to be inferred from mechanical measurements made on complex multicellular tissues, and because of this it is vitally important to know whether any mechanical advantages are conferred on cells as a result of tissue structure. The high force development of vascular smooth muscle tissues in spite of their limited myosin content [22], coupled with recurring suggestions that a mechanical advantage for muscle cells exists in the arterial wall (see Driska et al. [28]), led to an examination of this possibility. Two lines of evidence have ruled out the existence of mechanical advantages in the tissues examined. First, it was found that the force development of vascular smooth muscle strips did not depend on how long a segment of the strip was chosen for force measurement, i.e., force did not depend on how many cells long the preparation was [26]. The second type of experiment measured either the change in cell length or distance between features in the same cell in response to known changes in tissue length. In the absence of mechanical advantages, 10% shortening of the tissue would lead to a 10% reduction in mean cell length or distance between distinguishable cellular features. A 20% reduction in mean cell length would indicate a 2:1 mechanical advantage. Data of this type for hog carotid artery [27, 28], guinea pig taenia coli [40], and rabbit bladder [19] strips, and rings of small arteries [41] indicated that the cells do not have a mechanical advantage, and that cellular estimates of shortening velocity and active stress development made by proper normalization of tissue measurements are valid.

Contractile Properties of Single Smooth Muscle Cells. Single cells can be dispersed from vascular smooth muscle, and certain mechanical measurements such as extent and velocity of unloaded shortening can be made. However, it is necessary to fasten cells to a force transducer for studies of force development or shortening against external loads, and this has not yet been reported. Much progress has been made, however, on stomach muscle cells from the toad *Bufo marinus,* and even though these cells are neither vascular nor mammalian, the studies have produced data that are highly relevant to vascular tissue. The large size of these cells allows them to be tied around a microprobe and still have a portion of the cell left to generate force. The conclusions presented in the preceding section receive strong support from the fact that the active stress development for single *Bufo* cells is as high as that estimated from vascular smooth muscle tissue measurements [29]. These cells retain their cholinergic receptors and have been very useful in studies of pharmacology and electrophysiology. Another interesting finding is that after direct electrical stimulation there is a measurable latency before force develops [29], and the clear demonstration of it in a preparation free of agonist diffusion delays establishes this as a characteristic that all theories of regulation and excitation–contraction coupling must explain.

MECHANICAL PROPERTIES OF "SKINNED" PREPARATIONS

Various techniques have been applied to decrease or eliminate the permeability barrier of the plasma membrane of vascular smooth muscle strip preparations and allow direct activation of the contractile machinery by Ca^{2+} Sophisticated mechanical studies have not generally been performed with these preparations because force development usually declines with each contraction–relaxation cycle, and many such cycles would be necessary for a force–velocity curve. Usually isometric tension is the measured response and in some cases ATPase activity can be measured. A major contribution of these preparations is that they serve as a bridge between muscle protein biochemistry and muscle mechanics.

Methods of "Skinning" VSM Strips. The small size of VSM cells precludes true mechanical skinning of the sarcolemma, so the membrane is usually made permeable by dissolution with detergents [42] or glycerol [43], physical trauma by grinding [44] or freeze-glycerination [45], or through the action of specific agents such as staphylococcal alpha toxin [46] or ionophore A-23187 [47]. Nonionic detergents

like Triton X-100 attack all membranes, but saponin treatment has been reported to disrupt the plasma membrane but not the sarcoplasmic reticulum [48]. The freeze-glycerination technique is thought to involve membrane cracking, rather than dissolution [45]. Saida reported that the divalent cation ionophore A-23187 can be used to reversibly "skin" smooth muscle, allowing anions such as ATP to enter, with resealing of the membrane occurring on removal of the agent [47]. Two important criteria for skinned preparations are the active stress development and extracellular space measurements made with small solutes. Ideal preparations develop as much stress as the native tissue, and allow small solutes to equilibrate through the entire volume of the tissue.

Results with "Skinned" Preparations. Skinned preparations of smooth muscle have been used to demonstrate the Ca^{2+} dependence of force generation [42–48], ATPase [45], and myosin light-chain phosphorylation [44, 46]. Kerrick and co-workers have made extensive use of skinned preparations in their studies on the role of myosin light-chain phosphorylation in the regulation of contraction. They found that, when the myosin light chains in the preparations were irreversibly thiophosphorylated by ATP-γ-S, the force development was no longer dependent on Ca^{2+} [44]. This agreed with biochemical studies wherein ATP-γ-S had the same effect on actomyosin MgATPase activity [49]. Skinned preparations have also been used to demonstrate Mg^{2+} dependence of force development [43, 48], and that relaxation induced by vanadate occurs at a step following light-chain phosphorylation [45]. One practical disadvantage of skinned preparations is the amount of time required for a contraction–relaxation cycle, but it has been found that the relaxation rate can be increased by inorganic phosphate [50]. Using skinned preparations it has also been possible to demonstrate relaxation by the cAMP-dependent protein kinase [51]. This enzyme has many substrates, but here it was presumably acting by phosphorylating myosin light-chain kinase, which decreases the myosin kinase activity, leading to decreased levels of phosphorylated light chain and relaxation.

Biochemistry of the Contractile Proteins

In biochemical studies of dispersed proteins, the ability to measure force development or shortening is lost because the ordered structure of the muscle is lost. The biochemical correlate of contraction that is usually studied is the Ca^{2+}-dependent MgATPase activity. Here the substrate is MgATP (usually present in millimolar concentrations), but low concentrations of Ca^{2+} (10^{-5} *M*) are required for full activity. When $[Ca^{2+}]$ is very low (10^{-8} *M*), the MgATPase activity of good preparations is inhibited to less than 10% of its value at 10^{-5} *M* Ca^{2+}. Another biochemical correlate of contraction that is often studied is called superprecipitation. This is the ATP-dependent increase in light scattering that results from contraction of aggregates of actin and myosin molecules. Superprecipitation cannot be quantitated as precisely as ATPase activity, but it is free from interferences by other contaminating ATPases, and is a useful adjunct to ATPase measurements.

The protein preparations used in these studies range in complexity from myofibrils to actomyosin to mixtures of purified proteins. The term smooth muscle myofibrils is used to describe the insoluble material after homogenization of muscle in low-ionic-strength solutions to remove cytoplasmic proteins. Usually these preparations have to be washed with nonionic detergents to remove contaminating membranous ATPase activities. Myofibrils are not a simple system, but they are easily prepared and presumably the actin and myosin are present as native filaments. Actomyosin is a mixture of actin, myosin, tropomyosin, and other proteins which has been solubilized, extracted from the homogenized muscle tissue, and precipitated. Thick filaments are probably disrupted by solubilization and then reform on precipitation, so that even though the complement of proteins present in actomyosin is simpler than that in myofibrils, some native structure is lost.

Finally, individual proteins, (myosin, actin, etc.) can be prepared and purified separately and recombined in known stoichiometry. This approach is the most time-consuming, but leads to the most definitive results.

CONTRACTILE PROTEIN COMPOSITION OF SMOOTH MUSCLE

Like skeletal muscle, smooth muscle contains the structural proteins myosin, actin, and tropomyosin. It also appears to contain smaller but significant amounts of other structural proteins (α-actinin, desmin or vimentin, vinculin, and filamin), some of which may be present in skeletal muscle. The chief qualitative difference from skeletal muscle is that it does not contain stoichiometrically significant amounts of the regulatory protein troponin [52–54]. Smooth muscle has been reported to contain a different type of thin filament regulatory protein called leiotonin [55, 56], but its role as a regulatory protein is not at present widely accepted. All vertebrate muscles also contain enzymes known as myosin light-chain kinase (MLCK) and myosin light-chain phosphatase (MLCP), and in smooth muscle these enzymes appear to have an important role in the regulation of contraction.

Stoichiometry. Before considering specific properties of each of the purified proteins it is appropriate to consider the amounts present in the cell. The most striking quantitative feature of the protein composition of smooth muscle is the abundance of actin and scarcity of myosin relative to skeletal muscle [22]. The actin–myosin weight ratio in smooth muscle is about tenfold higher than in skeletal muscle, reflecting both a lower myosin content and a higher actin content [22]. These findings agree well with morphologic measurements made with the electron microscope. The rather high tropomyosin content of smooth muscle, which had led to some confusion in the early biochemical literature, was seen to be consistent with the high actin content, implying a thin filament structure like that of skeletal muscle with one tropomyosin molecule spanning about seven actin monomers. Surveys of the contractile protein contents of several mammalian smooth muscles have revealed a dichotomy between two groups of tissues, those which have very high amounts of actin and those which have less (but still much more than skeletal muscles) [57]. The tissues in the first group (arteries) seem to develop more force than those in the other group (veins and other nonvascular smooth muscle), although some anomalous examples have been found. The higher amounts of actin present in smooth muscle tissue carry over into myofibril and actomyosin preparations, and the preparation of myosin free from contaminating actin is more difficult than it is with skeletal muscle.

Specific Proteins

MYOSIN. Myosin is the major protein comprising the thick filaments of muscle, and possesses the ATPase activity that converts the chemical energy of ATP hydrolysis to mechanical work. Its native molecular weight is about 470,000 daltons, being composed of two heavy chains of 200,000 daltons each, and two of each of two classes of light chains, 20,000 and 17,000 daltons. The 20,000-dalton light chain can be phosphorylated by myosin light-chain kinase, and this will be discussed in a subsequent section. Like myosin from other muscles, the smooth muscle protein binds Ca^{2+}, and this may be involved in regulation. The myosin content of smooth muscle is about 16 mg/g cells (or about 10 mg/g tissue in a preparation where cells make up 60% of the tissue) [22]. The protein differs from that of skeletal muscle in amino acid composition, solubility, aggregation characteristics, and in the enzymatic properties of the ATPase (in that the ATPase activity of the smooth muscle enzyme is lower and usually cannot be activated by actin as dramatically). In a subsequent section, there is a more detailed discussion of myosin MgATPase in reference to regulatory mechanisms. For a recent comprehensive review article on myosin and the other contractile proteins of smooth muscle, see Hartshorne and Gorecka [58].

ACTIN. Actin is a globular protein with a molecular weight of about 42,000 daltons consisting of one polypeptide chain. Actin polymerizes to form a long-double-helical structure

known as F-actin, and this constitutes the backbone of the thin filaments in muscle. Actin activates the MgATPase activity of myosin in vitro and this is the basis for the increased energy usage in contracting muscle. Actin is present in larger quantities (on a weight basis) than any other cellular protein in vascular smooth muscle, there being about 30 mg/g tissue in the hog carotid artery [22]. Actins from all types of muscle are quite similar, but not identical. Isoelectric focusing reveals that there are three isoelectric variants in smooth muscle termed α, β, and γ [59]. The α subunit is most similar to skeletal actin, but the roles and significance of the isoelectric variants have yet to be unambiguously determined because of the difficulty in separating them without denaturation.

TROPOMYOSIN. Tropomyosin is a rod-shaped protein whose secondary structure is nearly 100% alpha helix. It has two subunits, an α subunit having a molecular weight of about 34,000 daltons, and a 36,000-dalton β subunit. There are different amounts of these two tropomyosin variants in striated muscle, depending on the fiber type. The corresponding tropomyosin subunits in smooth muscle seem to be slightly larger, having subunit molecular weights of 36,000 and 39,000 in chicken gizzard [53], but the significance of this is not yet understood. In striated muscles it is thought that the long tropomyosin molecules, which bind the regulatory protein troponin, lie in the grooves formed by the actin double helix and serve to control a block of 6–7 actins by moving further into the groove in response to Ca^{2+} binding by troponin. The absence of troponin in vertebrate smooth muscle means that this cannot be the role of tropomyosin, here, but it is often thought to have a structural role in maintaining thin filament rigidity. In biochemical studies tropomyosin has been shown to be an activator of actomyosin ATPase in systems containing purified myosin light-chain kinase and phosophatase [60], but the mechanism for this activation is not known. Tropomyosin does not seem to have a regulatory role in smooth muscle because it is not needed for Ca^{2+} -sensitive actin activation of smooth muscle myosin MgATPase. Native tropomyosin is a term for a crude mixture of proteins that is predominantly tropomyosin. In striated muscle, native tropomyosin preparations contain troponin, and therefore can confer Ca^{2+} sensitivity to mixtures of skeletal myosin and actin. The term native tropomyosin has also been applied to crude mixtures from smooth muscle, but here the active factor is not troponin, but rather either myosin light-chain kinase and phosphatase [61] or leiotonin [56].

TROPONIN. Troponin is not found in Ca^{2+}-sensitive actomyosin preparations from smooth muscle [53, 54], or thin filament preparations [53], nor could it be prepared from smooth muscle using skeletal muscle techniques. Most investigators believe it is not present, in spite of earlier [62] and recurring [63] reports of troponin or troponin-like components. The concept of thin filament regulation has been further broadened by reports of the phosphorylation of thin filament components [64]. Wider acceptance of these results awaits further purification and characterization of the active components. The word troponin appears in the earlier papers [e.g., 55] of several workers who now feel that leiotonin is the active component of their thin filament regulatory systems. After about 1977, they began to refer to this active component as leiotonin because it is not comparable to skeletal troponin.

LEIOTONIN. Ebashi and co-workers have reported that a thin filament protein they call leiotonin is responsible for regulation. This protein has two subunits, with molecular weights of about 80,000 (leiotonin A) and 18,000 (leiotonin C) [65]. They claim that the C subunit binds Ca^{2+} but is not calmodulin or troponin C, and that the purified protein, unlike crude preparations, does not have myosin light-chain kinase activity [55]. Estimates of the amount of leiotonin present in smooth muscle are very low, about one-tenth the amount of tropomyosin present [55]. Since it is supposed to bind to actin, it is difficult to picture a role for leiotonin in regulation unless it acts as an enzyme rather than as a structural protein like troponin.

MYOSIN LIGHT-CHAIN KINASE (MLCK). Myosin light-chain kinases are present in all types of muscle, where they catalyze the ATP-depen-

dent phosphorylation of a specific serine residue in one of the light chains. Smooth muscle is the type of muscle where this phosphorylation seems to have its most clear-cut role, allowing actin activation of myosin MgATPase activity [66]. The enzyme has a catalytic subunit with a molecular weight of 100,000–140,000 and calmodulin, the ubiquitous 17,000-dalton Ca^{2+}-binding protein [67, 68], is the regulatory subunit. The stochiometry is now established as one catalytic subunit per calmodulin as reported by Adelstein and Klee [69]. The enzyme is activated when the Ca^{2+}–calmodulin complex binds to the catalytic subunit. The 140,000-dalton subunit may itself be phosphorylated by the well-known cAMP-dependent protein kinase, reducing the MLCK activity at a constant level of Ca^{2+}–calmodulin [70]. This would tend to relax smooth muscle, and has attracted much attention as a possible mechanism for β-adrenergic relaxation. However, the phosphorylation of MLCK at the site decreasing MLCK activity does not take place when Ca^{2+}–calmodulin is bound (as it would be expected to be in a contracting muscle) [70]. Therefore, it seems that this mechanism could reduce vascular reactivity in a relaxed blood vessel, but not relax a constricted blood vessel. The MLCK catalytic subunit is subject to proteolysis, losing the ability to be inhibited by phosphorylation, then its Ca^{2+} requirement, and finally its activity. The first MLCK preparations studied had lower molecular weights (83,000) and were not Ca^{2+} dependent, [71] probably due to this fact.

MYOSIN LIGHT-CHAIN PHOSPHATASE (MLCP). The myosin light-chain phosphatases in muscle are difficult to purify without denaturation, so comparatively less is known about them. The enzyme removes the phosphate group from the phosphorylated 20,000-dalton light chain. The dynamic balance of the reactions catalyzed by MCLK and MLCP determines the fraction of the light chains that are phosphorylated, so knowledge about this enzyme is just as important as knowledge about the kinase. Two different enzymes have been studied in turkey gizzard [72]. Neither is thought to be Ca^{2+} dependent, but Mg^{2+} modulation of phosphatase activity has been reported [73]. One enzyme, myosin phosphatase I, has equimolar amounts of three subunits (60,000, 55,000, and 38,000 daltons), does not require Mg^{2+}, and is active on phosphorylated light chains and phosphorylated MLCK. The other enzyme, phosphatase II, has a single 43,000-dalton subunit, requires Mg^{2+}, and is relatively more specific for phosphorylated myosin light chain over phosphorylated MLCK, compared to phosphatase I [72].

ALPHA-ACTININ. The remaining proteins are structural proteins identified in smooth muscle. α-Actinin has a molecular weight of about 110,000 and is found in cytoplasmic dense bodies and plasma membrane dense patches in smooth muscle [74]. It is thought to be involved with anchoring of thin filaments to plasma membrane dense patches and cytoplasmic dense bodies, structures which are thought to be analogous to the Z lines of striated muscle.

VINCULIN. Vinculin is a protein with a subunit molecular weight of 130,000 daltons found in the brush border of epithelial cells and also smooth muscle. It, too, is thought to fasten thin filaments to the plasma membrane, but unlike α-actinin, it is not located in cytoplasmic dense bodies. Immunoelectron-microscopic techniques show that vinculin is located closer to the membrane than α-actinin is [75]. Vinculin binds to actin in vitro causing it to form bundles [76].

DESMIN AND VIMENTIN. Smooth muscle has a class of myofilaments known as intermediate filaments because their diameter of 10 nm is between that of the thin actin filaments (6–8 nm) and the thick myosin filaments (12–15 nm). The intermediate filaments are very resistant to solubilization by solutions used for extracting actomyosin. The protein component comprising these filaments was shown by Cooke to have a subunit molecular weight of 55,000 [77]. Two other groups of workers subsequently named this protein desmin [78] and skeletin [79], and now the term desmin is most widely used. A very similar protein called vimentin has been characterized as the 10-nm filament protein in nonmuscle cells, and also

occurs in smooth muscle. Desmin and vimentin are fairly similar in overall structure, vimentin being slightly larger (58,000 daltons) and having a lower apparent isoelectric point. Gabbiani et al. [80] have reported that vascular smooth muscle differs from other smooth muscle in having vimentin (rather than desmin) as its major intermediate filament protein. Other workers, however, have shown that both proteins are present in some blood vessels [81]. Some preliminary work has been done using the presence of vimentin or desmin to identify the nature of intimal smooth muscle cells that accumulate after endothelial injury to the rat aorta [82]. At present the role of intermediate filaments in smooth muscle is not known, but the most common supposition is that they form a cytoskeleton [77]. A comprehensive review of the ultrastructure of smooth muscle, including intermediate filaments, has appeared [83].

FILAMIN. Filamin is a protein with a subunit molecular weight of 250,000 that is present in reasonably large amounts in chicken gizzard (one-third as much as myosin on a weight basis [84]). This large protein is thought to function as an actin filament cross-linker [85], and it is very similar, if not identical, to the actin-binding protein isolated from rabbit macrophages [86]. The role of filamin in smooth muscle is not known, but based on its presence in large amounts in smooth muscle and other motile nonmuscle cells, it has been assumed to be involved in contraction.

Currently the structure of the cytoplasm is the subject of intense research in both smooth muscle and nonmuscle cells. For further details on α-actinin, vinculin, desmin, vimentin, and filamin, the reader should refer to the volume that includes the summary by Brinkely [87].

Regulation of the Contractile System by Ca^{2+}

INTRODUCTION

One of the most important questions in smooth muscle research is the nature of the regulatory systems governing contraction. The lack of troponin [52–54] meant that a different system must exist, and an obvious alternative was the myosin-linked system found in molluscs. (These molluscan muscles lack troponin, and Ca^{2+} causes contraction through binding to the myosin molecule.) However, the regulatory system in VSM is more complicated than the simple molluscan system, even though myosin Ca^{2+} binding might be involved. Most investigators believe that myosin light-chain phosphorylation is at least part of the system. The regulation of actomyosin ATPase activity by light-chain phosphorylation was first reported with contractile proteins from blood platelets [88] and subsequently was found in smooth muscle [60, 61, 89]. While the phosphorylation theory is certainly the most popular, it is not the only one still held. A list of the different regulatory mechanisms that have been proposed, and an assessment of their current popularity, is presented below.

STATUS OF PROPOSED MECHANISMS

Troponin. Early reports of troponin in smooth muscle [62, 90] have not been widely accepted and are generally thought to be the result of preparative artifacts. The concept of thin filament regulation has been revived recently [63] but as yet has found little support.

Myosin-linked Systems. In 1974 it was reported that vertebrate smooth muscle had myosin-linked regulation [52] like molluscan muscles. In these molluscan muscles, which lack troponin, Ca^{2+} binds to myosin to initiate contraction. The vertebrate system is now known to be more complicated, although the phosphorylation mechanism can be considered to be myosin-linked. Furthermore, there might be a physiologic role for myosin Ca^{2+} binding.

Leiotonin. Several prestigious research groups, mostly in Japan, believe that regulation of smooth muscle contraction is achieved through a thin-filament protein different from troponin, known as leiotonin [55]. Like phosphorylation, it confers Ca^{2+} sensitivity by activating in the presence of Ca^{2+} (rather than by inhibiting ATPase in the absence of Ca^{2+} like the skeletal troponin system). Thus it is a true activator. The difficulty in preparing this protein has

been an obstacle to its wide acceptance outside of Japan.

Thin Filament Phosphorylation. It has been reported that proteins on thin filaments from some (but not all) smooth muscles can be phosphorylated in a Ca^{2+}-dependent manner, which makes the activation of skeletal myosin by these preparations Ca^{2+} dependent [64]. The thin filament component that is phosphorylated has a molecular weight of 21,000, but it is claimed to not be the myosin light chain. Wider acceptance of this view hinges on isolation, purification, and characterization of the active components.

Myosin Light-Chain Phosphorylation. The wide acceptance of this hypothesis justifies a historical development and more detailed coverage. Phosphorylation of skeletal myosin light chains had been reported by Perrie and co-workers, but there was no detectable change in any of the ATPase activities on phosphorylation [91]. Adelstein's group then reported that, with myosin made from blood platelets, phosphorylation caused an increase in actin-activated MgATPase activity [88]. Soon several laboratories reported that smooth muscle myosin light chain was phosphorylated in a Ca^{2+}-dependent manner, and that this phosphorylation roughly paralleled the MgATPase activity in its Ca^{2+} dependence [60, 61, 68]. Subsequently, it was shown that phosphorylation of smooth muscle myosin was required for appreciable actin-activated MgATPase activity. [66] Numerous lines of biochemical evidence led to the hypothesis that contraction is regulated by Ca^{2+} only through the Ca^{2+} dependence of the phosphorylation step [49]. This hypothesis predicts that, if myosin can be maintained permanently phosphorylated, actin activation will no longer be Ca^{2+} dependent. Using different tissues and techniques, it was found that fully phosphorylated guinea pig vas deferens myosin was activated by actin in the absence of Ca^{2+}, but further activated in its presence [60]; chicken gizzard myosin, however, when irreversibly thiophosphorylated, is activated no more by actin in the presence of Ca^{2+} then in its absence [49]. The results with chicken gizzard were

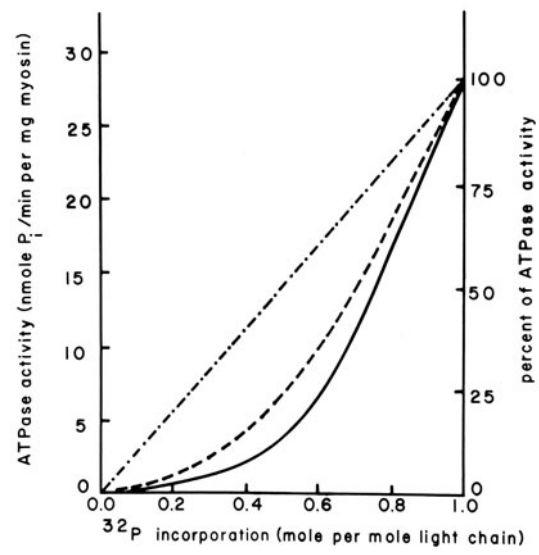

FIGURE 37–5. Dependence of actin-activated MgATPase activity of smooth muscle myosin on the extent of phosphorylation of the light chain. Solid line describes the experimental data; alternating dots and dashes show behavior expected if the two ATPase sites were independent and activated only by phosphorylation of their associated light chains; dashed line shows the result expected if phosphorylation was random and both light chains had to be phosphorylated before either ATPase site was activated. If phosphorylation were an ordered process and both light chains had to be phosphorylated for any ATPase activity, the plot would be a straight line from zero ATPase at 0.5 mol P/mol LC20 to full ATPase at full phosphorylation. From Persechini and Hartshorne [92] with permission of the American Association for the Advancement of Science.

consistent with the hypothesis that Ca^{2+} regulates contraction only through activation of the kinase, and that phosphorylation is both necessary and sufficient for full activation. The vas deferens results, while also pointing to the necessity (but not sufficiency) of phosphorylation for full activation, also suggested the existence of a second site for the action of Ca^{2+}. While this might be an example of a true species or tissue difference, it is also possible that during protein preparation certain aspects of a Ca^{2+} regulatory mechanism are lost or artifactually generated.

Recent reports indicate that the relationship between myosin phosphorylation and ATPase

activity might not be as simple as it was once thought to be. Because myosin is a hexamer, having two 200,000-dalton heavy chains and two each of 17,000- and 20,000-dalton light chains, a given myosin molecule can have 0, 1, or 2 of its 20,000-dalton light chains (LC20) phosphorylated. Each of the two 200,000-dalton heavy chains has an ATPase site, and thus the question arises of whether phosphorylation of one light chain activates the associated heavy chain's ATPase site, or whether both light chains must be phosphorylated before either of the ATPase sites are activated. Persechini and Hartshorne [92] recently reported data (shown in fig. 37–5) that they interpreted as supporting the second possibility, i.e., they claimed that the ATPase sites do not act independently. Thus a plot of MgATPase activity vs mol P/mol LC20 is not a straight line intercepting the origin (as it would be if the ATPase sites were independent), but rather a concave-up curve. The authors suggested that the results were consistent with phosphorylation being an ordered process, with one light chain being preferentially phosphorylated, resulting in only about 10% of the activity of the doubly phosphorylated myosin. Addition of the second phosphate group would then lead to a dramatic increase in ATPase, as both ATPase sites became maximally activated.

In vitro studies of the biochemistry of contractile proteins are very much affected by subtle alterations of proteins which are not easily detected but have important effects on enzymatic properties. Apparently under some conditions with some myosin preparations, phosphorylation by purified MLCK alone is not adequate to fully activate ATPase activity, and other factors (present in crude preparations of MLCK) seem to be needed [93]. This is surprising because in other work from the same laboratory, phosphorylation alone seems to result in full activation [92]. This then suggests that myosin could be very sensitive to preparative conditions, and that this could be the explanation for disagreements between the advocates of leiotonin and the advocates of the various mechanisms involving phosphorylation. If this is the reason for the disagreements, the next problem is determining which of these mechanisms is most important in vivo. Much progress has been made in this area through the study of phosphorylation as a regulatory mechanism in living smooth muscle preparations, and this will be discussed in the next section.

It is not known whether phosphorylation increases actomyosin MgATPase by increasing actin–myosin binding or by increasing $\dot{V}_{max}$, the maximum ATPase rate at saturating actin concentrations, or both. This would be useful to know because in living tissues, phosphorylation is thought to increase maximum shortening velocity [32, 33] which would predict an increased value of $\dot{V}_{max}$ of ATPase in vitro. Hopefully this question will soon be answered.

STUDIES ON THE ROLE OF MYOSIN LIGHT-CHAIN PHOSPHORYLATION IN THE REGULATION OF CONTRACTION OF INTACT SMOOTH MUSCLE

The hypothesis that smooth muscle contraction is regulated exclusively by myosin light-chain phosphorylation (LCP) makes several testable predictions: (a) on stimulation or relaxation, changes in LCP should precede or coincide with the mechanical response; (b) there should be low levels of phosphorylated LC20 in resting muscle; and (c) the magnitude of the mechanical response, whether force, shortening velocity, or stiffness, should be proportional to the extent of phosphorylation, although this proportionality need not be linear. Numerous workers have demonstrated that phosphorylation takes place on stimulation of intact smooth muscle [94–98], and that it coincides with or precedes the mechanical response. These findings support the hypothesis that phosphorylation is involved as a regulatory system in vivo. But phosphorylation does not always change on contraction of pig aortic strips [98] and phosphorylation cannot explain all the mechanical responses, because it reaches its peak level before isometric force does and then declines during the time that force reaches its peak [32, 33, 95, 99, 100]. During prolonged stimulation of the hog carotid, force is well maintained while phosphorylation falls to near-resting values [32, 33, 99]. This means that any proportionality between force and phosphorylation would have to have a time-depen-

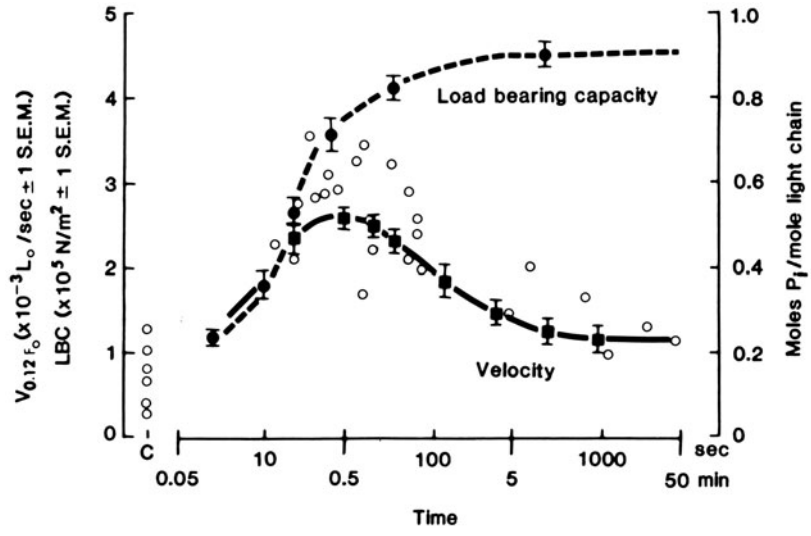

FIGURE 37–6. Time courses of LC20 phosphorylation, shortening velocity, and load-bearing capacity on K^+ stimulation of hog carotid artery strips. Open circles: LC20 phosphorylation; filled squares: shortening velocity against a load that was 12% of the maximum active isometric force; filled circles: load-bearing capacity. Load-bearing capacity is the peak force measured when a quick stretch of 0.025 L_o was applied at a rate of 0.1 L_o/s, and it provides a better estimate of the number of attached cross-bridges than does isometric force measurement. Error bars represent ± 1 SE; phosphorylation data are single points, and C denotes control, unstimulated muscle strips. Note the logarithmic time base. From Dillon et al. [32] with permission of the American Association for the Advancement of Science.

dent proportionality constant. By measurements of shortening velocities after varying periods of isometric stimulation it was found that velocity of shortening had a similar time course to light-chain phosphorylation [32, 33] as shown in figure 37–6. This led to the suggestion that shortening velocity (but not isometric force) was regulated by light-chain phosphorylation. To explain the decrease in shortening velocities during prolonged stimulation, it was proposed that phosphorylated cross-bridges cycled rapidly and that attached cross-bridges could be dephosphorylated, forming a so-called latch bridge that cycled very slowly, if at all [32]. These latch bridges could be similar to attached, noncycling cross-bridges in other smooth muscles [101]. These latch bridges were hypothesized to maintain force economically, but to provide an internal load which decreases the shortening velocities attained by phosphorylated cycling cross-bridges. The number of attached cross-bridges is thought to be regulated by some other Ca^{2+}-dependent mechanism. Some support for the latch-bridge hypothesis can be drawn from studies which show the rate of energy consumption decreases with time during isometric contraction [100]. This latch-bridge hypothesis has attracted much attention, but it is currently based on rather indirect evidence. The latch-bridge mechanism, if correct, would allow a vascular smooth muscle to shorten rapidly when stimulated, but then the cross-bridge cycling rate would fall, decreasing the energy usage required to maintain tension. This would be well suited to the role of vascular smooth muscle, allowing it to maintain the diameter of a blood vessel economically for long periods of time.

STUDIES ON THE REGULATION OF "SKINNED" PREPARATIONS BY LIGHT-CHAIN PHOSPHORYLATION

One of the strongest arguments for the hypothesis that only phosphorylation regulates contraction comes from studies on "skinned" smooth muscle preparations. The ATP ana-

logue ATP-γ-S is a substrate for the light-chain kinase, but once the light chain is thiophosphorylated it is a poor substrate for the phosphatase. After treatment of skinned preparations with ATP-γ-S, force development no longer requires Ca^{2+} [44]. Uncertainties about whether thiophosphorylated light chain is functionally the same as phosphorylated light chain were answered by the demonstration that phosphorylation by ATP and a modified MLCK that no longer required Ca^{2+} for activity could remove the Ca^{2+} requirement for force development [102]. This seems to be strong evidence for the primacy of phosphorylation as the regulatory mechanism in this skinned preparation. Unfortunately, mechanical responses of the skinned preparations are not as completely characterized as those of intact tissue. These studies [44, 46, 102] with skinned preparations have often been criticized because the amount of phosphate incorporated into the light chain from ATP was not as great as expected, increasing from 0.01 mol P/mol LC20 to 0.20 mol P/mol LC20 when the $[Ca^{2+}]$ was increased from 10^{-8} *M* to 1.6×10^{-4} *M* in gizzard preparations. With rabbit ileum, the increase was even less, from 0.00 to 0.05 [46]. When these preparations were incubated with ATP-γ-S, however, the incorporation of thiophosphate in the light chain increased from 0.10 to 0.80 mol thiophosphate/mol LC20 for gizzard, and from 0.04 to 0.75 for ileum, over the same range of Ca^{2+} concentrations. Force development was the same in both cases even though much higher levels of thiophosphorylation were achieved than of phosphorylation. Taken at face value, this data is difficult to reconcile with a model that has force production regulated by phosphorylation. The disagreement between these studies and those supporting the latch-bridge hypothesis and its postulation of a second site for Ca^{2+} action might be simply due to a species or tissue difference. Alternatively, certain aspects of the regulatory mechanism of living muscle might be lost on membrane disruption.

REGULATORY MECHANISMS: A SUMMARY

There is at present no uniformly accepted view of the mechanisms regulating smooth muscle contraction. Almost all researchers agree that the regulatory system is different than the troponin system of skeletal muscle, but there is little uniform agreement beyond this. Most researchers feel that myosin light-chain phosphorylation is involved as at least part of the system. Myosin light-chain phosphorylation appears to be the only regulatory mechanism in some isolated protein preparations and in some "skinned fiber" preparations, but additional mechanisms seem to operate in other protein preparations and in living smooth muscle tissues. Some prestigious laboratories deny the importance of light-chain phosphorylation and assert that a new thin filament protein named leiotonin is responsible for regulation. Other proposed and possible mechanisms include Ca^{2+} binding by myosin and phosphorylation of thin filament components.

A chapter such as this should provide some basis for the reader to see beyond all the disagreements toward some unified view of smooth muscle regulatory mechanisms. One approach, then, is to allow for the possibility that not all smooth muscles are identical in their regulatory mechanisms, just as they are not identical in many other respects. The diversity of smooth muscles has often been emphasized, and smooth muscle cells in chicken gizzard need not be regulated the same way as those in cow aorta. Another possible explanation is that, under different experimental conditions, different mechanisms are masked or unmasked as a different step in the cross-bridge cycle becomes rate-limiting for ATPase activity. This could be a result of the loss or even artifactual generation of regulatory mechanisms during the preparative procedures involved with each model system. If this possibility is accepted, it leads to the conclusion that the best preparations to study are the most physiologic ones. Since myosin light-chain phosphorylation can be demonstrated on stimulation of strips of intact smooth muscle, the physiologic *occurrence* of phosphorylation on contraction is established [94–97, 100], and biochemical work has demonstrated that it can act in a regulatory role [49, 60, 66, 102]. But because more thorough mechanical studies point to a role for phosphorylation in regulat-

ing velocity of shortening but not contractile force [32, 33], another regulatory mechanism is needed to explain regulation of force in the living tissue [32, 33, 95, 99]. The other proposed mechanisms (leiotonin, myosin Ca^{2+} binding, or thin filament phosphorylation), which apparently regulate ATPase under other conditions, might serve this purpose. The field of smooth muscle regulation is a very active one, and current research should soon tell us whether this speculative explanation of diverse and apparently conflicting results is correct. A more complete understanding of the mechanisms regulating vascular smooth muscle contraction is of great importance, and the results of current and future research should be just as interesting.

References

1. Carew TE, Vaishnav RN, Patel DJ: Compressibility of the arterial wall. Circ Res 23:61–68, 1968.
2. Murphy RA: Mechanics of vascular smooth muscle. In: Bohr DF, Somlyo AP, Sparks HV, Geiger SR (eds) Handbook of physiology. Sect 2: The cardiovascular system. Vol 2: Vascular smooth muscle. Bethesda MD: American Physiological Society, 1980, pp 325–351.
3. Middleman S: Transport phenomena in the cardiovascular system. New York: Wiley-Interscience, 1972.
4. Doyle JM, Dobrin PB: Stress gradients in the walls of large arteries. J Biomech 16:631–639, 1973.
5. Bergel DH: The static elastic properties of the arterial wall. J Physiol 156:445–457, 1961.
6. Dobrin PB, Rovick AA: Influence of vascular smooth muscle on contractile mechanics and elasticity of arteries. Am J Physiol 217:1644–1651, 1969.
7. Bunce DFM: Atlas of arterial histology. St Louis: Warren H Green, 1974.
8. Dobrin PB: Influence of initial length on length–tension relationship of vascular smooth muscle. Am J Physiol 225:664–670, 1973.
9. Dobrin PB: Mechanical properties of arteries. Physiol Rev 58:397–460, 1978.
10. Dobrin PB, Doyle JM: Vascular smooth muscle and the anisotropy of dog carotid artery. Circ Res 27:105–119, 1970.
11. Cox RH: Effects of age on the mechanical properties of rat carotid artery. Am J Physiol 233:H256–H263, 1977.
12. Cox RH: Alterations in active and passive mechanics of rat carotid artery with experimental hypertension. Am J Physiol 237:H597–H605, 1979.
13. Cox RH: Comparison of arterial wall mechanics in normotensive and spontaneously hypertensive rats. Am J Physiol 237:H159–H167, 1979.
14. Hudetz AG: Incremental elastic modulus for orthotropic incompressible arteries. J Biomech 12:651–655, 1979.
15. Doyle JM, Dobrin PB: Finite deformation analysis of the relaxed and contracted dog carotid artery. Microvasc Res 3:400–415, 1971.
16. Duling BR, Gore RW, Dacey RG, Damon DN: Methods for isolation, cannulation, and in vitro study of single microvessels. Am J Physiol 241:H108–H116, 1981.
17. Herlihy JT: Helically cut vascular strip preparation: geometrical considerations. Am J Physiol 238:H107–H109, 1980.
18. Furchgott RF: The requirement for endothelial cells in the relaxation of arteries by acetylcholine and some other vasodilators. Trends pharmacol sci 2:173–176, 1981.
19. Uvelius B: Isometric and isotonic length–tension relations and variations in cell length in longitudinal smooth muscle from rabbit urinary bladder. Acta Physiol Scand 97:1–12, 1976.
20. Gordon AM, Huxley AF, Julian FJ: The variation in isometric tension with sarcomere length in vertebrate muscle fibres. J Physiol 184:170–192, 1966.
21. Ashton FT, Somlyo AV, Somlyo AP: The contractile apparatus of vascular smooth muscle: intermediate high voltage stereo electron microscopy. J Mol Biol 98:17–29, 1975.
22. Murphy RA, Herlihy JT, Megerman J: Force generating capacity and contractile protein content of arterial smooth muscle J Gen Physiol 64:691–705, 1974.
23. Paul RJ: Chemical energetics of vascular smooth muscle. In: Bohr DF, Somlyo AP, Sparks HV, Geiger SR (eds) Handbook of physiology. Sect 2: The cardiovascular system. Vol 2: Vascular smooth muscle. Bethesda MD: American Physiological Society, 1980, pp 201–235.
24. Cornelius F, Lowy J: Tension–length behavior of a molluscan smooth muscle related to filament organization. Acta Physiol Scand 102:167–180, 1978.
25. Murphy RA: Contractile system function in mammalian smooth muscle. Blood vessels 13:1–23, 1976.
26. Driska SP, Murphy RA: Estimate of cellular force generation in an arterial smooth muscle with a high actin–myosin ratio. Blood vessels 15:26–32, 1978.
27. Murphy RA, Driska SP, Cohen DM: Variations in actin to myosin ratios and cellular force generation in vertebrate smooth muscles. In: Casteels R, Godfraind T, Ruegg JC (eds) Excitation–contraction coupling in smooth muscle. Amsterdam: Elsevier/North Holland, 1977, pp 417–424.
28. Driska SP, Damon DN, Murphy RA: Estimates of cellular mechanics in an arterial smooth muscle. Biophys J 24:525–540, 1978.
29. Fay FS: Isometric contractile properties of single

isolated smooth muscle cells. Nature 265:553–556, 1977.
30. Hellstrand P, Johansson B: The force–velocity relation in phasic contraction of venous smooth muscle. Acta Physiol Scand 93:157–166, 1975.
31. Uvelius B: Shortening velocity, active force, and homogeneity of contraction during electrically evoked twitches in smooth muscle from rabbit urinary bladder. Acta Physiol Scand 106:481–486, 1979.
32. Dillon PF, Aksoy MO, Driska SP, Murphy RA: Myosin phosphorylation and the crossbridge cycle in arterial smooth muscle. Science 211:495–497, 1981.
33. Dillon PF, Murphy RA: Tonic force maintenance with reduced shortening velocity in arterial smooth muscle. Am J Physiol 242:C102–C108, 1982.
34. Hellstrand P, Johansson B: Analysis of the length response to a force step in smooth muscle from rabbit urinary bladder. Acta Physiol Scand 106:221–238, 1979.
35. Mulvany MJ: The undamped and damped series elastic components of a vascular smooth muscle. Biophys J 26:401–414, 1979.
36. Bressler BH, Clinch NF: The compliance of contracting skeletal muscle. J Physiol 237:477–493, 1974.
37. Ford LE, Huxley AF, Simmons RM: Tension responses to sudden length change in stimulated frog muscle fibres near slack length. J Physiol 269:441–515, 1977.
38. Cecchi G, Griffiths PJ, Taylor S: Muscular contraction: kinetics of crossbridge attachment studied by high frequency stiffness measurements. Science 217:70–72, 1982.
39. Peterson JW: Relation of stiffness, energy metabolism, and isometric tension in a vascular smooth muscle. In: Vanhoutte PM, Leusen I (eds) Mechanisms of vasodilatation. Basel: S Karger, 1978, 79–88.
40. Cooke PH, Fay FS: Correlation between fiber length, ultrastructure, and the length–tension relationship of mammalion smooth muscle. J Cell Biol 52:105–116, 1972.
41. Mulvany MJ, Warshaw DM: The active tension–length curve of vascular smooth muscle related to its cellular components. J Gen Physiol 74:85–104, 1979.
42. Gordon AR: Contraction of detergent treated smooth muscle. Proc Natl Acad Sci USA 75:3527–3530, 1978.
43. Filo RS, Bohr DF, Ruegg JC: Glycerinated skeletal and smooth muscle: calcium and magnesium dependence. Science 147:1581–1583, 1965.
44. Hoar PE, Kerrick WGL, Cassidy PS: Chicken gizzard: relation between calcium activated phosphorylation and contraction. Science 204:503–506, 1979.
45. Peterson JW: Vandate ion inhibits actomyosin interaction in chemically skinned vascular smooth muscle. Biochem Biophys Res Commun 95:1846–1853, 1980.
46. Cassidy P, Hoar PE, Kerrick WGL: Irreversible thiophosphorylation and activation of tension in functionally skinned rabbit ileum strips by [^{35}S] ATPγS. J Biol Chem 254:11148–11153, 1979.
47. Saida K: A method of skinning smooth muscle fibers with A23187. Biomed Res 2:134–142, 1981.
48. Saida K, Nonmura Y: Characteristics of Ca^{2+} and Mg^{2+}-induced tension development in chemically skinned smooth muscle fibers. J Gen Physiol 72:1–14, 1978.
49. Sherry JMF, Gorecka A, Aksoy MO, Dabrowska R, Hartshorne DJ: Roles of calcium and phosphorylation in the regulation of the activity of gizzard myosin. Biochemistry 17:4411–4418, 1978.
50. Schneider M, Sparrow M, Ruegg JC: Inorganic phosphate promotes relaxation of chemically skinned smooth muscle of guinea-pig. *Taenia coli.* Experientia 37:980–982, 1981.
51. Ruegg JC, Paul RJ: Vascular smooth muscle calmodulin and cyclic AMP-dependent protein kinase alter calcium sensitivity in porcine carotid skinned fibers. Circ Res 50:394–399, 1982.
52. Bremel RD: Myosin linked calcium regulation in vertebrate smooth muscle. Nature 252:405–407, 1974.
53. Driska S, Hartshorne DJ: The contractile proteins of smooth muscle properties and components of a Ca^{2+} sensitive actomyosin from chicken gizzard. Arch Biochem Biophys 167:203–212, 1975.
54. Sobieszek A, Bremel RD: Preparation and properties of vertebrate smooth-muscle myofibrils and actomyosin. Eur J Biochem 55:49–60, 1975.
55. Mikawa T, Toyo-oka T, Nonomura Y, Ebashi S: Essential factor of gizzard "troponin" fraction: a new type of regulatory protein. J Biochem 81:273–275, 1977.
56. Ebashi S, Mikawa T, Hirata M, Toyo-oka T, Nonomura Y: Regulatory proteins of smooth muscle. In: Casteels R, Godfraind T, Ruegg JC (eds) Excitation–contraction coupling in smooth muscle. Amsterdam: Elsevier/North Holland, 1977, pp 325–334.
57. Cohen DM, Murphy RA: Differences in cellular contractile protein contents among porcine smooth muscles. J Gen Physiol 72:369–380, 1978.
58. Hartshorne DJ, Gorecka A: Biochemistry of the contractile proteins of smooth muscle. In: Bohr DF, Somlyo AP, Sparks HV, Geiger SR (eds) Handbook of physiology. Sect 2: The cardiovascular system. Vol 2: Vascular smooth muscle. Bethesda MD: American Physiological Society, 1980 pp 93–120.
59. Izant JG, Lazarides E: Invariance and heterogeneity in the major structural and regulatory proteins of chick muscle cells revealed by two-dimensional gel electrophoresis. Proc Natl Acad Sci USA 74:1450–1454, 1974.
60. Chacko S, Conti MA, Adelstein RS: Effect of phosphorylation of smooth muscle myosin on actin activation and Ca^{2+} regulation. Proc Natl Acad Sci USA 74:129–133, 1977.

61. Aksoy MO, Williams D, Sharkey EM, Hartshorne DJ: A relationship between Ca^{2+} sensitivity and phosphorylation of gizzard actomyosin. Biochem Biophys Res Commun 69:35–41, 1976.
62. Carsten ME: Uterine smooth muscle: troponin. Arch Biochem Biophys 147:353–357, 1971.
63. Marston SB, Trevett RM, Walters M: Calcium ion-regulated thin filaments from vascular smooth muscle. Biochem J 185:355–365, 1980.
64. Walters M, Marston SB: Phosphorylation of the calcium ion-regulated thin filaments from vascular smooth muscle: a new regulatory mechanism? Biochem J 197:127–139, 1981.
65. Mikawa T, Nonomura Y, Hirata M, Ebashi S, Kakiuchi S: Involvement of an acidic protein in regulation of smooth muscle contraction by the tropomyosin–leiotonin system. J Biochem 84:1633–1636, 1978.
66. Gorecka A, Aksoy MO, Hartshorne DJ: The effect of phosphorylation of gizzard myosin on actin activation. Biochem Biophys Res Commun 71:325–331, 1976.
67. Dabrowska R, Aromatorio D, Sherry JMF, Hartshorne DJ: Composition of the myosin light chain kinase from chicken gizzard. Biochem Biophys Res Commun 78:1263–1272, 1977.
68. Dabrowska R, Sherry JMF, Aromatorio D, Hartshorne DJ: Modulator protein as a component of the myosin light chain kinase from chicken gizzard. Biochemistry 17:253–258, 1978.
69. Adelstein RS, Klee CB: Purification and characterization of smooth muscle myosin light chain kinase. J Biol Chem 256:7501–7509, 1981.
70. Conti MA, Adelstein RS: The relationship between calmodulin binding and phosphorylation of smooth muscle myosin kinase by the catalytic subunit of 3′:5′ cAMP dependent protein kinase. J Biol Chem 256:3178–3181, 1981.
71. Daniel JL, Adelstein RS: Isolation and properties of platelet myosin light chain kinase. Biochemistry 15:2370–2377, 1976.
72. Pato MD, Adelstein RS: Dephosphorylation of the 20,000 dalton light chain of myosin by two different phosphatases from smooth muscle. J Biol Chem 255:6535–6538, 1980.
73. Moreland RS, Ford GD: The influence of Mg^{2+} on the phosphorylation of myosin by an actomyosin preparation from vascular smooth muscle. Biochem Biophys Res Commun 106:652–659, 1982.
74. Schollmeyer JE, Furcht LT, Goll DE, Robson RM, Stromer MH: Localization of contractile proteins in smooth muscle cells and in normal and transformed fibroblasts. In: Goldman R, Pollard T, Rosenbaum J (eds) Cell motility. Cold Spring Harbor NY: Cold Spring Harbor Laboratory, 1976, pp 361–388.
75. Geiger B, Dutton AH, Tokuyasu KT, Singer SJ: Immunoelectron microscope studies of membrane–microfilament interactions: distributions of α-actinin, tropomyosin, and vinculin in intestinal epithelial brush border and chicken gizzard smooth muscle cells. J Cell Biol 91:614–628, 1981.
76. Jockusch BM, Isenberg G: Vinculin and α-actinin: interaction with actin and effect on microfilament network formation. Cold Spring Harbor Symp Quant Biol 46:613–624, 1982.
77. Cooke PH: A filamentous cytoskeleton in vertebrate smooth muscle fibers. J Cell Biol 68:539–556, 1976.
78. Lazarides E, Hubbard B: Immunological characterization of the 100Å filaments from muscle cells. Proc Natl Acad Sci USA 73:4344–4348, 1976.
79. Small JV, Sobieszek A: Studies on the function and composition of the 10 nm (100Å) filaments of vertebrate smooth muscle. J Cell Sci 23:243–268, 1977.
80. Gabbiani G, Schmid E, Winter S, Chaponnier C, De Chastonay C, Vandekerckhove J, Weber K, Franke WW: Vascular smooth muscle cells differ from other smooth muscle cells: predominance of vimentin filaments and a specific α-type actin. Proc Natl Acad Sci USA 78:298–302, 1981.
81. Berner PF, Frank E, Holtzer H, Somlyo AP: The intermediate filament proteins of rabbit vascular smooth muscle immunofluorescent studies of desmin and vimentin. J Muscle Res Cell Motil 2:439–452, 1981.
82. Gabbiani G, Rungger-Brandle E, De Chastonay C, Franke WW: Vimentin-containing smooth muscle cells are responsible for intimal thickening after endothelial injury [abstr]. Fed Proc 41:269, 1982.
83. Somlyo AV: Ultrastructure of vascular smooth muscle. In: Bohr DF, Somlyo AP, Sparks HV, Geiger SR (eds) Handbook of physiology. Sect 2: The cardiovascular system. Vol 2: Vascular smooth muscle. Bethesda MD: American Physiological Society, 1980, pp 33–67.
84. Wang K, Ash JF, Singer SJ: Filamin, a new high molecular-weight protein found in smooth muscle and non-muscle cells. Proc Natl Acad Sci USA 72:4483–4486, 1975.
85. Wang K, Singer SJ: Interaction of filamin with F-actin in solution. Proc Natl Acad Sci USA 74:2021–2025, 1977.
86. Hartwig JH, Stossel TP: Isolation and properties of actin, myosin, and a new actin-binding protein in rabbit alveolar macrophages. J Biol Chem 250: 5696–5705, 1975.
87. Brinkely BR: Summary: organization of the cytoplasm. Cold Spring Harbor Symp Quan Biol 46:1029–1040, 1982.
88. Adelstein RS, Conti MA: Phosphorylation of platelet myosin increases actin-activated myosin ATPase activity. Nature 256:597–598, 1975.
89. Sobieszek A: Vertebrate smooth muscle myosin: enzymatic and structural properties. In: Stephens NL (ed) The biochemistry of smooth muscle. Balitmore: University Park Press, 1977, pp 413–443.
90. Ebashi S, Iwakura H, Nakajima H, Nakamura R,

Ooi Y: New structural proteins from dog heart and chicken gizzard. Biochem 345:201–211, 1966.
91. Perrie WT, Smillie LB, Perry SV: A phosphorylated light-chain component of myosin from skeletal muscle. Biochem J 135:151–164, 1973.
92. Persechini A, Hartshorne DJ: Phosphorylation of smooth muscle myosin: evidence for cooperativity between the myosin heads. Science 213:1383–1385, 1981.
93. Persechini A, Mrwa U, Hartshorne DJ: Effects of phosphorylation on the actin-activated ATPase activity of myosin. Biochem Biophys Res Commun 98:800–805, 1981.
94. Janis RA, Moats-Staats BM, Gualtieri RT: Protein phosphorylation during spontaneous-contraction of smooth muscle. Biochem Biophys Res Commun 96:265–270, 1980.
95. Driska SP, Aksoy MO, Murphy RA: Myosin light chain phosphorylation associated with contraction in arterial smooth muscle. Am J Physiol 240:C222–C233, 1981.
96. Barron JT, Barany M, Barany K: Phosphorylation of the 20,000 dalton light chain of myosin of intact arterial smooth muscle in rest and in contraction J Biol Chem 254:4954–4956, 1979.
97. DeLanerolle P, Stull JT: Myosin phosphorylation during contraction and relaxation of tracheal smooth muscle. J Biol Chem 255:9993–10000, 1980.
98. Murray KJ, England PJ: Contraction in intact pig aortic strips is not always associated with phosphorylation of myosin light chains. Biochem J 192:967–970, 1980.
99. Aksoy MO, Murphy RA, Kamm KE: Role of Ca^{2+} and myosin light chain phosphorylation in regulation of smooth muscle. Am J Physiol 242:C109–C116, 1982.
100. Butler TM, Siegman MJ: Chemical energetics of contraction in mammalian smooth muscle. Fed Proc 41:204–208, 1982.
101. Siegman MJ, Butler TM, Mooers SU, Davies RE: Calcium-dependent resistance to stretch and stress relaxation in resting smooth muscles. Am J Physiol 231:1501–1508, 1976.
102. Bridenbaugh RL, Walsh PM, Kerrick WGL, Hartshorne DJ: Phosphorylation-dependent activated tension in skinned gizzard muscle fibers in the absence of Ca^{2+}. Biophys J 37:121a, 1982.
103. Halpern W, Mongeon SA, Root DT: Stress, tension and myogenic aspects of small isolated extraparenchymal rat arteries. In: Stephens NL (ed) Smooth muscle contraction. New York: Dekker, 1984 (in press).
104. Herlihy JT, Murphy RA: Length–tension relationship of smooth muscle of the hog carotid artery. Circ Res 33:275–283, 1973.

38. METABOLISM AND ENERGETICS OF VASCULAR SMOOTH MUSCLE

John W. Peterson

Introduction

The metabolism and energetics of vascular smooth muscle contractility have been comprehensively reviewed in the past several years [1–8]. This short review attempts therefore only to summarize briefly what is rather widely accepted regarding the energy metabolism of vascular smooth muscle and the demands imposed upon that metabolism by contractile activity. In the latter part, I try to focus on several issues which are currently unresolved and topics of some debate.

Amphibian skeletal muscles and vascular smooth muscles represent two extreme modes of how chemical energy in the form of the terminal phosphate bond of adenosine triphosphate (ATP) might be provided to the contractile proteins of muscles to supply the motive power needed to drive muscular contraction (cf., Kushmerick [9] for a schematic summary). During contraction at 0°C, amphibian skeletal muscle utilizes ATP approximately 100 times faster than its aerobic metabolism can resynthesize ATP. During a brief isometric tetanus, therefore, the available preformed high-energy phosphate compounds decline rapidly, limiting the ability of the muscle to maintain the developed force. After some period of time, aerobic resynthesis of ATP is activated and, on a time scale greatly longer than the sustained contractile period itself, the original phosphagen content is restored. In order to support the brief but intense period of ATP hydrolysis associated with contraction before the onset of aerobic recovery metabolism, skeletal muscles possess a large pool of preformed high-energy phosphate compounds on the order of 15–25 μmol/g fresh muscle. While ATP (the substrate used directly by the contractile proteins) is present in only moderate concentration, ADP generated by the actomyosin ATPase is immediately rephosphorylated to ATP by phosphate transfer from a phosphocreatine (PCr) pool present at relatively high concentrations.

Vascular smooth muscle (VSM) operates on the opposite tack. The initiation of contractile activity is associated with virtually no measurable decline in the available ATP + PCr content of the muscle [10], since the rates of ATP utilization by the contractile apparatus and the rates of aerobic resynthesis are compatible. Only if aerobic and glycolytic metabolisms are blocked can a net decline in the tissue content of ATP and PCr be noted. This leads then to two distinct strategies to study the energetics of vascular smooth muscle contraction, both of which are represented in the literature.

One method relies on measuring steady-state metabolic rates (that is, the rate at which ATP is being resynthesized) during rest and contractile activity to estimate the usage of ATP. This method depends upon the assumption (verifiable, in most instances) that during the time of measurement the intracellular ATP + PCr pool is constant and that ATP utilization and production rates are in constant balance. This method is, of course, subject to the limitation that, on short time scales, such may not be the case. An alternative method is to block all ATP resynthesis (using combinations of oxygen- and substrate-free environments and various meta-

N. Sperelakis (ed.), PHYSIOLOGY AND PATHOPHYSIOLOGY OF THE HEART.

Martinus Nijhoff Publishing, Boston/The Hague/Dordrecht/Lancaster.

bolic poisons) and measure directly the decline in intracellular ATP + PCr at rest and during contractile activity. This method is also subject to inherent limitations. The use of metabolic poisons, in general, raises the issue of how representative the particular measurements are of the normal tissue (cf., Daemers-Lambert [11], for example). Also, since the method of determining tissue ATP content is inherently destructive, one is limited to one data point per tissue, thus requiring less direct statistical comparisons among a large population of tissues. The advantage of the method, however, is that it is not dependent on the steady-state assumption and can be applied, in principle, to arbitrarily short time periods. Limiting the time resolution of the method, however, is the extremely low ATPase rate manifest in vascular smooth muscle, even when taken in comparison to the small pool size of preformed high-energy phosphates. Both methods have been used in the study of smooth muscle energetics and, for the most part, the resulting data have proven complementary, so that methodologic limitations alone don't seem to play an important role in our understanding of the results.

These two energy-provision strategies appear to have evolved to meet the specific physiologic demands placed upon the various muscle types. Vascular smooth muscle's role in situ is to maintain blood vessel tone over long periods of time and to adjust tone gradually in response to changing conditions of the cardiovascular system. To do so economically, smooth muscle actomyosin possesses an extraordinarily low inherent ATPase and yet is capable of developing and maintaining forces quantitatively comparable to that of skeletal muscles. Paul has estimated that only 3%–5% of the total human basal metabolism is consumed by the vasculature and only about one-fifth of that is required to maintain circulatory regulation [4]. While the vascular mass, which distributes the cardiac output and plays an extremely important role in cardiovascular dynamics, is about ten times greater than that of the heart itself, it consumes less than one-half as much energy in fulfilling its role.

Content of High-Energy Phosphates

This chapter will throughout make no attempt to present an exhaustive compilation of data, but will instead focus on the most typical values of various parameters, with the observed ranges indicated when possible. Extreme values reported in the literature have, for the most part, been deleted. I hope, in this way, to concentrate on general features of vascular metabolism and energetics without the added complication of reconciling specific items of data from various tissues, species, and laboratories. While an extensive literature exists on the rat portal vein (Johansson, Hellstrand, and colleagues), this spontaneously active vessel seems atypical of the tonic vessels most frequently studied and has, therefore, not been included in numerical comparisons.

Table 38–1 summarizes the content of high-energy phosphates found in quiescent mammalian muscles. The most notable feature is simply that vascular smooth muscle has, in general, the lowest content of preformed high-energy stores; in some cases less than one-fiftieth of the preformed energy available to skeletal muscles.

These conditions set the stage then for the two modes of energy provision described above. At room temperature and at the maximum isometric tension that each muscle type is capable of producing, the mammalian skeletal muscles would consume their available preformed high-energy phosphates in about 2–3 s; while the smooth muscles would not substantially deplete their supplies, on the other hand, until 2–3 min. Daemers-Lambert and Roland [12] found no change in the ATP + PCr content of isolated oxygenated bovine carotid arteries after

TABLE 38–1. High-energy phosphate content of resting mammalian muscles

	[ATP]	[PCr]	[Total ~P]
Vascular smooth muscle	0.3–1	0.3–1	0.5–2
Other smooth muscles	1–2	1–3	2–5
Skeletal muscle	~5	10–15	15–25

All values in μmol/g wet tissue. The ranges have been estimated from tables of specific values contained in the reviews cited [1–7] and from references 22–25.

30 min of maximal activation with potassium chloride; whereas similar experiments with metabolically inhibited iodoacetate-treated arteries led to a complete depletion of high-energy phosphates. On a much shorter time scale, Krisanda and Paul [13] have been able to detect no change in the ATP or PCr content of well-oxygenated pig carotid arteries in times as short as 30 s following activation of isometric tension development. Clearly, in the case of vascular smooth muscle, the aerobic capacity to resynthesize ATP is capable of rapidly achieving a balance with the ATPases which activate, develop, and maintain contractile activity.

Respiration

As discussed above, it has been observed that the metabolic capacity of vascular smooth muscle is sufficient to resynthesize ATP at least as rapidly as ATP is utilized by the contractile machinery. The biochemical pathways for ATP synthesis appear to be similar to those found in mammalian skeletal muscles. Studies of the respiratory quotient [14, 15] indicate that the primary substrate for energy metabolism is carbohydrate, although the capacity to utilize a wide variety of substrates is present [16]. The necessary enzymes of glycolysis, the Krebs cycle, and the respiratory transport chain have been demonstrated in VSM [17–19]. Mitochondria isolated from vascular smooth muscle and characterized with respect to P/O ratio, respiratory control ratio, and substrate utilization appear not to differ substantially from the mitochondria of other mammalian tissues [20, 21].

The resting respiratory rates of mammalian smooth and skeletal muscles show relatively similar values. For both red and white skeletal muscles, basal respiratory rates are in the range 150–300 nmol O_2/min/g tissue [22–25], while the smooth muscles range from 50–200 nmol O_2/min/g tissue [1–7]. This suggests that, in the absence of an activated actomyosin ATPase and consequent contractile activity, the basal energy cost of maintaining life processes in mammalian muscle types is similar. A major difference arises, however, upon activation of contractile activity. In continuously twitching or tetanized mammalian skeletal muscle, for example, steady-state O_2 consumption rate increases by factors typically 25- to 50-fold [22, 25], as does recovery O_2 consumption rate following tetani of moderate (< 15 s) duration [22]. In isometrically contracted vascular smooth muscle, O_2 consumption rate increases typically no more than twofold [1–7]. This much lower maximum oxygen consumption rate is, of course, consistent with the above-mentioned differences in the inherent actomyosin ATPases, the pool size of preformed high-energy phosphates, and the different energy-provision strategies between the two muscle types.

A consistent finding in studies of isolated vascular smooth muscle is that the increases in the rate of aerobic metabolism are very tightly correlated with the levels of maintained isometric tension under a wide variety of conditions [26–33]. This is illustrated in figure 38–1 for studies using strips of hog carotid artery [31] stimulated to develop and maintain varying levels of isometric tension in response to graded isotonic increases in the ratio of K^+ to Na^+ in the bathing saline. The upper panel shows continuous recordings of the oxygen tension in the bathing solution determined polarographically by oxygen electrode. The slopes of the oxygen concentration records are proportional to the rates of oxygen consumption by the arterial segment. It is evident from figure 38–1 that the steady-state rate of O_2 consumption increases progressively as isometric tension increases and returns to the initial resting value when contractile activity ceases. The results of identical experiments with five artery segments are plotted in figure 38–2 (open circles), demonstrating the tight linear correlation between *supra*basal O_2 consumption rate and the level of maintained isometric tension.

In most cases, the quantitative correlation between isometric tension maintenance and increased O_2 consumption rate has been found not to change substantially over long periods of time (up to 12 h in vitro), nor to vary *significantly* with the mode of stimulation of the blood vessel whether ionic, pharmacologic, or

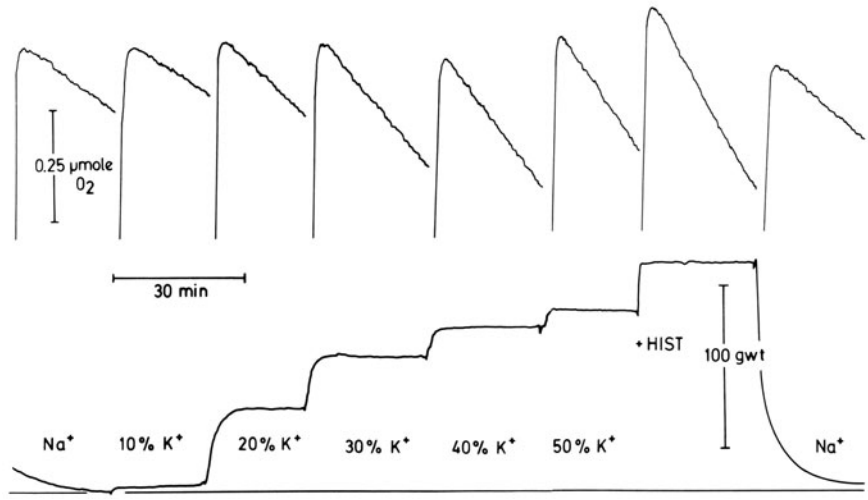

FIGURE 38–1. *(Top panel)* Records of O_2 concentration measured by O_2 electrode in a closed chamber containing a segment of hog carotid artery. The rapid vertical rises in the O_2 records correspond to changes of the bathing medium which both restored O_2 concentration to approximately the initial value and accomplished the change in ionic composition of the bathing physiologic saline solution. The downward slope of each trace is proportional to the O_2 consumption rate of the arterial segment in the chamber (cf., Paul et al. [29]) during the mechanical state directly below. *(Bottom panel)* Record of the isometric tension development of the arterial segment in response to the indicated increase in the percentage substitution of Na^+ by K^+ in the bathing solution. "Na^+" indicates normal saline (Krebs-Henseleit). "Hist" indicates the addition of 10^{-5} *M* histamine to the already K^+-depolarized artery segment.

electrical [1–7, 26–33]. Data illustrating this relative invariance are shown in figure 38–2. Additional data beyond that discussed above are shown for experiments with hog carotid arteries in which isometric tension was varied by maintaining a constant elevated ratio of K^+ to Na^+ in the bathing solution, but varying the extracellular Ca^{2+} concentration [31]. Over the range of $[Ca^{2+}]$ from 0.1 to 1.0 m*M*, graded isometric tension responses similar to those shown in the lower panel of figure 38–1 were obtained. The steady-state rates of O_2 consumption following this alternative mode of activating graded isometric contractions are shown in figure 38–2 for experiments with five artery samples (filled circles). Clearly, in this case at least, the response of aerobic metabolism to increasing isometric tension maintenance was essentially invariant to the particulars of how the muscle was activated to produce tension. Similar comparative data obtained in studies with bovine mesenteric vein [27–29] display a likewise invariant dependence of *su-prab*asal O_2 metabolism on graded isometric contractions produced by varying the concentration of three pharmacologic stimulants: epinephrine, norepinephrine, and histamine (cf. also fig. 38–3).

In comparing various vascular smooth muscles from a variety of species, the increases in O_2 consumption rate above basal levels to maintain the maximum level of isometric force is in the range of 50–100 nmol O_2/min/g tissue [1–7]. Because of the generally observed close correlation between isometric tension maintenance and *supra*basal aerobic metabolism, it is generally believed that the ATP hydrolyzed by vascular smooth muscle actomyosin is rapidly resynthesized through primarily oxidative pathways.

Aerobic Glycolysis

In well-oxygenated resting mammalian skeletal muscles, the steady production of lactic acid is rather small, ranging in the literature from 5–

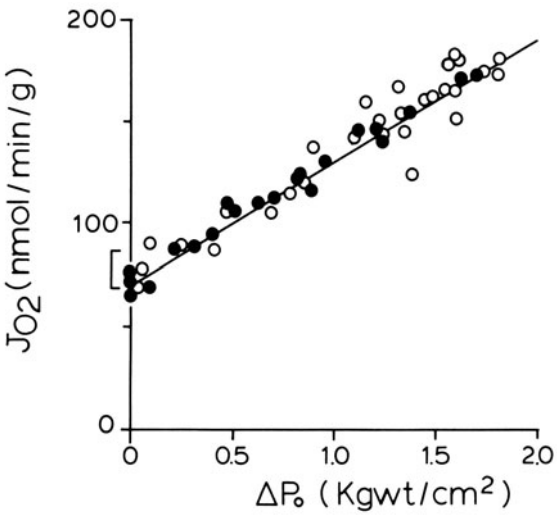

FIGURE 38–2. Observed rates of O_2 consumption (J_{O_2}) are plotted against maintained isometric force (ΔP_o) in five hog carotid artery samples in response to varying levels of K^+ for Na^+ substitution in the bathing medium, as described by figure 38–1 (open circles). In five other artery samples, maximal activation was maintained by 50% K^+-substituted saline, but extracellular [Ca^{2+}] was varied (after depletion using Ca^{2+}-free saline and 0.5 m*M* EGTA) between 0.1 and 1 m*M*. Again, O_2 consumption rate is plotted against the maintained isometric force under these conditions (filled circles). The linear relation between force and O_2 consumption is identical for the two sets of activating conditions. The mean (±SD) resting rate of O_2 consumption for the ten artery segments is shown by the bracket near the J_{O_2} axis. The fact that the linear regression through the force-dependent J_{O_2} data passes near the resting J_{O_2} value is suggestive that basal J_{O_2} was not substantially altered during isometric contraction.

50 nmol lactate/min/g tissue [22–24], as compared to a resting O_2 consumption rate of 150–300 nmol O_2/min/g tissue. In general, the contribution of aerobic glycolysis to total ATP production rate in the resting muscle does not exceed 5% and the bulk of the glucose or glycogen utilized is metabolized aerobically. In the early phase of skeletal muscular activity, before the onset of recovery metabolism, lactate production may increase substantially. Over longer-term tetani, however, or averaged over the full period of recovery metabolism (several minutes), lactate production increases by factors only 2–4 times over the basal production rate. O_2 consumption rates, on the other hand, increase by factors typically 20- to 100-fold, so that the energetics of both steady-state and/or recovery metabolism in support of mechanical activity in mammalian skeletal muscles is almost entirely oxidative.

In vascular smooth muscle, the situation is somewhat different. It has been known for some time that vascular smooth muscles maintain unusually high levels of lactic acid production [15], even in well-oxygenated in vitro preparations. While it was, early on, suspected that this reflected some sort of "tissue damage," most recent evidence obtained under conditions suitable to maintain healthy smooth muscle tissue in vitro observe this high level of aerobic glycolysis as a consistent finding (cf., Lundholm et al. [34] for a review). Substantial levels of aerobic glycolysis have been reported for a wide variety of smooth muscle types, including uterine, intestinal, and tracheal smooth muscles [1–7, 34, 35].

For blood vessels with basal O_2 consumption rates in the range of 50–200 nmol O_2/min/g, typical resting aerobic lactic acid production rates are in the range 100–250 nmol lactate/min/g with a steady-state ratio of 1–2 mol lactate produced per mol O_2 consumed being most common. In terms of the fate of utilized carbohydrate, this is a highly inefficient system in that a molar ratio of 1–2 means that 75%–85% of the glucose equivalents utilized are metabolized only to lactic acid. The 15%–25% of glucose completely oxidized nonetheless provides the bulk of the total ATP production (70%–80%) due to the much higher ATP production per glucose molecule of oxidative metabolism.

In the earliest study examining in detail the role of aerobic glycolysis in the support of mechanical activity in vascular smooth muscle, Peterson and Paul [28] found that both O_2 consumption and lactic acid production rates increased linearly in response to increasing isometric tension development and tissue ATPase. The molar stoichiometric proportion of ATP being produced oxidatively and glycolytically remained approximately constant (that is, 25%–30% of the total ATP production was due to lactic acid production), regardless of the level of mechanical activity. In addition, this

was found to be the case whether isometric force was varied by varying the level of pharmacologic activation or by varying the length of the muscle at fixed *supra*maximal pharmacologic activation.

These observations led to a fairly simple sort of picture in which the ATP produced by oxidative and glycolytic metabolism entered continuously into a pool of available ATP which was then drawn upon more-or-less uniformly by the various intracellular ATPases, as needed. The observed fixed stoichiometry between oxidative and glycolytic metabolism was then, hypothetically at least, due to some undefined metabolic regulatory features [34]. More recent studies, however, beginning with that of Glück and Paul [30], indicate that this naive picture is probably incorrect. In particular, evidence has accumulated that lactic acid production in VSM is a metabolic feature perhaps specifically coupled to the support of particular cellular activities. Precisely what activities and how this coupling is effected are currently matters of some debate and are dealt with in more detail in a subsequent section.

Chemical Energy Utilization and Contractile Activity

Resting vascular smooth muscle consumes ATP at a rate typically 0.5–1.0 μmol ATP/min/g tissue. The bulk of this ATP requirement is met through carbohydrate metabolism, typically 70%–90% from oxidative metabolism and 10%–30% from aerobic glycolysis [4]. Upon maximal activation of isometric tension development in isolated VSM preparations at lengths near optimal for force development, the total estimated ATP utilization rate increases by a factor of 2 or so. The difference between the initial resting metabolic rate and the maximally activated metabolic rate reflects the sum total of all energy-consuming processes activated in parallel with or consequent to the mechanical activation. An underlying assumption in this method of measuring contractile energetics is, of course, that the energy requirements of basal processes remain more-or-less constant during the period of mechanical activity. Most evidence, albeit indirect, indicates

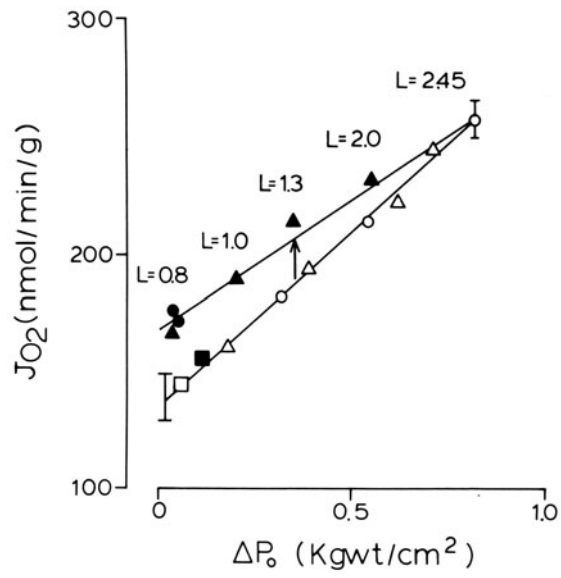

FIGURE 38–3. O_2 consumption rate (J_{O_2}) is plotted against active isometric force (ΔP_o) for an experiment with a single segment of bovine mesenteric vein. The bar indicates the mean (± SD) basal J_{O_2} measured periodically during the experiment. At a segment length L = 2.45 cm, the tissue was progressively activated with increasing concentrations of epinephrine (○), then relaxed in normal saline. The α-adrenergic blocker dihydroergotamine was applied (□) and supramaximal epinephrine readded (■). The contractile effect of epinephrine was about 90% inhibited, as was the metabolic effect. This is taken to indicate that "stimulus artifact" effects of β-adrenergic actions on the metabolic response were essentially negligible. The venous segment was then progressively activated with increasing concentrations of histamine (△), describing the same linear correlation between J_{O_2} and ΔP_o as epinephrine. The muscle was then shortened in the presence of supramaximal histamine in four steps, allowing a measurement of J_{O_2} at each progressively smaller level of isometric tension maintenance (▲) until, at L = 0.8 cm, active isometric tension was nearly fully abolished. At this "zero active force length," J_{O_2} remained somewhat elevated above the basal J_{O_2} level. This "tension-independent activation energy" was the same for both histamine and epinephrine (●), again suggesting that specific pharmacologic actions of the drugs used on aerobic metabolism were negligible. The vertical arrow between the two lines shown indicates an hypothetical isotonic contraction of the preparation from a state approximately one-half maximally activated at length L = 2.45 cm to a fully activated state at L = 1.30 cm against a constant load of 0.36 Kgwt/cm^2, as discussed in the text.

this to be the case for pharmacologic or ionic methods of stimulation [29–32] (cf., figs. 38–2 and 38–3).

The increased ATP utilization rate upon mechanical activation can be conceptualized, at least, as occurring in three separate parts: (1) actomyosin ATPase in support of mechanical activity, (2) ATP-dependent processes which play some role in activating and maintaining the activation of mechanical activity, and (3) all other ATPases activated through the particular means of stimulation chosen. In the more recent studies of smooth muscle energetics, some effort has been made to sort out the quantitative subdivision of the total increase in ATPase into these three categories. In many cases, the third category (which is roughly equivalent to a stimulus artifact) appears to make only a small-to-negligible contribution to the overall increase in tissue metabolism [29, 30, 32] (cf., also fig. 38–3). The first category is most frequently approximated by the *tension-dependent* metabolism, which is measured by determining how *supra*basal energy metabolism changes as the actomyosin interaction (i.e., force development) is varied. During such measurements, the level of stimulation (that is, in essence, the variable components of categories 2 and 3) is held fixed. If, at constant supramaximal stimulation for example, the muscle is lengthened or shortened to lengths where tension development is abolished, the tension-dependent ATPase by definition goes to zero and the remaining *supra*basal metabolism is called the *tension-independent* metabolism. An example of such measurements performed with a single segment of bovine mesenteric vein [36] is shown in figure 38–3, which additionally illustrates the invariance of such measurements to the particular pharmacologic agonist used. Upon supramaximal activation with epinephrine (10^{-6} *M*) at the optimal length for force generation (L = 2.45 cm for this sample), O_2 consumption rate increased by 110 nmol O_2/min/g over the initial resting O_2 consumption rate of about 140 nmol O_2/min/g. Progressive stepwise shortening of the muscle from this length with supramaximal histamine as stimulant caused a decline in isometric tension maintenance (i.e., the *force–length* relationship) which led to a linearly correlated decline in *supra*basal O_2 consumption rate (upper line). When the muscle had freely shortened to L = 0.8 cm so that no isometric tension was evident, O_2 consumption rate remained elevated over the basal rate by about 25 nmol O_2/min/g. This value, the tension-independent metabolism, is about 20% of the total *supra*basal ATPase at maximum isometric tension and was not dependent on whether epinephrine or histamine was used to effect the stimulation. Simultaneous measurements of *supra*basal aerobic glycolysis [6, 28] gave similar values for the tension-independent component of aerobic glycolysis in bovine mesenteric vein.

Figure 38–3 also provides an opportunity to demonstrate the economy of circulatory regulation by vascular smooth muscle. Suppose the vessel segment of figure 38–3 were at a vessel radius equivalent to the segment length L = 2.45 cm and partially activated so as to maintain that vessel caliber against a blood pressure equivalent to a wall tension of 0.36 Kgwt/cm^2. Maintaining the pressure in the vessel constant but maximally activating the vascular smooth muscle would, for the particular sample of fig. 38–3, cause the vessel to shorten to a length approximately L = 1.30 cm (as indicated by the vertical arrow). For the cylindrical blood vessel, this length change is equivalent to a reduction in caliber of about 45%. Using Pouiselle's law to compute the change in flow resistance of the vessel, this amounts to a 12-fold increase in flow resistance. In terms of energy cost, however, the increased energy metabolism necessary to support the muscular activity generating this circulatory regulation is less than 15% of the resting basal metabolism. Apparently the energy cost of regulating peripheral circulation is very low.

The tension-independent metabolism discussed above reflects terms in both categories 2 and 3, as well as the possibility of some residual activated ATP hydrolysis by actomyosin which nonetheless makes no contribution to tension development. Such a situation could arise, for example, through the generation of internally opposing forces which result in no net external force. That such might be the case

is indicated by studies of vascular smooth muscle stiffness. Using the notion of Huxley and Simmons [37] that muscle stiffness is a direct measure of the number of actin–myosin cross-bridges formed at any instant during mechanical activity, then a comparison of resting stiffness (due to inert structural components) with the stiffness found at the extremes of length where tension development is abolished would indicate the extent to which actin and myosin nonetheless interact. In studies of this sort with several arterial preparations, Pfitzer and Peterson [38] found that, during the rise of isometric tension following stimulation, arterial wall stiffness increased in direct proportion to the isometric force developed. The same linear proportionally also applied between stable isometric force and stiffness when isometric force was varied by varying the extracellular [Ca^{2+}] in the high-K^+ bathing medium [39]. These observations suggest that isometric tension and actomyosin interaction in VSM are indeed directly related. In hog carotid artery segments, maximally activated and at their freely shortened length so that no isometric tension was measurable, stiffness was elevated by some 10%–15% above the purely passive stiffness and this component required Ca^{2+} in the bathing medium (Peterson, unpublished observation). This is indicative that at least some component of the tension-independent ATPase could be an actomyosin ATPase.

Measurements of the *supra*basal energy metabolism and estimates of the actomyosin ATPase of vascular smooth muscles determined as the tension-dependent ATPase are presented in table 38–2. Comparisons of the contractile ATPase of the intact preparation determined in this way with that of the ATPase of purified isolated VSM actomyosin, while tentative at best, are in reasonable agreement [4, 5, 40, 42]. From studies of the above sorts, two principal conclusions arise: (a) Despite the ability to develop forces entirely comparable to skeletal and cardiac muscles, the activated ATPase of vascular smooth muscle actomyosin is extremely small, and (b) The investment of energy in processes necessary to maintain the activation of contractile activity is substantial, on the order of 15%–30% of the energy requirement of the actomyosin itself at maximal tension development.

The extraordinary economy of tension maintenance in vascular smooth muscle and the detailed nature of the "activation" processes mentioned above are areas of intense interest in VSM physiology. An additional discussion of *activation energetics* is given in a subsequent section. The very low *tension cost* (or, alternatively, the high *holding economy*) of vascular smooth

TABLE 38–2. *Supra*basal energy metabolism of isometrically contracted VSM

Preparation	(1) Total suprabasal metabolism μmol ATP/min/g Kgwt/cm² force	(2) Tension--dependent metabolism μmol ATP/min/g Kgwt/cm² force	(3) Tension--independent metabolism μmol ATP/min/g	Stimulus	Ref
Bovine mesenteric vein	1.64	1.28	0.20	Epi, NE, Hist	27–29
Hog carotid artery	0.68	0.43	0.27	Hist	30
	0.81	0.46	0.23	K^+	30
	0.40			K^+	31
	0.51			K^+ + Hist	32
Bovine mesenteric artery	1.22	1.12	0.11	Epi	54
	0.66			K^+	
Rat aorta	1.97			K^+	33
Bovine carotid artery	0.82			Electrical	12

In column (1), total *supra*basal metabolism has been divided by the observed isometric tension with the mode of stimulation indicated. Column (2) is that part of the total suprabasal metabolism which vanishes when isometric tension is abolished (but stimulation maintained), normalized to the isometric force. Column (2) is frequently taken as representative of the actomyosin ATPase, to the extent that force represents the quantity of activated actomyosin. Column (3) is the steady-state suprabasal metabolism required to maintain activation. Epi, epinephrine; NE, norepinephrine; Hist, histamine.

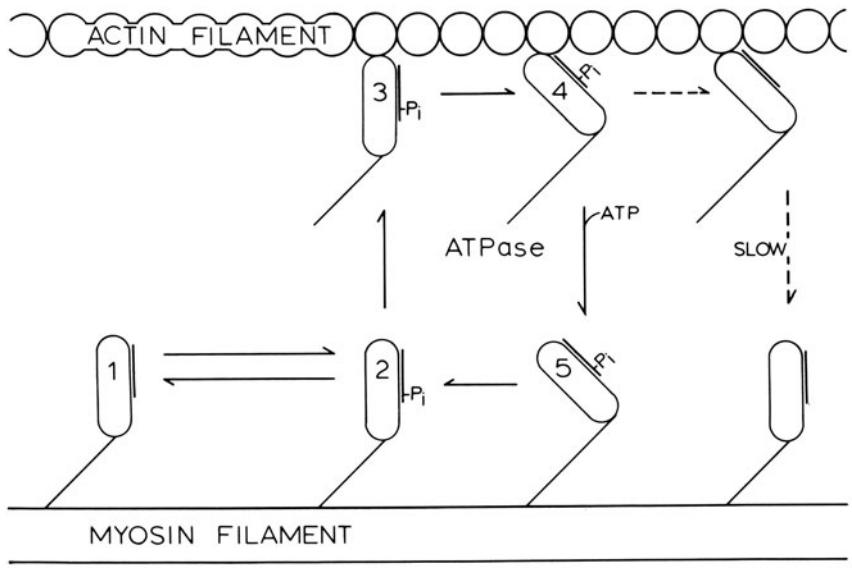

FIGURE 38–4. A schematic model of the smooth muscle myosin cross-bridge interaction with actin filaments is depicted. The transition from state 1 to state 2 represents the Ca^{2+}–calmodulin-dependent phosphorylation–dephosphorylation activation mechanism proposed for smooth muscle regulation. The cycle of interaction (states 2–5) hydrolyzes 1 ATP molecule and generates 1 "quantum" of tension with each pass. Only the angulated attached myosin cross-bridge (state 4), however, generates isometric force. The inherent speed of the cycle is much slower in smooth than in striated muscle, with the ATP-dependent dissociation step (state 4–5) apparently being slowest. The dashed lines indicate formation of a proposed dephosphorylated actomyosin cross-bridge [47, 48], which then dissociates only very slowly and may be responsible for the very high "holding economy" of vascular smooth muscle.

muscle appears to reside primarily in the molecular properties of the actomyosin itself, although structural and geometric factors may also play some part [5, 40–43]. Barany [44] first described an inherent correlation between the ATPase activities of various myosins and the contractile velocities of the muscles from which the myosins originated. Daemers-Lambert [11] observed in bovine carotid artery that DFNB treatment caused a sharp reduction in the rate of isometric tension development which corresponded with a fourfold decrease in the measured ATPase. Vascular smooth muscle appears to be the slowest of all mammalian muscles in terms of its shortening velocity [43] and this mechanical property appears to be a direct reflection of how slowly the actomyosin cross-bridges hydrolyze ATP in going through their repetitive cycle of interaction with actin filaments. From comparisons of the actomyosin content of vascular smooth muscles and the observed rates of the tension-dependent metabolism, it has been estimated that the VSM myosin cross-bridge goes through its cycle of interaction with actin filaments in about 0.75–1.5 s [5, 40–42]. This is an extraordinarily slow rate of interaction when compared to skeletal muscle cross-bridges, which are estimated to cycle at rates more like 100–150 times per second.

If the smooth muscle myosin cross-bridge spends a large fraction of this very long cycle time in contact with the actin filament in the force-generating configuration, then the high holding economy of the tissue is not difficult to appreciate. A schematic representation of this model of the actomyosin cross-bridge cycle is shown in figure 38–4. The steady-state ATPase rate of a single myosin cross-bridge is the reciprocal of the time required to make one full passage through states 2, 3, 4, 5, and back to state 2. Only state 4, however, generates

isometric tension, so that the average tension maintained by a large number of cross-bridges interacting asynchronously is proportional to the time spent in state 4 as a fraction of the total cycle time. Marston and Taylor [45], in comparing purified myosins from four different types of vertebrate muscles (including gizzard smooth muscle), have found that the time required for ATP to dissociate the smooth muscle cross-bridge from actin (state 4–5 in fig. 38–4) is by far the slowest, although not nearly slow enough to fully account for the very high holding economy of smooth muscle relative to the other muscle types. Precisely what molecular features of smooth muscle myosin are responsible for these inherent differences in the enzymatic activities and kinetics of otherwise apparently quite similar molecules is currently not understood.

Some Unresolved Issues

HOLDING ECONOMY

A picture of the actomyosin cross-bridge cycle in which the overall cycle time of the cross-bridge determines the actomyosin ATPase while the fraction of the cycle time spent in the tension-generating state determines the force developed yields, in a relatively direct way, the holding economy of the system. In this very simplified model, however, any factors (biochemical, mechanical, or otherwise) which alter the fraction of the full cycle time which the cross-bridge spends in the tension-generating state could alter the observed holding economy of the tissue (cf., fig. 38–4).

Although observed in a nonvascular mammalian muscle, Herzig et al. [46] have reported a behavior of cardiac muscle which is indicative of this sort of process. Using chemically skinned pig cardiac muscle fibers, it was found that low concentrations (20–100 μM) of vanadate ion ($H_2VO_4^-$), an endogenous compound in cardiac muscle, inhibited both isometric tension development and the actomyosin ATPase of Ca^{2+}-activated cardiac fibers. Observing a dose–response relationship for vanadate ion, however, it was seen that isometric tension fell more rapidly than the actomyosin ATPase, so that a new linear relation between tension and ATPase was established in the presence of vanadate ions, but with a holding economy some 25% less than the relationship previously observed with Ca^{2+} activation in the absence of vanadate ions. It was also observed that the rate of delayed tension development following an activating quick stretch was accelerated by the addition of vanadate. These observations are consistent with the hypothesis that the principal effect of vanadate in these experiments is a disproportionate shortening of the time the cross-bridges spend in the tension-generating state. A quickening of this step disproportionate to the whole cross-bridge cycle time would both increase actomyosin ATPase while decreasing the steady force, thus reducing the holding economy as observed.

Dillon and Murphy [47] have recently reported a phenomenon in vascular smooth muscle that would be similar in its effect on the holding economy. They determined the unloaded shortening velocity of hog carotid artery segments as a function of time during the development and maintenance of isometric tension. The maximum rate at which the muscle is capable of shortening, which is often taken as a direct index of the speed of the individual cross-bridge cycle rate, became progressively slower over a period of some 15–30 min following the activation of mechanical activity. Driska et al. [48] and Aksoy et al. [49] have found a similar temporal relation of the degree of myosin regulatory light-chain phosphorylation during isometric contraction in the same preparation. This temporal correlation is suggestive of the possibility that myosin phosphorylation (possibly in addition to its postulated role as the ultimate regulator of smooth muscle actomyosin interaction—cf., Hartshorne and Siemankowski [50] for a review) acts as a modulator of the speed of the smooth muscle actomyosin cross-bridge cycle. In their model, phosphorylated myosin cross-bridges are dissociated from actin filaments much more rapidly than dephosphorylated myosin cross-bridges. This model is illustrated schematically by the dashed lines in figure 38–4. If this is the case, one would expect the holding econ-

omy of highly phosphorylated VSM myosin to be much less than that of active but dephosphorylated VSM myosin.

This model could also possibly explain another observation regarding holding economy in vascular smooth muscle. Peterson [32] has recently observed in the same preparation that the addition of histamine to hog carotid arteries already stimulated with high K^+ leads to an approximate 25% increase in the tension cost of stable isometric force, even when compared at the identical isometric tension. Data from Aksoy et al. [49] indicate that in the steady phase of isometric contraction (< 15 min) myosin light-chain phosphorylation with high K^+ as activator is only about 18% of the total myosin. With histamine as activator, however, the more-or-less stable level of myosin phosphorylation is around 45%. If their model is correct, these extra, more rapidly cycling cross-bridges due to histamine activation could be the source of the excess tension cost in Peterson's experiments.

A mechanism which is similar in design, but opposite in end effect, has been suggested for myosin light-chain phosphorylation in mammalian skeletal muscles by Kushmerick and Crow [22]. In mouse soleus muscle, they have observed that increasing myosin light-chain phosphorylation during isometric tetani appears to decelerate rather than quicken the myosin cross-bridge cycle. It is possible then that the role of myosin light-chain phosphorylation is primarily that of a speed modulator of the myosin cross-bridge, but that the ultimate effect of phosphorylation on speed depends on the particular type of myosin involved. If this is, in fact, a general mode of regulation in muscles, then the simple notion that muscle stiffness, ATPase, and force development are all simply more-or-less equivalent measures of the number of activated myosin cross-bridges is no longer tenable.

AEROBIC GLYCOLYSIS

As described earlier, vascular smooth muscle manifests a high degree of lactic acid production, even in well-oxygenated in vitro preparations. This high inefficiency in terms of carbohydrate utilization seems, on the surface, somewhat anomalous since we have earlier stressed the extraordinary holding economy of the tissue. Early reports were suggestive that oxidative and glycolytic metabolisms operated in a more-or-less fixed stoichiometric relation, regardless of the mechanical state of the muscle or the method chosen to effect the mechanical activation [26, 28].

Glück and Paul [30], however, demonstrated in hog carotid arteries that, while histamine activation led to a tension-dependent increase in lactic acid production rate, stimulation with a 100% K^+ for Na^+ substituted bathing medium led to a distinct inhibition of aerobic glycolysis even though isometric tension development was near optimal. This dissociation of the ATP production due to lactic acid formation from the contractile actomyosin ATPase led to the conclusion that the observed tension-correlated increases in lactic acid production were possibly more closely related to activation processes than tension development itself. Although ATP levels remained essentially unaltered, so that energy stores to power contractility were available, Cremer-Lacuara et al. [51] found that 2-deoxyglucose, which inhibits glucose metabolism, abolished the spontaneous activity of rat portal vein. Again in hog carotid arteries, Peterson and Glück [31] have reported that relatively small substitutions of Na^+ by K^+ (up to 10%) in otherwise normal bathing medium appear to activate aerobic glycolysis. With progressively increasing substitutions of K^+ for Na^+ (up to 50%), however, aerobic glycolysis was neither stimulated nor inhibited.

In other studies, Paul et al. [52] have found in hog coronary arteries that hypertonic addition of K^+ stimulates aerobic glycolysis (i.e., at constant external Na^+); while ouabain and K^+-free or Na^+-free bathing medium both depress aerobic glycolysis. On this basis, it has been proposed that the energy production of aerobic glycolysis is somehow specifically coupled to the Na^+–K^+ transport system of vascular smooth muscles.

In hog carotid arteries, Peterson observed a similar dissociation of lactic acid production from the energy cost of isometric tension maintenance with high-K^+ activation. With main-

tained activation via high-K^+ depolarization (50% K^+ for Na^+ substitution), varying the level of isometric tension development by altering the concentration of extracellular Ca^{2+} exerted no consistent effect on aerobic glycolysis, which simply remained at or near the resting level [31]. Adding histamine to the already K^+-depolarized artery segment, however, led to a sharp increase in aerobic glycolysis [32] to nearly the same value as that reported for histamine activation alone [30]. During progressive removal and replacement of extracellular Ca^{2+} in arteries supramaximally stimulated with high K^+ plus added histamine, the level of aerobic glycolysis correlated linearly with the Ca^{2+}-activated stable isometric force. On this basis, it was suggested that the energy production of aerobic glycolysis may be coupled to intracellular or plasma membrane *Ca^{2+} pumps* which are responsible for the sequestration and homeostasis of intracellular [Ca^{2+}]. This was proposed, at least in part, since one well-known action of the H_2 receptor for histamine is predominantly vasodilatory, suggesting that histamine can activate intracellular Ca^{2+} sequestration or transmembrane extrusion (cf., Peterson [32]). In uterine smooth muscle, Kroeger [53] has reported that increased Ca^{2+} transport stimulates aerobic glycolysis.

These two proposals may not be at all mutually exclusive, since it has been argued that the Ca^{2+} pumps of smooth muscles operate exclusively through a $Na^+ - Ca^{2+}$ exchange mechanism powered by the ATP utilization of the Na^+–K^+ transport system [53].

ACTIVATION ENERGETICS

In the section on *Chemical energy utilization and contractile activity,* I described "tension-independent" metabolism as a component of the total *supra*basal energy metabolism observed during the steady maintenance of isometric force in vascular smooth muscle. This energy utilization is a durable component, persisting throughout contractile activity and apparently associated more closely with the maintenance of the activated state of the muscle than with the actual actomyosin ATPase which generates contractile activity. Most frequently, these energy costs are ascribed to processes such as ATP-dependent Ca^{2+} translocation, other altered energy-dependent ion fluxes, protein phosphorylation–dephosphorylation cycles, and other miscellaneous processes [4]. In this section, a second sort of *activation energy* will be discussed.

It has now been repeatedly observed using a variety of methodologies in vascular smooth muscles [12, 13, 54], other smooth muscles [55], fast mammalian skeletal muscles [22, 56], and in amphibian skeletal muscle [57] that the initiation and development of isometric tension is energetically far more costly than the steady-state maintenance of isometric tension (even when including the above-mentioned "steady-state activation energy").

In bovine carotid arteries poisoned with iodoacetate to block glycolysis, Daemers-Lambert and Roland [12] observed directly a five-fold greater rate of ATP + PCr utilization in the first 20 s of isometric tension development than during the subsequent several minutes of stable force maintenance. Using anaerobic metabolism as the index of overall energy metabolism, Lundholm and Mohme-Lundholm [54] found that lactic acid production in the first 15 min of isometric tension development in bovine mesenteric artery exceeded the steady-state lactic acid production rate by a factor of 2–12, depending on the stimulus used (epinephrine and high K^+, respectively). Using the rate of *supra*basal O_2 consumption in hog carotid artery, Krisanda and Paul [13] have reported that during the first 1–4 min of K^+-stimulated isometric contraction, the rate of metabolic energy utilization is approximately twice that found during the steady phase of tension maintenance.

In the rabbit taenia coli, a smooth muscle somewhat faster than most vascular smooth muscles with regard to shortening velocity, time to peak tension, and measured ATPase (typically factors of 2–4 at equitemperature comparison), Seigman et al. [55] have determined directly that high-energy phosphate utilization rate during the first 25 s of isometric tension development is about fourfold greater than the steady-state rate. In a specific comparison of the rate of energy utilization during the development of isometric force between rabbit taenia coli and frog skeletal muscle, Butler and

Davies [3] found that the net energy usage of the two muscles as a function of time is virtually identical once the approximately 45-fold inherent difference in speed of the two preparations (at different temperatures) is scaled away. This similarity of energy usage between two otherwise disparate (in terms of time scale and economy) muscle preparations might be taken to suggest that the observed excess energy utilization associated with the development of isometric tension is an inherent property of actomyosin systems. In their comparison, although time and ATPase scales differ by a factor of 50–100, the net excess high-energy phosphate consumed to reach similar maximum tensions was 0.35 μmol ~P/g muscle for both the smooth and skeletal muscles.

The suggestion, however, that this excess energy utilization represents some form of intrinsic internal work performed by the actomyosin systems in stretching internal elastic elements during the development of isometric force, a term which might be essentially similar in all muscle types, has proven unlikely. For both the taenia coli [55] and hog carotid artery [13], energy utilization has been measured during the redevelopment of isometric force following a fast shortening step which discharged all maintained isometric force. In both cases, the redevelopment of isometric force required no measurable excess energy utilization beyond the observed force maintenance rate. This argues that only the activation of tension development from the resting state requires excess high-energy phosphate utilization.

Furthermore, the similarity of excess energy utilization during initial isometric tension development observed for the taenia coli and frog sartorius muscles does not seem to apply, in general, to vascular smooth muscle. The excess energy utilization for this process in hog carotid artery is on the order of 2 μmol ~P/g, while that in bovine mesenteric artery ranges from 2 to 4 μmol ~P/g (calculated from the data of Krisanda and Paul [13] and Lundholm et al. [54], respectively). This excess energy utilization in vascular smooth muscles, while qualitatively similar, is some five-to tenfold greater than that observed in taenia coli. This higher level of "initial activation energy" in vascular smooth muscle may correlate, however, with the reported dependence of VSM contractile velocity on the degree of myosin regulatory light-chain phosphorylation.

Dillon and Murphy [47] have found in hog carotid artery that the contractile velocity during the early phase of isometric tension development is typically 50%–100% greater than the shortening velocity measured during the steady phase of isometric contraction. Peterson [36] found a similar difference in contractile velocities measured in bovine mesenteric vein. The maximum shortening velocity of "afterloaded" contractions (that is, shortening allowed from the time the muscle first develops an isometric force equal to the imposed load, usually < 30 s) averaged about eight times faster than the maximum shortening velocity measured by releases after isometric tension had become stable (>10 min). The time course of contractile velocity decrease in these preparations is similar to the time course of excess energy utilization described above. Both observations may be the consequence of the very much higher myosin regulatory light-chain phosphorylation levels which have been observed in the first 1–2 min following activation [48, 49].

At this time, it is not possible to state with any certainty whether this initial activation energy reflects purely activation processes (such as excess energy-dependent Ca^{2+} translocation) which are greater in the early phase of muscle contraction than during the steady phase, or varying kinetics of the myosin cross-bridge cycle during the early phase of its interaction with actin filaments, or some variable combination of both processes.

References

1. Hellstrand P, Paul RJ: Vascular smooth muscle: relations between energy metabolism and mechanics. In: Crass MF III, Barnes CD (eds) Vascular smooth muscle. New York: Academic, 1982, pp 1–35.
2. Paul RJ: Smooth muscle: mechanochemical energy conversion relations between metabolism and contractility. In: Johnson LR (ed) Physiology of the gastrointestinal tract. New York: Raven, 1981, pp 269–288.

3. Butler TM, Davies RE: High-energy phosphates in smooth muscle. In: Bohr DF, Somlyo AP, Sparks HV, Geiger SR (eds) Handbook of physiology. Sect 2: The cardiovascular system. Vol 2: Vascular smooth muscle. Bethesda MD: American Physiological Society, 1980, pp 237–252.
4. Paul RJ: Chemical energetics of vascular smooth muscle. In: Bohr DF, Somlyo AP, Sparks HV, Geiger SR (eds) Handbook of physiology. Sect 2: The cardiovascular system. Vol 2: Vascular smooth muscle. Bethesda MD: American Physiological Society, 1980, pp 201–235.
5. Paul RJ, Rüegg JC: Biochemistry of vascular smooth muscle: energy metabolism and proteins of the contractile apparatus. In: Kaley G, Altura BM (eds) Microcirculation, vol 2. Baltimore: University Park Press, 1978, pp 41—82.
6. Paul RJ, Peterson JW: Smooth muscle energetics. In: Casteels R, Godfraind T, Rüegg JC (eds) Excitation–contraction coupling in smooth muscle. Amsterdam: Elsevier/North-Holland Biomedical, 1977, pp 455–462.
7. Paul RJ, Peterson JW: The mechanochemistry of smooth muscle. In: Stephens NL (ed) The biochemistry of smooth muscle. Baltimore: University Park Press, 1977, pp 15–39.
8. Daemers-Lambert C: Mechanochemical coupling in smooth muscle. In: Stephens NL (ed) The biochemistry of smooth muscle. Baltimore: University Park Press, 1977, pp 51–82.
9. Kushmerick MJ: Chemical energy balance in amphibian and mammalian skeletal muscles: introduction. Fed Proc 41:147–148, 1982.
10. Daemers-Lambert C: Action du chlorure de potassium sur le metabolisme des esters phosphores et le tonus du muscle arteriel (carotide de bovide). Angiologica 1:249–274, 1964.
11. Daemers-Lambert C: Action du fluoronitrobenzene sur le metabolisme phosphore du muscle lisse arteriel pendant la stimulation electrique (carotide de bovide). Angiologica 6:1–12, 1969.
12. Daemers-Lambert C, Roland J: Metabolisme des esters phosphores pendant le developpement et le maintien de la tension phasique du muscle lisse arterial (carotides de bovide). Angiologica 4:69–87, 1967.
13. Krisanda JM, Paul RJ: Transient in phosphagen utilization during isometric contraction of vascular smooth muscle. Biophys J 37:186a, 1982.
14. Kosan RL, Burton AC: Oxygen consumption of arterial smooth muscle as a function of active tone and passive stretch. Circ Res 18:79–88, 1966.
15. Kirk JE, Effersoe PG, Chiang SP: The rate of respiration and glycolysis by human and dog aortic tissue. J Gerontol 9:10–35, 1954.
16. Chace KV, Odessey R: The utilization by rabbit aorta of carbohydrates, fatty acids, ketone bodies, and amino acids as substrates for energy production. Circ Res 48:850–858, 1981.
17. Zemplenyi T: Enzymes of the arterial wall. J Atheroscler Res 2:2–24, 1962.
18. Zemplenyi T, Lojda Z, Mrhova O: Enzymes of the vascular wall in experimental atherosclerosis in the rabbit. In: Sandler M, Bourne GH (eds) Atherosclerosis and its origin. New York: Academic, 1963, pp 459–513.
19. Kirk JE: Intermediary metabolism of human arterial tissue and its changes with age and atherosclerosis. In: Sandler M, Bourne GH (eds) Atherosclerosis and its origin. New York: Academic, 1963, pp 67–117.
20. Vallieres J, Scarpa A, Somlyo AP: Subcellular fractions of smooth muscle. I. Isolation, substrate utilization and Ca^{++} transport by main pulmonary artery and mesenteric vein mitochondria. Arch Biochem Biophys 170:659–669, 1975.
21. Wrogemann K, Stephens NL: Oxidative phosphorylation in smooth muscle. In: Stephens NL (ed) The biochemistry of smooth muscle. Baltimore: University Park Press, 1977, pp 41–50.
22. Kushmerick MJ, Crow M: Chemical energy balance in amphibian and mammalian skeletal muscles. Fed Proc 41:163–168, 1982.
23. Chapman JB, Gibbs CL, Loiselle DS: Myothermic, polargraphic, and fluorometric data from mammalian muscles. Fed Proc 41:176–184, 1982.
24. Cerretelli P, Di Prampero PE, Piiper J: Energy balance of anaerobic work in the dog gastrocnemius muscle. Am J Physiol 217:581–585, 1969.
25. Stainsby WN, Barclay JK: Relation of load, rest length, work and shortening to oxygen uptake by in situ dog semiteninosus. Am J Physiol 221:1238–1242, 1971.
26. Hellstrand P: Oxygen consumption and lactate production of the rat portal vein in relation to its contractile activity. Acta Physiol Scand 100:91–106, 1977.
27. Paul RJ, Peterson JW, Caplan SR: Oxygen consumption rate in vascular smooth muscle: relation to isometric tension. Biochim Biophys Acta 305:474–480, 1973.
28. Peterson JW, Paul RJ: Aerobic glycolysis in vascular smooth muscle: relation to isometric tension. Biochim Biophys Acta 357:167–176, 1974.
29. Paul RJ, Peterson JW, Caplan SR: A nonequilibrium thermodynamic description of vascular smooth muscle mechanochemistry. I. The rate of oxygen consumption: a measure of the driving chemical reaction. J Mechanochem Cell Motil 3:19–32, 1974.
30. Glück E, Paul RJ: The aerobic glycolysis of porcine carotid artery and its relation to isometric force. Pflugers Arch 370:9–18, 1977.
31. Peterson JW, Glück E: Energy cost of membrane depolarization in hog carotid artery. Circ Res 50:839–847, 1982.
32. Peterson JW: Effect of histamine on the energy metabolism of K^{+}-depolarized hog carotid artery. Circ Res 50:848–855, 1982.
33. Arner A, Hellstrand P: Energy turnover and me-

chanical properties of resting and contracting aortas and portal veins from normotensive and spontaneously hypertensive rats. Circ Res 48:539–548, 1981.
34. Lundholm L, Andersson RGG, Arnqvist HJ, Mohme-Lundholm E: Glycolysis and glycogenolysis in smooth muscle. In: Stephens NL (ed) The biochemistry of smooth muscle. Baltimore: University Park Press, 1977, pp 159–207.
35. Kroeger EA: Regulation of metabolism by cyclic adenosine 3′:5′-monophosphate and ion-pumping in smooth muscle. In: Stephens NL (ed) The biochemistry of smooth muscle. Baltimore: University Park Press, 1977, pp 315–327.
36. Peterson JW: Rates of metabolism and mechanical activity in vascular smooth muscle. PhD thesis, Harvard University, university microfilm no. 7424959, 1974.
37. Huxley AF, Simmons RM: Proposed mechanism of force generation in striated muscle. Nature 233:533–538, 1971.
38. Pfitzer G, Peterson JW: Stiffness of the arterial wall in response to potassium and pharmacological activation. In: Reinis Z, Pokorny J, Linhart J, Hild R, Schirger A (eds) Adaptability of vascular wall. Prague: Avicenum Czechoslovak Medical, 1980, pp 125–127.
39. Peterson JW: Relation of stiffness, energy metabolism, and isometric tension in a vascular smooth muscle. In: Vanhoutte PM, Leusen I (eds) Mechanisms of vasodilatation. Basel: S Karger, 1978, pp 79–88.
40. Paul RJ, Glück E, Rüegg JC: Cross bridge ATP utilization in arterial smooth muscle. Pflugers Arch 361:297–299, 1976.
41. Rüegg JC: Smooth muscle tone. Physiol Rev 51:201–248, 1971.
42. Mrwa U, Paul RJ, Kreye VAW, Rüegg JC: The contractile mechanism of vascular smooth muscle. In: Smooth muscle pharmacology and physiology. Paris: Inserm, 1976, pp 319–326.
43. Murphy RA: Mechanics of vascular smooth muscle. In: Bohr DF, Somlyo AP, Sparks HV, Geiger SR (eds) The handbook of physiology. Sect 2: The cardiovascular system. Vol 2: Vascular smooth muscle. Bethesda MD: American Physiological Society, 1980, pp 325–351.
44. Barany M: ATPase activity of myosin correlated with speed of muscle shortening. J Gen Physiol 50:197–218, 1967.
45. Marston SB, Taylor EW: Comparison of the myosin and actomyosin ATPase mechanisms of the four types of vertebrate muscles. J Mol Biol 139:573–600, 1980.
46. Herzig JW, Peterson JW, Rüegg JC, Solaro RJ: Vanadate and phosphate ions reduce tension and increase cross-bridge kinetics in chemically skinned heart muscle. Biochim Biophys Acta 672:191–196, 1982.
47. Dillon PF, Murphy RA: Tonic force maintenance with reduced shortening velocity in arterial smooth muscle. Am J Physiol 242:C102–C108, 1982.
48. Driska SP, Aksoy MO, Murphy RA: Myosin light chain phosphorylation associated with contraction in arterial smooth muscle. Am J Physiol 240:C222–C233, 1981.
49. Aksoy MO, Murphy RA, Kamm KE: Role of Ca^{2+} and myosin light chain phosphorylation in regulation of smooth muscle. Am J Physiol 242:C109–C116, 1982.
50. Hartshorne DJ, Siemankowski RF: Regulation of smooth muscle actomyosin. Annu Rev Physiol 43:519–530, 1981.
51. Cremer-Lacuara MG, Lacuara JL, Fiol de Cuneo M, Ruiz RD: Substrate supply and function of isolated venous smooth muscle under anoxia and metabolic inhibition. Can J Physiol Pharmacol 58:723–730, 1980.
52. Paul RJ, Bauer M, Pease W: Vascular smooth muscle: aerobic glycolysis linked to sodium and potassium transport processes. Science 206:1414–1416, 1979.
53. Lang S, Blaustein MP: The role of the sodium pump in the control of vascular tone in the rat. Circ Res 46:463–470, 1980.
54. Lundholm L, Mohme-Lundholm E: Energetics of isometric and isotonic contraction in isolated vascular smooth muscle under anaerobic conditions. Acta Physiol Scand 64:275–282, 1965.
55. Seigman MJ, Butler TM, Mooers SU, Davies RE: Chemical energetics of force development, force maintenance, and relaxation in mammalian smooth muscle. J Gen Physiol 76:609–629, 1980.
56. Awan MZ, Goldspink G: Energetics of the development and maintenance of isometric tension by mammalian fast and slow skeletal muscles. J Mechanochem Cell Motil 1:97–108, 1972.
57. Homsher E, Rall JA, Wallner A, Ricchiuti NV: Energy liberation and chemical change in frog skeletal muscle during single isometric tetanic contractions. J Gen Physiol 65:1–22, 1975.

39. CONTROL OF THE CORONARY CIRCULATION

Harvey V. Sparks, Jr.,
Roger D. Wangler, and
Donald F. DeWitt

Introduction

Normal function of the heart depends on an adequate coronary blood flow. Myocardial metabolism and coronary flow are mutually interactive so that any increase in the metabolism of the normal heart is matched by an increase in coronary blood flow, and any significant restriction of flow in pathophysiologic states results in the reduction of myocardial metabolism and cardiac performance. In this chapter we describe the determinants of coronary blood flow; these include physical factors, myocardial metabolism, humoral influences, and neural control. In addition, we discuss certain pathophysiologic conditions, such as vascular responses to cardiac hypertrophy and myocardial ischemia, and the significance of coronary collateral vessels.

Physical Factors

The aortic pressure is the inlet pressure for the coronary circulation. Because extravascular compression limits myocardial blood flow during systole (see below), diastolic aortic pressure is more important than systolic pressure in determining myocardial perfusion [1–6]. This means that in pathophysiologic states in which diastolic pressure is lowered (i.e., aortic insufficiency or arteriovenous fistula) the adequacy of myocardial perfusion is jeopardized [7, 8].

N. Sperelakis (ed.), PHYSIOLOGY AND PATHOPHYSIOLOGY OF THE HEART.

Martinus Nijhoff Publishing, Boston/The Hague/
Dordrecht/Lancaster.

In the simplest case, coronary blood flow would be calculated by the difference between aortic and coronary sinus pressure divided by the vascular resistance to flow. However, experimental evidence indicates that this is not true. Figure 39–1 shows data taken from a resting, unanesthetized dog [9]. Circumflex coronary blood flow, as well as aortic and circumflex coronary pressure, were measured during an unusually long diastolic interval. At the end of that interval, circumflex flow reached zero. Furthermore, the aortic and circumflex pressures were both well above zero at that point. In the lower panel, individual pressure–flow points have been plotted showing that the intercept at which zero flow occurred is approximately 45 mmHg. The right-hand lower panel shows two possible interpretations of these data. In one case, resistance is calculated as inlet pressure, P_C, divided by circumflex flow. Note that as flow goes to zero, 2½ s after the dicrotic notch, resistance approaches an infinitely high value. Another possible interpretation of these data is shown by plotting inlet pressure, P_C, minus the pressure at which flow reached zero, i.e., 45 mmHg. In this case, the calculated resistance is constant throughout the diastolic interval. The first calculation assumes that the downstream or outlet pressure of the coronary circulation is right atrial pressure, that is, zero. The second calculation assumes that the pressure gradient for coronary flow is coronary artery pressure minus a much higher pressure, which is located somewhere within the myocardium. Most investigators interpret

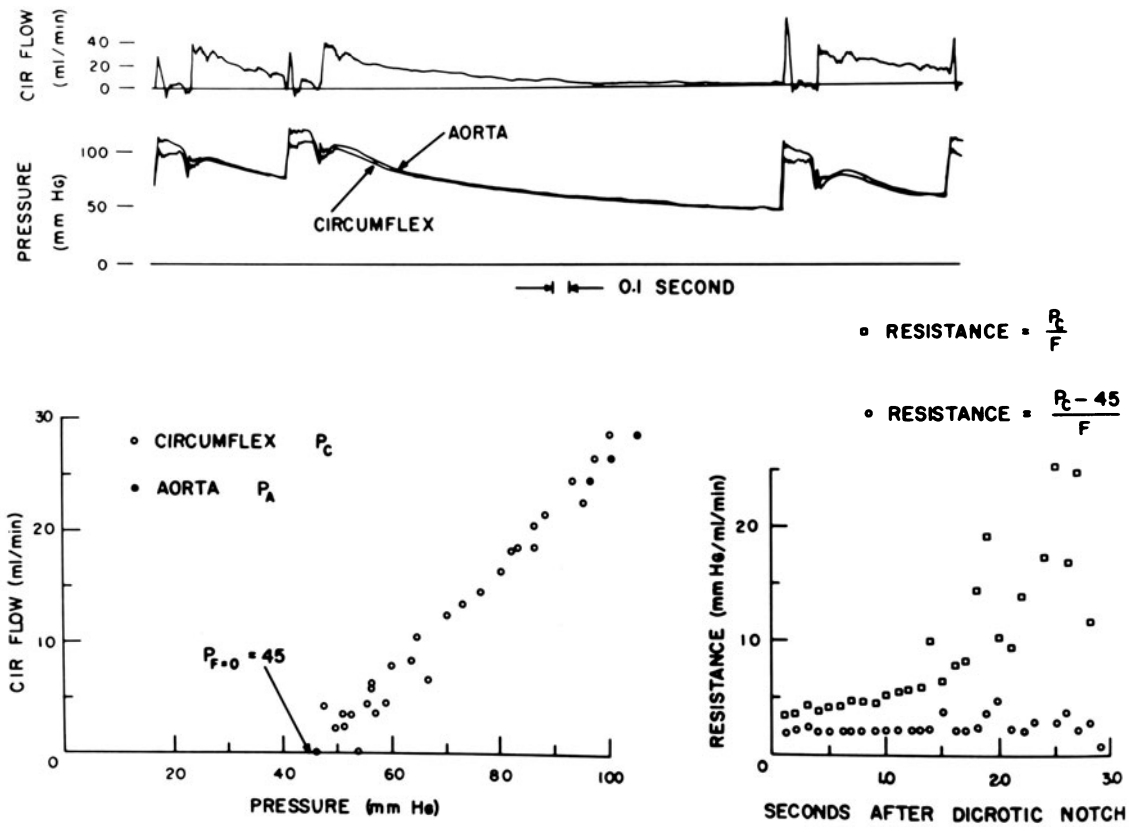

FIGURE 39–1. *(Top)* Circumflex coronary blood flow during a long diastolic interval. Circumflex and aortic pressure are also shown. (Lower left) pressure–flow relationship for this interval. (Lower right) Change in resistance calculated as indicated. Reproduced by permission from Bellamy [9].

this type of data as evidence that the outlet pressure for coronary circulation is well above coronary sinus or right atrial pressure [1, 9–11]. Its precise value depends on experimental circumstances, and it should be emphasized that the value of 45 mmHg, found in figure 39–1, would be at the high end of the range of values which have been found [12–16].

The current explanation for the high outlet pressure is that intramyocardial pressure is high enough to physically impinge on a portion of the vasculature so that intravascular pressure upstream to this point must exceed intramyocardial pressure in order for flow to pass through [1, 10, 11, 17, 18]. This results in a pressure gradient for flow which is equal to the inlet, or arterial, pressure minus the tissue pressure. In the case of the coronary circulation, this would mean that flow is not sensitive to right atrial or coronary sinus pressure, but instead to the pressure causing constriction of the microcirculation (the zero flow intercept as is shown in fig. 39–1). Pressure-flow plots have been obtained for a variety of experimental circumstances. In general, we can say that vasodilators cause the expected decrease in resistance, and a shift of the pressure intercept to the left, that is, a decrease in outlet pressure [9, 12, 19, 20]. Thus, the increased flow is caused both by decreased vascular resistance and an increased pressure gradient. Increased preload causes an increase in the zero pressure intercept [15]; that is, it acts to restrict flow by raising outlet pressure, thereby decreasing the pressure gradient for flow. The most extreme example of a rise in intramyocardial pres-

sure occurs during systole [12, 16, 17, 19–21]; the compressive forces on vessels within the subendocardium are so great that the pressure gradient for flow becomes very small and flow almost ceases. Flow continues at a somewhat reduced rate in the subepicardium where compressive forces are smaller [22–24]. Systolic attenuation of coronary flow is exaggerated by any event which raises intraventricular pressure, for example, elevated preload [15]. An increase in cardiac contractility has the same effect [25–30]. Increased heart rate limits coronary blood flow because the proportion of the cardiac cycle spent in systole increases, thereby limiting the time available for diastolic flow [27, 31–33]. Another factor which may contribute to the limitation of coronary flow during systole is the tendency of the contracting myocardium to distort microvessels. These sheer or traction forces may result in kinking of blood vessels and hinderance of flow. This is probably a relatively minor phenomenon in the coronary circulation [29, 34–36].

Changes in hematocrit influence coronary blood flow. In general, as hematocrit increases, viscosity increases, and so resistance to flow is elevated. The tendency toward a lower flow is offset by the greater oxygen-carrying capacity of the red-cell-enriched blood [37–40]. A limit on this process is reached when hematocrit exceeds 0.65, at which time the increase in viscosity is greater than the increase in oxygen-carrying capacity. At the other extreme, a reduction in hematocrit, as is found in hemorrhage, limits oxygen delivery when oxygen-carrying capacity is reduced proportionately more than viscosity [38, 40, 41].

Metabolic Control of Coronary Blood Flow

Myocardial metabolism normally exerts the single most important influence on coronary vascular resistance. There is a positive monotonic relationship between the extent of coronary vasodilation and myocardial oxygen consumption [42]. This means that oxygen delivery to the myocardium is closely matched to oxygen use. Despite the general importance of this relationship, significant alterations in coronary blood flow are possible at a given myocardial oxygen consumption. Although metabolism exerts a dominant influence on myocardial perfusion, changes in blood gases, neurogenic control mechanisms, and humoral mechanisms can exert a modulating effect on this relationship [2].

There are three commonly observed manifestations of metabolic control of coronary blood flow. The first is the reactive hyperemia which results from a brief period of occlusion of a coronary artery. The second is autoregulation of coronary blood flow; the tendency of blood flow to remain constant despite altered perfusion pressure. The third is functional hyperemia, or the increase in coronary blood flow associated with increased myocardial metabolism. Although earlier investigators often made the implicit assumption that the mechanisms responsible for all three of these phenomena were the same, it is now apparent that different mechanisms are involved. Therefore, we will consider these phenomena separately and evaluate the relative importance of each of the postulated mechanisms.

REACTIVE HYPEREMIA

When a major coronary vessel is occluded for a brief period of time, its release is followed by a dramatic increase in blood flow. The peak increase occurs within a few seconds after the release of the occlusion. The amplitude of this peak depends on the duration of the occlusion, up to approximately 15 s. Longer occlusions cause no further increase in the peak response [43–45]. The duration of the hyperemic response increases with the length of occlusion. The total excess flow which occurs during reactive hyperemia is greater than the flow "debt" incurred during the period of occlusion. Reactive hyperemia occurs in denervated and in isolated hearts; thus it is generally agreed that the mechanisms responsible must reside within the heart itself. These mechanisms can be divided into two general categories, myogenic and metabolic. The myogenic hypothesis states that resistance vessels distal to an occlusion dilate in response to the reduction in wall stress [46]. The metabolic hypothesis states that a reduction in blood flow resulting from occlusion of a major vessel causes release of vasodilator

substances either from myocardial cells or from the vessel wall itself [2].

The problem is the identification of the portion of reactive hyperemia caused by a myogenic response as opposed to the release of various vasodilator metabolites. A number of ingenious experiments have been performed in an effort to dissect these two phenomena. Eikens and Wilcken [47, 48] demonstrated that extremely short periods of occlusion (< 1 s) resulted in reactive hyperemia. They stated that the metabolic insult caused by such short periods of occlusion would be unlikely to result in release of metabolic vasodilators and concluded that their experiments supported the myogenic hypothesis. Later studies by Greenfield's [49] group showed that the magnitude of reactive hyperemia depended on the placement of a brief occlusion within the cardiac cycle. They found that diastolic coronary artery occlusions of duration greater than 100 ms resulted in reactive hyperemia. The magnitude of the hyperemia was dependent upon the duration of the occlusion, and the onset of the response was delayed until the first postocclusion systole. These investigators took this as evidence that a metabolic phenomenon may be responsible for the vasodilation because it seemed to be dependent on the increased metabolism which occurs during systole. In conclusion, the available data do not allow us to state with any degree of certainty what fraction of reactive hyperemia, following a very brief occlusion, is the result of a myogenic mechanism. In the absence of any specific blocker of a myogenic response, it would appear to be impossible to fully dissect these two phenomena.

Occlusions of longer duration appear to have a metabolic component. The evidence for this is that longer occlusions result in a reactive hyperemia of greater duration [43–45] and the release of several vasodilator metabolites [2]. Once the occlusion is released, the vasodilator substances cause an increased blood flow until they are metabolized, taken back up into cells, or washed out. Vessel wall P_{O_2} represents a variant of this hypothesis in which oxygen, a constrictor, is removed, resulting in vasodilation. There are several tests of the role of a particular vasodilator substance. If the vasodilator has a causal role, it should be present in the vicinity of the vascular smooth muscle in a concentration capable of resulting in vasodilation. Furthermore, agents capable of blocking the vasodilator's action should reduce reactive hyperemia and agents capable of altering the vasodilator's concentration around the vascular smooth muscle should cause an appropriate change in the hyperemic response.

Potassium is released into the coronary venous effluent following a brief occlusion [50, 51]. Furthermore, the time course of the return of potassium release to control levels is similar to the return of vascular resistance. This has led to the suggestion that potassium is responsible for at least a portion of reactive hyperemia. There are two arguments against this conclusion. First, Bunger and co-workers [52], using the crystalloid-perfused guinea pig heart, were unable to block reactive hyperemia with ouabain, which blocked the vasodilator response to potassium. Second, Sparks and co-workers [51] calculated the increase in interstitial potassium concentration resulting from a 15-s occlusion and concluded that the increase was not sufficient to cause more than a very small portion of the vasodilator response observed. Thus, it appears that potassium is released, but plays a minor role in causing reactive hyperemia.

Occlusion of a coronary artery results in a fall of tissue and microvascular wall P_{O_2} [53, 54]. The question is whether P_{O_2} falls far enough to cause relaxation of vascular smooth muscle. The results of studies of vascular smooth muscle sensitivity to changes in P_{O_2} are divided. Duling's group [55, 56] suggests that the vascular wall is not particularly sensitive to ambient P_{O_2}. However, other studies [57, 58] indicate that a wide range of vascular wall P_{O_2}'s may be able to influence vascular smooth muscle tone. One mechanism by which changes in vascular wall P_{O_2} may exert an influence is the release of prostaglandins [59]. Even if P_{O_2} falls to a level which results in dilation during occlusion, it is unlikely to be responsible for the dilation following the occlusion. Once flow is restored, effluent P_{O_2} quickly rises to a value far higher than control [60]. This suggests that microvascular wall P_{O_2} is also elevated by the increased flow delivery

of oxygen. Once microvascular wall P_{O_2} is elevated there would no longer be a stimulus for the continued vasodilation. The validity of this argument cannot be evaluated until more information is available on the mechanism by which altered vessel wall P_{O_2} influences vascular smooth muscle tone.

As mentioned above, vessel wall hypoxia results in release of prostaglandins. A number of studies have demonstrated that myocardial ischemia also results in release of prostaglandins into the venous effluent [61, 62]. This suggests a causal role for prostaglandins in reactive hyperemia. However, the use of compounds such as indomethacin, which decrease the production of prostaglandins via the cyclooxygenase pathway, has not yielded uniform results. Alexander and co-workers [61] employed indomethacin and observed a reduction in hyperemic flow following a 20-s occlusion. However, these results could not be confirmed by three other groups [63–65].

A number of investigators have demonstrated that coronary occlusion results in a rise in tissue adenosine content [66–69]. In addition, tissue adenosine content remains elevated after release of occlusion and returns to the control value with a time course very similar to that of the blood flow [69]. It is very likely that this increase in tissue content is at least partly the result of an increase in interstitial adenosine because adenosine can also be recovered from the venous effluent following coronary occlusion [66, 68]. Most studies show that administration of theophylline or aminophylline, adenosine receptor antagonists, results in a reduction in reactive hyperemia by approximately 30% [65, 70, 71, but see 72, 73]. In addition, infusion of the catalytic subunit of adenosine deaminase causes a reduction in reactive hyperemia by about 30% [74]. Theophylline in combination with adenosine deaminase causes no further decrease in reactive hyperemia. This result suggests that other factors are responsible for the remaining two-thirds of the reactive hyperemic response [74].

In summary, the available evidence strongly suggests that adenosine causes approximately one-third of the hyperemia resulting from a brief period of coronary occlusion. It also seems likely that the myogenic mechanism participates in the initiation of the hyperemic response. However, it appears that there are unidentified mechanisms which are equally important in causing reactive hyperemia. We think the available evidence rules out an important role for prostaglandins and potassium ion. Other substances which have been ruled out include calcium [2], magnesium [75], and osmolarity [50]. Substances which deserve further evaluation include vessel wall hypoxia, increased hydrogen ion concentration, and leukotrienes [76].

AUTOREGULATION

Autoregulation of blood flow is defined as the tendency of flow to remain constant despite alterations in perfusion pressure. When perfusion pressure is suddenly changed, flow tends to follow the change in perfusion pressure. Over a period of seconds, however, flow then returns toward the previous value. The range of perfusion pressure over which flow remains relatively constant is from 70 to 145 mmHg [77, 78].

When perfusion pressure drops below ~70 mmHg, flow begins to fall linearly until it stops at a perfusion pressure well above zero (see fig. 39–1). It is sometimes assumed that the descending limb of the autoregulation curve represents a region of perfusion pressures in which the coronary resistance vessels are maximally dilated. This is not true. Figure 39–2 shows an experiment in which adenosine was infused at each of several perfusion pressures and demonstrates that there is still residual vasodilator reserve despite the absence of autoregulation [79]. Studies with microspheres have demonstrated that both the subepicardium and subendocardium exhibit autoregulation [80, 81]. The mechanism of autoregulation is unknown. There are three generic theories: myogenic, tissue pressure, and metabolic. As in the case of reactive hyperemia there is no direct evidence in favor of the myogenic mechanism. On the other hand, there are no experiments which rule it out. The tissue-pressure hypothesis states that as perfusion pressure is lowered extravascular compression decreases and resistance vessels dilate. Once again there is no direct evidence supporting this hypothesis. Many

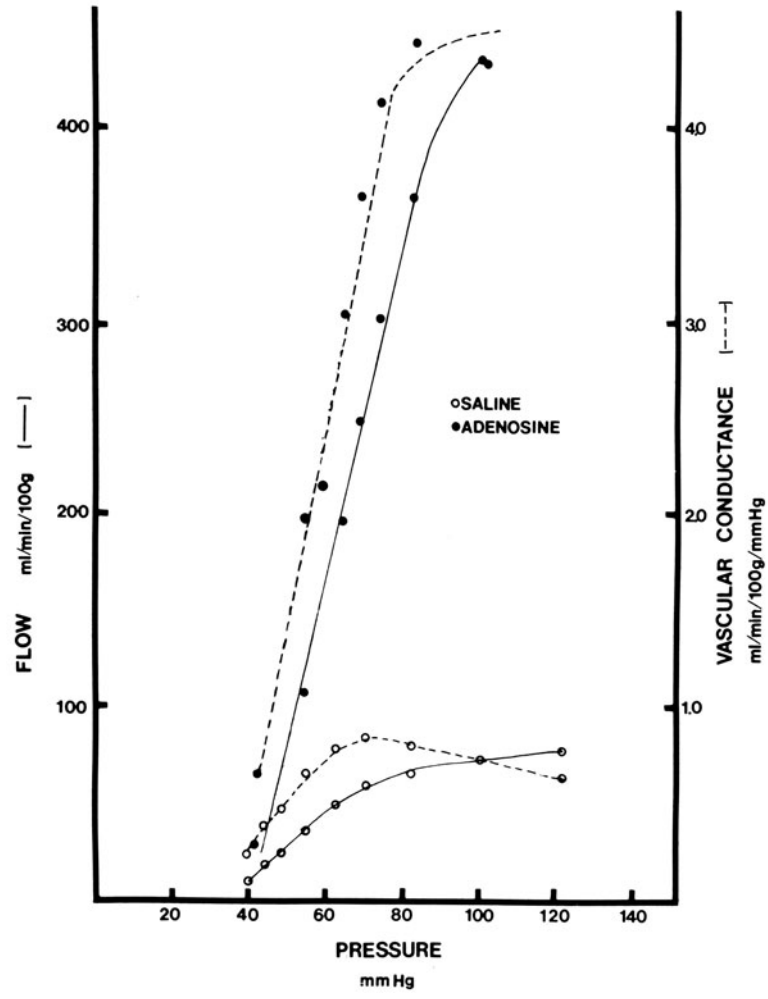

FIGURE 39–2. Mean left circumflex coronary blood flow of an anesthetized dog. Perfusion pressure was lowered with an inflatable cuff around the artery. Pressure was measured distal to the cuff. In the presence of saline, coronary blood flow did not decrease in proportion to the decrease in pressure between 120 and 60 mmHg because vascular conductance increased. Below 60 mmHg, flow and conductance decreased precipitously. At all perfusion pressures, adenosine infused directly into the artery caused an increase in flow and conductance. This shows that coronary vasodilator reserve was not exhausted at pressures associated with the precipitous fall in flow and conductance.

investigators have assumed that coronary autoregulation is the result of a metabolic mechanism. However, there are few studies which have tested the roles of specific vasodilator metabolites. Cyclooxygenase inhibitors do not affect autoregulation [82]. This would appear to rule out the participation of prostaglandins. In addition, Bunger and co-workers [52] found no evidence to support a role for potassium in coronary autoregulation. Reduced vessel wall P_{O_2} should accompany any fall in oxygen delivery resulting from reduced perfusion pressure [54]. However, there are no direct tests of the role of vessel wall P_{O_2} in autoregulation. Schrader and co-workers [68] showed that reduction of perfusion pressure from normal levels resulted in elevation of tissue and coronary effluent adenosine content, but elevation of perfusion pressure above normal produced no changes in tissue or effluent adenosine content. It is unlikely

that decreased adenosine release could be responsible for the vasoconstriction in response to increased perfusion pressure. This is because the available evidence indicates that adenosine release does not contribute a vasodilator influence under resting conditions [74].

FUNCTIONAL HYPEREMIA

Increased myocardial metabolism is normally matched by an increase in coronary blood flow and oxygen delivery. The relationship can be modulated by a number of stimuli, for example, sympathetic vasoconstrictor neural activity [83], angiotensin [84, 85], antidiuretic hormone [86], alterations in P_{CO_2} [89–90], and vasoactive drugs [91]. Any modulation in coronary blood flow at a given metabolic rate leads to a change in oxygen extraction. For example, adrenergic vasoconstriction causes lower oxygen delivery and higher extraction of oxygen for a given myocardial oxygen consumption [83].

The coupling of coronary vascular conductance to metabolism is easily observable in isolated hearts and so is not causally dependent upon nerves or hormones. Most investigators believe that increased metabolism is associated with release of a vasodilator substance from myocardial cells. It is postulated that this vasodilator elicits relaxation of coronary smooth muscle and thus increases flow to match the increase in metabolism. However, there is strong evidence favoring the participation of at least two vasodilator mechanisms, and it is probable that there are also other mechanisms which remain to be discovered. Several vasodilator systems which may be important in other contexts do not seem to be responsible for functional hyperemia. We doubt that vessel wall P_{O_2} falls during functional hyperemia. This is because coronary sinus P_{O_2} does not ordinarily change and because oxygen delivery to the resistance vessels is dramatically increased by the elevated blood flow [54]. Case and associates [87–89] have revived the hypothesis that an increase in vessel wall P_{CO_2} may be responsible for functional hyperemia. This idea is attractive because an increase in production of CO_2 should accompany an increase in oxygen metabolism. However, very large changes in arterial P_{CO_2} are necessary to elicit relatively modest changes in coronary vascular conductance. Given the very small changes which occur in coronary sinus P_{CO_2}, it is unlikely that there is a sufficient hypercapnic stimulus to result in the observed functional hyperemia [90]. Changes in arterial P_{CO_2} may have indirect effects on the relationship between myocardial blood flow and oxygen consumption. For example, it appears that elevated hydrogen ion concentration causes coronary vascular smooth muscle relaxation [92] and enhances its sensitivity to adenosine [92, 93]. Also, elevation in P_{CO_2} or hydrogen ion concentration results in unloading of oxygen from hemoglobin.

Functional hyperemia occurs in the presence of indomethacin and this argues against a causal role for prostaglandin release [42, 90]. In addition, the lack of changes in the hydrogen ion concentration [94, 95] and osmolarity [50] of the coronary sinus effluent would seem to rule out these two potential vasodilator influences.

Potassium is elevated transiently when myocardial metabolism increases. The increase is sufficient to cause approximately one-third of the initial increase in vascular conductance associated with increased heart rate [51]. If oxygenation of the myocardium is normal, however, potassium release quickly declines [96, 97]. Thus, although potassium is a coronary vasodilator, it cannot be responsible for steady-state increases in coronary blood flow associated with increased metabolism.

Adenosine is the most venerable candidate for the cause of functional hyperemia in the heart. The adenosine hypothesis [2] states that increased metabolism is associated with an increase in adenosine release from myocardial cells. This release raises the interstitial concentration of adenosine which in turn results in vasodilation of resistance vessels. Until recently it seemed likely that adenosine is formed as a result of the action of ecto 5′-nucleotidase on AMP. It was proposed that ecto 5′-nucleotidase with its active site facing the outer surface of the cell membrane somehow came in contact with intracellular AMP and this resulted in formation of extracellular adenosine. Recent studies have raised the possibility that adenosine formation occurs within the cell. The evidence

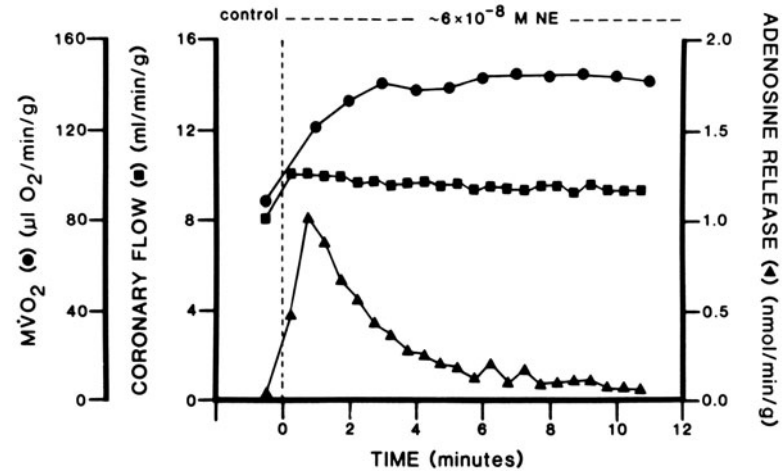

FIGURE 39–3. Myocardial oxygen consumption (MVO_2), coronary flow, and adenosine release in a representative experiment on an isolated Langendorf-perfused guinea pig heart. Norepinephrine ($\sim 6 \times 10^{-8}$ *M*) caused a steady increase in MVO_2 and flow, but adenosine release rose to a peak at 1 min and then fell to the control value over the next few minutes. This suggests that adenosine is not responsible for the *sustained* increase in flow.

in favor of this is: (a) AOPCP, a blocker of ecto 5′-nucleotidase does not diminish the release of adenosine in response to hypoxia [98, 99]. (b) Inhibitors of carrier-mediated adenosine transport reduce adenosine release in response to hypoxia [99, 100]. (c) Stimulation of the intracellular pathway which produces S-adenosylhomocysteine from adenosine lowers release of adenosine during a hypoxic stimulus [101]. (d) Adenosine deaminase fails to destroy all of the adenosine found in isolated cell suspensions, suggesting that a portion must be sequestered inside the cells away from the enzyme [102]. (e) Tissue content of adenosine is so high that, if all of the adenosine present in tissue were distributed in the interstitium, it would result in close to maximum coronary vasodilation [103]. Taken together, these arguments strongly suggest that, at least under conditions of hypoxia, adenosine is formed intracellularly and released into the interstitium. There are no comparable experiments which test whether this is also true for physiologic stimuli which result in increased myocardial metabolism.

There are three lines of evidence which lend support to the idea that adenosine is responsible for functional hyperemia. First, adenosine is a potent vasodilator. Second, metabolic machinery capable of rapid formation and destruction of adenosine is present in myocardium. Third, a number of studies have demonstrated that most stimuli which result in increased myocardial metabolism also result in increased adenosine release into venous effluent and/or pericardial fluid [91, 104–106]. In addition, most of these stimuli cause an increase in tissue content of adenosine [104, 107, 108]. However, there are other lines of evidence which confuse the issue. First, aminophylline, a methylxanthine which antagonizes the vasodilator action of adenosine, does not reduce functional hyperemia [109]. Second, it is possible to raise myocardial metabolism and coronary blood flow without increasing adenosine release when cardiac pacing is the stimulus [110]. Third, adenosine release in response to the administration of norepinephrine is phasic [111]. When norepinephrine is administered to an isolated guinea pig heart (fig. 39–3), adenosine release peaks within the first minute and then rapidly falls to a much lower level while myocardial oxygen consumption and coronary conductance remain elevated and constant. Although these results appear to contradict the adenosine hypothesis there are potential expla-

nations for each one. Another methylxanthine, theophylline, has been demonstrated to cause increased adenosine release [112]. Thus, it may be that administration of methylxanthines results in increased interstitial adenosine which in turn overcomes the adenosine blockade. It is also possible that blockers administered interarterially do not reach the extravascular receptor sites responsible for mediating adenosine's vasodilator effect. The lack of increased adenosine release associated with pacing might be consistent with the adenosine hypothesis if release of adenosine is not an accurate index of interstitial adenosine concentration. Because we know so little about the nature of the capillary barrier to adenosine transport, it is difficult to evaluate this possibility. Finally, the phasic release of adenosine observed in the guinea pig heart could be the result of multiple cellular sources of adenosine. For example, the large initial release of adenosine could be from endothelial cells which are known to contain a large amount of adenosine [113]. It could be that only the steady-state adenosine release observed at later time points actually reflects an increase in interstitial adenosine concentration. Again, lack of knowledge of the biology of in vivo endothelial cells prevents us from evaluating this possibility.

In summary, adenosine remains the strongest candidate for the cause of steady-state functional hyperemia.

Neural Control of Coronary Blood Flow

Both divisions of the autonomic nervous system innervate the coronary vessels [114–118]. Furthermore, coronary vascular smooth muscle cells have both alpha- and beta-adrenergic receptors [116, 117], as well as muscarinic cholinergic receptors [2]. Thus, the basic innervation of the coronary system allows for the full range of potential autonomic influence.

SYMPATHETIC CONTROL

Stimulation of sympathetic efferents to the heart causes transient coronary vasoconstriction followed by a steady-state vasodilation [121–124]. The steady-state increase in flow is proportional to the increase in myocardial metabolism. Furthermore, this increase in flow can be prevented by agents which selectively block $beta_1$ receptors which are thought to reside primarily on myocardial cells [121, 122, 124, 125]. With sympathetic activation in the presence of an alpha blocker, the initial vasoconstriction is abolished and the increase in steady-state flow is higher for any given level of myocardial metabolism [83, 126–128]. Sympathetic activation in the presence of beta blockade results in coronary vasoconstriction which can be blocked by various alpha-receptor blockers [121, 122, 125]. It appears that sympathetic stimulation results in a direct alpha-receptor-mediated constrictor effect which competes with an indirect, metabolic vasodilator influence resulting from stimulation of myocardial $beta_1$ receptors. It is also possible that beta receptors of coronary smooth muscle are activated and that this contributes a vasodilator influence. The available evidence is not adequate to allow any conclusion concerning this possibility. However, the data do suggest that the effect would be minor when compared to the influences of direct alpha-mediated constriction and indirect $beta_1$-mediated metabolic vasodilation [125].

Sympathetic nerve stimulation reduces coronary sinus oxygen content to approximately half the value obtained when coronary alpha receptors are blocked [83, 129, 130]. Although this represents a rather dramatic vasoconstrictor influence in the face of increased metabolic need, there is no evidence that this results in impaired function of normal myocardium. Buffington and Feigl [131] have investigated the possibility that sympathetic alpha constriction could have a deleterious effect in the presence of a critical coronary stenosis. Although the results of this study were negative, this idea should be subjected to further investigation in other preparations.

A number of studies have suggested that alpha receptors may be responsible for spasm of large coronary arteries [132–135]. This coincides with the observation that there is a relatively higher population of alpha receptors on large coronary arteries than on small coronary arteries [136–139].

PARASYMPATHETIC CONTROL

Stimulation of the vagus nerve, in paced hearts, causes a reduction in end-diastolic resistance. This reduction of resistance is blocked by atropine [71, 140, 141] and has led to the conclusion that parasympathetic cholinergic nerves innervate coronary resistance vessels. At present there is no known physiologic role for these nerves. A careful study by Feigl [142] has failed to demonstrate sympathetic cholinergic vasodilation in the heart. This result was substantiated in a later study by Brown [143].

REFLEX CONTROL OF THE CORONARY CIRCULATION

Bilateral carotid artery occlusion results in coronary blood flow changes which are similar to those observed during stellate ganglion stimulation; i.e., there is an increase in coronary blood flow which can be enhanced by alpha blockade. Bilateral carotid artery hypotension, in the presence of propranolol and vagotomy, results in increased coronary resistance [130, 144]. This increase in resistance can be prevented by sympathectomy or by an alpha blocker. If carotid sinus nerves are stimulated, coronary vascular resistance is reduced. This reduction in resistance can be prevented by pretreatment with an alpha blocker, which removes resting alpha-constrictor tone [145–147]. Thus, it appears that there is alpha-adrenergic vasoconstrictor coronary tone which is enhanced by carotid occlusion and abolished by increased baroreceptor nerve firing. When carotid body chemoreceptors are stimulated by nicotine, parasympathetic cholinergic vasodilation occurs in the coronary bed [146, 148, 149]. It is unclear whether physiologic stimulation of the carotid bodies by altered blood gases results in the same phenomenon [150].

Exercise is accompanied by dramatic increases in coronary blood flow. However, blockade of coronary alpha receptors demonstrates that, even under these conditions, flow is somewhat limited by a competing sympathetic alpha-receptor activation [127, 128]. This constrictor influence does not cause any decrement in ventricular performance of the normal myocardium [127, 128].

Cardiac Hypertrophy

Cardiac hypertrophy is associated with clinical signs of impaired myocardial perfusion, for example, angina pectoris [151–153] and electrocardiographic abnormalities [152–154]. Histologic studies of postmortem hearts demonstrating ventricular hypertrophy give evidence of decreased vascular density [155–158], increased collateralization [159], and subendocardial fibrosis [160, 161]. However, most studies of cardiac hypertrophy have shown that myocardial perfusion and oxygen consumption (per unit cardiac mass) are normal under resting conditions [162–170]. There is a notable exception to these observations; right ventricular hypertrophy has been consistently associated with an increased perfusion (per unit cardiac mass) of the resting right ventricle [171–174]. An increase in right ventricular wall stress may account for the augmented perfusion in that ventricle [174]. Most studies indicate that the transmural distribution of blood flow is also normal in hypertrophied hearts [163–167]. Exceptions have been noted in cases of severe hypertrophy [175, 176], or situations requiring utilization of vasodilator reserve, for example, coronary artery stenosis [177] or increased metabolic demand [163, 165, 167, 175]. In these cases a selective deficit in subendocardial blood flow is observed. Infusions of various coronary vasodilators indicate that global minimum coronary vascular resistance is unchanged in hypertrophied hearts [162, 167, 169, 171]. When resistance is normalized to the mass of perfused myocardium, however, there is an increase in minimum vascular resistance [163, 164, 167, 169, 171]. Taken together, these data suggest that there is a decrease in the available total cross-sectional area of resistance vessels. This decrement could result from a failure of resistance vessels to proliferate in proportion to the increased myocardial mass [173, 178–180] and/or an increase in arteriolar wall–lumen ratio subsequent to medial hypertrophy induced by arterial hypertension [181–184]. In either case, one would expect the functional results which have been observed; resting flow appears to be maintained by encroachment on the coronary vasodilator reserve, whereas maximum vasodilator capacity is reduced.

Several physiologic interventions give rise to perfusion abnormalities in hypertrophied hearts. For example, electrical pacing results in a maldistribution of blood flow across the wall of the heart with a relative decrease in subendocardial flow [165, 167]. As mentioned above, coronary occlusion results in severe subendocardial ischemia [177]. Furthermore, transient coronary occlusion is followed by an attenuated reactive hyperemic response [162, 163, 171, 185]. Several investigators have noted a significant redistribution of flow away from the subendocardium during intense exercise in experimental animals with ventricular hypertrophy [163, 175].

There are many crucial aspects of the coronary circulation in hypertrophied hearts which remain to be elucidated. First, almost nothing is known about the influence of the age of onset of hypertrophy on the maintenance of myocardial perfusion. Second, very few studies provide information about the relationship between the severity of ventricular hypertrophy and the degree of impairment of the coronary circulation. Third, only one study provides information on the effects of long-term, stable hypertrophy [169]. Fourth, further studies are needed in order to clarify the role of the stimulus for hypertrophy in the interaction between cardiac hypertrophy and the coronary bed. Finally, in view of the prevalence of coronary artery disease and arterial hypertension in man, important information may be gained from studies of the interactions among coronary stenosis, arterial hypertension, and cardiac hypertrophy.

Ischemia

RESPONSES TO ACUTE ISCHEMIA

When stenosis of a major coronary artery occurs, two compensatory events limit the potential fall in myocardial blood flow beyond the stenosis. First, vessels distal to the stenosis dilate [44] in response to the fall in transmural pressure and increased metabolic vasodilator stimulation (see discussion of autoregulation above). Second, flow from other major arteries reaches the region beyond the stenosis via preexisting collateral vessels linking arteries and arterioles of the two regions. The contribution of collateral flow to the potentially ischemic region depends on the species and on other unknown factors [186–188]. Some species such as dog have a higher number of preexisting collaterals than other species, such as pig and man [186, 187]. However, there appears to be a considerable variation in the number of collateral vessels within a given species and the reason for this variation is not known [188, 189].

When stenosis of a coronary artery reaches a critical level, the combination of autoregulatory dilation of resistance vessels and collateral flow is no longer sufficient to provide a normal resting flow. At this point, flow to the subendocardium begins to fall [190, 191]. The greater vulnerability of the subendocardium appears to be related to the higher intramyocardial forces which act on vessels supplying this region (see the above discussion of determinants of transmural blood flow). The subendocardium uses more of its vasodilator capacity under normal circumstances. For this reason, less vasodilator reserve remains to compensate for a fall in perfusion pressure caused by the stenosis. A reduction in ventricular contractile force occurs very soon after coronary blood flow is decreased [192–195]. Ultimately, ventricular contraction in the ischemic region becomes so weak that paradoxical bulging occurs during ventricular systole because of the increase in intracavitary pressure [192, 195].

PROLONGED ISCHEMIA

If a critical stenosis is maintained for several hours, blood flow in the ischemic region falls even if pressure beyond the stenosis is held constant [196–200]. Since it is unikely that major changes in collateral flow will occur if poststenotic pressure is constant, this finding suggests that distal vessels within the ischemic region progressively constrict. Guyton and coworkers [197] suggested that local ischemia can initiate a positive feedback cycle in which ischemia begets vasoconstriction and further ischemia (fig. 39–4) [198]. A portion of this progressive "ischemic vasoconstriction" may be the result of tissue swelling impinging on resistance vessels. This possibility is supported

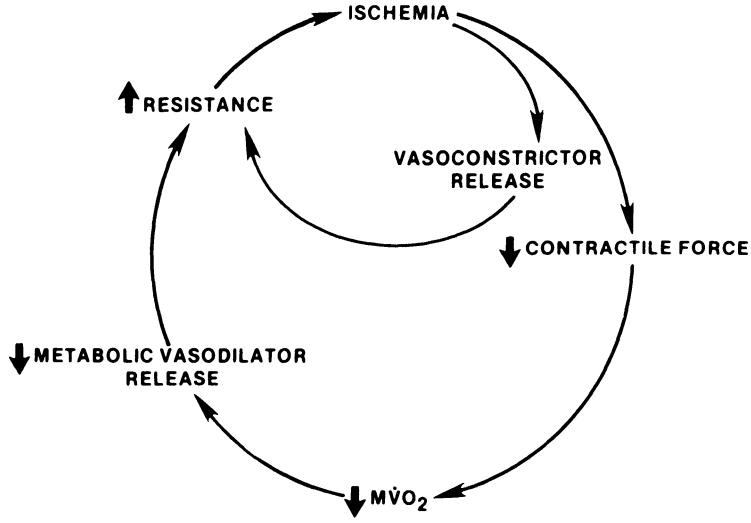

FIGURE 39–4. Proposed positive feedback relationship initiated by myocardial ischemia. Both vasoconstrictor release and decreased myocardial metabolism cause vasoconstriction and a further drop in blood flow. This leads to the observed increase in vasodilator reserve with time. Reproduced by permission from Sparks and Gorman [198].

by the observation that a mannitol infusion causes increased blood flow within the ischemic region [196, 201]. However, mannitol not only reduces cell swelling, but also causes vascular smooth muscle relaxation and so could be exerting part of its effect by dilating resistance vessels [202]. The possibility that active vasoconstriction occurs within the ischemic region was evaluated by infusing adenosine or norepinephrine after progressive vasoconstriction was allowed to occur for 3 h [199]. Both of these agents cause an increase in blood flow within the ischemic region, suggesting that active vasoconstriction had occurred. The increase in vascular tone does not appear to be the result of release of a vasoconstrictor metabolite of the cyclooxygenase pathway, because indomethacin causes vasoconstriction, not vasodilation after 3 h of ischemia [199]. Alpha-receptor blockade with phenoxybenzamine results in dilation and prevents ischemic vasoconstriction [199]. This does not appear to be the result of removal of alpha-receptor-mediated vasoconstriction because the vasodilation is blocked by the beta-receptor blocker, propranalol. Instead, it appears that phenoxybenzamine increases norepinephrine release by blockade of prejunctional alpha receptors and this in turn causes the observed vasodilation. One possibility is that progressive vasoconstriction is at least in part the result of reduced myocardial metabolism and reduced metabolic vasodilator release over the 3-h period. This idea is supported by the observation that, in an isolated guinea pig heart preparation, adenosine release is initially elevated when coronary flow is reduced, but then falls significantly over the next hour [203]. The above observations strongly suggest that it is not safe to assume that resistance vessels beyond a critical stenosis are maximally dilated. Instead, it appears that these resistance vessels are still responsive to local control mechanisms. In addition, these vessels appear to respond to certain pharmacologic interventions, including nitroglycerin [204].

If a coronary artery is occluded for 2 h and is then reopened (reflow preparation), there is an initial hyperemia. However, the hyperemic peak flow is not as great as it is following a 10-min occlusion [205]. This suggests that minimum vascular resistance has increased during the period of occlusion. In addition, resting flow and peak reactive hyperemic flow continue to decline over the next 2–4 h [206]. This in-

crease in vascular resistance occurs primarily in the subendocardium [205, 207]. Histologic examination reveals extensive tissue swelling [208], hemorrhage, and microthrombi [209, 210]. In addition, treatment with mannitol before release of 1- or 2-h occlusion results in higher initial reflow, less structural damage, and reduced areas of necrosis [205, 208, 211]. However, the beneficial hemodynamic effects of mannitol disapear after 4 h of reperfusion [208]. In summary, studies of prolonged stenosis and reflow suggest that a positive feedback loop develops in ischemic myocardium, in which reduced flow causes vasoconstriction and a further reduction in flow (fig. 39–4).

COLLATERAL BLOOD FLOW

As mentioned above, increased collateral flow provides a measure of immediate compensation when stenosis occurs. Furthermore, development of new collateral vessels can begin within 1–6 h, depending on the degree of occlusion [186, 212–214]. As a consequence, the blood pressure and flow distal to the occlusion begin to increase and continue to do so until basal needs of the tissue subserved are met. If an occlusion is released after full collateral development, the collateral vessels become nonfunctional within 24 h [215]. If the same coronary artery is reoccluded between three and 90 days, full collateral flow is reestablished within 1 h without myocardial damage.

It has been suggested that collateral vessel development occurs from preexisting microscopic vascular connections between major coronary arteries. Schaper and colleagues have provided support for this idea [186]. They propose that local release of vasodilators dilates the connecting microscopic collateral vessels and increases the pressure and wall stress on the thin wall vessels. This stress results in wall damage that induces cellular infiltration and breaks in the wall. Reparative processes then occur in which there is proliferation of endothelium and smooth muscle as well as progressive growth of the vessel. Thus there is a transition from the thin-walled microscopic collateral vessels to large, thick-walled, large-lumen vessels. The exact determinants of the development of these collateral vessels are not clear. The collateral development does not occur in response to exercise without preexisting ischemia [216–218], and is directed only toward ischemic areas [219]. Tissue hypoxia [220–222] and/or changes in transmural pressure may be involved [186]. At first, developing collateral vessels have no smooth muscle and behave passively. Later, with the development of smooth muscle, the vessels could be influenced by vasoactive drugs.

NITROGLYCERIN

The mechanism by which nitroglycerin relieves myocardial ischemia [223] is controversial and varies according to the experimental or clinical condition. Extrapolation from one situation to another may not be appropriate. The sites of action of nitroglycerin depend upon its concentration and the cause of the ischemia. Large coronary arteries, which are conduit vessels, are not influenced by adenosine [224, 225] or dipyridamole [226, 227]. They are affected by alpha- and beta-receptor stimulation [83, 136, 228–230] and are quite sensitive to low concentrations of nitroglycerin [224–229, 231]. The primary determinant of coronary resistance is arteriolar tone. The tone is affected by adenosine [224, 225], dipyridamole [226, 227], and beta-receptor stimulation [228, 230], but not by nitroglycerin in concentrations sufficient to dilate larger vessels [224–226, 228, 232, 233]. Arterioles dilate in response to much higher concentrations of nitroglycerin or to intracoronary injections of nitroglycerin.

Because of these relationships, therapeutic levels of nitroglycerin which dilate large coronary arteries produce no substantial increase in resting coronary flow. When arterioles are dilated by ischemia, the vasodilator reserve is reduced, and dilation of large arteries by nitroglycerin produces decreased vascular resistance and increased coronary blood flow [85, 204]. When larger arteries are narrowed by atherosclerotic lesions, a reduction in vascular tone in the large arteries by nitroglycerin can alleviate ischemia and angina [231, 234, 235]. In circumstances involving occlusion of a single large artery in which extensive collateral development supplies blood to distal areas, nitroglycerin increases flow to the ischemic area by di-

lating collaterals or the large vessels feeding them [236–239]. Finally, administration of nitroglycerin in high concentrations can result in "coronary steal" from the ischemic myocardium because dilation of vessels in the less ischemic epicardium, or in the relatively normal areas of neighboring myocardium, diverts blood flow away from the ischemic area [83, 232, 240].

Nitroglycerin can also produce beneficial effects on the heart by causing peripheral vasodilation and venodilation. As a result of venodilation there is a reduction in venous return and a decrease in left ventricular diastolic pressure [241], which is often elevated during ischemia [241, 242]. The peripheral vasodilation reduces preload and afterload [241, 243] and increases diastolic coronary flow. However, the reduction in arterial pressure elicits a reflex tachycardia which increases oxygen consumption unless inhibited by beta blockade or prevented by pacing [232, 244]. A reduction in cardiac work load decreases oxygen demand and extravascular compression, both of which increase the ratio of blood flow to oxygen use.

References

1. Hoffman JIE: The effect of intramyocardial forces on the distribution of intramyocardial blood flow. J Biomed Eng 1:33–40, 1979.
2. Berne RM, Rubio R: Coronary circulation. In: Berne RM, Sperelakis N, Geiger SR (eds) Handbook of physiology. Vol 1, sect 2: The cardiovascular system. Bethesda MD: American Physiological Society, 1979, pp 873–952.
3. Braunwald E, Ross J Jr, Sonnenblick EH: Myocardial hypoxia and ischemia. In: Mechanisms of contraction of the normal and failing heart. Boston: Little, Brown and Company, 1976, pp 357–397.
4. Bell JR, Fox AC: Pathogenesis of subendocardial ischemia. Am J Med Sci 268:2–13, 1974.
5. Moir TW: Subendocardial distribution of coronary blood flow and the effect of antianginal drugs. Circ Res 30:621–624, 1972.
6. Hoffman JIE, Buckberg GD: Transmural variations in myocardial perfusion. In: Yu PN, Goodwin JF (eds) Progress in cardiology, vol 5. Philadelphia: Lea and Febiger, 1976, pp 37–89.
7. Buckberg GD, Fixler DE, Archie JP, Hoffman JIE: Experimental subendocardial ischemia in dogs with normal coronary arteries. Circ Res 30:67–81, 1972.
8. Griggs DM Jr, Chen CC: Coronary hemodynamics and regional myocardial metabolism in experimental aortic insufficiency. J Clin Invest 53:1599–1606, 1974.
9. Bellamy RF: Diastolic coronary artery pressure flow relations in the dog. Circ Res 43:92–101, 1978.
10. Permutt S, Riley RL: Haemodynamics of collapsible vessels with tone: the vascular waterfall. J Appl Physiol 18:924–932, 1963.
11. Bellamy RF: Calculation of coronary vascular resistance. Cardiovasc Res 14:261–269, 1980.
12. Sherman IA, Grayson J, Bayliss CE: Critical closing and critical opening phenomena in the coronary. Am J Physiol 238:H533–558, 1980.
13. Grayson J, Parratt JR: A species comparison of the effects of changing perfusion pressure on blood flow and metabolic heat production in the myocardium. J Physiol (Lond) 187:465–488, 1966.
14. Archie JP, Brown R: Effect of preload on the transmural distribution of diastolic coronary blood flow. J Surg Res 16:215–223, 1974.
15. Ellis AK, Klocke FJ: Effects of preload on the transmural distribution of perfusion and pressure–flow relationships in the canine coronary vascular bed. Cir Res 46:68–77, 1979.
16. Panerai RB, Chamberlain JH, Sayers BM: Characterization of the extravascular component of coronary resistance by instantaneous pressure–flow relationships in the dog. Circ Res 45:378–390, 1979.
17. Downey JM, Kirk ES: Inhibition of coronary blood flow by a vascular waterfall mechanism. Circ Res 36:753–760, 1975.
18. Munch DF, Downey JM: Prediction of regional myocardial blood flow in dogs. Am J Physiol 239:H308–315, 1980.
19. Bellamy RF, Lowensohn HS: Effect of systole on coronary pressure–flow relations in the right ventricle of the dog. Am J Physiol 238:H481–486, 1980.
20. Bellamy RF, Lowensohn HS, Ehrlich W, Baer RW: Effect of coronary sinus occlusion on coronary pressure–flow relations. Am. J Physiol 239:H57–64. 1980.
21. Stein Pd, Marzilli M, Sabbah HN, Lee T: Systolic and diastolic pressure gradients within the left ventricular wall. Am J Physiol 238:H625–630, 1980.
22. Downey JM, Kirk ES: Distribution of coronary blood flow across the canine heart during systole. Circ Res 34:251–257, 1974.
23. Hess DS, Bache RJ: Transmural distribution of myocardial blood flow during systole in the awake dog. Circ Res 38:5–15, 1976.
24. Hess DS, Bache RJ: Transmural right ventricular myocardial blood flow during systole in the awake dog. Circ Res 45:88–94, 1979.
25. Marzilli M, Goldstein S, Sabbah NN, Lee T, Stein PD: Modulating effect of regional myocardial performance on local myocardial perfusion in the dog. Circ Res 45:634–641, 1979.
26. Raff WK, Kosche F, Lochner W: Coronary extravascular resistance and increase of maximal rate of intraventricular pressure rise by isoproterenol Pflugers Arch 325:323–333, 1971.
27. Raff WK, Kosche F, Lochner W: Extravascular cor-

onary resistance and its relation to the microcirculation. AM J Cardiol 29:598–603, 1972.
28. Raff WK, Kosche F, Goebel H, Lochner W: Coronary extravascular resistance at increasing left ventricular pressure. Pflugers Arch 333:352–361, 1972.
29. Snyder R, Downey JM, Kirk ES: The active and passive components of extravascular coronary resistance. Cardiovasc Res 9:1–6, 1975.
30. Trimble J, Downey J: Contribution of myocardial contractility to myocardial perfusion. Am J Physiol 236:H121–126, 1979.
31. Raff WK, Kosche F, Lochner W: Heart rate and coronary extravascular resistance. Pflugers Arch 323:241–249, 1971.
32. Bache RJ, Cobb FR: Effect of maximal coronary vasodilation on transmural myocardial perfusion during tachycardia in the awake dog. Circ Res 41:648–653, 1977.
33. Domenech RJ, Goich J: Effect of heart rate on regional coronary blood flow. Cardiovasc Res 10:224–231, 1976.
34. Downey JM, Downey HF, Kirk ES: Effect of myocardial strain on coronary blood flow. Circ Res 34:286–292, 1974.
35. Fenton TR, Cherry JM, Klassen GA: Transmural myocardial deformation in canine left ventricular wall. Am J Physiol 235:H523–530, 1978.
36. Feigl EO, Fry DL: Intramural myocardial shear during the cardiac cycle. Circ Res 14:536–540, 1964.
37. Surjadhana A, Rouleau J, Boerboom L, Hoffman JIE: Myocardial blood flow and its distribution in anesthetized polycythemic dogs. Circ Res 43:619–631, 1978.
38. Jan K-M, Chien S: Effect of hematocrit variations on coronary hemodynamics and oxygen utilization. Am J Physiol 233:H106–113, 1977.
39. Moret P, Covarrubias E, Coudert J, Duchosal F: Cardiocirculatory adaptation to chronic hypoxia: comparative study of coronary flow, myocardial oxygen consumption, and efficiency between sea level and high altitude residents. Acta Cardiol 27:283–305, 1972.
40. Jan K-M, Heldman J, Chien S: Coronary hemodynamics and oxygen utilization after hematocrit variations in hemorrhage. Am J Physiol 239:H326–332, 1980.
41. Holtz J, Bassenge E, Von Restorff W, Mayer E: Transmural differences in myocardial blood flow and in coronary dilatory capacity in hemodiluted conscious dogs. Basic Res Cardiol 71:36–46, 1977.
42. Harlan DM, Rooke TW, Belloni FL, Sparks HV: Effect of indomethacin on coronary vascular response to increased myocardial oxygen consumption. Am J Physiol 235:H372–378, 1978.
43. Coffman JD, Gregg DE: Reactive hyperemia characteristics of the myocardium. Am J Physiol 199:1143–1149, 1960.
44. Khouri EM, Gregg ED, Lowensohn HS: Flow in the major branches of the left coronary artery during experimental coronary insufficiency in the anesthetized dog. Circ Res 23:99–109, 1968.
45. Olsson RA, Gregg DE: Myocardial reactive hyperemia in the unanesthetized dog. Am J Physiol 208:224–230, 1965.
46. Johnson PC: The myogenic response. In: Bohr DF, Somlyo SR, Sparks HV (eds) Handbook of physiology. Vol 2, sect 2: The cardiovascular system. Bethesda MD: American Physiological Society, 1980, pp 409–442.
47. Eikens E, Wilcken DEL: Myocardial reactive hyperemia and coronary vascular reactivity in the dog. Circ Res 33:267–274, 1973.
48. Eikens E, Wilcken DEL: Reactive hyperemia in the dog heart: effects of temporarily restricting arterial inflow and of coronary occlusions lasting one and two cardiac cycles. Circ Res 35:702–712, 1974.
49. Schwartz GG, McHale PA, Greenfield GG: Hyperemic response of the coronary circulation to brief diastolic occlusion in the conscious dog. Circ Res 50:28–37, 1982.
50. Scott JB, Radawski D: Role of hyperosmolarity in the genesis of active and reactive hyperemia. Circ Res (Suppl 1) 28:I26–32, 1971.
51. Murray PA, Belloni FL, Sparks HV: The role of potassium in the metbolic control of coronary vascular resistance of the dog. Circ Res 44:767–780, 1979.
52. Bunger R, Haddy FJ, Querengasser A, Gerlach E: Studies on potassium induced coronary dilation in the isolated guinea pig heart. Pflugers Arch 63:27–31, 1976.
53. Winbury MM, Howe BB, Weiss HR: Effect of nitroglycerin and dipyridamole on epicardial and endocardial oxygen tension: further evidence for redistribution of myocardial blood flow. J Pharmacol Exp Ther 176:184–199, 1971.
54. Sparks HV: Effect of local metabolic factors on vascular smooth muscle. In: Bohr DF, Somlyo SR, Sparks HV (eds) Handbook of physiology. Vol 2, sect 2: The cardiovascular system. Bethesda MD: American Physiological Society, 1980, pp 475–513.
55. Duling BR: Microvascular responses to alterations in oxygen tension. Circ Res 31:481–489, 1972.
56. Duling BR, Pittman RN: Oxygen tension: dependent or independent variable in local control of blood flow? Fed Proc 34:2020–2024, 1975.
57. Gellai M, Detar R: Evidence in support of hypoxia but against high K^+ and hyperosmolality as possible mediators of sustained vasodilation in rabbit cardiac and skeletal muscle. Circ Res 35:681–691, 1974.
58. Coburn RF, Ploegmakers F, Gondrie P, Abboud R: Myocardial myoglobin oxygen tension. Am J Physiol 224:870–876, 1973.
59. Kalsner S: Intrinsic prostaglandin release: a mediator of anoxia-induced relaxation in an isolated coronary artery preparation. Blood Vessels 13:155–166, 1976.

60. McNeil TA: Venous oxygen saturation and blood flow during reactive hyperemia in the human forearm. J Physiol (Lond) 134:195–201, 1956.
61. Alexander RW, Kent KM, Pisano JJ, Keiser HR, Cooper T: Regulation of postocclusive hyperemia by endogenously synthesized prostaglandins in the dog heart. J Clin Invest 55:1174–1181, 1975.
62. Needleman P, Iskson PC: Intrinsic prostaglandin biosynthesis in blood vessels. In: Bohr DF, Somlyo SR, Sparks HV (eds) Handbook of physiology. Vol 2, sect 2: The cardiovascular system. Bethesda MD: American Physiological Society, 1980, pp 613–633.
63. Owen TL, Ehrhart IC, Weidner WJ, Scott JB, Haddy FJ: Effects of indomethacin on local blood flow regulation in canine heart and kidney. Proc Soc Exp Biol Med 149:871–876, 1975.
64. Hintze TH, Kaley G: Prostaglandins and the control of blood flow in the canine myocardium. Circ Res 40:313–320, 1977.
65. Giles RW, Wilcken DEL: Reactive hyperemia in the dog heart: inter-relations between adenosine, ATP, and aminophylline and the effect of indomethacin. Cardiovasc Res 11:113–121, 1977.
66. Rubio R, Berne RM, Katori M: Release of adenosine in reactive hyperemia of the dog heart. Am J Physiol 216:56–62, 1969.
67. Olsson RA: Changes in content of purine nucleoside in canine myocardium during coronary occlusion. Circ Res 26:301–306, 1970.
68. Schrader J, Haddy FJ, Gerlach E: Release of adenosine, inosine, and hypoxanthine from the isolated guinea pig heart during hypoxia, flow-autoregulation and reactive hyperemia. Pflugers Arch 369:1–6, 1977.
69. Olsson RA, Snow JA, Gentry MK: Adenosine metabolism in canine myocardial reactive hyperemia. Circ Res 42:358–362, 1978.
70. Curnish RR, Berne RM, Rubio R: Effect of aminophylline on myocardial reactive hyperemia. Proc Soc Exp Biol Med 141:593–598, 1972.
71. Schutz W, Zimpfer M, Raberger G: Effect of aminophylline on coronary reactive hyperemia following brief and long occlusion periods. Cardiovasc Res 11:507–511, 1977.
72. Juhran W, Voss EM, Dietmann K, Schaumann W: Pharmacologic effects on coronary reactive hyperemia in conscious dogs. Naunyn Schmiedbergs Arch Pharmacol 269:32–47, 1971.
73. Bittar N, Pauly TJ: Myocardial reactive hyperemia responses in the dog after aminophylline and lidoflazine. Am J Physiol 220:812–815, 1971.
74. Saito D, Seinhart CR, Nixon DG, Olsson RA: Intracoronary adenosine deaminase reduces canine myocardial reactive hyperemia. Circ Res 49:1262–1267, 1981.
75. Haddy FJ, Scott JB: Metabolic factors in peripheral circulatory regulation. Fed Proc 34:2006–2011, 1975.
76. Samuelsson B, Paoletti R (eds): Leukotrienes and other lipoxygenase products. Adv Prostaglandin Thromboxane Leukotriene Res 9, 1982.
77. Mosher P, Ross J, McFate PA, Shaw RF: Control of coronary blood flow by an autoregulatory mechanism. Circ Res 14:250–259, 1964.
78. Shaw RF, Mosher P, Ross J, Joseph JI, Lee ASJ: Physiologic principles of coronary perfusion. J Thorac Cardiovasc Surg 44:608–616, 1962.
79. Gorman MG, Sparks HV: Unpublished observations.
80. Rouleau J, Boerboom LE, Surjadhana A, Hoffman JIE: The role of autoregulation and tissue diastolic pressures in the transmural distribution of left ventricular blood flow in anesthetized dogs. Circ Res 45:804–815, 1979.
81. Boatwright RB, Downey HF, Bashour FA, Crystal GJ: Transmural variation in autoregulation of coronary blood flow in hyperperfused canine myocardium. Circ Res 47:599–609, 1980.
82. Rubio R, Berne RM: Regulation of coronary blood flow. Prog Cardiovasc Dis 18:105–122, 1975.
83. Mohrman DE, Feigel EO: Competition between sympathetic vasoconstriction and metabolic vasodilation in the canine coronary circulation. Circ Res 42:79–86, 1977.
84. Britton S, Di Salvo J: Effects of angiotensin I and angiotensin II on hindlimb and coronary vascular resistance. Am J Physiol 225:1226–1231, 973.
85. Cohen MV, Kirk ES: Differential response of large and small coronary arteries to nitroglycerin and angiotensin: autoregulation and tachyphylaxis. Circ Res 33:445–453, 1973.
86. Green HD, Kepchar JH: Control of peripheral resistance in major systemic vascular beds. Physiol Rev 39:617–686, 1959.
87. Case RB, Felix A, Wachter M, Kyriakidis G, Castellana F: Relative effect of CO_2 on canine coronary vascular resistance. Circ Res 42:410–418, 1978.
88. Case RB, Greenberg H: The response of canine coronary vascular resistance to local alterations in coronary arterial pCO_2. Circ Res 42:410–418, 1978.
89. Case RB, Greenberg H, Moskowitz R: Alterations in coronary sinus pO_2 and O_2 saturation resulting from pCO_2 changes. Cardiovasc Res 9:167–177, 1975.
90. Rooke T, Sparks HV: Arterial CO_2 myocardial consumption, and coronary blood flow in the dog. Circ Res 47:217–225, 1980.
91. Wiedmeier VT, Spell LH: Effects of catecholamines, histamine and nitroglycerin on flow, oxygen consumption and coronary blood flow during stellate ganglia stimulation. Circ Res 45:708–718, 1979.
92. Raberger G, Weissel M, Kraupp O: The dependence of the effects of intracoronary administered adenosine and of coronary conductance on the arterial pH, pCO_2, and buffer capacity in dogs. Naunyn Schmiedebergs Arch Pharmacol 271:;301–310, 1971.
93. Merrill GF, Haddy FJ, Dabney JM: Adenosine, theophylline, and perfusate pH in the isolated, perfused guinea pig heart. Circ Res 42:225–229, 1978.

94. Kittle CF, Aoki H, Brown E: The role of pH and CO_2 in the distribution of blood flow. Surgery 57:139–154, 1965.
95. Tarnow J, Bruckner JB, Eberlein HJ, Gethmann JW, Hess W, Patschke D, Wilde J: Blood pH and $PaCO_2$ as chemical factors in myocardial blood flow control. Basic Res Cardiol 70:685–696, 1975.
96. Gilmore JP, Nizolek JA, Jacob RJ: Further characterization of myocardial K^+ loss induced by changing contraction frequency. Am J Physiol 221:465–469, 1971.
97. Sybers HD, Helmer PR, Murphy QR: Effects of hypoxia on myocardial potassium balance. Am J Physiol 220:2047–2050, 1971.
98. Frick GP, Lowenstein JM: Studies of 5′-nucleotidase in the perfused rat heart: including measurements of the enzyme in perfused skeletal muscle and liver. J Biol Chem 251:6372–6378, 1976.
99. Schutz W, Shrader J, Gerlach E: Different sites of adenosine formation in the heart. Am J Physiol 240:H963–970, 1981.
100. Kukovitz WR, Poch G: Inhibition of hypoxia-induced rise in adenosine release and flow by coronary dilators. Cardiology 56:107–113, 1971/1972.
101. Schrader J, Schutz W, Bardenheuer H: Role of S-adenosylhomocysteine hydrolase in adenosine metabolism in mammalian heart. Biochem J 196:65–70, 1981.
102. Olsson RA, Saito D, Steinhart CR: Compartmentalization of the adenosine pool of dog and rat hearts. Circ Res 50:617–626, 1982.
103. Schrader J, Gerlach E: Compartmentation of cardiac adenine nucleotides and formation of adenosine. Pflugers Arch 367:129–135, 1976.
104. Miller WL, Belardinelli L, Bacchus A, Foley DH, Rubio R, Berne RM: Canine myocardial adenosine and lactate production, oxygen consumption and coronary blood flow during stellate ganglia stimulation. Circ Res 45:708–718, 1979.
105. Watkinson WP, Foley DH, Rubio R, Berne RM: Myocardial adenosine formation with increased cardiac performance in the dog. Am J Physiol 5:H13–21, 1979.
106. Degenring FH: Cardiac nucleotides and coronary flow during changes of cardiac inotrophy. Basic Res Cardiol 71:291–296, 1976.
107. Foley DH, Herlihy JT, Thompson CI, Rubio R, Berne RM: Increased adenosine formation by rat myocardium with acute aortic constriction. J Mol Cell Cardiol 10:293–300, 1978.
108. McKenzie JE, McCoy FP, Bockman EL: Myocardial adenosine and coronary resistance during increased cardiac performance. Am J Physiol 8:H509–515, 1980.
109. Jones CE, Hurst TW, Randall JR: Effect of aminophylline on coronary functional hyperemia and myocardial adenosine. Am J Physiol 243:H480–487, 1982.
110. Manfredi JP, Sparks HV: Adenosine's role in coronary vasodilation induced by atrial pacing and norepinephrine. Am J Physiol 243:H536–545, 1982.
111. DeWitt DF, Wangler RD, Thompson CI, Sparks HV: Phasic release of adenosine during steady state metabolic stimulation in the isolated guinea pig heart. Circ Res 53:636–643, 1983.
112. McKenzie JE, Steffan RP, Price RB, Haddy FJ: Effect of theophylline on adenosine and coronary vascular resistance during increased cardiac work. Physiologist 24:26, 1981.
113. Nees S, Gerbes AL, Willershausen-Zonnchen B, Gerlach E: Purine metabolism in cultured endothelial cells. Adv Exp Med Biol 122:25–30, 1980.
114. Randall WC, Armour JA: Gross and microscopic anatomy of the cardiac innervation. In: Randall WC (ed) Neural regulation of the heart. New York: Oxford University, 1977, pp 13–41.
115. Armour JA, Randall WC: Functional anatomy of canine cardiac fibers. Acta Anat 91:510–528, 1975.
116. Denn MJ, Stone HL: Autonomic innervation of dog coronary arteries. J Appl Physiol 41:30–35, 1976.
117. Dolezel S, Gerova J, Gero J, Sladek T, Vasku J: Adrenergic innervation of the coronary arteries and the myocardium. Acta Anat 100:306–316, 1978.
118. Schenk EA, Badawi AE: Dual innervation of arteries and arterioles: histochemical study. Z Zellforsch Mikrosk Anat 91:170–177, 1968.
119. Ross G: Adrenergic responses of the coronary vessels. Circ Res 39:461–465, 1976.
120. Parratt JR: Effects of adrenergic activators and inhibitors on the coronary circulation. In: Szekeres L (ed) Handbook of experimental pharmacology. Vol 54, part 1: Adrenergic activators and inhibitors. Berlin: Springer-Verlag, 1980, pp 735–822.
121. McRaven DR, Mark AL, Abboud FM, Mayer HE: Responses of coronary vessels to adrenergic stimuli. J Clin Invest 50:773–778, 1971.
122. Ek L, Ablad B: Effects of three beta adrenergic receptor blockers on myocardial oxygen consumption in the dog. Eur J Pharmacol 14:19–28, 1971.
123. Uchida Y, Murao S: Sustained decrease in coronary blood flow and excitation of cardiac sensory fibers following sympathetic stimulation. Jpn Heart J 16:265–279, 1975.
124. Mark AL, Abboud FM, Schmid PG, Heistad DD, Mayer HE: Differences in direct effects of adrenergic stimuli on coronary, cutaneous and muscular vessels. J Clin Invest 51:279–287, 1972.
125. Hamilton FN, Feigl EO: Coronary vascular sympathetic beta-receptor innervation. Am J Physiol 230:1569–1576, 1976.
126. Imai S, Otorii T, Takeda K, Katano Y: Coronary vasodilation and adrenergic receptors in the dog heart and coronary. Jpn J Pharmacol 25:423–432, 1975.
127. Murray PA, Vatner SF: Adrenoreceptor attenuation of the coronary vascular response to severe exercise in the conscious dog. Circ Res 45:654–660, 1979.
128. Heydrickx GR, Muylaert P, Pannier JL: Alpha-adrenergic control of oxygen delivery to myocardium during exercise in conscious dogs. Am J Physiol 242:H805–809, 1982.

129. Feigl EO: Control of myocardial oxygen tension by sympathetic coronary vasoconstriction in the dog. Circ Res 37:88–95, 1975.
130. Powell JR, Feigl EO: Carotid sinus reflex coronary vasoconstriction during controlled myocardial oxygen metabolism in the dog. Circ Res 44:44–51, 1979.
131. Buffington CW, Feigl EO: Adrenergic coronary vasoconstriction in the presence of coronary stenosis in the dog. Circ Res 48:416–423, 1981.
132. Yasue H, Touyama M, Shimamoto M, Kato H, Tanaka S, Akiyama F: Role of autonomic nervous system in the pathogenesis of Prinzmetal's variant form of angina. Circulation 50:534–539, 1974.
133. Yasue H, Touyama M, Kato H, Tanaka S, Akiyama F: Prinzmetal's variant form of angina as a manifestation of alpha adrenergic receptor-mediated coronary artery spasm: documentation by coronary arteriography. Am Heart J 91:148–155, 1976.
134. Levene DL, Freeman MR: Alpha-adrenergic mediated coronary artery spasm. JAMA 236:1018–1022, 1976.
135. Hillis LD, Braunwald E: Coronary artery spasm. N Engl J Med 299:695–702, 1978.
136. Zuberbuhler RC, Bohr DF: Responses of coronary smooth muscle to catecholamines. Circ Res 16:431–440, 1965.
137. Mekata H, Niu H: Electrical and mechanical responses of coronary artery smooth muscle to catecholamines. Jpn J Physiol 19:599–608, 1969.
138. Andersson R, Holmberg S, Svedmyr N, Aberg G: Adrenergic alpha- and beta-receptors in coronary vessels in man: an in vitro study. Acta Med Scand 191:241–244, 1972.
139. Bayer B-L, Mentz P, Forster W: Characterization of the adrenoceptors in coronary arteries of pigs. Eur J Pharmacol 29:58–69, 1974.
140. Feigl EO: Parasympathetic control of coronary blood flow in dogs. Circ Res 15:509–519, 1969.
141. Tiedt N, Religa A: Vagal control of coronary blood flow in dogs. Basic Res Cardiol 74:267–276, 1979.
142. Feigl EO: Sympathetic control of coronary circulation. Circ Res 20:262–271, 1967.
143. Brown AM: Motor innervation of the coronary arteries of the cat. J Physiol (Lond) 198:311–328, 1968.
144. Feigl EO: Carotid sinus reflex control of coronary blood flow. Circ Res 23:262–271, 1968.
145. Vatner SF, Franklin D, Van Critters RL, Braunwald E: Effects of carotid sinus nerve stimulation on the coronary circulation of the conscious dog. Circ Res 27:11–21, 1970.
146. Hackett JG, Abboud FM, Mark AL, Schmid PG, Heistad DD: Coronary vascular responses to stimulation of chemoreceptors and baroreceptors: evidence for reflex activation of vagal cholinergic innervation. Circ Res 31:8–17, 1972.
147. Religa Z, Trzebski A, Religa A, Glowienko A: Effect of the stimulation of afferent fibers in Hering's nerve on the blood flow and resistance in the coronary vessels of the dogs. Pol Med J 11:632–641, 1972.
148. Hashimoto K, Igakashi S, Uei I, Kumakura S: Carotid chemoreceptor reflex effects on coronary flow and heart rate. Am J Physiol 206:536–540, 1964.
149. Vatner SF, McRitchie RJ: Interaction of the chemoreflex and the pulmonary inflation reflex in the regulation of coronary circulation in conscious dogs. Circ Res 37:664–673, 1975.
150. Ehrhart IC, Parker PE, Weidner WJ, Dabney JM, Scott JB, Haddy FJ: Coronary vascular and myocardial responses to carotid body stimulation in the dog. Am J Physiol 229:754–760, 1975.
151. Fallen EL, Elliott WC, Gorlin R: Mechanisms of angina in aortic stenosis. Circulation 36:480–488, 1967.
152. Goodwin JF: Hypertrophic diseases of the myocardium. Prog Cardiovasc Dis 16:199–238, 1973.
153. Hurst JW, Logue RB, Schlant RO, Wenger NK: The heart, arteries and veins. New York: McGraw-Hill 1978, pp 1556–1590.
154. Harris CN, Aronow WS, Parker DP, Kaplan MA: Treadmill stress in left ventricular hypertrophy. Chest 63:353–357, 1979.
155. Roberts JT, Wearn TJ: Quantitative changes in the capillary muscle relationships in human heart during growth and hypertrophy. Am Heart J 21:617–633, 1941.
156. Linzbach AJ: Heart failure from the point of view of quantitative anatomy. Am J Cardiol 5:370–382, 1960.
157. Arai S, Machida A, Nakamura T: Myocardial structure and vascularization of hypertrophied hearts. Tohoku J Exp Med 95:35–54, 1968.
158. Rakusan K: Quantitative morphology of capillaries of the heart: number of capillaries in animal and human hearts under normal and pathological conditions. Methods Achiev Exp Pathol 5:272–286, 1971.
159. Zoll PM, Wessler S, Schlesinger MJ: Interarterial coronary anastomoses in the human heart, with particular reference to anemia and relative cardiac anoxia. Circulation 4:797–815, 1951.
160. Moller JH, Nakeb A, Edwards JE: Infarction of the papillary muscle and mitral insufficiency associated with congenital aortic stenosis. Circulation 34:87–91, 1966.
161. Buchner F: Qualitative morphology of heart failure: light and electron microscopic characteristics of acute and chronic heart failure. Methods Achiev Exp Pathol 5:60–120, 1971.
162. Marchetti GV, Merlo L, Noseda V, Visioli O: Myocardial blood flow in experimental cardiac hypertrophy in dogs. Cardiovasc Res 7:519–527, 1973.
163. Holtz J, Von Restorff W, Bard P, Bassenge E: Transmural distribution of myocardial blood flow and of coronary vascular reserve in canine left ventricular hypertrophy. Basic Res Cardiol 72:86–92, 1977.
164. O'Keefe DD, Hoffman JIE, Cheitlin R, O'Neill

MJ, Allard JR, Shapkin E: Coronary blood flow in experimental canine left ventricular hypertrophy. Circ Res 43:43–51, 1978.
165. Vrobel TR, Ring SW, Anderson RW, Emery RW, Bache RJ: Effect of heart rate on myocardial blood flow in dogs with left ventricular hypertrophy. Am J Physiol 239:H621–627, 1980.
166. Bache RJ, Vrobel TR: Effects of exercise on blood flow in the hypertrophied heart. Am J Cardiol 44:1029–1033, 1979.
167. Mueller TM, Marcus ML, Kerber RE, Young JA, Barnes RW, Abboud FM: Effect of renal hypertension and left ventricular hypertrophy on the coronary circulation in dogs. Circ Res 42:543–549, 1978.
168. Malik AB, Abe T, O'Kane H, Geha AS: Cardiac function, coronary flow, and oxygen consumption in stable left ventricular hypertrophy. Am J Physiol 225:186–191, 1973.
169. Wangler RD, Peters KG, Marcus ML, Tomanek RJ: Effects of duration and severity of arterial hypertension and cardiac hypertrophy on coronary vasodilator reserve. Circ Res 51:10–18, 1982.
170. Marcus ML, Mueller TM, Gascho JA, Kerber RE: Effects of cardiac hypertrophy secondary to hypertension on the coronary circulation. Am J Cardiol 44:1023–1028, 1979.
171. Murray PA, Vatner SF: Reduction of maximal coronary vasodilator capacity in conscious dogs with severe right ventricular hypertrophy. Circ Res 48:27–33, 1981.
172. Archie JP, Fixler DE, Ullyot DJ, Buckberg GD, Hoffman JIE: Regional myocardial blood flow in lambs with concentric right ventricular hypertrophy. Circ Res 34:143–154, 1974.
173. Murray PA, Baig H, Fishbein MC, Vatner SF: Effects of experimental right ventricular hypertrophy on myocardial blood flow in conscious dogs. J Clin Invest 64:421–427, 1979.
174. Manohar M, Thurmon JC, Tranquill WJJ, Devous MD, Theodorakis MC, Shawley RV, Feller DL, Benson JG: Regional myocardial blood flow and coronary vascular reserve in unanesthetized young calves with severe concentric right ventricular hypertrophy. Circ Res 48:785–796, 1982.
175. Bache RJ, Vrobel TR, Ring WS, Emery RW, Anderson RW: Regional myocardial blood flow during exercise in dogs with chronic left ventricular hypertrophy. Circ Res 48:76–87, 1981.
176. Rembert JC, Kleinman LH, Fedor JM, Wechsler AS, Greenfield JC Jr: Myocardial blood flow distribution in concentric left ventricular hypertrophy. J Clin Invest 62:379–386, 1978.
177. Mittman U, Bruckner UB, Keller HE, Kohler U, Vetter H, Waag K-L: Myocardial flow reserve in experimental cardiac hypertrophy. Basic Res Cardiol 75:199–206, 1980.
178. Breisch EA, Houser SR, Carey RA, Spann JF, Bove AA: Myocardial blood flow and capillary density in chronic pressure overload of the feline left ventricle. Cardiovasc Res 14:469–475, 1980.
179. Lund DD, Tomanek RJ: Myocardial morphology in spontaneously hypertensive and aortic-constricted rats. Am J Anat 152:141–151, 1978.
180. Henquell L, Odoroff CL, Honig CR: Intercapillary distance and capillary reserve in hypertrophied rat hearts beating in situ. Circ Res 41:400–408, 1977.
181. Mulvaney MJ, Hansen PK, Aalkjaer C: Direct Evidence that the greater contractility of resistance vessels in spontaneously hypertensive rats is associated with a narrowed lumen, a thickened media, and an increased number of smooth muscle cell layers. Circ Res 43:854–864, 1978.
182. Warshaw DM, Mulvaney MJ, Halpern W: Mechanical and morphological properties of arterial resistance vessels in young and old spontaneously hypertensive rats. Circ Res 45:250–259, 1979.
183. Noreson E, Hallback M, Hjalmarsson A: Structural "resetting" of the coronary vascular bed in spontaneously hypertensive rats. Acta Physiol Scand 101:363–365, 1977.
184. Yamori Y, Mori C, Nishio T, Ooshima A, Hork R, Ohtaka M, Soeda T, Saito M, Abe K, Nara Y, Nakao Y, Kihara M: Cardiac hypertrophy in early hypertension. Am J Cardiol 44:964–969, 1979.
185. Peters K, Wangler R, Tomanek R, Marcus M: Interaction of age and hypertrophy on coronary dilator capacity. Fed Proc 40:546, 1981.
186. Schaper W: The collateral circulation of the heart. Amsterdam: North-Holland, 1971.
187. Gregg DE: The natural history of collateral development. Circ Res 35:335–344, 1974.
188. Schwarz F, Wagner HO, Sesto M, Hofmann M, Schaper W, Kubler W: Native collaterals in the development of collateral circulation after chronic coronary stenosis in mongrel dogs. Circulation 66:303–308, 1982.
189. Schwarz F, Flameng W, Ensslen R, Sesto M, Thormann J: Effect of coronary collaterals on left ventricular function at rest and during stress. Am Heart J 95:570–577, 1978.
190. Kelly DT, Pitt B: Regional changes in intramyocardial pressure following myocardial ischemia. In: Bloor CM, Olsson RA (eds) Current topics in coronary research, vol 39. New York: Plenum, 1973, pp 115–130.
191. Bache RJ, Cobb FR, Greenfield JC: Myocardial blood flow distribution during ischemia-induced coronary vasodilation in the unanesthetized dog. J Clin Invest 54:1462–1472, 1974.
192. Tennant R, Wiggers CJ: The effect of coronary occlusion on myocardial contraction. Am J Physiol 112:351–361, 1935.
193. Katz AM: Effects of ischemia on the contractile process of heart muscle. Am J Cardiol 32:456–460, 1973.
194. Hillis LD, Braunwald E: Myocardial ischemia. N Eng J Med 296:971–978, 1977.

195. Theroux P, Franklin D, Ross J, Kemper WS: Regional myocardial function during acute coronary artery occlusion and its modificaiton by pharmacologic agents in the dog. Circ Res 35:896–908, 1974.
196. Frame LH, Powell WJ: Progressive perfusion impairment during prolonged low flow myocardial ischemia in dogs. Circ Res 39:269–276, 1976.
197. Guyton RA, McClenathan JH, Michaelis LL: Evolution of regional ischemia distal to a proximal coronary stenosis: self-propagation of ischemia. Am J Cardiol 40:381–392, 1977.
198. Sparks HV, Gorman MG: Ischemic vasodilation or ischemic vasoconstriction. In: Vanhoutte PM, Leusen I (eds) Vasodilation. New York: Raven, 1981, pp 193–204.
199. Gorman MG, Sparks, HV: Progressive coronary vasoconstriction during relative ischemia in canine myocardium. (ref. 199) Circ Res 51:4;;–420, 1983.
200. Harris JR, Overholser KA, Stiles RG: Concurrent increases in resistance and transport after coronary obstruction in dogs. Am J Physiol 240:H262–273, 1981.
201. Willerson JT, Powell WJ, Guiney TE, Stark JJ, Sanders CA, Leaf A: Improvement in myocardial function and coronary blood flow in ischemic myocardium after mannitol. J Clin Invest 51:2989–2998, 1972.
202. Krishnamurty VSR, Adams R, Smitherman T, Willerson JT: Influence of mannitol on isolated, in vitro smooth muscle vascular reactivity. Circulation (Suppl 2)52:II-7, 1975.
203. Wangler RD, DeWitt DF, Sparks HV: Phasic release of adenosine during ischemia. Fed Proc 42:462, 1983.
204. Gorman MG, Sparks HV: Nitroglycerin causes vasodilation within ischemic myocardium. Cardiovasc Res 14:515–521, 1980.
205. Willerson JT, Watson JT, Hutton I, Templeton GH, Fixler DE: Reduced myocardial reflow and increased coronary vascular resistance following prolonged myocardial ischemia in the dog. Circ Res 36:771–781, 1975.
206. Parker PE, Bashour FA, Downey HF, Kechejian SJ, Williams AF: Coronary hemodynamics during reperfusion following acute coronary ligation in dogs. Am Heart J 90:593–599, 1975.
207. Kloner RA, Ganote CE, Jennings RB: The "no-reflow" phenomenon after temporary coronary occlusion in the dog. J Clin Invest 54:1496–1507, 1974.
208. Parker PE, Bashour FA, Downey HF, Bouvros IS: Coronary reperfusion: effects of hyperosmotic mannitol. Am Heart J 97:745–752, 1979.
209. Krug A, De Rochemont WM, Korb G: Blood supply of the myocardium after temporary coronary occlusion. Circ Res 19:57–62, 1966.
210. Lang T, Corday E, Gold H, Meerbaum S, Rubins S, Constatini C, Hirose S, Osher J, Rosen V: Consequences of reperfusion after coronary occlusion: effects on hemodynamic and regional myocardial metabolic function. Am J Cardiol 33:69–81, 1974.
211. Powell WJ, Di Bona DR, Flores J, Frega N, Leaf A: Effects of hyperosmotic mannitol in reducing ischemic cell swelling and minimizing myocardial necrosis. Circulation (Suppl 1)53::I45–49, 1976.
212. Marcus ML, Kerber RE, Ehrhardt J, Abboud FM: Effects of time on volume and distribution of coronary collateral flow. Am J Physiol 230:279–285, 1976.
213. Jugdutt BI, Becker LC, Hutchins GM: Early changes in collateral blood flow during myocardial infarction in conscious dogs. Am J Physiol 237:H371–380, 1979.
214. Schaper W, Pasyk S: Influence of collateral flow on the ischemic tolerance of the heart following acute and subacute coronary occlusion. Circulation (Suppl 1)53:I57–62, 1976.
215. Khouri EM, Gregg DE, McGranahan GM: Regression and reappearance of coronary collaterals. Am J Physiol 220:655–661, 1971.
216. Eckstein RW: Effect of exercise and coronary artery narrowing on coronary collateral circulation. Circ Res 5:230–235, 1957.
217. Sanders M, White FC, Peterson TM, Bloor CM: Effects of endurance exercise on coronary collateral blood flow in miniature swine. Am J Physiol 234:H614–619, 1978.
218. Scheel KW, Ingram LA, Wilson JL: Effects of exercise on the coronary and collateral vasculature of beagles with and without coronary occlusion. Circ Res 48:523–530, 1981.
219. Scheel KW, Brody DA, Ingram LA, Keller F: Effects of chronic anemia on the coronary collateral vasculature in dogs. Circ Res 38:553–559, 1976.
220. Scheel KW, Rodriguez RJ, Ingram LA: Directional coronary collateral growth with chronic circumflex occlusion in the dog. Circ Res 40:384–390, 1977.
221. Eckstein RW: Development of interarterial coronary anastomoses by chronic anemia: disappearance following correction of anemia. Circ Res 3:306–310, 1955.
222. Blum RL, Alpern H, Jaffe H, Lang TW, Corday E: Determination of interarterial coronary anastomosis by radioactive spherules: effect of coronary occlusion and hypoxemia. Am Heart J 79:244–249, 1970.
223. McGregor M: The nitrates and myocardial ischemia. Circulation 66:689–692, 1982.
224. Harder DR, Belardinelli L, Sperelakis N, Rubio R, Berne RM: Differential effects of adenosine and nitroglycerin on the action potentials of large and small coronary arteries. Circ Res 44:176–182, 1979.
225. Schnaar RL, Sparks HV: Response of large and small coronary arteries to nitroglycerin, $NaNO_2$ and adenosine. Am J Physiol 223:223–228, 1972.
226. Fam WM, McGregor M: Effect of nitroglycerin and dipyridamole on regional coronary resistance. Circ Res 22:649–659, 1968.

227. Tomoike H, Ootsubo H, Sakai K, Kikuchi Y, Nahamura M: Continuous measurement of coronary artery diameter in situ. Am J Physiol 240:H73–79, 1981.
228. Torres EC, Brandi G: The effect of vasoactive drugs on local coronary flow. Can J Physiol Pharmacol 47:421–430, 1969.
229. Vatner SF, Pagani M, Manders WT, Pasipoularides AD: Alpha adrenergic vasoconstriction and nitroglycerin vasodilation of large coronary arteries in the conscious dog. J Clin Invest 65:5–14, 1980.
230. Cohen MV, Sonnenblick EH, Kirk ES: Coronary steal: its role in detrimental effect of isoproterernol after acute coronary occlusion in dogs. Am J Cardiol 38:880–888, 1976.
231. Feldman RL, Pepine CJ, Conti R: Magnitude of dilatation of large and small coronary arteries by nitroglycerin. Circulation 64:324–330, 1981.
232. Ganz W, Marcus HS: Failure of intracoronary nitroglycerin to alleviate pacing-induced angina. Circulation 46:880–889, 1972.
233. Macho P, Hintze TH, Vatner S: Regulation of large coronary arteries by increases in myocardial metabolic demands in conscious dogs. Circ Res 49:594–600, 1981.
234. Likoff W, Kasparin H, Lehman JS, Segal BL: Evaluation of "coronary vasodilators" by coronary angiography. Am J Cardiol 13:7–9, 1964.
235. Brown G, Bolson W, Peterson RB, Pierce CD, Dodge HT: The mechanisms of nitroglycerin action: stenosis vasodilation as a major component of drug response. Circulation 64:1089–1097, 1981.
236. Fam WM, McGregor M: Effect of coronary vasodilator drugs on retrograde flow in areas of chronic myocardial ischemia. Circ Res 15:355–365, 1964.
237. Goldstein RE, Stinson EB, Scherer JL, Senigen RP, Grehl TM, Epstein SE: Intraoperative coronary collateral function in patients with coronary occlusive disease: nitroglycerin responsiveness and angiographic correlations. Circulation 49:298–308, 1974.
238. Cohen MV, Downey JM, Sonnenblick EH, Kirk ES: Effects of nitroglycerin on coronary collaterals and myocardial contractility. J Clin Invest 52: 2836–2847, 1973.
239. Jugdutt BI, Becker LC, Huthchins GM, Bulkley BH, Reid PR, Kallman CH: Effect of intravenous nitroglycerin on collateral blood flow and infarct size in the conscious dog. Circulation 63:17–28, 1981.
240. Forman R, Kirk ES, Downey JM, Sonnenblick EH: Nitroglycerin and heterogeneity of myocardial blood flow: reduced subendocardial blood flow and ventricular contractile force. J Clin Invest 52:905–911, 1973.
241. Parker JO, Di Girogi S, West RO: A hemodynamic study of acute coronary insufficiency precipitated by exercise with observations on the effects of nitroglycerin. Am J Cardiol 17:470–483, 1966.
242. Muller O, Rorvik K: Haemodynamic consequences of coronary heart disease. Br Heart J 20:302–310, 1958.
243. Hoeschen RJ, Bousvaros GA, Klassen GA, Fam WM, McGregor M: Haemodynamic effects of angina pectoris, and of nitroglycerin in normal and anginal subjects. Br Heart J 28:221–230, 1966.
244. Frick MH, Balcon R, Cross D, Sowton E: Hemodynamic effects of nitroglycerin in patients with angina pectoris studied by an atrial pacing method. Circulation 37:160–168, 1968.

40. CORONARY ARTERY SPASM

Philip D. Henry

Historical Introduction

Allan Burns (1809) [1], medical school dropout and brilliant autodidact, was the first to propose that angina during exercise was due to myocardial ischemia. He believed that diseased coronary arteries acted as constricted rigid tubes which limited blood supply to the myocardium and generated a state in which the heart's "energy supply and its energy expenditure do not balance each other". According to this concept it is an increased work load on the heart that precipitates myocardial ischemia and anginal symptoms. However, already Herberden (1772) [2] had recognized that angina may occur at rest, often during the night, a phenomenon that cannot be readily explained on the basis of Burns' mechanism. During the 19th century, many authors felt that anginal pain was triggered by some distention of the aorta or left ventricle. Such cardiovascular distentions were sometimes thought to occur as a result of peripheral constrictor responses, a syndrome that had been outlined by Nothnagel (1867) [3] under the name "angina pectoris vasomotoria". Latham (1876) [4] and others believed that angina might reflect a cramp or spasm of the heart, but such a mechanism was not widely accepted, since it was thought that a cramp of the heart was not compatible with survival [5]. In the first edition of his textbook, Osler (1892) [6] discussed the possiblity that cardiac pain "resulted from the great stretching and tension of the nerves in the muscular substance". He added that "a modified form of this view is that there is a spasm of the coronary arteries with great increase in the intracardiac pressure". Osler was still under the influence of the mechanistic hypotheses of the 19th century. However, in his second Lumleian lecture on angina pectoris 18 years later (1910) [7], his "modified view" became explicit. He discussed the possible role of coronary artery spasm at great length, and indicated that angina may be associated with other vasomotor disturbances such as Raynaud disease or migraine. On the basis of his clinical observations, he concluded that there was "evidence that sclerotic arteries are specially prone to spasm". Also, he speculated that coronary vessels might be affected by a "perverted internal secretion which favours spasm of the arteries". Therefore, the 19th century, era of speculations and controversies, generated two seemingly contradictory "coronary theories": Burns' rigid arteries, an example of insufficient vasomotion, and Osler's atherosclerotic vasospasm, an example of excessive vasomotion.

In the 1920s, electrocardiography initiated a new era in clincial cardiology. Early experimental studies had demonstrated that myocardial injury was associated with typical electrocardiographic changes, and Smith [8] was the first to describe the electrocardiogram of acute myocardial infarction in dogs subjected to coronary ligation. Pardee [9] then observed ST elevations similar to those described by Smith in a patient undergoing acute myocardial infarction. Subsequently, many authors confirmed Pardee's electrocardiographic observations, and it became widely accepted that marked ST elevations and Q waves constituted signs of acute myocardial infarction. However, Parkinson and Bedford (1931) [10] were among the first to note that ST-segment elevations suggestive of coronary occlusion occurred transiently in some patients experiencing attacks of angina. They

N. Sperelakis (ed.), PHYSIOLOGY AND PATHOPHYSIOLOGY OF THE HEART.

Martinus Nijhoff Publishing, Boston/The Hague/Dordrecht/Lancaster.

suggested that in such instances the electrocardiogrpahic changes did not reflect coronary thrombosis and myocardial infarction, but represented "functional ischaemia". They concluded that "it is difficult to conceive a functional ischaemia arising otherwise than from coronary spasm". The phenomenon of transient ST elevation during episodes of anginal pain was subsequently documented by numerous investigators [11–13]. In a notable paper, Hausner and Scherf (1933) [14] made the following observations regarding angina with marked electrocardiographic abnormalities: (1) ECGs typical of sudden coronary occlusion including ST elevations and in one case Q waves appeared as a recurrent transient phenomenon during attacks of angina, (2) attacks occurred usually at rest, and symptoms and signs were relieved by nitroglycerin, (3) attacks with identical ECGs were precipitated by exercise testing (climbing of stairs), (4) attacks in the same patient ocurred with or without increases in blood pressure, (5) the electrocardiographic changes occurred in some instances without simultaneous chest pain, (6) attacks were accompanied by polymorphous ventricular extrasystoles in one patient, and (7) in two patients, there were frequent attacks which culminated in death after weeks or months of observation. These two patients exhibited no or minimal coronary atherosclerosis at autopsy. The authors discussed the possibility that the attacks were triggered by coronary constriction, and pointed out that insufficient coronary dilation during exercise may have the same effect as constriction at rest [14]. Brow and Holman (1933) [15] classified angina into two groups: exercise-induced angina due to a "disease-limited coronary circulation", and spontaneous angina possibly due to coronary vasospasm and associated with marked ST-T changes of the electrocardiogram. Many years later, Prinzmetal and collaborators (1959) [16] described a special syndrome of rest angina which they thought was attributable to coronary spasm and was specific enough to permit diagnosis in the absence of electrocardiography. Furthermore, they claimed that with this new syndrome "chemical changes in the myocardium differed from those occurring in classic angina pectoris". However, Prinzmetal and collaborators never summarized the data about the 20 cases they had reportedly collected, nor were any data provided regarding the specific chemical changes of the syndrome. The term variant angina proved to be a best-seller, however, and was subsequently widely applied to anginal syndromes which clearly lacked the specific features outlined by Prinzmetal. For instance, some authors used the term to characterize the syndrome of marked ST elevation during and after exercise, a syndrome first outlined by Hausner and Scherf [14].

The demonstration of coronary artery spasm in man was made possible by modern coronary arteriography. The early reports by Arnulf (1959) [17] and Gensini and collaborators (1962) [18] demonstrating spasm by nonselective coronary arteriography received initially little attention. A few years later, Demany et al. (1968) [19] and Dhurandhar et al. (1972) [20] related coronary artery spasm as visualized by selective arteriography to the anginal syndrome of Prinzmetal. However, with the increasing popularity of coronary arteriography, spasms were soon observed in a variety of anginal syndromes, including exercise-related angina and acute myocardial infarction. It became apparent that seemingly inappropriate coronary vasomotion occurred in patients with variable clinical presentation and coronary anatomy. Therefore, evidence that coronary spasm was usually associated with the eclectic features depicted by Prinzmetal and collaborators [16] was not completely confirmed. On the other hand, phenomena originally described by Hausner and Scherf [14] such as ST elevation without pain [21], transient Q waves [22], absence of increases in arterial pressure [23], and progressive deterioration culminating in acute myocardial infarction [24, 25] were rediscovered.

Definition of Coronary Artery Spasm

There is no universally accepted definition of coronary artery spasm. The term spasm in smooth muscle physiology usually refers to a strong and sustained contraction that impairs normal organ function. Since the demonstra-

tion of coronary artery spasms in man depends upon coronary arteriography, it is important to recognize the inherent limitations of this technique. First, the commonly used angiographic dyes act as potent vasodilators, a property of the dyes that may potentially obscure sustained coronary constrictor responses [26, 27]. Second, even with multiple angiographic views, it may be difficult to reconstruct with confidence the three-dimensional geometry of the lumen of coronary arteries, and claimed angiographic resolution at the 0.1-mm level cannot be accepted without reservation [28, 29]. Third, arteriography is effective in detecting localized distortions of the arterial lumen, whereas diffuse narrowing is more difficult to appreciate, since arterial lumen must be related to the myocardial mass supplied by the artery [29]. Fourth, segmental arterial tone should be related to the range of vasomotion at the level of constricted segments and nonconstricted neighboring segments. Therefore, pharmacologic manipulations such as vasodilation in response to nitroglycerin and vasoconstriction in response to ergonovine are necessary to assess abnormal vasomotion. Unfortunately, such maneuvers are rather elaborate and not without danger, and consequently are not performed routinely by arteriographers. Fifth, at the level of eccentric arterial lesions, normal constrictor tone might suffice to critically narrow the arterial lumen, a mechanism of dynamic obstruction that would not necessarily imply an abnormality of smooth muscle funtion [30]. Sixth, there is general agreement that the diagnosis of coronary spasm depends upon the transient nature of the coronary obstruction, and more specifically upon the relief of the obstruction by the administration of potent vasodilators such as nitroglycerin and nifedipine. However, there is no generally accepted definition regarding the extent of the relief of the narrowing required to establish the diagnosis of functionally important dynamic narrowing, and the efficacy of vasodilators in relieving enhanced coronary constrictor tone has not been defined in quantitative terms. Seventh, coronary arteriography is capable of visualizing only large (epicardial) coronary arteries, precluding the demonstration of spasms involving smaller (intramyocardial) arteries. In view of these radiologic difficulties, the definition of coronary artery spasm remains somewhat vague, a fact that may explain the rather striking variability of the incidence of coronary spasm in different catheterization laboratories.

Prevalence of Coronary Spasm

As mentioned above, the diagnosis of coronary spasm depends upon angiographic protocols and interpretations which vary from laboratory to laboratory [31]. Premedication with spasmolytic drugs such as nitroglycerin and diazepam, avoidance of coronary constrictors (ergonovine) when coronary lesions are thought to explain symptoms, and failure to obtain multiple views may contribute to the variability of the diagnosis of coronary spasm. Although some authors believe that coronary spasm is a rare event, others have suggested that abnormal coronary vasomotion may play an important role in patients suffering from myocardial ischemia [23]. Thus, coronary spasm has been implicated in a variety of syndromes, including sudden death [32], myocardial infarction with or without coronary thrombosis [33–38], various forms of rest angina [23], and exercise-related angina [39–45]. In Japan, coronary spasm appears to be more frequent than in North America, and the diagnosis of variant angina is made in a great percent (10%–70%) of patients with anginal symptoms referred to Japanese medical centers [46, 47]. Therefore, estimation of the prevalence of coronary artery spasm in various populations remains poorly defined.

Clinical Syndromes Associated with Coronary Artery Spasm

Electrocardiographers in the 1930s invoked coronary spasm to explain electrocardiographic changes of myocardial ischemia occurring at rest without apparent precipitating factors [10, 14, 15]. Prinzmetal and collaborators [16] delineated a specific anginal syndrome which was attributed to coronary artery spasm and had the following distinguishing features: (1) anginal pain occurs at rest or during "ordinary activ-

ity"; (2) anginal pain is similar in location compared to other anginal syndromes, but often longer in duration and more severe; (3) cyclical pain recurs every few minutes, forming a "sign wave pattern"; (4) attacks have distinct waxing and waning periods of equal duration (in contrast, classic angina was thought to have short waning periods compared to the waxing periods); (5) pain occurs often at the same hour of the day; (6) nitroglycerin promptly relieves pain; (7) the electrocardiogram during attacks exhibits striking ST elevations with reciprocal depressions; (8) ST elevations have a distribution corresponding to that of myocardial infarctions of defined electrocardiographic location; (9) electrocardiographic changes include alterations of the QRS complex; (10) anginal episodes are complicated by arrythmias and AV block; (11) infarction may develop in the distribution of previous ST elevations; (12) exercise fails to produce attacks; (13) there are distinct chemical disturbances different from those seen in classic angina; (14) diagnosis is possible only after careful study; (15) "acute emotional storms" do not precipitate attacks in contrast to classic angina; (16) patients are in greater distress compared to those suffering from classic angina; (17) nylidrin hydrochloride tends to prevent attacks; and (18) attacks involve only one area of the heart, in contrast to classic angina, which was thought to represent a "diffuse disturbance of the heart" [16]. One difficulty with Prinzmetal's picturesque description is that not all statements were supported by clinical data, and the numerous previoius reports on rest angina with infarct-like electrocardiograms were not adequately summarized.

As emphasized by Maseri et al. (1978) [23], arteriography visualizes spontaneous and ergonovine-induced coronary spasms in patients with variable history and coronary anatomy. ST elevation as described by Prinzmetal et al. is not a very specific sign, since ST elevation and depression in the same leads may occur with single or different episodes of chest pain or without chest pain in the same patient. Furthermore, it is important to rule out minor or incomplete myocardial infarctions in patients exhibiting rest angina and recurrent marked electrocardiographic changes [24, 25]. In Prinzmetal's material, 12 patients were reported to have ultimately developed myocardial infarction, but clinical data were not provided. It appears difficult to distinguish between Prinzmetal's variant angina culminating in infarction and so-called unstable angina [24, 25]. Prinzmetal's claim that angina with marked ST elevations did not occur in exercise-related angina was in contradiction with previous reports [14] and has not been confirmed in the recent literature. On the contrary, there is increasing evidence that coronary artery spasm may be precipitated by exercise [39–45].

The role of coronary spasm in precipitating acute myocardial infarction has been the subject of considerable controversy [23, 33–38]. Some authors have concluded that coronary spasm is not a pathogenic mechanism of acute myocardial infarction, since arteriographic and autopsy data reveal a coronary thrombosis in the majority of patients with transmural myocardial infarction [48]. This conclusion is somewhat surprising, since the precursor events precipitating coronary thrombosis are incompletely understood. In addition, it is possible that arterial injury after myocardial infarction may favor coronary spasm [49, 50].

It has been widely appreciated that coronary spasm may be associated with serious ventricular dysrhythmias and AV block [23, 46]. Therefore, there is little reason to doubt Leary's (1935) [32] hypothesis that coronary spasm is a factor in producing sudden death [51–53].

In summary, coronary spasm appears to occur in various syndromes of myocardial ischemia, and the notion that coronary spasm is associated with a specific anginal syndrome as detailed by Prinzmetal has not been generally confirmed.

Prognosis of Coronary Spasm

The prognosis of coronary artery spasm strongly depends upon the method of diagnosis and classification of patients. In centers in which ergonovine testing is used extensively in patients who present initially with occasional episodes of chest pain, the apparent prognosis

of variant angina appears to be quite favorable as initially emphasized by Japanese workers [46]. Waters et al. (1983) [54] and Bott-Silverman and Heupler (1983) [55] have recently reemphasized that remission is a frequent outcome of variant angina and that cardiac mortality is "relatively low" in medically treated patients. However, since most patients with variant angina exhibit signs of coronary atherosclerosis, it will be important to characterize the natural history of patients with apparent remission.

Anatomy of Coronary Artery Spasm

Coronary spasm frequently involves arterial segments exhibiting angiograhic signs of coronary atherosclerosis [23, 30]. However, coronary spasm has been claimed to occur with "normal" or "near-normal" coronary arteries [56, 57]. As mentioned above, coronary arteriography has certain limitations in detecting coronary artery disease, and numerous studies of coronary obstructive lesions in patients by angiographic and pathologic techniques have demonstrated that arteriography may underestimate obstructive lesions [28, 29]. Arteriography visualizes only narrowed or distorted vascular lumens, but fails to detect disease of the arterial wall associated without narrowing or expansion of the arterial lumen [58]. In addition, failure to demonstrate an abnormal angiographic coronary anatomy does not rule out microstructural and biochemical lesions of atherosclerosis. Therefore, to call an artery "normal" on the basis of a coronary arteriogram is misleading and reveals insufficient awareness of the cell biology of early atherogenesis.

There are relatively few studies on the pathologic anatomy of patients who exhibited coronary artery spasm on arteriography. Because of the prevalence of coronary atherosclerosis in countries where coronary arteriography is used extensively, it is not surprising that many patients with coronary spasm have demonstrated coronary atherosclerosis at autopsy [14, 16, 20, 59–63]. In some reports, patients with vasospastic angina demonstrated fibrous medial dysplasia [64, 65]. These findings are of some interest, since the vasospasm syndrome resulting from ergot intoxication (ergotism) is known to produce similar medial fibromuscular lesions [66].

Clinical Pharmacology of Coronary Artery Spasm

ERGOT DERIVATIVES

Chest pain is one of the major symptoms of ergotism [66–68]. Labbé (1929) [69] was one of the first to invoke coronary spasm to explain chest pain occurring after the intramuscular administration of ergotamine, a compound that had been isolated ten years before by Stoll. Later, some authors used ergotamine to suppress sympathetic tone in an attempt to relieve angina [70]. Master et al. (1948) [71] used ergotamine to enhance the specificity of the two-step exercise test for the diagnosis of coronary disease. They believed that the drug prevented the false positive test due to sympathetic overactivity. However, Scherf and Schlachman (1948) [72] investigated the effects of ergotamine in patients with coronary disease and concluded that the drug provoked angina and was contraindicated in these patients. Stein (1949) [73] used another ergot derivative, ergonovine, for the diagnostic provocation of angina in conjunction with Master's exercise test. Stein's ergonovine test was revived only many years later as a test for the provocation of coronary artery spasm during arteriography. Heupler et al. (1978) [74] demonstrated in nine patients with variant angina that ergonovine 1.3–4.0 μg/kg i.v. provoked episodes of coronary spasm. They concluded that the ergonovine test was safe and useful for the diagnosis of coronary artery spasm. Curry et al. (1979) [75] evaluated the ergonovine test in patients with variant angina and concluded that there were close similarities between ergonovine-induced and spontaneous attacks of angina. Théroux et al. (1979) [76] used graded intravenous doses of ergonovine (between 25 and 400 μg) to assess the antianginal efficacy of coronary dilators on the basis of increased tolerance to ergonovine. Cipriano et al. (1979) [77] demonstrated that ergono-

vine elicited mild diffuse coronary constriction in patients without vasospastic angina, but provoked marked (>85%) focal or diffuse vessel narrowing in patients suffering from variant angina. Recently, Cannon et al. (1983) [78] have provided evidence that in some patients with atypical chest pain ergonovine produces chest pain and reductions in coronary flow attributable to excessive constriction of the intramyocardial vasculature. Collectively, these findings appear to support the concept that the coronary arteries of patients with vasospastic angina are supersensitive to the constrictor effects of ergonovine.

The supersensitivity of patients with variant angina to ergonovine provides little specific receptor-pharmacologic information. Ergot derivatives are known to act on multiple monoaminergic receptors inluding alpha-adrenergic, serotonergic, histaminergic, and dopaminergic receptors [79]. In addition, ergot derivatives often exhibit dualistic or partial agonistic effects, i.e., low and high doses may produce agonistic and antagonistic effects, respectively [79]. To our knowledge, the mechanism of action of ergonovine in patients has not been investigated with specific monoaminergic blocking agents. In isolated canine coronary arteries, serotonin blocking agents (methysergide, cyproheptadine) are more effective than alpha blockers (phentolamine, prazosin) in antagonizing ergonovine, suggesting a serotonergic mechanism [80–83]. Similarly, we have recently observed that the serotonin blocking agent ketanserin, but not prazosin, was capable of relaxing isolated human coronary arteries contracted with ergonovine [84]. These findings suggest that ergonovine acts on canine and human coronary arteries by a similar mechanism.

ALPHA-ADRENERGIC AGENTS

Orlickj et al. (1977) [85] have demonstrated that administration of the alpha blocker phentolamine to patients with a normally innervated heart or a transplanted heart augments coronary sinus flow monitored by thermodilution. They concluded that resting coronary blood flow in man was regulated by alpha-adrenergic constrictor tone. Mudge et al. (1976) [86] performed cold pressor tests (immersion of one hand in ice water for 1 min) while monitoring coronary sinus flow by thermodilution. The test increased coronary vascular resistance in patients with coronary disease, but not in those without coronary disease, and the increases were blocked by phentolamine. They concluded that adrenergically mediated coronary vascular tone may contribute to ischemia in patients with coronary disease. Levene and Freeman (1976) [87] observed that coronary spasm in a patient with angina was relieved by phentolamine. In addition, prolonged oral administration of phenoxybenzamine improved the exercise tolerance assessed by bicycle ergometry and reduced or abolished electrocardiographic abnormalities after exercise. This suggested that coronary spasm was mediated by an alpha-adrenergic mechanism. Yasue et al. (1974) [88] were able to provoke anginal attacks in patients with variant angina by the administration of epinephrine, and phenoxybenzamine prevented spontaneous attacks in one patient. Isoproterenol and propranolol had no effect on the attacks. In another report (1976) [89], the same authors triggered attacks of variant angina with epinephrine after pretreatment with propranolol. These observations indicated that coronary spasm was in part mediated by the activation of alpha-adrenergic receptors. Ricci et al. (1979) [90] demonstrated in four patients with variant angina that phentolamine reversed coronary spasm visualized by arteriography and increased coronary sinus flow measured by thermodilution. Furthermore, oral administration of phenoxybenzamine caused disappearance of symptoms during follow-up periods of up to 12 months. Bertrand and collaborators (1980) [91] treated patients with partial denervation of the heart (plexectomy) and aortocoronary bypass, and observed a better relief of symptoms compared to that achieved in control patients receiving only coronary bypass. In another study (1981) [92], a patient after unsuccessful plexectomy was subjected to complete sympathetic denervation by autotransplantation, a procedure that provided symptomatic relief and suppressed electrocardiographic signs of ischemia. Collectively, these results are consistent with the concept

that coronary spasm may be neurogenic, and more specifically noradrenergic, in nature.

The notion that coronary artery spasm is mediated by an alpha-adrenergic mechanism has not been generally confirmed, however. Chierchia et al. (1983) [93] demonstrated in patients with variant angina that the cold pressor test, intravenous phenylephrine, and norepinephrine after beta blockade did not potentiate the coronary constrictor effects of ergonovine or reduce the number and severity of spontaneous attacks of ischemia detected by continuous electrocardiographic monitoring. In addition, continuous infusions of phentolamine titrated to effect a reduction in systolic arterial pressure of 15 mmHg failed to prevent ischemic attacks. Buda et al. (1981) [94] demonstrated a spontaneous coronary artery spasm by arteriography and thallium scintigraphy in a patient with transplanted heart, suggesting that autonomic innervation was not essential for the occurrence of coronary artery spasm. In a recent report, Weber et al. (1983) [95] found that plexectomy, despite adequate suppression of autonomic innervation, was ineffective in relieving symptoms and signs of ischemia in three patients with variant angina. Robertson et al. (1979) [96] studied catecholamine metabolism in three patients with variant angina, and demonstrated that episodes of variant angina were not associated with increases in plasma catecholamine levels at the onset and termination of the episodes. Furthermore, propranolol had no beneficial effects and increased the length of episodes of ST elevation in one patient, in agreement with other studies [97–99].

It is difficult to draw definitive conclusions from the conflicting reports cited above. However, the recent study by Chierchia et al. (1983) [93] casts some doubt about the importance of alpha-adrenergic mechanisms in variant angina. Additional studies with selective alpha blockers such as prazosin will be required to define the importance of alpha-adrenergic stimulation in provoking coronary artery spasm.

HISTAMINERGIC AGENTS

According to current concepts, histamine acts on two major subclasses of receptors referred to as H_1 and H_2 receptors. Among the agonists, 2-methyl-histamine is selective for H_1 receptors, whereas, 4-methyl-histamine, dimaprit, and impromidine are selective for H_2 receptors. The classic antihistamines such as benadryl, chlortrimeton, mepyramine, and pyrilamine block the H_1 receptors, whereas drugs such as cimetidine, tiotidine, metiamide, and burinamide exert selective blocking effects on H_2 receptors. Ginsburg et al. (1981) [100] have precipitated in patients exhibiting features of variant angina coronary artery spasm by the intravenous administration of histamine after pretreatment with cimetidine. Unfortunately, the authors failed to demonstrate that H_1 antihistamines were effective in blocking histamine-induced ischemic attacks. Consequently, definitive conclusions regarding the importance of histaminergic effects in precipitating coronary spasm will have to await further studies.

SEROTONERGIC AGENTS

Although serotonin has been implicated in various vasospasm syndromes, including vascular headaches, cerebral vasospasm, and Raynaud phenomenon, there is surprisingly little information available regarding the effects of serotonin and serotonin antagonists on vasospastic angina. This is somewhat surprising, since serotonin has proved to be a relatively potent constrictor of large coronary arteries isolated from dogs, monkeys, and man. In a preliminary study, we have demonstrated that serotonin is approximately ten times more potent than norepinephrine in the presence of beta blockade in contracting human epicardial coronary arteries [84]. To our knowledge, provocative tests with serotonin analogous to those performed with ergonovine and histamine have not been reported. One major difficulty in assessing serotonergic mechanisms in man is that antiserotonin agents with satisfactory selectivity and low toxicity are not available. Drugs such as ergot derivatives (methysergide), cyproheptadine, and pizotifen are nonselective and have appreciable alpha-adrenergic and histaminergic blocking effects [79, 101]. Long-term treatment with methysergide is not without hazard since the drug produces ergot toxicity including fibrogenic effects. The imipramine-like

drugs cyproheptadine and pizotifen produce typical antihistamine toxicity and are often poorly tolerated because of their central nervous system depressant effects. Ketanserin, a serotonin blocking agent with selectivity for smooth muscle and platelets, has little effect on the central nervous system and has proved useful for the differentiation of monoaminergic receptors in vitro [102]. However, the selectivity of this agent for serotonin versus alpha agonists is not sufficient, and relatively high doses of ketanserin are required to antagonize ergonovine in human arteries in vitro. Intravenous ketanserin has thus far proved ineffective in antagonizing ergonovine-induced coronary spasm in patients with variant angina [103].

PEPTIDERGIC AGENTS

Although vasoactive peptides such as angiotensin II and vasopressin are potent vasoconstrictors, their effects in patients with vasospastic angina have to our knowledge not been investigated.

CHOLINERGIC AGENTS

Yasue et al. (1974) [88] observed that methacholine, a muscarinic agonist, precipitated attacks in patients with variant angina. In addition, long-term administration of atropine appeared to suppress anginal attacks in these patients. Endo et al. (1976) [104] demonstrated by arteriography that methacholine provoked coronary spasms in susceptible patients. The angiographic demonstration of coronary spasm in response to methacholine is important, since subcutaneous methacholine may produce appreciable arterial hypotension and tachycardia, hemodynamic responses which alter angina threshold and may precipitate episodes of chest pain in the absence of coronary artery spasm.

Compared to the ergonovine test, provocation with methacholine has proved somewhat less reliable and has not been widely employed. It may be surprising that a muscarinic agonist, an agent expected to exert vasodilator effects, precipitates coronary spasm in patients with variant angina. Recent experiments with isolated arteries and veins in different laboratories have confirmed that an intact endothelium is required for nonneurogenic acetylcholine to exert its relaxing effects [105]. Mechanically deendothelialized vessels respond to acetylcholine with contraction, and apposition of a second vessel with intact endothelium against the deendothelialized surface of the test vessel has been reported to regenerate relaxation responses, suggesting that relaxation depends upon the release of a defusible factor from the endothelial cells [106]. The importance of this endothelial factor for vasomotion in vivo, and more specifically for neurogenic cholinergic vasodilation, has not been established, however.

WITHDRAWAL OF VASORELAXING AGENTS

The biochemical mechanisms underlying the development of tolerance to nitrates in the intact organism and in isolated arteries have not been completely elucidated [107]. Sudden withdrawal of nitrates from tolerant subjects may precipitate a vasospasm syndrome. Ammunition workers suddenly removed from their industrial exposure to nitrate have been reported to develop signs of vasospasms including myocardial ischemia and infarction [108]. It seems that the vasodilating influence of the nitrate evokes a counterregulatory constrictive hyperreactivity which is unmasked by the sudden withdrawal of the drug. However, the receptor pharmacologic and membrane biophysical mechanisms mediating the constrictive hyperreactivity have not been clarified.

Mechanism of Coronary Artery Spasm

In view of the limited and partly contradictory information available, the mechanism of coronary spasm in man remains to be clarified. However, experimental data on the contractile behavior of isolated human coronary arteries and on the altered reactivity of atherosclerotic arteries appear to provide a useful basis for further investigation.

RHYTHMIC CONTRACTILE ACTIVITY OF ISOLATED HUMAN CORONARY ARTERIES

Ross et al. [109] were the first to point out that isolated human coronary arteries exhibit striking oscillations in resting tone. The cycle length of the oscillations is slow, usually be-

tween 0.5 and 1.5 min. The oscillations are augmented by most constricting agonists, including potassium, calcium, norepinephrine, histamine, serotonin, acetylcholine, and thromboxane A_2. Monoaminergic blocking agents such as prazosin, propranolol, and ketanserin have little or no effect on the rhythmic activity [110]. On the other hand, withdrawal of calcium, calcium antagonists, local anesthetics, and nitroglycerin suppresses the rhythmic activity. Isolated epicardial coronary arteries from most common laboratory animals, including canine, porcine, ovine, and bovine arteries, fail to exhibit analogous rhythmic contractions. Rabbit coronary arteries ocassionally exhibit rhythmic contractions, but these intramyocardial arteries are small and difficult to isolate without damaging them (P.D. Henry, unpublished observations). Vascular smooth muscle (VSM) may be categorized into a group that generates action potentials in vitro ("spiking VSM") and another group that does not ("nonspiking VSM") [111]. Examples of spiking and nonspiking VSM are the rat portal vein and rabbit aorta, respectively. However, nonspiking VSM can be made to spike in vitro by lowering the K^+ conductance with barium and tetraethylammonium ions, indicating that the difference between spiking and nonspiking VSM is not a fundamental one. Unfortunately, there are no data available regarding the electrophysiologic properties of human coronary arterial smooth muscle. Therefore, it is not possible to make a statement about the possible relationship between electrical activity and rhythmic contractions in vitro or coronary spasm in vivo.

RELATIONSHIP BETWEEN ENDOTHELIUM, PLATELETS, AND VASOACTIVE LIPIDS

Endothelial cells are an important site of prostacyclin (PGI_2) synthesis, a prostanoid that relaxes smooth muscle and antagonizes platelet aggregation. Therefore, endothelial injury due to atherosclerotic changes [112, 113] or shear forces at the site of stenoses [114] may impair the ability of the vessel wall to generate PGI_2 and thereby favor constriction and platelet deposition [115]. Deposited platelets may amplify the response to endothelial injury by releasing constrictive and aggregating agents such as thromboxane A_2 and serotonin. It has been shown that angina, including vasospastic angina, may be associated with the release of thromboxane A_2 into the coronary venous blood [116, 117]. However, it has been difficult to establish a cause-and-effect relation between release of thromboxane A_2 and angina.

As mentioned above, endothelial injury may also modify arterial reactivity. Studies with isolated arteries have shown that relaxation in response to agents such as acetylcholine [105, 106], bradykinin [118], and thrombin [50] occurs only when the integrity of the endothelium is preserved. Deendothelialization of the arteries changes the response to these agents from dilation to constriction. Relaxations and constrictions evoked by acetylcholine are both blocked by atropine. The nature of the relaxing factor released from endothelial cells is not known. However, blockade of cyclooxygenase and lipooxygenase does not impair endothelium-dependent vasorelaxation, suggesting that the active principle is not an arachidonic acid metabolite of the prostaglandin and leucotriene series [106]. The recognition that endothelial cells may contribute to vasomotor regulation appears important, since various pathophysiologic processes in patients with coronary disease may impair endothelial function. The relationships between endothelial injury, altered vasomotion, and thrombogenesis will require further investigation.

RELATIONSHIP BETWEEN ATHEROSCLEROSIS AND VASOMOTOR REGULATION

An atherogenic environment may affect coronary regulation by factors other than the production of obstructive lesions or endothelial injury. Alterations in circulating lipids may potentially affect the lipid composition of the cell membrane of platelets [119] and vascular smooth muscle [120]. Hypercholesterolemia may alter platelet function and result in increased aggregability [119]. Similarly, hypercholesterolemia in rabbits may alter the reactivity of the arteries to various vasoactive agonists. For instance, aortas from hypercholesterolemic rabbits may be supersensitive to ergonovine and serotonin. This supersensitivity may be

mediated by alterations in the membrane receptors of smooth muscle cells. Radioligand binding experiments and receptor autoradiographic studies with atherosclerotic rabbit aortas have revealed an increased abundance of serotonergic receptors localized in the inner media and intima [121]. Acute exposure of isolated canine coronary arteries to a high-cholesterol environment appears to sensitize the arteries to the constrictor effects of calcium ions. Whether this phenomenon reflects predominantly excessive uptake of Ca^{2+} or deficient active extrusion of Ca^{2+} has not been established. In various membranes, an increased abundance of membrane cholesterol has been shown to suppress Na,K-ATPase activity [122]. The sensitivity of membrane transporters to changes in their lipid microenvironment is an important observation, since decreased Ca^{2+} extrusion might enhance the response to constictors that stimulate Ca^{2+} uptake. Recently, Shimokawa et al. (1983) [123] provoked coronary artery spasms in atherosclerotic miniature swine by the administration of histamine after pretreatment with cimetidine. The constrictor responses were blocked by the H_1 antihistamine diphenhydramine.

It is not known whether hypercholesterolemia in man is associated with alterations in arterial reactivity. It has been suggested that patients with atherosclerosis react excessively to the cold pressor test, a phenomenon that might indicate an altered noradrenergic responsiveness [124].

EFFECTS OF METALLIC IONS

Experiments with potassium-ion-selective electrodes have shown that potassium may increase up to 15 m*M* or higher in ischemic myocardium [125]. Although such concentrations of potassium exert potent constrictor effects on vascular smooth muscle, the role of potassium in the regulation of intramyocardial coronary resistance during ischemia has not been well characterized. Recently, we have demonstrated that potassium applied to the external surface of epicardial canine coronary arteries in situ exerts potent and sustained constrictor effects, whereas other agents, including norepinephrine and angiotensin II, applied similarly failed to evoke sustained constrictions [125].

It has been suggested that magnesium deficiency may contribute to the development of coronary spasm [126]. Isolated canine coronary arteries exposed to a medium containing no magnesium exhibited increased constrictions in response to a variety of agents, including norepinephrine, acetylcholine, serotonin, angiotensin II, and potassium [126].

EFFECT OF HYDROGEN IONS

Lowering the hydrogen ion activity by hyperventilation or infusion of tris base may provoke coronary artery spasm, and these maneuvers have been suggested as provocative tests for the diagnosis of vasospastic angina [127]. Coronary spasm after exercise might be related to hyperventilation, but there is little information available about acid–base changes in patients with exercise-related coronary spasm.

Therapeutic Interventions

The initial observation by Japanese workers that calcium antagonists are effective for the treatment of variant angina has been widely confirmed. An uncontrolled study from 11 institutions in Japan involving 243 patients has shown that nifedipine (30–60 mg/day), diltiazem (90–240 mg/day), and verapamil (120–320 mg/day) were effective in reducing or abolishing variant angina in 94%, 91%, and 86% of the patients, respectively [128]. In contrast, beta blockers alone produced relief in only 11% of the patients. In a similar open trial involving multiple American Centers, nifedipine produced symptomatic relief in 63% of the cases [129]. Nifedipine, diltiazem, and verapamil are effective in suppressing ergonovine-induced attacks of chest pain in patients thought to suffer from angiospastic angina [130]. In one recent report, calcium antagonists controlled symptoms in the majority of patients suffering from coronary artery spasm, whereas an average dose of 80 mg/day of isosorbide dinitrate was often ineffective [55]. However, in a randomized study, isosorbide dinitrate and nifedipine did not appear to differ in efficacy for the treatment of coronary artery spasm [131]. Such studies are difficult to evaluate, since they are based in part upon arbitrary dosing of drugs.

As mentioned above, it is possible that

membrane physiologic changes of atherosclerosis promote the net uptake of calcium, a process that might explain excessive constrictor responses. An abnormality of the uptake or extrusion of calcium has been recently invoked as a pathophysiologic mechanism of various hypertensive syndromes [132]. Therefore, if abnormalities in calcium uptake play a role in the pathogenesis of abnormal constrictor responses, the use of calcium antagonists might represent a specific therapeutic intervention. It should be emphasized, however, that calcium antagonists are effective in blocking numerous endogenous constrictors, including norepinephrine, serotonin, angiotensin II, and thromboxane A_2. Consequently, detailed receptor pharmacologic studies are required to clarify the mechanism of action of calcium antagonists in vivo [130].

Although platelets may play a role in precipitating or aggravating coronary artery spasm, intravenous prostacyclin or cyclooxygenase inhibitors have thus far not been shown to exert beneficial effects [116, 117, 133, 134].

Indications for mechanical interventions in patients with coronary spasm are similar to those without spasm. Therefore, fixed lesions may be considered for treatment by coronary bypass grafting [46] or percutaneous transluminal angioplasty [135]. However, these procedures do not appear to modify the vasospastic component of the disease [135].

Summary

The concept of coronary artery spasm derives from clinical coronary arteriographic observations demonstrating sustained, vasodilator-sensitive coronary constrictions during which patients suffer from symptoms and signs of myocardial ischemia. Most patients with coronary spasm exhibit angiographic signs of coronary atherosclerosis. Coronary spasm of a major epicardial coronary artery may produce marked electrocardiographic changes including transient ST elevations and Q waves. Although recurrent marked ST elevations may occur in patients with Prinzmetal variant angina, similar electrocardiographic changes may be observed in other anginal syndromes, including exercise-related angina, and angina before and after myocardial infarction. In addition, there is evidence that coronary spasm plays a pathogenic role in acute myocardial infarction and sudden death.

The vasomotor mechanisms underlying inappropriately sustained coronary constrictor responses are poorly understood. Provocation of coronary spasm with ergonovine and its relief with calcium antagonists provide little specific receptor-pharmacologic information, since ergonovine may act on multiple monoaminergic receptors and calcium antagonists are effective blockers of multiple endogenous constrictors.

Experimental studies suggest that vascular smooth muscle exposed to a high-cholesterol environment may undergo membrane physiologic changes involving monoaminergic receptors and ion transporters. Therefore, it is possible that coronary artery spasm reflects membrane physiologic changes of atherosclerosis.

References

1. Burns A: Observations on some account of the most frequent and important diseases of the heart. Edinburgh: J Muirhead, 1809, pp 136–163.
2. Herberden W: Some account of a disorder of the breast. R Coll Phys Med Trans 2:59–67, 1772.
3. Nothnagel H: Angina pectoris vasomotoria. Dts Arch Klin Med 3:309–322, 1867.
4. Latham PM: Collected works, vol 1. London: New Sydenham Society, 1876. Lecture 37, pp 445–463.
5. Hale EM: Lectures on diseases of the heart. New York: Boericke and Tafel, 1871, p 56.
6. Osler W: The principles and practice of medicine. New York: WD Appleton and Co, 1892, p 656.
7. Osler W: The Lumleian lectures on angina pectoris: lecture II. Lancet 1:839–844, 1910.
8. Smith FM: The ligation of coronary arteries with electrocardiographic study. Arch Intern Med 22:8–27, 1918.
9. Pardee HEB: An electrocardiographic sign of coronary artery obstruction. Arch Intern Med 26:244–257, 1920.
10. Parkinson J, Bedford DE: Electrocardiographic changes during brief attacks of angina pectoris. Lancet 1:15–19, 1931.
11. Wilson FN, Johnston FD: The occurrence in angina pectoris of electrocardiographic changes similar in magnitude and in kind to those produced by myocardial infarction. Am Heart J 22:64–74, 1941.
12. Sanazaro PJ: Transient electrocardiographic changes simulating acute myocardial infarction. Am Heart J 51:149–155, 1956.
13. Roesler H, Bressler W: Transient electrocardiographic changes identical with those of acute myo-

cardial infarction accompanying attacks of angina pectoris. Am Heart J 47:520–526, 1954.
14. Hausner E, Scherf D: Uber Angina Pectoris Probleme. Z Klin Med 126:166–193, 1933.
15. Brow GR, Holman DV: Electrocardiographic study during a paroxysm of angina pectoris. Am Heart J 9:259–264, 1933.
16. Prinzmetal J, Kennamer R, Merliss R, Wada T, Bor N: Angina pectoris. I. A variant form of angina pectoris: preliminary report. Am J Med 27:375–388, 1959.
17. Arnulf G: Étude artériographique de la vasomotricité coronarienne chez l'animal et chez l'homme. Presse Med 67:2055–2057, 1959.
18. Gensini GG, Di Giorgi S, Murad-Netto S, Black A: Arteriographic demonstration of coronary artery spasm and its release after the use of a vasodilator in a case of angina pectoris and in the experimental animal. Angiology 13:550–553, 1962.
19. Demany MA, Tambe A, Zimmerman HA: Coronary arterial spasm. Dis Chest 53:714–721, 1968.
20. Dhurandhar RW, Walt DL, Silver MD, Trimble AS, Adelman AG: Prinzmetal's variant form of angina with arteriographic evidence of coronary arterial spasm. Am J Cardiol 30:902–905, 1972.
21. Guazzi M, Olivari MT, Polese A, Fiorentini C, Margrini F: Repetitive myocardial ischemia of Prinzmetal type without angina pectoris. Am J Cardiol 37:923–927, 1976.
22. Meller J, Conde CA, Donoso E, Dack S: Transient Q waves in Prinzmetal's angina. Am J Cardiol 35:691–695, 1975.
23. Maseri A, Severi S, De Nes M, l'Abbate M, Chierchia A, Marzilli M, Ballestra A-M, Parodi O, Biagini A, Distante A: "Variant" angina: one aspect of a continuous spectrum of vasospastic myocardial ischemia. Am J Cardiol 42:1019–1035, 1978.
24. Madias JE: The syndrome of variant angina culminating in acute myocardial infarction. Circulation 59:297–306, 1979.
25. Boden WE, Bough EW, Benham I, Shulman RS: Unstable angina with episodic ST segment elevation and minimal creatine kinase release culminating in extensive, recurrent infarction. J Am Coll Cardiol 1:11–20, 1983.
26. Bentley KI, Clark M, Henry PD: Angiographic dye relaxes canine coronary artery by a non-osmotic mechanism. Am J Cardiol 47:407, 1981.
27. Morris TW, Katzberg RW, Fischer HW: A comparison of the hemodynamic responses to metrizamide and meglumine/sodium diatrizoate in canine renal angiography. Invest Radiol 13:74–78, 1978.
28. Arnett EN, Roberts WC: Acute myocardial infarction and angiographically normal coronary arteries: an unproven combination. Circulation 53:395–400, 1976.
29. Marcus ML, Armstrong ML, Heistad DD, Eastham CL, Mark AL: Comparison of three methods of evaluating coronary obstructive lesions: postmortem arteriography, pathologic examination and measurement of regional myocardial perfusion during maximal vasodilation. Am J Cardiol 49:1699–1706, 1982.
30. MacAlpin RN: Contribution of dynamic vascular wall thickening to luminal narrowing during coronary arterial constriction. Circulation 61:296–301, 1980.
31. Bennett KR: Coronary artery spasm: the effect of cardiovascular laboratory. Cathet Cardiovasc Diagn 2:321–327, 1976.
32. Leary T: Coronary spasm as a possible factor in producing sudden death. Am Heart J 10:338–344, 1935.
33. Sewell WH: Coronary spasm as a primary cause of myocardial infarction. Angiology 17:1–8, 1966.
34. Oliva PB, Breckinridge JC: Arteriographic evidence of coronary arterial spasm in acute myocardial infarction. Circulation 56:366–374, 1977.
35. Johnson AD, Detwiler JH: Coronary spasm, variant angina, and recurrent myocardial infarctions. Circulation 55:947–950, 1977.
36. Maseri A, l'Abbate A, Baroldi G, Chierchia S, Marzilli M, Ballestra AM, Severi S, Parodi O, Biagini A, Distante A, Pesola A: Coronary vasospasm as a possible cause of myocardial infarction. N Engl J Med 299:1271–1277, 1978.
37. El-Maraghi NRH, Sealey BJ: Recurrent myocardial infarction in a young man due to coronary arterial spasm demonstrated at autopsy. Circulation 61: 199–207, 1980.
38. Vincent GM, Anderson JL, Marshall HW: Coronary spasm producing coronary thrombosis and myocardial infarction. N Engl J Med 309:220–223, 1983.
39. Angoli L, Marinoni GP, Falcone C, Bramucci E, De Servi S, Specchia G, Montemartini C: Spasme coronarien a l'effort: demonstration coronarographique d'un cas. Arch Mal Coeur 71:823–826, 1978.
40. Yasue H, Omote S, Takizawa A, Nagao M, Miwa K, Tanaka S: Exertional angina pectoris caused by coronary arterial spasm: effects of various drugs. Am J Cardiol 43:647–652, 1979.
41. Broustet JP, Griffo R, Series E, Guern P, Laylavoix F: Angor de Prinzmetal déclenché par l'arrêt de l'effort: cinq cas a coronarographie normale. Arch Mal Coeur 72:391–400, 1979.
42. Waters DD, Chaitman BR, Dupras G, Théroux P, Mizgala HF: Coronary artery spasm during exercise in patients with variant angina. Circulation 52:580–585, 1979.
43. Yasue H, Omote S, Takizawa A, Nagao M, Miwa K, Tanaka S: Circadian variation of exercise capacity in patients with Prinzmetal's variant angina: role of exercise-induced coronary arterial spasm. Circulation 59:938–948, 1979.
44. Specchia G, De Servi S, Falcone C, Bramucci E, Angoli L, Mussini A, Marinoni GP, Montemartini C, Bobba P: Coronary arterial spasm as a cause of exercise-induced ST-segment elevation in patients

with variant angina. Circulation 59:948–954, 1979.
45. Waters DD, Szlachcic J, Bonan R, Miller DD, Dauwe F, Théroux P: Comparative sensitivity of exercise, cold pressor and ergonovine testing in provoking attacks of variant angina in patients with active disease. Circulation 67:310–315, 1983.
46. Kimura E, Hosoda S, Katoh K, Endo M, Yasue H, Asada S, Kuroiwa A: Panel discussion on the variant form of angina pectoris. Jpn Circ J 42:455–476, 1978.
47. Sakanashi M: Pharmacological aspects of coronary arterial spasm. TIPS 2:234–236, 1981.
48. Ganz W: Coronary spasm in myocardial infarction: fact or fiction? Circulation 63:487–488, 1981.
49. Koiwaya Y, Torii S, Takeshita A, Nakagaki O, Nakamura M: Postinfarction angina caused by coronary arterial spasm. Circulation 65:275–280, 1982.
50. Ku DD: Coronary vascular reactivity after acute myocardial ischemia. Science 218:576–578, 1982.
51. Kimura E, Tanaka K, Mizuno K, Honda Y, Hashimoto H: Suppression of repeatedly occurring ventricular fibrillation with nifedipine in variant form of angina pectoris. Jpn Heart J 18:736–742, 1977.
52. Campbell TJ, Hickie JB, Michell G, O'Rourke MF: Nifedipine in the treatment of life threatening Prinzmetal angina. Aust NZ J Med 9:293–294, 1979.
53. Miller DD, Waters DD, Szlachcic J, Théroux P: Clinical characteristics associated with sudden death in patients with variant angina. Circulation 66:588–592, 1982.
54. Waters DD, Bouchard A, Théroux P: Spontaneous remission is a frequent outcome of variant angina. J Am Coll Cardiol 2:195–199, 1983.
55. Bott-Silverman C, Heupler FA: Natural history of pure coronary artery spasm in patients treated medically. J Am Coll Cardiol 2:200–205, 1983.
56. Heupler FA: Syndrome of symptomatic coronary arterial spasm with nearly normal coronary arteriograms. Am J Cardiol 45:873–881, 1980.
57. Selzer A, Langston M, Ruggeroli C, Cohn K: Clinical syndrome of variant angina with normal coronary arteriogram. N Engl J Med 295:1343–1347, 1976.
58. Wissler RW, Vesselinovitch D: Atherosclerosis: relationship to coronary blood flow. Am J Cardiol 52:2A-7A, 1983.
59. Peretz DI: Variant angina pectoris of Prinzmetal. Can Med Assoc J 85:1101–1102, 1961.
60. Mériel P, Galinier F, Bounhoure J-P, Mignon J-P, Salvador M: Onde monophasique et tachycardie ventriculaire dans l'angor spontané de type Prinzmetal. Arch Mal Coeur 59:460–465, 1966.
61. Gianelly R, Mugler F, Harrison DC: Prinzmetal's variant of angina pectoris with only slight coronary atherosclerosis. Calif Med 108:129–132, 1968.
62. Benhaim R, Calvo G, Seban C, Tarrade T, Chiche P: Les aspects anatomiques de l'angor de Prinzmetal: à propos d'une observation anatomoclinique. Arch Mal Coeur 68:189–197, 1975.
63. Poggi L, Bory M, Djiane P, d'Journo J, Serradimigni A: Les lesions anatomiques dans l'angor spontané de Prinzmetal. Marseille Med 109:39–41, 1972.
64. Guermonprez JL, Gueret P, Camilleri JP, Guerinon J, Deloche A, Maurice P: Angor de Prinzmetal, Etude histologique coronaire de prélévements peroperatoires. Arch Mal Coeur 70:301–308, 1977.
65. Petitier H, De Lajartre AY, Geslin Ph, Godin JF, Victor J, Crochet D, Dupon H: Dysplasie fibreuse intimale coronaire et angor de Prinzmetal. Arch Mal Coeur 71:963–1438 and 1053–1059, 1978.
66. Fievez M, Philippart F, Hustin J: Communications to the editor. Angiology 26:491–498, 1975.
67. Von Storch TJC: Complications following the use of ergotamine tartrate. JAMA 111:293–300, 1938.
68. Goldfischer JD: Acute myocardial infarction secondary to ergot therapy. N Engl J Med 262:860–863, 1960.
69. Labbé M, Boulin R, Justin-Besancon G: L'Angine de poitrine ergotaminique. Presse Med 66:1069, 1929.
70. Nordenfelt O: Über functionelle Veränderungen der P und T-Zacken im Elektrokardiogramm. Acta Med Scand Suppl 119:1, 1941.
71. Master AM, Pordy L, Kolker J: Ergotamine tartrate and the "two step" exercise electrocardiogram in functional cardiac disturbance. J Mt Sinai Hosp 15:164–168, 1948.
72. Scherf D, Schlachman M: Electrocardiographic and clinical studies on the action of ergotamine tartrate and dihydro-ergotamine. Am J Med Sci 216:673–679, 1948.
73. Stein I: Observations on the action of ergonovine on the coronary circulation and its use in the diagnosis of coronary artery insufficiency. Am Heart J 37:36–45, 1949.
74. Heupler FA, Proudfit WL, Razavi M, Shirey EK, Greenstreet R, Sheldon WC: Ergonovine maleate provocative test for coronary arterial spasm. Am J Cardiol 41:631–640, 1978.
75. Curry RC, Pepine CJ, Sabom MB, Conti CR: Similarities of ergonovine-induced and spontaneous attacks of variant angina. Circulation 59:307–312, 1979.
76. Théroux P, Waters DD, Affaki GS, Crittin J, Bonan R, Mizgala HF: Provocative testing with ergonovine to evaluate the efficacy of treatment with calcium antagonists in variant angina. Circulation 60:504–509, 1979.
77. Cipriano PR, Guthaner DF, Orlick AE, Ricci DR, Wexler L, Silverman JF: The effects of ergonovine maleate on coronary arterial size. Circulation 59:82–89, 1979.
78. Cannon RO, Watson RM, Rosing DR, Epstein SE: Angina caused by reduced vasodilator reserve of the small coronary arteries. J Am Coll Cardiol 1:1359–1373, 1983.

79. Berde B, Sturmer E: Introduction to the pharmacology of ergot alkaloids and related compounds as a basis of their therapeutic application. In: Berde B, Schild HO (eds) Berlin: Ergot alkaloids and related compounds. Springer-Verlag, 1978, pp 1–23.
80. Müller-Schweinitzer E: The mechanism of ergometrine-induced coronary arterial spasm: in vitro studies on canine arteries. J Cardiovasc Pharmacol 2:645–655, 1980.
81. Sakanashi M, Yonemura K-I: On the mode of action of ergometrine in the isolated dog coronary artery. Eur J Pharmacol 64:157–160, 1980.
82. Brazenor RM, Angus JA: Ergometrine contracts isolated canine coronary arteries by a serotonergic mechanism: no role for alpha adrenoceptors. J Pharmacol Exp Ther 218:530–536, 1981.
83. Holtz J, Held W, Sommer O, Kühne G, Bassenge E: Ergonovine-induced constrictions of epicardial coronary arteries in conscious dogs: α-adrenoceptors are not involved. Basic Res Cardiol 77:278–291, 1982.
84. Henry PD: Coronary constriction as a pathogenic mechanism of myocardial ischemia. In: De Bakey ME, Gotto AM (eds) Factors influencing the course of myocardial ischemia. Amsterdam: Elsevier Biomedical, 1983, pp 123–133.
85. Orlick AE, Ricci DR, Alderman EL, Stinson EB, Harrison DC: Effects of alpha adrenergic blockade upon coronary hemodynamics. J Clin Invest 62:459–467, 1978.
86. Mudge GH, Grossman W, Mills RM, Lesch M, Braunwald E: Reflex increase in coronary vascular resistance in patients with ischemic heart disease. N Engl J Med 295:1333–1337, 1976.
87. Levene DL, Freeman MR: α-Adrenoceptor-mediated coronary artery spasm. JAMA 236:1018–1052, 1976.
88. Yasue H, Touyama M, Shimamoto M, Kato H, Tanaka S, Akiyama F: Role of autonomic nervous system in the pathogenesis of Prinzmetal's variant form of angina. Circulation 50:534, 1974.
89. Yasue H, Youyama M, Kato H, Tanaka S, Akiyama F: Prinzmetal's variant form of angina as a manifestation of alpha-adrenergic receptor-mediated coronary artery spasm: documentation by coronary arteriography. Am Heart J 91:148–155, 1976.
90. Ricci DR, Orlick AE, Cipriano PR, Guthaner DF, Harrison DC: Altered adrenergic activity in coronary arterial spasm: insight into mechanism based on study of coronary hemodynamics and the electrocardiogram. Am J Cardiol 43:1073–1079, 1979.
91. Bertrand ME, Lablanche JM, Rousseau MF, Warembourg HH, Stankowtak C, Soots G: Surgical treatment of variant angina: use of plexectomy with aortocoronary bypass. Circulation 61:877–882, 1980.
92. Bertrand ME, Lablanche JM, Tilmant PY, Ducloux G, Warembourg H, Soots G: Complete denervation of the heart (autotransplantation) for treatment of severe, refractory coronary spasm. Am J Cardiol 47:1375–1378, 1981.
93. Chierchia S, Davies G, Gerkenboom G, Crea F, Crean P, Maseri A: Alpha-adrenergic receptors and coronary spasm: an elusive link. Circulation 69:8–14, 1984.
94. Buda AJ, Fowles RE, Schroeder JS, Hunt SA, Cipriano PR, Stinson EB, Harrison DC: Coronary artery spasm in the denervated transplanted human heart. Am J Med 70:1144–1149, 1981.
95. Weber S, Donzeau-Gouge G-P, Chauvaud S, Picard G, Guerin F, Carpentier A, Degeorges M: Assessment of plexectomy in the treatment of severe coronary spasm in patients with normal coronary arteries. Am J Cardiol 51:1072–1076, 1983.
96. Robertson D, Robertson RM, Nies AS, Oates JA, Friesinger GC: Variant angina pectoris: investigation of indexes of sympathetic nervous system function. Am J Cardiol 43:1080–1085, 1979.
97. Yasue H, Omote S, Takizawa A, Nagao M, Miwa K, Kato H, Tanaka S, Akiyama F: Pathogenesis and treatment of angina pectoris at rest as seen from its response to various drugs. Jpn Circ J 42:1–10, 1978.
98. Robertson RM, Wood AJJ, Vaughn WK, Robertson D: Exacerbation of vasotonic angina pectoris by propranolol. Circulation 65:281–285, 1982.
99. Tilmant PY, Lablanche JM, Thieuleux FA, Dupuis BA, Bertrand ME: Detrimental effect of propranolol in patients with coronary arterial spasm countered by combination with diltiazem. Am J Cardiol 52:230–233, 1983.
100. Ginsburg R, Bristow MR, Kantrowitz N, Baim DS, Harrison DC: Histamine provocation of clinical coronary artery spasm: implications concerning pathogenesis of variant angina pectoris. Am Heart J 102:819–822, 1981.
101. Henry PD, Yokoyama M: Inappropriate coronary vasomotion: search for a local fault. In: Rafflenbeul W, Lichtlen PR, Balcon R (eds) Unstable angina pectoris. Stuttgart; G Thieme, New York, 1981, pp 18–23.
102. Van Nueten JM, Janssen PAJ, Van Beek J, Xhonneux R, Verbeuren TJ, Vanhoutte PM: Vascular effects of ketanserin (R 41 468), a novel antagonist of 5-HT_2 serotonergic receptors. J Pharmacol Exp Ther 218:217–230, 1981.
103. Personal communications: Drs ME Bertrand, Lille, France; DD Waters, Montreal, Canada; and S Chiercha, London, England.
104. Endo M, Hirosawa K, Kaneko N, Hase K, Inoue Y, Konno S: Prinzmetal's variant angina. N Engl J Med 294:252–255, 1976.
105. Furchgott RF, Zawadzki JV: The obligatory role of endothelial cells in the relaxation of arterial smooth muscle by acetylcholine. Nature 288:373–376, 1980.
106. Frank GW, Bevan JA: Electrical stimulation causes endothelium-dependent relaxation in lung vessels. Am J Physiol 244:H793–H798, 1983.
107. Ignarro LJ, Lippton H, Edwards JC, Baricos WH, Hyman AL, Kadowitz PJ, Gruetter CA: Mechanism of vascular smooth muscle relaxation by organic ni-

rates, nitrites, nitroprusside and nitric oxide: evidence for the involvement of S-nitrosothiols as active intermediates. J Pharmacol Exp Ther 218:739–749, 1981.
108. Lange RL, Reid MS, Tresch DD, Keelan MH, Bernhard VM, Coolidge G: Nonatheromatous ischemic heart disease following withdrawal from chronic industrial nitroglycerin exposure. Circulation 46:666–678, 1972.
109. Ross G, Stinson E, Schroeder J, Ginsburg R: Spontaneous phasic activity of isolated human coronary arteries. Cardiovasc Res 14:613–618, 1980.
110. Ginsburg R, Bristow MR, Harrison DC, Stinson EB: Studies with isolated human coronary arteries. Chest 78:180–186, 1980.
111. Speralakis N: Electrophysiology of vascular smooth muscle of coronary artery. In: Kalsner S (ed) The coronary artery. London: Croom Helm, 1982, pp 118–166.
112. Dembinska-Kiec A, Gryglewska T, Zmunda A, Gryglewski RJ: The generation of prostacyclin by arteries and by the coronary vascular bed is reduced in experimental atherosclerosis in rabbit. Prostaglandins 14:1025–1034, 1977.
113. Angelo VD, Villa S, Mysliwiec M, Donati MB, De Gaetaso G: Defective fibrinolitic and prostacyclin like activity in human atheromatous plaques. Thromb Diath Haem 39:535–536, 1978.
114. Folts JD, Gallagher K, Rowe GG: Blood flow reductions in stenosed canine coronary arteries: vasospasm or platelet aggregation? Circulation 65:248–255, 1982.
115. Martin TJ, Smith IL, Nolan RD, Dusting GJ: Prostanoids in platelet-vascular interactions. Am J Cardiol 52:22A–27A, 1983.
116. Robertson RM, Robertson D, Roberts LJ, Maas RL, FitzGerald GA, Friesinger GC, Oates JA: Thromboxane A_2 in vasotonic angina pectoris. N Engl J Med 304:998–1003, 1981.
117. Hirsh PD, Hillis LD, Campbell WB, Firth BG, Willerson JT: Release of prostaglandins and thromboxane into the coronary circulation in patients with ischemic heart disease. N Engl J Med 304:685–691, 1981.
118. Chand N, Altura BM: Acetylcholine and bradykinin relax intrapulmonary arteries by acting on endothelial cells: role in lung vascular diseases. Science 213:1376–1379, 1981.
119. Shattil SJ, Anaya-Galindo R, Bennett J, Colman RW, Cooper RA: Platelet hypersensitivity induced by cholesterol incorporation. J Clin Invest 55:636–643, 1975.
120. Henry PD, Yokoyama M: Supersensitivity of atherosclerotic rabbit aorta to ergonovine: mediation by a serotonergic mechanism. J Clin Invest 66:306–313, 1980.
121. Nanda V, Henry PD: Increased serotonergic and alpha adrenergic receptors in aortas from rabbits fed a high cholesterol diet. Clin Res 30:209A, 1982.
122. Yokoyama M, Henry PD: Sensitization of isolated canine coronary arteries to calcium ions after exposure to cholesterol. Circ Res 45:479–486, 1979.
123. Shimokawa H, Tomoike H, Nakeyama S, Yamamoto H, Araki H, Nakamura M: Coronary artery spasm induced in atherosclerotic miniature swine. Science 221:560–561, 1983.
124. Voudoukis IJ: Exaggerated cold-pressor response in hypertensive patients with superimposed arteriosclerosis. J Surg Oncol 2:83–87, 1970.
125. Perez JE, Saffitz JE, Gutierrez FA, Henry PD: Coronary artery spasm in intact dogs induced by potassium and serotonin. Circ Res 52:423–431, 1983.
126. Turlapaty PDMV, Altura BM: Magnesium deficiency produces spasms of coronary arteries: relationship to etiology of sudden death ischemic heart disease. Science 208:198–200, 1980.
127. Yasue H, Nagao M, Omote S, Takizawa A, Miwa K, Tanaka S: Coronary arterial spasm and Prinzmetal's variant form of angina induced by hyperventilation and tris-buffer infusion. Circulation 58:56–62, 1978.
128. Kimura E, Kishida H: Treatment of variant angina with drugs: a survey of 11 cardiology institutes in Japan. Circulation 63L:844, 1981.
129. Antman E, Muller JE, Goldberg S, MacAlpin R, Rubenfine M, Tabatznid B, Liang C, Heupler F, Achuff S, Reichek N, Geltman E, Kerin NZ, Neff RK, Braunwald E: Nifedipine therapy for coronary artery spasm: experience in 127 patients. N Engl J Med 302:1269–1273, 1980.
130. Henry PD, Perez JE: Clinical pharmacology of calcium antagonists. In: Brest AN (ed) Cardiovascular clinics. Philadelphia: FA Davis, 1984, 93–109.
131. Hill JA, Feldman RL, Pepine CJ, Conti CR: Randomized double-blind comparison of nifedipine isosorbide dinitrate in patients with coronary arterial spasm. Am J Cardiol 49:431–437, 1982.
132. Bühler FR, Hulthén L: Calcium channel blockers: a pathophysiologically based hypertensive treatment concept for the future? Eur J Clin Invest 12:1–3, 1982.
133. Chierchia S, Patrono C, Crea F, Ciabattoni G, De Caterina R, Cinotti GA, Distante A, Maseri A: Effects of intravenous prostacyclin in variant angina. Circulation 65:470–477, 1982.
134. Chierchia S, De Caterina R, Crea F, Patrono C, Maseri A: Failure of thromboxane A_2 blockade to prevent attacks of vasospastic angina. Circulation 66:702–705, 1982.
135. David PR, Waters DD, School J-M, Crepeau J, Szlachcic J, Lesperance J, Hudon G, Bourassa G: Percutaneous transluminal coronary angioplasty in patients with variant angina. Circulation 66:695–702, 1982.

INDEX